Modern Approaches in Solid Earth Sciences

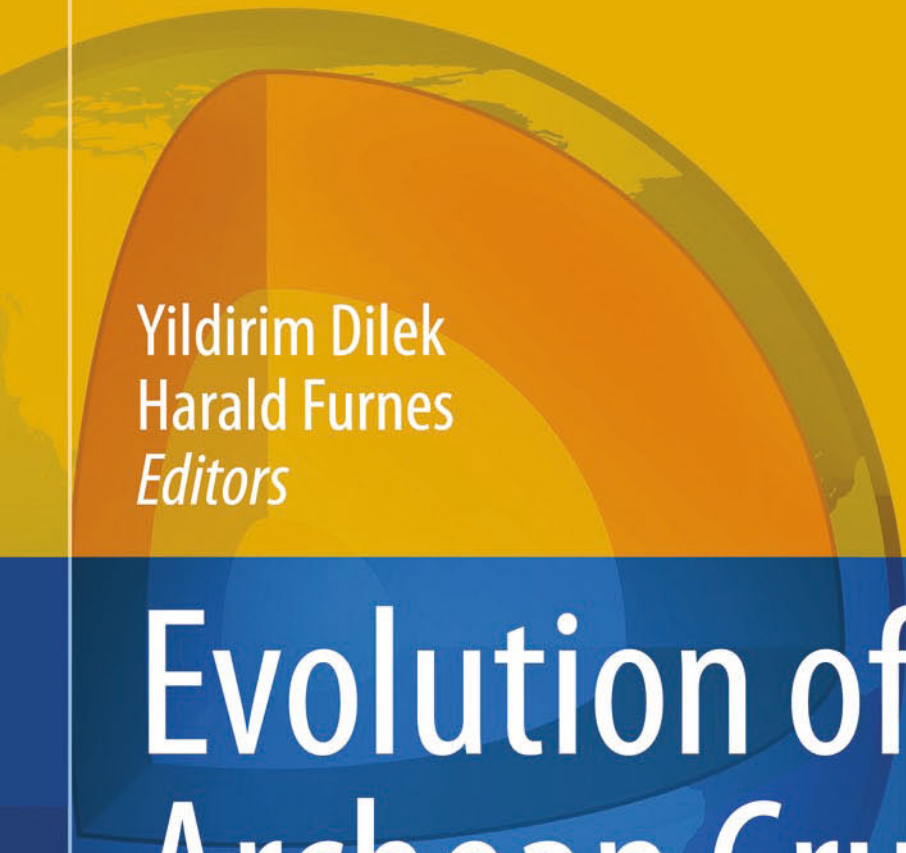

Yildirim Dilek
Harald Furnes
Editors

Evolution of Archean Crust and Early Life

Springer

Evolution of Archean Crust and Early Life

Modern Approaches in Solid Earth Sciences

VOLUME 7

Series Editors

For other titles published in this series, go to
www.springer.com/series/7377

Yildirim Dilek • Harald Furnes
Editors

Evolution of Archean Crust and Early Life

Springer

Editors
Yildirim Dilek
Dept. of Geology & Environmental Earth Science
Miami University
Oxford
Ohio
USA

Harald Furnes
Department of Earth Science & Centre for Geobiology
University of Bergen
Bergen
Norway

Responsible Series Editor: Y. Dilek

ISSN 1876-1682 ISSN 1876-1690 (electronic)
ISBN 978-94-007-7614-2 ISBN 978-94-007-7615-9 (eBook)
DOI 10.1007/978-94-007-7615-9
Springer Dordrecht Heidelberg London New York

Library of Congress Control Number: 2013954958

Credit cover figure: bubaone/istockphoto.com

Printed on acid-free paper

Springer is part of Springer Science+Business Media (www.springer.com)

Preface

The geological, geochemical and geodynamic processes involved in the formation of oceanic and continental crust during the Phanerozoic are well understood within the frameworks of plate and plume tectonics. However, processes and the mode (steady-state versus episodic) of oceanic and juvenile continental crust generation in the Precambrian, particularly during the Archean, are less understood and more controversial because of the ongoing debate about whether or not modern plate tectonics operated prior to the Neoarchean. The Phanerozoic ophiolite record shows that ancient oceanic crust developed in various tectonic settings, such as mid-ocean ridges, arc–back arc–forearc regions, and rifted continental margins, during the Wilson Cycle evolution of ocean basins. Unequivocal ophiolite occurrences in the Archean record are rare in the literature, but are potentially more widespread in the greenstone belts than our current estimates and considerations. Similarly, how large amounts of continental crust were produced and how much of it was recycled back into the mantle in the Archean, what role mantle plumes versus plate tectonics played in continental crust formation during the early Precambrian are some of the outstanding questions regarding Earth's crustal growth and evolution.

Archean greenstone belts constitute a significant component of the Precambrian geology and provide a window into deep time. They consist mainly of mafic-ultramafic lavas, calc-alkaline-felsic volcanic and volcaniclastic rocks, and sedimentary lithofacies assemblages. Most greenstone belts are spatially associated with TTG (tonalite, trondhjemite, granodiorite) terrains. Competing models on the origin and evolution of greenstone belts have important implications for the Archean Earth. The role of plate tectonics in the evolution of Phanerozoic and Proterozoic crust is well established, but is a subject of debate regarding the Archean history. Crustal growth and differentiation through punctuated events (i.e. emplacement of mantle 'superplumes') versus continuous subduction processes and whether Archean crust was too weak and mobile to behave as in rigid plates are fundamental questions in geodynamics and in Earth history. Recent studies have documented the occurrence of boninites, adakites, Mg-andesites, high-pressure rocks, and ophiolites in some of the Archean greenstone belts, suggesting that Phanerozoic-like subduction zone tectonics may have been operating as early as 3.8 Ga. Geophysical findings also show that many greenstone belts can be interpreted as horizontal thrust sheets, rather than deep synclinal keels, indicating that their unexposed bottoms are most likely defined by major shear

zones, and that many greenstone belts were involved in some type of fold-and-thrust and/or listric extensional tectonics.

Well-preserved bioalteration textures in Archean marine volcanic glass suggest an endolithic mode of microbial life in the early Earth. What role did submarine volcanoes play during the origin of early life remains a significant question and is being addressed nowadays through the integrated studies of Archean oceanic crust. The recently conducted Barberton *Scientific Drilling Program* (South Africa) has been designed to shed some light on these questions.

This book has emanated from a series of scientific sessions we convened during the International Geological Congress (IGC-33) in Oslo in 2008 and at the Geological Society of America Annual Meetings in Portland (2009) and Minneapolis (2011). The main objectives of these sessions were to evaluate and to discuss the diverse datasets from the Archean Earth, specifically the greenstone belts, in order to better understand the nature and tempo of physical, chemical and biological processes involved in development of the Archean Earth and their implications for the planetary evolution and early life. The book mostly contains some of the papers presented in these sessions, and provides an integrated approach to the study of the evolution of the Archaean lithosphere and biosphere. The structural and geochemical make-up of both the oceanic and continental crust of the Archaean Earth is documented in some case studies of various cratons, and the implications of the Phanerozoic plate and plume tectonic processes for the Archaean geology are discussed in several chapters. The last four chapters in the book investigate the record of microbial life in the Archean Earth and the recently developed techniques of decoding this record to better understand the evolution of the early life in marine and in some extreme environments. All chapters are process-oriented and data-rich, and reflect the most recent knowledge and information on the Archean Earth. The interdisciplinary approach of examining the evolution of the Archean crust and life in this book sets it apart from previous publications on Precambrian geology, and makes it a unique contribution to our understanding of the early Earth and life. The book is intended for students (upper-level undergraduate and graduate students) and researchers in the academia and industry in earth and natural sciences.

We thank the contributors to this book for their time and effort in preparing their papers. We are indebted to Dr. Petra D. van Steenbergen, Senior Publishing Editor at Springer, for her enthusiastic support and encouragement throughout the preparation of this book.

April 2013
Yildirim Dilek
Harald Furnes

Contents

Contributors

P.E.B. Armitage Paul Armitage Consulting Ltd, 55 Reedham Crescent, Cliffe Woods, Rochester, UK

Jean H Bédard Geological Survey of Canada, Québec, QC, Canada

Steffen G. Bergh Department of Geology, University of Tromsø, Tromsø, Norway

Alexander T. Brasier Faculty of Earth and Life Sciences, VU University Amsterdam, Amsterdam, The Netherlands

Darren A. Chevis Department of Earth and Environmental Sciences, Tulane University, New Orleans, Louisiana, USA

Kent C Condie Department of Earth and Environmental Science, New Mexico Tech, Socorro, NM, USA

F. Corfu Department of Geosciences, University of Oslo, Oslo, Norway

Yildirim Dilek Department of Geology & Environmental Earth Science, Miami University, Oxford, OH, USA

School of Earth Science and Mineral Resources, China University of Geosciences, Beijing, China

David A. Foster Department of Geological Sciences, University of Florida, Gainesville, FL, USA

David A. Foster Department of Geological Sciences, University of Florida, Gainesville, FL 32611–2120, USA

Harald Furnes Department of Earth Science & Centre for Geobiology, University of Bergen, Bergen, Norway

Ben D. Goscombe Integrated Terrane Analysis Research, Aldgate, South Australia, Australia

David R. Gray Geostructures, Deviot, Tasmania, Australia

Jaana Halla Finnish Museum of Natural History, University of Helsinki, Helsinki, Finland

Lyal B Harris Institut national de la recherche scientifique, Centre Eau Terre Environnement, Québec, QC, Canada

Esa Heilimo Geological Survey of Finland, Kuopio, Finland

Darrell J. Henry Department of Geology and Geophysics, Louisiana State University, Baton Rouge, LA, USA

Pentti Hölttä Geological Survey of Finland, Espoo, Finland

Hannu Huhma Geological Survey of Finland, Espoo, Finland

Karen H. Johannesson Department of Earth and Environmental Sciences, Tulane University, New Orleans, Louisiana, USA

Asko Kontinen Geological Survey of Finland, Kuopio, Finland

Anatoliy B. Kudryavtsev Department of Earth and Space Sciences and Molecular Biology Institute, University of California, Los Angeles, CA, USA

Center for the Study of Evolution and the Origin of Life, University of California, Los Angeles, CA, USA

NAI PennState Astrobiology Research Center, University Park, PA, USA

K. Kullerud Department of Geology, University of Tromsø, Tromsø, Norway

Matthew I. Leybourne ALS Geochemistry, North Vancouver, British Columbia, Canada

Satu Mertanen Geological Survey of Finland, Espoo, Finland

Perttu Mikkola Geological Survey of Finland, Kuopio, Finland

David W. Mogk Department of Earth Sciences, Montana State University, Bozeman, MT, USA

Paul A. Mueller Department of Geological Sciences, University of Florida, Gainesville, FL, USA

P.I. Myhre Department of Geology, University of Tromsø, Tromsø, Norway

Jorma Paavola Geological Survey of Finland, Kuopio, Finland

Petri Peltonen First Quantum Minerals Ltd, Sodankylä, Finland

Julia Semprich Physics of Geological Processes, University of Oslo, Oslo, Norway

Ali Polat Department of Earth and Environmental Sciences, University of Windsor, Windsor, ON, Canada

E.J.K. Ravna Department of Geology, University of Tromsø, Tromsø, Norway

Brad E. Rosenheim Department of Earth and Environmental Sciences, Tulane University, New Orleans, Louisiana, USA

J. William Schopf Department of Earth and Space Sciences and Molecular Biology Institute, University of California, Los Angeles, CA, USA

Alexander Slabunov Karelian Research Centre, RAS, Institute of Geology, Petrozavodsk, Russia

Peter Sorjonen-Ward Geological Survey of Finland, Kuopio, Finland

Katherine Telfeyan Department of Earth and Environmental Sciences, Tulane University, New Orleans, Louisiana, USA

David Wacey Centre for Geobiology and Department of Earth Sciences, University of Bergen, Bergen, Norway

Centre for Microscopy, Characterisation and Analysis, ARC Centre for Core to Crust Fluid Systems & Centre for Exploration Targeting, The University of Western Australia, Crawley, WA, Australia

Simon A. Wilde Department of Applied Geology, The Institute for Geoscience Research, Curtin University, Perth, Western Australia

Maarten de Wit AEON and Faculty of Science, Nelson Mandela Metropolitan University, Port Elizabeth, South Africa

Joseph L. Wooden Department of Earth Sciences, Stanford University, Stanford, CA, USA

K.B. Zwaan Geological Survey of Norway, Trondheim, Norway

Precambrian Greenstone Belts Host Different Ophiolite Types

1

Harald Furnes, Maarten de Wit and Yildirim Dilek

Abstract

We use in this study the new description and classification of ophiolites in order to identify potential ophiolite complexes in four Precambrian greenstone belts, ranging in age from 3.8 Ga to 2.0 Ga, and their tectonic origin. The mafic-ultramafic rock assemblages in the 3.8 Ga Isua (Greenland) and 3.5 Ga Barberton (South Africa) greenstone belts show geochemical signatures that are comparable to those of Phanerozoic suprasubduction-zone ophiolites. The 2.7 Ga greenstone belts of the Wawa greenstone belts of the Superior Province (Canada) and the 1.95 Ga Jormua Complex (Finland) display subduction-unrelated geochemical patterns, and represent plume- and continental margin-type ophiolites, respectively. This geochemical and tectonic diversity of the Precambrian greenstone belts is reminiscent of the Phanerozoic ophiolites, and suggests that the modern plate tectonics operated as far back as the early Archean, albeit perhaps in a different mode.

1.1 Introduction

The term *greenstone belt* has been in use for a long time to define the Archean and Proterozoic terranes that consist of spatially and temporally related, metamorphosed, intrusive and extrusive ultramafic, mafic to felsic rock assemblages commonly associated with different types of sedimentary rocks, and surrounded by granitoid plutons (de Wit 2004). The widespread occurrence in these rocks of a variety of green minerals such as serpentine, chlorite, epidote, actinolite and hornblende is the main reason for the name "greenstones". These mineral phases represent low- to medium-grade (most commonly), or even granulite facies metamorphic conditions. The areal extent of the greenstone belts varies widely from small (e.g. Isua, Greenland—75 km^2) to large (e.g. the Lap-

H. Furnes (✉)
Department of Earth Science & Centre for Geobiology, University of Bergen, Allegaten 41, 5007 Bergen, Norway
e-mail: harald.furnes@geo.uib.no

M. de Wit
AEON and Faculty of Science, Nelson Mandela Metropolitan University, Port Elizabeth 6031, South Africa

Y. Dilek
Department of Geology & Environmental Earth Science, Miami University, Oxford, OH 45056, USA

School of Earth Science and Mineral Resources, China University of Geosciences, 100083 Beijing, China

Y. Dilek, H. Furnes (eds.), *Evolution of Archean Crust and Early Life*, Modern Approaches in Solid Earth Sciences 7, DOI 10.1007/978-94-007-7615-9_1,

land Greenstone belt—50,000 km^2), and their mafic component is predominantly tholeiitic basalts. However, in some greenstone belts, such as in the Hattu greenstone belt of the Karelian Craton, Mg-rich komatiitic rocks may reach nearly 25 % of the exposed greenstone outcrop (de Wit and Ashwal 1995, 1997a; Hunter and Stowe 1997). For more detailed description of the greenstone belts we refer the reader to Windley (1977); Kröner (1981); Condie (1994); Goodwin (1996); de Wit and Ashwal (1995, 1997b); Eriksson et al. (2004); Kusky (2004); Van Kranendonk et al. (2007).

The usage of the term "ophiolite" has been rather restricted in connection with Precambrian greenstone belts (de Wit and Ashwal 1997a), and whether ophiolites occur in the Archaean greenstone belts has been a lively debate. Some researchers (e.g. Bickle et al. 1994; Hamilton 1998; Stern 2005; White 2005; Bedard 2006; Hamilton 2007; Stern 2008; Robin and Bailey 2009; Maurice et al. 2009; Hamilton 2011) have argued that no ophiolites are represented in the Archean greenstone belts, whereas some others (e.g. Dann 1991; Dann and Bowring 1997; de Wit and Ashwal 1997a; St-Onge et al. 1997; Sylvester et al. 1997; de Wit 1998; Kusky et al. 2001; Cavosie et al. 2007; Furnes et al. 2007; Nutman et al. 2007; Van Kranendonk 2007; Dilek and Polat 2008; Wyman et al. 2008; Friend and Nutman 2010; Van Kranendonk 2011; Shirey and Richardson 2011) have shown that ophiolites are significant components of the Archean greenstone belts. The general consensus is that ophiolites are widespread in the Proterozoic record. The middle Proterozoic (1,950 Ma) Jormua Complex in central Finland is, for example, one of the best documented Precambrian ophiolites, containing a well-defined sheeted dyke complex (Kontinen 1987; Peltonen et al. 1998). The debate on the existence of any Archean ophiolite is based largely on the question of whether Phanerozoic-type plate tectonics could have operated on the early Earth when the geothermal gradients and heat flow values were high, plates may have been smaller, and convection cells in the mantle were likely more rigorous in comparison to modern times.

In this paper we evaluate structural architecture and geochemical make-up of four well-known Precambrian greenstone belts (Fig. 1.1) ranging in age from Middle Proterozoic to Paleoarchean (Jormua—Finland, Wawa—Canada, Barberton—South Africa, and Isua—Greenland), in comparison to diverse Phanerozoic ophiolite types with different tectonic origins. We show that these Archean to Proterozoic greenstone belts include ophiolite complexes with distinctly different internal structures and lithological associations, reminiscent of their Phanerozoic counterparts. The corollary to this conclusion is that the modern plate tectonics likely operated as early as in the Paleoarchean, facilitating oceanic crust formation in different geodynamic environments. In the first part of the paper we provide a brief summary of the ophiolite types and their internal structure as background information for our assessment of the Precambrian greenstone belts. Next, we describe the internal structure, stratigraphy and geochemical characteristics of the four well-known Precambrian greenstone belts, which contain distinct ophiolite complexes. We then discuss the tectonic origin of these Precambrian ophiolites, using a generic model.

For more comprehensive information on these four greenstone belts, the reader is referred to the following literature: *Isua Supracrustal Belt* (Nutman et al. 1984, 1996; Rosing et al. 1996; Nutman et al. 1997; Komiya et al. 1999; Nutman et al. 2000; Myers 2001; Komiya et al. 2002; Polat et al. 2002; Polat and Hofmann 2003; Komiya et al. 2004; Nutman et al. 2007; Furnes et al. 2009); *Barberton greenstone belt* (Viljoen and Viljoen 1969; de Wit et al. 1987; Armstrong et al. 1990; de Wit et al. 1992; Kröner et al. 1996; Parman et al. 1997; Byerly 1999; Lowe and Byerly 1999; Vennemann and Smith 1999; Grove et al. 1999; Chavagnac 2004; Dann and Grove 2007; Lowe and Byerly 2007; de Wit et al. 2011; Furnes et al. 2011, 2012, 2013); *Wawa greenstone belts* (Williams et al. 1991; Polat et al. 1998,1999; Scott et al. 2002; Polat 2009); *Jormua Complex* (Kontinen 1987; Peltonen et al. 1996, 1998; Tsuru et al. 2000; Peltonen et al. 2003).

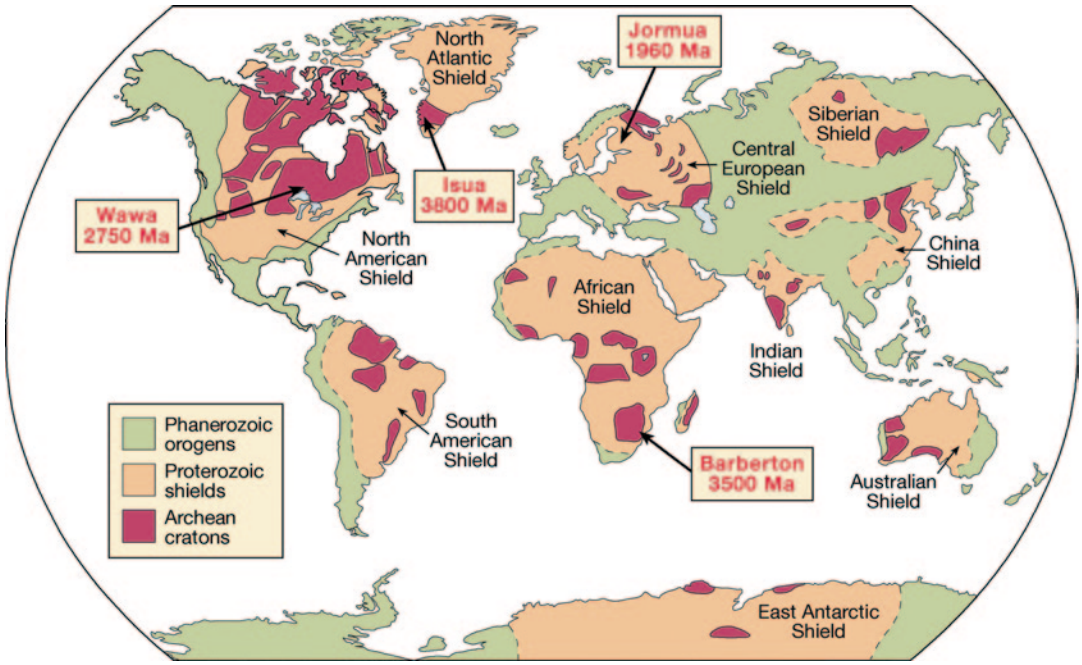

Fig. 1.1 Map showing the World distribution of Phanerozoic, Proterozoic Shields and Archean cratons, and the location of the volcano-magmatic complexes (Isua, Barberton, Wawa and Jormua) dealt with in this work. Modified from Marshak (2005)

1.2 Phanerozoic Ophiolite Types

Ophiolites preserve records of the evolution and destruction of lost oceanic lithosphere, and are thus important components for the understanding of the complex development of orogenic belts. The literature on the lithological, geochemical and petrological descriptions of Phanerozoic ophiolites is extensive. On the basis of increasing information on their internal structure and geochemical characteristics, ophiolites are now widely believed to have formed in different tectonic environments. Thus it is clear that the 1972 Penrose definition of ophiolites (Anonymous 1972) is not all inclusive, is too restrictive, and needs to be modified. To this end, Dilek and Furnes (2011) redefined ophiolite as "suites of temporally and spatially associated ultramafic to felsic rocks related to separate melting episodes and processes of magmatic differentiation in particular oceanic tectonic environments. Their geochemical characteristics, internal structure, and thickness vary with spreading rate, proximity to plumes or trenches, mantle temperature, mantle fertility, and the availability of fluids". In this definition, ophiolites basically are divided into two main groups, i.e., subduction-unrelated and subduction-related (Fig. 1.2). The subduction-unrelated ophiolites include **continental-margin-, mid-ocean-ridge-** (*plume-proximal, plume-distal, and trench-distal* subtypes), and **plume-type** (*plume-proximal ridge and oceanic plateaux* subtypes) ophiolites. These ophiolites represent the constructional (rift-drift to seafloor spreading) stage of oceanic crust formation and contain predominantly mid-ocean-ridge basalts. The subduction-related ophiolites, on the other hand, include **suprasubduction-zone** (*backarc to forearc, forearc, oceanic backarc, and continental backarc* subtypes) and **volcanic arc types**. These ophiolites represent destructive stages of ocean floor recycling (subduction with or without seafloor spreading), and their magmatic products show variable subduction influence in their melt evolution. The crustal geochemistry of the two main types shows pronounced differences

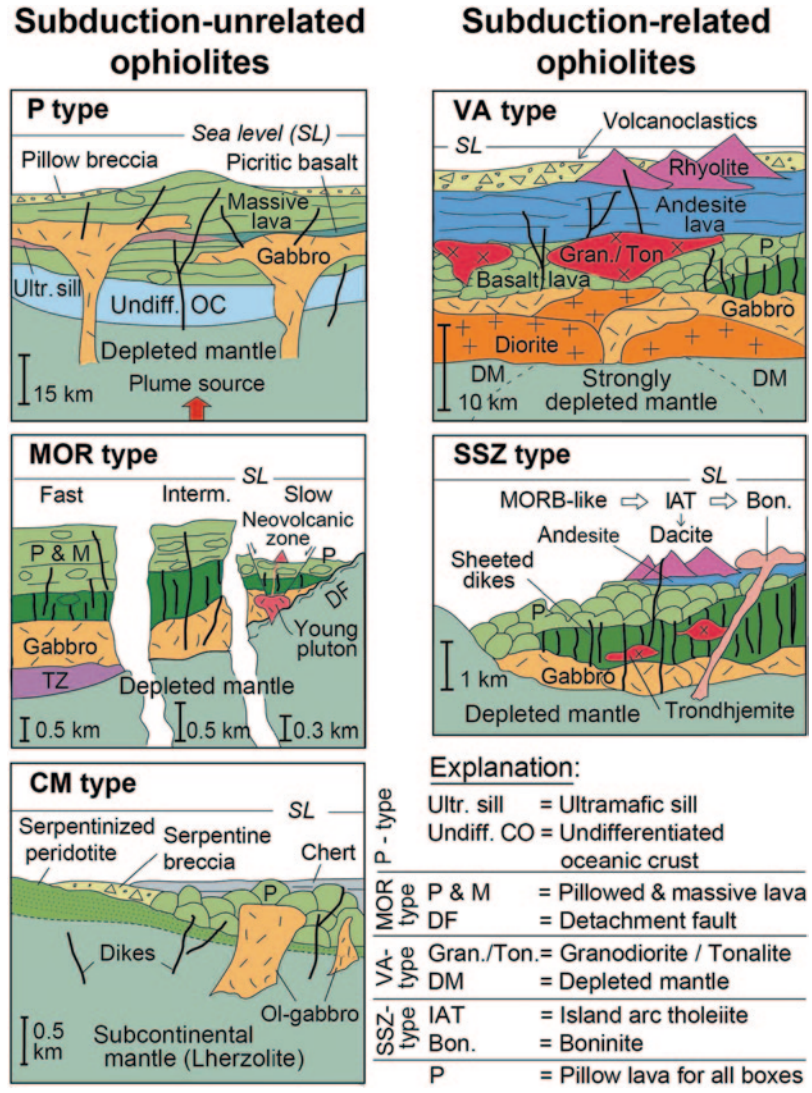

Fig. 1.2 Structural architecture and lithological development of subduction-unrelated and subduction-related ophiolites. Modified from Dilek and Furnes (2011)

in the concentration of subduction-sensitive elements (Cs, Pb, Rb, K, Ba, Th, U and LREE), and define contrasting patterns with respect to element-element-, element ratio-, and multi-element diagrams.

1.3 Geology of the Precambrian Greenstone Belts

There are about 260 known Precambrian greenstone belts world-wide. Geological and geochemical data from these greenstone belts demonstrate important differences in their internal structure and rock compositions (e.g. de Wit and Ashwal 1997a; de Wit 2004). The volcanic and magmatic diversity in their crustal sequences suggests a wide spectrum of tectonic settings that is preserved in the rock record of the greenstone belts. Below, we first describe the geology of four greenstone belts of different ages, and then discuss their geochemical features and affinities in the framework of the new ophiolite classification.

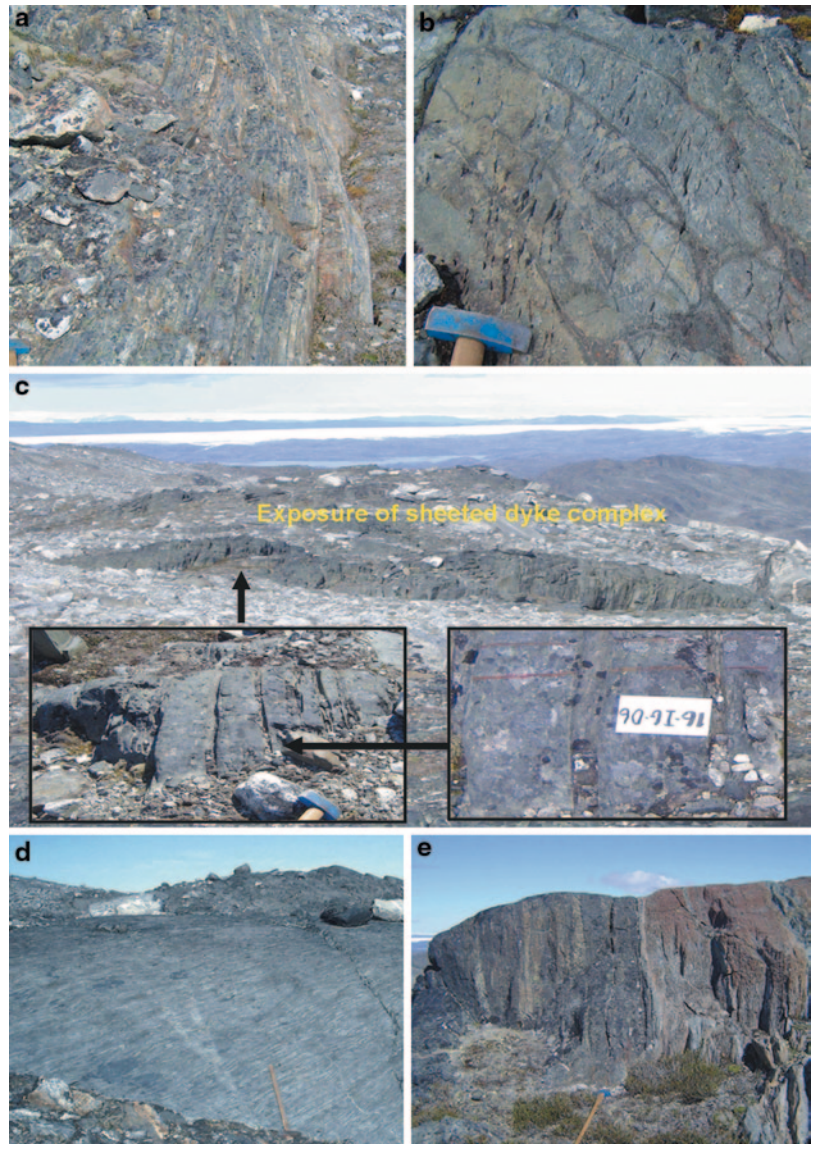

Fig. 1.3 Lithological components of the undifferentiated amphibolites (UA) of the Isua Supracrustal Belt (ISB), Greenland. **a** Grey chert; **b** non-vesicular pillow lava; **c** sheeted dyke complex; **d** strongly foliated gabbro; and **e** ultramafic rocks (dark pyroxenites and reddish-brown harzburgite/metadunite)

1.3.1 Isua Supracrustal Belt

The Paleoarchean (~3.8 Ga) Isua supracrustal belt (ISB) in southwestern Greenland contains one of the world's oldest intact submarine mafic volcanic sequences, and mafic intrusive rock complexes (Nutman et al. 1997). The mafic-ultramafic units of the ISB occur in two major tectonostratigraphic units: undifferentiated amphibolites (UA) and garbenschiefer amphibolites (GA) (e.g. Nutman et al. 1984; Rosing et al. 1996; Nutman et al. 1997; Komiya et al. 1999; Furnes et al. 2007, 2009). In the western part of the ISB, the UA occurs as two arched linear belts with the GA as a central belt. The UA contains all major lithological units of a typical Penrose-type complete ophiolite sequence, i.e., cherts, pillow lavas and minor pillow breccias/hyaloclastites, a sheeted dyke complex, layered gabbro and ultramafic rocks (Fig. 1.3) (Furnes et al. 2007, 2009). Based on their geochemistry and field appearance, the ultramafic rocks can be divided into metadunites and metaperidotites that may represent mantle-derived tectonic slivers, as well

as cumulates from mafic intrusions. The GA is composed dominantly of volcaniclastic, volcanic and intrusive metabasaltic rocks. The strongly deformed tholeiitic metabasites are derived from extrusive and shallow intrusive protoliths, and in places relic pillow structures (locally variole-bearing) and dike-in-dike relationships are well preserved (Gill and Bridgwater 1979; Nutman et al. 1984; Komiya et al. 2004). We have interpreted that the UA and GA complexes as genetically related (Furnes et al. 2009), a view that is dissented by Friend and Nutman (2010).

1.3.2 Barberton Greenstone Belt

The Paleoarchean (ca. 3.5–3.3 Ga) Onverwacht Suite (OS) of the Barberton Greenstone Belt (BGB) in South Africa consists of seven complexes of predominantly volcanic rocks and intrusions. These rocks define a 15-km-thick imbricate tectonic stack, including from base to top: Sandspruit, Theespruit, Komati, Hooggenoeg, Noisy, Kromberg and Mendon Complexes (e.g. de Wit et al. 2011). The Sandspruit Complex consists largely of basalt and komatiite, while the Theespruit Complex contains basaltic to dacitic lavas and intrusions. Both complexes have been extensively intruded by 3,460–3,440 Ma and 3,210–3,240 Ma tonalite to trondhjemite plutons and display higher-grade metamorphism than the structurally higher complexes (de Wit et al. 2011, and references therein). The ca. 3-km-thick volcanic and subvolcanic sequences of the Komati Complex are dominated by komatiites and komatiitic basalts in the lower part and by dominantly basalts and komatiitic basalts in the upper part (Dann 2000). The lavas are intruded by ultramafic (generally wehrlite), mafic and felsic minor intrusions, both concordant and discordant. Large, massive serpentinized peridotite bodies (mostly orthopyroxenites, dunites, wehrlites and local rodingites) occur in separate tectonic domains throughout the belt, but the contact relationships of these peridotite bodies with the above-mentioned complexes remain obscure (de Wit et al. 1987; MacLennan 2012).

The Hooggenoeg Complex, on the other hand, comprises a 2.7-km-thick pile of predominantly basaltic lavas, with minor occurrences of komatiitic basalts and komatiites in the middle part of the volcanic sequence (Furnes et al. 2012, 2013). The pillow lavas are variolitic, and range from slightly vesicular in the lower part of the sequence to non-vesicular in the upper part (Fig. 1.4a, b), indicative of eruption at water depths in the order of 2,000–4,000 m, respectively (Furnes et al. 2011). Dyke swarms, perpendicular to the upper surfaces of the pillow lava flows, have been observed in the lower and middle part of the volcanic sequence (Fig. 1.4c).

The structurally higher rock unit of the OS is the Noisy Complex, which rests unconformably on the deep water marine pillow lavas of the Hooggenoeg Complex. The Noisy Complex consists of dacitic to rhyolitic intrusive and volcanic rocks associated with shallow water clastic and volcaniclastic rocks and an up to 600-m-thick chert at the top (known as the Buck Ridge Chert) (de Vries et al. 2006; de Wit et al. 2011). Above the Noisy Complex and in tectonic contact with it is the ~2 km thick Kromberg Complex consisting of sheets of serpentinite and intrusive metagabbro (into chert) at its lowest structural level, and a volcanic sequence of pillowed and massive lavas in the middle part that is intruded by multiple sills of fine-grained basaltic and coarser-grained ultramafic rocks (see Fig. 1.7 of de Wit et al. 2011). The structurally highest and youngest unit (3.33 Ga; Kröner et al. 1996) in the OS is the Mendon Complex, separated from the Kromberg Complex by an extensive shear zone (de Wit et al. 2011; Grosch et al. 2012). Its magmatic rocks include basaltic to komatiitic lavas and intrusions (Byerly 1999), which are interlayered with chert horizons exhibiting graded beds of accretionary lapilli, interpreted as turbidite deposits originating from shallow water pyroclastic eruptions (Stanistreet et al. 1981; Heinrichs 1984; Thompson-Stiegler et al. 2008).

1.3.3 Wawa Greenstone Belts

The ca. 2.7 Ga greenstone belts (Schreiber-Hemlo greenstone belts) within the Wawa Subprovince (3,750–2,650 Ma) of the Superior Province in Canada include two distinct volcanic associations (Polat et al. 1998, 1999; Polat 2009). The early

Fig. 1.4 Lithological components of the Hooggenoeg Complex of the Barberton Greenstone Belt (GBG), South Africa. **a** Slightly vesicular pillow lava from lower part of the volcanic sequence; **b** non-vesicular, variole-bearing pillow from the upper part of the volcanic sequence; and **c** Dyke swarm perpendicular to the bedding of the pillow lava (lower part of the volcanic sequence)

volcanic complex (2,750–2,725 Ma) is mainly represented by voluminous tholeiitic basalts and Al-undepleted komatiites that are capped by basaltic lavas transitional to alkaline compositions and Al-depleted komatiites. This complex is interpreted to represent an oceanic plateau of a mantle plume origin. Pillow lavas and pillow breccias attest to the oceanic setting of this complex. The later magmatic phase (2,725–2,690 Ma) is characterised by calc-alkaline basalts, andesites, dacites, rhyolites, and trondhjemite, tonalite and granodiorite intrusions. The mafic volcanic rocks range from undeformed, greenschist-facies pillow lavas, to highly deformed amphibolites (Polat et al. 1999).

1.3.4 Jormua Complex

The mafic to ultramafic rocks of the Jormua Complex (JC), dated to 1,953 ± 3 Ma (Peltonen et al. 1996), occur the central part of a metasedimentary,

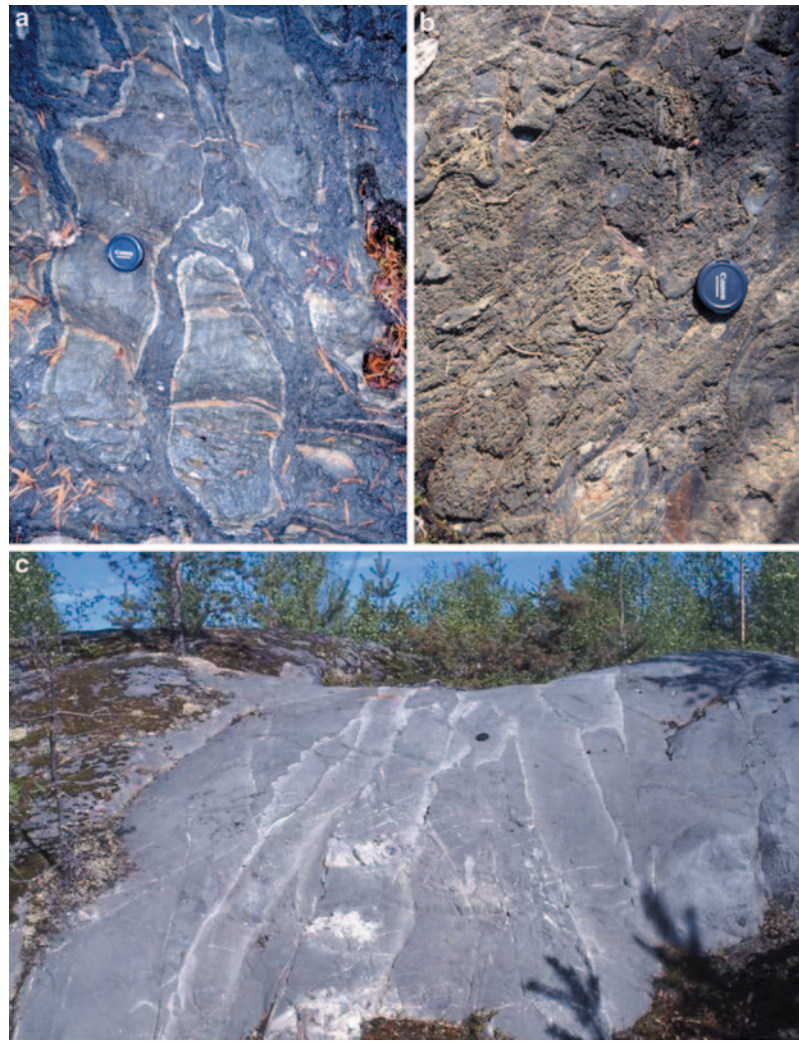

Fig. 1.5 Lithological components of the Jormua Complex, Finland. **a** Non-vesicular pillow lava; **b** pillow breccia; and **c** sheeted dyke complex

Mesoproterozoic (2.3–1.92 Ga) sequence, surrounded by Archean basement rocks in Northeastern Finland (Kontinen 1987; Peltonen et al. 1998). The rock units of the JC include pillow lavas and volcanic breccias, a well-preserved sheeted dyke complex (Fig. 1.5), as well as plagiogranites, gabbroic cumulates, and mantle peridotites. The thickness of the volcanic sequence varies from place to place, but the maximum thickness reaches about 500 m. Some of the pillows contain drain-out structures, which can be used as reliable indicators to determine the way-up in the pillow lava pile. Remnants of variolitic textures are still visible in the outer ~1 cm of the chilled pillow margins, and the consistently non-vesicular character of the pillows indicates eruption in relatively deep (>1,000 m) water (Furnes et al. 2005). The pseudostratigraphic position of the sheeted dyke complex is difficult to determine, but as a conservative estimate, a depth of between 500 m and 1,000 m below the top of the volcanic sequence has been proposed (Furnes et al. 2005).

All of the volcanic rocks and the dykes in the JOC have been metamorphosed in upper greenschist to lower amphibolite facies conditions. The peak of metamorphism has been estimated at ~500±20 °C (Peltonen et al. 1996). This metamorphic event completely recrystallized the rocks and erased their primary magmatic

textures. Despite the pervasiveness of the metamorphic overprint, the originally glassy rims of pillows, hyaloclastite breccias, and dyke margins are easily recognized (Fig. 1.5).The typical mineral assemblage in the metabasaltic rocks is oligoclase–andesine + actinolitic hornblende–hornblende + Fe-oxides ± chlorite ± epidote ± quartz ± biotite. The pillow lavas and pillow breccias are generally strongly foliated (Fig. 1.5a, b), whereas the sheeted dyke complex appears undeformed (Fig. 1.5c).

Although the sequence has been tectonically disrupted into several blocks, it contains all the components of a typical Penrose-style ophiolite (Kontinen 1987; Peltonen et al. 1996). The thickness of the JC varies, and the lava sequence locally rests directly on the ultramafic upper mantle rocks.

1.4 Geochemical Characteristics

In the Bowen diagrams (MgO-TiO_2) the garbenschiefer amphibolites of the Isua supracrustal belt plots exclusively in the field of subduction-related ophiolites, whereas the undifferentiated amphibolites plots in both the subduction-related and subduction–unrelated fields (Fig. 1.6a). Although the garbenschiefer amphibolites are highly schistose, their mafic volcaniclastic and pillow lava protoliths can be observed in the lowest-strain domains (Komiya and Maruyama 1995; Rosing 1999; Polat et al. 2002; Furnes et al. 2009). The undifferentiated amphibolites comprise mainly pillow lavas and dykes (Polat and Hofmann 2003; Furnes et al. 2009).

The mafic rocks (lavas and shallow intrusives) of oldest and the structurally lowest unit in the Barberton belt, the Komati Complex, as well as of the youngest and the structurally youngest, the Mendon Complex, plot in the high-MgO field, and straddle the boundary between the fields of the subduction-related and subduction-unrelated rocks in the MgO-TiO_2 diagram (Fig. 1.6b). The lavas of the Hooggenoeg Complex define a large spread in the MgO-TiO_2 diagram; their TiO_2 values in the MgO-range of ~8–4 wt.% show values between 0.5 and 1.7 wt.%, and a substantial part of these lavas plot exclusively in the subduction-related field. The lavas of the Kromberg Complex, on the other hand, display a much less variation, with TiO_2 values plotting mostly between 1–1.5 wt.% (Fig. 1.6). The earliest Wawa and the Jormua metabasalts plot predominantly in the fields of Plume-type and Continental margin-type ophiolites, respectively (Fig. 1.6c, d). The tholeiitic to calc-alkaline volcanic rocks and intrusions of the Wawa are generally more differentiated than most of the Barberton greenstones, with MgO values <5 wt.% (Fig. 1.6c), and they are closely related to subduction-unrelated and subduction-related environments, respectively.

In the N-MORB-normalised multi-element diagrams, the undifferentiated amphibolites of Isua show features of both subduction-related and subduction-unrelated rocks. The patterns defined from Lu through Nd show a steady increase in the normalised values towards the more-incompatible elements, reminiscent of the patterns defined by subduction-unrelated ophiolites, although the pronounced positive Pb-anomalies and negative Nb-anomalies reflect subduction-influence. Those of the garbenschiefer amphibolites, on the other hand, typically plot within the field of subduction-related ophiolites and display their characteristic features such as pronounced positive Pb-anomalies, negative Nb- and Ta-anomalies, strong enrichment of Ba and Th, and strong depletion of the MREEs. The last feature is most typical of boninites found in modern subduction zone environments (Fig. 1.7). In the N-MORB-normalised multi-element diagrams for the volcanic units of the Komati, Hooggenoeg, Kromberg and Mendon Complexes of the Onverwacht Suite, the envelopes for the maximum and minimum values of subduction-related and subduction-unrelated rocks are shown (Fig. 1.8). The volcanic rocks from these four complexes all show better comparison with subduction-related than subduction-unrelated patterns, by defining a near flat to slightly enriched pattern from Lu through Nd and the strong enrichment of the most incompatible, non-conservative elements (Cs, Ba and Pb). They also display variably negative Nb and Ta anomalies. The lavas of the Mendon Complex and the major part of the Hooggenoeg Complex show the

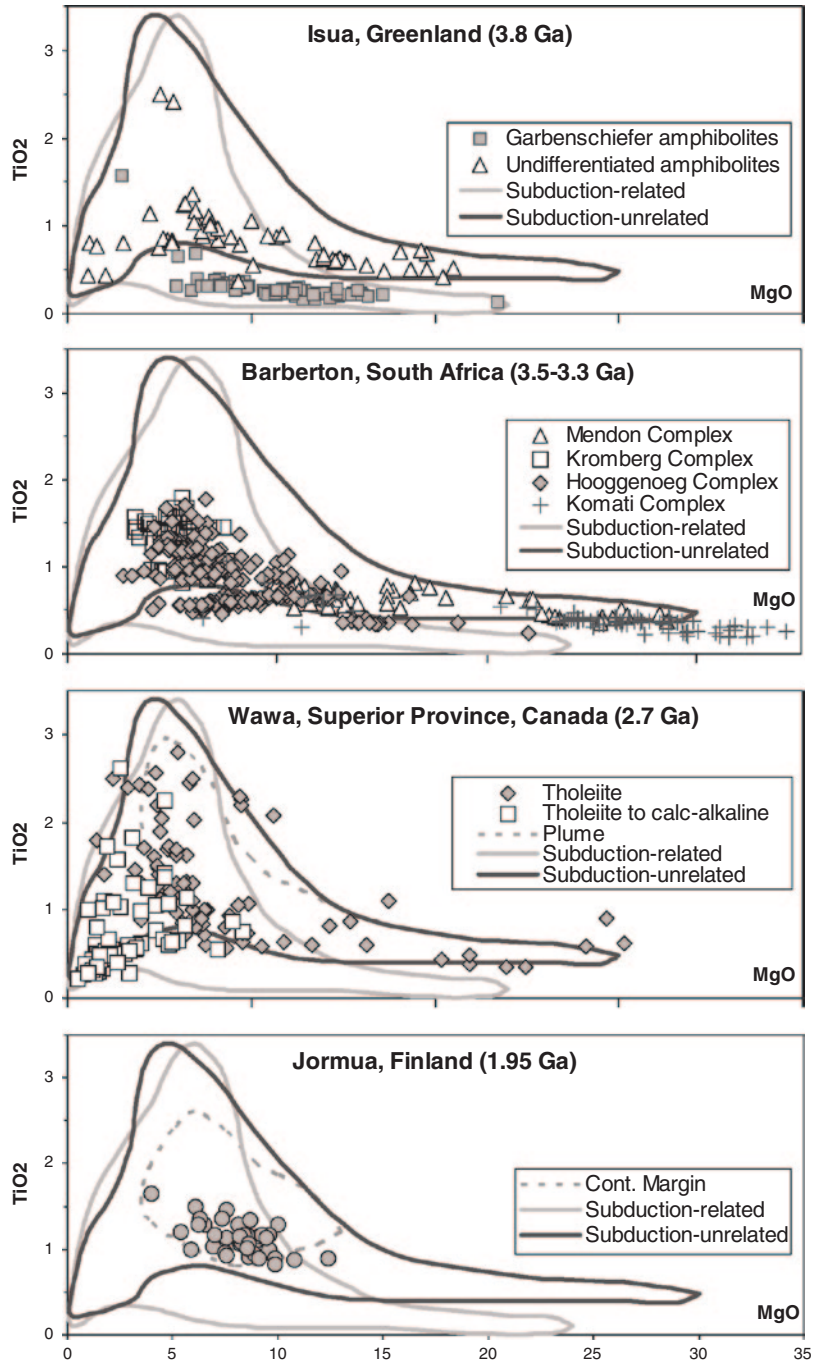

Fig. 1.6 MgO-TiO_2 relationships of the greenschist to amphibolite volcanic-intrusive complexes of the Isua, Barberton, Wawa and Jormua. The fields for subduction-related/unrelated ophiolites, and those of the plume and continental margin, are taken from Dilek and Furnes (2011). Data sources are: Isua: Polat et al. (2002), Polat and Hofmann (2003), Komiya et al. (2004), Furnes et al. (2009); Barberton: Jahn et al. (1982), Smith and Erlank (1982), Lahaye et al. (1995), Byerly (1999), Parman et al. (2003, 2004), Chavagnac (2004), Furnes et al. (2012); Wawa: Polat et al. (1999), Polat and Kerrich (2000); Polat (2009); Jormua: Kontinen (1987), Peltonen et al. (1996).

most pronounced negative Ta and Nb anomalies (Fig. 1.8a, c), whereas the same anomalies from the Kromberg Complex are minor and are hardly detectable in the rocks of the Komati Complex (Fig. 1.8b, d). The tholeiities and komatiites of the first magmatic phase, and the second phase of tholeiitic to calc-alkaline lavas of the Wawa magmatic rocks compare best with subduction-unrelated and subduction-related rocks, respectively (Fig. 1.9a, b). The metabasaltic rocks

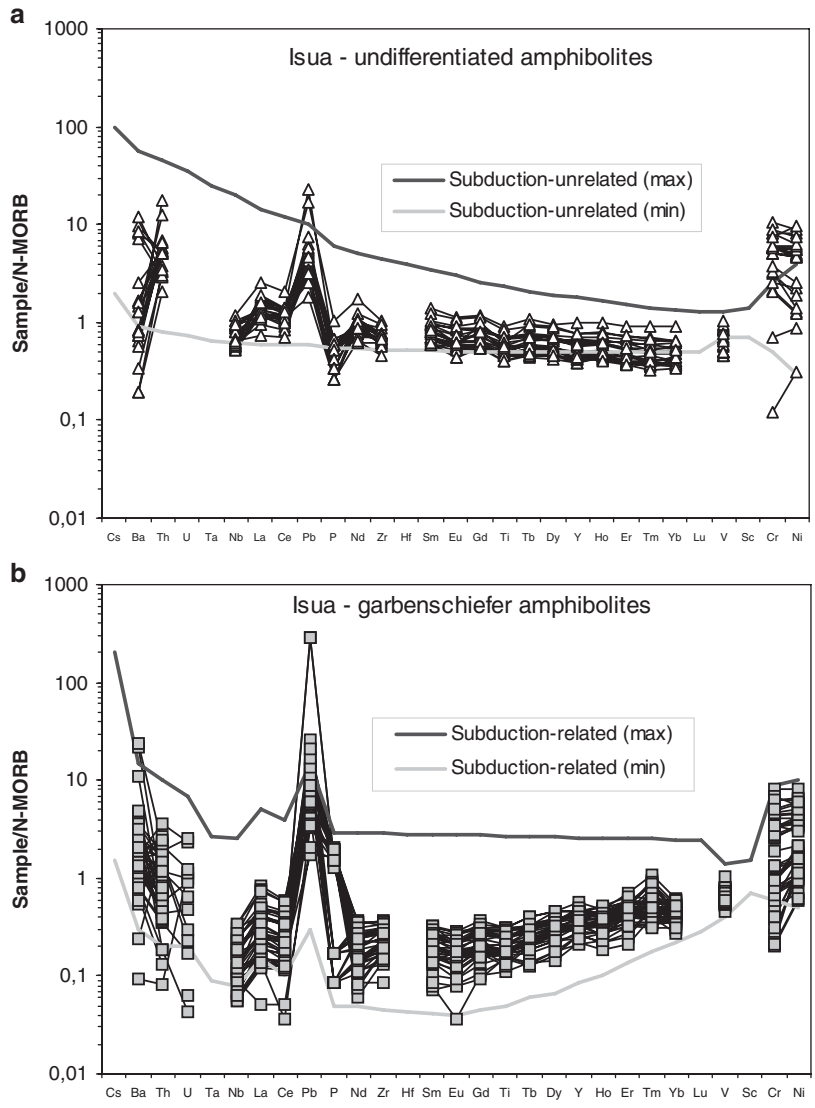

Fig. 1.7 MORB-normalised multi-element diagrams of the undifferentiated (**a**) and garbenschiefer (**b**) amphibolites of the Isua Supracrustal Belt. Data sources: as in Fig. 1.6. MORB-data are from Pearce and Parkinson (1993). Fields (max and min) of subduction-related/unrelated are from Dilek and Furnes (2011)

of Jormua plot within the field defined by the subduction-unrelated ophiolites (Fig. 1.10).

Figure 1.11 shows the Ta/Yb-Th/Yb and Ti-V discrimination diagrams for the four greenstone belts. In the Ta/Yb-Th/Yb diagrams all the Isua amphibolites indicate subduction influence, whereas the Barberton volcanic units plot along the boundary line between the subduction-related magmatic rocks and the MORB (N-MORB to E-MORB) field. The tholeiites and komatiites, representing the first phase of the Wawa greenstones, show a large spread from N-MORB to OIB, and about half of the Wava data plot within the field of subduction-unrelated rocks. The second magmatic phase in Wava, represented by the tholeiitic to calc-alkaline rocks fall all exclusively within the field of subduction-related rocks. The Jormua amphibolites cluster around the E-MORB field. In the Ti-V diagram the Isua data plot in two distinct fields: the garbenschiefer amphibolites plot exclusively around $Ti/V < 10$, whereas the undifferentiated amphibolites define Ti/V ratios of 20–30 (Fig. 1.11) typical of mixed MORB and island arc affinities (Shervais 1982). The Barberton data define a large scatter in the Ti/V ratios between 10 and 30, and the

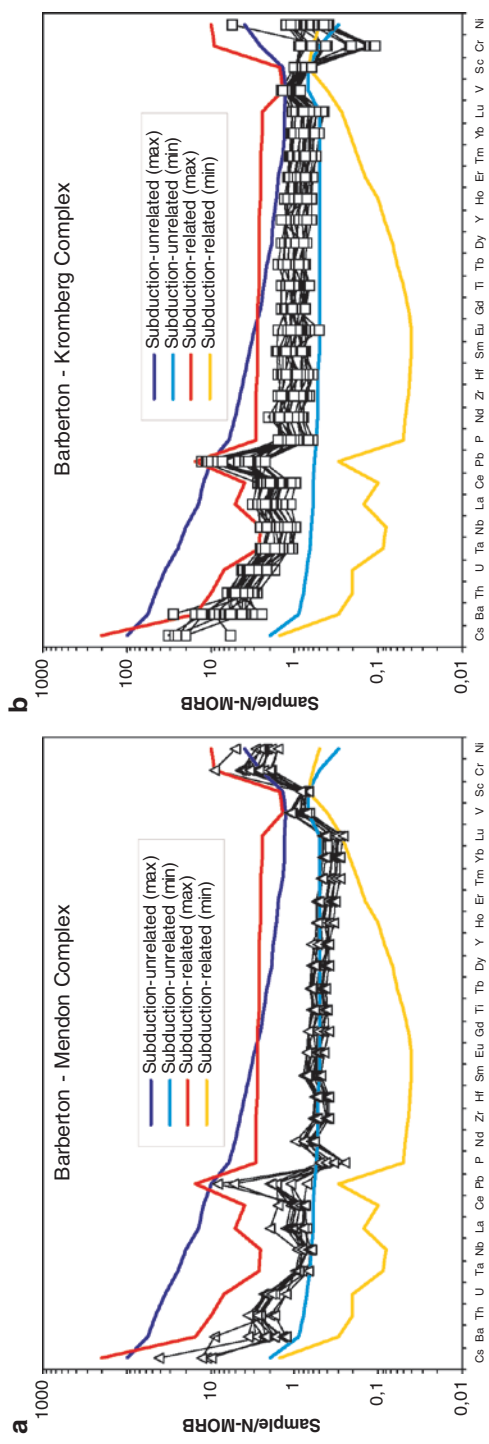

Fig. 1.8 MORB-normalised multi-element diagrams of the different complexes of the Onverwacht Suite of the Barberton Greenstone Belt. Data sources: Mendon, Kromberg and Hooggenoeg Complexes (Furnes et al. 2012), and from the Komati Complex (Chavagnac 2004; Parman et al. 2003). MORB data and subduction-related/unrelated fields: as in Fig. 1.7

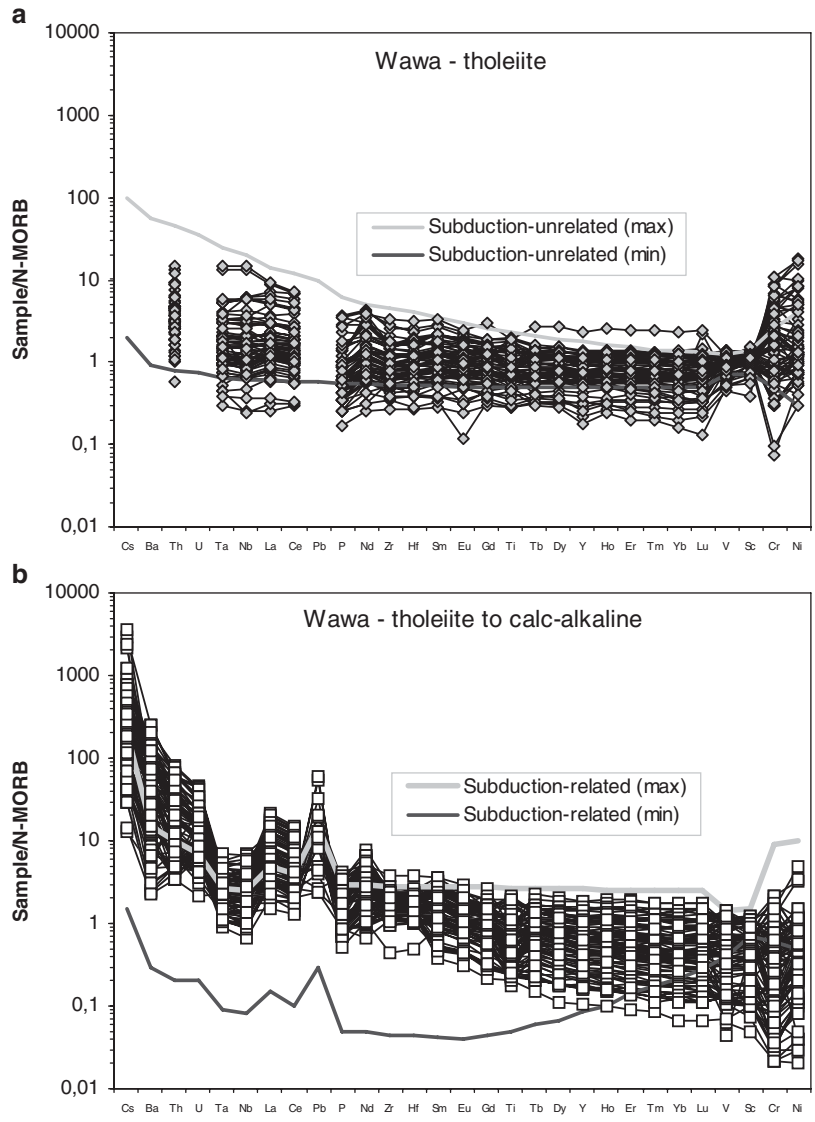

Fig. 1.9 MORB-normalised multi-element diagrams of the plume-related (**a**) and subduction-related (**b**) volcanic and subvolcanic rocks of the Wawa greenstones. MORB data and subduction-related/unrelated fields: as in Fig. 1.7

Wawa volcanic and intrusive rocks display an even wider scatter between10 and 50. The Ti/V ratios of the Jormua amphibolites mostly define a rather limited range, mostly around 30, a value typical of MORB affinities (Shervais 1982).

We have used N-MORB values as the normalisation values for the multi-element diagrams (Figs. 1.7, 1.8, 1.9, and 1.10). Alternatively we could have applied the primordial mantle (PM) values as reported in McDonough and Sun (1995). Due to the different element concentrations in N-MORB and PM, the normalised values of the most incompatible elements (e.g. Cs, Ba and Pb) would have been subdued, whereas the negative anomalies of Nb and Ta would remain nearly unchanged, as shown in Furnes et al. (2012, 2013).

1.5 Chemical Geodynamics of Ophiolites in the Greenstone Belts

The timing of the initiation of plate tectonics as we know from the Phanerozoic, and the indicators of those tectonic processes that led to the

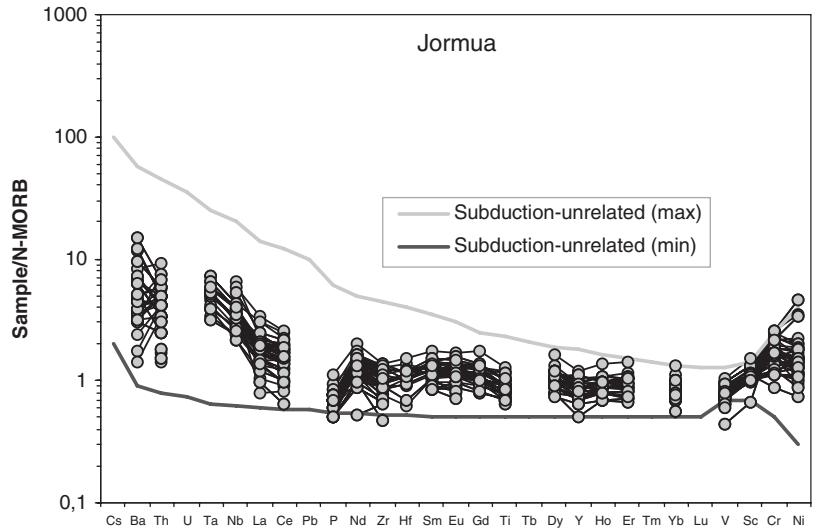

Fig. 1.10 MORB-normalised multi-element diagram of the pillow lava and dykes of the Jormua sequence. MORB data and subduction-related/unrelated fields: as in Fig. 1.7

formation of ophiolites, arc-backarc complexes, accretionary prisms and high-pressure metamorphic rocks are controversial questions in earth sciences (e.g. Cawood et al. 2006; Condie and Pease 2008; Dilek and Polat 2008; van Hunen and Moyen 2012). The mode and nature of continental crustal growth and the geothermal gradients in the Archean are also still poorly constrained. The engine of moving rigid plates today is mostly driven by subduction processes, a prerequisite to make plate tectonics work. Some researchers have proposed, based on some geochemical arguments, that plate tectonics was not in operation before 2.5–3.2 Ga (Shirey and Richardson 2011; Keller and Schoene 2012; Næraa et al. 2012). Some other scientists stated that lithospheric subduction might have been episodic in character in the early Archean (e.g. Watson and Harrison 2005), and that the subduction angles may have been highly steep (van Hunen and Moyen 2012) rather than shallow, as seen in most of the modern subduction zones (Gerya 2011; Gerya and Meilick 2011).

The geochemical fingerprint of the metavolcanic and intrusive rock assemblages from the four selected greenstone belts (Fig. 1.12) and their structural architecture indicate their magmatic evolution in different tectonic environments. Compared with the geochemical patterns of the Phanerozoic subduction-related ophiolites, the multi-element patterns of the Isua and Barberton lavas show similarities to those of supra-subduction-zone (SSZ) ophiolites (Fig. 1.12). The geological field relationships show that the undifferentiated amphibolites of Isua contain all the components of a typical SSZ-type ophiolite (Dilek and Furnes 2011). The pillow lavas and sheeted dike complex display a MORB-like geochemistry with a wide compositional range from primary to highly fractionated magmas (Polat and Hofmann 2003; Furnes et al. 2007, 2009). The presence of a sheeted dyke complex in the undifferentiated amphibolites (Fig. 1.3c) suggests oceanic crust formation via seafloor spreading (Fig. 1.12; Moores and Vine 1971; Coleman 1977; Dilek and Eddy 1992). The compositional range and geochemistry of its ultramafic to differentiated rocks is, however, comparable to those of plume-type, peri-Caribbean ophiolites (Dilek and Furnes 2011). Negative Nb-anomalies, as displayed in the MORB-normalised multi-element patterns (Figs. 1.7a and 1.12), on the other hand, suggest that the melt source region, from which the magmas of the undifferentiated amphibolite unit were derived, were influenced by subduction-related processes. We therefore infer that the undifferentiated amphibolites in Isua represent the products of subduction initiation magmatism.

The geochemical composition of the garberschiefer amphibolites defines a typical boninite-like

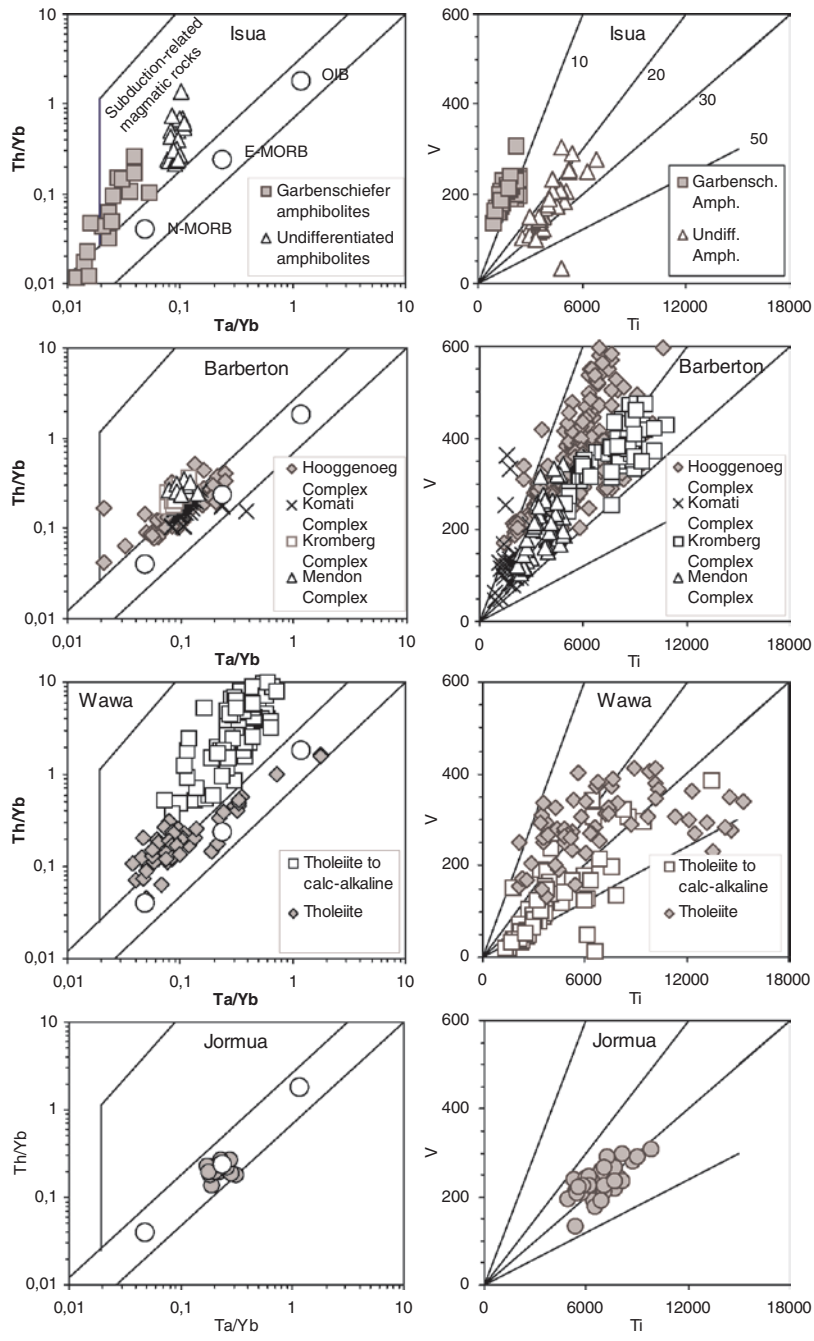

Fig. 1.11 Discrimination diagrams (Th/Yb-Ta/Yb and V-Ti) for the Isua, Barberton, Wawa and Jormua volcanic rocks

pattern, with strong depletion in incompatible elements MREE, P and Ti, pronounced negative Nb anomaly and enriched contents of U, Th, Ba and Pb (Fig. 1.7b). It thus differs from the undifferentiated amphibolite unit with respect to the lithological components, structural architecture, and geochemistry. We thus infer that the garbenschiefer amphibolite unit represents an advanced stage in the suprasubduction-zone development of the Isua ophiolite (Fig. 1.12). The undifferentiated amphibolites and garbenschiefer amphibolites of Isua most likely represent the early and late stages, respectively, in the formation of a SSZ type ophiolite, as previously suggested by Furnes et al. (2009).

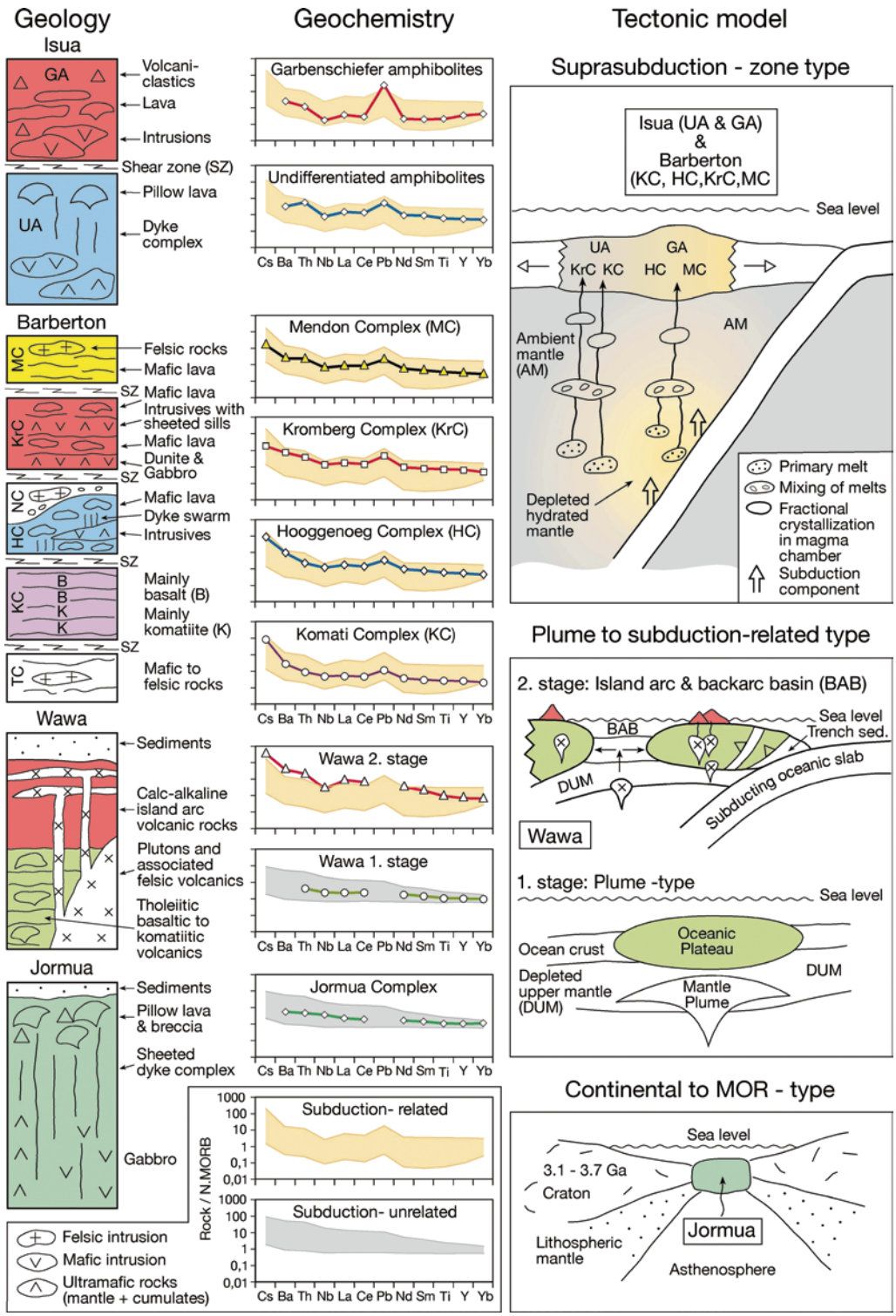

Fig. 1.12 Simplified summary of the geology, multi-element diagrams and tectonic models for the Isua, Barberton, Wawa and Jormua as different ophiolite complexes. The geological sections are based on: Isua: Furnes et al. (2009); Barberton: (de Wit et al. 2011; Furnes et al. 2011); Wawa (Polat et al. 1998; Polat 2009); Jormua (Kontinen 1987; Peltonen et al. 1996, 1998, 2003; Furnes et al. 2005). Abbreviation (Barberton): NC = Noisy Complex; TC = Theespruit Complex; GA = Garbenschiefer Amphibolites; UA = Undifferentiated Amphibolites

The nearly15-km-thick imbricate stack of lavas and intrusive rocks in the seven complexes of the Onverwacht Suite in the Barberton greenstone belt (the Sandspruit, Theespruit, Komati, Hooggenoeg, Noisy, Kromberg and Mendon Complexes; de Wit et al. 2011) also shows geochemical patterns (Fig. 1.8) comparable to those of SSZ-type ophiolites. Furnes et al. (2012, 2013) have proposed that the komatiitic to basaltic magmas of the Onverwacht Suite were generated from a subduction-metasomatized mantle as in modern volcanic arcs and back-arc basins (Fig. 1.12). The basaltic lavas and komatiites of the Sandspruit Complex and the tholeiitic to calc-alkaline, basaltic to dacitic lavas and intrusions of the Theespruit Complex are comparable to the volcano-plutonic units of a volcanic arc (Furnes et al. 2013), reminiscent of the Jurassic and older arc ophiolites in the Sierra Nevada metamorphic belt in California (Dilek 1989; Dilek et al. 1991).

The geochemical and tectonic affinities of the komatiites and komatiitic basalts of the Komati Complex have been interpreted differently both as subduction-related (e.g. Parman et al. 2004) and subduction-unrelated (e.g. Chavagnac 2004). Comparison between the patterns of MORB-normalised multi-element diagrams defined by the komatiites of the Komati Complex and those of subduction-related and subduction-unrelated ophiolites (Fig. 1.8d) suggests the formation of this complex in a subduction zone setting. Similarly, the mafic to ultramafic lavas of the Hooggenoeg, Kromberg and Mendon Complexes define subduction-related patterns, particularly demonstrated by the MORB-normalised multi-element patterns (Fig. 1.8a, c). Also, the lithological components, particularly of the Kromberg Complex, are largely comparable with those of Phanerozoic suprasubduction-zone ophiolites (e.g. Dilek and Furnes 2009, 2011). The crustal sequence in most Phanerozoic suprasubduction-zone ophiolites is made of lavas and dykes combined (~40–50 %), and gabbros and ultramafic intrusions (Dilek and Furnes 2009), whereas the exposed Kromberg Complex consists predominantly of mafic to ultramafic intrusions (Fig. 1.12). The Hooggenoeg Complex, on the other hand, with its relatively good exposure, has about equal amount of intrusive and extrusive rocks, as well as dyke swarms in the lower to middle part of the sequence (Fig. 1.12). Subduction-related contributions to the systematic variations in Th concentrations of the Hooggenoeg volcanic sequence may have been related to changes in the depth to the underlying subducting slab and hence possibly to variations in the angle of subduction (Furnes et al. 2012).

Considering the structural field relations, and the lithological and the geochemical characteristics of the lavas and intrusions of the Onverwacht Suite, we infer that the Komati, Hooggenoeg, Kromberg and Mendon Complexes collectively represent the remnants of a Paleoarchean oceanic crust formed in a back-arc basin. The Theespruit and Noisy Complexes likely represent an island arc system (de Wit et al. 2011; Furnes et al. 2011, 2012, 2013). The shallow-water clastic sedimentary rocks of the Noisy Complex unconformably overlying the deep-marine volcanic rocks and associated intrusions of the Hooggenoeg Complex indicate a significant episode of crust uplift and deep erosion, following the magmatic construction of the Onverwacht Suite.

The first stage in the geochemical evolution of the Wawa greenstones appears to have produced mafic rock assemblages that are comparable to the plume-type ophiolites in the peri-Caribbean region (Fig. 1.12; Dilek and Furnes 2011). These plume-type ophiolitic fragments in the Wava greenstone belts occur adjacent to subduction-accretion complexes (Polat et al. 1998; Polat 2009), which represent the later stage magmatic products. This later magmatic phase produced an intra-oceanic arc—backarc system that was developed on and across the previously constructed oceanic plateau in the Neoarchean (Polat 2009; Fig. 1.12).

The geochemistry of the Jormua amphibolites shows an E-MORB affinity and is reminiscent of the geochemical character of continental margin-type ophiolites (Figs. 1.6, 1.10, and 1.11). Chromites from the central part of the Jormua ophiolite have Re-Os isotopic systematics that indicate the incorporation of both ancient subcontinental lithospheric mantle and MORB-type mantle, a phenomenon that can be explained via continental

rift—drift tectonics (Tsuru et al. 2000), as in some Tethyan ophiolites (Rampone and Piccardo 2000; Dilek et al. 2005). However, the existence in Jormua of a well-developed sheeted dyke complex indicates that the rift-drift stage was followed by seafloor spreading and associated extensional tectonics, as also documented from some well-preserved Phanerozoic ophiolites (Dilek and Eddy 1992; Dilek et al. 1998). These features and interpretations collectively suggest that the Jormua ophiolite likely formed in a restricted ocean basin, analogous to the Ligurian Tethys and the modern Red Sea as previously suggested by Peltonen et al. (1996, 2003).

1.6 Conclusions

Our comparative study of the geological and geochemical features of mafic-ultramafic rock assemblages in four Precambrian greenstone belts (i.e. Isua, Barberton, Wawa, and Jormua) shows that these rock units represent ophiolite complexes that formed in different tectonic settings. Compared to the Phanerozoic ophiolites, the mafic-ultramafic rock sequences of the 3.8 Ga Isua (Greenland) and the 3.5 Ga Barberton (South Africa) greenstone belts are analogous to supra-subduction-zone ophiolites. The mafic-ultramafic rocks of the 2.7 Ga Wawa greenstone belts (Canada) represent a complex tectonic evolution, encompassing an earlier phase of plume-type ophiolite development, followed by an island arc construction. The amphibolites of the 1.95 Ga Jormua Complex (Finland) show the structural architecture and geochemical fingerprint of continental margin—type ophiolites, which form during the rift—drift and seafloor spreading stages of an embryonic ocean basin evolution.

This approach to identifying the Precambrian mafic-ultramafic rock associations as different ophiolite types through their distinct geochemical and tectonic fingerprints can be used effectively to decipher the geodynamic setting of the formation of ancient oceanic crust during the Precambrian, particularly in the Archaean. This insight can in turn help us better evaluate the mode and nature of plate tectonic processes in deep time. We posit that the term ‘greenstone belt’ and the connotation it generally carries are restrictive, anachronistic, and no longer helpful in developing a realistic understanding of the evolution of the early Earth.

Acknowledgements Financial support over many years of field work in Phanerozoic ophiolites and Precambrian greenstone belts, have been supported by the Norwegian Research Council and the Meltzer Foundation at the University of Bergen (HF), the National Research Foundation of South Africa (MdeW), and Miami University, USA (YD). Jane Ellingsen helped with some of the illustrations. This is AEON publication No. 107.

References

Anonymous (1972) Penrose field conference on ophiolites. Geotimes 17:24–25

Armstrong RA, Compston W, de Wit MJ, Williams IS (1990) The stratigraphy of the 3.5–3.2 Ga Barberton Greenstone Belt revisited: a single zircon ion microprobe study. Earth Planet Sci Lett 101:90–106

Bedard JH (2006) A catalytic delamination-driven model for coupled genesis of Archean crust and sub-continental lithospheric mantle. Geochim Cosmochim Acta 71:1188–1214

Bickle MJ, Nesbit EG, Martin A (1994) Archean greenstone belts are not oceanic crust. J Geol 102:121–128

Byerly GR (1999) Komatiites of the Mendon Formation: late-stage ultramafic volcanism in the Barberton Greenstone Belt. In: Lowe DR, Byerly GR (eds) Geologic evolution of the Barberton Greenstone Belt, South Africa, vol 329 (Geological Society of America Special Paper). Geological Society of America, pp 189–211

Cavosie AJ, Valley JW, Wilde SA (2007) The oldest terrestrial mineral record: a review of 4400–4000 Ma detrital zircons from Jack Hills, Western Australia. In: Van Kranendonk MJ, Smithies RH, Bennet VC (eds) Earth’s oldest rocks. Development in Precambrian geology, vol 15. Elsevier, Amsterdam, pp 91–111

Cawood PA, Kröner A, Pisarevsky A (2006) Precambrian plate tectonics: criteria and evidence. GSA Today 16(7):4–11

Chavagnac V (2004) A geochemical and Nd isotopic study of Barberton komatiites (South Africa): implication for the Archean mantle. Lithos 75:253–281

Coleman RG (1977) Ophiolites. Springer-Verlag, New York, pp 229

Condie KC (1994) Archean crustal evolution. Developments in Precambrian geology (advisory editor, Windley BF). Elsevier, Amsterdam, pp 528

Condie KC, Pease V (2008) When did plate tectonics begin on planet Earth? Geol Soc Am Spec Pap 440:294

Dann JC (1991) Early Proterozoic ophiolite, central Arizona. Geology 19:590–593
Dann JC (2000) The 3.5 Ga Komati Formation, Barberton Greenstone Belt, South Africa, Part I: new maps and magmatic architecture. S Afr J Geol 103:147–168
Dann JC, Bowring SA (1997) The Payson ophiolite and Yavapai-Mazatzal orogenic belt, central Arizona. In: de Wit MJ, Ashwal LD (eds) Greenstone belts. Oxford University Press, Oxford, pp 781–790
Dann JC, Grove TL (2007) Volcanology of the Barberton Greenstone Belt, South Africa: inflation and evolution of flow fields. In: Van kranendonk MJ, Smithies RH, Bennett VC (eds) Earth's oldest rocks. Developments in Precambrian geology, vol 15. Elsevier, Amsterdam, pp 527–570
de Vries ST, Nijman W, Armstrong RA (2006) Growth-fault structure and stratigraphic architecture of the Buck Ridge volcano-sedimentary complex, upper Hooggenoeg Formation, Barberton Greenstone Belt, South Africa. Precamb Res 149:77–98
de Wit MJ (1998) On Archean granites, greenstones, cratons and tectonics: does the evidence demand a verdict? Precamb Res 91:181–226
de Wit MJ (2004) Archean greenstone belts do contain fragments of ophiolites. In: Kusky TM (ed) Precambrian ophiolites and related rocks. Development in Precambrian geology, vol 13. Elsevier, Amsterdam, Archean green pp 599–614
de Wit MJ, Ashwal LD (1995) Greenstone belts: what are they? S Afr J Geol 98:504–519
de Wit MJ, Ashwal LD (1997a) Convergence towards divergent models of greenstone belts. In: de Wit MJ, Ashwal LD (eds) Greenstone belts. Oxford University Press, Oxford, pp ix–xvii
de Wit MJ, Ashwal LD (eds) (1997b) Greenstone belts. Clarendon Press, Oxford, pp 809
de Wit MJ, Hart RA, Hart RJ (1987) The Jamestown Ophiolite Complex, Barberton mountain belt: a section through 3.5 Ga oceanic crust. J Afr Earth Sci 6:681–730
de Wit MJ, Roering C, Hart RJ, Armstrong RA, de Ronde CEJ, Green RE, Tredoux M, Peberdy E, Hart RA (1992) Formation of an Archean continent. Nature 357:553–562
de Wit MJ, Furnes H, Robins B (2011) Geology and tectonostratigraphy of the Onverwacht Suite, Barberton Greenstone Belt, South Africa. Precamb Res 186:1–27
Dilek Y (1989) Tectonic significance of post-accretion rifting of a Mesozoic island-arc terrane in northern Sierra Nevada, California. J Geol 97:503–518
Dilek Y, Eddy CA (1992) The Troodos (Cyprus) and Kizildag (S. Turkey) ophiolites as structural models for slow-spreading ridge segments. J Geol 100:305–322
Dilek Y, Thy P, Moores EM (1991) Episodic dike intrusion in the northwestern Sierra Nevada, California: implications for multistage evolution of a Jurassic arc terrane. Geology 19:180–184
Dilek Y, Moores EM, Furnes H (1998) Structure of modern oceanic crust and ophiolites and implications for faulting and magmatism at oceanic spreading centers. In: Buck R, Karson JA, Delaney P, Lagabrielle Y (eds) Faulting and magmatism at mid-ocean ridges. Geophysical Monograph, vol 106. American Geophysical Union, Washington, DC, pp 219–266
Dilek Y, Furnes H, Shallo M (2005) Rift-drift, seafloor spreading, and subduction tectonics of Albanian ophiolites. Int Geol Rev 47:147–176
Dilek Y, Furnes H (2009) Structure and geochemistry of Tethyan ophiolites and their petrogenesis in subduction rollback systems. Lithos 113:1–20
Dilek Y, Furnes H (2011) Ophiolite genesis and global tectonics: geochemical and tectonic fingerprinting of ancient oceanic lithosphere. Geol Soc Am Bull 123:387–411
Dilek Y, Polat A (2008) Suprasubduction zone ophiolites and Archean tectonics. Geology 36:430–432. doi:10.1130/Focus052008.1
Eriksson PG, Alterman W, Nelson DR, Mueller WU, Catuneanu O (eds) (2004) The Precambrian earth: tempos and events. Developments in Precambrian geology, vol 12 (series editor, Condie KC). Elsevier, Amsterdam, pp 941
Friend CRL, Nutman AP (2010) Eoarchean ophiolites? New evidence for the debate on the Isua supracrustal belt, southern West Greenland. Am J Sci 310:826–861
Furnes H, Banerjee NR, Muehlenbachs K, Kontinen A (2005) Preservation of biosignatures in metaglassy volcanic rocks from the Jormua ophiolite complex, Finland. Precamb Res 136:125–137
Furnes H, de Wit MJ, Staudigel H, Rosing M, Muehlenbachs K (2007) A vestige of Earth's oldest ophiolite. Science 315:1704–1707
Furnes H, Rosing M, Dilek Y, de Wit MJ (2009) Isua supracrustal belt (Greenland)—A vestige of a 3.8 Ga suprasubduction zone ophiolite, and the implications for Archean geology. Lithos 113:115–132
Furnes H, de Wit MJ, Robins B, Sandstå NR (2011) Volcanic evolution of the upper Onverwacht Suite, Barberton Greenstone Belt, South Africa. Precamb Res 186:28–50
Furnes H, Robins B, de Wit MJ (2012) Geochemistry and petrology of lavas in the upper Onverwacht Suite, Barberton Mountain Land, South Africa. S Afr J Geol 115:171–210
Furnes H, de Wit MJ, Robins B (2013) A review of new interpretations of the tectonostratigraphy, geochemistry and evolution of the Onverwacht Suite, Barberton Greenstone Belt, South Africa. Gondwana Res 23:403–428
Gerya T (2011) Future directions in subduction modelling. J Geodynamics 52:344–378
Gerya TV, Meilick FI (2011) Geodynamic regimes of subduction under an active margin: effects of rheological weakening by fluids and melts. J Met Geol 29:7–31
Gill RCO, Bridgwater D (1979) Early Archaean basic magmatism in West Greenland—geochemistry of the Ameralik Dykes. J Petrol 20:695–726
Goodwin AM (1996) Principles of Precambrian geology. Academic Press, London, pp 327

Grosch EG, Vidal O, Abu-Alam T, McLoughlin N (2012) P-T constraints on the metamorphic evolution of the Paleoarchean Kromberg type-section, Barberton Greenstone Belt, South Africa. J Petrol 53:513–545

Grove TL, Parman SW, Dann JC (1999) Conditions of magma generation for Archean komatiites from the Barberton Mountain land, South Africa. In: Fei Y, Bertka CM, Mysen BO (eds) Mantle petrology: field observations and high pressure experimentation, vol 6 (special publication). Geochemical Society, pp 155–167

Hamilton WB (1998) Archean magmatism and deformation were not the products of plate tectonics. Precamb Res 91:109–142

Hamilton WB (2007) Earth's first two billion years—the era of internally mobile crust. Geol Soc Am Memoir 200:233–296

Hamilton WB (2011) Plate tectonics began in Neoproterozoic time, and plumes from deep mantle have never operated. Lithos 123:1–20

Heinrichs T (1984) The Umsoli chert, turbidite testament for a major phreatoplinian event in the Onverwacht/Fig Tree transition (Swaziland Supergroup, Archean, South Africa). Precamb Res 24:237–283

Hunter DR, Stowe CW (1997) A historical review of the origin, composition, and setting of Archean greenstone belts. In: de Wit MJ, Ashwal LD (eds) Greenstone belts. Oxford University Press, Oxford, pp 5–30

Jahn BM, Gruau G, Glikson AY (1982) Komatiities of the Onverwacht Group, S. Africa: REE geochemistry, Sm/Ng age, and mantle evolution. Contrib Min Petrol 80:25–40

Keller CB, Schoene B (2012) Statistical geochemistry reveals disruption in secular lithospheric evolution about 2.5 Ga. Nature 485:490–493

Komiya T, Maruyama S (1995) Geochemistry of the oldest MORB and OIB of the World, Isua (3.8 Ga), Greenland. EOS Trans 76:700

Komiya T, Maruyama S, Masuda T, Nohda S, Hayashi M, Okamoto K (1999) Plate tectonics at 3.8–3.7 Ga: field evidence from the Isua accretionary complex, southern West Greenland. J Geol 107:515–554

Komiya T, Hayashi M, Maruyama S, Yurimoto H (2002) Intermediate-P/T type Archean metamorphism of the Isua supracrustal belt: implications for secular change of geothermal gradients at subduction zones and for Archean plate tectonics. Am J Sci 302:806–826

Komiya T, Maruyama S, Hirata T, Yurimoto H, Nohda S (2004) Geochemistry of the oldest MORB and OIB in the Isua supracrustal belt, southern West Greenland: implications for the composition and temperature of early Archean upper mantle. Island Arc 13:47–72

Kontinen A (1987) An early Proterozoic ophiolite—the Jormua mafic-ultramafic complex, northeastern Finland. Precamb Res 353:13–334

Kröner A (ed) (1981) Precambrian plate tectonics. Developments in Precambrian geology, vol 4. Elsevier, Amsterdam, pp 781

Kröner A, Hegner E, Wendt JL, Byerly GR (1996) The oldest part of the Barberton granitoid-greenstone terrain, South Africa: evidence for crust formation between 3.5 and 3.7 Ga. Precamb Res 78:105–124

Kusky TM (ed) (2004) Precambrian ophiolites and related rocks. Developments in Precambrian geology, vol 13. Elsevier, Amsterdam, pp 772

Kusky TM, Li JH, Tucker RD (2001) The Archean Dongwanzi ophiolite complex, North China craton: 2.505-billion-year-old oceanic crust and mantle. Science 292:1141–1142

Lahaye Y, Arndt N, Byerly G, Chauvel C, Fourcade S, Gruau G (1995) The influence of alteration on the trace-element and Nd isotopic compositions of komatiites. Chem Geol 126:43–64

Lowe DR, Byerly GR (1999) Stratigraphy of the west-central part of the Barberton Greenstone Belt, South Africa. In: Lowe DR, Byerly GR (eds) Geologic evolution of the Barberton Greenstone Belt, South Africa, vol 329 (Geological Society of America Special Paper). Geological Society of America, pp 1–36

Lowe DR, Byerly GR (2007) An overview of the geology of the Barberton Greenstone Belt: implications for early crustal development. In: Van Kranendonk MJ, Smithies RH, Bennett VC (eds) Earth's oldest rocks. Developments in Precambrian geology, vol 15. Elsevier, Amsterdam, pp 481–526

MacLennan S (2012) Structural, geophysical and geochemical characterisation of an Archean paleosubduction zone, Barberton Greenstone Belt, South Africa. M.Sc. thesis, University of Cape Town, South Africa

Marshak S (2005) Earth: portrait of a planet. W.W. Norton & Company, New York, pp 747

Maurice C, David J, Bedard JH, Francis D (2009) Evidence for a mafic cover sequence and its implications for continental growth in the northeastern Superior Province. Precamb Res 168:45–65

McDonough WF, Sun S-S (1995) The composition of the Earth. Chem Geol 120:223–253

Moores EM, Vine FJ (1971) The Troodos massif, Cyprus, and other ophiolites as oceanic crust: evaluation and implications. Phil Trans Roy Soc London 268A:443–466

Myers JS (2001) Protoliths of the 3.8–3.7 Ga Isua greenstone belt, West Greenland. Precamb Res 105:129–141

Nutman AP, Allaart JH, Bridgwater D, Dimroth E, Rosing M (1984) Stratigraphic and geochemical evidence for the depositional environment of the early Archean Isua supracrustal belt, southern West Greenland. Precamb Res 25:365–396

Nutman AP, McGregor VR, Friend CRL, Bennett VC, Kinny PD (1996) The Itsaq Gneiss Complex of southern West Greenland; The world's most extensive record of early crustal evolution (3900–3600 Ma). Precamb Res 78:1–39

Nutman AP, Bennett VC, Friend CRL, Rosing MT (1997) ~3710 and ≥3790 Ma volcanic sequences in the Isua (Greenland) supracrustal belt; structural and Nd isotope implications. Chem Geol 141:271–287

Nutman AP, Bennett VC, Friend CRL, McGregor VR (2000) The early Archaean Itsaq Gneiss Complex of southern West Greenland: the importance of field observations in interpreting age and isotopic constraints for early terrestrial evolution. Geochim Cosmochim Acta 64:3035–3060

Nutman AP, Friend CRL, Horie K, Hidaka H (2007) The Itsaq Gneiss Complex of southern west Greenland and the construction of Eoarchaean crust at convergent plate boundaries. In: Van Kranendonk MJ, Smithies RH, Bennett VC (eds) Earth's oldest rocks. Developments in Precambrian geology, vol 15. Elsevier, Amsterdam, pp 187–218

Næraa T, Scherstén A, Rosing MT, Kemp AIS, Hoffmann E, Kokfelt TF, Whitehouse MJ (2012) Hafnium isotope evidence for a transition in the dynamics of continental growth 3.2 Gyr ago. Nature 485:627–630

Parman SW, Dann JC, Grove TL, de Wit MJ (1997) Emplacement conditions of komatiitic magmas from the 3.49 Ga Komati Formation, Barberton Greenstone Belt, South Africa. Earth Planet Sci Lett 150:303–323

Parman SW, Shimizu N, Grove TL, Dann JC (2003) Constraints on the pre-metamorphic trace element composition of Barberton komatiites from ion probe analyses of preserved clinopyroxene. Contrib Mineral Petrol 144:383–396

Parman SW, Grove TL, Dann J, de Wit MJ (2004) A subduction origin for komatiites and cratonic lithospheric mantle. S Afr J Geol 107:107–118

Pearce JA, Parkinson IJ (1993) Trace element models for mantle melting: application to volcanic arc petrogenesis. In: Prichard HM, Alabaster T, Harris NBW, Neary CR (eds) Magmatic processes and plate tectonics, vol 76 (Geological Society of London Special Publication). Geological Society, pp 373–403

Peltonen P, Kontinen A, Huhma H (1996) Petrology and geochemistry of metabasalts from the 1.95 Ga Jormua ophiolite, northeastern Finland. J Petrol 37:1359–1383

Peltonen P, Kontinen A, Huhma H (1998) Petrogenesis of the mantle sequence of the Jormua ophiolite (Finland): melt migration in the upper mantle during Palaeoproterozoic continental break-up. J Petrol 39:297–329

Peltonen P, Mänttäri I, Huhma H, Kontinen A (2003) Archean zircons from the mantle: the Jormua ophiolite revisited. Geology 31:645–648

Polat A (2009) The geochemistry of Neoarchean (ca. 2700 Ma) tholeiitic basalt, transitional to alkaline basalts, and gabbros, Wawa Subprovince, Canada: implications for petrogenetic and geodynamic processes. Precamb Res 168:83–105

Polat A, Hofmann AW (2003) Alteration and geochemical patterns in the 3.7–3.8 Ga Isua greenstone belt, West Greenland. Precamb Res 126:197–218

Polat A, Kerrich R (2000) Archean greenstone magmatism and the continental growth-mantle connection: constraints from Th-U-Nb-LREE systematics of the 2.7 Ga Wawa subprovince, Superior Province, Canada. Earth Planet Sci Lett 175:41–54

Polat A, Kerrich R, Wyman DA (1998) The late Archean Schreiber-Hemlo and White River-Dayohessarah greenstone belts, Superior Province: collages of oceanic plateaus, oceanic arcs, and subduction-accretion complexes. Tectonophysics 289:295–326

Polat A, Kerrich R, Wyman DA (1999) Geochemical diversity in oceanic komatiites and basalts from the late Archean Wawa greenstone belts, Superior Province, Canada: trace element and Nd isotope evidence for a heterogeneous mantle. Precamb Res 94:139–173

Polat A, Hofmann AW, Rosing M (2002) Boninite-like volcanic rocks in the 3.7–3.8 Ga Isua greenstone belt, West Greenland: geochemical evidence for intra-oceanic subduction zone processes in the Earth. Chem Geol 184:231–254

Rampone E, Piccardo GB (2000) The ophiolite-oceanic lithosphere analogue: new insights from the Northern Apennines (Italy). In: Dilek Y, Moores EM, Elthon D, Nicolas A (eds) Ophiolites and oceanic crust: new insights from field studies and the Ocean Drilling Program, vol 349 (Geological Society of America Special Paper). Geological Society of America, pp 21–34

Robin CMI, Bailey RC (2009) Simultaneous generation of Archean crust and subcratonic roots by vertical tectonics. Geology 37:523–526

Rosing MT (1999) ^{13}C-depleted carbon microparticles in >3700-Ma sea-floor sedimentary rocks from West Greenland. Science 283:674–676

Rosing MT, Rose NM, Bridgwater D, Thomsen S (1996) Earliest part of Earth's stratigraphic record: a reappraisal of the >3.7 Ga Isua (Greenland) supracrustal sequence. Geology 24:43–46

Scott CR, Mueller WU, Pilote P (2002) Physical volcanology, stratigraphy, and lithogeochemistry of an Archean volcanic arc: evolution from plume-related volcanism to arc rifting of SE Abitibi Greenstone Belt, Val d'Or, Canada. Precamb Res 115:223–260

Shervais JW (1982) Ti-V plots and the petrogenesis of modern and ophiolite lavas. Earth Planet Sci Lett 59:101–118

Shirey SB, Richardson S (2011) Start of the Wilson cycle at 3.0 Ga shown by diamonds from subcontinental mantle. Science 333:434–436

Smith HS, Erlank AJ (1982) Geochemistry and petrogeneis of komatiites from the Barberton greenstone belt, South Africa. In: Arndt NT, Nisbet EG (eds) Komatiites. Allen & Unwin, London, p 347–397

Stanistreet IG, de Wit MJ, Fripp REP (1981) Do graded units of accretionary spheroids in the Barberton Greenstone Belt indicate an Archean deep water environment? Nature 293:280–284

Stern RJ (2005) Evidence from ophiolites, blueschists, and ultra-high pressure metamorphic terranes that the modern episode of subduction tectonics began in Neoproterozoic time. Geology 33:557–560

Stern RJ (2008) Modern-style plate tectonics began in Neoproterozoic time: an alternative interpretation of Earth's tectonic history. In: Condie KC, Pease V (eds), When did plate tectonics begin on planet Earth? vol 440. Geological Society of America Special Paper, pp. 265–280

St-Onge MR, Lucas SB, Scott DJ (1997) The Ungava orogen and the Cape Smith thrust belt. In: de Wit MJ, Ashwal LD (eds) Greenstone belts. Oxford University Press, Oxford, pp 772–780

Sylvester PJ, Harper GD, Byerly GR, Thurston PC (1997) Volcanic aspects of greenstone belts. In: de Wit MJ, Ashwal LD (eds) Greenstone belts. Oxford University Press, Oxford, pp 55–90

Thompson-Stiegler M, Lowe DR, Byerly GR (2008) Abundant pyroclastic komatiitic volcanism in the 3.5–3.2 Ga Barberton Greenstone Belt, South Africa. Geology 36:779–782

Tsuru A, Walker RJ, Kontinen A, Peltonen P, Hanski E (2000) Re-Os isotopic systematics of the 1.95 Ga Jormua Ophiolite Complex, northeastern Finland. Chem Geol 164:123–141

van Hunen J, Moyen J-F (2012) Archean subduction: fact or fiction. Ann Rev Earth Planet Sci 40:195–219

Van Kranendonk MJ (2011) Cool greenstone drips and the role of partial convective overturn in Barberton greenstone belt evolution. J Afr Earth Sci 60:346–352

Van Kranendonk MJ, Smithies RH, Bennett VC (eds) (2007) Earth's oldest rocks. Developments in Precambrian geology, vol 15 (series editor, Condie KC). Elsevier, Amsterdam, pp 1307

Vennemann TW, Smith HS (1999) Geochemistry of mafic and ultramafic rocks in the Kromberg Formation in its type section, Barberton Greenstone Belt, South Africa. In: Lowe DR, Byerly GR (eds) Geologic evolution of the Barberton Greenstone Belt, South Africa, vol 329 (Geological Society of America Special Paper). Geological Society of America, pp 133–149

Viljoen MJ, Viljoen RP (1969) An introduction to the geology of the Barberton granite-greenstone terrain. Geol Soc S Afr Spec Publ 2:9–28

Watson EB, Harrison TM (2005) Zircon thermometer reveals minimum melting conditions on earliest Earth. Science 308:841–844

White DJ (2005) High-temperature, low-pressure metamorphism in the Kisseynew domain, Trans-Hudson orogen: crustal anatexis due to tectonic thickening? Can J Earth Sci 42:707–721

Williams RH, Stott GM, Heather K, Muir TL, Sage RP (1991) Wawa subprovince. In: Thurston PC, Williams HR, Sutclife HR, Stott GM (eds) Geology of Ontario, Ontario. Geol Surv Spec Volume 4, Part 1:485–539

Windley BF (1977) The Evolving Continents. Wiley, Chichester, pp 385

Wyman DA, O'Neill C, Ayer JA (2008) Evidence for moderen-style subduction to 3.1 Ga: a plateau-adakite-gold (diamond) association. In: Condie KC, Pease V (eds) When did plate tectonics begin on planet Earth? vol 440 (Geological Society of America Special Paper). Geological Society of America, pp 129–148

The Plume to Plate Transition: Hadean and Archean Crustal Evolution in the Northern Wyoming Province, U.S.A.

2

Paul A. Mueller, David W. Mogk, Darrell J. Henry, Joseph L. Wooden and David A. Foster

Abstract

The 2.8–4.0 Ga record of crustal evolution preserved in the northern Wyoming Province of western North America provides insight into the role of plume- and plate-regimes in the generation of Hadean and Archean continental crust, and the associated elemental depletion of the primitive mantle. The most complete record is exposed in the Beartooth Mountains (Montana-Wyoming), which lie within the Beartooth-Bighorn magmatic zone (BBMZ) sub-province of the Wyoming Province. The BBMZ (> 100,000 km^2) is characterized by a single, voluminous suite of Mesoarchean (~ 2.8–2.9 Ga) TTG (tonalite-trondhjemite-granodiorite) plutonic and metaplutonic rocks. In the Beartooth Mountains these Mesoarchean rocks are exposed along an ~ 100 km E-W cross-section, along which they intrude greenschist grade turbidites in the west (South Snowy block) and high grade, older gneisses in the east (Beartooth Plateau block). The most complete assemblage of pre-2.8 Ga crust is preserved as enclaves within the plutonic Mesoarchean rocks of the Beartooth Plateau block. These older gneisses consist of 3.1–3.5 Ga, tectonically interleaved

P. A. Mueller (✉)
Department of Geological Sciences, University of Florida, Gainesville, FL 32611, USA
e-mail: pamueller@ufl.edu

D. W. Mogk
Department of Earth Sciences, Montana State University, Bozeman, MT 59717 USA

D. J. Henry
Department of Geology and Geophysics, Louisiana State University, Baton Rouge, LA 70803 USA

J. L. Wooden
Department of Earth Sciences, Stanford University, Stanford, CA 94305 USA

D. A. Foster
Department of Geological Sciences, University of Florida, Gainesville, FL 32611 USA

Y. Dilek, H. Furnes (eds.), *Evolution of Archean Crust and Early Life*, Modern Approaches in Solid Earth Sciences 7, DOI 10.1007/978-94-007-7615-9_2,

meta-plutonic (principally TTG and associated migmatites) and metasupracrustal lithologies (e.g., quartzites, schists, banded iron formation, and a range of paragneisses).

The arc-like elemental abundances and enriched Pb and Nd isotopic systematics of the Mesoarchean magmatic suite and the 3.1–3.5 Ga older enclaves in conjunction with Lu-Hf data from 3.3 to 4.0 Ga detrital zircons suggest a model of crustal evolution that began with a Hadean, mafic proto-continent that likely developed over a zone of mantle upwelling. Lu-Hf systematics of the 3.6 to 4.0 Ga zircons suggest substantial recycling within the proto-continent in this interval, and that this recycling involved a low Lu/Hf (~0.1) system. A ubiquitous component of 3.2–3.4 Ga detrital zircons with more juvenile Hf isotopic compositions occurs throughout the northern Wyoming Province and suggests a major period of crustal growth and generation of TTG-suite rocks from more depleted sources. Following a period of relative quiescence (2.8–3.1 Ga) in the BBMZ, late Mesoarchean arc magmatism (TTG, adakites, etc.) largely reconstituted the older crust during a relatively brief period between 2.79 and 2.83 Ga; it has remained essentially undisturbed since that time.

Placing this history in a global context suggests that Hadean-Eoarchean crust formed in diachronous and spatially diverse environments that were both plume-like (e.g., Pilbara, northern Wyoming Province) and subduction-like (e.g., West Greenland). The relative importance of plume-type crustal growth declined and subduction-type growth increased through time as a consequence of a progressive decline in terrestrial heat production and mantle potential temperature, with a concomitant increase in hydrous mantle melting in subduction zones.

2.1 Introduction

One of the most poorly constrained and geochemically critical periods in earth history is the ~700 Ma between accretion (~4.5 Ga) and formation of the first well preserved felsic crust (~3.8 Ga). When considering the specific question of the formation of felsic crust, many authors have speculated about the nature of Hadean geodynamics and their relationship to modern geodynamic systems. Some hypotheses call upon extraterrestrial analogs (e.g., stagnant lid convection; Kamber et al. 2003; Debaille et al. 2013), while others call for modified versions of plate tectonics (e.g., thicker, more numerous, slower plates; faster plates, shallower subduction, etc.; Hargraves 1986; Abbott et al. 1994; Korenaga 2006; Herzberg and Rudnick 2012). These and many other studies (e.g., Wooden and Mueller 1988; Wyman and Kerrich 2002; Kamber et al. 2003; Smithies et al. 2005; Valley et al. 2005; Hamilton 2003; Harrison et al. 2008; Shirey et al. 2008; Wittig et al. 2008; Nutman and Friend 2009; Nebel-Jacobsen et al. 2010; Keller and Schoene 2012) have used both empirical and theoretical approaches to reach significantly different conclusions regarding the dominant geodynamic processes and related geochemical impacts associated with the creation of the earliest continental crust, sub-continental lithospheric mantle (e.g., tectosphere, keels, etc.), and elemental depletion of the primitive mantle.

In this contribution, we focus on the 4.0–2.8 Ga record of crustal evolution in the northern part of the Wyoming Province (NWP, Condie 1976; Wooden et al. 1988; Mogk et al. 1992; Figs. 2.1 and 2.2). Evidence from this crust supports the contention that Earth's earliest continents evolved in two separate, but contemporaneous, regimes: one driven by plate subduction and the other by mantle upwelling. Much as the planet forms crust today in both subduction and mantle plume

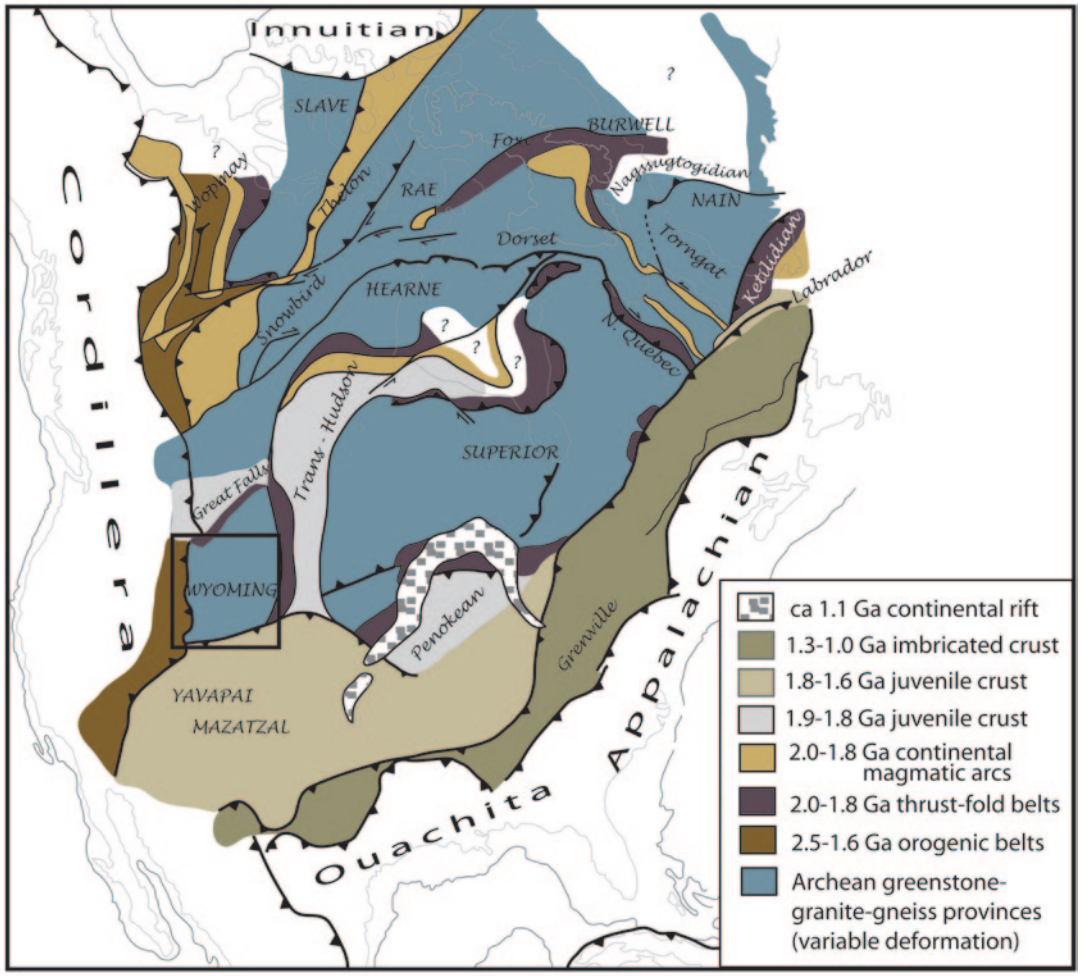

Fig. 2.1 Precambrian age-provinces of North America showing location of Wyoming Province (after Hoffman 1989)

systems, so it likely was in the Hadean-Eoarchean. The primary difference compared to tectonics on the modern Earth is the relative contributions of the two mechanisms, i.e., a higher proportion of subduction-derived crust today compared to the early Earth (e.g., Smithies et al. 2005; Van Kranendonk 2011; Mueller et al. 2010).

2.2 The Northern Wyoming Province

The northern part of the Wyoming Province comprises two primary subdivisions (Mogk et al. 1992; Chamberlain et al. 2003; Mueller et al. 2005; Mueller and Frost 2006; Fig. 2.2): (1) the BBMZ (Beartooth-Bighorn magmatic zone) extends over an area of more than 100,000 km^2 and is composed primarily of Mesoarchean metaplutonic rocks of the TTG (tonalite-trondhjemite-granodiorite) association, but contains enclaves of older rocks (as old as 3.5 Ga in the Beartooth Range); and (2) the MMT (Montana metasedimentary terrane) contains a range of Neoarchean metasedimentary associations interleaved with older (3.2–3.5 Ga) gneisses (e.g., Mueller et al. 1993, 1996, 2004; Krogh et al. 2011). A third tectonic domain, the GFTZ (Great Falls tectonic zone), is comprised primarily of MMT lithologies overprinted in the Paleoproterozoic (~1.8 Ga) during suturing of the NWP to the Medicine Hat block. Numerous authors (O'Neil and Lopez 1985; Mueller et al. 2002, 2005; Roberts et al. 2002;

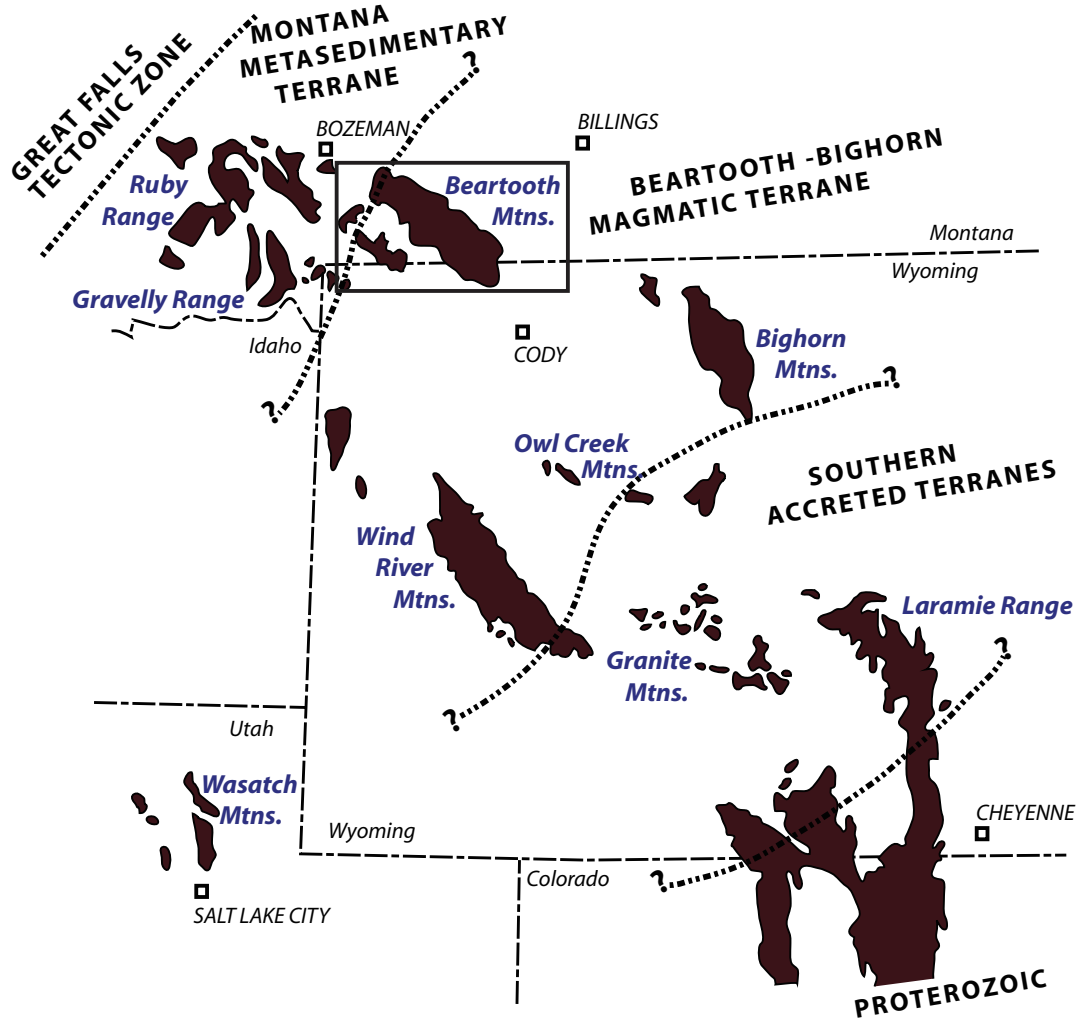

Fig. 2.2 Outline of major exposures of crystalline basement and generalized approximate sub-province boundaries in the Wyoming Province: Southern accreted terranes; Beartooth-Bighorn magmatic zone; and Montana metasedimentary terrane (Mogk et al. 1992; Chamberlain et al. 2003)

Brady et al. 2004; Foster et al. 2006, 2012) have discussed the evolution of the GFTZ and its impact on the MMT, so it will not be addressed here.

The most voluminous rocks formed during the Hadean-Archean in the northern Wyoming Province are the Mesoarchean TTG gneisses (metagranitoids) that dominate the BBMZ. The metagranitoids of the BBMZ are linked by several important characteristics in addition to their primary Mesoarchean age: (1) uniquely enriched Pb isotopic compositions (elevated $^{207}Pb/^{204}Pb$ for a given $^{206}Pb/^{204}Pb$) and negative initial Nd isotopic compositions; (2) current exposures and parageneses that reflect amphibolite to granulite grade metamorphism, indicative of upper- to mid-crustal conditions; and (3) seismic images that show a continuity of relatively thick crust (~50 km) with a distinctive, thick (10–25 km), high velocity lower crust (Vp > 7 km/sec), and (4) a mantle keel of > 250 km thickness (e.g., Wooden and Mueller 1988, Mueller and Wooden 1988; Frost 1993; Frost et al. 1998; Henstock et al. 1998; Clowes et al. 2002; Gorman et al. 2002; Chamberlain and Mueller 2007; Yuan and Romanowicz 2010; Tian and Zhao 2012).

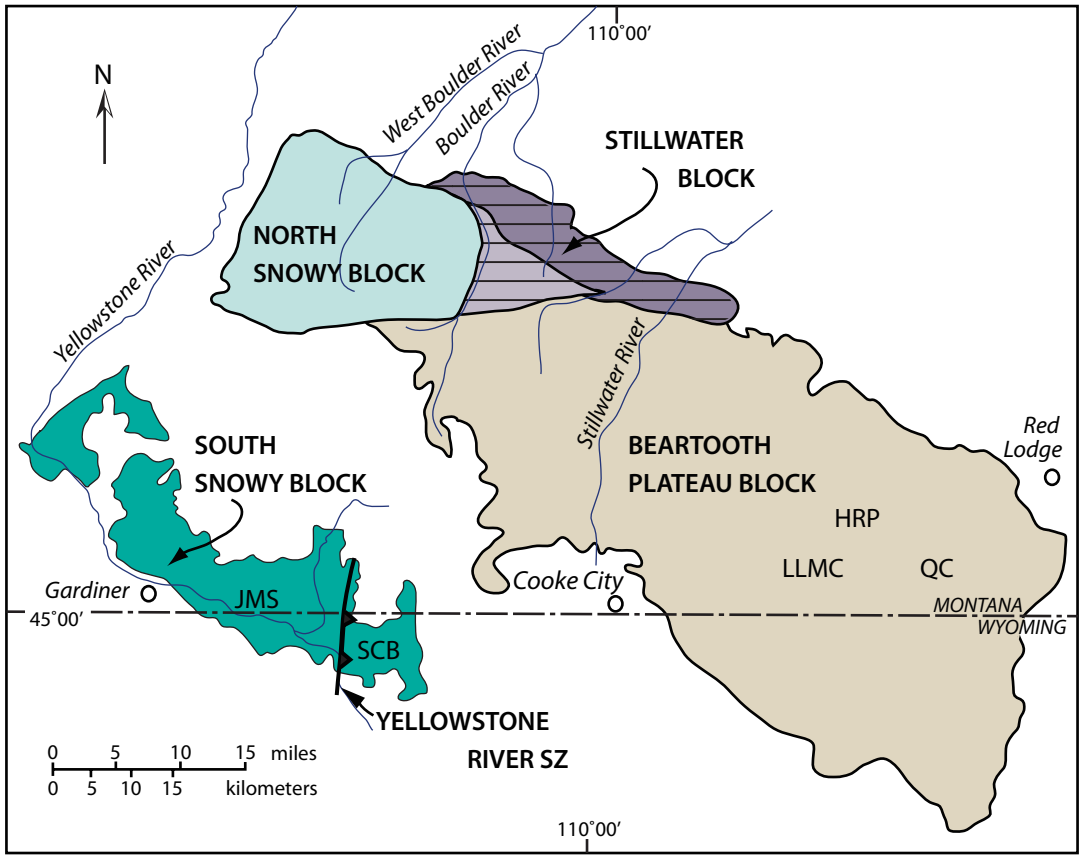

Fig. 2.3 Outline of the Beartooth uplift with individual blocks labeled. The *darker color* in the Stillwater block is the Stillwater Layered Igneous Complex (2.7 Ga). The LLMC and its temporal equivalents occur throughout the Beartooth Plateau and South Snowy blocks. See text for discussion of SCB (Slough Creek batholith), JMS (Jardine Metasedimentary Sequence), and Yellowstone River shear zone (SZ); *white areas* indicate Phanerozoic cover

These geochemical and geophysical characteristics are all applicable to crust comprising the Beartooth Mountains (Montana-Wyoming). Although Mesoarchean crust is contiguous throughout the Beartooth Mountains, this crust can be divided into several blocks with distinct geology (Fig. 2.3). This contribution will focus on two of the major blocks: the Beartooth Plateau and South Snowy blocks. The Beartooth Plateau block comprises most of the southeastern part of the Range and is lithologically dominated by Mesoarchean TTG plutonic and metaplutonic igneous rocks typical of the BBMZ. This association is exemplified by the 2.79–2.83 Ga Long Lake magmatic complex (LLMC; Fig. 2.3; Mueller et al. 2010). The LLMC contains enclaves of older, high-grade, metamorphic rocks (to 3.5 Ga); some of which contain detrital zircons to 4.0 Ga (Mueller et al. 1998; Valley et al. 2005; Mueller and Wooden 2012; Maier et al. 2012). The South Snowy block comprises most of the southwestern part of the Range. It is similar to the Beartooth plateau block in terms of its plutonic components, which were emplaced coevally with the LLMC, but distinct because these plutons intruded and partially assimilated metasedimentary rocks of greenschist-to-amphibolite grade (Mogk et al. 2012). Consequently, the South Snowy and Beartooth Plateau blocks expose a cross section of crustal levels that reflect the development of a Mesoarchean marginal arc built on Eoarchean-Hadean crust.

Beartooth Plateau Block Early work by Poldervaart and students (e.g., Eckelmann and Poldervaart 1957; Harris 1959; Larsen et al. 1966; Rowan 1969; Skinner 1969; Spencer 1969; Butler 1969) described and mapped the varied lithologies and structures throughout the Beartooth Plateau block. They interpreted the quartzofeldspathic gneisses as classic products of "granitization". Application of modern analytical approaches, primarily ion probe (specifically SHRIMP) for U-Pb geochronology and ICP techniques for trace elements, however, has led to the recognition and characterization of a very different history for these Archean rocks (e.g., Mueller et al. 2010; Mueller and Wooden 2012). The Hadean-to-Archean geologic evolution of the Beartooth Plateau block is discussed below in three general sections: (1) the earliest or "pre-rock" record interpreted from the chemical and isotopic compositions of detrital zircons; (2) the transitional period from ~3.1 to ~3.6 Ga that is dominant in the detrital zircon record; and (3) the well-characterized evolution of the 2.8 Ga, arc-related, magmatic and deformational event.

1. The earliest record of crustal evolution preserved in the Wyoming Province is derived from detrital zircons from the Beartooth Plateau block (Fig. 2.3; Mueller et al. 1992; Mueller et al. 1998; Mueller and Wooden 2012; Maier et al. 2012). These zircons occur in quartz-rich metasedimentary rocks that are intercalated within multilithologic metamorphic assemblages intruded by the prevalent Mesoarchean plutonic rocks of the LLMC (Mueller et al. 1998, 2010). Lithologies include quartzofeldspathic gneisses, metapelites, banded iron formation, migmatites, quartzites, and mafic and ultramafic amphibolites (Henry et al. 1982; Mueller and Wooden 2012; Maier et al. 2012).

U-Pb ages determined for detrital zircons via ion microprobe (SHRIMP) are dominated by 3.2–3.4 Ga grains in all samples (Mueller et al. 1998). Detrital grains younger than 3.1 Ga were not documented, which implies deposition after 3.1 Ga, but before unroofing of the extensive 2.8 Ga plutonic rocks. The critical observations noted in previous work on detrital zircons from these rocks and pertinent to Hadean and Mesoarchean crustal evolution include: (1) zircons > 3.5 Ga are relatively abundant (~25% of the zircons analyzed by Mueller et al. 1998) and ages extend in a continuum from ~3.3 Ga to 4.0 Ga (Mueller et al. 1998); (2) O-isotopic compositions of zircons from a sub-set of these same quartzites have δO^{18} values that are: (i) only slightly elevated relative to zircons from mantle-derived melts, (ii) similar to those in the ancient 4.0–4.4 Ga zircons from Australia (Jack Hills), and (iii) consistent with very limited intracrustal recycling of surface materials into the magmas from which the zircons originally crystallized (Valley et al. 2005); and (3) Hf isotopic data for several multi-grain zircon separates from these rocks (Stevenson and Patchett 1990) implied the presence of older Archean crust in the Beartooth area.

More recently, Mueller and Wooden (2012) reported extensive U-Pb, trace element, and Lu-Hf data for 3.3–4.0 Ga detrital zircons from quartzites within these metamorphic enclaves. In that study trace-element analyses were performed at the same locations within individual zircons that were used for the U-Pb geochronologic analyses. Analyses of Lu-Hf systematics were then made at the same locations used for U-Pb and/or trace element measurements in order to maximize the probability that all measurements were made on material in the same domain of the zircon (identified using cathodoluminescense). These analyses revealed a clear pattern of continuously decreasing minimum εHf values (parts in 10^4 deviation from the chondritic reservoir of Bouvier et al. 2008) in each 100 Ma segment between 4.0 and 3.6 Ga (Fig. 2.4). Subsequent to about 3.5–3.6 Ga, the minimum εHf values begin to increase, reaching a maximum at ~3.3 Ga. Utilization of the recently proposed BSE (bulk silicate earth) Lu-Hf parameters of Bizzaro et al. (2012), rather than those of Bouvier et al. (2008), would alter the absolute values of εHf, but would not change the pattern of decreasing values with decreasing age in Fig. 2.4.

The most important aspect of the positive correlation of initial εHf and age in Fig. 2.4 is that a single evolution line conforms to the minimum εHf values of individual zircons for the period from 3.6–4.0 Ga. Using these minimum values along with the constraint that there was no crust

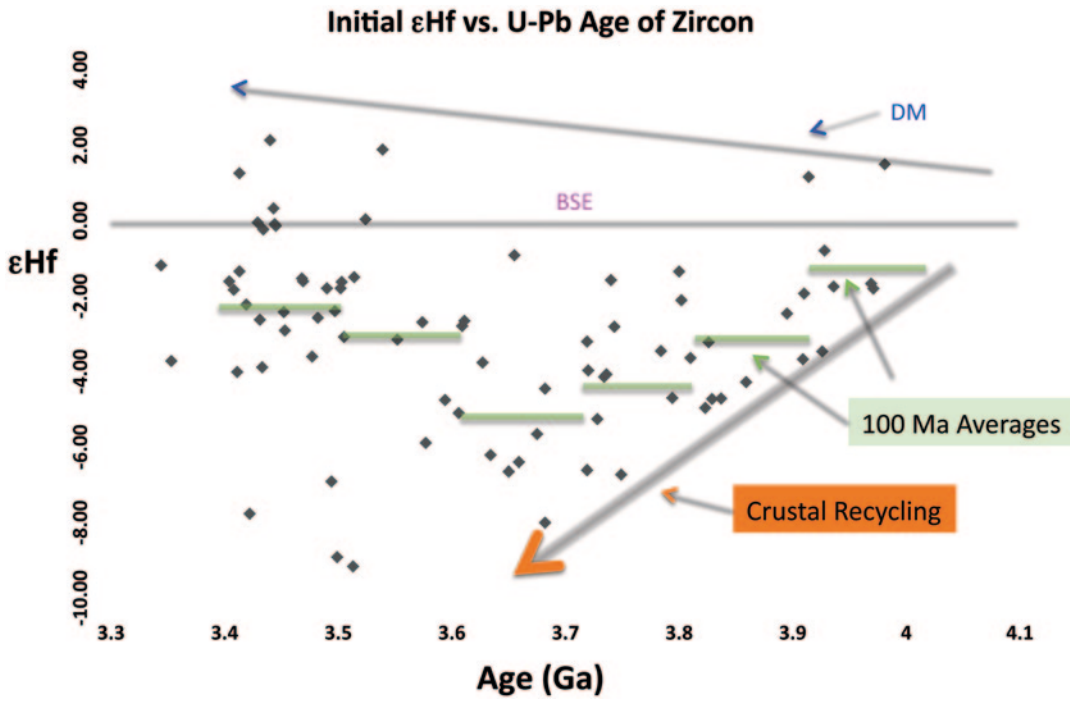

Fig. 2.4 Age ($^{207}Pb/^{206}Pb$ of zircon) vs. initial εHf showing the continuity of ages for detrital zircons during the 3.3–4.0 Ga period, the consistently decreasing values of εHf from 4.0 to 3.5 Ga, and the increasing initial εHf values post-3.5 Ga. The line along the lower limit of εHf values corresponds to a Lu/Hf ratio of 0.09. DM line is from Mueller et al. (2008) and CHUR/BSE from Bouvier et al. (2008). Horizontal bars are the averages of the initial εHf values for each 100 Ma increment. After Mueller and Wooden (2012)

significantly older than ~4.0 Ga in the system (i.e., the evolution line should not intersect the primitive or depleted mantle curves much older than the age of the oldest zircon, 4.0 Ga), yields a slope corresponding to a Lu/Hf ratio of ~0.10. This is a critical value for four reasons: (1) Using the most negative values provides the best approximation of the evolution of pre-existing crust (i.e., closest to 100% crustal melt), (2) It is only slightly above the value for current, average continental crust (0.081) proposed by Rudnick and Gao (2003), (3) It suggests a similar evolution path to the older zircons from the Jack Hills (e.g., Harrison et al. 2008; Kemp et al. 2010), and (4) It is lower than the typical values for modern arc or MORB magmas (~0.20; e.g., Pfander et al. 2007; Porter and White 2009; Wilbold et al. 2009; Arevalo and McDonough 2010; Nebel et al. 2011).

The difference between modern arc, MORB, and crustal Lu/Hf values is expected in light of the continual depletion in incompatible elements, including HFSE (high field-strength elements), characteristic of the evolution of the depleted mantle (e.g., Salters and Stracke 2004). Consequently, the modeled Lu/Hf value of ~0.1 for the period from 3.5–4.0 Ga in the NWP strongly suggests the source rocks for these zircons were derived from a more primitive (much less depleted) mantle than modern MORB or arc melts, or that garnet formed in the residuum of these melts and led to lower Lu concentrations (and lower Lu/Hf ratios). Trace element data for these zircons, however, suggest it is unlikely that parent magmas were in equilibrium with garnet (Mueller and Wooden 2012).

A second significant aspect of these data is that they define an overlapping continuum of ages with no significant peaks. Although the lack of discernable age-concentrations may reflect inadequate sampling for the time interval, the lack of strong age-concentrations is similar to the data from the Jack Hills (e.g., Harrison et al. 2008),

but contrasts with other ancient detrital zircon suites such as those from the Rae Province, Canada (Hartlaub et al. 2006); Tanzania (Kapete et al. 2012); and the Limpopo Belt (Zeh et al. 2008) that also show continua of ages, but with discernable age-concentrations. The presence or absence of discernable concentrations (peaks) in the age spectra has implications for whether magmatic additions to individual segments of Hadean-Eoarchean crust followed a pattern of long-term episodicity similar to the patterns derived from younger detrital zircon suites that have been interpreted to reflect episodic plate tectonic-driven orogeny on the 100 Ma time-scale (e.g., Condie 2000) or to extended periods of diapiric upwelling. Although extended episodes of mantle upwelling (>100 Ma) are rare on Earth today, numerical simulations by Robin and Bailey (2009) show that repeated diapiric upwellings and associated density driven overturns of Hadean-Eoarchean crust can be expected to occur at intervals of as few as 10 Ma, which would yield a record that would be difficult to discern from an absolute continuum of ages. Similarly, Moyen and van Hunen (2012) suggest that Archean plate tectonics was characterized by short-lived subduction cycles of only a few million years, which could also produce an essentially continuous record.

2. The transition from the positive age-εHf relationship defined by the 3.6–4.0 Ga detrital zircons to the negative age-εHf from 3.2–3.5 Ga marks increasing contributions from more depleted (juvenile) sources to crustal growth. Gneissic and migmatitic rocks (TTG suite) and a range of metasupracrustal rocks (meta-igneous and metasedimentary) that formed during this transitional period are preserved at varying scales within the ~2.8 Ga LLMC, particularly in the Beartooth Plateau block. In the Beartooth Plateau block these metamorphosed supracrustal rocks include metabasites, peraluminous gneisses (migmatites), meta-ironstones, meta-ultramafic rocks, pelitic to psammatic schists, and quartzites, in addition to metaplutonic quartzofeldspathic gneisses (e.g., James 1946; Henry et al. 1982; Maier et al. 2012). The individual lithologies have been tectonically mixed along high-grade ductile shear zones, and multiple stages of disharmonic folding developed prior to emplacement of the LLMC. Many of these lithologies preserve petrologic evidence of one, and possibly two, stages of granulite facies metamorphic events with an amphibolite facies overprint that is commonly associated with local mylonitization (Fig. 2.5).

Ages for these pre-2.8 Ga rocks throughout the Range are difficult to determine because of the multiple metamorphic events and complex paragenetic sequences (e.g., Mogk and Henry 1988; Mueller et al. 1996). Quartzofeldspathic gneisses and migmatites that have been examined for their U-Pb zircon systematics suggest a range of ages from 3.5 Ga to 3.1 Ga (Fig. 2.6). Whole-rock Sm-Nd data yield a range of depleted mantle model ages (T_{dm}) that are often older than the intrusion age of individual lithologies with a maximum of 4.1 Ga (Fig. 2.7). Uranogenic common Pb (^{207}Pb-^{206}Pb) isotopic ratios show a general correlation on an isochron diagram along a reference line corresponding to an age of ~3.2 Ga (Fig. 2.8). This "age" is clearly the result of mixing among rocks of different ages as well as partial re-equilibration during metamorphism(s), but still provides a strong indication that these rocks are older than 2.8 Ga. The combination of the Pb-Pb array, which lies above the average crust of Stacey and Kramers (1975), and Sm-Nd whole-rock data (T_{dm} much older than crystallization age in some cases) shown in Figs. 2.7 and 2.8 indicate that some of the rocks that formed in the 3.1–3.5 interval interacted strongly with even older crust, while others did not (Wooden and Mueller 1988; Chamberlain and Mueller 2007).

In aggregate, the rocks that formed during this transitional period (3.1–3.5 Ga) range in composition from basaltic to rhyolitic (Irvine and Baragar 1972; Fig. 2.9). The mafic rocks (48–52 % SiO_2) follow a tholeiitic trend (Fig. 2.10) and are both olivine- and quartz-normative. Tectonic variation diagrams reveal chemical affinities with calc-alkaline basalts and island arc tholeiites (Mullen 1983; Fig. 2.11). Rocks of intermediate composition (52–63 % SiO_2) include both tholeiitic and calc-alkaline varieties, whereas felsic rocks (>63 % SiO_2) are calc-alkaline. Most of the felsic gneisses are weakly peraluminous

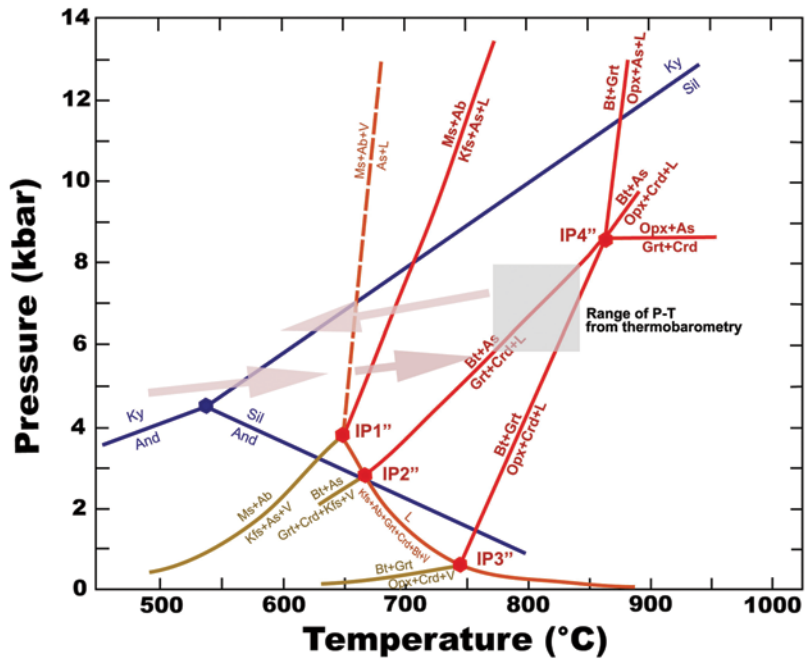

Fig. 2.5 Petrogenetic grid adapted from Spear et al. (1999) showing dehydration reactions (*gold*), water-saturated melting reactions (*orange*), dehydration melting reactions (*red*),and aluminosilicate polymorph boundaries (*blue*) in pressure-temperature space. The *gray-pink* arrows suggest the approximate pressure/temperature path experienced by these rocks. The *gray* box indicates the results and standard deviation of the geothermobarometry for peak metamorphic conditions

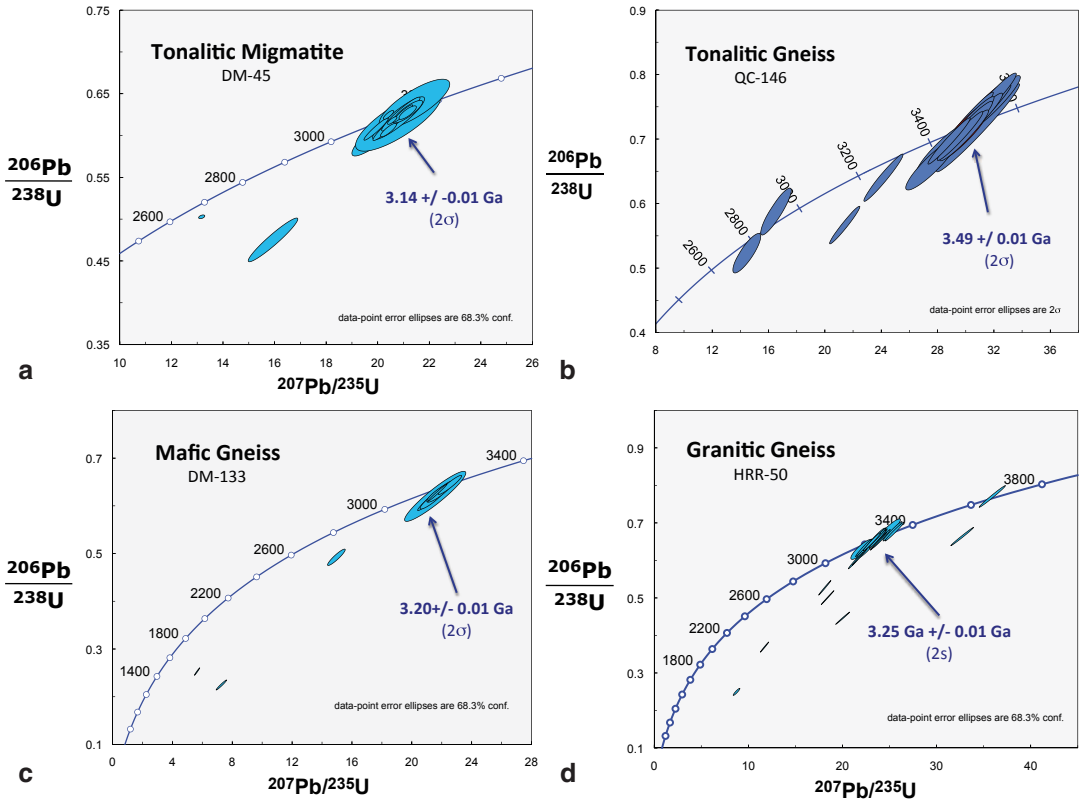

Fig. 2.6 U-Pb concordia plots for four pre-2.8 Ga gneisses: **a** tonalitic gneiss, **b** tonalitic migmatite, c mafic gneiss, and **d** granitic gneiss. All from the Beartooth Plateau block and determined using the SHRIMP-RG ion microprobe. Pb-loss is evident in all samples, and xenocrysts > 3.6 Ga in (d)

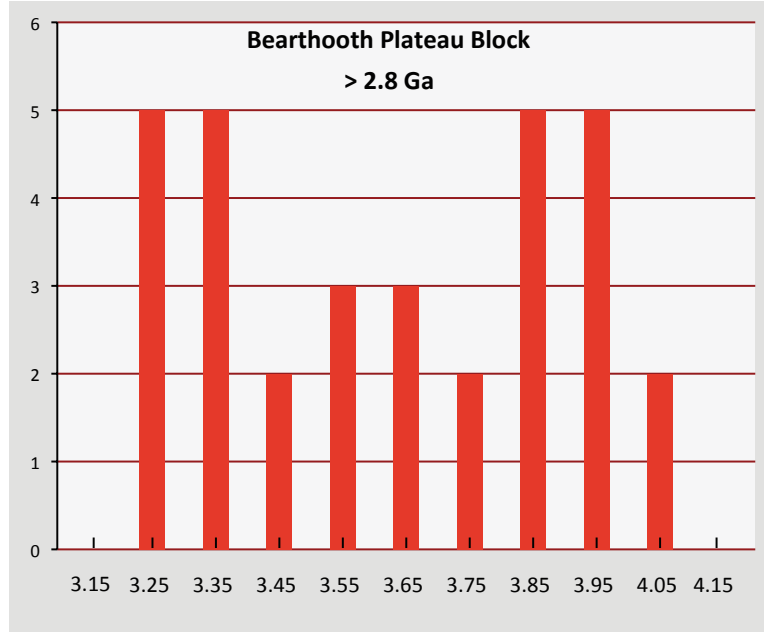

Fig. 2.7 Distribution of Tdm (Sm-Nd depleted mantle model ages; DePaolo 1981) for pre-LLMC lithologies from the Beartooth Plateau block

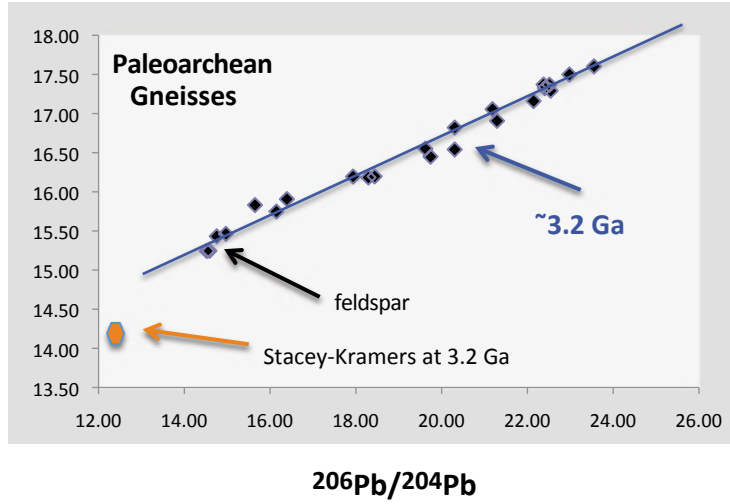

Fig. 2.8 Plot of common, uranogenic, whole-rock Pb isotopes and one feldspar from pre-LLMC rocks from the Beartooth Plateau block. Bulk-rock compositions range from 56 to 78 wt.% SiO_2

(normative corundum < 2%). The protoliths of the felsic gneisses are difficult to determine due to the lack of original minerals and potential redistribution of elements during metamorphism, but the majority of these rocks appear to have an igneous origin (Fig. 2.12; Leyreloup et al. 1977). Tectonic variation diagrams reveal that the felsic gneisses have compositions of volcanic arc or syn-collisional granites (Fig. 2.13; Pearce et al. 1984). We do not imply that all of these rocks are genetically related due to the uncertainty of their ages of formation; however, their compositions collectively do fall within the range of rocks from well-characterized, contemporary, tectonic environments.

3. The Mesoarchean TTG rocks and granites (Wooden et al. 1988a, b; Mueller et al. 2010) that volumetrically dominate the Beartooth Mountains are the basis for designating this region as part of the BBMZ (e.g., Mogk et al. 1992;

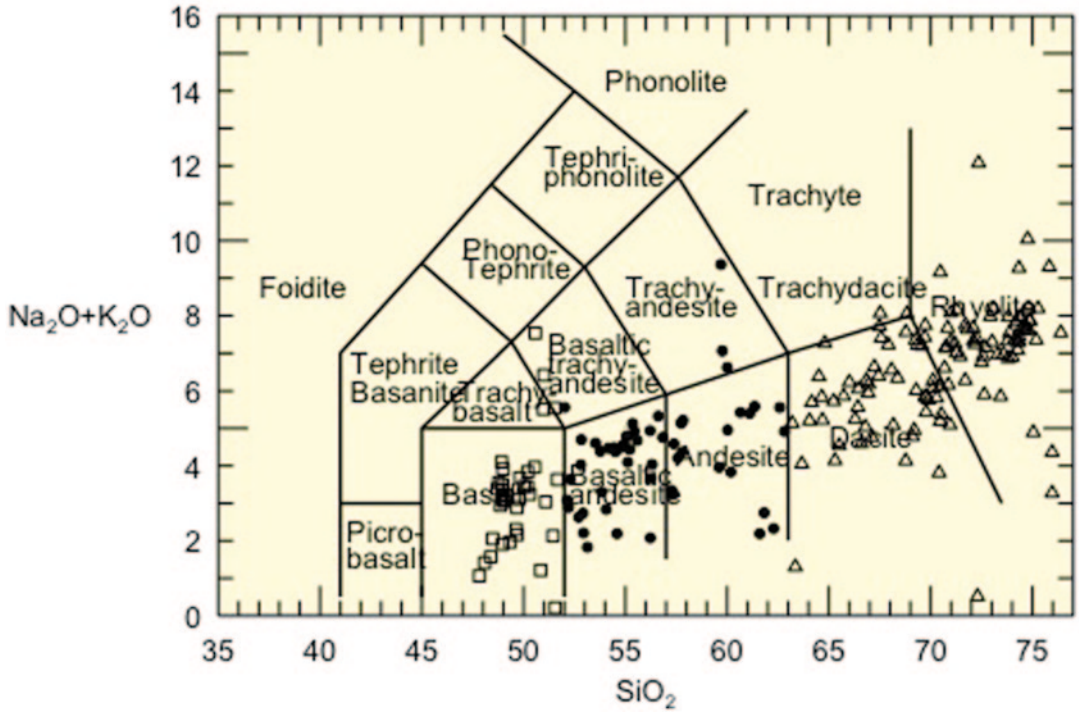

Fig. 2.9 Total alkali-silica diagram showing primary compositional variety among the 3.1–3.5 Ga xenoliths within the Long Lake magmatic complex (Irvine and Baragar 1972). Samples plotted do not include quartzites or banded iron formation lithologies. Symbols are: *squares*, 48–52 % SiO_2; *solid circles*, 52–63 % SiO_2; *triangles*, 63–80 % SiO_2

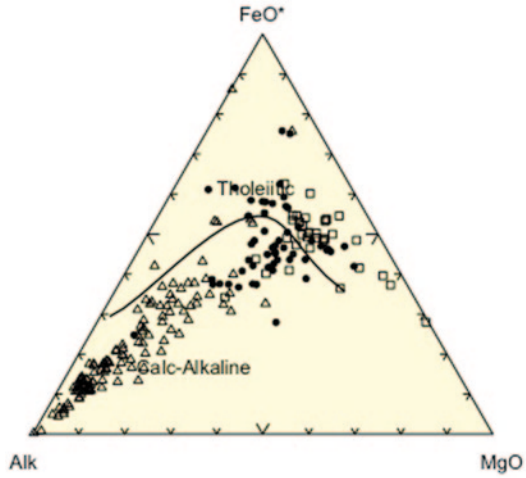

Fig. 2.10 Normalized alkali-iron-magnesium diagram showing tholeiitic character of mafic lithologies (48–52 % SiO_2) from the Beartooth plateau block. Symbols as in Fig. 2.9

Chamberlain et al. 2003; Mueller and Frost 2006). Tonalitic to trondhjemitic plutonic rocks and derivative gneisses formed at ~2.8 Ga (U-Pb zircon ages) are exposed extensively throughout the Range, but are most comprehensively studied in the Beartooth Plateau block, where they are designated as the Long Lake magmatic complex (LLMC; Fig. 2.3). The LLMC constitutes a diverse assemblage of Mesoarchean rocks that range from amphibolites and amphibole-bearing gneisses of dioritic-tonalitic compositions to more evolved TTG-suite rocks that range from granodiorite to trondhjemite to granite, including many with adakitic affinity (Mueller et al. 1983, 2010; Fig. 2.14). More mafic components may exist, but the difficulty of determining reliable ages for these lithologies prevents confirming their presence as part of the LLMC suite. The Mesoarchean rocks were intruded both syn- and post-kinematically so that metamorphic foliations and lineations were imparted variably across compositions and locations.

In areas that exhibit the most deformation, e.g., gneissic banding, lineation, etc., the granoblastic

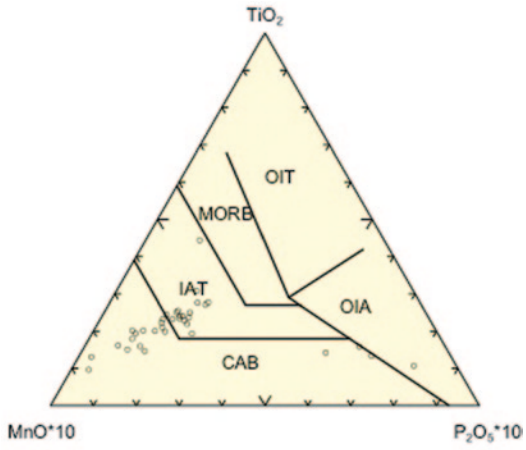

Fig. 2.11 Normalized Mn-Ti-P diagram showing indications of calc-alkaline and island arc tholeiitic character of samples with 48–52 wt.% SiO_2

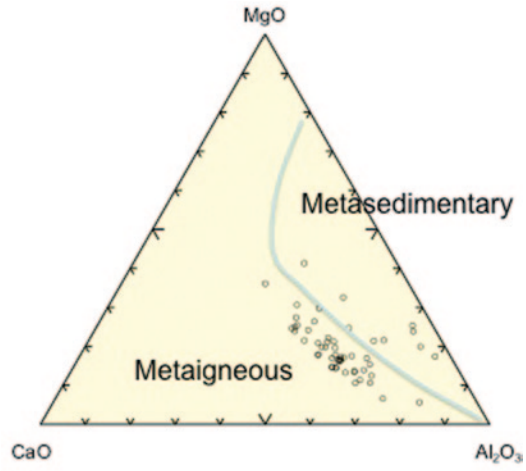

Fig. 2.12 Normalized Ca-Mg-Al diagram with proposed fields for metamorphic rocks with igneous vs. sedimentary protoliths for samples with 52–63 wt.% SiO_2 (Leyerdoup et al. 1977)

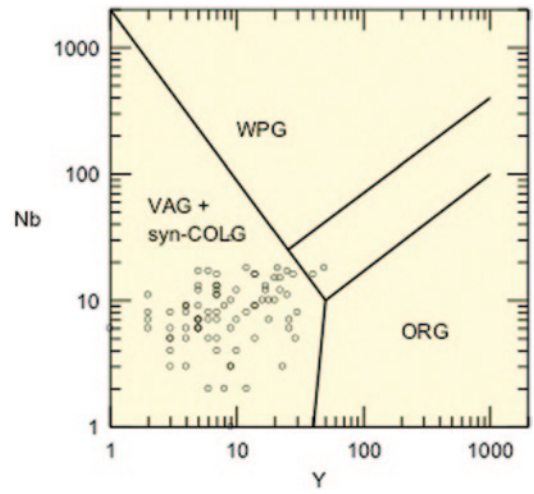

Fig. 2.13 Plot of Nb vs. Y (in ppm) proposed by Pearce et al. (1984) to identify the tectonic environment of granitoids (63–80 wt.% SiO_2)

texture of the recrystallized quartz and feldspars suggests that deformation and recrystallization must have developed at relatively high temperatures to allow this extent of ductile deformation and recovery. Peak metamorphism was generally in the amphibolite facies, but did reach granulite grade in some locations (e.g., Mueller et al. 2010). In areas where intrusive relations are evident, individual rock types do not exhibit consistent field relationships (e.g., granodiorites intrude granites, and vice versa). These mutual intrusive relationships are compatible with, and supportive of, geochemical and petrologic data that show that the LLMC lithologies do not represent a sequence of progressively more mafic or more granitic compositions with time. It is also clear that the various compositions do not represent sequential differentiates of a single parent magma, i.e., the granites are not differentiates of the granodiorites, the granodiorites are not differentiates of the diorites, etc. (Wooden and Mueller 1988; Mueller et al. 2010).

These complex field and petrologic relationships, combined with the limited time span of magmatism (2.79–2.83 Ga), suggest that multiple, independent sources were important to the development of the LLMC at any given time (Mueller et al. 2010). For example, it is difficult to envisage a fractional crystallization scenario in which the most silicic samples (e.g., granites and trondhjemites up to 78% SiO_2) can be derived from the intermediate samples (e.g., granodiorites) because of the difficulty of increasing silica content without raising incompatible element contents (e.g., La, Fig. 2.15). In addition, some granodiorites show clear evidence of equilibration with garnet (Yb, Lu < 10x chondrites), but none of the more silicic samples exhibit this trait (Mueller et al. 2010). Combined with bulk

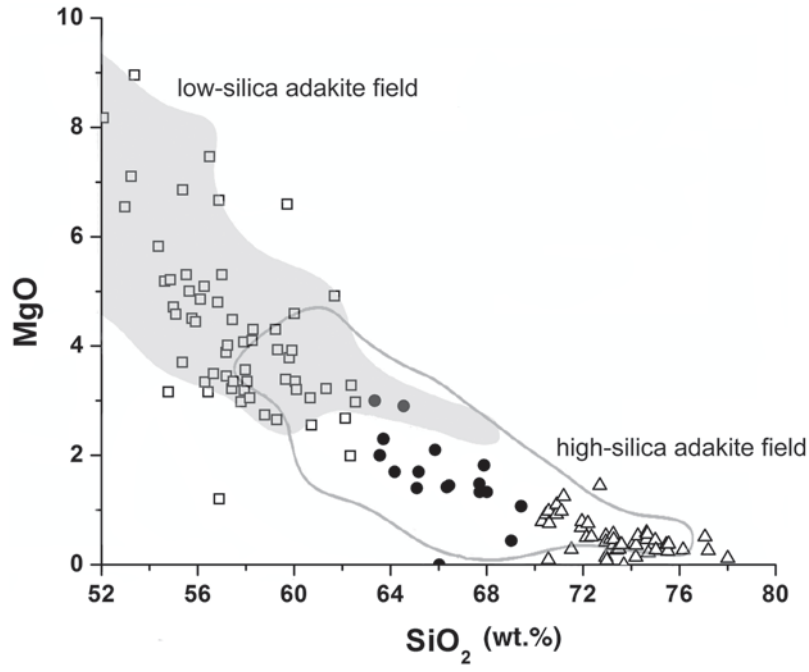

Fig. 2.14 Plot of weight percent oxides of MgO and SiO_2 for LLMC lithologies with reference fields from Martin et al. (2005). Symbols are: *solid circle* = granodiorites, *open triangle* = granites (s.l.), *open square* = diorites

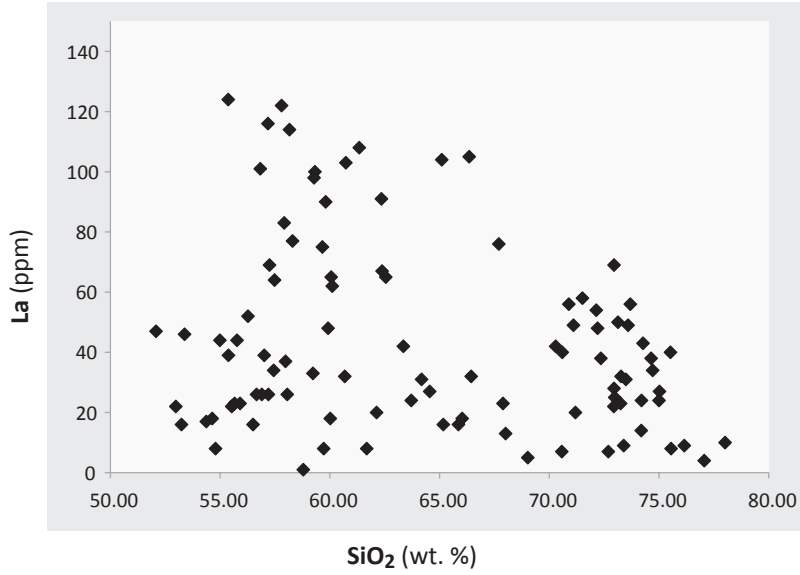

Fig. 2.15 La vs. SiO_2 for LLMC lithologies showing largely random relationship between the parameters, which rules out extensive fractional crystallization as the cause of compositional variation in the LLMC

compositions that range from 52–78 % SiO_2, it is apparent that the source regions of individual magmas in the LLMC likely ranged from lithospheric mantle to mid-crustal levels. For the most mafic samples, the normalized trace element abundances (Fig. 2.16).) show traits typical of magmas from modern arcs (e.g., relative depletion of HFSE, positive anomaly for Pb, etc.).

Considering the different sources that must have been involved in LLMC magma genesis, it is surprising that initial Sr, Pb, and Nd isotopic compositions for all LLMC rocks (regardless of

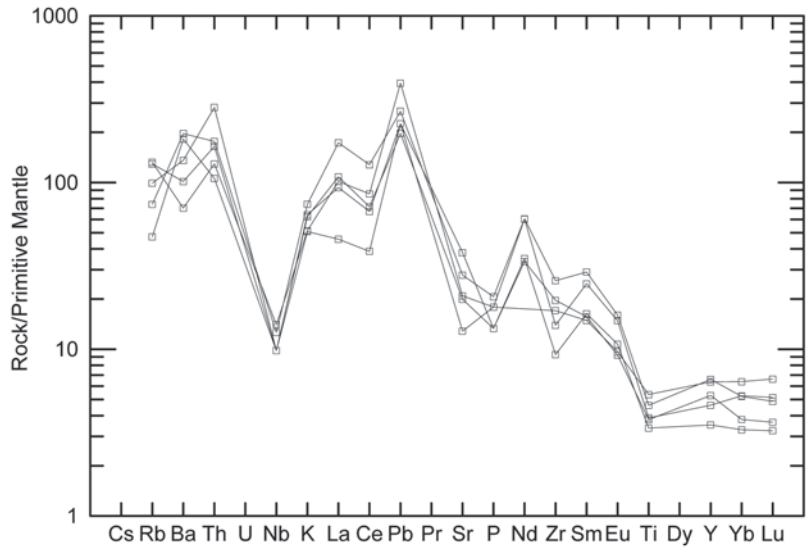

Fig. 2.16 Plot of primitive-mantle-normalized trace element abundances for LLMC diorites showing the relative depletion of the HFSE and positive anomaly for Pb typical of modern subduction-related magmatism

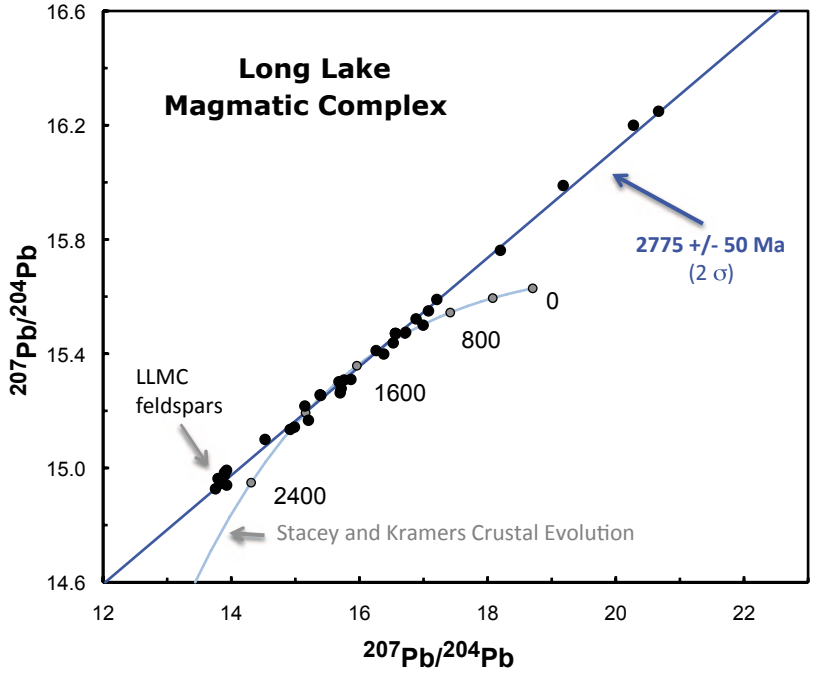

Fig. 2.17 Plot of common, uranogenic Pb isotopes from a full range of LLMC compositions (52–78 wt.% SiO_2) and feldspars that yield an age within error of the U-Pb zircon ages for the same rocks (Mueller et al. 2010). Note the initial Pb isotopic composition suggested by the feldspar data lies well above the Stacey and Kramers (1975) average crustal growth curve, indicating interaction with an older, high-μ reservoir

SiO_2 content) do not reflect the range of values expected for the isotopic compositions of ancient crust or depleted mantle at 2.8 Ga (Wooden and Mueller 1988). As shown in Fig. 2.17, whole-rock Pb isotopic compositions yield a linear array that, when regressed, results in an age indistinguishable from the ages of the youngest intrusives of the LLMC (2.79 Ga; Mueller et al. 2010), effectively recording the cooling of the complex. In addition, the fact that these Pb (and Sr data, Wooden and Mueller 1988) define near-isochrons means that radioelement parent-daughter ratios have remained largely intact since the end of LLMC magmatism and, more significantly, that

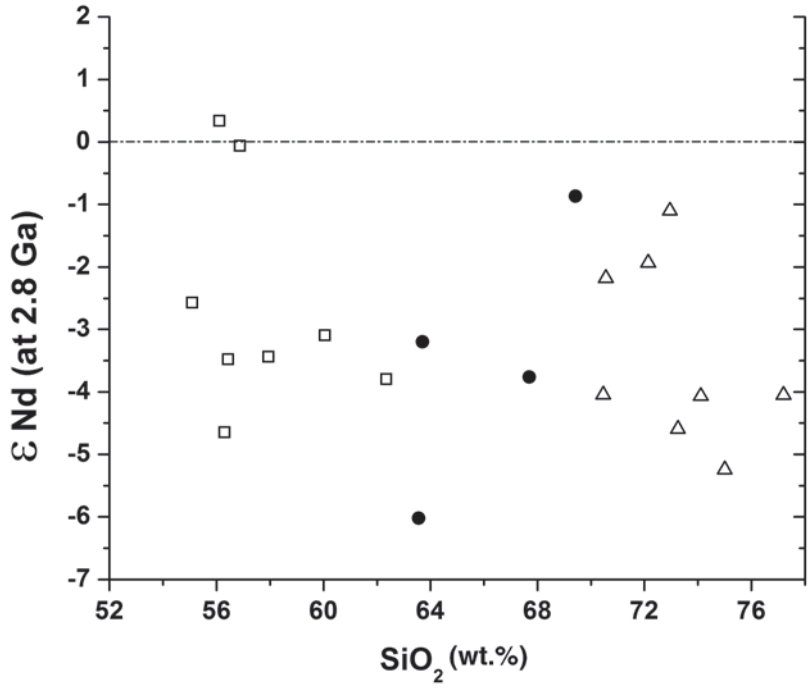

Fig. 2.18 Plot of initial Nd isotopic composition of LLMC samples vs. SiO_2 showing the lack of consistent relationship between SiO_2 (as an index of differentiation) and initial Nd isotopic composition, indicating that in-situ contamination is an unlikely explanation for the limited variation of initial values (av. -3 +/- 1, 1s). Pre-2.8 Ga crust would have had a range of εNd from −2 to −16 at 2.8 Ga. Symbols as in Fig. 2.13

the samples shared common initial isotopic compositions. The coherence of radiometric systems based on highly mobile elements such as Rb, Sr, and Pb also implies that the overall geochemistry of LLMC rocks has not been significantly disturbed since the rocks formed. In addition to the common initial ratios implied by the Rb-Sr and Pb-Pb arrays, the apparent lack of relationship between SiO_2 and initial Nd isotopic compositions (average of -3 εNd; Fig. 2.18) suggests that initial ratios in all systems are unlikely to be related to bulk rock composition or the composition of the immediate host rocks (e.g., lowest initial Nd isotopic compositions are not found exclusively in rocks with the highest SiO_2 contents or in specific locations). Consequently, observed elemental abundances and calculated initial isotopic compositions provide strong constraints for LLMC petrogenesis.

The large volume of rock generated, the range of bulk compositions, the limited interval of magmatism, the normalized trace element patterns, and limited range of initial isotopic compositions strongly suggest that the LLMC formed along an Archean continental margin as a consequence of the subduction of oceanic lithosphere and continental detritus (Wooden and Mueller 1988; Mueller et al. 2010). The homogeneity of initial isotopic compositions suggests these ratios were not derived from interactions between individual magmatic units and older host rocks, but that detritus shed from this ancient continent ("Beartoothia") was subducted and at least partially equilibrated with fluids that permeated the melt-zones in the upper mantle (wedge) and lower crust (Fig. 2.19). Because the enriched initial isotopic compositions of the LLMC rocks are not equivalent to juvenile 2.8 Ga values (i.e., 2.8 Ga depleted mantle) or older Beartooth crust at 2.8 Ga, it appears that most of the mass of the LLMC was derived from contemporary mantle lithosphere or oceanic crust, not from recycling of pre-existing crust (Mueller et al. 2010). The LLMC melting environment, therefore, is similar to the classic MASH zone (mixing, assimilation, storage, hybridization) proposed for isotopic homogenization of Andean magmatism by Hildreth and Moorbath (1988).

The impact of an extensive flux of relatively juvenile material on bulk crustal composition is most readily seen in the U-Pb systematics of the LLMC. In particular, the average μ-value ($^{238}U/^{204}Pb$) of the LLMC rocks calculated

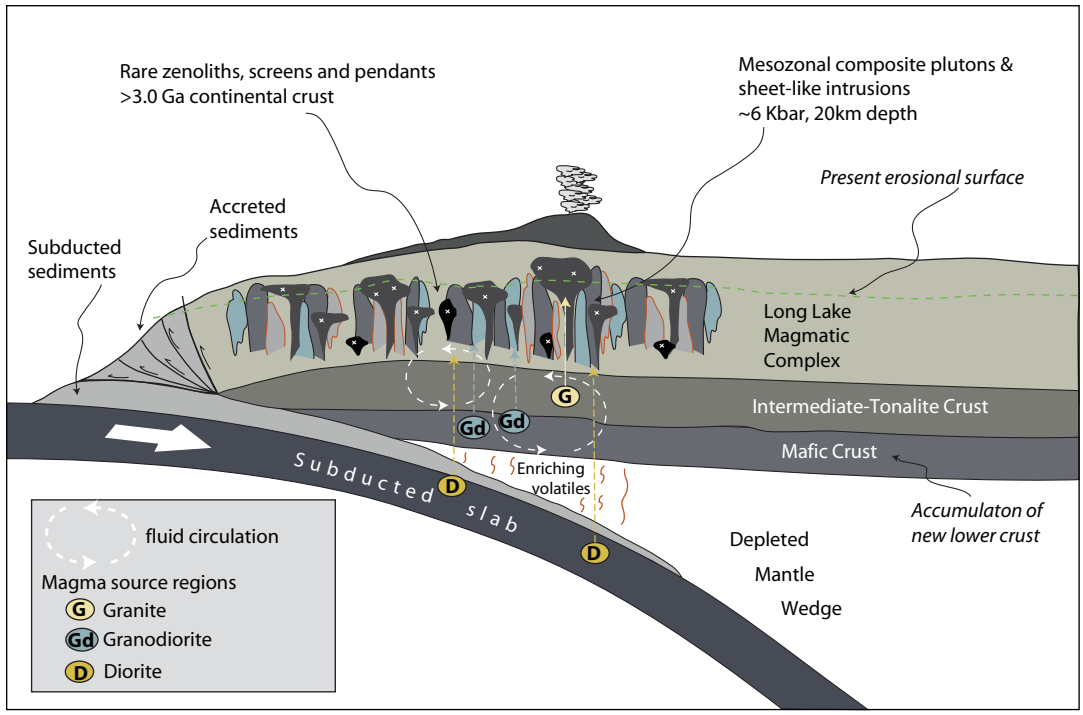

Fig. 2.19 Schematic depiction of tectono-magmatic framework for LLMC magmatism emphasizing the presence of older crust and multiple sources for the LLMC magmas. Basaltic magmatism was no doubt concurrent, but they are not depicted because of the lack of confirmed 2.8 Ga mafic rocks

from their measured Pb isotopic compositions at 2.8 Ga (Wooden and Mueller 1988) and the average μ-value measured in LLMC rocks today (Staffenberg et al. 2011) are both ~5, and are not sufficient to produce the average Pb isotopic composition of the LLMC rocks in the age of the Earth. Consequently, the LLMC and other Mesoarchean rocks in the BBMZ (e.g., Frost et al. 2006) exhibit a "crustal Pb paradox". This paradox is similar to that posited for the modern depleted mantle (e.g., White 1993; Kramers and Tolstikhin 1997; Hofmann 2003) in which the Pb isotopic compositions of MORB cannot be produced by the μ-values of the modern depleted mantle in the age of the earth. In both cases (paradoxes), the Pb isotopic compositions must be inherited from an older, higher-μ source. The composition and age of this older crust in the NWP can be partially constrained by the Lu-Hf systematics of the Eoarchean-Hadean detrital zircons as discussed above (~4.0 Ga; Wooden and Mueller 1988; Mueller and Wooden 2012).

2.3 South Snowy Block

The South Snowy block (Fig. 2.3), which comprises the pre-volcanic basement in the northern part of Yellowstone National Park and the Absaroka volcanic field, contains numerous exposures of Mesoarchean plutonic rocks that intruded a thick sequence of metasedimentary rocks (e.g., pelitic schists, quartzites, and banded iron formation); historically, these rocks are referred to as the Jardine Metasedimentary Sequence (JMS, Fig. 2.3; Casella et al. 1982; Montgomery and Lytwyn 1984; Mogk et al 2011; Osborne et al. 2011). The metaclastic lithologies exhibit a systematic coarsening from west to east and preserve primary sedimentary structures typical of middle-to-distal fan turbidites (e.g., graded beds, cross beds, sole marks, etc.). The JMS was likely deposited as a sequence of turbidites on oceanic crust or thin continental crust along an active continental margin (Thurston 1986; Goldstein et al. 2011; Foster et al. 2011).

Table 2.1 1 U-Pb ages of zircons from igneous and meta-igneous rocks of the South Snowy block

Sample	Lithology	Age (Ma)
10-BW-7-2-01	Muscovite granite	2816 +/− 27
10-PM-7-14-01	Hornblende quartz diorite	2815 +/− 9
10-DM-7-3-03	Hornblende-biotite quartz diorite	2798 +/− 4
10-PM-7-2-01	Biotite quartz monzonite	2808 +/− 7
11DM-7-08-01	Augen gneiss	2791 +/− 7
11MH-7-01-02	Biotite granite gneiss	2816 +/− 13
11MN-7-05-01	Biotite-hornblends granodiorite	2794 +/− 10
11MN-7-15-01	Quartz hornblende diorite	2806 +/− 13
11SPM-7-18-02	Biotite tonalite gneiss	2832 +/− 7
11SRM-7-06-01	Biotite granite gneiss	2810 +/− 6
11TG-7-16-01	Biotite tonalite	2802 +/− 2
11TG-7-06-01	Hornblende-biotite tonalite	2804 +/− 3
10-AL-7-13-01	Quartzofeldspathic gneiss	3243 +/−22

Metamorphic assemblages in the JMS schists exposed in the western part of the South Snowy block along the Yellowstone River (Fig. 2.3) range from chlorite-zone (greenschist facies) to staurolite-andalusite-garnet zone (lower amphibolite facies). Metamorphic grade increases from west to east and north-to-south toward the Beartooth Plateau block. Thermobarometry indicates metamorphic temperatures of 572–609 °C and pressures of 3.4–5.9 kbar for the lower amphibolite facies rocks; epidote-bearing plutonic rocks to the west suggest pressures of ~8 kbar. These variations in metamorphic conditions from west to east are not smooth, however, because a major shear zone (Yellowstone River shear zone) separates the 3–5 kbar rocks on the west from the ~8 kbar rocks to the east (Fig. 2.3). This shear zone is a major crustal discontinuity (ductile shear zone) that separates the JMS of the western South Snowy block (volumetrically dominated by metasedimentary rocks) from the eastern South Snowy block (volumetrically dominated by the TTG plutons of the Slough Creek batholith). The shear zone developed partly in the Slough Creek batholith and partly within 3.2 Ga basement gneisses, which are similar to the older gneisses in the Beartooth Plateau block (Table 2.1). Kinematic indicators in the shear zone suggest that older (~3.2 Ga) high-grade gneisses and components of the Slough Creek batholith were thrust over the western part of the JMS with a cumulative vertical throw of 10–15 km (Marks et al. 2012). In the footwall, the lower grade JMS turbidites show progressive deformation characterized by bedding parallel fabrics overprinted by isoclinal folds and then several generations of kink and chevron folds in domains separated by high-strain zones with intense crenulation cleavage. Late-stage, greenschist facies, retrograde zones overprint amphibolite facies mylonite in the Yellowstone River shear zone, suggesting that the thrust was overprinted as a normal fault. This fault zone now juxtaposes different crustal levels of the 2.8 Ga arc crust.

Major and trace element abundances of the JMS are generally consistent with a bimodal mixture of mafic-ultramafic and felsic sources based on both high transition metal contents and consistent, negative Eu-anomalies (e.g., Thurston 1986). For example, abundances of Cr (up to 550 ppm, average 280) and Ni (up to 200 ppm, average 92) are significantly higher than the values of average crust, but comparable to average Archean crust (230 ppm Cr and 130 ppm Ni; Taylor and McLennan 1995; Fig. 2.20). Although absolute abundances can be lowered as a result of quartz-dilution, the JMS samples show a distinctly higher Cr/Ni ratio compared to average Archean crust. Samples with the highest Cr and Ni values are comparable to the high transition metal contents reported for Onverwacht metasedimentary rocks (e.g., Fig Tree and Moodies; Hofmann 2005), suggestive of an ultramafic component in the provenance.

Whether the transition metal contents are viewed as high or average for Archean

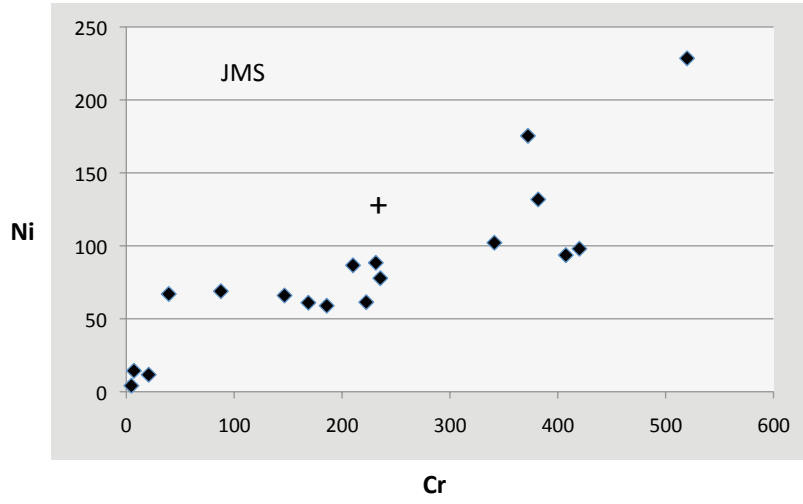

Fig. 2.20 Distribution of Cr and Ni values (ppm) for JMS with (+) plotted to show average values of Archean crust (Taylor and McLennan 1995)

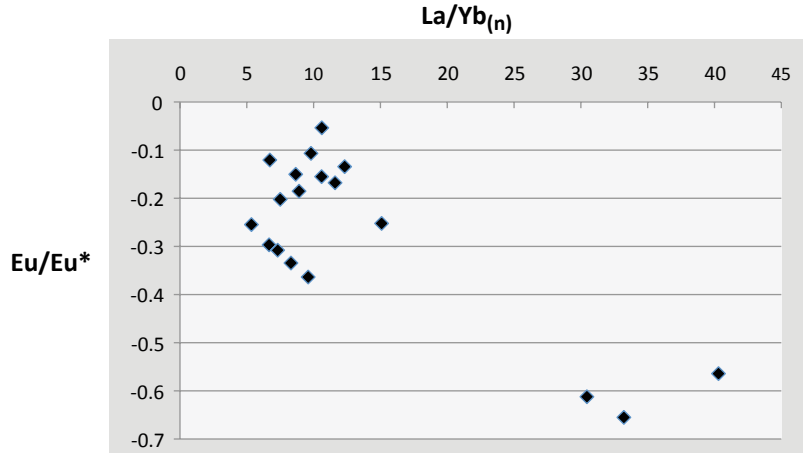

Fig. 2.21 Distribution of $(La/Yb)_n$ relative to Eu anomaly (Eu/Eu*) for JMS lithologies

sedimentary rocks, the consistently negative Eu-anomalies (Eu/Eu* from −0.1 to −0.6; Fig. 2.21) are more typical of Proterozoic than Archean (meta)sedimentary rocks as discussed by Taylor and McLennan (1995). The development of strong negative Eu-anomalies and the association of the most negative anomalies with the highest $(La/Yb)_n$ ratios are consistent with a petrologically mature provenance in which crustal melting was prevalent (i.e., melting and/or crystallization in the plagioclase stability field). The low $Yb_{(n)}$ values (<10) observed in many samples are consistent with derivation from typical Archean TTG rocks (e.g., Martin et al. 2005). Although Taylor and McLennan (1995) generally attribute the negative Eu-anomalies in sediments to crustal thickening and melting that occurred after the Archean-to-Proterozoic transition, negative Eu-anomalies in (meta) sedimentary rocks can occur at any time when crustal thickness and geodynamics favor emplacement of crustally derived melts in the upper crust. In the case of the South Snowy block's (JMS) sedimentary protoliths, the presence of older detrital zircons, relatively high transition metal contents, and consistent negative Eu-anomalies are compatible with a bimodal provenance consisting of crustally derived felsic and mantle-derived mafic/ultramafic components.

Plutonic rocks comprise a major part of the crust exposed in the South Snowy block. In the western South Snowy block two 10 km-scale,

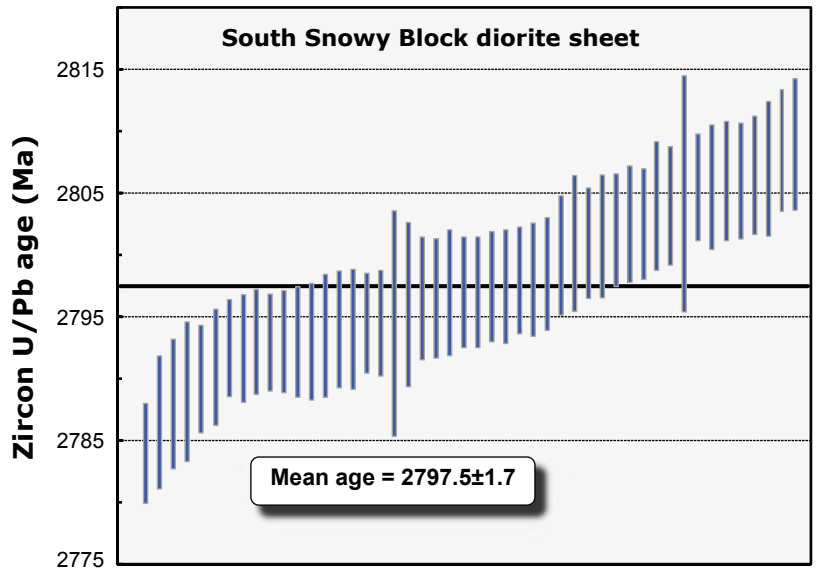

Fig. 2.22 Distribution of U-Pb ages for individual zircons analyzed by laser ablation ICP-MS for a diorite pluton that intruded the Jardine Metasedimentary Sequence in the South Snowy block; error bars are 2 sigma

bulbous, locally muscovite-bearing, peraluminous granitic plutons (Crevice Mountain and Hellroaring Creek stocks) intruded the JMS; Table 1 shows U-Pb zircon ages of 2.80–2.81 Ga for these plutons (Philbrick et al. 2011; Foster et al. 2011). These granitic rocks are associated with a suite of dioritic and granodioritic sheets that created injection migmatites in parts of the JMS. U-Pb zircon ages for these sheets (leucosomes) also range from 2.79 to 2.81 Ga, and have TTG compositions (Fig. 2.22; Foster et al. 2011). A second, distinct suite of intrusive rocks is exposed in the eastern South Snowy block and referred to as the Slough Creek batholith (SCB, Fig. 2.3). These rocks range in composition from diorite to granite with TTG suite affinities and comprise a composite plutonic suite of sheet-like intrusions with compositional variations on the 10–100 m scale; magmatic epidote in hornblende-bearing plutons indicate crystallization at ~8 kbar. Crystallization ages determined from U-Pb zircon geochronology are also ~2.8 Ga (Berndt et al. 2012; Table 2.1). The ages of the oldest plutons (~2.81 Ga) and the youngest detrital zircons (~2.9 Ga) constrain the depositional age of the JMS (Fig. 2.23).

The intermediate-to-felsic igneous suites in the eastern and western South Snowy block were emplaced in the same time-interval as the LLMC in the Beartooth Plateau block and have a range of major element compositions similar to the LLMC. In terms of important trace element abundances, the plutonic rocks in the South Snowy block share the low U/Pb ratios common to the Mesoarchean plutonic suite throughout the northern Wyoming Province (i.e., less than the crustal average). Ratios in the South Snowy plutonic suites are slightly higher than those in the LLMC (7.5 vs. 5.0), but this difference is likely to be at least partly related to the assimilation of the host meta-turbidites (average $^{238}U/^{204}Pb = 13$), as evident in the zones of injection migmatite and the overall prevalence of peraluminous compositions.

For less mobile trace elements (e.g., REE), the plutonic rocks of the South Snowy block resemble granodioritic rocks of the LLMC (Mueller et al. 2010) because they have similar, strongly depleted HREE contents (average $Yb(n) < 5$; $n = 37$) indicative of residual garnet in their source(s). Overall REE patterns, however, are not strongly fractionated with La/Yb(n) from 4 to 150; only two have ratios > 100. The western South Snowy block stocks (west of the Yellowstone River shear zone) and the Slough Creek batholith in the eastern South Snowy block are, therefore, interpreted to be upper and middle crustal equivalents

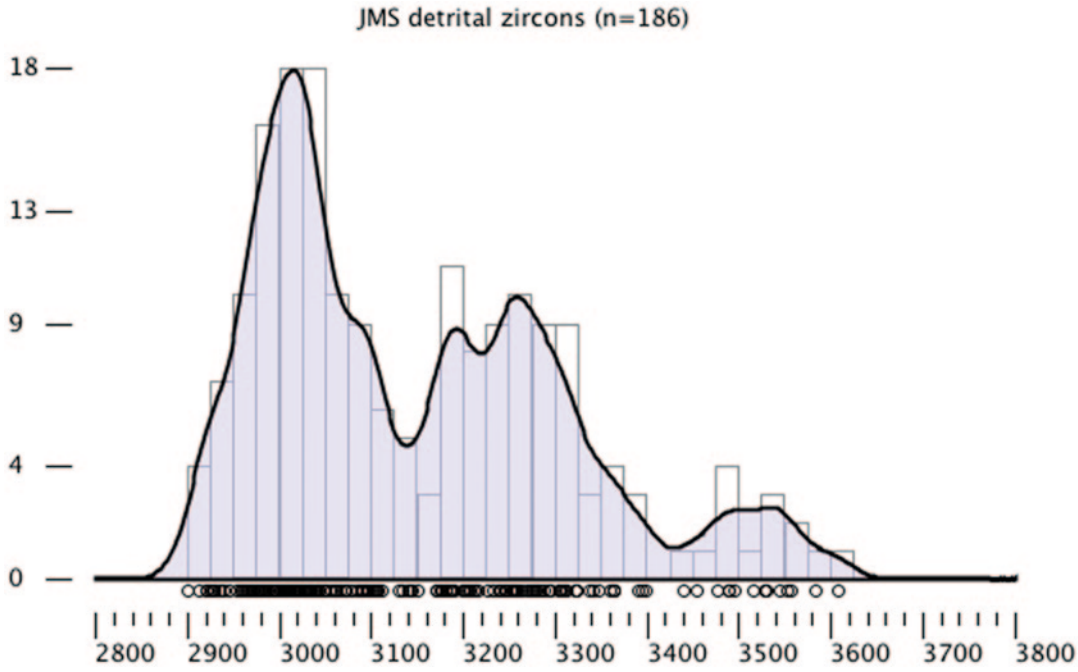

Fig. 2.23 Distribution of $^{207}Pb/^{206}Pb$ ages for 200 detrital zircons from four samples from the Jardine Metasedimentary Sequence expressed as a histogram (40 Ma bins) and as a probability density function; small circles below the x-axis represent the individual data points

of the LLMC intruded at about 12 km and 24 km depth, respectively.

The connection between these plutonic suites is particularly strong in terms of whole-rock Pb isotopic compositions, which are one of the most diagnostic geochemical features of the Wyoming Province (e.g. Mueller and Wooden 1988; Mueller and Frost 2006; Frost and Fanning 2006). Figure 2.24 shows the coherence of uranogenic common Pb for the JMS plutonic suites and that they, like the LLMC, indicate an age indistinguishable from their range of U-Pb zircon ages (~2.8 Ga). Equally significant, these data lie well above the Stacey and Kramers (1975) evolution curve for average continental crust and any initial Pb isotopic composition associated with these rocks also must lie above this curve. This unique compositional feature and the U-Pb zircon ages provide a strong genetic link between the LLMC and JMS plutonic suites.

Although the continuity of intrusive ages from the Beartooth Plateau block to the South Snowy block suggests a common heritage for the plutonic rocks at 2.8 Ga, detrital zircons from the JMS suggest an exotic origin for these metasedimentary rocks prior to 2.8 Ga. The ages of detrital zircons from the JMS range from ~3.6 Ga to 2.9 Ga with a significant population of 3.0–3.1 Ga grains (Fig. 2.23; Mueller et al. 1998; Goldstein et al. 2011). A limited, but distinct, concentration of ages from 3.2 to 3.3 Ga correlates with a similar age-maximum in detrital suites throughout the NWP, but is much less prominent in the JMS (Mueller et al. 1998). The presence of younger grains (2.9–3.1 Ga), which are not present or show very minor abundances in other Archean metapsammites from the NWP, suggests the JMS was not derived from crystalline basement preserved in the Beartooth Range, or any Archean exposures in southwestern Montana (e.g., Mogk 1988; Mueller et al. 1993, 1996, 2004; Mueller and Frost 2006; Chamberlain and Mueller 2007). Potential sources with ages of ~2.9–3.0 Ga, however, are present ~250 km to the south in the Owl Creek Mountains (Mueller et al. 1985) and in the Bighorn Mountains (Frost and Fanning 2006). Rocks from the

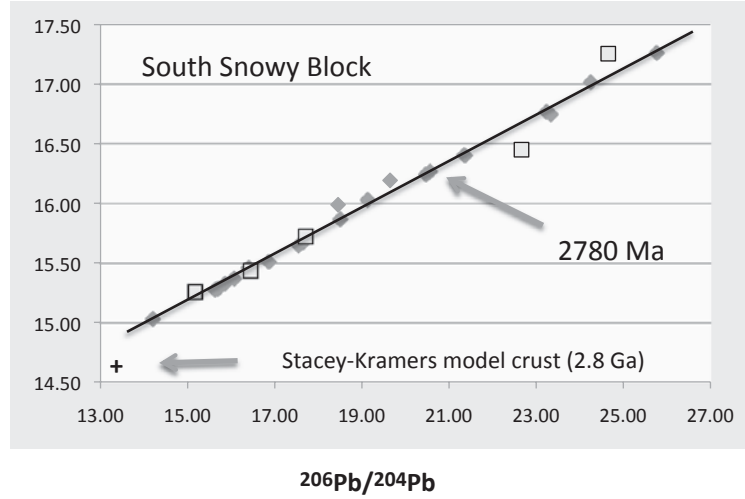

Fig. 2.24 Plot of common, uranogenic Pb isotopes from plutonic rocks emplaced in the Jardine Metasedimentary Sequence (*diamonds*) and the host metasedimentary rocks (*squares*). A line corresponding to an age of 2.78 Ga is provided for reference. Plus (+) indicates the Pb isotopic composition of Stacey and Kramers (1975) average crust at 2.8 Ga

Owl Creek and Bighorn Ranges have Sm-Nd model ages (Tdm) in excess of 3.0 Ga, which compare favorably with Tdm (Sm-Nd) from the JMS (3.04–3.76 Ga). More significantly, uranogenic, whole-rock Pb isotopic compositions for the JMS are coherent and share the very diagnostic enriched signatures of igneous and meta-igneous rocks of the Wyoming Province (e.g. Mueller and Wooden 1988; Mueller and Frost 2006; Frost et al. 2006; Fig. 2.15). Like the plutonic data, Pb isotopic compositions of the JMS lie well above the Stacey and Kramers (1975) crustal evolution curve, strongly indicating an origin internal to the Wyoming Province. Regardless of its original location, the JMS formed part of the upper crust of the Beartooth area by 2.8 Ga.

The structural style in the JMS is very similar to Phanerozoic accretionary complexes developed within thick turbidite sequences (e.g., Gray and Foster 1998, 2003), as is the association with orogenic gold mineralization at nearby Jardine (Thurston 1986; Foster and Gray 2008). We, therefore, interpret the western South Snowy block assemblage as a subduction-accretion complex that filled with turbidite scraped off of the subducting oceanic crust against a continental magmatic arc built on considerably older crust. The deformed lithologies of the JMS turbidite wedge were accreted to Beartoothia prior to 2.8 Ga, when they were intruded by TTG-suite magmas. Intrusion led to partial melting of the JMS, perhaps accompanied by assimilation at depth. The Yellowstone River shear zone developed at this time and displaced older basement, JMS lithologies, and components of the Mesoarchean intrusive suite (Slough Creek batholith). Consequently, a transect from the western South Snowy block to the eastern limit of the Beartooth Plateau block reveals a classic, composite, crustal section of a Mesoarchean (~2.8 Ga) arc complex that grew by both magmatic and tectonic accretion and displays variations in structure (brittle, to semi-ductile, to ductile), in metamorphism (greenschist to granulite facies), and in granitoid intrusive style (epizonal to catazonal).

2.4 Discussion

The diverse and well-preserved record of Mesoarchean crustal genesis combined with inferences drawn from the ages and compositions of detrital zircons in the Beartooth Mountains offer insight into progressive changes in modes of crust formation in the NWP, and by extension, in the early Earth, including the relationship between ancient continental crust and mantle. Data from the Beartooth region suggest the following sequence of events:

In the Beginning Mafic (and perhaps ultramafic) magmas began to accumulate and form a section of thickened lithosphere over a zone of mantle upwelling 4.0–4.1 Ga ago. Melting within this

thickened lithosphere produced zircon-bearing magmas (e.g., tonalites), although the higher Zr contents of primordial mantle (e.g., McDonough and Sun 1995) may have led to zircon formation in magmas derived directly from the mantle as reported from some modern mid-ocean ridge systems (e.g., Grimes et al. 2009). The initial Hf isotopic compositions show a pattern of decreasing initial εHf with decreasing age from 4.0 to 3.5–3.6 Ga (Fig. 2.4). The Lu/Hf inferred from this pattern is the maximum value likely to pertain to the lithosphere (including crust) because the most negative εHf values may not represent 100% crustal melts, in which case the average value of the crust would be lower. In the modern Earth, Rudnick and Gao (2003) suggest a Lu/Hf value of 0.081 for bulk continental crust, comparable to the value derived here. A similar value (~0.1) also describes the trend of minimum initial εHf data from the more ancient zircons from western Australia (e.g., Harrison et al. 2008; Nebel-Jacobsen et al. 2010; Mueller and Wooden 2012).

Despite the similarity in the inferred Lu/Hf of the sources of both the NWP and Jack Hills zircons, Guitreau et al. (2012) argue that these age-εHf patterns do not imply long-lived, enriched reservoirs, but are an artifact of improper age assignments (negative εHf caused by young ages resulting from Pb-loss). As such, they would not provide a valid basis for inferring the Lu/Hf of the source of the zircon-bearing magmas. In contrast, Mueller and Wooden (2012) showed that Hf isotopic compositions in the Beartooth suite of detrital, magmatic zircons (i.e., those with Th/U > 0.1) do not correlate with U-Pb discordance, i.e., the most positive or negative εHf values in any given period are not defined by zircons with discordant U-Pb ages. Consequently, we consider the initial Hf isotopic compositions calculated for the ancient detrital zircons from the Beartooth Plateau block to be reliable indicators of original magmatic values.

Although the exact chemical and mineralogic composition of the mantle source of the proposed mafic crust cannot be specified, the viability of the proposed low Lu/Hf composition can be evaluated using modern analogs. For example, in modern mantle melting regimes the Lu/Hf ratios of anhydrous mantle melts are always less than the Lu/Hf of their source because Hf is less compatible than Lu in all major mantle minerals (olivine, orthopyroxene, and clinopyroxene+/-garnet). Salters and Stracke (2004) used these relationships to estimate 1) an ~60% reduction in Lu/Hf of MORB compared to its source in the modern depleted mantle, 2) that the Lu/Hf of the depleted mantle has increased continuously over geologic time, and 3) that the Lu/Hf of the depleted mantle is more than twice the consensus value of 0.24 for the primitive mantle (e.g., McDonough and Sun 1995; Palme and O'Neill 2003; Lyubetskaya and Korenaga 2007). Accepting this value (0.24) for primordial mantle and applying the bulk distribution coefficients suggested by Workman and Hart (2005) for the formation of modern MORB yields a Lu/Hf value of 0.07 for "Hadean MORB". More Mg-rich melts (e.g., komatiites) may have also formed in this interval, and would likely reflect higher degrees of melting (e.g., Grove and Parman 2004) and, therefore, higher Lu/Hf. Komatiites typically have low absolute abundances of Lu and Hf which, combined with their limited abundance in greenstone belts, suggest it is unlikely that they had a material impact on the overall Lu and Hf budgets of the protocrust (e.g., Kerrich and Xie 2002). Partial melting of komatiitic compositions in this crust could, however, contribute to some of the less negative εHf values recorded in the 3.5–4.0 detrital zircons.

Discerning whether this accumulation of largely mafic crust and/or lithosphere was derived from a plume-like mantle upwelling or a subduction system akin to modern systems cannot be resolved definitively using Lu-Hf systematics. For example, Porter and White (2009) estimate the average Lu/Hf ratio in primary arcs magmas from nine major arcs is ~0.20. Although distinctly higher than the "Hadean MORB" value (0.07), it is similar to values characteristic of modern MORB (average value of ~0.20; Arevalo and McDonough 2010; Jenner and O'Neill 2012). This lack of contrast in Lu-Hf fractionation between anhydrous melting regimes and those in which a significant fraction of the melts likely formed in hydrous systems simply reflects the fact that the characteristic, relative depletion in high field

strength elements that characterize much of modern arc magmatism primarily reflects enrichment in fluid mobile elements, rather than absolute depletion in HFSE or Lu (e.g., Munker et al. 2004). True depletion in HFSE does occur, however, in environments in which Ti-rich phases (hydrous or anhydrous; Wang et al. 2000) such as rutile are retained in an eclogitic residuum. Retention of Ti-rich phases in an eclogitic (slab) residuum occurs over a fairly narrow range of T and P (e.g., 1200–1300 °C, 3 GPa; Klemme et al. 2002), so it is unlikely that extreme HFSE depletions will be common features of these rocks. Likewise, extremely low Lu/Hf, which would reflect garnet in the residuum, is also rare in the >1000 entries in the MORB databases noted above. In particular, the HREE abundances of the 3.6–4.0 Ga detrital zircons from the NWP are not compatible with garnet in the residuum of their original host magmas (Mueller and Wooden 2012).

Evolution of the protocrust Once formed, this original mafic-to-felsic protocrust must evolve isotopically with, or without, external input. During the 3.5–3.6 to 4.0 Ga interval in the NWP, the range of initial εHf values for detrital zircons shows that intracrustal evolution was augmented by the addition of more juvenile material; a similar pattern was discerned for the Archean zircons from the Jack Hills (e.g., Bell et al. 2011). "More juvenile" in this sense refers to contributions from a source characterized by Lu/Hf>0.1, which could be the primitive mantle and/or the evolving depleted mantle and/or a komatiitic component in the proto-continent. The mechanism by which these additions were made is not clear because it is impossible to judge the volume of crust that produced these zircons, or what volume of non-zircon-bearing crust may have formed in the same time frame. The continuity of ages across the 3.5–4.0 Ga interval, however, does not favor the intermittent episodes of suprasubduction magmatism typically observed in global patterns of crustal growth that have been related to plate tectonic phenomena (e.g., Condie 2000). In addition, the shallow subduction regime envisioned for the early earth (e.g., Abbott et al. 1994; Hansen 2007; Martin et al. 2005) would not be compatible with development of the >250 km mantle keel (tectosphere) present beneath the NWP (e.g., Yuan and Romanowicz 2009).

Although extended evolution of an upwelling system (i.e., for several hundred million years) has not been documented on the modern earth, it has been suggested for Archean mafic rocks of the Pilbarra and Yilgarn cratons (e.g., Smithies et al. 2005; Van Kranendonk et al. 2013). Similar continua of ancient detrital zircon ages have also been reported for other Archean terranes (e.g., Harrison et al. 2008, Kapete et al. 2012). In addition, there are indications of very long-lived (100's of Ma) upwelling systems on Mars and Venus (e.g., Wilson et al. 2001; Reese et al. 2004; Basilevsky and Head 2007; Hynek et al. 2011; Xiao et al. 2012; Richardson et al. 2013). The potential similarity between the early earth and Mars is that Mars has remained in a non-plate tectonic state throughout its history (e.g., Breuer and Spohn 2003), which is favorable for long term, spatially restricted upwelling and melting. Even without spatial restriction, the migrating plume model of Hynek et al. (2011) for Tharsis (Mars), for example, also describes a possible evolution of the northern Wyoming Province, i.e., an initial, rapid, large outpouring of lava followed by intermittent new additions from new sources as the structure migrated within the convecting mantle system. For Earth, if a planetary-scale plate tectonic regime was not fully functioning (e.g., limited deep circulation of oceanic lithosphere, formation of eclogitic slabs, steep subduction, etc.) or not functioning at all (e.g., stagnant lid convection; Kamber et al. 2003, 2007) during the Hadean and Eoarchean, then perhaps long-lived up-welling-derived structures behaved similarly to Tharsis (e.g., Robin and Bailey 2009).

Discerning between the up-welling and subduction options, neither of which has a modern terrestrial analog, cannot be done directly. The evolution of this ancient crustal component can be constrained, however, by examining the Pb isotopic compositions of the Mesoarchean magmatic rocks. As noted by Wooden and Mueller (1988) and Mueller et al. (2010), Mesoarchean magmatic rocks in the NWP exhibit a "crustal Pb paradox". This paradox arises because the initial

Pb isotopic compositions of the Mesoarchean rocks are too enriched to have been generated by their U/Pb ratios in the age of the earth (Fig. 2.8). Consequently, these rocks must have inherited their enriched signature from a pre-existing reservoir characterized by higher $^{238}U/^{204}Pb$ (μ) than the Mesoarchean rocks themselves. Alternative explanations, e.g., that the μ-values measured in the Mesoarchean rocks today are not indigenous to the rocks, are not viable because the array of Pb isotopic values of the Mesoarchean rocks yield the same age (within error) as the U-Pb ages measured on zircons from the same rocks (e.g., Frost et al 2006; Mueller et al. 2010). In addition, direct measurement of U and Pb concentrations in the Mesoarchean rocks yield the same μ-values as those calculated from the observed Pb isotopic compositions at 2.8 Ga (Wooden and Mueller 1988; Frost et al. 2006; Staffenberg et al. 2011). Only through inclusion of Pb from an older, high-μ reservoir can we account for the Pb isotopic compositions of the Mesoarchean rocks. Consequently, the NWP must contain (or have contained) an ancient crustal component characterized by above average U/Pb ratios (i.e., greater than the value of 9.7 of Stacey and Kramers (1975) model), and this crust could have existed for as little as one hundred million years and still generated the elevated Pb isotopic compositions needed (Mueller et al. 2010).

Formation of the ancient high-μ reservoir Accepting that an ancient, high-μ reservoir must have formed in the NWP early in its history makes it necessary to identify how this reservoir formed and how it influenced the Mesoarchean igneous rocks. As noted in step 1 above, the Lu-Hf systematics of the 3.5–3.6–4.0 Ga detrital zircons (Fig. 2.4) strongly suggest that the development of an early enriched reservoir in the NWP began with melting of primitive or only slightly depleted mantle. Although the inferred Lu/Hf ratio of this reservoir could be indirectly tied to melting of a primitive or near-primitive mantle composition by analogy with modern mantle melting, these data do not allow distinction between anhydrous (MORB) or hydrous (arc) melting systems. In the case of U-Pb, however, there is a significant distinction between hydrous (arc) and anhydrous (MORB) melting in the modern earth. Anhydrous melts of the modern depleted mantle (MORB) have distinctly higher U/Pb ratios than typical arc magmas and typically greater fractionation of U from Pb. For example, Porter and White (2009) indicate an average μ of ~6 for 8 of 9 primary arc magmas (excluding one extreme value of 35 for the southern Antilles). In contrast, data from over 1000 analyses of modern MORB suggest a μ-value of ~15 (13 from Arevalo and McDonough 2010; 17 from Jenner and O'Neill 2012).

The difference in U/Pb ratios between arc and MORB magmas contrasts with the lack of fractionation of Lu and Hf because of the redox-sensitive mobility of U and the fluid mobile nature of Pb. The petrologic influence of a reducing, or at least non-oxidizing, surficial environment for the early earth, was likely significant for U-Pb systematics in sub-marine, subduction driven, melting systems. For example, a primary pathway for U to enter a modern subducting slab involves: 1) oxidation of U from the +4 (insoluble) to the +6 (soluble) state during surficial weathering; 2) transporting and retaining U in +6 form in surface waters, which leads to high μ-values in modern seawater (~ 10,000); 3) reduction in oxidation potential due to circulation of seawater in marine hydrothermal systems fixes U as the +4 ion, which produces μ-values in oceanic lithosphere much higher than in average crust (up to 200; e.g., Chauvel et al. 1995; Kelly et al. 2005); and (4) subduction and melting of this lithosphere occurs in an environment too reducing to extensively oxidize and mobilize the U (e.g., Foley 2010; Evans 2012). While U is held largely in the slab, Pb is not similarly affected. Consequently modern arc magmas generally have low U/Pb ratios and the subducted lithosphere is characterized by relatively high U/Pb ratios, which are ultimately responsible for producing the HIMU component of the modern mantle (e.g., Kramers and Tolstikhin 1997). The expectation for U/Pb ratios in Hadean and Archean arcs should, therefore, be no higher than the values observed in modern arcs, and probably lower.

The transition from recycling to juvenile crustal growth The pattern of decreasing, minimum εHf values in detrital zircons appears to end ~3.5 Ga with the lowest recorded εHf values (Fig. 2.4). Beginning ~3.5 Ga, a transitional period shows a progressively higher proportion of more positive εHf values until a maximum at ~3.3 Ga. Zircons at ~3.3 Ga record initial εHf values in the narrow range between BSE and the depleted mantle, with some recording values as high as expected for the contemporaneous depleted mantle. These εHf values clearly indicate that the 3.2–3.4 Ga zircons, in particular, crystallized in magmas that received a much more prominent input from more depleted sources (e.g., asthenosphere) than previous generations of magmas in the NWP. Although the primary signal has some ambiguity because it is derived from detrital zircons (rather than rocks), the dominance of zircons of this age-range in detrital suites throughout the NWP (Mueller et al. 1998) and their positive initial εHf values must be the products of a major infusion of new crust derived from a more depleted source (Mueller and Wooden 2012).

The last subduction The final step in the development of the Mesoarchean crust of the NWP is the initiation of subduction-driven, continental margin, magmatism (Fig. 2.19). The case for Mesoarchean arc magmatism has been made previously (Wooden and Mueller 1988; Frost et al. 2006; Mueller et al. 2010) and relies on (1) a relatively short episode of magmatism (<100 Ma overall and <50 Ma for the LLMC), (2) relative HFSE depletion in normalized trace element plots indicative of hydrous melting for rocks of 50–55% SiO_2, (3) low average μ-values (~5) at 2.8 Ga, comparable to modern arcs, 4) a high proportion of TTG compositions, 5) crustal production rates comparable to modern arcs, and 6) a limited range of enriched initial (2.8 Ga) eNd values (av. of −3 vs. the depleted mantle value of +5; DePaolo 1981) and initial $^{87}Sr/^{86}Sr$ values (isochron intercept of 0.7022; Wooden and Mueller 1988) vs. the depleted mantle value of <0.701; Workman and Hart 2005).

A significant aspect of the Mesoarchean arc model is that it provides a mechanism for imparting the enriched Pb, Nd, and Sr initial isotopic compositions to this lithosphere and crust. As should be expected for a suite of rocks with such limited ranges of initial isotopic compositions (LLMC for example), there is no regular relationship between initial isotopic composition of any individual rock and that rock's composition or location (Mueller et al. 2010). Considering the age (at least 3.5 Ga) and compositional diversity of pre-existing crust, the only way to impart a uniform isotopic signature to the volume and variety of Mesoarchean rock types in the NWP is by exchange with fluids in the subduction channel (subducting mantle and overlying mantle wedge), and newly formed lower crust (Mueller et al. 2010; Fig. 2.19). These fluids likely facilitated isotopic exchange between subducted sediment derived from the ancient continental margin upon which the Mesoarchean arc was built and the various melt sources, including ancient (contemporary) mantle.

The resultant "paradoxical" isotopic-elemental relationships simply reflect two distinct processes, one that controls elemental abundances and one that controls isotopic compositions. Because the majority of new crust was derived from melting new material (e.g., oceanic mantle and lithosphere) brought into the melting zone via plate motion and subduction, the elemental compositions of these magmas were controlled by crystal-liquid partitioning in the melt zone. Their isotopic compositions, however, do not reflect contemporaneous mantle or oceanic lithosphere because of interaction (mixing) with fluids that were in equilibrium (or nearly so) with detritus from the older crust. This detritus had sufficiently enriched isotopic ratios to change the isotopic compositions of the various melts through isotopic/elemental exchange with the sediment-derived fluids, with a lesser impact on elemental abundances. This situation is analogous to modern arcs in which elemental abundances (e.g., Sr) are controlled by crystal-liquid distribution coefficients, but isotopic compositions (e.g., $^{87}Sr/^{86}Sr$) can be altered by interaction with fluids with distinctly enriched isotopic compositions, but low elemental abundances (e.g., seawater) as suggested by DePaolo

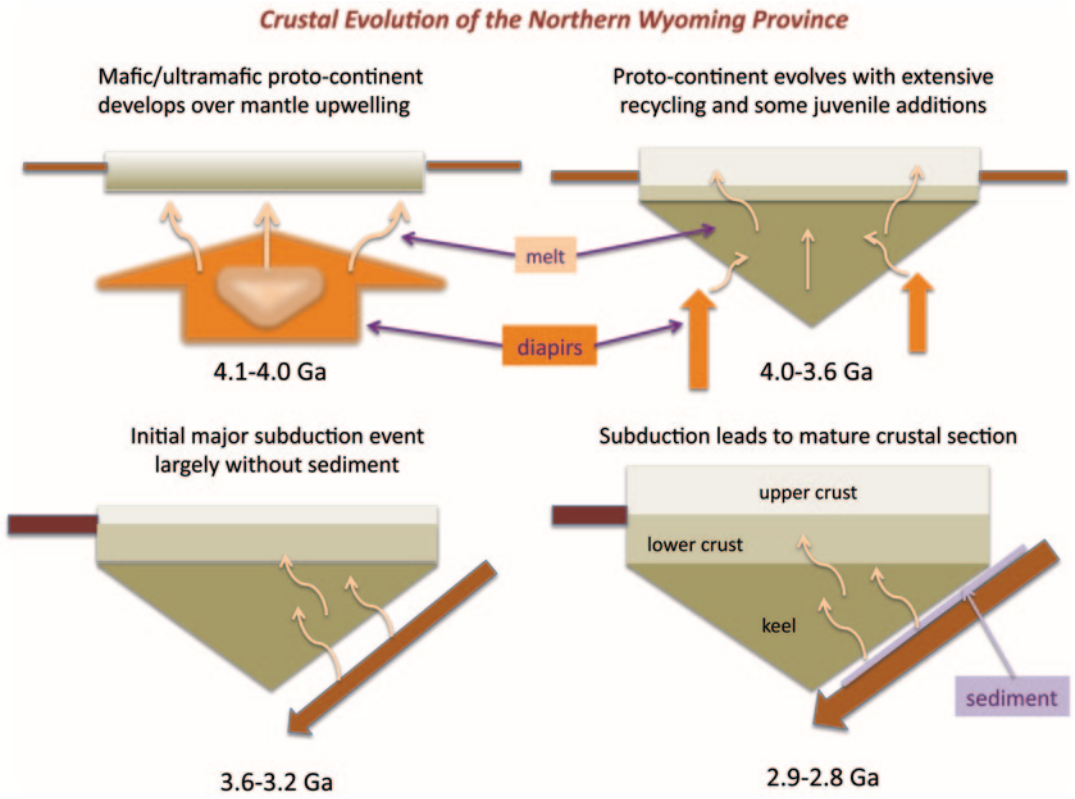

Fig. 2.25 Schematic (not to scale) depiction of the four main stages of crustal evolution in the northern Wyoming Province

and Wasserburg (1977) among others. Empirical, experimental, and theoretical evidence continues to support the viability of decoupling elemental and isotopic compositions in such environments (e.g., Hildreth and Moorbath 1988; Lesher 1990; Keleman et al. 1990; Bindeman et al. 2013).

2.5 Conclusions

The implications of the Hadean-Eoarchean record in the northern Wyoming Province for global geodynamic systems rests on both the nature of the record and its length (2.8–4.0 Ga), which allows insight into both reservoirs and processes operative on at least one part of the early Earth. In the case of the NWP, data discussed here suggest three main episodes of crustal genesis as schematically depicted in Fig. 2.25: (1) 4.0–4.1 Ga: mantle up-welling characterized by anhydrous melting begins the formation of a mafic-ultramafic proto-continent; (2) 4.0–3.5–3.6 Ga: crustal maturation begins as mantle upwelling continues to add some juvenile material while the proto-continent and lithosphere differentiate internally to form an incipient lower crust/upper crust structure; (3) 3.4–3.2 Ga: first major pulse of subduction-driven crustal growth with a minor recycled component; (4): 3.1–2.8 Ga: a period that began with an ~300 Ma period of post-orogenic quiescence, but ended with the second major episode of crustal growth in the NWP that included a diagnostic, well distributed component of recycled crust via interaction with subducted continental detritus.

In this scenario, a clear change in tectonic environment of crustal genesis is indicated with the advent of subduction driven crustal growth beginning ~3.4 Ga ago. From different perspectives, numerous authors have used a variety

of similar local and global data to suggest that the observed changes reflect global changes in Earth's geodynamics. For example, (1) Kamber et al. (2003, 2007) suggested a rapid, global conversion from stagnant lid convection to mobile lid convection at 3.8 Ga based on Pb isotopic compositions in ancient gneisses from SW Greenland; (2) Debaille et al. (2013) proposed the same transition, but for 3.0 Ga, not 3.8 Ga, based on ^{142}Nd abundances in a 2.7 Ga basalt from the Abitibi Belt; (3) Naerra et al. (2012) suggested a broad period of conversion (3.2–3.5 Ga) from one plate tectonic regime to another based on Lu-Hf systematics of Archean zircons from SW Greenland; and (4) Keller and Schoene (2012) used a global database of igneous rocks to propose a major transition in mantle melting at 2.5 Ga. In contrast, other workers (e.g., Brown 2006; Ernst 2009) have argued for more gradual changes tied to Earth's continuously declining heat production that required bottom-up convection in the hotter early earth, but top-down convection (slab-pull) in the modern Earth; stagnant-lid convection was limited to regions beneath supercontinents in the Proterozoic. By the end of the Archean, cratonic units were able to accumulate into supercontinents and form contrasting (paired) metamorphic belts that formed under distinctly different thermal gradients (e.g., ultra-high-temperature and eclogite-high-pressure granulites; Brown 2006).

Among the proposals for major, global-scale changes in the tectonic and geochemical record, the record in the NWP fits most closely with the 3.2–3.5 Ga interval suggested by Naerra et al. (2012). There is a significant difference, however, between the 3.2–3.5 Ga record from SW Greenland (changing plate tectonic regimes) and that from the NWP (change from plume-driven to subduction driven crustal genesis). As pointed out by Mueller and Wooden (2012), this difference in tectonic environments between NWP and SW Greenland is evident in the contrast between the initial Hf isotopic compositions of 3.8 Ga zircons from the Wyoming province (av. $\varepsilon Hf = -3$) and SW Greenland (av. $\varepsilon Hf = 0$). This difference seems best interpreted to indicate that continental crust was forming and evolving simultaneously in both subduction-driven and plume-driven environments at 3.8 Ga.

Globally and over time, the proportion of plume-driven crustal genesis declined from a higher, but poorly constrained, fraction to its present proportion of ~5–10% of mantle heat loss (Coffin and Eldholm 1994). This decline in the proportion of plume-driven crustal genesis and the attendant fraction of global heat loss are a reflection of both (1) decreasing heat production and declining mantle potential temperatures that favor a decreasing contribution from anhydrous mantle melting (e.g., Arndt 2003; Ernst 2009; Herzberg and Rudnick 2012) and (2) increased access of the mantle to water via subduction, which can lower the peridotite solidus by several hundred degrees (e.g., Katz et al. 2003; van Keken et al. 2011; Parai and Mukhopadhyay 2012). In terms of a relationship between early, plume-like accumulations of crust and the initiation of plate tectonic-like processes on the early Earth, numerous authors have pointed to the role that these Archean-Hadean equivalents of modern LIPs (e.g., Ontong-Java) may have played as precursors, perhaps even critically necessary precursors, to the initiation of subduction (e.g., Smithies et al. 2005; Nair and Chacko 2008). Whether the interplay of such structures (plateaus) and processes (plate subduction) reflect either continuous or step-like, global-scale, tectonic transitions remains an open question.

Acknowledgements We acknowledge the financial support of the N.S.F. (EAR-8211828, 8618885, 9219645, 0538133, 0546751, and 0609948), NASA, and the U.S.G.S. Data and observations pertinent to the South Snowy block benefited from the contributions of 24 undergraduate students supported by an NSF REU site project (EAR-0851934, 0851752, and 0852025). The support and cooperation of the staff of Yellowstone National Park are also gratefully acknowledged.

References

Abbott D, Drury R, Smith W (1994) Flat to steep transition in subduction style. Geol 22:937–940

Arevalo R, McDonough W (2010) Chemical variations and regional diversity of MORB. Chem Geol 271:70–85

Arndt N (2003) Komatiites, kimberlites, and boninites. J Geophys Res. doi:10 1029/2002JB002157

Basilevsky A, Head J (2007) Beta Regio, Venus: Evidence for uplift, rifting, and vocanism due to a mantle plume. Icarus 192:167–186

Bell E, Harrison T, McCulloch M, Young E (2011) Early Archean crustal evolution of the Jack Hills zircon source terrane inferred from Lu-Hf, $^{207}Pb/^{206}Pb$, and $d^{18}O$ systematics of Jack Hills zircons. Geochim Cosmochim Acta 75:4816–4829

Berndt TR, Hanson MH, Kotash AK, Mogk DW, Henry DJ, Mueller PA, Foster DA (2012) Precambrian geology of Yellowstone National Park (YNP) and surrounding areas: plutonic rocks of the Slough Creek area. Geol Soc Am Abst Progr 44:70

Bindeman I, Lundstrom C, Bopp C, Huang F (2013) Stable isotope fractionation by thermal diffusion through partially molten wet and dry silicate rocks. Earth Planet Sci Lett 365:51–62

Bizzaro M, Connelly J, Thrane K, Borg L (2012) Excess hafnium-176 in meteorites and the early Earth zircon record. Geochem Geophys Geosys. doi:10 10929/2011GC004003

Brady JB, Kovaric DN, Cheney JT, Jacob LJ, King JT (2004) $^{40}Ar/^{39}Ar$ ages of metamorphic rocks from the tobacco root mountains, Montana. In: Brady JB, Burger HR, Cheney JT, Harms TA (eds) Precambrian geology of the tobacco root mountains, Montana: Geol Soc Am Spec Pap 377:131–150

Breuer D, Spohn T (2003) Early plate tectonics versus single-plate tectonics on Mars: evidence from magnetic field history and crust evolution J Geophys Res. doi:10 1029/2002JE001999

Butler J (1969) Origin of precambrian granite gneisses in the Beartooth mountains, Montana and Wyoming. In: LH Larsen (ed) Igneous and metamorphic Geology. Geol Soc Am Mem 115:73–101

Casella CJ, Levay J, Eble E, Hirst B, Huffman K, Lahti V, Metzger R (1982) Precambrian geology of the southwestern Beartooth mountains, Yellowstone National Park, Montana and Wyoming. In: Mueller P, Wooden J (eds) Precambrian geology of the Beartooth Mountains, Montana and Wyoming. Montana Bur Mines Geol Spec Publ 84:1–24

Chamberlain K, Frost C, Frost BR (2003) Early Archean to Mesoproterozoic evolution of the Wyoming province: Archean origins to modern lithospheric structure. Can J Earth Sci 40:1357–1374

Chamberlain KR, Mueller PA (2007) Oldest rocks of the Wyoming Craton. In: Van Kranendonk MJ, Smithies RH, Bennett V (eds) Earth's oldest rocks, developments in precambrian geology series vol 3, Condie K, (series ed). Elsevier, pp 775–791

Chauvel C, Goldstein S, Hofmann A (1995) Hydration and dehydration of oceanic crust controls Pb evolution in the mantle. Chem Geol 126:65–75

Clowes R, Burianyk M, Gorman A, Kanasewich E (2002) Crustal velocity structure from SAREX, the Southern Alberta refraction experiment. Can J Earth Sci 39:351–373

Coffin M, Eldholm O (1994) Large igneous provinces: crustal structure, dimensions, and external consequences. Rev Geophys 32:1–36

Condie KC (1976) The Wyoming Archean province in the western United States. In: Windley BF (ed) The early history of the Earth. Wiley, London, p 499–511

Condie K (2000) Episodic continental growth models: After thoughts and extensions. Tectonophys 322(1–2):153–162

Debaille V, O'Neill C, Brandon A, Haenecour P, Yin Q-Z, Mattielli N, Treiman A (2013) Stagnant-lid tectonics in early Earth revealed by ^{142}Nd variations in late Archean rocks. Earth Planet Sci Lett (in press)

DePaolo D (1981) Neodymium isotopes in the Colorado Front Range and crust-mantle evolution in the Proterozoic. Nature 291:193–196

DePaolo D, Wasserburg G (1977) The sources of island arcs as indicated by Nd and Sr isotopic studies. Geophys Res Lett 4:465–468

Eckelmann FD, Poldervaart A (1957) Geologic evolution of the Beartooth Mountains, Montana and Wyoming, Part 1 Archean history of the Quad Creek area. Geol Soc Am Bull 68:1225–1262

Ernst G (2009) Archean plate tectonics, rise of Proterozoic supercontinentality and onset of regional, episodic stagnant-lid behavior. Gond Res 15:243–253

Evans K (2012) The redox budget of subduction zones. Earth Sci Rev 113:11–32

Foley S (2010) A reappraisal of redox melting in the Earth's mantle as a function of tectonic setting and time. J Petrol 52:1363–1391

Foster DA, Mogk DW, Henry DJ, Mueller PA (2011) Evolution of Archean rocks of the south snowy block, Yellowstone National Park: results of an REU site project. Geological Society of America Annual Meeting, Minneapolis 9–12 October. Geol Soc Am Abst Progr 43:435

Foster DA, Mueller P, Heatherington A, Gifford J, Kalakay T (2012) Lu-Hf systematics of magmatic zircons reveal a Proterozoic crustal boundary under the cretaceous pioneer batholith, Montana. Lithos. doi: 10 1016/j lithos 2012 03 005

Foster D, Mueller P, Vogl J, Mogk D, Wooden J (2006) Proterozoic evolution of the western margin of the Wyoming Craton: Implications for the tectonic and magmatic evolution of the northern Rocky Mountains. Can J Earth Sci 43:1601–1619

Foster D, Gray D (2008) Paleozoic crustal growth, structure, strain rate, and metallogeny in the Lachlan Orogen, Eastern Australia. In: Spencer JE, Titley SR (eds) Ores and orogenesis: circum-pacific tectonics, geological evolution, and ore deposits, Arizona. Geol Soc Digest 22:213–225

Frost CD, Frost BR, Chamberlain KR, Hulsebosch TP (1998) The late archean history of the Wyoming province as recorded by granitic magmatism in the Wind River Range, Wyoming. Precambrian Res 89:145–173

Frost C (1993) Nd isotopic evidence for antiquity of the Wyoming Province. Geol 21:351–354

Frost C, Fanning (2006) Archean geochronological framework of the Bighorn Mountains, Wyoming. Can J Earth Sci 43:1391–97

Frost C, Frost B, Kirkwood R, Chamberlain K (2006) The tonalite-trondhjemite-granodiorite (TTG) to granodiorite-granite (GG) transition in the late Archean plutonic rocks of the central Wyoming province. Can J Earth Sci 43:1399–1418

Goldstein EH, Sauer K, Harwood J, Mogk D, Henry D, Mueller P, Foster D (2011) Evolution of the precambrian rocks of Yellowstone National Park (YNP): metasedimentary rocks. Geol Soc Am Abst Progr 43(4):61

Gorman A, Clowes R, Ellis R, Henstock T, Spence G, Keller G, Levander A, Snelson C, Burianyk M, Kanasewich E, Asudeh I, Zoltan H, Miller K (2002) Deep probe: imaging the roots of western North America. Can J Earth Sci 39:375–398

Grimes C, John B, Cheadle M, Mazdab F, Wooden J, Swapp S, Schwartz J (2009) On the occurrence, trace element geochemistry, and crystallization history of zircon from in situ ocean lithosphere. Contrib Mineral Petrol 158:757–783

Grove T, Parman S (2004) Thermal evolution of the earth as recorded by komatiites. Earth Planet Sci Lett 219:173–187

Guitreau M, Blichert-Toft J, Martin H, Mojzsis S, Albarede F (2012) Hafnium isotope evidence from Archean granitic rocks for deep-mantle origin of continental crust. Earth Planet Sci Lett 337–338:211–223

Hamilton WB (2003) An alternative earth. GSA Today 13:4–12

Hansen V (2007) Subduction origin on early earth: a hypothesis. Geol 3:1059–1062

Hargraves R (1986) Faster spreading or greater ridge length in the Archean. Geol 14:750–752

Harrison T, Schmitt A, McCulloch M, Lovera O (2008) Early (> 4 5 Ga) formation of terrestrial crust: Lu-Hf, $\delta^{18}O$, and Ti thermometry results for Hadean zircons. Earth Planet Sci Lett 268:476–486

Harris RL Jr (1959) Geologic evolution of the Beartooth Mountains, Montana and Wyoming, Part 3: Gardner lake area, Wyoming. Geol Soc Am Bull 70:1185–1216

Hartlaub R, Heaman L, Simonetti A, Bohm C (2006) Relicts of Earth's earliest crust: U-Pb, Lu-Hf, and morphological characteristics of > 3.7 Ga detrital zircon of the western Canadian Shield. Geol Soc Am Spec Pap 405:75–89

Henry DJ, Mueller PA, Wooden JL, Warner JL, Lee-Berman R (1982) Granulite grade supracrustal assemblages of the Quad Creek area, eastern Beartooth Mountains, Montana. In: Mueller PA, Wooden JL, (eds) Precambrian geology of the Beartooth Mountains, Montana and Wyoming. Montana Bur Mines Geol Spec Publ 84:147–159

Henstock T, Levander A, Deep Probe Working Group (1998) Probing the Archean and Proterozoic lithosphere of western North America. GSA Today 8:16–17

Herzberg C, Rudnick R (2012) Formation of cratonic lithosphere: an integrated thermal and chemical model. Lithos 149:4–15

Hildreth W, Moorbath S (1988) Crustal contribution to arc magmatism in the Andes of Central Chile. Contrib Mineral Petrol 98:455–489

Hoffman PF (1989) Speculations on Laurentia's first gigayear (2.0–1.0 Ga). Geol 17:135–138

Hofmann A (2003) Sampling mantle heterogeneity through oceanic basalts: isotopes and trace elements. In: Carlson R, Holland H, Turekian K (eds) The mantle and core treatise on Geochemistry v2:pp 61–101

Hofmann A (2005) The geochemistry of sedimentary rocks from the Fig Tree Group, Barberton greenstone belt: Implications for tectonic, hydrothermal, and surface processes during mid-Archean time. Precambrian Res 143:23–49

Hynek B, Robbins S, Sramek O, Zhong S (2011) Geological evidence for a migrating Tharsis plume on early Mars. Earth Planet Sci Lett. doi:10.1016/j.epsl.2011.08.020

Irvine TN, Baragar WRA (1971) A guide to the chemical classification of the common volcanic rocks. Can J Earth Sci 8:523–548

James HL (1946) Chromite deposits near Red Lodge, Carbon County, Montana. US Geol Surv Bull 945-F:151–189

Jenner F, O'Neill H (2012) Analysis of 60 elements in 616 ocean floor basaltic glasses. Geochem Geophys Geosys. doi:10 1029/2011GC0040009

Kabete J, McNaughton N, Groves D, Mruma A (2012) Reconnaissance SHRIMP U-Pb zircon geochronology of the Tanzania Craton: evidence for neoarchean granitoid-greenstone belts in the Central Tanzania region and the southern East Africa orogen. Precambrian Res 216–219:232–266

Kamber BS (2007) The enigma of the terrestrial protocrust: Evidence for its former existence and the importance of its complete disappearance. In: Van Kranendonk MJ, Smithies RH, Bennett V (eds) Earth's oldest rocks. Developments in Precambrian Geology. Elsevier, Amsterdam. doi:10 1016/S0166–2635(07)15024–6

Kamber B, Collerson K, Moorbath S, Whitehouse M (2003) Inheritance of early Archean Pb-isotope variability from long-lived Hadean protocrust. Contrib Mineral Petrol 45:25–46

Katz R, Spiegelman M, Langmuir (2003) A new parameterization of hydrous mantle melting. Geochem Geophys Geosys. doi:10.1029/2002GC000433

Kelemen P, Johnson K, Kinzler R, Irving A (1990) High field-strength element depletions in arc basalts due to mantle-magma interaction. Nature 345:521–524

Keller C, Schoene B (2012) Statistical geochemistry reveals disruption in secular lithospheric evolution about 2.5 Gyr ago. Nature 485:490–493

Kelly K, Plank T, Farr L, Ludden J, Staudigel H (2005) Subduction cycling of U, Th, and Pb. Earth Planet Sci Lett 234:369–383

Kemp A, Wilde S, Hawkesworth C, Coath C, Nemchin A, Pidgeon R, Vervoort J, Dufrane S (2010) Hadean crustal evolution revisited: New constraints from Pb-Hf systematics of the Jack Hills zircons. Earth Planet Sci Lett 296:45–56

Kerrich R, Xie Q (2002) Compositional recycling structure of an Archean superplume: Nb-Th-U-LREE systematics of Archean komatiites and basalts revisited. Contrib Mineral Petrol 142:476–484

Klemme S, Blundy J, Wood B (2002) Experimental constraints on major and trace element partitioning during partial melting of eclogite. Geochim Cosmochim Acta 66:3109–3123

Kortenaga J (2006) Archean geodynamics and thermal evolution of the Earth. Amer Geophys Union Monograph 164:7–32

Kramers J, Tolstikhin I (1997) Two terrestrial lead isotope paradoxes, forward transport modeling, core formation and the history of the continental crust. Chem Geol 139:75–110

Krogh T, Kamo S, Hanley T, Hess D, Dahl P, Johnson R (2011) Geochronology and geochemistry of Precambrian gneisses, metabasites, and pegmatite from the Tobacco Root Mountains, northwestern Wyoming craton, Montana. Can J Earth Sci 46:161–185

Larsen LH, Poldervaart A, Kirchmeyer M (1966) Geologic evolution of the Beartooth Mountains, Montana and Wyoming, Part 7. Structural homogeneity of gneisses in the Lonesome Mountain area. Geol Soc Am Bull 77:1277–1292

Lesher C (1990) Decoupling of chemical and isotopic exchange during magma mixing. Nature 237:235–237

Leyreloup A, Dupuy C, Andriambololona R (1977) Catazonal xenoliths in French Neogene volcanic rocks: Constitution of the lower crust. Contrib Mineral Petrol 63:283–300

Lyubetskaya T, Korenaga J (2007) Chemical composition of earth's primitive mantle and its variance: 1 methods and results. J Geophys Res. doi: 10 1029/2005JB004223

Maier A, Cates N, Trail D, Mojzis S (2012) Geology, age and field relations of Hadean zircon-bearing supracrustal rocks from Quad Creek, eastern Beartooth Mountains (Montana-Wyoming). Chem Geol. doi: 10 1016/j chemgeo 2012 04 005

Marks S, Mogk D, Henry D, Mueller P, Foster D, Davidson C (2012) Precambrian geology of Yellowstone National Park (YNP) and surrounding areas: Mylonites and shear zones. Geol Soc Am Abst Progr 44:71

Martin H, Smithies R, Rapp R, Moyen JF, Champion D (2005) An overview of adakite, tonalite-trondhjemite-granodiorite (TTG) and sanukitoid: relationships and some implications for crustal evolution. Lithos 79:1–24

McDonough W, Sun S-S (1995) The composition of the earth. Chem Geol 120:223–253

Mogk DW (1988) Archean allochthonous units in the northern and western Beartooth Mountains, Montana. In: Lewis S, Berg R (eds) Precambrian and mesozoic plate margins, Montana, Idaho, and Wyoming. Montana Bur Mines Geol Spec Publ 96:43–52

Mogk DW, Henry DJ (1988) Metamorphic petrology of the northern Archean Wyoming Province, SW Montana: evidence for Archean collisional tectonics. In: Ernst W (ed) Metamorphism and crustal evolution in the western United States, proceedings of the VII Rubey colloquium on metamorphic terranes. Prentice Hall, NY, pp 362–382

Mogk DW, Mueller PA, Wooden JL (1992) The nature of Archean terrane boundaries: An example from the northern Wyoming Province. Precambrian Res 55:155–168

Mogk D, Henry D, Mueller P, Foster D (2011) Evolution of the Precambrian rocks of Yellowstone National Park (YNP): overview of an NSF/REU site project. Geol Soc Am Abst Progr 43:61

Mogk DW, Henry DJ, Mueller PA, Foster D (2012) Precambrian geology of Yellowstone National Park (YNP) and surrounding areas: emerging science and scientists at an REU site project. Geol Soc Am Abst Progr 44:70

Montgomery C, Lytwyn J (1984) Rb-Sr systematics and ages of principal Precambrian Lithologies in the South Snowy block. J Geol 92:103–112

Moyen J-F, van Hunen J (2012) Short-term episodicity of Archean plate tectonics. Geol 40:451–454

Mueller PA, Wooden JL, Schulz K, Bowes DR (1983) Incompatible-element-rich andesitic amphibolites from the Archean of Montana and Wyoming: evidence for mantle metasomatism. Geology 11:203–206

Mueller PA, Peterman ZE, Granath JW (1985) A bimodal Archean volcanic series, Owl Creek Mountains, Wyoming. J Geol 93:701–712

Mueller PA, Wooden JL, Nutman AP (1992) 3.96 Ga zircons from an Archean quartzite, Beartooth Mountains, Montana. Geol 20:327–330

Mueller PA, Wooden JL, Mogk DW, Nutman AP, Williams IS (1996) Extended history of a 3.5 Ga trondhjemitic gneiss, Wyoming Province, USA: Evidence from U-Pb systematics in zircon. Precambrian Res 78:41–52

Mueller PA, Wooden JL, Nutman AP, Mogk DW (1998) Early Archean crust in the northern Wyoming province—Evidence from U-Pb ages of detrital zircons. Precambrian Res 91:297–307

Mueller P, Burger H, Wooden J, Brady J, Cheney J, Harms T, Heatherington A, Mogk D (2005) Age and tectonic implications of Paleoproterozoic metamorphism in the northern Wyoming Province. J Geol 111:169–179

Mueller PA, Wooden JL (1988) Evidence for Archean subduction and crustal recycling, Wyoming Province, USA. Geol 16:871–874

Mueller PA, Shuster R, Wooden J, Erslev E, Bowes D (1993) Age and composition of Archean crystalline rocks from the southern Madison Range: Implications for crustal evolution in the Wyoming craton. Geol Soc Am Bull 105:437–446

Mueller P, Heatherington A, Kelley D, Wooden J, Mogk D (2002) Paleoproterozoic Crust within the Great Falls Tectonic Zone: Implications for the Assembly of Southern Laurentia. Geol 30:127–130

Mueller P, Wooden J, Heatherington A, Burger H, Mogk D, D'Arcy K (2004) Age and evolution of the Precambrian crust of the Tobacco Root Mountains. In: Brady JB, Burger HR, Cheney JT, Harms TA (eds) Precambrian geology of the Tobacco Root Mountains, Montana. Geol Soc Am Spec Pap 377:181–202

Mueller P, Frost C (2006) The Wyoming Province: A distinctive Archean craton in Laurentian North America. Can J Earth Sci 43:1391–97

Mueller PA, Wooden JL, Mogk DW, Henry DJ, Bowes DR (2010) Rapid growth of an Archean continent by arc magmatism. Precambrian Res 183:70–88

Mueller PA, Wooden JL (2012) Trace element and Lu-Hf systematics in Hadean-Archean detrital zircons: implications for crustal evolution. J Geol 120:15–29

Mullen ED (1983) $MnO/TiO_2/P_2O_5$: a minor element discriminant for basaltic rocks of oceanic environments and its implications for petrogenesis. Earth Planet Sci Lett 62:53–62

Munker C, Worner G, Yogodzinski G, Churikova T (2004) Behaviour of high field strength elements in subduction zones: constraints from Kamchatka-Aleutian arc lavas. Earth Planet Sci Lett 204:275–293

Naeraa T, Schersten A, Rosing M, Kemp A, Hofmann J, Kokfelt T, Whitehouse M (2012) Hafnium isotope evidence for a transition in the dynamics of crustal growth 3.2–3.5 Gyr ago. Nature Geosci 485:627–630

Nair R, Chacko T (2008) Role of oceanic plateaus in the initiation of subduction and origin of continental crust. Geol 36:583–586

Nebel O, Vroon P, van Westreren M, Iizuka T, Davies G (2011) The effect of sediment recycling in subduction zones on the Hf isotope character of new arc crust, Banda arc, Indonesia. Earth Planet Sci Lett 303:240–250

Nebel-Jacobsen Y, Munker C, Nebel O, Gerdes A, Mezger K, Nelson D (2010) Reworking of Earth's first crust: constraints from Hf isotopes in Archean zircons form Mt Narryer, Austalia. Precambrian Res 182:175–186

Nutman A, Friend C (2009) New 1:20,000 scale geological maps, synthesis and history of investigation of the Isua supracrustal belt and adjacent orthogneisses, southern West Greenland: a glimpse of Eoarchean crust formation and orogeny. Precambrian Res 172:189–211

O'Neill J, Lopez D (1985) Character and regional significance of Great Falls tectonic zone, east-central Idaho and west-central Montana. Am Assoc Petroleum Geol Bull 69:437–447

Osborne C, Baldwin J, Henry D, Mogk D, Mueller P, Foster D (2011) Evolution of the precambrian rocks of Yellowstone National Park (YNP): low-pressure metamorphism of the Jardine metasedimentary sequence. Geol Soc Am Abst Progr 43:62

Palme H, O'Neill H (2003) Cosmochemical estimates of mantle composition. In: Carlson R (ed) The mantle and core, In: Holland H, Turekian K (eds), Treatise on Geochemistry 2:1–38

Parai R, Mukhopadhyay S (2012) How large is the subducted water flux? New constraints on mantle regassing rates. Earth Planet Sci Lett 317–318:396–406

Pearce JA, Harris NBW, Tindle AG (1984) Trace element discrimination diagrams for the tectonic interpretation of granitic rocks. J Petrol 25:959–978

Pfander J, Munker C, Stracke A, Mezger K (2007) Nb/Ta and Zr/Hf in ocean island basalts—Implications for crust-mantle differentiation and the fate of Niobium. Earth Planet Sci Lett 254:158–172

Philbrick K, Ware B, Henry D, Mogk D, Mueller P, Foster D (2011) Evolution of the Precambrian rocks of Yellowstone National Park (YNP): late Archean felsic plutons. Geol Soc Am Abst Progr 43:62

Porter K, White W (2009) Deep mantle subduction flux. Geochem Geophys Geosys. doi: 10 1029/2009GC002656

Reese C, Solomatov V, Baumgardner J, Stegman J, Vezolainen A (2004) Magmatic evolution of impact-induced Martian mantle plumes and the origin of Tharsis. J Geophys Res. doi: 10 1029/2003JE002222

Richardson J, Bleacher J, Glaze L (2013) The volcanic history of Syra Planun, Mars. J Vol Geotherm Res. doi.org/10.1016/j.jvolgeores.2012.11.007

Roberts H, Dahl P, Kelley S, Frei R (2002) New ^{207}Pb-^{206}Pb and ^{40}Ar-^{39}Ar ages from SW Montana, USA: constraints on the Proterozoic and Archean tectonic and depositional history of the Wyoming Province. Precambrian Res 117:119–143

Robin C, Bailey R (2009) Simultaneous generation of Archean crust and sub-cratonic roots by vertical tectonics. Geol 37:523–526

Rowan LC (1969) Structural geology of the Quad-Wyoming-Line Creeks area, Beartooth Mountains, Montana. Geol Soc Am Mem 115:1–18

Rudnick R, Gao S (2003) Composition of the continental crust. In: Rudnick R (ed) The crust. In: Holland H, Turekian K (eds) Treatise on geochemistry 3:1–64

Salters V, Strracke A (2004) Composition of the depleted mantle. Geochem Geophys Geosys. doi: 10 1029/2003GC000597

Shirey S, Kamber B, Whitehouse M, Mueller P, Basu A (2008) A review of the geochemical evidence for mantle and crustal processes in the Hadean and Archean: Implications for the onset of plate tectonic subduction. Geol Soc Am Mem 440:1–29

Skinner WR (1969) Geologic evolution of the Beartooth Mountains, Montana and Wyoming: part 8. Ultramafic rocks in the Highline Trail Lakes area, Wyoming. Geol Soc Am Mem115:19–52

Smithies R, Van Krankendonk M, Champion D (2005) It started with a plume-early Archean basaltic protocrust. Earth Planet Sci Lett 238:284–397

Spencer EW (1969) Geologic evolution of the Beartooth Mountains, Montana and Wyoming, Part 2. Fracture patterns. Geol Soc Am Bull 70:467–508

Stacey JS, Kramers JD (1975) Approximation of terrestrial lead isotope evolution by a two-stage model. Earth Planet Sci Lett 26:381–399

Staffenberg J, Mueller P, Mogk D, Henry D, Wooden J (2011) Testing a model of 2 8 Ga arc genesis with trace elements. Geol Soc Am Abst Progr 43:435

Stevenson RK, Patchett PJ (1990) Implications for the evolution of continental crust from the Hf isotope systematics of Archean detrital zircons. Geochim Cosmochim Acta 54:1683–1698

Taylor S, McLennan S (1995) The geochemical evolution of the continental crust. Rev Geophys 33:241–265

Thurston PB (1986) Geochemistry and provenance of Archean metasedimentary rocks in the southwestern Beartooth Mountains. MS thesis, Montana State University

Tian Y, Zhao D (2012) P-wave tomography of the western United States: insights into the Yellowstone hotspot and Juan de Fuca slab. Phys Earth Planet Int 200–201:72–84

Valley J, Lackey J, Cavosie A, Clechenko C, Spicuzza M, Basei M, Bindeman L, Frerreira V, Sial A, King E, Peck W, Sinha A, Wei C (2005) 4.4 billion years of crustal maturation: oxygen isotope ratios of magmatic zircons. Contrib Mineral Petrol 150:561–580

Van Keken P, Hacker B, Syracuse E, Abers G (2011) Subduction factory: 4. depth-dependent flux of H_2O from subducting slabs worldwide. J Geophys Res. doi:10.1029/2010JB007922

Van Kranendonk M, Ivanic T, Wingate M, Kirkland C, Wyche S (in press) long-lived, authocthonous development of the Archean Murchison Domain and implications for Yilgarn Craton tectonics. Precamb Res

Van Kranendonk M (2011) Two types of Archean continental crust: plume and plate tectonics on early Earth. Am J Sci 310:1187–1209

Wang L, Rouse R, Essene E, Peacor D, Zhang Y (2000) Carmichaelite, a new hydroxyl-bearing titanite from Garnet Ridge, Arizona. Am Mineral 85:1792–2000

White W (1993) $^{238}U/^{204}Pb$ in MORB and open system evolution of the depleted mantle. Earth Planet Sci Lett 115:211–226

Wilson L, Scott E, Head J (2001) Evidence for episodicity in the magma supply to the large Tharsis volcanoes. J Geophys Res 106:1423–1433

Wittig N, Pearson DG, Webb M, Ottley CJ, Irvine GJ, Kopylova M, Jensen SM, Nowell GM (2008) Origin of cratonic lithospheric mantle roots: A geochemical study of peridotites from the North Atlantic Craton, West Greenland. Earth Planet Sci Lett. doi:10 1016/j epsl 2008 06 034

Wooden JL, Mueller PA (1988) Pb, Sr, and Nd isotopic compositions of a suite of Late Archean igneous rocks, eastern Beartooth Mountains: implications for crust-mantle evolution. Earth Planet Sci Lett 87:59–72

Wooden JL, Mueller PA, Mogk DW (1988) A review of the geochemistry and geochronology of the Archean rocks of the northern part of the Wyoming Province. In Ernst WG (ed) Metamorphism crustal evolution of the Western United States vol 7:pp 383–410

Wooden JL, Mueller PA, Mogk DW, Bowes DR (1988) A review of the geochemistry and geochronology of Archean rocks of the Beartooth Mountains, Montana and Wyoming. In: Lewis SE, Berg RB (eds) Precambrian and mesozoic plate margins, Montana Bur Mines. Geol Spec Publ 96:23–42

Workman R, Hart S (2005) Major and trace element composition of the depleted MORB mantle. Earth Planet Sci Lett 231:53–72

Wyman D, Kerrich R (2002) Formation of Archean lithospheric roots: the role of mantle plumes. Geol 30:543–546

Xiao L, Huang J, Christensen P, Greely R, Williams D, Zhao J, He Q (2012) Ancient volcanism and its implications for thermal evolution of Mars. Earth Planet Sci Lett 323–324:9–18

Yuan H, Romanowicz B (2010) Lithospheric layering in the North American craton. Nature 466:1063–1067

Zeh A, Gerdes A, Klemd R, Barton J (2008) U-Pb and Lu-Hf isotope record of detrital zircon grains from the Limpopo belt-evidence for crustal recycling at the Hadean to early-Archean transition. Geochim Cosmochim Acta 72:5304–5329

The Archaean Karelia and Belomorian Provinces, Fennoscandian Shield

3

Pentti Hölttä, Esa Heilimo, Hannu Huhma, Asko Kontinen, Satu Mertanen, Perttu Mikkola, Jorma Paavola, Petri Peltonen, Julia Semprich, Alexander Slabunov and Peter Sorjonen-Ward

Abstract

The Archaean bedrock of the Karelia and Belomorian Provinces is mostly composed of granitoids and volcanic rocks of greenstone belts whose ages vary from c. 3.50 to 2.66 Ga. Neoarchaean rocks are dominant, since Paleoarchaean and Mesoarchaean granitoids (>2.9 Ga) are only locally present. The granitoid rocks can be classified, based on their major and trace element compositions and age, into four main groups: TTG (tonalite-trondhjemite-granodiorite), sanukitoid, QQ (quartz diorite-quartz monzodiorite) and GGM (granodiorite-granite-monzogranite) groups. Most ages obtained from TTGs are between 2.83–2.72 Ga, and they seem to define two age groups separated by a c. 20 m.y. time gap. TTGs are 2.83–2.78 Ga in the older group and 2.76–2.72 Ga in the younger group. Sanukitoids have been dated at 2.74–2.72 Ga, QQs at c. 2.70 Ga and GGMs

P. Hölttä (✉) · H. Huhma · S. Mertanen · P. Peltonen
Geological Survey of Finland, P.O. Box 96, 02151, Espoo, Finland
e-mail: pentti.holtta@gtk.fi

E. Heilimo · A. Kontinen · P. Mikkola · J. Paavola · P. Sorjonen-Ward
Geological Survey of Finland, P.O. Box 1237, 70211, Kuopio, Finland

P. Peltonen
First Quantum Minerals Ltd, Kaikukuja 1, 95600, Sodankylä, Finland

A. Slabunov
Karelian Research Centre, RAS, Institute of Geology, Pushkinskaya St. 11, 185910, Petrozavodsk, Russia

J. Semprich
Physics of Geological Processes, University of Oslo, Blindern, P.O. Box 1048, 0316, Oslo, Norway

Y. Dilek, H. Furnes (eds.), *Evolution of Archean Crust and Early Life,* Modern Approaches in Solid Earth Sciences 7, DOI 10.1007/978-94-007-7615-9_3, © Springer Science+Business Media Dordrecht 2014

at 2.73–2.66 Ga. Based on REE, the TTGs fall into two major groups: low-HREE (heavy rare earth elements) and high-HREE TTGs, which originated at various crustal depths. Sanukitoids likely formed from partial melting of subcontinental metasomatized mantle, whereas the GGM group from partial melting of pre-existing TTG crust.

The Karelia and Belomorian Provinces include a large number of generally NNW-trending greenstone belts, whose tectonic settings of origin may include an oceanic plateau, island arc and/or continental rift. The ages of volcanic rocks in these greenstone belts vary from 3.05 to 2.70 Ga.

Migmatized amphibolites occur as layers and inclusions in TTGs and fall into two main groups on the basis of their trace element contents. Rocks of the first group have flat or LREE-depleted trace element patterns, resembling the modern mid-ocean ridge basalts. Rocks of the second group are enriched in LILE and LREE may in part represent metamorphosed dykes with assimilated and/or diffused crustal signatures from their TTG country rocks.

Metamorphism of the TTG complexes occurred under upper amphibolite and granulite facies conditions at c. 2.70–2.60 Ga. The pressures of the regional metamorphism were mostly c. 6.5–7.5 kbar as constrained by geobarometry, and the corresponding temperatures were c. 650–740 °C. The granulites near the western boundary of the Karelia Province were equilibrated at c. 9–11 kbar and 800–850 °C. Subduction-related eclogites in the Belomorian Province were metamorphosed at pressures up to 20 kbars in two stages around 2.88-2.81 Ga and c. 2.72 Ga. In other greenstone belts the observed metamorphic conditions show significant variations. In the central parts of the Ilomantsi greenstone belt the observed metamorphic P and T values are c. 3–4 kbars and 550–590ºC, and in the Kuhmo greenstone belt 16–17 kbar and 650–690 °C, respectively.

Neoarchaean accretion of exotic terranes at c. 2.83–2.75 Ga and the subsequent collisional stacking at ~2.73–2.68 Ga were instrumental in the construction of the current crustal architecture of the Karelia Province. The Svecofennian orogeny strongly modified, however, this Neoarchaean crustal structure during the early Proterozoic

3.1 Introduction

There is no a widely accepted geodynamic framework for the Archaean eon, as exists for the modern Earth via plate tectonics and the Wilson cycle (Benn et al. 2006). Nevertheless, it is commonly thought that plate tectonics has been operating in some form at least since the Neoarchaean (e.g. deWit 1998; Condie and Benn 2006). However, there is considerable controversy concerning many of the fundamental aspects of the Archaean tectonics, including serious doubts about the applicability of the concept at all (Hamilton 1998, 2011). Some views emphasize the likelihood of a much faster convection and ocean floor spreading rate in the Archaean than in the Phanerozoic, whereas some researchers suggest that plate velocities have been fairly similar throughout geological time (Blichert-Toft and Albarede 1994; Kröner and Layer 1994; Blake et al. 2004; van Hunen et al. 2004; Strik et al. 2003; Korenaga 2006). Some recent simulations indicate that only after the development of the post-perovskite layer above the core-mantle boundary and after

sufficient cooling of the early Earth, could the core have been able to release enough heat to the upper mantle to enable the rapid motion of plates. The earliest this event could probably have occurred is inferred to be in the early Palaeoproterozoic (Tateno et al. 2009; Hirose 2010).

It is generally thought that the Archaean mantle was hotter than today, and the critical petrological evidence for this is komatiites and their much higher abundance in the Archaean than in the younger geological environments. Komatiites have been related to mantle plumes and reported to record very high mantle temperatures and melting pressures. On the other hand, it has also been argued that komatiites were, similarly to modern boninites, produced by hydrous melting at relatively shallow mantle depths in a subduction environment. This alternative interpretation predicts that the Archaean mantle was only slightly hotter than the present one (Grove and Parman 2004; Condie and Benn 2006).

Complete ophiolite sequences that would attest to the existence of Phanerozoic-style oceanic crust are rare in the Archaean rock record. A Neoarchaean, 2.51 Ga ophiolite complex has been described from the North China craton (Kusky et al. 2004), and greenstone occurrences that share many—although not all—characteristics of Phanerozoic ophiolites have also been found in other Archaean cratons, including the Belomorian province of the Fennoscandian shield (Kusky and Polat 1999; Corcoran et al. 2004; Puchtel 2004; Shchipansky et al. 2004). Archaean oceanic crust could have been thicker than the Proterozoic and Phanerozoic oceanic crust, resembling that of modern oceanic plateaux. This would explain the scarcity of MORB-type ophiolites, as in this case only the upper basaltic, pillow lava-dominated sections of the oceanic crust were likely to be accreted or obducted and thus preserved in the rock record (Kusky and Polat 1999). Şengör and Natal'in (2004) pointed out that in many Phanerozoic accretionary orogens, as in the western Altaids, evidence of closed oceans also only occurs in the form of separated fragments of variably complete ophiolitic sequences, without a single example of well-preserved major ophiolite nappe such as those in Oman or Newfoundland. Moreover, as the Altaids cover about as much of the Earth's land area as the Archaean crust, the rarity of indisputable Archaean ophiolite sequences already appears a less forceful argument against modern-style plate tectonism. Dilek and Polat (2008) and Dilek and Furnes (2011) also argued that the structure of the Archaean oceanic crust differed from that of the modern one; for example the Archaean sheeted dyke systems could be rare because spreading rates and magma supply budgets were necessarily not in such a balance that is needed for their generation.

Tonalite-trondhjemite-granodiorite (TTG) gneisses are the major constituent of the Archaean crust, and more widespread in the Archaean than in the younger rock record (Condie and Benn 2006). The petrogenesis of HREE-depleted Archaean TTGs have been interpreted in terms of a process that begins with tectonic thickening and subduction of oceanic crust, followed by progressive metamorphism and partial melting of the basaltic rocks, producing TTG melts that for the most part were in equilibrium with anhydrous, eclogitic residues (Rapp et al. 2003). Foley et al. (2002) argued that even the earliest continental crust might have formed by melting of amphibolites in subduction zone environments rather than by the melting of eclogites or magnesium-rich amphibolites in the lower parts of thick oceanic crust. Nair and Chacko (2008) proposed a model where oceanic plateaux served as the nuclei for Archaean cratons, and that TTGs originated in intraoceanic subduction systems where thinner oceanic lithosphere subducted beneath the thick oceanic plateaux.

On the basis of isotopic age distribution and εNd data, the most important Archaean crust-forming event was at c. 2.70 Ga, when large volumes of continental crust were produced worldwide. In some theories, this flare-up in crust formation was related to a large-scale mantle overturn event, which gave rise to a large number of plumes (Condie 1998, 2000; Condie and Benn 2006). The period of 2.75–2.65 Ga was also a time period during which the pre-existing continental crust was intensively reworked in various Archaean provinces, as in the Kola and Karelia

Provinces in the Fennoscandian and Superior Province in the Canadian Shield.

Archaean rocks cover roughly one-third of the Precambrian region in the Fennoscandian shield. Most of these rocks are Neoarchaean in age (2.8–2.5 Ga). Mesoarchaean (3.2–2.8 Ga) juvenile or reworked units are essential constituents of the bedrock only locally, and Palaeoarchaean rocks (3.6–3.2 Ga) are, overall, rare. The Neoarchaean (2.75–2.65 Ga) crust-forming event was very strong, including juvenile TTG magmatism, sedimentation, metamorphism and crustal melting producing granites. In this chapter we provide a review of the extant literature on the geology of the Fennoscandian Shield and present new data on the geochemistry, age determinations, metamorphism and palaeomagnetism of the Archaean Karelia Province and the adjacent Belomorian Province in Finland and in Russia. We then discuss the magmatic and tectonic processes that strongly controlled the evolution of these provinces and their present constitution and structure, with an emphasis on the Neoarchaean evolution. All ages referred to are U-Pb zircon ages, unless otherwise stated.

3.2 Geological Setting

The Archaean of Fennoscandia is traditionally divided into Norrbotten, Murmansk, Kola, Belomorian and Karelia Provinces (Fig. 3.1; Slabunov et al. 2006a, b; Hölttä et al. 2008). Lobach-Zhuchenko et al. (2000b, 2005) and Hölttä et al. 2008 subdivided the Karelia Province into three terranes: the Vodlozero, the Central Karelia and the Western Karelia (Fig. 3.1), which they observed with several singular lithological, structural and age characters. We have adopted this provincial division, but use instead the term subprovince to reflect the uncertainty about the nature of the unit contacts. By definition, a tectonostratigraphic terrane should be a fault-bounded crustal block whose geological history differs from that of the surrounding areas (Jones et al. 1983; Jones 1990). The Karelia subprovinces clearly differ in their geological histories, but there is as yet little evidence that they are all bounded by major accretionary faults.

The Karelia subprovinces include Mesoarchaean 3.2–2.8 Ga volcanic rocks and granitoids that are also common in the Vodlozero subprovince, and Neoarchaean (≤2.8 Ga) granitoids and greenstones with locally occurring, recycled Mesoarchaean crustal material (Vaasjoki et al. 1993). The Belomorian province east of the Karelia Province largely consists of 2.93–2.72 Ga TTG gneisses, greenstones and paragneisses, and local occurrences of ophiolite-like rocks and eclogites, which have not been discovered elsewhere in the Archaean parts of the Fennoscandian Shield (Shchipansky et al. 2004; Volodichev et al. 2004; Slabunov 2008; Slabunov et al. 2006a, b). Reflection seismic studies suggest that the Belomorian province comprises a stack of eastward-dipping subhorizontal nappes and thrusts that is separated from the underlying Karelia Province by a major detachment zone (Mints et al. 2004). These nappes probably developed during the Palaeoproterozoic (Mints et al. 2004; Sharov et al. 2010).

3.3 Geochemistry of Granitoids and Migmatitic Amphibolites

Figure 3.2 presents a lithological map of the Finnish part of the Karelia Province, showing that most of the area (c. 80 %) consists of TTGs. The rest is mainly comprised of supracrustal rocks in greenstone belts and sedimentary gneisses, and migmatitic amphibolites in enclaves in the gneissic granitoids. The gneissic granitoids include both true orthogneisses and TTG migmatites with amphibolite and paragneiss mesosomes, as observed in the field.

3.3.1 Granitoids

Archaean granitoids in the Karelia Province can be divided into four main groups on the basis of their field and petrographic characters, major and trace element compositions and age. These are the TTG (tonalite-trondhjemite-granodiorite), sanukitoid, QQ (quartz diorite-quartz monzodiorite) and the GGM (granodiorite-granite-monzo-

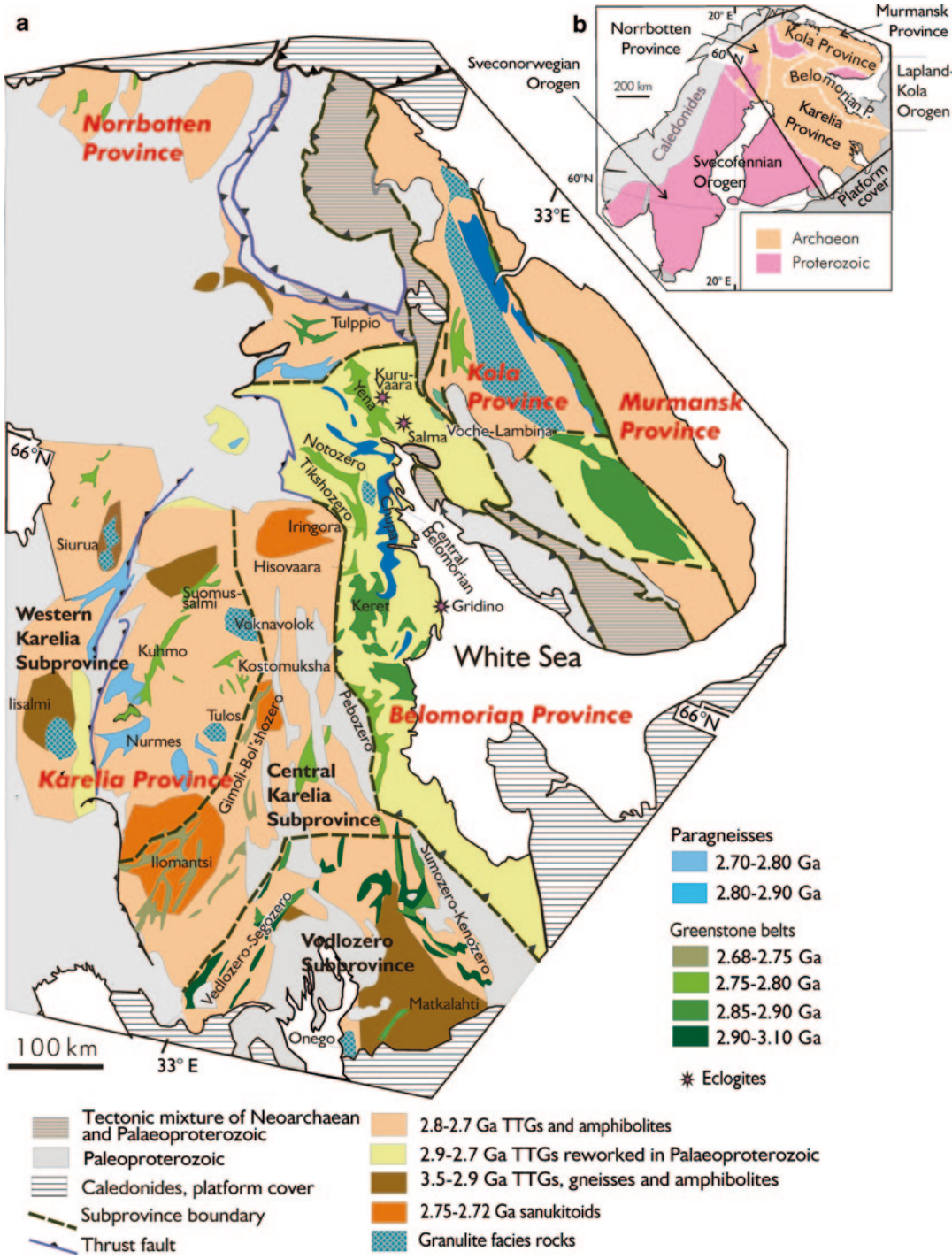

Fig. 3.1 A generalised geological map of the Archaean **a** of the Fennoscandian shield (**b**, inset), modified after Slabunov et al. (2006a) and Hölttä et al. (2008)

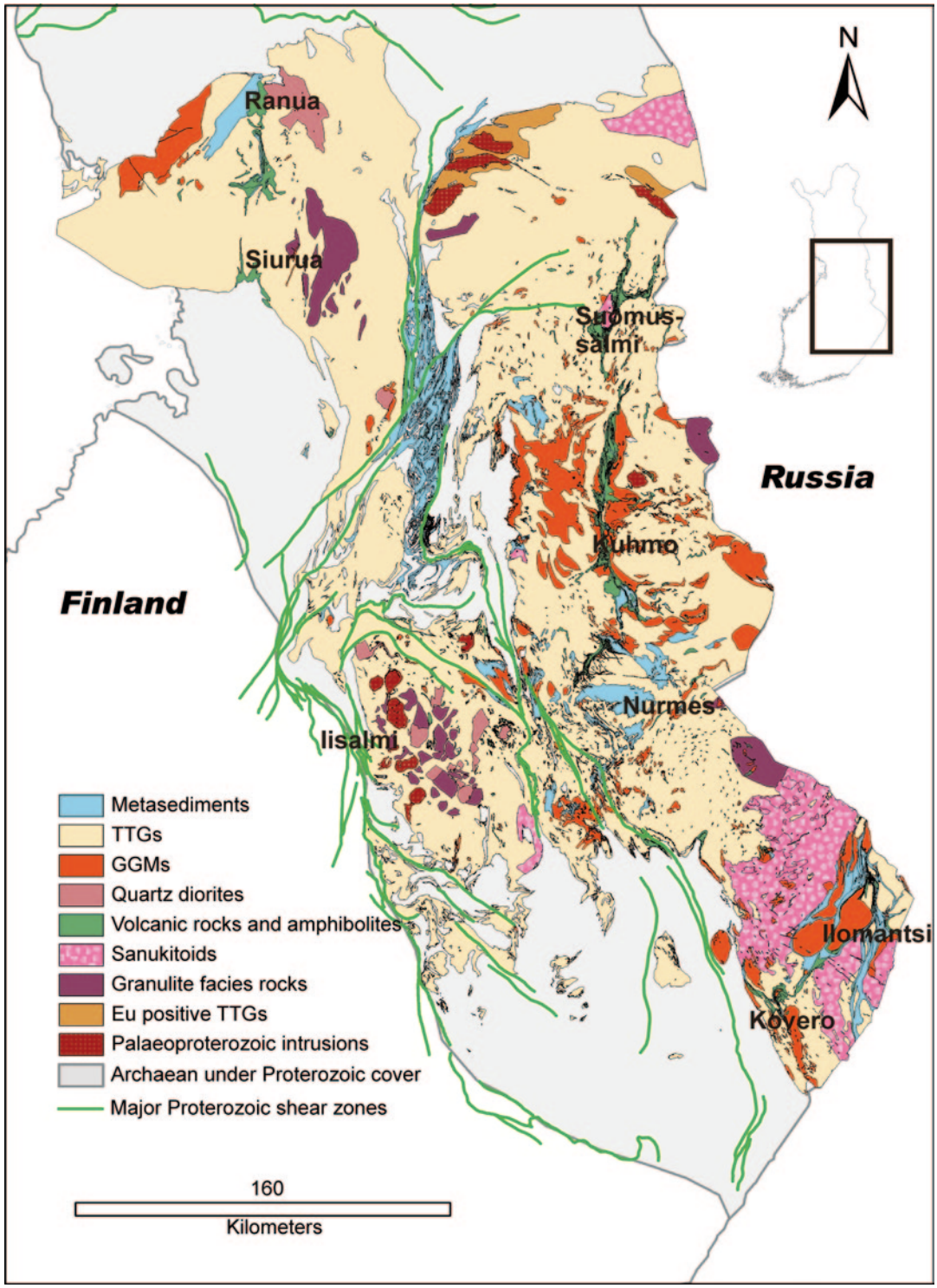

Fig. 3.2 A generalised geological map of the Finnish part of the Karelia Province. The inset shows the location of the map area in Finland

granite) groups (Käpyaho et al. 2006; Mikkola et al. 2011a).

3.3.1.1 TTGs

TTGs represent the majority of the Archaean bedrock in the Karelia, and understanding of their origin is thus crucial. It is well recognized that Archaean TTGs share many geochemical features with adakites, silica-rich volcanic and plutonic rocks in volcanic arcs, which are strongly depleted in Y and heavy rare earth elements, low in high-field-strength elements (HFSE) and high in their Sr/Y and La/Yb ratios (Defant and Drummond 1990). The chemical criteria for adakites are listed in the original paper by Defant and Drummond (1990), and later, for example, in Richards and Kerrich (2007), who use the following critical composition to define an adakite: $SiO_2 \geq 56$ wt%, $Al_2O_3 \geq 15$ wt%, MgO < 3 wt%, Mg number ~50, $Na_2O \geq$ wt 3.5 %, $K_2O \leq 3$ wt%, K_2O/Na_2O ~0.42, Rb ≤ 65 ppm, Sr ≥ 400 ppm, Y ≤ 18 ppm, Yb ≤ 1.9 ppm, Ni ≥ 20 ppm, Cr ≥ 30 ppm, Sr/Y ≥ 20 and $La_N/Yb_N \geq 20$. Martin and Moyen (2003) divided the adakites into the low silica (< 60 wt% SiO_2) and high silica (HSA, > 60 wt% SiO_2) groups, relating the HSA group to slab melting with some interaction with mantle-wedge peridotite and the LSA group to melting of wedge peridotites, which were previously metasomatised by slab-derived melts.

Most TTGs at least in the Western Karelia Province fulfil the adakite criteria, apart from the Cr and Ni contents, which are normally below the detection limits of the XRF analysis used, 30 and 20 ppm, respectively. Mg contents are also normally low, in most of the TTGs in the range of Mg# 0.35–0.45, suggesting that they gained minor components from mantle peridotites (Halla 2005; Lobach-Zhuchenko et al. 2005, 2008). Halla et al. (2009) divided the TTGs into two major groups, low-HREE (heavy rare earth elements) and high-HREE TTGs, which likely originated at different lithospheric depths. Here, we follow the proposal of Halla et al. (2009), but instead of the HREE contents—which depend on the source composition and post-melting fractionation, besides melting pressure—we use the $(La/Yb)_N$ ratio, as low-HREE rocks generally have high $(La/Yb)_N$ ratios. We further divide the low-HREE group into Eu-positive and Eu-negative subgroups. Our dataset demonstrates that the two TTG groups are not separated in compositional space, but rather represent the end-members of a full compositional continuity (Fig. 3.3).

Moyen (2011) studied a large set of analyses from rocks generally regarded as TTGs, ultimately dividing these rocks into four groups: the potassic group and the high-, medium- and low-pressure groups of 'proper' juvenile TTGs. The high-pressure group, equivalent to the low-HREE group, has TTGs with high Al_2O_3, Na_2O, Sr and low Y, Yb, Nb and Ta. The TTGs of the low-pressure group, equivalent to the high-HREE group, show opposite values in these respects. The potassic group rocks that show enrichment in K and LIL elements are thought Moyen (2011) to have formed by melting of pre-existing crustal rocks (Moyen 2011). If the criteria for true TTGs include $K_2O/Na_2O < 0.5$ (Martin et al. 2005), approximately 20 % of our samples collected in the field as TTG suite rocks would actually belong to the potassic or transitional TTGs, as originally described by Champion and Smithies (2007). On the other hand, this is a definitional problem, because in granodiorites the K_2O/Na_2O ratio is typically 0.5–1, and those rocks whose K_2O/Na_2O is < 0.5 are tonalites and trondhjemites, i.e. TTs rather than TTGs.

The rocks in the low-HREE group are trondhjemitic and tonalitic when classified using normative compositions and the QAPF diagram in Streckeisen and Le Maitre (1979) or the Ab-An-Or diagram in O'Connor (1965).In the Eu-negative subgroup, SiO_2 is generally 62–74 wt%, mg# 30–55 and Al_2O_3 15–17 wt%. Most of the samples have fractionated REE patterns with low HREE and high Sr/Y (median 81). They also have high La_N/Yb_N ratios of 20–120 with a median of 49, showing negative Eu anomalies (Fig. 3.5) and low abundances of compatible elements.

The SiO_2 values in the Eu-positive, low-HREE TTGs typically vary from 68–76 wt%, and they commonly have low abundances of FeO and MgO, as reflected in their near-white to light grey colour in outcrops and samples. Mg# is generally 28–55 and Al_2O_3 14.5–17.5 wt%. These TTGs

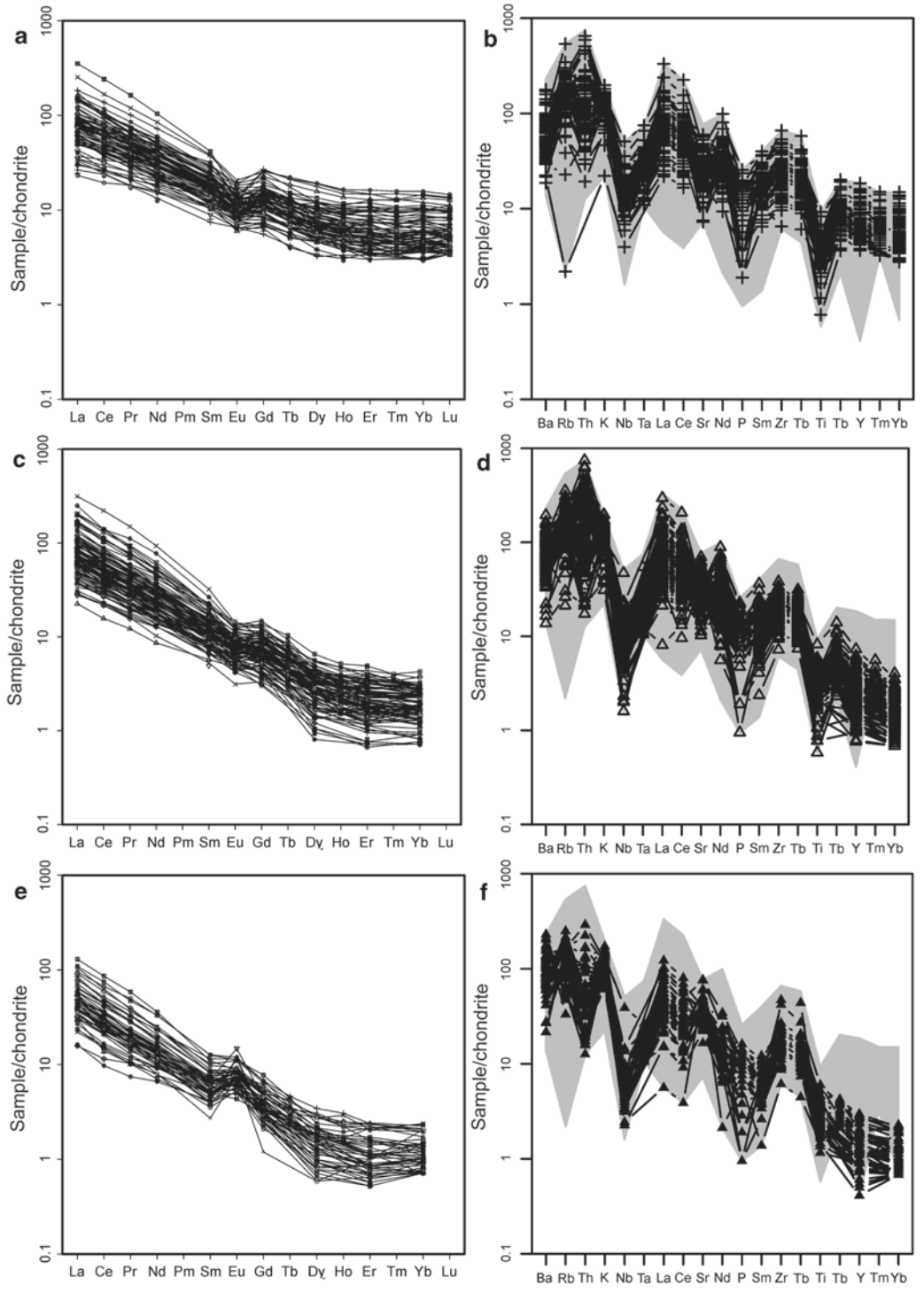

Fig. 3.3 Trace element patterns of TTGs: **a**, **b** = high HREE group, **c**, **d** = low HREE group, **e**, **f** = Eu-positive group. Diagrams represent 255 analyses where the K_2O/Na_2O ratio is <0.5, taken from the Rock Geochemical Database of Finland (Rasilainen et al. 2007). Normalizing values in the REE diagrams (a, c, e) are from Boynton (1984) and in the trace element diagrams (b, d, f) from Thompson (1982). The *shaded* area is for all data. Normalising factors are as in Fig. 3.3

are associated with negative magnetic anomalies on airborne magnetic maps, and especially in the northern part of the Karelia Province in Finland they cover large areas (Fig. 3.2). Most samples show, apart from positive Eu anomalies, strongly fractionated REE patterns with HREE mostly below the detection limits, low Y, Sc and Nb, high Sr/Y, La_N/Yb_N and Zr/Sm ratios and low abundances of compatible elements. In outcrops, part of these rocks show diatexitic migmatite structures and seem to represent almost complete fusion of amphibolites, but there are also many occurrences of this group that appear to be homogeneous orthogneisses.

The high-HREE group is normatively granodioritic and tonalitic. Its SiO_2 content is c. 60–72 wt%, mg# generally 30–55 and Al_2O_3 15–17 wt%. The Al_2O_3/SiO_2 ratio is generally lower in samples of this than the other TTG groups. Rocks in this group have low Sr/Y ratios (median 22) and higher abundances of compatible elements and HREE than the other TTGs. The La_N/Yb_N is <20 with a median of 10. On average, the high-HREE group has higher Nb contents (c. 5–15 ppm) than the low HREE group (c. 1–8 ppm).

3.3.1.2 Sanukitoids

The late tectonic, Neoarchaean sanukitoid intrusions occur in the Western and Central Karelia subprovinces, commonly associated with major shear zones (e.g. Lobach-Zhuchenko et al. 2005; Heilimo et al. 2010, Fig. 3.1). To this date ~20 sanukitoid intrusions have been described from the Karelia Province. The size of the intrusions is generally small, exceptions being the Koitere, Kuusamo and Njuk sanukitoids. The rocks are variably even-grained or K-feldspar porphyritic, and form a series from diorites to tonalites and granodiorites. U–Pb age determinations give an age of 2.74–2.72 Ga for the sanukitoid magmatism, which falls between the last peak of TTG (tonalite-trondhjemite-granodiorite) magmatism, ~2.75 Ga (Käpyaho et al. 2006; Mikkola et al. 2011a) and the age of the GGMs, ~2.70 Ga (granodiorite-granite-monzogranite) and QQ (quartz diorite- quartz monzonites) in the Karelia Province (Käpyaho et al. 2006; Lauri et al. 2011; Mikkola et al. 2011a, 2012).

The geochemistry of the sanukitoids is contradictory: they are enriched in the compatible elements Mg, Ni, and Cr and are also enriched in the incompatible elements LILE (Ba, Sr, and K), and LREE. Stern et al. (1989) gave a strict geochemical definition of sanukitoids: SiO_2 = 55–60 wt.%, MgO = 6 wt.%, Mg# = 60, Sr = 600–1800 ppm, Ba = 600–1800 ppm, Cr = 100 ppm, and Ni = 100 ppm. More recent studies (Lobach-Zhuchenko et al. 2005; Halla 2005) consider sanukitoids as a series of granitoids with high contents of compatible and incompatible elements, at a given SiO_2 content, that separates sanukitoids from the TTG series. The sanukitoid intrusions in the western Karelian Subprovince in Finland are alkali-calcic to calc-alkalic, magnesian, mostly metaluminous, and show geochemical features typical for the sanukitoid series: high content of LILE (K, Ba, and Sr), and high content of mantle-compatible elements (Mg, Cr, and Ni) and high Mg#.

Bibikova et al. (2005) and Lobach-Zhuchenko et al. (2005) have argued that sanukitoid intrusions in the Russian side of the Karelia Province occur as two temporally, spatially, and geochemically different groups, termed as the eastern and western sanukitoid zones. Compiled single-grain zircon U–Pb age data of the Finnish side of the Karelian Province confirm the occurrence of two temporally differing sanukitoid zones throughout the Province (Heilimo et al. 2011). The western zone shows a younger average age of ~2718 Ma, and the eastern zone an older average age of ~2740 Ma with an apparent age difference of ~20 Ma between the zones. Most felsic sanukitoids contain inherited zircon cores with ages up to ~3.2 Ga reflecting the importance of inheritance processes in the petrogenesis of sanukitoids (Bibikova et al. 2005; Heilimo et al. 2011).

The available isotope data from the Neoarchaean mantle-derived sanukitoids of the Karelia Province of the Fennoscandian Shield indicate well-mixed sources and reflect recycling of sediments from crustal reservoirs of different age in subduction processes. Oxygen isotope data from zircon show variable $\delta^{18}O$ values indicating a mantle input and also contributions from sources with high $\delta^{18}O$ values, such as sediments and altered upper oceanic crust (Mikkola et al. 2011a;

Heilimo et al. 2012, 2013). Slab breakoff at the end-stage of subduction has been proposed as a plausible trigger mechanism for sanukitoid magmatism in Karelia Province because it allows contributions from different $\delta^{18}O$ sources as well as explaining the contradictory elemental compositions (Heilimo et al., 2013)

3.3.1.3 QQs

Another important group of non-TTG granitoids comprises rocks whose normative composition is mostly quartz dioritic and quartz monzonitic (QQ), but locally also dioritic and monzodioritic. Rocks belonging to this group are especially found in the Western Karelia subprovince. Most QQ intrusions are located west of the sanukitoids described above, but whether there is a genetic link between the sanukitoid and QQ groups is not yet clear. The QQs include the enderbites in the Iisalmi complex (Hölttä 1997), the Ranua diorite (Mutanen and Huhma 2003) and some smaller plutons (Mikkola et al. 2011a). The QQs have zircon U-Pb ages close to 2.70 Ga. The ε_{Nd} values at 2.7 Ga are positive, for example +1 in the two analyzed enderbites of the Iisalmi complex (Hölttä et al. 2000a) and +0.8 in the Ranua diorite (Mutanen and Huhma 2003). Many compositional features in these rocks also fulfil the definition of adakites, as the SiO_2 content in most analysed samples is 52–62 wt%, Al_2O_3 a high 15.4–20.1 wt%, MgO 2.5–4.0 wt%, mg# 44–54, Na_2O 3.3–5.4 wt%, K_2O 0.8–1.8 wt%, Rb 13–52 ppm, Sr 630–1170 ppm, Sr/Y 21–80, Ba 200–800 ppm, Y < 18 ppm and Yb < 1.9 ppm. Furthermore, Cr in most samples is > 30 ppm and Ni > 20 ppm, except for the values of 10–28 ppm and 6–13 ppm, respectively, in the Ranua diorite. However, the QQs have only moderately fractionated REE patterns with La_N/Yb_N ratios of 6–15, and the enderbites in the Iisalmi area have a typically flat HREE (Fig. 3.4). This type of REE pattern is a distinctive feature of the enderbites and was not observed in other Archaean igneous rocks, apart from 2.74 Ga alkaline rocks in Suomussalmi, which have a similar REE distribution but generally higher REE abundances (Mikkola et al. 2011b). The enderbites have lower Rb, U and Th contents than the other quartz diorites, probably because of the loss in these elements during the granulite facies metamorphism that they underwent at 2.70–2.60 Ga (Mänttäri and Hölttä 2002).

3.3.1.4 GGMs

Granodiorite-granite-monzogranite (GGM) suite rocks dated to 2.73–2.66 Ga are the youngest Neoarchaean rocks occurring in large volumes in the Western Karelia subprovince (Käpyaho et al. 2006). They are relatively weakly deformed, reddish and medium- to coarse-grained rocks. Many of the granites have highly fractionated, HREE-depleted patterns with negative or no Eu anomalies, but some are less fractionated with relatively high HREE (Mikkola et al. 2012). At least part of the granites could represent the melting products of sedimentary gneisses. On the other hand, according to experimental studies, dehydration melting of sodic TTG gneisses can also produce granitic to granodioritic melts (Patiño Douce 2004; Watkins et al. 2007). Skjerlie et al. (1993) have shown experimentally that when interlayered, the melt productivity of tonalite and pelite increases via the interchange of components that lower the required melting temperatures. Anatectic granites, therefore, tend to contain material from two or more different source rocks, which is reflected in their isotopic and chemical compositions (Skjerlie et al. 1993). This could also be the case with the Archaean GGMs, which could represent the melting products of TTGs and paragneisses, and mixing of the derived melts with contemporaneous mafic magmas. The range in the ε_{Nd} (2700 Ma) values of the GGMs is c. −1.5 to +1.0 (Hölttä et al. 2012), indicating that some of them might represent the melting of juvenile 2.72–2.78 TTGs, whereas others could originate from older material. However, in the Suomussalmi area, the average $\delta^{18}O$ values of zircon from GGMs are normally only slightly higher (6.42 ± 0.10) than that of the TTGs, 6.10 ± 0.19. This means that at least in Suomussalmi the GGMs do not necessarily have a significant sedimentary input in their source but rather represent melting products of TTGs (Mikkola et al. 2012). However, in the Suomussalmi area the abundance of exposed

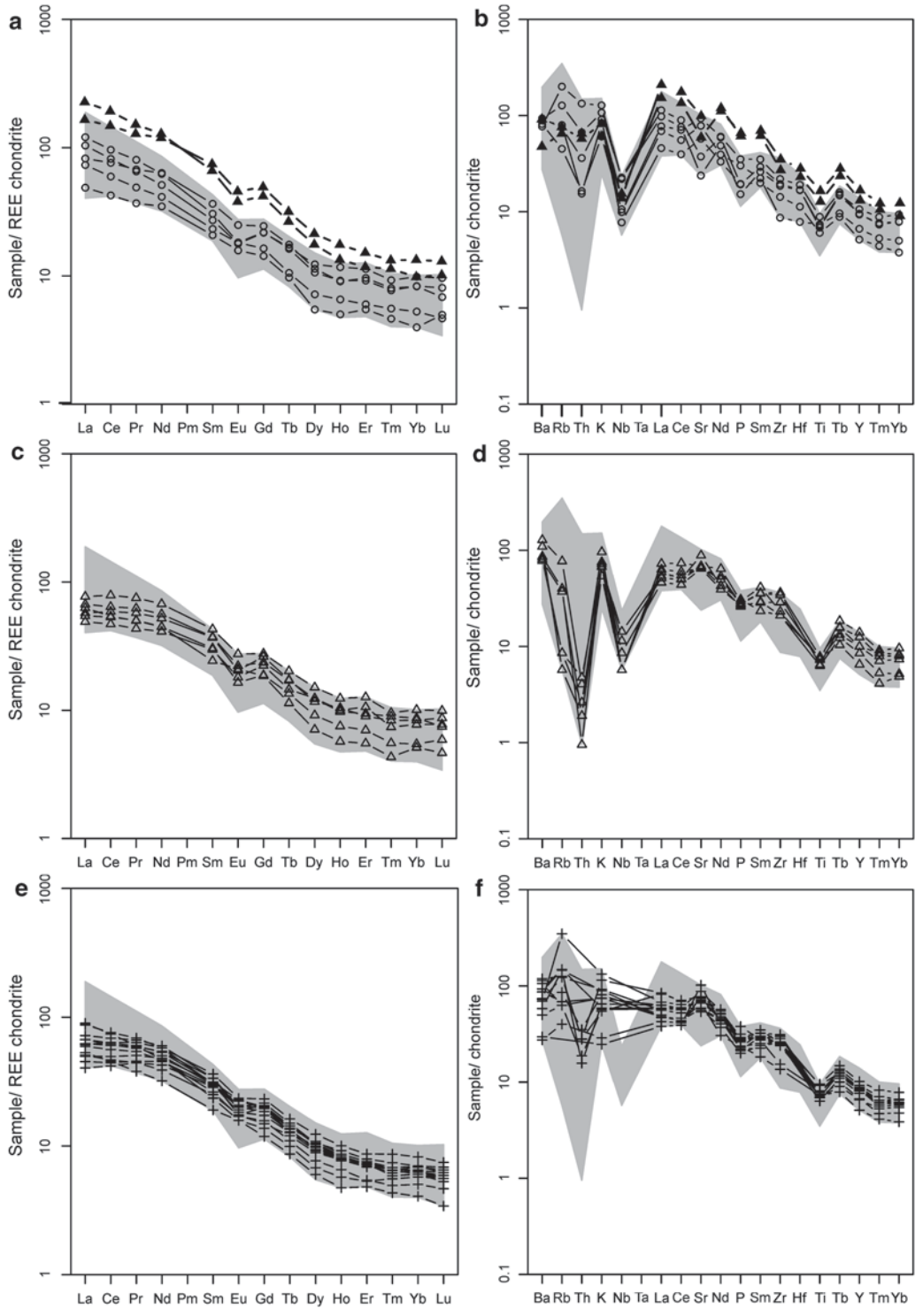

Fig. 3.4 Trace element patterns of QQs. **a**, **b** = Ranua, *black triangles* denote alkali gabbroic inclusions in quartz diorite; **c**, **d** = enderbites of the Iisalmi complex; **e**, **f** = opx-free QQs in Iisalmi north of the granulites. The *shaded* area is for all data

sedimentary gneisses is also low, whereas in other areas they may have had a more significant contribution to GGM genesis.

3.3.2 Amphibolites in gneissic complexes

In the Western Karelia subprovince amphibolites are a ubiquitous component of TTGs in which they can typically be found as layers and inclusions whose widths vary from a few tens of centimetres to tens of metres. Normally, the gneiss-associated amphibolites are all migmatized, the volume of felsic neosome ranging in the exposures from < 10 % up to c. 90 %. Extensively melted and deformed amphibolites closely resemble strongly deformed, plutonic TTGs with amphibolite rafts, making their distinction difficult. In metatexitic amphibolites, palaeosomes have mostly amphibolite facies mineral assemblages, typically hornblende-plagioclase-quartz, commonly with retrograde epidote. In granulite facies areas, amphibolites commonly have coexisting orthopyroxene and clinopyroxene. Garnet-bearing two-pyroxene mafic and intermediate granulites, which are common in the Iisalmi complex, represent high-temperature/medium-pressure equivalents of the common hornblende amphibolites.

The ages of the amphibolites are problematic to resolve, because they commonly appear to contain predominantly metamorphic zircon grains (e.g. Mutanen and Huhma 2003). Intermediate granulites and amphibolites in the Iisalmi complex have been dated for their protoliths at c. 3.2 Ga (Paavola 1986; Mänttäri and Hölttä 2002; Lauri et al. 2011), but this complex is older overall than most other areas in the western part of the Karelia Province.

On the basis of major element composition and using the TAS classification, the amphibolites are classified mostly as basalts and andesitic-basalts. Some amphibolites are andesitic and some have a slightly alkaline character. In the Jensen cation plot, most compositions are in the field of high-Mg tholeiites, and some even in the komatiitic basalt field, the latter probably because of the existence of cumulus olivine.

Basaltic amphibolites (SiO_2 < 52 wt%) fall into two main groups on the basis of their trace element contents. Samples of the first group have flat or LREE-depleted trace element patterns, resembling those of the modern mid-ocean ridge basalts. Further characteristics of these samples are high $(Nb/La)_N$ ratios, low Zr/Y ratios and high Ni and Cr contents (Hölttä 1997; Nehring et al. 2009; Hölttä et al. 2012). Samples of the second group are enriched in LILE and LREE and have lower Nb/La_N ratios and higher Zr/Y ratios than those in the first group (Fig. 3.5). Compatible elements, especially Ni but also Cr, are lower in the LREE-enriched than in the group of LREE-depleted samples.

Condie (2005) used the high field strength element (HFSE) ratios of Archaean basalts to demonstrate their possible mantle source domains, assuming that their magmatectonic framework was broadly similar to that of young oceanic basalts. He noted that on the basis of the Nb/Th, Zr/Nb, Nb/Y and Zr/Y ratios, most non-arc-type Archaean basalts from greenstone belts resemble oceanic plateau basalts, which are thought to originate from plumes variably comprising deep primitive and shallow depleted mantle. Figure 3.6 shows a plot of Nb/Y vs. Zr/Y for the basaltic amphibolites in the Finnish part of the Karelia Province. Given the depletion of granulite facies rocks in U and Th, thorium-based ratios are probably useless for the high-grade migmatitic amphibolites. As Zr/Nb ratios in all samples of the amphibolites are c. 10–30, they probably do not contain recycled oceanic lithospheric material. Most of the analysed amphibolites have LREE-depleted or flat REE patterns, relatively low Zr/Y ratios of c. 1–2, and tendency to plot between the primitive and deep depleted mantle compositions in the diagram in Fig. 3.6. A smaller number of the amphibolites are LREE enriched, have Zr/Y ratios of c. 3–5 and define on the Nb/Y vs. Zr/Y diagram a trend towards enriched sources that could be the lithospheric mantle or the continental crust. In the field, some of the amphibolites show dyke-like relationships with the host TTGs, suggesting that amphibolites in the second group could represent metamorphosed and deformed dykes, whose magmas were chemically reacted with the TTG crust.

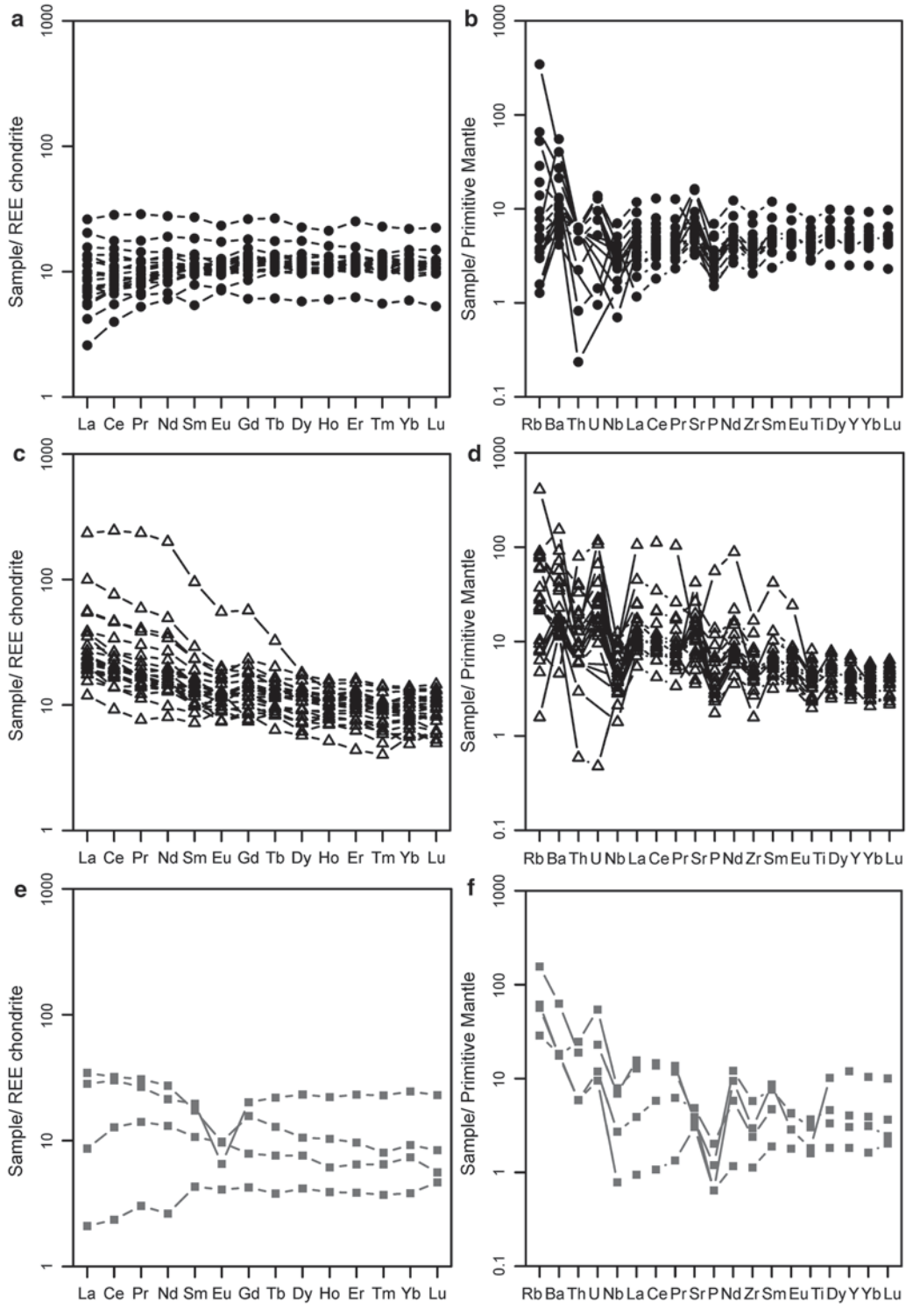

Fig. 3.5 Trace element patterns of basaltic amphibolites. **a**, **b** = LREE-depleted group; **c**, **d** = LREE-enriched group; **e**, **f** = komatiitic basalts. Normalising factors are as in Fig. 3.3

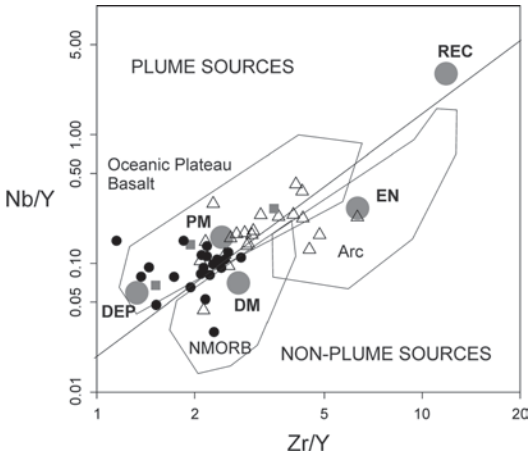

Fig. 3.6 Nb/Y vs. Zr/Y of basaltic amphibolites. *Black circles* = LREE depleted basalts, *triangles* = LREE enriched basalts, *grey squares* = komatiitic basalts. Abbreviations: *PM* primitive mantle; *DM* shallow depleted mantle; *ARC* arc-related basalts; *NMORB* normal ocean ridge basalt; *DEP* deep depleted mantle; *EN* enriched component; *REC* recycled component

This interpretation is supported by the higher LILE contents in these amphibolites compared with the first group of amphibolites, which could be restites of the plateau basalts after melting that produced the TTGs.

3.4 Greenstone Belts

The Karelia and Belomorian Provinces include numerous, generally NNW-trending greenstone belts (Slabunov et al. 2006a). Case studies have proposed distinct formative settings for the individual belts, i.e. an oceanic plateau setting for the Kostomuksha belt (Puchtel et al. 1998), an island arc setting for the Sumozero-Kenozero belt (Puchtel et al. 1999) and a continental rift setting for the Suomussalmi-Kuhmo and Matkalahti belts (Luukkonen 1992; Papunen et al. 2009; Kozhevnikov et al. 2006). A brief description of the best-known belts is given here.

3.4.1 Vedlozero–Segozero Greenstone Belt

The Vedlozero–Segozero greenstone belt is located at the western margin of the Vodlozero subprovince and consists of three volcanic complexes whose ages are 3.05–2.95 Ga, 2.90-2.85 Ga and 2.76-2.74 Ga (Svetov and Svetova 2011). The 3.05–2.95 Ga complex comprises two suites (Svetov 2009). The basalt–andesite–dacite–rhyolite (BADR) suite contains pillow and amygdaloid lavas, fragmental intermediate and felsic lavas, tuffs and dikes. The age of subvolcanic dacitic andesite is 2995 ± 20 Ma (Sergeev 1982); andesitic lavas are dated at 2945 ± 19 Ma (Ovchinnikova et al. 1994) and 2971 ± 59 Ma (Svetov 2010). The rocks belong to the calc-alkaline series with adakitic geochemical characteristics (Svetov 2009). This association is a relict of the oldest volcanic island arc system known in the Fennoscandian Shield (Svetov 2005, 2009).

Another suite consists of komatiites and basalts. The Sm–Nd isochron age of this association is 2921 ± 55 Ma; ε Nd (t) = +1.5 (Svetov et al. 2001). The sequence is composed of diverse lavas, including pillow, variolitic, and spinifex varieties. Pyroclastic interlayers occupy less than 5% of the sequence's volume (Svetova 1988; Svetov et al. 2001). The Al-undepleted pyroxenites and basaltic komatiites and tholeiitic basalts are predominant, their intrusive equivalents consisting of magnesian gabbro and serpentinized ultramafic rocks. This association is interpreted to have evolved in a backarc basin of a suprasubduction zone environment (Svetov 2005).

The 2.90–2.85 Ga complex consists of andesites, dacitic andesites, dacites and rhyolites—i.e. ADR-type volcanic rocks and various kind of metasediments. The Janis palaeovolcano, for example, consists of lava breccias, lavas, and block agglomerate tuffs; a feeder is filled with subvolcanic dacite. The chemogenic silicites were deposited in the crater lake. Tuffs, tuffites, tuffstones, tuffaceous conglomerates, and silicites occur at the periphery of the paleovolcano. The subvolcanic intrusions are composed of dacite and rhyolite. The dacitic andesites erupted in a subaerial environment (Svetova 1988). Lavas were inferior in abundance to the products of volcanic explosions. Existing dates for the felsic volcanic rocks give ages of 2860 ± 15 Ma (Samsonov 2004) and 2866 ± 11 Ma (Svetov 2010); dykes are dated at 2862 ± 45 Ma (Ovchinnikova et al. 1994). The ADR-type volcanic rocks belong

to the calc-alkaline series, the same rocks with adakitic and Nb-enriched andesite geochemical characteristics (Svetov 2005, 2010. This complex was evidently formed in a suprasubduction setting of the Andean type active continental margin (Svetov 2005).

The ADR-type, 2.76–2.74 Ga volcanic complex is found in the Malasel'ga area. The existing dates for these felsic volcanic rocks reveal zircon ages of 2765 ± 13 and 2743 ± 12 Ma (Svetov 2010).

3.4.2 Sumozero–Kenozero Greenstone Belt

The Sumozero– Kenozero greenstone belt is located at the eastern margin of the Vodlozero subprovince. Two volcanic complexes of different ages are recognized in Sumozero–Kenozero greenstone belt, the c. 3.00–2.90 Ga komatiite–basalt complex and the 2.88 Ga complex consisting of BADR and adakitic volcanic rocks (Rybakov et al. 1981).

The Sm–Nd whole rock isochrons for komatiite- basalt associations yield ages of 2.91–2.96 Ga (Sochevanov et al. 1991; Lobach-Zhuchenko et al. 1999; Puchtel et al. 1999). The komatiite–basalt complex consists mainly of metakomatiitic lavas, locally with spinifex texture, and pillowed tholeiitic basalts. Interlayers of felsic volcanic and tuffaceous rocks, and graphite-bearing schists, as well as crosscutting mafic and felsic dykes and plagiogranite bodies are found. Komatiites (~30 wt % MgO in the spinifex zone) belong to the Al-undepleted group. The komatiites and tholeiitic basalts have positive Nb anomalies and their REE patterns are similar to those of the MORB-type rocks. In terms of isotopic and geochemical signatures, the komatiite–basalt association is comparable with oceanic plateau complexes, genetically related to the mantle plumes (Puchtel et al. 1999).

The younger complex of Sumozero–Kenozero greenstone belt consists of metavolcanic BADR rocks with interlayers of carbonaceous and carbonate schists and quartzite. There also exist subvolcanic rhyolites and adakites (Rybakov et al. 1981; Puchtel et al. 1999). The ages of the BADR and adakitic rocks are 2875 ± 2 Ma and 2876 ± 5 Ma, respectively. The BADR and adakitic rocks are thought to have formed in a subductional setting as the products of melting of a mantle wedge and a subducting slab, respectively (Puchtel et al. 1999).

3.4.3 Matkalahti Greenstone Belt

The Matkalahti greenstone belt is situated in the central, poorly exposed part of the Vodlozero subprovince. The belt is composed of alternating metasedimentary rocks (quartz arenite, graywacke, carbonaceous schist) and mylonitized basaltic–komatiitic metavolcanic rocks with rare interlayers of foliated felsic metavolcanic rocks (Kozhevnikov et al. 2006). The age of detrital zircon grains from quartz arenite and graywacke varies from 3.33 to 2.82 Ga indicating that this complex is younger than 2.82 Ga. The complex may represent an intracratonic rift assemblage (Kozhevnikov et al. 2006).

3.4.4 Kuhmo Greenstone Belt

The Kuhmo greenstone belt forms the central part of the c. 220-km-long Suomussalmi-Kuhmo-Tipasjärvi greenstone belt in the Western Karelia subprovince (Fig. 3.2). The supracrustal succession in the Kuhmo belt starts with rhyolitic-dacitic lavas and pyroclastic rocks, whose depositional basement and original thickness are unknown. Felsic volcanic rocks occur in two age groups, 2.84–2.82 Ga and c. 2.80 Ga (Huhma et al. 2012a). The felsic volcanics are overlain by an up to one-kilometre-thick sequence of tholeiitic pillow lavas and hyaloclastites, with sporadic layers of Algoma-type BIFs. The tholeitic strata are overlain by a sequence of komatiites (total thickness ~500 m), komatiitic basalts (~300 m), interlayered high-Cr basalts (~250 m) and komatiites, high-Cr basalts (~250 m) and finally pyroclastic intermediate-mafic volcanics (Papunen et al. 2009).

The Kuhmo greenstone belt is bounded by TTGs, sanukitoids, QQ and GGM suite plutons. Several studies have suggested that the Kuhmo

greenstone succession was deposited on older continental crust represented by the TTGs (Martin et al. 1984; Luukkonen 1992; Papunen et al. 2009). However, no unconformity or superposition relationship between the TTGs and the greenstone belt supracrustal units has ever been demonstrated. Nor is the concept of an old sialic basement supported by the more recent isotope geochemical and age data (e.g. Käpyaho et al. 2006; Huhma et al. 2012a). With the exception of one sample from the palaeosome of a migmatite c. 30 km east of the Kuhmo greenstone belt (2942 ± 6 Ma; Käpyaho et al. 2007), all samples from the surrounding TTGs yield crystallisation ages younger than the volcanic rocks of the greenstone belt. Furthermore, Käpyaho et al. (2006) concluded, based on an extensive Sm-Nd isotope study, that the plutonic rocks in the Kuhmo area represent relatively juvenile material without a major input from significantly older crust. Neither do the εNd from +1.2 to +2.4 of intermediate and felsic volcanic rocks in Kuhmo (Huhma et al. 2012b) indicate that they would contain significant amounts of older crustal material, as one could expect if they originated in a narrow continental rift setting as suggested by Papunen et al. (2009).However, in the northern part, the Suomusalmi section of the belt both volcanic rocks and granitoids display negative initial εNd values and oldest volcanic rocks yield ages close to 2.95 Ga (Mikkola et al. 2011a; Huhma et al. 2012a, b).

The Kuhmo komatiites and komatiitic basalts have generally flat primitive mantle normalised patterns showing only moderate depletion in LREE (Fig. 3.7), as is common for Al-undepleted komatiites. Owing to multiple episodes of post-eruption alteration, the Kuhmo komatiites are disturbed to various degrees in their isotope systems. For example, a Sm-Nd isotope study by Gruau et al. (1992) has shown that the Kuhmo komatiites produce a Sm-Nd isochron yielding an age of c. 1.9 Ga, indicative of resetting of the Sm-Nd isotope system of these Archaean rocks during a Proterozoic metamorphic event.

In terms of Nb/Y and Zr/Y ratios, Kuhmo komatiites plot close to the demarcation line between plume and non-plume source compositions (Fig. 3.8c). Most samples cluster between primitive mantle (PM) and shallow depleted mantle (DM) compositions, and there are many plottings towards the deep depleted plume component (DEP). In the Zr/Nb vs. Nb/Th plot (Fig. 3.8d), the Kuhmo komatiites also plot close to the oceanic plateau basalts, but at somewhat higher Zr/Y values, probably indicating minor pre-eruption fractionation of chromite. Overall, the Kuhmo komatiites show an affinity to oceanic plateau basalts derived from a slightly depleted primitive mantle (PM)-type source, with a minor deep plume signature. Importantly, these komatiites clearly have not been derived from a depleted MORB-type source, and there is also little indication of enriched and recycled mantle components in their source, or input from continental crust during their ascent and eruption.

3.4.5 Kostomuksha Greenstone Belt

The Kostomuksha greenstone belt consists of basalt–komatiite, rhyolite–dacite and banded iron formation (BIF) suites (Kozhevnikov 2000; Lobach-Zhuchenko et al. 2000a; Rybakov et al. 1981; Rayevskaya et al. 1992). The belt hosts an economic BIF that is under active mining.

Existing Sm–Nd isochron ages of basalt and komatiite are 2.84 (Puchtel et al. 1998) and 2.81 Ga, respectively, and the zircon age (SHRIMP-II) of the tuff coeval with the this basalts is 2792 ± 6 Ma (Kozhevnikov et al. 2006). In their geochemical signatures tholeiitic basalts and komatiites are comparable with oceanic plateau basalts.They are depleted in Th and LREE ((La/Sm)N = 0.66), characterized by a flat HREE pattern ((Gd/Yb)N = 1), a chondritic Ti/Zr ratio, a slightly positive Nb anomaly, and an average εNd(*t*) of +2.8 (Puchtel et al. 1998). The evolved and unfractionated komatiitic lavas host rare tuffaceous units, and peridotitic sills are widespread. The Al-depleted komatiites are depleted in LREE ((La/Sm)N = 0.48; (Gd/Yb)N = 1.2, Puchtel et al. 1998). The Re–Os isotopic data (γ^{187}Os = +3.6 ± 1.0) suggest that they were derived from a plume that arose at the core-mantle boundary (Puchtel et al. 2001).

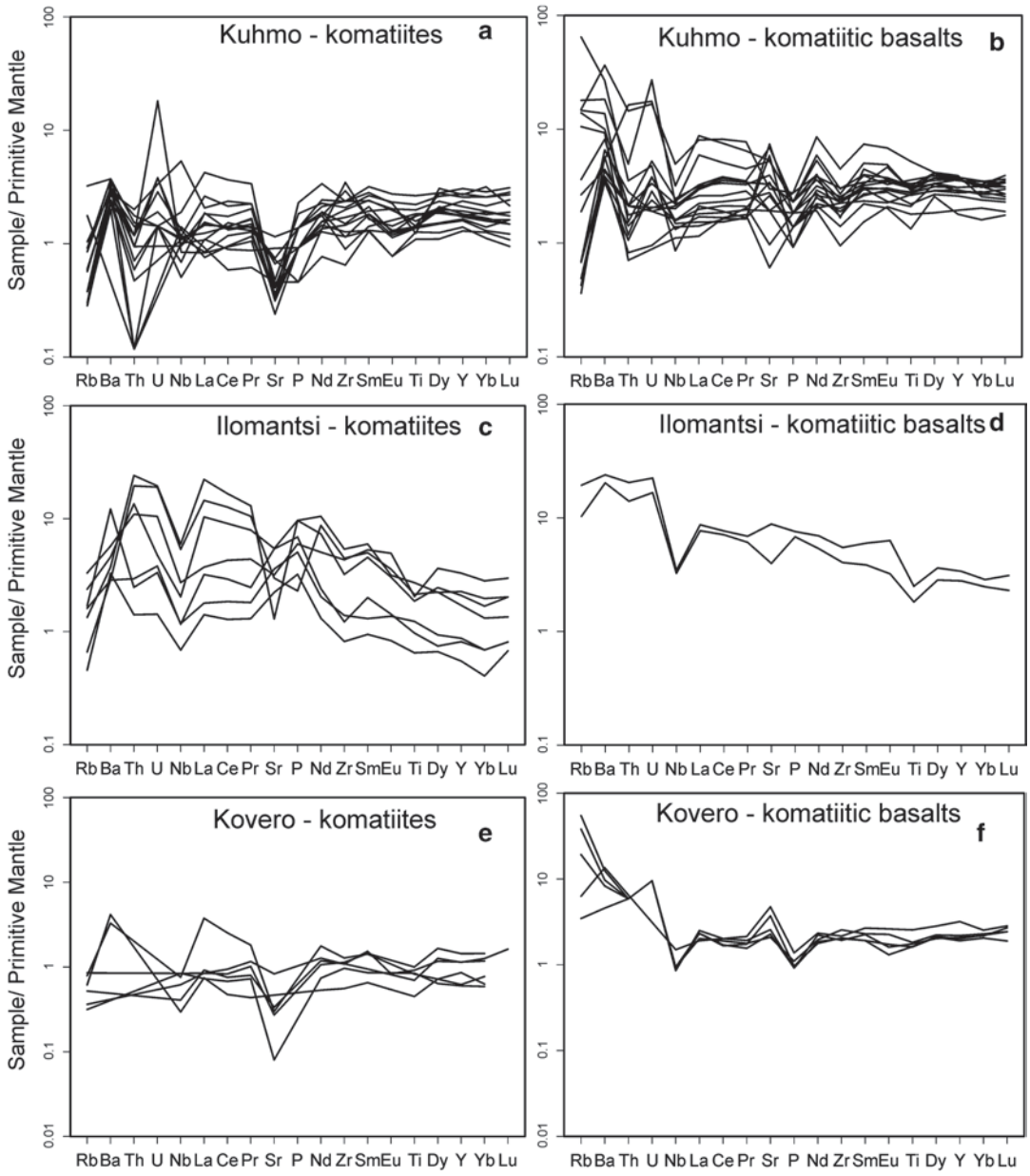

Fig. 3.7 Primitive mantle-normalized trace element patterns of komatiites and komatiitic basalts in Kuhmo, Ilomantsi and Kovero. Normalizing values are from Sun and McDonough (1989)

The rhyolite–dacite suite consists of various lavas, tuffs, and tuffites with interlayers of carbonaceous schist and jaspilite; dikes and subvolcanic intrusions also exist. Age estimates of 2790±21 Ma (Bibikova et al. 2005) and 2795±10 Ma (Lobach-Zhuchenko et al. 2000a) have been obtained for this suite. Rayevskaya et al. (1992) classified the volcanic rocks as calc-alkaline rhyolites and dacites (sporadic andesites) with distinct negative Nb anomalies. Two geochemically different groups of rocks are distinguished: (1) high-K rocks with highly fractionated REE patterns ((La/Sm)N = 4.9–6.2, (Gd/Yb)N = 2.5–3.7) and low Al_2O_3, Sr, and Y and

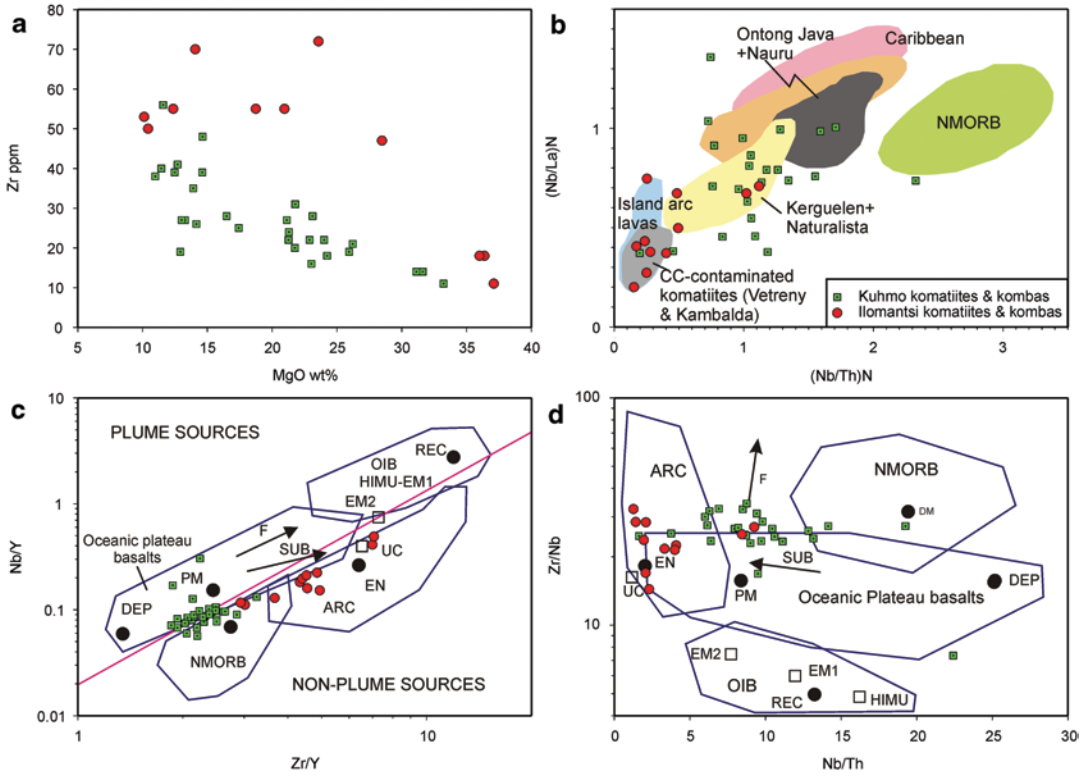

Fig. 3.8 Zr-Nb-Y-Th-La ratios in the komatiites and komatiitic basalts of Kuhmo and Ilomantsi. Abbreviations (Condie 2005): *UC* upper continental crust; *PM* primitive mantle; *DM* shallow depleted mantle; *HIMU* high mu (U/Pb) source; *EM1* and *EM2* enriched mantle sources; *ARC* arc-related basalts; *NMORB* normal ocean ridge basalt; *OIB* oceanic island basalt; *DEP* deep depleted mantle; *EN* enriched component; *REC* recycled component. *Arrows* indicate the effects of batch melting (F) and subduction (SUB)

(2) an adakitic group with fractionated REE patterns ((La/Sm)N = 2.9–5.3, (Gd/Yb)N = 1.4–2.1)) and high Y and Sr (Samsonov et al. 2005). These rocks have plutonic analogues in the area. The εNd(t) values are from −6.21 to +1.59 (Bibikova et al. 2005). These geochemical signatures indicate that the volcanic rocks were related to at least two mantle and ancient crustal sources, and that they likely formed in an arc setting (Samsonov et al. 2005; Kozhevnikov 2000).

The sedimentary suite consists of conglomerates, jaspilites including the BIFs and greywackes with thin interlayers of andesite–dacite–rhyolite tuffs and komatiite bodies. The terrigenous sedimentary rocks are poorly differentiated, immature, and comparable with graywackes from the Neoarchean greenstone belts. The provenance was composed of approximately equal abundances of basic and felsic rocks (Mil'kevich and Myskova 1998). The U-Pb age on zircon from dacitic tuffite interlayered with the sedimentary suite is 2787 ± 8 Ma (Bibikova et al. 2005), indicating the deposition time of the sedimentary suite.

All three rock suites in the Kostomuksha greenstone belt were formed at c. 2.80–2.79 Ga but evidently in different geodynamic settings. It is widely thought that the greenstone belt is a tectonic collage that arose as a result of accretion of almost coeval mantle- plume volcanic plateau and subduction-related igneous and sedimentary rocks (Kozhevnikov et al. 2006; Kozhevnikov 2000; Puchtel et al. 1998; Samsonov 2004).

3.4.6 Ilomantsi and Gemoli-Bol'shozero Greenstone Belts

In the Ilomantsi greenstone belt and in its NNE continuation, the Gemoli-Bol'shozero greenstone belt are located in the southwestern part of the

Central Karelia subprovince. The supracrustal sequence is dominated by sedimentary rocks intercalated with less abundant komatiites, tholeiites, low-Ti tholeiites, andesites, dacites and banded iron formations. The lowermost unit in Ilomantsi starts with mafic pillow lavas, but predominantly consists of felsic pyroclastic and epiclastic sedimentary rocks. The depositional environment was dominated by two distinct but overlapping felsic volcanic complexes, probably locally subaerial, but nevertheless developed within relatively deep, turbidite-dominated basins (Sorjonen-Ward 1993). Thin tholeiitic intercalations and komatiitic sheet flows occur in the upper part of the succession, typically associated with banded iron formations. The komatiites are generally massive recrystallized in structure, and only locally preserve such relict features as cumulus textures or flow top breccias (O'Brien et al. 1993). No primary silicate minerals are preserved in the komatiites, as they have been pervasively altered and recrystallised to tremolite-chlorite-serpentine rocks or chlorite-talc-rich schists. Locally, the komatiites are demonstrably intercalated with felsic volcanic rocks.

Komatiitic rocks from Ilomantsi have the characteristics of the aluminium-undepleted, Munro-type komatiites, having average Al_2O_3/TiO_2 ratios of c. 17.4, but there is considerable scatter. Komatiites and komatiitic basalts of the Kovero greenstone belt, which flanks the Ilomantsi belt in the SW, have high Al_2O_3/TiO_2 ratios, reflecting their low TiO_2 content at a given Al_2O_3 and MgO level (Hölttä et al. 2012). Ni, Co and Cr increase as a function of MgO and Mg# in a way that is indicative of low-pressure fractionation of olivine and chromite being the main factor controlling the compositional variation. This is consistent with the relatively differentiated nature of the lavas, as chromite is generally undersaturated in komatiites with >c. 25% MgO (Barnes and Roeder 2001). Kovero komatiites seem to differ from the Ilomantsi and Kuhmo komatiites, having overall higher Cr/MgO ratios.

Ilomantsi komatiites have highly fractionated patterns with high LREE/HREE ratios and distinct negative Nb-Ta and Ti-anomalies (Fig. 3.7). The close similarity in trace element patterns between the komatiites and associated rhyolites and dacites (O'Brien et al. 1993) is a clear indication of extensive interaction of the komatiites with the felsic volcanics. Interestingly, the komatiitic basalts from Ilomantsi show less fractionated incompatible trace element patterns than the komatiites, inconsistent with derivation of the basaltic magmas from the komatiites by crystal fractionation. A likely explanation is that the komatiitic basalts evolved from the komatiitic magma already prior to the eruption, within transient storage chamber(s) at depth. During the subsequent eruptions, the komatiites assimilated more felsic magmas than the komatiitic basalts, possibly due to their higher eruption temperatures.

Vaasjoki et al. (1993) reported a TIMS U-Pb age of 2754 ± 6 Ma on zircon from a plagioclase-phyric andesite that represents the stratigraphically lowermost units of the Ilomantsi greenstone belt. The majority of detrital zircon grains in the nearby metasedimentary rocks are of the same age (Huhma et al. 2012a). Previous studies on the Ilomantsi belt have documented a close relationship between volcanism, sedimentation, deformation and pluton emplacement (Sorjonen-Ward 1993), implying rapid c. 2.75 Ga crustal growth in the region. All exposed contacts between the supracrustal rocks and granitoids have been interpreted as intrusive (Sorjonen-Ward and Luukkonen 2005), and the granitoids cannot, therefore, represent the basement to the Ilomantsi greenstone belt, nor a dominant source of the material in the supracrustal sequences.

3.4.7 Keret Greenstone Belt

The Keret greenstone belt is located in the western part of Belomorian Province and consist of three complexes whose ages are 2.88–2.82 Ga, 2.80–2.78 Ga and c. 2.70 Ga. The Keret'ozero greenstone complex is the oldest. It consists of three metavolcanic suites which are komatiite-tholeiite suite, intermediate-felsic suite and andesite basalt-basalt suite (Slabunov 1993, 2008).

Komatiite-tholeiite metabasalts are classified as Na-tholeiite series. High-Mg rocks are classified as Al-undepleted LREE-enriched komatiites and komatiitic basalts having 10–37 wt.% MgO, 0.19–0.9 wt.% TiO_2, $Al_2O_3/TiO_2 \approx 20$,

$CaO/Al_2O_3 = 0.64–0.9$ and $Zr/Y = 2–3$. This suite represents an oceanic plateau setting (Slabunov 2008).

The intermediate and felsic suite consists of metatuffs, metalava and subvolcanic bodies. The rocks vary in composition from andesite-basalt to rhyolite, with andesites and dacites being predominant. Geochemically the rocks in this suite are classified as calc-alkaline island-arc volcanic rocks, which were produced in a subduction zone. U-Pb datings on zircon give ages of 2877 ± 45 and 2829 ± 30 Ma (Bibikova et al. 1999).

The andesite basalt-basalt suite differs from the underlying unit in the predominance of basalts. Essential constituents are Cr- and Ni-rich metasedimentary interbeds, which could have been produced by breakdown of intermediate-felsic volcanic rocks, basaltic lavas and komatiites. These rocks are geochemically comparable with mature island-arc volcanic rocks. Greywackes of such composition are typically formed in ensimatic island-arc settings (Slabunov 2008, 2010).

Hisovaara greenstone complex is located in the northern part of the Keret belt and is dated at c. 2.80–2.78 Ga. It is subdivided into six suites (Thurston and Kozhevnikov 2000; Bibikova et al. 2003; Kozhevnikov et al. 2005; Kozhevnikov and Shchipansky 2008). The ultrabasic-boninitic-basaltic suite is composed of ultrabasic rocks (peridotitic cumulates), tholeiitic metabasalts, high-Mg basalts and komatiites with a 0.5–1 m thick metaboninite interbed and high-Ti ferrobasalts (Shchipansky et al. 2004). This suite is interpreted as a fragment of a suprasubduction ophiolite, the best-preserved portion of which has been described from the adjacent Irinogora area of the Tikshozero belt.

The andesitic suite consists of biotite-epidote-amphibole schists, in which amygdaloidal, massive and glomeroporphyric textures are locally preserved. The age of these andesites is 2777 ± 5 Ma (Bibikova et al. 2003). These rocks are extremely rich in Na_2O (Kozhevnikov 2000). In geochemical characteristics they are similar to tholeiitic andesites from initial intraoceanic island arcs (Bibikova et al. 2003).

The age of volcanic-sedimentary suite is estimated at 2778 ± 21 Ma (Bibikova et al. 2003). Thin intercalations of carbonaceous varieties and iron-cherty and aluminosilicate rocks and lenses of homogeneous metasomatic quartz-kyanite rocks are encountered. The latter are assumed to have been produced by hydrothermal processes that accompanied volcanism (Kozhevnikov 2000; Bibikova et al. 2001b). The U-Pb dating on zircon grains from quartz-kyanite rocks shows give an age of c. 2.77 Ga (Bibikova et al. 2001c). Abundant subvolcanic andesite, dacite and rhyolite bodies or dykes were identified in volcanic-sedimentary suite. These felsic rocks are compositionally comparable to adakites (Bibikova et al. 2003).

The suite of coarse clastic volcanics consists of agglomerate tuffs, oligomictic conglomerates, volcanic conglomerates with tuffaceous matrix and lava breccias that vary in composition from andesite to rhyodacite (Kozhevnikov 2000; Kozhevnikov and Shchipansky 2008). This suite is interpreted to represent a pull-apart basin (Kozhevnikov 2000).

An upper mafic suite consists of metabasalts with a well-preserved pillow texture. Sheet-like bodies of ultramafic composition occur only locally. Metabasalts rest on the underlying rocks along an angular unconformity (Kozhevnikov 2000).

A sedimentary-volcanic suite of c. 2.70 Ga consisting mainly of quartz arenites was identified in the Hisovaara area (Thurston and Kozhevnikov 2000). The protolithis of the sandstones were deposited between 2.71–2.69 Ga, as shown by U-Pb ages of detrital zircon grains (Kozhevnikov et al. 2006).

3.4.8 Tikshozero Greenstone Belt

The Tikshozero greenstone belt is located in the western part of the Belomorian province north of the Keret belt, and it consists of three complexes whose ages are 2.80–2.78 Ga, c. 2.75 Ga and 2.74–2.72 Ga.

The 2.80–2.78 Ga greenstone complex consists of intermediate-felsic volcanic and subvolcanic suite, suprasubduction ophiolite suite, metabasalt suite, metagreywacke suite, coarse clastic suite and sedimentary-volcanic suite. Well-preserved ophiolitic fragments constitute

an important part of this complex (Shchipansky et al. 2004) and make up a significant component of gently NNE-dipping thrust sheets. These sheets consist of mafic metavolcanics which are analogues to the upper tholeiites and boninites of Hisovaara. Ophiolitic rocks are thrust over on island-arc type intermediate and felsic calc-alkaline metavolcanic rocks and related volcanosedimentary rocks, which may be regarded as a paraautochthonous basement for the ophiolitic thrust sheets. Supracrustal rocks of the Iringora areal unit were subjected to intense deformation and metamorphism, but their primary volcanic and sedimentary structures are locally preserved.

A c. 2.75 Ga unit within the Hisovaara greenstone complex consists predominantly of intermediate volcanic rocks. Amygdaloidal and pillow lavas, sedimentary-volcanic rocks, and minor metabasalts and high-Mg basic rocks make up this unit. Porphyritic basalts from this units are dated at 2.75 Ga (Alekseev et al. 2004).

The 2.74–2.72 Ga units in the Hisovaara greenstone complex, Tikshozero belt consists of three suites represented by the komatiite-tholeiite suite, intermediate-felsic volcanic suite and sedimentary-volcanic suite (Stepanov and Slabunov 1989; Levchenkov et al. 2003). On the basis of their composition, the tholeiitic basalts of the komatiite-tholeiite suite are similar to modern N-MORB basalts, with their REE content 8–15 times chondritic with almost flat REE patterns ($(La/Yb)_N = 0.9–1.0$). Komatiites in this suite represent Al-undepleted type (Al_2O_3/TiO_2 18–25, $CaO/Al_2O_3 = 0.7–1.6$; $Zr/Y = 2–2.8$), and they are depleted in LREE $(La/Sm)_N = 0.7–0.8$).

The intermediate-felsic volcanic suite consists of amphibole-biotite schists. Well-preserved agglomerate-tuff and thinly-laminated felsic tuffaceous rocks are common. On the basis of their chemical compositions, intermediate-felsic rocks are calc-alkaline andesite basalts, andesites and rhyolites. They show a low Sr/Y ratio (about 20–25), Y concentration varying from 20 to 30 ppm. They exhibit a differentiated REE spectrum ($(La/Yb)_N$ c. 11–17) and a negative Nb anomaly relative to Th and La, typical of island-arc volcanic rocks. The intermediate-felsic volcanic rocks are dated at 2.74 Ga (Levchenkov et al. 2003). The volcanic rocks were slightly contaminated with older crustal material, as indicated by their Sm-Nd systematics (ε_{Nd} (2.73) ranging from +0.9 to −1.1; t_{DM} = ca. 3.0 Ga) and by the presence of c. 2.80 Ga zircon cores (Mil'kevich et al. 2007).

The sedimentary-volcanic suite consists of leucocratic (garnet-kyanite)-biotite-muscovite schist—greywacke that is locally tourmaline-bearing, with interbeds of biotite-amphibole schist—intermediate-felsic tuffs or lavas. The age of the lavas is estimated at 2.72 Ga Ma (Mil'kevich et al. 2007).

3.4.9 Central Belomorian Greenstone Belt

The Central Belomorian greenstone belt consists of amphibolites with intercalated serpentinite, orthopyroxene and hornblendite bodies. They contain no relics of primary textures, and are therefore classified on the basis of petrographic and geochemical characteristics.

Metabasalts (amphibolites) are similar in chemical composition to tholeiites, and are comparable in many respects to MORB, although some varieties of metabasalts are comparable with oceanic-island basalts (Bibikova et al. 1999; Slabunov 2008). The Sm-Nd systematics of these metabasalts (ε_{Nd} (2.85 Ga) = +2.3) shows that their protolith was not contaminated with older crustal material. This inference is consistent with their formation in an oceanic setting (Slabunov 2008).

Relict olivine (86–81 % *Fo*), orthopyroxene (89–85 % *En*) and spinel (iron-rich ferrichromite with 21 % Cr_2O_3) grains are preserved in serpentinites. The olivines are comparable in composition with those from the cumulate peridotites of a gabbroid ophiolite complex and deep cumulate peridotites. The serpentinites seem to have been formed after dunites and harzburgites (Stepanov et al. 2003). They are depleted in LREE ($(La/Yb)_N = 0.52$), but some varieties show a U-shaped REE distribution pattern. The Sm-Nd isotopic characteristics of the serpentinites (ε_{Nd} (2.85 Ga) = +1.9) rule out any crustal contamination, and suggest that they were derived from a depleted mantle, which is also consistent with

their origin as part of an oceanic lithosphere (Slabunov 2008).

The age of the oceanic lithosphere of the Central Belomorian greenstone belt is estimated at 2.88–2.84 Ga on the basis of the U-Pb age on zircon from oceanic trondhjemites (2878 ± 13 Ma, Bibikova et al. 1999) and of the age of early metamorphism in metagabbroic amphibolites from the Lake Seryak area (2836 ± 49 Ma, Slabunov et al. 2009). This age agrees within analytical error with the age of the diorite massif (2.85 ± 0.01 Ga), which crosscuts the unit (Borisova et al. 1997). Based on geological, isotopic and other geochemical data from mafic-ultramafic rocks the Central Belomorian greenstone belt is interpreted as a fragment of a Mesoarchaean oceanic association (Lobach-Zhuchenko et al. 1998; Bibikova et al. 1999; Slabunov 2008).

3.4.10 Chupa Paragneiss Belt

The Chupa paragneiss belt of the Belomorian province consists of migmatized kyanite-garnet-biotite and biotite gneisses. Fine-grained garnet-biotite gneisses, relics of the least altered primary rocks, occur as small lenses of metasediments (Bibikova et al. 1999, 2001a, 2004; Myskova et al. 2003). Based on geochemical characteristics (enrichment in Ni, V, Co and Cr), paragneisses are reconstructed as metagraywackes produced by breakdown of felsic volcanics and mafic–ultramafic rocks in a fore-arc basin environment. Small intermediate and felsic volcanic (dacite-dominated) calc-alkaline interbeds, comparable with island-arc volcanics, and scarce tholeiite bodies are encountered in the graywackes. These observations collectively support the fore-arc basin deposition interpretation (Bibikova et al. 1999; Myskova et al. 2003).

Greywackes in the Chupa paragneiss belt likely formed in the interval 2.87–2.85 Ga, because the age of the cores of detrital zircons is 3.2–2.9 Ga, and the age of the earliest metamorphogenic zircons is 2.86–2.78 Ga. The U-Pb zircon age of the metadacites in the belt is 2870 ± 20 Ma (Bibikova et al. 2004).

3.5 Radiometric Age Determinations from the Karelia Province in Finland

3.5.1 U-Pb

During the past decades, a large number of thermal ionisation mass spectrometry (TIMS) U-Pb age determinations on zircon from Archaean rocks have been carried out at the Isotope Laboratory of the Geological Survey of Finland (GTK). Recently, the secondary ion mass spectrometer (SIMS) of the Nordsim laboratory and multiple-collector inductively coupled plasma mass spectrometer (LA-MC-ICPMS) of GTK have also been used in the age determination of Archaean rocks. Figure 3.9 presents most of the zircon age data available from plutonic and volcanic rocks in the Finnish part of the Karelia Province. It is evident from the diagram that the ages of the TTGs range mostly between 2.83–2.72 Ga, and within this range cluster are two groups separated by a c. 20 Ma time gap; in the older group, TTGs are 2.83–2.78 Ga, and in the younger group 2.76–2.72 Ga. The >2.78 Ga TTGs occur almost exclusively outside the Ilomantsi complex (Fig. 3.9). In the Ilomantsi greenstone belt, volcanic rocks and related dykes are 2.76–2.72 Ga. From the Ilomantsi complex there have thus far been only two observations of Mesoarchaean rocks (Huhma et al. 2012a), consistent with observations from the Central Karelia subprovince in Russia (Lobach-Zhuchenko et al. 2005; Bibikova et al. 2005; Slabunov et al. 2006a), suggesting that most of the Central Karelian crust is relatively young, c. 2.76–2.72 Ga. However, some porphyritic dykes that intruded into mafic volcanic rocks have older, c. 3.0 Ga zircon populations (Vaasjoki et al. 1993). Two datings for felsic volcanic rocks from the Kovero greenstone belt SW of Ilomantsi give ages of c. 2.88 Ga (Huhma et al. 2012a). These results indicate that the Ilomantsi greenstone belt is not a completely juvenile Neoarchaean formation, but includes at least some reworked Mesoarchaean material. Volcanic rocks in the other greenstone belts are dated mostly at 2.84–2.80 Ga (Huhma et al. 2012a). Mesoarchaean c. 2.95 Ga ages are

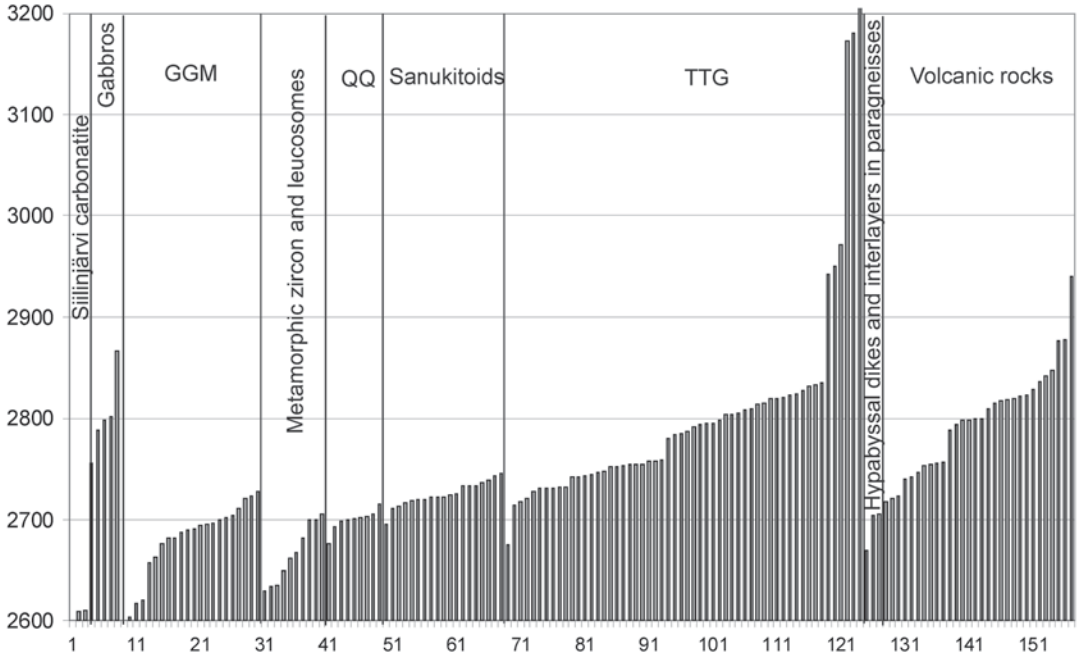

Fig. 3.9 Histogram showing the distribution of the U-Pb ages on zircon of various Archaean lithologies in the Finnish part of the Karelia Province

yielded by some volcanic rocks and TTGs in the northwestern part of the Western Karelia subprovince. In the Western Karelia subprovince, rocks whose zircon ages are > 3.0 Ga to exist only in its western part (Hölttä et al. 2000a; Mutanen and Huhma 2003; Lauri et al. 2011). The GGM suite rocks, mostly of c. 2.73–2.66 Ga, occur all over in the subprovince. In the Western Karelia subprovince the youngest Neoarchaean zircon ages are from granulites and leucosomes of migmatites giving ages of c. 2.65–2.63 Ga and c. 2.71–2.65 Ga, respectively. These ages have been interpreted to date the high-grade metamorphism of lower and mid-crust (Mutanen and Huhma 2003; Mänttäri and Hölttä 2002; Käpyaho et al. 2007; Lauri et al. 2011).

3.5.2 Sm-Nd

The TIMS/SIMS/LA-MC-ICPMS U-Pb zircon age determination localities do not yet evenly cover the Archaean area of Finland, and some relatively large areas remain untouched. Hence, some surprises may arise as the future studies fill up the existing gaps. Sm-Nd analyses have been carried out from most of the samples used for the U-Pb zircon analyses. For this work, many additional TTG samples were analysed to improve the regional cover of the Sm-Nd data. These samples are partly from our own sample sets and partly from the Rock Geochemical Database of Finland (Rasilainen et al. 2007). Whole rock chemistry was used to select samples with the least obvious metamorphic alteration. The analytical data are presented by Huhma et al. (2012b). Figure 3.10 shows the distribution of the T_{DM} model ages on a geological map of Finland.

The various geochemical groups of TTGs observed in this work do not correlate with Sm-Nd model ages or ε_{Nd} values in any simple way. The diagrams in Fig. 3.11 show the REE patterns and the Sm-Nd (T_{DM}) model ages of a large number of the analysed TTGs. Even in the youngest age group, the model ages are < 2.8 Ga and ε_{Nd} values range from + 0.9 to + 2.4, and the samples by and large represent juvenile Neoarchaean materials. Hence, all geochemical types are represented in our study, and the same pattern also holds true in the oldest model age group.

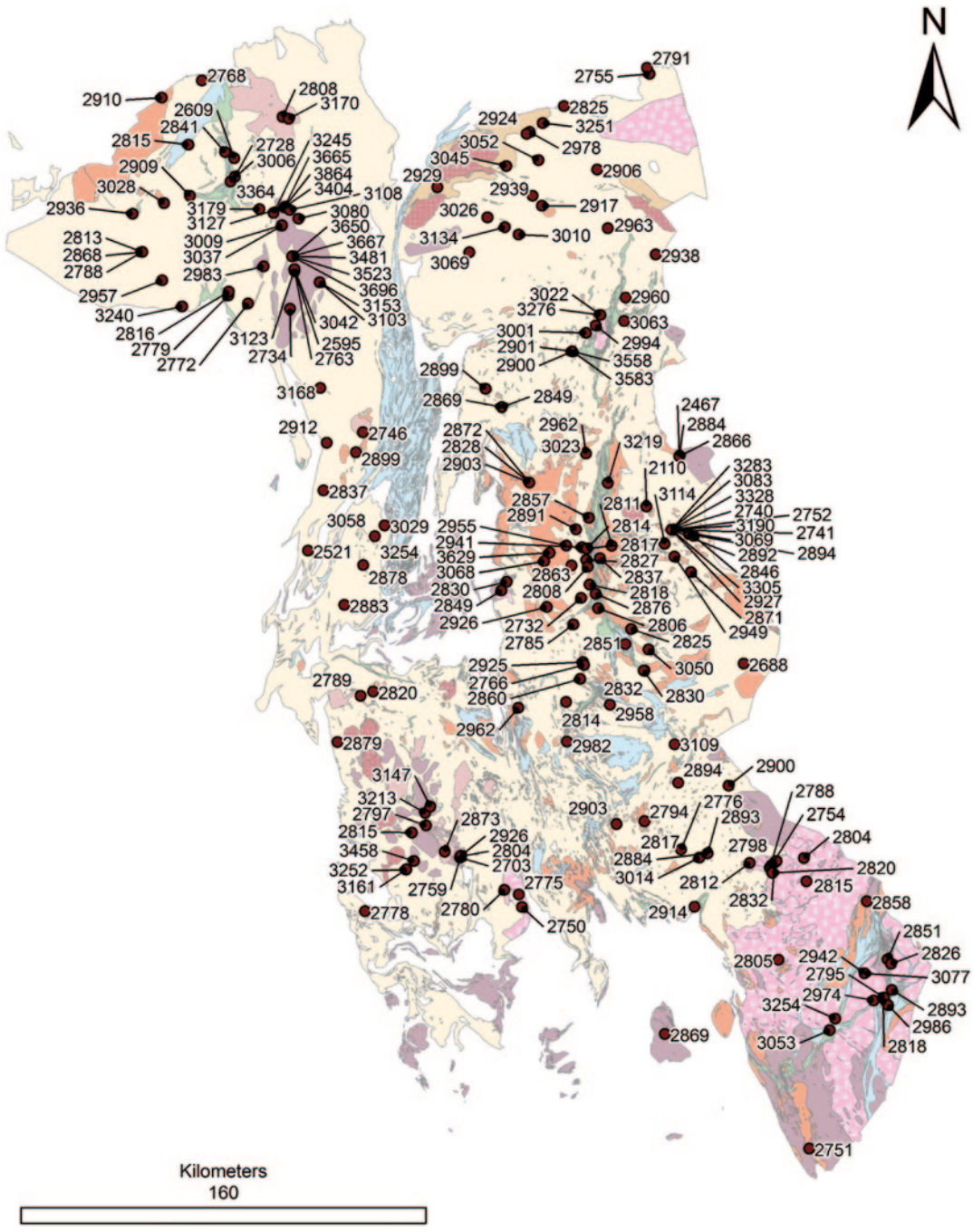

Fig. 3.10 Distribution of the T_{DM} model ages. The lithological base map is from Fig. 3.2

3.5.3 SIMS Ages on Detrital Zircon in Paragneisses

Kontinen et al. (2007) concluded in their study on the Nurmes paragneisses in the Western Karelia subprovince that the deposition of the protolith wackes took place at c. 2.70 Ga, which is in the range observed in U-Pb ages of the youngest dated detrital zircon grains. Nearly 50% of the grains were dated at 2.75–2.70 Ga. The whole

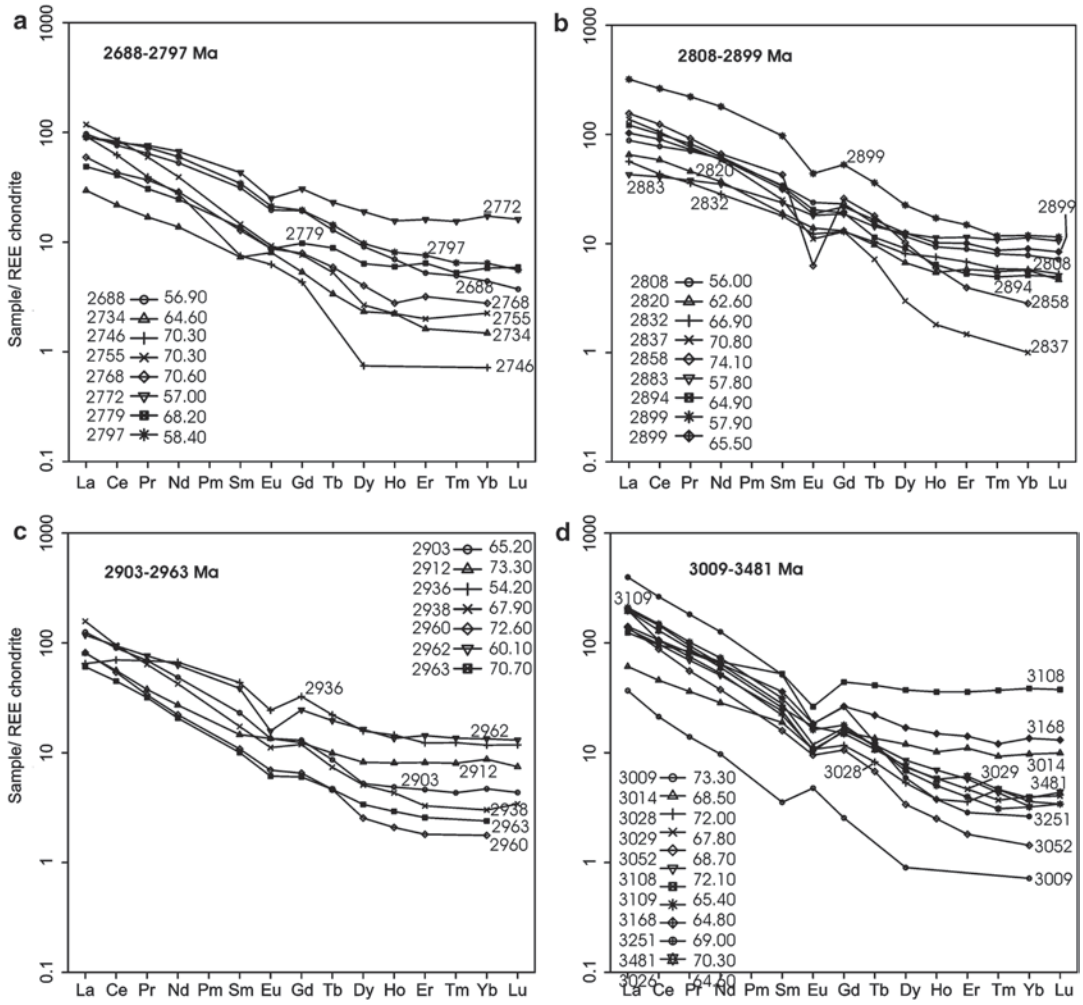

Fig. 3.11 REE patterns of the samples used for Sm-Nd analyses. The numbers next to the *curves* are for the model ages and the insets in the *upper right* corner of the *boxes* show the model age and the SiO_2 content of the sample

rock compositions of the Nurmes paragneisses suggest that the source terrains mainly comprised TTGs and sanukitoid-type plutonic and mafic volcanic rocks. Huhma et al. (2012a) analysed detrital zircon in metasediments from five other localities in the Karelia Province, and the results were similar to those from the previous studies. Most of these samples predominantly contain c. 2.73–2.75 Ga zircon grains, which suggests that the Neoarchaean intrusions of this age produced most of the sedimentary detritus. Mesoarchaean 3.2–2.8 Ga zircon grains were rare in all paragneiss and also other metasedimentary samples.

According to Bibikova et al. (2005), zircon from sanukitoids has higher Th/U ratios (>0.5) than zircon in TTGs (<0.5). Given that most 2.75–2.72 Ga zircon grains from paragneisses have Th/U ratios >0.5, sanukitoids indeed may have been one of their main sources, although it has to be noted that high Th/U in zircon is not restricted to sanukitoids, but is also found in samples of the other main rock groups.

3.6 Lower Crustal Xenoliths

Mantle and lower crustal xenoliths recovered from c. 500- to 600-Ma-old kimberlites near the southwestern boundary of the Western Karelia subprovince provide pertinent information on the

petrology and physical properties of the lower crust (Hölttä et al. 2000b; Peltonen et al. 2006). The lower crustal xenoliths are almost exclusively mafic granulites. Mineral thermobarometry, together with isotopic, petrological and seismic velocity constraints, imply that the lower crustal xenoliths are derived from the weakly reflective, high-V_p layer at the base of the crust (40–58 km depth; Hölttä et al. 2000b; Peltonen et al. 2006). Single grain zircon U–Pb dates and Nd model ages (T_{DM}) from the xenoliths imply that the bottom high velocity layer is a hybrid layer consisting of both Archaean and Proterozoic mafic granulites. Many of the studied xenoliths record only Proterozoic zircon ages (2.5–1.7 Ga) and Nd model ages (2.3–1.9 Ga), implying that the lower crust contains a significant juvenile Palaeoproterozoic component (Hölttä et al. 2000b; Peltonen et al. 2006). Only a small fraction of zircon grains separated from the xenoliths give Archaean ages typically in the range of 2.7–2.6 Ga. Mesoarchaean zircon grains are almost absent. The oldest zircon ages, up to c. 3.5 Ga, and Nd T_{DM} model ages of c. 3.7 Ga of the xenoliths are similar to those from the oldest gneisses in the Siurua complex. Based on these data, the lowermost crust probably originated as Archaean mafic gneisses, but was repeatedly intruded by Proterozoic mafic magmas 2.5–1.80 Ga ago.

3.7 Metamorphism

3.7.1 Amphibolites and Paragneisses in the Western Karelia Subprovince

Ubiquitous evidence of melting and migmatisation of felsic but also mafic rocks within the TTGs of the Western Karelia Province implies that they were mostly metamorphosed in upper amphibolite and granulite facies conditions. Partial melting was commonly extensive, leading to the intense migmatisation characterizing so many localities. Lower grade rocks are found in the inner parts of the Kuhmo-Suomussalmi and Ilomantsi greenstone belts that commonly show mid- or low amphibolite facies mineral assemblages, well preserved primary structures and only a little or no migmatisation. Because of the dominance of the mineralogically monotonous gneissic TTG rocks, suitable mineral assemblages—especially garnet-bearing paragenesis—for the study of pressure-temperature evolution are not common. However, amphibolites and paragneisses locally have a garnet-hornblende-plagioclase-quartz or garnet-biotite-plagioclase-quartz mineral assemblages that can be used for geothermometry and geobarometry. Pressures and temperatures have been obtained using Thermocalc (Powell et al. 1998) and TWQ (Berman 1988, 1991) average PT calculations and grt-bt-pl-qtz thermobarometry (Wu et al. 2004). Metamorphic pressures obtained for the paragneisses and for the amphibolites around are mostly c. 4.7–7.5 kbar, and corresponding temperatures c. 650–740 °C (Hölttä et al. 2012). Many samples give lower temperatures of c. 600 °C, but they probably record post-peak cooling or Proterozoic metamorphism of the Archaean bedrock, because these rocks are normally migmatised, indicating high metamorphic temperatures.

Low P/T orthopyroxene-bearing, normally garnet-free granulite facies rocks occur slocally in the Western Karelia Province, but medium-pressure granulites, metamorphosed at c. 9–11 kbar and 800–850 °C, are only found in the Iisalmi complex near the western border of the Western Karelia subprovince (Hölttä and Paavola 2000). Sanukitoid suite granodiorites north of the Ilomantsi greenstone complex locally contain orthopyroxene, but it is not clear whether the mineral assemblages in these rocks were metamorphic or magmatic (Halla and Heilimo 2009). Amphibolites and paragneisses near these charno-enderbites were metamorphosed in upper amphibolite and granulite facies at c. 6.5–7.5 kbar and 670–750 °C (Hölttä et al. 2012).

3.7.2 Greenstone Belts

Garnet-bearing samples form supracrustal rocks in the Ilomantsi belt that typically have the assemblage grt-bt-pl-qtz±ms, locally with andalusite and staurolite or more commonly their muscovite-filled pseudomorphs. Grt-bt thermometry for these samples indicates in most

cases crystallization at c. 550–590 °C (Hölttä et al. 2012), similarly to the results of O'Brien et al. (1993) and Männikkö (1988), and these temperatures are in accordance with the observed mineral associations. In the NE part of the Ilomantsi greenstone belt, sillimanite is also present in pelitic rocks, and temperatures from grt-bt thermometry are also higher than in the SE, being c. 600–625 °C. Pressures indicated by the grt-bt-pl-qtz barometer are c. 3.5–5.5 kbar in the central parts of the greenstone belt but > 6 kbar in the NW in the sillimanite-bearing metasediments (Hölttä et al. 2012). The lower pressures are of the same order as those obtained by Männikkö (1988) using sphalerite barometry for samples from the Kovero greenstone belt SW of Ilomantsi. Garnet grains in the Ilomantsi belt samples are commonly zoned, with cores richer in Mg than rims, indicating decreasing PT conditions during garnet growth.

Previous studies on the Kuhmo-Suomussalmi greenstone belt have resulted in evidence of a decrease in metamorphic grade from outer to inner parts of the belt. According to Tuisku (1988), geothermometry suggests metamorphic temperatures as low as 500 °C for the inner and up to 660 °C for the outer parts of the belt. Pressures obtained using the sphalerite barometer applied to sphalerite inclusions in pyrite are mostly between 6–7 kbar but range in some cases as high as c. 13 kbar (Tuisku 1988).

An interesting observation was made for a patch of garnet-bearing amphibolites east of the Kuhmo greenstone belt. Noting the standard tholeiite basaltic whole-rock composition of these amphibolites, it is surprising that they do not comprise any matrix plagioclase, but only minor albite and oligoclase inclusions in garnet. The observed ranges of the anorthite content in the plagioclase inclusions in two microanalysed samples are An_{10}–An_{30} and An_1–An_{20}, indicating that some of the inclusions are almost pure albite. The garnet hosts are rich in grossular (X_{grs} 0.25–0.35, $X_{grs} = Ca/(Fe+Mn+Mg+Ca)$) and spessartine ($X_{sps}$ 0.10–0.12) but Mg-poor (X_{prp} 0.05–0.09), which indicates that the metamorphic temperatures were not very high during garnet crystallization. These rocks generally contain epidote, commonly only as inclusions in garnet but locally also in the matrix. If an albitic composition An_1 of plagioclase is used in the average P calculation, the Thermocalc gives average pressures of c. 16–17 kbar at 600–700 °C.

3.7.3 Age of Archaean High-Grade Metamorphism

Because the bulk of TTGs and volcanic rocks in the greenstone belts are from juvenile Neoarchaean additions to the crust, it is not surprising that signs of Mesoarchaean metamorphic events are difficult to distinguish in the preserved small enclaves of Mesoarchaean rocks. Mänttäri and Hölttä (2002) interpreted a c. 3.1 Ga zircon population to be metamorphic in the 3.2 Ga rocks of the Iisalmi complex. Käpyaho et al. (2007) found an obviously metamorphic zircon population of 2.84–2.81 Ga in a palaeosome of a 2.94 Ga migmatite west of the Kuhmo greenstone belt. However, most of the observed high-grade metamorphism and deformation appears Neoarchaean in age.

In the Western Karelia subprovince the ion probe U-Pb data on zircon and monazite from granulites and from leucosomes of migmatites appear to indicate partial melting over a broad time interval from 2.72–2.61 Ga (Hölttä et al. 2000a; Mänttäri and Hölttä 2002; Mutanen and Huhma 2003; Käpyaho et al. 2007; Lauri et al. 2011). Titanite from amphibolite facies rocks also yields broadly similar U-Pb ages. Zircon grains from leucosomes in the Iisalmi granulites give ages from 2.71–2.65 Ga. These age data indicate that migmatisation was a long-lasting event, and mostly coeval with GGM magmatism. The youngest Sm-Nd garnet-whole rock ages in the Iisalmi complex granulites are < 2.5 Ga, which indicates that cooling to the closure temperatures of the Sm-Nd system lasted until the Proterozoic era (Hölttä et al. 2000a).

3.7.4 Eclogites of the Belomorian Province

Archaean eclogites are found in the Belomorian Province at Gridino and Salma (Fig. 3.1).

Eclogites fall into three age groups. Mesoarchaean 2.88–2.86 Ga and 2.82–2.81 Ga eclogites are found only from the Salma area in the northern Belomorian province but Neoarchaean 2.72 Ga eclogites are known from both Gridino and Salma (Volodichev et al. 2004; Shchipansky and Konilov 2005; Mints et al. 2010a, b; Shchipansky et al. 2012a, b). Eclogites form up to tens of metres sized fragments and layers in TTG gneisses.

In the northern Belomorian province Mesoarchaean eclogites are found in fault bounded mélange zones whose length is several tens of kilometres. Some of the eclogites are rich in Fe and Ti and some are high-Mg picritic rocks. Garnetites and kyanite-bearing trondhjemites are associated with eclogites. Eclogites Garnetites are assumed to have been produced by the metasomatic alteration of eclogites (Shchipansky et al. 2012a, b; Mints et al. 2010b). Based on their composition (FeO*/MgO—0.5–2.5) eclogites are classified as tholeiitic basic rocks. Their REE concentration is 2–12 times that of chondrite, and their REE distribution pattern is either flat or weakly fractionated (La_N/Sm_N—0.99–1.8; Ga_N/Yb_N—0.77–1.17). Some of them are slightly enriched in Nb relative to Th and La (Shichipansky et al. 2012b). Compositionally, eclogites represent MORB and oceanic plateau basalts or gabbros. Kyanite-bearing trondhjemites have adakitic compositions, and they form small veins in eclogites. They are interpreted as melting products of eclogites in a subductional setting (Shchipansky and Konilov 2005).

In the northern Belomorian province metamorphic conditions for the eclogite-facies metamorphism are estimated at P ~ 13–14 kbar and T ~ 700–750 °C (Konilov et al. 2010; Mints et al. 2010b). However, signs of "pre-eclogite-facies" metamorphism in the form of inclusions of chlorite, zoisite and even pumpellyite-actinolite-albite intergrowth in garnet have been observed. Commonly the primary eclogite mineral assemblages (omphacite-garnet-amphibole-quartz-rutile) are replaced by diopside-plagioclase symplectites during decompression and later eclogites have partly altered into amphibolites. Younger granulite facies overprints have also been identified in eclogitic rocks (Shchipansky and Konilov 2005; Konilov et al. 2010).

Geochronological studies of eclogites suggest that Mesoarchaean oceanic rocks were metamorphosed at eclogite facies at 2.88–2.87 Ga and 2.82–2.81 Ga. The early retrograde alterations of eclogites were close in time to eclogitization. Symplectitic eclogites were metamorphosed at 2.72–2.70 Ga, 2.53–2.08 Ga and 1.91–1.89 Ga (Konilov et al. 2010; Kaulina 2010; Shchipansky et al. 2012b; Mints et al. 2010a, b).

Neoarchaean eclogites have been described from the Gridino and Salma areas. Neoarchaean eclogites in the Gridino area, together with amphibolites, ultrabasic rocks, TTG gneisses and zoisitites, form a part of a metamorphosed melange which constitutes a fault-bounded zone (Slabunov 2008). This zone is cross-cut by a swarm of near-N-S-trending Palaeoproterozoic mafic dykes whiche were also eclogitized to a varying degree.

In the Gridino area eclogites have the mineral assemblage omphacite-garnet-quartz-rutile ± kyanite, thermobarometric studies show that they were metamorphosed at c. 14–17.5 kbars and 740–865 °C (Volodichev et al. 2004). Pre-eclogite amphibolite-facies mineral assemblages (epidote, amphibole, carbonate, quartz and albite inclusions in cores of garnet grains) have been identified in the eclogites (Perchuk and Morgunova 2011; Volodichev and Slabunov 2011). Retrograde plagioclase-diopside symplectites after omphacite and amphibole-plagioclase-biotite assemblages after garnet are common in the Gridino eclogites. They were produced by decompression during the exhumation of the rocks (Volodichev et al. 2004), probably simultaneously with intrusion of small enderbite stocks and veins.

An ion microprobe study of zircon from Gridino eclogite gave an age of 2720 ± 8 Ma Ma, which probably is the age of eclogite facies metamorphism (Volodichev et al. 2004). This age is in good agreement with the geological data: the mélange is cross-cut by massive 2701 Ma trondhjemite veins (Volodichev et al. 2004). Geochronological data are difficult to interpret because eclogite-facies metamorphism was not the only metamorphic event. The area was also metamorphosed during the Palaeoproterozoic, as shown by c. 1.9 Ga zircon generations (Bibikova et al.

2003; Skublov et al. 2011) and by re-equilibration of Sm-Nd isotopic systems in minerals at that time (Kaulina and Apanasevich 2005).

Zircon grains of 2.72 Ga have been described also from eclogites in Salma (Konilov et al. 2010; Shchipansky et al. 2012a, b; Mints et al. 2010b). These Neoarchaean eclogites seem to be separated by a fault from Mesoarchaean eclogites. A contact between these two complexes is visible in the Kuru-Vaara quarry (Shchipansky et al. 2012a). Neoarchaean eclogites in the Kuru-Vaara area are classified as amphibole eclogites (omphacite + garnet + amphibole + rutile), metamorphosed at peak temperatures of 680–720 °C and pressures of up to 20 kbar (Shchipansky et al. 2012a). Based on their chemical composition, these eclogites are classified as low-K tholeiitic basalts whose REE concentration is similar with N-MORB. Some of them show an U-shaped or boninite-like REE distribution pattern. The formation of Neoarchaean eclogites is attributed to subduction where the oceanic crust submerged to a depth of at least 50 km.

3.7.5 Proterozoic Metamorphism

The Archaean bedrock in the western part of the Karelia Province underwent strong reheating during the Palaeoproterozoic Svecofennian orogeny. Evidence of this includes, for example, that biotite and hornblende sampled from the Archaean rocks have K-Ar ages typically in the range 1.8–1.9 Ga. Archaean K-Ar mineral ages are only present in samples from the Iisalmi and Taivalkoski granulites and the Ilomantsi complex (Kontinen et al. 1992; O'Brien et al. 1993). The heating of the Archaean crust has been explained by its burial under a massive overthrust nappe complex ca. 1.9 Ga ago (Kontinen et al. 1992).

Numerous ductile shear zones were developed in the Archaean bedrock during the Svecofennian orogeny. The widths of these shear zones vary from tens of metres to several kilometres (Kohonen et al. 1991). In many places the Proterozoic shearing was associated with high hydrous fluid flows and related chemical alteration, which is reflected, for instance, in alkali-deficient compositions and kyanite- and cordierite-bearing assemblages in originally TTG rocks (Pajunen and Poutiainen 1999). In some zones almost all Archaean rocks were ductilely deformed during the Svecofennian orogeny. West of the Iisalmi granulite complex, Archaean granulite facies mineral assemblages were decomposed in the Proterozoic metamorphism that took place at c. 550–650 °C and 5–6 kbar (Mänttäri and Hölttä 2002). Similar temperatures and pressures for the Proterozoic metamorphic overprint have also been reported near the Kuhmo greenstone belt (Pajunen and Poutiainen 1999). Deformation microstructures in the sanukitoid granodiorites near the Ilomantsi complex indicate temperatures of 400–500 °C during Proterozoic metamorphism (Halla and Heilimo 2009).

3.8 Palaeomagnetism

Several palaeomagnetic studies on Archaean rocks have been carried out in the Karelia Province, but only in a few cases has stable Archaean remanent magnetization unaffected by Proterozoic overprinting been revealed. The main use of palaeomagnetic data in Archaean geology has been in reconstructing the past positions and movement of the craton at different times and comparing its position with other similar-aged cratons. Continental reconstructions have been made particularly with the Superior Province because of the considerable geological similarity between these two cratonic masses. This section reviews the palaeomagnetic data from Archaean rocks in Finland and NW Russia, and present models of the Archaean plate configurations of the Karelia and the Superior Provinces.

The 2913 ± 30 Ma Shilos metabasaltic rocks located NW of Lake Onega in NW Russia, with preserved remanent magnetization estimated at 2800 Ma (Arestova et al. 2000 and references therein), are the oldest rocks from the Karelia Province for which palaeomagnetic data are presently available. Another case of old remanence is from the NW of Lake Onega, where the 2890 Ma Semch River gabbro-diorite is interpreted to preserve its primary magnetic remanence (Gooskova

and Krasnova 1985). However, in both cases the age of remanence is defined based on comparison to the APWP (Elming et al. 1993). Therefore, due to poor age constraints, the data are not used in either case for continental reconstructions.

The most reliable Neoarchaean palaeomagnetic data from the Western Karelia Province are obtained from the granulite facies enderbites in the Iisalmi area (Neuvonen et al. 1981, 1997; Mertanen et al. 2006a), from the orthopyroxene-bearing sanukitoids NW of the Ilomantsi area (Mertanen and Korhonen 2008, 2011) and from the Panozero sanukitoid in the Vodlozero subprovince (Lubnina and Slabunov 2009). Younger, well-defined Neoarchaean data come from the Shalskiy gabbronorite dyke and granulite-grade gneisses in the Vodlozero subprovince in NW Russia (Krasnova and Gooskova 1990; Mertanen et al. 2006b). Common to all these cases is that they are generally well-preserved from the 1.9–1.8 Ga Svecofennian overprinting, they show high magnetic anomalies compared to surrounding TTG gneisses and their remanence has high stability, the directions of remanence clearly differing from the known Proterozoic remanences.

The sanukitoids NW of the Ilomantsi complex and the Iisalmi enderbites show a steep characteristic remanence component, but in the former inclination is negative and in the latter positive (Mertanen et al. 2006a; Mertanen and Korhonen 2011). It is interpreted that the steep remanence directions record the long-lasting Neoarchaean metamorphic event at different times, during which the polarity of the Earth's magnetic field has reversed at least once. The remanence of the sanukitoids NW of Ilomantsi is regarded as ca. 2.7 Ga ($^{207}Pb/^{206}Pb$ monazite age of 2685 Ma, Halla 2002) and the Iisalmi granulite complex as ca. 2.6 Ga (Sm-Nd garnet-whole rock ages 2590–2480, Hölttä et al. 2000a). Based on these data the Karelia Province moved from a high polar palaeolatitude of 83° to the palaeolatitude of c. 68°, respectively. The overall data from Ilomantsi and Iisalmi thus imply that at c. 2.7–2.6 Ga the Western Karelia subprovince was located at high palaeolatitudes.

The palaeomagnetic pole of Panozero differs significantly from those NW of Ilomantsi and in Iisalmi (Lubnina and Slabunov 2009). The difference between the poles can be explained by the different locations of the Vodlozero and Western Karelia subprovinces during the early Neoarchaean. It is possible that in the time interval of 2.77–2.74 Ga the Karelian subprovinces were separated, and the final joining of separate terranes took place at 2.70–2.65 Ga (Slabunov et al. 2011). Alternatively, it is also possible that the two terranes were joined already at ca. 2.77–2.74 Ga, and the amalgamated craton drifted from low palaeolatitudes to higher palaeolatitudes between 2.74 and 2.68 Ga.

3.9 Discussion

3.9.1 Adakitic Features of TTGs

The mutual compositional similarity of TTGs and modern adakites has been the basis of a suggestion of petrogenetic kinship between the two rock suites (Martin 1999; Martin et al. 2005). Adakites are spatially related to subduction, and the most likely source of their parental magmas has been the basaltic part of a subducted oceanic slab. They seem to be related to an environment where the subduction zone is abnormally hot, allowing the subducting slab to melt (Moyen 2009). Numerical and petrological models suggest that partial melting of a subducting slab is possible at 60–80 km depth, but only when the subducting oceanic crust is very young (<5 Ma), and therefore hot, or as a consequence of heating under abnormally high stresses in the subduction shear zone (Defant and Drummond 1990, 1993; Peacock et al. 1994). However, according to Gutscher et al. (2000), most of the known Pliocene-Quaternary adakite occurrences are related to the subduction of 10–45 Ma lithosphere, which, according to numerical models, should not produce melt under normal subduction zone thermal gradients. Gutscher et al. (2000) addressed this by flat subduction that can produce the temperature and pressure conditions necessary for the fusion of moderately old oceanic crust. Variation in the subduction angle has been proposed as a critical factor also controlling the variation observed

in geochemical features of the Archaean TTGs. Smithies et al. (2003) proposed that Archaean subduction was predominantly flat and that the subduction regimes thus lacked well-developed mantle wedges that would produce melts or interact with possible slab-derived melts, in the latter case increasing the compatible element content and Mg contents of the slab melts.

Recently, the usage of the terms adakite, and especially adakite-like, has been expanded to encompass a wide range of rocks that exhibit the high Sr/Y and La/Yb ratios but not necessarily the other criteria of the original adakite definition. This loose usage has led Moyen (2009) to recommend that separate, more precise terms should be used to describe these "adakitic" rocks, and the term adakite should be reserved only for the high-silica adakites that closely correspond to the rocks originally described as adakites by Defant and Drummond (1990). Halla et al. (2009) argued that the term adakite should only be used for unmistakable slab melts, and therefore not for such rocks as the TTGs in the Karelia Province. Smithies (2000) also argued that despite the many compositional similarities, most Archaean TTGs actually differ from Cenozoic adakites, especially in that they have on average lower Mg# and higher SiO_2 contents, suggesting that, unlike adakitic melts, the TTG melts did not interact with mantle peridotite.

High Sr/Y and La/Yb ratios can have several causes, such as high Sr/Y sources, garnet-present melting and interactions with the mantle (Moyen 2009). Melts with an adakitic geochemical signature can also be generated by normal crystal fractionation processes from andesitic parental melts, and slab melting is not compulsory for adakite petrogenesis; but, adakites or adakite-like rocks can instead originate in various geodynamic settings (Castillo et al. 1999; Castillo 2006; Richards and Kerrich 2007; Petrone and Ferrari 2008).

Modelling by van Hunen et al. (2004) suggests that if mantle temperatures were indeed higher during the Archaean than presently, even flat subduction was an unlikely process. If this was the case, the obvious lack of interaction with mantle in many TTGs must be explained in some other way. Halla et al. (2009) attributed the low-HREE TTG group to high-pressure partial melting (>20 kbar) of a garnet-bearing basaltic source with little evidence of subsequent mantle contamination. The high-HREE group was generated by significantly lower pressure melting (c. 10 kbar) of a garnet-poor basaltic crust and shows interaction with the mantle by its higher Mg#, Cr and Ni contents. Halla et al. (2009) proposed that the high-HREE TTGs were produced in an incipient, hot subduction zone underneath a thick oceanic plateau/protocrust. For the low-HREE TTGs, they saw a non-subduction setting as probable, proposing that these rocks were generated by deep melting in the lower parts of thick domains of basaltic oceanic crust.

3.9.2 TTG Melts and PTX Relations of their Protoliths

There is a general agreement that the Archaean TTG suite rocks were formed by partial melting from a compositionally basaltic-gabbroic source. The process was evidently fluid-absent partial melting of amphibolites at temperatures of 900–1100 °C and over a large pressure range from 10 to 25 kbar. The composition of products from partial melting is controlled by pressure and temperature, the composition of the source, water availability during the process and the degree of melting. The composition of the partial melts is further modified, for instance, by magma mixing, fractional crystallization and wall rock contamination on their way from the loci of melting to the crystallization sites (Rapp et al. 1991; Martin 1995; Martin and Moyen 2002; Foley et al. 2002; Rapp et al. 2003; Moyen and Stevens 2006; Moyen 2011).

During the fusion process, pressure and temperature control the assortment and abundance of the residual minerals, such as garnet and plagioclase, and consequently the major and trace element content of the TTG melts. For example, the heavy REE is controlled by residual garnet, which is stable in mafic rocks at pressures above c. 9–12 kbar and increases in abundance with increasing pressure. Sr is controlled by plagioclase, which is stable below c. 15–20 kbar. Nb and Ta

depend on the presence of residual rutile, which is stable above c. 16–18 kbar (Foley et al. 2002; Moyen and Stevens 2006; Moyen 2011).

In the low-HREE TTG group with positive Eu anomalies, Sr and Sr/Y ratios are high and Nb low. Positive Eu could be explained by plagioclase accumulation, but as TTGs in this group are no more enriched in Al_2O_3, CaO or Na_2O than the other low-HREE TTGs, it is more probable that they represent melting with residual rutile and garnet. In dacitic and rhyolitic melts, the garnet-melt partition coefficients are higher for Sm (2.66) and Gd (10.5) than for Eu (1.5) (Rollinson 1993). Thus, high pressure melting with abundant garnet in the residue would obviously lead to melts that are HREE poor, and show a positive Eu/Eu* ratio, which is also predicted by experimental work (e.g. Springer and Seck 1997).

The melting temperature strongly depends on the starting composition, and the solidus temperatures for arc basalts; tholeiitic basalts and komatiitic basalts are thus highly different (Moyen and Stevens 2006). The trace element composition of melts principally depends on their protolith concentrations, but through control of the mineral composition of the restite, the major element content of the protolith also affects the trace element composition of the coexisting melt. According to Nair and Chacko (2008), the increase in residual garnet from 5 to 15 wt% changes the La/Yb ratio in the melt fraction from c. 12 to c. 24. Variation in the La/Yb ratio of the melts may be considerable, even under constant P and T, if there is enough compositional variation in the source. Figure 3.12 shows simplified pseudosections with melting curves and breakdown curves of amphibole, orthopyroxene, garnet and rutile for two compositionally deviating samples analysed from amphibolite intercalations in TTGs, representing tholeiitic and komatiitic basalts with 1 wt.% H_2O. The pseudosections were constructed using the Perple_X 6.6.6 software (Connolly 1990, 2005; Connolly and Petrini 2002, http://www.perplex.ethz.ch/). The composition has a strong influence on the melting temperature but also on the mineral stability fields. In Na_2O and Al_2O_3-poor komatiitic basalt, plagioclase decomposes at pressures that are c. 7–10 kbar lower than in the case of basaltic composition (Fig. 3.12). This means that in >800ºC temperatures komatiitic basalt can produce melts with elevated Sr at pressures that are far below the c. 19–21 kbar range that is broadly the upper stability limit of plagioclase in tholeiitic basalts in these temperatures. Also, in komatiitic basalt rutile is present at several kbar lower pressures than in tholeiitic basalt, and consequently komatiitic basalt can produce Nb and Ta depleted melts at lower pressures than tholeiitic basalt.

According to the model calculations, also the abundance of garnet is strongly dependent on the composition so that at above c. 10 kbar the komatiitic basalt produces roughly twice as much garnet as the tholeiitic basalt (Fig. 3.12). Consequently in TTG melts the La/Yb ratio may significantly differ only on the basis of the composition of the protolith.

Sanukitoids and quartz diorites are partly too Mg-rich to represent melts from crustal sources. The high Sr content and low La_N/Yb_N ratio indicate that the quartz diorites originated from a hot and shallow mantle environment, where the temperature was so high that plagioclase was not stable, and the pressure so low that little garnet was present in the residue. Figure 3.13 shows the proportion of residual garnet during the dehydration melting of amphibolite, and the corresponding La/Yb ratios in the derived melts, according to the experimental work of Nair and Chacko (2008). The garnet mode in the residue in the case of QQs and high-HREE TTGs would have been 5–15 wt%, and much higher in low-HREE TTGs. This could reflect higher pressures of melting in the case of the low-HREE TTGs, but could also indicate a compositionally different source, which would promote a higher garnet mode in the residue.

In the Archaean Earth, low pressure TTGs could have formed, for example, at the base of thick oceanic plateaus (deWit and Hart 1993; Moyen and Stevens 2006). In the greenstone belts, most sequences of mafic volcanic rocks of plateau basalt signatures are not compositionally homogeneous, but typically comprise a variety of compositionally different tholeiitic and komatiitic basalts and komatiites. In addition,

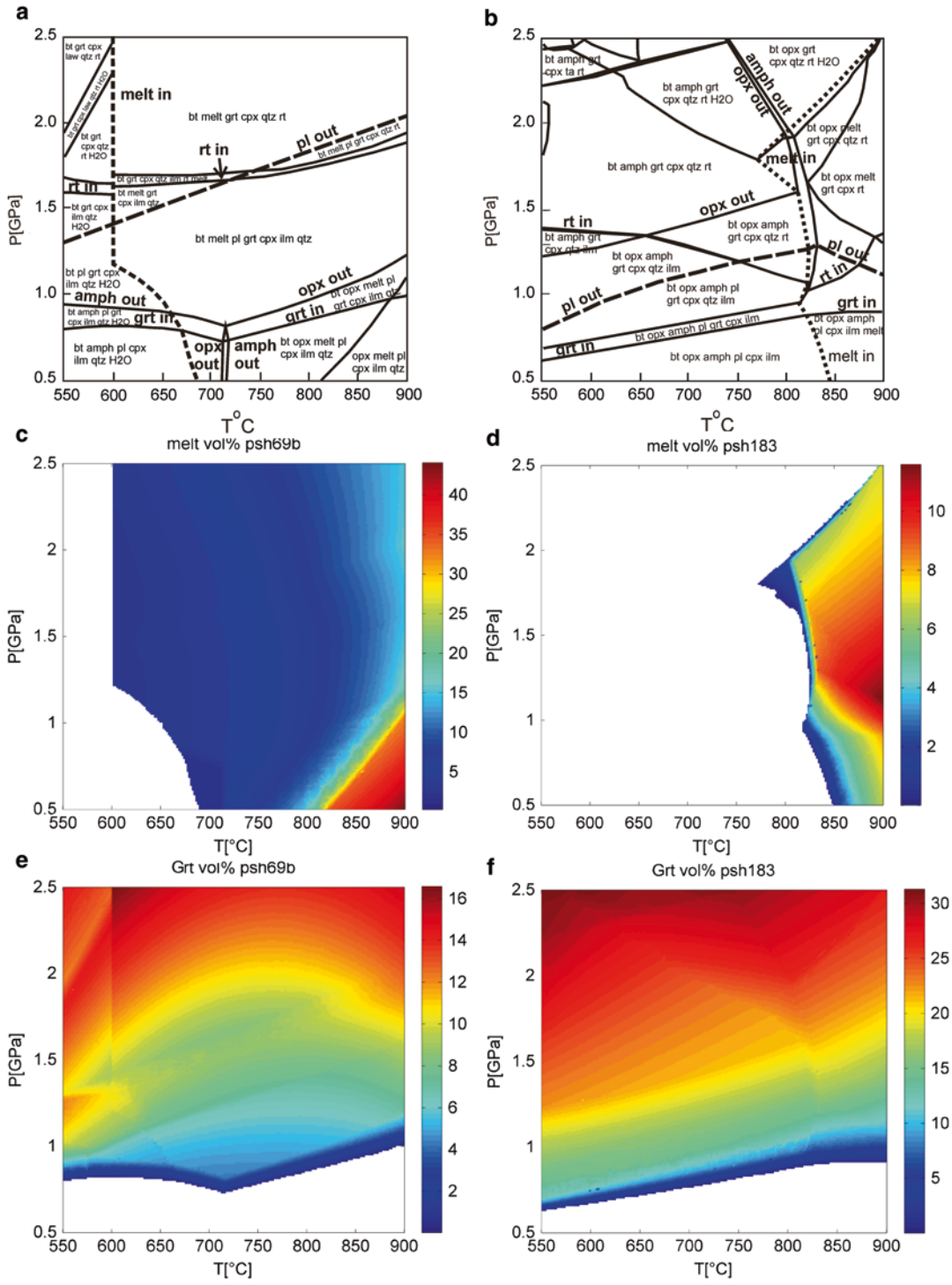

Fig. 3.12 NCKFMASHTi pseudosections for Fe-rich basaltic granulite (psh69b) and komatiitic basalt (psh183) and lower and upper stability limits of various minerals in these two whole-rock compositions. The solution models used in calculations were: biotite (TCC), amphibole (GlTrTsPg), garnet (HP), orthopyroxene (HP), clinopyro-

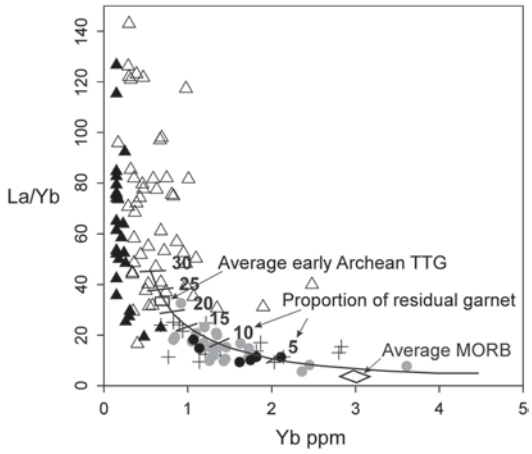

Fig. 3.13 La/Yb ratios of Karelian TTGs plotted on the La/Yb diagram after Nair and Chacko (2008), showing the effect of the abundance of residual garnet on the La/Yb ratio of the melt in 20 % melt fraction during dehydration melting of amphibolite. *Black triangles* = low-HREE TTGs, *crosses* = high-HREE TTGs, *grey dots* = QQs, *black dots* = orthopyroxene-bearing QQs (enderbites)

many greenstone belts also contain calc-alkaline basalts and andesites-dacites. Modern oceanic plateaux, such as the Kerguelen Plateau, consist of intermediate, felsic and alkaline volcanic rocks, as well as sediments (Frey et al. 2000). It is evident from the above discussion that melting of such heterogeneous packages would produce melts that would also be compositionally heterogeneous and show variable trace element patterns, even in cases where the melting depth was not very high or highly variable.

3.9.3 Greenstone Belts

A picture emerging from previous research suggests that the Karelia Province was a collage of TTG and greenstone complexes that originated in various tectonic settings related to subduction, collision, continental rifting and mantle plumes (Bibikova et al. 2003; Samsonov et al. 2005; Slabunov et al. 2006a, b; Papunen et al. 2009). The greenstone belts have also been interpreted as composite terranes comprising magmatic products from various tectonic settings involving plumes and arc magmatism (Puchtel et al. 1998, 1999). Archaean greenstone belts can be divided into autochthonous to parautochthonous and allochthonous based on their relationship with the underlying basement rocks (Polat and Kerrich 2000, 2006). According to Thurston (2002), evidence from the Superior Province suggests that many, if not all, greenstone sequences were in autochthonous or parautochthonous units fed from mantle plumes either in continental rift or continental platform settings. Allochthonous models favour the assembly of greenstone belts by horizontal tectonic transport and accretion of various types of oceanic crust in a plate-tectonic geodynamic regime (e.g. Puchtel et al. 1998, 1999; Percival et al. 2004, 2006; Polat and Kerrich 2006). The presence of such features as fold and thrust complexes, orogen-parallel strike-slip faults and tectonically juxtaposed terranes from different tectonic settings, as well as subduction zone geochemical signatures in part of the plutonics and volcanics in the greenstone belts, supports the concept that the accretion of alloch-

xene (HP), plagioclase (h), ilmenite (WPH), melt (HP). For the original references see http://www.perplex.ethz.ch/PerpleX_solution_model_glossary.html. Compositions used (in wt.%) are:

	psh69b	psh183
SiO_2	59.63	47.3
TiO_2	1.00	0.347
Al_2O_3	13.53	11.5
FeO	9.68	8.54
MgO	2.65	14.2
CaO	5.49	11.7
Na_2O	3.45	1.16
K_2O	1.97	0.918
H_2O	1.0	1.0

thonous terranes was elemental in the growth of many greenstone belts (Polat and Kerrich 2006).

Many komatiite-bearing sequences in Archaean greenstone belts have been interpreted as pieces of dismembered Archaean oceanic plateaux (Kusky and Kidd 1992; Abbott and Mooney 1995; Puchtel et al. 1998). Many greenstone belts are characterized by assemblages that suggest roughly coeval plume-type komatiite-tholeiitic basaltic and arc-type calc-alkaline volcanism. This situation has been explained in the Karelia Province in terms of a subduction setting where the arc-type plutonic volcanic rocks formed at the margins of plume-generated thick basalt plateaux that were not able to subduct because of their buoyant nature (Puchtel et al. 1998, 1999). Interlayering of komatiites with subduction-related volcanic rocks has been explained by the interaction of plume and subduction related magmas in such a subduction regime (Grove and Parman 2004).

Grove and Parman (2004) proposed that Archaean komatiites could have been formed by hydrous melting in a subduction environment, which would easily explain the close spatial and temporal association of many komatiites and island arc type volcanic rocks. This idea, which is supported by the experimental work of Barr et al. (2009), is still disputable, however. For example, based on their work on komatiites in Ontario and Barberton, Arndt et al. (2004) and Stiegler et al. (2010) saw little evidence for the hypothesis of hydrous melting.

3.9.3.1 The Kuhmo Greenstone Belt—an Oceanic Plateau?

The basic-ultrabasic volcanic assemblages in the Kuhmo greenstone belt consist of komatiites and their evolved counterparts, i.e. komatiitic basalts. The komatiite-basalt sequence is completely devoid of epiclastic and chemical interflow sediments, and it lacks geochemical evidence of contamination by any significantly older continental material. These data suggest an eruptive setting far from continental land masses and hydrothermal vents at oceanic ridges, and argues against the origin of the Kuhmo greenstone belt within a continental rift zone, as has been proposed, for instance, by Papunen et al. (2009). Immobile trace element (Zr, Y, Nb, Th) systematics are also inconsistent with the formation in a back-arc setting, but rather suggest an oceanic plateau setting and magma derivation from a mantle plume. The Al-undepleted nature and the trace element characters of the komatiites indicate that they were derived from a source more similar to primitive upper mantle rather than that of depleted MORBs. Furthermore, there is negligible geochemical evidence for the involvement of crust or enriched or recycled mantle sources (EM1, EM2, HIMU). Condie (2005) stressed the clustering of non-arc-related Archaean basalts, in terms of HFSE ratios, close to the primitive mantle values, and suggested on this basis that Archaean mantle plumes had their main source in the "primitive mantle". Our findings support this conclusion, indicating that the late Archaean mantle was less fractionated, or better stirred, than either the early Archaean and post-Archaean mantle.

The U-Pb zircon data (Huhma et al. 2012a) and the Sm-Nd data (Huhma et al. 2012b) on the Kuhmo volcanic rocks provide no evidence for their deposition on a significantly older basement in the Kuhmo region. Felsic volcanic rocks in the central part of the Kuhmo belt formed 2.80 Ga ago, giving the minimum age for the mafic-ultramafic magmatism (Huhma et al. 2012a). We conclude that the Kuhmo komatiites represent fissure-controlled eruptions onto a pre-existing rhyolitic-dacitic-tholeiitic oceanic plateau.

3.9.3.2 The Ilomantsi Greenstone Belt—a Volcanic Arc within an Attenuated Continental Margin?

Komatiites within the Ilomantsi greenstone belt, which is located c. 150 km SSE of the Kuhmo belt, were emplaced within a volcano-sedimentary basin. Magmatism was dominated by felsic volcanism in two major pulses and coeval granitoid plutons. The komatiites were emplaced as thin but extensive sheet flows, and probably also as sills beneath the felsic volcanic edifices. The komatiites and dacites-rhyolites occur intercalated, suggesting that ultrabasic and felsic volcanism was coeval. Both the komatiites and the felsic volcanic rocks have distinctly low

Nb/Th, suggesting that the komatiites contain a significant component assimilated from the felsic volcanic rocks. Alternatively, the komatiites could have inherited their arc-signature from a subduction-enriched mantle wedge. However, we consider this model less likely, because the samples enriched in lithophile-incompatible elements are depleted in PGE, which is best explained by the segregation of a sulphide melt from the magma in response to contamination by sulphidic metasediments during emplacement. There is evidence of a significantly older cryptic granitoid basement in the region in the form of inherited c. 3.0 Ga zircon grains in plutonic and subvolcanic felsic rocks and old T_{DM} ages of metasedimentary units in the Ilomantsi belt (Vaasjoki et al. 1993; Huhma et al. 2012a, b). We suggest that the Ilomantsi volcanic rocks represent arc magmatism within an attenuated continental margin where older basement rocks were assimilated by younger arc magmatism.

3.9.4 The Greenstone Belts of the Belomorian Province—an Archaean Subduction System?

The Keret belt arc-type volcanic rocks, the Chupa belt metagraywackes, interpreted as fore-arc basin sediments, an ophiolite-like Central Belomorian greenstone belt and the Salma eclogite-bearing mélange form the 2.88–2.82 Ga lateral sequence. This sequence likely represents an arc-subduction-accretion system, in which arc-type volcanic rocks and metagreywackes belong to the suprasubduction zone whereas the ophiolitic and eclogites are part of a subducting slab. This system vanished at 2.82 Ga, and the accretion of the arc-ophiolite complexes gave rise to the first fragment of a continental crust.

The 2.81–2.78 Ga sequence consists of basalt-komatiite, suprasubduction ophiolite and island-arc complexes that include a large fraction of adakite-series rocks, TTGs, fore-arc basin metagraywackes, a medium pressure granulite-enderbite-charnockite complex and eclogites. These complexes mark an oceanic plateau, a back-arc spreading basin, a volcanic island-arc zone, a fore-arc basin, a deep section of a suprasubduction zone and fragments (2.82–2.80 Ga eclogites) of a subducting slab (Slabunov 2013). The fact that adakites are abundant among the island-arc volcanics formed in this period is consistent with the subduction concept.

After a short, c. 25 Ma period of no tectonic activity, subduction continued and a new island-arc complex was formed. A new continental crust was not generated over the next 20 Ma. The last growth event of the sialic crust began at 2.73 Ga and continued for 25–30 Ma. During this period the Gridino and Shirokaya Salma-Kuru-Vaara eclogites, calc-alkaline island-arc volcanics, molybdenum-bearing gabbro-diorite-granodiorite intrusions and a granulite-enderbite complex were formed, probably at a convergent boundary during subduction in an active continental margin setting (Slabunov 2013).

3.9.5 Supercontinent Reconstruction

Several similarities in their geological evolutions can be cited in support of the concept that the Archaean Superior, Hearne and Karelia Provinces were parts of the Neoarchaean-Palaeoproterozoic supercontinent Superia (Bleeker and Ernst 2006).

Comparison of palaeomagnetic data from the Karelia Province with similar-aged poles from the Superior Province (Mertanen and Korhonen 2011, and references therein) shows that Superior was also located at relatively high palaeolatitudes at 2.68–2.60 Ma (Figs. 3.14a, b). However, the Karelia and Superior Provinces were significantly separated, as there is a c. 30° difference between the latitudes both at 2.68 Ga and 2.60 Ga. Taking into account the maximum errors of the poles from both cratons, the latitudinal distances become shorter, and it may be possible that they were even joined at that time. The relative palaeopositions of the two cratons cannot be resolved unequivocally, especially at 2.68 Ga, due to the nearly polar position of the Karelia Province, which allows its rotation in several directions with respect to Superior.

The steeply inclined remanence of the Iisalmi and Ilomantsi rocks differs distinctly from the

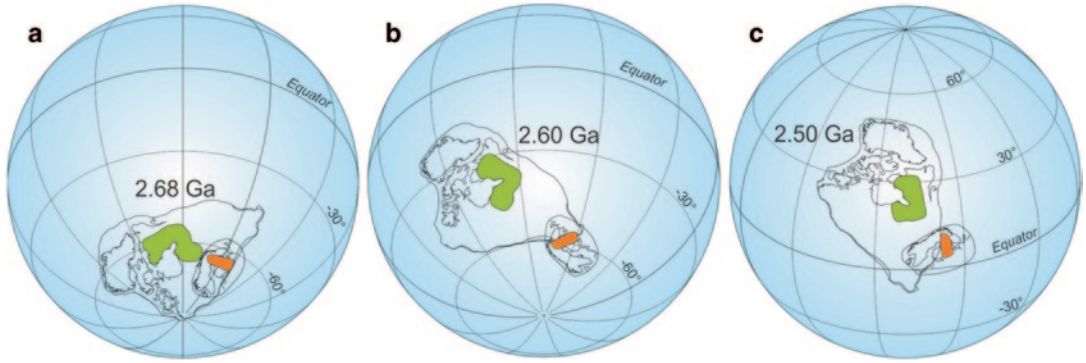

Fig. 3.14 Continental reconstructions between the Karelia and Superior cratons at 2.68 Ga (**a**), 2.60 Ga (**b**) and 2.50 Ga (**c**)

2.50 Ga remanence of the Shalskiy gabbronorite dyke dated at 2510 ± 1.6 Ma in the Vodlozero subprovince (Bleeker et al. 2008). The Shalskiy dyke, as well as the Shalskiy basement gneisses and Vodla River gneisses ca. 50 km east of the Shalskiy dyke, has a shallow southwards pointing remanence direction (Krasnova and Gooskova 1990; Mertanen et al. 2006b) which is interpreted to be 2.50 Ga. This remanence direction positions the Karelia Province at a low equatorial palaeolatitude. The data thus suggest substantial movement of the Karelia Province between the time of cooling at c. 2.60 Ga after the high grade metamorphism and subsequent rifting and minor reworking of the craton at c. 2.50 Ga.

Palaeomagnetic reconstruction between Karelia and Superior Provinces at 2.50 Ga is presented in Fig. 3.14c. Compared with the 2.6 Ga configuration, the palaeopositions between Karelia and Superior are now completely different. The Superior Province had drifted across the equator to the latitude of approximately 20° and rotated clockwise by about 45°, so that at 2.50 Ga both provinces were located near the equator, and the Karelia Province along the southern margin of the Superior Province. This (Slabunov 2008, 2010) reconstruction is in close agreement with the Superia model of Bleeker and Ernst (2006), who suggested that the provinces were together at 2.50 Ga.

3.9.6 Tectonic Evolution of the Karelia Province

If the Karelia province was indeed once a part of the supercontinent Superia, then many of the observations and models presented for the evolution of the Superior and Hearne Provinces must also be applicable to the Karelia Province. Several major characteristics in the crustal architecture and composition of the Superior province have long been considered to provide strong support for the operation of modern-style plate tectonics during the Neoarchaean (e.g. Goodwin 1968; Langford and Morin 1976; Card 1990). Tectonic build-up of the province, mostly between 2.72–2.68 Ga, is interpreted in terms of accretionary growth process that involved collisions of many microcontinental blocks and juvenile volcanic arcs (Percival et al. 2006).

Accretionary-type orogeny is commonly considered one of the main processes behind growth of continental crust with time (Şengör and Natal'in 1996; Cawood et al. 2003; Brown 2009). It may also be applicable to Archaean granite–greenstone complexes, as these are commonly characterized by linear belt structures in which early accretion of formations from various oceanic tectonic environments and microcontinents is followed by arc-type magmatism (e.g. Kusky and Polat 1999; Bibikova et al. 1999, 2003; Samsonov et al. 2005). Neoarchaean accretion of exotic terranes at c. 2.83–2.75 Ga, culminating in a subsequent major collisional event/orogeny at around 2.73–2.67 Ga, may have been the mecha-

nism that generated the basic structure of the Karelia Province, and which was then strongly reworked during the Svecofennian orogeny. The subduction events enriched the lithospheric mantle in LIL elements. At c. 2.76 Ga, a new volcanic arc began to form above a subduction zone at the margin of the Western Karelia Province, represented now by the Ilomantsi plutonic-volcanic complex. A subsequent slab breakoff or some other subduction-related process at c. 2.72 Ga led to melting of the enriched wedge mantle, producing voluminous sanukitoids and also small amounts of TTGs (Lobach-Zhuchenko et al. 2008; Halla et al. 2009; Heilimo et al. 2010, 2011).

Kontinen et al. (2007) interpreted SHRIMP and TIMS U-Pb age determinations on zircon grains from the paragneiss mesosomes and cross-cutting granitoid plutons to constrain the deposition of protolith wackes to c. 2.70 Ga. Some caution should be taken with this interpretation, as the newly obtained precise age of 2715 ± 2 Ma for the Loso sanukitoid intrusion (Huhma et al. 2012a), which crosscuts the local Nurmes type paragneisses, suggests that metamorphic effects may have influenced the youngest ages obtained for detrital zircon grains in the paragneisses. Deposition more likely took place in a short (10 Ma or less) period just before 2715 Ma, and it is possible that deposition of the Nurmes sediments and sanukitoid plutonism were partly overlapping events. Trace element and U–Pb data suggest that the source comprised mainly 2.75–2.70 Ga TTG and/or sanukitoid-type plutonic and mafic volcanic rocks. The close similarity of the paragneiss and sanukitoid compositions is an important clue to the timing and tectonic setting of the deposition. It is clear that TTG-dominated crust, presently characterizing the Western Karelia subprovince, was not the dominant source of the Nurmes sediments. The presence of MORB-type volcanic intercalations in Nurmes wackes suggests that they were deposited in a back arc or intra-arc setting (Kontinen et al. 2007). The exotic nature of the Nurmes sediments as overthrust must be considered as a serious option.

After the intrusion of the last juvenile granitoids, the QQ quartz diorites at 2.70 Ga, the crust was deformed and metamorphosed. The related process could have been collisional stacking after closure of ocean basins, which thickened the crust between 2.71–2.64 Ga. Vibroseismic images of the crust, as well as tectonic observations from the exposed bedrock, indicate ductile thrusting and related crustal stacking with tectonic transportation from southeast to northwest (Kontinen and Paavola 2006; Korja et al. 2006; Sorjonen-Ward 2006). A similar seismic structure characterised by gently dipping, commonly listric reflections, is also common in other Neoarchaean cratons, and it is interpreted to result from horizontal compression (van der Velden et al. 2006). Fragments of Mesoarchaean (micro) continents, such as the Siurua and Iisalmi complexes, are present as slices in the thickened Neoarchaean crust. Reflecting heat production by radioactive decay in the thickened, predominantly felsic-granitoid crust, a Barrovian-type medium P/T metamorphic framework was developed. The middle and lower parts of the crust were partially melted, producing migmatites and the GGM suite intrusions (Mänttäri and Hölttä 2002; Käpyaho et al. 2007; Lauri et al. 2011).

The thickness of the Neoarchaean crust in the Iisalmi complex was at least c. 40 km on the basis of c. 10–11 kbar pressures from the granulites that represent lower crust and bear evidence of long-term residence at high-temperatures (Mänttäri and Hölttä 2002). The significance of the amphibolite facies high-pressure rocks from the other areas is more problematic to interpret as these rocks record a geothermal gradient that is lower than the normal continental gradient. Apart from Kuhmo garnet-amphibolites, other examples of Archaean high P/T rocks in the Fennoscandian Shield are the eclogites in the Belomorian Province which were metamorphosed at c. 700–800 °C and c. 14–17 kbar, possibly even at pressures exceeding 20 kbar (Volodichev et al. 2004; Mints et al. 2010a; Shchipansky et al. 2012b), i.e. in an eclogite–high-pressure granulite (E-HPG)-type environment, which is consistent with subduction of crustal rocks into the mantle depths (Brown 2007). In Kuhmo the rocks metamorphosed under high pressure only seem to occur in a restricted area surrounded by amphibolite facies rocks that were metamorphosed at c. 6–7 kbar. Therefore, their exhumation might

be explained by similar subduction-related tectonic processes that exhume high-pressure rocks at present convergent margins (Beaumont et al. 1996, 1999; Agard et al. 2009).

The Ilomantsi greenstone belts shows low pressure metamorphism at 3.5–5.5 kbar and 550–600 °C, which indicates a gradient that is warmer than the normal continental geotherm. These rocks are juxtaposed with migmatites that normally show pressures of c. 6–8 kbar, and in the Kuhmo amphibolite even 15–16 kbar, which represents the amphibole-epidote eclogite facies in the classification of Brown (2009). The duality of thermal environments is typical for modern plate tectonics, where the belts representing different gradients are juxtaposed by plate tectonic processes (Brown 2009). Although the metamorphic structure in the Karelia Province is not quite similar to that in modern subduction-related orogenic belts, the significant differences in the metamorphic gradient between adjacent domains is easy to explain by subductional/collisional processes that assembled rocks representing various geodynamic settings.

One major problem is that we do not currently have a clear conception of the extent to which the present crustal structure is due to Archaean accretion/thickening or to Palaeoproterozoic orogenic events. Nevertheless, at least the western and eastern parts of the Karelia Province were strongly reworked in the Palaeoproterozoic Svecofennian and Lapland–Kola orogenies, when it was compressionally thickened and subjected to medium P/T type amphibolite facies metamorphism at 1.9–1.8 Ga (Kontinen et al. 1992; Daly et al. 2001, 2006; Bibikova et al. 2001b).

3.10 Conclusions

1. The Western Karelia Province mostly consists of Neoarchaean gneissic granitoids, whereas Palaeoarchaean and Mesoarchaean granitoids (>2.9 Ga) are only locally present. The granitoid rocks are classified into four main groups, which are the TTG (tonalite-trondhjemite-granodiorite), sanukitoid, QQ (quartz diorite-quartz monzodiorite) and GGM (granodiorite-granite-monzogranite) groups. Most ages obtained from TTGs are between 2.83–2.72 Ga, and they define two age groups separated by a c. 20 Ma time gap. TTGs are 2.83–2.78 Ga in the older group and 2.76–2.72 Ga in the younger group. Sanukitoids have been dated at 2.74–2.72 Ga, QQs at c. 2.70 Ga and GGMs at 2.73–2.66 Ga. Based on REE, the TTGs fall into two major compositional groups, low-HREE TTGs and high-HREE TTGs, which originated at different crustal depths; but, the compositions of their protoliths had a significant effect on the REE patterns. Sanukitoids are interpreted as products of melting of subcontinental metasomatized mantle. The GGM group represents partial melting of pre-existing TTG crust that also caused high-grade metamorphism and migmatisation.
2. Existing isotope data on volcanic rocks of the Kuhmo greenstone belt do not provide much evidence for their deposition on significantly older basement in intracratonic environment. The composition of the komatiites in Kuhmo indicates that they were derived from primitive upper mantle, representing fissure-controlled eruptions onto a pre-existing oceanic plateau. The volcanic rocks in the Ilomantsi greenstone belt represent arc magmatism within an attenuated continental margin where older basement rocks were assimilated by younger arc magmatism. Metamorphic evolution of the greenstone belts differs from that of the surrounding migmatites, indicating late-tectonic juxtaposition of greenstone belts and TTG migmatites.
3. At least four discrete subductional systems of 2.88−2.82 Ga, 2.81−2.78 Ga, c. 2.75 Ga and 2.74–2.72 Ga were identified in the greenstone belts of the Belomorian Province. Greywacke units were formed in fore-arc basins at 2.88−2.82 Ga and at c. 2.78 Ga. Volcanic rocks were generated at c. 2.70 Ga in extensional settings which arose fom the orogenic collapse. In the Belomorian Province there are three age groups (2.88−2.87 Ga, 2.82−2.80 Ga and 2.72 Ga) of crustal eclogites which were derived from oceanic basalts and high-Mg rocks in subductional processes.

4. Neoarchaean accretion of exotic terranes at c. 2.83–2.75 Ga and subsequent crustal stacking at around 2.73–2.68 Ga is a possible mechanism that largely generated the present structure of the Karelia Province, although it was again strongly reworked during the Svecofennian orogeny.

Acknowledgements Yildirim Dilek and Jaana Halla are thanked for reviews that greatly improved the manuscript. This work was partly supported by the Russian Foundation for Basic Research (grant nr 11-05-00168-a).

References

Abbott DH, Mooney WD (1995) Crustal structure and evolution: support for the oceanic plateau model of continental growth. Rev Geophys (Supplement, US National Report to the IUGG):231–242

Agard P, Yamato P, Jolivet L, Burov E (2009) Exhumation of oceanic blueschists and eclogites in subduction zones: timing and mechanisms. Earth-Sci Rev 92:53–79

Alekseev NL, Balagansky VV, Zinger TF et al (2004) Late Archean History of the Belomorian Mobile Belt and the Karelia Craton Junction Zone, Baltic Shield. Doklady Earth Sci 397A:743–746

Arestova NA, Gooskova EG, Krasnova AF (2000) Palaeomagnetism of the Shilos Structure rocks in the Southern Vygozero greenstone belt, East Karelia. Fizika Zemli (Earth Physics—English translation) 5:70–75

Arndt NT, Lesher CM, Houl MG, Lewin E, Lacaze Y (2004) Intrusion and crystallization of a Spinifex-textured komatiite sill in Dundonald Township, Ontario. J Petrol 45:2555–2571

Barnes SJ, Roeder PL (2001) The range of spinel compositions in terrestrial mafic and ultramafic rocks. J Petrol 42:2279–2302

Barr JA, Grove TL, Wilson AH (2009) Hydrous komatiites from commondale, South Africa: an experimental study. Earth Planetary Sci Lett 284:199–207

Beaumont C, Ellis S, Hamilton J, Fullsack P (1996) Mechanical model for subduction-collision tectonics of Alpine-type compressional orogens. Geology 24:675–678

Beaumont C, Ellis S, Pfiffner A (1999) Dynamics of sediment subduction-accretion at convergent margins: short-term modes, long-term deformation, and tectonic implications. J Geophys Res 104:17573–17602

Benn K, Mareschal J-C, Condie KC (2006) Introduction: archean geodynamics and environments. In: Benn K, Mareschal J-C, Condie KC (eds) Archean geodynamics and environments. Geophysical monograph 164:1–5

Berman RG (1988) Internally-consistent thermodynamic data for stoichiometric minerals in the system Na_2O-K_2O-CaO-MgO-FeO-Fe_2O_3-Al_2O_3-SiO_2-TiO_2-H_2O-CO_2. J Petrol 29:445–522

Berman RG (1991) Thermobarometry using multiequilibrium calculations: a new technique with petrologic applications. Can Mineral 29:833–855

Bibikova EV, Slabunov AI, Bogdanova SV et al (1999) Early magmatism of the Belomorian mobile belt (Baltic Shield):lateral zonation and isotopic age. Petrology 7:123–146

Bibikova EV, Glebovitskii VA, Claesson S et al (2001a) New isotopic data on the protolith age and evolutionary stages of the Chupa formation, Belomorian belt. Geochem Int 39(1):12–17

Bibikova E, Skiöld T, Bogdanova S et al (2001b) Titanite-rutile thermochronometry across the boundary between the Archaean Craton in Karelia and the Belomorian Mobile Belt, eastern Baltic Shield. Precambrian Res 105:315–330

Bibikova EV, Ihlen PM, Marker M (2001c) Age of hydrothermal alteration leading to garnetite and kyanite pseudo-quarzite formation in the Khizovaara segment of the archaean Keret greenstone belt, Russian Karelia In: SVEKALAPKO. 6th Workshop. Lammi. Finland. University of Oulu, Finland, Department of Geophysics report p 15.

Bibikova EV, Samsonov AV, Shchipansky AA, Bogina MM, Gracheva TV, Makarov VA (2003) The Hisovaara Structure in the Northern Karelian Greenstone Belt as a Late Archean Accreted Island Arc:isotopic geochronological and petrological evidence. Petrology 11(3):261–290

Bibikova EV, Bogdanova SV, Glebovitskii VA et al (2004) Evolution of the Belomorian Belt: NORDSIM U-Pb zircon dating of the Chupa Paragneisses, magmatism and metamorphic stages. Petrology 12(3):195–210

Bibikova EV, Petrova A, Claesson S (2005) The temporal evolution of sanukitoids in the Karelian Craton, Baltic Shield:an ion microprobe U–Th–Pb isotopic study of zircons. Lithos 79:129–145

Blake TS, Buick R, Brown SJA et al (2004) Geochronology of a Late Archaean flood basalt province in the Pilbara Craton, Australia: constraints on basin evolution, volcanic and sedimentary accumulation, and continental drift rates. Precambrian Res 133:143–173

Bleeker W, Ernst R (2006) Short-lived mantle generated magmatic events and their dyke swarms:the key unlocking Earth's palaeogeographic record back to 2.6 Ga. In: Hanski E, Mertanen S, Rämö OT and Vuollo J (eds) Dyke Swarms—time markers of crustal evolution: proceedings of the fifth international Dyke conference 2005 Rovaniemi, 31 July–3 Aug 2005, Fourth International Dyke Conference, Kwazulu-Natal, 26–29 June 2001. Taylor, Francis Group, London, pp 3–26

Bleeker W, Hamilton MA, Ernst RE, Kulikov VS (2008) The search for Archean-Paleoproterozoic supercratons; new constraints on Superior-Karelia-Kola correlations within supercraton Superia including the

first ca 2504 Ma (Mistassini) ages from Karelia. 33rd international geological congress abstracts
Blichert-Toft J, Albarede F (1994) Short-lived chemical heterogeneities in the Archean mantle with implications for mantle convection. Science 263:1593–1596
Borisova EYu, Bibikova EV et al (1997) U–Pb age and nature of magmatic complex of Seryak mafic zone (the Belomorian Mobile Belt) Baltic Shield. Terra Nova Abstracts 9, P:132
Boynton WV (1984) Cosmochemistry of the rare earth elements: meteorite studies. In: Henderson P (ed) Rare earth element geochemistry. Elsevier, Amsterdam, pp 63–114
Brown M (2007) Metamorphic conditions in orogenic belts: a record of secular change. International Geology Review 49:193–234
Brown M (2009) Metamorphic patterns in orogenic systems and the geological record. In: Cawood PA, Kröner A (eds) Earth accretionary systems in space and time vol 318. The geological society London special publications, pp 37–74
Card KD (1990) A review of the superior province of the Canadian shield, a product of Archean accretion. Precambrian Res 48:99–156
Castillo PR (2006) An overview of adakite petrogenesis. Chinese Science Bulletin 51(3):257–268
Castillo PR, Janney PE, Solidum RU (1999) Petrology and geochemistry of Camiguin Island southern Philippines:insights to the source of adakites and other lavas in a complex arc setting. Contrib Mineral Petrol 134:33–51
Cawood P, Kröner A, Windley B (2003) Accretionary orogens:definition character significance. Geophys Res Abs 5:04856
Champion DC, Smithies RH (2007) Geochemistry of Paleoarchean granites of the East Pilbara Terrane, Pilbara Craton, Western Australia: implications for early Archean crustal growth. Dev Precambrian Geol 15:369–409
Condie KC (1998) Episodic continental growth and supercontinents:a mantle avalanche connection? Earth Planetary Sci Lett 163:97–108
Condie KC (2000) Episodic continental growth models: afterthoughts and extensions. Tectonophysics 322:153–162
Condie KC (2005) High field strength element ratios in Archean basalts:a window to evolving sources of mantle plumes? Lithos 79:491–504
Condie KC, Benn K (2006) Archean geodynamics: similar to or different from modern geodynamics. In: Benn K, Mareschal J-C, Condie KC (eds) Archean Geodynamics and Environments Geophysical Monograph 164:47–60
Connolly JAD (1990) Multivariable phase-diagrams—an algorithm based on generalized thermodynamics. Am J Sci 290:666–718
Connolly JAD (2005) Computation of phase equilibria by linear programming: a tool for geodynamic modeling and its application to subduction zone decarbonation. Earth Planetary Sci Lett 236:524–541
Connolly JAD, Petrini K (2002) An automated strategy for calculation of phase diagram sections and retrieval of rock properties as a function of physical conditions. J Metamorphic Geology 20:697–708
Corcoran PL, Mueller WU, Kusky TM (2004) Inferred ophiolites in the Archean Slave Craton. In: Kusky TM (ed) Precambrian ophiolites and related rocks. Dev in Precambrian Geology 13:363–404
Daly JS, Balagansky VV, Timmerman MJ, Whitehouse MJ et al (2001) Ion microprobe U-Pb zircon geochronology and isotopic evidence supporting a trans-crustal suture in the Lapland Kola Orogen, northern Fennoscandian Shield. Precambrian Res 105:289–314
Daly JS, Balagansky VV, Timmerman MJ et al (2006) The Lapland-Kola Orogen: Palaeoproterozoic collision and accretion of the northern Fennoscandian lithosphere. In: Gee DG, Stephenson RA (eds) European lithosphere dynamics. Geological Society of London Memoir 32:579–598
Defant MJ, Drummond MS (1990) Derivation of some modern arc magmas by melting of young subducted lithosphere. Nature 367:662–665
Defant MJ, Drummond MS (1993) Mount St Helens:potential example of the partial melting of the subducted lithosphere in a volcanic arc. Geology 21:547–550
deWit MJ, Hart RA (1993) Earth's earliest continental lithosphere hydrothermal flux and crustal recycling. Lithos 30:309–335
deWit MJ (1998) On Archean granites greenstones cratons and tectonics: does the evidence demand a verdict? Precambrian Res 91:181–226
Dilek Y, Polat A (2008) Suprasubduction zone ophiolites and Archean tectonics. Geology 36:431–432
Dilek Y, Furnes H (2011) Ophiolite genesis and global tectonics: geochemical and tectonic fingerprinting of ancient oceanic lithosphere. Geol Soc Am Bull 123:387–411
Elming S-Å, Pesonen LJ, Leino MAH et al (1993) The drift of the Fennoscandian and Ukrainian Shields during the Precambrian: a Palaeomagnetic analysis. Tectonophysics 223:177–198
Foley S, Tiepolo M, Vannucci R (2002) Growth of early continental crust controlled by melting of amphibolite in subduction zones. Nature 417:837–840
Frey FA, Coffin MF, Wallace PJ et al (2000) Origin and evolution of a submarine large igneous province: the Kerguelen Plateau and Broken Ridge, southern Indian Ocean. Earth and Planetary Sci Lett 176:73–89
Goodwin AM (1968) Archean protocontinental growth and early crustal history of the Canadian shield. 23rd International Geological Gongress. Prague 1:69–89
Gooskova EG, Krasnova AN (1985) Palaeomagnetism of the basic Archean and Proterozoic intrusions of the eastern part of the Baltic Shield. Izvestia Akademii Nauk SSSR ser Fizika Zemli (Earth Physics—English translation) 21:366–373
Grove TL, Parman SW (2004) Thermal evolution of the Earth as recorded by komatiites. Earth and Planetary Sci Lett 219:173–187

Gruau G, Tourpin S, Fourcade S et al (1992) Loss of isotopic (Nd, O) and chemical (REE) memory during metamorphism of komatiites: new evidence from eastern Finland. Contrib Mineral Petrol 112:66–82

Gutscher M-A, Maury R, Eissen J-P et al (2000) Can slab melting be caused by flat subduction? Geology 28(6):535–538

Halla J (2002) Origin and Paleoproterozoic reactivation of Neoarchean high-K granitoid rocks in eastern Finland. PhD thesis, University of Helsinki, Finland. Annales Academica Scientiarium Fennicae, Geologica-Geographica, vol 163

Halla J (2005) Late Archean high-Mg granitoids (sanukitoids) in the southern Karelian domain eastern Finland:Pb and Nd isotopic constraints on crust-mantle interactions. Lithos 79:161–178

Halla J, Heilimo E (2009) Deformation-induced Pb isotope exchange between Kfeldspar and whole rock in Neoarchean granitoids:implications for assessing Proterozoic imprints. Chem Geol 265:303–312

Halla J, van Hunen J, Heilimo E et al (2009) Geochemical and numerical constraints on Neoarchean plate tectonics. Precambrian Res 174:155–162

Hamilton WB (1998) Archean magmatism and tectonics were not products of plate tectonics. Precambrian Res 91:143–179

Hamilton WB (2011) Plate tectonics began in Neoproterozoic time and plumes from deep mantle have never operated. Lithos 123:1–20

Heilimo E, Halla J, Hölttä P (2010) Discrimination and origin of the sanukitoid series: geochemical constraints from the Neoarchean western Karelian Province (Finland). Lithos 115:27–39

Heilimo E, Halla J, Huhma H (2011) Single-grain zircon U–Pb age constraints of the western and eastern sanukitoid zones in the Finnish part of the Karelian Province. Lithos 121:87–99

Heilimo E, Halla J, Mikkola P (2012) Neoarchean sanukitoid series intrusions in the Karelian domain eastern Finland. Geological Survey of Finland Special Paper 54:213–224

Heilimo E, Halla J, Andersen T et al (2013) Neoarchean crustal recycling and mantle metasomatism: Hf–Nd–Pb–O isotope evidence from sanukitoids of the Fennoscandian shield. Precambrian Res 228:250–266

Hirose K (2010) The Earth's missing ingredient. Scientific American 302(6):58–65

Hölttä P (1997) Geochemical characteristics of granulite facies rocks in the Varpaisjärvi area central Fennoscandian Shield. Lithos 40:31–53

Hölttä P, Paavola J (2000) P-T-t development of Archaean granulites in Varpaisjärvi Central Finland I: effects of multiple metamorphism on the reaction history of mafic rocks. Lithos 50:97–120

Hölttä P, Huhma H, Mänttäri I et al (2000a) P-T-t development of Archaean granulites in Varpaisjärvi, Central Finland II: Dating of high-grade metamorphism with the U-Pb and Sm-Nd methods. Lithos 50:121–136

Hölttä P, Huhma H, Mänttäri I et al (2000b) Petrology and geochemistry of mafic granulite xenoliths from the Lahtojoki kimberlite pipe, eastern Finland. Lithos 51:109–133

Hölttä P, Balagansky V, Garde AA et al (2008) Archean of Greenland and Fennoscandia. Episodes 31(1):1–7

Hölttä P, Heilimo E, Huhma H et al (2012) The Archaean of the Karelia Province in Finland. Geological Survey of Finland Special Paper 54:21–72

Huhma H, Mänttäri I, Peltonen P et al (2012a) The age of the Archaean greenstone belts in Finland. Geological Survey of Finland Special Paper 54:73–174

Huhma H, Kontinen A, Mikkola P et al (2012b) Nd isotopic evidence for Archaean crustal growth in Finland. Geological Survey of Finland Special Paper 54:175–212

Jones DL (1990) Synopsis of late Palaeozoic and Mesozoic terrane accretion within the Cordillera of western North America. In: Dewey JF, Gass IG, Curry GB, Harris NBW, Sengör AMC (eds) Allochthonous Terranes. Cambridge University Press, Cambridge, pp 23–30

Jones DL, Howell PG, Coney PJ et al (1983) Recognition character and analysis of tectonostratigraphic terranes in western North America. J of Geol Educ 31:295–303

Kaulina TV (2010) Obrazovanie i preobrazovanie zirkona v polimetamorficheskizh kompleksazh (Formation and recrystallization of zircons in polymetamorphic complexes). KNC RAN, Apatity pp 1–114

Kaulina T, Apanasevich E (2005) Late archaean eclogites of the Kola Peninsula (NE Baltic shield): U-Pb and Sm-Nd data. In: Proyer A, Ettinger K (eds) 7nd International Eclogite Conference. Mitteilungen der Österreichischen Mineralogischen Gesellschaft, vol 150, p 64

Käpyaho A, Mänttäri I, Huhma H (2006) Growth of Archaean crust in the Kuhmo district, eastern Finland: U-Pb and Sm-Nd isotope constraints on plutonic rocks. Precambrian Res 146:95–119

Käpyaho A, Hölttä P, Whitehouse M (2007) U-Pb zircon geochronology of selected Neoarchaean migmatites in eastern Finland. Bull of the Geol Soc of Finland 79(1):95–115

Kohonen J, Luukkonen E, Sorjonen-Ward P (1991) Nunnanlahti and Holimäki shear zones in North Karelia: evidence for major early Proterozoic ductile deformation of Archean basement and further discussion of regional kinematic evolution. In: Geological Survey of Finland, Current Research 1989-1990. Geological Survey of Finland. Special Paper 12:11–16

Konilov A, Shchipansky AA, Mints MV et al (2010) The Salma Eclogites of the Belomorian Province, Russia: HP/UHP Metamorphism through the subduction of Mesoarchean oceanic crust). In: Dobrzhinetskaya LF, Faryad SW, Wallis S, Cuthbert S (eds) Ultrahigh-pressure metamorphism 25 years after the discovery of Coesite and Diamond. Elsevier, London p 623

Kontinen A, Paavola J (2006) A preliminary model of the crustal structure of the eastern Finland Archaean complex between Vartius and Vieremä based on constraints from surface geology and FIRE 1 seismic survey. Geological Survey of Finland Special Paper 43:223–240

Kontinen A, Paavola J, Lukkarinen H (1992) K-Ar ages of hornblende and biotite from Late Archaean rocks of eastern Finland—interpretation and discussion of tectonic implications. Geological Survey of Finland Bulletin 365:31

Kontinen A, Käpyaho A, Huhma H et al (2007) Nurmes paragneisses in eastern Finland Karelian craton: provenance tectonic setting and implications for Neoarchaean craton correlation. Precambrian Res 152:119–148

Korenaga J (2006) Archean geodynamics and the thermal evolution of Earth. In: Benn K, Mareschal J-C, Condie KC (eds) Archean Geodynamics and Environments. Geophysical Monograph 164:7–32

Korja A, Lahtinen R, Heikkinen P et al (2006) A geological interpretation of the upper crust along FIRE 1. Geological Survey of Finland Special Paper 43:45–76

Kozhevnikov VN (2000) Arzheiskie zelenokamennie pojsa Karel'skogo kratona kak akkreshionnie orogeni (Archean greenstone belts of the Karelian Craton as accretionary orogens). KNC RAN, Petrozavodsk, pp 1–223

Kozhevnikov VN, Samsonov AV, Shchipansky AA (2005) Arzheiskii Zhizovarskii zelenokamennii kompleks v raione ozera Verzhnee (Archean greenstone complex of the Hisovaara structure, Lake Verzhnee area). In: Volodichev OI, Slabunov AI (eds) Belomorian mobile belt and its analogues: geology, geochronology, geodynamics and metallogeny. Extended Abstracts and Field Trip Guide Book. KarRC RAS, Petrozavodsk, pp 31–52

Kozhevnikov VN, Berezhnaya NG, Presnyakov SL et al (2006) Geochronology (SHRIMP-II) of zircon from archean lithotectonic associations in the greenstone belts of the Karelia craton: implications for stratigraphic and geodynamic reconstructions Stratigraphy and Geological Correlation 14:240–259

Kozhevnikov VN, Shchipansky AA (2008) Neoarchean Khizovaara Greenstone complex in the lake Verkhneye area. In: Peltonen P, Hölttä P, Slabunov A (eds) Karelian Craton transect (Finland, Russia): Precambrian greenstone belts, ophiolites and eclogites. 33rd International Geological Congress, Excursion No 18. Oslo, p 33

Krasnova AF, Gooskova EG (1990) Geodynamic evolution of the Vodlozero block of Karelia according to palaeomagnetic data. Izvestiya Earth Physics 26:80–85

Kröner A, Layer PW (1994) Crust formation and plate motion in the early Archean. Science 256:1405–1411

Kusky TM, Kidd WSF (1992) Remnants of an Archean oceanic plateau Belingwe greenstone belt, Zimbabwe. Geology 20:43–46

Kusky TM, Polat A (1999) Growth of granite-greenstone terranes at convergent margins and stabilization of Archean cratons. Tectonophysics 305:43–73

Kusky TM, Li JH, Raharimahefa T et al (2004) Origin and emplacement of Archean ophiolites of the Central Orogenic Belt, North China Craton. In: Kusky TM (ed) Precambrian ophiolites and related rocks. Dev in Precambrian Geol 13:223–282

Langford FF, Morin JA (1976) The development of the Superior Province of northwestern Ontario by merging island arcs. Am J of Sci 276:1023–1034

Lauri LS, Andersen T, Hölttä P et al (2011) Evolution of the Archaean Karelian Province in the Fennoscandian Shield in the light of U–Pb zircon ages and Sm–Nd and Lu–Hf isotope systematics. J of the Geol Soc London 167:1–18

Levchenkov OA, Mil'kevich RI, Miller YuV et al (2003) U–Pb isotope age of metaandesites in the upper sequence of the Tikshozero Greenstone Belt (Lake Verkhnie Kichany, Northern Karelia). Doklady Earth Sciences 389A:384–387

Lobach-Zhuchenko SB, Chekulaev VP, Stepanov VS et al (1998) The white sea foldbelt—late Archean accretion- and collision-related zone of the Baltic Shield. Doklady Earth Sciences 358:34–37

Lobach-Zhuchenko SB, Arestova NA, Chekulaev VP et al (1999) Evolution of the Yuzhno-Vygozero greenstone belt, Karelia. Petrology 7(2):160–176

Lobach-Zhuchenko SB, Arestova NA, Mil'kevich RI et al (2000a) Stratigraphy of the Kostomuksha Belt in Karelia (Upper Archean) as Inferred from Geochronological, Geochemical, and Isotopic Data. Stratigraphy and Geological Correlation 8(4):319–326

Lobach-Zhuchenko SB, Chekulaev VP, Arestova NA et al (2000b) Archean terranes in Karelia: geological and isotopic–geochemical evidence. Geotectonics 34(6):452–466

Lobach-Zhuchenko SB, Rollinson HR, Chekulaev VP et al (2005) The Archaean sanukitoid series of the Baltic Shield: geological setting, geochemical characteristics and implications for their origin. Lithos 79:107–128

Lobach-Zhuchenko SB, Rollinson H, Chekulaev VP et al (2008) Petrology of a late Archaean highly potassic sanukitoid pluton from the Baltic Shield: insights into late Archaean mantle metasomatism. J of Petrol 49(3):393–420

Lubnina NV, Slabunov AI (2009) Paleomagnetism in the Neoarchean Polyphase Panozero Intrusion in the Fennoscandian Shield. Moscow University Geology Bulletin 64(6):346–353

Luukkonen EJ (1992) Late Archaean and early Proterozoic structural evolution in the Kuhmo-Suomussalmi terrain eastern Finland. Publications of the University of Turku, Series A II Biologica—Geographica—Geologica, University of Turku, vol. 78

Männikkö KH (1988) Myöhäisarkeeisen Koveron liuskejakson länsiosan deformaatio ja metamorfoosi. Pohjois-Karjalan malmiprojekti, Raportti 15. Oulu: Oulun yliopisto (Metamorphism and deformation of the late Archaean Kovero schist belt. North Karelian Ore Project, Report 15, University of Oulu, in Finnish)

Mänttäri I, Hölttä P (2002) U-Pb dating of zircons and monazites from Archean granulites in Varpaisjärvi central Finland: evidence for multiple metamorphism and Neoarchean terrane accretion. Precambrian Res 118:101–131

Martin H (1995) The Archean grey gneisses and the genesis of the continental crust. In: Condie KC (ed) The Archean crustal evolution. Elsevier, Amsterdam, pp 205–259

Martin H (1999) The adakitic magmas: modern analogues of Archaean granitoids. Lithos 46:411–429

Martin H, Moyen J-F (2002) Secular changes in tonalite-trondhjemite-granodiorite composition as markers of the progressive cooling of Earth. Geology 30(4):319–322

Martin H, Auvray B, Blais S et al (1984) Origin and geodynamic evolution of the Archean crust of eastern Finland. Bullet Geol Soc Finland 56:135–160

Martin H, Smithies RH, Rapp R et al (2005) An overview of adakite tonalite–trondhjemite–granodiorite (TTG) and sanukitoid: relationships and some implications for crustal evolution. Lithos 79:1–24

Mertanen S, Pesonen LJ, Hölttä P et al (2006a) Palaeomagnetism of Palaeo-proterozoic dolerite dykes in central Finland. In: Hanski E, Mertanen S, Rämö OT, Vuollo J (eds) Dyke Swarms—time markers of crustal evolution. Proceedings of the fifth international Dyke Conference IDC5 Rovaniemi Finland 31 July–3 August 2005. Taylor Francis Group/Balkema, pp 243–256

Mertanen S, Vuollo JI, Huhma H et al (2006b) Early Paleoproterozoic-Archean dykes and gneisses in Russian Karelia of the Fennoscandian Shield—new paleomagnetic isotope age and geochemical investigations. Precambrian Res 144(3–4):239–260

Mertanen S, Korhonen F (2008) Archean-Paleoproterozoic configuration of Laurentia and Baltica focusing on paleomagnetic data from Baltica. 33rd International Geological Congress 6–14 August 2008 Oslo, Abstracts

Mertanen S, Korhonen F (2011) Paleomagnetic constraints on an Archean-Paleoproterozoic Superior-Karelia connection; new evidence from Archean Karelia. Precambrian Res 186:193–204

Mikkola P, Huhma H, Heilimo E et al (2011a) Archean crustal evolution of the Suomussalmi district as part of the Kianta Complex, Karelia; constraints from geochemistry and isotopes of granitoids. Lithos 125:287–307

Mikkola P, Salminen P, Torppa A et al (2011b) The 2.74 Ga Likamännikkö complex in Suomussalmi East Finland: lost between sanukitoids and truly alkaline rocks? Lithos 125:716–728

Mikkola P, Lauri LS, Käpyaho A (2012) Neoarchean leucogranitoids of the Kianta Complex Karelian Province, Finland: source characteristics and processes responsible for the observed heterogeneity. Precambrian Res 206–207:72–86

Mil'kevich RI, Myskova TA (1998) Pozdnefrzheiskii metaterrennie porodi Zapadnoi Karelii: litologia, geozhimia, proiszhozhdenie (Late Archean Metaterrigenous rocks of the Western Karelia: Lithology, Geochemistry and Provenances). Lithology and Mineral Res 33(2):155–171

Mil'kevich RI, Myskova TA, Glebovitsky VA (2007) Kalikorva structure and its position in the system of the Northern Karelian Greenstone Belts: geochemical and geochronological data. Geochem Int 45:428–450

Mints MV, Berzin RG, Suleĭmanov AK et al (2004) The deep structure of the early Precambrian crust of the Karelian craton, southeastern Fennoscandian shield: results of investigation along CMP profile 4B. Geotectonics 38(2):87–102

Mints MV, Belousova EA, Konilov AN et al (2010a) Mesoarchean subduction processes: 2.87 Ga eclogites from the Kola Peninsula, Russia. Geol 38:739–742

Mints MV, Blokh YuI, Gusev GS et al (eds) (2010b) Glubinnaj stroenie, evoluchij i poleznie iskopaemie rannedokembriiskogo fundamenta Vostochno-Evropeisoi platformi. Tom 1. (Deep structure, evolution and useful minerals of the Early Precambrian basement of the East European Platform. Interpretation of data from reference profile1-EB and profiles 4B and TATSEIM. Vol. 1). GEOMAP, GEOS, Moscow, pp 1–408

Moyen J-F (2009) High Sr/Y and La/Yb ratios: the meaning of the "adakitic signature". Lithos 112:556–574

Moyen J-F (2011) The composite Archaean grey gneisses: petrological significance and evidence for a non-unique tectonic setting for Archaean crustal growth. Lithos 123:21–36

Moyen J-F, Stevens G (2006) Experimental constraints on TTG petrogenesis:implications for Archean geodynamics. In: Benn K, Mareschal J-C, Condie KC (eds) Archean Geodynamics and Environments. Geophysical Monograph 164:149–176

Mutanen T, Huhma H (2003) The 3 5 Ga Siurua trondhjemite gneiss in the Archaean Pudasjärvi Granulite Belt, northern Finland. Bulletin of the Geological Society of Finland 75:51–68

Myskova TA, Glebovitskii VA, Miller YuV et al (2003) Supracrustal sequences of the Belomorian mobile belt: primary composition age and genesis. Lithol Mineral Resour 11:3–19

Nair R, Chacko T (2008) Role of oceanic plateaus in the initiation of subduction and origin of continental crust. Geology 36(7):583–586

Nehring F, Foley SF, Hölttä P et al (2009) Internal differentiation of the Archean continental crust: fluid-controlled partial melting of granulites and TTG-amphibolite associations in central Finland. J of Petrol 50(1):3–35

Neuvonen KJ, Korsman K, Kouvo O et al (1981) Paleomagnetism and age relationship of the rocks in the Main Sulphide Ore Belt in central Finland. Bulletin of the Geological Society of Finland 53:109–133

Neuvonen KJ, Pesonen LJ, Pietarinen H (1997) Remanent Magnetization in the Archaean Basement and Cutting Diabase Dykes in Finland, Fennoscandian Shield. Geophysica 33(1):111–146

O'Brien H, Huhma H, Sorjonen-Ward P (1993) Petrogenesis of the late Archean Hattu schist belt Ilomantsi eastern Finland:geochemistry and Sr Nd isotopic composition. Geological Survey of Finland Special Paper 17:147–184

O'Connor JT (1965) A classification for Quartz-rich igneous rocks based on feldspar ratios. U.S. Geological Survey Professional Paper 525-B: B79–B84

Ovchinnikova GV, Matrenichev VA, Levchenkov OA et al (1994) U-Pb and Pb-Pb isotopic studies of felsic volcanics from the Hautavaara greenstone structure, Central Karelia. Petrology 2(3):266–281

Paavola J (1986) A communication on the U-Pb and K-Ar age relations of the Archaean basement in the Lapinlahti-Varpaisjärvi area central Finland. Geological Survey of Finland Bulletin 339:7–15

Pajunen M, Poutiainen M (1999) Palaeoproterozoic prograde metasomatic-metamorphic overprint zones in Archaean tonalitic gneisses eastern Finland. Bull of the Geol Soci of Finland 71(1):73–132

Papunen H, Halkoaho T, Luukkonen E (2009) Archaean evolution of the Tipasjärvi-Kuhmo-Suomussalmi Greenstone Complex Finland. Geol Survey of Finland Bulletin 403:1–68

Patiño Douce AE (2004) Vapor-absent melting of tonalite at 15–32 kbar. J of Petrol 46(2):275–290

Peacock SM, Rushmer T, Thompson AB (1994) Partial melting of subducting oceanic crust. Earth and Planetary Sci Lett 121:227–244

Peltonen P, Mänttäri I, Huhma H et al (2006) Multi-stage origin of the lower crust of the Karelian craton from 3.5 to 1.7 Ga based on isotopic ages of kimberlite-derived mafic granulite xenoliths. Precambr Res 147:107–123

Perchuk AL, Morgunova AA (2011) Contrasting basic rock eclogitization regimes in the Gridino high-pressure complex, Karelia. In: Slabunov AI, Perchuk AL (eds) Granulite and eclogite complexes in the Earth's history. Extended Abstracts and Field Guide. Institute of Geology, Karelian Research Centre (KRC), Russian Academy of Sciences (RAS), Petrozavodsk, pp 162–164

Percival JA, McNicoll V, Brown JL et al (2004) Convergent margin tectonics, central Wabigoon subprovince, Superior Province, Canada. Precambrian Res 132:213–244

Percival J, Sanborn-Barrie M, Skulski T et al (2006) Tectonic evolution of the western Superior Province from NATMAP and Lithoprobe studies. Can J of. Earth Sci 43:1085–1117

Petrone CM, Ferrari L (2008) Quaternary adakite—Nb-enriched basalt association in the western Trans-Mexican Volcanic Belt: is there any slab melt evidence? Contrib Mineral Petrol 156:73–86

Polat A, Kerrich R (2000) Archean greenstone belt magmatism and the continental growth-mantle evolution connection: constraints from Th-U-Nb-LREE systematics of the 2.7 Ga Wawa subprovince, Superior Province, Canada. Earth and Planetary Sci Lett 175:41–54

Polat A, Kerrich R (2006) Reading the geochemical fingerprints of Archean hot subduction volcanic rocks. In: Benn K, Mareschal J-C, Condie KC (eds) Archean Geodynamics and Environments. Geophysical Monograph 164:198–213

Powell R, Holland TJB, Worley B (1998) Calculating phase diagrams involving solid solutions via non-linear equations with examples using THERMOCALC. J of Metamorphic Geol 16:577–588

Puchtel I (2004) 3.0 Ga Olondo Greenstone Belt in the Aldan Shield E Siberia. In: Kusky T (ed) Precambrian ophiolites and related rocks. Dev in Precambrian Geol, vol. 13. Elsevier, Amsterdam, pp 405–423

Puchtel IS, Hofmann AW, Mezger K et al (1998) Oceanic plateau model for continental crustal growth in the Archaean: a case study from the Kostomuksha greenstone belt, NW Baltic shield. Earth and Planetary Sci Lett 155:57–74

Puchtel IS, Hofmann AW. Amelin YuV et al (1999) Combined mantle plume–island arc model for the formation of the 2.9 Ga Sumozero-Kenozero greenstone belt, SE Baltic Shield: isotope and trace element constraints. Geochimica et Cosmochimica Acta 63:3579–3595

Puchtel IS, Brügmann GE, Hofmann AW (2001) ^{187}Os-enriched domain in an Archean mantle plume:evidence from 28 Ga komatiites of the Kostomuksha greenstone belt, NW Baltic Shield. Earth and Planetary Sci Lett 186:513–526

Rapp RP, Watson EB, Miller CF (1991) Partial melting of amphibolite/eclogite and the origin of Archaean trondhjemites and tonalites. Precambrian Res 51:1–25

Rapp RP, Shimizu N, Norman MD (2003) Growth of early continental crust by partial melting of eclogite. Nature 425(9):605–609

Rasilainen K, Lahtinen R, Bornhorst T (2007) Rock geochemical database of Finland, Manual. Geological Survey of Finland, Report of Investigation 164

Rayevskaya MB, Gor'kovets VY, Svetova AI, Volodichev OI (1992) Stratigrafij dokembria Karelii. Opornii razrezi verzhnearcheiskzh otlozhenii (Precambrian stratigraphy of Karelia. Reference sections of Upper Archean deposits). Karelian Research Centre, Russian Academy of Sciences, Petrozavodsk, pp 1–191

Richards JP, Kerrich R (2007) Adakite-like rocks: their diverse origins and questionable role in metallogenesis. Economic Geol 102(4):537–576

Rollinson H (1993) Using geochemical data: evaluation, presentation, interpretation. Pearson Education Limited, Essex

Rybakov SI, Svetova AI, Kulikov VS et al (1981) Vulkanizm arzheiskizh zelenokamennizh pojsov Karelii (Volcanism in the Archean Greenstone Belts of Karelia). Nauka, Leningrad, pp 1–154

Samsonov AV (2004) Evoluchij magmatizma granit-zelenokamennizh oblastei Vostochno-Evropeiskogo kratona (Evolution of magmatism in the granite–greenstone domains of the East European Craton), Doctoral Dissertation. Institute of Geology of Ore deposits (IGEM), Russian Academy of Sciences, Moscow, pp 1–48

Samsonov AV, Bogina MM, Bibikova EV et al (2005) The relationship between adakitic calc-alkaline volcanic rocks and TTGs: implications for the tectonic setting of the Karelian greenstone belts, Baltic Shield. Lithos 79:83–106

Şengör AMC, Natal'in BA (1996) Turkic-type orogeny and its role in the making of the continental crust. Ann Rev of Earth and Planetary Sci 24:263–337

Şengör AMC, Natal'in BA (2004) Phanerozoic analogues of Archaean oceanic basement fragments:Altaid ophiolites and ophirags. In: Kusky T (ed) Precambrian Ophiolites and Related Rocks. Dev in Precambrian Geol, vol 13. Elsevier, Amsterdam, pp 675–726

Sergeev SA (1982) Geologia i izotopnaj geologia granit-zelenokamennizh kompleksov arzhej Chentral'noi I Ugo-Vostochnoi Karelii (Geology and isotopic geochronology of Archean granite-greenstone complexes in Central and Southeast Karelia). Dissertation, University of St Petersburg, St Petersburg, pp 1–24

Sharov NV, Slabunov AI, Isanina EV et al (2010) Sejsmogeologicheskij razrez zemnoj kory po profilju GSZ—OGT "Susha-More" Kalevala-Kem'-gorlo Belogo morja (Seismic simulation of the Earth's crust on the profiles DSS–CDP Kalevala-Kem'-White Sea). Geophys J (Ukraina) 32:21–34

Shchipansky AA, Konilov AN (2005) Archean eclogites, Shirokaya Salma area. In: Volodichev OI, Slabunov AI (eds) Belomorian mobile belt and its analogues: geology, geochronology, geodynamics and metallogeny. Extended Abstracts and field trip guide book. Karelian Research Centre (KRC), Russian Academy of Sciences (RAS), Petrozavodsk, pp 15–19

Shchipansky AA, Samsonov AV, Bibikova EV et al (2004) 2.8 Ga boninite-hosting partial suprasubduction ophiolite sequences from the North Karelian greenstone belt, NE Baltic Shield, Russia. In: Kusky T (ed) Precambrian Ophiolites and related rocks. Dev in Precambrian Geol, Elsevier, Amsterdam, 13:425–487

Shchipansky AA, Khodorevskaya LI, Konilov AN, Slabunov AI (2012a) Eclogites from the Belomorian Mobile Belt (Kola Peninsula): geology and petrology. Russian Geol and Geophys 53:1–21

Shchipansky AA, Khodorevskaya LI, Slabunov AI (2012b) The geochemistry and isotopic age of eclogites from the Belomorian Belt (Kola Peninsula):evidence for subducted Archean oceanic crust. Russian Geol and Geophys 53:262–280

Skjerlie KP, Patiño Douce AE, Johnston AD (1993) Fluid absent melting of a layered crustal protolith: implications for the generation of anatectic granites. Contrib Mineral Petrol 114:365–378

Skublov SG, Herwartz D, Berezin AV (2011) Pervii dannii Lu-Hf datirovanij eklogitov v Belomorskom podvizhnom pojse (The first Lu-Hf age dates of eclogites from the Belomorian mobile belt). In: Kozakov IK (ed). Proceedings of the 3rd Russian conference on Precambrian geology and geodynamics. Problems in Precambrian plate- and plume tectonics. IGGD, Russian Academy of Sciences, St.Petersburg, pp 166–168

Slabunov AI (1993) Verzhnearzheiskaj Keretskaj granit-zelenokamennaj sistema Karelii (Upper Archean Keret granite–greenstone system in Karelia). Geotectonics 28:61–74

Slabunov AI (2008) Geologij I Geodinamika arzheiskizh podvizhnizh pojsov (na primere Belomorskoi provincii Fennoskandinavskogo schita) (Geology and geodynamics of Archean mobile belts (example from the Belomorian province of the Fennoscandian Shield)). Karelian Research Centre (KRC), Russian Academy of Sciences (RAS), Petrozavodsk, pp 1–296

Slabunov AI (2010) Archean evolution of the Belomorian province: from an ocean to a collision orogen. In: Teyler IM and Knox-Robinson CM (eds) 5th International Archean Symposium. Abstracts. Perth: Geological Survey of Western Austalia. 2010/18:212–215

Slabunov AI (2011) Archaean eclogite-bearing and granite-greenstone complexes of the Belomorian province: correlation and geodynamic interpretation. In: Slabunov AI, Perchuk AL (eds) Granulite and eclogite complexes in the Earth's history. Extended Abstracts and Field Guide. Karelian Research Centre (KRC), Russian Academy of Sciences (RAS), Petrozavodsk, pp 210–214

Slabunov A. (2013) Archaean associations of volcanics, granulites and eclogites of the Belomorian province, Fennoscandian Shield and its geodynamic interpretation. Geophysical Research Abstracts. Vena. 6782

Slabunov AI, Lobach-Zhuchenko SB, Bibikova EV et al (2006a) The Archaean nucleus of the Baltic/Fennoscandian Shield. In: Gee DG, Stephenson RA (eds) European lithosphere dynamics. Geological Society of London Memoir 32:627–644

Slabunov AI, Lobach-Zhuchenko SB, Bibikova EV et al (2006b) The Archean of the Baltic Shield: geology, geochronology, and geodynamic settings. Geotectonics 40:409–433

Slabunov AI, Stepanova AV, Bibikova EV (2009) Mezoarzheiskii fragment okeanicheskoi kori (Shentral'no-Belomorskii zelenokamennii pojs Belomorskoi provinchii) (Mesoarchean segment of ocean crust (Central-Belomorian Greenstone Belt of the Belomorian Province). In: Slabunov AI, Svetov SA (eds) Archean granite-greenstone systems and their younger analogues, Extended abstracts and Guidebook of field trips. Karelian Research Centre (KRC), Russian Academy of Sciences (RAS), Petrozavodsk, pp 154–156

Slabunov AI, Hölttä P, Sharov NV, Nesterova NS (2011a) 4-D model' formirovanija zemnoj kory Fennoskandinavskogo schita v arhee kak sintez sovremennyh geologicheskih dannyh (A 4-D framework of the Fennoscandian Shield earth Crust growth in Archean:synthesis of off-the-shelf geological data) In: Proceedings of the All-Russian Conference convened to celebrate the 50th anniversary of the founding of the Institute of Geology. 24–26 May. Geology of Karelia from the Archaean to the present. Karelian Research Centre (KRC), Russian Academy of Sciences (RAS), Petrozavodsk, pp 13–21

Smithies RH (2000) The Archaean tonalite-trondhjemite-granodiorite (TTG) series is not an analogue of Cenozoic adakite. Earth and Planetary Sci Lett 182:115–125

Smithies RH, Champion DC, Cassidy KF (2003) Formation of Earth's early Archaean continental crust. Precambrian Res 127:89–101

Sochevanov NN, Arestova NA, Matrenichev VA et al (1991) Pervii dannie o Sm-Nd vozraste arzheiskizh

bazal'tov v Karel'skoi granit-zelenokamennoi oblasti (First Data on the Sm–Nd Age of Archean Basalts in Karelia Granite–Greenstone Region) Doklladi Akademii Nauk SSSR 318(1):175–180

Sorjonen-Ward P (1993) An overview of structural evolution and lithic units within and intruding the late Archean Hattu schist belt Ilomantsi eastern Finland. Geological Survey of Finland Special Paper 17:9–102

Sorjonen-Ward P (2006) Geological and structural framework and preliminary interpretation of the FIRE 3 and FIRE 3A reflection seismic profiles central Finland. Geological Survey of Finland Special Paper 43:105–159

Sorjonen-Ward P, Luukkonen E (2005) Archean rocks. In: Lehtinen M, Nurmi PA, Rämö OT (eds) The Precambrian Geology of Finland—key to the evolution of the Fennoscandian Shield. Elsevier, Amsterdam, pp 19–99

Springer W, Seck HA (1997) Partial fusion of basic granulites at 5 to 15 kbar: implications for the origin of TTG magmas. Contrib Mineral Petrol 127:30–45

Stern RA, Hanson GN, Shirey SB (1989) Petrogenesis of mantle-derived, LILE-enriched Archean monzodiorites and trachyandesites (sanukitoids) in southwestern Superior Province. Canadian J Earth Sci 26:1688–1712

Stepanov VS, Slabunov AI (1989) Dokembriiskii amfiboliti i bazit-ul'trabaziti Severnoi Karelii (Precambrian Amphibolites and early mafic–ultramafic rocks in Northern Karelia). Nauka, Leningrad, pp. 11–175

Stepanov VS, Slabunov AI, Stepanova AV (2003). Porodoobrazuuschii i acchessornii minerali pozdnearzheiskizh peridotitov raiona ozera Seriak (Belomorskii podvizhnii pojs Fennoskandinavskogo schita) (Rock-forming and accessory minerals of Late Archaean peridotites from the Lake Seryak area, Belomorian mobile belt, Fennoscandian Shield). In: Geology and Useful minerals of Karelia, vol 6. Petrozavodsk, p. 17–25

Stiegler MS, Lowe DR, Byerly GR (2010) The petrogenesis of volcaniclastic komatiites in the Barberton Greenstone Belt, South Africa: a textural and geochemical study. J of Petrol 51:947–972

Streckeisen A, Le Maitre RW (1979) A chemical approximation to the modal QAPF classification of the igneous rocks. Neues Jb Miner Abh 136:169–206

Strik G, Blake TS, Zegers TE et al (2003) Palaeomagnetism of flood basalts in the Pilbara Craton Western Australia: Late Archaean continental drift and the oldest known reversal of the geomagnetic field. J of Geophys Res 108 (B12):21

Sun SS, McDonough WF (1989) Chemical and isotopic systematics of oceanic basalts: implications for mantle composition and processes. Geological Society of London Special Publication 42:313–345

Svetova AI (1988) Arhejskij vulkanizm Vedlozersko-Segozerskogo zelenokamennogo pojasa Karelii (Archean Volcanism in the Vedlozero–Segozero Greenstone Belt of Karelia), Karelian Research Centre (KRC), Russian Academy of Sciences (RAS), Petrozavodsk, pp 1–148

Svetov SA (2005) Magmaticheskie sistemy zony perehoda okean-kontinent v arhee vostochnoj chasti Fennoskandinavskogo wita (Magmatic systems in the ocean-continent transition zone in the Archean of the eastern Fennoscandian Shield). Karelian Research Centre (KRC), Russian Academy of Sciences (RAS), Petrozavodsk, pp 1–230

Svetov SA (2009) Drevnejshie adakity Fennoskandinavskogo schita (The oldest adakites of the Fennoscandian Shield). Karelian Research Centre (KRC), Russian Academy of Sciences (RAS), Petrozavodsk, pp 1–115

Svetov SA (2010) Arhitektura arhejskih konvergentnyh sistem v sravnenii s fanerozojskimi analogami (po dannym FME-sistematiki vulkanitov (Architecture of Archaean convergent systems in comparison with Phanerozoic analogues, as shown by data on the FME-systematics of volcanites). Lithospere 3:12–20

Svetov SA, Svetova AI (2011) Archaean subduction: marker rock assemblages and architecture. In: Proceedings of the All-Russian Conference convened to celebrate the 50th anniversary of the founding of the Institute of Geology. 24–26 May. Geology of Karelia from the Archaean to the present. Karelian Research Centre (KRC), Russian Academy of Sciences (RAS), Petrozavodsk, pp 22–32

Svetov SA, Svetova AI, Huhma H (2001) Geochemistry of the komatiite-tholeiite rock association in the Vedlozero-Segozero Archean greenstone belt, Central Karelia. Geochem Int 39(1):24–38

Tateno S, Hirose K, Sata N et al (2009) Determination of post-perovskite phase transition boundary up to 4400 K and implications for thermal structure in D″ layer. Earth and Planetary Sci Lett 277:130–136

Thompson RN (1982) British Tertiary province. Scottish J of Geol 18:49–107

Thurston P (2002) Autochthonous development of Superior Province greenstone belts? Precambrian Res 115:11–36

Thuston HC, Kozhenvnikov VN (2000) An Archean quartz arenite–andesite association in the eastern Baltic Shield, Russia: implications for assemblage types and Shield history. Precambrian Res 101:313–340

Tuisku P (1988) Geothermobarometry in the Archean Kuhmo-Suomussalmi greenstone belt eastern Finland. Geological Survey of Finland Special Paper 4:171–172

Vaasjoki M, Sorjonen-Ward P, Lavikainen S (1993) U-Pb age determinations and sulfide Pb-Pb characteristics from the late Archean Hattu schist belt, Ilomantsi, eastern Finland. Geological Survey of Finland Special Paper 17:103–131

van der Velden AJ, Cook FA, Drummond BJ et al (2006) Reflections of the Neoarchean: a global perspective. In: Benn K, Mareschal J-C, Condie KC (eds) Archean geodynamics and environments. Geophysical Monograph 164:255–265

van Hunen J, van den Berg AP, Vlaar NJ (2004) Various mechanisms to induce present-day shallow flat

subduction and implications for the younger Earth: a numerical parameter study. Phys Earth and Planetary Interiors 146:179–194

Volodichev OI, Slabunov AI, Bibikova EV et al (2004) Archean eclogites in the Belomorian mobile belt, baltic shield. Petrology 12(6):540–560

Volodichev OI, Slabunov AI (2011) Superposition of two age and genetic groups of eclogites in the Gridino area, Belomorian province, Fennoscandian Shield. In: Slabunov AI, Perchuk AL (eds) Granulite and eclogite complexes in the Earth's history. Extended Abstracts and Field Guide. Karelian Research Centre (KRC), Russian Academy of Sciences (RAS), Petrozavodsk, pp 46–48

Watkins JM, Clemens JD, Treloar PJ (2007) Archaean TTGs as sources of younger granitic magmas: melting of sodic metatonalites at 0.6–1.2 GPa. Contrib Mineral Petrol 154:91–110

Wu C-M, Zhang J, Ren L-D (2004) Empirical garnet–biotite–plagioclase–quartz (GBPQ) geobarometry in medium- to high-grade metapelites. J of Petrol 45(9):1907–1921

4 Archaean Elements of the Basement Outliers West of the Scandinavian Caledonides in Northern Norway: Architecture, Evolution and Possible Correlation with Fennoscandia

Steffen G. Bergh, K. Kullerud, P.I. Myhre, F. Corfu, P.E.B. Armitage, K.B. Zwaan and E.J.K. Ravna

Abstract

Meso- and Neoarchaean basement rocks occur in two coastal outliers west of the Scandinavian Caledonides in North Norway, i.e. in western Troms (West Troms Basement Complex) and the Lofoten-Vesterålen area. When restored, these two outliers appear to have been assembled together in a cratonic-marginal position at the northern edge of the Fennoscandian shield in the Neoarchaean, and they share a similar tectono-magmatic history prior to Palaeoproterozoic events. This is confirmed by radiometric dating and similarity of sedimentary/volcanic units, intrusive/magmatic events, structural architecture and metamorphic events, and the mechanisms of amalgamation.

Distinctive tonalite-trondhjemite-granodiorite (TTG) gneisses (2.92-2.67 Ga) and intervening meta-volcanic and sedimentary units, e.g. the Ringvassøya greenstone belt (2.83–2.6 Ga), make up a significant portion of the West Troms Basement Complex. The TTG gneisses, likely magmatic in origin, were deformed, metamorphosed up to granulite facies and locally migmatized during periods of accretion and collisional/convergent tectonism at c. 2.9–2.8 Ga, 2.75–2.7 and 2.7–2.67 Ga. The final Neoarchaean stage (c. 2.67 Ga) caused high-grade metamorphism, resetting and comprehensive migmatization along presumed Neoarchaean terrane boundary

S. G. Bergh (✉) · K. Kullerud · P.I. Myhre · E.J.K. Ravna
Department of Geology, University of Tromsø, 9037 Tromsø, Norway
e-mail: steffen.bergh@uit.no

F. Corfu
Department of Geosciences, University of Oslo, P.O. Box 1047 Blindern, 0316 Oslo, Norway

P.E.B. Armitage
Paul Armitage Consulting Ltd, 55 Reedham Crescent, Cliffe Woods, Rochester ME3 8HT, UK

K.B. Zwaan
Geological Survey of Norway, 7491, Trondheim, Norway

Y. Dilek, H. Furnes (eds.), *Evolution of Archean Crust and Early Life,* Modern Approaches in Solid Earth Sciences 7, DOI 10.1007/978-94-007-7615-9_4,

shear zones prior to intrusion of an extensive Palaeoproterozoic mafic dyke swarm (2.4–2.2 Ga). The subsequent Palaeoproterozoic evolution involved rifting and basin formation (2.4–1.9 Ga), intrusion of an extensive magmatic suite of anorthosite-mangerite-charnockite-granite (1.8–1.7 Ga) and Svecofennian accretion and collisional orogenesis at c. 1.8–1.67 Ga.

In terms of correlation of the Archaean components with Fennoscandia and/or Laurentia, a closer connection to Fennoscandia is inferred from gravity-magnetic trends beneath the Caledonides, age constraints and tectono-magmatic evolution, and extrapolation of intervening tectonic basement windows present in the Caledonides. Provinces such as the Kola-Norwegian, Belomorian and Karelian provinces of the northwestern Fennoscandian shield of Russia, Finland and north Sweden, display obvious similarities with respect to supracrustal units of similar age and geological setting and their tectono-magmatic evolution.

4.1 Introduction

Archaean and Palaeoproterozoic continental crust (2.9–1.67 Ga) is preserved in the West Troms Basement Complex and Lofoten-Vesterålen islands of northern Norway (Fig. 4.1). This basement crustal segment defines an emerged horst bounded to the east by thrust nappes of the Scandinavian Caledonides (Griffin et al. 1978; Olesen et al. 1997; Corfu 2004a, b), in a similar setting to the Western Gneiss Region of South Norway (Andersen et al. 1991), and to the west by Mesozoic basins offshore (Fig. 4.2) (Blystad et al. 1995). In spite of the internal position relative to the Caledonides, and in great contrast to the basement outliers in South Norway, where Caledonian high-grade metamorphic reworking is widespread, the geo-transects from Lofoten-Vesterålen into western Troms display only modest Caledonian reworking and can therefore be used to characterize the Archaean components and structural architecture (e.g. Griffin et al. 1978; Corfu 2004; Corfu et al. 2003; Bergh et al. 2010).

A framework for the Archaean and Palaeoproterozoic geological units in the West Troms Basement Complex has recently been established (see Table 4.1) (Zwaan 1995; Zwaan et al. 1998; Corfu et al. 2003; Kullerud et al. 2006; Bergh et al. 2007, 2010; Myhre 2011; Myhre et al. 2013), as well as for Lofoten-Vesterålen (Corfu 2004a, b 2007), and new advances have highlighted and resolved aspects of the tectono-magmatic evolution (Bergh et al. 2010). The question of regional correlation of these cratonic-marginal provinces with respect to the cratonic Fennoscandia in the Neoarchaean (Bleeker & Ernst 2006; Mertanen & Korhonen 2011) and the situation prior to Palaeoproterozoic events (e.g. Bridgwater et al. 1990; Connelly et al. 2000; Hölttä et al. 2008; Myhre 2011) still remains enigmatic.

This paper reviews the current knowledge of the Archaean bedrock components and tectono-metamorphic history in the West Troms Basement Complex and Lofoten-Vesterålen area of North Norway (Griffin et al. 1978; Corfu et al. 2003; Corfu 2004a, b, 2007; Armitage & Bergh 2005; Kullerud et al. 2006; Bergh et al. 2007; Bergh et al. 2010; Myhre et al. 2010, 2011), with emphasis on supracrustal units and adjacent blocks of relatively rigid tonalitic (TTG) gneisses and magmatic rocks, and attempts to correlate them with crustal provinces in the Fennoscandian Shield farther east. Questions specifically raised for the Archaean basement suites concern (1) the age, origin and significance of the TTG gneisses including high-grade metamorphism and localized migmatization, (2) the components, structure and ore potential of the supracrustal units, and (3) the Archaean tectono-magmatic and metamorphic history. The presence of Neoarchaean terrane boundaries has been suggested and may help to restore the outline and cratonic margin characteristics of Fennoscandia, and to unravel cycles of tectono-magmatic events prior to the Palaeoproterozoic orogenesis.

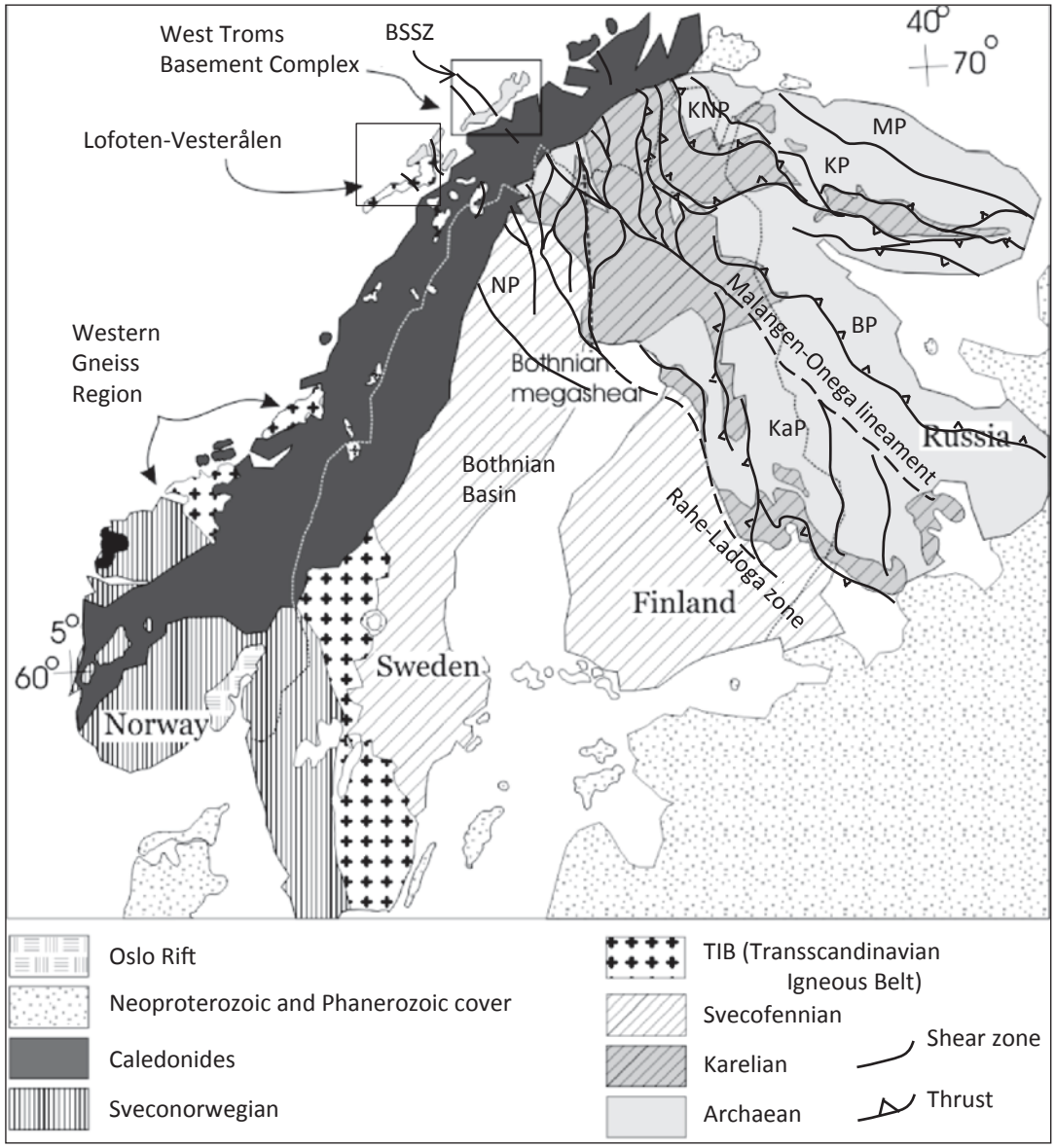

Fig. 4.1 Geological overview map of the Fennoscandian Shield with location (frames) of the West Troms Basement Complex (Fig. 4.3) and the Lofoten-Vesterålen area (Fig. 4.6) representing tectonic outliers to the west of the Scandinavian Caledonides. Archaean and younger provinces and major ductile shear zones are included for the Fennoscandian Shield to the east of the Caledonides. The map is modified from Corfu et al. (2003) and Hölttä et al. (2008). Abbreviations are: *BP* = Belomorian province, *BSSZ* = Bothnian-Senja shear zone, *MP* = Murmansk province, *KaP* = Karelian province, *KNP* = Kola-Norwegian province, *KP* = Kola province, *NP* = Norrbotten province

4.2 Geological Setting

Archaean and Palaeoproterozoic crust underlies much of the northeastern part of the Fennoscandian Shield in Kola, Finland and northern Sweden (Gaál & Gorbatchev 1987; Hölttä et al. 2008), and incorporates basement outliers west of the much younger Palaeozoic Scandinavian Caledonides to the northwest (Fig. 4.1). Here, the West Troms Basement Complex (Bergh

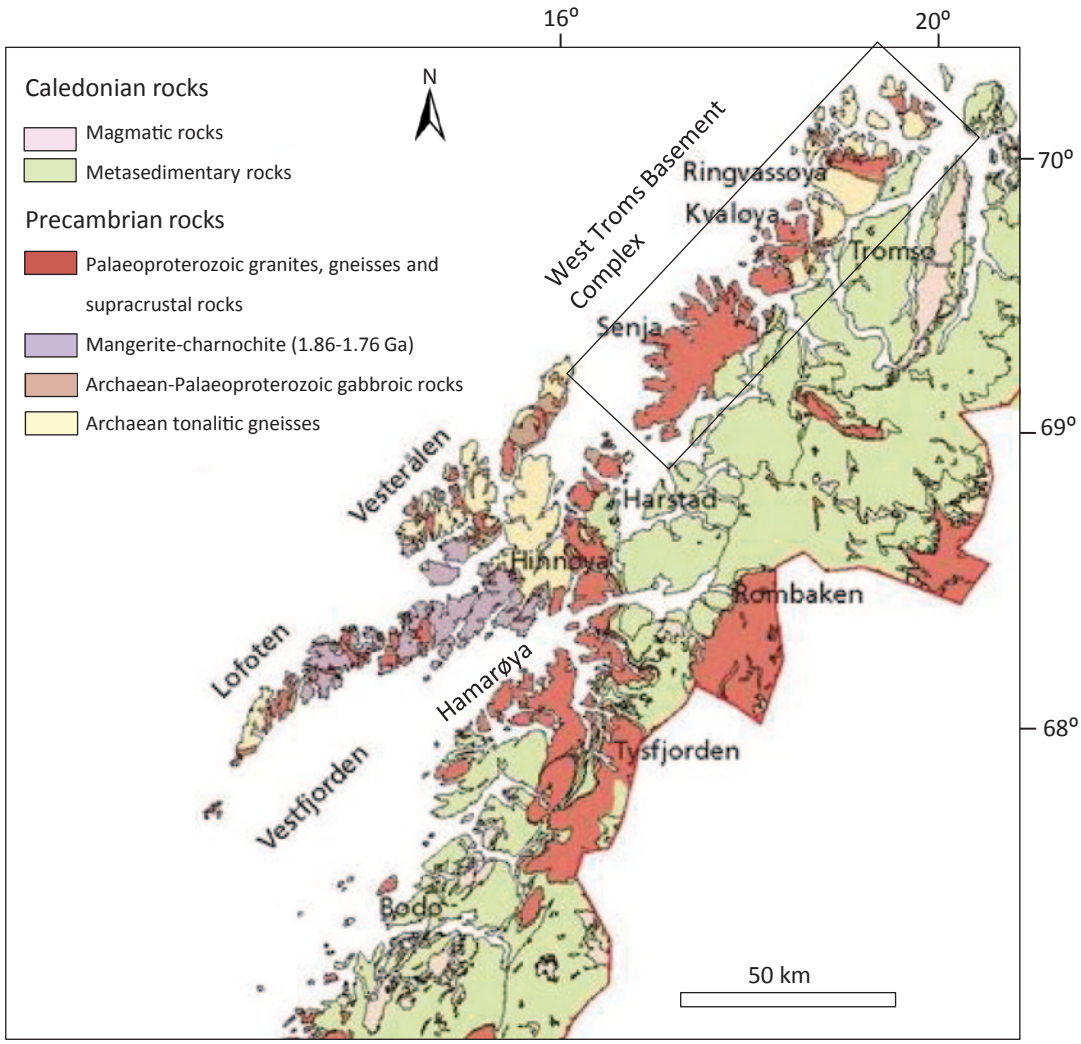

Fig. 4.2 Regional geological map of parts of northern Norway showing Archaean-Palaeoproterozoic basement rocks present as outliers to the west of the Caledonian nappe stack, in the West Troms Basement Complex and the Lofoten-Vesterålen area. Also shown are nearby tectonic basement windows within the Caledonides, mostly composed of Palaeoproterozoic intrusive rocks as in the Rombak Tectonic Window and on Hamarøya and in Tysfjorden farther south. The map is from Ramberg et al. (2006)

et al. 2010) and a suite of basement rocks in the Lofoten-Vesterålen area to the southwest (Griffin et al. 1978; Corfu 2004a) emerge as a c. 300 km long transect of a basement horst west of the NE-trending axis of the Scandinavian Caledonides (Fig. 4.2), and is separated from the Caledonian nappes by Mesozoic normal faults to the east (Andresen & Forslund 1987; Blystad 1995; Olesen et al. 1997).

The oldest, Neoarchaean components of these basement outliers are believed to be an autochthonous part of the Archaean-Palaeoproterozoic Fennoscandian Shield (e.g. Gaál & Gorbatchev 1987; Henkel 1991; Olesen et al. 1997) that stretches from Finnmark in North Norway, through Russia, Finland and Sweden (Fig. 4.1). This correlation is based on the tracing of NW-SE gravity-magnetic anomalies beneath the Caledonian cover (Olesen et al. 1997) in a direction parallel to the Bothnian-Senja shear zone system of Sweden (Henkel 1991; Doré et al. 1997; Olesen et al. 1997), and is also inferred from similarities with basement rocks in tectonic windows within the nearby Caledonian nappes (Fig. 4.2).

Table 4.1 Summary and tentative correlation of age constraints, main component characteristics and tectonic events in the West Troms Basement Complex and Lofoten-Vesterålen area, compiled from Griffin et al. (1978), Corfu (2004), Corfu et al. (2007), Bergh et al. (2010) and Myhre et al. (2011b)

West Troms Basement Complex		Lofoten-Vesterålen province	
Age (Ga)	**Components and events**	**Age (Ga)**	**Components and events**
2.92–2.77 Ga	*Neoarchaean cratonization:*		*Neoarchaean cratonization:*
	Tonalite crystallization (Dåfjord & Kvalsund gneisses)	2.85–2.7 Ga	Accretion, convergence and crustal thickening
2.85–2.83 Ga	*Volcanism and sedimentation*:		
	Ringvassøya greenstone belt: calc-alkaline and tholeiitic metabasalts, paragneisses and sulphide-rich schists	2.75–2.68 Ga	Tonalite magmatism
2.75–2.7 Ga	*Continued Neoarchaean cratonization*		
2.75–2.67 Ga	Mafic plutonism (Bakkejord diorite) in the southwest	2.72–2.66 Ga	*Neoarchaean deformation and metamorphism:*
2.73–2.58 Ga	*Main Neoarchaean deformation and metamorphism:*		Various orthogneisses (e.g. Bremnes gneiss) formed by crustal shortening
	Magmatism, migmatization (Gråtind migmatite) and ductile shearing (in *Dåfjord* and *Kvalsund* gneisses)		
	Main gneissic foliation (initially flat-lying), ductile shear zones, tight folds and ENE-directed stretching lineation		
	Medium/high-grade metamorphism, ENE-WSW crustal contraction and thickening by accretion and/or underplating		
2.69-2.58 Ga	High-grade granulite facies metamorphism and resetting	2.64 Ga	Emplacement of tonalites, followed by high-grade metamorphism and localized migmatization and ductile crustal shearing (*Sigerfjord migmatite, Ryggedalen granulite*)
2.69 Ga	Granitoid and alkaline intrusions		
2.58–2.57 Ga	Late-stage mafic intrusion (*Bakkejord pluton*)		
2.40 Ga	*Crustal extension and intrusion* of the *Ringvassøya* mafic dyke swarm	?	
2.4–2.2 Ga	*Deposition* of *Vanna group* clastic sediments in a marine subsiding basin	?	*Deposition* of supracrustal units, heterogeneous mafic gneisses, banded iron formations, quartzite, marbles, graphite schists
2.22 Ga	*Intrusion* of Vanna diorite sill	?	
2.2–1.9 Ga	*Deposition of Mjelde-Skorelvvatn*, Torsnes and possibly the *Astridal* supracrustal belts		
1.993 Ga	*Intrusion/volcanism* in the Mjelde-Skorelvvatn belt	1.87-1.86 Ga	Precursory stage magmatism, AMCG-suite
1.80 Ga	*Magmatism/intrusion* of granites and norite in Senja	1.8-1.79 Ga	Main stage intrusion of AMCG-suite plutonic rocks
1.79 Ga	*Magmatism/intrusion* of *Ersfjord Granite* in Kvaløya	1.77 Ga	Intrusion of granite pegmatite dykes
c. 1.9–1.7 Ga	*Palaeoproterozoic/Svecofennian deformation*		*Svecofennian deformation*

The West Troms Basement Complex comprises various Meso- and Neoarchaean TTG gneisses (2.9–2.67 Ga), supracrustal rocks/greenstone belts (2.8–1.9 Ga) and igneous rocks that suffered polyphase Neoarchaean ductile deformation and high-grade metamorphism (Myhre et al. 2013). The basement suite of Lofoten-Vesterålen (Fig. 4.4) consists of a similar metamorphic Neoarchaean basement and supracrustal rocks (2.8–2.67 Ga) intruded by a very extensive suite of 1.8–1.7 Ga plutonic rocks of the AMCG suite (Griffin et al. 1978; Corfu 2004a, b). Both of these basement suites display dominant NW-SE structural trends which are largely parallel with Archaean and Palaeoproterozoic orogenic belts of the Fennoscandian Shield that stretches from Kola through Finland and Sweden into the Bothnian Basin of central Scandinavia (Gaál and Gorbatchev 1987), while the AMCG suite appears to link up with the Transscandinavian Igneous Belt of southern Sweden (Fig. 4.1).

4.3 Archaean Rocks of the West Troms Basement Complex

Meso-and Neoarchaean rocks comprise relatively rigid blocks between the thin supracrustal belts in the West Troms Basement Complex (Fig. 4.3, Table 4.1) and are composed of various tonalite-trondhjemite and anorthositic gneisses (2.92–2.7 Ga) with mafic and ultramafic layers and intercalated apparent banded ironstones, and overlying (2.85–2.7 Ga) supracrustal units or greenstone belt rocks (Bergh et al. 2010; Myhre et al. 2011). The TTG gneisses have been intruded by mafic, ultramafic and felsic plutons and deformed and metamorphosed during the Neoarchaean (2.7–2.67 Ga) and were later strongly affected by Palaeoproterozoic (1.9–1.75 Ga) tectono-thermal events. In the northeast, on Ringvassøya, tonalitic orthogneisses and granitoids (Dåfjord gneiss) have yielded U-Pb zircon crystallization ages of 2.92–2.77 Ga (Zwaan and Tucker 1996; Myhre et al. 2013), and these rocks are considered to be related to tonalite plutons on the island of Vanna farther north (Fig. 4.3), where a U-Pb crystallization age of 2885 ± 20 Ma is obtained (Bergh et al. 2007). The island of Kvaløya in the central part is dominated by slightly younger Neoarchaean gneisses, i.e. the Kvalsund gneiss and Gråtind migmatite (Zwaan et al. 1998; Bergh et al. 2010). The Kvalsund gneiss and the remainder of the Neoarchaean rocks southward record important events of crustal magmatism and reworking at 2.75–2.70 and 2.70–2.67 Ga, concluding with the emplacement of mafic dykes at c. 2.67 Ga into the Bakkejord pluton (Myhre et al. 2013). A main intrusion age of 2.75–2.70 Ga and later pulses of 2.58–2.57 Ga were obtained for the crystallization of the Bakkejord pluton (Myhre et al. 2013), while granitoid rocks intruded and caused migmatization of the gneisses at 2.70–2.67 Ga. Granodiorite in central parts of Senja crystallized at 2.69 Ga, and a granite near Torsnes at 2689 ± 6 Ma. Minor alkaline intrusions (Mikkelvik alkaline massif) intruded at 2695 ± 15 Ma on Ringvassøya (Zozulya et al. 2009). A similar age span is recorded in southwestern Senja, where magmatism and metamorphism occurred during distinct events around 2.8, 2.7 and 2.6 Ga (Zwaan & Tucker 1996; Motuza et al. 2001; Corfu et al. 2003; Myhre et al. 2013). There is also evidence of a latest Neoarchaean high-grade metamorphic event at c. 2.6 Ga in the TTG gneisses (Myhre et al. 2013).

The only supracrustal unit in the West Troms Basement Complex that evidently is of Neoarchaean age is the Ringvassøya greenstone belt (Fig. 4.3). This up to 15 km wide and 40 km long greenstone belt is sandwiched (thrusted) between segments of the tonalitic Dåfjord gneiss (Figs. 4.4 and 4.5a), and is made up of a lower unit of low-grade mafic and intermediate felsic meta-volcanic rocks (Motuza et al. 2001), and an upper unit of amphibolite-facies quartz-feldspathic gneisses (Zwaan 1989; Motuza et al. 2001). Felsic meta-volcanics (keratophyre), amphibolite schists, sulphide-rich mica schists and magnetite-rich banded quartzites (Fig. 4.5b), some of which have gained high concentrations of sulphides and epigenetic gold (Zwaan 1989; Sandstad & Nilsson 1998; Bergh et al. 2010), make up a significant portion of the lower unit. U-Pb crystallization ages of 2848.5 ± 4 Ma and 2835 ± 14 Ma (Motuza et al. 2001) have been

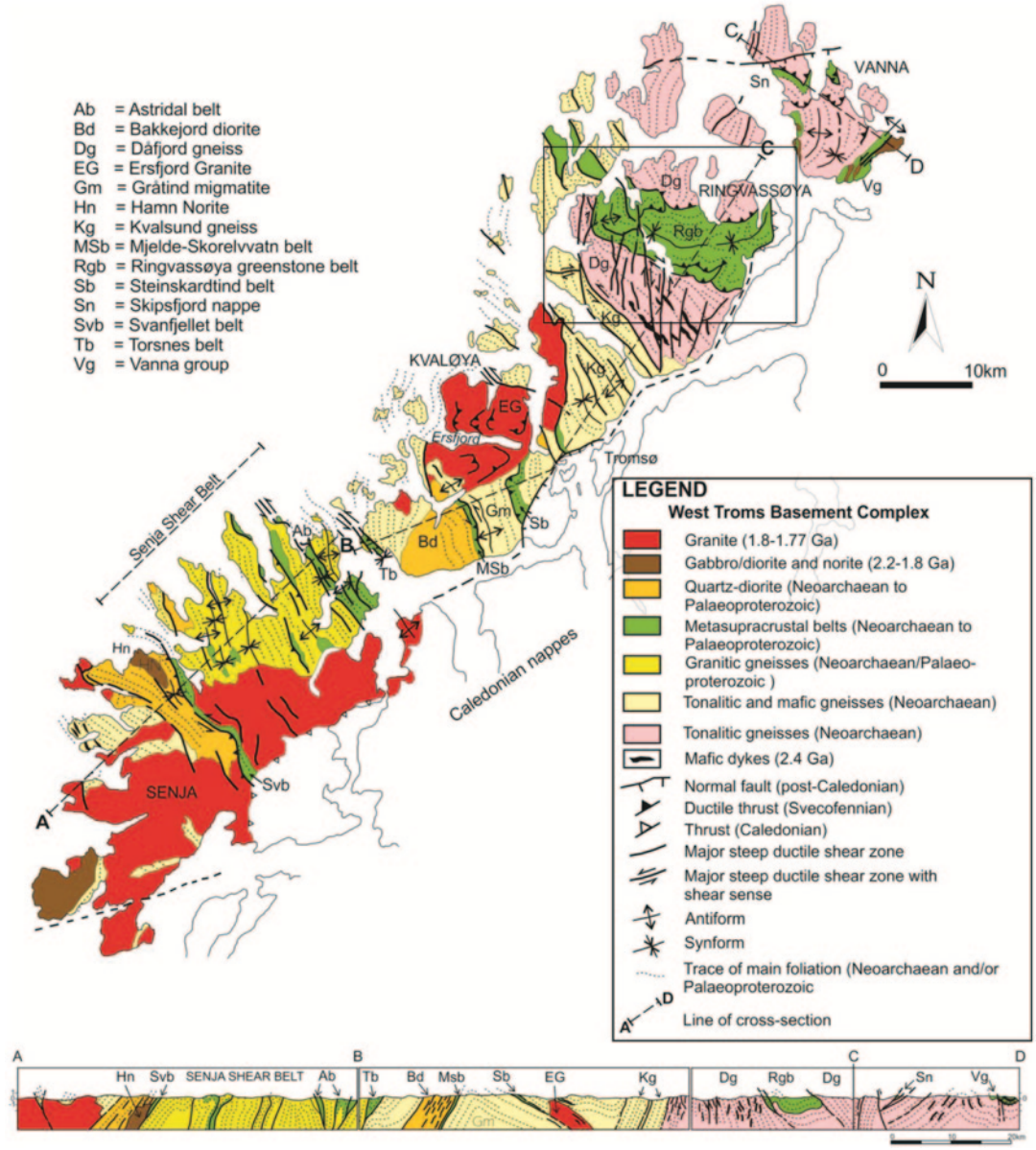

Fig. 4.3 Geological and tectonic map of the West Troms Basement Complex, with cross-section. The framed area covers Fig. 4.4. The map is revised after Kullerud et al. (2006) and Bergh et al. (2010)

determined for the felsic meta-volcanic rocks in the lower unit, while minimum ages of 2832 Ma for a quartz-keratophyre and c. 2.83 Ga for a thin syn-tectonic granitoid dyke are obtained in the eastern part (Kullerud et al. 2006). The age of the upper gneiss unit is unknown. The geochemistry of the Neoarchaean layered supracrustal rocks of the Ringvassøya greenstone belt indicates a transition to continental origin (Zwaan 1989), e.g. arc-related meta-volcanic rocks with a MORB-transitional, tholeiitic to calc-alkaline affinity (Motuza et al. 2001).

The Archaean TTG gneisses and some of the intercalated mafic bodies (Fig. 4.5c) in the West Troms Basement Complex are deformed and metamorphosed up to granulite facies, locally

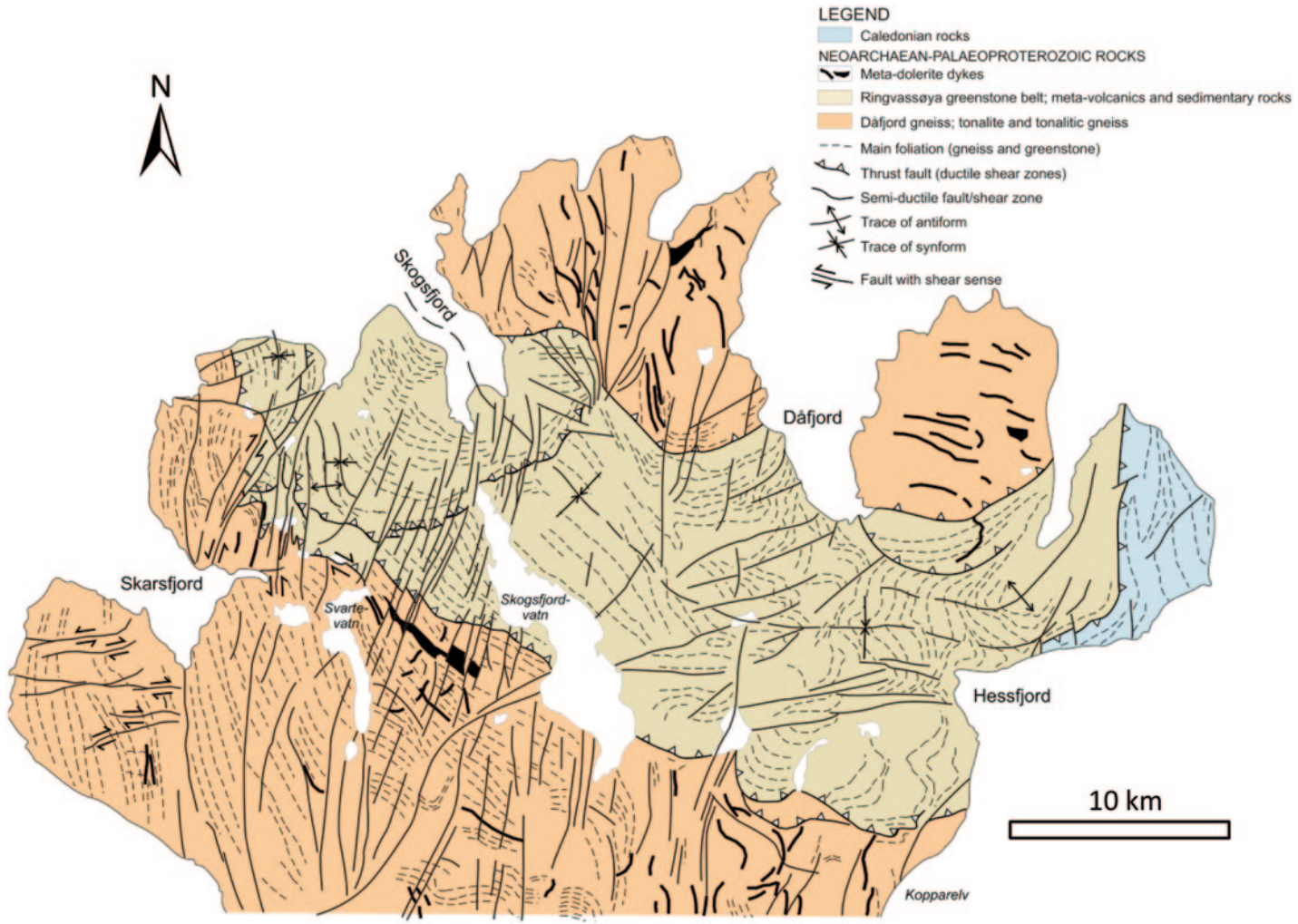

Fig. 4.4 Geological and structural map of the Ringvassøya greenstone belt and the surrounding Neoarchaean Dåfjord gneiss modified after Zwaan (1989) and Bergh et al. (2010). The trend of the Neoarchaean gneiss fabric and main foliation in the greenstone belt rocks is shown as stippled lines. Note the presence of synform-antiformal folds, thrust contacts and younger shear zones within the greenstone belt rocks that offset the gneiss-greenstone contact. A widespread mafic dyke swarm (2.4 Ga) occurs in the adjacent tonalitic gneisses

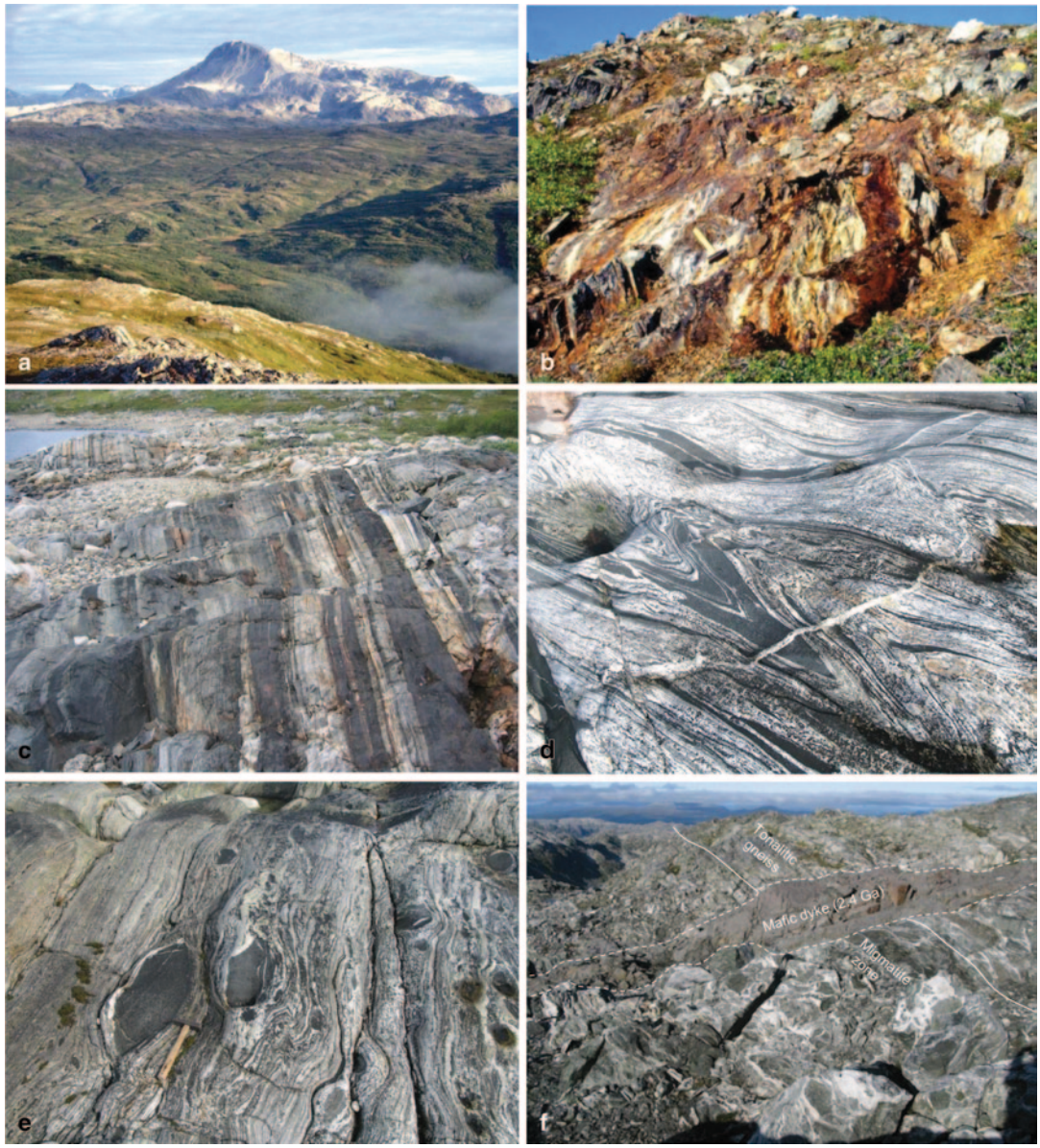

Fig. 4.5 Outcrop features of the Meso-Neoarchaean Ringvassøya greenstone belt and surrounding tonalitic gneisses in the West Troms Basement Complex: **a** View of mafic meta-volcanic rocks of the Ringvassøya greenstone belt (*lower part*) surrounded by TTG gneisses (distal mountains). View is toward SE along strike with the belt. **b** Presumed Neoarchaean siliciclastic schists with extremely oxidized sulphides (rust) in the northwestern part of the Ringvassøya greenstone belt. **c** Banded tonalitic gneiss (*light-coloured*) with foliation-parallel mafic intercalations (Dåfjord gneiss in central part of Ringvassøya). **d** Tonalitic gneiss with intrafolial, asymmetric ENE-verging folds cut by 1.79 Ga pegmatite veins. Locality: Western Ringvassøya. View is to the NW. **e** Zone of highly migmatized Kvalsund gneiss at the boundary to the Dåfjord gneiss in the southwestern part of Ringvassøya. Note mafic pods. **f** Major migmatized shear zone in the south-central parts of Ringvassøya, cut by a 2.4 Ga mafic dyke. View towards SE

with migmatites, prior to deposition of younger supracrustal units throughout the West Troms Basement Complex (Fig. 4.3), and also prior to intrusion of an extensive 2.4 Ga mafic dyke swarm (Kullerud et al. 2006; Bergh et al. 2010). A steep NW-SE trending transposed gneissic

foliation with dip-slip stretching lineations and tight ENE-vergent intrafolial folds (Fig. 4.5d) attests for WSW-ENE contraction. Foliation-parallel, granulite-facies migmatite zones, interpreted as major ductile shear zones (Fig. 4.5e, f), separate compositionally different gneisses (Zwaan et al. 1998; Bergh et al. 2010). The most prominent shear zones occur between the Dåfjord and Kvalsund gneisses on Ringvassøya and within the Senja Shear Belt (Fig. 4.3). Deformation along the former took place at rather high grade conditions as evidenced by partial melting of mafic enclaves in dilatant sites within the Kvalsund gneiss (Fig. 4.3), and lobate grain boundaries in the sheared tonalite. Polyphase refolding prior to and synchronously with thrusting in the migmatite zones is common and suggests protracted Neoarchaean deformation (Bergh et al. 2010). This Neoarchaean deformation, however, is not well constrained by age determinations, but a U-Pb crystallization age of 2733 ± 1 Ma for the tonalitic precursor of the Kvalsund gneiss and reset ages of 2.69–2.56 Ga, which may represent the duration of the metamorphic gneiss-forming event (Myhre et al. 2013) and a 2587 ± 1.5 Ma U-Pb zircon age for a syn-tectonic granite dyke on Ringvassøya (Kullerud et al. 2006), support a Neoarchaean age for the deformation.

4.4 Archaean Rocks in the Lofoten-Vesterålen Area

The Lofoten and nearby Vesterålen islands (Fig. 4.6) were shown to be composed of Precambrian rocks by Herr et al. (1967), and Heier and Compston (1969) documented major tectono-metamorphic events at 2.8 and 1.8 Ga. Subsequent work based primarily on Pb-Pb, Rb-Sr and Sm-Nd dating, broadly confirmed the two-stage evolution, expanding it to include older events and introducing a number of other sub-stages (Taylor 1975; Griffin et al. 1974, 1978; Jacobsen & Wasserburg 1978; Andresen & Tull 1983; Wade 1985). The chronology of the basement complex and the Palaeoproterozoic anorthosite-mangerite-charnockite-granite suite has now been refined by modern U-Pb geochronology (Corfu 2004a, b, 2007).

The basement rocks in western parts of Lofoten and Vesterålen (Fig. 4.6 and Table 4.1) comprises TTG gneisses, meta-supracrustal gneisses (Fig. 4.7a, b) and younger AMCG igneous rocks metamorphosed to granulite facies. The distribution of Neoarchaean rocks also coincides with a major magnetic and gravity high (Fig. 4.6) caused by the presence of dense rocks in the crust and an elevated Moho discontinuity (Heier 1960; Griffin et al. 1978; Mjelde et al. 1993; Olesen et al. 1997). The eastern part of the region consists instead of various amphibolite-facies gneisses, migmatites, greenstone belts and granitic plutons. The portion of the rocks with Neoarchaean ages occupies large parts of the islands of Langøy in Vesterålen and Hinnøy farther east (Fig. 4.6), and small remnants are also present at the southwestern tip of Austvågøy (Wade 1985). The Neoarchaean rocks of Langøy (Fig. 4.7c, d) consist mainly of high-grade gneisses interpreted to represent supracrustal rocks of intermediate composition, while Neoarchaean gneisses on Hinnøy define an amphibolite-facies metamorphic domain that was migmatized in the Neoarchaean and subsequently deformed and metamorphosed at granulite-facies conditions in the Palaeoproterozoic (Griffin et al. 1978). The boundary between the two metamorphic domains corresponds to the eastern limit of the magnetic high defined by Heier (1960) who mapped the first appearance of orthopyroxene along a line running north-south in eastern Langøy (Fig. 4.6). In the south he linked the line to a local thrust that juxtaposes the Eidsfjord anorthosite on retrogressed mangerite (Heier 1960; Markl 1998), but subsequent studies modified the trajectory, suggesting that the orthopyroxene isograd is folded and continues southeastward across Hinnøy (Fig. 4.6; Griffin et al. 1978). The appearance of orthopyroxene to the west of the amphibolite-facies domain on Hinnøy has been interpreted as either a prograde metamorphic transition (Heier 1960; Griffin et al. 1978), or an abrupt transition marked by a crustal scale ductile shear zone of presumed Neoarchaean age. The zone east of the metamorphic boundary (Fig. 4.6) is dominated

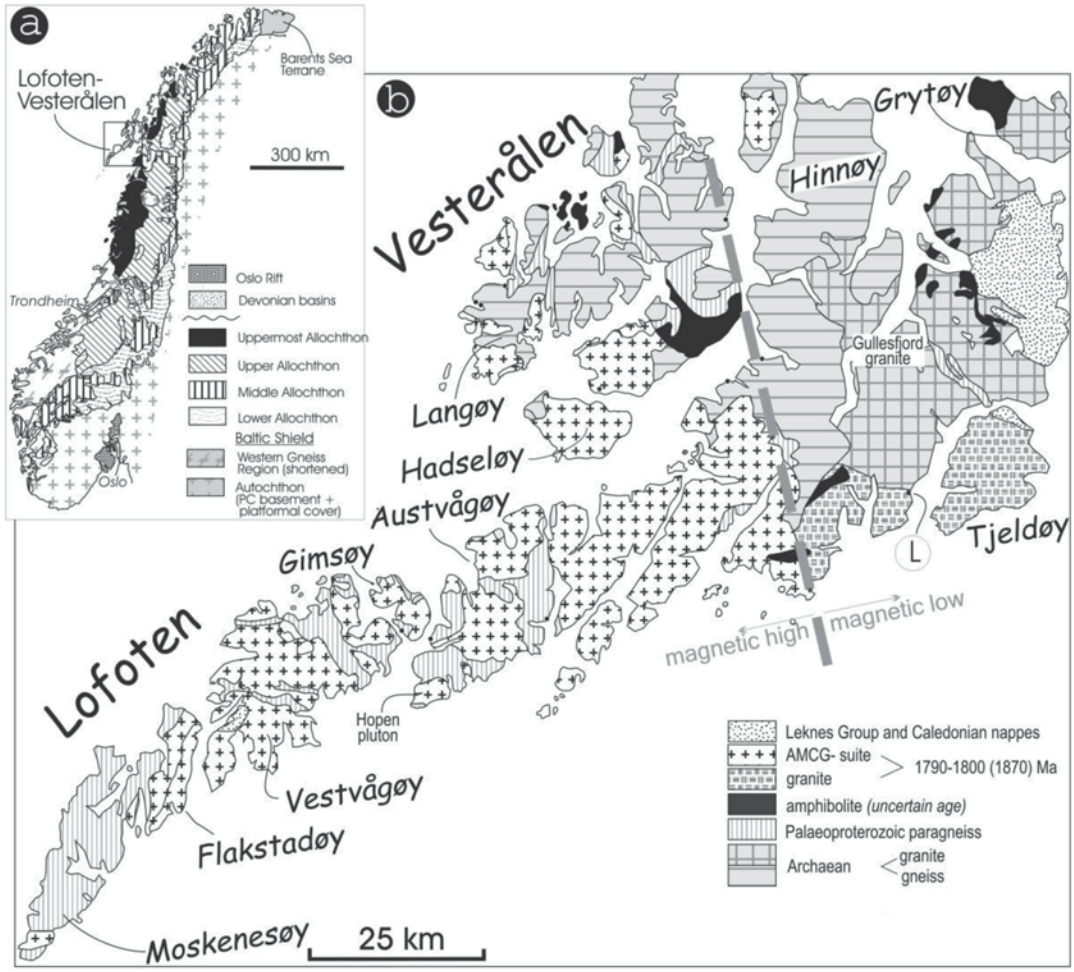

Fig. 4.6 Geological map of the Lofoten and Vesterålen islands, North Norway, showing the Neoarchaean basement gneisses and the Palaeoproterozoic anorthosite-mangerite-charnochite-granite igneous suite. The map is modified from Tveten (1978), Andresen & Tull (1983) and Corfu (2004)

by intrusive rocks of tonalitic to granitic composition, migmatitic domains and local greenstone belt remnants, all considered to be Neoarchaean in age (Taylor 1974; Griffin et al. 1978).

U-Pb dating largely confirms the general understanding of the Lofoten-Vesterålen crustal history (Heier & Compston, 1969; Griffin et al. 1978) providing additional evidence for two major periods of crustal accretion and stabilization in the Neoarchaean and Late Palaeoproterozoic. Neoarchaean U-Pb ages are found in zircon and monazite both in the high- and medium-grade parts of the region and define distinct events of magmatism in the period c. 2.75–2.68 Ga with a subsequent event at about 2.64 Ga involving the emplacement of tonalite and high-grade metamorphism including migmatization, thus adding new magmas and reworking the existing crust. The ages and component characteristics of the Lofoten-Vesterålen region largely correspond to observations farther north, in the West Troms Basement Complex, where crust-forming episodes were in operation during a major accretion event at 2.75–2.67 Ga (Corfu et al. 2003; Bergh et al. 2010; Myhre et al. 2013), thus supporting a link between the two basement outliers in North Norway.

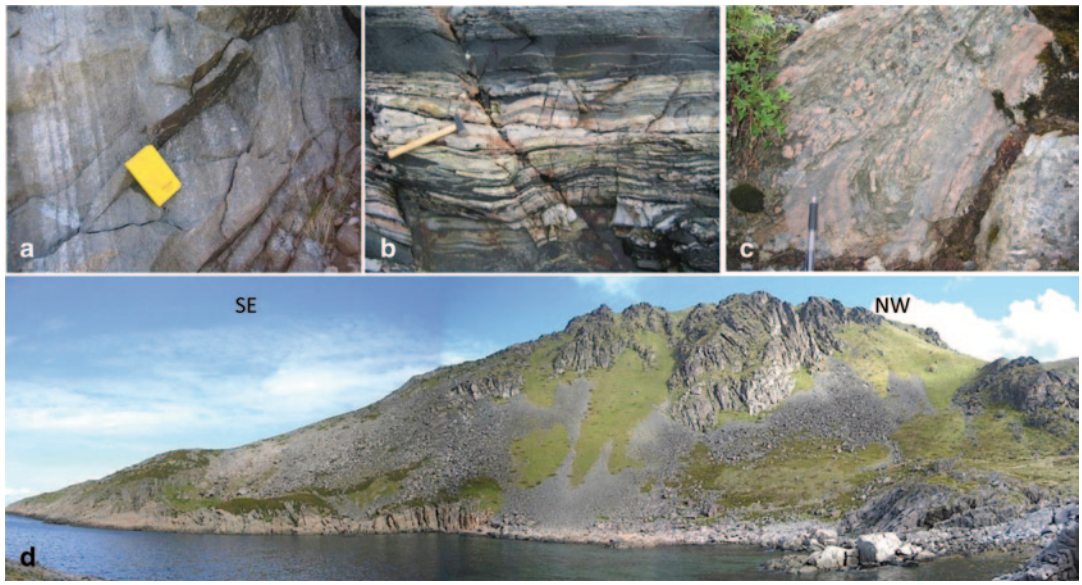

Fig. 4.7 Outcrop photographs of Archaean basement rocks in Lofoten and Vesterålen. **a** Banded tonalitic gneiss of the Neoarchaean gneiss suite in Vesterålen. **b** Foliated Neoarchaean paragneiss composed of alternating quartz-rich and mafic meta-volcanic rocks; Langøy, Vesterålen. **c** Retrogressed migmatite zone in tonalitic gneisses on Langøya, Vesterålen. **d** Panorama of tonalitic gneisses on Langøya, Vesterålen

4.5 Discussion

The Archaean portion of the West Troms Basement Complex and adjacent Lofoten-Vesterålen area, west of the Scandinavian Caledonides, are similar in terms of Neoarchaean lithologies, i.e. tonalitic TTG gneisses, supracrustal units, magmatic rocks, radiometric ages, and tectono-metamorphic evolution (Table 4.1) which make them very likely part of the same Archaean geotransect (Bergh et al. 2010; Myhre et al. 2013). In the West Troms Basement Complex, the TTG gneisses were formed and variously deformed during at least three main Neoarchaean tectono-magmatic events in spatial domains at 2.92–2.80 Ga (tonalite crystallization in the northeast), 2.75–2.70 Ga (mafic plutons in the central and southwestern parts) and at c. 2.7–2.67 Ga (magmatism, regional high-grade metamorphism and migmatization), followed by a high-grade metamorphic resetting at c. 2.6 Ga (Myhre et al. 2013). The 2.7–2.67 Ga event is considered the main orogenic event that formed the main gneissic foliation and subsequent localized migmatization and high-grade ductile shearing (Bergh et al. 2010). Crustal accretion caused by plate convergence is a favourable process for this deformation, which may have involved juxtaposition of different crustal portions or *terranes* (Fig. 4.8a; Bergh et al. 2010; Myhre et al. 2013). Notably, the high-grade migmatitic shear zone that was responsible for juxtaposition of the 2.75–2.67 Ga gneisses in the southwest against 2.8 Ga and older rocks to the northeast, may represent a major intracratonic break or a suture zone between two tonalitic gneiss *terranes*, or alternatively an intracratonic zone of weakness in an extensive Neoarchaean basement. The juxtaposition of 2.8–2.7 Ga tonalites against the oldest 2.92–2.8 Ga province may also reflect a Neoarchaean suture zone, since the fabric along the docking shear zone between the Dåfjord and Kvalsund gneisses is cut by 2.4 Ga mafic dykes (Myhre et al. 2013). Such sutures, however, are hard to detect elsewhere due to the superimposed Svecofennian events (Fig. 4.8c, d).

In this Neoarchaean scenario, the intercalated mafic and siliciclastic rocks of e.g. the Ringvassøya greenstone belt, with ages of 2.85 -2.83 Ga, may be remnants of amalgamated ocean floor deposits, arc-related mafic/ultramafic

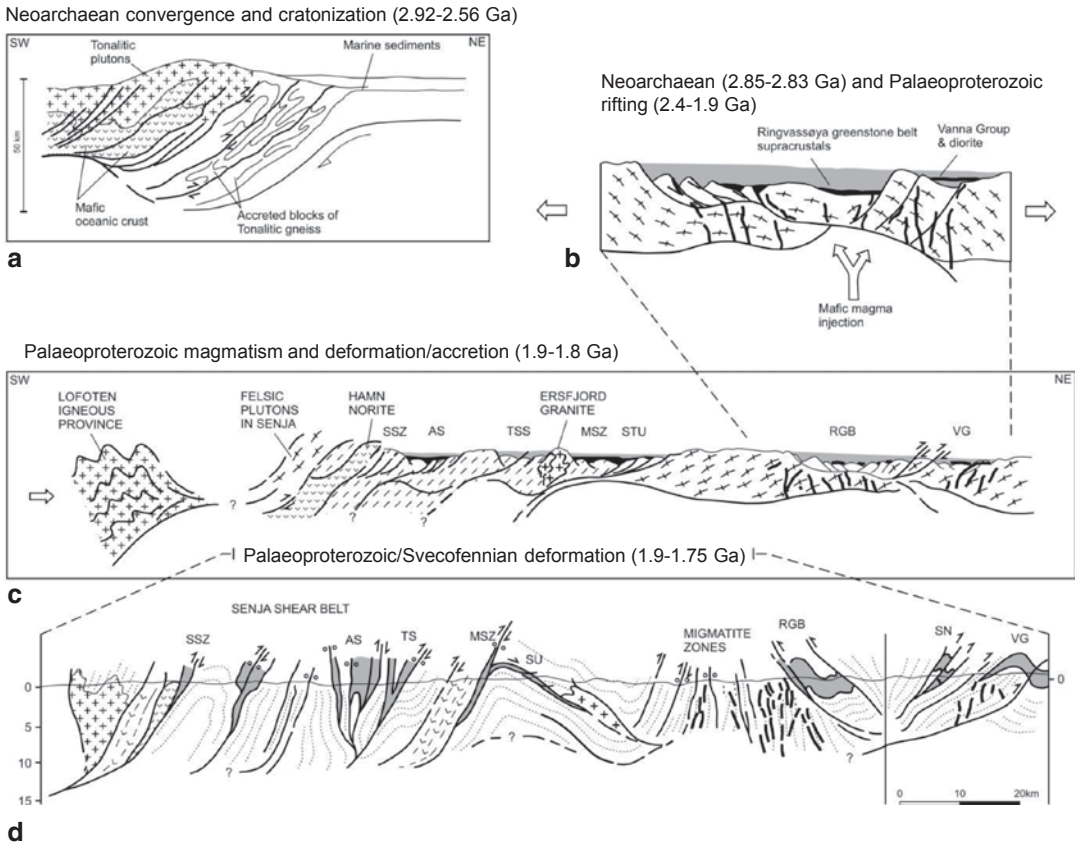

Fig. 4.8 Tectonic diagrams illustrating the Meso-Neoarchaean to Palaeoproterozoic tectonic evolution of the West Troms Basement Complex, after Bergh et al. (2010): **a** Meso-Neoarchaean (2.92–2.56 Ga) tonalitic gneiss-forming event with crustal accretion and thickening. Note position of possible precursory volcanic basin deposits of the 2.85–2.83 Ga Ringvassøya greenstone belt. **b** Neoarchaean and Early Palaeoproterozoic (2.5–1.9 Ga) crustal extension, basin formation and intrusion of the 2.4 Ga Ringvassøya mafic dyke swarm. **c** Palaeoproterozoic (1.9–1.8 Ga?) continental contraction and probable magmatic arc accretion in the southwest (including the Lofoten AMCG suite). **d** Detailed section illustrating the composite result of Archaean and Palaeoproterozoic crustal contraction and transpressive deformation through time. Abbreviations are shown in Fig. 4.3

and metasedimentary rocks, and/or continental basalts and siliciclastic units formed in the intervals of major accretion (Fig. 4.8a, b; Motuza et al. 2001; Bergh et al. 2010; Myhre et al. 2011). Importantly, the transitional tholeiitic to calc-alkaline geochemistry of the greenstone belt rocks is reminiscent of the chemostratigraphy and magmatic evolution of island arc ophiolites, and thus may provide important clues to understanding the evolution of Archaean oceanic crust evolution (cf. Dilek & Furnes 2009, 2011).

The main Neoarchaean crust formation to the southwest of the Dåfjord/Kvalsund gneiss *terrane* boundary took place at 2.75–2.67 Ga, but this region also contains older rocks (Myhre et al. 2013). Thus, there is no obvious major break in the ages of the rocks associated with the structural architecture of the West Troms Basement Complex, suggesting that large parts of the Neoarchaean rocks here record a single but complex amalgamation event (Myhre et al. 2013). The U-Pb and structural data suggest that Neoarchaean accretionary processes (Fig. 4.8a) were responsible for many of the internal structures of the gneisses in the West Troms Basement Complex prior to Palaeoproterozoic orogenesis (Fig. 4.8c, d), and that it constituted a coherent

crustal segment at the end of the Neoarchaean (Myhre et al. 2013).

In the Lofoten-Vesterålen area, U-Pb data provide clear evidence for two major periods of crustal accretion and stabilization in the Neoarchaean (Heier & Compston 1969; Griffin et al. 1978). The earliest crust formed during a major crustal accretion event recorded at 2.85–2.7 Ga throughout the region (Corfu et al. 2003; Kullerud et al. 2006). Neoarchaean U-Pb ages are also found in zircon and monazite both in the high- and medium-grade parts of the region and define another distinct tectono-magmatic event. The available data indicate magmatism in the period c. 2.75–2.68 Ga with a subsequent event at about 2.64 Ga involving the emplacement of tonalite and high-grade metamorphism and migmatization, thus adding new magmas and reworking the existing crust (cf. Jacobsen & Wasserburg 1978; Wade 1985).

The termination of the Neoarchaean crustal amalgamation event (c. 2.6 Ga) was followed by the intrusion of the extensive Ringvassøya mafic dyke swarm and a dioritic sill into meta-sedimentary rocks of the Vanna Group in the period 2.4–2.2 Ga (Fig. 4.8b; Bergh et al. 2007). This adds a clear time limit for the onset of Palaeoproterozoic rift-magmatic events (Fig. 4.8c, d) in the West Troms Basement Complex. In the Lofoten-Vesterålen area, there is also clear evidence of mafic dykes, supracrustal units and widespread tectono-magmatic events at c. 1.8–1.7 Ga that post-date the Neoarchaean activity (Griffin et al. 1978). The mafic dyke swarms and supracrustal units are coeval in age with a global event that involved crustal extension (Fig. 4.8b) and break-up of a Neoarchaean supercontinent between about 2.4 and 1.9 Ga (Williams et al. 1991). Later, the intrusion of mafic and granitoid plutons in the West Troms Basement Complex and the AMCG suite in Lofoten (Griffin et al. 1978; Corfu 2004a) marked the onset of an intensive magmatic event (1.87–1.79 Ga) corresponding to arc-related tectonism during the early stages of the collisional Svecofennian orogeny in Fennoscandia (Gaál & Gorbatchev 1987; Nironen 1997). During this event the Neoarchaean rocks were variably deformed and metamorphosed up to granulite facies (Griffin et al. 1978; Corfu et al. 2007; Bergh et al. 2010). In the West Troms Basement Complex, this deformation occurred at c. 1.79–1.75 Ga and was localized mainly along the boundaries to supracrustal belts and superimposed on pre-existing Neoarchaean structures. The deformation involved NE-directed thrusting, macroscopic upright folding and combined late-stage partitioned deformation (Bergh et al. 2010), which created the overall lens-shaped structural pattern that characterizes these basement suites (Fig. 4.3) (Bergh et al. 2010).

4.6 Neoarchaean Terrane Amalgamation

The Neoarchaean basement outliers west of the Caledonides in North Norway belong to a crustal segment with a variety of ages, major metamorphic breaks and a protracted tectono-magmatic history (Bergh et al. 2010; Myhre et al. 2013) with periods of Neoarchaean amalgamation at c. 2.9–2.8 Ga, 2.75–2.7 and 2.7–2.67 Ga (Fig. 4.9a). The final Neoarchaean stage (c. 2.67 Ga) caused high-grade metamorphism, resetting and comprehensive migmatization along presumed Neoarchaean terrane boundary shear zones prior to the intrusion of an extensive Palaeoproterozoic mafic dyke swarm at 2.4–2.2 Ga (Fig. 4.8b). The aftermath of Palaeoproterozoic evolution involved rifting and basin formation at 2.4–1.9 Ga (Fig. 4.8b), accretion and intrusion of magmatic suites at 1.8–1.7 Ga (Fig. 4.8c) and the Svecofennian orogeny at c. 1.8–1.67 Ga (Fig. 4.8d).

This paper addresses the Neoarchaean events, and one way to explore them further is to identify different Neoarchaean crustal segments, then to identify possible sutures formed by the juxtaposition of these terranes and, finally, to discuss the process of their assembly in order to explain metamorphic and petrological characteristics (cf. Griffin et al. 1978; Corfu 2004, 2007; Bergh et al. 2010; Myhre et al. 2013). The host rocks of the geotransect include age-equivalent TTG gneisses with a range of structural and metamorphic assemblages, but only modest variations exist at peak metamorphic grades in the differ-

ent parts of the suite (Myhre et al. 2013). This indicates that at the end of the Neoarchaean the TTG gneisses and accompanying magmatic and supracrustal units were assembled as a single large terrane, formed during one prolonged cratonization event (2.92–2.67 Ga), though with considerable complexity in detail (Myhre et al. 2013). In this scenario, the migmatized ductile shear zones bounding the Dåfjord and Kvalsund gneisses on Ringvassøya (Fig. 4.3; Bergh et al. 2010; Myhre et al. 2013) and potentially the major tectonic and metamorphic boundary in the Lofoten area (Fig. 4.6; Corfu 2004a) may reflect Neoarchaean crustal boundaries between contrasting terranes or blocks that were assembled in the late Neoarchaean. However the presence of metasupracrustal units with highly contrasting ages, e.g. 2.85–2.83 Ga for the Ringvassøya greenstone belt, 2.4–2.2 Ga for the Vanna Group (Bergh et al. 2007) and c. 1.9 Ga for the Torsnes belt (Myhre et al. 2011), would support multiple terranes and not a unified supracrustal belt at the end of the Neoarchaean. The slight contrast in U-Pb ages of the Neoarchaean basement rocks in the southwest (2.7–2.6 Ga) compared to the northeast (2.92–2.8 Ga) could indicate the presence of two terranes (Bergh et al. 2010).

A major tectono-metamorphic break also exists in the Lofoten area (Fig. 4.6), and a similar abrupt change is thought to occur between the islands of Vesterålen and Senja (Fig. 4.2), in a region that separates dominantly amphibolite-facies Neoarchaean gneisses from Palaeoproetrozoic granulite-facies AMCG suite rocks of the Lofoten province (Griffin et al. 1978; Corfu 2004a). This major boundary is inferred by contrasting gravity and magnetic signatures. This boundary, however, is Palaeoproterozoic in age (cf. Henkel 1991; Doré et al. 1997; Olesen et al. 1997), as evidenced by the U-Pb age of peak metamorphism at 1.87–1.78 Ga in Lofoten and c.1.78 Ga in the West Troms Basement Complex (Table 4.1). This suture could be a reactivation of the Neoarchaean terrane boundary shear zones (Corfu 2004a; Bergh et al. 2010) formed by SW-directed convergence/accretion toward an orogenic front near Lofoten involving an oppositely NE-dipping accretion/subduction-derived shear zone situated in the Senja Shear Belt in the northeast (cf. Bergh et al. 2010).

4.7 Neoarchaean Correlation with Fennoscandia

A major unresolved problem in the Archaean to Palaeoproterozoic basement outliers in North Norway is their potential correlation with other cratonic-marginal crustal segments in the North Atlantic realm (Fig. 4.9). Their location just west of the Scandinavian Caledonides makes it difficult to attribute them to Fennoscandia and/or Laurentia (Fig. 4.9), and therefore they have usually been assigned an uncertain or exotic tectonostratigraphic status (Hölttä et al. 2008; Koistinen et al. 2001). However, a first step toward a valid correlation requires a geological and geodynamic understanding of the region, and such a framework has recently been established for the West Troms Basement Complex (Bergh et al. 2010). Similar frameworks exist for the Fennoscandian Shield of Finland, Sweden and northwestern Russia (Gaál & Gorbatchev 1987; Gorbatchev & Bogdanova 1993; Hölttä et al. 2008; Lahtinen et al. 2008), for Greenland/Laurentia (van Gool et al. 2002; Sidgren et al. 2006) and the Lewisian of NW Scotland (Friend & Kinney 2001; Park 2005).

Previous reconstructions show that the Karelian and Superior cratons of Fennoscandia and Laurentia in the North Atlantic realm (Fig. 4.9) were in close vicinity to each other or connected in the Neoarchaean as a supercontinent (Mertanen & Korhonen 2011) and that breakup of this supercontinent along Neoarchaean shear zones led to the formation of several micro-continents which were later reassembled with juvenile terranes during the Palaeoproterozoic (Williams et al. 1991; Daly et al. 2006) (Fig. 4.9).

Most workers agree that the Neoarchaean components of the basement outliers west of the Caledonides in North Norway are an autochthonous part of the Fennoscandian Shield (Gaál & Gorbatchev 1987; Park et al. 2001; Hölttä et al. 2008). The critical local evidence arrives from tracing Neoarchaean and/or Palaeoproterozoic

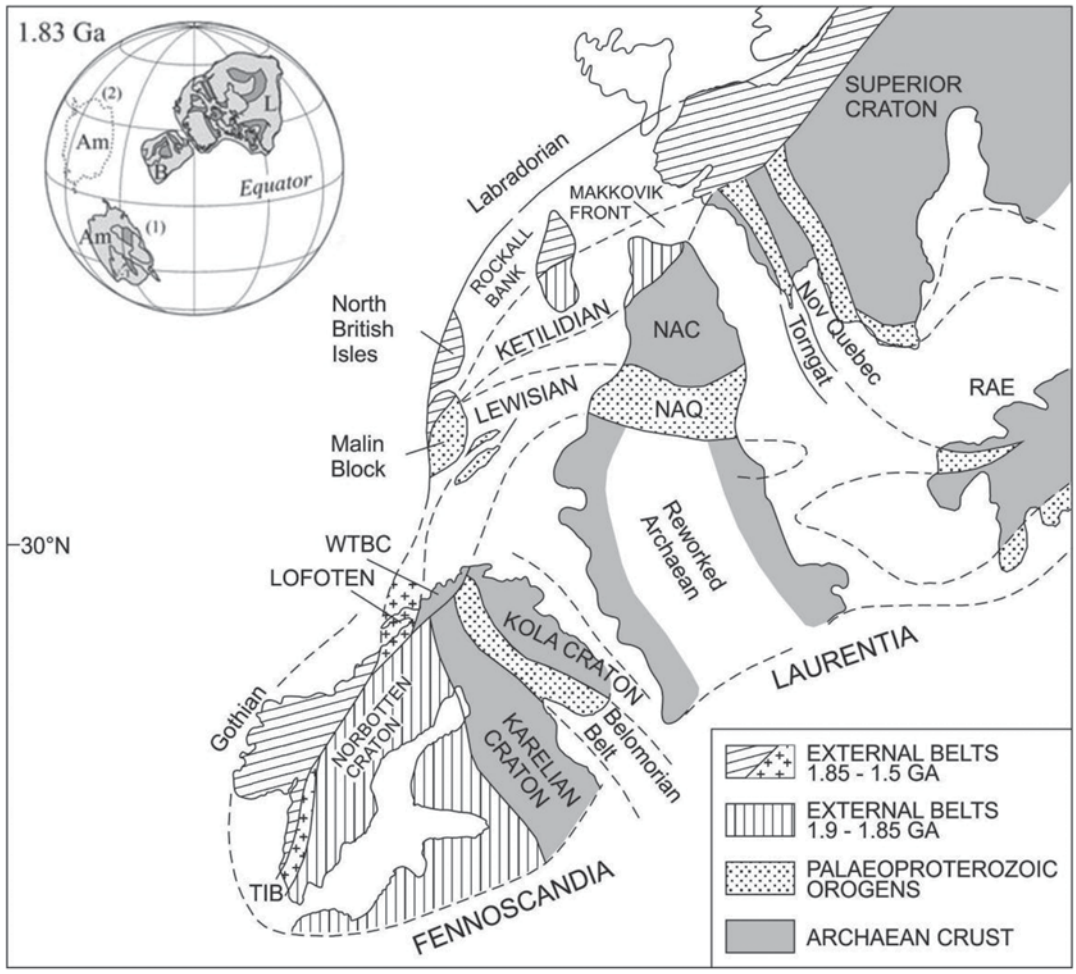

Fig. 4.9 Reconstruction of Fennoscandia and Laurentia prior to the onset of Palaeoproterozoic orogeny (1.83 Ga) based on the palaeomagnetic fit of Pesonen et al. (2003). Note that the West Troms Basement Complex (including Lofoten-Vesterålen) lies within a continuous Palaeoproterozoic belt extending from the Torngat orogen of Laurentia through the Ketilidian and Nagssugtoqidian orogens to link up with the Kola and Karelian/Belomorian provinces of Fennoscandia. The map is modified from Park et al. (2001) and Lahtinen et al. (2008). Abbreviations: *WTBC* = West Troms Basement Complex

NW-SE shear zones and greenstone belts in the basement rocks beneath the Caledonian nappes in northern Nordland, central Troms and Finnmark in a direction parallel to the Bothnian-Senja shear zone system of northern Sweden and Finland (Fig. 4.1 and 4.10; Henkel 1991; Doré et al. 1997; Olesen et al. 1997). The basement suite in Lofoten and Vesterålen lies very close to a suite of similar magmatic rocks in Hamarøya and Tysfjord on the mainland (Tveten 1978), but still within the Caledonides (Fig. 4.2). In addition, several tectonic basement windows occur inside the Caledonian nappe pile, the largest and closest of which is the Rombak Tectonic Window (Figs. 4.2 and 4.10) (Korneliussen et al. 1986; Korneliussen & Sawyer 1989; Bargel et al. 1995). The Rombak Tectonic Window is dominated by Palaeoproterozoic metavolcanic and sedimentary rocks (<2.3 Ga), defining N-S and NW-SE trending narrow belts and shear zones, and intruded by mafic to intermediate 1.9–1.7 Ga granitic batholiths (Korneliussen et al. 1986; Romer 1987, Korneliussen & Sawyer 1989; Bargel et al. 1995; Larsen et al. 2011), while

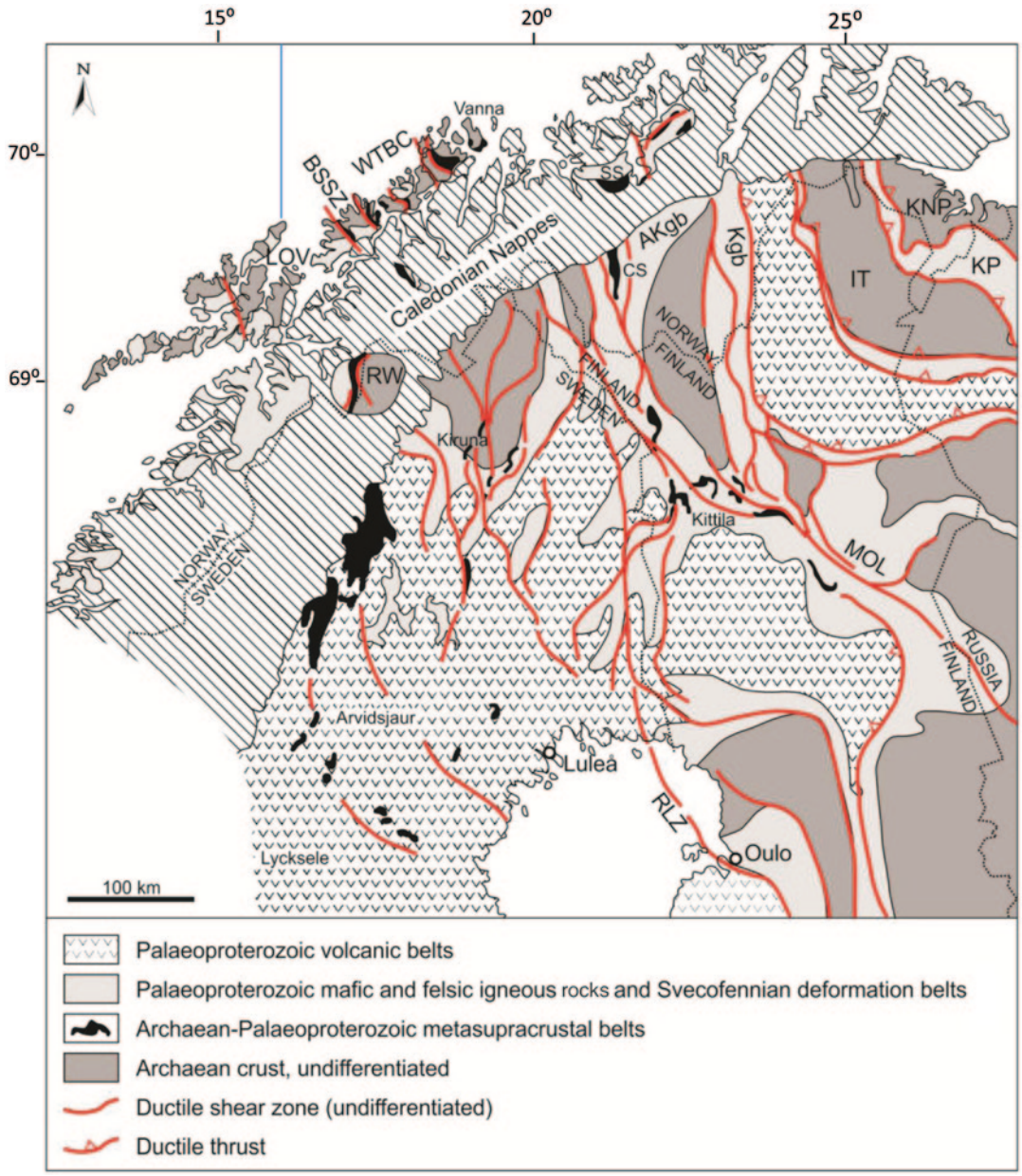

Fig. 4.10 Regional map of the northern Fennoscandian Shield showing the distribution of Archaean and Palaeoproterozoic crust and the basement outliers within and to the west of the Scandinavian Caledonides. Note the presence of various metasupracrustal belts, magmatic rocks and major ductile shear zones that may represent terrane boundaries between Archaean and/or Palaeoproterozoic crustal fragments. This map provides the basis for correlation of the West Troms Basement Complex and Lofoten-Vesterålen with the autochthonous northern part of Fennoscandia, through transitional tectonic windows within the Caledonides. Note also the parallelism of ductile shear zones in the West Troms Basement Complex, including the Bothnian-Senja shear zone with the Malangen-Onega lineament of the Karelian province (Fig. 4.1), and the characteristic NW-SE and N-S trending network of ductile shear zones of the region. For details of names and units of the Fennoscandian shield, see Hanski et al. (2001). The map is modified from Gaál & Gorbatchev (1987), Gorbatchev & Bogdanova (1993), Kärki et al. (1993), Hanski et al. (2001), Koistinen et al. (2001) and Bergh et al. (2007). Abbreviations are: *AKgb* = Alta-Kautokeino greenstone belt, *BSSZ* = Bothnian-Senja shear zone *KaP* = Karelian province, *Kgb* = Karasjok greenstone belt, *KNP* = Kola-Norwegian province, *KP* = Kola province, *LOV* = Lofoten-Vesterålen, *MOL* = Malangen-Onega lineament, *RLZ* = Rahe-Ladoga shear zone, *RW* = Rombak Tectonic Window, *SS* = Skoadduvarri Sandstone, *CS* = Caravarri Sandstone, *WTBC* = West Troms Basement Complex

older basement TTG gneisses may exist. Thus, it is reasonable to conclude that these basement suites may be connected and that they link the Caledonian basement outliers of western Troms and Lofoten to the northern and outermost Fennoscandian Shield (Fig. 4.10: Bergh et al. 2010).

In a larger context, dominantly Neoarchaean rocks make up much of the northeastern parts of the Fennoscandian Shield and include provinces such as the Karelian, Belomorian, Kola, Kola-Norwegian, Murmansk and Norrbotten provinces (Fig. 4.1; Hölttä et al. 2008). TTG gneisses cover about 80 % of these areas, in addition to greenstone belts, paragneisses, granulite complexes and migmatitic amphibolites (Table 4.2; Hölttä et al. 2008). Notably, these provinces comprise major NW-SE and N-S trending mega-shear zones and aligned meta-supracrustal belts similar to those of the West Troms Basement Complex and Lofoten-Vesterålen area (Fig. 4.10). The closest province to be linked to the basement outliers west of the Caledonides would be the Neoarchaean components of the Karelian province (Table 4.2; Slabunov et al. 2006), which cover the same age span of TTG gneisses (>2.8–2.7 Ga) and greenstone belts (2.85–2.73 Ga). This province also appears to line up directly along strike with the basement suites of western Troms and corresponds well with the extension of the Bothnian-Senja shear zone into the Malangen-Onega lineament (Fig. 4.10). An alternative correlation is with the Belomarian, Kola, Kola-Norwegian and/or Murmansk provinces (Kozlov et al. 2006) which extend southeastward from Finnmark into Finland and the Kola peninsula (Fig. 4.1, Table 4.2).

In Kola, Neoarchaean TTG gneisses of the Murmansk province (Hölttä et al. 2008) have the same ages as those of the West Troms Basement Complex (2.77–2.72 Ga), including greenstone belts of the Kola-Norwegian province that have been dated at c. 2.87–2.76 Ga (Hölttä et al. 2008). Three greenstone belt associations are present in the Belomorian province (Fig. 4.1), dated at 2.88–2.82 Ga, 2.82–2.78 Ga and 2.75–2.66 Ga (Table 4.2; Hölttä et al. 2008). The oldest 2.88–2.82 Ga greenstone belts consist of arc-type BADR rocks, basaltic andesites with forearc meta-greywackes, oceanic komatiites and basalts and mafic-ultramafic complexes that may be fragments of e.g. suprasubduction zone ophiolites (Slabunov et al. 2006; Dilek & Polat 2008). These compositional features to some extent resemble those of the Ringvassøya greenstone belt (Motuza et al. 2001), although komatiites have not yet been recorded there.

Additionally, in the period c. 2.75–2.62 Ga all these provinces were intensely deformed and underwent high-grade metamorphism during accretional and collisional processes (Hölttä et al. 2008). Synchronous arc volcanism and deposition of greywacke/mudstones is recorded as meta-supracrustal suites throughout the Karelian, Belomorian and Kola-Murmansk provinces, which makes correlation to Fennoscandia highly possible and warrants further regional comparison (Hölttä et al. 2008).

Farther northeast in Norway, the Karasjok and Kautokeino greenstone belts (Fig. 4.10) of presumed Palaeoproterozoic age (Krill 1985; Krill et al. 1985; Bergh & Torske 1988; Braathen & Davidsen 2000) may be analogues to at least the youngest greenstone belts in the West Troms Basement Complex (Armitage & Bergh 2005; Myhre et al. 2011). Notably, all these metasupracrustal rocks have been reworked by the Palaeoproterozoic orogenic events in the period 1.9–1.7 Ga (Lahtinen et al. 2008). A correlation of the meta-supracrustal sequences in the Vanna Group with the Skoadduvarri and Caravarri Sandstone Formations of the Kautokeino greenstone belt (Zwaan & Gautier 1981; Bergh & Torske 1986; Torske & Bergh 2004) also seems plausible (Fig. 4.10), and would add valid constraints to the debate on regional correlation of the West Troms Basement Complex with Fennoscandia or Laurentia (Bergh et al. 2010; Myhre et al. 2011). Furthermore, if a correlation between the Kautokeino Greenstone Belt and parts of the Kittila Greenstone Complex in the Karelian province of central Finland (Fig. 4.10: Hanski et al. 1997; Rastas et al. 2001) and related meta-supracrustal (greywacke) sequences (Räsanen et al. 1995; Hanski et al. 1997, 2000: Lehtonen et al. 1998) is valid, as proposed by Torske & Bergh (2004), this would favour a direct

Table 4.2 Summary of the main ages, components and events in the Karelian, Belomorian and Kola-Murmansk provinces of the Fennoscandian Shield, after Kozlov et al. (2006), Slabunov et al. (2006), Hölttä et al. (2008) and Lahtinen et al. (2008)

Karelian province		Belomorian province		Kola-Norwegian & Murmansk province	
Age (Ga)	**Components and events**	**Age (Ga)**	**Components and events**	**Age (Ga)**	**Components and events**
3.5 Ga	Trondhjemitic gneisses (Western Karelian, Siurua)				
3.2–2.8 Ga	Neoarchaean TTG-gneisses (Western Karelian)	2.93–2.72 Ga	Meso and Neoarchaean granitoids and TTG gneisses	2.92 Ga	Gabbro-anorthosite
2.85–2.78 Ga	Tonalitic gneisses, migmatites and volcanic rocks (Kianta Complex)	2.88–2.82 Ga	Greenstone belt 1: Arc-type basalt-andesite, komatiite, ultramafic volcanics and forearc greywackes	2.87 Ga	Felsic metavolcanic rocks, alkaline rocks and schists
2.85–2.83 Ga	Orthogneisses			2.8 Ga	Greenstone belt: greywackes and mudstones
2.84–2.79 Ga	Greenstone belts: Oceanic-type komatiites and arc-basalts with sedimentary rocks (Western Karelian)	2.82–2.78 Ga	Greenstone belt 2: Arc-type calc-alkaline volcanic rocks, ophiolites, komatiite-basalt and greywacke.	2.76 Ga	Greenstone belt: basalt and rhyodacite
2.76–2.7 Ga	TTG gneisses and greenstone belts (Central Karelian)	2.75–2.66 Ga	Greenstone belt 3: Molasse-type meta-sedimentary and volcanic rocks, including subalkaline dacite-basalts	2.77—2.72 Ga	TTG gneisses, granitoids, diorites and supracrustal rocks (Murmansk province)
2.75-2.73 Ga	Arc basalt and andesites, felsic volcanic rocks (Eastern Karelian)				
	Neoarchaean deformation and metamorphism				*Neoarchaean deformation and metamorphism*
2.74–2.7 Ga	Subduction-related granitoid rocks		*Neoarchaean deformation and metamorphism:*	2.9–2.7 Ga	Growth of continental masses by subduction of oceanic crust
2.7 Ga	Crustal collision and NE-thrusting	2.73–2.72 Ga	Granulite charnockite complex	2.72 Ga	Collision with the Karelian and Belomorian provinces
2.71–2.69 Ga	Back-arc greywackes/paragneisses and MORB-type volcanics	2.72 Ga	Eclogites	2.67-2.6 Ga	Intraplate crustal growth

Table 4.2 (continued)

Karelian province		Belomorian province		Kola-Norwegian & Murmansk province	
2.72–2.62 Ga	Granulite facies metamorphism and magmatism		Polyphase deformation and high- and moderate-pressure metamorphism due to accretion, subduction and collision with the Kola-Murmansk province		
2.71–2.68 Ga	Post-kinematic granitic rocks	2.68-2.64 Ga	Granitoid rocks, tonalite, trondhjemite, diorite and post-kinematic subalkaline granites	2.77–2.63 Ga	Granitoid rocks
2.5–2.1 Ga	Palaeoproterozoic rifting, dyke swarm intrusion and basin sedimentation				
2.1–2.05 Ga	Formation of the Kola ocean and Svecofennian sea and seafloor spreading				
2.1–1.92 Ga	Arc-related sedimentation				
1.9–1.79 Ga	Arc-related magmatism				
1.94–1.86 Ga	Lappland-Kola orogen: island arc and collision				
1.92–1.79 Ga	Svecofennian orogen; arcretion and continental collision (Lappland-Savo, Fennian, Sveco-baltic and Nordic orogeny)				
1.71–1.67 Ga	Transscandinavian Igneous Belt: Batholitic granitoid				
1.6 Ga	Gothian orogen				

link between the adjacent Neoarchaean rocks of the basement outliers in North Norway and the Karelian province (Figs. 4.1 and 4.10). This correlation is further supported by meta-supracrustal units of many of the supracrustal belts in the West Troms Basement Complex and Rombak Tectonic Window containing auriferous sulphide deposits (Bergh & Armitage 1998; Sandstad & Nilsson 1998; Henderson & Kendrick 2003; Larsen et al. 2011), similar to the auriferous meta-supracrustal belt in the Lycksele-Arvidsjaur region of northern Sweden (Bark & Weihed 2007; Korneliussen & Nilsson 2008), i.e. just south of the Norrbotten province (Fig. 4.10).

4.8 Conclusions

1. Neoarchaean basement rocks occur in two coastal outliers west of the Scandinavian Caledonides in North Norway, in western Troms and the Lofoten-Vesterålen area. The West Troms Basement Complex consists of Meso- and Neoarchaean TTG gneisses (2.9–2.6 Ga) and a major supracrustal unit, the Ringvassøya greenstone belt (2.85–2.83 Ga), in addition to younger, Palaeoproterozoic rift-magmatic dyke swarms (2.4–2.2 Ga) supracrustal rocks (2.4–1.9 Ga), and igneous granitic and mafic rocks (1.8–1.77 Ga) whereas in the Lofoten province to the southwest, similar Neoarchaean TTG gneisses have been intruded by an extensive 1.8–1.7 Ga magmatic suite composed of anorthosites, mangerites, charnockites, gabbros and granites. In both regions, the TTG gneisses and related rocks were intensively reworked during the Palaeoproterozoic orogenesis (1.9–1.7 Ga).
2. The TTG gneisses of the West Troms Basement Complex crystallized as tonalitic magmas and were deformed and metamorphosed up to granulite facies during three tectono-magmatic events at 2.92–2.80 Ga, 2.75–2.70 Ga and at c. 2.7–2.67 Ga, followed by a high-grade metamorphic resetting at c. 2.6 Ga. The 2.7–2.67 Ga event was the main amalgamation event with high-grade ductile shearing and migmatization, most probably due to crustal accretion and plate convergence/collision with juxtaposition of one or more crustal terranes in an extensive Neoarchaean basement. Possible terrane boundaries exist (1) between the Dåfjord and Kvalsund gneisses in the West Troms Basement Complex, (2) along a major tectono-metamorphic break in eastern Lofoten, and (3) between the islands of Vesterålen and Senja. The mafic transitional tholeiitic to calc-alkaline meta-volcanic rocks and intercalated siliciclastic rocks of the Ringvassøya greenstone belt (2.85–2.83 Ga) may be remnants of arc-related ophiolites and meta-sedimentary deposits formed in the intervals between major accretion.
3. The Neoarchaean basement rocks in western Troms and Lofoten share a similar early Neoarchaean history of: (1) tonalite magmatism (2.92–2.8 Ga), (2) convergent tectonism (c. 2.7–2.67 Ga) including high-grade metamorphism, partial melting, and formation of crustal-scale ductile shear zones and a gently dipping gneissic fabric, and (3) a terminal metamorphic stage (c. 2.6–2.5 Ga) characterized by retrogression and crustal rejuvenation. The existence of a Neoarchaean stage of tectonic assembled terranes is not well constrained due to the superimposed Palaeoproterozoic (Svecofennian) orogeny (1.9–1.7 Ga), which may also have involved multiple terrane boundaries.
4. Regional correlation of the basement outliers in North Norway with the Karelian province of the Fennoscandian Shield seems most likely. Gravity-magnetic linkage of NW-SE trending ductile shear zones and greenstone belts from the western outliers via transitional tectonic basement windows within the Caledonides, to the autochthonous Belomorian and Kola-Norwegian/Murmansk provinces farther east, is also highly relevant in that these suites record temporally similar components that share similar geological settings and Archaean evolution.

Acknowledgements This paper is based on several years of research in the West Troms Basement Complex and the Lofoten-Vesterålen area. The ongoing research is an interdisciplinary study at the University of Tromsø, the University of Oslo and the Geological Survey of Norway, aimed at resolving aspects of the Precambrian development of provinces along the northern margin of Fennoscandia.

References

Andresen A, Tull JF (1983) The age of the Lødingen granite and its possible regional significance. Norsk Geologisk Tidsskrift 63:269–276

Andresen A, Forslund T (1987) Post-Caledonian brittle faults in Troms: geometry, age and tectonic significance (Abstract). The Caledonian and related Geology of Scandinavia. Symposium. Cardiff, Sept 1987

Andersen TB, Jamtveit B, Dewey JF, Swensson E (1991) Subduction and eduction of continental crust: major mechanisms during continent-continent collision and

orogenic extensional collapse, a model based on the south Norwegian Caledonides. Terra Nova 3:303–310

Armitage PEB, Bergh SG (2005) Structural development of the Mjelde-Skorelvvatn Zone on Kvaløya, Troms: a metasupracrustal shear belt in the Precambrian West Troms Basement Complex, North Norway. Norwegian Journal of Geology 85:117–132

Bargel T, Bergstrøm B, Boyd R, Karlsen TA (1995) Geologisk kart, Narvik kommune M 1:100 000, Norges geologiske undersøkelse

Bark G, Weihed P (2007) Orogenic gold in the Lycksele–Storuman ore province, northern Sweden; the Palaeoproterozoic Faboliden deposit. Ore Geology Reviews 32:431–451

Bergh SG, Armitage PEB (1998) Structural reconnaissance field work on western Ringvassøy. (Unpublished report), p 32

Bergh SG, Torske T (1986) The Proterozoic Skoadduvarri Sandstone Formation, Alta, Northern Norway: a tectonic fan delta complex. Sedimentary Geol 47:1–25

Bergh SG, Torske T (1988) Palaeovolcanology and tectonic setting of a Proterozoic meta-tholeiitic sequence near the Baltic Shield margin, northern Norway. Precambr Res 39:227–246

Bergh SG, Kullerud K, Corfu F, Armitage PEB, Davidsen B, Johansen HW, Pettersen T, Knudsen S (2007) Low-grade sedimentary rocks on Vanna, North Norway: a new occurrence of a Palaeoproterozoic (2.4–2.2 Ga) cover succession in northern Fennoscandia. Norwegian Journal of Geology 87:301–318

Bergh SG, Kullerud K, Armitage PEB, Zwaan KB, Corfu F, Ravna EJK, Myhre PI (2010) Neoarchaean to Svecofennian tectono-magmatic evolution of the West Troms Basement Complex, North Norway. Norwegian Journal of Geology 90:21–48

Bleeker W, Ernst R (2006) Short-lived mantle generated magmatic events and their dyke swarms: the key unlocking Earth's paleogeographic record back to 2.6 Ga. In: Hanski E, Mertanen S, Rämö T, Vuollo J (eds) Dyke swarms—time markers of crustal evolution. Balkema Publishers, Rotterdam, pp 3–26

Blystad P, Brekke H, Færseth RB, Larsen BT, Skogseid J, Tørudbakken B (1995) Structural elements of the Norwegian continental shelf. Part II: the Norwegian sea region. Norwegian Petroleum Directorate Bulletin 8:1–45

Braathen A, Davidsen B (2000) Structure and stratigraphy of the Palaeoproterozoic Karasjok Greenstone Belt, north Norway—regional implications. Norsk Geologisk Tidsskrift 80:33–50

Bridgewater D, Austrheim H, Hansen BT, Mengel F, Pedersen S, Winter J (1990) The Proterozoic Nagssugtoqidian mobile belt of southeast Greenland: a link between the Eastern Canadian and Baltic Shields. Geosci Can 17:305–310

Connelly JN, Van Gool JAM, Mengel FC (2000) Temporal evolution of a deeply eroded orogen: the Nagssugtoqidian Orogen, West Greenland. Can J Earth Sci 37:1121–1142

Corfu F (2004a) U-Pb age, setting, and tectonic significance of the anorthosite-mangerite-charnockite-granite-suite, Lofoten-Vesterålen, Norway. J of Petrol 45:1799–1819

Corfu F (2004b) U-Pb geochronology of the Leknes Group: an exotic Early-Caledonian metasedimentary assemblage stranded on Lofoten basement, N-Norway. J Geol Soc London 161:619–627

Corfu F (2007) Multistage metamorphic evolution and nature of the amphibolite–granulite facies transition in Lofoten–Vesterålen, Norway, revealed by U–Pb in accessory minerals. Chem Geol 241:108–128

Corfu F, Armitage PEB, Kullerud K, Bergh SG (2003) Preliminary U-Pb geochronology in the West Troms Basement Complex, North Norway: Archaean and Palaeoproterozoic events and younger overprints. Norges geologiske undersøkelse Bulletin 441:61–72

Daly JS, Balagansky VV, Timmerman MJ, Whitehouse MJ (2006) The Lapland-Kola orogen: Palaeoproterozoic collision and accretion of the northern Fennoscandian lithosphere. Geological Society London Memoirs 32:579–598

Dilek Y, Polat A (2008) Suprasubduction zone ophiolites and Archean tectonics. Geology 36:431–432

Dilek Y, Furnes H (2009) Structure and geochemistry of Tethyan ophiolites and their peterogenesis in subduction rollback systems. Lithos 113:1–20

Dilek Y, Furnes H (2011) Ophiolite genesis and global tectonics: Geochemical and tectonic fingerprinting of ancient oceanic lithosphere. Geological society of America Bulletin 123:387–411

Doré AG, Lundin ER, Fichler C, Olesen O (1997) Patterns of basement structure and reactivation along the NE Atlantic margin. J Geol Soc London 154:85–92

Friend PD, Kinny PD (2001) A reappraisal of the Lewisian Gneiss Complex: geochronological evidence for its tectonic assembly from disparate terranes in the Proterozoic. Contribution Mineral Petrology 142:198–218

Gaál G, Gorbatschev R (1987) An outline of the Precambrian evolution of the Baltic Shield. Precambr Res 35:15–52

Gorbatschev R, Bogdanova S (1993) Frontiers in the Baltic Shield. Precambr Res 64:3–21

Griffin WL, Heier KS, Taylor PN, Weigand PW (1974) General geology, age and chemistry of the Raftsund mangerite intrusion, Lofoten-Vesterålen. Norges geologiske undersøkelse Bulletin 312:1–30

Griffin WL, Taylor PN, Hakkinen JW, Heier KS, Iden IK, Krogh EJ, Malm O, Olsen KI, Ormaasen DE, Tveten E (1978) Archaean and Proterozoic crustal evolution in Lofoten-Vesterålen, N. Norway. J Geol Soc London 135:629–647

Hanski EJ, Huhma H, Lehtonen MI, Rastas P (1997) Isotope (Srn-Nd, U-Pb) and geo-chemical evidence for an oceanic crust to molasse evolution of the Palaeoproterozoic Kittilä greenstone complex, northern Finland. Norges geologiske undersøkelse Report 97.131, COPENA conference, Abstracts and Proceedings

Hanski EJ, Manttari I, Huhma H, Rastas P (2000) Post-1.88 Ga deposits of the Kumpu and Laino group molasse-type sediments in northern Finland: evidence from conventional NORDSIM zircon dating. Abstract, 24, Nordisk geologisk vintermøte, Trondheim 2000. Geonytt 1,75

Heier KS (1960) Petrology and geochemistry of high-grade metamorphic and igneous rocks on Langøy, Northern Norway. Norsk Geologisk tidsskrift 207:1–246

Heier KS, Compston W (1969) Interpretation of Rb-Sr age patterns in high grade metamorphic rocks, north Norway. Norsk geologisk tidsskrift 49:257–283

Henderson I, Kendrick M (2003) Structural controls on graphite mineralisation, Senja, Troms. Geological Survey of Norway Report 2003.011, p 111

Henkel H (1991) Magnetic crustal structures in Northern Fennoscandia. Tectonophysics 192:57–79

Herr W, Wolfe R, Kopp E, Eberhardt P (1967) Development and recent applications of the Re/Os dating method. In: Radioactive dating and methods of low-level counting. International Atomic Energy Agency, Vienna, pp 499–508

Hölttä P, Balagansky V, Garde A, Mertanen S, Peltonen P, Slabunov A, Sorjonen-Ward P, Whitehouse M (2008) Archaean of Greenland and Fennoscandia. Episodes 31:13–19

Jacobsen SB, Wasserburg GJ (1978) Interpretation of Nd, Sr and Pb isotope data from Archaean migmatites in Lofoten-Vesterålen, Norway. Earth Planet Sci Lett 41:245–253

Koistinen T, Stephens MB, Bogatchev V, Nordgulen Ø., Wennerström M, Korhonen J (compilers) (2001) Geological map of the Fennoscandian Shield, scale 1:2 000 000. Espoo, Geological Survey of Finland; Geological Survey of Norway, Trondheim; Geological Survey of Sweden, Uppsala; Ministry of Natural Resources of Russia, Moscow

Korneliussen A, Sawyer E (1989) The geochemistry of lower Proterozoic mafic to felsic igneous rocks, Rombak Window, North Norway. Norges geologiske undersøkelse Bulletin 415:7–21

Korneliussen A, Tollefsrud J. i, Flood B, Sawyer E (1986) Precambrian volcano-sedimentary sequences and related ore deposits, with special reference to the Gauteslifjell carbonate-hosted gold deposits, Rombak basement window, Northern Norway. Norges geologiske undersøkelse, Report 86 193, p 46

Kozlov N.Ye, Sorokhtin NO, Glaznev VN, Kozlova N.Ye, Ivanov AA, Kudryashov NM, Martynov Ye.V, Tyuremnov VA, Matyushkin AV, Osipenko LG (2006) Geology of the Archean of the Baltic Shield. Saint Petersburg, Nauka Publishers, p 239 [in Russian]

Krill A (1985) Svecokarelian thrusting with thermal inversion in the Karasjok-Levajok area of the northern Baltic Shield. Norges geologiske undersøkelse Bulletin 403:89–101

Krill A, Bergh SG, Lindahl I, Mearns E, Often M, Olerud S, Olesen O, Sandstad JS, Siedlecka A, Solli A (1985) Rb-Sr, U-Pb and Sm-Nd isotopic dates from Precambrian rocks of Finnmark. Norges geol Undersøkelse Bulletin 403:37–54

Kullerud K, Skjerlie KP, Corfu F, DeLaRosa J (2006) The 2.40 Ga Ringvassøy mafic dykes, West Troms Basement Complex, Norway: the concluding act of Early Palaeoproterozoic continental breakup. Precambr Res 150:183–200

Lahtinen R, Garde A, Melezhik VA (2008) Palaeoproterozoic evolution of Fennoscandia and Greenland. Episodes 31:20–28

Larsen T, Henderson IHC, Sandstad JS, Bergh SG, Sundblad K (2011) Svecofennian deformation and associated shear zone related sulphide mineralization in the Rombak Tectonic Window, North Norway. NGF Abstracts and Proceedings of the Geological Society of Norway, No.1, p 58

Lehtonen M, Airo M-L, Eilu P, Hanski E, Kortelainen V, Lanne E, Manninen T, Rastas P, Rasanen J, Virransalo P (1998) The stratigraphy, petrology and geochemistry of the Kittila greenstone area, northern Finland. Geological Survey of Finland, Report 140, p 144

Markl G (1998) The Eidsfjord anorthosite, Vesterålen, Norway: field observations and geochemical data. Norsk geologisk tidsskrift 434:51–73

Mertanen S, Korhonen F (2011) Paleomagnetic constraints on an Archean-Paleoproterozoic Superior-Karelia connection: new evidence from Archean Karelia. Precambr Res 186:193–204

Mjelde R, Sellevoll MA, Shimamura H, Iwasaki T, Kanazawa T (1993) Crustal structure beneath Lofoten, N. Norway from vertical incidence and wide-angle seismic data. Geophysical Journal International 114:116–126

Motuza G, Motuza V, Beliatsky B, Savva E (2001) The Ringvassøya greenstone belt (Tromso, North Norway): implications for a Mesoarchaean subduction zone. EUROPROBE time-slice symposium "Archaean and Proterozoic plate Tectonics: geological and geophysical records". St. Petersburg, Russia, October 1–November 3, 2001, pp 43–44

Myhre PI (2011) U-Pb geochronology along a Meso-Neoarchean geotransect in the West Troms Basement Complex, North Norway. Unpublished PhD thesis, University of Tromsø, Norway

Myhre PI, Heaman LM, Bergh SG (2010) Svecofennian (c. 1780 Ma) metamorphic zircon ages from the West Troms Basement Complex, northern Norway. In: NGF Abstract, Proceedings Geological Society Norway pp 128–129

Myhre PI, Corfu F, Bergh S (2011) Palaeoproterozoic (2.0–1.95 Ga) pre-orogenic supracrustal sequences in the West Troms Basement Complex, North Norway. Precambr Res 186:89–100

Myhre PI, Corfu F, Bergh SG, Kullerud K (2013) U-Pb geochronology along a Meso-Neoarchean geotransect in the West Troms Basement Complex, North Norway. Norwegian Journal of Geology, (in press)

Nironen M (1997) The Svecofennian Orogen: a tectonic model. Precambr Res 86:21–44

Olesen O, Torsvik T, Tveten E, Zwaan KB, Løseth H, Henningsen T (1997) Basement structure of the continental margin in the Lofoten-Lopphavet area, northern Norway: constraints from potential field data, on-land structural mapping and paleomagnetic data. Norwegian Journal of Geology 77:15–30

Park RG (2005) The Lewisian terrane model: a review. Scot J Geol 41:105–118

Park RG, Tarney J, Connelly JN (2001) The Loch Maree Group: Palaeoproterozoic subduction-accretion complex in the Lewisian of NW Scotland. Precambr Res 105:205–226

Pesonen LJ, Elming S, Mertanen S, Pisarevsky S, D'Agrella-Filho MS, Meert JG, Schmidt PW, Abrahamsen N, Bylund G (2003) Palaeomagnetic configuration of continents during the Proterozoic. Tectonophysics 375: 289–324

Ramberg IB, Bryhni I, Nøttvedt A (2006) The making of a land. Norsk Geologisk Forening

Rásanen J, Hanski E, Juopperi H, Kortelainen V, Lanne E, Lehtonen MI, Manninen T, Rastas P, Vaananen J (1995) New stratigraphical map of Central Finnish Lappland, 22nd Nordic Geological Winter meeting, Turku, 1996, Abstract, p 182

Rastas P, Huhma H, Hanski EJ, Lehtonen MI, Harkonen I, Kortelainen V, Manttari I, Paakkola J (2001) U-Pb isotopic studies on the Kittilä greenstone area, central Finland. In: Vaasjoki M (ed) Radiometric age determinations from Finish Lapland and their bearing on the timing of Precambrian volcano-sedimentary sequences. Geological Survey of Finland Special Paper 33:95–141

Romer RL (1987) The geology, geochemistry and metamorphism of the Sjangeli area, a tectonic window in the Caledonides of Northern Sweden. Research Report, Luleå University, Sweden. LULEÅ, 16, p 124

Sandstad JS, Nilsson LP (1998) Gullundersøkelser på Ringvassøya; sammenstilling av tidligere prospektering og feltbefaring i 1997. Norges geologiske undersøkelse Report 98. 07, p 61

Sidgren A-S, Page L, Garde AA (2006) New hornblende and muscovite 40Ar/39Ar cooling ages in the central Rinkian fold belt, West Greenland. Geological Survey Denmark-Greenland Bulletin 11:115–123

Slabunov AI, Lobach-Zhuchenko SB, Bibikova EV, Sorjonen-Ward P, Balagansky VV, Volodichev OI, Shchipansky AA, Svetov SA, Chekulaev VP, Arestova NA, Stepanov VS (2006) The Archean nucleus of the Baltic/Fennoscandian Shield. In: Gee DG, Stephenson RA (eds) European lithosphere dynamics, Geological Society of London. Memoirs 32:627–644

Taylor PN (1974) Isotope geology and related geochemical studies of ancient high-grade metamorphic basement complexes: Lofoten and Vesterålen, North Norway. PhD thesis, Oxford University, pp 1–187

Taylor PN (1975) An early Precambrian age for Migmatitic Gneisses from Vikan i Bø, Vesterålen, North Norway. Earth Planet Sci Lett 27:35–42

Torske T, Bergh SG (2004) The Caravarri Formation of the Kautokeino Greenstone Belt, Finnmark, North Norway; a Palaeoproterozoic foreland basin succession. Norges geologiske undersøkelse Bulletin 442:5–22

Tveten E (1978) Geologisk kart over Norge, berggrunns kart Svolvær 1:250 000, Norges geologiske undersøkelse

Van Gool JAM, Connelly JN, Marker M, Mengel FC (2002) The Nagssugtoqidian orogen of West Greenland: tectonic evolution and regional correlation from a West Greenland perspective. Can J Earth Sci 39:665–686

Wade SJR (1985) Radiogenic isotope studies of crust-forming processes in the Lofoten-Vesterålen Province of North Norway. PhD Thesis, University of Oxford (vol I, 1–285, vol II, 1–292)

Williams H, Hoffman PF, Lewry JF, Monger JWH, Rivers T (1991) Anatomy of North America: thematic geological portrayals of the continent. Tectonophysics 187:117–134

Zozulya D, Kullerud K, Ravna EK, Corfu F, Savchenko Y (2009) Geology, age and geochemical constraints on the origin of the Late Archaean Mikkelvik alkaline massif, West Troms Basement Complex in Northern Norway. Norwegian Journal of Geology 89:327–340

Zwaan KB (1989) Berggrunnsgeologisk kartlegging av det prekambriske grønnsteinsbeltet på Ringvassøy, Troms. Norges geologiske undersøkelse Rapport 89.101

Zwaan KB (1995) Geology of the Precambrian West Troms Basement Complex, northern Norway, with special emphasis on the Senja Shear Belt: a preliminary account. Norges geologiske undersøkelse Bulletin 427:33–36

Zwaan KB, Gautier AM (1980) Alta og Gargia. Beskrivelse til de berggrunnsgeologiske kart 1834 I og 1934 IV, 1:50,000. Norges geologiske undersøkelse 357:1–47

Zwaan KB, Tucker RD (1996) Absolute and relative age relationships in the Precambrian West Troms Basement Complex, northern Norway (Abstract). 22nd Nordic Geol. Winter Meeting, Åbo, Finland, p 237

Zwaan KB, Fareth E, Grogan PW (1998) Geologisk kart over Norge, berggrunnskart Tromsø, M 1:250.000. Norges geologiske undersøkelse

A Review of the Geodynamic Significance of Hornblende-Bearing Ultramafic Rocks in the Mesoarchean Fiskenæsset Complex, SW Greenland

5

Ali Polat

Abstract

The Fiskenæsset Complex, SW Greenland, is characterized by layered anorthosite, leucogabbro, gabbro, and ultramafic rock association. Ultramafic rocks consist mainly of hornblendite, hornblende peridotite, hornblende pyroxenite, and dunite. Despite upper amphibolite to granulite facies metamorphism, poly-phase deformation and multiple granitoid intrusions, primary igneous layers and mineral assemblages have been well preserved. Petrographic studies, including SEM-BSE imaging, reveal the presence of igneous hornblende occurring as an interstitial mineral to olivine, clinopyroxene, orthopyroxene, plagioclase, and chromite, as well as inclusions in these minerals, consistent with a hydrous mantle source. Large negative Nb-anomalies in whole-rock samples and hornblende grains suggest that the magmas of the Fiskenæsset Complex originated from a hydrous subarc mantle peridotite. Water was recycled to the source of the Fiskenæsset rocks through subduction of hydrated oceanic crust. Phanerozoic hornblende-bearing mafic and ultramafic rocks are typically associated with supra-subduction zone ophiolites and magmatic arcs. Recycling of water to the upper mantle via subduction of oceanic crust not only resulted in the generation of hornblende-rich rocks, but also played an important role in the formation of TTG-dominated Archean continental crust.

5.1 Introduction

The world's best preserved Archean layered anorthosites and related rocks occur in SW Greenland (Myers 1985; Ashwal and Myers 1994; Windley and Garde 2009; Polat et al. 2009, 2011; Hoffmann et al. 2012). The Fiskenæsset Complex, SW Greenland, is the largest Archean layered intrusive complex in the world, consisting of well exposed layers of anorthosite, leucogabbro, gabbro, and ultramafic rocks (Windley et al. 1973; Windley and Smith 1974; Myers 1985; Polat et al. 2009, 2011, 2012). This complex occurs within a poly-deformed amphibolite to granulite facies orthogneissic (TTG) terrane (Fig. 5.1; Bridgwater et al. 1976; Windley et al. 1973; Myers 1985), and yet it retains well-preserved

A. Polat (✉)
Department of Earth and Environmental Sciences, University of Windsor, Windsor, ON, Canada
e-mail: polat@uwindsor.ca

Y. Dilek, H. Furnes (eds.), *Evolution of Archean Crust and Early Life*, Modern Approaches in Solid Earth Sciences 7, DOI 10.1007/978-94-007-7615-9_5, © Springer Science+Business Media Dordrecht 2014

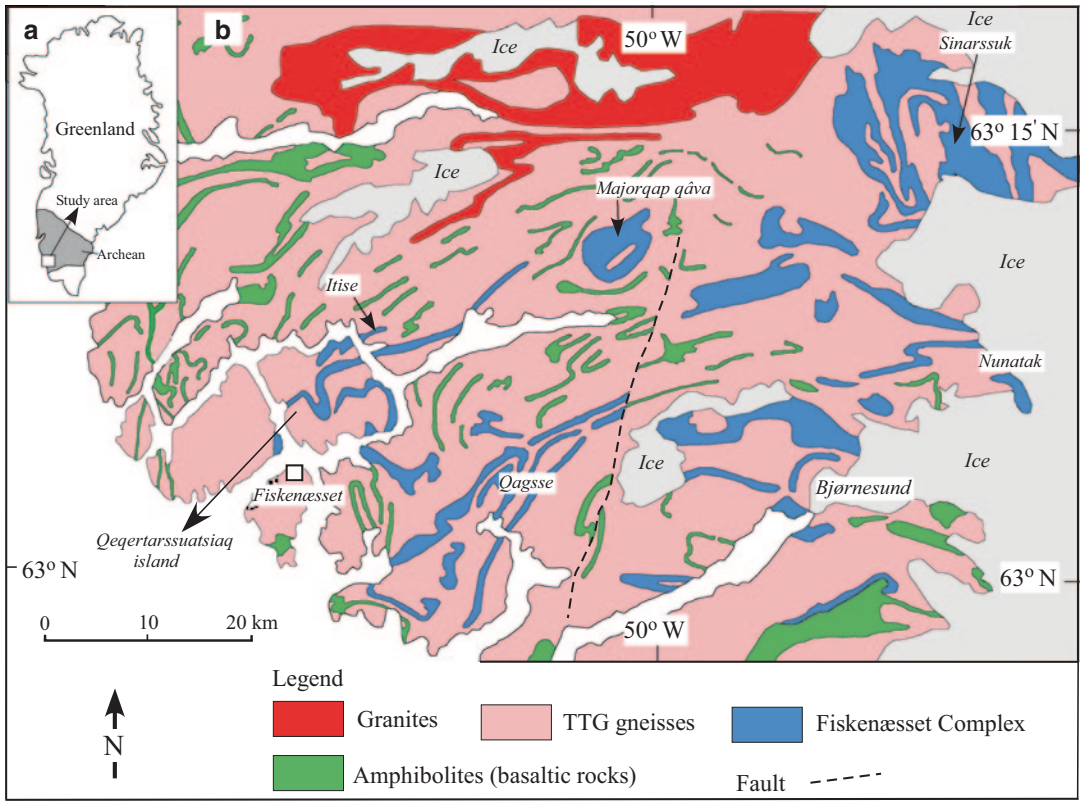

Fig. 5.1 **a** Map of Greenland showing general location of the study area in the Archean craton; and **b** simplified geological map of the Fiskenæsset region (Myers 1976)

primary igneous structures, stratigraphy, textures, and geochemical signatures (Windley et al. 1973; Myers 1985; Polat et al. 2009, 2011, 2012; Huang et al. 2012).

This contribution reviews the recently published (Polat et al. 2009, 2010, 2011, 2012; Huang et al. 2012) field, petrographic, and geochemical data for ultramafic rocks of the Mesoarchean (2.97 Ga) Fiskenæsset Complex, SW Greenland, to make inferences on the mantle source characteristics and the geodynamic processes that played an important role in the formation of the complex as well as on the generation of Mesoarchean continental crust in the study area. Although ultramafic rocks in the Fiskenæsset Complex occur in many locations, this study focuses on those exposed at northern Qeqertarssuatsiaq, Itise, and Sinarssuk (Fig. 5.1b). Forty-five to sixty metres-thick ultramafic rocks at northern Qeqertarssuatsiaq are composed of olivine-pyroxene hornblendite, pyroxene hornblendite, and hornblende pyroxenite (Polat et al. 2012). At Itise and Sinarssuk they consist mainly of hornblende peridotites, hornblende pyroxenites, pyroxene hornblendites, and dunites. In addition, at Sinarssuk dunites and peridotites contain 1 to 15 cm thick chromite layers. In the northern Qeqertarssuatsiaq and Itise areas the ultramafic rocks are intruded by a network of 1–30 cm-thick hornblendite veins (Polat et al. 2010, 2012).

Hornblendites are rare magmatic rocks and typically associated with Phanerozoic ophiolites (Irvine 1974; Koepke and Seidel 2004; Ishimaru et al. 2007; Greene and Giaramita 2008; Dilek and Furnes 2011) and magmatic arcs (Dhuime et al. 2007; Payot et al. 2009; Smith et al. 2009). Given their mantle-derived origin, petrographic and geochemical characteristics of the hornblende-bearing ultramafic rocks in the Fiskenæsset Complex can be used to gain insights into Archean petrogenetic and geodynamic processes.

5.2 Regional Geology, Metamorphism, Field Relationships, and Geochronology

The Fiskenæsset region of SW Greenland consists mainly of TTG gneisses (*ca.* 85 %), amphibolites (*ca.* 10 %), and layered intrusive rocks (*ca.* 5 %) including anorthosite, leucogabbro, gabbro, and ultramafic units (Kalsbeek and Myers 1973; Windley and Smith 1974; Myers 1985). The association of layered anorthosite, leucogabbro, gabbro, and ultramafic rocks constitutes the Fiskenæsset Complex. All these rocks were variably subjected to granulite facies metamorphism and retrogressed to amphibolite facies (Myers 1985; McGregor and Friend 1992). Metamorphic ages are best constrained between 2950 and 2660 Ma (Pidgeon and Kalsbeek 1978; Kalsbeek and Pidgeon 1980; McGregor and Friend 1992; Polat et al. 2010). Riciputi et al. (1990) showed that peak metamorphic conditions in the region reached about 780 °C and 8.9 kbar.

The Fiskenæsset Complex occurs as layers within TTG gneisses and amphibolites (Myers 1985). Single layers range in width from 2 km to less than a metre, occur as trains of inclusions in TTG gneisses, and extend in outcrop for up to at least 50 km (Fig. 5.1b). Throughout the study area exposed layers of the Fiskenæsset Complex have a total strike-length of at least 500 km, typically with the same layer being repeated several times by a combination of folding and thrusting (Kalsbeek and Myers 1973; Myers 1985). Three phases of isoclinal to tight folding resulted in spectacular km-scale fold interference patterns (Myers 1976, 1985).

In many outcrops the Fiskenæsset Complex retains its igneous stratigraphy, cumulate textures, layering, mineral grading, channel deposits, and crosscutting relationships, despite the extensive folding and regional metamorphism (Myers 1985; Polat et al. 2009, 2011, 2012; Huang et al. 2012 and references therein).

The Fiskenæsset Complex has a present mean thickness of ca. 550 m (Myers 1985). The main stratigraphic units, from bottom to top, are: Lower Gabbro, Ultramafic, Lower Leucogabbro, Middle Gabbro, Upper Leucogabbro, Anorthosite, and Upper Gabbro Units (Fig. 5.2; Myers 1985). Chromitite layers that are up to 20 m thick in their undeformed state (Ghisler 1976) occur typically in the Anorthosite Unit and at the top of the Upper Leucogabbro Unit (Myers 1985). Thinner chromitite layers, several centimetres to several tens of centimetres thick, occur in dunites and hornblende peridotites in the Sinarssuk area (Fig. 5.4d; see also Polat et al. 2011).

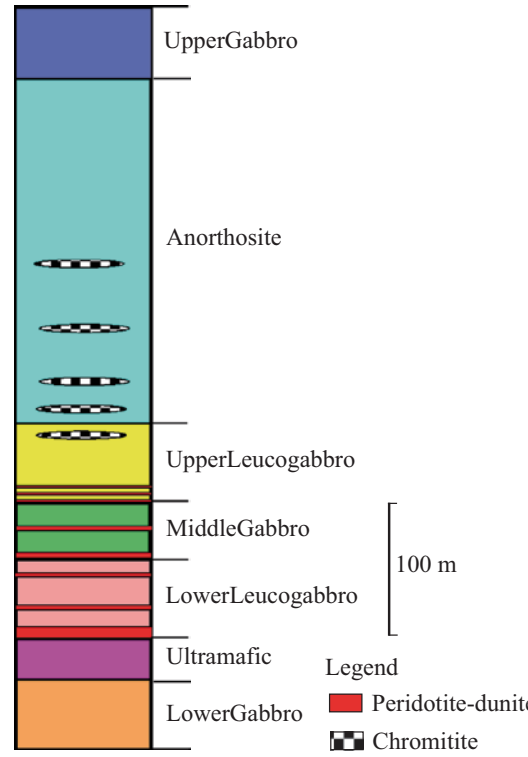

Fig. 5.2 Simplified stratigraphy of the Fiskenæsset Complex (modified after Myers 1985)

Anorthosites and leucogabbros are the two dominant lithologies in the complex. The size of plagioclase crystals in leucogabbros varies from a few millimetres to 40 cm (Polat et al. 2009, 2011). Some large plagioclase crystals are composed of aggregates of smaller crystals, containing hornblende inclusions. Interstitial minerals between cumulate plagioclases are dominated by hornblende and relic pyroxene (Polat et al. 2009, 2011). Ultramafic rocks consist predominantly of hornblendite, hornblende peridotite, hornblende

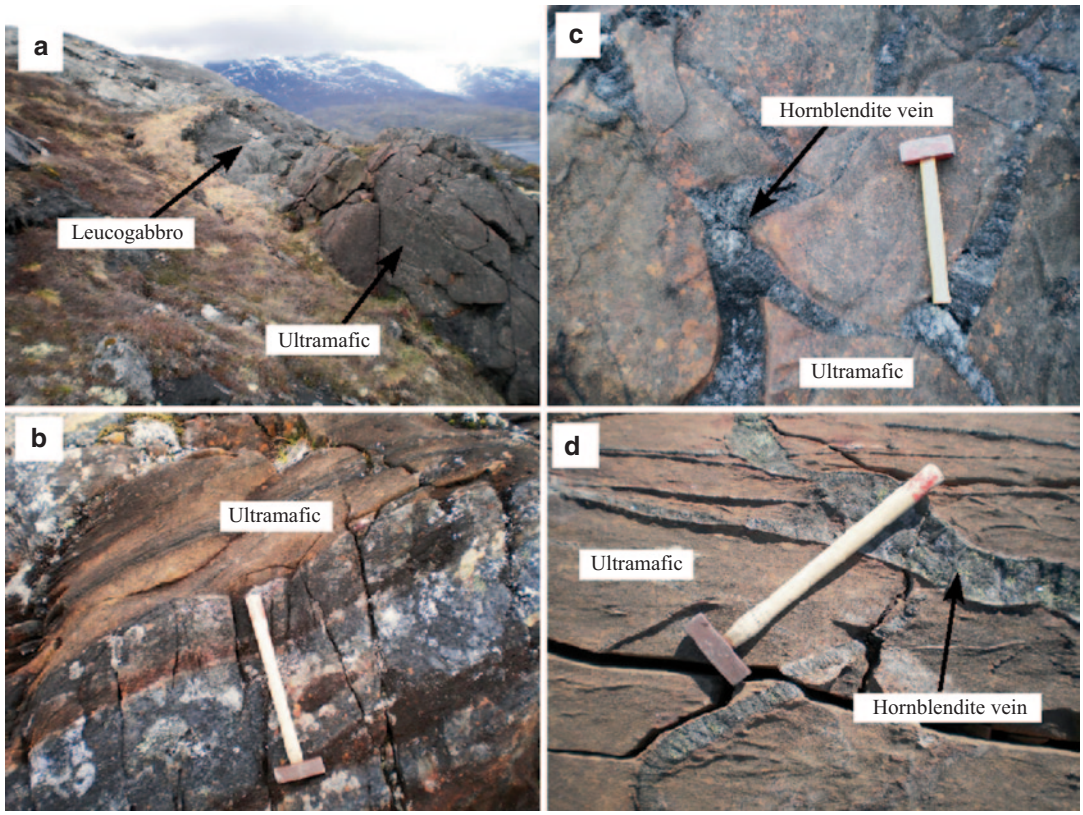

Fig. 5.3 Field photographs illustrating lithological characteristics and field relationships of the ultramafic layers and cross-cutting hornblendite veins at Northern Qeqertarssuatsiaq and Itise: **a** ultramafic sill and overlying leucogabbros; **b** layered ultramafic sill; **c** hornblendite veins cutting and containing lenses of brown orthopyroxene-rich ultramafic rocks; and **d** a network of hornblendite veins cutting orthopyroxene-rich ultramafic rocks (modified from Polat et al. 2012)

pyroxenite, and dunite, which mainly occur as sills, ranging in thickness from several tens of centimetres to several tens of metres. Some of the thickest layers of the Ultramafic Unit occur at Majorqap qâva, northern Qeqertarssuatsiaq, and Itise (Figs. 5.1b, 5.3, and 5.4; see also Huang et al. 2012 and Polat et al. 2009, 2011, 2012). Igneous layering is characterized by intercalated dunite, peridotite, pyroxenite, hornblendite, gabbro, leucogabbros, and anorthosite in the Majorqap qâva and Sinarssuk areas (Figs. 5.3 and 5.4; see also Polat et al. 2009, 2011). Ultramafic sills in the northern Qeqertarssuatsiaq and Itise areas do not display distinct igneous compositional layers and are devoid of chromitite layers.

In several locations at Qeqertarssuatsiaq and Itise, ultramafic layers are intruded by a network of several centimetre - to several tens of centimetre-thick hornblendite veins (Fig. 5.3c, and d), which are commonly characterized by mainly 1–2 cm long hornblende crystals and well-preserved reaction rims with the host ultramafic sill and locally grade into leucogabbros and massive hornblendites; all these features are consistent with an igneous origin.

Intrusive contacts between the Fiskenæsset Complex and the bordering orthogneisses are best exposed in the Sinarssuk and Majorqap qâva areas (Fig. 5.1). As shown by Myers (1976, (1985), the protoliths of TTG gneisses were emplaced as syn-tectonic sheets into the stratigraphic units of the Fiskenæsset Complex and associated basaltic rocks. The emplacement of these rocks occurred mainly along thrust faults (Myers 1976, 1985).

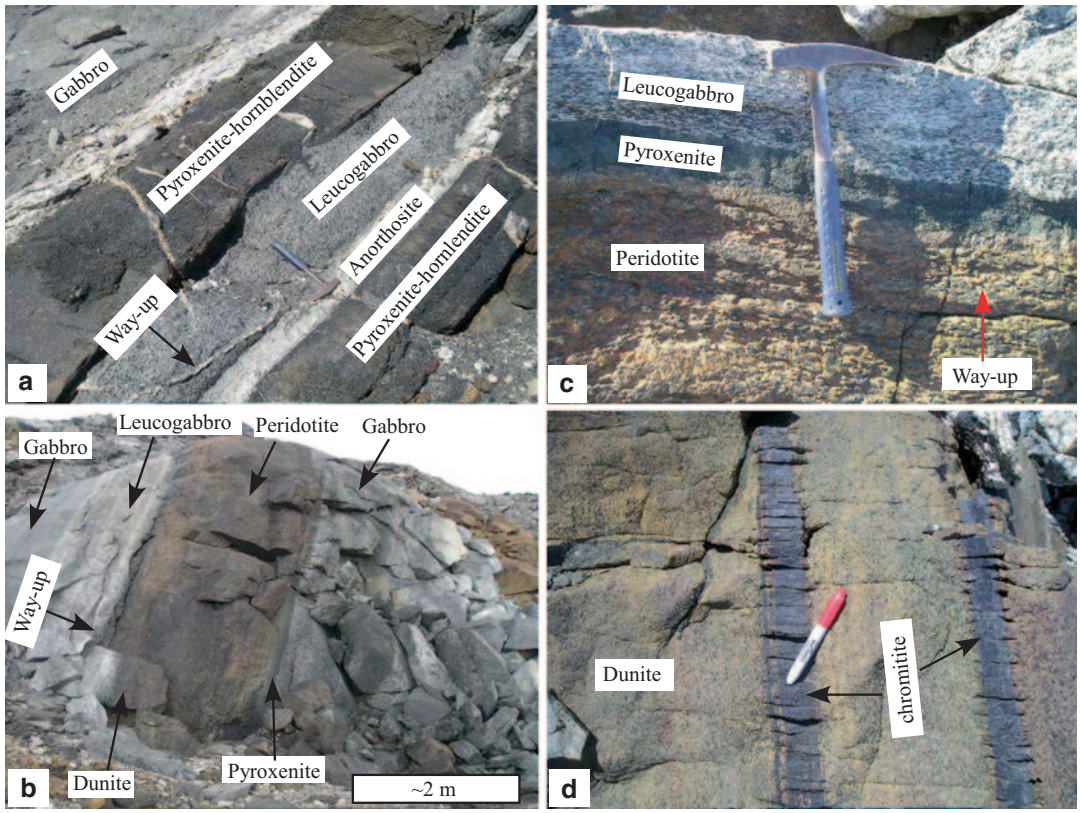

Fig. 5.4 Field photographs illustrating igneous layering in the Sinarssuk area: **a** Igneous layering characterized by pyroxenite, leucogabbro, and anorthosite layers; **b** Igneous layering characterized by dunite, peridotite, gabbro and leucogabbro layers; **c** Igneous layering characterized by peridotite, pyroxenite and leucogabbro layers; and **d** Chromitite (Cr-spinel) layers within dunites (modified from Polat et al. 2011). Hornblende-bearing peridotites in Polat et al. (2011) are re-classified as hornblende peridotites. Similarly, hornblende-bearing pyroxenites in Polat et al. (2011) are re-classified as hornblende pyroxenites and pyroxene hornblendites on the basis of the modal abundance of hornblende

Herr et al. (1967) obtained a Re-Os age of 3080 ± 70 Ma from molybdenites in the Fiskenæsset anorthosites, and Gancarz (1976) reported a Pb-Pb isochron age of 2750 Ma from plagioclase and mafic matrix separates from anorthosites and leucogabbros. Ashwal et al. (1989) reported an Sm-Nd isochron age of 2860 ± 50 Ma for the Fiskenæsset Complex. Keulen et al. (2010) presented U-Pb ($^{207}Pb/^{206}Pb$) zircon ages in the range of 2950 to 2700 Ma for a hornblendite dyke at Majorqap qâva, interpreting the 2950 Ma age as the time of dyke intrusion. Polat et al. (2010) showed that anorthosites, leucogabbros, gabbros and ultramafic rocks at Qeqertarssuatsiaq have 2973 ± 28 Ma (MSWD = 33) and 2945 ± 36 Ma (MSWD = 44) Sm-Nd and Pb isotope regression ages, respectively. Magmatic zircon grains from anorthosite samples collected from Majorqap qâva yielded a mean U-Pb age of 2936 ± 13 Ma (Souders et al. 2013), which is within error similar to the whole-rock Sm-Nd and Pb-Pb regression ages.

5.3 Petrography

5.3.1 Northern Qeqertarssuatsiaq Ultramafic Sill

Scanning Electron Microscope-Energy Dispersive X-ray Spectrometry (SEM-EDS) analyses indicate that the majority of samples from the

ultramafic sill are dominated by hornblende (40–80%). In abundance, pyroxene ranges from 10 to 60%, olivine from 1 to 20%, opaque minerals from 1 to 10%, and spinel between 0 to 5%. These rocks are classified as olivine-pyroxene hornblendite (*ca.* 75%), pyroxene hornblendite (*ca.* 15%), and hornblende pyroxenite (*ca.* 10%). In the field these rock types do not occur as distinct lithological units. Instead, pyroxene hornblendites and hornblende pyroxenites occur as lens-shaped to irregular patches within olivine-pyroxene hornblendites (Polat et al. 2012).

Olivine grains are anhedral to euhedral. They display sharp, straight to curved and indented boundaries. In some samples olivine occurs as inclusions within hornblende and clinopyroxene. Some grains contain hornblende, magnetite and clinopyroxene inclusions. Some olivine - hornblende contacts display magnetite-rich reaction rims (Fig. 5.5). Many olivine-hornblende boundaries are marked by a train of small magnetite grains (Figs. 5.5 and 5.6). Olivine is widely replaced by hornblende, orthopyroxene and clinopyroxene and to a lesser extent by spinel. Some grains have serpentine veins originating from olivine-hornblende contacts (Figs. 5.5 and 5.6).

Orthopyroxene is characterized by anhedral to euhedral grains, and exhibits straight to indented grain boundaries. Some boundaries between orthopyroxene and olivine are curved (Figs. 5.5 and 5.6). Orthopyroxene is partly replaced by hornblende. Many orthopyroxene grains occur between hornblende and olivine grains and contain an intergrowth of symplectitic (vermicular) magnetite (Figs. 5.5 and 5.6). These orthopyroxene-magnetite intergrowths appear to have grown at the expense of olivine (Figs. 5.5 and 5.6).

Clinopyroxene grains have anhedral to euhedral habits. Grain boundaries are straight, curved, and indented (Figs. 5.5 and 5.6). Clinopyroxene-orthopyroxene boundaries tend to be sharp. Clinopyroxene-hornblende boundaries are straight to indented and commonly marked by a magnetite-hosting reaction rim. Some clinopyroxene-olivine boundaries also display reaction rims. Clinopyroxene is variably replaced by hornblende.

Like other minerals, hornblende displays anhedral to euhedral crystal habits. Grain boundaries vary from straight to variably indented. Hornblende grains mainly constitute the interstitial phase between olivine-olivine, olivine-orthopyroxene, olivine-clinopyroxene and clinopyroxene-orthopyroxene grains. In some samples, olivine and clinopyroxene occur as inclusions within hornblende, and similarly some olivine and pyroxene grains enclose small hornblende grains. Hornblende replaces olivine, orthopyroxene and clinopyroxene. Many hornblende-olivine, hornblende-orthopyroxene and hornblende-clinopyroxene contacts exhibit a thin layer of magnetite-hosting reaction rim (Figs. 5.5 and 5.6).

The predominant opaque phase is magnetite, and sulphide occurs 1 to 3% in some samples. Magnetite grains range in shape from euhedral to symplectitic. Euhedral to subhedral magnetite typically occurs as interstitial grains between olivine-olivine, olivine-clinopyroxene, olivine-hornblende, and pyroxene-hornblende, whereas symplectitic magnetite occurs predominantly within orthopyroxene located between hornblende and olivine (Fig. 5.6). Magnetite also occurs as thin layers, or trains of small grains, along olivine-hornblende, pyroxene-hornblende, and hornblende-hornblende grain boundaries (Fig. 5.6).

The hornblendite veins mainly consist of 90–95% hornblende, 5–10% plagioclase, and 0–5% pyroxene (Polat et al. 2012). In addition, there are 150 to 250 μ Cl- and F-bearing apatite inclusions in hornblende. Plagioclase and pyroxene grains mainly form rounded inclusions within hornblende, and appear to have been resorbed by hornblende-forming melt. The size of hornblendes in the veins varies from 1 to 2 cm.

5.3.2 Sinarssuk

Ultramafic rocks at Sinarssuk are composed of dunite, horblende peridotite, hornblende pyroxenite, and pyroxene hornblendite. Dunite is composed of olivine (*ca.* 90%), pyroxene (5–10%), and chromite (2–5%) (Fig. 5.7). Chromite locally reaches up to 20%. Hornblende peridotites

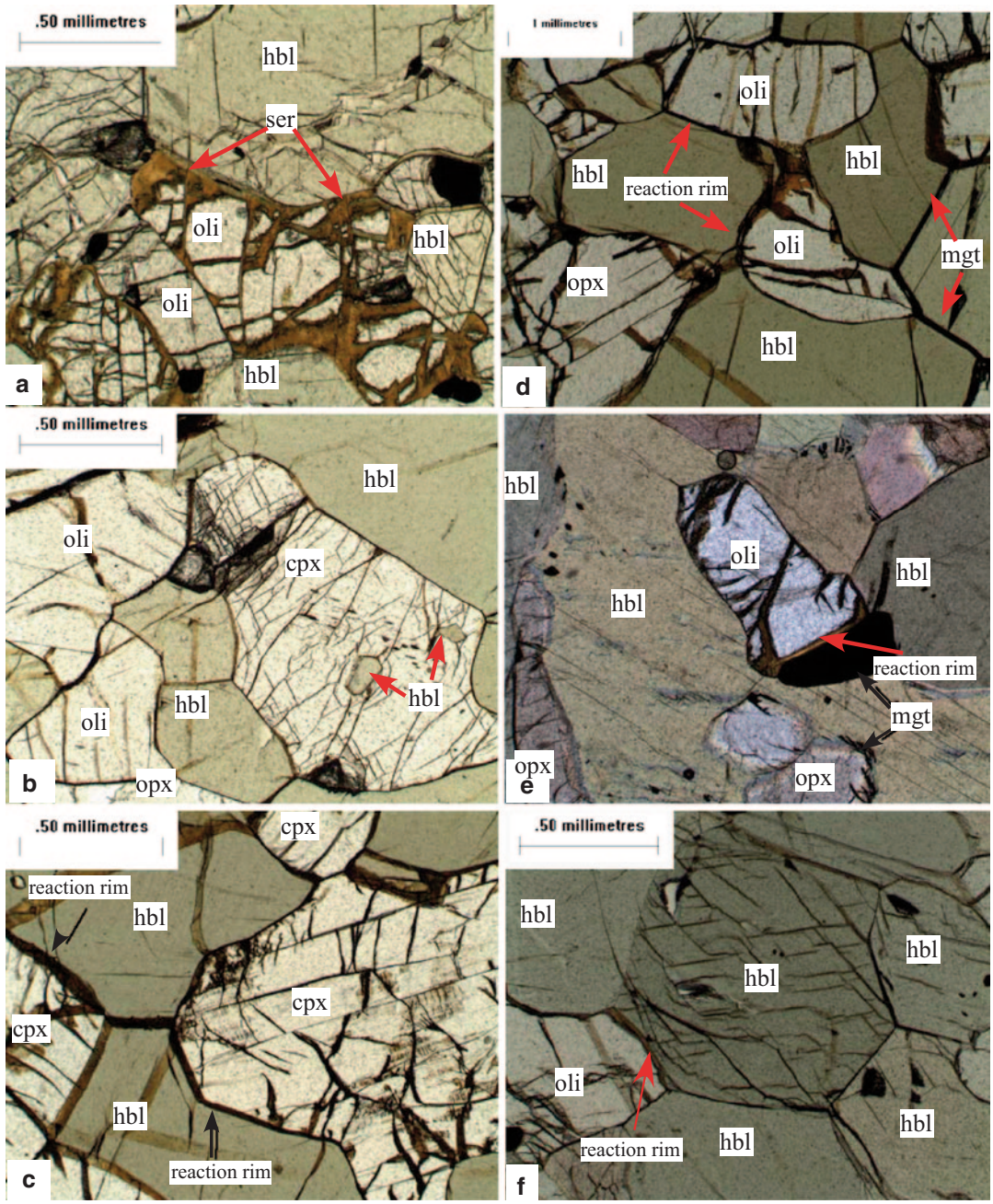

Fig. 5.5 Photomicrographs illustrating the petrographic characteristics of the ultramafic sill at Northern Qeqertarssuatsiaq: **a** hornblende (hbl) and serpentinized olivine (oli) grains; **b** Polygonal hornblende (hbl), clinopyroxene (cpx) and olivine (oli) grains, with sharp, straight to rounded boundaries. Clinopyroxene contains small hornblende (hbl) inclusions; **c** polygonal hornblende (hbl) and clinopyroxene (cpx) grains, with sharp, straight boundaries and reaction rims; **d** Polygonal hornblende (hbl), olivine (oli), and orthopyroxene (opx) grains, with sharp, straight to rounded boundaries and narrow reaction rims. Magnetite (mgt) grains tend to occur between hornblende-olivine and hornblende-orthopyroxene grains; **e** relict olivine (oli) and orthopyroxene (opx) grains in a matrix of hornblende (hbl). Magnetite (mgt) grains tend to occur between hornblende-olivine and hornblende -orthopyroxene grains; and **f** Polygonal hornblende (hbl) grains, with sharp, straight grain boundaries, displaying a granoblastic texture. Boundary between olivine (oli) and hornblende (hbl) is marked by a reaction rim (modified from Polat et al. 2012)

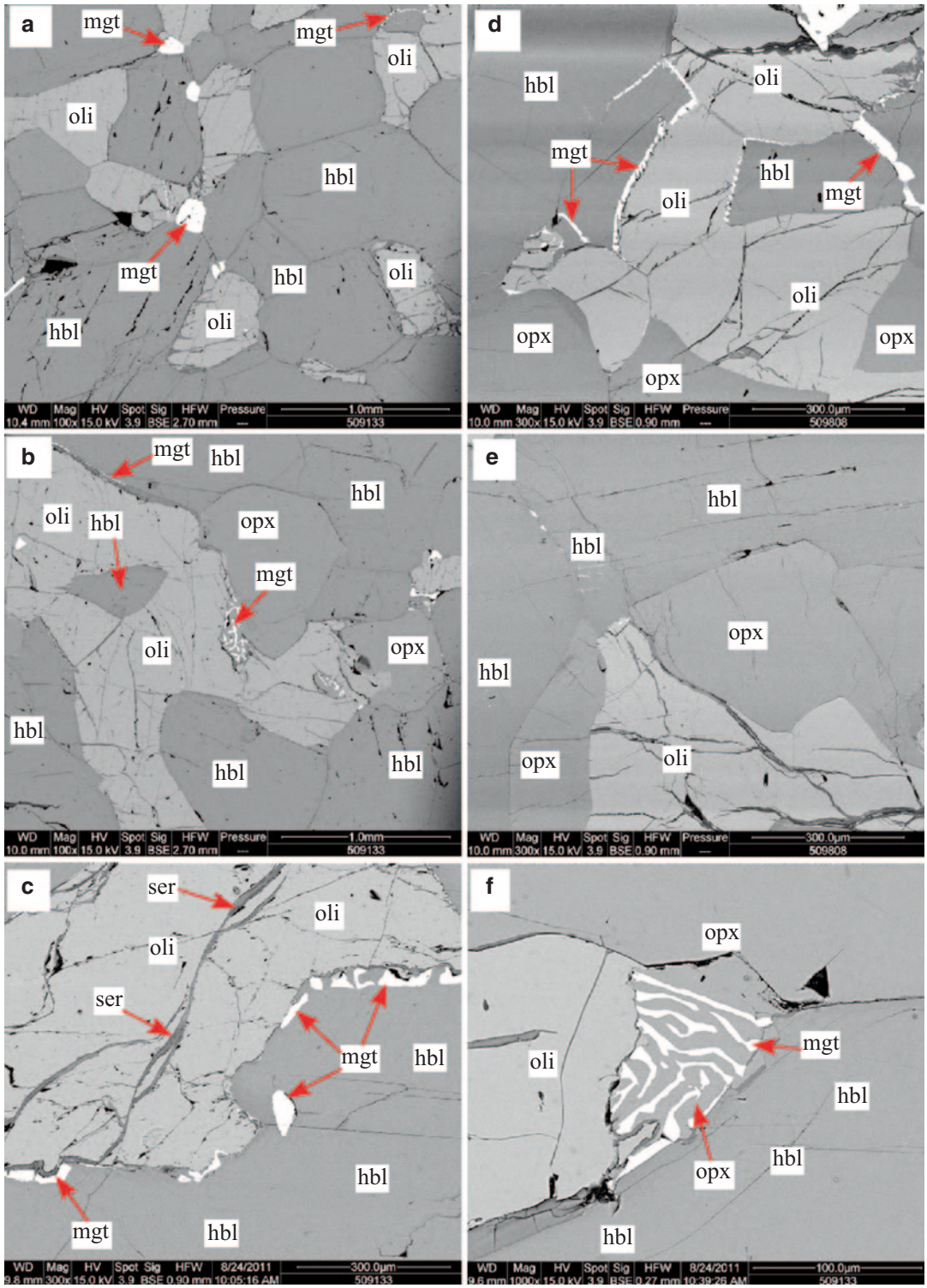

Fig. 5.6 SEM backscatter electron (BSE) images showing the petrographic characteristics of the ultramafic sill at Northern Qeqertarssuatsiaq: **a** Polygonal hornblende (hbl) and olivine (oli) grains, with sharp straight boundaries; **b** polygonal hornblende (hbl), orthopyroxene (opx) grains, displaying sharp to indented grain boundaries with olivine (oli); **c** Olivine (oli) and hornblende (hbl) grains displaying an indented grain boundary marked by a train of anhedral magnetite (mgt) grains; **d** Olivine (oli), hornblende (hbl), orthopyroxene (opx), and magnetite (mgt) grains,

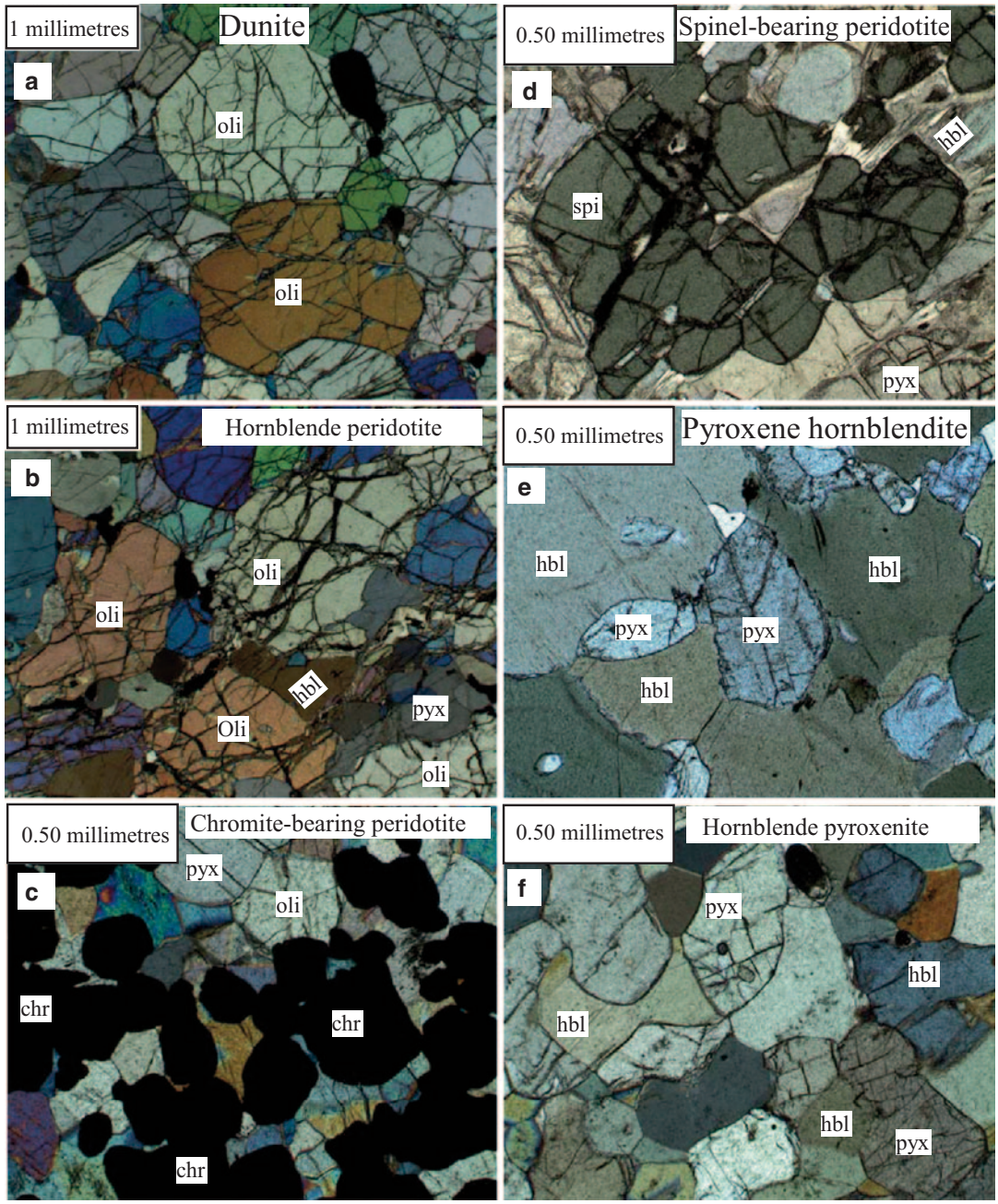

Fig. 5.7 Photomicrographs illustrating petrographic characteristics of ultramafic rocks at Sinarssuk: **a** dunite; **b** peridotite containing olivine, pyroxene (pyx) and hornblende (hbl); **c** a chromite (Cr-spinel, chr) layer in peridotite; **d** peridotite including large spinel (spi), pyroxene (pyx) and hornblende (hbl); **e** pyroxene hornblendite containing; and **f** Hornblende pyroxenite including pyroxene (pyx) inclusions within hornblende (hbl) (modified from Polat et al. 2011). Hornblende-bearing pyroxenites in Polat et al. (2011) are re-classified as hornblende pyroxenites and pyroxene hornblendites on the basis of the modal abundance of hornblende

Fig. 5.6 (continued) with sharp, planar, curved and indented boundaries; **e** growth of orthopyroxene (opx) at the expense of olivine (oli) between olivine and hornblende (hbl) grains; and **f** an intergrowth of symplectitic (vermicular) magnetite (mgt) and orthopyroxene (opx) situated between hornblende (hbl) and olivine (oli) (modified from Polat et al. 2012)

consist mainly of olivine (40–60%), pyroxene (30–40%), hornblende (10–30%), serpentine (0–10%), and accessory minerals (<5%) such as spinel and chromite (Fig. 5.7). Chromite, magnetite, and spinel are up to 50% in some peridotite layers. Olivine has been partially altered to serpentine, and pyroxene is replaced by hornblende. Hornblende pyroxenites and pyroxene hornblendites occur in the same layers and grade to each other, with increasing hornblende content.

Hornblende pyroxenites contain 50–70% pyroxene, 30–50% hornblende, 0–5% plagioclase, and 5–10% spinel (Fig. 5.7), whereas pyroxene hornblendites consist of 50–70% hornblende, 30–50% pyroxene, 0–5% plagioclase, and (5–10%) spinel (Fig. 5.7). Some pyroxene grains occur as relict inclusions in hornblendes, consistent with the replacement of pyroxene by hornblende (Fig. 5.7). Many pyroxene grains display sharp contacts with hornblendes.

Chromite (Cr-spinel) cumulates occur in dunites and hornblende peridotites (Fig. 5.4d). In these cumulates, hornblende occurs both as an interstitial mineral and as small rounded inclusions in chromite (Cr-Fe-spinel) grains (Fig. 5.8). There is no obvious sign of recrystallization of chromite and hornblende grains, implying that hornblende and chromite grains crystallized simultaneously from the same magma.

5.4 Geochemistry

5.4.1 Northern Qeqertarssuatsiaq Ultramafic Rocks

Ultramafic rocks at northern Qeqertarssuatsiaq were sampled along a traverse (Traverse 1) for petrographic and geochemical investigations (Polat et al. 2012). Rocks in the traverse are characterized by moderately variable SiO_2 (42.0–53.2 wt. %), MgO (16.2–31.3 wt. %), Fe_2O_3 (10.0–22.5 wt. %), Ni (488–1350 ppm), Sc (19–46 ppm), Co (50–144 ppm), and V (61–140 ppm) contents and Mg-numbers (72–79) (Table 5.1). They have large variations in Al_2O_3(1.3–9.8 wt. %), CaO (2.3–17.4 wt. %), TiO_2 (0.10–0.32 wt. %), Na_2O (0.12–0.87 wt. %), K_2O (0.02–0.66 wt.

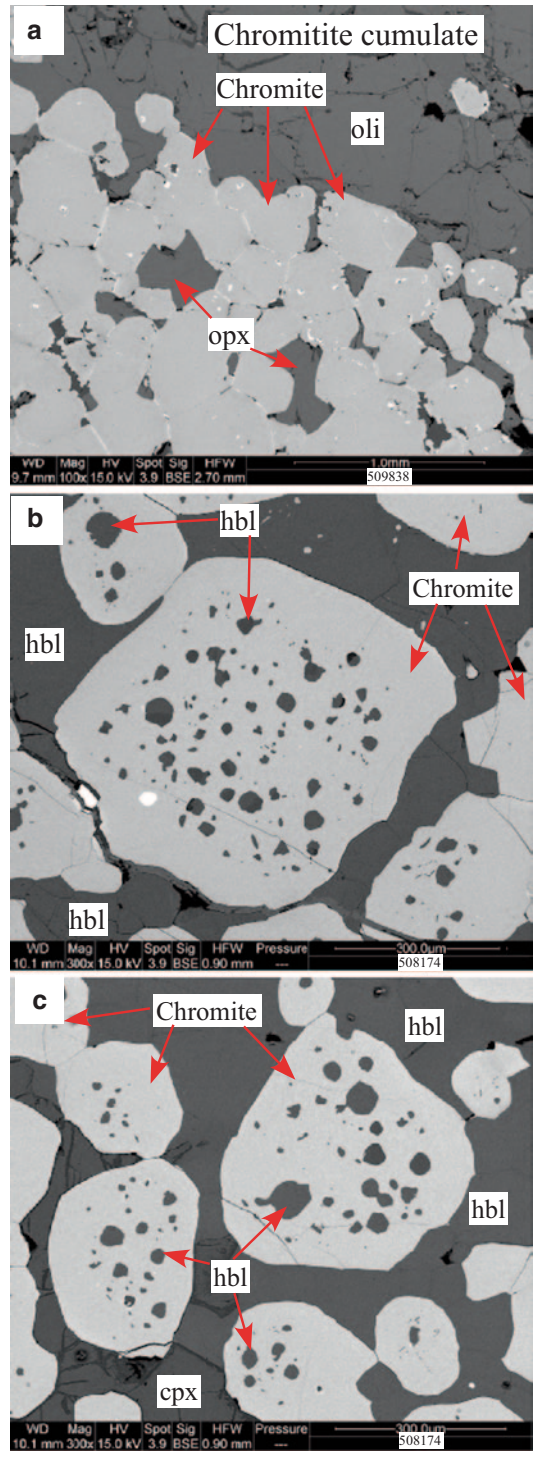

Fig. 5.8 Scanning electron microscope (SEM) backscatter electron (BSE) images of ultramafic rocks at Sinarssuk: **a** Chromite (Cr-spinel) cumulate layer in dunite. **b** and **c** Chromite cumulates containing hornblende (hbl) grains as inclusions and an interstitial phase (modified from Polat 2012)

Table 5.1 Summary of the ranges of significant compositional values and element ratios for the ultramafic sill and hornblendite veins at Qeqertarssuatsiaq[a]

	Ultramafic sill			Hornblendite veins
	Group 1	Group 2	Group 3	
SiO_2 (wt. %)	48.0–53.2	42.0–48.3	43.8–46.9	42.9–46.8
TiO_2	0.25–0.36	0.16–0.33	0.10–0.16	0.25–0.85
Al_2O_3	2.42–4.64	1.28–6.07	4.13–9.81	9.61–16.92
Fe_2O_3	10.0–15.4	13.3–22.5	12.2–17.7	11.6–13.7
MgO	16.2–22.3	21.5–31.3	22.6–28.4	11.7–15.0
CaO	8.2–17.4	2.3–12.2	4.7–8.3	11.8–14.2
Na_2O	0.37–0.66	0.12–0.46	0.23–0.78	1.24–1.70
Mg-number	73–77	72–76	76–79	65–72
Cr (ppm)	495–1201	403–883	83–135	195–377
Co	50–107	78–144	73–118	61–74
Ni	488–1350	586–1162	640–955	205–371
Sc	19–41	12–46	23–30	48–67
V	99–140	71–204	61–87	169–341
Sr	22–67	7–23	12–28	87–245
Ba	2–41	2–12	1–8	37–88
Zr	12–31	10–17	5–10	12–61
Nb	0.18–1.17	0.08–1.00	0.16–0.49	1.03–2.26
Y	3.2–5.9	1.4–6.9	1.8–3.0	5.4–12.8
Th	0.02–0.60	0.09–0.21	0.09–1.55	0.51–1.32
U	0.01–0.14	0.01–0.12	0.03–0.20	0.06–0.15
Pb	1.25–22.0	1.1–4.2	0.66–3.50	3.04–4.64
La	0.57–3.24	0.17–0.85	0.39–0.95	2.18–16.86
Ce	1.77–7.56	0.47–2.45	0.88–2.88	4.72–37.47
Nd	1.55–4.29	0.41–1.88	0.55–1.35	2.63–17.11
Sm	0.51–1.11	0.11–0.51	0.16–0.32	0.70–2.89
Gd	0.58–1.26	0.21–1.09	0.23–0.40	0.90–2.54
Yb	0.35–0.58	0.19–0.79	0.25–0.37	0.65–1.46
La/Sm_n	0.72–1.97	0.52–0.96	1.16–2.59	1.29–3.76
Gd/Yb_n	1.38–1.81	0.86–1.26	0.71–0.93	1.14–1.65
Eu/Eu*	0.84–0.89	0.65–0.98	0.64–1.16	0.81–1.01
Nb/Nb*	0.15–0.66	0.11–0.63	0.04–0.30	0.10–0.32
Zr/Zr*	0.48–2.17	0.58–1.12	0.66–1.82	0.15–1.18
Ti/Ti*	0.73–1.79	0.78–2.34	0.95–1.37	0.57–1.22
Zr/Y	2.67–9.66	1.59–2.90	2.52–4.80	1.51–4.75
Ti/Zr	68–124	108–234	67–116	86–216
Al_2O_3/TiO_2	9–13	7–24	41–84	14–61

* Modified from Polat et al. (2012)

%), Rb (0.5–4.6 ppm), Sr (6.5–66.8 ppm), and Cr (83–1021 ppm) (Table 5.1). Most elements display zigzag patterns with stratigraphic height (see Polat et al. 2012). SiO_2, TiO_2, Zr, and Cr tend to decrease upward in the traverse, whereas other elements do not show an obvious trend.

The Qeqertarssuatsiaq ultramafic rocks display depleted to enriched chondrite-normalized REE patterns (Fig. 5.9). On the basis of their REE patterns, these ultramafic rocks are divided into three groups (Fig. 5.9; Polat et al. 2012). Locations of these groups in the reconstructed stratigraphic column are given in Fig. 5.2 of Polat et al. (2012). Group 1 occurs in the lower part of the stratigraphy and is characterized by slightly convex-upward LREE (La/Sm_n = 0.72–1.13) and

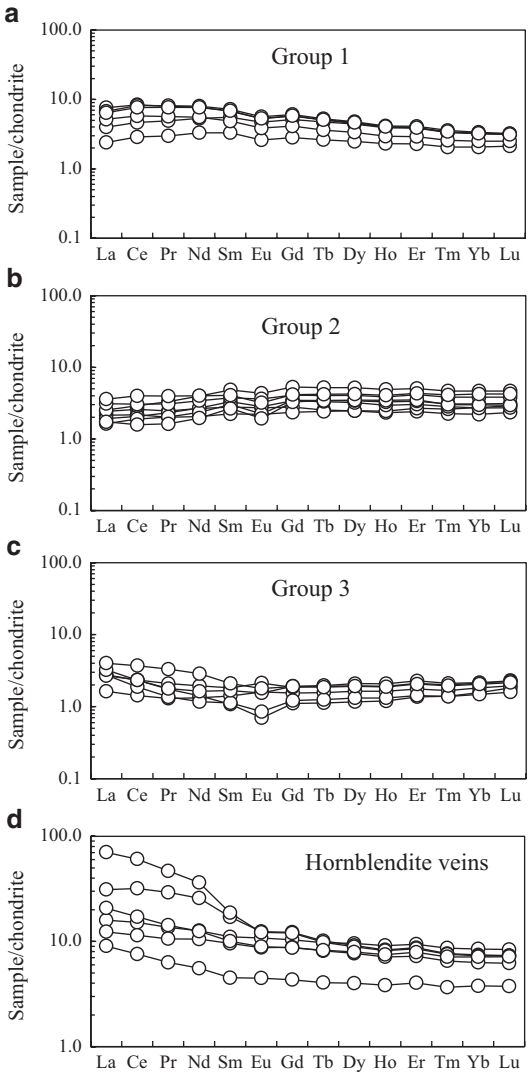

Fig. 5.9 Chondrite-normalized REE patterns for ultramafic rocks in the sill **a–c** and cross-cutting hornblendite veins **d** at Northern Qeqertarssuatsiaq. Normalization values are from Sun and McDonough (1989)

depleted HREE (Gd/Yb_n = 1.38–1.81) patterns. Group 2 samples come from the middle section of the stratigraphy and have depleted LREE (La/Sm_n = 0.52–0.96) and near-flat HREE (Gd/Yb_n = 0.86–1.14) patterns. Group 3 rocks are located in the upper part of the sequence and exhibit slightly concave-upward REE patterns (La/Sm_n = 1.16–2.59; Gd/Yb_n = 0.71–0.93). On N-MORB-normalized diagrams, samples in all groups display large negative Nb (Nb/Nb* = 0.04–0.66) anomalies. Zirconium (Zr/Zr* = 0.48–2.17) and Ti (Ti/Ti* = 0.73–2.34) anomalies are negative to positive (Fig. 5.10; Table 5.1).

5.4.2 Northern Qeqertarssuatsiaq and Itise Hornblendite Veins

The hornblendite veins exposed at Qeqertarssuatsiaq and Itise are characterized by a moderate range of SiO_2 (42.9–46.8 wt. %), MgO (11.7–15.0 wt.%), Al_2O_3 (9.6–16.9 wt. %), Cr (195–377 ppm), Ni (205–371 ppm), and V (169–326 ppm) contents (Table 5.1). They display a restricted range of CaO (11.8–14.2 wt. %), Fe_2O_3 (11.6–13.7 wt. %), Na_2O (1.2–1.7 wt. %), Co (61–74 ppm), and Sc (48–67 ppm) contents and Mg-numbers (65–72). Concentrations of K_2O (0.18–0.76 wt. %), Rb (5.6–23.1 ppm), Sr (87–245 ppm), and Ba (37–88 ppm) exhibit large variations (Table 5.1).

On chondrite- and N-MORB-normalized trace element diagrams, the hornblendite veins have the following characteristics: (1) variably enriched LREE patterns (La/Sm_n = 1.29–3.76; La/Yb_n = 1.88–9.65) and depleted HREE patterns (Gd/Yb_n = 1.11–1.65); (2) minor negative Eu (Eu/Eu* = 0.81–1.01) anomalies; (3) large negative Nb (Nb/Nb* = 0.10–0.32) anomalies; and (4) Ti (Ti/Ti^a = 0.57–1.22) anomalies are negative to positive (Figs. 5.9d and 5.10d).

5.4.3 Sinarssuk Ultramafic Rocks

Dunites display a restricted range of SiO_2 (38–40 wt. %), MgO (39.5–40.0 wt. %), Al_2O_3(1.9–4.1 wt. %), Fe_2O_3 (15.4–17.0 wt. %) and TiO_2 (0.03–0.09 wt. %) contents, and Mg-number ranges from 82 to 84 (Table 5.2). They have small variations of V (24–25 ppm), Sc (10–11 ppm), and Co (169–193 ppm) contents, but display moderate to large variations in Al_2O_3/TiO_2 (43–68), Ti/Zr (39–195), Zr/Y (3.1–6.8), and Nb/Ta (9.4–16.3) ratios (Table 5.2).

Hornblende peridotites have higher SiO_2 (42–43 wt. %), Al_2O_3 (8.7–12.4 wt. %), CaO

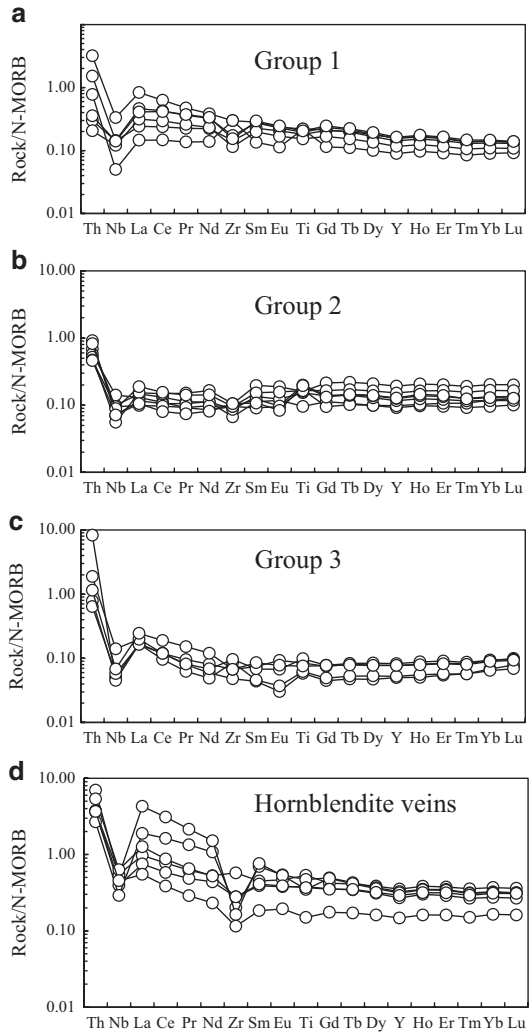

Fig. 5.10 N-MORB-normalized trace element patterns for ultramafic rocks in the sill **a–c** and cross-cutting hornblendite veins **d** at Northern Qeqertarssuatsiaq. Normalization values are from Hofmann (1988)

(5.2–7.2 wt. %), Sc (11–15 ppm) and V (37–55 ppm), and Al_2O_3/TiO_2 (92–315) ratios, but lower MgO (25–29 wt. %) and Mg-numbers (79–81) than dunites (Table 5.2).

Hornblende pyroxenites and pyroxene hornblendites have moderate variations in SiO_2 (40–52 wt. %), MgO (16–20 wt. %), CaO (8.1–11.8 wt. %) and Fe_2O_3 (8.4–11.1 wt. %), but larger variations in TiO_2 (0.04–0.06 wt. %), Al_2O_3 (4.2–21.2 wt. %), Sc (4–71 ppm), and V (19–213 ppm). Mg-numbers (76–82) in hornblende pyroxenites are comparable to those in hornblende peridotites.

These ultramafic lithologies have the following respective Ni (1713; 1261–955; 800–575 ppm) and Cr (9506–110; 108; 116–958 ppm) contents. All ultramafic lithologies display similar normalized trace element patterns characterized by concave-upward REE patterns, negative Nb but positive Zr anomalies, and systematic normalised enrichments of Th over La; hornblende pyroxenites and pyroxene hornblendites record relatively subdued concave patterns (Fig. 5.11).

5.5 Implications for Archean Petrogenesis, Geodynamics and Continental Growth

5.5.1 Evidence for an Igneous Origin of Hornblende

Despite poly-phase deformation and amphibolite to granulite facies metamorphism, primary cumulate textures and igneous layers are well preserved in the Fiskenæsset Complex (Figs. 5.3 and 5.4). Hornblende in the complex occurs both as a magmatic and a metamorphic mineral (see Polat et al. 2009; Rollinson et al. 2010). Due to metamorphic overprint it is not always easy to petrographically distinguish the metamorphic hornblendes from their magmatic counterparts. The sharp, straight to curved grain boundaries are interpreted as representing equilibrium conditions resulting from either magmatic or metamorphic crystallization, whereas the indented boundaries marked by alteration are interpreted as stemming from disequilibrium reactions (Polat et al. 2012).

Symplectitic intergrowths are common in retrogressed high-grade metamorphic rocks (e.g., eclogites, granulites), marking incomplete metamorphic reactions (Best 2003). Accordingly, they are generally considered as products of metamorphic reactions between neighboring minerals (e.g., plagioclase and olivine). Many studies, however, documented the development of symplectitic intergrowths in unmetamorphosed layered mafic to ultramafic intrusions and

Table 5.2 Summary of the ranges of significant compositional values and element ratios for the ultramafic rocks at Sinarssuk[a]

	Dunite	Hornblende peridotite	Hornblende pyroxenite and pyroxene hornblendite
SiO_2	38.4–39.8	41.9–42.9	40.3–43.9
TiO_2	0.003–0.09	0.04–0.09	0.04–0.05
Al_2O_3	1.9–4.1	8.7–12.4	15.6–21.2
Fe_2O_3	15.4–17.0	11.6–14.9	8.4–11.3
MgO	39.5–40.0	25–28	15.1–19.1
CaO	1.4–1.7	5.2–7.2	8.1–11.2
Na_2O	0.12–0.15	0.62–0.90	0.96–2.13
Mg-number	82–84	79–81	76–82
Cr	110–9506	108	116
Co	169–193	108–133	83–93
Ni	1713–1740	955–1261	682–800
Sc	10–11	11–15	4–20
V	24–25	37–55	19–49
Sr	3–5	5–26	12–30
Zr	2.9–4.3	4.1–15.1	3.1–6.0
Nb	0.077–0.101	0.071–0.125	0.090–0.199
Y	0.6–0.9	0.9–2.3	0.9–1.3
Th	0.052–0.385	0.208–0.267	0.045–0.068
U	0.017–0.254	0.187–0.297	0.042–0.068
Pb	0.5–0.6	0.50–0.83	0.9–4.2
La	0.104–0.339	0.300–0.423	0.155–0.797
Ce	0.221–0.619	0.569–0.815	0.362–1.157
Nd	0.165–0.242	0.291–0.456	0.261–0.470
Sm	0.057–0.063	0.081–0.167	0.091–0.118
Gd	0.067–0.116	0.122–0.269	0.128–0.157
Yb	0.107–0.148	0.124–0.316	0.114–0.170
La/Sm_n	1.06–3.82	1.63–2.39	0.99–4.34
Gd/Yb^n	0.52–0.65	0.70–0.81	0.76–1.14
Eu/Eu*	0.97–1.29	1.44–2.04	1.81–3.37
Ce/Ce*	0.93–1.03	0.96–0.97	0.91–1.02
Al_2O_3/TiO_2	43–68	92–315	322–487
Nb/Ta	9.4–16.3	9.5–13.2	12.8–35.3
Nb/Nb*	0.07–0.26	0.07–0.09	0.08–0.58
Zr/Zr*	1.76–2.26	1.64–3.39	1.17-1.32
Ti/Ti*	1.22–2.97	1.07–1.20	0.82–1.13

* Data from Polat et al. (2011)

in mantle xenoliths (Ambler and Ashley 1977; Otten 1983; Johnston and Stout 1984; Hooper and Hatcher 1985; Barton and van Gaans 1988; Claeson, 1998; Efimov and Malitch 2012). These studies suggest that symplectitic texture can originate as a product of chemical reaction between cumulus crystals and late stage melts or residual hydrous fluids, involving subsolidus oxidation of olivine (see Ambler and Ashley 1977; Gill 2010; Efimov and Malitch 2012). Magnetite is a very common mineral in layered intrusions (Wager and Brown 1967) and in Alaskan-type ultramafic rocks (Irvine 1974), and the occurrence of small magnetite grains between cumulate crystals has been reported from the Skærgaard intrusion (Wager and Brown 1967).

Symplectitic magnetite and orthopyroxene tend to have formed between olivine and hornblende grains at the expense of olivine (Fig. 5.6), indicating a possible reaction be-

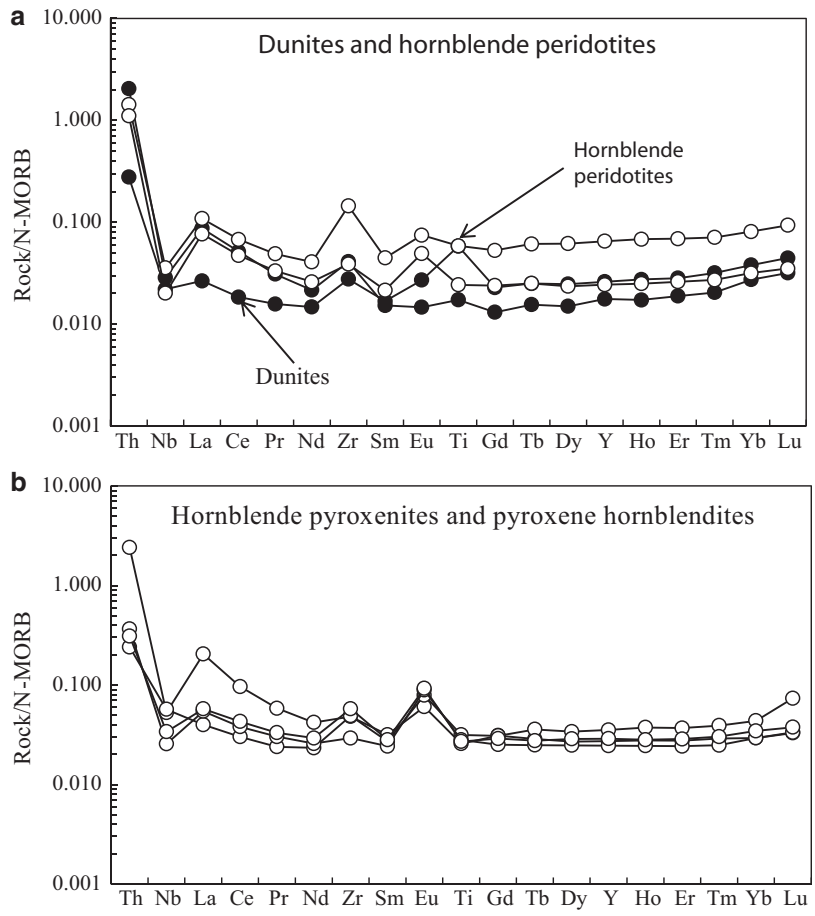

Fig. 5.11 N-MORB-normalized trace element patterns for dunites (solid circle) and hornblende peridotites (open circle) **a** and hornblende pyroxenites and pyroxene hornblendites at Sinarssuk. **b** Normalization values are from Hofmann (1988). Hornblende-bearing pyroxenites in Polat et al. (2011) are re-classified as hornblende pyroxenites and pyroxene hornblendites on the basis of the modal abundance of hornblende (hbl)

tween hornblende-forming, residual, hydrous melt and olivine (hydrous melt + olivine → orthopyroxene + magnetite) (cf., Ambler and Ashley 1977). Serpentinization of olivine grains can also be attributed to the reaction between olivine and hydrous melts. Alternatively, although less likely, the orthopyroxene-magnetite symplectite intergrowth might have developed through hornblende-olivine reaction during granulite facies metamorphism.

The ultramafic sill in northern Qeqertarssautsiaq is composed dominantly of hornblende (40–80 %). Hornblende also occurs in ultramafic rocks exposed in other parts of the complex, as well as in gabbros, leucogabbros and anorthosites throughout the complex (Polat et al. 2009, 2011; Huang et al. 2012). There are two likely explanations for the origin of hornblende grains in the complex: (1) they resulted from the metasomatic alteration of pyroxenes by metamorphic fluids that were derived from the neighbouring TTGs during either their intrusion or retrograde amphibolite facies metamorphism (see McGregor and Friend 1997); or (2) they originated as an igneous mineral but were recrystallized during prograde granulite facies metamorphism. The presence of hornblende inclusions in chromite (Rollinson et al. 2010; Polat et al. 2009; Huang et al. 2012), olivine, clinopyroxene and orthopyroxene (Figs. 5.5–5.8) is consistent with an igneous origin for this mineral. Furthermore, igneous hornblende is an abundant mineral in Alaskan-type ultramafic rocks, including peridotite, hornblende-olivine clinopyroxenite, hornblende clinopyroxenite, hornblende-magnetite clinopyroxenite, and hornblendites (Irvine 1974).

Polat et al. (2011) showed that magmas parental to the Fiskenæsset Complex had an average

MgO value of 20 wt. %. High MgO (16–31 wt. %) and Ni (490–1350 ppm) contents in the Qeqertarssautsiaq ultramafic rocks suggest that the ultramafic layer was emplaced as a hydrous crystal mush (Liquid + olivine ± amphibole ± opx ± cpx) rather than as a pure primary liquid.

Cross-cutting field relationship between the hornblendite veins and ultramafic sill (Fig. 5.3c and d) is consistent with a hydrous igneous origin of the former rock type (Fig. 5.3; Polat et al. 2012). The following petrographic observations suggest that the precursor of recrystallized hornblende grains in the ultramafic sill formed as a primary igneous phase: (1) the presence of hornblende inclusions in olivine, orthopyroxene, and clinopyroxene (Figs. 5.5–5.7); (2) the occurrence of hornblende grains as an interstitial phase between olivine-olivine, olivine-pyroxene, and pyroxene-pyroxene grains (Figs. 5.5–5.7); and (3) formation of orthopyroxene through hornblende-olivine reaction requires the presence of hornblende in the system prior to the granulite facies metamorphism. The presence of hornblende inclusions in olivine and pyroxene is interpreted by Polat et al. (2012) as trapped hornblende-forming liquid. Accordingly, it is inferred that the ultramafic rocks in the Fiskenæsset Complex were derived from a hydrous magma, originating from a metasomatized mantle source.

5.5.2 Geochemical Evidence for Sub-arc Source

Outcrops of ultramafic rocks studied by Polat et al. (2009, 2011, 2012) and Huang et al. (2012) are devoid of weathering, have relict igneous textures, and contain abundant fresh igneous olivine, pyroxene, and hornblende (Figs. 5.5–5.8). They display coherent chondrite-normalized REE (except Eu) and multi-element, including HFSE, patterns, indicating that these elements were relatively immobile during metamorphism. Exceptions are domains of calc-silicate, epidote-clinozoisite alteration and brecciated anorthosites that are characterized by large Ce anomalies ($Ce/Ce^* < 0.9$ and > 1.1) and significant ($> 50\%$) recrystallization (see Polat et al. 2009, 2011).

Contamination of the Fiskenæsset rocks by continental crust during magma emplacement was ruled out by Polat et al. (2009, 2010) on the basis of geological, geochemical, and Nd isotopic considerations. Mantle-like oxygen isotope characteristics ($\delta^{18}O = +5.6$) of the complex are also consistent with the absence of crustal contamination (Polat and Longstaffe, unpublished data). In addition, Polat et al (2011, 2012) and Huang et al. (2012) showed that positive anomalies of Zr and Ti in some samples, combined with flat HREE to convex REE patterns, are not features of Archean continental crust (Taylor and McLennan 1995). These lines of evidence are consistent with the emplacement of the Fiskenæsset Complex at ~ 2970 Ma into oceanic crust far away from continental lithosphere.

Different REE patterns (e.g., convex- and concave-upward patterns) in the Qeqertarssautsiaq and Sinarssuk ultramafic rocks are consistent with heterogeneous mantle source and variable amount of hornblende in these rocks. Polat et al. (2012) suggest that the three different REE patterns in the Qeqertarssautsiaq ultramafic rocks resulted from the emplacement of three different batches of crystal mush, having different melt (hornblende)/crystal (olivine + orthopyroxene + clinopyroxene) ratios. Both the Qeqertarssautsiaq and Sinarssuk ultramafic rocks share negative Nb anomalies (Figs. 5.10 and 5.11), suggesting a common mantle source and petrogenetic origin.

Current evidence indicates that the magmas of the Fiskenæsset Complex were derived from a long-term depleted mantle source and emplaced as multiple sills into Mesoarchean oceanic crust, forming an association of ca. 550 m-thick anorthosite, leucogabbro, gabbro, and ultramafic layers (Polat et al. 2009, 2010, 2012,; Souders et al. 2013). Field, petrographic, whole-rock data with BSE images from olivine-pyroxene hornblendites, hornblende pyroxenites and pyroxene hornblendites in the sill and cross-cutting hornblendite veins on the island of Qeqertarssuatsiaq suggest that these rocks crystallized from hydrous mantle-derived melts. On the basis of Th-REE-HFSE systematics, Polat et al. (2009, 2011, 2012) concluded that the Fiskenæsset Complex

formed as part of an Archean juvenile oceanic island arc system (cf., Saunders et al. 1991; Pearce and Peate 1995; Hawkins 2003; Murphy 2007).

The presence of igneous hornblende in the in the Fiskenæsset Complex implies a hydrous mantle source. The questions are: (1) where did this water come from; and (2) how did water end up in the Mesoarchean upper mantle? Given that all rock types, including anorthosites, gabbros, leucogabbros, and ultramafic rocks, in the Fiskenæsset Complex display present-day subduction zone geochemical signatures, it is argued that water was recycled to the mantle source of the Fiskenæsset rocks through subduction of hydrated Archean oceanic crust (Polat et al. 2012). It is well established that water plays an important role in subduction zone magmatism (see McInnes et al. 2001; Cervantes and Wallace 2003; Claeson and Meurer 2004; Maruyama et al. 2009; Kelley et al. 2010; Wada et al. 2012). Upon their release from the subducting hydrated oceanic crust and sediments, hydrous fluids and melts migrate into the overlying mantle wedge beneath magmatic arcs (Zellmer et al. 2003; Arai and Ishimaru 2008). Interaction between subduction-derived fluids and melts and the mantle wedge results in metasomatism and melting of sub-arc mantle peridotites (Murphy 2007; Dilek et al. 2008; Dilek and Thy 2008; Dilek and Polat 2008; Klimm et al. 2008). The currently available, multi-disciplinary data from the Fiskenæsset Complex likewise provide a robust model for the hydrous nature of the magmas that were derived from partial melting of a subduction-metasomatized Mesoarchean sub-arc mantle wedge that led to hydrous arc magmatism, resulting in the formation of igneous hornblende.

5.5.3 Growth of Archean Continental Crust

Understanding the origin of the continental crust is one of the main objectives of earth sciences because as a land species we owe our existence to the formation of continents. Similarly, change in the volume of the continental crust and distribution of continents on Earth's surface have profound effects on major geologic, atmospheric and hydrospheric processes that have regulated climate change and biological evolution throughout the history of Earth (Condie 2005; Polat 2012). Phanerozoic continental crust grew mainly along subduction zones by tectonic accretion and emplacement of juvenile magmatic rocks (Şengör et al. 1913; Burke 2011). However, the nature of petrogenetic and geodynamic processes that generated Archean continental crust still remains controversial (Foley et al. 2002; Rapp et al. 2003; Hawkesworth et al. 2010).

Recently, Nagel et al. (2012) and Adam et al. (2012) used two different geochemical approaches to explain the geodynamic origin of Archean continental crust (TTGs), but reached similar conclusions. These studies show that the geochemical characteristics of Archean TTGs are consistent with melting of hydrous mafic arc lavas, such as tholeiitic basalts and boninites, in the lower part of thickened oceanic island arcs. These studies reinforce a genetic link between subduction zone tectonic and petrogenetic processes and formation of Archean TTGs from metamorphosed arc lavas, implying that recycled water played a crucial role in the growth of Archean continents (see Campbell and Taylor 1983). Water is likely to have been transported into the Archean upper mantle by hydrated and metamorphosed oceanic crust (Fig. 5.12). Hydration of modern oceanic crust occurs mostly at spreading centers, where rising magmas provide a heat source for the circulation of seawater through oceanic crust via extensional faults and fractures. Collectively, geological, petrographic, and geochemical data from the Fiskenæsset Complex suggest that the origin of the Archean continental crust in the Fiskenæsset region, SW Greenland, can be viably explained by Phanerozoic-like plate tectonic processes (Fig. 5.12).

The Qeqertarssuatsiaq ultramafic sill consists of *ca.* 75% olivine-pyroxene hornblendite, ca. 15% pyroxene hornblendite, and *ca.* 10% hornblende pyroxenite. The sill is intruded by a network of several centimetre- to several tens of centimeter-thick hornblendite veins (Figs. 5.3 and 5.4). Petrographic observations suggest an igneous origin for the majority of hornblende

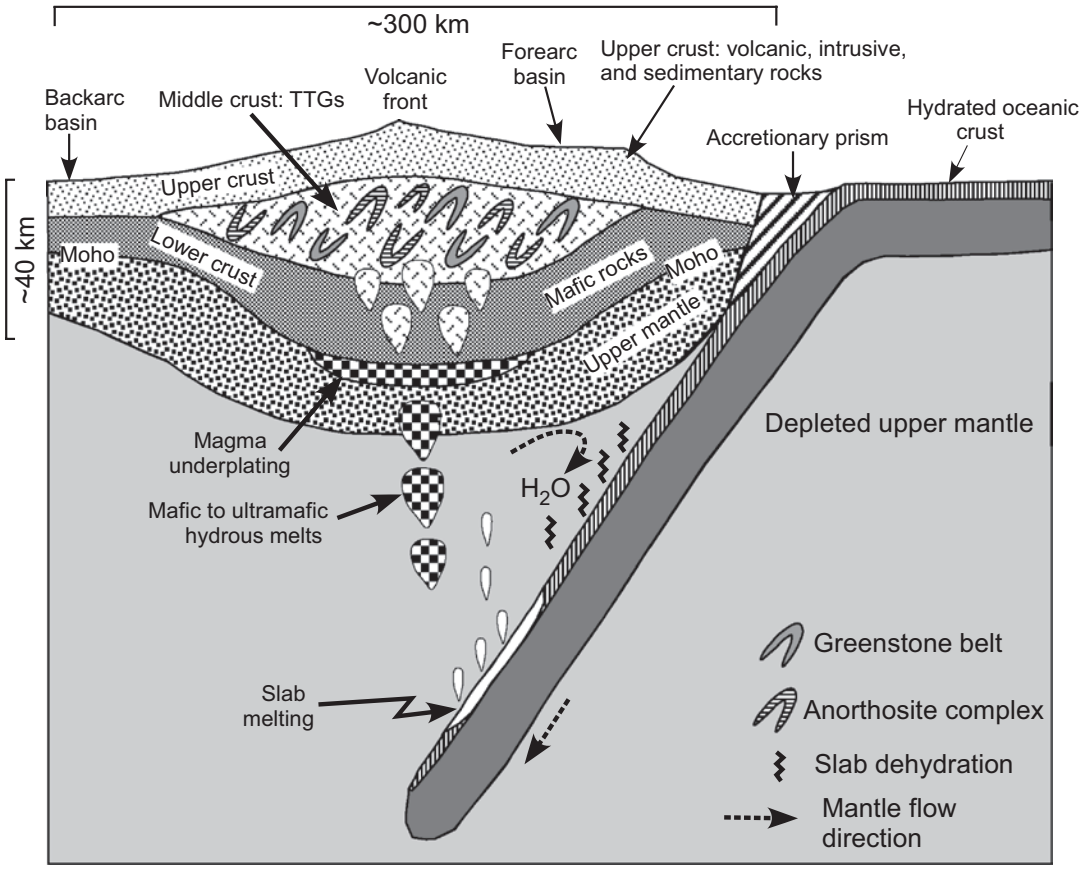

Fig. 5.12 A simplified geodynamic model for the generation of Archean continental crust (tonalite-trondhjemite-granodiorite, TTG) through partial melting of mafic lower crust at the base of an oceanic arc (modified after Davidson and Arculus 2006 and Polat 2012)

grains in the Fiskenæsset hornblendites, consistent with a hydrous mantle source(s). Phanerozoic hornblendites and hornblende-bearing mafic to ultramafic rocks occur predominantly in supra-subduction zone ophiolites (Koepke and Seidel 2004; Ishimaru et al. 2007; Greene and Giaramita 2008; Dilek and Furnes 2011) and in the roots of magmatic island arcs (Bradshaw 1989; Dhuime et al. 2007; Payot et al. 2009; Smith et al. 2009; Kiddle et al. 2010; Tiepolo et al. 2011), suggesting that the Fiskenæsset Complex originated at a Mesoarchean subduction zone. Both Nd (average initial $\varepsilon_{Nd}=+3.3$; Polat et al. 2010) and O (average $\delta^{18}O=5.6‰$; Polat and Longstaffe, unpublished data) isotope data are consistent with the formation of the Fiskenæsset Complex as part of a juvenile oceanic island arc complex. The Fiskenæsset Complex was intruded by voluminous TTGs, generating the Archean continental crust in the region. The bordering TTGs were derived from partial melting of the basaltic amphibolites in a thickened magmatic arc (Huang et al. 2013).

In the modern Earth flux of water into the mantle is controlled by subduction zone processes (Hirschmann and Kohlstedt 2012; Savage 2012) and the growth of the continental crust takes place predominantly at subduction zones (Şengör et al. 1993; Burke 2011). Polat (2012) suggested that similar water recycling and crustal growth processes also occurred in the Archean. Recycling of water into Archean upper mantle could not only have triggered the arc magmatism, but also played an important role in the forma-

tion of early continents at subduction zones (see Maruyama et al. 2009; Rollinson 2010). Basically, continental crust cannot grow, and arcs cannot generate melts over millions of years without subduction, recycling of water, and slab dehydration or melting.

Acknowledgments Dr. Y. Dilek is acknowledged for the invitation of this paper. The research was supported by NSERC grants and the fieldwork by the Bureau of Minerals and Petroleum in Nuuk and the Geological Survey of Denmark and Greenland (GEUS).

References

Ambler EP, Ashley PM (1977) Vermicular orthopyroxene-magnetite symplectites from the Wateranga layered mafic intrusion, Queensland, Australia. Lithos 10:163–172

Adam J, Rushmer T, O'Neil J, Francis D (2012) Hadean greenstones from the Nuvvuagittuq fold belt and the origin of the Earth's early continental crust. Geology 40:363–366

Arai S, Ishimaru S (2008) Insights into petrological characteristics of the lithosphere of mantle wedge beneath arcs through peridotite xenoliths: a review. J Petrol 49:665–695

Ashwal LD, Jacobsen SB, Myers JS, Kalsbeek F, Goldstein SJ (1989) Sm-Nd age of the Fiskenæsset anorthosite complex, west Greenland. Earth Planet Sc Lett 91:261–270

Ashwal LD, Myers JS (1994) Archean anorthosites. In: Condie KC (ed) Archean crustal evolution. Elsevier, Amsterdam, pp 315–355

Barton M, Van Gaans C (1988) Formation of orthopyroxene-Fe-Ti oxide symplectites in precambrian intrusive, Rogaland, southwestern Norway. Am Mineral 73:1046–1059

Best MG (2003) Igneous and metamorphic petrology. Blackwell Publishing, Malden, MA, USA pp 729

Bradshaw JY (1989) Early Cretaceous vein-related garnet granulite in Fiordland, southwest New Zealand: a case for infiltration of mantle-derived CO_2-rich fluids. J Geol 97:697–716

Bridgwater D, Keto L, McGregor VR, Myers JS (1976) Archean gneiss complex of Greenland. In: Escher A, Watt WS (eds) Geology of Greenland. Grønlands Geologiske Undersøgelse, pp 18–75

Burke K (2011) Plate tectonics, the Wilson cycle, and Mantle plumes: geodynamics from the top. Annu Rev Earth Pl Sc 39:1–29

Campbell IH, Taylor SR (1983) No water, no granites—no granites, no continents. Geophys Res Lett 10:1061–1064

Cervantes P, Wallace PJ (2003) Role of H_2O in subduction-zone magmatism: new insights from melt inclusions in high-Mg basalts from central Mexico. Geology 31:235–238

Claeson DT (1998) Coronas, reaction rims, symplectites and emplacement depth of the Rymmen gabbro, Transscandinavian igneous belt, southern Sweden. Mineral Mag 62:743–757

Claeson DT, Meurer WP (2004) Fractional crystallization of hydrous basaltic "arc-type"' magmas and the formation of amphibole-bearing gabbroic cumulates. Contrib Mineral Petr 147:288–304

Condie KC (2005) Earth as an evolving planetary system. Elsevier, Burlington, pp 447

Davidson JP, Arculus RJ (2006) The significance of Phanerozoic arc magmatism in generating continental crust. In: Brown M, Rushmer T (eds) Evolution and differentiation of the continental crust. Cambridge University Press, New York, pp 135–172

Dilek Y, Furnes H (2011) Ophiolite genesis and global tectonics: geochemical and tectonic fingerprinting of ancient oceanic lithosphere. Geol SocAm Bull 123:387–411

Dilek Y, Furnes H, Shallo M (2008) Geochemistry of the jurassic mirdita ophiolite (Albania) and the MORB to SSZ evolution of a marginal basin oceanic crust. Lithos 100:174–209

Dilek Y, Polat A (2008) Suprasubduction zone ophiolites and Archean tectonics. Geology 36:431–432

Dilek Y, Thy P (2009) Island arc tholeiite to boninitic melt evolution of the Cretaceous Kizildag (Turkey) ophiolite; model for multi-stage early arc/fore-arc magmatism in Tethyan subduction factories. Lithos 113:68–87

Dhuime B, Bosch D, Bodinier JL, Garrido CJ, Bruguier O, Hussain SS, Dawood H (2007) Multistage evolution of the Jijal ultramafic–mafic complex (Kohistan, N Pakistan): Implications for building the roots of island arcs. Earth Planet Sc Lett 261:179–200

Efimov AA, Malitch KN (2012) Magnetite–orthopyroxene symplectites in gabbros of the Urals: A structural track of olivine oxidation. Geol Ore Deposit 54:531–539

Foley S, Tiepolo M, Vannucci R (2002) Growth of early continental crust controlled by melting of amphibolite in subduction zones. Nature 417:837–840

Gancarz AJ (1976) Isotopic systematic in archean rocks, west Greenland, PhD thesis. California Institute of Technology, Pasadena, pp 378

Ghisler M (1976) The geology, mineralogy and geochemistry of the pre-orogenic archean stratiform chromite deposits at Fiskenæsset, west Greenland. Monogr Ser Miner Depos 14:156

Gill R (2010) Igneous rocks and processes a practical guide. Wiley-Blackwell, Malaysia, pp 428

Greene EL, Giaramita MJ (2008) Layered mafic to ultramafic intrusives in the eastern Elk outlier of the western Klamath Terrane; ophiolitic crust or syn-Nevadan intrusives? Abstracts with programs. Geol Soc Am 41(5):14

Hawkins JW (2003) Geology of supra-subduction zones-Implications for the origin of ophiolites. In: Dilek Y, Newcomb S (eds) Ophiolite concept and the evolution of geological thought. Geol Soc Am Spec Pap 373:227–268

Hawkesworth CJ, Dhuime B, Pietranik AB, Cawood PA, Kemp AIS, Storey CD (2010) The generation and evolution of the continental crust. J Geol Soc 167:229–248

Herr W, Wolfle R, Eberhardt P, Kopp E (1967) Development and recent application of the Re/Os dating method. In: Radioactive dating and methods of low-level counting. International Atomic Energy Agency, Vienna, pp 499–508

Hirschmann M, Kohlstedt D (2012) Water in Erath's mantle. Phys Today 65:40–45

Hoffmann JE, Svahnberg H, Piazolo S, Scherstén A, Münker C (2012) The geodynamic evolution of Mesoarchean anorthosite complexes inferred from the Naajat Kuuat complex, southern west Greenland. Precambrian Res 196–197:149–170

Hofmann AW (1988) Chemical differentiation of the Earth: the relationship between mantle, continental crust, and oceanic crust. Earth Planet Sc Lett 90:297–314

Huang H, Polat A, Fryer BJ, Appel PWU, Windley BF (2012) Geochemistry of the Mesoarchean Fiskenæsset complex at Majorqap qâva, sw Greenland: evidence for two different magma compositions. Chem Geol 314–317:66–82

Huang H, Polat A, Fryer BJ (2013) Origin of the archean tonalite–trondhjemite–granodiorite (TTG) suites and granites in the Fiskenæsset region, southern west Greenland: implication for the continental growth. Gondwana Res 23:452–470

Hooper RJ, Hatcher RD (1985) The origin of orthopyroxene-magnetite symplectites in the Gladesville gabbro, central Georgia Pidemont. Abstracts with Programs. Geol Soci Am 17:95–95

Irvine TN (1974) Petrology of the Duke Island ultramafic complex southeastern Alaska. Geol SocAm Mem 138:240

Ishimaru S, Arai S, Ishida Y, Shirasaka M, Okrugin VM (2007) Melting and multi-stage metasomatism in the mantle wedge beneath a frontal arc inferred from highly depleted peridotite xenoliths from the Avacha Volcano, southern Kamchatka. J Petrol 48:395–433

Johnston AD, Stout JH (1984) Development of orthopyroxene-Fe/Mg ferrite symplectites by continuous olivine oxidation. Contrib Mineral Petr 88:196–202

Kalsbeek F, Myers JS (1973) The geology of the Fiskenæsset region. Grønlands Geologiske Undersøgelse Rapport 51: 5–18

Kalsbeek F, Pidgeon RT (1980) The geological significance of Rb-Sr whole-rock isochrons of polymetamorphic Archean gneisses, Fiskenæsset area, southern west Greenland. Earth Planet Sc Lett 50:225–237

Kelley AK, Plank T, Newman S, Stopler EM, Grove TL, Parman S, Hauri E (2010) Mantle melting as a function of water content beneath the Mariana Arc. J Petrol 51:1711–1738

Keulen N, Næraa T, Kokfelt TF, Schumacher JC, Scherstén A (2010) Zircon record of the igneous and metamorphic history of the Fiskenæsset anorthosite complex in southern west Greenland. Geol Surv Den Greenl Bull 20:67–70

Kiddle EJ, Edwards BR, Loughlin SC, Petterson M, Sparks RSJ, Voight B (2010) Crustal structure beneath Montserrat, Lesser Antilles, constrained by xenoliths, seismic velocity structure and petrology. Geophys Res Lett 37:L00E11. doi:10.1029/2009GL042145

Klimm K, Blundy JD, Green TH (2008) Trace element partitioning and accessory phase saturation during H_2O-saturated melting of basalt with implications for subduction zone chemical fluxes. J Petrol 49:523–553

Koepke J, Seidel E (2004) Hornblendites within ophiolites of Crete, Greece; evidence for amphibole-rich cumulates derived from an iron-rich tholeiitic melt. Ofioliti 29:157–175

Maruyama S, Hasegawa A, Santosh M, Kogiso T, Omori S, Nakamura H, Kawai K, Zhao D (2009) The dynamics of big mantle wedge, magma factory, and metamorphic–metasomatic factory in subduction zones. Gondwana Res 16:414–430

McGregor VR, Friend CRL (1992) Late Archean prograde amphibolite to granulite-facies relations in the Fiskenæsset region, southern west Greenland. J Geol 100:207–219

McGregor VR, Friend CRL (1997) Field recognition of rocks totally retrogressed from granulite facies: an example from Archean rocks in the Paamiut region. South-West Greenland. Precambrian Res 86:59–70

McInnes BIA, Gregoire M, Binns RA, Herzig PM, Hannington MD (2001) Hydrous metasomatism of oceanic sub-arc mantle, Lihir, Papua New Guinea: petrology and geochemistry of fluid-metasomatized mantle-wedge xenoliths. Earth Planet Sc Lett 188:169–183

Murphy JB (2007) Arc magmatism II: geochemical and isotopic characteristics. Geosci Can 34:7–35

Myers JS (1976) Granitoid sheets, thrusting, and Archean crustal thickening in west Greenland. Geology 4:265–268

Myers JS (1985) Stratigraphy and structure of the Fiskenæsset complex, southern west Greenland. Geol Surv Greenl Rep 150:72

Nagel TJ, Hoffmann JE, Münker C (2012) Generation of Eoarchean tonalite-trondhjemite-granodiorite series from thickened mafic arc crust. Geology 40:375–378

Otten MT (1983) Formation of orthopyroxene-magnetite symplectites by oxidation of olivine; a magmatic or subsolidus process? Eos, Transactions. Am Geophys Union 64:870

Payot BD, Arai S, Tamayo Jr. RA, Yumul Jr., GP (2009) What underlies the Philippine island arc? Clues from the Calaton Hill, Tablas island, Romblon (Central Philippines). J Asian Earth Sci 36:371–389

Pearce JA, Peate DW (1995) Tectonic implications of the composition of volcanic arc magmas. Ann Rev Earth Pl Sc 23:251–285

Pidgeon RT, Kalsbeek F (1978) Dating of igneous and metamorphic events in the Fiskenæsset region of southern west Greenland. Can J Earth Sc 15:2021–2025

Polat A (2012) Growth of Archean continental crust in oceanic island arcs. Geology 40:383–384

Polat A, Appel PWU, Fryer B, Windley B, Frei R, Samson IM, Huang H (2009) Trace element systematics of the Neoarchean Fiskenæsset anorthosite complex and associated meta-volcanic rocks, sw Greenland: evidence for a magmatic arc origin. Precambrian Res 175:87–115

Polat A, Frei R, Scherstén A, Appel PWU (2010) New age (ca. 2970 Ma), mantle source composition and geodynamic constraints on the Archean Fiskenæsset anorthosite complex, sw Greenland. Chem Geol 277:1–20

Polat A, Fryer B, Appel PWU, Kalvig P, Kerrich R, Dilek Y, Yang Z (2011) Geochemistry of anorthositic differentiated sills in the Archean (~ 2970 Ma) Fiskenæsset complex, sw Greenland: implications for parental magma compositions, geodynamic setting, and secular heat flow in arcs. Lithos 123:50–72

Polat A, Fryer B, Samson IM, Weisener C, Appel PWU, Frei R, Windley BF (2012) Geochemistry of ultramafic rocks and hornblendite veins in the Fiskenæsset layered anorthosite complex, SW Greenland: Evidence for hydrous upper mantle in the Archean. Precambrian Res 214–215:124–153

Rapp RP, Shimizu N, Norman MD (2003) Growth of early continental crust by partial melting of eclogite. Nature 425:605–609

Riciputi LR, Valley JW, McGregor VR (1990) Conditions of Archean granulite metamorphism in the Godthåb-Fiskenæsset region, southern west Greenland. J Metamorph Geol 8:171–190

Rollinson H (2010) Coupled evolution of Archean continental crust and subcontinental lithospheric mantle. Geology 38:1083–1086

Rollinson H, Reid C, Windley BF (2010) Chromitites from the Fiskenæsset anorthositic complex, West Greenland: clues to late Archaean mantle processes. In: Kusky TM, Zhai M, Xiao W (eds) The evolving continents: understanding processes of continental growth. Geol Soc London, Spec Publ 338:197–212

Saunders AD, Norry MJ, Tarney J (1991) Fluid influence on the trace element compositions of subduction zone magmas. Philos T Roy Soc A 335:377–392

Savage B (2012) Seismic constraints on the water flux delivered to the deep Earth by subduction. Geology 40:235–238

Şengör AMC, Natal'in BA, Burtman VS (1993) Evolution of the Altaid tectonic collage and Palaeozoic crustal growth in Eurasia. Nature 364:299–307

Smith DJ, Petterson MG, Saunders AD, Millar IL, Jenkin GRT, Toba T, Naden J, Cook JM (2009) The petrogenesis of sodic island arc magmas at Savo volcano, Solomon Islands. Contrib Mineral Petr 158:785–790

Souders AK, Sylvester PJ, Myers JS (2013) Mantle and crustal sources of Archean anorthosite: a combined in situ isotopic study of Pb–Pb in plagioclase and Lu–Hf in zircon. Contrib Mineral Petr 165:1–24

Sun SS, McDonough WF (1989) Chemical and isotopic systematics of oceanic basalts: implications for mantle composition and processes. In: Saunders AD, Norry MJ (eds) Magmatism in the Ocean Basins. Soc London, Spec Publ 42:313–345

Taylor SR, McLennan SM (1995) The geochemical evolution of the continental crust. Rev Geophys 33:241–265

Tiepolo M, Tribuzioi R, Langone A (2011) High-magnesian andesite petrogenesis by amphibole crystallization and ultramafic crust assimilation: evidence from Adanello hornblendites (Central Alps, Italy). J Petrol 52:1011–1045

Wada I, Behn MD, Shaw AM (2012) Effects of heterogeneous hydration in the incoming plate, slab rehydration, and mantle wedge hydration on slab-derived H_2O flux in subduction zones. Earth Planet Sc Lett 353–354:60–71

Wager LR, Brown GM (1967) Layered Igneous Rocks. W.H. Freeman and Company, San Francisco, pp 588

Windley BF, Smith JV (1974) The Fiskenæsset Complex, West Greenland, part 2. General mineral chemistry from Qeqertarssuatsiaq. Grønlands Geologiske Undersøgelse Bulletin 108:54

Windley BF, Garde AA (2009) Arc-generated blocks with crustal sections in the North Atlantic craton of West Greenland: new mechanism of crustal growth in the Archean with modern analogues. Earth Sci Rev 93:1–30

Windley BF, Herd RK, Bowden AA (1973) The Fiskenæsset Complex, west Greenland, part 1; a preliminary study of the stratigraphy, petrology and whole-rock chemistry near Qeqertarssuatsiaq. Geol Surv Greenl Bull 106:80

Zellmer GF, Hawkesworth CSJ, Thomas LE, Harford CL, Brewer TS, Loughlin SC (2003) Geochemical evolution of the Sourière Hills volcano, Montserrat, Lesser Antilles volcanic arc. J Petrol 44:1349–1374

The Precambrian Geology of the North China Craton: A Review and Update of the Key Issues

6

Simon A. Wilde

Abstract

This paper reviews current thinking with respect to the main issues concerning the nature and evolution of the North China Craton (NCC). Because literature on the NCC is so voluminous, it of necessity focuses on specific aspects that have wider applicability to the nature of Precambrian cratons in general. The assembly of the craton is examined and opposing views evaluated. The overall distribution of Precambrian rocks is placed within the favoured model for subdividing the craton, and recent advances in determining the ages of key lithological associations are presented. The more controversial topic of where the NCC was placed in the Nuna/Columbia and Rodinia supercontinents is canvassed, although no definitive conclusions can be drawn. Finally, the removal of continental lithosphere from beneath the eastern part of the craton in the Phanerozoic is briefly examined, since this phenomenon has wider implications for the global preservation of Precambrian crust.

6.1 Introduction

A considerable amount of data have been compiled on the Precambrian rocks of the North China Craton and it is impossible to give due recognition to all sources in an overview paper such as this. In particular, there has been a proliferation of new geochronological data following installation of the first ion-microprobe in China in 2001 at the Beijing SHRIMP Center, and the results have been published both in international journals and in many local publications with restricted international access. Instead, what I intend to do is to identify several key issues that have arisen through work undertaken principally in the past ten years and thereby expand upon our earlier reviews (Zhao et al. 2001a, 2005; Wilde et al. 2002), highlighting current issues where a general consensus exists, as well as those that remain controversial. In particular, areas that will be addressed include: (1) the general configuration of the North China Craton, including its assembly; (2) the nature and distribution of the Precambrian rocks; (3) the role and position of

S. A. Wilde (✉)
Department of Applied Geology, The Institute for Geoscience Research, Curtin University, PO Box U1987 Perth 6845 Western Australia
e-mail: s.wilde@curtin.edu.au

Y. Dilek, H. Furnes (eds.), *Evolution of Archean Crust and Early Life*, Modern Approaches in Solid Earth Sciences 7, DOI 10.1007/978-94-007-7615-9_6, © Springer Science+Business Media Dordrecht 2014

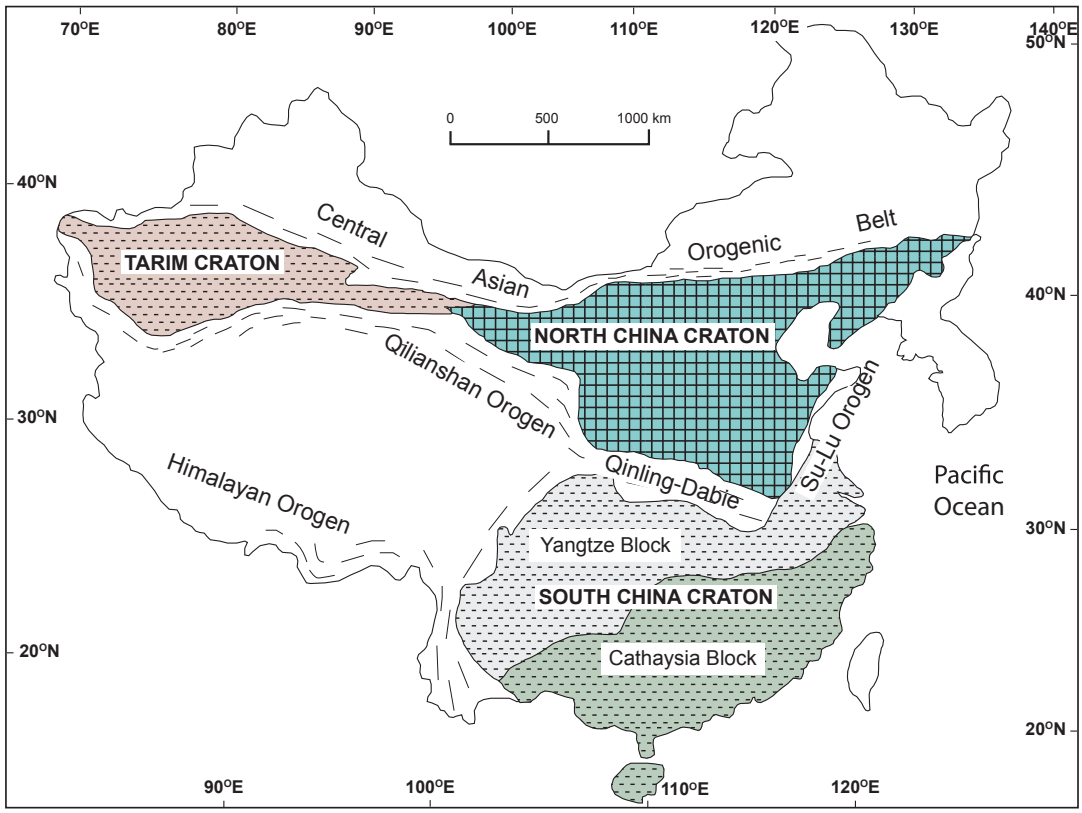

Fig. 6.1 Setting of the North China Craton within China, emphasizing the three Precambrian cratonic nuclei and surrounding orogenic belts. (modified from Zhao et al. 1999a)

the North China Craton within the Proterozoic supercontinents; and (4) the effects of lithospheric thinning on craton stability. Whilst the latter event has taken place in the Phanerozoic, it is still germane to briefly comment upon it here, since it affects the Precambrian crust and lithosphere and the very stability of the craton.

6.2 Background

The North China Craton (NCC) covers an area of ~1.5 million square kilometers of northern China. It is bounded to the north by the Neoproterozoic-Phanerozoic Central Asian Orogenic Belt (CAOB), to the west by the Paleozoic Qilianshan Orogen, and is separated from the Archean-Proterozoic South China Craton by the Mesozoic Qinling-Dabie-Sulu ultrahigh-pressure (UHP) metamorphic belt; to the east it is bounded by the Pacific Ocean (Fig. 6.1). In earlier literature, the NCC was commonly referred to as part of the 'Sino-Korean Craton'. However, although some modern geochronological results are now available for North Korea (Zhao et al. 2006a; Wu et al. 2007a, b), information is sparse and any direct extension of the NCC into Korea remains speculative, although it is likely the Rangnim (Nangrim) massif may link-up, based on the similarity of limited zircon U-Pb ages (Zhao et al. 2006a; Wu et al. 2007a).

The basement of the NCC has been studied in detail since the late 1980s and consists of variably-exposed Archean and Paleoproterozoic rocks that include tonalite-trondhjemite-granodiorite (TTG) gneiss, calc-alkaline granite, charnockite, migmatite, amphibolite- and greenschist-facies mafic rocks, pelitic and psammitic

schist, Al-rich gneiss (khondalite), banded iron formation (BIF), calc-silicate, and marble (e.g. Huang et al. 1986; Jahn et al. 1987; Ma et al. 1987; Qiao et al. 1987; Kröner et al. 1988; He et al. 1992; Liu et al. 1992; Shen et al. 1992; Sun et al. 1992; Shen and Qian 1995; Song et al. 1996; Bai and Dai 1998; Wu et al. 1991, 1998). An unmetamorphosed Mesoproterozoic cover of volcano-sedimentary successions, referred to collectively as the Changcheng-Jixian-Qingbaikou 'system', unconformably overlies these basement rocks, together with locally-extensive Phanerozoic cover.

In the pre-plate tectonics scenario, the North China Craton was traditionally considered to comprise a unified Archean to Paleoproterozoic basement that evolved during four tectonic cycles, separated by distinct 'movements' defined by 'unconformities'; a view that persisted with some workers until more recent times. These were named the Qianxi (>3.0 Ga), Fuping (3.0–2.5 Ga), Wutai (2.5–2.4 Ga) and Lüliang (2.4–1.8 Ga) cycles (Huang 1977; Ma and Wu 1981; Wu et al. 1991; Zhao 1993; Shen and Qian 1995) and they were terminated by 'movements' of the same name, considered to have occurred at ~3.0 Ga, ~2.5 Ga, ~2.2 Ga and ~1.8 Ga, respectively (Ma et al. 1987; Cheng 1994; Bai and Dai 1998). As outlined in Zhao et al., (2005), these tectonic cycles/movements were defined on either meager or spurious evidence, that included K–Ar, Rb–Sr and limited conventional multigrain U–Pb zircon geochronology; the view that high-grade metamorphic rocks were older than low-grade rocks; a common misinterpretation of shear zones as 'unconformities' and an assumption that supracrustal rocks were dominant over orthogneisses throughout the craton. However, modern studies carried out since the late 1980s, especially high quality geochronology and geochemistry, have corrected many of these misconceptions.

These more recent developments have led to a general acceptance that the basement of the NCC is composed of several different blocks, separated by major shear zones, which developed independently and eventually collided to form the craton. However, there was still debate as to how the craton should be subdivided, where the boundaries were located, and the nature and the timing of amalgamation (Wu et al. 1998; Wu and Zhong 1998; Zhang et al. 1998; Zhao et al. 1998, 2001a, Li et al. 2000; Zhai et al. 2000, 2005; Zhai and Liu 2003; Wu et al. 2000; Kusky and Li 2003). However, since 2005 there has been a general acceptance of the model proposed by Zhao et al. (1998, 1999a, b, 2001a, 2005) and, following presentation of the evidence, this will form the basis for discussion in this overview.

6.3 Configuration and Assembly of the North China Craton

6.3.1 Block Model for the NCC

In one of our earlier studies (Zhao et al. 2005), we outlined and illustrated various models that had been proposed for subdividing the NCC and readers are referred to this paper for further details. In essence, the number of blocks ranged from 15 (Zhang et al. 1998) to 5 (Wu et al. 1998), but with little explanation of the nature of their boundaries. Zhao et al. (1998, 1999a, b) initially proposed a 3-fold subdivision of the craton, based on lithological, structural, metamorphic and geochronological differences between the central part of the craton and its eastern and western parts. Their key argument was the differences in metamorphic P/T paths within the various supracrustal assemblages. The paths were anticlockwise in the eastern part of the craton, clockwise in the central part of the craton and changed from anticlockwise to clockwise in the western part at the Archean/Proterozoic boundary (Zhao et al. 1999a, b). The late Archean anticlockwise pattern was interpreted to be related to a series of mantle plumes that resulted in magmatic underplating and high-grade metamorphism at ~2.5 Ga (Zhao et al. 1999a), whereas the clockwise paths were considered to reflect continent-continent collisional orogenesis related to the Paleoproterozoic assembly of the NCC at ~1.85 Ga (Zhao et al. 2001a).

This model was further refined following more detailed field and laboratory studies and led to

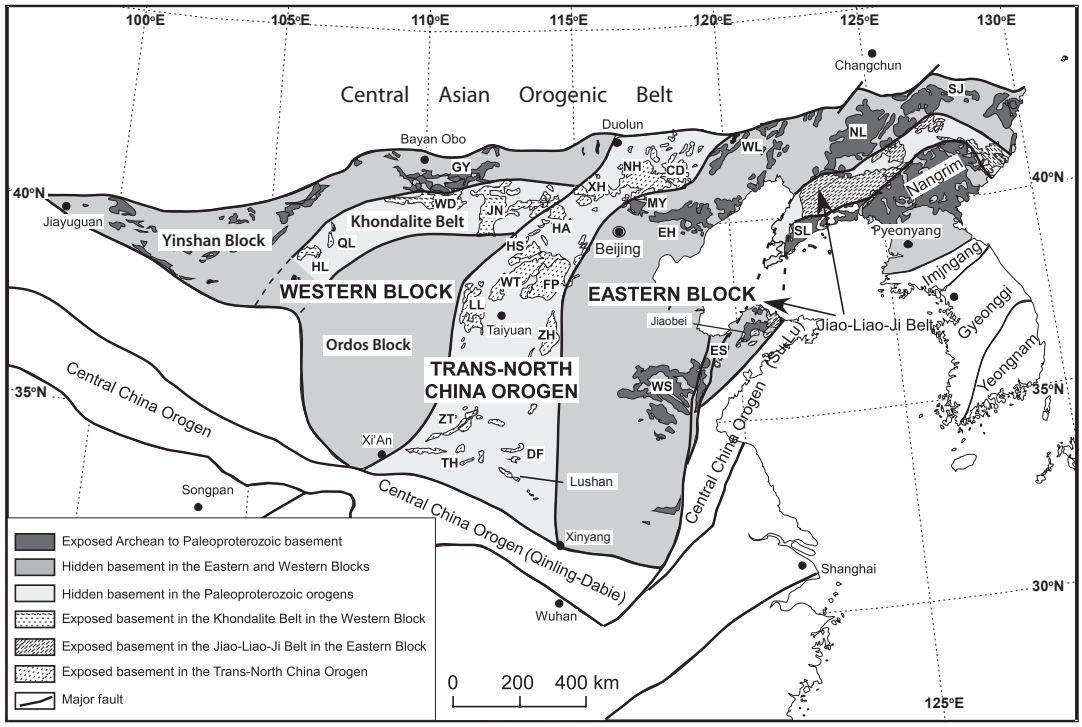

Fig. 6.2 Subdivision of the North China Craton, modified from Zhao et al. (2005). Abbreviations of metamorphic domains/complexes: *CD*: Chengde; *DF*: Dengfeng; *EH*: Eastern Hebei; *ES*: Eastern Shandong; *GY*: Guyang; *HA*: Huai'an; *HL*: Helanshan; *JN*: Jining; *LL*: Lüliang; *MY*: Miyun; *NH*: Northern Hebei; *NL*: Northern Liaoning; *QL*: Qianlishan; *SJ*: Southern Jilin; *SL*: Southern Liaoning; *TH*: Taihua; *WD*:Wulashan-Daqingshan; *WL*: Western Liaoning; *WS*: Western Shandong; *WT*: Wutai; *XH*: Xuanhua; *ZH*: Zanhuang; *ZT*: Zhongtiao

the current 6-fold subdivision of the craton (Zhao et al. 2005) (Fig. 6.2). This revision was based on the recognition of the importance of major collisional zones within the Eastern and Western blocks. In the eastern block, the Jiao-Liao-Ji belt trends generally NE-SW and separates the block into two segments. Paleoproterozoic volcano-sedimentary rocks of the Jiao-Liao-Ji belt are associated with granitoids and were metamorphosed to greenschist/amphibolite facies. These rocks were considered to be deposited in a rift setting (Yang et al. 1988; Li et al. 2005) that was closed at ~1.85 Ga, although other workers have favoured either continent-arc collision (Bai 1993; Faure et al. 2004; Luo et al. 2004) or continent-continent collision (He and Ye 1998) without prior rifting. In the western block, the Khondalite belt extends E-W and likewise separates the block into two component parts (Zhao et al. 2005). The dominant rocks are khondalitic sediments, associated with minor TTG gneiss, mafic granulite, charnockite and S-type granite. The rocks were deposited in the Paleoproterozoic and metamorphosed to granulite facies at ~1.92 Ga (Santosh et al. 2007). Thus, the general consensus is that the NCC consists of an Archean Eastern Block that includes the Paleoproterozoic Jiao-Liao-Ji collisional belt; a Western Block composed of the Yinshan Block in the north and the Ordos Block to the south, separated by the Paleoproterozoic Khondalite Belt; and a central Paleoproterozoic collisional zone referred to as the Trans-North China Orogen along which the craton is considered to have amalgamated at ~1.85 Ga (Fig. 6.2).

However, not all workers have accepted the model outlined above in its entirety and the arguments have focused around two main issues: the location and nature of the internal block

boundaries and the timing of amalgamation of the Eastern and Western blocks. In particular Kusky and Li (2003), although recognizing the veracity of eastern and western blocks with a central orogenic belt between, proposed that the blocks collided at ~2.5 Ga in the same basic configuration of Zhao et al. (2001a), but that they subsequently underwent extension along the combined northern margin, followed by arc development and arc collision at ~2.3 Ga, resulting in the Inner Mongolia-Northern Hebei Orogen. To the south of this orogen, an extensive granulite facies terrain known as the North China Granulite-Facies Belt (see also Shen et al. 1992; Shen and Qian 1995; Li et al., 1997) developed. This included an accretionary terrain in the north and re-worked Archean rocks of the craton to the south, both deformed and metamorphosed at ~2.3 Ga. The northern margin of the NCC then evolved into an Andean-type margin at 2.20–1.85 Ga and, from 1.85 Ga, Kusky and Li (2003) considered the NCC underwent extension. In this model, the ongoing activity at the northern margin led to a rotation of the main tectonic elements formed at 2.5 Ga, causing them to swing to the NE (see Fig. 6.2 of Kusky and Li 2003). A strong rebuttal of this model was presented by Zhao et al. (2006b), based mainly on evidence obtained from the so-called North China Granulite-Facies Belt. Instead of recording a consistent sequence of metamorphic events, it was shown that the 'belt' recorded P/T paths and ages consistent with a simple northward extension of the Western, Eastern and Trans-North China Orogen domains of the NCC (Zhao et al. 2001a, 2005, 2006b). It is important to note that the 'Central Orogenic Belt' of Kusky and Li (2003), although it has a similar location to the Trans-North China Orogen in the south of the NCC, is different in the northern part. Indeed, the northern extension of the Central Orogenic Belt cuts further to the east and includes the area to the east of Beijing that forms part of the Eastern Hebei domain of the Eastern Block in the model of Zhao et al. (2001a, 2005).

Notwithstanding the above, there is a requirement to slightly modify at least one of the boundaries proposed by Zhao et al. (2005), based on recently-published geophysical data (Zheng et al. 2009). A series of seismic profiles extending across the central part of the NCC reveal that the boundary between the Western block and the Trans-North China Orogen most likely extends N-S for a greater distance than originally proposed (note this modification has been incorporated into Fig. 6.2). Importantly, the available seismic data are broadly consistent with the block model proposed by Zhao et al. (2005), although the question of subduction polarity will be discussed in a following section.

6.3.2 Timing of Amalgamation

As indicated above, based on lithological, structural, metamorphic and geochronological constraints, Zhao et al. (2001a, 2005) concluded that the Trans-North China Orogen represents a Paleoproterozoic collisional zone along which the Eastern and Western blocks of the NCC were amalgamated at ~1.85 Ga. This was in broad agreement with the views of Wu et al. (1998) and Wu and Zhong (1998) who, although their subdivision of the craton was markedly different (see Zhao et al. 2005), suggested their two NE blocks (Jiaoliao and Qianhuai) amalgamated at 2.5 Ga, but that the remaining blocks did not collide until 1.8 Ga during the Lüliang orogeny. However, several workers have suggested that all blocks had collided by 2.5 Ga and that the 1.8 Ga Lüliang 'event' represented merely a re-working of the craton. For example, Zhai et al. (2000), Zhai and Liu (2003), and Zhai and Santosh (2011) favoured collision of the blocks at 2.5 Ga, as did Li et al. (2000) and Polat et al. (2005, 2006). Although Kusky and Li (2003) supported the subdivision of the NCC into three major blocks, they considered that the Eastern and Western blocks were already amalgamated by a ~2.5 Ga collisional event and that the ~1.85 Ga Lüliang event was the result of intracontinental rifting. A later model proposed a variation on these ideas (Faure et al., 2007; Trap et al. 2007, 2008, 2009a, b) whereby an earlier collisional event at ~2.1 Ga led to amalgamation of the Eastern Block with a microcontinental block they called the 'Fuping

Block'. This was followed by final collision between the Eastern and Western blocks along the Trans-North China Orogen to form the North China Craton at 1.9–1.8 Ga.

6.3.2.1 Why no Collision at 2.5 Ga?

The arguments in favour of a 2.5 Ga collision essentially revolve around the way the metamorphic data are interpreted, as well as an understanding of the strength and distribution of the 1.8 Ga event across the NCC. Kusky and Li (2003) argued against placing too much emphasis on the P/T and geochronological data, whereas Zhao et al. (2001a, 2005) argued these were the key to resolving the issue. One of the main weaknesses of the Kusky and Li (2003) argument appears to be a failure to appreciate the importance of the 1.8 Ga Lüliang event. It is evident from the regional reviews of metamorphism across the craton (Zhao et al., 1998, 1999b, 2000a) that the strong recrystallization and growth of new zircon, when coupled with a consistent clockwise P/T path, requires doubling of the crust along the lines proposed by Thompson and England (1984) and cannot be achieved during a later extensional event. Likewise, where data are available (see Zhao et al. 1998, 1999a, b, 2000, 2002a for further references), the consistent anticlockwise P/T paths of rocks metamorphosed at 2.5 Ga cannot be explained by collisional processes. Furthermore, there is no evidence throughout the full extent of the Trans-North China Orogen to indicate that Archean rocks older than 2.5 Ga underwent collisional metamorphism at ~2.5 Ga (see below).

In the southern part of the Trans-North China Orogen at Lushan (Fig. 6.2), Wan et al. (2006a) reported that 1.85 Ga metamorphism affected both Archean detrital zircons and ~2.1 Ga granitoids; there was no evidence in support of a high-grade Archean metamorphic event. Farther north in the Zanhuang complex (Fig. 6.2), Wang et al. (2003) identified four phases of deformation and applied $^{40}Ar/^{39}Ar$ dating of amphibole to define the timing of the D_1, D_2 and D_3 events at 1870 Ma, 1870–1826 Ma and 1826–1793 Ma, respectively. They concluded that the major tectonothermal event affecting the Zanhuang complex occurred between 1870–1793 Ma. More recent work has established that the lower part of the succession is Archean in age and was metamorphosed to upper amphibolite facies. Trap et al. (2009a) obtained hornblende and biotite Ar-Ar ages between 1827–1792 Ma and metamorphic monazite with an age of 1824 ± 6 Ma whereas Xiao et al. (2011) obtained a U-Pb zircon age of 1821 ± 17 Ma for the metamorphic event. In contrast, the upper sedimentary sequence is at greenschist facies and thus detrital zircons are devoid of metamorphic rims (Liu et al. 2011a); however, their age constrains sedimentation to between ~2.09 and ~1.85 Ma. Farther north in the Fuping complex (Fig. 6.2), high-grade regional metamorphism occurred at 1.85 Ga and affected both rocks >2.5 Ga and others ~2.0 Ga in age (Zhao et al. 2002a, 2005). At Wutaishan to the north of Fuping (Figs. 6.2 and 6.3), greenschist/amphibolite facies volcanic and sedimentary rocks show no evidence of zircon growth at 1.8 Ga (Wilde et al. 1997, 2004a), presumably because temperatures remained too low. However, Ar-Ar data on amphibolites from the Wutai complex (Wang et al. 1996; Wilde et al., unpublished data) reveal ages between 1.85–1.70 Ga, consistent with the effects of the 1.85 Ga Lüliang event.

To the north of Wutaishan, the Hengshan complex (Fig. 6.3) is composed of amphibolite- to granulite-facies granitoid gneisses, high-pressure granulites and retrograde eclogites and minor supracrustal rocks (Zhao et al. 2001a, b). Zircon dating reveals major granitoid emplacement between 2.52 Ga and 2.48 Ga, with younger granitoids emplaced in the Early Paleoproterozoic at ~2360–2330 Ma, 2250 Ma and 2115 Ma (Kröner et al. 2005a). Importantly, the Paleoproterozoic granitoids show the same metamorphic and deformational fabrics as seen in the Archean gneisses, demonstrating that the high-grade event occurred in the Proterozoic and not the Archean (Kröner et al. 2005a; O'Brien et al. 2005). Still further north in the Huai'an Complex (Fig. 6.2), metamorphic zircons in high-pressure mafic granulite record a SHRIMP U-Pb age of 1817 ± 12 Ma (Guo et al. 2003), again indicating that the main metamorphic event did not occur in

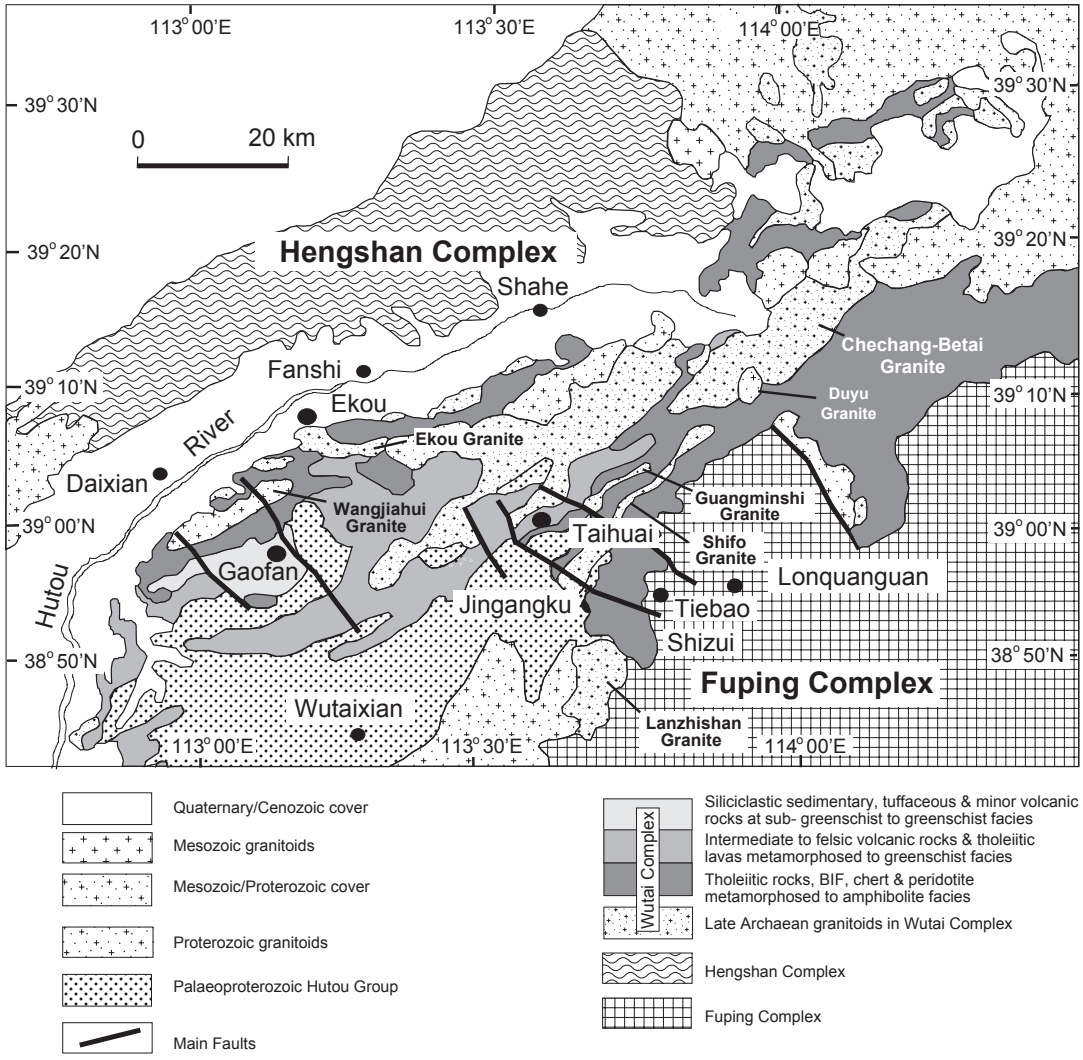

Fig. 6.3 Simplified geological map of the Hengshan-Wutai-Fuping area, emphasizing the main subdivisions of the Wutai complex and the associated granitoids. (based on Wilde et al. 2004a)

the Archean. Together, these data thus preclude 2.5 Ga being the time of high-grade metamorphism in the Trans-North China Orogen. Instead it occurred at ~1.85 Ga, supporting the Paleoproterozoic collisional model for the amalgamation of the NCC (Zhao et al. 2005).

Other arguments that have been canvassed to support formation of an integrated NCC at 2.5 Ga include (a) the presence of high-pressure granulite facies rocks only in the northern part of the Trans-North China Orogen, and extending perpendicular to the orogenic grain, (b) the fact that both the Eastern and Western blocks record metamorphism at 2.5 Ga, and (c) the question of how island arc and ophiolitic rocks that formed at 2.55 Ga could avoid deformation and metamorphism until 1.8 Ga (see Kusky and Li 2003). With respect to (a), this certainly has not been adequately addressed in recent studies. However, it is not unusual for tilting to occur on a cratonic scale, as exemplified by the Dharwar Craton of India that shows a distinct southward increase in metamorphic grade from greenschist- to granulite-facies (see Condie et al. 1982). The nature of

the 2.5 Ga metamorphism (b) has already been discussed above and the fact that in both the Eastern and Western blocks it is associated with anticlockwise P/T paths indicates it is not the result of continent-continent collision. The argument that rocks cannot remain unmetamorphosed for considerable periods of time (c) was partly addressed by Zhao et al. (2005), who pointed out that the Andes has been evolving as a continental margin for ~500 Ma (Howell 1995; Dalziel 1997; Rivers and Corrigan 2000). However, it is noted this is not a common phenomenon, although the width of the ocean that once separated the Eastern and Western blocks is currently unknown. Overall, none of these arguments appear to invalidate the model of Zhao et al. (2005).

6.3.2.2 Complex Paleoproterozoic Collisional Events

Further evidence in support of collision at ~1.85 Ga in the Trans-North China Orogen comes from the identification of two high-grade Paleoproterozoic metamorphic events in the Huai'an complex, located in the Khondalite Belt (Western Block) near the boundary with the orogen (Zhao et al. 2010a). However, these data also have implications for the timing of collision between the Yinshan and Ordos blocks to form the Western Block of the NCC and this whole issue of inter-block amalgamation within the Western and Eastern blocks is discussed below.

Western Block: One of the main problems with elucidating the history of the Western Block is that exposure is virtually confined to the northern part, since the Ordos Block in the south is covered by Mesozoic-Cenozoic strata and details are restricted to limited drill core samples (Wu et al. 1986) and to geophysical interpretation (Wu et al. 1998; Zheng et al. 2009). Zhao et al. (2005) suggested that collision between the Yinshan and Ordos blocks along the Khondalite Belt may have occurred at ~2.0–1.9 Ga, based on evidence available at the time (Hu 1994; Wang et al. 1995; Wu and Li 1998; Wan et al. 2000). Wan et al. (2006b) reported detrital zircon data from sedimentary rocks distributed across the whole NCC, including the Khondalite Belt. They reported a few ages of 2.33-2.02 Ga from sillimanite-bearing gneiss north of Datong, close to boundary between the Khondalite Belt and the Trans-North China Orogen (Fig. 6.2). The zircon population was strongly affected by metamorphism at 1.87–1.84 Ga. However, whether this was related to metamorphism of the Khondalite Belt or the Trans-North China Orogen was uncertain. Indeed, similar ages centred around 1.85 Ga were reported from this area by Zhao et al. (2008a) and interpreted to be components of the Trans-North China Orogen that forms part of the Huai'an complex. Later work (eg. Santosh et al. 2007) indicated metamorphism of the khondalite rocks south of Jining, ca. 100 km west of this contact, occurred at 1.92 Ga, with remnants of detrital cores recording ages of 3.09–1.94 Ga (clustering at 1.97 Ga), and thus indicating a short time-span between sedimentation and high-grade metamorphism. Importantly, Zhao et al. (2010a) found evidence of two high-grade metamorphic events in zircons from graphite–garnet–sillimanite gneiss from the Huai'an complex at the boundary between the Khondalite Belt and the Trans-North-China Orogen. Here, several zircon grains contained inner growth rims that recorded ages of ~1.95 Ga, similar within their error to the results of Santosh et al. (2007) from Jining, and outer rims with an age of ~1.85 Ga, interpreted to record the time of high-grade metamorphism in the Trans-North China Orogen. This provided conclusive evidence not only of the earlier timing of metamorphism in the Khondalite Belt, and by implication the timing of collision of the Yinshan and Ordos blocks to form the Western Block of the NCC, but that the 1.85 Ga event is ubiquitous throughout the Trans-North China Orogen.

The precise timing of high-grade metamorphism in the Khondalite Belt is still open to debate. Guo et al. (2008) and Zhao (2009) suggested that the presence of ultra-high temperature (UHT) rocks at Jining were likely the result of contact metamorphism due to the emplacement of massive gabbroic/noritic dykes with an age of 1.92 Ga, thus implying that collision between the Yinshan and Ordos blocks occurred prior to 1.92 Ga. Zhao (2009) further argued that collision occurred at ~1.95 Ga, based on the presence

of the double zircon rims discussed above (Zhao et al. 2010a) and the fact that ~1.95 Ga ages were obtained by Yin et al. (2009) from pelitic granulites of the Qianlishan complex in the westernmost part of the Khondalite Belt (Fig. 6.2). However, it should be noted that errors on both these data sets are large and range from 12–26 Ma. Furthermore, the zircon rims in the study of Zhao et al. (2010a) are extremely narrow and smaller than the analytical beam, so that it was almost impossible to locate analytical sites so that overlap onto adjacent zircon domains was completely avoided (hence the large errors). Thus, these studies do not preclude the age of 1919±10 Ma favoured by Santosh et al. (2007) as being close to the true age of UHT metamorphism. Of course, how precisely this coincides with the time of collision is currently unknown.

Eastern Block: Events within the Jiao-Liao-Ji belt that separates the Eastern Block into two component parts (Fig. 6.2), as alluded to previously, are more complicated with various interpretations as to the tectonic evolution. One of the key points of contention has revolved around the relationship between the North and South Liaohe 'groups' and their associated granitoids (Fig. 6.2). Both groups consist of sedimentary and volcanic successions metamorphosed from greenschist- to lower amphibolite-facies, whereas the Liaoji granitoids can be subdivided into two groups: a pretectonic suite of monzogranitic gneisses with ages of 2.2–2.1 Ga and 1.88–1.85 Ga (post-tectonic) porphyritic monzogranites and alkaline syenites (Li and Zhao 2007; Luo et al. 2008). Contrary to earlier opinions, it appears that the detrital zircon provenance of both the North and South Liaohe 'groups' are comparable, with a minor zircon population at 2.5 Ga and a main population at 2.2–2.0 Ga (Wan et al. 2006b; Luo et al. 2008). This implies that the basement beneath the two groups is similar, and that the North and South Liaohe 'groups' did not evolve independently on two discrete continental blocks; a conclusion also supported by the zircon Lu-Hf data of Luo et al. (2008). These data have therefore been used to support the rift model (see Li et al. 2005) for the Jiao-Liao-Ji belt (Luo et al. 2008).

Another important piece of information is whether the North and South Liaohe 'groups' underwent metamorphism at a common time. In the western Liaodong Peninsula, Yin and Nie (1996) obtained a biotite $^{40}Ar/^{39}Ar$ age of 1896±7 Ma from a major shear zone that cuts the North Liaohe 'group', suggesting peak metamorphism must have been earlier. Luo et al. (2004) suggested that the Jiao-Liao-Ji belt underwent regional metamorphism at ~1.9 Ga; however, the study of Lu et al. (2006) found no evidence of this event in the Ji'an 'Group' (Fig. 6.2), considered to be an equivalent of the South Liaohe 'group'. Significantly, a metamorphic zircon age of ~1.9 Ga was recorded in the study of the South Liaohe 'group' by Luo et al. (2008), Thus metamorphism in the Jiao-Liao-Ji belt is bracketed by 1.93–1.90 zircon ages from the study of Luo et al. (2008), being remarkably similar to the ages recorded for granulite-facies metamorphism in the Khondalite Belt in the Western Block of the NCC.

If the rift model for the Jiao-Liao-Ji Belt is correct, then there is no need to consider the two Archean components of the Eastern Block as representing discrete cratonic blocks. However, it should be noted that this is not the case if the North and South Liaohe 'groups' had been shown to be different in terms of age and provenance. In the models invoking continent-arc(-continent) collision (Bai 1993; Faure et al. 2004), the northern block (Longgang block) is separated from the southern block (Langrim block) by the Jiao-Liao-Ji Belt, which is interpreted as an intervening arc and back-arc basin (Bai 1993). The Longgang block was considered to be the active margin of the eastern NCC, with the Langrim block having a passive northern margin and the intervening ocean subducting northward below the Longgang block. Importantly, the new structural data of Li et al. (2005) and the geochronological results of Li et al. (2006), Li and Zhao (2007) and Luo et al. (2008), together with the lack of calc-alkaline magmatism in the Jiao-Liao-Ji Belt, do not support this model. However, recent studies in the southern part of the belt (Tam et al. 2012) have identified high-pressure pelitic granulites in the Jiaobei massif (Fig. 6.2) with clockwise P/T paths, thus providing evidence that the belt was

the result of collisional orogenesis, at least in its later stages of evolution. This is another area of the NCC where further work is required to clarify the geological history.

Trans-North China Orogen: Events here have already been covered with respect to amalgamation with the Western Block; the question that remains is whether other collisions might have occurred between ~2.5 and 1.8 Ga. In this regard, there has been the suggestion that major activity occurred within the Trans-North China Orogen at ~2.1–2.0 Ga, possibly involving either continent-arc or continent-continent collision. The abundance of ~2.0 Ga magmatic zircon is many of the sedimentary successions (Wan et al. 2006b) appear disproportionate to the number of igneous rocks of this age currently exposed in the area, and the release and incorporation of these detrital zircons may reflect extensive erosion following a significant orogenic event.

Studies on this issue have been largely focused in the Hengshan-Wutaishan-Fuping region (Figs. 6.2 and 6.3) which is one of the best exposed sections in the Trans-North China Orogen (Wilde et al. 1997, 2002). Faure et al. (2007) and Trap et al. (2007) presented structural evidence that suggested there may have been a major collisional event at 2.1 Ga, and this was developed further in Trap et al. (2008, 2009a, b). The gist of their model is that an ill-defined eastern continental block (referred to as the 'Fuping block') collided with the main Eastern Block of the NCC at ~2.1 Ga and that the Wutai and Hengshan complexes (Figs. 6.2 and 6.3) that resided to the west in the 'Lüliang Ocean', were thrust over the 'Fuping block' between 1.9–1.88 Ga, followed by NW-directed subduction of this combined block beneath the Western Block of the NCC at ~1.8 Ga (Fig. 6.4c).

Variants of the Faure et al. (2007) model have been proposed by Wang (2009) and Wang et al. (2010). Wang (2009) proposed that a major ocean, named the Proto-North China Ocean, developed between the Western and Eastern blocks prior to ~2565 Ma. Northwestward intra-oceanic subduction resulted in the formation of a proto-arc, represented by the ~2565–2540 Ma Wutai granitoids. The proto-arc then underwent rifting, propagating a back-arc basin that was extended to form an intra-oceanic arc-basin at ~2540–2525 Ma and formation of the precursors to the Wutai complex volcano-sedimentary sequence. Multiple subduction zones developed between ~2525–2475 Ma, resulting in closure of the Wutai back-arc basin. Final collision between the Eastern and Western blocks most likely took place at ~1.9–1.8 Ga. Furthermore, Wang (2009) argued that the tectonic evolution of the Trans-North China Orogen is characterized by subduction-accretion processes and the development of arc-basins and is more likely to be a Cordilleran-type orogen than a simple continent-continent collisional orogen. A number of criticisms can be made of this model (see Zhao et al. 2010c), and these will be discussed more fully in the following section.

In the Wang et al. (2010) paper, an Alaskan-type mafic-ultramafic intrusion in the Hengshan complex, with an age of 2193 ± 15 Ma, was interpreted to be derived from the mantle wedge above a subduction zone and emplaced within a continental arc. When combined with additional data on 2.3–2.0 Ga rocks from the Fuping complex (Zhao et al. 2000b, 2002a) and the Lüliang complex south of Wutaishan (Fig. 6.2) (Liu et al. 2006; Faure et al. 2007; Zhao et al. 2008b), the following scenario was constructed: (1) development of a ~2.5 Ga intra-oceanic arc-back arc basin system (Wutai complex) and its accretion to the Hengshan and Fuping complexes at the end of the Neoarchean; (2) an hiatus in magmatism and tectonism between ~2.5–2.3 Ga; (3) ~2.3–2.1 Ga marginal arc-back arc basin magmatism developed in the accreted Hengshan-Wutai-Fuping arc terranes and the Lüliang terrane; (4) ~2.1 Ga collision, resulting in closure of the ~2.3–2.1 Ga Lüliang back-arc basin, accretion of the Lüliang-Hengshan-Wutai-Fuping arc terranes, and their attachment to the Western Block of the North China Craton; (5) the intrusion of ~1970–1910 Ma post-collisional mafic dykes during extension; (6) final collision of the Western and Eastern blocks between ~1.9–1.8 Ga, resulting in extensive magmatism, tectonism and metamorphism; and lastly (7) post-1.8 Ga crustal

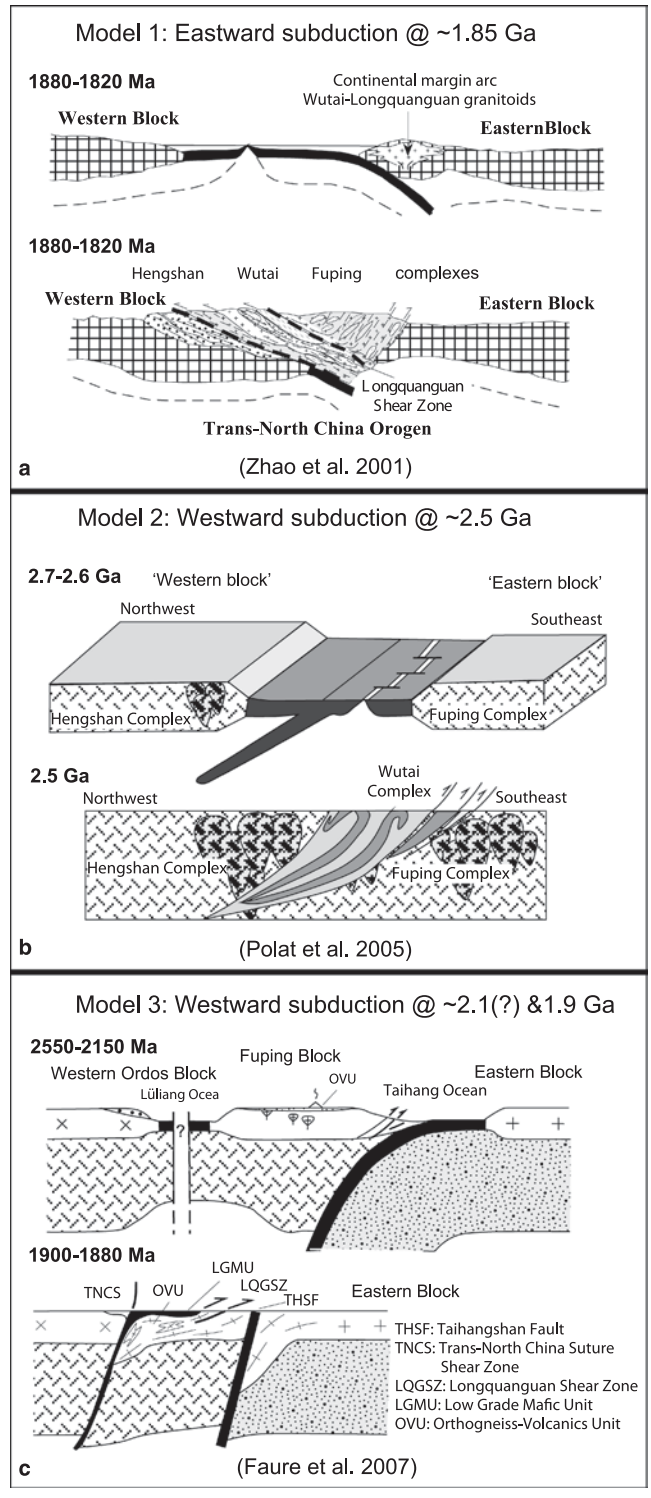

Fig. 6.4 The three main models that have been proposed for subduction polarity and timing of collision between the Eastern and Western blocks of the North China Craton. **a** eastward subduction after Zhao et al. (2001); **b** westward subduction based on Polat et al. (2005); and **c** two episodes of westward subduction following Faure et al. (2007), with collision of the Eastern and Fuping blocks at ~ 2.1 Ga and of these combined blocks with the Western Block between ~ 1.9–1.88 Ga. Modified from Zhang et al. (2012) (in press)

extension. The key points in this model are the inference of westward-directed subduction; the renewal of arc magmatism between 2.3 to 2.1 Ga in the Hengshan-Wutaishan-Fuping accreted arc, with coeval development of a back-arc basin in the Lüliang-area; the lack of volcanism after ~2.1 Ga in the Hengshan-Wutaishan-Fuping-Lüliang arcs, suggesting collision at this time; however, from the geometry it is suggested this collision was with the Western Block of the NCC; following this collision, syn- and post-collisional granitoids intruded all areas. Wang et al. (2010) favoured collision of the Eastern and Western blocks at ~1.88 Ga, but did not discuss the subduction polarity.

There thus seems to be growing evidence for a major event at ~2.1 Ga, but the full details have yet to be resolved. So far, no evidence has been presented of metamorphism at this time, which means that these models remain speculative. Both models outlined above invoke NW-directed subduction at some stage during the collisional process. This contrasts with the view of Zhao and co-workers, who have consistently favoured SE-directed subduction beneath the Eastern block. This controversial issue is discussed in more detail below.

6.3.3 Subduction Polarity

One of the longest-standing issues of contention between workers in the NCC in recent times has been the direction of subduction. In the original version of the current consensus model (Zhao et al. 1998), it was inferred that closure of the ocean between the Eastern and Western blocks was the result of subduction beneath the Eastern Block (Fig. 6.4a). This was based partly on initial structural studies, but principally on the fact that ~2.7 Ga inherited zircons were recorded in granitoids from the Wutai and Fuping complexes (Wilde et al. 1997), whereas only younger ages were known from the western part of the craton. Since components of the Eastern Block were known to extend back beyond 2.6 Ga, this was considered the most likely source. In addition, the oldest granitoids were dated at 2560–2540 Ma (Wilde et al. 1997, 2005) and were therefore older than the volcano-sedimentary rocks of the Wutai complex (2540–2515; Wilde et al. 2004a) with which many are in sheared contact (Wilde et al. 2005; Wang et al. 2010). These observations required their emplacement into pre-existing crust and hence it was considered that the western margin of the Eastern Block was an active continental margin at this time. Further investigation over the years utilizing structural, geochemical and geochronological data has led to substantiation of this model to the satisfaction of many workers (e.g. Zhao et al. 1999a, b, Wilde et al. 2002; Kröner et al. 2005a, 2006; Zhang et al. 2007, 2009, 2012, in press; Li et al. 2010).

In contrast, Kusky et al. (2001) and Kusky and Li (2003) originally presented sketchy evidence for westward subduction of the Central Orogenic Belt (Trans-North China Orogen) beneath the Western Block. This was initially based on the view that a Neoarchean magmatic arc was built on the western margin of the Eastern Block with a fore-arc to the west, of which the Dongwanzi ophiolite (also a subject of great controversy, see below) lay to the west (Kusky et al., 2001). These authors reported sheeted dykes with single chilled margins mainly on the NE sides. Later, Kusky and Li (2003) suggested a foreland basin (Qinglong Basin) was developed on the western edge of the Eastern Block in the Fuping area and that to the west lay an extensive granulite terrane (the Hengshan high-pressure granulite belt) interpreted to have formed on the eastern margin of the Western Block during a 2.5 Ga collision.

More substantial evidence based on structural geological observations has been presented in favour of westward subduction by Michel Faure and co-workers (Faure et al. 2007; Trap et al. 2007, 2008, 2009a, b), although this has been countered by equally strong structural arguments for eastward directed subduction below the Eastern Block (see Zhang et al. 2007, 2009, 2012; Li et al. 2010). Most of this work has been undertaken in the well-exposed Hengshan-Wutai-Fuping area (Fig. 6.3) and hinges on opposing interpretations of the basic geology. It also somewhat clouds the issue, since the Hengshan block has commonly been seen as synonymous with the

Western Block and the Fuping with the Eastern Block (see Kusky and Li 2003); both erroneous assumptions. The view in the Chinese literature prior to c.1998 was that the Wutai, Hengshan and Fuping complexes were separate crustal entities that had amalgamated either at ~2.5 or 1.8 Ga. This view has also been expressed in more recent international studies (e.g. Kusky et al. 2001; Kusky and Li 2003; Polat et al. 2005, 2006; Li and Kusky 2007; Faure et al. 2007; Trap et al. 2007, 2008, 2009a, b). However, an alternative model based on geochemical, geochronological and structural studies is that they form part of a single ~2.5 Ga arc that evolved marginal to the Eastern Block (Wilde et al. 2002, 2004a, 2005; Guan et al. 2002; Wilde and Zhao 2005; Zhao et al. 2005; Kröner et al. 2005a, 2006). Structural arguments relate to whether thrusting was top-to-the-SE or to the NW in the various blocks and to which deformational event various structures belong. This is not as straightforward as it may seem, since unpublished field studies by the author and Peter Cawood found evidence of movement in both directions along many dislocation planes throughout the area, related to early thrusting followed by later extension. Also, the structural data can be interpreted in several ways (see Zhang et al. 2009) and cannot on their own lead to a resolution of the polarity question.

Polat et al. (2005) used their geochemical data to infer west-directed ridge-subduction carrying the Wutai complex beneath the Hengshan complex; note this does not necessarily imply that it reflects the overall subduction polarity of the Trans-North China Orogen, although they do use 'Fuping complex' as synonymous with 'Eastern block' (Fig. 6.4b). In Polat et al. (2006), further geochemical work on rocks of the Wutai and Zunhua complexes is presented, but has little direct bearing on the direction of subduction, although they do show the ocean subducting to the NW below the Western Block. Wang et al. (2004), also based on geochemical data from the Wutai complex, favoured its development as an intra-oceanic arc-back arc association—possibly with multiple arcs—that accreted with the Hengshan-Fuping magmatic arc at ~2.5 Ga to form a single arc system; subduction polarity was not discussed, although in a subsequent paper that includes structural data, Wang (2009) inferred it was to the NW. This was further refined in Wang et al. (2010), with the suggestion of a NW-directed collision of the combined Hengshan-Wutaishan-Fuping- Lüliang arcs with the Western Block at ~2.1 Ga, as discussed in the previous section. But it should be re-stated that Wang et al. (2010) favoured major collision of the Eastern and Western blocks at ~1.8 Ga and that subduction polarity for this event was not discussed.

The debate about the Dongwanzi ophiolite is also relevant to this issue of subduction polarity and the reader is referred to the following for full details and references (Kusky et al. 2001, 2007a; Li et al 2002; Zhao et al 2007; Li and Kusky 2007). Essentially, the key argument revolves around the age and origin of mafic-ultramafic rocks in the Dongwanzi and Zunhua areas (Fig. 6.5) of the Eastern Block (but grouped in the 'Central Orogenic Belt' of Kusky et al. 2001). They were interpreted as ophiolites by Kusky et al. (2001), but this was questioned by a number of workers and culminated in Zhao et al. (2007) dating gabbros that were incorporated in the ophiolite at ~300 Ma. This led to a further exchange of opposing views (Kusky and Li 2008; Zhao et al. 2008c). Chromite with a Re-Os model age of 2547±10 Ma at Zunhua (Kusky et al. 2004) was interpreted to have formed in Alpine-type podiform chromitite, thus suggesting derivation in an oceanic setting to the west of their Eastern block. However, geochemical data (Zhou and Bai 1992; Zhang et al. 2004) suggested the chromites plotted outside the Alpine-peridotite field (but see Kusky et al. 2007a for further discussion). Whatever may be the correct interpretation, Li and Kusky (2007) have argued that a major collisional zone extends through the central part of their Central Orogenic Belt and is related to westward subduction of the Eastern Block of the NCC beneath the Western Block at 2.5 Ga.

The most recent evidence relevant to this question of subduction polarity of the Trans-North China Orogen is from the seismic data presented in Zheng et al. (2009). Here, two low-velocity zones (identified as L1 and L2) were recognized

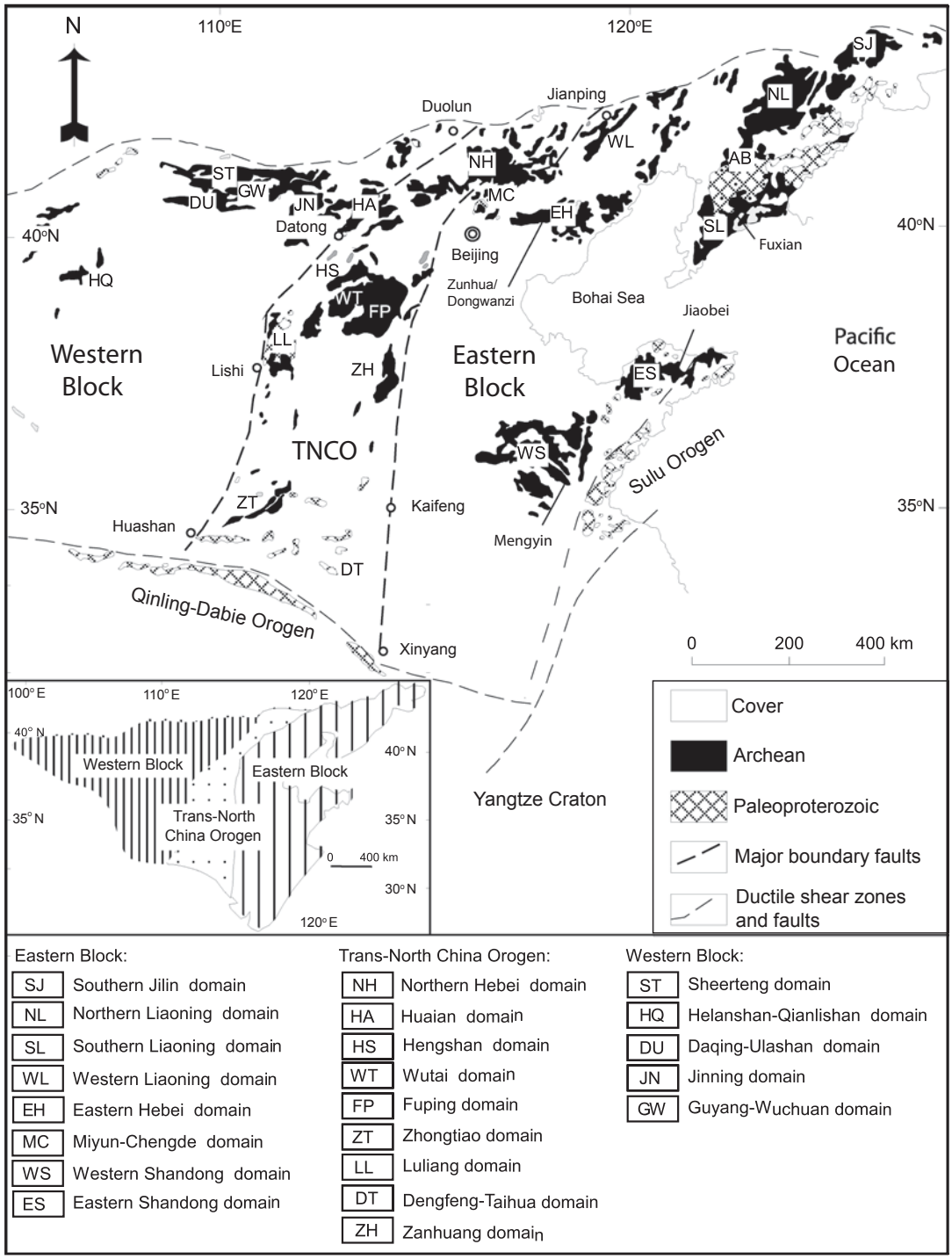

Fig. 6.5 Simplified geological map of the North China Craton showing the distribution of Archean and Proterozoic metamorphic domains. (modified from Zhao et al. 1999a)

in seismic sections that extend from the Western Block, through the Trans-North China Orogen, into the Eastern Block. Zone L1 was interpreted as remnants of upper-middle crustal material associated with westward-dipping subduction beneath the Western Block, and L2 as slices of upper-middle crustal material associated with westward-dipping subduction beneath their 'Fuping block' located between the Western and Eastern blocks, as earlier proposed by Faure et al. (2007) and Trap et al. (2007). Zheng et al. (2009) thus concluded that the seismic reflection data support the westward subduction model of two subduction zones in the Trans-North China orogen; the older one beneath the 'Fuping block' that collided with the Eastern Block at ~2.1 Ga, and the younger one beneath the Western Block that finally collided with the combined 'Fuping and Eastern block' at 1.9–1.8 Ga (see also Faure et al. 2007; Trap et al. 2007, 2008; Kusky 2011). But, as argued by Zhao et al. (2010b), since the low-velocity zones do not extend into the mantle it is uncertain if L1 represents subduction or overthrusting of the Western Block over the Trans-North China Orogen. Furthermore, Zhao et al. (2010b) again pointed-out that there is no metamorphic evidence for a ~ 2.1 Ga collisional event in the Fuping area, hence the interpretation of L2 remains speculative.

Clearly, the whole question of subduction polarity of the Trans-North China Orogen and its various component parts still requires resolution.

6.4 Nature and Distribution of the Precambrian Rocks

In the previous sections, emphasis has been placed on cratonic-scale features and on how the major units may have come together. Since our 2005 model (Zhao et al. 2005) has largely withstood the test of time, albeit with some need to more fully recognize the significance of events at 2.3–2-1 Ga in the Trans-North China Orogen, I will use this as a template in which to outline the major rock units that occur in each of the component blocks of the NCC. In particular, emphasis will be placed on identifying significant features and relationships, and on discussing any current divergences of opinion.

As noted above, the NCC can be divided into three major component parts: the Eastern and Western blocks, separated by the Trans-North China Orogen (e.g. Zhao et al. 2001).The Eastern Block consists predominantly of deformed and metamorphosed Neoarchean tonalite- trondhjemite-granodiorite (TTG) batholiths surrounded by anastomosing networks and linear belts of volcanic and sedimentary rocks metamorphosed from greenschist- to granulite-facies at ~2.5 Ga (see Zhao et al. 1998 for details). Rare Eoarchean to Mesoarchean rocks are locally present in the Eastern Block near Anshan (Liu et al. 1992, 2008). The recognition that the rift/collisional Jiao-Liao-Ji Belt splits the Eastern Block into two (Zhao et al. 2005) adds an additional complexity. In contrast, the Western block differs through the absence of Eoarchean to Mesoarchean rocks, the development of Paleoproterozoic khondalitic rocks and the predominance of Neoarchean granitoids, although a 2.5 Ga metamorphic event is also recognized (see Zhao et al. 1999b for details). The linear structural style and clockwise P–T path of rocks in the Khondalite Belt indicate it is a collisional belt between the Ordos Block to the south and the Yinshan Block to the north (Zhao et al. 2005).

The Trans-North China Orogen lies between these two major blocks and is composed of TTG gneisses and linear metamorphic belts that were originally equated with typical Archean greenstone belts, although only the Wutai complex fully meets this criterion (Wilde et al. 2004a). The best exposures are in the Hengshan-Wutai-Fuping area, located in the central segment of the orogen (Figs. 6.2 and 6.3) and most tectonic models have been based on studies in this general area (e.g. Wilde et al. 2002; Kröner et al. 2005a, b; Polat et al. 2005; Zhao et al. 2005; Faure et al. 2007).

A map outlining the distribution of the main exposures of Precambrian rocks in the NCC, including supracrustal belts, is presented as Fig. 6.5. They have been subdivided into various 'domains', named after local towns or their location within the various provinces (see also

Zhao et al. 2001a, 2005). Domain boundaries are either faulted or obscured by younger cover, including local Proterozoic sedimentary rocks.

6.4.1 Western Block

The Western Block is poorly exposed in the south and outcrop is restricted to the northern part. Based partly on geophysical data, it is separated into the Ordos Block in the south, the Yinshan Block in the north, with the Khondalite Belt in between (Fig. 6.2). The Ordos Block is entirely covered by the Mesozoic Ordos sedimentary basin and the nature of the basement rocks is known only from limited drill holes. Although it has generally been assumed that the basement is Archean in age, unpublished work (Y.S. Wan personal communication 2012) suggests that Paleoproterozoic ages predominate. Work is currently in progress to confirm this.

Rocks of the Yinshan Block have been grouped, from east to west, into the Sheerteng, Wuchuan, and Guyang domains (Fig. 6.5) (Zhao et al. 1999b, 2001), although those farthest to the west appear to have been little studied. They consist of TTG gneisses and ultramafic to felsic volcanic rocks, metamorphosed from greenschist to granulite facies. In general, the high-grade TTG gneisses are associated with mafic granulites and charnockite, dominantly in the Wuchuan and Guyang domains, whereas the lower grade volcanic assemblages form linear greenstone belts associated with low-grade TTG rocks, notably in the Sheerteng domain (see Zhao et al. 1999b and references therein). Metamorphism in all domains is characterized by anti-clockwise P/T paths (Zhao et al. 1999b) and occurred at ~2.5 Ga.

The Khondalite Belt contains the Helanshan-Qianlishan, Daqingshan-Ulashan and Jining domains (Fig. 6.5). The basic features of the khondalites have been described in an earlier section and are not repeated here, but there are a number of key points to stress. Besides khondalites, there are widespread syn-tectonic S-type granites invading the supracrustal rocks with ages of ~1.9 Ga. The khondalitic rocks themselves are interpreted to have formed along the passive northern margin of the Ordos Block, with subduction to the north below the Yinshan Block (Zhao et al. 2005). The metamorphic assemblages all define tight clockwise P/T paths (see Zhao et al. 1999b and references therein) and rocks attained UHT conditions, at least locally (Santosh et al. 2006, 2007; Guo et al. 2008). These events occurred around 1.92 Ga and represent the collision of the Ordos and Yinshan blocks.

6.4.2 Eastern Block

The main exposures of Precambrian rocks in the Eastern Block are located in two main areas: in its northern part to the north and east of Beijing, and in the central part in Shandong Province: there are no known outcrops in the southern part of the block (Fig. 6.5).

The northern area contains the Southern Jilin, Northern Liaoning, Southern Liaoning, Western Liaoning, Miyun-Chengde, Anshan-Benxi, and Eastern Hebei domains (Fig. 6.5). The rocks are Eo- to Neoarchean TTG gneisses intruded by variably-deformed ~2.5 Ga granitoids. Supracrustal rocks are not abundant but are present in all domains, including the more extensive and economically important Neoarchean banded iron formations (BIF) in the Anshan-Benxi domain. The oldest rocks in China are located near Anshan (Liu et al. 1992) and consist of a variety of TTG gneisses with ages ranging from 3.8 to 3.3 Ga (Liu et al. 2008). There has been some controversy regarding the precise age of the oldest rocks. Liu et al. (2008) recollected material from the Baijiafen quarry and Dongshan scenic park at Anshan and established that the oldest rock at Baijiafen was a 10 cm-wide band of TTG gneiss with an age of 3800±5 Ma (in agreement with the original age determined in 1992), whereas the oldest material at Dongshan scenic park was a quartz diorite boudin with a weighted mean $^{207}Pb/^{206}Pb$ age of 3794±4 Ma (younger than the trondhjemite age of 3811±4 Ma obtained by Song and others (1996) from the same area). They concluded that the ancient rocks were less widespread than previously believed and this

was reconfirmed by Wu et al. (2008), who determined the oldest age at Baijiafen quarry was 3822 ± 7 Ma, with a subsequent magmatic event at 3799 ± 6 Ma. However, these authors considered that most rocks in the Baijiafen quarry and Dongshan scenic park were younger and emplaced between 3.3 and 3.1 Ga, although they contain zircon xenocrysts with ages of ~3.8 Ga. Both these recent studies established that the hafnium in zircon was chondritic, with Hf model ages only extending back to ~3.9 Ga, which is close to the emplacement age of the oldest rocks. Whole-rock Nd model ages presented by Wu et al. (2005a) and Wan et al. (2005) are overall slightly younger, although the oldest ages are ~4.1 Ga.

Old ages have also been reported from the Eastern Hebei domain, where Jahn et al. (1987) reported a Sm-Nd whole-rock isochron age of ~3.5 Ga for amphibolites from the Qianxi complex, although this has subsequently been questioned (Liu et al. 2007). However, there is no doubting the antiquity of detrital zircons in the Caozhuang quartzite in the Qianxi complex (Liu et al. 1992), where recent work (Wilde et al. 2008) has indicated ages up to 3858 ± 3 Ma. Importantly, the > 3.8 Ga zircon population also records elevated $\delta^{18}O$ values that average 6.5‰, which is 0.3‰ higher than the average for the Jack Hills detrital zircons, indicating recycling of > 3.8 Ga continental crust in the NCC.

The central area consists of the Eastern and Western Shandong domains (Fig. 6.5). In Eastern Shandong, 90% of the rocks are TTG gneisses (Zhao et al. 1998), with minor enclaves and lenses of supracrustal rocks. The latter consist of mafic granulite, amphibolite and pelitic gneiss. The granulites and amphibolites record anticlockwise P/T paths (Z.L. Li 1993 quoted in Zhao et al. 1998) resulting from metamorphism at 2.5 Ga.

The rocks in Western Shandong have been widely regarded as forming an Archean granite-greenstone terrane (Bai 1993). Overall, they are of lower metamorphic grade than in Eastern Shandong, ranging from greenschist- to amphibolite-facies, with only local granulite-facies rocks. The granitic rocks include both TTG and calc-alkaline varieties. The supracrustal rocks include komatiite (Xu and Dong 1992; Cheng and Kusky 2007), metabasalt, quartzite, BIF, amphibolite, and biotite-rich paragneiss (Wan et al. 2010, 2012). The recent work by Wan et al. (2010, 2012) has thrown new light on the geology of the Western Shandong domain, with the recognition of three discrete belts: a northeastern belt of Late Neoarchean (2.53–2.50 Ga) age composed of crustally-derived monzogranite and syenogranite, with abundant migmatite; a central belt composed mainly of Early Neoarchean (2.7–2.6 Ga) TTG gneiss and supracrustal rocks; and a southwestern belt comprising juvenile Late Neoarchean (2.56–2.50 Ga) granitoids and gabbros (Wan et al. 2010). Although these younger monzogranites and syenogranites also occur in the southwestern belt, they form only a minor component. The importance of these results is the recognition of 2.7–2.6 Ga supracrustal rocks and granitoids in the NCC, since they are notably absent from the northern part of the Eastern Block, the Trans-North China Orogen and the Western Block. Further work is required to determine the full extent of the Early Neoarchean granitoids.

All domains in the Eastern Block underwent high-grade metamorphism with anticlockwise P/T paths at ~2.5 Ga (Zhao et al. 1999a). For further details on the metamorphic history of the various domains the reader is referred to Zhao et al. (1998) and references therein.

The Jiao-Liao-Ji Belt has been discussed earlier with respect to its position and significance within the Eastern Block (Fig. 6.2), especially with regard to the evidence obtained from the North and South Liaohe 'groups'. Besides the latter, it also contains the volcano-sedimentary successions of the Fengzishan and Jingshan groups of Eastern Shandong in its southern part and the Ji'an and Laoling groups in Jilin Province to the north; perhaps also including the Macheonayeong Group in North Korea (Zhao et al. 2005). All groups are lithologically similar, consisting of a basal clastic sequence that is overlain by a bimodal volcanic succession, followed by a carbonate-rich sequence, with an upper pelite-rich unit (Li et al. 2005). The Fengzishan and Laoling groups have been correlated with the

North Liaohe 'group' and the Jingshan and Ji'an groups with the South Liaohe 'group'. The rocks were deposited at ~2.0 Ga, and post-date the 2.2–2.1 Ga Liaoji gneissic granitoids (Luo et al. 2004). The rocks were metamorphosed to greenschist/amphibolite facies at ~1.9 Ga and intruded by alkaline granitoids at ~1.88 Ga (Zhao et al. 2005).

6.4.3 Trans-North China Orogen

This area has been the focus of much attention by local and international geoscientists over the past two decades, although, as discussed above, there is still no general consensus regarding the timing and polarity of subduction of the orogen in respect to the amalgamation of the North China Craton. Much of the early work concentrated on resolving the nature of the three best-exposed tectonic units: the Hengshan, Fuping and Wutai complexes (Fig. 6.3). More recently, work has extended to the adjacent Lüliang complex (Liu et al. 2006; Zhao et al. 2008b), to the high-pressure granulite terrane to the north (Guo et al. 2005), and to the Zanhuang, Dengfeng and Taihua domains in the far south (Fig. 6.2) (Wang et al. 2003; Wan et al. 2006a).

The Hengshan and Fuping complexes consist mainly of TTG gneiss, with local amphibolite and supracrustal rocks. U-Pb zircon dating indicates that the TTG gneisses in both complexes were emplaced between ~2525 and 2475 Ma (Guan et al. 2002; Zhao et al. 2002a; Kröner et al. 2005a, b). Geochemical and isotopic data, together with evidence for earlier basement (xenocrystic zircons with an age of ~2.7 Ga) in both complexes, suggest that they developed in a continental arc setting (e.g. Liu et al. 2004; Kröner et al. 2005a, b), possibly along the western margin of the Eastern Block of the NCC (e.g. Wilde et al. 1997, 2002; Wilde and Zhao 2005; Zhao et al. 2001, 2005).

The Wutai complex is a Late Neoarchean granite-greenstone domain. The greenstones are composed of volcanic and sedimentary rocks at sub-greenschist- to amphibolite-facies. Their age is constrained by SHRIMP U-Pb zircon dating of intermediate and felsic volcanic rocks at ~2530–2515 Ma (Wilde et al. 2004a). Field and geochronological investigations indicate that units of different metamorphic facies are in tectonic contact (Wilde et al. 2004a; Kröner et al. 2005a), and occur as complex stacked thrust sheets that have jumbled the original stratigraphy. Mafic volcanic rocks have diverse geochemical compositions, ranging from MORB-, BABB-, to IAB-type (Wang et al. 2004; Polat et al. 2005, 2006) and the greenstone belt is interpreted to have formed in an intra-oceanic arc-basin, although opinion is divided as to whether it was in a fore-arc setting, perhaps involving ridge-subduction (Polat et al. 2005) or a back-arc setting (Wang 2009). Unconformably overlying the Wutai greenstone belt is the Paleoproterozoic Hutuo Group (Fig. 6.3), which is composed of unmetamorphosed to low-grade metasedimentary rocks, including conglomerate, quartzite, phyllite, slate, dolomitic marble, with rare intermediate volcanic rocks. SHRIMP U-Pb zircon dating of a felsic tuff indicates a crystallisation age of 2087±9 Ma, with an earlier inherited zircon population of 2180±5 Ma (Wilde et al. 2004b). A study of detrital zircons (Liu et al. 2011a) indicates that much of the material was derived from erosion of the underlying Wutai granitoids. But besides the dominant 2550–2500 Ma zircons, a minor detrital population at 2250–2000 Ma is also present, substantiating the Paleoproterozoic age of the Hutuo Group. Detrital zircons as young as ~1810 Ma were obtained from the upper part of the group (Liu et al. 2011b), indicating this succession was deposited during the main 1.8 Ga collisional event.

The Wutai granitoids are mainly granodiorite and monzogranite and U-Pb zircon dating indicates that most were intruded between 2566 and 2517 Ma (Wilde et al. 1997, 2005), the earliest phases therefore pre-dating the Wutai greenstone sequence with which they are in tectonic contact. The geochemistry and Nd isotopes suggest that the granitoids formed in an intra-oceanic arc setting (Liu et al. 2004; Wang 2009), although this may not apply to the oldest components that are geochemically more involved and contain 2.7 Ga inherited zircons (Wilde et al. 1997).

The Hengshan-Wutai-Fuping complexes were originally considered to represent separate crustal

blocks (e.g. Bai 1993), and some recent workers (Polat et al. 2005, 2006) have perpetuated this view. Conversely, Wang et al. (2004) considered that the Wutai back-arc basin evolved separately, with the rocks thrust over the Hengshan and Fuping continental arc to form a combined entity at ~2.5 Ga, whereas other workers have considered the Hengshan and Fuping complexes to represent the basal part and the Wutai complex the upper part of a single arc complex (see Kröner et al. 2005a, b).

The geology of the Lüliang complex, lying to the southwest of the Hengshan-Wutai-Fuping area (Fig. 6.2), has recently been investigated in detail (e.g. Liu et al. 2006; Faure et al. 2006, 2007; Zhao et al. 2008b). It consists mainly of supracrustal rocks and granitoids that formed between 2.3 and 1.8 Ga (Yu et al. 1997; Geng et al. 2000; Zhao et al. 2008b). The earliest magmatic rocks are TTG gneisses with an age of 2499 ± 9 Ma (Zhao et al. 2008b), comparable to certain TTG gneisses in the Hengshan and Fuping complexes. Younger gneisses with a magmatic age of 2375 ± 10 Ma are locally present, and these are coeval with volcanic rocks in the supracrustal component of the Lüliang complex (Faure et al. 2006) and with granitoids in both the Zhongtiao domain to the east (Fig. 6.2) (Sun et al. 1992) and in the Hengshan complex to the north (Kröner et al. 2005a, b). The most widespread granitoids in the Lüliang complex have ages ranging from 2199–2173 Ma (Zhao et al. 2008b) and are similar to granitoids identified in both the Hengshan (Kröner et al. 2005a) and Fuping complexes (Guan et al. 2002; Zhao et al. 2002a). So, although the Lüliang complex differs in being largely Paleoproterozoic in age, the timing of granitic magmatism is not unique and points to a uniformity of events in the central part of the Trans-North China Orogen: rocks in all complexes underwent high-grade metamorphism at ~1.85 Ga.

6.5 Age of the Precambrian Lithosphere

The general composition of the lower crust beneath the NCC has been discussed by Gao et al. (1998a, b) and Rudnick and Gao (2003). A combination of seismic and xenolith data have been used to conclude that the crust has four layers and that the upper part of the lower crust is intermediate granulite in composition whereas the lowermost crust is mafic (Gao et al. 1998a, b). The total crust is considered to have an average composition of granodiorite (Gao et al. 1998b). However, the question of when it formed is an important issue, especially when much of the eastern part of the craton has undergone lithospheric thinning, with possible delamination of the lowermost crust and lithospheric mantle (see later section).

Wu et al. (2005a) presented a compilation of all the reliable Nd data for the North China Craton available at that time. They concluded that there were differences between the Eastern and Western blocks and the Trans-North China Orogen. The Eastern Block recorded two peaks in the Ndt_{DM2} data: at 3.4 Ga and 2.8 Ga, with the latter being dominant. Fewer data were available from the Western Block but they had an average Ndt_{DM2} age of 2.74 Ga, with no model ages greater than 3.2 Ga. Data from basement rocks in the Trans-North China Orogen recorded a single population between 2.8 and 2.4 Ga, with an average Ndt_{DM2} model age of 2.7 Ga. When considered as a whole, the NCC Nd data give a mean model age of 2.8 Ga for extraction from the mantle. This is notably older than the majority of U-Pb zircon ages recorded from magmatic rocks in the NCC which concentrate between 2.55 and 2.00 Ga (Wilde et al. 1997, 2005). Significantly, many of the Paleoproterozoic rocks gave negative $\varepsilon_{Nd}(t)$ values, indicative of crustal reworking rather than a new episode of crustal growth (Wu et al. 2005a).

A recent review of all the available zircon Hf model age data for the North China Craton (Geng et al. 2012) indicates a number of key features that overall mirror the Nd data. In the Eastern Block, two-stage model ages show a concentration at 4.0–3.5 Ga, indicating a short crustal residence time for the earliest crustal components, and a major peak at 2.75 Ga, marking the main period of crustal growth in the Eastern Block. The latter zircon group also record mainly positive $\varepsilon_{Hf}(t)$ values, indicating the input of juvenile material to the crust at this time. Zircon Hf data from the Western Block are few, but show

a similar concentration of two-stage model ages at 2.7 Ga for the TTG and greenstone rocks. The khondalites are distinct and show a peak at 2.3 Ga, with negative $\varepsilon_{Hf}(t)$ values indicating reworking of pre-existing crust. Two-stage model ages from the Trans-North China Orogen show a peak at ~2.7 Ga, broadly similar to the Eastern Block although slightly younger, but nonetheless substantiating the intimate connection of these two blocks from Neoarchean times. Overall, the Hf data substantiate the view that the main period of crustal growth in the NCC was at 2.8–2.7 Ga and that the abundance of 2.55–2.50 Ga granitoids reflects reworking of this crust with only limited new additions.

6.6 The Position of the North China Craton within the Precambrian Supercontinents

At the start of the Phanerozoic, the North China Craton is generally considered to lie somewhere to the north of Australia in a peri-Gondwana position (see Metcalfe 1996), based on limited paleomagnetic data (Li et al. 1996; Zhao et al. 1996). Its subsequent northward movement, along with the Tarim and South China blocks, has ultimately resulted in its collision with the Siberia Craton along the Central Asian Orogenic Belt. The precise timing and location of final closure of the paleo-Asian Ocean that lay between the two cratons is the subject of considerable debate, although the weight of evidence indicates that the Solonker-Xra Moron-Changchun zone marks the site and that suturing appears to have occurred in the Late Permian (Wu et al. 2007c).

However, data relevant to its earlier position within Rodinia are sparse and, indeed, the North China Craton was not even discussed or shown in the original reconstructions of McMenamin and McMenamin (1990), Hoffman (1991) and Dalziel (1991). Attempts have been made (see Zhai et al. 2003) to identify events in the NCC at 1200–950 Ma that might be related to supercontinent formation, but these are extremely tenuous. Yang et al. (2004a) also suggested that certain Triassic dolerite dykes in the Liaodong Peninsula that incorporated Mesoproterozoic zircons with ages of 1.1–0.9 Ga might be tapping crust generated during the amalgamation of Rodinia, though the evidence is far from convincing.

With respect to the Paleoproterozoic supercontinent Nuna/Columbia, there is considerably more evidence available from the North China Craton. Indeed, it was the driver behind the original attempt at reconstruction of a global pre-Rodinian supercontinent (Zhao et al. 2002b); the aim being to identify and then link all 2.1–1.8 Ga collisional belts that recorded events similar to those identified in the North China Craton (see Fig. 6.6). In this model, geological similarities—especially the dominance of 2.55–2.50 Ga granitic magmatism—in the North China and India blocks suggest a possible link, an idea first suggested by Kröner et al. (1998). However, the connection proposed was between the Trans-North China Orogen and the Central Indian Tectonic Zone (Fig. 6.6) and this no longer appears viable given the dominance of 1.65 Ga events in the latter (see Bhowmik et al. 2011). A possible link between the North China Craton and Baltica has also been suggested (Qian 1997; Wilde et al. 2002), based mainly on lithological and geochronological data available at the time, with possible linking of the Trans-North China Orogen with the Kola-Karelian Orogen. A connection with the Siberia Craton along the Akitkan orogen has also been suggested as a possibility (Condie 2002).

Although there has been little advance in establishing which, if, any of the 2.1–1.8 Ga orogenic belts might link-up with the Trans-North China Orogen, further work has been undertaken to establish the breakup history of the North China Craton from Nuna/Columbia. One of the key indicators is the development of major mafic dyke swarms related to mantle plumes beneath the supercontinent. The oldest mafic dykes identified in the NCC intruded at ~1915 Ma (Kröner et al. 2006), but these are boudinaged within TTG gneisses of the Hengshan complex and pre-date the major 1.85 Ga high-grade metamorphic event; they have also not been established as forming part of a major dyke swarm. However, several swarms that post-date the Paleoproterozoic metamorphic event in the Trans-North

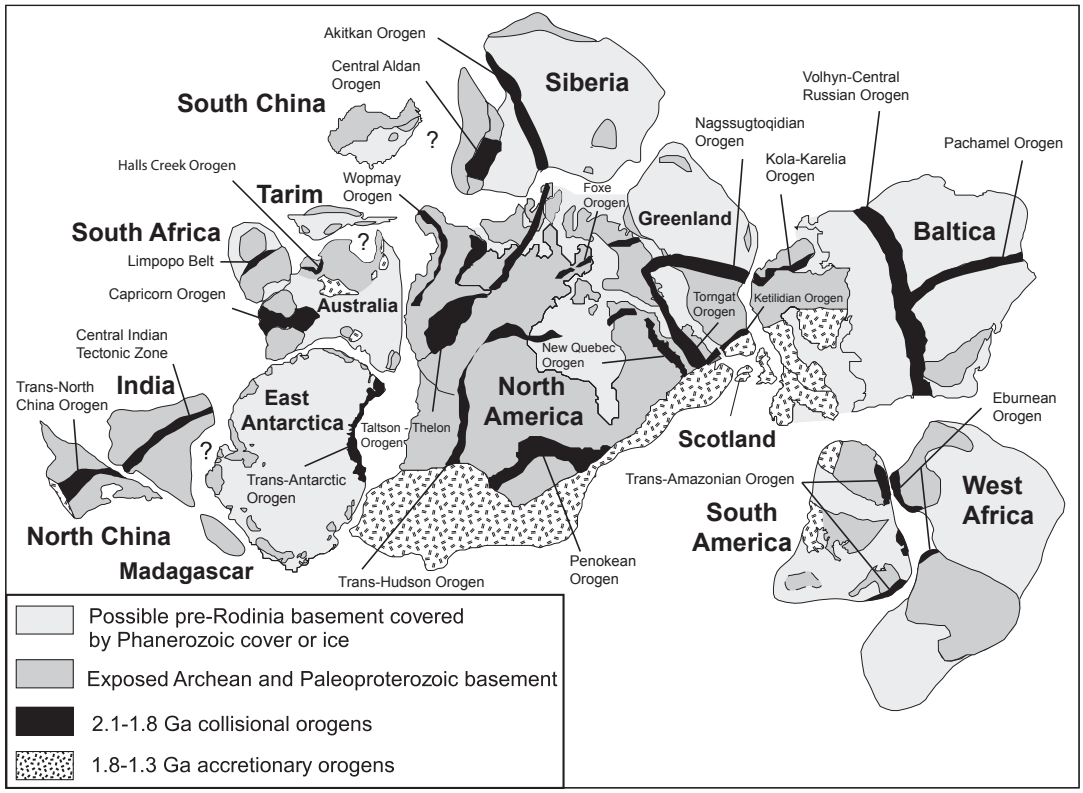

Fig. 6.6 Possible configuration of the main cratonic masses in the Nuna/Columbia supercontinent as proposed by Zhao et al. (2004), with slight modifications. These were linked on mainly geological grounds, based on evidence from 2.1 and 1.8 Ga collisional belts

China Orogen have been identified and range in age from 1.8 to 1.75 Ga (Peng et al. 2005, 2007, 2008). These are widespread in the Hengshan-Wutai-Fuping-Lüliang area (Figs. 6.2 and 6.3) and are considered to form a Large Igneous Province (LIP) related to a mantle plume that was associated with the breakup of Nuna/Columbia (Peng et al. 2007).

Another feature that has been associated with the breakup of Nuna/Columbia is the Xiong'er Group of dominantly andesitic volcanics and related dykes at the southern extremity of the Trans-North China Orogen—although there are two widely-divergent interpretations. Peng et al. (2008) consider the Xiong'er volcanic belt to be a rift that formed part of a triple-junction, activated by a mantle plume at ~1.78 Ga. They further suggest that this records the breakup of the NCC from an unknown continent to the south. Alternatively, several other workers consider that the Xiong'er Group, based on its geochemistry, is an arc sequence that extends in age from 1.8–1.4 Ga (Zhao et al. 2003; He et al. 2008). In this model, the southern margin of the NCC would be margined by an arc system from the Late Paleoproterozoic through much of the Mesoproterozoic, thus indicating an open ocean to the south.

The northern margin of the North China Craton also records events that have been related to the breakup of Nuna/Columbia (Zhao et al. 2003). Here, the Zhaertai-Bayan Obo-Huade-Weichang Rift Zone extends right across the northern part of the NCC and records ages from 1.6–1.2 Ga. The rocks include bimodal volcanics and extensive sedimentary sequences recording the transition from a rapidly subsiding ensialic basin or continental marginal environment to a stable continental shelf environment. Furthermore, Kusky et al. (2007b) have used their model of the North Hebei Orogen, developed across the

whole of the northern part of the NCC, to propose that granulite facies metamorphism at 1.93–1.92 Ga was related to collision between Baltica and Amazonia between 2.0–1.7 Ga.

Finally, the interior of the North China Craton shows strong evidence for rifting and anorogenic magmatism throughout most of the Mesoproterozoic (Zhao et al. 2004, 2006c; Kusky et al 2007b), commonly equated with the ultimate breakup of the Paleoproterozoic supercontinent of which the NCC was part. In addition a major sedimentary sequence (the Changcheng-Jixian-Qingbaikou 'series') is widely developed in the central part of the NCC and unconformably overlies the basement rocks. It consists of clastic and carbonate sediments with minor shale, bentonite and rare volcanic horizons. The age of the sequence ranges from ~1. 8 to 1.32 Ma (see discussion in Wan et al. 2011), attesting to the stability of the North China Craton throughout most of the Mesoproterozoic.

6.7 Lithospheric Thinning in the Phanerozoic

As indicated at the start of this review, the fact that the North China Craton has undergone lithospheric thinning requires comment, since the potential loss of Precambrian lithosphere and lower crust has important implications for the overall survival of cratons and hence the long term preservation of Precambrian rocks. The occurrence of ~450 Ma diamondiferous kimberlites at Fuxian and Mengyin (Fig. 6.5), coupled with evidence from xenolith data for much thinner lithosphere in the Cenozoic, indicates the loss of >120 km of lithospheric mantle from beneath the eastern part of the North China Craton (Menzies et al. 1993; Griffin et al. 1998). Subsequent studies by numerous workers have substantiated this view, with widespread evidence from the rock record (see Wu et al. 2005b and references therein), Re-Os isotopic data (Gao et al. 2002; Wu et al. 2003), mineralization (Yang et al. 2003), development of core complexes (Davis et al. 1996; Yang et al. 2007a) and magma mingling (Yang et al. 2004b). More recently, surface wave tomography has indicated that large tracts of East Asia have thin lithospheres (McKenzie and Priestley 2008), including not only the North China Craton, but South China and parts of Far East Russia as far north as Lake Baikal: India too has thinner lithosphere than is typical below most cratons.

It is not appropriate here to delve deeper into the reasons for lithospheric thinning in the NCC: rather, it is necessary to address two questions: (1) when did thinning start and (2) how complete was it? There is considerable debate regarding both issues. In terms of timing, it is generally agreed that the main manifestation of lithospheric thinning was in the Cretaceous. This has been referred to as a 'giant igneous event' by Wu et al. (2005b) and granitic magmatism was widespread throughout northern China at this time. However, there is some evidence that the onset of thinning may have occurred earlier. Gao et al. (2004) interpreted certain Upper Jurassic lavas in NE China as the result of foundering and melting of lower crustal eclogite into the mantle, where it interacted with peridotite. Furthermore Yang et al. (2007b) considered that certain Late Triassic dolerite dykes in the Liaodong Peninsula formed in a similar manner to those described by Gao et al. (2004), although an added complication here is the proximity of the Sulu collision zone that marks the collision of the North and South China cratons, where slab break-off is considered to have occurred at around this time. However, detailed study of Late Triassic granites and their enclaves from the Liaodong Peninsula (Yang et al. 2007c) provided further evidence in support of crust-mantle interaction in the Triassic.

Although the surface wave tomographic data show thin lithosphere beneath much of East Asia (McKenzie and Priestley 2008), in detail there appears to be considerable variation. O'Reilly et al. (2001) suggested that there was transformation of the lithospheric mantle beneath the North China Craton, involving dispersion and dilution rather than wholesale delamination. This was based on seismic tomography that showed alternating blocks of high- and low-velocity material (interpreted, respectively, as Archean and Phanerozoic lithosphere) extending to depths of ~150 km (Yuan 1996). Wilde et al. (2003) supported this interpretation, based on their study of mantle xenoliths from Hannuoba in the northern part of the Trans-North China Orogen

and the fact that Proterozoic lithosphere was preserved in the southern part of the craton (Zheng et al. 2001). More recent evidence also appears to support this view, with 3.6 Ga zircons being reported from felsic granulite xenoliths in an Early Jurassic volcanic diatreme at Xinyang at the southern boundary of the Trans-North China Orogen (Zheng et al. 2004). It thus appears that ancient crust and/or lithosphere was preserved after the Paleozoic at least in some parts of the North China Craton, and that it is still available for incorporation in mantle-derived magmas.

Notwithstanding the exceptions noted above, the replacement or removal of lithospheric mantle and part of the lower crust from beneath the NCC was widespread and has led to extensive modification of the craton. This process has been referred to as 'decratonization' (Yang et al. 2008) and it remains to be established how widespread this phenomenon is in other cratons. Although the mechanisms for 'decratonization' are not canvassed here, the reader is referred to the elegant paper of Windley et al. (2010) which reviews the evidence and then outlines a possible scenario involving multiple subduction and the role of water in nominally anhydrous minerals.

Acknowledgements I wish to thank two important ladies of Chinese Geology—both now retired—for first introducing me to the geology of China. Prof. Kaiyi Wang of the Chinese Academy of Sciences invited me to work in the North China Craton at Wutaishan and Prof Jinglan Liu of the Harbin Institute of Geology introduced me to the Central Asian Orogenic Belt via the Jiamusi Massif. This was in 1992—and I am pleased to say that I have had the most rewarding experience of working regularly in both areas over the past twenty years. I also want to acknowledge Fuyuan Wu, Guochun Zhao, Jinhui Yang and Jianbo Zhou for their friendship, encouragements and invaluable assistance over many years.

References

Bai J (1993) The Precambrian geology and Pb–Zn mineralization in the northern margin of North China Platform. Geological Publishing House, Beijing, pp 47–89 (in Chinese with English abstract)

Bai J, Dai FY (1998) Archean crust of China. In: Ma XY, Bai J (eds) Precambrian crust evolution of China. Springer–Geological Publishing House, Beijing, pp 15–86

Bhowmik SK, Wilde SA, Bhandari A (2011) Zircon U-Pb/Lu-Hf and monazite chemical dating of the Tirodi biotite gneiss: implication for latest palaeoproterozoic to early mesoproterozoic orogenesis in the Central Indian Tectonic Zone. Geological Journal 46:1–23

Cheng SU, Kusky T (2007) Komatiites from west Shandong, North China craton: implications for plume tectonics. Gondwana Res 12:77–83

Cheng YQ (1994) Outline of regional geology of China. Geological Publishing House, Beijing, p 517

Condie KC (2002) Breakup of a paleoproterozoic supercontinent. Gondwana Res 5:41–43

Condie KC, Allen P, Narayana BL (1982) Geochemistry of the Archean low- to high-grade transition zone, southern India. Contrib Mineral Petrol 81:157–167

Dalziel IWD (1991) Pacific margins of Laurentia and East Antarctic–Australia as a conjugate rift pair: evidence and implications for an Eocambrian supercontinent. Geology 19:598–601

Dalziel IWD (1997) Neoproterozoic-paleozoic geography and tectonics: review, hypothesis, environmental speculation. Geological Society America Bulletin 108:16–42

Davis GA, Qian X, Zheng Y, Yu H, Wang C, Mao TH, Gehrels GE, Muhammad S, Fryxell JE (1996) Mesozoic deformation and plutonism in the Yunmeng Shan: a Chinese metamorphic core complex north of Beijing, China. In: Yin A, Harrison TM (eds) The tectonic evolution of Asia. Cambridge University Press, New York, pp 253–280

Faure M, Lin W, Monie P, Bruguier O (2004) Palaeoproterozoic arc magmatism and collision in Liaodong Peninsula (north-east China). Terra Nova 16:75–80

Faure M, Trap P, Lin W, Le Breton N, Bruguier O, Monie P (2006) Structure and tectonic evolution of the Lüliangshan (Shanxi Province, China): a key area for the understanding of the Paleoproterozoic. Trans-North China Belt. 2006 IAGR Annual convention and international conference, Hong Kong, (Abstracts), pp 53–54

Faure M, Trap P, Lin W, Monie P, Bruguier O (2007) Polyorogenic evolution of the paleoproterozoic trans-north China belt, new insights from the Lüliangshan-Hengshan-Wutaishan and Fuping massifs. Episodes 30:1–12

Gao S, Luo T-C, Zhang B-R, Zhang H-F, Han Y-W, Hu Y-K, Zhao Z-D (1998a) Chemical composition of the continental crust as revealed by studies in East China. Geochim Cosmochim Acta 62:1959–1975

Gao S, Zhang B-R, Jin Z-M, Kern H, Luo T-C, Zhao Z-D (1998b) How mafic is the lower continental crust? Earth Planet Sci Lett 161:101–117

Gao S, Rudnick RL, Carlson RW, McDonough WF, Liu YS (2002) Re-Os evidence for replacement of ancient mantle lithosphere beneath the North China Craton. Earth Planet Sci Lett 198:307–322

Gao S, Rudnick RL, Yuan H-L, Liu X-M, Liu Y-S, Xu W-L, Ling W-L, Ayers J, Wang X-C, Wang Q-H (2004) Recycling lower continental crust in the North China craton. Nature 432:892–897

Geng YS, Wan YS, Shen QH, Li HM, Zhang RX (2000) Chronological framework of the early Precambrian

important events in the Lüliang Area, Shanxi Province. Acta Geol Sin 74:216–223
Geng YS, Du LL, Ren LD (2012) Growth and reworking of the early Precambrian continental crust in the North China Craton: constraints from zircon Hf isotopes. Gondwana Res 21:517–529
Griffin WL, Zhang AD, O'Reilly SY, Ryan CG (1998) Phanerozoic evolution of the lithosphere beneath the Sino-Korean craton. In: Flower MFJ, Chung SL, Lo CH, Lee TY (eds) Mantle dynamics and plate interactions in East Asia, vol 100. American Geophysical Union, Washington, D. C., (Geodynamics Series) pp 107–126.
Guan H, Sun M, Wilde SA, Zhou XH, Zhai MG (2002) SHRIMP U-Pb zircon geochronology of the fuping complex: implications for formation and assembly of the North China Craton. Precambr Res 113:1–18
Guo JH, Sun M, Chen FK, Zhai MG (2003) SHRIMP U-Pb zircon geochronology of high-pressure granulites in the Sanggan area, North China Craton: Timing of Paleoproterozoic continental collision. In: Kehelpannala KVW (ed) Proceedings of the IGCP-440 and legends international symposium and field workshop on "The role of Sri Lanka in Rodinia and Gondwana assembly and breakup". Centenary Publication, Geological Survey & Mines Bureau, Sri Lanka, pp. 56–61
Guo JH, Sun M, Zhai MG (2005) Sm-Nd and SHRIMP U-Pb zircon geochronology of high-pressure granulites in the Sanggan area, North China Craton: timing of Paleoproterozoic continental collision. J Asian Earth Sci 24:629–642
Guo JH, Zhao GC, Chen Y, Peng P, Windley BF, Sun M (2008) Highly silica- undersaturated sapphirine granulites from the Daqingshan area of the Western Block, North China Craton: Palaeoproterozoic UHT Metamorphism and Tectonic Implications. Gondwana 13, September 2008, China, pp. 63–64 (program & abstracts)
He GP, Ye HW (1998) Two types of early proterozoic metamorphism in the Eastern Liaoning and Southern Jilin provinces and their tectonic implications. Acta Petrologica Sinica 14:152–162 (in Chinese with English abstract)
He GP, Lu LZ, Ye HW, Jin SQ, Ye TS (1992) Metamorphic evolution of early precambrian rocks in the eastern Hebei and Inner Mongolia regions. Jilin University Press, Changchun
He YH, Zhao GC, Sun M, Wilde SA (2008) Geochemistry, isotope systematics and petrogenesis of the volcanic rocks in the Zhongtiao Mountain: an alternative interpretation for the evolution of the southern margin of the North China Craton. Lithos 102:157–178
Hoffman FP (1991) Did breakout of Laurentia turn Gondwana inside-out? Science 252:1409–1411
Howell DG (1995) Principles of Terranes analysis, second edition. Chapman and Hall, London, pp 232
Hu NG (1994) Evolution of Helanshan complex. Xi'an Atlas Press, Xi'an
Huang JQ (1977) The basic outline of China tectonics. Acta Geol Sin 52:117–135
Huang X, Bai Z, DePaolo DJ (1986) Sm-Nd isotope study of early Archean rocks, Qianan, Hebei Province, China. Geochim Cosmochim Acta 50:625–631
Jahn BM, Auvray B, Cornichet J, Bai YD, Shen QH, Liu DY (1987) 3.5 Ga old amphibolites from eastern Hebei Province, China: field occurrence, petrography, Sm–Nd isochron age and REE geochemistry. Precambr Res 34:311–346
Kröner A, Compston W, Zhang GW, Guo AL, Todt W (1988) Ages and tectonic setting of late Archean greenstone–gneiss terrain in Henan Province, China, as revealed by single-grain zircon dating. Geology 16:211–215
Kröner A, Cui WY, Wang SQ, Wang CQ, Nemchin AA (1998) Single zircon ages from high-grade rocks of the Jianping Complex, Liaoning Province, NE China. J Asian Earth Sci 16:519–532
Kröner A, Wilde SA, Li JH, Wang KY (2005a) Age and evolution of a late Archaean to early Palaeozoic upper to lower crustal section in the Wutaishan/Hengshan/Fuping terrain of northern China. J Asian Earth Sci 24:577–595
Kröner A, Wilde SA, O'Brien PJ, Li JH, Passchier CW, Walte NP, Liu DY (2005b) Field relationships, geochemistry, zircon ages and evolution of a late Archaean to Palaeoproterozoic lower crustal section in the Hengshan terrain of northern China. Acta Geol Sin 79:605–629
Kröner A, Wilde SA, Zhao GC, O'Brien PJ, Sun M, Liu DY, Wan YS, Liu SW, Guo JH (2006) Zircon geochronology and metamorphic evolution of mafic dykes in the Hengshan complex of northern China: evidence for late Palaeoproterozoic extension and subsequent high-pressure metamorphism in the North China Craton. Precambr Res 146:45–67
Kusky TM (2011) Geophysical and geological tests of tectonic models of the North China Craton. Gondwana Res 20:26–35
Kusky TM, Li JH (2003) Paleoproterozoic tectonic evolution of the North China Craton. J Asian Earth Sci 22:383–397
Kusky TM, Li ZH, Glass A, Huang HA (2004) Archean ophiolites and ophiolite fragments of the North China Craton. In: Kusky TM (ed) Precambrian ophiolites and related rocks: developments in precambrian geology. Elsevier, Amsterdam, pp. 223–274
Kusky TM, Li JH (2008) Note on the paper by G.C. Zhao, S. A. Wilde, S.Z. Li, M. Sun, M. L. Grant and X.P. Li, 2007, "U–Pb zircon age constraints on the Dongwanzi ultramafic–mafic body, North China, confirm it is not an Archean ophiolite". Earth Planet Sci Lett 273:227–230
Kusky TM, Li JH, Tucker RD (2001) The Archean Dongwanzi ophiolite complex, North China Craton: 2.505-billion-year-old oceanic crust and mantle. Science 292:1142–1145
Kusky TM, Zhi XC, Li JH, Xia QX, Raharimahefa T, Huang XN (2007a) Chondritic osmium isotopic composition of Archean ophiolitic mantle, North China craton. Gondwana Res 12:67–76
Kusky TM, Li JH, Santosh M (2007b) The Paleoproterozoic North Hebei Orogen: North China craton's collisional suture with the Columbia supercontinent. Gondwana Res 12:4–28

Li JH, Kusky TM (2007) A late Archean foreland fold and thrust belt in the North China Craton: implications for early collisional tectonics. In: Zhai MG, Xiao WJ, Kusky TM, Santosh M (eds) Tectonic evolution of China and adjacent crustal fragments. Gondwana Research 12:47–66

Li SZ, Zhao GC (2007) SHRIMP U–Pb zircon geochronology of the Liaoji granitoids: constraints on the evolution of the Paleoproterozoic Jiao-Liao-Ji belt in the Eastern Block of the North China Craton. Precambr Res 158:1–16

Li X, Zhang L, Powell CMc (1996) Positions of the East Asian cratons in the Neoproterozoic supercontinent Rodinia. Aust J Earth Sci 43:593–604

Li JH, Qian XL, Zhai MG (1997) The tectonic division of North China granulite facies belt and its early Precambrian tectonic evolution. Scientia Geologica Sinica 32:254–266

Li JH, Kröner A, Qian XL, O'Brien P (2000) Tectonic evolution of an early Precambrian high-pressure granulite belt in the North China Craton. Acta Geol Sin 74:246–258

Li JH, Kusky TM, Huang XN (2002) Archean podiform chromitites and mantle tectonites in ophiolitic mélange, North China Craton: a record of early oceanic mantle processes. GSAToday 12:4–11

Li SZ, Zhao GC, Sun M, Han ZZ, Hao DF, Luo Y, Xia XP (2005) Deformation history of the Paleoproterozoic Liaohe Group in the Eastern Block of the North China Craton. J Asian Earth Sci 24:659–674

Li SZ, Zhao GC, Sun M, Han ZZ, Zhao GT, Hao DF (2006) Are the South and North Liaohe groups of North China Craton different exotic terranes? Nd isotope constraints. Gondwana Res 9:198–208

Li SZ, Zhao GC, Wilde SA, Zhang J, Sun M, Zhang GW, Dai LM (2010) Deformation history of the Hengshan–Wutai–Fuping complexes: implications for the evolution of the Trans-North China Orogen. Gondwana Res 18:611–631

Liu DY, Nutman AP, Compston W, Wu JS, Shen QH (1992) Remnants of 3800 crust in the Chinese Part of the Sino-Korean craton. Geology 20:339–342

Liu SW, Pan PM, Xie QL, Zhang J, Li QG (2004) Archean geodynamics in the central zone, North China Craton: constraints from geochemistry of two contrasting series of granitoids in the Fuping and Wutai complexes. Precambr Res 130:229–249

Liu SW, Zhao GC, Wilde SA, Shu GM, Sun M, Li QG, Tian W, Zhang J (2006) Th-U-Pb monazite geochronology of the Lüliang and Wutai Complexes: constraints on the tectonothermal evolution of the Trans-North China Orogen. Precambr Res 148:205–225

Liu DY, Wan YS, Wu JS, Wilde SA, Zhou HY, Dong CY, Yin XY (2007) Eoarchean rocks and zircons in the North China Craton. In: van Kranendonk M, Smithies RH, Bennett V (eds) Earth's oldest rocks. Elsevier Series 'Developments in Precambrian Geology' 15:251–273.

Liu DY, Wilde SA, Wan YS, Wu JS, Zhou HY, Dong CY, Yin XY (2008) New U-Pb and Hf isotopic data confirm Anshan as the oldest preserved part of the North China Craton. Am J Sci 308:200–231

Liu CH, Zhao GC, Sun M, Zhang J, He YH, Yin CQ, Wu FY, Yang JH (2011a) U-Pb and Hf isotopic study of detrital zircons from the Hutuo group in the Trans-North China Orogen and tectonic implications. Gondwana Res 20:106–121

Liu CH, Zhao GC, Liu FL, Sun M, Zhang J, Yin CQ (2011b) Zircons U-Pb and Lu-Hf isotopic and whole-rock geochemical constraints on the Gantaohe Group in the Zanhuang complex: implications for the tectonic evolution of the Trans-North China Orogen. Lithos 146–147:80–92

Lu XP, Wu FY, Guo JH, Wilde SA, Yang JH, Liu XM, Zhang XO (2006) Zircon U–Pb geochronological constraints on the Paleoproterozoic crustal evolution of the Eastern block in the North China Craton. Precambr Res 146:138–164

Luo Y, Sun M, Zhao GC, Li SZ, Xu P, Ye K, Xia XP (2004) LAICP- MS U–Pb zircon ages of the Liaohe Group in the Eastern Block of the North China Craton: constraints on the evolution of the Jiao-Liao-Ji Belt. Precambr Res 134:349–371

Luo Y, Sun M, Zhao GC, Li SZ, Ayers JC, Xia XP, Zhang JH (2008) A comparison of U–Pb and Hf isotopic compositions of detrital zircons from the North and South Liaohe Groups: Constraints on the evolution of the Jiao-Liao-Ji Belt, North China Craton. Precambr Res 163:279–306

Ma XY, Wu ZW (1981) Early tectonic evolution of China. Precambr Res 14:185–202

Ma XY, Bai J, Shuo ST, Lao QY, Zhang JS (1987) The early Precambrian tectonic framework of China and research methods. Geological Publishing Press, Beijing

McKenzie D, Priestley K (2008) The influence of lithospheric thickness variations on continental evolution. Lithos 102:1–11

McMenamin MAS, McMenamin DLS (1990) The emergence of animals: the Cambrian breakthrough. Columbia University Press, New York, pp 217

Menzies MA, Fan WM, Zhang M (1993) Palaeozoic and Cenozoic lithoprobe and the loss of >120km of Archean lithosphere, Sino-Korean craton, China. In: Prichard HM, Alabaster T, Harris NBW, Neary CR (eds) Magmatic processes and plate tectonics. Geological Society London, Special Publication 76:71–81

Metcalfe I (1996) Gondwanaland dispersion, Asian accretion and evolution of eastern Tethys. Aust J Earth Sci 43:605–623

O'Brien PJ, Walte N, Li JH (2005) The petrology of two distinct granulite types in the Hengshan Mts, China, and tectonic implications. J Asian Earth Sci 24:615–627

O'Reilly SY, Griffin WL, Poudjom Djomani YH, Morgan P (2001) Are lithospheres forever? Tracking changes in subcontinental lithospheric mantle through time. GSA Today 11:4–10

Peng P, Zhai M-G, Zhang H-F, Guo J-H (2005) Geochronological constraints on the Paleoproterozoic evolution of the North China craton: SHRIMP zircon ages

of different types of mafic dikes. International Geology Review 47:492–508

Peng P, Zhai MG, Guo JH, Kusky T, Zhao TP (2007) Nature of mantle source contributions and crystal differentiation in the petrogenesis of the 1.78 Ga mafic dykes in the central North China craton. Gondwana Res 12:29–46

Peng P, Zhai MG, Ernst RE, Guo JH, Liu F, Hu B (2008) The 1.78 Ga large igneous province in the North China craton: the Xiong'er volcanic province and the North China dyke swarm. Lithos 101:260–280

Peng P, Zhai M-G, Guo J-H (2006) 1.80–1.75 Ga mafic dyke swarms in the central North China craton: implications for a plume-related break-up event. In: Hanski E, Mertanen S, Ramö T, Vuollo J (eds) Dyke Swarms—time markers of crustal evolution. A.A. Balkema Publishers

Polat A, Kusky TM, Li JH, Fryer B, Kerrich R, Patrick K (2005) Geochemistry of Neoarchean (ca. 2.55–2.50 Ga) volcanic and ophiolitic rocks in the Wutaishan Greenstone Belt, Central Orogenic Belt, North China Craton: implications for geodynamic setting and continental growth. Geol Soc Am Bull 117:1387–1399

Polat A, Herzberg C, Munker C, Rodgers R, Kusky T, Li JH, Fryer B, Delany J (2006) Geochemical and petrological evidence for a suprasubduction zone origin of Neoarchean (ca. 2.5 Ga) peridotites, central orogenic belt, North China craton. Bulletin of the Geological Society of America 118:771–784

Qian XL (1997) Tectonic correlations of the Precambrian evolution of the North China Craton with the baltic shield. In: Qian XL, You ZD, Halls HC (eds) Precambrian geology and metamorphic petrology. Utrcht, pp 43–58

Qiao GS, Wang KY, Guo QF, Zhang GC (1987) Sm–Nd isotopic dating of the Paleoarchean rocks in Eastern Hebei, China. Scientia Geologica Sinica 22:158–165

Rivers T, Corrigan D (2000) Convergent margin on southeastern Laurentia during the Mesoproterozoic: tectonic implications. Can J Earth Sci 37:359–383

Rudnick RL, Gao S (2003) Composition of the continental crust. In: Rudnick RL (ed) Treatise on geochemistry 3. The crust, Elsevier, pp 1–64

Santosh M, Sajeev K, Li JH (2006) Extreme crustal metamorphism during Columbia supercontinent assembly: Evidence from North China Craton. Gondwana Res 10:256–266

Santosh M, Wilde SA, Li JH (2007) Timing of Paleoproterozoic ultrahigh-temperature metamorphism in the North China Craton: evidence from SHRIMP U-Pb zircon geochronology. Precambr Res 159:178–196

Shen QH, Qian XL (1995) Archean rock assemblages, episodes and tectonic evolution of China. Acta Geoscientia Sinica 2:113–120

Shen QH, Xu HF, Zhang ZQ, Gao JF, Wu JS, Ji CL (1992) Early Precambrian granulites in China. Geological Publishing House, Beijing

Song B, Nutman AP, Liu DY, Wu JS (1996) 3800 to 2500 Ma crustal evolution in Anshan area of Liaoning Province, Northeastern China. Precambr Res 78:79–94

Sun M, Armstrong RL, Lambert RStJ (1992) Petrochemistry and Sr, Pb and Nd isotopic geochemistry of early Precambrian rocks, Wutaishan and Taihangshan areas, China. Precambr Res 56:1–31

Tam PY, Zhao GC, Zhou XW, Sun M, Guo JH, Li SZ, Yin CQ, Wu ML, He YH (2012) Metamorphic P–T path and implications of high-pressure pelitic granulites from the Jiaobei massif in the Jiao-Liao-Ji Belt, North China Craton. Gondwana Res 22:104–117

Thompson AB, England PC (1984) Pressure–temperature–time paths of regional metamorphism, II. Their influences and interpretation using mineral assemblages in metamorphic rocks. J of Petrology 25:929–55

Trap P, Faure M, Lin W, Monié P (2007) Late Paleoproterozoic (1900–1800 Ma) nappe stacking and polyphase deformation in the Hengshan-Wutaishan area: implications for the understanding of the Trans-North-China Belt. North China Craton. Precambr Res 156:85–106

Trap P, Faure M, Lin W, Bruguier O, Monie P (2008) Contrasted tectonic styles for the Paleoproterozoic evolution of the North China Craton. Evidence for a ~2.1 Ga thermal and tectonic event in the Fuping Massif. J Struct Geol 30:1109–1125

Trap P, Faure M, Lin W, Monie P, Meffre S, Melleton J (2009a) The Zanhuang Massif, the second and eastern suture zone of the Paleoproterozoic Trans-North China Orogen. Precambr Res 172:80–98

Trap P, Faure M, Lin W, Monie P, Meffre S (2009b) The Lüliang Massif: a key area for the understanding of the Palaeoproterozoic. In: Evans D, Reddy S, Collins A. (eds). Palaeoproterozoic supercontinents and global evolution. Geological Society of London Special Publication 323:99–125

Wan YS, Geng YS, Shen QH, Zhang RX (2000) Khondalite series-geochronology and geochemistry of the Jiehekou Group in the Lüliang area, Shanxi Province. Acta Petrologica Sinica 16:49–58

Wan YS, Liu DY, Song B, Wu JS, Yang CH, Zhang ZQ, Geng YS (2005) Gechemical and Nd isotopic compositions of 3.8 Ga meta-quartz dioritic and tronhjemitic rocks from the Anshan area and their geological significance. J Asian Earth Sci 24:563–575

Wan YS, Wilde SA, Liu DY, Yang CX, Song B, Yin XY (2006a) Further evidence for ~1.85 Ga metamorphism in the Central Zone of the North China Craton: SHRIMP U–Pb dating of zircon from metamorphic rocks in the Lushan area. Henan Province. Gondwana Res 9:189–197

Wan YS, Song B, Liu DY, Wilde SA, Wu JS, Shi YR, Yin XY, Zhou HY (2006b) SHRIMP U–Pb zircon geochronology of Palaeoproterozoic metasedimentary rocks in the North China Craton: evidence for a major late Palaeoproterozoic tectonothermal event. Precambr Res 149:249–271

Wan YS, Liu DY, Wang SJ, Dong CY, Yang EX, Wang W, Zhou HY, Du LL, Yin XY, Xie HQ, Ma MZ (2010) Juvenile magmatism and crustal recycling at the end of Neoarchean in western Shandong province, north China Craton: evidence from SHRIMP zircon dating. Am J Sci 310:1503–1552

Wan YS, Liu DY, Wang W, Song TR, Kröner A, Dong CY, Zhou HY, Yin XY (2011) Provenance of Meso- to Neoproterozoic cover sediments at the Ming Tombs, Beijing, North China Craton: an integrated study of U–Pb dating and Hf isotopic measurement of detrital zircons and whole-rock geochemistry. Gondwana Res 20:219–242

Wan YS, Wang SJ, Liu DY, Wang W, Kröner A, Dong CY, Yang EX, Zhou HY, Hangqian X, Ma MZ (2012) Redefinition of depositional ages of Neoarchean supracrustal rocks in western Shandong Province, China: SHRIMP U–Pb zircon dating. Gondwana Res 21:768–784

Wang ZH (2009) Tectonic evolution of the Hengshan–Wutai–Fuping complexes and its implication for the Trans-North China Orogen. Precambr Res 170:73–87

Wang J, Lu SN, Li HM, Wang RZ, Sun YF, Li HK, Li SQ (1995) Geochronological framework of metamorphic rocks in the middle part of Inner Mongolia. Bull. Tianjin Institute of Geology and Mineral Resources 29:1–76

Wang KY, Li JL, Hao J, Li JH, Zhou SP (1996) The Wutaishan Orogenic belt within the Shanxi Province, northern China: a record of late Archaean collisional tectonics. Precambr Res 78:95–103

Wang YJ, Fan WM, Zhang Y, Guo F (2003) Structural evolution and $^{40}Ar/^{39}Ar$ dating of the Zanhuang metamorphic domain in the North China Craton: constraints on Paleoproterozoic tectonothermal overprinting. Precambr Res 122:159–182

Wang ZH, Wilde SA, Wang KY (2004) A MORB-arc basalt-adakite association in the 2.5 Ga Wutai greenstone belt: late Archean magmatism and crustal growth in the North China Craton. Precambr Res 131:323–343

Wang ZH, Wilde SA, Wan JL (2010) Tectonic setting and significance of 2.3–2.1 Ga magmatic events in the Trans-North China Orogen: New constraints from the Yanmenguan mafic–ultramafic intrusion in the Hengshan–Wutai–Fuping area. Precambr Res 178:27–42

Wilde SA, Zhao GC (2005) Archean to Paleoproterozoic evolution of the North China Craton. J Asian Earth Sci 24:519–522

Wilde SA, Cawood PA, Wang K (1997) The relationship and timing of granitoid evolution with respect to felsic volcanism in the Wutai Complex, North China Craton. Proceedings of the 30th International Geological Congress: Precambrian Geology and Metamorphic Petrology 17:75–87. VSP Scientific Publisher, Netherlands

Wilde SA, Zhao GC, Sun M (2002) Development of the North China Craton during the Late Archaean and its final amalgamation at 1.8 Ga; some speculations on its position within a global Palaeoproterozoic Supercontinent. Gondwana Res 5:85–94

Wilde SA, Zhou XH, Nemchin AA, Sun M (2003) Mesozoic Crust-Mantle interaction beneath the North China Craton: a consequence of the dispersal of Gondwanaland and accretion of Asia. Geology 31:817–820

Wilde SA, Cawood PA, Wang KY, Nemchin A, Zhao GC (2004a) Determining Precambrian crustal evolution in China: a case-study from Wutaishan, Shanxi Province, demonstrating the application of precise SHRIMP U-Pb geochronology. In: Malpas J, Fletcher CJN, Ali JR, Aitchison JC (eds), Aspects of the tectonic evolution of China. Special Publication Geological Society of London 226:5–25

Wilde SA, Zhao GC, Wang KY, Sun M (2004b) First precise SHRIMP U-Pb zircon ages for the Hutou Group, Wutaishan: further evidence for the Palaeoproterozoic amalgamation of the North China Craton. Chin Sci Bull 49:83–90

Wilde SA, Cawood PA, Wang KY, Nemchin AA (2005) Granitoid evolution in the late Archean Wutai complex, North China Craton. J Asian Earth Sci 24:597–613

Wilde SA, Valley JW, Kita NT, Cavosie AJ, Liu DY (2008) SHRIMP U-Pb and CAMECA 1280 oxygen isotope results from ancient detrital zircons in the Caozhuang quartzite, Eastern Hebei, North China Craton: evidence for crustal recycling 3.8 Ga ago. Am J Sci 308:185–199

Windley BF, Maruyama S, Xiao WJ (2010) Thinning of sub-continental lithospheric mantle under eastern China: the role of water and multiple subduction. Am J Sci 310:1250–1293

Wu CH, Li HM (1998) The ages of zircons and rutiles from khondalite in the Huangtuyao area Inner Mongolia. Geology Review 44:618–626 (in Chinese)

Wu CH, Zhong CT, 1998. The Paleoproterozoic SW–NE collision model for the central North China Craton. Progress in Precambrian Research 21:28–50 (in Chinese)

Wu CH, Li SX, Gao JF (1986) Archean and Paleoproterozoic metamorphic regions in the North China Craton. In: Dong SB (ed) Metamorphism and crustal evolution of China. Geological Publishing House, Beijing, pp 53–89

Wu JS, Geng YS, Shen QH, Liu DY, Li ZL, Zhao DM (1991) The early Precambrian significant geological events in the North China Craton. Geological Publishing House, Beijing

Wu JS, Geng YS, Shen QH, Wan YS, Liu DY, Song B (1998) Archean geological characteristics and tectonic evolution of China-Korea Paleo-Continent. Geological Publishing House, Beijing

Wu CH, Li HM, Zhong CT, Zhuo YC (2000) TIMS U–Pb single zircon ages for the orthogneisses and paragneisses of Fuping Complex. Progress in Precambr Res 23:130–139

Wu FY, Walker RJ, Ren XW, Sun DY, Zhou XH (2003) Osmium isotopic constraints on the age of lithospheric mantle beneath northeastern China. Chem Geol 197:107–129

Wu FY, Zhao GC, Wilde SA, Sun DY (2005a) Nd isotopic constraints on crustal formation in the North China Craton. J Asian Earth Sci 24:523–545

Wu FY, Lin JQ, Wilde SA, Zhang XO, Yang JH (2005b) Nature and significance of the early cretaceous giant igneous event in eastern China. Earth Planet Sci Lett 233:103–119

Wu FY, Han RH, Yang JH, Wilde SA, Zhai MG (2007a) Initial constraints on granitic magmatism in North Korea using U-Pb zircon geochronology. Chem Geol 238:232–248

Wu FY, Yang JH, Wilde SA, Liu XM, Guo JH, Zhai MG (2007b) Detrital zircon U-Pb and Hf isotopic constraints on the crustal evolution of Northern Korea. Precambr Res 159:155–177

Wu FY, Zhao GC, Sun DY, Wilde SA, Zhang GL (2007c) The Hulan group: its role in the evolution of the Central Asian Orogenic Belt of NE China. J Asian Earth Sci 30:542–556

Wu FY, Zhang YB, Yang JH, Xie LW, Yang YH (2008) Zircon U–Pb and Hf isotopic constraints on the Early Archean crustal evolution in Anshan of the North China Craton. Precambr Res 167:339–362

Xiao LL, Wu CM, Zhao GC, Guo JH, Ren LD (2011) Metamorphic P–T paths of the Zanhuang amphibolitic gneisses and metapelitic gneisses: constraints on the tectonic evolution of the Paleoproterozoic Trans-North China Orogen. Int J Earth Sci (Geol Rundsch) 100:717–739

Xu H, Dong Y (1992) Granite-Greenstone Belt in West Shandong. Geological Press, Beijing

Yang ZS, Li SG, Yu BX, Gao DH, Gao CG (1988) Structural deformation and mineralization in the early Proterozoic Liaojitite suite, eastern Liaoning province, China. Precambr Res 39:31–38

Yang JH, Wu FY, Wilde SA (2003) A review of the geodynamic setting of large-scale late Mesozoic mineralization in the North China Craton: an association with lithospheric thinning. Ore Geology Reviews 23:125–152

Yang JH, Wu FY, Zhang YB, Zhang Q, Wilde SA (2004a) Identification of Mesoproterozoic zircons in a Triassic dolerite from the Liaodong Peninsula, Northeast China. Chin Sci Bull 49:1958–1962

Yang JH, Wu FY, Chung SL, Wilde SA, Chu MF (2004b) Multiple sources for the origin of granites: geochemical and Nd/Sr-isotopic evidence from the Gudaoling granite and its mafic enclaves, northeast China. Geochim Cosmochim Acta 68:4469–4483

Yang JH, Wu FY, Chung SL, Lo CH, Wilde SA, Zhao Y, Liu W, Zhai MG (2007a) Rapid exhumation and cooling of the Liaonan metamorphic core complex inferred from 40Ar/39Ar thermochronology: implications for late Mesozoic extension in the North China Craton. Bulletin Geological Society of America 119:1405–1414

Yang JH, Sun JF, Chen FK, Wilde SA, Wu FY, Liu XM (2007b) Sources and petrogenesis of Late Triassic dolerite dykes in the Liaodong Peninsula: implications for post-collisional lithospheric thinning of the Eastern North China Craton. J of Petrology 48:1973–1997

Yang JH, Wu FY, Wilde SA, Liu XM (2007c) Sources and petrogenesis of Late Triassic granitoids in the Liaodong Peninsula and their relationship to post-collisional lithospheric thinning of the southeast North China Craton. Chem Geol 242:155–175

Yang JH, Wu FY, Wilde SA, Belousova E, Griffin WL (2008) Mesozoic decratonization of the North China block. Geology 36:467–470

Yin A, Nie S (1996) Phanerozoic palinspastic reconstruction of China and its neighboring regions. In: Yin A, Harrison TM (eds) The tectonic evolution of Asia. Cambridge Univ. Press, NewYork, pp 285–442

Yin CQ, Zhao GC, Sun M, Xia XP, Wei CJ, Leung WH (2009) LA-ICP-MS U–Pb zircon ages of the Qianlishan Complex: constrains on the evolution of the Khondalite Belt in the Western Block of the North China Craton. Precambr Res 174:78–94

Yu JH, Wang DZ, Wang XY (1997) Ages of the Lüliang Group and its main metamorphism in the Lüliang Mountains, Shanxi: evidence from single grain zircon U–Pb ages. Geological Review 43:403–408

Yuan XC (1996) Velocity structure of the Qinling lithosphere and mushroom cloud model: Science in China, Series D: Earth Sciences 39:235–244

Zhai MG, Liu WJ (2003) Paleoproterozoic tectonic history of the north China Craton: a review. Precambr Res 122:183–199

Zhai MG, Santosh M (2011) The early Precambrian odyssey of North China Craton: a synoptic overview. Gondwana Res 20:6–25

Zhai MG, Bian AG, Zhao TP (2000) The amalgamation of the supercontinent of North China Craton at the end of Neo-Archaean and its breakup during late Palaeoproterozoic and Mesoproterozoic. Science in China (Series D) 43:219–232

Zhai MG, Shao JA, Hao J, Peng P (2003) Geological signature and possible position of the North China block in the supercontinent Rodinia. Gondwana Res 6:171–183

Zhai MG, Guo JH, Liu WJ (2005) Neoarchean to Paleoproterozoic continental evolution and tectonic history of the North China Craton: a review. J Asian Earth Sci 24:547–561

Zhang FQ, Liu JZ, Ouyang ZY (1998) Tectonic framework of greenstones in the basement of the North China Craton. Acta Geophysica Sinica 41:99–107

Zhang Q, Wang Y, Zhou GQ, Qian Q, Robinson PT (2004) Ophiolites in China: their distribution, ages and tectonic settings. In: Dilek Y, Robinson PT (eds) Ophiolites in Earth History. Geological Society of London Special Publication 218:541–566

Zhang J, Zhao GC, Li SZ, Sun M, Liu SW, Wilde SA, Kröner A, Yin CQ (2007) Deformation history of the Hengshan Complex: implications for the tectonic evolution of the Trans-North China Orogen. J Struct Geol 29:933–949

Zhang J, Zhao GC, Li SZ, Sun M, Liu SW, Yin CQ (2009) Deformational history of the Fuping Complex and new U-Th-Pb geochronological constraints: implications for the tectonic evolution of the Trans-North China Orogen. J Struct Geol 31:177–193

Zhang J, Zhao GC, Li SZ, Sun M, Chan LS, Shen WL, Liu SW (in press) Structural pattern of the Wutai Complex and its constraints on the tectonic framework of the Trans-North China Orogen. Precambrian Res doi:10.1016/j.precamres.2011.08.009

Zhang HF, Yang YH, Santosh M, Zhao XM, Ying JF, Xiao Y (2012) Evolution of the Archean and Paleoproterozoic lower crust beneath the Trans-North China Orogen and the Western Block of the North China Craton. Gondwana Res 22:73–85

Zhao ZP (1993) Evolution of Precambrian crust of Sino-Korean Platform. Scientific Press, Beijing

Zhao XX, Coe RS, Gilder SA, Frost GM (1996) Palaeomagnetic constraints on the Palaeogeography of China: implications for Gondwanaland. Aust J Earth Sci 43:643–672

Zhao GC, Wilde SA, Cawood PA, Lu LZ (1998) Thermal evolution of the Archaean basement rocks from the eastern part of the North China Craton and its bearing on tectonic setting. Int Geol Review 40:706–721

Zhao GC, Wilde SA, Cawood PA, Lu LZ (1999a) Thermal evolution of two types of mafic granulites from the North China craton: implications for both mantle plume and collisional tectonics. Geol Mag 136:223–240

Zhao GC, Wilde SA, Cawood PA, Lu LZ (1999b) Tectonothermal history of the basement rocks in the western zone of the North China Craton and its tectonic implications. Tectonophysics 310:37–53

Zhao GC, Cawood PA, Wilde SA, Lu LZ (2000a) Metamorphism of basement rocks in the Central Zone of the North China Craton: implications for Paleoproterozoic tectonic evolution. Precambr Res 103:55–88

Zhao GC, Wilde SA, Cawood PA, Lu LZ (2000b) Petrology and P–T path of the Fuping mafic granulites: Implications for tectonic evolution of the central zone of the North China Craton. J Metamorph Geol 18:375–391

Zhao GC, Wilde SA, Cawood PA, Sun M (2001a) Archean blocks and their boundaries in the North China Craton: lithological, geochemical, structural and P-T path constraints and tectonic evolution. Precambr Res 107:45–73

Zhao GC, Cawood PA, Wilde SA, Lu LZ (2001b) High-pressure granulites (retrograded eclogites) from the Hengshan Complex, North China Craton: petrology and tectonic implications. J of Petrology 42:1141–1170

Zhao GC, Wilde SA, Cawood PA, Sun M (2002a) SHRIMP U-Pb zircon ages of the Fuping Complex: implications for accretion and assembly of the North China Craton. Am J Sci 302:191–226

Zhao GC, Sun M, Wilde SA (2002b) Reconstruction of a pre-Rodinia supercontinent: New advances and perspectives. Chin Sci Bull 47:1585–1588

Zhao GC, Sun M, Wilde SA, Li SZ (2003). Assembly, accretion and break-up of the Palaeo-Mesoproterozoic supercontinent Columbia and its records in the North China Craton. In: Kehelpannala KVW (ed) The role of Sri Lanka in Rodinia and Gondwana assembly and breakup. Geological Survey & Mines Bureau, Sri Lanka, pp 53–55

Zhao GC, Sun M, Wilde SA, Li SH (2004) A Paleo-Mesoproterozoic supercontinent: assembly, growth and breakup. Earth-Sci Rev 67:91–123

Zhao GC, Sun M, Wilde SA, Li SZ (2005) Late Archean to Paleoproterozoic evolution of the North China Craton: key issues revisited. Precambr Res 136:177–202

Zhao GC, Cao L, Sun M, Wilde SA, Choe WJ, Li SZ (2006a) Implications based on the first SHRIMP U-Pb dating on Precambrian granitoid rocks in North Korea. Earth and Planetary Sci Lett 251:365–379

Zhao GC, Sun M, Wilde SA, Li SZ, Liu SW, Zhang J (2006b) Composite nature of the North China Granulite-Facies Belt: tectonothermal and geochronological constraints. Gondwana Res 9:337–348

Zhao GC, Sun M, Wilde SA, Li SZ, Zhang J (2006c) Some key issues in reconstructions of Proterozoic supercontinents. J of Asian Earth Sci 28:3–19

Zhao GC, Wilde SA, Li SZ, Sun M, Grant ML, Li XP (2007) U–Pb zircon age constraints on the Dongwanzi ultramafic–mafic body, North China, confirm it is not an Archean ophiolite. Earth Planet Sci Lett 255:85–93

Zhao GC, Wilde SA, Sun M, Guo JH, Kröner A, Li SZ, Li XP, Zhang J (2008a) SHRIMP U-Pb zircon geochronology of the Huai'an Complex: constraints on the Late Archean to Paleoproterozoic magmatic and metamorphic events in the Trans-North China Orogen. Am J Sci 308:270–303

Zhao GC, Wilde SA, Sun M, Li SZ, Li XP, Zhang J (2008b) SHRIMP U–Pb zircon ages of granitoid rocks in the Lüliang complex: implications for the accretion and evolution of the Trans-North China Orogen. Precambr Res 160:213–226

Zhao GC, Wilde SA, Li SZ, Sun M, Grant ML, Li XP (2008c) Response to note on "U–Pb zircon age constraints on the Dongwanzi ultramafic–mafic body, North China, confirm it is not an Archean ophiolite" by Kusky and Li. Earth Planet Sci Lett 273:231–234

Zhao GC (2009) Metamorphic evolution of major tectonic units in the basement of the North China Craton: key issues and discussion. Acta Petrol Sin 25: 1772–1792

Zhao GC, Wilde SA, Guo JH, Cawood PA, Sun M, Li XP (2010a) Single zircon grains record two Paleoproterozoic collisional events in the North China craton. Precambr Res 177:266–276

Zhao GC, Wilde SA, Zhang J (2010b) New evidence for seismic imaging for subduction during assembly of the North China craton: COMMENT. Geology 38:e206

Zhao GC, Li SZ, Zhang J, Sun M, Xia XP (2010c) A comment on "Tectonic evolution of the Hengshan–Wutai–Fuping complexes and its implication for the Trans-North China Orogen". Precambr Res 176:94–98

Zheng J, O'Reilly SY, Griffin WL, Li F, Zhang M, Pearson NJ (2001) Relict refractory mantle beneath the eastern North China block: significance for lithosphere evolution. Lithos 57:43–66

Zheng J, Griffin WL, O'Reilly SY, Lu FX, Wang CY, Zhang M, Wang FZ, Li HM (2004) 3.6 Ga lower crust in central China: New evidence on the assembly of the North China craton. Geology 32:229–232

Zheng TY, Zhao L, Zhu RX (2009) New evidence from seismic imaging for subduction during assembly of the North China craton. Geology 37:395–398

Zhou MF, Bai WJ (1992) Chromite deposit in China and their origin. Mineralia Deposita 27:192–199

How to Make a Continent: Thirty-five Years of TTG Research

7

Kent C. Condie

Abstract

After more than 35 years of TTG (tonalite-trondhjemite-granodiorite) research, we still face many questions about the origin and tectonic significance of these peculiar rocks. What we do know is that TTGs are similar in composition regardless of age, they have high La/Yb, Sr/Y, Sr and Eu/Eu*, they decrease in abundance relative to calc-alkaline granitoids at the end of the Archean, and they are not made in oceanic arcs, shallow levels of oceanic plateaus or at ocean ridges. Furthermore, oxygen isotopes in TTG zircons require interaction of TTG sources with the hydrosphere, and the existence of Hadean continental crust inferred from detrital zircon suites remains problematic. Although we now realize that TTGs require amphibole and garnet fractionation and sources that are at least 50 km deep, what we do not know are the relative roles of (1) melting versus fractional crystallization and (2) melting of slabs versus melting of thickened mafic crust. The mechanisms and rates of slab dehydration control the stability of garnet and amphibole in subduction zones. From what we know about early Archean greenstones, they are more altered than later ones, and thus they would appear to bring more water and fluid-mobile elements into subduction zones, at least by the late Archean when plate tectonics became widespread. Hotter slabs in the Archean should contribute to higher volatile release rates. This may explain the trace element changes we see in TTGs at the end of the Archean.

To make continental crust today we need to start at a continental subduction zone where we produce both calc-alkaline (CA) and TTG magmas, and combine the felsic components in a ratio of about 3 parts CA to 2 parts TTG. In contrast, to make an Archean continent, we need nearly 100 % of the TTG component, and may begin, at least before about 3 Ga, by melting the roots of oceanic plateaus.

7.1 Introduction

Since the term TTG (tonalite-trondhjemite-granodiorite) was introduced by Fred Barker (1979) as a name for the most abundant pluton-

K. C. Condie (✉)
Department of Earth and Environmental Science, New Mexico Tech, 87801, Socorro, NM, USA
e-mail: kcondie@nmt.edu

Y. Dilek, H. Furnes (eds.), *Evolution of Archean Crust and Early Life*, Modern Approaches in Solid Earth Sciences 7, DOI 10.1007/978-94-007-7615-9_7, © Springer Science+Business Media Dordrecht 2014

ic suite in the Archean, there have been an increasing number of publications aimed at better understanding these rocks and why they are so abundant in Archean crust. At one time it was thought that TTGs were limited to the Archean, but we now realize that they occur throughout the preserved geologic record and that some are still forming in young arc systems (Drummond and Defant 1990). TTGs, however, decrease in abundance after the end of the Archean.

There is an ongoing discussion as to whether TTGs are slab melts and hence should be referred to as adakites. The term "adakite" was originally proposed by Defant and Drummond (1990) for unusual volcanic rocks from Adak Island in the Aleutians first described by Kay (1978). These rocks have unusually high Sr, Mg, Ni, Cr and high La/Yb and Sr/Y ratios, and were suggested to be slab melts, with garnet in the restite (Kay 1978). Thus the name adakite became synonymous with slab melt, and high La/Yb and Sr/Y ratios were proposed to identify such rocks. It is now clear, however, that rocks that have been described as adakites in the literature encompass a range of compositions, some of which may be slab melts and many others that are not slab melts (Kamber et al. 2002; Richards and Kerrich 2007; Coldwell et al. 2011). Because of some geochemical similarities of TTGs to young "adakites", TTGs have been considered by some investigators as slab melts (Martin 1999). Trace element signatures of these rocks reflect source processes and restite mineralogy, including the presence of garnet and amphibole, but the absence of plagioclase. Because such conditions are satisfied by a variety of melting and fractional crystallization conditions found in thick mafic crust, adakites and TTGs need not be slab melts (Smithies 2000; Condie 2005; Bedard 2006; Richards and Kerrich 2007). Hence, due to the ambiguity of the term "adakite", it will not be used in this paper.

So where do TTGs form and what do they tell us about continental growth? Studies of young TTGs, especially at sites around the Pacific Basin, show that they are produced in continental margin arc systems such as the Andes and the Philippines, often but not always in association with buoyant subduction of relatively hot slabs (Drummond and Defant 1990; Petford and Atherton 1996; Kay et al. 1999; Coldwell et al. 2011). They dominate in the plutonic suites of the Archean, decreasing significantly in abundance thereafter. In this review, we will focus on six important constraints for the production of TTGs and changes in their abundance with time.

7.2 Constraints on TTG Production

7.2.1 TTGs are Similar in Composition Regardless of Age

Although in terms of a major element and rock type distribution, TTGs are highly variable (Moyen 2011), ranging from diorite to leucotrondhjemite in composition, incompatible trace element distributions are remarkably uniform as a function of both rock type and age (Fig. 7.1a; Append. 1). TTGs show enrichment in incompatible elements with a rather uniform decrease in enrichment with increasing compatibility. They all show striking negative anomalies at Nb, Ta and Ti, a feature often related to subduction, although other tectonic scenarios also may give rise to these depletions (Bedard 2006). The low concentrations of Y and heavy REE reflect the role of restitic garnet, and to a lesser extent amphibole (Rapp and Watson 1995). The same incompatible element pattern characterizes TTGs of all ages, which suggests that the same type of source and the process of TTG production have operated for the last 4 Ga. This does not, however, mean that all TTGs through time have been produced in the same tectonic setting. Average incompatible element distributions in TTGs are also similar to average upper continental crust (Fig. 7.1b; Append. 1). The main difference is that average upper crust is less depleted in heavy REE. This is controlled by the ratio of TTG to calc-alkaline (CA) components in the continental crust, which is about 40/60 assuming Ybn (primitive mantle normalized value) in TTG and CA of 1.5 and 7.0, respectively (Fig. 7.1b; Condie 1993). In contrast, average Archean upper continental crust is essentially identical to Archean TTG, reflecting a strong Archean TTG component (Figs. 7.2 and 7.3; Condie 1993, 2005).

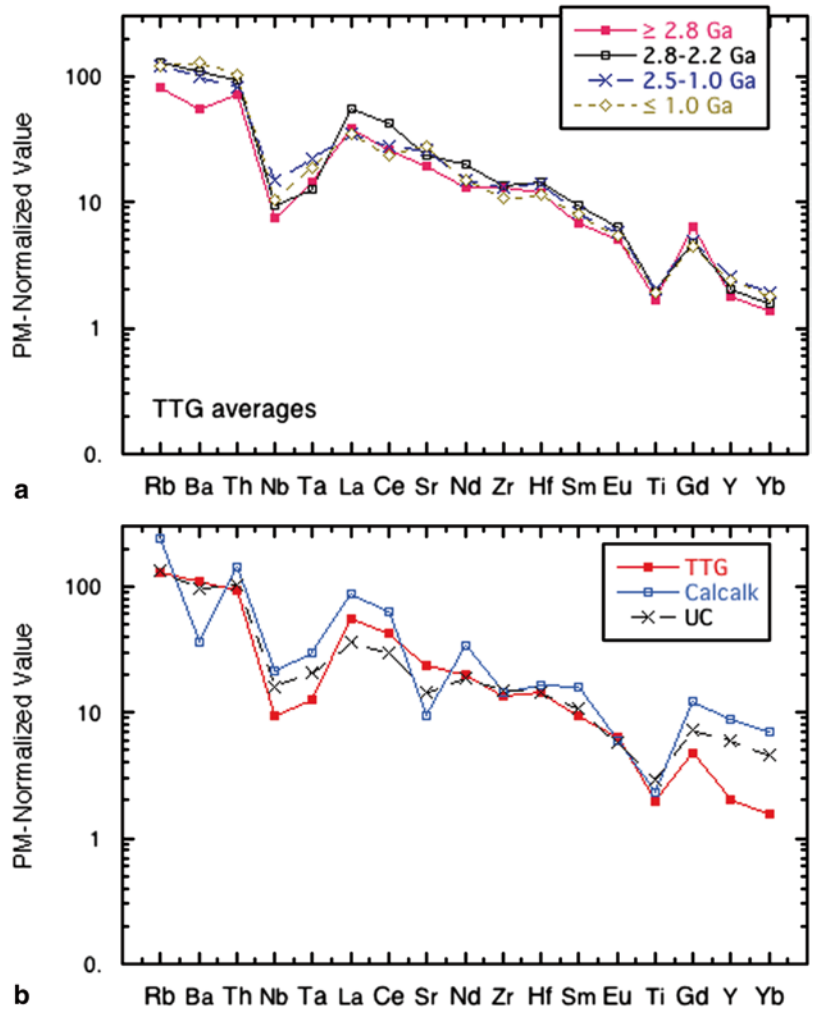

Fig. 7.1 **a** Normalized incompatible element distributions in average TTGs. Data from Condie (2005). Primitive mantle normalizing values from Sun and McDonough (1989). **b** Normalized incompatible element distributions in average late Archean TTG, average calc-alkaline granitoid (Calcalk), and average upper continental crust (UC). TTG from Condie (2005), UC from Rudnick and Gao (2004), and Archean UC from Condie (1993)

The calc-alkaline (CA) series also characterizes subduction zones, with the ratio of CA/TTG increasing with time (Condie 2008). In Archean gray gneiss terranes, there is a complete spectrum of suites from low to high-pressure sodic compositions as well as a potassic group (Moyen 2011). The low-pressure sodic suite and the potassic suite belong to the CA series, whereas the medium to high pressure sodic suites are equivalent to TTGs as used in this study. Coeval CA and TTG suites at 2.8 Ga have been described in the same granitoid complex in Karelian greenstone terrains (Samsonov et al. 2005). Although the incompatible element distribution patterns are similar in CA and TTG suites, there are three very important differences (Fig. 7.1b): (1) CA suites are not depleted in Y and heavy REE; (2) they show negative Sr and Eu anomalies (Eu anomaly masked by the Ti anomaly in Fig. 7.1b); and overall, (3) CA suites exhibit higher absolute concentrations of incompatible elements.

The bottom line is that there are five geochemical features of TTGs that must be explained by any model for their production (Fig. 7.1; Append. 1):

1. they show over-abundances in slab-derived LIL-elements (such as K, Rb, Th, and La);
2. they show striking depletions in Nb, Ta and Ti;
3. they also exhibit strong light to heavy REE fractionation;
4. they do not show depletions in Sr or Eu, which characterize the calc-alkaline suites; and
5. many TTGs, especially Archean examples, show relatively high and correlated contents of compatible elements such as Ni, Cr and Co.

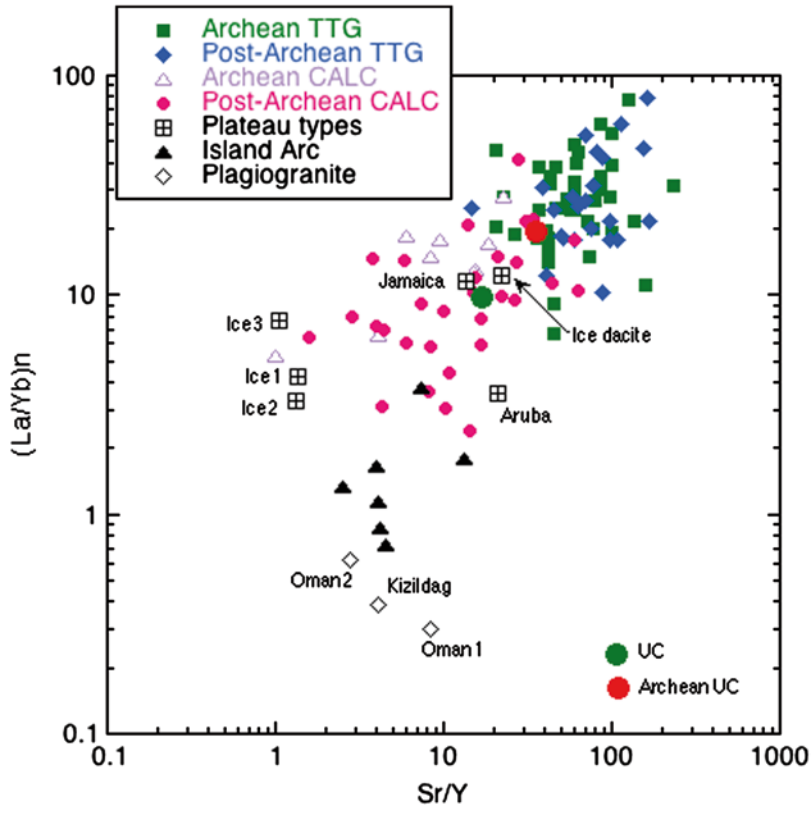

Fig. 7.2 (La/Yb)n versus Sr/Y graph comparing TTGs with other felsic rock types. Data from Condie (2005, 2008) and sources given in Fig. 7.5. (La/Yb)n is the normalized ratio relative to primitive mantle (Sun and McDonough 1989). CALC, calc-alkaline granitoids; Ice, Iceland. All plotted points are average values from different geographic locations. Other information in Fig. 7.1

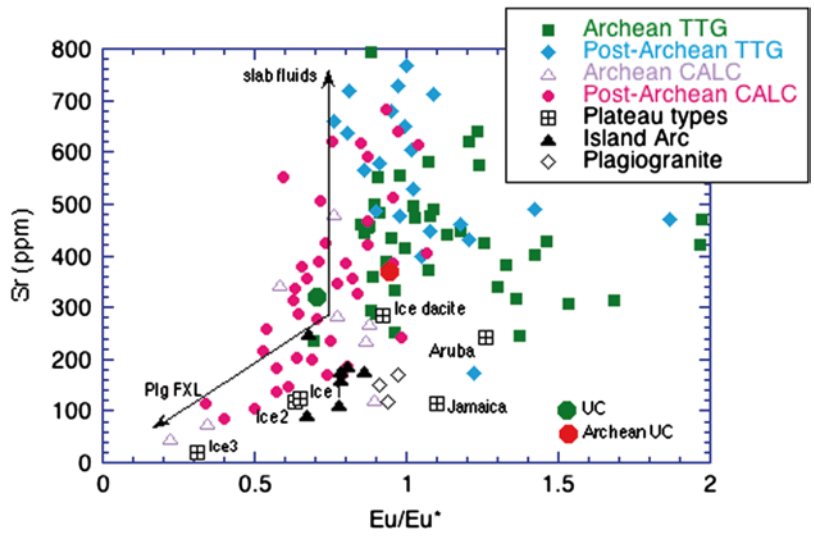

Fig. 7.3 Sr versus Eu/Eu* graph comparing TTGs with other felsic rock types. Data from Condie (2005, 2008) and sources given in Figs. 7.2 and 7.5. All plotted points are average values from different geographic locations. Eu/Eu* = Eu/(Sm x Gd)$^{1/2}$, with values normalized to primitive mantle (Sun and McDonough 1989). Plg FXL, plagioclase-dominated fractional crystallization trajectory; CALC, calc-alkaline granitoids; Ice, Iceland

7.2.2 TTGs Have High La/Yb, Sr/Y, Sr and Eu/Eu*

A great deal has been published about the strong light to heavy REE fractionation and the fractionation of Sr from Y in TTGs (Rapp et al. 1991; Martin 1999; Smithies 2000; Richards and Kerrich 2007). All models have one thing in common: a major role of amphibole and/or garnet fractionation. An important role for gar-

net, furthermore, requires source depths of 50 km or more. Basically, there are three scenarios all of which require garnet and amphibole as restitic phases: (1) melting of thickened mafic crust in the upper plate in subduction zones, (2) melting of descending slabs, or (3) fractional crystallization of wet mafic melts in which garnet and amphibole are the major fractionating phases (Kamber et al. 2002). So far, no one has come up with an unambiguous test or tests to distinguish between these three scenarios, although the behavior of compatible trace elements should be useful in identifying igneous rock suites related by fractional crystallization (Kleinhanns et al. 2003). Proponents of slab melting argue that the high Sr (≥400 ppm) and low Y (≤18 ppm) and Yb (≤1.9 ppm) are diagnostic of slab melting (Martin 1999). These geochemical features, however, can also be satisfied by dehydration melting of garnet amphibolite or eclogite in overthickened mafic crust at depths ≥50 km. Recent experimental work shows that the garnet stability field expands in the lower crust in moderately hydrous magmas (Zellmer et al. 2012).

Other experimental studies have shown that hydrous crystallization of basaltic magma with garnet, amphibole and pyroxenes as major liquidus phases rapidly depletes a TTG magma in Y and heavy REE, while enriching it in Sr and Eu due to the instability of plagioclase (Rapp et al. 1991; Rapp and Watson 1995; Muntener et al. 2001; Moyen 2011). Nb/Ta ratios in most TTGs are <16 suggesting that the mafic sources did not contain rutile (Foley et al. 2002; Condie 2005). However, Nb/Ta ratios range from 7–42 in Archean TTGs from SW Greenland indicating that some formed in the rutile stability field and some in the garnet stability field (Hofmann et al. 2011). The Nb/Ta ratio is also sensitive to the rutile/titanite ratio of the source, and this ratio is depth sensitive in the range of 30–70 km (John et al. 2011). Clearly TTG magmas must form at a range of depths, either or both, at progressively increasing pressures in thick mafic crust, or in descending slabs.

Three populations of data are apparent on a La/Yb versus Sr/Y graph for average granitoid compositions (Fig. 7.2; Append. 1): (1) TTGs, which show relatively high (La/Yb)n (generally ≥15) and Sr/Y (≥30) ratios; (2) calc-alkaline suites, which for the most part have low values of these ratios [(La/Yb)n and Sr/Y each ≤20)], and (3) oceanic arc granitoids, which have strikingly low ratios [(La/Yb)n≤5; Sr/Y≤10)] (Condie and Kroner 2012) (the low sodic and potassic suites of Moyen (2011) belong to the calc-alkaline group). These three populations cannot be related by varying degrees of melting of the same source or by fractional crystallization of the same minerals. Although all three are subduction-related, they must reflect some combination of different sources, different volatile release patterns, or/and different depths of melting. If wet fractional crystallization is the primary means by which high La/Yb and Sr/Y ratios are achieved in TTGs, it is necessary to have water saturation in primary melts in the mantle wedge. This relates to the mechanism and controls of water release during slab dehydration, neither of which is well known. Subduction zones must have diverse characteristics to support all three igneous suites, in some cases overlapping in space and time. Average upper continental crust (UC) (Rudnick and Gao 2004) plots at the upper end of the calc-alkaline group, consistent with both CA and TTG contributing to the average composition of continental crust today (Fig. 7.2). It is noteworthy that average Archean upper continental crust plots with Archean TTGs indicating the importance of the TTG component in the Archean continents.

On a Eu/Eu*versus Sr graph, TTGs define a field of relatively high Sr and variably positive Eu anomalies (Eu/Eu*≥1), indicating the absence of plagioclase in the restite (Fig. 7.3). High Sr contents reflect the dominance of slab fluids, since Sr is a fluid-mobile element. In contrast, calc-alkaline suites often exhibit low Sr and negative Eu anomalies, plotting near the plagioclase fractionation line (Plg FXL, Fig. 7.3). Some post-Archean examples, however, fall in the slab fluid region, but mostly with negative Eu anomalies, again controlled by plagioclase fractionation. In addition, there is a strong correlation of Sr and Sr/Y ratio in calc-alkaline suites showing that plagioclase

Table 7.1 Summary of the ratio of TTG to calc-alkaline (CA) granitoids with age (updated from Condie 2008)

Age (Ma)	>2800	2800–2500	2500–1000	<1000
Map TTG/CA[a]	8 (4–10)	15	0.10	0.37
By number of sites				
TTG	28	25	12	18
Calc Alk	5	2	13	26
TTG/CA	5.6	12.5	0.92	0.70
By number of samples				
TTG	386	328	138	171
Calc Alk	169	20	242	374
TTG/CA	2.7	9.4	0.55	0.65

[a] scaled from geologic maps

fractionation is a major control on the Sr/Y ratio (Condie 2008). As in Fig. 7.2, the average composition of upper continental crust and Archean upper continental crust plot in the CA and TTG fields, respectively (Fig. 7.3).

As pointed out by Kamber et al. (2002) and Kleinhanns et al. (2003), the strong arc signature of fluid-mobile elements (such as Pb, Li, B, As) in TTGs is difficult to reconcile with the view that TTGs form by direct slab melting. In particular, the overabundance of such fluid-mobile elements as B and As requires large volumes of fluid liberated by descending slabs into mantle wedges (Mohan et al. 2008). Thus, it seems unavoidable that TTGs are produced in refertilized mantle wedges. Although correlations of Sr and Eu/Eu* with major elements such as K, Ca and Na support fractional crystallization (Kamber et al. 2002), the large range in major element contents required to explain the variation in Sr and Yb contents is not observed in most TTG suites (Moyen and Stevens 2006). Another potential obstacle for fractional crystallization to explain strong La/Yb fractionation in TTGs is that there should be large volumes of cumulus minerals in the lower crust. This, of course, is a problem only if the cumulate rocks have not delaminated and sank into the mantle. If garnet and amphibole are the dominant cumulus phases (rather than olivine, pyroxenes and plagioclase) as shown by experimental studies, they are clearly dense enough to sink into the mantle, and thus the missing cumulate problem goes away (Kleinhanns et al. 2003).

7.2.3 TTGs Decrease in Abundance Relative to Calc-alkaline Granitoids at the End of the Archean

Condie (2008) showed that the ratio of TTG to calc-alkaline granitoids (CA) decreases remarkably at the end the Archean (Table 7.1). The distinction between CA and TTG suites is based chiefly on major element trends on such diagrams as the K-Na-Ca graph (Martin 1994), various silica variation diagrams, Sr and Eu anomaly distributions, and low contents of Y and heavy REE (as summarized above). Although there are few examples of CA suites older than 2.8 Ga, the data suggest that the ratio of TTG/CA reached a maximum in the late Archean. As recorded by both the TTG average and maximum values, La/Yb, Sr, Eu/Eu* and Ni also seem to have broad peaks in the late Archean (2.8—2.5 Ga) (Fig. 7.4; Condie 2005). A plot of La and Yb against La/Yb shows that the high values defining the La/Yb peak are controlled chiefly by high La values (Condie 2008). Because La is an example of a fluid-mobile element, this clearly favors a metasomatic cause for the high La/Yb ratios in the late Archean. The control of the decreasing TTG/CA ratio on the composition of upper continental crust with time is clearly evident in Figs. 7.2 and 7.3

Both K/La and Th/La ratios increase in TTGs between the late Archean and the Paleoproterozoic (Condie 1993). This change could reflect subduction of Archean K-rich sediments beginning at the end of the Archean (Condie 2008). In any case, it would appear that after the Archean,

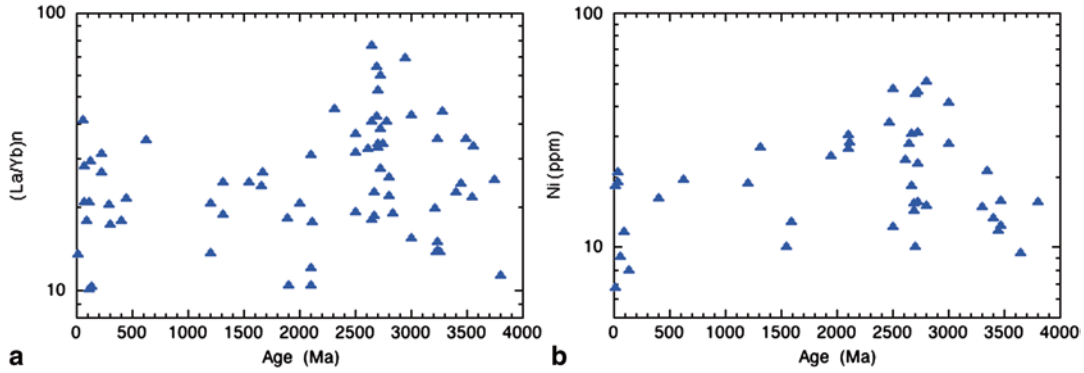

Fig. 7.4 (La/Yb)n (**a**) and Ni (**b**) versus age in TTGs. All plotted points are average values from different geographic locations. Data from Condie (2005) with updates

subduction-related magmatism shifted from deep to shallow levels and involved both the metasomatized mantle wedge and the lower to middle crust, producing CA suites, which dominate in continental-margin subduction systems from 2.5 Ga onwards. Although an increase in the Mg number of TTGs between 4 and 2.5 Ga is proposed by Martin and Moyen (2002), no such trend is apparent in the database of Condie (2005). However, there does seem to be a broad peak in Ni coincident with the La/Yb peak in the late Archean (Fig. 7.4b). This could record interaction of TTGs with the mantle wedge or overlying mantle lithosphere, both of which are Ni-rich.

It is interesting and perhaps not unexpected that the peak in La/Yb and Ni approximately coincides with a proposed widespread propagation of plate tectonic processes in the late Archean (Condie and Kroner 2008; Condie and O'Neill 2010). For the hotter Archean mantle, buoyant subduction should have been more widespread than it is today. Experimental studies confirm that the size and location of the melt region in the mantle wedge varies linearly and inversely with slab dip (Grove et al. 2009), and thus during the late Archean the amount of TTG melt produced may have been greater. Melting may have occurred both in the mantle wedge and in thickened mafic crust or/and in the descending slab. High-grade metamorphic rocks of late Archean age show that at least part of the late Archean crust exceeded 50 km in thickness (Rapp and Watson 1995). Alternatively, or in addition to buoyant-subduction triggered melting, widespread release of volatiles from the descending slabs may have triggered melting of mafic components in thickened crust and/or fractional crystallization of garnet/amphibole leading to TTG magmas. Supportive of this idea is the fact that many early Archean greenstones are intensely altered (Hofmann and Harris 2008), and if subducted in the late Archean, these greenstones should liberate large volumes of water into mantle wedges. In either case, it is the widespread onset of plate tectonics that would be responsible for the enhanced production rates of TTGs in the late Archean.

A closely related question is the appearance of sanukitoids in the Archean. Sanukitoids are a group of unusual plutonic rocks first described by Shirey and Hanson (1984) and named after sanukites, which are andesitic volcanics from the Setouchi belt in Japan. They are unusual in that they are enriched in both compatible and incompatible elements (Heilimo et al. 2010). As plutonic rocks, they first appear in the geologic record at about 3 Ga, followed by a peak in abundance in the latest Archean (2.8-2.5 Ga), and then the virtual disappearance of these unusual rocks (Kovalenko et al. 2005; Rapp et al. 2010; Martin et al. 2010). Sanukitoids have major and trace element distributions intermediate between typical Archean TTGs and young arc granitoids and have relatively high Mg numbers and trace metal contents (Ni, Cr, Co) and high Ba and Sr (Martin et al. 2010; Heilimo et al. 2010). They also retain the high La/Yb and Sr/Y ratios

characteristic of TTGs. Experiments show that sanukitoids can form by (1) partial melting of mantle that was previously metasomatized by TTG magmas (perhaps in a mantle wedge), or (2) by reactions between TTG magmas and mantle lherzolites (Rapp et al. 2010). However, other melting experiments show that mantle wedge processes may not be necessary and that elevated Mg number and trace metals in both sanukitoids and TTGs can be produced by chemical changes as felsic magmas migrate through, and segregate from a partially molten restite in the lower crust at convergent margins (Getsinger et al. 2009). The restriction of sanukitoids chiefly to the latest Archean would appear to somehow be tied to the increase in TTG abundance at this time, and thus be subduction related.

But what about the remarkable drop in the TTG/CA ratio after the end of the Archean? We need not only a turn-on switch for enhanced TTG production (widespread subduction), but also a turn-off switch. As pointed out by Condie and O'Neill (2010), the widespread onset of plate tectonics would send many slabs into the mantle, cooling the mantle, with a resultant shift from dominantly buoyant subduction to normal subduction with a well-developed mantle wedge. With cooling, dehydration rates of descending slabs may have decreased, and wet garnet/amphibole fractionation (melting and crystallization) became less important at convergent margins. Also, widespread cooling of the mantle in the late Archean would lead to less mantle wedge metasomatism and reactions with TTG magmas, and thus to a drop in abundance to sanukitoids.

7.2.4 TTGs are Not Made in Oceanic Arcs, Shallow Levels of Oceanic Plateaus or at Ocean Ridges

Although TTGs are clearly produced in some young continental-margin arc systems (e. g., the Andes), what we do not know is whether they can be produced in other tectonic settings. Oceanic arcs are commonly thought to be the building blocks of continents, and yet if TTG is the earmark of continental crust, oceanic arcs are missing that earmark (Condie and Kroner 2012). Unlike TTGs, oceanic arc granitoids have very low La/Yb and Sr/Y ratios (typically ≤ 5 and ≤ 10, respectively; Fig. 7.2) (Smith et al. 2006; Shukuno et al. 2006; Leat et al. 2007; Condie and Kroner 2012). They also typically have very low Sr and light REE contents (Figs. 7.3 and 7.5a), the former probably recording plagioclase fractionation at shallow depths and latter reflecting a depleted mantle source. So what is different about an oceanic arc convergent margin and a TTG convergent margin like the Andes? It would appear to be some combination of two factors: (1) the amount of dehydration of the descending slab, and (2) the depth to the magma source. Whereas in oceanic arcs the intensity of volatile release and LILE metasomatism must be relatively small, in TTG margins it must be large and source depths must be greater. Because young examples of TTG-type convergent margins are mostly continental margins, most continental growth must occur at continental subduction zones, which in turn implies that it is necessary to have older continental crust to make new continental crust (Condie and Kroner 2012). Although some oceanic arcs are accreted to continental convergent margins (Jagoutz et al. 2009), the volume must be small since the frequency of accreted oceanic arcs in young accretionary orogens is relatively small (Condie and Chomiak 1996; Condie 2007; Condie and Kroner 2012). Although Jagoutz and Schmidt (2012) propose that continental granitoids formed in the Late Cretaceous Kohistan oceanic arc, it is likely they were produced either during or after collision with Asia.

Another tectonic setting that has received considerable attention in terms of making continental crust is oceanic plateaus (Nair and Chacko 2008; Willbold et al. 2009). Two approaches have been used to test oceanic plateaus as sources for TTG: (1) studying felsic igneous rocks generated at modern oceanic plateaus, principally Iceland, and (2) studying granitoids and rhyolites generated in ancient oceanic plateaus and flood basalt provinces (Turner and Rushmer 2009). Geochemical studies of both felsic volcanics and shallow granitoids in Iceland clearly indicate they are not TTGs, (Figs. 7.2, 7.3 and 7.5a).

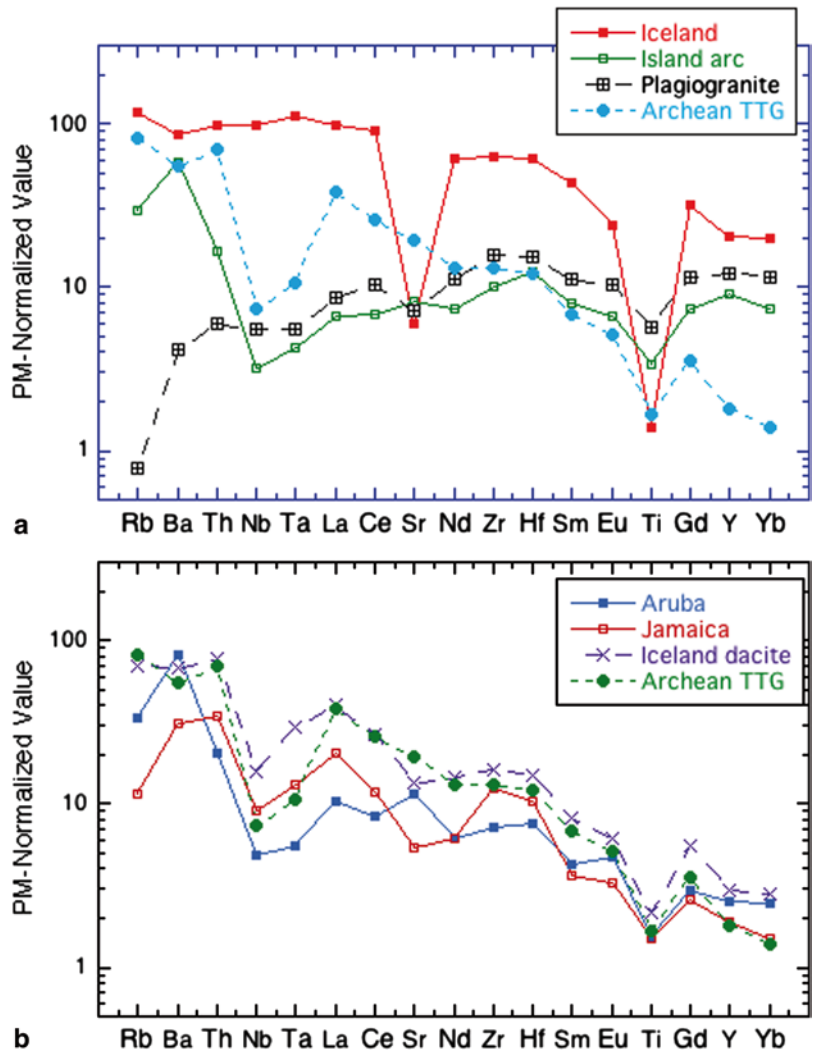

Fig. 7.5 **a** Normalized incompatible element distributions in felsic igneous rocks. Data sources: Iceland rhyolites (Martin and Sigmarsson 2007); oceanic arc dacite, Raoul Island, Kermadec arc (Smith et al. 2006); plagiogranite, Rajmi type, Oman ophiolite (Rollinson 2009); Kizildag ophiolite (Dilek and Thy 2009); other data sources in Fig. 7.2. **b** Normalized incompatible element distributions in young oceanic plateau type TTGs. Data sources: Aruba batholith, Dutch Antilles (White et al. 1999); rhyodacite, Newcastle Volcanic Formation, Jamaica (Hastie et al. 2010); Iceland dacite (Willbold et al. 2009); others as in Fig. 7.2

Rhyolites and related shallow-level felsic igneous rocks from Iceland do not show fractionation of REE and typically show large negative Sr and Ti anomalies and small Eu anomalies (Fig. 7.5a), attesting to the role of shallow fractional crystallization of plagioclase and magnetite (Martin and Sigmarsson 2007). In terms of La/Yb and Sr/Y ratios they are typical calc-alkaline or tholeiitic suites that are the products of either shallow fractional crystallization or partial melting of mafic precursors (Martin and Sigmarsson 2007, 2010; Fig. 7.2). There is no evidence for TTG formation at shallow levels in Iceland.

Another group of Iceland felsic volcanics, however, has TTG-like geochemistry: these are the dacites of the Kroksfjordur volcanic complex (Willbold et al. 2009). Although not as strongly depleted in heavy REE as Archean TTGs (Fig. 7.5b), the Kroksfjordur dacites plot near the CA-TTG transition zone on both the La/Yb-Sr/Y and Sr-Eu/Eu* graphs (Figs. 7.2 and 7.3). They appear to have been produced in a source composed chiefly of plagioclase, clinopyroxene, orthopyroxene, amphiboles and iron oxides (Willbold et al. 2009). Although garnet was not stable during their formation, amphiboles played a major role, indicating that wet sources may exist in some oceanic plateaus at depths <50 km, especially in cooler parts of the lithosphere around plateau margins (Martin et al. 2008). So all we

need is some way to produce TTG melts in the garnet stability field in oceanic plateaus to generate Archean-type TTGs. One way to double the thickness of Archean lithosphere is to subduct oceanic crust (up to 30 km thick in the Archean) beneath an oceanic plateau (Nair and Chacko 2008). Two alleged TTG suites (80–60 Ma) are associated with the Cretaceous Caribbean oceanic plateau: the Aruba batholith in the Dutch Antilles and rhyodacite lavas from Jamaica (White et al. 1999; Hastie et al. 2010). Although the Jamaican rocks show strong depletion in heavy REE like Archean TTGs, both suites show some features that are not typical of older TTGs (Figs. 7.2, 7.3 and 7.5b). Jamaican volcanics have unusually low Sr contents, but both Jamaican and Aruba rocks have Eu/Eu* values >1 suggesting a lack of plagioclase control; Aruba granitoids show a small positive Sr anomaly (Fig. 7.5b). Both sites fall with the calc-alkaline granitoids on the La/Yb-Sr/Y graph (Fig. 7.2). Anomalously high Ba and Rb at Aruba may be due to secondary processes (White et al. 1999). Aruba and Jamaica felsic igneous rocks may have formed in response to subduction-related underthrusting around the margins of the Caribbean plateau, and thus may not be derived from sources in the roots of the plateau.

And lastly, can we produce TTGs at ocean ridges as recorded by plagiogranites in ophiolites? The answer appears to be an emphatic No. It has been known for many years that plagiogranites from ophiolites have both major and trace element compositions very different from TTGs (Coleman and Donato 1979; Rollinson 2009). Not only are they less potassic, they typically show MORB-like incompatible element patterns with strong depletion in the most incompatible elements (Fig. 7.5a). Plagiogranites from suprasubduction zone ophiolites, however, differ from ocean ridge plagiogranites in that they generally show a subduction geochemical signature characterized by depletion in Nb, Ta and Ti (Dilek and Thy 2006, 2009; Dilek et al. 2008). Plagiogranites appear to be the products of either shallow fractional crystallization or shallow melting at ocean ridges.

7.2.5 Oxygen Isotopes in TTG Zircons Require Interaction of TTG Sources with the Hydrosphere

Oxygen isotopic compositions of zircons from TTGs typically have $\delta^{18}O$ values above the mantle value of 5.3‰, often in the range of 5.5–6.5‰, and in the case of TTGs from the Superior Province in Canada, in the range of 7–9‰ (Whalen et al. 2002; Bindeman et al. 2005). The relatively high $\delta^{18}O$ values are generally interpreted to show that TTGs are produced by partial melting of oceanic crust that was hydrothermally altered before subduction (Valley et al. 2005). Such an interpretation favors melting of descending slabs, although this is not the only possibility. Dehydration of descending slabs could also carry the enriched oxygen isotopic signature into the overlying mantle wedge and lower mafic crust, and thus partial melting of a thickened mafic crust may also inherit the higher $\delta^{18}O$ values. In either case, the oxygen isotopic data provide a major constraint on the origin the mafic source of TTGs: it would appear that this source must come from the top down and not the bottom up. In subduction zones it is the descending plate that controls the $\delta^{18}O$ of the rising fluids. However, if TTGs can be formed in the root zones of oceanic plateaus, the enriched $\delta^{18}O$ signature indicates that the mafic source started out life at or near the crust-ocean interface and was buried to greater depths where melting occurred. These source rocks cannot have come from mafic underplating by a mantle plume, unless the plume contained recycled altered oceanic crust that retained its original oxygen isotopic signature.

Bedard (2006) presented an unusual model for TTG production in an evolving and delaminating oceanic plateau, which also has relevancy for possible TTG production in a stagnant lid thermal regime during the Hadean. Heat is supplied in the model from a mantle plume and residual eclogite continues to sink and to refertilize the refractory mantle, allowing extraction of a continuing supply of TTG melts. Pulses in mantle melting are triggered by catastrophic delamination events that underplate new TTG crust resulting in new melting and TTG production. Smithies et al.

(2009) have presented a similar model for the evolution of the Pilbara craton in Western Australia from 3.5 to 3.32 Ga. Both plateau models may also apply to a widespread oceanic lithosphere in the Hadean, where crust and lithosphere are recycled by vertical rather than horizontal plate motions. Although neither the Bedard (2006) nor the Smithies et al. (2009) models are unique, they clearly show that TTGs may not require subduction. And perhaps the most important result, these models show that geochemistry *alone* cannot be used to identify ancient tectonic settings.

7.2.6 The Existence of Hadean Continental Crust Inferred from Detrital Zircon Suites Remains Problematic

Archean and Hadean detrital zircons from Western Australia plot chiefly in the field of continental zircon on a U/Yb–Y graph, distinct from zircons from young oceanic crust (Grimes et al. 2007). However, trace element distributions in zircons from gabbros from young oceanic crust show that it is not possible to distinguish between the Hadean zircons and zircons derived from oceanic crust (Coogan and Hinton 2010). Also, zircon compositions can vary significantly between different grains in the same sample and from zone to zone in the same zircon grain, complicating the interpretation of trace element distributions in zircons (Claiborne et al. 2010). Several studies show that Hadean detrital zircons have $\delta^{18}O$ values of 6.5–7.5 ‰, well above the mantle value of 5.3‰ (Valley et al. 2005). The elevated $\delta^{18}O$ values are generally interpreted to indicate that the source of the zircons had undergone low temperature hydrothermal alteration. In any case, these zircons provide no unambiguous evidence for continental crust older than 4 Ga, the age of some components in the Acasta gneisses in Canada (Bowring and Williams 1999).

Furthermore, the trace element patterns in Hadean zircons may have been generated by fractional crystallization of oceanic basalts at ocean ridges or some other oceanic setting, and should not be used as evidence for Hadean continental crust. The muscovite inclusions typical in Hadean zircons have been interpreted to reflect a pelitic protolith for the granitoids from which the zircons came (Harrison 2009). This in turn, implies weathering on continental crust, perhaps a Hadean craton. However, if a submarine mafic source underwent intense hydrothermal alteration producing clays, and these altered sources were later partially melted to produce granitoids, the zircons might carry with them micaceous inclusions indicative of the peraluminous (clay-rich) altered protolith. Hence, muscovite inclusions in Hadean zircons do not require a cratonic source.

Calculated compositions of felsic melts in equilibrium with Hadean zircons from the Jack Hills area in Western Australia also show a striking similarity to young plagiogranites from ophiolites (Rollinson 2008). Heavy REE patterns, for instance, are relatively flat very much like trondhjemites from the Oman ophiolite. No evidence of depleted heavy REE characteristic of TTGs is found in the calculated parent magma compositions of Hadean zircons. However, $\delta^{18}O$ in zircons from ophiolitic plagiogranites show that these rocks were in equilibrium with ocean ridge basalts with mantle oxygen isotope signatures, very different from Hadean zircons (Grimes et al. 2011). Hence, it would appear that Hadean zircons cannot be derived from oceanic plagiogranites. However, there is no evidence for Hadean TTG in the zircon suites, and if TTG is the earmark of Archean continental crust, then the evidence for Hadean continental crust is still not convincing.

7.3 So Where Do We Go from Here?

After more than 35 years of research on TTGs involving input from the field, geochemistry, isotopic dating, and experimental studies, we still face many questions about the origin and tectonic significance of these peculiar rocks. Although we now realize that TTGs require amphibole and garnet fractionation with sources that are at least 50 km deep for the medium and high pressure types, what we do not know is the relative roles of melting versus fractional

crystallization (Zellmer et al. 2012). Both are capable of explaining the high La/Yb and Sr/Y ratios of TTGs. Slabs obtain their water by alteration at ocean ridges. The mechanisms and rates of slab dehydration clearly control the stability of garnet and amphibole in subduction zones, yet we still do not have a complete understanding of these variables (Kleinhanns et al. 2003; Zellmer et al. 2012). From what we know about early Archean greenstones (≥3.5 Ga), they are more altered than later ones, and thus they would appear to bring more water and fluid-mobile elements into subduction zones, at least by the late Archean when plate tectonics became widespread. This may explain the trace element changes we see in TTGs in the late Archean. Hotter slabs in the Archean should also contribute to higher volatile release rates. These variables need to be quantified and modeled for Archean and post-Archean thermal regimes. The variation in thermal gradients required to explain the entire spectrum of TTGs and calc-alkaline suites allows, if not requires, a diversity of tectonic settings (Moyen 2011).

Another important question we are on the verge of learning more about is whether or not TTGs formed in the Hadean (>4 Ga). As reviewed above, REE distributions in detrital zircon suites suggest that TTGs were not produced in the Hadean. However, the zircon suites studied thus far may or may not be representative of the distribution of felsic crustal sources in the Hadean. Comparisons need to be made between Archean and Hadean zircon suites in terms of REE distributions, zircon crystallization temperatures and other geochemical tracers (Harrison 2009). A related and equally important question is whether the felsic magma compositions calculated from Hadean detrital zircons reflect oceanic plagiogranites or K-rich granites possibly from Hadean cratons. Zircons from both sources may have relatively flat REE patterns and large negative Eu anomalies. We need to look for other geochemical and isotopic tracers in zircons that can distinguish between these two tectonic settings. Also, it would appear that a great deal of work is needed to understand the significance of large variations in trace element distributions between and within zircon grains (Claiborne et al. 2010).

If TTGs are the earmark of upper continental crust, in how many different tectonic settings can TTG be produced and how have these settings evolved with time? We have a long list of tectonic settings in which felsic magmas can be generated (continental rifts, island arcs, shallow levels of oceanic plateaus, ocean ridges), yet no TTGs are generated and hence, no average upper continental crust. In fact, during the Phanerozoic the only tectonic setting in which TTG is being produced is the continental margin arc. The thick crust or lithosphere at continental subduction zones may be a requirement for TTG production, and if so, it would appear that we need older continental crust to produce new continental crust. Of course before continents, this could not have been the case, and oceanic plateaus may have been proxies for continents. To answer the question made in the title of this contribution, "How do we make continental crust?", today we need to start at a continental margin subduction zone where we produce both CA and TTG magmas, and combine the felsic components in the ratio of about 3 parts CA to 2 parts TTG. In the Archean the process differed in two ways: (1) we use close to 100 % of the TTG component (TTG/CA≥90), and (2) we possibly could begin by partial melting of the roots of oceanic plateaus, with or without subduction around their margins.

And one last problem that relates to the evolution of plate tectonics with time, is that of how and if mantle wedges have changed. Presumably when plate tectonics started, buoyant subduction must have been more widespread and hence mantle wedges were small or non-existent. As the mantle cooled and plates subducted at steeper angles, normal mantle wedges would develop. We see three major igneous rock series that are associated with mantle wedges, as well as several minor series: the most widespread today is the calc-alkaline series in continental arcs and the tholeiite series in oceanic arcs. The TTG series is relatively minor, and is virtually limited to continental arcs. These three igneous rock series are recognized throughout the geologic record (≤4 Ga) although the proportions change with age. In the Archean, tholeiite and TTG series clearly dominate, whereas in the post-Archean,

the calc-alkaline series dominates in continental-margin arcs and the tholeiite series in oceanic arcs. Some young mantle wedges give rise to both the calc-alkaline and tholeiite series, in some cases at the same location and at nearly the same time (George et al. 2004; Tatsumi and Suzuki 2009); a few continental-margin mantle wedges produce all three series, such as the Andes. Experimental results indicate that at depths < 50 km the calc-alkaline series is produced at magma water contents of 2–4 % and the tholeiite series at < 2 % water (Hamada and Fujii 2008; Tatsumi and Suzuki 2009). At depths ≥ 50 km and high water contents, we have production of the TTG series. Although we know from experimental studies that water content, source depth, and temperature are important in determining which series dominates, we still do not understand the relative roles of these variables nor how these roles may have changed with time. As a starting point, we need more detailed studies, including experimental as well as isotopic and geochemical input, that focus on young mantle wedges that produce more than one igneous-rock series.

References

Barker F (1979) Trondhjemites, dacites and related rocks. Elsevier, New York

Bedard JH (2006) A catalytic delamination-driven model for coupled genesis of Archean crust and sub-continental lithospheric mantle. Geochim Cosmochim Acta 70:1188–1214

Bindeman IN, Eiler JM, Yogodzinski GM, Tatsumi Y, Stern CR, Grove TL, Portnyagin M, Hoernle K, Danyushevsky LV (2005) Oxygen isotope evidence for slab melting in modern and ancient subduction zones. Earth Planet Sci Lettr 235:480–496

Bowring SA, Williams IS (1999) Priscoan (4.00-4.03 Ga) orthogneisses from northwestern Canada. Contib Mineral Petrol 134:3–16

Claiborne LL, Miller CF, Wooden JL (2010) Trace element composition of igneous zircon: a thermal and compositional record of the accumulation and evolution of a large silicic batholith, Spirit Mountain, Nevada. Contrib Mineral Petrol 160:511–531

Coldwell B, Clemens J, Petford N (2011) Deep crustal melting in the Peruvian Andes: felsic magma generation during delamination and uplift. Lithos 125:272–286

Coleman RG, Donato MM (1979) Oceanic plagiogranite revisited. In: Barker F (ed) Trondhjemites, dacites and related rocks. Elsevier, Amsterdam, pp 149–168

Condie KC (1993) Chemical composition and evolution of the upper continental crust: contrasting results from surface samples and shales. Chem Geol 104:1–37

Condie KC (2005) TTGs and adakites: are they both slab melts? Lithos 80:33–44

Condie KC (2007) Accretionary orogens in space and time. Geol Soc America Mem 200:145–158

Condie KC (2008) Did the character of subduction change at the end of the Archean? Constraints from convergent-margin granitoids. Geology 36(8):611–614

Condie KC, Chomiak B (1996) Continental accretion: contrasting Mesozoic and Early Proterozoic tectonic regimes in North America. Tectonophys 265:101–126

Condie KC, Kroner A (2008) When did plate tectonics begin? Evidence from the geologic record. Geol Society America Spec Paper 440:281–295

Condie KC, O'Neill C (2010) The Archean-Proterozoic boundary: 500 My of tectonic transition in Earth history. Amer J Sci 310:775–790

Condie KC, Kroner A (2012) The building blocks of continental crust: evidence for a major change in the tectonic setting of continental growth at the end of the Archean. Gondwana Res. doi:10.1016/j.gr.2011.09.011

Coogan LA, Hinton RW (2010) Do the trace element compositions of detrital zircons require Hadean continental crust? Geology 34(8):633–636

Dilek Y, Thy P (2006) Age and petrogenesis of plagiogranite intrusions of the Ankara mélange, central Turkey. Island Arc 15:44–57

Dilek Y, Thy P (2009) Island arc tholeiite to boninitic melt evolution of the Cretaceous Kizildag (Turkey) ophiolite: model for milti-stage early arc-forearc magmatism in Tethyan subduction factories. Lithos 113:68–87

Dilek Y, Furnes H, Shallo M (2008) Geochemistry of the Jurassic Mirdita ophiolite (Albania) and the MORB to SSZ evolution of a marginal basin oceanic crust. Lithos 100:174–209

Defant MJ, Drummond MS (1990) Derivation of some modern arc magmas by melting of young subducted lithosphere. Nature 347:662–665

Drummond MS, Defant MJ (1990) A model for trondhjemite-tonalite-dacite genesis and crustal growth via slab melting: Archean to modern comparisons. J Geophys Res 95:21503–21521

Foley S, Tlepolo M, Vannucci R (2002) Growth of early continental crust controlled by melting of amphibolite in subduction zones. Nature 417:837–840

George R, Turner S, Hawkesworth C, Bacon CR, Nye C, Stelling P, Dreher S (2004) Chemical versus temporal controls on the evolution of tholeiitic and calc-alkaline magmas at two volcanoes in the Alaska-Aleutian arc. J Petrol 45:203–219

Getsinger A, Rushmer T, Jackson MD, Baker D (2009) Generating high Mg-numbers and chemical diversity in tonalite-trondhjemite-granodiorite (TTG) magmas during melting and melt segregation in the continental crust. J Petrol 50:1935–1954

Grimes CB et al. (2007) Trace element chemistry of zircons from oceanic crust: a method for distinguishing detrital zircon provenance. Geology 35(7):643–646

Grimes CB, Ushikubo T, John BE, Valley JW (2011) Uniformly mantle-like $\delta^{18}O$ in zircons from oceanic plagiogranites and gabbros. Contrib Mineral Petrol 161:13–33

Grove TL, Till CB, Lev E, Chatterjee N, Medard E (2009) Kinematic variables and water transport control the formation and location of arc volcanoes. Nature 459:694–697

Hamada M, Fujii T (2008) Experimental constraints on the effects of pressure and H_2O on the fractional crystallization of high-Mg island arc basalt. Contrib Mineral Petrol 155:767–790

Harrison TM (2009) The Hadean crust: evidence from >4 Ga zircons. Annu Rev Earth Planet Sci 37:479–505

Hastie AR, Kerr AC, McDonald I, Mitchell SF, Pearce JA, Millar IL, Barfod D, Mark DF (2010) Geochronology, geochemistry and petrogenesis of rhyodacite lavas in eastern Jamaica: a new adakite subgroup analogous to early Archean continental crust? Chem Geol 276:344–359

Heilimo E, Halla J, Holtta P (2010) Discrimination and origin of the sanukitoid series: geochemical constraints from the Neoarchean western Karelian Province (Finland). Lithos 115:27–39

Hofmann A, Harris C (2008) Silica alteration zones in the Barberton greenstone belt: a window into subseafloor processes 3.5-3.3 Ga. Chem Geol 257:221–239

Hofmann JE, Munker C, Naeraa T et al. (2011) Mechanisms of Archean crust formation inferred from high-precision HFSE systematics in TTGs. Geochim Cosmochim Acta 75:4157–4178

Jagoutz OE, Schmidt ME (2012) The formation and bulk composition of modern juvenile continental crust: the Kohistan arc. Chem Geol 298–299:79–96

Jagoutz OE, Burg JP, Hussain S, Dawood H, Pettke T, Iizuka T, Maruyama S (2009) Construction of the granitoids crust of an island arc part I: geochronological and geochemical constraints from the plutonic Kohistan (NW Pakistan). Contrib Mineral Petrol 158:739–755

John T, Klemd R, Klemme S et al. (2011) Nb-Ta fractionation by partial melting at the titianite-rutile transition. Contrib Mineral Petrol 161:35–45

Kamber BS, Ewart A, Collerson KD, Bruce MC, McDonald GD (2002) Fluid-mobile trace element constraints on the role of slab melting and implications for Archean crustal growth models. Contrib Mineral Petrol 144:38–56

Kay RW (1978) Aleutian magnesian andesites: melts from subducted Pacific Ocean crust. J Volcanol Geotherm Res 4:117–132

Kay SM, Mpodozis C, Coira B (1999) Magmatism, tectonism, and mineral deposits of the central Andes. In: Skinner B (ed) Geology and ore deposits of the central andes, vol 7. Society Economic Geologists Special Publication, pp 27–59

Kleinhanns IC, Kramers JD, Kamber BS (2003) Importance of water for Archean granitoid petrology: a comparative study of TTG and potassic granitoids from Barberton Mountain Land, South Africa. Contrib Mineral Petrol 145:377–389

Kovalenko A, Clemens JD, Savatenkov V (2005) Petrogenetic constraints for the genesis of Archean sanukitoid suites: geochemistry and isotopic evidence from Karelia, Baltic shield. Lithos 79:147–160

Leat PT, Larter RD, Millar IL (2007) Silicic magmas of Protector shoal, South Sandwich arc: indicators of generation of primitive continental crust in an island arc. Geol Mag 144:179–190

Martin H (1994) The Archean grey gneisses and the genesis of the continental crust. In: Condie KC (ed) Archean crustal evolution. Elsevier, Amsterdam, pp 205–259

Martin H (1999) Adakitic magmas: modern analogues of Archean granitoids. Lithos 46:411–429

Martin H, Moyen J-F (2002) Secular changes in tonalite-trondhjemite-granodiorite composition as markers of the progressive cooling of Earth. Geology 30:319–322

Martin E, Sigmarsson O (2007) Crustal thermal state and origin of silicic magma in Iceland: the case of Torfajokull, Ljosufjoll and Snaefellsjokull volcanes. Contrib Mineral Petrol 153:593–605

Martin E, Sigmarsson O (2010) Thirteen million years of silicic magma production in Iceland: likes between petrogenesis and tectonic settings. Lithos 116:129–144

Martin E, Martin H, Sigmarsson O (2008) Could Iceland be a modern analogue for the Earth's early continental crust? Terra Nova 20:463–468

Martin H, Moyen J-F, Rapp R (2010) The sanukitoid series: magmatism at the Archean-Proterozoic transition. Earth Environ Science, Transact Roy Society Edinburgh 100:15–33

Mohan MR, Kamber B, Piercey SJ (2008) Boron and arsenic in highly evolved Archean felsic rocks: implications for Archean subduction processes. Earth Planet Sci Lettr 274:479–488

Moyen J-F (2011) The composite Archean grey gneisses: petrological significance, and evidence for a non-unique tectonic setting for Archean crustal growth. Lithos 123:21–36

Moyen J-F, Stevens G (2006) Experimental constraints of TTG petrogenesis: implications for Archean geodynamics: American Geophysical Union, Geophys. Mon 164:149–175

Muntener O, Kelemen PB, Grove TL (2001) The role of H_2O during crystallization of primitive arc magmas under uppermost mantle conditions and genesis of igneous pyroxenites: and experimental study. Contrib Mineral Petrol 141:643–658

Nair R, Chacko T (2008) Role of oceanic plateaus in the initiation of subduction and origin of continental crust. Geology 36(7):583–586

Petford N, Atherton M (1996) Na-rich partial melts from newly underplated basaltic crust: the Cordillera Blanca batholith, Peru. J Petrol 37:1491–1521

Rapp RP, Watson EB (1995) Dehydration melting of metabasalt at 8–32 kbar: implications for continental growth and crust-mantle recycling. J Petrol 36:891–931

Rapp RP, Watson EB, Miller CF (1991) Partial melting of amphibolite/eclogite and the origin of Archean trondhjemites and tonalites. Precambrian Res 51:1–25

Rapp RP, Norman MD, Laporte D, Yaxley GM, Martin H, Foley SF (2010) Continent formation in the Archean and chemical evolution of the cratonic lithosphere: melt-rock reaction experiments at 3–4 GPa and petrogenesis of Archean Mg-diorites. J Petrol 51(6):1237–1266

Richards JP, Kerrich R (2007) Special paper: Adakite-like rocks: their diverse origins and questionable role in metallogenesis. Econ Geol 102:537–576

Rollinson H (2008) Ophiolitic trondhjemites: a possible analogue for Hadean felsic crust. Terra Nova 20:364–369

Rollinson H (2009) New models for the genesis of plagiogranites in the Oman ophiolite. Lithos 112:603–614

Rudnick RL, Gao S (2004) Composition of the continental crust. In: Rudnick RL (ed) Treatise on Geochemistry, Vol 3. Elsevier, Amsterdam, pp 1–64

Samsonov AV, Bogina MM, Bibikova EV, Petrova AYu, Shchipansky AA (2005) The relationship between adakitic, calc-alkaline volcanic rocks and TTGs: implications for the tectonic setting of the Karelian greenstone belts, Baltic shield. Lithos 79:83–106

Shirey SB, Hanson GH (1984) Mantle-derived Archean monzodiorites and trachyandesites. Nature 310:222–224

Shukuno H, Tamura Y, Tani K, Chang Q, Suzuki T, Fiske RS (2006) Origin of silicic magmas and the compositional gap at Sumisu submarine caldera, Izu-Bonin arc, Japan. J Volcanol Geotherm Res 156:187–216

Smith IEM, Worthington TJ, Price RC, Stewart RS, Maas R (2006) Petrogenesis of dacite in an oceanic subduction environment: Raoul Island, Kermadec arc. J Volcanol Geotherm Res 156:252–265

Smithies RH (2000) The Archean tonalite-tondhjemite-granodiorite (TTG) series is not an analogue of Cenozoic adakite. Earth Planet Sci Letters 182:115–125

Smithies RH, Champion DC, Van Kranendonk MJ (2009) Formation of Paleoarchean continental crust through infracrustal melting of enriched basalt. Earth Planet Sci Lettr 281:298–306

Sun SS, McDonough WF (1989) Chemical and isotopic systematics of oceanic basalts: implications for mantle composition and processes. In: Saunders AS, Norry MJ (eds) Magmatism in Ocean Basins. Geol Society London, Spec Public 42:313–345

Tatsumi Y, Suzuki T (2009) Tholeiitic vs calc-alkalic differentiation and evolution of arc crust: constraints from melting experiments on a basalt from the Izu-Bonin-Mariana arc. J Petrol 50:1575–1603

Turner SP, Rushmer T (2009) Similarities between mantle-derived A-type granites and voluminous rhyolites in continental flood basalt provinces. Earth Environ Science Trans. Roy Soc Edinburgh 100:1–10

Valley JW et al. (2005) 4.4 billion years of crustal maturation: oxygen isotope ratios of magmatic zircon. Contrib Mineral Petrol 150:561–580

Whalen JB, Percival JA, McNicoll VJ, Longstaffe FJ (2002) A mainly crustal origin for tonalitic granitoid rocks, Superior province, Canada: implications for Late Archean tectonomagmatic processes. J Petrol 43:1551–1570

White RV, Tarney J, Kerr AC, Saunders AD, Kempton PD, Pringle MS, Klaver GT (1999) Modification of an oceanic plateau, Aruba, Dutch Caribbean: implications for the generation of continental crust. Lithos 46:43–68

Willbold M, Hegner E, Stracke A, Rocholl A (2009) Continental geochemical signatures in dacites from Iceland and implications for modes of early Archean crust formation. Earth Planet Sci Lettr 279:44–52

Winther KT (1996) An experimentally based model for the origin of tonalitic and trondhjemitic melts. Chem Geol 127:43–59

Zellmer GF, Iizuka Y, Miyoshi M, Tamura Y, Tatsumi Y (2012) Lower crustal H_2O controls on the formation of adakitic melts. Geology 10 April 2012. doi:10.1130/G32912.1

Recycling of Lead at Neoarchean Continental Margins

8

Jaana Halla

Abstract

A time-fixed Pb-Pb model of 2.7 ± 0.1 Ga mantle-derived granitoids from different Archean cratons suggests that the Pb isotope heterogeneity of Neoarchean granitoids can be explained by sediment recycling and subduction at oceanic and continental margins consisting of different-aged crustal segments. Recycling of crustal Pb to the mantle wedge gave rise to increasingly radiogenic mantle sources for the granitoids as the accretion of oceanic island arcs (OIA) and Mesoarchean microcontinents proceeded, leading to the formation of young (< 3.2 Ga) continental margins (YCM). Materials recycling at old (> 3.2 Ga) continental margins (OCM) encompassing fragments of Paleo- and Eoarchean protocrust provided the high- or low-μ Pb isotope signatures, depending on the age and U/Pb ratio of the crustal lead sources.

8.1 Introduction

Recycling of continental crust is a tectonic process that operates at the convergent plate boundaries. Surface material from the continental lithosphere is eroded and recycled in the mantle by subduction. Continental crust develops isotopic signatures (Hf, Nd, and Pb) that are different from those of the primitive mantle. Identification of these signatures in the mantle can be regarded as a proof of crustal recycling and subduction processes.

J. Halla (✉)
Finnish Museum of Natural History, University of Helsinki, Helsinki, Finland
e-mail: jaana.halla@helsinki.fi

Pb isotopes are especially suitable in studying crustal recycling in the Archean because of the strong decoupling of U and Pb between crust and mantle reservoirs and the shorter half-life of the ^{235}U isotope (parent to ^{207}Pb) compared with that of ^{238}U (parent to ^{206}Pb). As a consequence of the higher abundance of the ^{235}U in the Archean, the $^{207}Pb/^{204}Pb$ ratios increased rapidly and are thus a sensitive indicator of involvement of Pb derived from long-lived sources with different U/Pb ratio. The U/Pb ratio of a system is described by a μ-value (present-day $^{238}U/^{204}Pb$). Pb that evolves in a high-μ system develops a more radiogenic Pb isotope signature with high $^{207}Pb/^{204}Pb$ ratios with respect to $^{206}Pb/^{204}Pb$ ratios. Respectively, Pb isolated in a low-μ system carries a less-radiogenic Pb isotope signature with low $^{207}Pb/^{204}Pb$ ratios. In addition to the decoupling of U and Pb

Y. Dilek, H. Furnes (eds.), *Evolution of Archean Crust and Early Life*, Modern Approaches in Solid Earth Sciences 7, DOI 10.1007/978-94-007-7615-9_8, © Springer Science+Business Media Dordrecht 2014

between crust and mantle, also intracrustal (magmatic or metamorphic) differentiation of U from Pb may cause heterogeneity within the continental crust (e.g. Dickin 1998).

Kamber et al. (2003), among many others, documented the Early Archean isotope heterogeneity, particularly in the $^{207}Pb/^{204}Pb$ ratio. They concluded that the isotope heterogeneity could reflect the separation of a high-μ terrestrial protocrust from ca. 4.3 Ga basaltic crust, which had evolved with a higher U/Pb ratio than coeval mantle in the absence of subduction.

This paper presents a time-fixed Pb-Pb model based on the idea that if the Early Archean high-μ component exists, it should appear also in later granitoids as a consequence of interactions with Early Archean protocrust, possibly through recycling of older crust into the mantle in subduction zones. To resolve if the early Archean isotope heterogeneity was inherited in late Archean granitoids, this paper investigates the Pb isotope systematics of 2.7 ± 0.1 Ga granitoids following the idea of plumbotectonics of Zartman and Doe (1981). According to their model, orogenies extracted U, Th, and Pb from three sources (mantle, high-μ upper crust and low-μ lower crust), mixed them in the orogene reservoir, and redistributed them back to the crustal and mantle sources. The contributing older crustal material may carry a high- or low-μ Pb isotope signature, depending on the age and U/Pb ratio of the crustal segment participating in the orogeny.

The following hypothesis for Archean plate tectonics is to be tested with the model: Meso- to Eoarchean protocratons (> 2.8 Ga) acted as nuclei around which the Neoarchean (2.8–2.5 Ga) island arcs and oceanic plateaus were accreted. Recycled material from the high- or low-U/Pb portions of the protocratons with high- or low-μ Pb isotope signatures contributed to the formation of granitoids. Therefore, the isotope compositions of Neoarchean granitoids reflect the age of the crustal segments of the continental margin at which they were formed. To test the hypothesis, a time-fixed Pb isotope model for 2.7 ± 0.1 Ga granitoids is presented and tested with 500 Pb isotope analyses compiled from several publications.

8.2 Principles of the Pb-Pb Method

This section describes the basic principles of the isotope geology of lead. The Introduction-part and the description of the Holmes–Houtermans model along with Eq. 8.1–8.8 are based on the text of Faure (1986). Sect. 8.2.2 presents the most important models describing the average evolution of terrestrial lead: the Holmes–Houtermans model (Holmes 1946; Houtermans 1946), the two-stage model of Stacey and Kramers (1975), and the plumbotectonic model of Zartman and Doe (1981).

8.2.1 Introduction to Pb Isotopes

Lead has four naturally occurring stable isotopes: ^{204}Pb, ^{206}Pb, ^{207}Pb, and ^{208}Pb. Of these, only ^{204}Pb is nonradiogenic; the others are the final decay products of three complex decay chains from uranium (U) and thorium (Th). The relatively short-lived intermediate members of the decay series can usually be ignored. The most important naturally occurring isotopes of uranium, ^{238}U and ^{235}U, decay to ^{206}Pb and ^{207}Pb, respectively. Thorium exists primarily as one long-lived radioactive isotope, ^{232}Th, which decays to ^{208}Pb.

The isotope composition of lead is constantly changing owing to the radioactive decay of uranium and thorium. The lead isotopic composition of a mineral in a closed system depends on the initial lead isotopic ratios and the U/Pb and Th/Pb ratios of the mineral at the time of crystallization. The Pb isotopic composition of rocks and minerals varies widely from the highly radiogenic Pb in very old U- and Th-bearing minerals to the common lead occurring in minerals that have very low U/Pb and Th/Pb ratios. The term common lead thus refers to the lead in a mineral in which no significant radiogenic lead has been produced since the mineral formed. Examples of such minerals are galena (PbS) and K-feldspar ($KAlSi_3O_8$), in which Pb^{2+}replaces K^+. Common lead consists of lead that existed at the time of the formation of the Earth (primordial lead) and lead that formed by radioactive decay of

uranium and thorium (radiogenic lead) and later separated from uranium and thorium.

The evolution of lead in the Earth occurs in chemical environments (mantle, crust, Pb ores) having different U/Pb and Th/Pb ratios due to geochemical differentiation. The lead isotopic composition of a rock or a mineral may be changed both by decay of uranium and thorium and by mixing with lead from other sources having different isotope compositions.

8.2.2 Evolution of Lead

8.2.2.1 The Holmes–Houtermans Single-Stage Model

Holmes (1946) and Houtermans (1946) formulated independently a simple model for the evolution of lead in the Earth. This Holmes–Houtermans model, described e.g. by Faure (1986), is based on the following assumptions: (1) the Earth was originally fluid and homogeneous, (2) U, Th, and Pb were distributed uniformly, (3) the isotopic composition of the primordial lead was the same everywhere, (4) the subsequent differentiation of the Earth caused small regional differences in the U/Pb and Th/Pb ratios, (5) radiogenic Pb is produced only by decay of uranium and thorium in the source regions, and (6) the resulting Pb was later separated from the U- and Th-bearing source and incorporated into the common mineral that retained the same lead isotopic composition since its formation. This model is referred to as a single-stage evolution model because lead has evolved in a single source before isolation from uranium.

Equations The equations describing the Holmes–Houtermans model can be used to determine the ages of common leads with single-stage histories. The chemical environment of the source of the lead is described by milieu indexes μ, ω, and κ representing present-day $^{238}U/^{204}Pb$, $^{232}Th/^{204}Pb$, and $^{232}Th/^{238}U$ ratios, respectively.

The change in the isotopic composition of lead relative to the stable index isotope ^{204}Pb in a U-bearing system of age T (starting time of the system) that has remained closed to uranium and lead until the time t of separation of Pb from U (ending time of the system) can be described by the following equation:

$$\left(\frac{^{206}Pb}{^{204}Pb}\right)_t = \left(\frac{^{206}Pb}{^{204}Pb}\right)_T + \mu\left(e^{\lambda_{238}T} - e^{\lambda_{238}t}\right), \quad (8.1)$$

where λ_{238} is the decay constant of ^{238}U, μ is the term referred to as the milieu index describing the present-day $^{238}U/^{204}Pb$ ratio of the source, and

$\left(\frac{^{206}Pb}{^{204}Pb}\right)_t$ = isotope ratio of Pb of age t, and

$\left(\frac{^{206}Pb}{^{204}Pb}\right)_T$ = isotope ratio of Pb of age T.

If $t = 0$, Eq. 8.1 reduces to

$$\left(\frac{^{206}Pb}{^{204}Pb}\right)_t = \left(\frac{^{206}Pb}{^{204}Pb}\right)_T + \mu\left(e^{\lambda_{238}T} - 1\right). \quad (8.2)$$

Similar equations can be written for the two other decay schemes:

$$\left(\frac{^{207}Pb}{^{204}Pb}\right)_t = \left(\frac{^{207}Pb}{^{204}Pb}\right)_T + \frac{\mu}{137.88}\left(e^{\lambda_{235}T} - e^{\lambda_{235}t}\right) \text{ and} \quad (8.3)$$

$$\left(\frac{^{208}Pb}{^{204}Pb}\right)_t = \left(\frac{^{208}Pb}{^{204}Pb}\right)_T + \omega\left(e^{\lambda_{232}T} - e^{\lambda_{232}t}\right), \quad (8.4)$$

where λ_{235} is the decay constant of ^{235}U, λ_{232} is the decay constant of ^{232}Th, and ω is the milieu index describing the present-day $^{232}Th/^{204}Pb$ ratio of the source.

If $t = 0$, Eq. 8.3 reduces to

$$\left(\frac{^{208}Pb}{^{204}Pb}\right)_t = \left(\frac{^{208}Pb}{^{204}Pb}\right)_T + \omega\left(e^{\lambda_{232}T} - 1\right). \quad (8.5)$$

The evolution of lead can be described on a $^{207}Pb/^{204}Pb$ vs. $^{206}Pb/^{204}Pb$ or $^{208}Pb/^{204}Pb$ vs. $^{206}Pb/^{204}Pb$ diagram in terms of *growth curves*, based on Eq. 8.1 and 8.3 or 8.1 and 8.4. A growth curve originates at the point representing the isotope composition of the primordial lead. Each

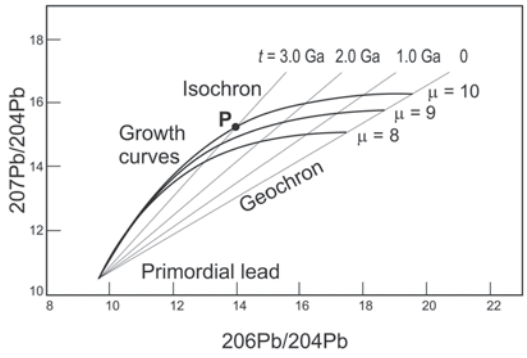

Fig. 8.1 The Holmes-Houtermans model for the evolution of single-stage lead. Lead growth curves represent systems with μ values of 8, 9, and 10. The straight line are isochrons for selected values of *t*. Point P represents lead, which was separated at 3.0 Ga from source region with μ value of 10

growth curve represents the change in lead isotope ratios over time for a system with a particular value of μ or ω (Fig. 8.1).

Equations 8.1 and 8.3 may be combined and μ eliminated because the $^{235}U/^{238}U$ ratio is known to be constant, equal to 1/137.88 for all U of normal isotopic composition in the Earth at the present time.

$$\frac{\left(\frac{^{207}Pb}{^{204}Pb}\right)_t - \left(\frac{^{207}Pb}{^{204}Pb}\right)_T}{\left(\frac{^{206}Pb}{^{204}Pb}\right)_t - \left(\frac{^{206}Pb}{^{204}Pb}\right)_T} = \frac{1}{137.88}\left[\frac{e^{\lambda_{235}T} - e^{\lambda_{235}t}}{e^{\lambda_{238}T} - e^{\lambda_{238}t}}\right]. \tag{8.6}$$

When the values of *t* are constant, a family of straight lines is formed on a $^{207}Pb/^{204}Pb$ vs. $^{206}Pb/^{204}Pb$ diagram according to Eq. 8.6. These straight lines, each corresponding to a particular value of *t*, are termed *isochrons*. All the isochrons pass through a common point representing the primordial lead isotope ratio (Fig. 8.1). The slope of a given isochron depends only on times *T* and *t*. The slope of the isochron can be calculated by the equation

$$m = \frac{1}{137.88}\left[\frac{e^{\lambda_{235}T} - e^{\lambda_{235}t}}{e^{\lambda_{238}T} - e^{\lambda_{238}t}}\right]. \tag{8.7}$$

This transcendental equation cannot be solved for an age by conventional algebraic methods, but it can be solved by a graphical method, by means of table giving the slopes of the isochrons as a function of *t*, or by computer, e.g. Isoplot/Ex version 2.2 (Ludwig 2000).

If $t = 0$, Eq. 8.7 reduces to

$$m = \frac{1}{137.88}\left[\frac{e^{\lambda_{235}T} - 1}{e^{\lambda_{238}T} - 1}\right]. \tag{8.8}$$

Single stage leads in the Earth and in meteorites plot on an isochron corresponding to $t = 0$, termed a *geochron*. The slope of the geochron was first determined by Patterson (1956). The isotope ratios of primordial lead and the age of the Earth were determined by analyzing iron and stony meteorites (Patterson 1956; Tatsumoto et al. 1973). The primordial composition of lead is assumed to be that of troilite (FeS) in iron meteorites, which contain negligible uranium and thorium (Patterson 1956). Assuming that the meteorites formed at the same time as the Earth, the age of the Earth can be calculated from Eq. 8.8.

Multi-stage lead, as explained by Faure (1986), has evolved in different systems with different milieu indexes (μ and ω). Lead can move from one system to another or the milieu indexes of the system may change. The present isotope composition of multi-stage lead is the cumulative result of different growth stages. A two-stage lead plots on a secondary isochron passing through a point on the growth curve of the first system. The slope of the secondary isochron depends solely on the time interval, during which the lead evolved in the second system. The time elapsed since final homogenization of the lead isotopic composition is defined by the slope of the Pb-Pb isochron obtained from Eq. 8.8. This equation can be used even if the initial composition and earlier evolution stages of the lead are not known. However, it is important to realize that not all linear arrays on Pb-Pb diagrams are isochrons; mixing of lead from different sources having different isotopic compositions may also produce linear correlations of lead isotopic ratios.

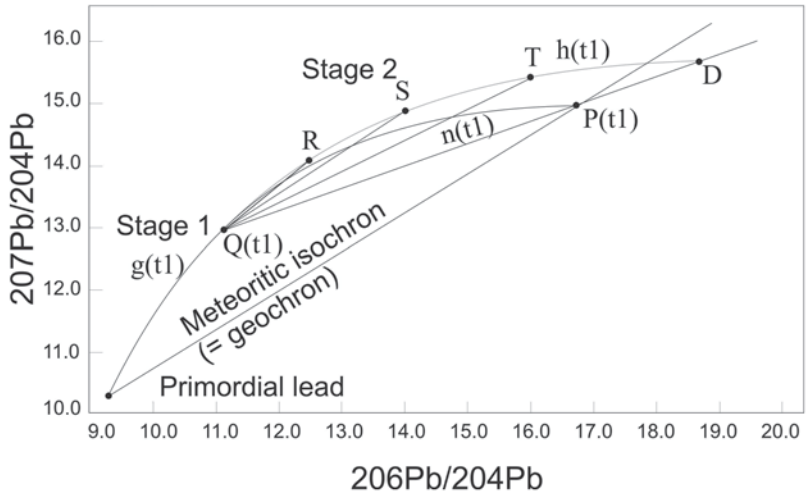

Fig. 8.2 Two-stage model of lead evolution constructed by Stacey and Kramers (1975). In the first stage, the lead evolves from the primordial lead isotopic composition to the composition of point Q ($t1$) in a uniform reservoir with a μ value indicated by a single-stage growth curve g($t1$) leading to present-day point P($t1$). At the beginning of the second stage, geochemical differentiation changes the μ value and the lead continues to evolve along the second-stage growth curve h($t1$) from point Q to point D representing the average present-day crustal Pb. Isochron lines connect points on the evolution line (e.g. R, S, T are compositions of conformable leads) to Q. The slopes of isochrons indicate the time elapsed since Pb was isolated from the reservoir

8.2.2.2 Two-Stage Model of Stacey and Kramers

The single-stage model ages of many ore deposits do not agree with the ages obtained by other methods, which indicates that the single-stage model is not adequate to explain the evolution of terrestrial lead. Stacey and Kramers (1975) suggested a two-stage model for average terrestrial lead (Fig. 8.2). According to their model, the first-stage evolution of lead began at 4.57 Ga with the primordial lead isotopic composition of Canyon Diablo troilites ($^{206}Pb/^{204}Pb = 9.307$, $^{207}Pb/^{204}Pb = 10.294$, and $^{208}Pb/^{204}Pb = 29.476$) in a homogeneous reservoir ($\mu_1 = 7.19$, $\omega_1 = 32.21$). At 3.7 Ga (T'), the values of chemical milieu indexes μ and ω changed due to geochemical differentiation and have remained constant until the present-day. At the beginning of the second stage, the lead, now having a isotopic composition of $^{206}Pb/^{204}Pb = 11.152$, $^{207}Pb/^{204}Pb = 12.998$, and $^{208}Pb/^{204}Pb = 31.230$, continued to evolve in the new chemical environment with $\mu_2 = 9.74$ and $\omega_2 = 36.84$.

At some point the lead separated from the source into a crystallizing common-lead mineral, in which the lead isotopic composition that prevailed at the time of crystallization has been preserved until the present day. The evolution of lead from the beginning of the second stage to the time of isolation of the source can be described by Eq. 8.6, and the age of the rock is obtained from the slope of the isochron according to Eq. 8.7 by replacing T by T'. Stacey and Kramers estimated the isotopic composition of average present-day lead ($^{206}Pb/^{204}Pb = 18.700$, $^{207}Pb/^{204}Pb = 15.628$, and $^{208}Pb/^{204}Pb = 38.630$) on the basis of intersections of whole-rock isochrons of granitic rocks and the lead isotopic compositions of oceanic sediments and volcanic rocks. The starting time of the second-stage evolution was defined on the basis of the accepted ages for well-known conformable galenas.

Alternatively, Cumming and Richards (1975) constructed a linear model for the evolution of lead in which U/Pb and Th/Pb ratios of the reservoir increase continuously with time instead of changing abruptly.

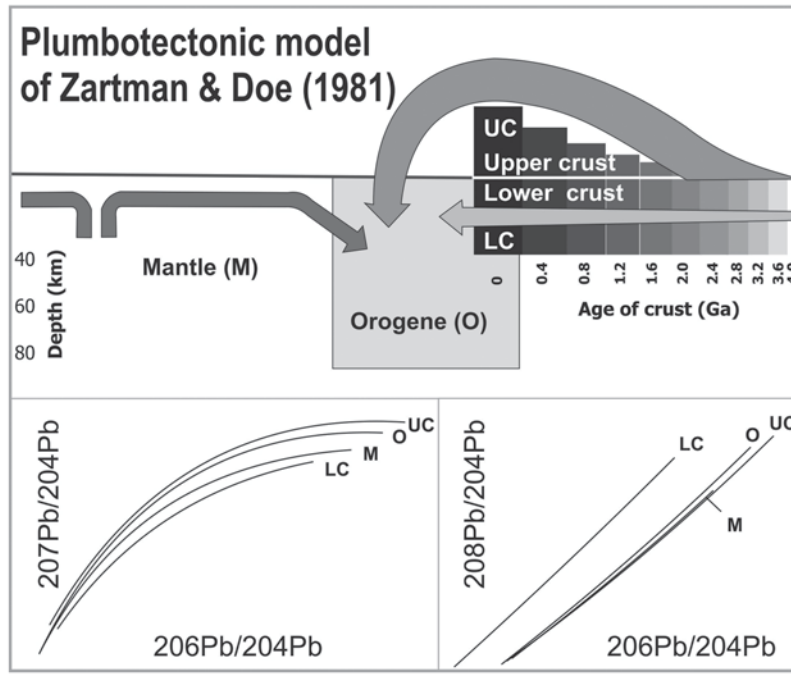

Fig. 8.3 Schematic drawing and Pb-Pb diagrams of the basic principles of the plumbotectonic model showing mixing of crustal and mantle reservoirs into the orogene reservoir and the resulting Pb isotopic evolution curves. Modified from Zartman and Doe (1981)

8.2.2.3 Plumbotectonic Model of Zartman and Doe

Doe and Zartman (1979) and Zartman and Doe (1981) combined the evolution of lead with plate tectonics and distinguished three broad sources for lead: upper mantle, upper continental crust and lower continental crust, and an additional short-lived mixing reservoir termed orogene. Based on observational data, they modelled the geochemical behaviour of U, Th, and Pb among these reservoirs. They also estimated the average present-day concentrations of U, Th, and Pb in the sources.

The basic scheme of the *plumbotectonic model* based on recycling (bi-directional transport) of material in plate tectonic processes is illustrated in Fig. 8.3. Orogenies occurring at 400 Ma intervals extracted U, Th, and Pb from the three sources (with a decreasing mantle contribution through time), mixed them in the orogene reservoir, and redistributed them back to the crustal and mantle sources. The contributing crustal material comprises a vertically recycled component from the upper crust (erosional processes) and a horizontally recycled component (continental collapsing) representing the total crust. The low U/Pb ratio of the lower crust is due to the fractionation of uranium into the upper crust during granulite-facies metamorphism. Chemical fractionation (U, Th, and Pb tend to fractionate to the upper crust) and radioactive decay create isotopic differences in the isolated sources during the interval of time between the orogenies. Tectonic processes evenly spaced in time allow mixing between the previously isolated sources with heterogeneous isotopic composition and tend to reduce the isotopic differences.

Zartman and Haines (1988) refined the plumbotectonic model and calculated the orogenies at 100 Ma intervals. During each orogeny, an orogene reservoir consisting of proximal, distal, and mantle wedge components receives material from preexisting continental crust and subcrustal lithosphere.

8.2.3 Lead Isotope Composition of K-Feldspar

The feldspars of igneous and metamorphic rocks are enriched in Pb and depleted in U and Th; the lead isotopic composition of K-feldspar thus remains unchanged over long periods of time and preserves the composition of the lead that was in-

corporated into the rocks during crystallization or metamorphism. The small amount of radiogenic lead that grows *in situ* in the feldspar may be corrected for by determining the μ ($^{238}U/^{204}Pb$) value chemically. Lead isotopes of K-feldspar can provide valuable information on the origin of rocks.

8.2.4 Pb-Pb Mantle-Crust Mixing Lines

A mantle—crust mixing line is a linear array in the Pb-Pb diagram that results from mixing of an older crust-derived component with the mantle material on a regional scale. For example, the lead isotopic compositions of the Tertiary continental flood basalts occurring along the SE Greenland continental margin define long linear trends in Pb-Pb diagrams, which have been suggested to reflect a contribution from Archean continental crust (Fitton et al. 1998; Saunders et al. 1999). The crustal contribution is easily recognized because of the low concentration of Pb in the mantle compared to the crust and the distinct low-μ signature of the Archean crust in SE Greenland. Similar results were obtained by Moorbath and Welke (1969) from lower Tertiary igneous rocks from the Isle of Skye, northwest Scotland. They suggested that the lead in the Tertiary igneous rocks were derived from mantle and underlying Lewisian basement.

Mantle-derived magmas may obtain a crustal Pb component from older crustal precursors through sediment subduction or underthrusting, mixing with melts from older crust, crustal assimilation, or contamination. In the case of subduction, the initial isotopic composition of the lead should be rather homogeneous because of the effective mixing processes operating in subduction zones (Wooden and Mueller 1988), whereas crustal contamination through the remelting or assimilation of preexisting crust would produce heterogeneous initial Pb isotope compositions due to the contribution of Pb from U-rich radiogenic accessory minerals during partial melting (Hogan and Sinha 1991).

The mixing with crustal and mantle Pb may occur in the mantle-wedge above a subduction zone by dehydration or melting of subducted continental sediments. Preferential transfer of Pb to the mantle wedge from fluids/melts that originated through the dehydration/melting of a subducted slab results in over-enrichment of island arc magmas and the continental crust in Pb (e.g. Miller et al. 1994; Brenan et al. 1995; Scambelluri et al. 2001). Subducted continental sediments are highly enriched in Pb relative to the mantle, and may add considerably to the amount of Pb available for hydrothermal/melt transport from the slab to the overlying mantle wedge. Considerably higher concentrations of sediment-derived radiogenic Pb in the mantle wedge may overwhelm the mantle Pb.

Rapid production of ^{207}Pb with respect to ^{206}Pb in the Archean (due to the shorter half-life of ^{235}U than ^{238}U) provides a constraint for evaluation of the existence of an older crustal component. The effects of crustal contamination, assimilation and magma mixing processes on the mantle melts may have been enhanced by 1) rapid recycling of the crustal material resulting in higher U/Pb ratios and 2) higher Pb concentrations in the crust than in the mantle. These factors may have generated very high $^{207}Pb/^{204}Pb$ ratios with respect to $^{206}Pb/^{204}Pb$ ratios in a relatively short time span and contributed to the high $^{207}Pb/^{204}Pb$ ratios with respect to $^{206}Pb/^{204}Pb$ ratios obtained for many Archean mantle-derived granitoids.

The mobility of uranium relative to Pb and Th during high-grade metamorphism causes stratification of the U/Pb (and Th/U) ratio and subsequently the Pb isotopic ratios in the continental crust. Dickin (1998) concluded that Pb isotopic mapping may be a useful tool in studies concerning the exhumation of Archean crust in highly metamorphosed orogenic belts.

8.3 Pb Isotope Modeling

The time-fixed (at 2.7 Ga) modeling presented in this section is based on the idea of plumbotectonics presented in Sect. 8.2.2.3.

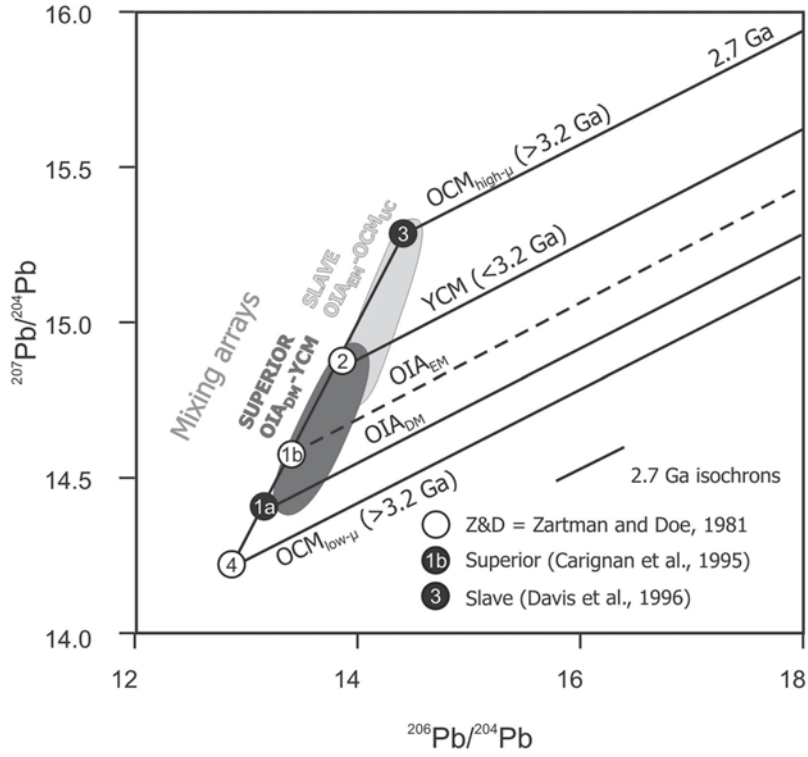

Fig. 8.4 Model initial Pb/Pb ratios (source end-members represented by numbered circles), the source mixing array (line drawn through the end-members) and model lines (hypothetical whole-rock 2.7 Ga isochrons). See detailed explanation in text (Sect. 8.3). Numbered model source end-members (*1–4*) are explained in Table 8.1. The Superior Province K-feldspar array (dark gray field) reflects the evolution of an island arc-type subduction zone with a depleted mantle source (OIA_{DM}) into a continental-type convergent margin (YCM). The Slave array (light gray field) indicates the presence of significantly older crust reflecting the evolution from mature island arcs (OIA_{EM}) to old continental margin with high-μ upper crust ($OCM_{high-\mu}$) segments

8.3.1 Model Source End-Members

At convergent margins, the possible sources for lead are the mantle and continental crust. The *mantle* source can be *depleted*, or *enriched* in radiogenic lead showing high ^{207}Pb with respect to ^{206}Pb. The isotope composition of lead deriving from the continental crust sources depends critically on the age and U/Pb ratio of the lead source. Relatively *young upper crust* (<3.2 Ga) has had less time to produce radiogenic lead than significantly *old upper crust* (>3.2 Ga). Long evolution of lead in high U/Pb (high μ) upper crust produces very radiogenic isotope compositions. On the contrary, U-depleted (low μ) lower crust that has been isolated from U for a long time retains very low radiogenic lead character with low ^{207}Pb with respect to ^{206}Pb. Thus an old continental margin (>3.2 Ga) can have two strikingly contrasting source end-members, the so called *old low-μ and high-μ* crust.

Model initial Pb/Pb ratios (at 2.7 Ga) that represent the source end-members at Neoarchean convergent oceanic or continental margins with different-aged crustal segments are listed in Table 8.1 and plotted in Fig. 8.4. The selected end-members are thought to represent the following *convergent tectonic settings*: oceanic island arc with a depleted mantle source (OIA_{DM}) or enriched mantle source (OIA_{EM}), young continental margin (YCM) with <3.2 Ga (upper) crustal sources, and old continental margins containing fragments of >3.2 Ga high-μ ($OCM_{high-\mu}$) or low-μ ($OCM_{low-\mu}$) crustal sources.

The ***oceanic island arc (OIA)*** tectonic setting includes two mantle end-members (numbers in parenthesis refer to Fig. 8.4): a primitive depleted mantle (DM) at oceanic margins or plateaus (1a) and an enriched mantle (EM) below mature island arcs (1b). The Pb/Pb ratios of the DM end-member are defined on the basis of the Pb isotope composition of the 2787 ± 14 Ma Mulcachy layered intrusion representing an early magmatic stage of the Wabigoon greenstone belt in the Superior Province, Canada (Carignan

Table 8.1 Model initial Pb/Pb ratios (source end-members) at 2.7 Ga

Source end-members (Nr. in Fig. 8.4)	Model Pb initial ratios			Tectonic setting		Reference
	$^{207}Pb/^{204}Pb$	$^{206}Pb/^{204}Pb$	$^{208}Pb/^{204}Pb$			
Depleted mantle (DM) (1a)	13.33	14.42	n.d.	Oceanic island arc (primitive)	OIA_{DM}	Carignan et al. (1995)
Enriched mantle (EM) (1b)	13.42	14.58	33.17	Oceanic island arc (mature)	OIA_{EM}	Zartman and Doe (1981)
Young (< 3.2 Ga) upper crust (2)	13.90	14.87	33.52	Young continental margin	YCM	Zartman and Doe (1981)
Old (> 3.2 Ga) high-μ crust (3)	14.36	15.27	34.26	Old continental margin with high U/Pb	$OCM_{high-\mu}$	Davis et al. (1996)
Old (> 3.2 Ga) low-μ crust (4)	12.87	14.22	33.23	Old continental margin with low U/Pb	$OCM_{low-\mu}$	Zartman and Doe (1981)

et al. 1995). The selected value is supported by the least radiogenic compositions of the Superior Province K-feldspar Array (dark grey field in Fig. 8.4). The model DM end-member composition is equivalent to the initial Pb/Pb ratios of granitoids formed from depleted mantle, without signs of crustal recycling, in a primitive oceanic island arc tectonic setting (OIA). This ratio is lower than the mantle value of Zartman and Doe (1981), which is here selected to represent the EM source in a more mature island arc system.

The more radiogenic young (< 3.2 Ga) upper crust source end-member (2) at the ***young continental margin (YCM)*** setting, is represented by the upper crust Pb isotope ratios of Zartman and Doe (1981).

The most and least radiogenic end-members of the model reflect the isotope signatures of material derived from significantly old continental crust at ***old continental margin settings (OCM)***. The most radiogenic end-member (an average Pb/Pb ratio of highly radiogenic K-feldspars from the Slave province, Canada; Davis et al. 1996) represents an old (> 3.2 Ga) high-μ upper crust source (3) of the model. The least radiogenic end-member (Zartman and Doe, 1981) corresponds to an old (> 3.2 Ga) low-μ lower crust source (4).

8.3.2 Source Mixing Arrays

Mixing and homogenization of older crust-derived Pb with the mantle on a regional scale would result in a linear array in a $^{207}Pb/^{204}Pb$–$^{206}Pb/^{204}Pb$ diagram, termed a mantle—crust mixing line. The line drawn through the model source end-members in Fig. 8.4 forms a mixing line between these sources. Classical examples of Archean mantle—crust mixing arrays are the *Superior* and *Slave arrays* (Fig. 8.4; data from Gariépy and Allègre 1985; Carignan et al. 1993; Carignan et al.1995; Henry et al.1998; Stevenson et al. 1999; Yamashita et al. 1999; Ayer and Dostal 2000; Isnard and Gariépy 2004). K-feldspar Pb isotope compositions, which are considered to represent the initial compositions of ca. 2.7 Ga granitoids from the Superior Province, plot on the model OIA_{DM}—YCM array (the Superior Array), reflecting the evolution of an oceanic island arc-type subduction zone into a young continental-type convergent margin. Another mixing array is defined by the more radiogenic K-feldspar data from the Slave Province in the northwestern Canadian Shield. The data plot on the model OIA_{EM}—$OCM_{high-\mu}$ mixing line reflecting progressive involvement of Pb from older high-μ crust. This is consistent with the presence of the oldest rocks in the world, the ca. 4.03 Acasta gneisses, in the western part of the Slave Province.

8.3.3 Model Lines: 2.7 Ga Isochrons

Figure 8.4 shows five hypothetical 2.7 Ga whole-rock isochrons starting from the five model initial Pb/Pb ratios. These isochrons define the borderlines of fields for whole-rock data from different oceanic and continental margin settings: the oceanic island arc (OIA) lines, the young continental margin (YCM) line, and the old continental mar-

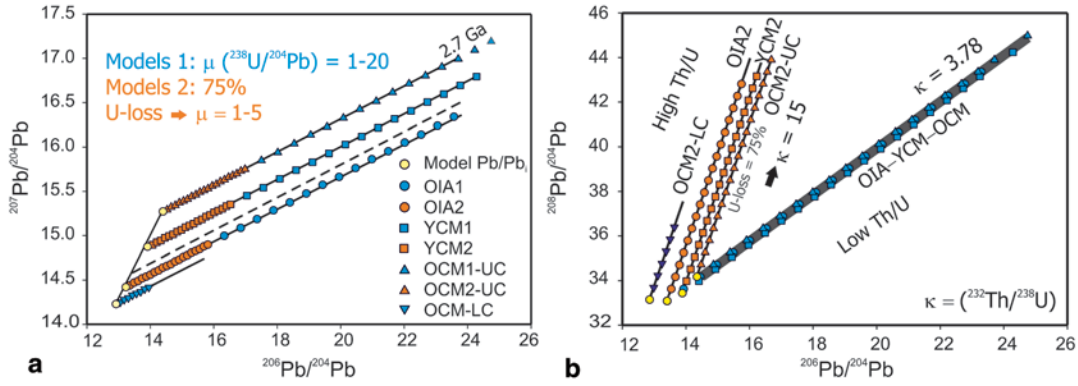

Fig. 8.5 Hypothetical (**a**) $^{207}Pb/^{204}Pb$ vs. $^{206}Pb/^{204}Pb$ and (**b**) $^{208}Pb/^{204}Pb$ vs. $^{206}Pb/^{204}Pb$ plots of 2.7 Ga whole-rock samples of granitoids generated in different convergent tectonic settings. The plots are calculated for two sets of μ-values 1–20 (*Models 1*) and 1–5 (Models 2), describing a U loss of 75 %. The model initial ratios (same as in Fig. 8.4) plot on the intersections of whole-rock isochrons and the source mixing line. The diagram can be used as a time-fixed tectonic discrimination diagram based on Pb isotope compositions of whole-rock granitoid samples. Model lines (2.7 Ga whole-rock isochrons) define the borders for different tectonic settings. UC = upper crust, LC = lower crust. Other acronyms in Table 8.1

gin (OCM) lines for high-μ and low-μ sources. The isochrons intersect the source mixing line at a point that represents the model initial Pb/Pb ratios at the time of granitoid formation. Consequently, the present-day whole-rock Pb/Pb isotope ratios of granitoids generated in a particular tectonic setting should plot in the field between the respective model lines (2.7 Ga isochrons), and the Pb/Pb ratios of K-feldspars (representing the initial Pb isotope ratios of the system) on the mixing line between the respective source end-members. For example, whole-rock Pb isotope data of granitoids formed at a young continental margin by mixing with enriched mantle and young continental crust material should plot between the OIA_{EM} and YCM lines, and the K-feldspar data on the mixing line between the enriched mantle (1b) and young upper crust (2) end-members.

8.4 Testing the Model

To see how the plots should behave theoretically, Fig. 8.5 shows hypothetical Pb/Pb plots of 2.7 Ga rocks from different settings and with different μ values for the whole rock system. The plots are calculated from all model initial compositions with two sets of μ-values 1–20 and 1–5, the latter describing a U loss of 75 % at the time of formation. The first set assumes a "normal" U/Pb ratio, and the second describes a situation in which the rock has been depleted in U e.g. during high-grade metamorphism. Figure 8.5a shows that the second set plots relatively close to the source mixing line. Figure 8.5b shows that a loss of U changes the κ (present-day $^{232}Th/^{238}U$) value significantly. Average Stacey and Kramers (1975) κ value is 3.78, whereas many Archean rocks show κ values as high as 15.

To test the model, a total number of 472 analyses from different Archean cratons is compiled and plotted in Figs. 8.6–8.8. Most data is plotted as fields for the sake of simplicity. The age of the cratons from where Pb isotope analyses are plotted are given in parenthesis in the following text.

8.4.1 Oceanic Island Arc setting (OIA)

The low-radiogenic end of the Superior Province (2.72–2.68 Ga with minor < 3.2 Ga fragments) K-feldspar Array plots on the depleted mantle values of the mixing line (Fig. 8.4). This points to an initial magmatic stage at an oceanic island arc (or plateau) setting, which is indicated by the OIA line in Fig. 8.6. The dashed line between OIA and YCM (young continental margin) represents a mature oceanic island arc.

The oceanic island arc (OIA) line is tested with plagioclase and whole-rock Pb isotope data of

3.0 Ga TTG granitoids from the Amnunnakta and Oldongso massifs in the Olekma granite-greenstone terrain of the *Aldan Shield*, eastern Siberia (Fig. 8.6a; the model parameters are recalculated to 3.0 Ga; data from Neymark et al. 1993). All the data plots below the OIA line indicating an oceanic arc tectonic setting, which is consistent with the results of Neymark et al. (1993). Based on a geochemical and isotope study (e.g. low $\delta^{18}O$ values similar to mantle), they concluded that there is no evidence of recycled crustal material in the granitoids and suggested a depleted source, e.g. melting of oceanic crust generated in mid-ocean ridges. The geochemical characteristics of Amnunnakta (gabbro-diorite-tonalite-trondhjemite) massif (lower SiO_2, high Mg, high HREE) are consistent with a depleted mantle source, whereas the composition of the Oldongso (tonalite-trondhjemite) massif (higher SiO_2, low Mg, low HREE) indicates partial melting of a basaltic source such as descending slab or lower parts of thickened mafic crust (e.g. oceanic plateaus or stacked oceanic crust).

8.4.2 Young Continental Margin Setting (YCM)

Pb isotope data of K-feldspars in the 2.7 ± 0.1 Ga granitoids of the Superior Province (2.72–2.68 Ga with minor < 3.2 Ga fragments) plot on the OIA_{DM}—YCM mixing line forming an array of compositions from those typical of primitive mantle to those typical of upper crust (Fig. 8.4). This is thought to reflect the evolution of an island arc-type subduction zone into a young continental-type convergent margin. This agrees with the common interpretation of increasing crust—mantle interactions during the accretion of the Superior craton.

Figures 8.6b–d show testing of the young continental margin (YCM) line. Data from Archean high-grade terrains of the *Karelian* (2.83–2.66 Ga, with < 3.2 Ga fragments) (Fig. 8.6b; data from Halla 2005) and *Grenville* provinces (Fig. 8.6c; data from Gariépy et al. 1990; Dickin 1998) show similar low U/Pb whole-rock isotope characteristics and plot between mature oceanic island arc (dashed line) and young continental margin lines. The results from Karelian granitoids in eastern Finland are consistent with their suggested origin in an enriched mantle wedge below a mature island arc or young continental margin (Halla 2005; Halla and Heilimo 2009; Halla et al. 2009; Heilimo et al., 2010; Heilimo et al. 2011; Heilimo et al. 2013). Pb isotopes of granitoid rocks from the *Yilgarn* craton (Fig. 8.6d; data from Oversby 1975; Bickle et al. 1983; McNaughton and Bickle 1987) point to young continental margin tectonic setting. According to the studies of Oversby (1975), continental type rocks have been present in the area at 3.3 Ga.

8.4.3 Old Continental Margin Setting (OCM)

Paleoarchean (> 3.2 Ga) and Eoarchean (> 3.6 Ga) crustal fragments are the possible sources of the most and least radiogenic ends of the mixing array (Fig. 8.4), as explained in the Introduction-part. The Slave Province (4.03–2.60 Ga) in the northwestern Canadian Shield represents a granite-greenstone province assembled by the accretion of oceanic island arcs to an older protocraton, followed by extensive plutonism at ca. 2.7 Ga. The western part of the province consists of rocks older than 3.2 Ga, including the oldest rocks in the world, the ca. 4.03 Acasta gneisses. The Pb isotope data of K-feldspars from the granitoids of the Slave province range up to the YCM—$OCM_{high\text{-}\mu}$ mixing line (Fig. 8.4) pointing to a significant recycling of pre-3.6 Ga high-μ crust (Davis et al. 1996). The Pb isotope data is consistent with the evolution history of the province and fits the model presented here.

Old Continental Margin (OCM) models are tested in Fig. 8.6e–g. The data from the *Wyoming* (North America) and *Pilbara* (Western Australia) cratons with Paleoarchean fragments up to 3.6 Ga are consistent with the model indicating the presence of an upper crustal Pb source older than 3.2 Ga (Fig. 8.6e–f; data from Rosholt et al. 1973; Wooden and Mueller 1988; Oversby 1975). Wooden and Mueller (1998) attributed the crustal signature of 2.74–2.79 Ga mantle-derived granitoids from Wyoming to subduction of continental sediments from older high-μ crustal source and

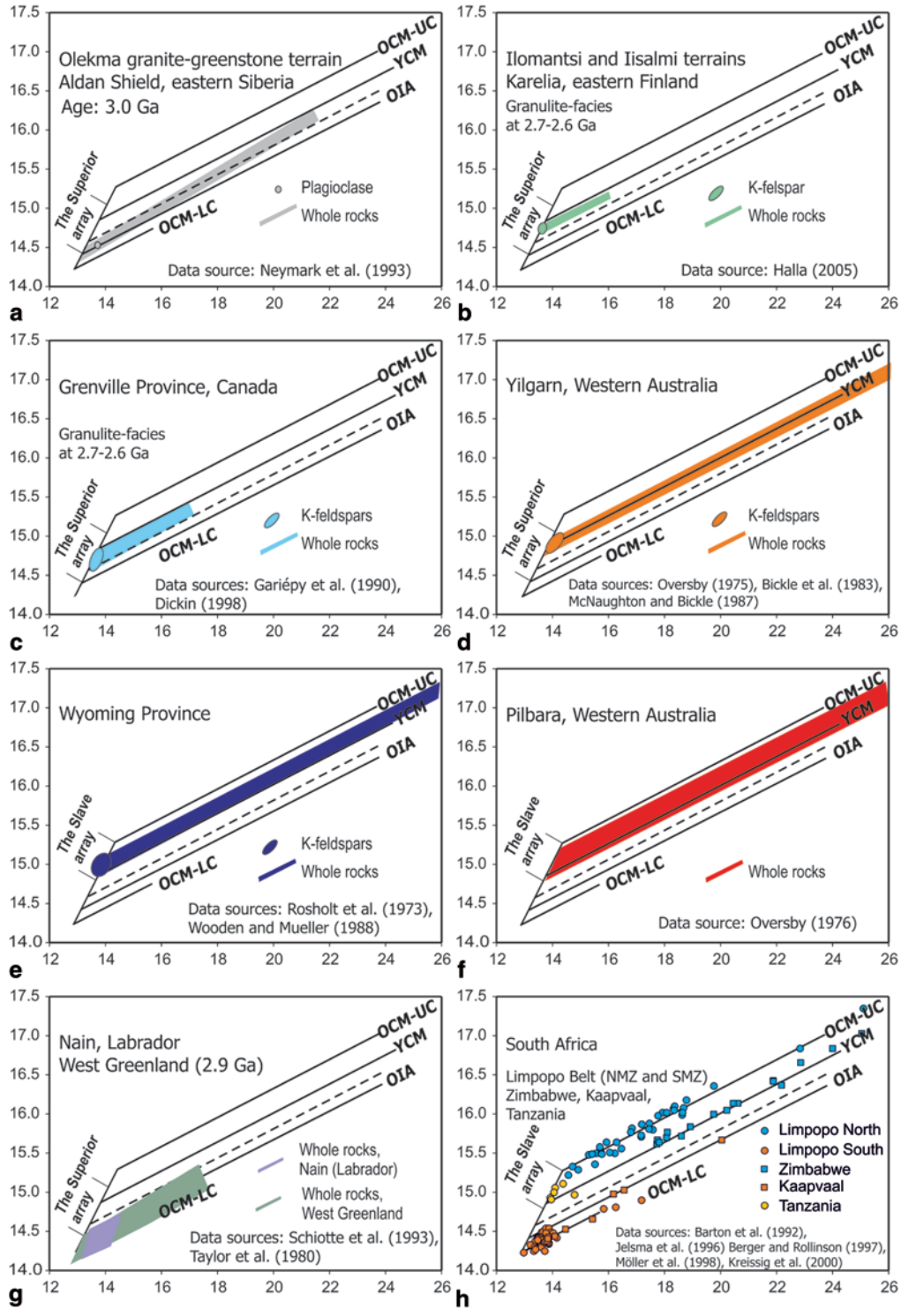

Fig. 8.6 $^{207}Pb/^{204}Pb$ (y-axis) vs. $^{206}Pb/^{204}Pb$ (x-axis) plot of whole rocks and K-feldspars of 2.7 ± 0.1 Ga granitoids from different Archean cratons. The dashed line between OIA and YCM lines represents a mature oceanic island arc. UC = upper crust, LC = lower crust. Other acronyms in Table 8.1. Granitoids (ca. 3.0 Ga) from Aldan Shield,

contamination of the overlying mantle wedge. They also noted the high Th/U characteristics of the source and related it to the effects of Th-enriched fluids. Data from *West Greenland* and *Nain* Province, Labrador (Fig. 8.6g; data from Schiøtte et al. 1993; Taylor et al. 1980) indicate the presence of > 3.2 Ga low-μ crust. This is consistent with the Eoarchean ages up to 3.8 Ga obtained from the North Atlantic craton.

In South Africa (Fig. 8.6h; data from Barton et al. 1992; Jelsma et al. 1996; Berger and Rollinson 1997; Kreissig et al. 2000), both high- and low-radiogenic Pb isotope sources are found in the orogenic Limpopo belt between the the Zimbabwe craton in the north and Kaapvaal craton in the south. The data from Northern Marginal Zone indicate the presence of > 3.2 Ga high-μ crust, whereas data from the Southern Marginal Zone of the Limpopo Belt indicate the presence of > 3.2 Ga low-μ crust.

The Kaapvaal craton (3.7–2.7 Ga) also shows contribution from old low-μ crust, whereas the Zimbabwe (3.5–2.6 Ga) and Tanzanian (mainly 2.9–2.4 Ga, < 3.2 Ga fragments) cratons are partly affected by lead derived from old high-μ crust.

Figure 8.7 shows plots of whole-rock samples on $^{208}Pb/^{204}Pb$ vs. $^{206}Pb/^{204}Pb$ diagrams. High Th/U (high κ) trends on the diagram suggest that the rocks have lost about 75% of their U at the time of formation. Highly metamorphosed terrains such as Karelia, Grenville and Limpopo show high Th/U trends whereas other terrains, e.g. Yilgarn and Zimbabwe, show lower Th/U trends. In Fig. 8.8, all rocks that show high Th/U characteristics are plotted on a $^{208}Pb/^{204}Pb$ vs. $^{207}Pb/^{204}Pb$ diagram with the model lines.

8.5 Interpretation of the Modeling

The results of the Pb isotope modeling are summarized in Fig. 8.9. The change in the Pb isotope composition between different cratons is transitional, but a pattern following the known evolutional history of the cratons can be clearly observed. The pattern in Fig. 8.9a is suggested to describe the rapid recycling of crustal material through subduction processes. The evolution starts with an oceanic island arc setting with a depleted mantle source (OIA_{DM}) that do not show any sign of mantle enrichment or crustal recycling (low-radiogenic end of the Superior Array, Aldan). However, it should be kept in mind that recycling of young crustal material during accretion of primitive island arcs or oceanic plateaus does not affect the mantle Pb isotope compositions.

In the next stage, progressive recycling of crustal sediments generated a more mature island arc setting with an enriched mantle wedge source (OIA_{EM}) with more radiogenic Pb isotope compositions. Further on, mature island arcs and small Mesoarchean microcontinents (< 3.2 Ga) were assembled resulting in young continental margins of mostly newly accreted crust (Karelia, Grenville, Yilgarn, Zimbabwe, and the high-radiogenic end of the Superior Array). As a consequence of increasing crust-mantle interactions, more radiogenic mantle sources were developed.

Fig. 8.6 (continued) eastern Siberia, and the low-radiogenic end of the Superior Array show a primitive oceanic island arc (OIA) tectonic setting without signs of mantle enrichment and crustal recycling (**a**). High-grade granitoids from the westernmost part of the Karelian craton in eastern Finland (**b**) and from the Grenville Province (Canada) (**c**) show similar isotope compositions plotting between mature island arc (dashed line above OIA) and young continental margin (YMC) lines showing minor contributions from Mesoarchean crust. The granitoids from the Yilgarn (Western Australia) (**d**) and Zimbabwe (South Africa) cratons (**h**) as well as the more radiogenic end of the Superior Array indicate the existence of a young continental margin tectonic setting with Mesoarchean fragments. The data from the Wyoming (North America) (**e**) and Pilbara, (Western Australia) cratons (**f**) are consistent with the old continental margin (OCM) with the presence of a Paleoarchean upper crustal (UC) Pb source older than 3.2 Ga. Data from West Greenland and Nain Province, Labrador (**g**) as well as data from the Kaapvaal craton and Southern Marginal Zone of the Limpopo Belt, South Africa (**h**) indicate lead contributions from Eoarchean low-μ crust. The most radiogenic Pb isotope compositions are found from the western Slave Province, Canada, and from the Northern Marginal Zone of the Limpopo belt between the Zimbabwe and Kaapvaal cratons in South Africa (**h**) indicating recycling of Eoarchean high-μ upper crust

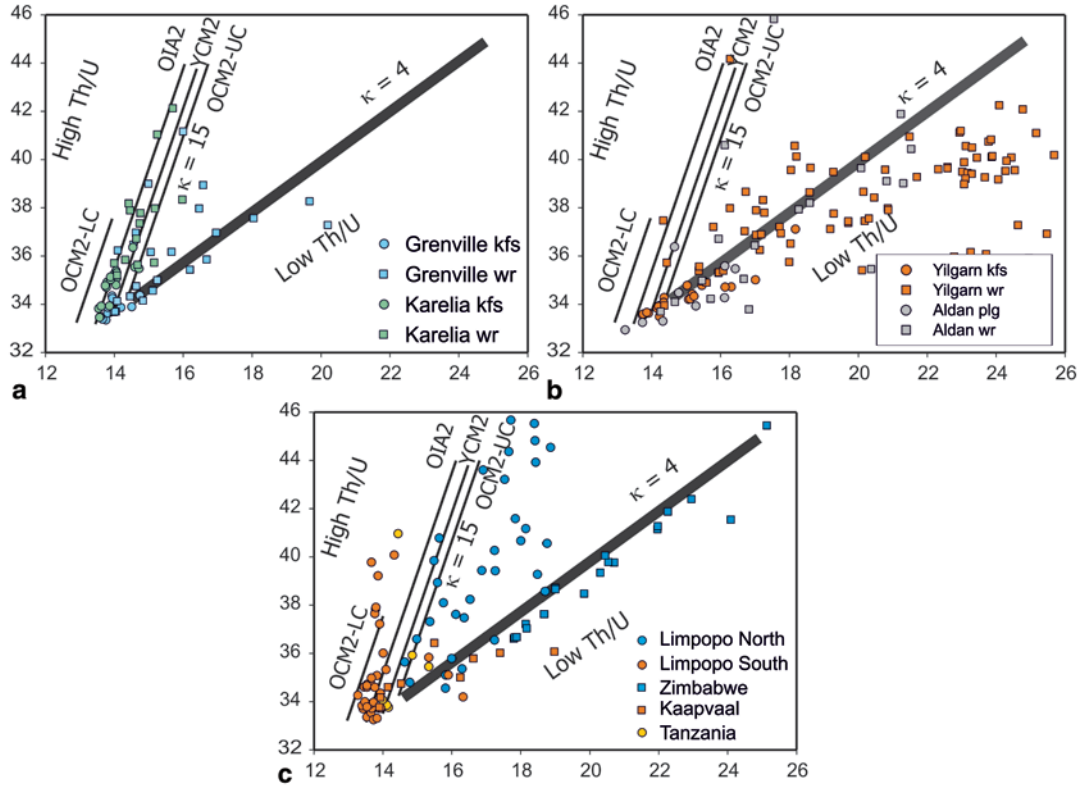

Fig. 8.7 $^{208}Pb/^{204}Pb$ (*y-axis*) vs. $^{206}Pb/^{204}Pb$ (*x-axis*) plots of whole rocks and K-feldspars of 2.7±0.1 Ga granitoids from different Archean cratons. High-grade granitoids from the westernmost part of the Karelian craton and from the Grenville Province (**a**) have similar high Th/U affinities (κ~15). Their Pb isotope compositions suggest a U-depletion event at the time of their formation. Data from Aldan and Yilgarn cratons (**b**) show low Th/U trends (κ~4), as well as the data from Zimbabwe (**c**). Data from the Kaapvaal craton, Southern Limpopo Belt, and Tanzania (**c**) indicate high Th/U trends. See Fig. 8.5 for acronyms

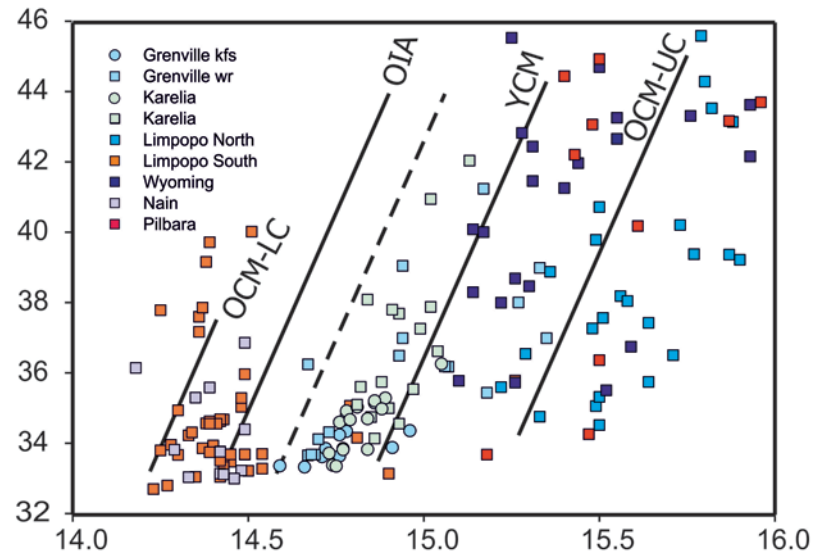

Fig. 8.8 $^{208}Pb/^{204}Pb$ (*y-axis*) vs. $^{207}Pb/^{204}Pb$ (*x-axis*) plot of selected whole rocks and K-feldspars of 2.7±0.1 Ga granitoids from different Archean cratons. The data from Karelia, Grenville, Limpopo, Wyoming, Nain and Pilbara show high Th/U trends indicating a U-loss event at the time of granitoid formation, probably during high-grade metamorphism. See Fig. 8.5 for acronyms

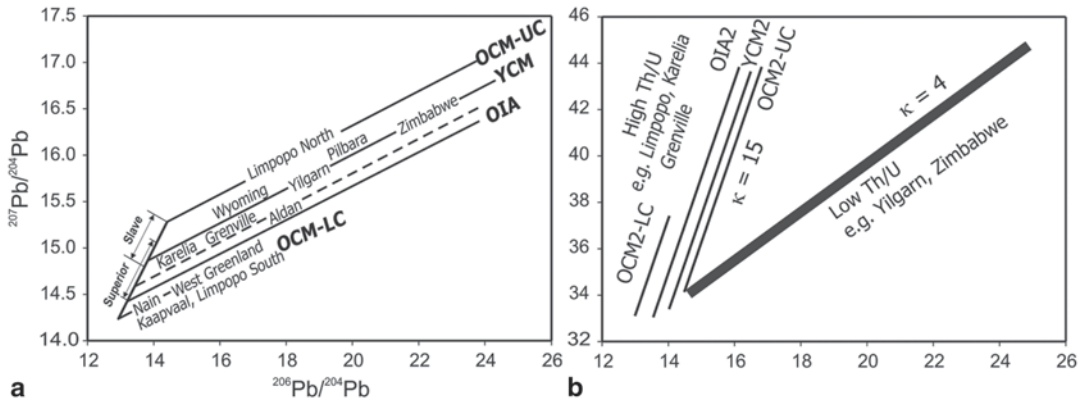

Fig. 8.9 A summary diagram of (**a**) $^{207}Pb/^{204}Pb$ (*y-axis*) vs. $^{206}Pb/^{204}Pb$ (*x-axis*) and (**b**) $^{208}Pb/^{204}Pb$ (*y-axis*) vs. $^{206}Pb/^{204}Pb$ (*x-axis*) plots of whole rocks and K-feldspars of 2.7 ± 0.1 Ga granitoids from different Archean cratons

Finally, collisions at continental margin embodying fragments of Paleo- to Eoarchean protocrust (>3.2 Ga) led to the formation of an old continental margin (OCM) tectonic settings with high- or low-μ signatures representing the most and least radiogenic Pb isotope compositions, respectively. Materials recycling at continental margins with very old high-μ segments can carry very high-radiogenic signatures (Wyoming, Pilbara, Slave, Limpopo North), depending on the age of the source. Low radiogenic signatures indicate the presence of low-μ segments (Nain, West Greenland, Kaapvaal, and Limpopo South). The source of the low-μ component may be a U depleted part of an early Archean protocrust, which have formed through intracrustal differentiation of U from Pb. Figure 8.9b shows that highly metamorphic terrains (e.g. Limpopo, Karelia, and Grenville) show very high Th/U trends indicating a significant U loss at the time of formation. Less metamorphic terrains (e.g. Yilgarn and Zimbabwe) have retained their "average" Th/U ratio.

This study suggests that late Archean granitoid magmas that formed at continental margins encompassing fragments of Early Archean protocrust, inherited their high-μ or low-μ signatures from the protocrust. Thus the Pb isotope systematics of Neoarchean granitoids can be used to reveal the age of the continental margin at which they were formed and to study increasing crust—mantle interactions during the assembly of Neoarchean supercraton(s). Consequently, the Pb isotopes can be a powerful tool for craton correlations and identification of metamorphic collisional belts.

8.6 Implications of the Model

The types of potassic granitoids that are the target of this study appeared in the Archean rock record in a restricted time period between 3.0 and 2.5 Ga. The variety of rock types included in the study consists of 2.7 ± 0.1 Ga diorites, granodiorites, monzodiorites, granites, monzonites, quartz monzonites, and syenites. They are found in all major Archean cratons embedded as batholiths and stocks in granite-greenstone terrains that consist of voluminous sodic tonalite-trondhjemite-granodiorite (TTG) suites and greenstone sequences. The group of the potassic granitoids share several common geochemical characteristics in their element concentrations, such as high contents of incompatible elements (especially high K and LILE as well as elevated Ba, Sr, and P), most often contradictorily combined with elevated compatibles (Mg, Cr, and Ni). Such a combination of high incompatible and high compatible geochemical characteristics requires both crustal and mantle input in the granitoid petrogenesis. This is also consistent with the requirement of crustal involvement to explain Pb isotope systematics of the granitoids.

The emergence of high K granitoid magmatism in the transition from Meso- to Neoarchean has invoked the debate of the onset of modern

plate tectonics, since the enrichment of the sub-continental lithospheric mantle with incompatible elements requires recycling of crustal material into the mantle, which, in turn, is a process generally attributed to subduction. The mechanism involves melting of sub-continental lithospheric mantle that has been variably enriched in incompatible elements and Hf, Nd, and Pb isotopes with crustal signatures (derived from subducted sediments), accompanied by extensive crystal fractionation and crustal contamination of the magma en route to the emplacement. It has been argued that the appearance of mantle-derived granitoids marks the initiation of deep subduction and the mantle wedge formation at convergent margins. The mantle wedge, which has been regarded as the primary source of many Archean granitoids, was enriched by subduction of oceanic crust and terrigenous sediments. The metasomatizing agents may have been fluids or melts from subducted slab and/or sediments. The strength of the crustal isotope signature inherited from sediments depends on the age of the crustal source and the amount of the respective element recycled. High Nd and Hf model ages and low respective epsilon values as well as high $^{207}Pb/^{204}Pb$ ratios of granitoids would point to the presence of significantly older crustal material within the host terrane.

The isotopic work carried out on high-potassium granitoids is relatively sparse and data is fragmented in diverse publications, waiting to be compiled, but, in general, the Hf, Pb, Nd, and Sr isotope systematics of granitoids sustain a variable but significant contribution from older crustal material, indicating an increasing role of crustal recycling in the evolution of granitoid magmas towards the end of the Archean. An important implication of the time-fixed Pb isotope modeling on 2.7±0.1 Ga granitoids presented here is the observation that geochemically and petrologically similar granitoid suites from different provinces/cratons may carry strikingly different Pb isotope signatures, which seem to reflect the environment where the granitoids were generated. In other words, the evolution of the host province is registered in the isotope composition of the granitoids.

Previous research of Davis et al. (2005) has also revealed the correlation of the isotope compositions of granitoids and the age of the surrounding terrains. A detailed study of Hf isotopes in zircon from the western Superior Province revealed distinct terranes with components of different age; young juvenile terranes (2.75–2.68 Ga) in the Western Wabigoon subprovince, slightly older (up to 3.0 Ga) reworked terranes in the south-central Wabigoon and the Sachigo subprovince, and strongly reworked terrane (up to 3.3 Ga) in the Winnipeg River subprovince. The different terranes probably accreted between 2.71–2.75 when TTG magmatism was ongoing in different terranes. Mantle-derived potassic granitoid suites show enriched Hf isotope signatures that appear to correlate with the age of the surrounding terrane, often implicating a crustal contribution from Mesoarcehan crust. Davis et al. (2005) suggested that terrain accretion by convergent tectonics is coeval with emplacement of high-K granitoid suites that become younger from north to south.

The generation of the observed differences in the isotope systematics of Neoarchean granitoids requires, firstly, the presence and contribution of continental margins with different-aged crust with different isotope signatures and, secondly, a process that transported crustal material into the mantle source of the granitoids. The best-fit tectonic scenario for the Neoarchean is the modern-type convergent plate margins with subduction zones, leading to the (1) accretion of juvenile island arcs, (2) collision of the arcs with older continents, and (3) continent-continent collisions. Taking as an example, the granitoids from the Superior and Karelia provinces show similar Pb isotope characteristics, pointing to the model tectonic setting of young continental margin. This is consistent with the general agreement that the Superior and Karelia provinces were formed between ca. 2.8 and 2.6 Ga by accretion of Neoarchean island arcs or oceanic terranes and minor Mesoarchean continental nuclei (>3.0 Ga). On the other hand, the very radiogenic Pb isotope systematics of the granitoids of the Slave Province and the strikingly contracting isotope compositions (with respect to radiogeneity) of the northern and southern Limpopo belt between the Kaapvaal and Zimbabwe cratons suggest the tectonic setting of old continental margin. This fits with the interpretation that the Slave province formed as a consequence of continent-arc colli-

sion whereas the Limpopo Belt is a result of a continent-continent collision.

The fime-fixed modeling of Pb isotope systematics of Neoarchean granitoids shows the power of Pb isotopes in tracking accretion of island arcs, collisions of continents and the recycling of material into the mantle, which all are processes included in the present-day plate tectonic model. The implication of the model is that the Pb isotopes can be used as a tool to 1) trace the oldest continental areas in Earth, 2) correlate mantle keels with distinct isotope compositions that reflect the evolution of the overlying craton, leading to possible supercontinent correlations, and 3) identifying zones of continental collisions and high-metamorphic belts, which are characterized by the most distinct isotope signatures and high Th/U trends.

8.7 Conclusions

The Pb isotope modeling suggests that in the Neoarchean, rapid recycling of crustal Pb through subduction-related processes gave rise to more radiogenic Pb isotope compositions in the mantle wedge and created an increasingly radiogenic mantle source as the accretion of island arcs along convergent plate boundaries proceeded and led to the formation of a young convergent continental margin.

Collisions with significantly older continental nuclei consisting of long-lived U-enriched or U-depleted sections (old continental margins) produced the most distinctive (high- and low-radiogenic) mantle sources for granitoids.

In general, the Pb isotope models indicate increasing crust–mantle interactions at convergent continental margins during the formation of Neoarchean supercontinents. Identification of high and low Th/U trends of rocks helps to recognize high grade terrains and, consequently, locate the zones where continents have collided.

Acknowledgements This study is a contribution to IGCP-SIDA 599 Project "The Changing Early Earth" sponsored by UNESCO and SIDA (Swedish International Development Cooperation Agency).

References

Ayer JA, Dostal J (2000) Nd and Pb isotopes from the Lake of the Woods greenstone belt, northwestern Ontario: implications for mantle evolution and the formation of crust in the southern Superior Province. Can J Earth Sci 37:1677–1689

Barton Jr JM, Doig R, Smith CB, Bohlender F, van Reenen DD (1992) Isotopic and REE characteristics of the intrusive charnoenderbite and enderbite geographically associated with the Matok pluton, Limpopo Belt, southern Africa. Precambr Res 55:451–467

Berger M, Rollinson H (1997) Isotopic and geochemical evidence for crust-mantle interaction during late Archean crustal growth. Geochim Cosmochim Acta 61:4809–4829

Bickle MJ, Chapman HJ, Bettenay LF, Groves DI, Laeter JR de (1983) Lead ages, reset rubidium-strontium ages and implications for the Archaean crustal evolution of the Diemals area, Central Yilgarn Block, Western Australia. Geochim Cosmochim Acta 47:907–914

Brenan JM, Shaw HF, Ryerson FJ (1995) Experimental evidence for the origin of lead enrichment in convergent-margin magmas. Nature 378:54–56

Carignan J, Gariépy N, Machado N, Rive M (1993) Pb isotopic geochemistry of granitoids and gneisses from the late Archean Pontiac and Abitibi Subprovinces of Canada. Chem Geol 106:299–316

Carignan J, Machado N, Gariépy C (1995) Initial Pb isotope composition of silicate minerals from the Mulcahy layered intrusion: Implications for the nature of the Archean mantle and the evolution of greenstone belts in the Superior Province, Canada. Geochim Cosmochim Acta 59:97–105

Cumming GL, Richards JR (1975) Ore lead isotope ratios in a continuously changing Earth. Earth Planet Sci Lett 28:155–171

Davis WJ, Gariépy C, Breemen O van (1996) Pb isotope composition of late Archaean granites and the extent of recycling early Archean crust in the Slave Province, northwest Canada. Chem Geol 130:255–269

Davis DW, Amelin Y, Nowell GM, Parrish RR (2005) Hf isotopes in zircon from the western Superior province, Canada: Implications for Archean crustal development and evolution of the depleted mantle reservoir. Precambr Res 140:132–156

Dickin AP (1998) Pb isotope mapping of differentially uplifted Archean basement: a case study from the Grenville Province, Ontario. Precambr Res 91:445–454

Doe BR, Zartman RE (1979) Plumbotectonics, The Phanerozoic. In: Barnes HL (ed.) Geochemistry of Hydrothermal Ore Deposits 22–70. 2nd edition. John Wiley & Sons, New York

Faure G (1986). Principles of Isotope Geology. John Wiley & Sons, New York, pp 589

Fitton JG, Hardarson BS, Ellam RM, Rogers G (1998). Sr-, Nd-, and Pb-isotopic composition of volcanic rocks from the Southeast Greenland margin at 63° N: temporal variation in crustal contamination during continental breakup. Proceedings of the Ocean Drilling Program. Sci Res 152:351–357

Gariépy C, Allégre J (1985) The lead isotope geochemistry and geochronology of late-kinematic intrusives from the Abitibi greenstone belt, and the implications for late Archaean crustal evolution. Geochim Cosmochim Acta 49:2371–2383

Gariépy C, Verner D, Doig R (1990) Dating Archean metamorphic minerals southeast of the Grenville front, western Quebec, using Pb isotopes. Geology 18:1078–1081

Halla J (2005) Late Archean high-Mg granitoids (sanukitoids) in the southern Karelian Domain, eastern Finland: Pb and Nd isotope constraints on crust—mantle interactions. Lithos 79:161–178

Halla J, Heilimo E (2009) Deformation-induced Pb isotope exchange between K-feldspar and whole rock in Neoarchean granitoids: Implications for assessing Proterozoic imprints. Chem Geol 265:303–312

Halla J, van Hunen J, Heilimo E, Hölttä P (2009) Geochemical and numerical constraints on Neoarchean plate tectonics. Precambr Res 174:155–162

Henry P, Stevenson RK, Gariépy C (1998) Late Archean mantle composition and crustal growth in the Western Superior Province of Canada: Neodymium and lead isotopic evidence from the Wawa, Quetico, and Wabigoon subprovinces. Geochim Cosmochim Acta 62:143–157

Heilimo E, Halla J, Hölttä P (2010) Discrimination and origin of the sanukitoid series: Geochemical constraints from the Neoarchean western Karelian Province (Finland), Lithos 115:27–39

Heilimo E, Halla J, Huhma H (2011) U-Pb SIMS geochronology of sanukitoid affinity intrusions in the Finnish part of the Karelian Province. Lithos 121:87–99

Heilimo E, Halla J, Andersen T, Huhma H (2013). Neoarchean crustal recycling and mantle metasomatism: Hf-Nd-Pb-O isotope evidence from sanukitoids of the Fennoscandian shield. Precambrian Research 228:250–266

Hogan JP, Sinha AK (1991). The effect of accessory minerals on the redistribution of lead isotopes during crustal anatexis: a model. Geochimica et Cosmochimica Acta:335–348

Holmes A (1946) An estimate of the age of the earth. Nature 157:680–684

Houtermans FG (1946). Die Isotopenhäufigkeiten im natürlichen Blei und da Alter des Urans. Naturwissenschaften 33:185–186, 219

Isnard H, Gariépy C (2004) Sm-Nd, Lu-Hf and Pb-Pb signatures of gneisses and granitoids from the La Grande belt: Extent of Archean crustal recycling in the northeastern Superior Province, Canada. Geochim Cosmochim Acta 68:1099–1113

Jelsma HA, Vinyu ML, Valbracht PJ, Davies GR, Wijbrans JR, Verdurmen EAT (1996) Constraints on Archaean crustal evolution of the Zimbabwe craton: a U-Pb zircon, Sm-Nd and Pb-Pb whole-rock isotopic study. Contrib Mineral Petrol 124:55–70

Kamber BS, Collerson KD, Moorbath S, Whitehouse MJ (2003) Contributions to Mineralogy and Petrology 145:25–46

Kreissig K, Nägler TF, Kramers JD, Reenen DD van, Smit CA (2000) An isotopic and geochemical study of the norhtern Kaapvaal Craton and the Southern Marginal Zone of the Limpopo Belt: are they juxtaposed terranes? Lithos 50:1–25

Ludwig KR (2000) User´s Manual for Isoplot/Ex version 2.2. A Geochronological Toolkit for Microsoft Excel. Berkeley Geochronology Center, Special Publication No. 1 a.

McNaughton NJ, Bickle MJ (1987) K-feldspar Pb-Pb isotope systemtatics Archaean post-kinematic granitoid intrusions of the Diemals area, central Yilgarn Block, Western Australia. Chem Geolo Isoto Geosci Sect 66:193–208

Miller DM, Goldstein SL, Langmuir CH (1994) Cerium/lead and lead isotope ratios in arc magmas and the enrichment of lead in the continents. Nature 368:514–520

Moorbath S, Welke H (1969) Lead isotope studies on igneous rocks from the Isle of Skye, northwest Scotland. Earth Planet Sci Lett 5:217–230

Neymark LA, Kovach VP, Nemchin AA, Morozova IM, Kotov AB, Vinogradov DP, Gorokhovsky BM, Ovchinnikova GV, Bogomolova LM, Smelov AP (1993) Late Archean intrusive complexes in the Olekma granite-greenstone terrain (eastern Siberia): geochemical and isotope study. Precambr Res 62:453–472

Oversby VM (1975) Lead isotopic systematics and ages of Archaean acid intrusives in the Kalgoorlie—Norseman area, Western Australia. Geochim Cosmochim Acta 39:1107–1125

Patterson C (1956) Age of meteorites and the Earth. Geochimica Cosmochimica Acta 10:230–237

Saunders AD, Kempton PD, Fitton JG, Larsen LM (1999) Sr, Nd, and Pb isotopes and trace element geochemistry of basalts from the Southeast Greenland margin. Proceedings of the Ocean Drilling Program. Scientific Res 163:77–93

Scambelluri M, Bottazzi P, Trommsdorff R, Vannucci R, Hermann J, Gòmez-Pugnaire MT, Vizcaino VLS (2001) Incompatible element-rich fluids released by antigorite break-down in deeply subducted mantle. Earth Planet Sci Lett 192:457–470

Schiøtte L, Hansen BT, Shirey SB, Bridgwater D (1993) Petrological and whole rock isotopic characteristics of tectonically juxtaposed Archaean gneisses in the Okak area of the Nain Province, Labrador: relevance for terrane models. Precambr Res 63:293–323

Stacey JS, Kramers JD (1975) Approximation of terrestrial lead isotope evolution by a two-stage model. Earth Planet Sci Lett 26:207–221

Stevenson R, Henry P, Gariépy C (1999) Assimilation—fractional crystallization origin of Archean Sanukitoid Suites: Western Superior Province, Canada. Precambr Res 96:83–99

Tatsumoto M, Knight RJ, Allègre (1973) Time differences in the formation of meteorites as determined from the ratio of lead-207 to lead-206. Science 180:1279–1283

Taylor PN, Moorbath S, Goodwin R, Petrykowski AC (1980) Crustal contamination as an indicator of the extent of early Archean continental crust: Pb isotopic

evidence from the late Archean gneisses of West Greenland. Geochim Cosmochim Acta 44:1437–1453
Wooden JL, Mueller PA (1988) Pb, Sr, and Nd isotopic compositions of a suite of Late Archean, igneous rocks, eastern Beartooth Mountains: implications for crust—mantle evolution. Earth Planet Sci Lett 87:59–72
Yamashita K, Creaser RA, Stemler JU, Zimaro TW (1999) Geochemical and Nd-Pb isotopic systematics of late Archean granitoids, southwestern Slave Province, Canada: constraints for granitoid origin and crustal isotopic structure. Can J Earth Sci 36:1131–1147
Zartman RE, Doe BR (1981) Plumbotectonics—the model. Tectonophysics 75:135–162
Zartman RE, Haines SM (1988) The plumbotectonic model for Pb isotopic systematics among major terrestrial reservoirs—A case for bi-directional transport. Geochim Cosmochim Acta 52:1327–1339

Crustal Evolution and Deformation in a Non-Plate-Tectonic Archaean Earth: Comparisons with Venus

9

Lyal B Harris and Jean H Bédard

Abstract

Evidence for modern plate tectonics in the Archaean is equivocal to absent, and alternative environments for formation and deformation of greenstone sequences are summarized. We focus on proposals for an unstable stagnant lid basaltic plateau crust, with cratonization occurring initially above major mantle plumes. Archaean continental drift initiated as a result of mantle traction forces acting on newly-formed subcontinental mantle keels, with further cratonic growth occurring as a result of terrane accretion to the leading edges of the migrating cratonic nuclei.

Venus is presented as an analogue for a non-plate-tectonic Archaean Earth. Despite the absence of evidence for characteristic plate tectonic environments on Venus (i.e. subduction = trenches and volcanic arcs; seafloor-spreading = volcanic ridges and transforms), the form, scale, and geometry of folds, brittle-ductile shear zones, and faults interpreted on the surface of Venus from radar imagery are comparable to mid-upper crustal structures on Earth. Anastomosing rifts link coronae interpreted to form above upwelling mantle plumes. The Lakshmi Planum highland plateau in the western Ishtar Terra region of Venus lacks extensive, regional-scale internal deformation structures, but a fold-thrust belt produced mountains on its northern margin, folds and sinistral strike-slip faults occur on its NW margin, and both regional dextral and sinistral strike slip belts occur in a zone of lateral escape to its NE. Rift zones are present along the southern margin to Lakshmi Planum. The scale and kinematics of structures in western Ishtar Terra closely resemble those of the Indian-Asia collision zone, and we propose that lateral displacement of some coronae and

L. B. Harris (✉)
Institut national de la recherche scientifique,
Centre Eau Terre Environnement, 490 de la Couronne,
G1K 9A9 Québec, QC, Canada
e-mail: lyal.harris@ete.inrs.ca

J. H. Bédard
Geological Survey of Canada, 490 de la Couronne,
G1K 9A9 Québec, QC, Canada

Y. Dilek, H. Furnes (eds.), *Evolution of Archean Crust and Early Life*, Modern Approaches in Solid Earth Sciences 7, DOI 10.1007/978-94-007-7615-9_9,

'craton-like' highlands or plana result from mantle tractions at their base in a stagnant lid convection regime, i.e. a similar regime as interpreted to have preceded development of plate tectonics on Earth.

In the Wawa-Abitibi Subprovince of the Superior Craton in Canada, the formation of granite greenstone sequences in a plume-related volcanic plateau and subsequent deformation can be generated through geodynamic processes similar to those on Venus without having to invoke modern-style plate tectonics. 3D S-wave seismic tomographic images of the Superior Province reveal a symmetrical rift in the sub-continental lithospheric mantle (SCLM) beneath the Wawa-Abitibi Subprovince, with no evidence for 'fossil' subduction zones. Major gold deposits and kimberlites are located above rift-bounding faults in the SCLM. Early rift structures localized subsequent deformation and hydrothermal fluid flow during N-S shortening and lateral escape ahead of a southwardly moving indenter (the Northern Superior Craton—Hudson's Bay terrane) in the ca. 2696 Ma Shebandowanian orogeny. The geometry of reverse and strike-slip shear zones in the Abitibi Subprovince of the SE Superior Province is similar to that of shear zones developed in western Ishtar Terra, Venus, which also formed ahead of a rigid indenter whose displacement is attributed to mantle tractions. Similarly, shortening and rift inversion in the Abitibi is ascribed to cratonic mobilism where displacement of the N Superior Province 'protocraton' resulted from mantle flow acting upon its deep lithospheric keel. Deformation in other Archaean cratons previously interpreted in terms of plate tectonics may also be the result of similar, mantle-driven processes.

9.1 The Archaean Earth

9.1.1 Nature of the Archaean Crust

Although much of the Archaean crust has been reworked by younger orogens or is buried beneath younger cover, fragments of it are preserved in cratons, protected by their inherent buoyancy and a stiff sub-continental lithospheric mantle (Davies 1979; Jordan 1988; Abbott et al. 1997; De Smet et al. 2000; Moser et al. 2001; Poudjom-Djomani et al. 2001; Lenardic et al. 2003; Lee et al. 2011). Most of the preserved cratonic crust is composed of granite-greenstone terrains (Anhaeusser et al. 1969; Goodwin 1981, 1996; Windley 1984; Kröner 1985; Ayres and Thurston 1985; Bickle et al. 1995; Choukroune et al. 1995; Hamilton 1998; Bleeker 2002), which have no modern terrestrial analogues. These are underlain by ancient subcontinental lithospheric mantle (SCLM) that differs from Phanerozoic mantle (Boyd 1998; Kelemen et al. 1998; MacKenzie and Canil 1999; Zheng et al. 2001; Arndt et al. 2002; Griffin et al. 2003, 2010; Herzberg 1999, 2004; Lee 2006; Canil 2008; Griffin et al. 2010), suggesting that the SCLM formed through geodynamic mechanisms such as mantle overturns or very large plumes that were unique to the Archaean. However, there is no consensus about the origin of the components of the cratonic crust and mantle, nor is there agreement about how they came to be associated. Much of our sampling of cratonic mantle comes from low velocity material on craton margins included in kimberlite xenoliths and less is known about high-velocity cratonic SCLM beneath cores of cratons (Griffin et al. 2003, 2010). The nature of the vanished non-cratonic Archaean 'oceanic' crust (e.g. Flament 2009) and mantle is even less well known, and has mostly been deduced on the basis of geochemical or geophysical arguments.

The most common supracrustal rocks of Archaean age are subaqueous tholeiitic basalts that occur as thick (< 20 km) piles with subordinate

plume-related komatiites (Goodwin 1981, 1996; Campbell et al. 1989; Tomlinson et al. 1999; Ayer et al. 2002; Kerrich and Xie 2002; Wyman and Kerrich 2002; Wyman et al. 2002; Sproule et al. 2002; Arndt 2003; Connolly et al. 2011). The closest modern geochemical analogue for such lavas are the basalts, picrites and komatiites of oceanic plateaux (Condie 2005; Herzberg and Rudnick 2012). These Archaean mafic-ultramafic sequences are separated at ca. 3–30 My intervals by thin horizons (generally < 1 km) of calc-alkaline volcanic rocks (dacite, soda-rhyolite, and rare andesite) that have negative Nb-Ta-Ti anomalies and show LILE-enrichment (Ayer et al. 2002; Smithies et al. 2007; Van Kranendonk et al. 2007a; Rollinson 2007; Leclerc et al. 2011; see review in Moyen and Van Hunen 2012). These calc-alkaline packages are commonly interpreted as arc sequences, but Bédard (2006) and Bédard et al. (2013) argue that most (with a few exceptions, e.g. Smithies et al. 2005a) formed by reworking older TTGs and tholeiitic basalts, with the andesites representing hybrids formed in a complex conduit system (e.g. Bédard et al. 2009). The calc-alkaline sequences are typically succeeded by chert, BIF (banded iron formations), and volcanogenic turbidites that commonly lack a terrigenous component, i.e. consistent with an oceanic plateau-type environment (e.g. Thurston 2002; Thurston et al. 2008; Leclerc et al. 2011). Unconformities may correspond to the bases or tops of the sedimentary packages (Donaldson and de Kemp 1998; Mueller and Pickett 2005; Thurston et al. 2008).

Supracrustal rocks generally occur in the cores of anastomosing synclines that wrap around domiform granitoid intrusions 10 to 50 km wide (MacGregor 1951; Anhaeusser et al. 1969; Choukroune et al. 1995; Goodwin 1996; Chardon et al. 1996, 1998; Hickman 1984; Collins et al. 1998; Van Kranendonk et al. 2007a, b; Thurston et al. 2008; Van Kranendonk 2011a). The synclines may be narrow and the structural history is typically complex, with a variety of older fabrics that are difficult to interpret because of the younger overprints, but in most cases kinematic indicators show the granitoids have risen compared to the sinking greenstones. Contacts and deformation fabrics are, commonly, intensely folded within marginal shear zones and may be intruded by satellite dykes. The stratigraphy is more recognizable in the lower-grade cores of synclines. The stratigraphic patterns imply that younger mafic basaltic lavas must have continuously been erupting onto this unstable submarine landscape.

The 'granitic' component of these terrains is dominated by TTGs (tonalites, trondhjemites, and granodiorites), with K-rich granites becoming more abundant with time (Barker and Arth 1976; Jahn et al. 1981; Condie 1981, 2005; Martin 1987, 1999; Luais and Hawkesworth 1994; Smithies 2000; Martin et al. 2005; Moyen and Stevens 2006; Bédard 2006; Moyen 2009, 2011; Moyen et al. 2010). Typically, these terrains have undergone numerous pulses of felsic plutonism, which may precede, accompany, and post-date deformation (Champion and Sheraton 1997; Chown et al. 2002; Boily et al. 2009). Most felsic volcanic rocks are geochemically similar to the plutons and may be coeval (Hill et al. 1989; Van Kranendonk et al. 2004), suggesting one may be the eruptive equivalent of the other, although in some cases, there are subtle geochemical differences that indicate non-unique evolution paths (Van Kranendonk pers. comm. 2012). The proportion of plutonic rock in the crust increases downwards, such that in the middle and deep crust (10–40 km) the supracrustal rocks occur only as strongly deformed and metamorphosed slivers (e.g. Bédard et al. 2003). Strong, ductile, high-temperature fabrics transform these TTG-supracrustal rock packages into gneisses at the deepest structural levels (Nutman and Friend 2007). Fabrics tend to be steep at shallow crustal levels, and flatter at deeper levels (Bédard et al. 2013).

9.1.2 Origins of Archaean Terrains

There are many schools of thought about the origin and evolution of these archetypal Archaean terrains. The strict uniformitarian approach applies the plate tectonic paradigm to interpret the TTGs as the roots of continental or oceanic arcs

against which oceanic plateaux were accreted during orogenic episodes driven by subduction (Dimroth et al. 1982; Card 1990; Williams 1990; Poulsen et al. 1992; Card and Poulsen 1998; Desrochers et al. 1993; Kimura et al. 1993; de Wit 1998; Kusky 1998; Kusky and Polat 1999; Lowe 1999; Polat and Kerrich 2001; Daigneault et al. 2002; Chown et al. 2002; Percival et al. 2004). The larger cratonic blocks are composites of smaller blocks with contrasting plutonic, volcanic, and sedimentary histories (e.g. Smithies and Witt 1997; Percival et al. 2004; Tomlinson et al. 2004; Van Kranendonk et al. 2007a; Smithies et al. 2005a; Nutman and Friend 2007, 2009; Boily et al. 2009; Friend and Nutman 2010; Windley and Garde 2009; Stott and Mueller 2009; Kisters et al. 2010; Czarnota et al. 2010). This has led to proposals that cratons grew by accreting marginal terranes. The zonation is imperfect in detail, and shown to be false in some cases (e.g. NE Superior Province; Boily et al. 2009), since many of the outboard blocks have inheritance and crystallization ages that overlap with those of the inboard blocks, and older blocks may be interleaved with more juvenile domains (e.g. W Superior; Percival et al. 2012). Despite these complexities, the stratigraphic relationships and age data from the W Superior (for example) imply sequential accretion of terranes from N to S, with collisions (orogenies) spaced at 10–20 My intervals (Percival et al. 2012). The majority of Archaean cratons show strong overprinting contractional and shear fabrics, where bulk shortening in many cases has led to tightening and flattening of older dome-and basin structures (Daigneault et al. 2002; Bleeker et al. 2008; Windley and Garde 2009; Chardon et al. 2011; Leclerc et al. 2012), and multiple reactivation of regional-scale shear zones (e.g. Harris 1987; Mueller and Harris 1988; Mueller et al. 1988; Daigneault 1996; Lacroix 1998; Groves et al. 2000; Erickson 2010; Hronsky et al. 2012; Leclerc et al. 2012).

This combination of terrane accretion and regional ‘compressional’ deformation has led many to posit the operation of Phanerozoic-style plate tectonics and orogenesis as an explanation. However, other essential features of Archaean cratons appear to be inconsistent with this interpretation. Fossil sutures are difficult or impossible to locate, since there are few of the rock assemblages that typify modern convergent plate margins, such as blueschists, accretionary mélanges, ophiolites, paired metamorphic belts, and thrust-and-fold belts (Chardon et al. 1999; Bleeker 2002; Kröner 1991; Hamilton 1998, 2007; McCall 2003; Stern 2005, 2008; Brown 2007). The voluminous mafic volcanism, and the high eruption temperatures of komatiites especially, are difficult to fit into an arc interpretation and are more commonly associated with ascending deep mantle plumes or jets (Bickle 1978; Sleep and Windley 1982; Campbell et al. 1989; Nisbet et al. 1993a; Green and Falloon 1998; Arndt 2003; Herzberg 2004; Herzberg et al. 2007; Connolly et al. 2011). Komatiitic metavolcanics have geochemical signatures that appear incompatible with a subduction-related origin (e.g. Camiré et al. 1993; Puchtel et al. 2009). Archaean intermediate volcanics (andesites) are some of the least common rocks in greenstone belts (Condie 1981; Goodwin 1981, 1996; Ayres and Thurston 1985; Laflèche et al. 1992a, b; Kerrich et al. 1999; Ayer et al. 2002; Leclerc et al. 2011), in stark contrast with the fact that andesites are among the most common volcanics at Phanerozoic convergent margins (e.g. Gill 1981; Kelemen et al. 2005). The intimate and long-lived association of magmas attributed to both arcs and plumes in the uniformitarian interpretation of the rocks from Archaean cratons (Polat and Kerrich 2001; Daigneault et al. 2002; Kerrich and Polat 2006; Wyman and Kerrich 2009) poses a severe challenge for plate tectonic interpretations (Bédard 2006; 2013; Bédard et al. 2013), since repeated and continuous arrival of hot ascending plumes, which correspond to the source of komatiites and associated tholeiites, should obliterate any subducted slab that was present (e.g. as interpreted for the Pacific Northwest by Obrebski et al. 2010 from high-resolution seismic tomography). The brief intervals between these intermittent ‘arc’ events (3–20 My) would require that a segment of oceanic crust could repeatedly become unstable and make it down to the necessary 100–150 km depth on very short timescales.

Although Archaean felsic igneous rocks show some similarities to Phanerozoic calc-alkaline rocks, the geochemistry of the TTGs does not closely resemble that of most Phanerozoic arc-related granitoids. For example, the strongly fractionated REE patterns of the Archaean TTGs imply near ubiquitous equilibration with garnet-pyroxenite restites at depths of 40–60 km (Martin 1987; Smithies 2000; Bédard 2006; Moyen 2009, 2011). In contrast, Phanerozoic arc-related batholiths are much more potassic on average, and mostly have flatter REE profiles implying shallower melting (e.g. Arth et al. 1978; Pitcher 1985; Martin 1987; Luais and Hawkesworth 1994; Atherton and Petford 1996). Some cordilleran batholiths do show such deep melting signatures (e.g. Girardi et al. 2012), which is interpreted to reflect melting of tectonically or magmatically thickened upper plate metabasite crust, a context analogous to what has been proposed for accreted Archaean oceanic terranes (Bédard et al. 2013). Overall, Archaean volcanic rocks show an absence of the source-metasomatic trace element signatures that typify arc suites (Hawkesworth and Kemp 2006; Pearce 2008; Bédard et al. 2013). When considered together with modelling results that suggest that Archaean basaltic crust was probably unsubductable (Bickle 1986; Davies 1992; van Thienen et al. 2004b; Davies 2006, 2008; van Hunen and van den Berg 2008; Sizova et al. 2010), the case for Phanerozoic- or modern -style subduction in the Archaean seems very weak. As an alternative explanation for these differences between Archaean and Phanerozoic suites that retains the plate tectonic framework, it has been proposed that Archaean arcs were somehow different, such that the subducting ocean crust either melted as it encountered the hotter Archaean mantle wedge (adakite model), or failed to subduct and subcreted to the craton edge, only to melt later (subcretion model). It has been suggested (e.g. Defant and Drummond 1990) that the rare adakitic magmas of the Phanerozoic Earth represent basaltic slab melts formed during subduction, and since the adakites have geochemical signatures very similar to those of the TTGs, an 'adakite' model for TTGs has become popular (Martin 1993, 1999; Moyen and Stevens 2006). However, this hypothesis fails simple mass balance tests, since it is essentially impossible to pass enough basaltic crust through the putative subduction zones in the time available to generate the requisite amount of TTG (Bédard 2006; Bédard et al. 2013) and it is difficult to explain the coeval emplacement of intrusions over several hundreds of km in width from a postulated subduction zone (e.g. Yilgarn Craton; Mole et al. 2012, and Dharwar Craton, Southern India; Peucat et al. 2013). This hypothesis also requires that subduction operate smoothly and continuously, despite the absence of any corroborative evidence for subduction. Furthermore, comparison of the predicted PT-path of the basaltic crust with a basaltic phase diagram suggests that very little of the slab would ever generate melt (e.g. Peacock et al. 1994; van Keken et al. 2002; Bédard 2006; Syracuse et al. 2010). Since the slab melting scenario was proposed, numerous studies have argued that most Phanerozoic adakites are not, in fact, formed by anatexis of the subducted basaltic crust, but are melts from the base of a very thick upper plate (Hawkesworth and Kemp 2006; Petford and Atherton 1996; Petford and Gallagher 2001; Annen 2011; Coldwell et al. 2011; Girardi et al. 2012), which removes the last remaining leg supporting the adakite model for Archaean TTG genesis.

The subcretion model (Fig. 9.1) is not new (Oxburgh 1972; de Wit 1982; Helmstaedt and Schultze 1986; Griffin et al. 2004; Lee 2006; Griffin and O'Reilly 2007; Lee et al. 2008), but hitherto has always been considered in the context of failed subduction of oceanic lithosphere formed by seafloor spreading. In a sense, the process has always been viewed through uniformitarian-tinted spectacles. The 'uniformitarian' subcretion model suffers from the following fundamental problem. If the subducting slabs stall and get imbricated at depth due to their buoyancy, then why were they subducting in the first place? Since there is no slab pull force acting on any of the slices in the series, what would induce the next slice of buoyant Archaean simatic plateau lithosphere in the series to subduct? Bédard et al. (2013) proposed that cratonic drift in re-

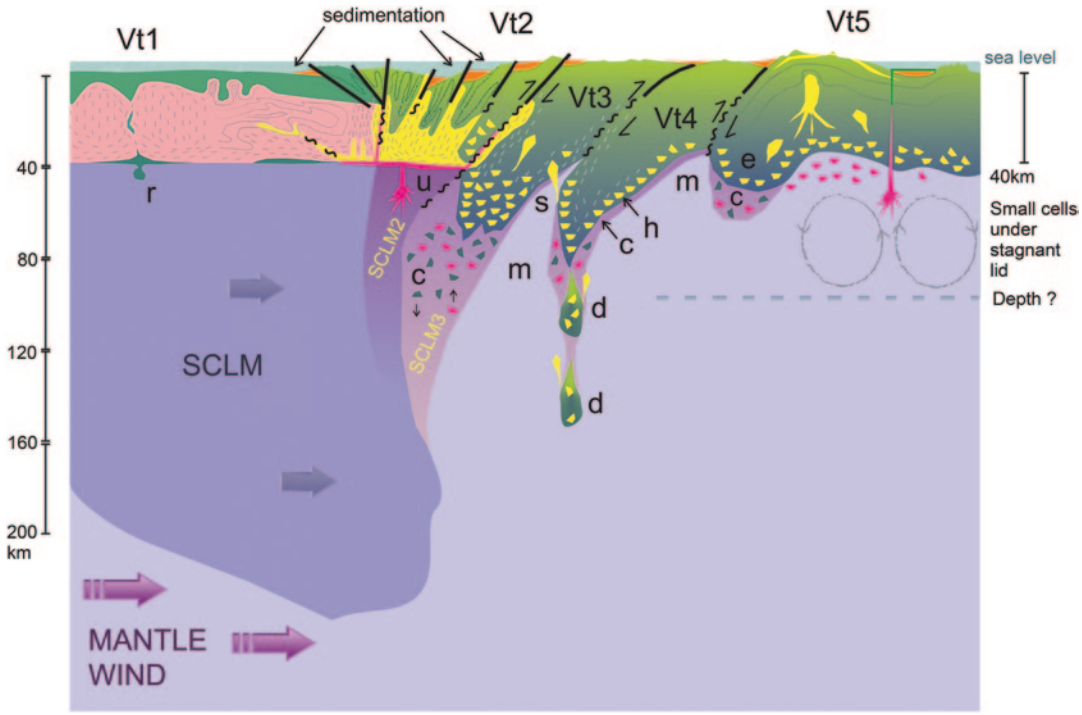

Fig. 9.1 Cartoon illustrating and developing the cratonic mobilism model of Bédard et al. (2013), emphasizing the sequential development of subcreted basaltic slivers ahead of the migrating cratonic mass (adapted from fig. 11 in Bédard et al. 2013): An older craton has an old sub-continental lithospheric mantle keel (SCLM) that is affected by mantle traction forces and is moving towards the right in the figure. The upper crust is composed of basalt-dominated lava sequences (*green Vt1 = volcanic terrain 1*) that have partly foundered into the soft granitoid lower crust (*pink*). Dashed lines highlight the zone of vertical mass transfer of the middle crust *vs* the flat foliations of the lower crust. The craton's leading edge is a region of compressional tectonics, with extensive flattening in the mid and lower crust, and horizontal translation in the distal ductile lower crust. Tectonic uplift and erosion generate flysch basins (*orange*). Volcanic terrains 2 to 5 mark a gradation between distal, essentially undeformed oceanic plateau-type crust (*Vt5*), to strongly deformed crust that is now welded onto the leading edge of the craton, which is rooted in a younger belt of lithospheric mantle (SCLM2). Vt3 and Vt4 are two slivers of 'subcreted' basaltic crust, separated locally by thin slivers of mantle (m). Vt5 shows a roughly steady state oceanic plateau type crust, with underplating and eruption of juvenile basalt (*red*) building up a thick plateau. Lower crustal anatexis generates juvenile TTG magmas (*yellow*), while delamination of densified lower crustal restites and cumulates (dark green) thins the crust. The subjacent convecting mantle melts to form normal Archaean tholeiites (*red blobs*). The down warped edge of this basaltic plateau crust (**e**) is melting at high P (*yellow blobs*) and releasing garnet pyroxenite restites into the subjacent mantle, which may generate additional increments of basalt (**c**), as per Bédard (2006).Vt4 shows a more advanced stage of subcretion of a segment of crust originally similar to Vt5. Melting is concentrated at the edges of the downthrust mass as a result of thermal conduction from the mantle (**h**) and internal radioactive heating. TTG melts that segregate might react with the intercalated septa of mantle rocks (m). Thermal softening could allow the end of this basaltic wedge to drip off into the mantle (**d**), where it might experience enhanced melting, allowing felsic melt to pass through mantle rocks and react with them (*yellow blebs escaping* **d**). As for Vt5, the mantle beneath the downthrust basalt (**c**) would be a zone of eclogite pollution and 2nd stage mantle melting. Vt3 shows a more advanced stage where melting of the downthrust basalt is far advanced. Large bodies of TTG melt have segregated and restitic eclogite has extensively polluted the subjacent mantle, allowing extraction of 2nd stage basaltic melts, and forming a domain of strongly depleted mantle that will cause the SCLM to grow outwards (SCLM3). Vt2 represents a plateau basalt terrane that has been completely integrated into the craton. All deeply thrust basalt has melted and differentiated. Anatectic TTG has isostatically reequilibrated with the subjacent mantle to form a flat Moho. The delaminated garnet pyroxenite restites have reacted with the convecting mantle beneath to form a belt of strongly depleted SCLM (SCLM2)

sponse to basal traction can provide the driving force for the leading-edge imbrication of oceanic lithospheric slabs and tectonic thickening of oceanic-plateau type crust, obviating this problem (Fig. 9.1). If the subcreted material is dominated by fertile Archaean tholeiites (with isolated intercalated felsic horizons), then this would provide an ideal source for voluminous TTG pulses. The new subcretion model yields a geochemical product that is very similar to the adakite model (e.g. Martin et al. 2005). However, unlike the adakite model, we do not think that the subcreted basalt melts as a result of diffusive heat transfer into a subducting oceanic slab from a superjacent convecting mantle wedge. Instead, we suggest that it would melt in response to radioactive heating and thermal diffusion/advection from the underlying and adjoining convecting mantle. Similar TTG-like magmas form in some Phanerozoic plutonic belts (e.g. Girardi et al. 2012), but these are cases where continental drift (due to mantle traction forces?) have led to high-P melting of a thickened basaltic welt, and so are more like Archaean environments than 'normal' subduction-related magmas. Our revised interpretation of the subcretion model presented in Fig. 9.1 comprises the following elements:

- An older craton has an old sub-continental lithospheric mantle keel (SCLM) that is affected by mantle traction forces and is moving towards the right in the figure. The upper crust is covered by basalt-dominated lava sequences that have partly foundered into the soft granitoid lower crust. The continental crust located closest to the craton's leading edge is a region of compressional tectonics, with extensive flattening in the mid and lower crust, and horizontal translation in the distal ductile lower crust. Transient tectonic uplift and erosion generate localized flysch basins. Volcanic terrains 2 to 5 mark a gradation between distal, essentially undeformed oceanic plateau-type crust (Vt5), to strongly deformed crust that is now welded onto the leading edge of the craton, which is rooted in a younger belt of lithospheric mantle (SCLM2). Vt3 and Vt4 are two slivers of 'subcreted' basaltic crust, separated locally by thin slivers of mantle (m).
- Vt5 shows a roughly steady state oceanic plateau type crust, with underplating and eruption of juvenile basalt building up a thick plateau. This stagnant lid domain would be underlain by small-scale convection cells; and would not show systematic differentiation since the basal crust would be recycled as fast as new crust is generated by eruption. The absence of a stable lithospheric mantle would allow thermal erosion of the lower crust. Anatexis of the basal crust would generate juvenile TTG magmas that develop incipient dome-and-keel structures, while delamination of densified lower crustal restites and cumulates thins the crust. The subjacent convecting mantle melts to form 'normal' Archaean tholeiites. The downwarped edge of a basaltic plateau crust (e) would be preferentially heated by the surrounding mantle and melt more. Delaminated garnet pyroxenite restites would contaminate the subjacent mantle and may generate small additional increments of basaltic melt (c), as per Bédard (2006).
- Vt4 shows a more advanced stage of subcretion of a segment of crust originally similar to Vt5. Melting is concentrated at the edges of the downthrust mass as a result of thermal conduction from the mantle (h) and internal radioactive heating. TTG melts that segregate might ascend and could locally (s) react with the intercalated septa of mantle rocks (m). Thermal softening (cf. van Hunen and Moyen 2012) may allow the end of this basaltic wedge to drip off into the mantle (d), where it might experience enhanced melting, allowing felsic melt to pass through mantle rocks and react with them. As for Vt5, the mantle beneath the downthrust basalt (c) would be a zone of eclogite pollution and 2nd stage mantle melting.
- Vt3 shows a more advanced stage. Melting of the downthrust basalt is more advanced, and large bodies of TTG melt segregate. Much of the deeply thrust crust has melted and restitic eclogite has extensively polluted the subjacent mantle, allowing extraction of 2nd stage basaltic melts, and forming a domain of strongly depleted mantle that may cause the SCLM to grow outwards (SCLM3). Gravita-

tional instability following delamination of the lowermost material may result in exhumation of down-thrusted material, explaining the extremely rare high-P assemblages described in the Barberton terrane of South Africa by Moyen et al. (2006).

- Vt2 represents a plateau basalt terrane that has been completely integrated into the craton. All deeply thrust basalt has melted and differentiated. Anatectic TTG has isostatically reequilibrated with the subjacent mantle to form a flat Moho. The delaminated garnet pyroxenite restites have reacted with the convecting mantle beneath to form a belt of strongly depleted SCLM (SCLM2).

The internal structure of Archaean cratons also seems inconsistent with what is expected during Phanerozoic-style orogenesis. Almost without exception, the older parts of cratons are characterized by the dome-and-basin pattern of the granite-greenstones, a pattern that is not seen in Phanerozoic orogens (MacGregor 1951; Anhaeusser et al. 1969; Choukroune et al. 1995; Goodwin 1996; Chardon et al. 1996, 1998; Hickman 1984; Collins et al. 1998; Van Kranendonk et al. 2007b; Van Kranendonk 2011a; Thurston et al. 2008). The widespread steeply dipping foliations with sub-vertical stretching lineations found in many Archaean TTG terrains and distributed thickening, folding, and transpressional shearing during ductile flow of the deep crust (e.g. Cagnard et al. 2006b), are not consistent with Phanerozoic accretionary or Alpine-style tectonics, where thrust-and-fold belts and thick-skinned structures that exhume deeply-buried crust and mantle rocks are ubiquitous, or where metamorphic domes form due to crustal extension during post-orogenic collapse. Instead, the widespread vertical and horizontal stretching (Chardon et al. 2011) and evidence for synchronous magmatism imply a very soft Archaean crust and/or SCLM (Chardon et al. 2002, 2008, 2011; Rey and Houseman 2006; Cagnard et al. 2006b; Bédard et al. 2013). The dome-and basin pattern is commonly explained as the result of partial convective overturn, with thick accumulations of dense basaltic rocks erupted above soft buoyant TTG crust going unstable and foundering as Rayleigh-Taylor instabilities (Mareschal and West 1980; Collins et al. 1998; Bailey 1999; de Brémond d'Ars et al. 1999; Bédard et al. 2003; Robin and Bailey 2009; Thébaud and Rey 2012; Van Kranendonk 2011a). Where strong overprints are lacking, the textures and structures attendant to vertical motion are clear and generally imply that the synclinal basins were sinking, while the felsic domes were rising and sometimes broached the surface to be eroded into the adjoining troughs. Opening out and reorientation of early-formed, regular antiforms during extrusive channel flow is proposed by Harris et al. (2012) as an alternative mechanism for forming dome and basin structures in Neoarchaean terrains. Channel flow induced by erosion of an orogenic front may also explain the juxtaposition of granite-greenstone and high-grade gneiss terrains (Harris et al. 2012).

Since the evidence for Phanerozoic-style subduction, seafloor spreading, and orogenesis is essentially absent, while evidence against these processes is abundant, alternative non-uniformitarian mechanisms are needed to generate the cratonic crust and lithospheric mantle, and for the development of contractional fabrics, regional shear zones, and for the accretion of terranes. In this paper we will not reiterate the case against Phanerozoic-style plate tectonics (see Bédard 2003, 2006, 2013; Bédard et al. 2003, 2013 and references therein), but adopt the alternative tectonic interpretation for Archaean orogenesis and terrane accretion of Bédard et al. (2013). We suggest that some Neoarchaean greenstones are samples of the Archaean Earth's non-cratonic crust and discuss implications of this. Parallels are made with deformation on Venus where structures similar to those of Archaean terrains formed in the absence of plate tectonics. We show that plate tectonics is not required to produce the constituent lithologies of greenstone belts, nor is it needed to explain the regional deformation of Archaean granite-greenstone terrains. The SE Superior Craton of Canada is presented as an example.

9.1.3 Origin of Cratonic Crust

Experimental data and trace element signatures of Archaean TTGs imply they were ultimately

derived by anatexis of metabasalt at pressures sufficient to stabilize residual garnet and titanate minerals at a depth of 40–60 km (see reviews in Moyen 2009, 2011). The secular increase in K-content of Archaean felsic plutons is thought to reflect buildup of incompatible elements like K during repeated anatexis of the sialic component of the crust (Davis and Edwards 1986; Taylor and McClennan 1986; Stern and Hanson 1991; Collins 1993; Wyborn 1993; Champion and Sheraton 1997; Stevenson et al. 1999; Moyen et al. 2001; Whalen et al. 2004; Martin et al. 2005; Bédard 2006). Isotopic and inherited zircon data are consistent with this concept, and require repeated addition of juvenile mafic magma to a TTG crust that remelts frequently (McCulloch and Wasserburg 1978; Gariépy and Allègre 1985; Bickle et al. 1989; Hill et al. 1989; Collins 1993; Wyborn 1993; Stern et al. 1994; Champion and Sheraton 1997; Ridley et al. 1997; Whitehouse et al. 1998; Leclair et al. 2001; Tomlinson et al. 2004). If there were no subduction zones to focus heat and magma, what options remain for the generation of such thick basaltic piles, and for melting them in bulk? There are three main hypotheses:

1. Bolide impact. This suggests that a large impactor generated a very large amount of melt and complementary residual mantle (e.g. Abbott and Isley 2002; Elkins-Tanton et al. 2004; Elkins-Tanton and Hager 2005; Jones 2005; Hansen 2007a; Darling et al. 2009). While this is not unrealistic in terms of generating a large first pulse, it does not explain the magmatic cyclicity that characterizes most cratonic suites (e.g. Ayer et al. 2002; Van Kranendonk et al. 2002, 2007b; Leclerc et al. 2011), or the progressive development of recycling signatures in volcanics (e.g. Champion and Sheraton 1997; Ayer et al. 2002; Boily et al. 2009).
2. Tectonic thickening of supracrustal packages. This could occur above double-sided Rayleigh-Taylor instabilities (Davies 1992; Chardon et al. 1996; Pysklywec et al. 2010). In this scenario, the lithosphere does indeed go unstable, but unlike Phanerozoic, one-sided convection, both 'plates' sink together, leaving an accumulation of supracrustal rocks above the convergence zone, while the dense lithospheric mantle that drives 'subduction' plunges into the deeper mantle (Elkins-Tanton, 2007; Pysklywec et al. 2010; Gorczyk et al. 2012; Moyen and van Hunen 2012). These gravity-driven processes may have produced shortening in the upper crust as it piles up above a downwelling zone (Houseman and Houseman 2010). However, this model predicts a pattern of outward younging and the development of outwardly-vergent thrusts around an orogenic core, a pattern that is unlike Archaean cratonic collages. This model also presupposes the existence of an oceanic crust and lithosphere that has the capacity to founder in an organized way into the underlying lower mantle; which is at odds with thermomechanical models (e.g. Sizova et al. 2010). Alternatively, tectonic thickening of basaltic plateau-type crust could occur at the leading edge of a migrating Archaean craton (Fig. 9.1), or by 'pop-down thrusting' of the brittle crust during flow of the ductile crust±SCLM (c.f. analogue models of Cagnard et al. 2006a).
3. Development of an unusually thick (>40 km) constructional volcanic pile above major mantle upwelling zones leading to anatexis of the basal crust, perhaps triggering initiation of an auto-catalytic differentiation cycle as suggested by Bédard (2006). The Ontong-Java basaltic plateau has a ca. 35 km thick crust (up to 38 km according to Richardson et al. 2000), and it seems reasonable to suppose that in a hotter Archaean Earth, significantly thicker basaltic piles might have formed, allowing basal anatexis in the garnet field. Calculations by Bédard et al. (2013) suggest that a magmatic flux similar to that of Hawaii might have constructed a 60 km thick crust in less than 20 My. This scenario also accounts for coeval generation of the continental crust and mantle, magmatic cyclicity, secular K-enrichment of the TTGs, and disposes of the eclogitic restites (Bédard 2006). Alternatively, catastrophic breakdown of layered convection, or avalanches of perched basaltic slabs into the lower mantle have been suggested (Stein and Hofmann 1994; Condie 1998; Rino et al. 2004; Davies 2008) to explain unusually large melt delivery pulses.

We think that repeated melting events focussed above a long-lived, plume-like mantle upwelling zone represent the most likely mechanism for the development of an early cratonic nucleus (hypothesis iii). Bédard et al. (2003), Bédard (2006), Smithies et al. (2005b), Van Kranendonk et al. (2007b), and Champion and Smithies (2007) suggested that the recycling seen in the TTGs is probably the result of repeated under- and intraplating of the sialic crust by coeval basaltic and komatiitic magmas, coupled with thermal incubation of radioactive elements. Repeated foundering of the basaltic volcanics erupted atop this maturing craton into the underlying TTGs would have generated the early dome-and-basin pattern. In mature cratons repeated recycling events would have obliterated the original protoliths, such that all that would remain is a super-mature association of young TTG and granite generated by remelting of older TTGs (cf. Hoffmann et al. 2011), and young basalts with strong crustal contamination signatures. Foundering of crustal restites into the mantle might have catalyzed development of the SCLM (Bédard 2006) from the top-down. These early events would have generated a cratonic block with a deep, stiff keel.

9.1.4 Ophiolites, Oceanic Plateaux, and Greenstone Belts

Dilek and Furnes (2011) defined an ophiolite as: 'an allochthonous fragment of upper-mantle and oceanic crustal rocks that is tectonically displaced from its primary igneous origin of formation as a result of plate convergence. Such a slice should include a suite of, from bottom to top, peridotites and ultramafic to felsic crustal intrusive and volcanic rocks (with or without sheeted dikes) that can be geochronologically and petrogenetically related; some of these units may be missing in incomplete ophiolites.'

The two most recent proposals for Archaean ophiolites formed by seafloor-spreading are the Dongwanzi (ca. 2.5 Ga) and Isua (ca. 3.8 Ga) complexes. The reason why these have received so much attention is that both were proposed to have sheeted dyke complexes, which represent a strong argument in favour of a seafloor spreading origin, which in turn implies the operation of plate tectonics. In the Isua case, Friend and Nutman (2010) showed that the sheeted dykes of Furnes et al. (2007a, b) are highly deformed ca. 3510 Ma Ameralik dykes emplaced into a previously deformed, older sequence of meta-volcanics, and that there are few connections between proposed plutonic, dyke, or volcanic components. The small, refractory (Fo_{92-96}) peridotite boudins embedded in a complex meta-volcanic schist that were interpreted as mantle rocks by Friend and Nutman (2010) could simply be olivine-rich cumulates formed in sub-volcanic sills (e.g. Bédard et al. 2007, 2009). Consequently, we must conclude that Isua is not an ophiolite by any definition. Dongwanzi is presented as a 2.505 Ga ophiolite by Kusky et al. (2001), Kusky (2002), and Kusky and Li (2008), which is supported by the interpreted sheeted dykes and refractory mantle containing nodular chromite deposits. Its age is, however, problematic (Zhao et al. 2008), and the interpretation of sheeted dykes is questioned by Zhai et al. (2002). If the proposed age and designation as an ophiolite are indeed correct, then 2.5 Ga (i.e. the Archaean-Proterozoic transition) is the most ancient preserved manifestation of seafloor-spreading.

Dilek and Furnes (2011) argue that fragments of oceanic plateaux may also be obducted/ accreted to a continent and propose that these be called 'plume ophiolites'. They state: 'Typically, a plume-related ophiolite is characterized by massive basaltic lava flows with subordinate pillowed flows, the occurrence of picritic basalts, and minor sedimentary deposits, all intruded by gabbroic plutons and sills and locally by ultramafic sills'. Many greenstone belt packages fit this description and have been likened to oceanic plateau-type crust. The main reason for the comparison is that oceanic plateaux (e.g. Coffin and Eldholm 1994; Coffin and Gallagan 1995; Neal et al. 1997; Hoernle et al. 2010; Kamber 2010) are the closest modern analogues to simatic supracrustal sequences dominated by basalt with subordinate komatiite, and starved of terrigenous input like the Abitibi and many other greenstone belts (e.g. Campbell et al. 1989; Kusky and Kidd 1992; Ernst and Buchan 2003; Arndt 2003; Condie 2003; Sandiford et al.

2004; Chavagnac 2004; Benn and Moyen 2008; Furnes et al. 2011).

The problem here is that very similar packages also form in clearly ensialic contexts (e.g. Nisbet et al. 1993b; Van Kranendonk et al. 2007a; Maurice et al. 2009; Smithies et al. 2009; Tessalina et al. 2010), so that in tectonically disrupted greenstone belts, any thick basaltic pile can be misidentified as a plume-type ophiolite. An additional problem is the nature of the 'common' Archaean tholeiites, many of which are interbedded with felsic magmas, have negative Nb-Ta anomalies, and show weak LILE and LREE enrichment. While many interpret the chemical signatures of these tholeiites (e.g. Polat and Kerrich 2000, 2001; Wyman and Kerrich 2009) as evidence of their formation in an arc context, the systematics of their elemental trends differs from that of Phanerozoic arcs and is better explained as the result of crustal assimilation (e.g. Pearce 2008; Maurice et al. 2009; Bédard et al. 2013).

Although it is clear that many Archaean shields represent tectonic collages, we believe that terrane accretion occurred at the leading edge of migrating cratonic nucleii (Fig. 9.1), not as a result of terrane accretion during conveyer-belt subduction beneath the craton. These accreted basaltic plateau-type crustal blocks could be considered as plume-type ophiolites as per the Dilek and Furnes (2011) definition, but we think that applying this classification to Archaean packages would be very subjective. Furthermore, we suspect that use of the term 'ophiolite' for juvenile simatic basaltic plateau crust would give the incorrect impression that uniformitarian-type plate tectonic processes were active.

9.1.5 Generation of Voluminous Felsic Magmas in the Absence of Abundant Water.

The subduction of hydrated oceanic crust plays an important role in the generation of voluminous convergent margin felsic magmas today. The efflux of water and other components is thought to trigger mantle melting, and generates basalts, boninites and andesites with significant water-contents (2–8% H_2O; Zimmer et al. 2010; Parman et al. 2011), which propagate to even higher water contents in derivative fractionation products. Anatexis of arc-related magmatic rocks generates 2nd-stage melts (granites, granodiorites) that are also water-rich. Proponents of Archaean subduction apply this actualistic model to explain the presence of voluminous felsic magmas in Archaean terrains, an interpretation that we dispute.

Although many voluminous post-Archaean felsic plutonic and volcanic suites are arc-related, there are also areas where voluminous water-poor felsic magmas exist. In many cases, there is no association with active margins and an ultimate plume source is posited. For example, large volumes of hot (800–1000 °C) rhyolitic lava are associated with the Snake River Plain and Yellowstone systems (Cathey and Nash 2004; Branney et al. 2008; McCurry et al. 2008; Ellis et al. 2011). Weakly hydrous felsic melts coexist and commonly mix with the dry ones and are thought to represent remelts of surrounding host rocks, or reworking of older consanguineous intrusions that interacted with the hydrosphere. The generation of voluminous felsic melts in these contexts is due either to extensive fractional crystallization, or to dry anatexis. Either way, the voluminous dry hot felsic magmas require a correspondingly large basaltic flux to provide the requisite heat energy (e.g. Annen 2011)

The other voluminous occurrence of dry granitoid magma is the so-called Proterozoic AMCG suite (AMCG=anorthosite-mangerite-charnockite-granite/gabbro). The huge anorthositic massifs are commonly surrounded by sheaths/ caps of pyroxene granitoids (e.g. Frost and Frost 2008; Bédard et al. 2010; Frost et al. 2010; Hegner et al. 2010). In some cases it is possible to demonstrate that the px-granitoids are the residues of extensive fractionation (or AFC) of basaltic-jotunitic magmas (e.g. Duchesne and Wilmart 1997; Wilson and Overgaard 2005; Namur et al. 2011). Whether or not plumes are involved in generating some AMCG suite rocks is still uncertain, and formation of Proterozoic AMCG massifs during post-orogenic collapse (e.g. Grenville Province; Corrigan and Hanmer 1997) suggests that a convective thinning or delamination origin is also involved. It is clear that many of the felsic rocks are the result of (at least) 2-stage histories, involv-

ing lower crustal anatexis of older rocks (Bédard 2001, 2010; Hegner et al. 2010), while many of the associated gabbroic to troctolitic plutons are plutonic equivalents of continental flood basalts (Bédard 2001; Namur et al. 2011). This implies that, like the Yellowstone-Snake River Plain rhyolites, the voluminous pyroxene-granitoids of the AMCG suite require the voluminous emplacement of basalt into the lower-middle crust.

A third voluminous occurrence of hot, dry pyroxene-granitoids is the Archaean enderbite-charnockite plutonic suite (enderbite = px tonalite). The best documented example is from the North Eastern Superior Province (NESP), where about 25 % of the exposed crust is enderbitic, with subordinate charnockite, mostly emplaced at 2.74-2.72 Ga (Percival and Mortensen 2002; Bédard 2003; Bédard et al. 2003; Leclair 2005). Geothermometric calculations imply emplacement at temperatures of about 900–1100 °C (Bédard et al. 2003), while Percival and Mortensen (2002) infer a low H_2O content. The enderbite suite was emplaced synchronously with an equally large pulse of more conventional TTGs (ca. 850 °C emplacement temperature) which contain hornblende and biotite. Bédard (2010) suggested that the NESP enderbites represent bulk remelts of older TTGs, triggered by large-scale under- and intra-plating by primitive basaltic to komatiitic magmas. Here too, the essential element seems to be a very large flux of primitive mantle-derived melt.

9.2 Venus—An Analogue for the Archaean Earth

9.2.1 Similarities and Differences between Venus and an Archaean Earth

Venus[1] (Fig. 9.2) is commonly proposed as an analogue for the Archaean Earth (e.g. Anderson 1981; McGill 1983; Morgan 1983; Sorohtin and Ushakov 2002; Stern 2004; Hansen 2007b; Head et al. 2008; Van Kranendonk 2010). Differences between Venus and Earth are summarized in Appendix 1. The most significant differences for comparative geological studies are:

- Characteristic features of Earth-like plate tectonics, such as 'modern-style', single-sided subduction (as defined by Sizova et al. 2010 and Bédard et al. 2013), arcuate chains of volcanoes and deep trenches indicative of subduction zones, linear volcanic rises offset by transform faults (as developed during seafloor-spreading on Earth), and 'jigsaw' fits between continent-like 'plana', have never been identified on Venus, nor is there evidence that plate tectonics occured in Venus' past[2] (Anderson 1981; Kaula and Phillips 1981; Phillips et al. 1981; Solomon et al. 1991, 1992; Phillips and Hansen 1994; Grimm 1998; Nimmo and McKenzie 1998; Smrekar et al. 2007).
- Surface temperatures for an Archaean Earth are estimated at -0.15 °C to ca. 20 °C (Haqq-Misra et al. 2008) compared to present temperature of ca. 460 °C on Venus (NASA undated). These values are consistent with evidence for surface water being present on an Archaean Earth (Sagan and Mullen 1972; Valley et al. 2002) whereas surface water is absent on Venus. Water is, however, detected in Venus' atmosphere (Bézard et al. 2009) and hence there may be, or have been, hydrous minerals present in the crust. Because of the elevated surface temperature, at least half the thickness of Venus' crust may exhibit semi-brittle (i.e. brittle-ductile) behaviour (Kohlstedt and Mackwell 2009), so structures observed in radar imagery of the surface of Venus are equivalent to structures that would occur at deeper crustal levels for Earth.

[1] See reviews by Phillips et al. (1981); Nikishin (1990); Schaber and Kozak (1990); Solomon et al. (1991, 1992), Phillips and Hansen (1994), Basilevsky and Head (2003); Hansen and Young (2007); and Ivanov and Head (2011) for descriptions of the geology and tectonics of Venus and Ivanov and Head (2011) for a global Venus geological map.

[2] Venus may, however, theoretically have had a period of plate tectonics during its early history (van Thienen et al. 2005), for which no evidence remains following its resurfacing.

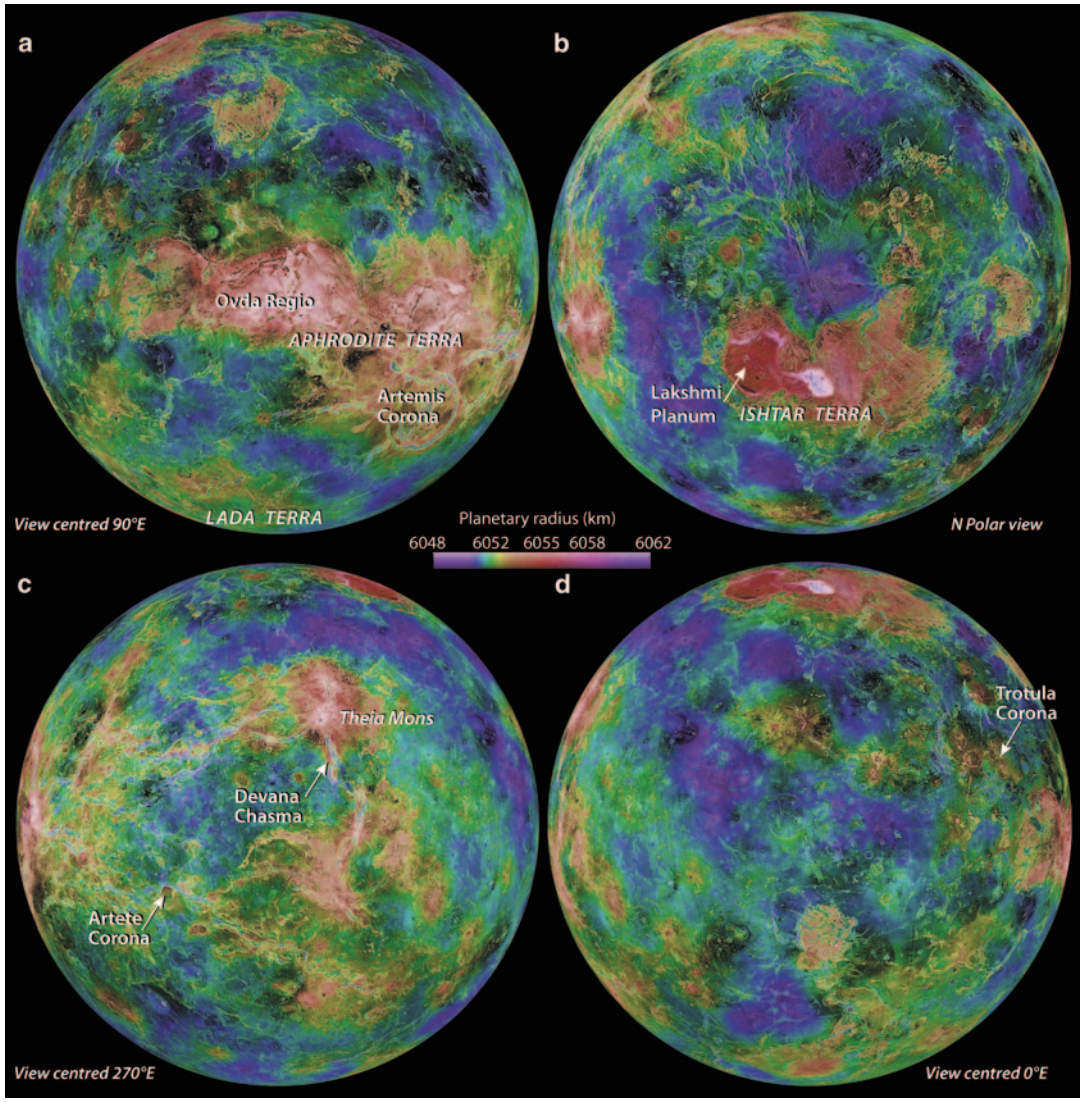

Fig. 9.2 Hemispherical views of Venus derived from a mosaic of Magellan radar imagery, with topography from Magellan radar altimetery. Labelled features are referred to in the text. Images were produced by the U.S. Geological Survey Astrogeology Science Center and made available through NASA Jet Propulsion Laboratory, California Institute of Technology

- Due to the lack of seismic studies on Venus, its deep structure and rheological strength profiles are uncertain. Venus is thought by some to lack an aesthenosphere (Phillips and Hansen 1994; Smrekar et al. 2007) as is present on Earth. Weertman (1979) and Bindschadler et al. (1992) propose that Venus has a more ductile crust and upper mantle, with less of a rheological contrast between lithosphere and underlying mantle than on Earth. Kiefer (1991), however, suggests that upper mantle viscosities are greater on Venus than for the present-day Earth and similarly, Smrekar et al. (2007) propose a stronger lithosphere for Venus based on the low water content of its interior. Until further exploration is undertaken that includes surface seismometers capable of withstanding the high temperatures (as pro-

posed by Crisp et al. 2002) and/or balloon EM sounding (Grimm et al. 2012), Venus' crustal thickness and rheological profile will remain the subject of debate. Even for Earth where so much data exists, 'crème brûlée' and 'jelly sandwich' strength profiles are still debated (e.g. Burov and Watts 2006; Burov 2010), so uncertainties on Venus are not unexpected.

- The thickness of Venusian thermal lithosphere also remains a subject of contention, with both Phanerozoic Earth-like (ca. 100 km) and greater (>200 km) thicknesses, i.e. comparable to Archaean cratonic keels, being proposed (Brown and Phillips 1999). Progressive cooling and thickening of the Venusian lithosphere is thought to have occurred over the past several hundred million years (Grimm 1998; Brown and Grimm 1999; Krassilnikov et al. 2012).

A resurfacing event ca. 500 My ago is proposed for Venus based on analysis of impact crater density (Schaber et al. 1992; Namiki and Solomon 1994; Turcotte et al. 1999). Catastrophic resurfacing of the whole of Venus' surface is, however, questioned by Hansen and Young (2007) based on their detailed geologic mapping and analysis. Without catastrophic resurfacing, the lack of plate tectonics on Venus means that features formed early in its history may be preserved (Hansen 2007a, b). A model of 'pulsating continents' and 'global, instantaneous subduction' proposed by Romeo and Turcotte (2008) also calls for the preservation of crustal plateaux. 'Global, instantaneous subduction' of Romeo and Turcotte (2008) has no similarity to present-day subduction on Earth, and appears equivalent to models for catastrophic resurfacing and convective overturn cited above. In the model of Romeo and Turcotte (2008), continent-like plateaux survive this 'convective overturn', and may undergo radial shortening during inward-directed flow during delamination of lithospheric mantle beneath the centre of plateaux, akin to 'mantle drip' models of Pysklywec et al. (2010), Gorczyk et al. (2012), and Moyen and van Hunen (2012). Radial extension is proposed by Romeo and Turcotte (2008) after the 'mantle drip' detaches.

In the following sections, we review the form, scale, and geometry of folds, brittle-ductile shear zones and faults on Venus, and conclude that they are much like crustal structures on Earth, permitting direct comparisons to be made. Although subduction, arc magmatism, and arc accretion are proposed for the Archaean Earth (as reviewed by Cawood et al. 2006 and discussed above), others contend that arc tectonics and modern-style subduction processes did not take place in the Archaean (e.g. Hamilton 1998; Sorohtin and Ushakov 2002; Bédard et al. 2013, and references therein). As expressed by Hansen (2007b), comparisons between the geology of Venus and Archaean granite-greenstone belts on Earth may thus help resolve the debate whether plate tectonics is required to produce the structures observed in Archaean terrains on Earth.

9.2.2 Mantle Plumes on Venus and Earth

Mantle plume-driven deformation and plate tectonics result from two distinct modes of convection (Hill et al. 1992). In contrast to an active lid convective regime with mobile plates on Earth, only ascending hot and descending cold plumes develop under the stagnant or fixed lid convection regime on Venus (Solomatov and Moresi 1996; Kameyama and Ogawa 2000; Schubert et al. 2001). Lithospheric deformation and mantle convection on Venus are strongly mechanically coupled (Herrick and Phillips 1992; Bindschadler et al. 1992; Kohlstedt and Mackwell 2009) as there is no low viscosity zone equivalent to the aesthenosphere on Earth. Regional and planetary-scale tectonics should therefore directly reflect underlying mantle convective processes (Kohlstedt and Mackwell 2009).

A mantle plume (Phillips and Hansen 1994; Ernst and Desnoyers 2004) or hot mantle diapir (Krassilnikov et al. 2012) origin is proposed for many volcanic features on Venus, such as novae and coronae[1,3] (Fig. 9. 2c, d) and mantle plumes and plume-related volcanism are the main mech-

[3] Tectonic features interpreted from Magellan radar imagery (Saunders 1992) and definitions of terms used are summarized by Stofan et al. (1993).

anisms for lithospheric heat transfer on Venus (Solomon and Head 1982; Schubert et al. 2001). Evidence for mantle plumes on Venus also comes from analysis of Venus' gravity field and topography (Smrekar and Sotin 2012). Uplift above plumes has been proposed as the mechanism for equatorial highlands on Venus (Kiefer 1991; Kiefer and Hager 1991a; Phillips et al. 1991; Ghent and Hansen 1999; Vezolainen 2003). Upwelling mantle plumes have also been proposed for crustal thickening and formation of crustal plateaux (Phillips et al. 1991), although these are attributed to 'coldspots' or mantle down-welling by Bindschadler et al. (1992). The existence of mantle plumes is, however, rejected by Hamilton (2005) who proposes an impact origin for features attributed to plumes on Venus. Whilst there is evidence for bolide impact on Venus, as well as on an Archaean Earth (e.g. Anhaeusser et al. 2010), we adhere to the non-impact interpretations for the formation of coronae.

Although subject to debate (e.g. the presence of plumes on Earth is also denied by Hamilton 2005, 2011), like Venus, mantle plumes are proposed to have played an important role in the formation of many Archaean granite-greenstone terrains on Earth (Tomlinson and Condie 2001; Rey et al. 2003; Pirajno 2007), especially in the formation of oceanic plateaux from which the cratons ultimately formed (e.g. Smithies et al. 2005a). Mantle plume-related komatiite—basalt volcanism is proposed for the Yilgarn Craton and Superior Province (Polat et al. 1999; Polat and Kerrich 2000; Dostal and Mueller 2013) and for the NW Baltic Shield by Puchtel et al. (1998). The Palaeoarchaean Pilbara Craton, the Mesoarchaean Superior Craton and elements of the Baltic Shield and areas of Neoarchaean crust are proposed by Van Kranendonk (2010) as examples of thick volcanic plateaux formed over hot, upwelling mantle plumes. Rey et al. (2003) suggest that thermal blanketing created by greenstone sequences above mantle plumes led to extensive reworking of continental crust between 2.75 and 2.65 Ga in Archaean cratons, such as the Superior and Yilgarn. Whilst plume activity in the Archaean Earth is thought to co-exist with plate tectonics by some researchers (e.g. Barley et al. 1998; Mueller et al. 1996), plumes, and gravitational potential resulting from uplift above plumes, are generally regarded as the sole driving forces for deformation on Venus. Venus therefore provides a unique opportunity to establish what types, scales, and geometries of structures are possible in the absence of modern plate tectonics and thence to determine if subduction and accretion at convergent margins are required to produce comparable structures on the Archaean Earth.

9.2.3 Upland Plateaux and Highlands on Venus—Equivalent to Early Continents or (proto-) Cratons on Earth?

Although the crust of Venus is thought to be composed dominantly of basalt (Head 1990a; Grimm and Hess 1997), the presence of felsic 'continental-like' crust is also postulated (Nikolayeva 1990; Jull and Arkani-Hamed 1995; Turcotte 1996; Romeo and Turcotte 2008; Bonin et al. 2002). Upland plateaux or highlands (defined as areas ca. > 2 km greater than the mean planetary radius; Phillips and Hansen 1994), including Ishtar Terra and Aphrodite Terra (Fig. 9.2a, b), are suggested as possible equivalents to continents on Earth (Marchenkov et al. 1990; Nikishin 1990; Turcotte 1996; Schubert et al. 2001 chapter 14; Romeo and Turcotte 2008). Jull and Arkani-Hamed (1995) and Turcotte (1996) liken the highland areas Ishtar Terra and Aphrodite Terra (Fig. 9.2a, b) to Archaean cratonic nuclei. As for cratons on Earth, analysis of gravity data by Janle and Jannsen (1986) and Marchenkov et al. (1990) suggests areas of thick crust are present beneath them (estimated at 60–80 km deep under Ishtar Terra and 70–80 km under Aphrodite Terra[4]). These values agree with estimates of Bleamaster and Hansen (2004) of average plateau thicknesses of 35–80 km compared to ca. 20 km for plains. Despite the absence of plate tectonics, relative displacement of 'continent-like' high-

[4] Such gravity interpretations are not, however, unique as the subsurface density distribution is unknown.

land areas without subduction is proposed by Nikishin (1990 and references therein; discussed in Sect. 3) in a fashion analogous to polar 'icepack tectonics' (Noltimier and Sahagian 1992), i.e. similar to the cratonic mobilism model of Bédard et al. (2013) for the Archaean Earth.

Analyses of Russian (Venera and Vega mission) samples collected in plains and 'wrinkle ridges'[3] suggest the presence of subalkaline tholeiitic basalts, the melting of which may produce rocks similar to Archaean trondhjemites (Bonin 2012). Hess and Head (1990) demonstrate that melting basalt, even under anhydrous conditions, may generate a SiO_2-rich melt and hence trondhjemites, andesites and basaltic andesites may form through melting of the deep crust at the base of thick plateaux and the roots of mountain belts, such as Ishtar Terra. The 'pancake dome' (or 'farrum') form of some lava flows suggests extrusion of silicic magma, and their presence is taken as support for the existence of granitoid batholiths on Venus (see discussions in Bonin et al. 2002 and Bonin 2012).

Near-infrared spectrometer data from the more recent Galileo satellite point towards the highland areas of Venus being composed of felsic rocks while lowlands are dominated by mafic rocks (Hashimoto et al. 2008; Müller et al. 2008), further supporting models where they are compared, respectively, to areas of continental and oceanic crust on Earth. These authors suggest possible implications of there being granite terrains on Venus are that (i) water was present, and (ii) that subduction processes, and hence plate tectonics, operated[5]. The tectonic implications presented by Hashimoto et al. (2008) and Müller et al. (2008) are, however, based largely on the model of Campbell and Taylor (1983) which states that water is required for granite produced during melting of subducted oceanic crust. Models for granite classification and formation have considerably evolved since 1983 and it is now accepted that granite can: (i) be produced in all tectonic settings on Earth and other planetary bodies, and (ii) may be formed under dry conditions, such as established for the formation of lunar granites (Bonin et al. 2002; Bonin 2012; see also Sect. 1.5). On Earth, I-type granites produced by partial melting of igneous rocks may be produced through crustal underplating unrelated to subduction processes (Chappell and Stephens 1988). Dehydration-melting of lower crustal hydrous silicates may generate water-undersaturated granite magma (Whitney 1988) and so water addition from a subduction zone is not required (see also Sect. 1.5 above). Of particular importance to Venus, given the inferred preponderance of plume activity there, is that voluminous, dry granitoids may be formed through differentiation and crustal melting above mantle plumes (Hill et al. 1992; Hill 1993; Campbell 2001; Rey et al. 2003, see above, sect. 1.5). The recent spectrometric evidence for felsic rocks on Venus does not, therefore, imply the existence of subduction processes and plate tectonics there. This agrees with conclusions from other studies of Venus tectonics (cited above) that show no evidence for subduction.

9.2.4 Faulting and Folding on Venus

Because of the limited extent of surface erosion processes on Venus (Ernst et al. 1995), radar imagery from Veneras 15 and 16 (Barsukov et al. 1986), and especially the 1990–1994 Magellan missions (Solomon et al. 1992), where the horizontal resolution of Synthetic Aperture Radar

[5] These interpretations, although contrary to current views on granite genesis, received considerable world-wide press coverage (e.g. Amos 2009; CBC News 2009; Dorminey 2009), especially as the European Space Agency (2009) quotes Müller as saying 'If there is granite on Venus, there must have been an ocean and plate tectonics in the past'. Treiman (2007) also stated that granites 'required abundant water to form', pushing this conjecture even further by suggesting that if granite were discovered on Ishtar Terra it would 'yield evidence on whether Venus once had an ocean, and thus the possibility of life'. A Nature editorial (Dorminey 2009) similarly reported 'granite highlands point to past water — and perhaps life'… Granite (s.l.) genesis does not require plate tectonics and recycling of water between mantle and atmosphere as stated by Dorminey (2009). Similarly, there is no basis from the presence of granites on Venus for comments that 'Venus might have once been almost entirely underwater' (N. Sleep, Stanford University, quoted in Dorminey 2009, and similarly proposed by Gramling (2009).

(SAR) images is 150 m (JPL undated), enables detailed structural interpretation using standard remote sensing techniques (e.g. Drury 1993; Weijermars undated; see Appendix 2). Radar images of Venus' surface reveal complex fault, fracture and fold geometries, volcanoes, lava flows, and impact craters. Folds, thrusts and strike-slip faults identified on Venus since the first radar images became available (e.g. Crumpler et al. 1988) provide unique examples of deformation structures formed without plate tectonics, and hence assist in making and validating tectonic interpretations for a non-uniformitarian Archaean Earth[6].

9.2.4.1 Plume, Intrusion, and Diapir-related Extensional Structures

Radar imagery highlights prominent radiating extensional fractures and/or faults forming novae and arachnoids[3] that radiate over 40 to > 2,000 km from the centre of volcanic uplifts (Janes et al. 1992; Squyres et al. 1992; Stofan et al. 1992; Ernst et al. 1995; Fig. 9.2). Dyke emplacement into radial extension fractures or faults (Parfitt and Head 1993; Ernst et al. 1995) resembles dyke swarms interpreted as radiating outward from mantle plumes on Earth in Archaean (e.g. Olsson et al. 2011) and younger terrains (e.g. Ernst et al. 1995).

Complex circular to elliptical volcano-tectonic features called coronae (Figs. 9.2, 9.3) are common features on Venus (Stofan et al. 1992). Their diameter varies from 60 to 2100 km for the composite coronae Artemis (Figs. 9.3, 9.4a; Sect. 3.3), with an average diameter of 230 km (DeLaughter and Jurdy 1999). Coronae are characterized by an elevated interior, an annular graben and/or ridges (outer rim) 10 to 150 km across and radiating fractures and/or graben (Pronin and Stofan 1990; Stofan et al. 1992, 1993) and may exhibit volcanic features such as lava domes and flows. Corona formation is generally thought to form in response to stresses in the crust developed above an up-welling thermal mantle plume, followed by gravitational relaxation or collapse due to magma withdrawal (Grimm and Phillips 1992; Janes et al. 1992; Squyres et al. 1992; Stofan et al. 1992, 1993; Herrick et al. 2005; Krassilnikov et al. 2012) ± delamination of the lower lithosphere (Smrekar and Stofan 1997). Coronae thus show a similar geometry to ring complexes and calderas on Earth (Glukhovskiy et al. 1986; Bowden et al. 1987; Petters 1991; Obaje 2009). Koch and Manga (1996) and Hoogenboom and Houseman (2006), however, propose an alternative tectonic model where, instead of being created through plume tectonics, domal features on Venus such as coronae may form due to gravitational (Rayleigh–Taylor) instabilities.

9.2.4.2 Rifts and Regionally Extended 'Ribbon' Terrains

Normal faults and graben (chasmata) radiate from and link novae and some coronae (Phillips and Hansen 1994; Krassilnikov et al. 2012; Figs. 9.2, 9.3), although the majority of coronae are not spatially associated with rifts (Krassilnikov et al. 2012). Faults, fractures and dykes radiating from novae are compared to dyke swarms on Earth (Head et al. 1991; McKenzie et al. 1992; Ernst et al. 1995) radiating from hotspots or mantle plumes (Le Cheminant and Heaman 1989; Ernst et al. 1995). These deep rift systems on Venus show geometrical similarities to rifts on Earth (Foster and Nimmo 1996), although there may be less crustal extension across them (Nimmo and McKenzie 1998) since they cannot evolve to a drift stage. In addition to well defined chasmata radiating from or linking novae, broad areas of rifting (e.g. the 115 to 630 km wide Lada Terra highland; Magee and Head 1995) and 'ribbon terrain'[7] are also developed on Venus, and have been compared to the Basin and Range Province of the western USA by Spiricheva and Nikishin (1990).

A consequence of the hotter, more ductile lithosphere on Venus (and for an Archaean Earth) is that homogeneous lithospheric deformation is distributed over large areas (Choukroune et al.

[6] All comparative planetology is, naturally, fraught with inherent uncertainties, as addressed by Baker (2013), so interpretations must remain speculative.

[7] = alternating long (ca. 50–100 km), narrow (ca. 1–3 km), shallow (< 0.5 km) flat-bottomed graben (Hansen and Willis 1998; Phillips and Hansen 1998; Ghent and Hansen 1999; Hansen et al. 1999)

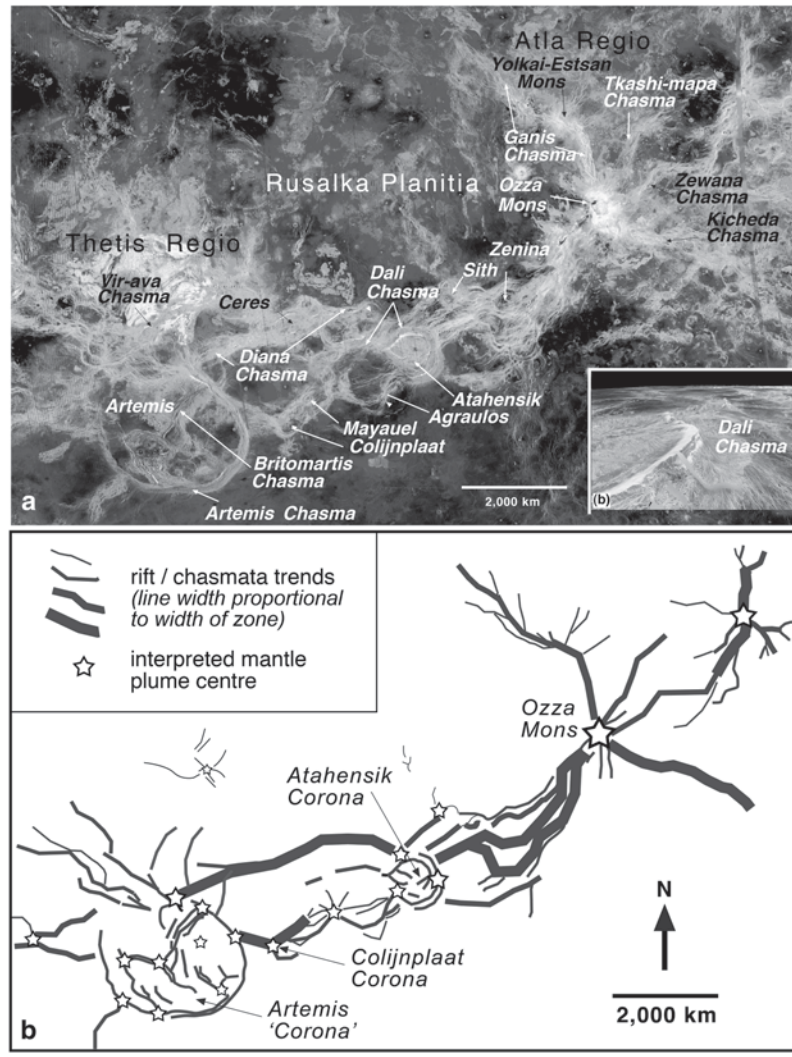

Fig. 9.3 Magellan radar image (**a**) and interpretation (**b**) of rifting between and radiating outward from interpreted mantle plume centres SE of Thetis Regio and Rulalka Planita, Venus. Artemis (located in the SW part of the area) is enlarged in Fig. 9.4a. See Fig. 9.2a for location.

1995; Flament 2009). Our ideas for plume related rift geometries on Earth come largely from plate reconstructions and observations of modern rifts such as the Afars and East African rift system where discrete graben intersect as triple point junctions. Triple point junctions are defined as an important criteria for the recognition of ancient rifts (Ernst and Buchan 2003) and it is considered (e.g. Shervais 2006) that if Archaean greenstone belts were formed by plume-related rifting, they should likewise have initially defined a triple point geometry. However, the 'classical' triple point geometry is produced in elastic, homogeneous lithospheric plates (Bhattacharji and Koide 1975). Whilst this is a valid approximation for a brittle crust capable of fracturing and deforming as individual plates (as on the Phanerozoic Earth), we cannot necessarily extrapolate a simple triple point, localized rift geometry back to the Archaean where the crust was hotter and hence more ductile, and so probably did not behave as a series of large rigid plates (Flament 2009). Notably, triple point geometries were not observed in numerical models with a more ductile lithosphere performed by Coltice et al. (2009), and 3 to 6 radiating rifts developed over simulated plume centres in analogue models with a ductile substrate by Harris et al. (2004). Broad areas with single or intersecting sets of closely spaced extensional faults and fractures formed

in late stages of models resemble ribbon and star terrain in tesserae on Venus (Harris et al. 2004).

In Archaean terrains, early rift±synvolcanic faults play a crucial role in localizing subsequent deformation. As plume-related rifting results in broad areas of normal faulting, then craton-wide networks of transcurrent shear zones may form when a previously rifted craton is shortened. For example, in the NESP, NNW- to N-striking rifts that control formation of an autochthonous sequence of 2.88 Ga and 2.72 Ga greenstone and sedimentary rocks across the NESP (Maurice et al. 2009) cut boundaries of previously assembled terranes with markedly different mantle extraction ages, metamorphic, and prior structural histories (Boily et al. 2009). These greenstone belts were then deformed during subsequent regional strike-slip faulting and intruded by granodiorite and enderbite bodies ca. 2.74–2.71 Ga.

9.2.4.3 Fold Belts and Transcurrent Shear Zones on Venus

Fold belts that are 100+km wide and thousands of kilometres long are interpreted from radar images of Venus, especially along portions of margins of crustal blocks such as plateaux, tessera highlands, and some coronae (Suppe and Connors 1992; Phillips and Hansen 1994). Fold belts also contain thrust imbricates and show characteristics of terrestrial fold-and-thrust belts (e.g. Maxwell Montes; Ansan and Vergely 1995). Wrinkle ridges (long, low-amplitude anticlines) occur over vast regions (Bilotti and Suppe 1999).

Regional transcurrent fault or brittle-ductile shear zones (Bruegge and Head 1990; Pohn and Schaber 1992; Solomon et al. 1992; Ansan et al. 1996; Koenig and Aydin 1998; Chetty et al. 2010; Fernández et al. 2010) up to 400 km long (Tuckwell and Ghail 2003) or more (as we show in Sect. 3), are interpreted from radar imagery. Wrench shear zones, as illustrated by Hansen and Willis (1996), Kumar (2005), Fernández et al. (2010), show the same geometry of subsidiary structures as developed in wrench systems in Archaean greenstone belts (e.g. South Africa; Stanistreet et al. 1986; Yilgarn Craton; Mueller and Harris 1988; Mueller et al. 1988). Conjugate shear fractures and faults (Willis and Hansen 1996; Hansen 2007b; Yin and Taylor 2011) have also been interpreted on Venus, suggesting regions may be dominated by either non-coaxial and coaxial deformation. Regrettably, strike-slip shear arrays are not commonly shown on many recent USGS geological maps of Venus, so that recent maps fail to portray the true extent of lateral displacements. The absence of interpreted strike-slip faults on many recent geological maps of Venus concurs with the comments of Fernández et al. (2010; who portray spectacular examples of wrench-style deformation in the lowland plains of Lavinia Planitia), that there is a perceived 'resistance in planetary geology to recognize strike-slip faults in planets outside the Earth'. This resistance is likely rooted in the preconception that plate tectonics is required to produce large regional lateral displacements.

Hansen (2007b) highlights similarities between patterns of folding and shearing around elongate domal structures in the Atalanta-Vinmara and Lavinia regions of Venus to structures within granite-greenstone belts on Earth. Her interpretations agree with those of Suppe and Connors (1992) for regional consistency of tectonic stresses, although evidence for superposed folding and reversal of shear displacement on faults elsewhere (e.g. Chetty et al. 2010; Sect. 3.2) indicates stress fields have varied throughout time.

9.3 Horizontal Displacements on Venus—A Precursor to Plate Tectonics?

Although there is no evidence on Venus for modern plate tectonic processes (Sect. 2.1), the geometry of shear zones and interpreted displacement above mantle plumes provides evidence that the largest corona, Artemis (Figs. 9.2a, 9.3, 9.4a) and the 'craton-like' Laksmi Planum in western Ishtar Terra (Fig. 9.2b) and Ovda Regio (Figs. 9.2a, 9.5) have experienced 'plate-like' relative horizontal displacements of several hundreds of kilometres. Large horizontal displacements on Venus and the resulting structures can be used as analogues to interpret structures

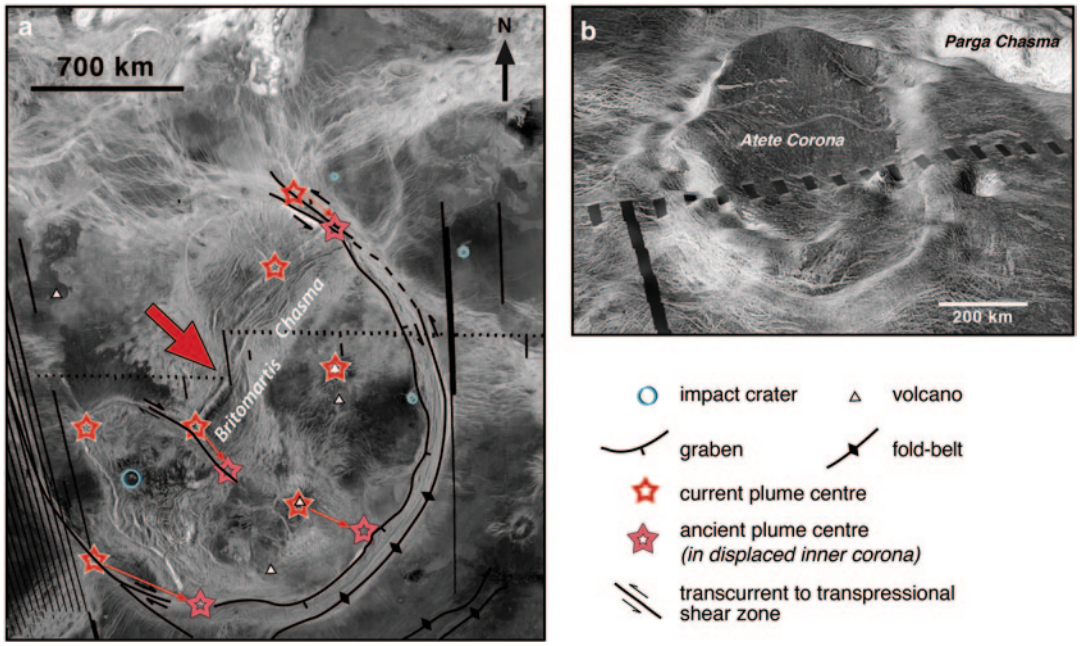

Fig. 9.4 Examples of lateral translation and possible incipient subduction on Venus (Magellan radar images). (**a**) Artemis. (**b**) Atete Corona. See Fig. 9.2 for location. Black bars = areas with no data

formed in Archaean terrains affected by cratonic mobilism (Bédard et al. 2013).

9.3.1 Atete Corona—Incipient Underthrusting

Asymmetrical coronae provide important illustrations for exhumation, horizontal translation, block tilting, folding, and rifting that may represent the earliest stage in an evolution that, whilst not reached on Venus, may have led to modern plate tectonics on Earth. Reconstructed 3D views of Atete Corona (Fig. 9.4b), a 500–600 km wide asymmetrical body in the Galindo (V-40) quadrangle of Venus (Fig. 9.2), show that its lava flow surface is tilted. Positive gravity anomalies under such arcuate, rift segments of Parga Chasma on coronae margins led Schubert et al. (1994) to propose incipient subduction, however no evidence for this is seen in more recent detailed gravity analysis (Smrekar et al. 2010), although its tilt-block geometry suggests that underthrusting occurred.

9.3.2 Shear Zone Reactivation and Refolding in Ovda Regio

Refolding of early regional isoclinal folds and of thrust or reverse faults, and changes in displacement on cross-cutting transcurrent shear zones is well illustrated in the Ovda Regio region of Venus (Fig. 9.2a), a crustal plateau proposed as an example of highly deformed continental-like crust on Venus by Romeo and Capote (2011). Whilst Romeo and Capote (2011) present detailed interpretations of structures formed in a series of superposed deformation events in small, representative areas of Ovda Regio, a regional interpretation is presented in Fig. 9.5. Ghent and Hansen (1999) recognised fold interference patterns in central Ovda Regio, although structures are interpreted as the result of a single progressive deformation event by Chetty et al. (2010).

Our interpretation in Fig. 9.5d shows spectacular regional isoclinal folds, with 500 to ca. 1,000 km long limbs indicative of episodes of considerable ca. N-S (D1) and ca. E-W (D2) regional shortening. F1 folds in the western half of

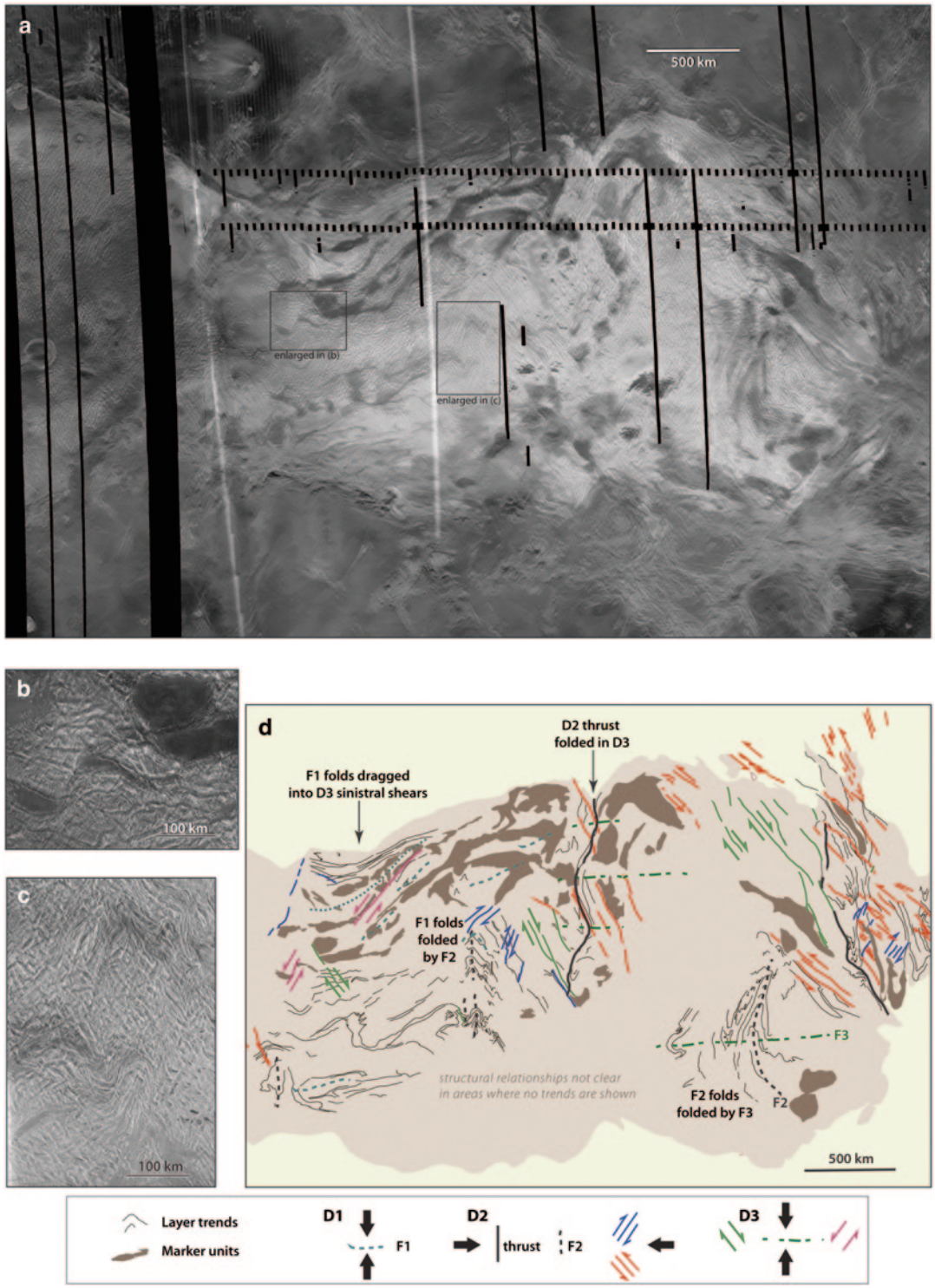

Fig. 9.5 Refolding and shearing implying superposed deformation events in Ovda Regio, Venus. See Fig. 9.2b for location. (**a**) Magellan radar image. Black bars = areas with no data. (**b**) Example of displacement of a volcanic horizon by a transcurrent brittle-ductile shear zone. (**c**) Example of regional folding. (**d**) Structural interpretation. Structures similar to those on Earth have formed in multiple deformation events, requiring systematic changes in regional stresses, despite the absence of plate tectonics on Venus

the map are locally refolded by open (F2) folds. NW-striking sinistral shear zones in the eastern map area, and along the N boundary of tessera terrain in the northwestern part of the map, also indicate E-W shortening in D2. A thrust or reverse fault is interpreted to separate the western block (dominated by F1 folds) from the eastern block (dominated by F2 folds), suggesting that the eastern block has impacted upon the western block. Reverse or thrust faults (D2) and tight F2 folds are folded by open folds with E-W axial traces. NNW-striking dextral shear zones indicate superposition by a third event (D3) where regional shortening is again N-S. Three phases of bulk shortening were also identified by Romeo and Capote (2011); the slight differences in interpreted principal strain axes may reflect rotation of their localized study areas during supeposed deformation. Romeo and Capote (2011) also interpret superposed structures formed during late NE-SW extension.

Overprinting of folds and shear zones requires successive changes in regional stress orientations (and/or rotation of crustal block with respect to consistent regional stress fields) and a crust rigid enough to transmit crustal stresses from one block to another during their convergence, although the blocks are also internally deformed. As shortening and extension arise from mantle flow generated by upwelling and downwelling plumes in a stagnant lid convection régime, the effective flow direction acting at the base of these bodies and/or the location of plumes must have thus changed with time. Numerical modelling by Tackley (2000a, b) suggests that plate-like surface mobility may occur even without an aesthenosphere (as is the case for Venus), and that this behaviour is episodic, which may explain the variability in implied shortening interpreted from the superposition of structures.

Juxtaposition of blocks with different fold patterns and overprinting of folds formed during tectonic juxtaposition of two blocks on Earth, as in Archaean high-grade gneiss terrains such as the NESP (Lin et al. 1996; Berclaz et al. 2004; Simard et al. 2008) and Greenland (Windley and Garde 2009), is taken by many as evidence for subduction and collision-related terrane assembly. The evidence from Ovda Regio on Venus, however, implies that such structures may develop despite the absence of modern-style plate-tectonics. Reactivation and changes in the displacement of strike-slip shear zones similar to those interpreted in Ovda Regio and refolding have also been documented in low grade Archaean terrains, e.g. in the Pilbara Craton (Blewett et al. 2002; Huston et al. 2002; Beintema et al. 2003, following formation of regional granitoid gneiss domes) and in the Archaean Itacaiúnas Belt in Brazil (Pinheiro and Holdsworth 1997).

9.3.3 SE Translation of Artemis

With the ca. 2100 km internal diameter of its internal trough and the 2600 km diameter of the full circular feature (Spencer 2001; Bannister and Hansen 2010), Artemis (Figs. 9.2a, 9.4a) is transitional in size between other coronae and volcanic rises or plateaux. Artemis is possibly the largest circular structure in the solar system (Bannister and Hansen 2010) and defies clear classification (Hansen 2001; Bannister and Hansen 2010), thus possibly representing a unique mode of corona formation (Stofan et al. 1992). Artemis has been recently mapped in detail by Bannister and Hansen (2010). Artemis has a U-shaped annular trough, Artemis Chasma, postdating NE-trending fractures within and outside, radiating fractures away from the annulus (Stofan et al. 1992), and a curved fold belt on its SE margin (Fig. 9.4a). Intersecting fractures and/or graben in its interior radiate from internal coronae (Fig. 9.4a). A numerical model of asymmetrical delamination of lithosphere thickened on the Artemis' SE margin by one or more plume heads is proposed by Smrekar and Stofan (1997).

Numerical modelling (Smrekar and Stofan 1997) suggest Artemis' general form may be derived from the linking of chasmata generated above several mantle plumes. That several plumes constitute Artemis is consistent with the following observations:

- Artemis' size is greater than would be expected above a single central mantle plume.
- There is no elevation difference between most of the interior of Artemis and the surrounding

plains, as is common to most large coronae (Janes et al. 1992; Stofan et al. 1993), which does not support formation by a young superplume. Its internal features also do not suggest collapse from a central uplift, as would be expected if it had formed over an ancient former superplume.
- The localized topographic highs and volcanic centres in southeastern Artemis from which fractures radiate are similar to features developed elsewhere on Venus above interpreted plumes.
- Britomartis (Fig. 9.4a) and other rifts/chasmata which define triple and other multiple junctions within the interior of Artemis are again similar to those developed over smaller mantle plumes, suggesting the presence of several plumes beneath the interior of Artemis.

Transcurrent to transpressional shear zones along Artemis' NE and SW margins link with fold-belts along its southeastern margin and within Artemis Chasma (Brown and Grimm 1995). In addition to folds and shear zones described by these authors, translation of the interior of Artemis towards the SE by ca. 300 km (Fig. 9.4a) is supported by:
- Chasmata that are interpreted as initially intersecting above a mantle plume and the interpreted plume centres are offset in the same sense as deduced by Brown and Grimm (1995) from *en échelon* fold patterns along transcurrent shear zones.
- Pairs of mantle plume centres (interpreted from a combination of radiating normal faults and chasmata and volcanoes) appear to be spaced by approximately the same amount along a northwest-southeast orientation (i.e. sub-parallel to the inferred displacement of the interior of Artemis). This is interpreted as representing the southeasterly displacement of structures formed above plumes, followed by the formation of younger structures and/or volcanoes above the fixed mantle plume following SE horizontal displacement, i.e. analogous to formation of 'hotspot trails' developed as plates move over mantle plumes on Earth (Wilson 1965; Morgan 1971; Duncan 1981).

The SE margin of Artemis is proposed to be an arcuate, zone of downwelling equivalent to an incipient subduction zone (McKenzie et al. 1992; Sandwell and Schubert 1992; Fowler and O'Brien 2003; Bannister and Hansen 2010) which may also have counterparts in the Archaean Earth (c.f. Van Kranendonk 2010).

9.3.4 'Himalayan-style' Indentation and Lateral Escape in Western Ishtar Terra

'Himalayan-style' indentation and lateral escape structures are associated with the northward displacement of the ca. 1400 km in diameter, craton-like Lakshmi Planum[1,3] on western Ishtar Terra in the northern polar region of Venus (Figs. 9.2b, 9.6a). As illustrated in Fig. 9.6a, b, a wide zone of folding, reverse faulting, and trancurrent shear zones striking sub-parallel to the indenter margin is developed in front of an interpreted indenter. Northwards displacement of Lakshmi Planum was accommodated by folding, reverse faulting or thrusting, and formation of transcurrent shear zones sub-parallel to the indenter margin up to 1000 km N of the planum boundary. A fold and thrust belt, Freyja Montes, is developed along the N margin of Lakshmi Planum. North Polar Plains units N of Freyja Montes may under-thrust northern Ishtar Terra and Freyja Montes along S-dipping faults forming a series of thrust imbricates (Head 1990b). Areas of intense faulting SE of Itzpapaloti Tessera appear to represent reactivation of early rifts.

Margins of the indenter are dominated by shear zones with dominantly strike-slip displacement. A zone of sinistral trancurrent shearing up to ca. 2,000 km long located NE to E of the Lakshmi Planum indenter resembles the Jiall-Red River shear system associated with lateral escape during indentation of Eurasia by India (Fig. 9.6c; Tapponnier and Molnar 1976; Molnar and Tapponnier 1977; Tapponnier et al. 1982) in both scale and geometry. Dextral shear zones developed closer to the interpreted eastern indenter margin are in a similar position as the Sagaing Fault in the Himalayan lateral escape system (Fig. 9.6c). A ca. 450 km wide regional transpressional shear system is developed in Akna Montes on the western margin of the indenter.

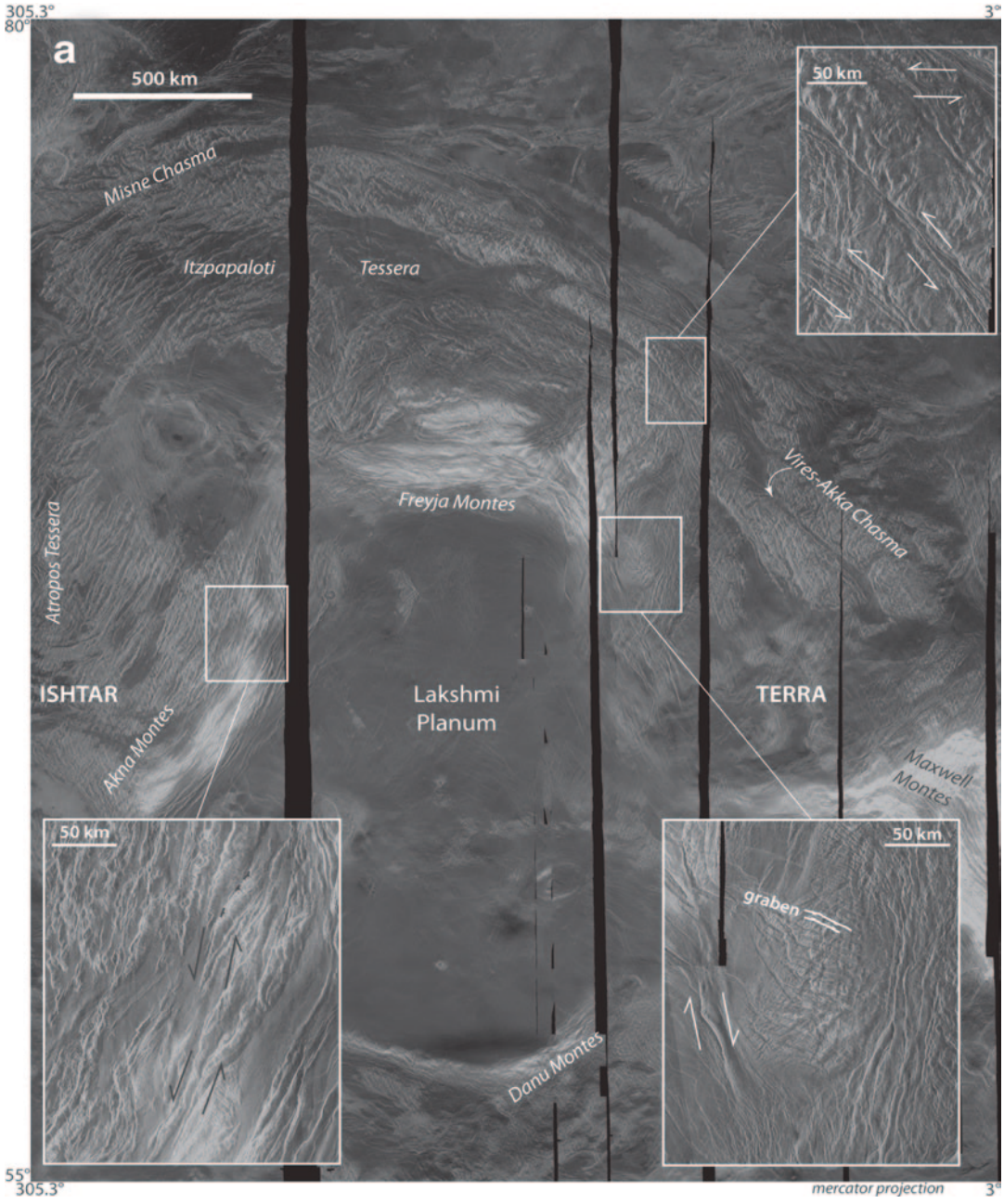

Fig. 9.6 (**a**) Magellan radar imagery over part of western Ishtar Terra, Venus. Insets provide enlarged examples of folds, transcurrent to transpressional shear zones, and reverse and normal faults. See Fig. 9.2 for location. (**b**) Shear zones interpreted from Magellan radar imagery in (**a**), illustrating indentation of the craton-like Lakshmi Planum into Itzpapaloti Tessera. The Freyja Montes mountain range dominated by reverse faults cut by ENE-striking dextral shears formed immediately N of the interpreted indenter. Deformation further N comprises orogen-parallel reverse and sinistral transcurrent or transpressional shears. Sinistral transpression is interpreted in

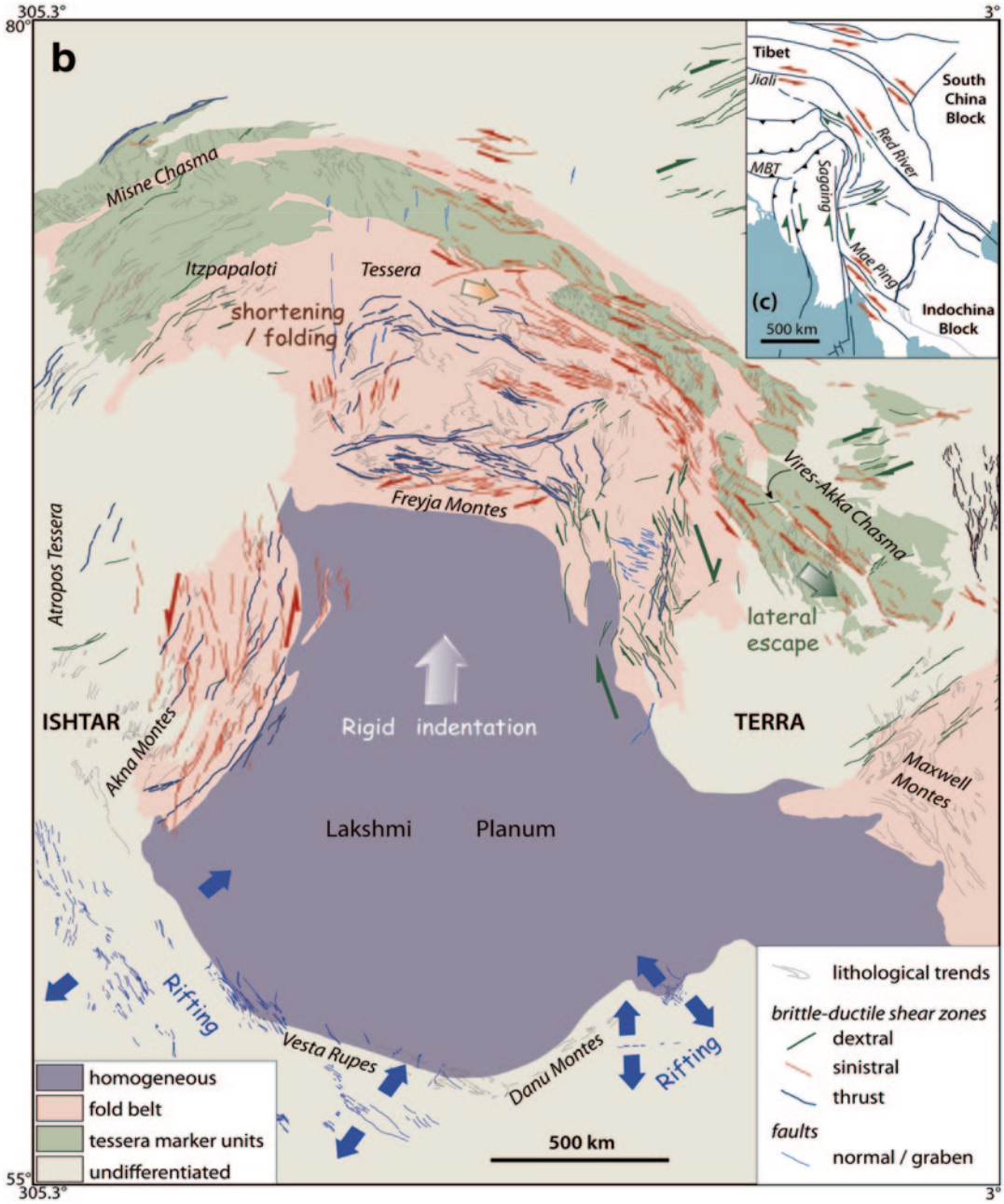

Akna Montes on the W margin of the indenter and dextral shears are developed close to the E indenter margin. Sinistral shearing in Vires-Akka Chasma represents lateral escape on the E margin of the indenter. Northwards displacement of Lakshmi Planum is interpreted as creating rifts on its southern margins. The dashed rectangle = the area enlarged and reoriented to match trends in the SE Superior Craton in Fig. 9.14. (**c**) Indentation and escape structures in the eastern Himalaya and SE Asia due to collision of India into Eurasia illustrate the same geometry and displacement senses as in the E half of (**a**)

The geometry of structures N of Lakshmi Planum resembles that of the Quebec Abitibi (developed further in Sect. 4.3). Linear belts of transcurrent shearing on the NE and E margins of the interpreted indenter are locally localized along previous rifts, and the resultant geometry resembles Archaean terrains such as the Yilgarn Craton that are dominated by regional transcurrent shear zones that reactivate early-formed rifts (Harris 1987; Blewett et al. 2010a; Czarnota et al. 2010). Sinistral transpressional shears on the Western margin of Lakshmi Planum are equivalent to Archaean shear zones in the Limpopo Belt of South Africa (Roering et al. 1992; Kamber et al. 1995; Kreissig et al. 2001; Schoene et al. 2008) where, similarly, a Himalayan-style indentation model has been proposed by Treloar et al. (1992).

9.3.5 Progressive 'Plate-like' Behaviour on Venus

The above examples illustrate a progressive evolution in deformation styles as crustal areas of Venus show progressively more 'plate-like' behaviour:

- Although juxtaposition of blocks with apparent different structural histories along a thrust or reverse fault contact occurred in Ovda Regio, both blocks were rigid enough that stresses were transferred across a wide area. Both blocks underwent considerable internal deformation during the three bulk shortening events interpreted from refolded folding and superposed faulting.
- Artemis represents an example of a large region that has undergone horizontal displacement, forming transcurrent shear zones with opposite senses of displacement on opposite margins. While the edges of this moving 'terrane' are strongly deformed and constitute a discrete fold belt, there is little internal deformation of Artemis, suggesting it was behaving as a rigid 'cratonic' block.
- Lakshmi Planum appears to have acted as a rigid indenter, much like India's impact on Asia, but without a plate tectonic 'engine'. Although Lakshmi Planum shows little internal deformation, stresses transmitted due to large horizontal displacements induced broad areas of shortening and transcurrent shearing in adjacent, weaker terrains.

A similar progressive evolution in tectonic style may have occurred on Earth, from purely stagnant lid and episodic convective overturn (c.f. Armann and Tackley 2012) in the Hadean, through intermediate stages where plate-like behaviour starts to develop in the Archaean (as suggested on Venus), to eventual 'modern' subduction and plate tectonics. This intermediate stage could be associated with possible double-sided zones of downwelling as produced in models of Tackley (2000a, b) and Pysklywec et al. (2010), mantle drips (c.f. Gorczyk et al. 2012), or plume-related mantle downthrusting as modelled by Burov and Cloetingh (2010), but without modern-style one-sided subduction.

Interpretation of 'Himalayan-style' indentation and lateral escape on Venus has significant implications. It implies that structures identical to those formed through plate tectonic processes on the Phanerozoic Earth may also develop in the absence of plate tectonics due to coupling between the lithosphere and flowing mantle (cf. Alvarez 2010; Becker and Facenna 2011). Therefore, crustal evolution and formation of structures commonly attributed to convergence and collision on an Archaean Earth do not require the operation of plate tectonics. This is illustrated in the following section using the SE Superior Craton (Fig. 9.7) as an example.

9.4 The South-Eastern Superior Craton—Formation and Deformation of Archaean Juvenile Mafic-Rich Crust Without Modern Plate Tectonics

9.4.1 Critique of Previous Models for Subduction and Accretion

The SE Superior Province illustrated in Figs. 9.7 and 9.8 comprises, from N to S, the Opinaca, Opatica, Abitibi, and Pontiac subprovinces. The Pontiac, Abitibi and Opatica subprovinces have

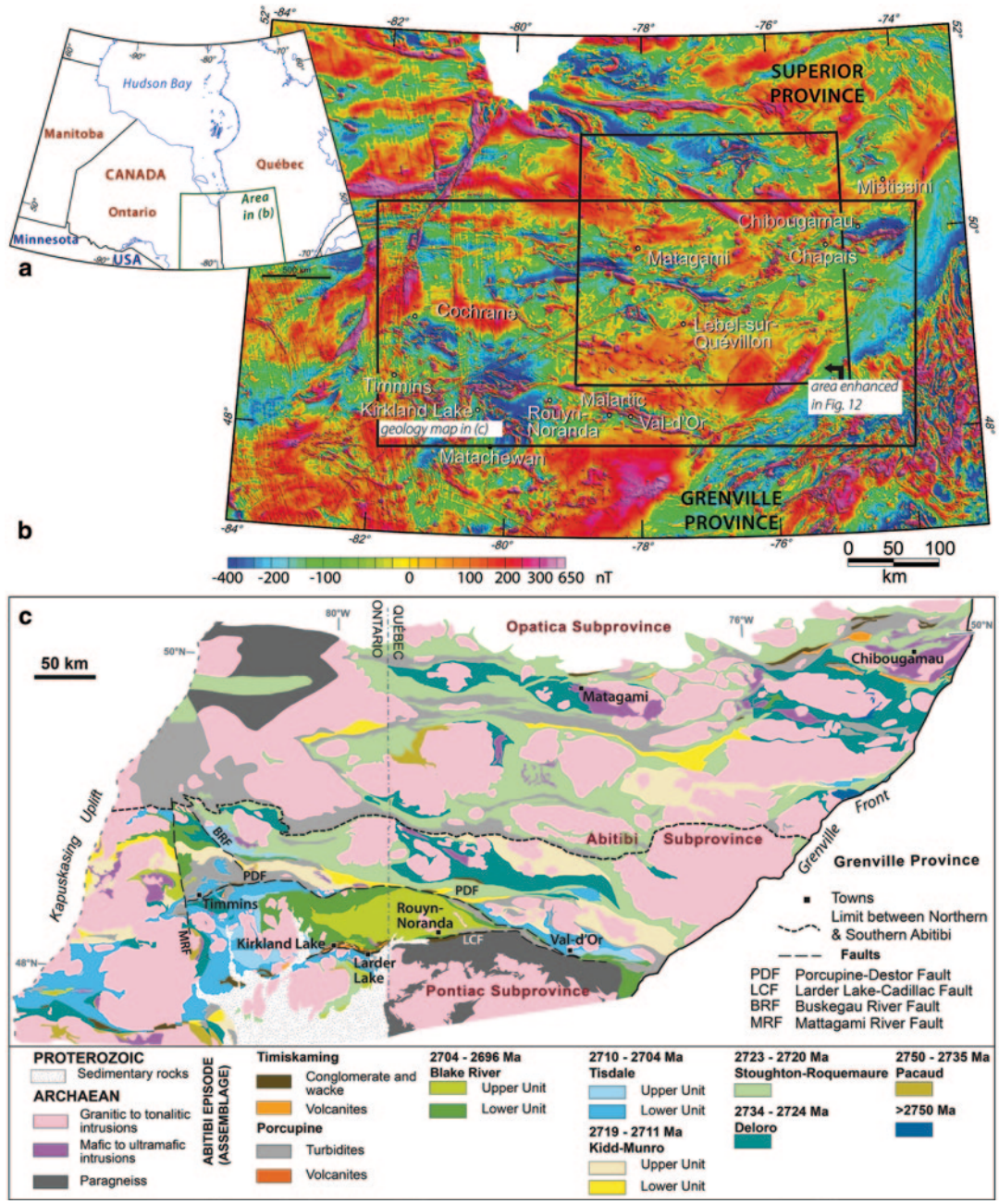

Fig. 9.7 The SE Superior Province, Canada. (**a**) Location. (**b**) Regional Geological Survey of Canada aeromagnetic imagery over the SE Superior Province and NW Grenville Province. (**c**) Geological map of the Abitibi and Pontiac subprovinces modified after Thurston et al. (2008; also incorporated in Goutier and Melançon 2007)

previously been regarded as accreted terranes, based on (i) arc (Dimroth et al. 1982, 1983; Jackson and Cruden 1995) or mantle plume–island arc (Wyman et al. 2002) models for formation of greenstone assemblages, (ii) models for accretion of oceanic plateaux and arcs through oblique subduction (Desrochers et al. 1993; Kusky and Polat 1999; Daigneault et al. 2002), and (iii) interpreta-

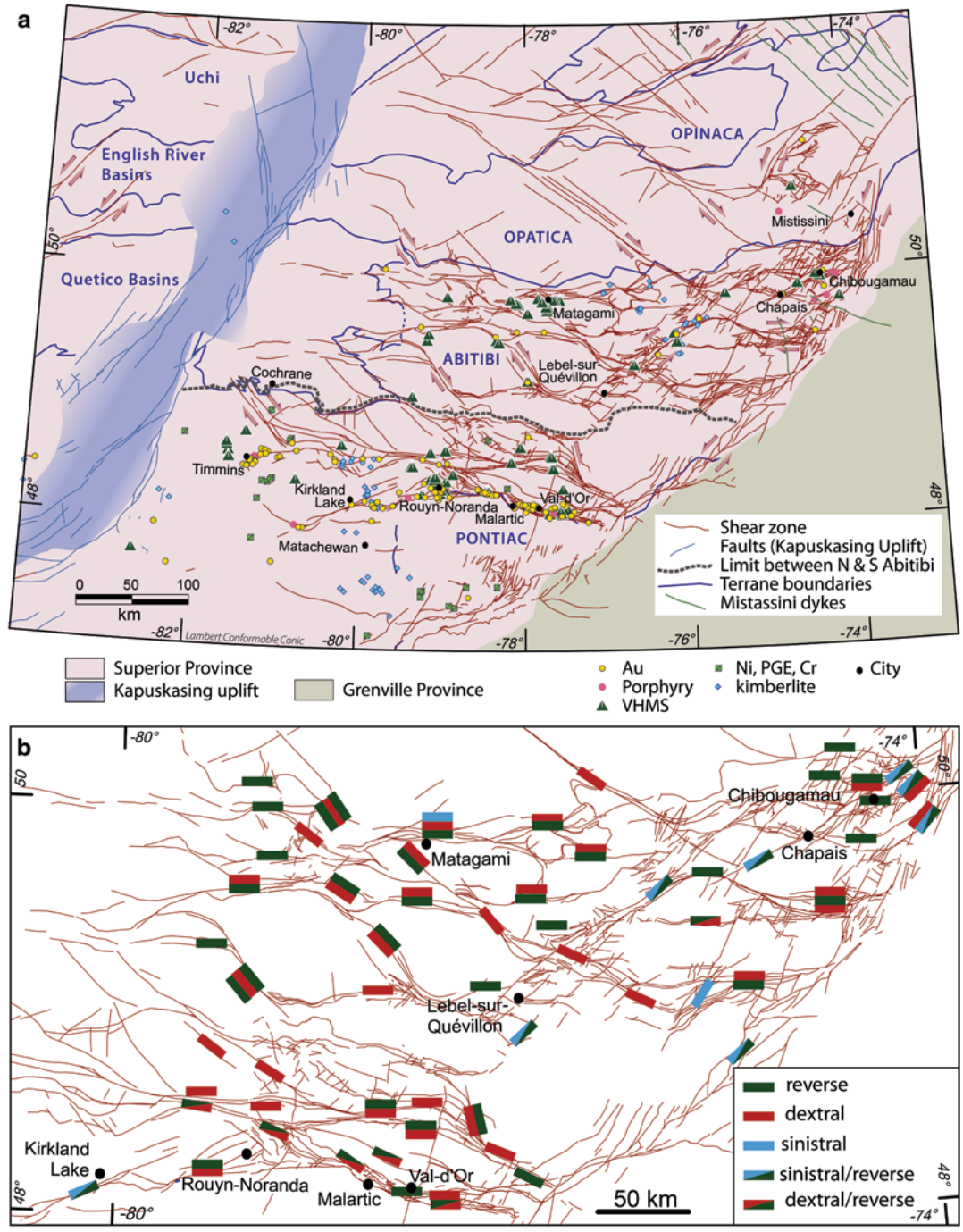

Fig. 9.8 (**a**) Terrane boundaries (from Stott et al. 2007) and discrete shear zones in the SE Superior Province compiled and simplified from Theriault (2002) and Daigneault (1996), with additional structures interpreted from aeromagnetic imagery. (**b**) Synthesis of Archaean displacement history along shear zones in the Abitibi Subprovince showing there is no simple sequence of discrete deformation events; however, such changes typify areas combining bulk shortening and lateral escape in younger orogens. Superposed symbols show oldest (*upper*) to youngest (*lower*) interpreted senses of displacement from field studies of Daigneault (1996), Lacroix (1998), Leclerc (2011), and Leclerc et al. (2012)

tions of fossil subduction zones on a deep crustal reflection seismic profile across the Abitibi and Opatica subprovinces of the SE Superior Province (Calvert et al. 1995; Calvert and Ludden 1999; van der Velden et al. 2006; Clowes et al. 2010). Similar, subduction zone interpretations are presented for the Western Superior Province (Calvert et al. 1995; White et al. 2003; van der Velden et al. 2006).

Bédard et al. (2013), however, provide geochemical, petrological, and tectonic arguments against the operation of uniformitarian subduction and accretion processes in the Archaean, concluding that Archaean arcs are "imaginary constructs with no objective existence". Interpretations of fossil subduction zones are also highly speculative, non-unique, and largely 'model-based':

- Dipping reflectors marking shear zones in the upper mantle do not *per se* imply subduction. The Abitibi-Opatica seismic profile differs greatly from reflection seismic profiles across younger collisional orogens (McBride et al. 1996; Cook and van der Velden 2012) in that lower crustal reflectors continue across the section above the interpreted relict subduction zone and there are no clear hinterland and foreland verging thrusts intersecting at the interpreted subduction zone. As noted by van der Velden and Cook (2005), the surface suture between the Opatica and Abitibi is located almost directly above the dipping mantle reflections interpreted as the relict subduction zone (which would normally correspond to a position within the hinterland, with the surface position of the suture offset due to the dip of the contact between terranes).
- Benn (2006) interprets the dipping mantle reflectors on the same profile across the Abitibi and Opatica subprovinces as thrust faults associated with imbrication of the lower crust without subduction, a geometry subsequently reproduced in numerical models of shortening of Archaean lithosphere by Gray and Pysklywec (2010). Mantle structures interpreted as fossil subduction zones in the Superior Province may alternatively record early (subsequently inverted?) normal shear zones, as identical mantle reflectors and crustal architecture are imaged across rifts, e.g. North Sea and Viking Graben (Reston 1990; Brun and Tron 1993) and Great Lakes (Clowes et al. 2010), and comparable extensional mantle shear zones are developed in numerical models by Frederiksen and Braun (2001).
- Garnet bearing amphibolite at the base of the crust interpreted from seismic and gravity data across the interpreted subduction zones in the W Superior Province by White et al. (2003) may simply represent mafic rocks underplated or intruded during plume-related rifting, instead of a 'large slab of remnant oceanic crust preserved at the base of the crust', as White et al. (2003) propose. Alternative origins proposed by White et al. (2003) are all based on the premise of arc accretion, and plume-related rifting was not considered or discussed.
- Although gravity studies in the Western Superior show there is no evidence for lateral density changes across the interpreted sutures (Nitescu et al. 2006), these authors invoke 'post-accretionary thermal softening…. through vertical mass transfer and ductile extensional flow' to explain why there is no gravity evidence for the putative suture. A simpler explanation is that there never was one…

We therefore believe that previous seismic interpretations fail to provide definitive evidence for subduction in either the SE or W Superior Province.

The Opinaca Subprovince (that lies immediately N of the Opatica Subprovince; Fig. 9.7) comprises granulite facies paragneisses and metavolcanics intruded by 2747 to 2710 Ma synvolcanic 2710 to 2697 Ma syn-tectonic and 2697 to 2618 Ma post- or late-tectonic TTG suites (Simoneau et al. 2007; Ravenelle et al. 2010). Ravenelle et al. (2010) interpret the Opatica Subprovince as a lateral extension of synorogenic flysch and accretionary prism deposits of the English River and/or Quetico subprovinces of the western Superior Province. Cadéron (2003) however interprets sedimentary and volcanic rocks of

the Opatica Subprovince as being deposited in a marginal basin on thinned continental crust. We concur with Benn (2006) and Benn and Moyen (2008) that the Abitibi and Opatica subprovinces constitute a single terrane, most likely the vestige of an oceanic plateau (as discussed in Sect. 4.2), where the Opatica subprovince represents a mid-crustal, extensively reworked equivalent to the Abitibi (Benn et al. 1992). Harris et al. (2012) suggest that juxtaposition of the two different crustal levels may result from exhumation of the Opatica Subprovince during extrusive channel flow, aided by wedging of the lower crust during thrusting of the upper mantle interpreted by Benn (2006).

9.4.2 Seismic Tomographic Interpretation for Rifting of a Continuous Sub-Crustal Lithospheric Mantle Layer (and not Subduction)

Surface- (Rayleigh-) wave seismic tomographic data of Godey (2002), presented in Godey et al. (2003, 2004) and Faure et al. (2011), was processed to visualize the structure of the SCLM of the Superior Province from 30 to 250 km depth (Figs. 9.9–9.11). Gridded velocity perturbations (dVs %) relative to the PREM reference earth model (Dziewonski and Anderson 1981) are shown in map view for a depth of 120 km (Fig. 9.9a), as 3D isosurfaces (Figs. 9.9b–e), and as 'ribbon sections' (i.e. ca. 50 km wide vertical slices through the 3D model; Fig. 9.10). An interactive 3Dpdf representation is also available to download (Harris 2013). These images portray major differences between the Paleo-Mesoarchaean Northern and Neoarchaean Southern Superior Craton and provide further evidence against subduction and accretion processes.

The N Superior Province—Hudson's Bay terrane (i.e. N of the Opinaca Subprovince) in Quebec is underlain by thick (generally 220 km+) cratonic SCLM. The 3D form of the 6% dVs isosurface (the 'high-velocity perturbation shell' representing highly depleted SCLM; Faure et al. 2011) defines an irregular surface with three pronounced cratonic keels (also portrayed by Faure et al. 2008, 2011 using the same data set). Irregular blocks of thicker SCLM containing smaller cores of SCLM with 6%$^{+}$dVs also occur in the SW of the Superior Craton in the Minnesota River Valley and beneath Proterozoic orogens in the northern USA.

As noted by Faure et al. (2008, 2010a, 2011), a ca. 1400 km long E-W and ca. 400 km wide zone of low velocity perturbations in the Superior Province occurs beneath the Neoarchaean Abitibi Subprovince. This generally E-W zone (i.e. sub-parallel to general lithological trends in the S Superior Province) changes to a NW-SE orientation in the easternmost Abitibi and beneath the Archaean Grenville Province parautochthon (Faure et al. 2008, 2010a; Fig. 9.11). Although Faure et al. (2008, 2010a) suggest the N and S margins of the E-W trending portion of this low velocity zone both equate to N-verging subduction zones interpreted from reflection seismic profiles, we interpret the 3D and cross-sectional views in Figs. 9.9–9.11 to illustrate apparent necking, boudinage and rifting apart of the SCLM, as portrayed by the 4.5% (yellow, Figs. 9.9 and 9.10) and 4.2% (orange; Fig. 9.10) isosurfaces. Isosurfaces above and below the interpreted rift bend towards the necking axis, supporting this extensional interpretation. The geometry imaged from seismic tomographic data is identical to that produced in numerical models by Gueydan et al. (2008) for rifting of a high strength SCLM, and differs significantly from seismic tomographic images of ancient subduction zones (e.g. Palaeoproterozoic North China Craton; Santosh et al. 2010). We do not see any evidence for shallowly N-dipping seismic feature interpreted to reflect subduction by Faure et al. (2008). There is similarly no evidence for remnant subducted slabs, as were proposed from a 2D section of limited extent in the western Superior by Sol et al. (2002), and which may instead image part of the rift-bounding structure.

The resultant geometry is thus akin to crustal rifts (but here it is the competent SCLM that has extended and symmetrically necked or boudi-

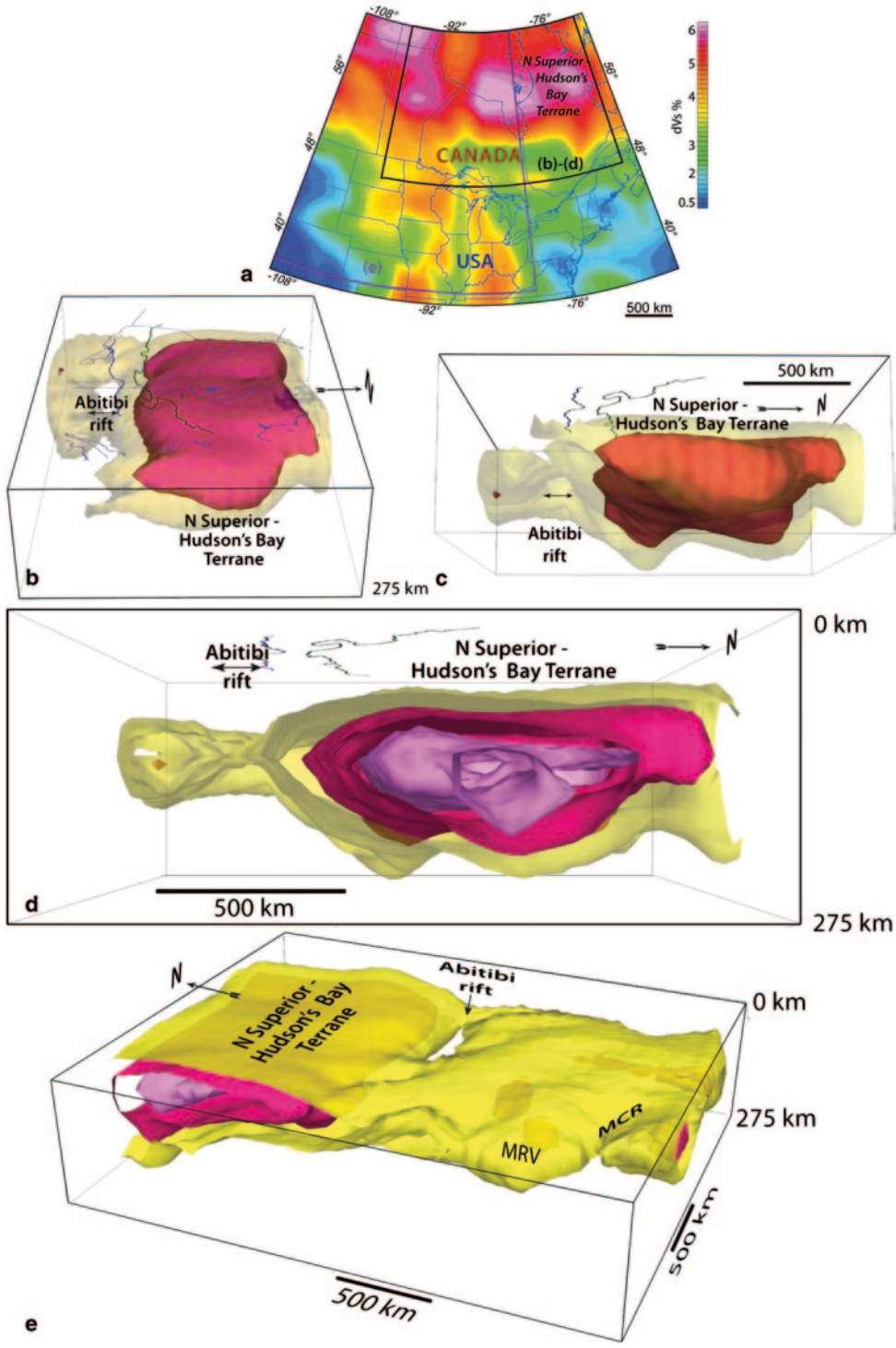

Fig. 9.9 2D and 3D representation of S-wave seismic tomography over the Superior Craton produced from data of Godey (2002) providing evidence for Archaean rifting of SCLM in the S Superior Craton. There is no evidence for remnant subducted slabs that may be expected in a subduction and accretion model. Colour changes in 3D views of the same isosurfaces (c.f. legend to Fig. 9.10) are due to variable transparency of surrounding layers

naged), and the 4.5 and 4.2% isosurfaces are bowed upwards beneath the zones of necking. The E-W and NW-SE low velocity zones intersect at the Grenville Front, making at an angle of ca. 120° to each other. The features imaged in the SE Superior Craton thus define a classical 'triple-point' geometry produced during rifting above mantle plumes. We speculate that, given this geometry, structures that subsequently localize the Grenville Front (defining the limit between the Mesoproterozoic Grenville Province and Superior Craton) may be controlled by an Archaean aulacogen. Propositions arising from other S- and P-wave tomographic studies over SE Quebec and Ontario that the NW-SE trending low velocity corridors mark the trail of the Cretaceous Great Meteor hotspot[8], and hence are superposed on E-W Archaean features (Rondenay et al. 2000, 2002; Aktas and Eaton 2006; Frederiksen et al. 2007; Villemaire et al. 2012), are improbable since:

- The large difference in seismic velocities which create the NW-SE trending anomaly cannot be produced in the mantle solely by thermal effects during displacement over a hot-spot and require the presence of prior NW-SE trending SCLM structures (Chen and Li 2012).
- There is no evidence for pervasive, regional extension across the SE Abitibi Subprovince following Archaean N-S shortening that would be expected during formation of such a broad feature in the underlying mantle.
- Archaean to Palaeoproterozoic plate tectonic reconstructions based on radiating dyke swarms and palaeomagnetic studies (Bleeker and Ernst 2006; Ernst 2007; Ernst and Bleeker 2010) place the Kola and Karelia cratons of Baltica against the SE Superior Craton. In these reconstructions, the Belomorian belt between the Kola and Karelia cratons, the contact between the Murmansk and Kola cratons, and many Neoarchaean greenstone belts (that show similarities in ages of Archaean events to the Superior Province; Card 1991; Slabunov et al. 2006) are oriented ca. NW-SE (in present-day coordinates), and thus parallel the NW-SE low velocity zone.
- Deep crustal to upper mantle structures striking NW-SE beneath the Grenville Province in SW Quebec and upstate New York interpreted from Bouguer gravity influenced sedimentation, mineralization, deformation, and plutonism during the Mesoproterozoic Grenvillian orogenic cycle (Harris et al. 2010; Dufréchou 2011; Dufréchou and Harris 2013) and correspond to margins of promontories of higher velocity Archaean mantle (Fig. 9.11). Reactivation during Palaeoproterozoic rifting and separation of the Kola and Karelia cratons is also postulated (Harris et al. 2010; Dufréchou 2011; Dufréchou and Harris 2013).
- Dufréchou and Harris (2013) also show that the interpreted NW-SE structures in Archaean basement are offset from, and at an angle to, the hotspot trail interpreted by Rondenay et al. (2000, 2002), and the interpreted hotspot trail is coincident with the 0.59 Ga (Kamo et al.

[8] The existence of a Great Meteor hotspot trail is questioned by Bédard (1985) and Matton and Jébrak (2009).

and the orientation of view with respect to the direction of artificial illumination. (**a**) Velocity perturbations (dVs %) relative to the PREM reference earth model of Dziewonski and Anderson (1981) for 120 km. This level presents the maximum horizontal extent of depleted ancient mantle (taken as the 6% isosurface following Faure et al. 2011). Locations of 3D figures are shown. (**b**) and (**c**) Upper and lower 3D views of the 6% [deep pink in (**b**) and orange-pink in (**c**)] and 4.5% (pale yellow) isosurfaces illustrating rifting of the SCLM in the Wawa-Abitibi Subprovince and the presence of a deep keel beneath the N Superior Province (Sachigo Superterrane in the W Superior Province). (**d**) W-looking view of the rift geometry in the SCLM beneath the Abitibi Subprovince with 7.5% (bright pink), 6% (deep pink), and 4.5% (yellow) isosurfaces. (**e**) View of the same isosurfaces as in (**d**) looking NE of the W Superior Province, extending further S to include the Minnesota River Valley area (MRV). Note (i) thinning and necking of the 4.5% (yellow) isosurface of SCLM beneath the Wawa Subprovince whereas this surface has completely rifted apart beneath the central Abitibi Subprovince, and (ii) NW-SE trending features within the Wawa and W Abitibi subprovinces. Rifting in the SW corner of the image corresponds to part of the Proterozoic Mid Continent Rift (MCR; Van Schmus 1992)

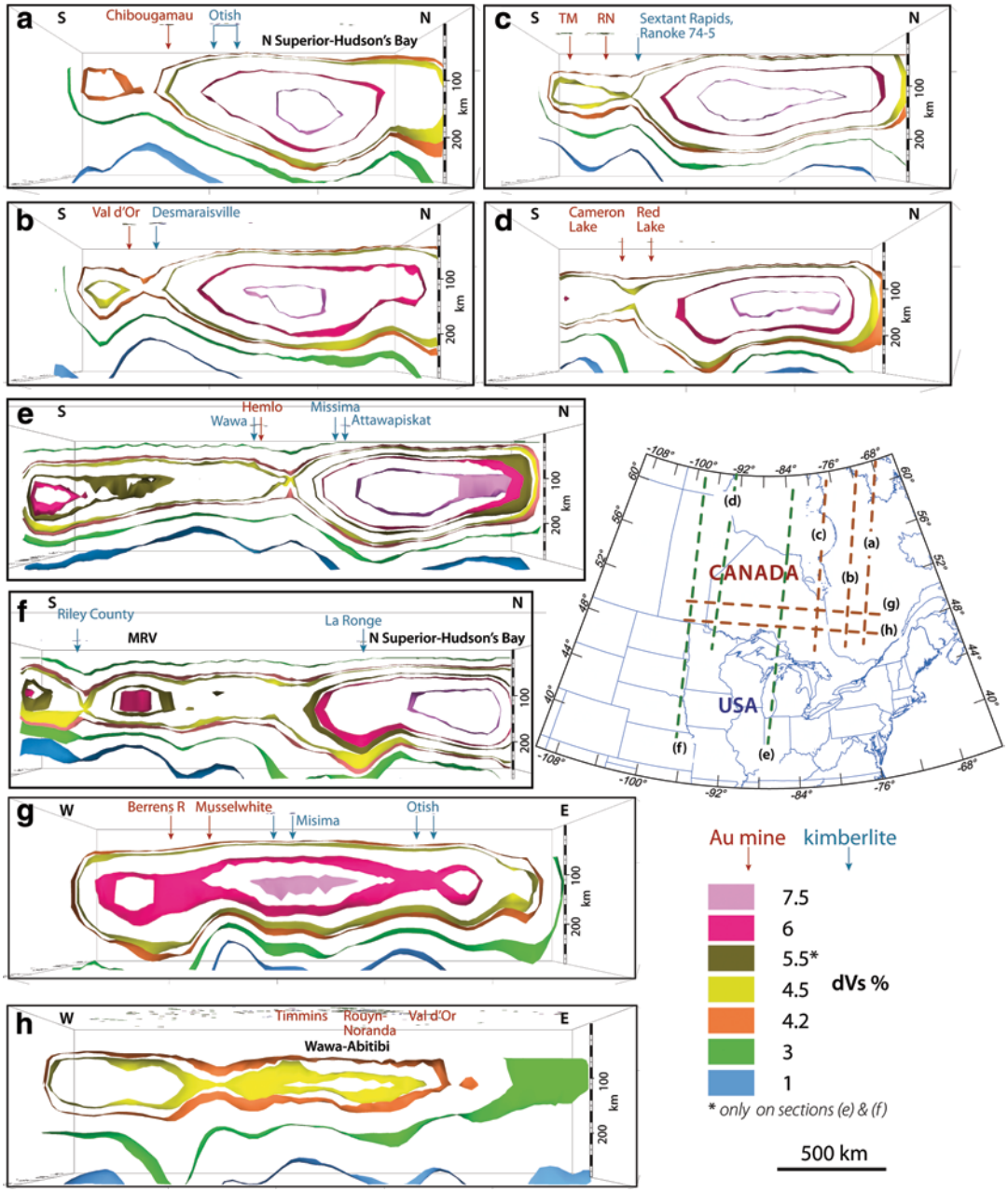

Fig. 9.10 'Ribbon sections' (horizontal views of ca. 50 km wide vertical slices, i.e. direct representations of uninterpreted data) through the 3D S-wave tomographic model presented in Fig. 9.9 (3x vertical exaggeration). Sections (**a–f**) illustrate necking and rift separation of SCLM beneath the Wawa-Abitibi Subprovince. Insert map shows location of sections. Approximately ESE-WNW sections in (**g**) and (**h**) show the presence of ca. N-S trending zones of deep necking that affect both the N and S Superior SCLM but that are not well expressed from surface mapping. Major gold deposits (*red*) occur above margins of interpreted rifts in SCLM. This is also the case for some kimberlites (*blue*). Whilst kimberlites above juvenile SCLM are barren, diamondiferous kimberlites of the Otish cluster in (**g**) occur in an area of necking of the 6% isosurface corresponding to the older, depleted SCLM. Gold deposits are taken from Gosselin and Dubé (2005), and kimberlite locations are from Faure (2010)

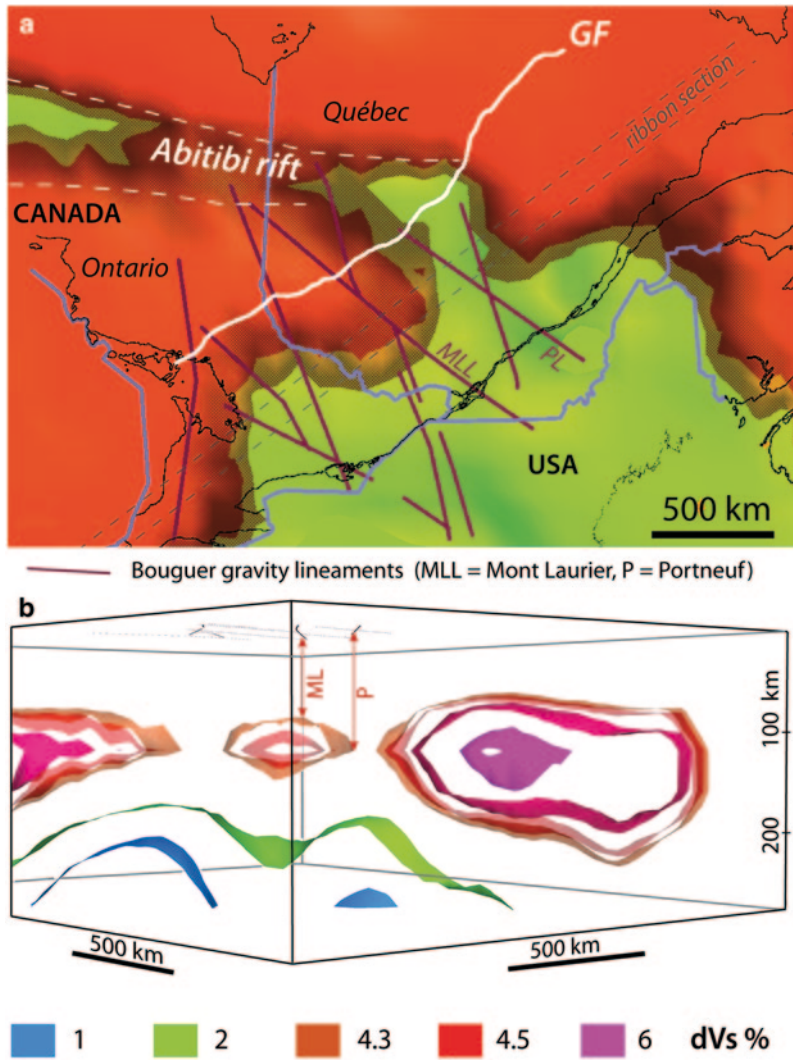

Fig. 9.11 (**a**) Vertical view of the 4.5% (*dark orange*), 4.3% (*transparent pale orange*), and 2% (*green*) isosurfaces centred on the contact between the SE Abitibi and Mesoproterozoic Grenville Province showing the ca. 120° change in orientation of the interpreted rift in SCLM. GF = Grenville Front marking the contact between the Superior and Grenville provinces. Mauve lines = province (*Canada*) and state (USA) boundaries, black lines = coastline and rivers. Fine dashed lines show the location of the ribbon section in (**b**). Lineaments interpreted from Bouguer gravity after Dufréchou and Harris (2013). (**b**) NE-SW oriented ribbon section across promontories of rifted Archaean SCLM beneath the Grenville Province showing that the most significant transverse lineaments, which correspond to basement structures beneath Grenvillian nappes that were active during Grenvillian orogenesis and collapse (Dufréchou 2011; Dufréchou and Harris 2013), are located on upper and lower margins of SCLM discontinuities. The low velocity corridor interpreted as a SCLM rift therefore existed prior to Cretaceous displacement over the inferred Great Meteor hotspot (see Sect. 4.2)

1995; Buchan and Hamilton 2009) Grenville (-Rideau) dyke swarm, a Neoproterozoic, Iapetan rift (as also suggested by Faure et al. 2010b).

We conclude that the low velocity features in the SCLM to the SE Superior Craton represent extensional structures that predate regional Archaean folding and shearing. The Wawa-Abitibi

Subprovince, located above this zone of focused SCLM extension, is therefore interpreted as a lithospheric-scale rift, developed during impingement of mantle plume(s) at the base of an older cratonic block, the roots of which were either rafted apart or largely assimilated along the rift axis. Volcanological interpretations for formation of greenstones of the Abitibi Subprovince also support a rift model (Goodwin 1977; Gibson et al. 1986; Thurston and Ayres 1986). Whilst the main rift corresponding to the Wawa-Abitibi Subprovince trends approximately E-W, orthogonal sections (Figs. 9.10g, h) show ca. N-S corridors of necking that affect the N Superior Province—Hudson's Bay Terrane.

Major gold deposits such as Val d'Or, Hemlo, Red Lake and Cameron Lake and the Chibougamau mineral district project onto the flanks of the interpreted rift zone (Fig. 9.10), suggesting that crustal to possibly lithospheric-scale extensional faults developed throughout rifting channelled hydrothermal fluids in their inversion and reactivation as reverse and transpressional structures during N-S shortening (discussed in Sect. 4.4). We show that giant gold deposits in the interpreted inverted rifts are preferentially localized above the rift margins. Several non-diamondiferous kimberlites are also located on the interpreted rift margins. The 2690 ± 9 Ma (Biczok et al. 2012) Musselwhite gold deposit within the North Caribou Terrane is situated on the flank of a ca. N-S zone of necking, suggesting that even in older terranes, SCLM extensional structures have played an important role in localizing gold mineralization, and that mineralization is not related to supra-subduction zone processes envisaged by Biczok et al. (2012). Diamond-bearing kimberlites of the Cambrian Otish kimberlite swarm (Stevenson et al. 2004) occur also in an area of necking of thick, highly depleted SCLM (Fig. 9.10g).

Support for rifting of an older continental lithosphere also comes from:

- Evidence for sialic crust up to 2.93 Ga in the Wawa Subprovince and inherited ca. 2.85 Ga zircons in felsic plutons, taken by Ketchum et al. (2008) as indicative of rifting of an older continental block.
- Evidence from analysis of diamonds in ca. 2.7 Ga volcaniclastic rocks and lamprophyre dykes and metaconglomerate in the Wawa Subprovince for the existence of a thick package of depleted lithospheric mantle (Stachel et al. 2006; Kopylova et al. 2011). Stachel et al. (2006) interpret this as support for the autochthonous formation of the Abitbi–Wawa greenstone belt on fragments of old continental crust.
- Sedimentological evidence against deposition in linear troughs that typify arc settings (Fralick et al. 1992) and sedimentological and stratigraphic analysis combined with detailed geochronology indicating autochthonous volcanism and sedimentation in formation of the Abitibi greenstone sequence (Ayres and Thurston 1985; Thurston 2002; Thurston et al. 2008).

9.4.3 Crustal Evolution of the Abitibi Subprovince

It is useful at this juncture to briefly review the geology of The Abitibi Subprovince (Fig. 9.7), so as to gain insight into the nature of the structures that develop during progressive rift inversion/basin closure and accretion to an advancing craton.

The stratigraphy, age, and general geometry of volcano-sedimentary sequences comprising the Abitibi Subprovince has been described in detail in previous studies (e.g. Ayres and Thurston 1985; Dimroth et al. 1986; Daigneault et al. 1990, 2002; Calvert and Ludden 1999; Thurston 2002; Thurston et al. 2008; Ross et al. 2011a, b). An early rift geometry is characterized by synvolcanic faults striking ca. E-W, ENE-WSW, and WNW-ESE (e.g. Faure 2009) and E-W trending normal faults are subsequently inverted as reverse faults (e.g. Dimroth et al. 1986). The development of an autochthonous volcanic stratigraphy is documented by Thurston et al. (2008). The picture that emerges from these studies is of a shallow-marine lava plain, periodically resurfaced by eruptions of tholeiitic to komatiitic

lava channelled by sill-dominated, probably normal fault-controlled, feeder systems. The closest modern analogues of these types of basalt-dominated environments are oceanic basaltic plateaux (as reviewed by Kerr et al. 2000). The high temperatures inferred for Archaean komatiites (Nisbet et al. 1993a; Herzberg et al. 2007; Connolly et al. 2011) suggest that they formed from hot mantle plumes, which agrees with our rift interpretation presented in the previous section (and developed further in Sect. 6). In the common Archaean volcanic cycles, waning magmatism led to the development of small felsic volcanic centres, followed by hiatuses, where chert, BIF, and locally-derived sediments were deposited (Ayer et al. 2002). The felsic centres may be explosive, and magmas typically have TTG-like compositions appropriate to high-pressure anatexis of metabasalt (Bédard et al. 2013). This suggests that they were (often) the eruptive equivalents of the ascending TTG domes, which occasionally broached the surface and were eroded into the adjoining gravity-driven downsags. Variable degrees of interaction between the older rocks that melted and juvenile mafic-ultramafic inputs also led to more complicated, AFC (assimilation and fractional crystallisation) differentiation paths. Other felsic lava types appear to represent low-pressure re-melts of basaltic roof rocks (the Type 3 soda-rhyolites), implying emplacement of hot mafic magma in high-level chambers (Thurston and Fryer 1983; Lesher et al. 1986; Hart et al. 2004; Bédard et al. 2013). Hydrothermal cooling of this volcanic crust led to the development of metal-rich VHMS deposits (reviewed by Galley et al. 2008). Mafic-felsic cycles were repeated on a 3–20 My time-interval.

9.4.4 Regional Deformation of the SE Superior Province

The Abitibi Subprovince, along with the Opatica and Opinaca subprovinces, subsequently underwent regional-scale bulk shortening producing regional folds and broad ductile shear corridors overprinted by a network of discrete shear zones (Figs. 9.8, 9.12, and 9.13) synchronous with TTG magmatism. The change from ductile to brittle deformation and the diachronous onset of compressive tectonism from N to S is outlined by Poulsen et al. (1992). The following sections describe a reinterpretation of deformation of the SE Superior Province in Québec, integrating the results of regional mapping (Theriault 2002) and other field studies (especially Daigneault 1996; Lacroix 1998; Leclerc et al. 2012) with those derived from our interpretation of enhanced aeromagnetic (Fig. 9.12) and gravity (Fig. 9.13) data. Comparisons are made with deformation on Venus to illustrate that plate tectonics is not required to produce the structures seen in the SE Superior Province.

9.4.4.1 Early Folding

In areas away from major shear corridors (discussed in the next section), such as the Chibougamau region of the NE Abitibi (Fig. 9.7), the earliest folds recognized are close to isoclinal, with NW- to NE-striking axial traces (Leclerc et al. 2012). Although previously interpreted as local features developed during syn-volcanic pluton emplacement and/or upwelling of basement gneiss (Dimroth et al. 1986; Daigneault 1991), interpretation of enhanced high-resolution aeromagnetic imagery shows these folds to be more extensive than suspected, and to have also deformed the Chibougamau pluton, implying (at least local) ca. E-W shortening (Leclerc 2011; Leclerc et al. 2012). The earliest fabrics and folds in the Opatica (Benn et al. 1992) and Opinaca (Cadéron 2003) subprovinces also trend approximately N-S, and an early N-S reverse fault and folds with NNW-striking axial traces are mapped by Lacroix (1998) in the Matagami area (location in Fig. 9.7b). In the central Québec Abitibi, similar early folds with ca. N-S axial traces are not apparent on enhanced aeromagnetic imagery.

9.4.4.2 Penetrative Ductile Shearing Interpreted from Enhanced Aeromagnetic Imagery

Previous structural compilations have focussed on mapping discrete brittle-ductile shear zones and faults (e.g. Daigneault 1996; Fig. 9.8a).

Enhanced aeromagnetic imagery (Canadian Aeromagnetic Data Base 2012) illustrates that penetrative dextral ductile shearing within broad (ca. 100 km^+), ESE-WNW trending corridors (Fig. 9.12) predates formation of brittle-ductile shear zones hundreds of metres in width striking E (reverse), ENE (sinistral) and WNW (dextral) (the 'linéaments d'entraînement' of Faure 2001) and discrete NE- and SE-striking faults (the 'linéaments sécants' of Faure 2001), in agreement with field observations (e.g. Pilote et al. 1990; Daigneault 1996; Gosselin 1998; Lacroix et al. 1998). Enhanced images in Fig. 9.12b, c show:

- Zoned, internally fractured granitic plutons constitute domes enwrapped by lithological layering in greenstone sequences.
- Folds are commonly developed against granitoid intrusions that have acted as rigid bodies during penetrative shearing. Complex fold interference patterns develop in the lee of some granitoid intrusions (e.g. in the W of Fig. 9.12c).
- Greenstones in the centre of the imaged area define a continuous regional deformation corridor that is offset sinistrally by the NE-striking Wedding-Lamarck Fault (enlarged inset, Fig. 9.12b).
- The enlarged inset in Fig. 9.12c shows a dextral ductile shear zone striking NW-SE that is the southern part of a regional shear zone that displaces the Abitibi-Opatica contact (Fig. 9.8a).
- Several generations of Palaeoproterozoic dolerite dykes (narrow, linear magnetic highs striking N, ENE, NNE, and NW on Fig. 9.12b) cut Archaean ductile structures.

Structures developed during ductile deformation resemble those in thin sections of mylonitic orthogneiss, as shown in the enlarged inset in Fig. 9.12b where axial surfaces of close to isoclinal folds trend NE-SW, striking at 45° to the margins of a broad ESE-WNW trending shear zone. Regional lithological layering enwraps the granitoid intrusion asymmetrically (comparable to a σ porphyroclast in mylonites). A second set of "drag" folds, overturned in a dextral sense and with E-W axial surfaces (i.e. striking at a slight angle anticlockwise to the shear direction) develop in the lee of a granitoid intrusion. Note that the southernmost layers affected by this fold are truncated and displaced along a sinistral antithetic shear zone striking ENE. A second ductile sinistral shear zone striking NE is localized on the SE margin of the granitoid where a fold with N-S axial surface is also formed due to a combination of displacement on the sinistral shear zone and interference with a smaller granitoid intrusion. Development of these sinistral ductile shears suggest that there may be a component of bulk N-S shortening across E-W shear corridors, i.e. dextral displacement may be transpressional. A younger, NE-striking brittle ductile shear zone (the Wedding-Lamarck Fault, inset Fig. 9.12b) truncates the fold with N-S axial surface in the S of the enlarged area.

9.4.4.3 Regional Shear Zones Interpreted from Regional Bouguer Gravity

The Bouguer anomaly grid of regional ground gravity data (Canadian Geodetic Information System 2012; Fig. 9.13a) across the same area as covered in Fig. 9.8a was filtered to isolate anomalies from the surface to ca. 25 km depth in Fig. 9.13b[9]. A simplified interpretation of this image in Fig. 9.13c portrays:

- Several blocks of higher density material (=areas dominated by mafic crust) in the Abitibi Subprovince in comparison to areas dominated by less dense TTG plutons. Edges in the horizontal gradient of the total Bouguer gravity data, upward continued to series of levels between the surface and 10 km (i.e. "gravity worms"; simplified on the map as dashed lines) coincide with the margins of interpreted mafic-dominated blocks. Elliptical gravity lows within these high density blocks correspond to granitoid batholiths (which have been omitted from this figure aimed at portraying regional-scale structures only).

[9] Using a Butterworth filter to separate shallow source components determined from the radially averaged energy/power spectrum. Depth estimates are calculated by Geosoft Oasis Montaj™ software using the algorithm of Spector and Grant (1970).

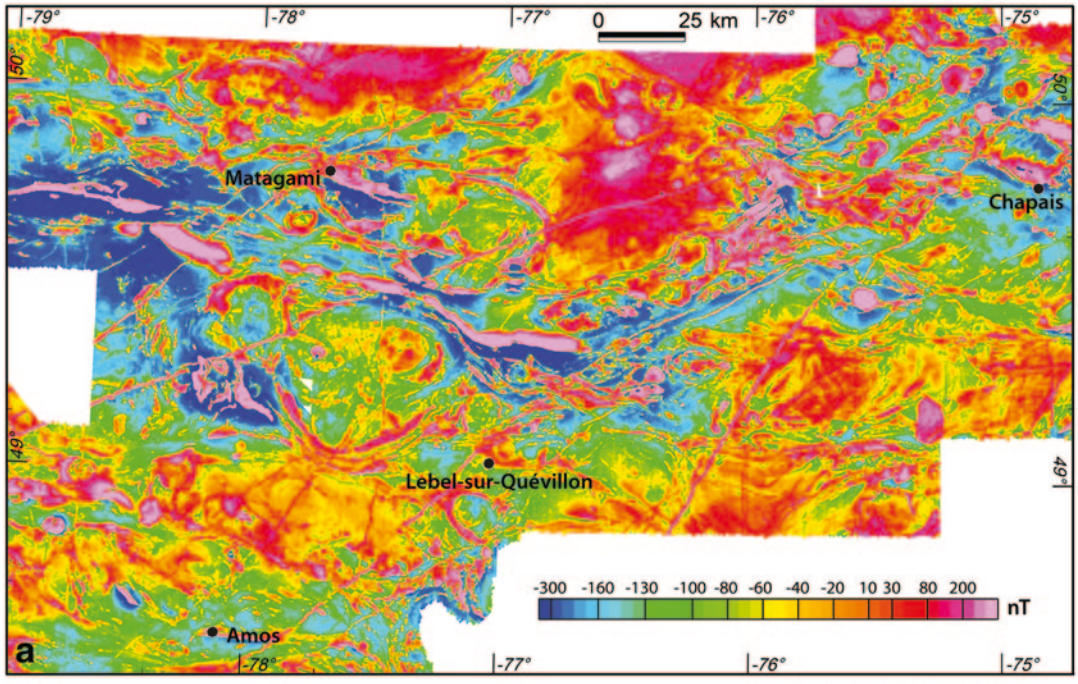
-79°
-78°
-77°
0 25 km
-76°
-75°
50°
49°
Matagami
Chapais
Lebel-sur-Quévillon
Amos
-300 -160 -130 -100 -80 -60 -40 -20 10 30 80 200
nT
a

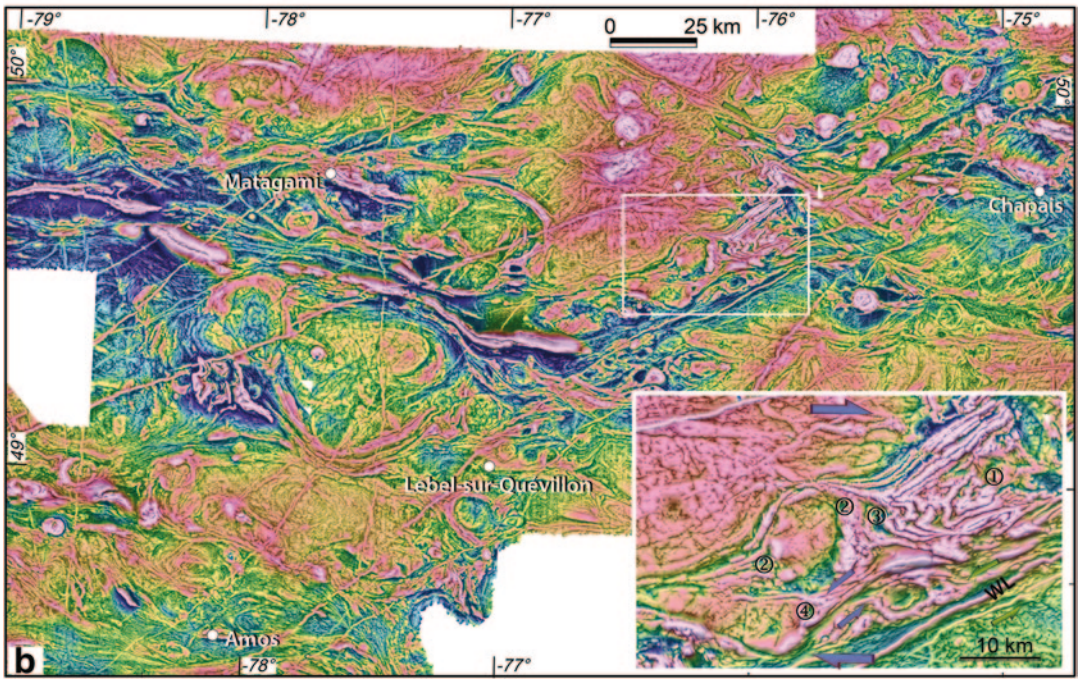
-79°
-78°
-77°
0 25 km
-76°
-75°
50°
49°
Matagami
Chapais
Lebel-sur-Quévillon
Amos
①
②
③
②
④
WL
10 km
b

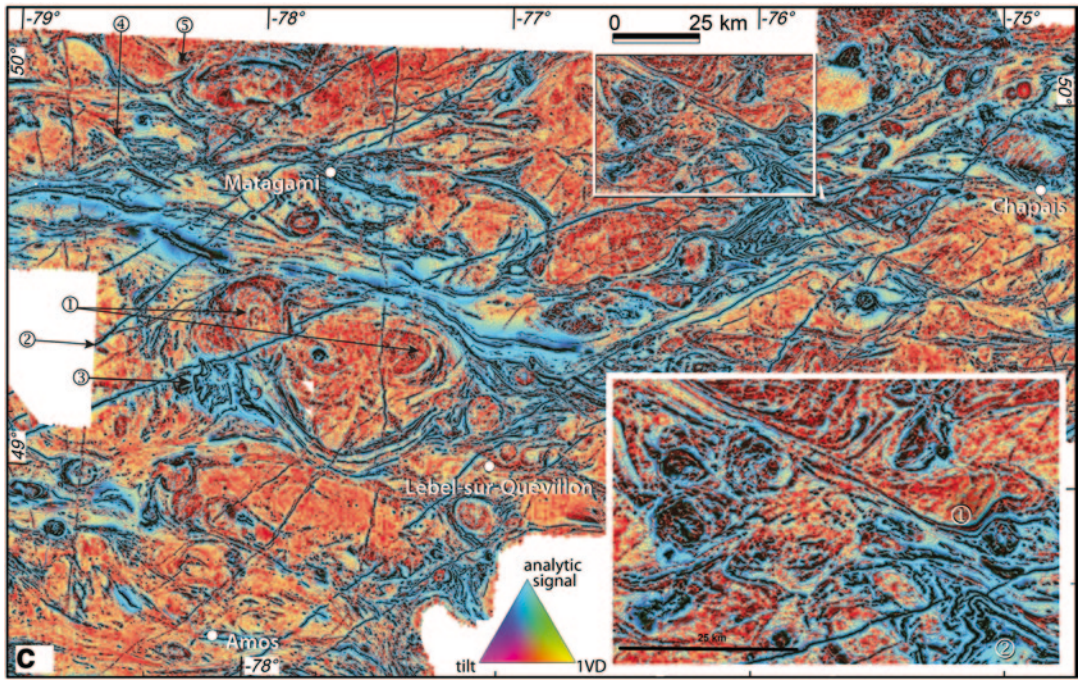

Fig. 9.12 High resolution aeromagnetic data (Canadian Aeromagnetic Data Base 2012) over the north-central Abitibi Subprovince enhanced to portray structural features illustrating penetrative ductile shearing. See Fig. 9.8a for location. (**a**) Total magnetic intensity (reduced to the pole). (**b**) Grayscale tilt image (= $\tan^{-1}$ [vertical gradient/total horizontal gradient]) superposed on an image of total magnetic intensity (TMI) reduced to the pole, with automatic gain control/correction (AGC). The enlarged inset shows criteria for broadly distributed dextral ductile shearing prior to formation of discrete ductile to brittle-ductile shear zones. (*1*) Axial traces of close to isoclinal folds strike NE, i.e. at 45° to the interpreted principal shear orientation in an S/C relationship. (*2*) Stratigraphic layering asymmetrically wraps a granitoid pluton in a similar manner to σ porphyroblasts in thin sections of mylonites. (*3*) 'Drag folds' developed in the lee of the granitoid body are also similar to structures developed in mylonites. (**c**) Ternary image combining horizontal and vertical gradients highlighting folds and shear zones defined by marker horizons in greenstone sequences (mainly blue and black) and primary layering (*1*) and fracturing within syn-volcanic TTG plutons (mainly yellow and orange colours). Smaller, circular, reddish-black anomalies correspond to mapped 'post-volcanic' or 'syn-tectonic' plutons, however most clearly intrude prior to regional ductile shearing. Long, linear features that cross the image (e.g. at locations 2) are Proterozoic dolerite dykes. Complex refolded folds occur between granitoids (e.g. at location 3). Examples of ductile deformation of granitoids where margins are 'dragged' into cross-cutting shear zones are shown at locations 4 and 5. The enlarged inset shows 'drag' of lithological layering in greenstones and granitoids (e.g. at location 1) into a dextral ductile shear zone. Deflection of layering has produced folds with NW-striking axial surfaces (e.g. location 2)

- Offset of the interpreted mafic-dominated areas occurs along ESE-WNW trending dextral and NNE- to NE-sinistral shear zones. The western part of the interpreted ESE-WNW dextral shear zone corresponds to the contact between the northern ('internal') and southern ('external') Abitibi Subprovince based on stratigraphic and structural features (Dimroth et al. 1982; 1984; Ludden et al. 1986; Chown et al. 1992; Thurston et al. 2008), although further E, whilst sub-parallel, the interpreted shear zone is situated slightly to the S of the boundary portrayed by Thurston et al. (2008).
- Abrupt changes in the orientation of gravity worms marking significant shear zones or faults in the Opatica and Opinaca subprovinces coincide with regional transcurrent shear zones interpreted from aeromagnetic imagery (Fig. 9.8a).

- Progressive curvature and offset of positive gravity anomalies in the parautochthon of the Grenville Province (i.e. rocks of the Superior Province that have been overprinted by Mesoproterozoic deformation and metamorphism during the Grenvillian orogenic cycle) occurs along structures marking or sub-parallel to the Grenville Front.

Whilst there is evidence for Proterozoic overprinting close to the Grenville Front (superposition of a new foliation and front-parallel, brittle-ductile to brittle structures; Allard 1976), the NNE to NE-striking sinistral ductile shear zones along the SE margin to the Abitibi Subprovince are, however, clearly Archaean in age:

- The primary lithological layering E of Chibougamau and ESE of Val d'Or (the main areas in the Abitibi Subprovince where greenstones abut the Grenville Front) is reoriented from regional E- and ESE- strikes (respectively) into a NE-SW orientation, as mapped in previous studies (e.g. Dimroth et al. 1986; Leclerc 2011; Leclerc et al. 2012). Sinistral ductile reorientation of greenstones into a NE-orientation adjacent to the Grenville Front is clearly seen on regional aeromagnetic imagery for both areas in Fig. 9.7a and, in the Chibougamau area, on the regional map (Fig. 9.7b) and especially on enhanced aeromagnetic imagery presented by Leclerc (2011) and Leclerc et al. (2012).
- SE of Chibougamau, the early-formed, regionally significant, Kapunapotagen Shear Zone is similarly reoriented from its E-W orientation into parallelism to the Grenville Front where it is overprinted by sinistral Archaean ductile shear zones striking NE (Leclerc 2011; Leclerc et al. 2012).
- Enhanced aeromagnetic imagery also illustrates that sinistral shear zones adjacent to the Grenville Front are cut by Palaeoproterozoic dykes (Leclerc 2011), and hence pre-date Mesoproterozoic deformation in the adjacent Grenville Province.
- NE-striking sinistral shear zones in the Chapais-Chibougamau area control some Archaean gold deposits (Dubé and Guha 1992; Leclerc 2011; Leclerc et al. 2012).
- Mesoproterozoic Grenvillian, 'Himalayan-style' inverted metamorphism is superposed on Archaean peak metamorphic assemblages recognized only along the SE margin to the N Abitibi Subprovince (Cadéron 2003; Cadéron and Rivers 2006).

This regional *Archaean* structure is named the "proto-Grenville shear zone" (Harris, unpublished report for Laurentian Goldfields 2008).

The overall pattern of regional ductile to brittle-ductile shear zones interpreted from Bouguer gravity in Fig. 9.13c is for conjugate transcurrent to transpressional structures implying ca. N-S bulk shortening. Whilst dextral transpressional shearing in the S Abitibi has been previously documented, our gravity interpretation provides the first indication for significant Archaean sinistral displacement along the SE Abitibi margin. Whilst our study has focussed on interpreting regional shear zones, folds with E-W axial traces with half-wavelengths of 10 to 40 km that deform the upper and middle crust are also interpreted from Bouguer gravity by Peschler et al. (2006).

9.4.4.4 Displacement History Along Discrete Shear Zones

The dominant displacements on faults and discrete ductile to brittle-ductile shear zones that cut both the Abitibi, Opatica and Opinaca subprovinces in Fig. 9.8a is reverse ± dextral on E-W striking structures and dextral displacement on NW-striking and sinistral displacement on NE-striking transcurrent to transpressional structures. Bulk ca. NNW-SSE to N-S shortening across the Abitibi has been interpreted from field studies in Québec (e.g. Dimroth et al. 1986; Robert 1989; Daigneault 1996; Lacroix 1998; Daigneault et al. 2002; Leclerc et al. 2012) and in SE Ontario (e.g. Wilkinson et al. 1999), numerical palaeostress modelling (Faure and Rafini 2004; Faure et al. 2010b), and the overall map pattern of regional shear zones interpreted from Bouguer gravity and aeromagnetic imagery. The field studies cited above, however, illustrate that the detailed history of displacement and reactivation along discrete shear zones is far more complex than would be expected during simple regional coaxial deformation and conjugate

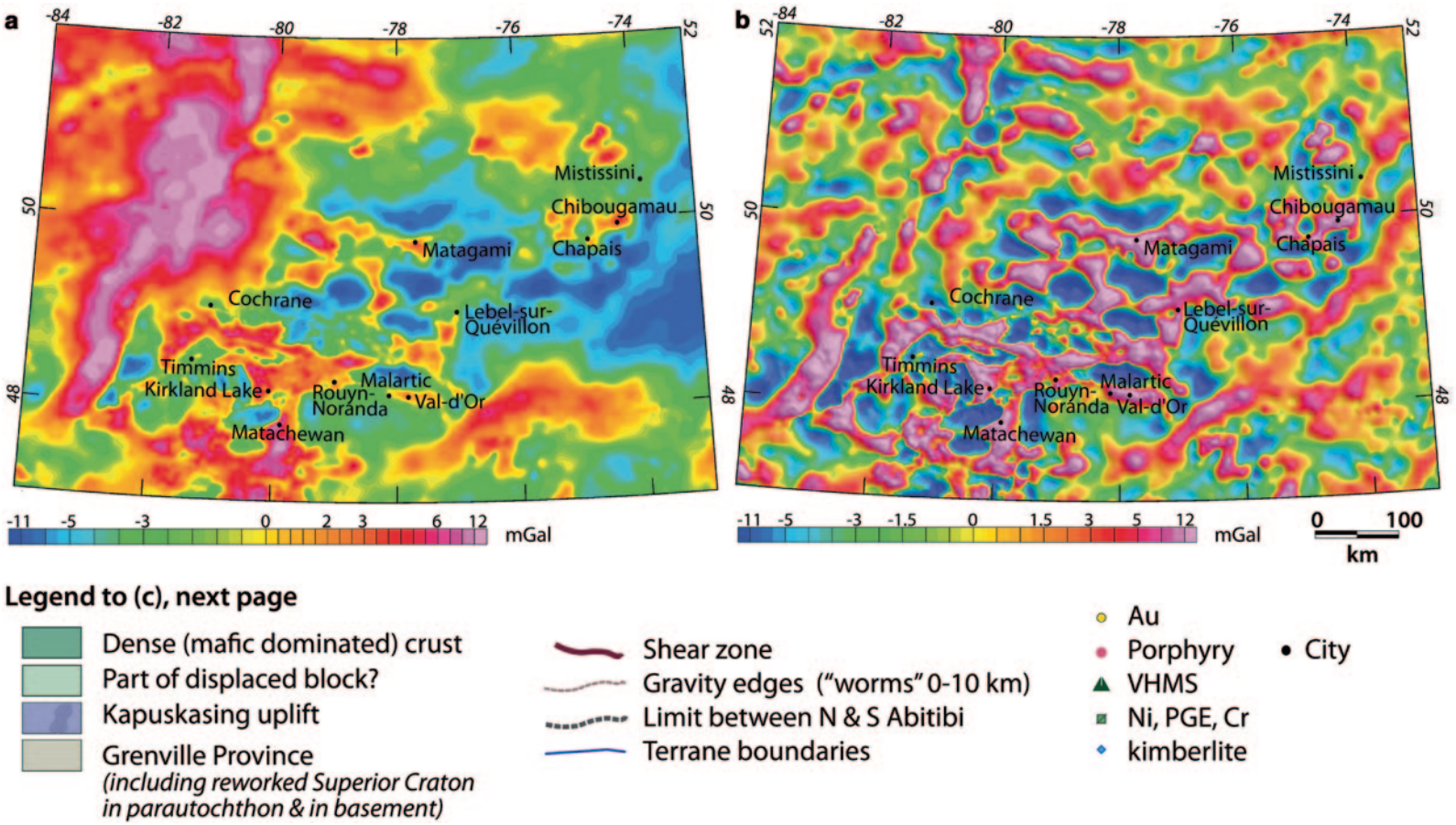

Fig. 9.13 (**a**) Bouguer gravity anomalies over the SE Superior Province (data from Canadian Geodetic Information System 2012). See Fig. 9.7a for location. The NNE-SSW gravity high in the W of the image corresponds to exhumed high grade Archaean rocks of the late Neoarchaean (?) to Palaeoproterozoic Kapuskasing uplift. (**b**) Short wavelength component of Bouguer gravity highlighting features in the upper crust to a depth of ca. 25 km. (**c**) Simplified interpretation of the image in (**b**) highlighting displacement of denser (mafic-dominated) blocks (i.e. gravity highs) by regional transcurrent to transpressional shear zones. Elliptical negative anomalies corresponding to TTG intrusions are not shown for simplicity as we wish to highlight the most significant crustal features and not plutons. Major structures [simplified from calculations of edges in the horizontal gradient of upward continued Bouguer gravity data (= gravity 'worms', shown by brown dashed lines)] in the Opinaca and Opitica terranes are displaced by ductile shear zones. Gravity worms also provide an indication of dip direction on some structures. Ductile deflection ('drag') of gravity highs in the SE part of the image within

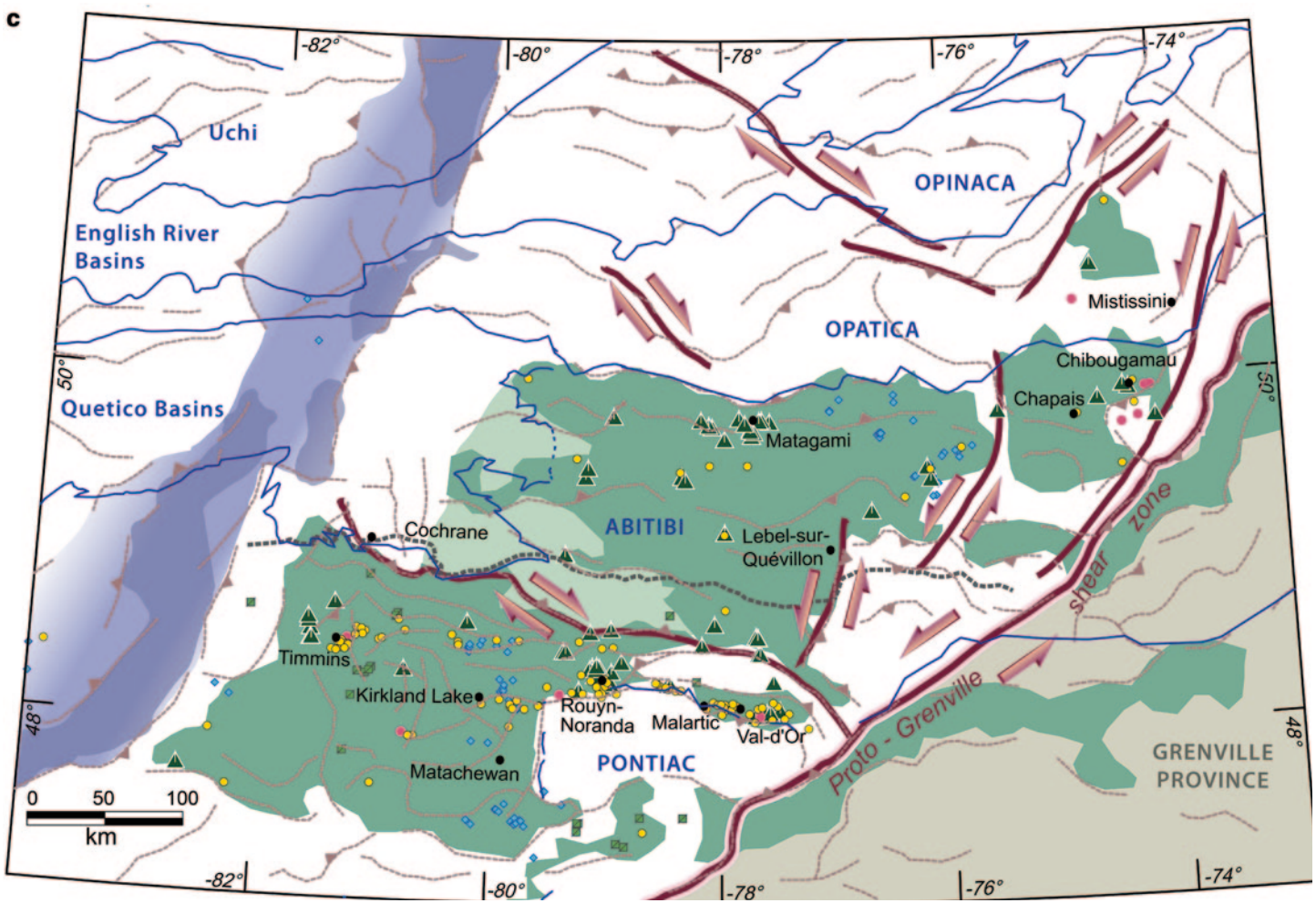

the Superior Province parautochthon to the Grenville province is interpreted as defining a regional sinistral shear zone, the 'Proto-Grenville shear zone' (PGSZ). Sinistral transcurrent shear zones within the eastern part of the Superior Province step *en échelon* N of the PGSZ. The PGSZ was reactivated as a thrust (the Grenville Front) during Grenvillian orogenesis and as an extensional shear zone during post-orogenic collapse. Shear zones define a conjugate array indicative of ca. N-S bulk shortening

shearing. Figure 9.8b presents a simplified representation of the changes in displacement recognized by these authors along the main structures. Furthermore, changes in calculated or inferred palaeostresses vary across the Abitibi, and show considerable heterogeneity:

- A series of changes in the direction of bulk shortening from NE-SW to N-S, back to NE-SW, and then to NW-SE, is proposed by Lacroix (1998) in the NW Abitibi.
- Palaeo-stress determinations in the Rouyn-Noranda district of the SE Abitibi by Carrier et al. (2000) document progressive changes in the orientation of maximum compressive stress from NW-SE to NE-SW and then to N-S.
- A progressive rotation of far-field regional stresses from NW-SE shortening to N-S shortening is inferred for the central Québec Abitibi by Fayol et al. (2011, 2012).
- Early sinistral displacement along the Larder Lake-Cadillac and Porcupine Destor faults in the southern Abitibi was proposed by Hubert et al. (1984) based on fold-fault relationships, although subsequent studies (e.g. Daigneault et al. 2002) documented thrust and dextral displacements.
- Shallowly-dipping, S-to SW-verging imbricate thrusts in the mid-crust underlie steep S-directed reverse faults and younger-N-verging out of sequence and back thrusts are interpreted from field and seismic data by Lacroix and Sawyer (1995) in the northern Abitibi near its contact with the Opatica Subprovince. Thrusts have been steepened, folded and reactivated during subsequent dextral shearing. Sinistral shearing is documented in a segment of the Abitibi-Opatica contact striking ENE (Goutier 2006). On the opposite margin to the Abitibi Subprovince, shallowly dipping, S-directed thrusts accompanied by upright to recumbent folds emplace metavolcanics over sedimentary strata in the NW Pontiac Subprovince (Camiré and Burg 1993).

Local extensional sites occur along both ductile and more brittle dextral shear zones within an overall transpressional regime in areas of curvature (‘releasing bends’), Riedel splays, and extension ‘stepovers’ or ‘jogs’ in which some syntectonic plutons are emplaced (e.g. Lacroix et al. 1998). Late-tectonic basins in which subareal conglomerates, sandstones, and shoshonitic lavas were deposited (Timiskaming-type assemblages; Hewitt 1963; Fig. 9.7b) developed either in dilatational sites along strike-slip faults (Card 1990; Thurston and Chivers 1990; Poulsen et al. 1992) or along the margins of basement heterogeneities interpreted from gravity data as in Fig. 9.13c (Fayol et al. 2011, 2012) and were intruded by syenite plutons (Robert 2001) during bulk ca. N-S shortening, or during an intervening period of extension and normal faulting (Bleeker 2012).

The Opatica Subprovince records tectonothermal events synchronous with those in the Abitibi (Davis et al. 1995) and the tectonically thickened boundary between the two subprovinces (Telmat et al. 2000) is displaced by NW dextral shear zones (Fig. 9.8a; Benn et al. 1992). Although a fossil subduction zone is interpreted between the Abitibi and Opatica by Calvert et al. (1995) and Calvert and Ludden (1999), no evidence for density changes in the deep crust consistent with this interpretation is shown by gravity data (Telmat et al. 2000), as is also the case for the W Superior Province described above. The structure imaged on the Lithoprobe seismic profile may simply define a crustal-scale shear zone similar to those produced in numerical models of shortening of Archaean lithosphere by Gray and Pysklywec (2010b), as discussed by Harris et al. (2012).

Early ductile, orogen-parallel shearing and the regional and temporal variability and changes in displacements along subsequent discrete shear zones cannot readily be explained by simple tectonic models of bulk shortening without lateral escape. Application of simple homogeneous shortening models would require superposition of several deformation events. However, a consistent sequence of superposed deformation events cannot be established across the subprovince. Late sinistral transcurrent shearing identified in our study along the SE Abitibi margin is not produced in physical and numerical ‘vice’ models of Cruden et al. (2006). Temporal and spatial changes in deformation characterizing the Abitibi are, however, consistent with a model

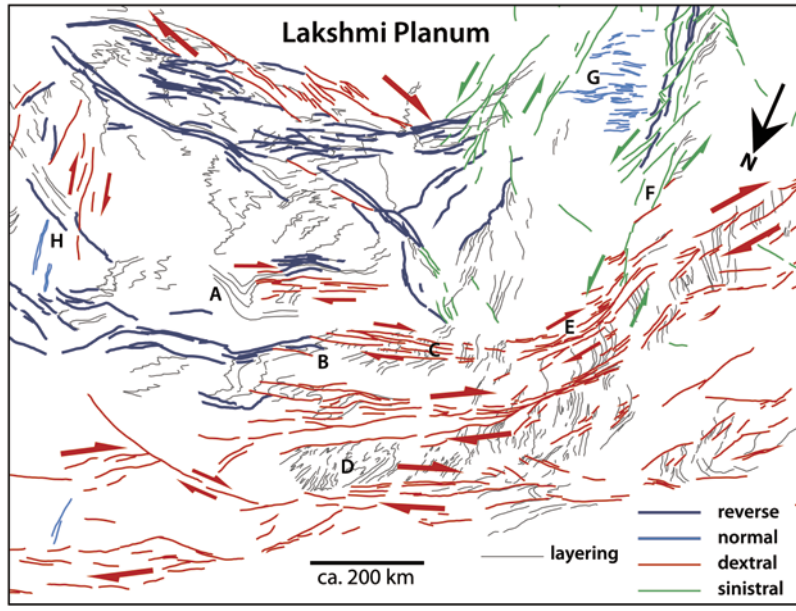

Fig. 9.14 Enlargement of the area N of the interpreted Lakshmi Planum indenter, Venus (see Fig. 9.4a for location), flipped horizontally and slightly rotated to correspond to the orientation of structures in the SE Superior Province. This interpretation portrays a similar geometry and displacement senses along shear zones as in the SE Superior Province in Fig. 9.8a. Arrow shows the N orientation on Venus (c.f. Fig. 9.5). Orogen-parallel transcurrent and reverse shears and cross-cutting transcurrent shears on Venus formed without plate tectonics, subduction and collision, suggesting that these processes were not required to produce structures in the SE Superior province. Note that the reorientation into a NNE-SSW orientation and sinistral offset of orogen-parallel shear zones along the right side of this map (sub-parallel to the Lakshmi Planam indenter margin) is also interpreted in the SE Superior Province. In the SE Superior Province, this major regional *Archaean* structure, the proto-Grenville shear zone, has been overlooked and/or has been regarded as Mesoproterozoic. See text for further details and comparisons between labelled features with the SE Superior Province

where there is both combined shortening and orogen-parallel shearing during lateral escape, as developed in front of an indenting body (e.g. Davy and Cobbold 1988; Cobbold and Davy 1988; Ratschbacher et al. 1991a, b), as along the Proterozoic NW Superior boundary (Kuiper et al. 2011).

Previously described Proterozoic and Phanerozoic examples of indentation and lateral escape (e.g. Himalaya; Tapponnier and Molnar 1976; Tapponnier et al. 1982; Fig. 9.6c) clearly involved plate tectonic processes of subduction and collision. However, as described in Sect. 3.4, the western Ishtar Terra region of Venus provides an excellent example of regional deformation accompanying indentation and lateral escape without plate tectonics. The geometry of shear zones developed in the region ahead of the Ishtar Terra indenter (Fig. 9.6b) is therefore compared in the next section to the SE Superior Province to ascertain whether there are similarities between the two regions, and thus to determine if plate tectonics is required to produce the geometry of structures mapped in the Superior Province.

9.4.5 Comparison Between Deformation in the SE Superior Province and the Freyja Montes-Itzpapaloti Tessera Area (western Ishtar Terra), Venus

9.4.5.1 Geometry and Displacement along Archaean Shear Zones

The geometry, scale and displacement sense on structures in the Freyja Montes-Itzpapaloti Tes-

sera area in front of the interpreted Lakshmi Planum indenter in western Ishtar Terra (Fig. 9.6), flipped horizontally and rotated to match orientations of features in the SE Superior Province in Fig. 9.14, are very similar to those of shear zones in the the SE Superior Province (Fig. 9.8a), suggesting similar modes of formation.

Application of the indenter and escape geometry established from western Ishtar Terra explains many features that have been hard to reconcile in existing models of bulk shortening or dextral transpression for the Québec Abitibi, and accounts (in a single progressive deformation event) for observations that would traditionally require the superposition of several discrete, deformation phases:

- At location A on Fig. 9.14, a regional fold with a N-S axial trace is located at the termination of an orogen-parallel shear dextral zone. Folds with ca. N-S axial traces, as described in Sect. 4.2.1, previously interpreted as requiring early regional E-W shortening for their formation, may instead have similarly formed due to local shortening at the termination of E-W, orogen-parallel, broad ductile dextral shear zones.
- Whilst the lower half of Freyja Montes-Itzpapaloti Tessera area (as oriented in Fig. 9.14) is dominated by dextral shear zones, reverse faults dominate the area closer to the interpreted indenter. In the Abitibi Subprovince, there are similar regional changes from areas dominated by bulk N-S flattening, where reverse faults and conjugate NW-striking dextral and NE-striking sinistral shears are developed (as in the Chibougamau area of the NE Abitibi; Daigneault et al. 1990; Dubé 1990; Daigneault 1991; Dubé and Guha 1992; Leclerc 2011; Leclerc et al. 2012), to areas dominated by E- to SE-striking dextral transpressional shear zones, such as the Destor-Porcupine-Manneville and Cadillac-Larder-Lake fault zones in the Val d'Or region of SE Abitibi (Daigneault et al. 2002).
- The Freyja Montes-Itzpapaloti Tessera area in Fig. 9.14 shows both orogen parallel and oblique shear zones where both reverse and dextral displacements are interpreted on-strike along the same belt (location B), or on parallel structures (locations C). Similarly, in the Abitibi Subprovince, changes from reverse to dextral displacement are documented on both E-W and NW-SE striking shear zones (summarized in Fig. 9.8b). Intense imbrication along S- to SW-vergent thrusts in the NW Abitibi and their reactivation and truncation by younger, E- and NW striking dextral strike-slip faults (Lacroix 1998) is similar to that in the top left of Fig. 9.14.
- Regional folds show both axial trends at ca. 45° to dextral shear zones (c.f. an S/C relationship), as at location D, or subparallel to reverse shears, as near the indenter margin (top of figure).
- Offset of NE-striking dextral transpressional shear zones by NNE-to N-striking sinistral faults is documented in the Urban Barry area of the east-central Abitibi NE of Val d'Or (Kitney et al. 2011). A dextral component of displacement along NE-striking shears is difficult to explain in the conventional model of N-S shortening and dextral transpression, since a sinistral strike-slip component is apparent on similarly oriented, coeval shear zones elsewhere in the Québec Abitibi. Dextral displacements are, however, precisely what is shown on our Venus interpretation in an equivalent position at location E, where E-W dextral shear zones swing to a NE orientation and are overprinted by sinistral shear zones (Fig. 9.14).
- The right hand side of Fig. 9.14 shows a corridor of reverse and sinistral shear zones, as discrete structures (e.g. at location F) or as a broad zone across which E-W shears are reoriented (location E). These shear zones subparallel to the indenter margin are in an equivalent position in the Freyja Montes-Itzpapaloti Tessera area in its orientation in Fig. 9.14 as the interpreted Proto-Grenville shear zone along the SE margin of the Abitibi Subprovince (Fig. 9.13), described in Sect. 4.2.3.

Fault zones superposed on aeromagnetic imagery (Minnesota Minerals Coordinating Committee 2012) show the same overall geometry in the Minnesota River Valley sector of the Superior

Province to that of shear zones in the Abitibi Subprovince. Our model for indentation and lateral escape ahead of an indenter shows many features similar to the interpretations of Mueller et al. (1996). However, as the same geometry of structures was produced across the Québec Abitibi as in Ishtar Terra on Venus, then there is no requirement for subduction along the northern (Calvert et al. 1995; Lacroix 1998) or southern margins of the Abitibi Subprovince (Mueller et al. 1996), to provide a driving mechanism for regional shortening.

9.4.5.2 Proterozoic Reactivation of Archaean Structures?

The structures described above in the SE Superior Province developed at ca. 2.69 Ga (Percival et al. 2004, 2012). Surprisingly, several 2.5 to 2.45 Ga features also match structures interpreted to have formed during indentation and orogen-parallel escape in western Ishtar Terra shown in Fig. 9.14:

i. NW-striking mafic dykes of the Mistassini dyke swarm dated at 2505–2445 Ma (unpublished report by M.A. Hamilton, Jack Satterly Geochronology Laboratory) occur precisely in an area of rifting interpreted on Ishtar Terra (location G) which (based on overprinting relationships) appears to be a late feature.
ii. Rifts and dextral transcurrent shears strike sub-parallel to the interpreted displacement direction in the Freyja Montes-Itzpapaloti Tessera area on the left side of the reoriented interpretation in Fig. 9.14 (location H). These features are in a similar relative position and strike parallel to the enigmatic, ca. 500 km long Kapuskasing 'zone' or 'uplift' (Fig. 9.8a). Extensional, dextral, and reverse displacements are interpreted along the Kapuskasing uplift (Percival et al. 1991; Percival and West 1994). Although dextral displacement along the Kapuskasing uplift is younger than emplacement of the 2.45 Ga Matachewan dykes (Halls and Zhang 1998), dating of granulite gneisses by Krogh and Moser (1994) suggest that the earliest displacements along the Kapuskasing uplift took place at ca. 2.5 Ga. A Rb-Sr age of ca. 1.95 Ga and 340Ar/39Ar biotite ages between 2.42 Ga and 1.89 Ga (Percival et al. 1991) corroborate a multiple reactivation history along this structural zone (Bursnall et al. 1994). Our model suggests that:
   - This significant crustal feature may have initiated at a late stage of progressive deformation associated with indentation in a similar position and with the same rift and dextral displacements as in western Lakshmi Planum, and was subsequently reactivated at 2.5 Ga and in the Palaeoproterozoic and Mesoproterozoic.
   - The ca. 2.5 Ga age marks initiation of this structure during N-S shortening as a continuation of the main tectonothermal event in the Abitibi. Further displacements along the Kapuskasing uplift are likely to have occurred during a separate, Palaeoproterozoic shortening event, with further reactivation until ca. 1.14 Ga (Bursnall et al. 1994).

9.5 Tectonics of Venus and the Archaean Earth

9.5.1 Mechanisms for Regional Shortening

Lithospheric shortening on Venus is interpreted as resulting from either:

- Mantle downwelling (Kiefer 1991; Kiefer and Hager 1991b; Simons et al. 1994; Koenig and Aydin 1998; Mège and Ernst 2001) or similarly, delamination and negative diapirism or 'drips' (Head 1990b; Davies 1992; Pysklywec and Cruden 2004; van Hunen et al. 2008). Mantle downwelling or drips accommodate crustal extension at rifts without modern subduction. A similar, pre-subduction model for the Archaean Earth is discussed by Brown (2009 and references therein) and negative diapirs, similar to those proposed for Venus, have corollaries in an Archaean Earth (Bédard 2006; Bédard et al. 2013).
- Gravitationally induced compression in geoid lows (Bilotti and Suppe 1999), e.g. in forming wrinkle ridges.

- Gravitationally induced stresses acting radially from uplifted areas (Simons et al. 1994) forming folds and thrusts rimming domes and coronae (i.e. similar to the 'vertical tectonics' model of Collins et al. 1998 for Archaean tectonics).

We favour an interpretation whereby large, 'plate-like' horizontal displacements on Venus result from tractions due to strong coupling between the lithosphere and mantle. Tectonic models for large horizontal displacements of rigid 'terranes' on Venus support the cratonic mobilism hypothesis presented by Bédard et al. (2013) for the Archaean Earth. As suggested for India and Africa (Alvarez 2010; Becker and Faccenna 2011; Sokolov and Trifonov 2012), the Australian Plate (Harig et al. 2010) and the Americas (Liu and Bird 2002; Eaton and Frederiksen 2007; Forte et al. 2010; Husson et al. 2012), Bédard et al. (2013) propose that deep seated mantle currents pushing against the deep keels of Archaean cratons caused them to drift across the Earth's surface, accreting simatic lithosphere to their leading edges. Bédard et al. (2013) contend that the overprinting shortening and accretion of terranes recorded the beginning of continental drift in the Archaean. The leading edges show reverse faulting, verticalization of accreted basaltic terranes, uplift and erosion to form turbidites and metasedimentary belts. The overridden basaltic plateau crust would not subduct but subcrete (Fig. 9.1), and melt as pulses, so contributing to craton growth. Although subcretion of basaltic crust in a plate tectonic framework seems implausible (see discussion above), a mobile craton provides the necessary driving force for subcretion. The craton sides would mostly be strike-slip faults, while the lees would be tensional low-standing areas. Craton interiors would be flat, shallow-water platforms, cut by large oblique strike slip faults that reactivate early structures. Bédard et al. (2013) also suggest that asymmetric keels could allow craton rotation, allowing changes of structural grain and reversals of shear sense on major faults.

In the tectonic model of Bédard et al. (2013), contrary to popular views, Archaean cratons are not stable nuclei against which mobile belts were accreted, but are themselves the active tectonic agents. Previous tectonic models for western Ishar Terra similarly explain the formation of fold belts by displacement of surrounding lava plains against an immobile, craton-like Lakshmi Planum, whereas our indentation and escape model implies that the opposite has occurred, i.e. that Lakshmi Planum is the mobile, indenting body, whose displacement is driven by mantle flow against its lithospheric root.

9.5.2 Configuration of Constituent Blocks on an Archaean Earth

If juvenile mafic-rich crust like that found in the E Yilgarn and Abitibi belt are samples of the non-cratonic part of Earth, then we can infer a mosaic of small, basalt-dominated terranes. The size of these terranes is poorly controlled. The largest isotopically coherent Archaean domain we know is from the NESP middle crust, and is only ca. 200–300 km wide (Boily et al. 2009). In contrast, the Ontong-Java plateau is over 1000 km wide. Since there is no clear evidence for subduction or seafloor spreading in Archaean assemblages, the evidence seems most consistent with a largely static mosaic of shield volcanos forming a stagnant lid over most of the planet. Stagnant lid convection (Solomatov and Moresi 1996, 1997, 2000; Sleep 2000; van Thienen et al. 2005; Ernst 2007; Whittington et al. 2009) is typified by a stiff (immobile) lid dominated by conductive cooling, while the underlying mantle develops a series of convection cells to evacuate heat. The vertical scale of these mantle cells is poorly constrained, but may be proportional to the thickness of the lid, which would imply layered mantle convection in the Archaean. In a stable stagnant lid regime like Mars, the thick, cold lid is occasionally pierced by massive outpourings of magma. In an unstable regime like early Venus, hot spot volcanism is the primary heat loss mechanism (Phillips et al. 1991; Noltimier and Sahagian 1992) and there are frequent volcanic resurfacing events where most of the pre-existing crust is buried and recycled (Hansen 2007a, b; cf. Van Thienen et al. 2004a, b). Structural patterns on Venus suggest

that jostling of small surface plates as a result of basal traction led to deformation of plate edges (Noltimier and Sahagian 1992; Phillips and Hansen 1998). Radiogenic and stable isotope data suggest that during most of the Archaean, the Earth efficiently recycled most of its crust (Bennett 2004; Valley et al. 2005; Kemp et al. 2010; Debaille et al. 2012) which is consistent with an unstable stagnant lid regime as discussed here.

In the Archaean context, it seems reasonable to posit that the basaltic crust was thickest above the ascending limbs of convection cells because more lava would have erupted there. The absence of garnet signatures in most Archaean basalts (e.g. Hollings and Kerrich 2004; Kerrich et al. 2008) implies that most of the melting occurred at shallow levels in the subjacent mantle, implying that the convection cells were not vertically extensive. This may explain why the plateau type crust was static, since it did not have a deep root capable of being affected by the flow patterns of the deeper mantle. The absence of a lithospheric root also explains why Archaean felsic melts have TTG-like signatures, whilst Iceland does not. The modern oceanic lithospheric mantle thickens as the crust drifts away from the hot ridge axis. This protects the crust from subjacent convection cells or rolls, and so prevents extensive lower crustal anatexis. Crustal anatexis in Phanerozoic oceanic plateaux would mostly occur at shallow levels, where central complex volcanoes (and magma chambers) focussed heat advection to high levels.

Most komatiites, particularly the Al-depleted Barberton-type, are thought to have formed from unusually hot upwellings that initiated at depths in the garnet or majorite-garnet fields (Barley et al. 2000; Sproule et al. 2002; Kerrich and Xie 2002; Arndt 2003; Blichert-Toft et al. 2004). In these cases the absence of garnet signatures is due to its exhaustion from the source during batch melting. The upwellings that generate komatiites may be superimposed on the 'background' cooling system, and represent instabilities that originate from greater depths. In other words, komatiites may represent products of deep-sourced plumes that may have helped trigger initiation of cratons, whereas normal Archaean 'oceanic' crust would be dominated by tholeiitic melts derived from smaller-scale shallow convection cells.

Because each oceanic terrane would have formed above an upwelling zone, it would have been buoyed up and have been in tension, while the junctions of the different terranes would have been low-standing depocentres, may have been in compression, and could have been tectonically thickened during subsequent compression. Because most of the crust formed by extrusion, it would have been hydrated through seafloor metamorphism and hydrothermal cooling, and then have been buried by the next volcanic pulse. With time the lavas would get buried deeper and deeper until the heat conducted and advected from below metamorphosed them, and eventually induced widespread lower crustal anatexis. The dense pyroxene-garnet restites from basalt anatexis would have foundered and been recycled into the mantle (Herzberg et al. 1983; Vlaar et al. 1994; Ducea and Saleeby 1998; Jull and Kelemen 2001; van Thienen et al. 2004a, b). This lower-crustal attrition would have hindered the development of a stable lithospheric mantle root capable of protecting the basaltic crust from recycling.

In this scenario, these oceanic micro-terranes would have formed largely by extrusive processes, and would have been recycled by piece-by-piece attrition from below. Since heat was lost not only by conduction, but by partial melting of the mantle (consuming latent heat) and advection of magma to the surface, the system may have reached a self-regulating near-steady state. If heat ever built up due to systemic inefficiencies, then the system would go through a localized 'convulsion' (eruption, overturn, assimilation; c.f. numerical models of Armann and Tackley 2012 for Venus) so as to evacuate the excess heat. We posit that this is the 'background' upon which was superimposed the effect of a) major deep seated mantle plumes leading to craton formation, and b) craton migration leading to terrane accretion. The SE Superior Craton provides an example of these tectonic processes.

9.6 Summary and Discussion

9.6.1 Formation and Deformation of the SE Superior Province without Modern-Style Subduction

Polat and Kerrich (2001) interpret components of the Abitibi-Wawa belt as 'part of a continental-scale subduction-accretion complex that formed along an Archaean convergent plate margin during the trenchward migration of the magmatic arc axis'. They infer that the komatiites and associated depleted tholeiitic basalt sequences are dismembered fragments of oceanic plateaux, whilst LREE-enriched and HFSE-depleted TTG plutons and associated bimodal (basalt/dacite) volcanic sequences are fragments of volcanic arcs. They consider that 70–80 % of the magmas are arc-related and only 20–30 % oceanic plateau related. We disagree with the interpretation that the LREE-enriched and HFSE-depleted basaltic/dacitic magmas are arc-related, and see these as crustally-contaminated plume magmas or as high-P remelts of such basalts (e.g. see Bédard 2006, 2013; Bédard et al. 2013).

Deformation of the Superior Province (described in Sect. 4) is traditionally interpreted in terms of progressive terrane accretion/docking of subduction-related arcs and oceanic plateaux with older cratonic elements of the N Superior Province or Hudson's Bay Terrane (e.g. Dimroth et al. 1983; Ludden et al. 1986; Card 1990; Mueller et al. 1996; Calvert and Ludden 1999; Percival et al. 2004, 2012). Terrane accretion is interpreted as occurring in distinct orogenic episodes (Percival et al. 2004, 2012), formerly grouped as the Kenoran Orogeny. In this plate tectonic model, N-S shortening in the Abitibi-Wawa terrane is interpreted as resulting from collision with and subduction beneath the N Superior Province in the Shebandowanian orogeny at ca. 2696 Ma (Percival et al. 2004, 2012). Further N-S shortening of the Abitibi-Wawa terrane is inferred during its subsequent collision with the Minnesota terrane to the S in the 2680 Ma Minnesotan orogeny (Percival et al. 2004, 2012).

We propose an alternative model, applying the concepts discussed in the previous section, where the formation and deformation of the southern Superior Province occurred without modern-style subduction. The series of events is depicted schematically in Figs. 9.15 (map view) and 9.16 (cross-section):

1. Rifting of early-formed and assembled Archaean lithosphere (Figs. 9.15a and 9.16a; now comprising the N Superior Province and Minnesota River Valley domain) started at ca. 2.78–2.75 Ga due to initial impingement of one or more large mantle plumes (Fig. 9.16a). The Wawa-Abitibi-Opatica rift (Fig. 9.15b) is thought to have been similar to broad, long, linear rifts on Venus as shown in Fig. 9.3, and may comprise parallel graben linking several plume centres. The Western Superior would similarly have been extended and broken up into a series of 'terranes'.
2. Continued mantle plume activity led to focussed thermal erosion, destruction, and assimilation of ancient lithosphere (as modelled numerically by Sobolev et al. (2011; Fig. 9.16b, e) at ca. 2.75 Ga, and metasomatic "re-fertilization" of SCLM (c.f. Griffin et al. 2009). Although mostly destroyed, analyses of Archaean diamonds (described above) implies that some blocks of highly depleted SCLM are preserved within the newly formed, post-rift sub-Abitibi-Wawa lithospheric mantle. Above the most intense plume activity, older blocks were rafted apart and mafic-dominated volcanism produced isotopically juvenile crust similar to that formed at a volcanic/oceanic plateau (Fig. 9.16c, f). This could generate segments like the Abitibi-Wawa or part of the Wabigoon subprovinces. As a result of the high magmatic flux, older, basal lavas melted and voluminous syn-volcanic TTG plutons were emplaced into the base of the volcano-sedimentary sequence. Minor rifts orthogonal to the main rift axis (Fig. 9.15c) developed at a late stage of plume-related rifting (or alternatively during subsequent N-S shortening).
3. Rifting of both the crust and newly formed SCLM (Fig. 9.16d) continued during waning phase of plume activity ca. 2.73 Ga, due either to a decrease in plume 'strength' or, more likely, due to southward displacement of the

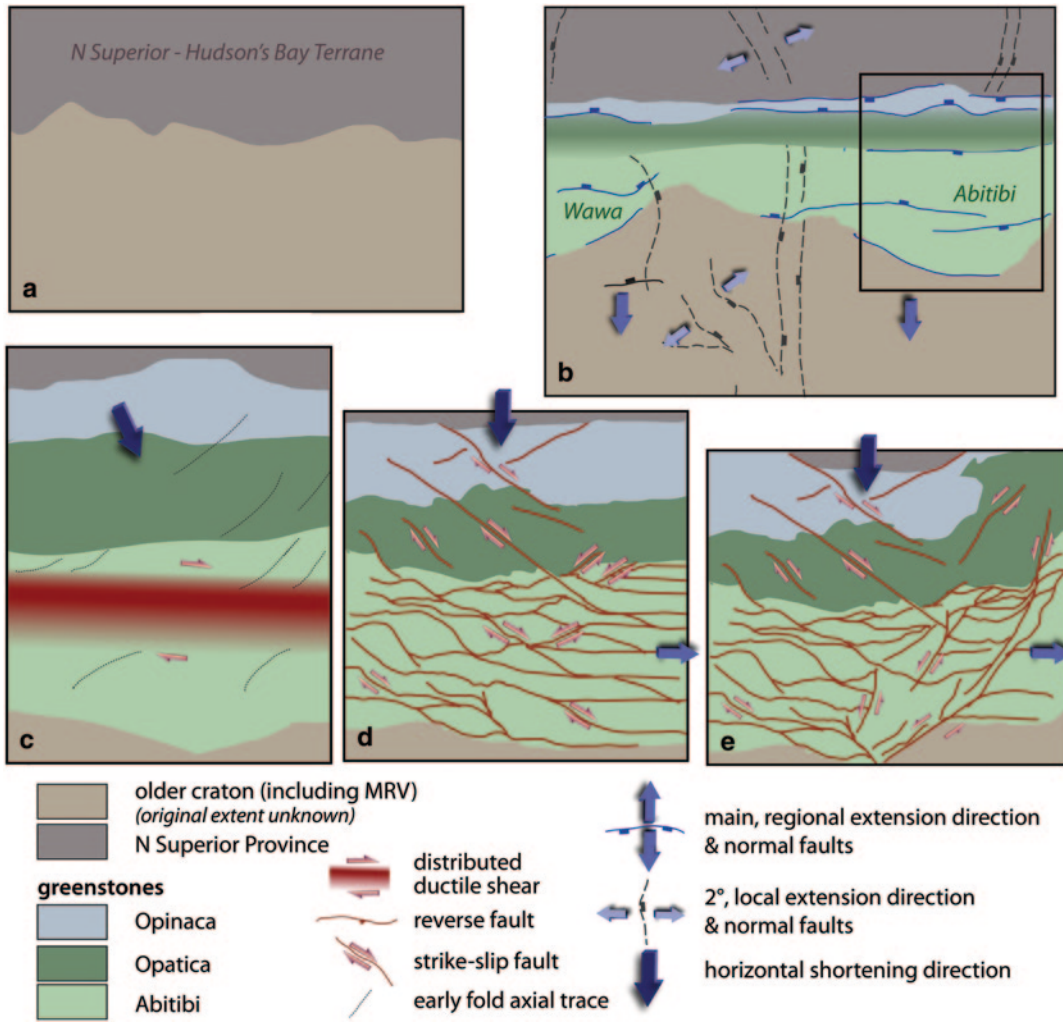

Fig. 9.15 Schematic model of events in the SE Superior Province in map view. (**a**) Configuration prior to rifting. (**b**) Rifting and formation of greenstones during impingement of one or several mantle plumes at ca. 2.75. The Wawa-Abitibi, Opatica, and Opinaca subprovinces developed in the main, E-W trending rift zone. Seismic tomography suggests minor, lithospheric necking/rifting producing secondary extensional features trending N-S to NW-SE (although their age is uncertain). (**c**–**e**) Enlargements of structures developed during subsequent shortening and eastwards lateral extrusion in the SE Superior Craton (area indicated by a rectangle in (**b**)). (**c**) Distributed ductile dextral shearing in the northern to central Abitibi. (**d**) Network of discrete ductile to brittle ductile shear zones that cut the Abitibi, Opatica, and Opinaca subprovinces. (**e**) Late reorientation of structures on the present-day E margin of the Abitibi Subprovince and bending of the eastern Opatica and Opinaca subprovinces into a NE orientation through indentation of the N Superior province and displacement along NE-striking sinistral shear zones. Formation of the proto-Grenville shear zone (subsequently reactivated as the Grenville Front during the Mesproterozoic)

N Superior Craton driven by regional mantle flow acting against its thick keel (c.f. the cratonic mobilism model of Bédard et al. 2013, as discussed in Sect. 5).

4. Southward translation of the N Superior Craton enhanced through combined regional mantle flow and the lateral flow associated with a mantle plume led to sequential southwards accretion of crustal fragments and

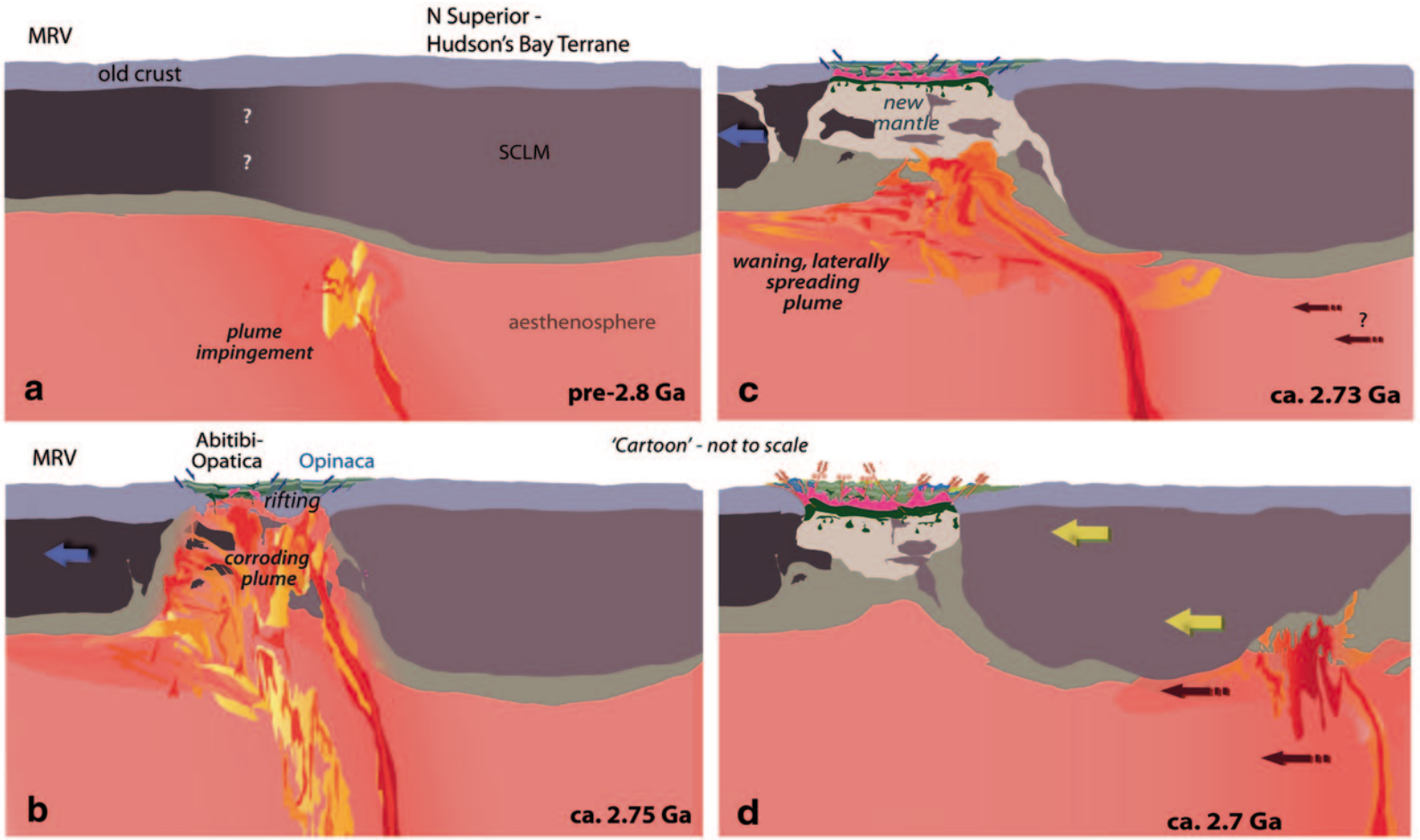

Fig. 9.16 Highly simplified and schematic cross-sections portraying interpreted events in the SE Superior Province. Representations of the form of thermal anomalies defining mantle plumes are based on numerical simulations of Sobolev et al. (2011). (**a**) Initial configuration prior to ca. 2.78 Ga. (**b**) Impingement of a mantle plume at ca. 2.75 Ga led to rifting in which greenstone sequences of the Wawa-Abitibi-Opatica subprovinces formed (note stratigraphic relationships are far more complex than portrayed). Greenstones were intruded by mafic and TTG plutons. Fragmentation, erosion and extensive destruction of ancient crust and SCLM occurred above the plume head. (**c**)

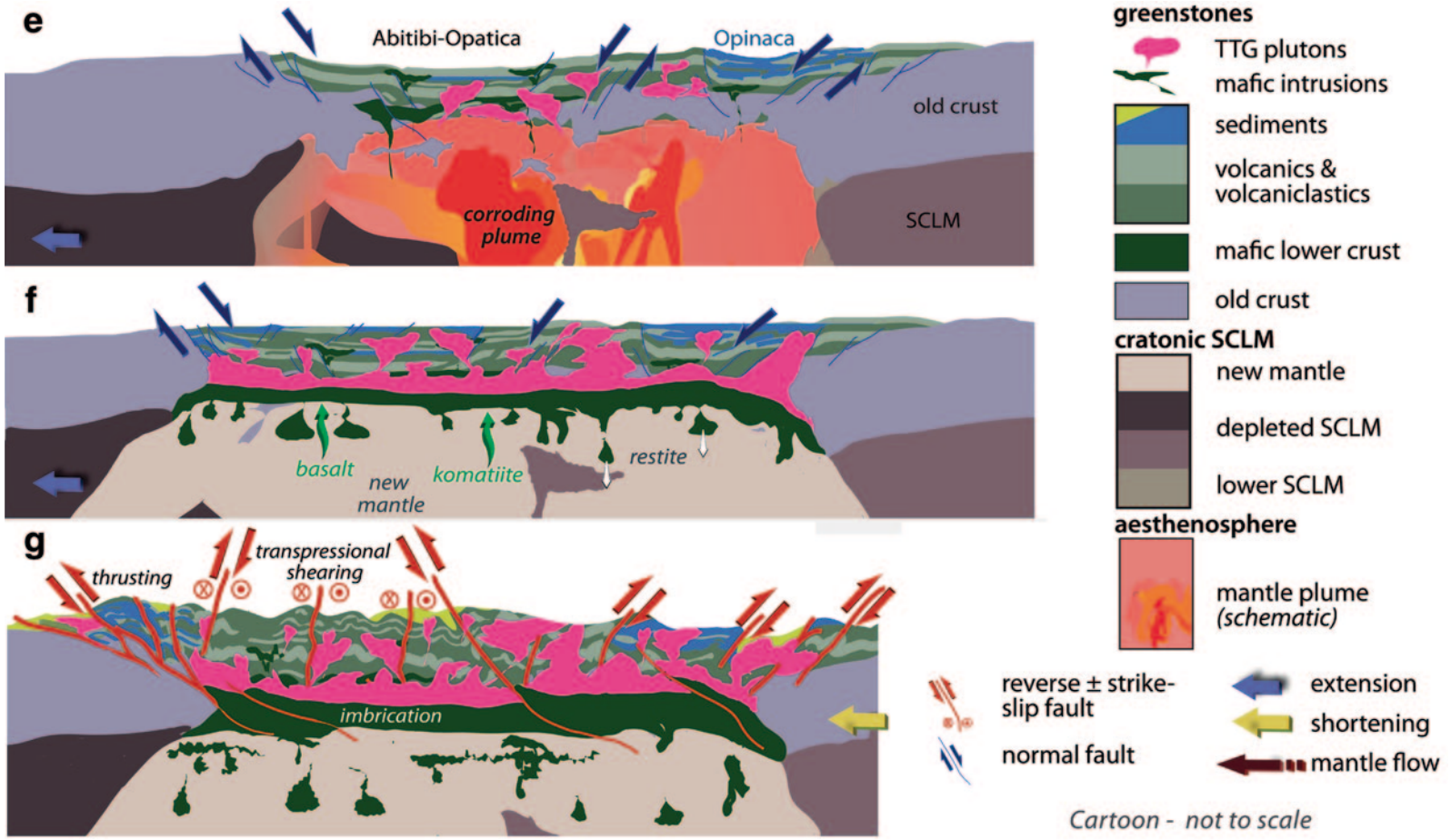

Continued rifting of crust and newly-formed SCLM, waning in intensity of a mantle plume, and displacement of the Superior Province due to regional mantle flow acting on the deep keel of the N Superior Province at ca. 2.73 Ga. Further deposition of volcanics, volcaniclastics, and sedimentary sequences in rift/thermal sag basins. Continued TTG intrusion. (**d**) Horizontal shortening and inversion of the Abitibi rift during southwards displacement and indentation of the N Superior Province through regional mantle flow, accentuated by a spreading plume beneath the northern Superior Province. Reverse±dextral shearing and intrusion of syn-tectonic plutons at ca. 2.7 Ga. See text for details. (**e–g**). Enlargements of (**b**) to (**d**) respectively

oceanic plateaux-like segments, culminating in indentation of the N Superior Province into the Opatica and Abitibi subprovinces (Figs. 9.15c–e, 9.16d, g). Post-volcanic plutons were intruded across the Abitibi and Opatica subprovinces. Broad corridors of dextral ductile shearing accompanied initial eastward ductile flow and lateral extrusion (i.e. orogen-parallel flow; Fig. 9.15c). With time, cooling, and exhumation to shallower crustal levels, deformation was subsequently localized into discrete ductile to brittle-ductile shear zones that occur within and cross-cut dextral ductile shear corridors (Fig. 9.15d). Heterogeneous strains due to combined shortening and lateral extrusion, further complicated by the geometry of large TTG plutons, resulted in spatial and temporal variability in displacement senses on discrete shear zones. The overall geometry, however, is of E-W reverse shears and conjugate NW-striking dextral and NE-striking sinistral shears with variable reverse components, as determined in the many previous structural studies cited in Sect. 4.3.1. Thurston et al. (2008) note that significant thrust repetition of greenstone assemblages has not been extensively recognized in the Abitibi. An exception is the folded Pipestone thrust (Dinel et al. 2008; Bleeker et al. 2008) in the south-central Abitibi belt of Ontario. Southward thrusting of greenstones is also documented on the northern margin of the Pontiac Subprovince (Camiré et al. 1993). Bulk N-S shortening was accommodated by displacement on moderate to steeply dipping reverse and transpressional to transcurrent faults over an extremely wide area, instead of large amounts of localised reverse or thrust displacement as in modern collisional orogens.

5. Late-tectonic ('Timiskaming') basins formed in dilational sites created by stepping of transcurrent shear zones or on the margins of major crustal discontinuities during continued regional shortening.
6. Reorientation of domains and E-W structures occurred through late displacement along NE-striking sinistral∓reverse shear zones, including the proto-Grenville shear zone (Fig. 9.15e).

9.6.2 Implications for Mineralization

A plume-related rift environment for formation of greenstone sequences is consistent with tectonic models for VHMS deposits presented by Galley et al. (2008), and thus does not require arc-related rifting (c.f. Bierlein et al. 2006). As in many Archaean granite-greenstone terrains, epigenetic ('orogenic' or 'lode') gold mineralization is late in the structural history, within subsidiary structures to main regional shear zones (e.g. Pilote et al. 1990; Groves et al. 2000; Goldfarb et al. 2005; Robert et al. 2005, 2007; Dubé and Gosselin 2007) that are commonly long-lived, lithospheric-scale structures (McCuaig and Kerrich 1998; Bierlein et al. 2006; Blewett et al. 2010b; Hronsky et al. 2012). Whilst these authors interpret the tectonic history of the Superior Province (and other Archaean terrains such as the Yilgarn Craton[10]) in terms of subduction and arc accretion models, we show above that this is not the case for the S Superior Craton where the major late, 'orogenic' gold deposits are preferentially located in reactivated early structures above the 'fossil' rift margins identified in tomographic images of SCLM. Proximity of gold deposits to our interpreted SCLM discontinuities may also help explain the common association between gold mineralization and (mantle-sourced) lamprophyres (Rock et al. 1987; Rock and Groves 1988; McCuaig and Kerrich 1998; Hronsky et al. 2012), as both hydrothermal fluid flow and lamprophyre emplacement may be controlled by the same lithospheric-scale faults. As discussed by Faure et al. (2011), definition of the form of keels to Archaean cratons aids in targeting prospective areas for diamondiferous kimberlites.

Our reinterpretations of the deep structure and tectonic evolution of the Abitibi Subprovince also have tectonic and metallogenic implications for once contiguous Archaean terrains in Baltica whose Archaean evolution is presently explained by subduction and accretion models (Weihed et al. 2005). The likely extension of the gold-endowed Abitibi Subprovince, and the interpreted fossil SCLM rift beneath it, into the Be-

[10] Arc-accretion models for the Yilgarn Craton are similarly questioned by Van Kranendonk (2011b).

lomorian and/or other Archaean greenstone belts in the Kola and Karelia cratons, an area where only a few Neoarchaean orogenic gold deposits (e.g. Oleninskoe; Lukonin 2008; O'Donovan and Armitage undated) have been discovered (Weihed et al. 2005), increases their prospectivity for Archaean orogenic gold.

9.6.3 Do Late Archaean and Palaeoproterozoic Structures Reflect Ongoing Mantle Flow?

Orogen-parallel mid-crustal extension along shallowly dipping shear zones between 2660 and 2645 Ma is documented in exhumed Wawa gneisses in the southern Wawa Subprovince (west of the Kapuskasing uplift) 10 to 25 My after the cessation of regional folding and shearing (Moser et al. 1996). These authors suggest that extensional strain in the ductile crust was decoupled from the upper crust. Although Moser et al. (1996) do not identify late structures in the overlying crust formed during orogen parallel flow, areas of E-W shortening responsible for late dextral reactivation of some NE-striking shear zones and the formation of conjugate kinks, as described in the Chibougamau area by Daigneault et al. (1990), Daigneault (1991), Leclerc (2011), and Leclerc et al. (2012) may be a consequence of deeper E-directed ductile flow, i.e. towards the orogen margin.

Localized rifting at ca. 2.5 Ga in the NE Abitibi and SE Opatica (to form the Mistassini dyke swarm and possibly as a precursor to the Kapuskasing uplift) occurs in areas where late rifting is also interpreted on western Ishtar Terra (Fig. 9.14). Although this is ca. 200 My younger than the main tectonothermal event in the Abitibi (and hence may be coincidental), displacement of cratons through interaction with mantle flow may occur over a long time-frame. Northward displacement of India and eastwards lateral extrusion of the eastern Himalaya and Tibet continue to the present day (Zhang et al. 2004; Meade 2007), 50 My after the main period of collision with Eurasia, as a result of continued northward mantle flow (Alvarez 2010; Becker and Faccenna 2011). It is hence possible that continued, southwards displacement of the N Superior Province after the cessation of the main period of regional deformation (in which orogen-parallel flow in the ductile crust may have initiated; c.f. Cagnard et al. 2006b), is similarly responsible for late mid-crustal, orogen-parallel flow, initiation of the Kapuskasing uplift, and development of the broad area of crustal thinning and dyke emplacement in the eastern Abitibi (c.f. Cunningham 2001). Such speculations, nevertheless, require testing through numerical and/or physical modelling.

9.7 Conclusions

We have shown that the formation and deformation of granite greenstone terrains in the Archaean does not require the operation of plate tectonic processes of subduction and seafloor spreading. An unstable stagnant lid model better fits available data. The Archaean Earth would have been a mosaic of oceanic plateau-type crustal domains, underlain by small scale convection cells that yielded the normal tholeiites. Large plume-like mantle instabilities would have focussed delivery of abundant, commonly hotter (komatiitic) magmas, and triggered initiation of cratonization. Once a craton with a lithospheric root formed, it would have begun to drift as a result of mantle currents, accreting terranes to its leading edge, and contributing to craton growth.

Venus provides a likely analogy for an Archaean Earth. Many deformation features of Venus, including regional horizontal displacements of craton-sized plana, plateaux, and coronae that produce refolded folds, regional shear zones, and Himalayan-style indentation and lateral escape, are similar to those found on Earth despite the absence of plate tectonics on Venus. Given the lack of definitive evidence for extensive, modern-style subduction in the Archaean, we consider that Venus-style tectonics, where regional folding and shearing result from ascending and descending mantle plumes and lithospherically coupled mantle flow acting against the thick cratonic keels, best explains regional fold and shear zone geometries and terrane accretion for an Archaean Earth.

Our representations of seismic tomography, spectrally filtered gravity data, and enhanced high-resolution aeromagnetic imagery for the SE Superior Craton provide a new context in which previous detailed mapping and structural studies can be placed. Comparison between the geometry of structures developed ahead of an interpreted indenter on western Ishtar Terra on Venus with those in the Southern Superior Province explains the formation of structures within a progressive deformation event that does not require the operation of plate tectonic processes. We propose that the Superior craton was extended and partly disaggregated due to the arrival of large plumes at ca 2.8–2.75 Ga, with fragments being rafted apart by mantle flow. Where the preexisting SCLM was destroyed or ruptured (e.g. the Abitibi-Wawa belt) magmas would bear no imprint of older crust. We further propose that the stabler cratonic block to the north (Hudson's Bay-Northern Superior terrane), which has the deepest lithospheric roots in North America, then began drifting southward as a result of mantle traction forces, and sequentially re-accreted the partly disaggregated fragments to create the existing architecture of the South and West Superior Shield.

Acknowledgements NASA Venus radar imagery was provided by the U.S. Geological Survey Astrogeology Science Center and the Jet Propulsion Laboratory at the California Institute of Technology. Stéphanie Godey is thanked for making available online her seismic tomographic database for North America. Geophysical data were processed using Geosoft's Oasis Montaj™ software and software developed and kindly provided by Pierre Keating (GSC), who also provided the detailed GSC aeromagnetic grid for the central Québec Abitibi enhanced by LH. Our ideas for the Abitibi benefited from previous studies (too numerous to cite all) and discussions with colleagues, notably Phil Thurston, who is also thanked for providing the Abitibi geological map, François Leclerc, Patrick Lengyel, and Sandrine Cadéron (who sadly passed away before publishing her research on Archaean tectonics adjacent to the Grenville Front). Initial gravity interpretations in the central Abitibi were undertaken by Noémie Fayol. LH acknowledges NSERC for funding of early stages of this research through a Discovery Grant, Laurentian Goldfields for funding initial research in the SE Superior Craton and NW Grenville Province, and the CFI, MELS-Québec, INRS-ETE, and Sun Microsystems for funding computing facilities and software used for processing of geophysical data. Yildirim Dilek, Benoît Dubé, Michel Jébrak, and Jean Goutier are thanked for their comments on an earlier draft. This is NRCAN/ESS/GSC contribution number 20120436.

Appendix 1 Differences between Venus and Earth

Despite its similar size (0.94 times the Earth's diameter), average density, and surface gravity (8.87 m/s^2 on Venus compared to 9.81 m/s^2 on Earth), Venus differs from Earth (McGill 1983; Schaber and Kozak 1990; Bonin 2012; Mocquet et al. 2011; NASA undated) in:

- The presence of a dense atmosphere (atmospheric pressure is 9.8 MPa compared to 0.1 MPa on Earth). Because of the dense clouds, visual means cannot be used to study Venus' surface (hence radar is used for imaging surface features).
- Absence of surface water on Venus; note that liquid water was present on the surface of an Archaean Earth (Sagan and Mullen 1972).
- An atmosphere of mainly carbon dioxide and nitrogen.
- Differences in surface processes and chemical weathering.
- Absence of plate tectonics—mantle plumes dominate the tectonics of Venus.
- Likely absence of an asthenosphere (weak layer in mantle).
- Its high surface temperature of 460 °C, with variations of ca. 100° depending on altitude. The difference in thermal structure results in a different rheological profile to Earth (Kohlstedt and Mackwell 2009).
- A liquid, instead of a solid, core.
- The absence of a magnetic field (either because a core dynamo does not exist or because temperatures are close to the Curie temperature).

Head (1990a) and Hansen (2007b) add the additional differences that:

- Although Earth presents a bimodal hypsometric curve (i.e. cumulative elevation frequency curve), that for Venus is unimodal.
- Venus lacks obvious evidence of weathering, erosion, and sediment transport and deposi-

tion processes, or extensive sedimentary layers clearly deposited by wind or water.
- The thickness of crust on Venus is generally uniform and variations in topography are due to crustal thickening processes (e.g. in orogenic/fold belts) and due to local variations in the thermal structure.
- Differences in relative average crustal thickness between Earth (continental = 40 km/oceanic 5 km) and Venus (upland plateaus/highlands = 'continents' 30 km compared to lowlands at ca. 15 km.
- The Earth has a larger percentage of 'continents'. (Venus has two main highlands that are likened to continents on Earth: Ishtar Terra and Aphrodite Terra.)
- Lithospheric thickness estimates vary on Venus and may be equal or less than on Earth: 100–150 km is estimated by Smrekar and Parmentier (1996) and 100–200 km by Pauer (2004), however Kucinskasl and Turcotte (1994) estimate a lithospheric thickness of ca. 300 km beneath equatorial highlands of Venus. In comparison, lithospheric thicknesses of continental areas on Earth vary between 90 to 300 km (Conrad and Lithgow-Bertelloni 2006).

Appendix 2 Interpretation criteria for structural interpretation of Venus radar imagery

Interpretation criteria of SAR images for Venus in our study follow techniques used in previous SAR interpretations (e.g. Tuckwell and Ghail 2003; Romeo et al. 2005; Fernández et al. 2010; Romeo and Capote 2011):
- Marker horizons (i.e. with distinctive dark or light tones and/or textures) are used to trace regional fold closures and to interpret fold axial traces. Folds of tectonic origin are separated from volcanic flow features due to their similar orientation over 100s of kilometres, the regular wavelength of regional structures that are accompanied by superposed folds of shorter wavelength, their association with reverse, thrust, and strike-slip faults, and the formation of classical fold interference patterns; see discussion on folding by Romeo and Capote (2011).
- Faults with dominant strike-slip displacement are interpreted where marker layers or other structural features (e.g. fold closures or linear features in tessera terrains) are consistently offset in the same sense along the fault's strike.
- Identical features as mapped on Earth (e.g. Wilcox et al. 1973; Sylvester 1988) are used to interpret brittle-ductile transcurrent shear zones. Folds or linear features progressively curve towards, and are offset across, linear structures. Faults with consistent lateral offset at a small angle (15° to 30°) to large, throughgoing structures are interpreted as Riedel shear arrays (c.f. Riedel 1929; Tchalenko 1968, 1970).
- Reverse or thrust faults or shear-zones are interpreted where linear features sub-parallel to axial traces of regional folds locally cross-cut folded lithological layering.
- Normal faults are linear features truncating lithological layering or other structural elements that bound down-thrown blocks (i.e. graben).
- Venus interpretations are aided by comparisons with radar interpretations of folds and shear zones on Earth that are constrained by field mapping (e.g. Rivard et al. 1999; Raharimahefa and Kusky 2006).

References

Abbott DH, Drury R, Mooney WD (1997) Continents as lithological icebergs: The importance of buoyant lithospheric roots. Earth Planet Sci Lett 149:15–27

Abbott DH, Isley AE (2002) Extraterrestrial influences on mantle plume activity. Earth Planet Sci Lett 205:53–62

Aktas K, Eaton DW (2006) Upper-mantle velocity structure of the lower Great Lakes region. Tectonophysics 420:267–281

Allard GO (1976) Doré Lake Complex and its importance to Chibougamau geology and metallogeny. Ministère des Richesses naturelles du Québec Report DP-368, 484 pp

Alvarez W (2010) Protracted continental collisions argue for continental plates driven by basal traction. Earth Planet Sci Lett 296:434–442

Amos J (2009) Probe hints at past Venus ocean. BBC News. http://news.bbc.co.uk/2/hi/8149361.stm. Accessed 3 Feb 2013

Anderson DL (1981) Plate tectonics on Venus. J Geophys Res 8:309–311

Anhaeusser CR, Mason R, Viljoen MJ, Viljoen RP (1969) Reappraisal of some aspects of Precambrian shield geology. Geol Soc Am Bull 80:2175–2200

Anhaeusser CR, Stettler E, Gibson RI, Cooper GRJ (2010) A possible Mesoarchaean impact structure at Setlagole, North West Province, South Africa: aeromagnetic and field evidence. S Afr J Geol 113:413–436

Annen C (2011) Implications of incremental emplacement of magma bodies for magma differentiation, thermal aureole dimensions and plutonism-volcanism relationships. Tectonophysics 500:3–10

Ansan V, Vergely P (1995) Evidence of vertical and horizontal motions on Venus: Maxwell Montes. Earth Moon Planets 69:285–310

Ansan V, Vergely P, Masson P (1996) Model of formation of Ishtar Terra, Venus. Planet Space Sci 44:817–831

Armann M, Tackley PJ (2012) Simulating the thermochemical magmatic and tectonic evolution of Venus's mantle and lithosphere: two-dimensional models. J Geophys Res 117:E12003. doi:10.1029/2012JE00423

Arndt N (2003) Komatiites, kimberlites, and boninites. J Geophys Res Solid Earth 108[B6]. doi:10.1029/2002JB002157

Arndt NT, Lewin É, Albarède F (2002) Strange partners: formation and survival of continental crust and lithospheric mantle. In: Fowler CMR, Ebinger CJ, Hawkesworth CJ (eds) The early Earth: physical, chemical and biological development. Spec Publ, Geol Soc London, 199:91–103

Arth JG, Barker F, Peterman ZE, Frideman I (1978) Geochemistry of the gabbro-diorite-tonalite-trondhjemite suite of southwest Finland and its implications for the origin of tonalitic and trondhjemitic magmas. J Petrol 19:289–316

Atherton MP, Petford N (1996) Plutonism and the growth of Andean crust at 9°S from 100 to 3 Ma. J S Am Earth Sci 9:1–9

Ayer J, Amelin Y, Corfu F, Kamo S, Ketchum J, Kwok K, Trowell N (2002) Evolution of the southern Abitibi greenstone belt based on U-Pb geochronology: autochthonous volcanic construction followed by plutonism, regional deformation and sedimentation. Precamb Res 115:63–95

Ayres LD, Thurston PC (1985) Archean supracrustal sequences in the Canadian Shield: an overview. In: Ayres LD, Thurston PC, Card KD, Weber W (eds) Evolution of Archean Supracrustal Sequences. Geol Assoc Can Spec paper 28:343–380

Bailey RC (1999) Gravity-driven continental overflow and Archaean tectonics. Nature 398:413–415

Baker VR (2013) Terrestrial analogs, planetary geology, and the nature of geological reasoning. Planet Space Sci (in press). doi:10.1016/j.pss.2012.10.008

Bannister RA, Hansen VL (2010) Geologic map of the Artemis Chasma quadrangle (V-48) Venus: U.S. Geological Survey Scientific Investigations Map 3099. http://pubs.usgs.gov/sim/3099/sim3099_map.pdf (map) and http://pubs.usgs.gov/sim/3099/sim3099_pamphlet.pdf. Accessed 19 July 2012

Barker F, Arth JG (1976) Generation of trondhjemitic-tonalitic liquids and Archean bimodal trondhjemite-basalt suites. Geology 4:596–600

Barley ME, Krapež B, Groves DI, Kerrich R (1998) The Late Archaean bonanza: metallogenic and environmental consequences of the interaction between mantle plumes, lithospheric tectonics and global cyclicity. Precamb Res 91:65–90

Barley ME, Kerrich R, Reudavy I, Xie Q (2000) Late Archaean Ti-rich, Al-depleted komatiites and komatiitic volcaniclastic rocks from the Murchison Terrane in Western Australia. Aust J Earth Sci 47:873–883

Barsukov VL et al (1986) The geology and geomorphology of the Venus surface as revealed by the radar images obtained by Veneras 15 and 16. J Geophys Res 91D (supplement):378–398

Basilevsky AT, Head JW (2003) The surface of Venus. Rep Prog Phys 66:1699–1734

Becker TW, Faccenna C (2011) Mantle conveyor beneath the Tethyan collisional belt. Earth Planet Sci Lett 310:453–46

Bédard JH (1985) The opening of the Atlantic, the Mesozoic New England igneous province, and mechanisms of continental breakup. Tectonophysics 113:209–232

Bédard JH (2001) Parental magmas of the Nain Plutonic Suite anorthosites and mafic cumulates: a trace element modelling approach. Contrib Mineral Petrol 141:747–771

Bédard JH (2006) A catalytic delamination-driven model for coupled genesis of Archaean crust and sub-continental lithospheric mantle. Geochim Cosmochim Acta 70:1188–1214

Bédard JH (2010) Parental magmas of Grenville Province massif-type anorthosites, and conjectures about why massif anorthosites are restricted to the Proterozoic. Earth Environ Sci Trans R Soc Edin 100:77–103

Bédard JH (2013) How many arcs can dance on the head of a plume? A 'Comment' on: a critical assessment of Neoarchean 'plume only' geodynamics: Evidence from the Superior province, by Derek Wyman, Precambrian Research, 2012. Precamb Res. 229, 189–197 doi:10.1016/j.precamres.2012.05.004

Bédard JH, Brouillette P, Madore L, Berclaz A (2003) Archaean cratonization and deformation in the northern Superior Province, Canada: an evaluation of plate tectonic versus vertical tectonic models. Precamb Res 127:61–87

Bédard JH, Harris LB, Thurston P (2013) The hunting of the snArc. Precamb Res 229: 20–48 http://dx.doi.org/10.1016/j.precamres.2012.04.001

Bédard JH, Leclerc F, Harris LB, Goulet N (2009) Intrasill magmatic evolution in the Cummings Complex, Abitibi greenstone belt: Tholeiitic to calc-alkaline

magmatism recorded in a subvolcanic conduit system. Lithos 111:47–71

Bédard JH, Marsh BD, Hersum TG, Naslund HR, Mukasa SB (2007) Large-scale mechanical redistribution of orthopyroxene and plagioclase in the Basement Sill, Ferrar dolerites, Antarctica: Petrological, mineral-chemical and field evidence for channelized movement of crystals and melt. J Petrol 48:2289–2326

Begg GC, Griffin WL, Natapov LM, O'Reilly SY, Grand SP, O'Neill CJ, Hronsky JMA, Djomani YP, Swain CJ, Deen T, Bowden P (2009) The lithospheric architecture of Africa: Seismic tomography, mantle petrology, and tectonic evolution. Geosphere 5:23–50

Beintema KA, Mason PRD, Nelson DR, White SH, Wijbrans JR (2003) New constraints on the timing of tectonic events in the Archaean central Pilbara Craton, Western Australia. J Virtual Explorer 13, pp 21. http://goo.gl/P9xEM. Accessed 3 Feb 2013

Benn K (2006) Tectonic delamination of the lower crust during Late Archean collision of the Abitibi-Opatica and Pontiac Terranes, Superior Province, Canada. In: Benn K, Mareschal J-C, Condie KC (eds) Archean Geodynamics and Environments, Geophysical Monograph Series 164:267–282

Benn K, Moyen J-F (2008) The Late Archean Abitibi-Opatica terrane, Superior Province: A modified oceanic plateau. GSA Special Papers 440:173–197

Benn KB, Sawyer EW, Bouchez J-L (1992) Orogen parallel and transverse shearing in the Opatica belt, Quebec: implications for the structure of the Abitibi Subprovince. Can J Earth Sci 29:2429–2444

Bennett VC (2004) Compositional evolution of the mantle. Treatise on Geochemistry 4, chapter 13:493–519

Berclaz A, Leclair A, Far NT (2004) Structural evolution of the Northeastern Superior Province (NESP) over 1 billion years, with emphasis on greenstone belts and their relation with enclosing granitoids. American Geophysical Union, Spring Meeting 2004, abstract #V31A–03

Bézard B, Tsang CCC, Carlson RW, Piccioni G, Marcq E, Drossart P (2009) Water vapor abundance near the surface of Venus from Venus Express/VIRTIS observations. J Geophys Res 114:E00B39. doi:10.1029/2008JE003251

Bhattacharji S, Koide H (1975) Mechanistic model for triple junction fracture geometry. Nature 255:21–24

Bickle MJ (1978) Heat loss from the Earth: a constraint on Archaean tectonics from the relation between geothermal gradients and the rate of heat production. Earth Planet Sci Lett 40:301–315

Bickle MJ (1986) Implications of melting for stabilization of the lithosphere and heat loss in the Archean Earth Planet. Sci Lett 80:314–324

Bickle MJ, Bettenay LF, Chapman HJ, Groves DI, McNaughton NJ, Campbell IH, de Laeter JR (1989) The age and origin of younger granitic plutons of the Shaw batholith in the Archaean Pilbara Block, Western Australia. Contrib Mineral Petrol 101:361–376

Bickle MJ, Nisbet EG, Martin A (1995) Archean greenstone belts are not oceanic crust. J Geol 102:121–138

Biczok J, Hollings P, Klipfel P, Heaman L, Maas R, Hamilton M, Kamo S, Friedman R (2012) Geochronology of the North Caribou greenstone belt, Superior Province Canada: Implications for tectonic history and gold mineralization at the Musselwhite mine. Precamb Res 192–195:209–230

Bierlein FP, Groves DI, Goldfarb RJ, Dubé B (2006) Lithospheric controls on the formation of provinces hosting giant orogenic gold deposits. Miner Deposita 40:874–886

Bilotti F, Suppe J (1999) The global distribution of wrinkle ridges on Venus. Icarus 139:37–157

Bindschadler DL, Schubert G, Kaula WM (1992) Coldspots and hotspots: global tectonics and mantle dynamics of Venus. J Geophys Res 97:13495–13532

Bleamaster LF, Hansen VL (2004) Effects of crustal heterogeneity on the morphology of chasmata, Venus. J Geophys Res 109: E02004. doi:10.1029/2003JE002193

Bleeker W (2002) Archaean tectonics: a review, with illustrations from the Slave Craton. In: Fowler CMR, Ebinger CJ, Hawkesworth CJ (eds) The Early Earth: Physical, Chemical and Biological Development. Geol Soc London Spec Publ 199:151–181

Bleeker W (2012) Targeted Geoscience Initiative 4. Lode gold deposits in ancient deformed and metamorphosed terranes: the role of extension in the formation of Timiskaming basins and large gold deposits, Abitibi Greenstone Belt—A discussion. Summary of Field Work and Other Activities 2012, Ontario Geological Survey. Open File Report 6280:47-1–47-12

Bleeker W, Ernst R (2006) Short-lived mantle generated magmatic events and their dyke swarms: The key unlocking Earth's paleogeographic record back to 2.6 Ga. In: Hanski E, Mertanen S, Rämö T, Vuollo J (eds) Dyke Swarms—time markers of crustal evolution. Taylor and Francis/Balkema, London, pp 3–26

Bleeker W, Breemen O van, Berger B (2008). The Pipestone Thrust and the fundamental architecture of the south-central Abitibi greenstone belt, Superior craton, Canada. Quebec 2008 GAC-MAC-SEG-SGA Joint annual meeting, session SY8: Abitibi (Québec, May 27–30, 2008). http://goo.gl/9BVmT. Accessed 3 Feb 2013

Blewett RS, Champion DC, Whitaker AJ, Bell B, Nicoll M, Goleby BR, Cassidy KF, Groenewald PB (2002) Three dimensional (3D) model of the Leonora-Laverton transect area: implications for Eastern Goldfields tectonics and mineralisation. In: Cassidy KF (ed) Geology, geochronology and geophysics of the north eastern Yilgarn Craton, with an emphasis on the Leonora-Laverton transect area. Geoscience Australia, Record 2002/18:83–100

Blewett RS, Czarnota K, Henson PA (2010a) Structural-event framework for the eastern Yilgarn Craton, Western Australia, and its implications for orogenic gold. Precamb Res 183:203–229

Blewett RS, Henson PA, Roy IG, Champion DC, Cassidy KF (2010b) Scale-integrated architecture of a world-class gold mineral system: the Archaean eastern Yilgarn Craton, Western Australia. Precamb Res 183:230–250

Blichert-Toft J, Arndt NT, Gruau G (2004) Hf isotopic measurements on Barberton komatiites: effects of incomplete sample dissolution and importance for primary and secondary magmatic signatures. Chem Geol 207:261–275

Boily M, Leclair A, Maurice C, Bédard JH, David J (2009) Paleo- to Mesoarchean basement recycling and terrane definition in the Northeastern Superior Province, Québec, Canada. Precamb Res 168:23–44

Bonin B (2012) Extra-terrestrial igneous granites and related rocks: A review of their occurrence and petrogenesis. Lithos 153:3–24. doi: 10.1016/j.lithos.2012.04.007

Bonin B, Bébien J, Masson P (2002) Granite: A planetary point of view. Gondwana Res 5:261–273

Bowden P, Black R, Martin RF, Ike EC, Kinnaird JA, Batchelor RA (1987) Niger-Nigerian alkaline ring complexes: a classic example of African Phanerozoic anorogenic mid-plate magmatism. In: Fitton JG, Upton BGJ (eds) Alkaline Igneous Rocks. Geol Soc London Spec Pub 30:357–379

Boyd FR (1998) The origin of cratonic peridotites: A major-element approach. Int Geol Rev 40:755–764

Branney MJ, Bonnichsen B, Andrews GDM, Ellis B, Barry TL, McCurry M (2008) 'Snake River (SR)-type' volcanism at the Yellowstone hotspot track: distinctive products from unusual. high-temperature silicic supereruptions. Bull Volcanol 70:293–314

Brown CD, Grimm RE (1995) Tectonics of Artemis Chasma: a Venusian 'plate' boundary. Icarus 117:219–249

Brown CD, Grimm RE (1999) Recent tectonic and lithospheric thermal evolution of Venus. Icarus 139:40–48

Brown CD, Phillips RJ (1999) Recent tectonic and lithospheric thermal evolution of Venus. Icarus 139:40–48

Brown M (2007) Metamorphic conditions in orogenic belts: A record of secular change. Int Geol Rev 49:193–234

Brown M (2009) Metamorphic patterns in orogenic systems and the geological record. In: Cawood PA, Kröner A (eds) Earth Accretionary Systems in Space and Time. Geol Soc London Special Pub 318:37–74

Bruegge RWV, Head JW (1990) Orogeny and large-scale strike-slip faulting on Venus: Tectonic Evolution of Maxwell Montes. J Geophys Res 95:8357–8381

Brun J-P, Tron V (1993) Development of the North Viking Graben; inferences from laboratory modelling. In: Cloetingh S, Sassi W, Horvath F, Puigdefabregas C (eds) Basin Analysis and Dynamics of Sedimentary Basin Evolution. Sediment Geol 86:31–51

Buchan KL, Hamilton MA (2009). New geochronologic and paleomagnetic results for the Grenville Dyke Swarm and implications for the Ediacaran APWP for Laurentia. EOS 90, n. 22, Jt. Assem. Suppl., Abstract GA12A–04

Bursnall JT, Leclair AD, Moser DE, Percival JA (1994) Structural correlation within the Kapuskasing uplift. Can J Earth Sci 31:1081–1095

Burov EB (2010) The equivalent elastic thickness (Te), seismicity and the long-term rheology of continental lithosphere: Time to burn-out "crème brûlée"? Insights from large-scale geodynamic modeling. Tectonophysics 484:4–26

Burov EB, Cloetingh S (2010) Plume-like upper mantle instabilities drive subduction initiation. Geohys Res Lett 37:L03309. doi:10.1029/2009GL041535

Burov EB, Watts AB (2006) The long-term strength of continental lithosphere: "jelly sandwich" or "crème brûlée"? GSA Today 16:4–10

Cadéron S (2003) Interpretation tectonometamorphique du nord de la province du Supérieur, Québec, Canada. PhD thesis, l'Université du Québec à Chicoutimi. http://constellation.uqac.ca/493/1/24684368.pdf. Accessed 3 Feb 2013

Cadéron S, Rivers T (2006) Inverted metamorphism at the eastern margin of the Superior Province: new insights on regional metamorphic overprinting along the Grenville Front in Québec, Canada. Abstract Volume, Montreal 2006, GAC-MAC: 22–23. www.gac.ca/activities/abstracts/ABSTRACT_VOLUME31.pdf. Accessed 3 Feb 2013

Cagnard F, Brun J-P, Gapais D (2006a) Modes of thickening of analogue weak lithospheres. Tectonophysics 421:145–160

Cagnard F, Durrieu N, Gapais D, Brun J-P, Ehlers C (2006b) Crustal thickening and lateral flow during compression of hot lithospheres, with particular reference to Precambrian times. Terra Nova 18:72–78

Calvert AJ, Ludden JN (1999) Archean continental assembly in the southeastern Superior Province of Canada. Tectonics 18:412–429

Calvert AJ, Sawyer EW, Davis WJ, Ludden JN (1995) Archean subduction inferred from seismic images of a mantle suture in the Superior Province. Nature 375:670–674

Camiré GE, Burg J-P (1993) Late Archaean thrusting in the northwestern Pontiac Subprovince, Canadian Shield. Precamb Res 61:51–66

Camiré GE, Ludden JN, Camiré GE, La Flèche MR, Burg J-P (1993) Mafic and ultramafic amphibolites from the northwestern Pontiac Subprovince: chemical characterization and implications for tectonic setting. Can J Earth Sci 30:1110–1122

Campbell IH (2001) Identification of ancient mantle plumes. In: Ernst RE, Buchan KL (eds) Mantle Plumes: their identification through time. Geol Soc Am Spec paper 352:5–21

Campbell IH, Griffiths RW, Hill RI (1989) Melting in an Archaean mantle plume: heads it's basalts, tails it's komatiites. Nature 339:697–699

Campbell IH, Taylor SR (1983) No water, no granites—no oceans, no continents. J Geophys Res 10:1061–1064

Canadian Aeromagnetic Data Base (2012) Abitibi, Quebec-Ontario Compilation. Geoscience Data Repository, Geological Survey of Canada, Earth Sciences Sector, Natural Resources Canada, Government of Canada

Canadian Geodetic Information System (2012) Geoscience Data Repository, Geodetic Survey Division, Earth Sciences Sector, Natural Resources Canada, Government of Canada

Canil D (2008) Canada's craton: a bottoms-up view. GSA Today 18:4–10

Card KD (1990) A review of the Superior Province of the Canadian Shield, a product of Archean accretion. Precamb Res 48:99–156

Card KD (1991) General comparison of the Canadian and Baltic shields. In: Ojakangas RW (ed) Precambrian Geology Of The Southern Canadian Shield and the eastern Baltic Shield, Minnesota Geological Survey Information Circular 34, iv–v

Card KD, Poulsen KH (1998) Geology and mineral deposits of the Superior Province of the Canadian Shield: Geology of the Precambrian Superior and Grenville Provinces and Precambrian Fossils in North America. In: Lucas, SB, St-Onge MR (eds) Geology of North America vol. 3-1, Geological Survey of Canada, Ottawa, pp. 13–204

Carrier A, Jébrak M, Angelier J, Holyland P (2000) The Silidor deposit, Rouyn-Noranda District, Abitibi Belt: Geology, structural evolution, and paleostress modeling of an Au quartz vein-type deposit in an Archean trondhjemite. Econ Geol 95:1049–1055

Cathey HE, Nash BP (2004) The Cougar Point Tuff: Implications for thermochemical zonation and longevity of high-temperature, large-volume silicic magmas of the Miocene Yellowstone hotspot. J Petrol 45:27–58

Cawood PA, Kröner A, Pisarevsky S (2006) Precambrian plate tectonics: Criteria and evidence. GSA Today 16:4–11

CBC News (2009) Venus probe images hint at ancient ocean. Quirks and Quarks Blog. http://www.cbc.ca/news/technology/story/2009/07/14/venus-ocean-water-express.html. Accessed 3 Feb 2013

Champion DC, Sheraton JW (1997) Geochemistry and Nd isotope systematics of Archaean granites of the Eastern Goldfields, Yilgarn Craton, Australia: Implications for crustal growth processes. Precamb Res 83:109–132

Champion DC, Smithies RH (2007) Geochemistry of Paleoarchean granites of the East Pilbara Terrane, Pilbara Craton, Western Australia: Implications for early Archean crustal growth. In: Van Kranendonk M, Smithies RH, Bennett VC (eds) Earth's Oldest rocks, Developments in Precambrian Geology. Elsevier, Amsterdam, pp 369–409

Chappell BW, Stephens WE (1988) Origin of infracrustal (I-type) granite magmas. In: Brown PE, Chappel BW (eds) Second Hutton Symposium: The Origin of Granites and Related Rocks, Trans Royal Soc Edin Earth Sci 83:71–86

Chardon D, Andronicos CL, Hollister LS (1999) Large-scale transpressive shear zone patterns and displacements within magmatic arcs: The coast plutonic complex, British Columbia. Tectonics 18:278–292

Chardon D, Choukroune P, Jayananda M (1996) Strain patterns, décollement and incipient sagducted greenstone terrains in the Archaean Dharwar craton (south India). J Struct Geol 18:991–1004

Chardon D, Choukroune P, Jayananda M (1998) Sinking of the Dharwar Basin (south India): implications for Archaean tectonics. Precamb Res 91:15–39

Chardon D, Jayananda M, Chetty TRK, Peucat JJ (2008) Precambrian continental strain and shear zone patterns: South Indian case. J Geophys Res 113:B08402. Doi:10.1029/2007JB005299

Chardon D, Jayananda M, Peucat JJ (2011) Lateral constrictional flow of hot orogenic crust: Insights from the Neoarchean of South India, geological and geophysical implications for orogenic plateaux. Geochem Geophys Geosyst 12. Doi:10.1029/2010GC003398

Chardon D, Peucat JJ, Jayananda M, Choukroune P, Fanning CM (2002) Archean granite-greenstone tectonics at Kolar (South India): interplay of diapirism and bulk inhomogeneous contraction during juvenile magmatic accretion. Tectonics 21(3) art. 1016

Chavagnac V (2004) A geochemical and Nd isotopic study of Barberton komatiites (South Africa): implication for the Archean mantle. Lithos 75:253–281

Chen C-W, Li A (2012) Shear wave structure in the Grenville Province beneath the lower Great Lakes region from Rayleigh wave tomography. J Geophys Res 117: B01303. doi:10.1029/2011JB008536.

Chetty TRK, Venkatrayudu M, Venkatasivappa V (2010) Structural architecture and a new tectonic perspective of Ovda Regio, Venus. Planet Space Sci 58:1286–1297

Choukroune P, Bouhallier H, Arndt NT (1995) Soft lithosphere during periods of Archaean crustal growth or crustal reworking. Geol Soc London Spec Pubs 95:67–86

Chown EH, Daigneault R, Mueller W, Mortensen JK (1992) Tectonic evolution of the Northern Volcanic Zone, Abitibi Belt, Quebec. Can J Earth Sci 29:2211–2225

Chown EH, Harrap R, Moukhsil A (2002) The role of granitic intrusions in the evolution of the Abitibi belt, Canada. Precamb Res 115:291–310

Clowes RM, White DJ, Hajnal Z (2010) Mantle heterogeneities and their significance: Results from Lithoprobe seismic reflection and refraction/wide-angle reflection studies. Can J Earth Sci 47:409–443

Cobbold PR, Davy P (1988) Indentation tectonics in nature and experiment. 2. Central Asia. Bull Geol Instit Uppsala 14:143–162

Coffin MF, Eldholm O (1994) Large igneous provinces: Crustal structure, dimensions, and external consequences. Rev Geophys 32:1–36

Coffin MF, Gahagan LM (1995) Ontong Java and Kerguelen plateaux: Cretaceous Icelands? J Geol Soc London 152:1047–1052

Coldwell B, Clemens J, Petford N (2011) Deep crustal melting in the Peruvian Andes: felsic magma generation during delamin Geological Survey of Canada, ation and uplift. Lithos 125:272–286

Collins WJ (1993) Melting of Archaean sialic crust under high aH2O conditions: genesis of 3300 Ma Na-rich granitoids in the Mount Edgar Batholith, Pilbara Block, Western-Australia. Precamb Res 60:151–174

Collins WJ, Van Kranendonk MJ, Teyssier C (1998) Partial convective overturn of Archaean crust in the east Pilbara Craton, Western Australia: driving mechanisms and tectonic implications. J Struct Geol 20:1405–1424

Coltice N, Bertrand H, Rey P, Jourdan F, Phillips BR, Ricard Y (2009) Global warming of the mantle beneath continents back to the Archaean. Gondwana Res 15:254–266

Condie KC (1981) Archean Greenstone Belts. Elsevier, Amsterdam, 434 pp

Condie KC (1998) Episodic continental growth and supercontinents: a mantle avalanche connection? Earth Planet Sci Lett 163:97–108

Condie KC (2003) Incompatible element ratios in oceanic basalts and komatiites: Tracking deep mantle sources and continental growth rates with time. Geochem Geophys Geosyst 4. Doi:2002GC000333

Condie KC (2005) High field strength element ratios in Archean basalts: a window to evolving sources of mantle plumes? Lithos 79:491–504

Connolly BD, Puchtel IS, Walker RJ, Arevalo R, Piccoli PM, Byerly G, Robin-Popieul C, Arndt N (2011) Highly siderophile element systematics of the 3.3 Ga Weltevreden Komatiites, South Africa: implications for early Earth history. Earth Planet Sci Lett 311:253–263

Conrad CP, Lithgow-Bertelloni C (2006) Influence of continental roots and asthenosphere on plate-mantle coupling, Geophys Res Lett 33: L05312. doi:10.1029/2005GL025621

Cook FA, van der Velden AJ (2012) Crustal seismic reflection profiles of collisional orogens. In: Roberts DG, Bally AW (eds) Regional Geology and Tectonics: Principles of Geologic Analysis, Elsevier, 179–213. doi:10.1016/B978-0-444-53042-4.00007-8

Corrigan D, Hanmer S (1997) Anorthosites and related granitoids in the Grenville orogen: A product of convective thinning of the lithosphere? Geology 25:61–64

Crisp D et al (2002) Divergent Evolution Among Earth-like Planets: The Case for Venus Exploration. In: Sykes MV (ed) The Future of Solar System Exploration (2003–2013) Astronomical Society of the Pacific Conference Proceedings 272: 5–34

Cruden AR, Nasseri MHB, Pysklywec R (2006) Surface topography and internal strain variation in wide hot orogens from three-dimensional analogue and two-dimensional numerical vice models. In: Buiter SJH, Schreurs G (eds). Analogue and Numerical Modelling of Crustal-Scale Processes. Geol Soc London Spec Pubs 253:79–104

Crumpler LS, Head JH, Campbell DB (1988) Orogenic belts on Venus. Geology 14:1031–1034

Cunningham WD (2001) Cenozoic normal faulting and regional doming in the southern Hangay region, Central Mongolia: implications for the origin of the Baikal rift province. Tectonophysics 331:389–411

Czarnota K, Champion DC, Cassidy KF, Goscombe B, Blewett RS, Henson PA, Groenewald PB (2010) The geodynamics of the Eastern Goldfields Superterrane. Precamb Res 183:175–202

Daigneault R (1991) Évolution structurale du segment de roches vertes de Chibougamau, Sous-Province archéenne de l'Abitibi, Québec. PhD thesis, Université Laval. 352 p. doi:01–1494946

Daigneault R (1996) Couloirs de déformation de la Sous-Province de l'Abitibi. MB 96–33, Ministère des Ressources naturelles, Secteur des mines, Québec, 128 pp

Daigneault R, St-Julien P, Allard GO (1990) Tectonic evolution of the northeast portion of the Archean Abitibi greenstone belt, Chibougamau area, Quebec. Can J Earth Sci 27:1714–1736

Daigneault R, Mueller WU, Chown EH (2002) Oblique Archean subduction: accretion and exhumation of an oceanic arc during dextral transpression, Southern Volcanic Zone, Abitibi Subprovince Canada. Precamb Res 115:261–290

Darling J, Storey C, Hawkesworth C (2009) Impact melt sheet zircons and their implications for the Hadean crust. Geology 37:927–930

Davies GF (1979) Thickness and thermal history of continental crust and root zones. Earth Planet Sci Lett 44:231–238

Davies GF (1992) On the emergence of plate tectonics. Geology 20:963–966

Davies GF (2006) Gravitational depletion of the early Earth's upper mantle and the viability of early plate tectonics. Earth Planet Sci Lett 243:376–382

Davies GF (2008) Episodic layering of the early mantle by the 'basalt barrier' mechanism. Earth Planet Sci Lett 275:382–392

Davis DW, Edwards G (1986) Crustal evolution of Archean rocks in the Kakagi Lake area, Wabigoon subprovince, northwest Ontario. Can J Earth Sci 23:182–192

Davis WJ, Machado N, Gariépy C, Sawyer EW, Benn K (1995) U—Pb geochronology of the Opatica tonalite-gneiss belt and its relationship to the Abitibi greenstone belt, Superior Province, Quebec. Can J Earth Sci 32:113–127

Davy P, Cobbold PR (1988) Indentation tectonics in nature and experiment. 1. Experiments scaled for gravity. Bull Geol Inst Uppsala 14:129–141

Debaille V, O'Neill C, Brandon AD, Haenecour P, Yin Q-Z, Mattielli N, Treiman AH (2012) Stagnant-lid tectonics in early Earth revealed by ^{142}Nd variations in late Archean rocks. 22nd VM Goldschmidt Conference, Earth in Evolution, June 24–29, Montreal, Canada, Abstract, session 5, p 35

de Brémond d'Ars J, Lécuyer C, Reynard B (1999) Hydrothermalism and diapirism in the Archean: gravitational instability constraints. Tectonophysics 304:29–39

Defant MJ, Drummond MS (1990) Derivation of some modern arc magmas by melting of young subducted lithosphere. Nature 347:662–665

DeLaughter JE, Jurdy DM (1999) Corona classification by evolutionary stage. Icarus 139:81–92

De Smet J, Van den Berg AP, Vlaar NJ (2000) Early formation and long-term stability of continents resulting

from decompression melting in a convecting mantle. Tectonophysics 322:19–33

Desrochers J-P, Hubert C, Ludden JN, Pilote P (1993) Accretion of Archean oceanic plateau fragments in the Abitibi greenstone belts, Canada. Geology 21:451–454

de Wit MJ (1982) Gliding and overthrust nappe tectonics in the Barberton greenstone belt. J Struct Geol 4:117–136

de Wit MJ (1998) Early Archean processes: evidence from the South African Kaapvaal craton and its greenstone belts. Geol Mijnbouw 76:369–373

de Wit MJ, de Ronde CEJ, Tredoux M, Roering C, Hart RJ, Armstrong RA, Green RWE, Pebedy E, Hart RA (1992) Formation of an Archaean continent. Nature 357:553–562

Dilek Y, Furnes H (2011) Ophiolite genesis and global tectonics: Geochemical and tectonic fingerprinting of ancient oceanic lithosphere. Bull Geol Soc Am 123:387–411

Dimroth E, Imreh L, Rocheleau M, Goulet N (1982) Evolution of the south-central segment of the Archean Abitibi Belt, Quebec. Part I: Stratigraphy and paleogeographic model. Can J Earth Sci 19:1729–1758

Dimroth E, Imreh L, Goulet N, Rocheleau M (1983) Evolution of the south-central segment of the Archean Abitibi Belt, Quebec. Part III: Plutonic and metamorphic evolution and geotectonic model. Can J Earth Sci 20:1374–1388

Dimroth E, Rocheleau M, Mueller W (1984) Paleogeography, isostasy and crustal evolution of the Archean Abitibi Belt: a comparison between the Rouyn-Noranda and Chibougamau areas. Guha J Chown EH (eds) Chibougamau—Stratigraphy Mineralization Can Inst Mining Spec 34:73–91

Dimroth E, Mueller W, Daigneault R, Brisson H, Poitras A, Rocheleau M (1986) Diapirism during regional compression: the structural pattern in the Chibougamau region of the Archean Abitibi Belt, Quebec: Geol Rund 75:715–736

Dinel E, Bleeker W, Ayer J, Dubé B (2008) Structural investigation and mineral potential of the Kidd-Munro assemblage in Clergue and Walker townships. Geo Surv Canada Current Res 2008-23, pp 10

Donaldson JA, de Kemp EA (1998) Archaean quartz arenites in the Canian Shield; examples from the Superior and Churchill provinces. Sediment Geol 120:153–176

Dorminey B (2009) Venus may have had continents and oceans. Nature. doi:10.1038/news.2009.24. http://www.nature.com/news/2009/090113/full/news.2009.24.html. Accessed 3 Feb 2013

Dostal J, Mueller WU (2013) Deciphering an Archean mantle plume: Abitibi greenstone belt, Canada. Gondwana Res 23:493–505

Dubé B (1990) Metallogénie aurifere du filon-couche de Bourbeau, région de Chibougamau, Québec. PhD Thesis, Université du Quebec à Chicoutimi. http://constellation.uqac.ca/1590/1/1458270.pdf. Accessed 3 Feb 2013

Dubé B, Gosselin P (2007) Greenstone-hosted quartz-carbonate vein deposits. In: Goodfellow WD (ed). Mineral Deposits of Canada: A Synthesis of Major Deposit-Types, District Metallogeny, the Evolution of Geological Provinces, and Exploration Methods: Geological Association of Canada, Mineral Deposits Division, Spec Pub 5:49–73

Dubé B, Guha J (1992) Relationship between NE trending regional faults and Archean mesothermal gold-copper mineralization: Cooke mine, Abitibi greenstone belt, Quebec, Canada. Econ Geol 87:1525–1540

Ducea M, Saleeby J (1998) A case for delamination of the deep batholithic crust beneath the Sierra Nevada, California. Int Geol Rev 40:78–93

Duchesne JC, Wilmart E (1997) Igneous charnockites and related rocks from the Bjerkreim-Sokndal layered intrusion (Southwest Norway). A jotunite (hypersthene monzodiorite)-derived A-type granitoid suite. J Petrol 38:337–369

Dufréchou G (2011) Origine et implications tectoniques de structures transverses profondes interprétées à partir de données de champ potentiel, Province de Grenville, Canada. PhD Thesis, INRS-ETE, Québec. http://www1.ete.inrs.ca/pub/theses/T000603.pdf

Dufréchou G, Harris LB (2013) Tectonic models for the origin of regional transverse structures in the SW Grenville Province interpreted from regional gravity. J. Geodynamics 64:15–39

Duncan RA (1981) Hotspots in the southern oceans—An absolute frame of reference for motion of the Gondwana continents. Tectonophysics 74:29–42

Drury SA (1993) Image Interpretation in Geology, 2nd Edition. Chapman and Hall, London

Dziewonski AM, Anderson DL (1981) Preliminary reference Earth model. Phys Earth Planet Inter 25:297–356

Eaton DW, Frederiksen A (2007) Seismic evidence for convection-driven motion of the North American plate. Nature 446:428–431

Ellis BS, Barry T, Branney MJ, Wolff JA, Bindeman I, Wilson R, Bonnichsen B (2011) Petrologic constraints on the development of a large-volume, high temperature, silicic magma system the Twin Falls eruptive centre, central Snake River Plain. Lithos 120:475–489

Elkins-Tanton LT (2007) Continental magmatism, volatile recycling, and a heterogeneous mantle caused by lithospheric gravitational instabilities. J Geophys Res Solid Earth 112(B3) doi 10.1029/2005JB004072

Elkins-Tanton LT, Hager BH (2005) Giant meteoroid impacts can cause volcanism. Earth Planet Sci Lett 239:219–232

Elkins-Tanton LT, Hager BH, Grove TL (2004) Magmatic effects of the lunar late heavy bombardment. Earth Planet Sci Lett 222:17–27

Erickson EJ (2010) Structural and kinematic analysis of the Shagawa Lake Shear Zone, Superior Province, Northern Minnesota: Implications for the role of vertical versus horizontal tectonics in the Archean. Can J Earth Sci 47:1463–1479

Ernst RE (2007) Large Igneous Provinces (LIPs) in Canada through time and their metallogenic potential. In: Goodfellow WD (ed) Mineral Deposits of Canada: a synthesis of major deposit-types, district metallogeny, the evolution of geological provinces, and exploration methods, geological association of Canada, mineral deposits division, Special Publication 5, pp 929–937.

Ernst RE, Bleeker W (2010) Large igneous provinces (LIPs), giant dyke swarms, and mantle plumes: significance for breakup events within Canada and adjacent regions from 2.5 Ga to present. Can J Earth Sci 47:695–739

Ernst RE, Buchan KL (2003) Recognizing mantle plumes in the geological record. Ann Rev Earth Planet Sci 31:469–523

Ernst RE, Desnoyers DW (2004) Lessons from Venus for understanding mantle plumes on Earth. Phys Earth Planet Int 146:195–229

Ernst RE, Head JW, Parfitt E, Grosfils E, Wilson L (1995) Giant radiating dyke swarms on Earth and Venus. Earth Sci Rev 39:1–58

Ernst WG (2007) Speculations on evolution of the terrestrial lithosphere-asthenosphere system—Plumes and plates. Gondwana Res 11:38–49

European Space Agency (2009) New map hints at Venus' wet volcanic past. http://goo.gl/9HRwX. Accessed 3 Feb 2013

Faure S (2001) Analyse des linéaments géophysiques en relation avec les minéralisations en or et métaux de base de l'Abitibi. Rapport, Projet CONSOREM 2000-03A, 26 p

Faure S (2009) Reconnaissance des structures synvolcaniques fertiles pour les minéralisations de sulfures massifs volcanogènes (Cu-Zn) dans le groupe de Blake River, Abitibi. Rapport du projet CONSOREM 2007-03, 48p

Faure S (2010) World Kimberlites CONSOREM Database (Version 3), Consortium de Recherche en Exploration Minérale CONSOREM, Université du Québec à Montréal

Faure S, Rafini S (2004) Modélisation des paléocontraintes et des paléopressions le long de la Faille Porcupine-Destor: Implication pour la formation de bassins sédimentaires, d'intrusions et de minéralisations aurifères. Rapport du projet CONSOREM 2003-03, 47 pp. https://consorem.uqac.ca/production_scien/2003_03/2003-03_paleo_fpdm.pdf. Accessed 1 Feb 2013

Faure S, Daigneault R, Godey S (2008) La géométrie et la fertilité des ceintures de roches vertes archéennes de la Province du lac Supérieur: Reflet de l'architecture et de la modification du manteau lithosphérique. Abstract, Québec Exploration 2008. http://goo.gl/fKlcA and poster http://goo.gl/EvrVO. Accessed 3 Feb 2013

Faure S, Godey S, Fallara F (2010a) Tomographie sismique des cratons et des ceintures de roches vertes: exploration régionale pour le diamant et l'or. Ateliers CONSOREM: Utilisation des outils et méthodes du CONSOREM, Québec Exploration 2010, http://goo.gl/61dOX. Accessed 1 Feb 2013

Faure S, Rafini S, Trépanier S (2010b) Modélisation géomécanique des paléocontraintes pour l'exploration de l'or orogénique en Abitibi. Québec Exploration 2010– Ateliers CONSOREM: Utilisation des outils et méthodes du CONSOREM. http://goo.gl/kbevC Accessed 1 Feb 2013

Faure S, Godey S, Fallara F, Trépanier S (2011) Seismic architecture of the Archean North American mantle and its relationship to diamondiferous kimberlite fields. Econ Geol 106:223–240

Fayol N, Harris LB, Jébrak M (2011) Dynamique transpressive et rôle des hétérogénéités crustales dans la localisation du bassin de Desmaraisville (Abitibi): étude géophysique et modélisation analogique. Résumés des conférences et des photoprésentations, Québec Exploration 2011, DV 2011-03, 41

Fayol N, Harris LB, Jébrak M (2012) Transpressional dynamics and the role of crustal heterogeneities in the localization of the Desmaraisville basin (Abitibi): Geophysical study and analogue modelling. Abstract, PDAC 2012 International Convention, Trade Show and Investors Exchange, Toronto. http://goo.gl/uhxqx. Accessed 1 Feb 2013

Fernández C, Anguita F, Ruiz J, Romeo I, Martín-Herrero ÁI, Rodríguez A, Pimentel C (2010) Structural evolution of Lavinia Planitia, Venus: Implications for the tectonics of the lowland plains. Icarus 206:210–228

Flament N (2009) Secular cooling of the solid Earth, emergence of the continents, and evolution of Earth's external envelopes. PhD thesis, U Sydney. http://goo.gl/2fN20. Accessed 3 Feb 2013

Forte AM, Moucha R, Simmons NA, Grand SP, Mitrovica JX (2010) Deep-mantle contributions to the surface dynamics of the North American continent. Tectonophysics 481:3–15

Foster A, Nimmo F (1996) Comparisons between the rift systems of East Africa, Earth and Beta Regio, Venus. Earth Planet Sci Lett 143:183–195

Fowler AC, O'Brien SBG (2003) Lithospheric failure on Venus. Proc R Soc Lond 459:2663–2704

Fralick P, Wu J, Williams HR (1992) Trench and slope basin deposits in an Archean metasedimentary belt, Superior Province, Canadian Shield. Can J Earth Sci 29:2551–2557

Frederiksen S, Braun J (2001) Numerical modelling of strain localisation during extension of the continental lithosphere. Earth Planet Sci Lett 188:241–251

Frederiksen AW, Miong S-K, Darbyshire FA, Eaton DW, Rondenay S, Sol S (2007) Lithospheric variations across the Superior Province, Ontario, Canada: Evidence from tomography and shear wave splitting. J Geophys Res 112:B07318. doi:10.1029/2006JB004861

Friend CRL, Nutman AP (2010) Eoarchean ophiolites? New evidence for the debate on the Isua Supracrustal Belt, Southern West Greenland. Am J Sci 310:826–861

Frost BR, Frost CD (2008) On charnockites. Gondwana Res 13:30–44

Frost CD, Frost BR, Lindsley DH, Chamberlain KR, Swapp SM, Scoates JS (2010) Geochemical and isotopic evolution of the anorthositic plutons of the Laramie Anorthosite Complex: Explanations for variations in silica activity and oxygen fugacity of massif anorthosites. Can Mineral 48:925–946

Furnes H, de Wit M, Staudigel H, Rosing M, Muehlenbachs K (2007a) A vestige of Earth's oldest ophiolite. Science 315:1704–1707

Furnes H, de Wit M, Staudigel H, Rosing M, Muehlenbachs K (2007b) Response to comments on "A vestige of Earth's oldest ophiolite". Science 318:U4–U5

Furnes H, de Wit M, Robins B, Sandsta NR (2011) Volcanic evolution of the upper Onverwacht Suite, Barberton Greenstone Belt, South Africa. Precamb Res 186:28–50

Galley A, Hannington M, Jonasson I (2008) Volcanogenic Massive Sulphide Deposits. In: Goodfellow WD (ed) Mineral Deposits of Canada: A Synthesis of Major Deposit Types. Geological Association of Canada, Mineral Deposits Division and Geological Survey of Canada Special Publication 5 ISBN-13: 978-1-897095-24-9, pp 141–162

Gariépy C, Allègre CJ (1985) The lead isotope geochemistry of late kinematic intrusives from the Abitibi greenstone belt, and their implications for late Archean crustal evolution. Geochim Cosmochim Acta 49:2371–2384

Ghent R, Hansen V (1999) Structural and kinematic analysis of eastern Ovda Regio, Venus: implications for crustal plateau formation. Icarus 139:116–136

Gibson IL, Roberts RG, Gibbs A (1986) An extensional fault model for the early development of greenstone belts, with reference to a portion of the Abitibi belt, Ontario, Canada. Earth Planet Sci Lett 79:159–167

Gill JB (1981) Orogenic andesites and plate tectonics. Springer Verlag, Berlin, p 390

Girardi JD, Patchett PJ, Ducea MN, Gehrels GE, Cecil MR, Rusmore ME, Woodsworth GJ, Pearson DM, Manthei C, Wetmore P (2012) Elemental and isotopic evidence for granitoid genesis from deep-seated sources in the Coast Mountains Batholith, British Columbia. J Petrol 53:1505–1536

Glukhovskiy MZ, Pavlovskiy YeV, Moralev VM (1986) Ring structures and granite-gneiss domes. Int Geol Rev 28:1202–1212

Godey S (2002) Structure of the uppermost mantle beneath North America: Regional surface wave tomography and thermo-chemical interpretation, Tekst Proefschrift Universiteit Utrecht. http://goo.gl/pB5Lw. Accessed 1 Feb 2013

Godey S, Deschamps F, Trampert J, Snieder R (2004) Thermal and compositional anomalies beneath the North American continent, J Geophys Res 109, B01308. doi:10.1029/2002JB002263

Godey S, Snieder R, Villaseñor A, Benz HM (2003) Surface wave tomography of North America and the Caribbean using global and regional broad-band networks: phase velocity maps and limitations of ray theory. Geophys J Int 152:620–632

Goldfarb RJ, Baker T, Dubé B, Groves DI, Hart CJR, Robert F, Gosselin P (2005) World distribution, productivity, character, and genesis of gold deposits in metamorphic terranes. In: Hedenquist JW, Thompson JFH, Goldfarb RJ, Richards JP (eds) Econ Geol 100th Anniversary Volume 407–450

Goodwin AM (1977) Archean volcanism in Superior Province, Canadian Shield. Geol Assoc Can Spec Pap 16:205–241

Goodwin AM (1981) Archaean plates and greenstone belts. In: Kröner A (ed) Precambrian Plate Tectonics, Elsevier Amsterdam, pp 105–135

Goodwin AM (1996) Principles of Precambrian Geology. Academic Press, London, pp 327

Gorczyk W, Hobbs B, Gerya TV (2012) Initiation of Rayleigh–Taylor instabilities in intra-cratonic settings. Tectonophysics 514–517:146–155

Gosselin G (1998) Veines de quartz aurifères précoces à la zone ouest de la mine Doyon, Canton de Bousquet, Preissac, Abitibi. Mémoire, Université du Québec à Chicoutimi. http://constellation.uqac.ca/1029/1/11644776.pdf Accessed 1 Feb 2013

Gosselin P, Dubé B (2005) Gold deposits and gold districts of the world. Geological Survey of Canada, Open File, 4893

Goutier J (2006) Géologie de la région du lac au Goéland (32F/15). RG 2005-05, Géologie Québec, Ministère des Ressources naturelles et de la Faune, Québec

Goutier J, Melançon M (2007) Compilation géoologique de la Sous-province de l'Abitibi (version préliminaire): Ministère des Ressources naturelles et de la Faune du Québec, Report RP2010-04 (1:250,000)

Gramling C (2009) Venus' gentler, Earth-like past. Earth Magazine. http://www.earthmagazine.org/article/venus-gentler-earth-past. Accessed 3 Feb 2013

Gray R, Pysklywec RN (2010) Geodynamic models of Archean continental collision and the formation of mantle lithosphere keels. Geophys Res Lett 37:L19301. doi:10.1029/2010GL043965

Green DH, Falloon TJ (1998) Pyrolite: a Ringwood concept and its current expression. In: Jackson I (ed) The Earth's Mantle: Composition, Structure and Evolution. Cambridge University Press, Cambridge, UK, pp 311–378

Griffin WL, O'Reilly SY (2007) Cratonic lithospheric mantle: Is anything subducted? Episodes 30:43–53

Griffin WL, O'Reilly SY, Abe N, Aulbach S, Davies RM, Pearson NJ, Doyle BJ, Kivi K (2003) The origin and evolution of Archean lithospheric mantle. Precamb Res 127:19–41

Griffin WL, O'Reilly SY, Afonso JC, Begg GC (2009) The composition and evolution of lithospheric mantle: a re-evaluation and its tectonic implications. J Petrol 50:1185–1204

Griffin WL, O'Reilly SY, Afonso JC, Begg GC (2010) The evolution and extent of Archean continental lithosphere: implications for tectonic models. In: Planet Formation, Crustal Growth and the Evolving Lithosphere: 5th International Archean Symposium. http://goo.gl/GTvz1. Accessed 3 Feb 2013

Griffin WL, O'Reilly SY, Doyle BJ, Pearson NJ, Coopersmith H, Kivi K, Malkovets V, Pokhilenko N (2004)

Lithosphere mapping beneath the north American plate. Lithos 77:873–922
Grimm RE (1998) What do we really know about the heat flow of Venus (or anyplace else we can't stick with probes?). The Leading Edge, Nov. 1998:1,544-1,546
Grimm RE, Phillips RJ (1992) Anatomy of a Venusian hot spot: Geology, gravity, and mantle dynamics of Eistla Regio. J Geophys Res 97E:16,035–16,054
Grimm RE, Hess PC (1997) The Crust of Venus. In: Bougher SW, Hunten DM, Phillips RJ (eds) Venus II: Geology, Geophysics, Atmosphere, and Solar Wind Environment. University of Arizona Press, Tucson, 1205–1244
Grimm RE, Barr AC, Harrison KP, Stillman DE, Neal KL, Vincent MA, Delory GT (2012) Aerial electromagnetic sounding of the lithosphere of Venus. Icarus 217:462–473
Groves DI, Goldfarb RJ, Knox-Robinson CM, Ojala J, Gardoll S, Yun GY, Holyland P (2000) Late-kinematic timing of orogenic gold deposits and significance for computer-based exploration techniques with emphasis on the Yilgarn Block, Western Australia. Ore Geol Rev 17:1–38
Gueydan F, Morency C, Brun J-P (2008) Continental rifting as a function of lithosphere mantle strength. Tectonophysics 460:83–93
Halls HC, Zhang B (1998) Uplift structure of the southern Kapuskasing zone from 2.45 Ga dike swarm displacement. Geology 26:67–70
Hamilton WB (1998) Archean tectonics and magmatism. Int Geol Rev 40:1–39
Hamilton WB (2005) Plumeless Venus has ancient impact-accretionary surface. In: Foulger GR, Natland JH, Presnall DC, Anderson DL (eds) Plates, Plumes, and Paradigms, GSA Spec Paper 388: 781–814
Hamilton WB (2007) Earth's first two billion years—The era of internally mobile crust. In: Hatcher RD Jr, Carlson MP., McBride JH., Martinez-Catalan JR (eds) 4-D Framework of Continental Crust, Geol Soc Amer Memoir 200:233–296
Hamilton WB (2011) Plate tectonics began in Neoproterozoic time, and plumes from deep mantle have never operated. Lithos 123:1–20
Hansen VL (2007a) Subduction origin on early Earth: A hypothesis. Geology 35:1059–1062
Hansen VL (2007b) Venus: a thin-lithosphere analog for early Earth? In: Van Kranendonk MJ, Smithies RH, Bennett VC (eds) Earth's Oldest Rocks, Developments in Precambrian Geology 15, Chapter 8.1, 987–1012
Hansen VL, Willis JJ (1996) Structural analysis of a sampling of tesserae: Implications for Venus geodynamics. Icarus 123:296–312
Hansen VL, Willis JJ (1998) Ribbon terrane formation, southwestern Fortuna Tessera, Venus: Implications for lithospheric evolution. Icarus 132:321–343
Hansen VL, Young DA (2007) Venus's evolution: a synthesis. In: Cloos M, Carlson WD, Gilbert MC, Liou JG, Sorensen SS (eds) Convergent Margin Terranes and Associated Regions: a Tribute to W.G. Ernst: GSA Special Paper 419:255–273
Hansen VL, Banks BK, Ghent RR (1999) Tessera terrain and crustal plateaus, Venus. Geology 27:1,071-1:074
Haqq-Misra JD, Domagal-Goldman SD, Kasting PJ, Kasting JF (2008) A revised, hazy methane greenhouse for the Archean Earth. Astrobiology 8:1127–1137
Harig C, Zhong S, Simons FJ (2010) Constraints on upper mantle viscosity from the flow-induced pressure gradient across the Australian continental keel. Geochem Geophys Geosys 11, Q06004. doi:10.1029/2010GC003038
Harris LB (1987) A tectonic framework for the Western Australian Shield and its significance to gold mineralisation—a personal view. In: Ho SE, Groves DI (eds) Recent Advances in the Understanding of Precambrian Gold Deposits. Geology Department and University Extension, University of Western Australia Publication 11:1–27
Harris LB (2013) Interactive 3D S-wave tomographic isosurfaces for the Superior Province, Canada, http://goo.gl/U8fMh
Harris LB, Byrne DR, Wetherly S, Beeson J (2004) Analogue modelling of structures developed above single and multiple mantle plumes: applications to brittle crustal deformation on Earth and Venus. In: Bertotti G, Buiter S, Ruffo P, Schreurs G (eds) GeoMod 2004–From mountains to sedimentary basins: modelling and testing geological processes. Boll Geofis teorica applicata 45(Supp. 1):301–303
Harris LB, Dufréchou G, Armengaud C, Johnson E (2010) The role of deep-crustal transverse structures interpreted from regional gravity in the localization and deformation of zinc deposits in the North American Grenville Province. In: Archibald SM (ed) Zinc2010, Proceedings of the Zinc2010 Meeting, Cork, Irish Association for Economic Geology, 49–52. http://www.iaeg.org/docs/2010/Zinc2010_Abstracts.pdf. Accessed 1 Feb 2013
Harris LB, Godin L, Yakymchuk (2012) Regional shortening followed by channel flow induced collapse: A new mechanism for "dome and keel" geometries in Neoarchaean granite-greenstone terrains. Precamb Res 212–213,139–154
Hart TR, Gibson HL, Lesher CM (2004) Trace element geochemistry and petrogenesis of felsic volcanic rocks associated with volcanogenic massive Cu-Zn-Pb sulfide deposits. Econ Geol 99:1003–1013
Hashimoto GL, Roos-Serote M, Sugita S, Gilmore MS, Kamp LW, Carlson RW, Baines KH (2008) Felsic highland crust on Venus suggested by Galileo near-infrared mapping spectrometer data, J Geophys Res 113, E00B24. doi:10.1029/2008JE003134
Hawkesworth CJ, Kemp AIS (2006) Evolution of the continental crust. Nature 443:811–817
Head JW (1990a) Processes of crustal formation and evolution on Venus: an analysis of topography, hypsometry, and crustal thickness variations. Earth Moon Planets 50/51:25–55
Head JW (1990b) Formation of mountain belts on Venus: Evidence for large-scale convergence, underthrusting,

and crustal imbrication in Freyja Montes, Ishtar Terra. Geology 18:99–102

Head JW, Campbell DB, Elachi C, Guest JE, McKenzie D, Saunders RS, Schaber GG, Schubert G (1991) Venus volcanism: initial analysis of Magellan data. Science 252:276–288

Head JW, Hurwitz DM, Ivanov MA, Basilevsky AT, Kumar PS (2008) Geological mapping of Fortuna Tessera (V-2): Venus and Earth's Archean process comparisons. Abstracts of the Annual Meeting of Planetary Geologic Mappers, Flagstaff, AZ. http://hdl.handle.net/2060/20080040991. Accessed 3 Feb 2013

Hegner E, Emslie RF, Iaccheri LM, Hamilton MA (2010) Sources of the Mealy Mountains and Atikonak River anorthosite-granitoid complexes, Grenville Province, Canada. Can Mineral 48:787–808

Helmstaedt HH, Schulze DJ (1986) Southern African kimberlites and their mantle sample: implications for Archean tectonics and lithosphere evolution. In: Ross J (ed) Kimberlites and Related Rocks, Blackwell, Carleton, Spec Publ Geol Soc Aust 14:358–368

Herrick RR, Phillips RJ (1992) Geological correlations with the interior density structure of Venus. J Geophys Res 97:16,017–16,034

Herrick RR, Dufek J, McGovern PJ (2005) Evolution of large shield volcanoes on Venus. J Geophys Res 110:E01002, pp 19. doi:10.1029/2004JE002283

Herzberg C (1999) Phase equilibrium constraints on the formation of cratonic mantle. In: Fei Y, Bertka CM, Mysen BO (eds) Mantle Petrology, Field Observations and High Pressure Experimentation: A Tribute to Francis R. (Joe) Boyd, The Geochemical Society Special Publication, Washington DC 6:241–257

Herzberg C (2004) Geodynamic information in peridotite petrology. J Petrol 45:2507–2530

Herzberg C, Asimow PD, Arndt N, Niu Y, Lesher CM, Fitton JG, Cheadle MJ, Saunders AD (2007) Temperatures in ambient mantle and plumes: Constraints from basalts, picrites, and komatiites. Geochem Geophys Geosys 8:2006GC001390

Herzberg CT, Rudnick R (2012) Formation of cratonic lithosphere: An integrated thermal and petrological model. Lithos 149:4–15. doi:10.1016/j.lithos.2012.01.010

Herzberg CT, Fyfe WS, Carr MJ (1983) Density constraints on the formation of the continental Moho and crust. Contrib Mineral Petrol 84:1–5

Hess PC, Head JW (1990) Derivation of primary magmas and melting of crustal materials on Venus: some preliminary petrogenetic considerations. Earth Moon Planets 50/51:57–80

Hewitt DF (1963) The Timiskaming series of the Kirkland Lake area. Can Mineral 7:497–523

Hickman AH (1984) Archaean diapirism in the Pilbara Block, Western Australia. In: Kröner A; Greiling R (eds) Precambrian Tectonics Illustrated, E.Schweizerbart'sche Verlagsbuchhandlung, Stuttgart, 113–127

Hill RI (1993) Mantle plumes and continental tectonics. Lithos 30:193–206

Hill RI, Campbell IH, Compston W (1989) Age and origin of granitic rocks in the Kalgoorlie-Norseman region of Western Australia: Implications for the origin of Archaean crust. Geochim Cosmochim Acta 53:1259–1275

Hill RI, Campbell IH, Davies GF, Griffiths RW (1992) Mantle plumes and continental tectonics. Science 256:186–193

Hoernle K, Hauff F, Van Den Bogaard P, Werner R, Mortimer N, Geldmacher J, Garbe-Schönberg D, Davy B (2010) Age and geochemistry of volcanic rocks from the Hikurangi and Manihiki oceanic plateaus. Geochim Cosmochim Acta 74:7196–7219

Hoffmann JE, Carsten MC, Næraa T, Rosing MT, Herwartz D, Garbe-Schönberg D, Svahnberg H (2011) Mechanisms of Archean crust formation inferred from high-precision HFSE systematics in TTGs. Geochim Cosmochim Acta 75:4157–4178

Hollings P, Kerrich R (2004) Geochemical systematics of tholeiites from the 2.86 Ga Pickle Crow Assemblage, northwestern Ontario: arc basalts with positive and negative Nb-Hf anomalies. Precamb Res 134:1–20

Hoogenboom T, Houseman GA (2006) Rayleigh–Taylor instability as a mechanism for corona formation on Venus. Icarus 180:292–307

Houseman GA, Houseman DK (2010) Stability and periodicity in the thermal and mechanical evolution of the early continental lithosphere. Lithos 120:42–54

Hronsky JMA, Groves DI, Loucks RR, Begg GC (2012) A unified model for gold mineralisation in accretionary orogens and implications for regional-scale exploration targeting methods. Mineral Deposita 47:339–358

Hubert C, Trudel P, Gélinas L (1984) Archean wrench fault tectonics and structural evolution of the Blake River Group, Abitibi Belt, Quebec. Can J Earth Sci 21:1024–1032

Husson L, Conrad CP, Faccenna C (2012) Plate motions, Andean orogeny, and volcanism above the South Atlantic convection cell. Earth Planet Sci Lett 316–317:126–135

Huston DL, Blewett RS, Keillor B, Standing J, Smithies RH, Marshall A, Mernagh TP, Kamprad J (2002) Lode gold and epithermal deposits of the Mallina Basin, North Pilbara Terrain, Western Australia. Econ Geol 97:801–818

Ivanov MA, Head JW (2011) Global geological map of Venus. Planet Space Sci 59:1559–1600

Jackson SL, Cruden AR (1995) Formation of the Abitibi greenstone belt by arc-trench migration. Geology 23:471–474

Jahn BM, Glikson AY, Peucat JJ, Hickman AH (1981) REE geochemistry and isotopic data of Archean silicic volcanics and granitoids from the Pilbara Block, Western Australia: implications for early crustal evolution. Geochim Cosmochim Acta 45:1633–1652

Janes DM, Squyres SW, Bindschadler DL, Baer G, Schubert G, Sharpton VL, Stofan ER (1992) Geophysical models for the formation and evolution of coronae on Venus. J Geophys Res 97E:16,055–16,068

Janle P, Jannsen D (1986) Gravity studies of Aphrodite Terra on Venus. Earth Moon Planets 36:275–287
Jones AP (2005) Meteorite impacts as triggers to large igneous provinces. Elements 1:277–281
Jordan TH (1988) Structure and formation of the continental tectosphere. J Petrol Special Lithosphere Issue:11–37
JPL (undated) Magellan Mission at a Glance, NASA Jet Propulsion Laboratory, California Institute of Technology. http://www2.jpl.nasa.gov/magellan/fact.html. Accessed 3 Feb 2013
Jull MG, Arkani-Hamed J (1995) The implications of basalt in the formation and evolution of mountains on Venus. Phys Earth Planet Int 89:163–175
Jull MG, Kelemen PB (2001) On the conditions for lower crustal convective instability. J Geophys Res Solid Earth 106:6423–6446
Kamber BS (2010) Archean mafic-ultramafic volcanic landmasses and their effect on ocean-atmosphere chemistry. Chem Geol 274:19–28
Kamber BS, Kramers JD, Napier R, Cliff RA, Rollinson HR (1995) The Triangle Shear zone, Zimbabwe, revisited: an important event at 2.0 Ga in the Limpopo Belt. Precamb Res 70:191–213
Kameyama M, Ogawa M (2000) Transitions in thermal convection with strongly temperature-dependent viscosity in a wide box. Earth Planet Sci Lett 180:355–367
Kamo S, Krogh T, Kumarapeli P (1995) Age of the Grenville dyke swarm, Ontario-Quebec: implications for the timing of Iapetan rifting. Can J Earth Sci 32:273–280
Kaula WM, Phillips RJ (1981) Quantitative tests for plate tectonics on Venus. Geophys Res Lett 8:1187–1190
Kelemen PB, Hart SR, Bernstein S (1998) Silica enrichment in the continental upper mantle via melt/rock reaction. Earth Planet Sci Lett 164:387–406
Kelemen PB, Hanghøj K, Greene AR (2005) One view of the geochemistry of subduction-related magmatic arcs, with an emphasis on primitive andesite and lower crust. In: Rudnick RL (ed) The Crust, Treatise on Geochemistry. Elsevier, Pergamon San Diego, v. 3:593–659
Kemp AIS, Wilde SA, Hawkesworth CJ, Coath CD, Nemchin A, Pidgeon RT, Vervoort D, DuFrane SA (2010) Hadean crustal evolution revisited: New constraints from Pb-Hf isotope systematics of the Jack Hills zircons. Earth Planet Sci Lett 296:45–56
Kerr AC, White RV, Saunders AD (2000) LIP Reading: Recognizing oceanic plateaux in the geological record. J Petrol 41:1041–1056
Kerrich R, Xie Q (2002) Compositional recycling structure of an Archean super-plume: Nb-Th-U-LREE systematics of Archean komatiites and basalts revisited. Contrib Mineral Petrol 142:476–484
Kerrich R, Polat A (2006) Archean greenstone-tonalite duality: Thermochemical mantle convection models or plate tectonics in the early Earth global dynamics? Tectonophysics 415:141–165
Kerrich R, Polat A, Wyman D, Hollings P (1999) Trace element systematics of Mg-, to Fe-tholeiitic basalt suites of the Superior Province: implications for Archean mantle reservoirs and greenstone belt genesis. Lithos 46:163–187
Kerrich R, Polat A, Xie Q (2008) Geochemical systematics of 2.7 Ga Kinojevis Group (Abitibi) and Manitouwadge and Winston Lake (Wawa) Fe-rich basalt-rhyolite associations: Backarc rift oceanic crust? Lithos 101:1–23
Ketchum JWF, Ayer JA, Breemen O van, Pearson NJ, Becker JK (2008) Pericontinental Crustal Growth of the Southwestern Abitibi Subprovince, Canada—U-Pb, Hf, and Nd Isotope Evidence. Econ Geol 103:1151–1184
Kiefer WS (1991) Models for the formation of highland regions on Venus. PhD thesis, California Institute of Technology. http://thesis.library.caltech.edu/4744/1/Kiefer_ws_1991.pdf. Accessed 3 Feb 2013
Kiefer WS, Hager BH (1991a) A mantle plume model for the equatorial highlands of Venus. J Geophys Res 96:E4. doi:10.1029/91JE02221
Kiefer WS, Hager BH (1991b) Mantle downwelling and crustal convergence: a model for Ishtar Terra, Venus. J Geophys Res 96:20,967-20,980. doi:10.1029/91JE02219
Kimura G, Ludden JN, Desrochers JP, Hori R (1993) A model of ocean-crust accretion for the Superior Province, Canada. Lithos 30:337–355
Kisters AFM, Belcher RW, Poujol M, Dziggel A (2010) Continental growth and convergence-related arc plutonism in the Mesoarchaean: Evidence from the Barberton granitoid-greenstone terrain, South Africa. Precamb Res 178:15–26
Kitney KE, Olivo GR, Davis DW, Desrochers J-P, Tessier A (2011) The Barry Gold Deposit, Abitibi Subprovince, Canada: A greenstone belt-hosted gold deposit coeval with Late Archean deformation and magmatism. Econ Geol 106:1129–1154
Koch DM, Manga M (1996) Neutrally buoyant diapirs: A model for Venus coronae. Geophys Res Lett 23:225–228
Koenig E, Aydin A (1998) Evidence for large-scale strike-slip faulting on Venus. Geology 2:551–554
Kohlstedt DL, Mackwell SJ (2009) Strength and deformation of planetary lithospheres. In: Watters TR, Schultz, RA (eds) Planetary Tectonics, Cambridge University Press, 397–456
Kopylova MG, Afanasiev VP, Bruce LF, Thurston PC, Ryder J (2011) Metaconglomerate preserves evidence for kimberlite, diamondiferous root and medium grade terrane of a pre-2.7 Ga Southern Superior protocraton. Earth Planet Sci Lett 312:213–225
Krassilnikov AS, Kostama V-P, Aittola M, Guseva EN, Cherkashina OS (2012) Relationship of coronae, regional plains and rift zones on Venus. Planet Space Sci 68:56–75. doi:10.1016/j.pss.2011.11.017
Kreissig K, Holze L, Frei R, Villa IM, Kramers JD, Kröner A, Smit CA, van Reenen DD (2001) Geochronology of the Hout River Shear Zone and the metamorphism in the Southern Marginal Zone of the Limpopo Belt, Southern Africa. Precamb Res 109:145–173

Krogh TE, Moser DE (1994) U-Pb zircon and monazite ages from the Kapuskasing uplift: age constraints on deformation within the Ivanhoe Lake fault zone. Can J Earth Sci 31:1096–1103

Kröner A (1985) Evolution of the Archaean continental crust. Annual Rev Earth Planet Sci 13:49–74

Kröner A (1991) Tectonic evolution in Archaean and Proterozoic. Tectonophysics 187:393–410

Kucinskas AB, Turcotte DL (1994) Isostatic compensation of equatorial highlands on Venus. Icarus 112:27–33

Kuiper YD, Lin S, Böhm CO (2011) Himalayan-type escape tectonics along the Superior Boundary Zone in Manitoba, Canada. Precamb Res 187:248–262

Kumar PS (2005) An alternative kinematic interpretation of Thetis Boundary Shear Zone, Venus: Evidence for strike-slip ductile duplexes. J Geophys Res 110:E07001. doi:10.1029/2004JE002387

Kusky TM (1998) Tectonic setting and terrane accretion of the Archean Zimbabwe craton. Geology 26:163–166

Kusky TM (2002) Is the Dongwanzi complex an Archean ophiolite? Response. Science 295:923. doi:10.1126/science.295.5557.923a

Kusky TM, Kidd WSF (1992) Remnants of an Archean oceanic plateau, Belingwe Greenstone Belt, Zimbabwe. Geology 20:43–46

Kusky TM, Li JH (2008) Note on the paper by Guochun Zhao, Simon A. Wilde, Sanzhong Li, Min Sun, Matthew l. Grant and Xuping Li (2007) 'U-Pb zircon age constraints on the Dongwanzi ultramafic-mafic body, North China, confirm it is not an Archean ophiolite'. Earth Planet Sci Lett 273:227–230

Kusky TM, Li JH, Tucker RD (2001) The Archean Dongwanzi Ophiolite Complex, North China Craton: 2.505-Billion-Year-Old Oceanic Crust and Mantle. Science 292:1142. doi:10.1126/science.1059426

Kusky TM, Polat A (1999) Growth of granite-greenstone terranes at convergent margins, and stabilization of Archean cratons. Tectonophysics 305:43–73

Lacroix S (1998) Géométrie Structurale et Evolution Tectonique de la Ceinture de Roches Vertes de L'Abitibi (Partie Nord-ouest): L'influence des Failles à Faible Pendage. PhD Thesis, L'Université du Québec à Chicoutimi. http://constellation.uqac.ca/1028/1/11647000.pdf. Accessed 3 Feb 2013

Lacroix S, Sawyer EW (1995) An Archean fold—thrust belt in the northwestern Abitibi Greenstone Belt: structural and seismic evidence. Can J Earth Sci 32:97–112

Lacroix S, Sawyer EW, Chown EH (1998) Pluton emplacement within an extensional transfer zone during dextral strike-slip faulting: an example from the late Archaean Abitibi Greenstone Belt. J Struct Geol 20:43–59

Laflèche MR, Dupuy C, Bougault H (1992a) Geochemistry and petrogenesis of Archean mafic volcanic rocks of the southern Abitibi Belt, Québec. Precamb Res 57:207–241

Laflèche MR, Dupuy C, Dostal J (1992b) Tholeiitic volcanic rocks of the late Archean Blake River Group, southern Abitibi greenstone belt: Origin and geodynamic implications. Can J Earth Sci 29:1448–1458

LeCheminant AN, Heaman LM (1989) Mackenzie igneous events, Canada: Middle Proterozoic hotspot magmatism associated with ocean opening. Earth Planet Sci Lett 96:38–48

Leclair A (2005) Géologie du nord-est de la province du Supérieur, Québec: Ministère des Ressources naturelles, Québec DV 2004–04, pp 19

Leclair A, Berclaz A, David J, Percival JA (2001) Regional geological setting of Archean rocks in the northeastern Superior Province. Geol Assoc Can/Mineral Assoc Can Meeting, Abstract volume 26:84

Leclerc F (2011) Géochimie et contexte tectonique du Groupe de Roy et du Complexe de Cummings dans la région de Chibougamau, Québec. PhD Thesis, INRS-ETE, Québec. http://www1.ete.inrs.ca/pub/theses/T000572.pdf. Accessed 3 Feb 2013

Leclerc F, Bédard JH, Harris LB, McNicoll VJ, Goulet N, Roy P, Houle P (2011) Tholeiitic to calc-alkaline cyclic volcanism in the Roy Group, Chibougamau area, Abitibi greenstone belt—Revised stratigraphy and implications for VHMS exploration. Can J Earth Sci 48:661–694

Leclerc F, Harris LB, Bédard JH, van Breemen O, Goulet N (2012) Structural and stratigraphic controls on magmatic, volcanogenic, and syn-tectonic mineralization in the Chapais-Chibougamau Mining Camp, northeastern Abitibi, Canada. Econ Geol 107:963–989

Lee CTA (2006) Geochemical/petrologic constraints on the origin of cratonic mantle. In: Benn K., Mareschal J-C, Condie KC (eds) Archean Geodynamics and Environments, AGU Geophys Monogr 164:89–114

Lee CTA, Luffi P, Hoink T, Li ZXA, Lenardic A (2008) The role of serpentine in preferential craton formation in the late Archean by lithosphere underthrusting. Earth Planet Sci Lett 269:96–104

Lee CTA, Luffi P, Chin EJ (2011) Building and destroying continental mantle. Ann Rev Earth Planet Sci 39:59–90

Lenardic A, Moresi LN, Muhlhaus H (2003) Longevity and stability of cratonic lithosphere: insights from numerical simulations of coupled mantle convection and continental tectonics. J Geophys Res, Solid Earth 108[B6], art. no. 2303. Doi:10.1029/2002JB001859

Lesher CM, Goodwin AM, Campbell IH, Gorton MP (1986) Trace element geochemistry of ore-associated and barren, felsic metavolcanic rocks in the Superior province, Canada. Can J Earth Sci 23:222–237

Liu Z, Bird P (2002) North America plate is driven westward by lower mantle flow. Geophys Res Lett 29(24):2164. doi:10.1029/2002GL016002

Lin S, Percival JA, Skulski T (1996) Structural constraints on the tectonic evolution of a late Archean greenstone belt in the northeastern Superior Province, northern Quebec (Canada). Tectonophysics 265:151–167

Lowe DR (1999) Geologic evolution of the Barberton greenstone belt and vicinity. In: MacGregor AM (1951) Some milestones in the Precambrian of Southern Africa. Proc Geol Soc South Africa 54:27–71

Lowe DR, Byerly GR (eds) (1999) Geologic Evolution of the Barberton Greenstone Belt, South Africa, Geol Soc Am Spec Paper 329:87–312

Luais B, Hawkesworth CJ (1994) The generation of continental crust: an integrated study of crust-forming processes in the Archaean of Zimbabwe. J Petrol 35:43–93

Lukonin D (2008) Archean and Proterozoic Gold Deposits of the Fennoscandian Shield, MSc Thesis, Luleå University of Technology, epubl.ltu.se/1653-0187/2008/083/LTU-PB-EX-08083-SE.pdf

Ludden JN, Hubert C, Gariépy C (1986) The tectonic evolution of the Abitibi greenstone belt of Canada. Geol Mag 123:153–166

MacGregor AM (1951) Some milestones in the Pre-Cambrian of Southern Rhodesla. Trans Proc Geol Soc S Africa 54, pp xxvii–lxxi

MacKenzie JM, Canil D (1999) Composition and thermal evolution of cratonic mantle beneath the central Archean Slave Province, NWT, Canada. Contrib Mineral Petrol 134:313–324

Magee KP, Head JW (1995) The role of rifting in the generation of melt: Implications for the origin and evolution of the Lada Terra-Lavinia Planitia region of Venus. J Geophys Res 100E:1527–1552

Marchenkov KI, Zharkov VN, Nikishin AM (1990) The stress state of Venusian crust and variations of its thickness: implication for tectonics and geodynamics. Earth Moon Planets 50–51:81–98

Mareschal J-C, West GF (1980) A model for Archaean tectonism: numerical models of vertical tectonism in greenstone belts. Can J Earth Sci 17:60–71

Martin H (1987) Petrogenesis of Archean trondhjemites, tonalites, and granodiorites from eastern Finland: major and trace element geochemistry. J Petrol 28:921–953

Martin H (1993) The mechanisms of petrogenesis of the Archean continental crust—Comparison with modern processes. Lithos 30:373–388

Martin H (1999) Adakitic magmas: modern analogues of Archaean granitoids. Lithos 46:411–429

Martin H, Smithies RH, Rapp R, Moyen JF, Champion D (2005) An overview of adakite, tonalite-trondhjemite-granodiorite (TTG), and sanukitoid: relationships and some implications for crustal evolution. Lithos 79:1–24

Matton G, Jébrak M (2009) The Cretaceous peri-Atlantic alkaline pulse (PAAP): Deep mantle plume origin or shallow lithospheric break-up? Tectonophysics 469:1–12

Maurice C, David J, Bédard JH, Francis D (2009) Evidence for a widespread mafic cover sequence and its implications for continental growth in the Northeastern Superior Province. Precamb Res 168:45–65

McBride JH, Snyder DB, England RW, Hobbs RW (1996) Dipping reflectors beneath old orogens: A Perspective from the British Caledonides. GSA Today 6:1–5

McCall GJH (2003) A critique of the analogy between Archaean and Phanerozoic tectonics based on regional mapping of the Mesozoic-Cenozoic plate convergent zone in the Makran, Iran. Precamb Res 127:5–17

McCuaig TC, Kerrich R (1998) P-T-t-deformation-fluid characteristics of lode gold deposits: evidence from alteration systematics. Ore Geol Rev 12:381–453

McCulloch MT, Wasserburg GJ (1978) Sm-Nd and Rb-Sr chronology of continental crust formation. Science 200:1003–1011

McCurry M, Hayden K, Morse LH, Mertzman S (2008) Genesis of post-hotspot, A-type rhyolite of the Eastern Snake River Plain volcanic field by extreme fractional crystallization of olivine tholeiite. Bull Volcanol 70:14835–14855

McGill GE (1983) The Geology of Venus. Episodes 1983:10–17

McKenzie D, McKenzie JM, Saunders RS (1992) Dike emplacement on Venus and on Earth. J Geophys Res 97E:15,977–15,990

Meade BJ (2007) Present-day kinematics at the India-Asia collision zone. Geology 35:81–84

Mège D, Ernst RE (2001) Contractional effects of mantle plumes on Earth, Mars, and Venus. In: Ernst RE, Buchan KL (eds) Mantle Plumes: Their Identification Through Time, GSA Spec Paper 352:103–140

Minnesota Minerals Coordinating Committee (2012) Explore Minnesota: Diamonds, files.dnr.state.mn.us/lands_minerals/mcc_docs/2012_diamonds.pdf

Mocquet A, Rosenblatt P, Dehant V, Verhoeven O (2011) The deep interior of Venus, Mars, and the Earth: A brief review and the need for planetary surface-based measurements. Planet Space Sci 59:1048–1061

Mole DR, Fiorentini ML, Thébaud N, McCuaig TC, Cassidy KF, Kirkland CL, Wingate MTD, Romano SS, Doublier MP, Belousova EA (2012) Spatio-temporal constraints on lithospheric development in the southwest—central Yilgarn Craton, Western Australia. Aust J Earth Sci 59:625–656

Molnar P, Tapponnier P (1977) Relation of the tectonics of eastern China to the India-Eurasia collision: application of slip-line field theory to large-scale continental tectonics. Geology 5:212–21

Morgan P (1983) Hot spot heat loss and tectonic style on Venus and in the Earth's Archean. Lunar Planet Sci 14:515–516

Morgan WJ (1971) Convection plumes in the lower mantle. Nature 230:42–43

Moser DE, Flowers RM, Hart RJ (2001) Birth of the Kaapvaal tectosphere 3.08 billion years ago. Science 291:465–468

Moser DE, Heaman LM, Krogh TE, Hanes JA (1996) Intracrustal extension of an Archean orogen revealed using single-grain U-Pb zircon geochronology. Tectonics 15:1093–1109

Moyen JF (2009) High Sr/Y and La/Yb ratios: The meaning of the "adakitic signature". Lithos 112:556–574

Moyen JF (2011) The composite Archaean grey gneisses: Petrological significance, and evidence for a non-unique tectonic setting for Archaean crustal growth. Lithos 123:21–36

Moyen JF, Champion D, Smithies RH (2010) The geochemistry of Archaean plagioclase-rich granites as a marker of source enrichment and depth of melting. Earth Environ Sci Trans Roy Soc Edin 100:35–50

Moyen JF, Martin H, Jayananda M (2001) Multi-element geochemical modelling of crust-mantle interactions during late-Archaean crustal growth: the Closepet granite (South India). Precamb Res 112:87–105

Moyen JF, Stevens G (2006) Experimental constraints on TTG petrogenesis: implications for Archaean geodynamics. In: Benn K, Condie K, Mareschal JC (eds) AGU Geophysical Monograph 164; Archaean Geodynamics and Environments, Chapter 10:149–175

Moyen JF, Stevens G, Kisters A (2006) Record of mid-Archaean subduction from metamorphism in the Barberton terrain, South Africa. Nature 442:559–562. doi:10.1038/nature04972

Moyen JF, Van Hunen J (2012) Short-term episodicity of Archaean plate tectonics. Geology 40:451–454

Mueller A, Harris LB (1988) Application of wrench tectonic models to mineralized structures in the Golden Mile, Kalgoorlie. In: Ho SE, Groves DI (eds) Recent Advances in the Understanding of Precambrian Gold Deposits. University of Western Australia Geology Department and University Extension, University of Western Australia Publication 11:97–108

Mueller A, Harris LB, Lungan A (1988) Structural control of greenstone-hosted gold mineralization by transcurrent shearing: a new interpretation of the Golden Mile district, Kalgoorlie, Western Australia. Ore Geol Rev 3:359–387

Mueller WU, Daigneault R, Mortensen JK, Chown EH (1996) Archean terrane docking: upper crust collision tectonics, Abitibi greenstone belt, Quebec, Canada. Tectonophysics 265:127–150

Mueller W, Pickett C (2005) Relative sea level change along the Slave craton coastline: characteristics of Archean continental rifting. Sedim Geol 176:97–119

Müller N, Helbert J, Hashimoto GL, Tsang CCC, Erard S, Piccioni G, Drossart P (2008) Venus surface thermal emission at 1 micron in VIRTIS imaging observations: evidence for variation of crust and mantle differentiation conditions. J Geophys Res 113:E00B17, pp 21. doi:10.1029/2008JE003118

Namiki N, Solomon SC (1994) Impact crater densities on volcanoes and coronae on Venus: Implications for volcanic resurfacing. Science 265:929–933

Namur O, Charlier B, Toplis MJ, Higgins MD, Hounsell V, Liegeois JP, Vander Auwera J (2011) Differentiation of tholeiitic basalt to A-type granite in the Sept Iles layered intrusion, Canada. J Petrol 52:487–539

NASA (undated) Venus: Facts & Figures. http://sse.jpl.nasa.gov/planets/profile.cfm?Object=Venus&Display=Facts&System=Metric. Accessed 3 Feb 2013

Neal CR, Mahoney JJ, Kroenke LW, Duncan RA, Petterson MG (1997) The Ontong Java Plateau. In: Mahoney JJ, Coffin MF (eds) large igneous provinces: continental, Oceanic and Planetary Flood Volcanism. Am Geophys Union Geophys Monog 100, pp. 183–216

Nikishin AM (1990) Tectonics of Venus: a review. Earth Moon Planets 50–51:101–125

Nikolayeva OV (1990) Geochemistry of the Venera 8 material demonstrates the presence of continental crust on Venus. Earth Moon Planets 50–51:329–341

Nimmo F, McKenzie D (1998) Volcanism and tectonics on Venus. Annu Rev Earth Planet Sci 26:23–51

Nisbet EG, Cheadle MJ, Arndt NT, Bickle MJ (1993a) Constraining the potential temperature of the Archaean mantle—a review of the evidence from komatiites. Lithos 30:291–307

Nisbet EG, Martin A, Bickle MJ, Orpen JL (1993b) The Ngezi Group: Komatiites, basalts and stromatolites on continental crust. In: Bickle MJ, Nisbet EG (eds) Geology of the Belingwe Greenstone Belt, Zimbabwe, Rotterdam, Netherlands, Balkema. Geol Soc Zimbabwe Spec Publ Series 2, p 121–165

Nitescu B, Cruden AR, Bailey RC (2006) Crustal structure and implications for the tectonic evolution of the Archean Western Superior craton from forward and inverse gravity modeling. Tectonics 25, TC1009. doi:10.1029/2004TC001717

Noltimier H, Sahagian D (1992) Tectonic style of venus: An analog to polar "icepack tectonics". J Geodyn 16:65–79

Nutman AP, Friend CRL (2007) Adjacent terranes with ca. 2715 and 2650 Ma high-pressure metamorphic assemblages in the Nuuk region of the North Atlantic Craton, southern West Greenland: complexities of neoarchaean collisional orogeny. Precamb Res 155:159–203

Nutman AP, Friend CRL (2009) New 1:20,000 scale geological maps, synthesis and history of investigation of the Isua supracrustal belt and adjacent orthogneisses, southern West Greenland: a glimpse of Eoarchaean crust formation and orogeny. Precamb Res 172:189–211

Obaje NG (2009) Geology and Mineral Resources of Nigeria, Lecture Notes in Earth Sciences 120, Springer-Verlag Berlin Heidelberg, pp 31–48

Obrebski M, Allen RM, Xue M, Hung S-H (2010) Slab-plume interaction beneath the Pacific Northwest. Geophys Res Lett 37:L14305. doi:10.1029/2010GL043489

O'Donovan G, Armitage M (undated) Technical Report on Norplat Limited Exploration Properties in the Kola Peninsula, SRK Consulting. In: Ovoca Resources PLC, Admission to trading on AIM. http://goo.gl/P9gjS Accessed 1 Feb 2013

Olsson JR, Söderlund U, Hamilton MA, Klausen MB, George R, Helffrich GR (2011) A late Archaean radiating dyke swarm as possible clue to the origin of the Bushveld Complex. Nature Geosci 4:865–869

O'Reilly SY, Zhang M, Griffin WL, Begg G, Hronsky J (2009) Ultradeep continental roots and their oceanic remnants: A solution to the geochemical "mantle reservoir" problem? Lithos 211:1043–1054

Oxburgh R (1972) Flake tectonics and continental collisions. Nature 239:202–204. doi:10.1038/239202a0

Parfitt EA, Head JW (1993) Buffered and unbuffered dyke emplacement on Earth and Venus: Implictions

for magma reservoir size, depth and rate of magma replenishment. Earth Moon Planets 61:249–261

Parman SW, Grove TL, Kelley KA, Plank T (2011) Along-arc variations in the pre-eruptive H2O contents of Mariana arc magmas inferred from fractionation paths. J Petrol 52:257–278

Pauer M (2004) The Gravity Field of Venus and Its Relationship to the Dynamic Processes in the Mantle. Research report to the Czech National Grant No. 205/02/1306, diploma thesis, Charles University, Prague, geo.mff.cuni.cz/theses/2004-Pauer-Mgr.pdf

Peacock SM, Rushmer T, Thompson AB (1994) Partial melting of subducting oceanic crust. Earth Planet Sci Lett 121:227–244

Pearce JA (2008) Geochemical fingerprinting of oceanic basalts with applications to ophiolite classification and the search for Archean oceanic crust. Lithos 100:14–48

Percival JA, Bursnall JT, Moser DE, Shaw DM (1991) Site survey for the Canadian continental drilling program's pilot project in the Kapuskasing Uplift; Ontario Geol Surv Ontario. Open File Report 5790:34 pp

Percival JA, Mortensen JK (2002) Water-deficient calc-alkaline plutonic rocks of northeastern Superior Province, Canada: Significance of charnockitic magmatism. J Petrol 43:1617–1650

Percival JA, McNicoll V, Brown JL, Whalen JB (2004) Convergent margin tectonics, central Wabigoon subprovince, Superior Province, Canada. Precamb Res 132:213–244

Percival JA, West GF (1994) The Kapuskasing uplift: a geological and geophysical synthesis. Can J Earth Sci 31:1256–1286

Percival JA, Skulski T, Sanborn-Barrie M, Stott GM, Leclair AD, Corkery MT, Boily M, (2012) Geology and tectonic evolution of the Superior Province, Canada. In: Percival JA, Cook FA, Clowes RM (eds) Tectonic Styles in Canada: The Lithoprobe Perspective. Geol Assoc Canada Spec Paper 49:321–378

Percival JA, western SNATMAPworkinggroup (2004) Orogenic framework for the Superior Province: Dissection of the "Kenoran Orogeny". The LITHOPROBE Celebratory Conference: From Parameters to Processes—Revealing the Evolution of a Continent. http://www.lithoprobe.ca/about/events/CC-Abs-Vol-CD-reduced%20size.pdf. Accessed 3 Feb 2013

Peschler AP, Benn K, Roest WR (2006) Gold-bearing fault zones related to Late Archean orogenic folding of upper and middle crust in the Abitibi granite-greenstone belt, Ontario. Precamb Res 151:143–159

Petford N, Atherton M (1996) Na-rich partial melts from newly underplated basaltic crust: The Cordillera Blanca Batholith, Peru. J Petrol 37:1491–1521

Petford N, Gallagher K (2001) Partial melting of mafic (Amphibolitic) lower crust by periodic influx of basaltic magma. Earth Planet Sci Lett 193:483–499

Petters S (1991) Regional Geology of Africa, Lect Notes Earth Sci 40, Springer-Verlag, Berlin Heidelberg, pp 722

Peucat J-J, Jayananda M, Chardon D, Capdevila R, Fanning CM, Paquette J-L (2013) The lower crust of the Dharwar Craton, Southern India: Patchwork of Archean granulitic domains. Precamb Res 227:4–28. doi:10.1016/j.precamres.2012.06.009,

Phillips RJ, Hansen VL (1994) Tectonic and magmatic evolution of Venus. Annu Rev Earth Planet Sci 22:597–654

Phillips RJ, Hansen VL (1998) Geological evolution of Venus: Rises, plains, plumes, and plateaus. Science 279(5356):1492–1497

Phillips RJ, Grimm RT, Makin MC (1991) Hot-spot evolution and the global tectonics of Venus. Science 252:651–658

Phillips RJ, Kaula WM, McGill GE, Malin MC (1981) Tectonics and evolution of Venus. Science 212:879–887

Pilote P, Guha J, Daigneault R, Robert F, Golightly JP (1990) Contexte structural et minéralisations aurifères des gîtes Casa-Berardi, Abitibi, Québec. Can J Earth Sci 27:1672–1685

Pinheiro RVL, Holdsworth RE (1997) Reactivation of Archaean strike-slip fault systems, Amazon region, Brazil. J Geol Soc London 154:99–104

Pirajno F (2007) Ancient to Modern Earth: The Role of Mantle Plumes in the Making of Continental Crust. Developments in Precambrian Geology 15:1037–1064

Pitcher WS (1985) Magmatism at a plate edge: the Peruvian Andes. Glasgow: Blackie Academic & professional, pp 328

Pohn HA, Schaber GG (1992) Indenter type deformation on Venus as evidence for large-scale tectonic slip, and multiple strike-slip events as a mechanism for producing tesselated terrain. Lunar Planet Sci 23:1095. www.lpi.usra.edu/meetings/lpsc1992/pdf/1539.pdf. Accessed 3 Feb 2013

Polat A, Kerrich R (2000) Archean greenstone belt volcanism and the continental growth–mantle evolution connection: constraints from Th–U–Nb–LREE systematics of the 2.7 Ga Wawa Subprovince, Superior Province, Canada. Earth Planet Sci Lett 175:41–54

Polat A, Kerrich R (2001) Geodynamic processes, continental growth, and mantle evolution recorded in late Archean greenstone belts of the southern Superior Province, Canada. Precamb Res 112:5–25

Polat A, Kerrich R, Wyman DA (1999) Geochemical diversity in oceanic komatiites and basalts from the late Archean Wawa greenstone belts, Superior Province, Canada: trace element and Nd isotope evidence for a heterogeneous mantle. Precamb Res 94:139–173

Poudjom-Djomani YH, O'Reilly SY, Griffin WL, Morgan P (2001) The density structure of subcontinental lithosphere through time. Earth Planet Sci Lett 184:605–621

Poulsen KH, Card KD, Franklin JM (1992) Archean tectonic and metallogenic evolution of the Superior Province of the Canadian Shield. Precamb Res 58:25–54

Pronin AA, Stofan ER (1990) Coronae on Venus: Morphology and distribution. Icarus 87:452–474

Puchtel IS, Hofmann AW, Mezger K, Jochum KP, Shchipansky AA, Samsonov AV (1998) Oceanic plateau model for continental crustal growth in the Archaean: A case study from the Kostomuksha greenstone belt, NW Baltic Shield. Earth Planet Sci Lett 155:57–74

Puchtel IS, Walker RJ, Anhaeusser CR, Gruau G (2009) Re-Os isotope systematics and HSE abundances of the 3.5 Ga Schapenburg komatiites, South Africa: hydrous melting or prolonged survival of primordial heterogeneities in the mantle? Chem Geol 262:355–369

Pysklywec RN, Cruden AR (2004) Coupled crust-mantle dynamics and intraplate tectonics: two-dimensional numerical and three-dimensional analogue modeling, Geochem Geophys Geosyst 5, Q10003. doi:10.1029/2004GC000748

Pysklywec RN, Gogus O, Percival J, Cruden AR, Beaumont C (2010) Insights from geodynamical modeling on possible fates of continental mantle lithosphere: collision, removal, and overturn. Can J Earth Sci 47:541–563

Raharimahefa T, Kusky TM (2006) Structural and remote sensing studies of the southern Betsimisaraka Suture, Madagascar. Gondwana Res 10:186–197

Ratschbacher L, Frisch W, Linzer H-G, Merle O (1991a) Lateral extrusion in the eastern Alps, Part 2: Structural analysis. Tectonics 10:257–271. doi:10.1029/90TC02623.

Ratschbacher L, Merle O, Davy P, Cobbold P (1991b) Lateral extrusion in the eastern Alps, Part 1: Boundary conditions and experiments scaled for gravity. Tectonics 10:245–256. doi:10.1029/90TC02622

Ravenelle J-F, Dubé B, Malo M, McNicoll V, Nadeau L, Simoneau J (2010) Insights on the geology of the world-class Roberto gold deposit, Éléonore property, James Bay area, Quebec. Geological Survey of Canada, Current Research 2010–1, 26 p.

Reston TJ (1990) Mantle shear zones and the evolution of the northern North Sea basin. Geology 18:272–275

Rey PF, Houseman G (2006) Lithospheric scale gravitational flow: the impact of body forces on orogenic processes from Archaean to Phanerozoic. In: Buiter SJH, Schreurs G (eds) Analogue and Numerical Modelling of Crustal-Scale Processes. Geol Soc London Spec Pub 253:153–167

Rey PF, Philippot P, Thébaud N (2003) Contribution of mantle plumes, crustal thickening and greenstone blanketing to the 2.75-2.65 Ga global crisis. Precamb Res 127:43–60

Richardson WP, Okal EA, Van der Lee S (2000) Rayleigh-wave tomography of the Ontong-Java Plateau. Phys Earth Planet Int 118:29–51

Ridley JR, Vearncombe JR, Jelsma HA (1997) Relations between greenstone belts and associated granitoids. In: de Wit MJ, Ashwal LD (eds) Greenstone Belts. Oxford Science Publications, Oxford, pp 376–397

Riedel W (1929) Zur Mechanik Geologischer Brucherscheinungen. Zentral-blatt fur Mineralogie, Geolo Paleontol B:354–368

Rino S, Komiya T, Windley BF, Katayama I, Motoki A, Hirata T (2004) Major episodic increases of continental crustal growth determined from zircon ages of river sands; implications for mantle overturns in the Early Precambrian. Phys Earth Planet Int 146:369–394

Rivard B, Corriveau L, Harris LB (1999) Structural reconnaissance of a deep crustal orogen using RADARSAT and Landsat satellite imagery and airborne geophysics. Can J Remote Sensing 25:258–267

Robert F (1989) Internal structure of the Cadillac tectonic zone southeast of Val d'Or, Abitibi greenstone belt, Quebec. Can J Earth Sci 26:2661–2675

Robert F (2001) Syenite-associated disseminated gold deposits in the Abitibi greenstone belt, Canada. Mineral Deposita 36:503–516

Robert F, Brommecker R, Bourne BT, Dobak PJ, McEwan CJ, Rowe RR, Zhou X (2007) Models and Exploration Methods for Major Gold Deposit Types. In: Milkereit B (ed) Proceedings of Exploration 07: Fifth Decennial International Conference on Mineral Exploration, 691–711

Robert F, Poulsen KH, Cassidy KF, Hodgson CJ (2005) Gold Metallogeny of the Superior and Yilgarn Cratons. Econo Geolo 100th Anniversary Volume:1001–1034

Robin CMI, Bailey RC (2009) Simultaneous generation of Archean crust and subcratonic roots by vertical tectonics. Geology 37:523–526

Rock NMS, Duller P, Haszeldine RS, Groves DI (1987) Lamprophyres as potential gold exploration targets: some preliminary observations and speculations. In: Ho SE, Groves DI (eds) Recent Advances in Understanding Precambrian Gold Deposits, Geology Dept. and University Extension, Univ WA Publ 11:271–286

Rock NMS, Groves DI (1988) Can lamprophyres resolve the genetic controversy over mesothermal gold deposits? Geology 16:538–541

Rondenay S, Bostock MG, Hearn TM, White DJ, Ellis R (2000). Lithospheric assembly and modification of the SE Canadian Shield: Abitibi-Grenville teleseismic experiment. J Geophys Res 105(B6): doi:10.1029/2000JB900022

Rondenay S, Bostock MG, Hearn TM, White DJ, Wu H, Sénéchal G, Ji S, Mareschal M (2002) Teleseismic studies of the lithosphere below the Abitibi—Grenville Lithoprobe transect. Can J Earth Sci 37:415–426

Roering C, van Reenen DD, Smit CA, Barton Jr JM, de Beer JH, de Wit MJ, Stettler EH, van Schalkwyk JF, Stevens G, Pretorius S (1992) Tectonic model for the evolution of the Limpopo Belt. Precamb Res 55:539–552

Rollinson H (2007) Early Earth Systems, A Geochemical Approach. Blackwell Publishing Oxford, pp 285

Romeo I, Turcotte DL (2008) Pulsating continents on Venus: an explanation for crustal plateaus and tessera terrains. Earth Planet Sci Lett 276:85–97

Romeo I, Capote R (2011) Tectonic evolution of Ovda Regio: An example of highly deformed continental crust on Venus? Planetary Space Sci 59:1428–1445

Romeo I, Capote R, Anguita F (2005) Tectonic and kinematic study of a strike-slip zone along the southern margin of Central Ovda Regio, Venus: Geodynamical

implications for crustal plateaux formation and evolution. Icarus 175:320–334
Ross PS, Goutier J, Mercier-Langevin P, Dubé B (2011a) Basaltic to andesitic volcaniclastic rocks in the Blake River Group, Abitibi Greenstone Belt: 1. Mode of emplacement in three areas. Can J Earth Sci 48:728–756
Ross PS, McNicoll V, Goutier J, Mercier-Langevin P, Dubé B (2011b) Basaltic to andesitic volcaniclastic rocks in the Blake River Group, Abitibi Greenstone Belt: 2. Origin, geochemistry, and geochronology. Can J Earth Sci 48:757–777
Sagan C, Mullen G (1972) Earth and Mars: evolution of atmospheres and surface temperatures. Science 177:52–56
Sandwell DT, Schubert G (1992) Evidence for retrograde lithospheric subduction on Venus In: Papers presented to the international colloquium on Venus. LPI Contribution 789. Lunar and Planetary Institute, United States, pp 97–99
Sandiford M, Van Kranendonk M, Bodorkos S (2004) Conductive incubation and the origin of granite-greenstone dome and keel structure: the Eastern Pilbara Craton, Australia. Tectonics 23, C1009. doi:10.1029/2002TC001452
Santosh M, Zhao D, Kusky Y (2010) Mantle dynamics of the Paleoproterozoic North China Craton: A perspective based on seismic tomography. J Geodyn 49:39–53
Saunders RS et al (1992) Magellan Mission Summary. J Geophys Res 97(E8):13,067–13,090. doi:10.1029/92JE01397
Schaber GG, Kozak RC (1990) Geologic/Geomorphic and Structure Maps of the Northern Quarter of Venus. US Geol Surv Open-File Report 90–24
Schaber GG, Strom RG, Moore HJ, Soderblom LA, Kirk RL, Chadwick DJ, Dawson DD, Gaddis LR, Boyce JM, Russel J (1992) Geology and distribution of impact craters on Venus: What are they telling us? J Geophys Res 97:13,257–13,301
Schoene B, de Wit MJ, Bowring SA (2008) Mesoarchean assembly and stabilization of the eastern Kaapvaal craton: a structural-thermochronological perspective. Tectonics 27, TC5010. doi:10.1029/2008TC002267
Schubert G, Moore WB, Sandwell DT (1994) Gravity over Coronae and Chasmata on Venus. Icarus 112:130–146
Schubert G, Turcotte DL, Olson P (2001) Mantle convection in the Earth and planets. Cambridge University Press
Shervais JW (2006) Plumes, plateaux, and the significance of subduction-related accretionary complexes in early Earth processes. In: Reimold U, Gibson R (eds) Early Earth Processes, GSA Special Paper 405:173–192
Simard M, Labbé J-Y, Maurice C, Lacoste P, Leclerc A, Boily M (2008) Synthèse du nord-est de la Province du Supérieur. Géologie Québec, MRNF Québec, MM 2008–02, pp 196
Simoneau J, Prud'homme N, Bourassa Y (2007) Mineral resource estimation Eleonore gold project, Quebec. Report Prepared for Goldcorp Inc., SRK Consulting (Canada) Inc., 209.89.176.189/_resources/eleonore_tech_report_aug9.pdf
Simons M, Hager BH, Solomon SC (1994) Global Variations in the geoid/topography admittance of Venus. Science 264:798–803
Sizova E, Gerya T, Brown M, Perchuk LL (2010) Subduction styles in the Precambrian: insight from numerical experiments. Lithos 116:209–229
Slabunov AI, et al (2006) The Archean of the Baltic Shield: Geology, geochronology, and geodynamic settings. Geotectonics 40:409–433
Sleep NH (2000) Evolution of the mode of convection within terrestrial planets. J Geophys Res 105(E7):17563–17578
Sleep NH, Windley BF (1982) Archean plate tectonics: constraints and inferences. J Geol 90:363–379
Smithies RH (2000) The Archaean tonalite-trondhjemite-granodiorite (TTG) series is not an analogue of Cenozoic adakite. Earth Planet Sci Lett 182:115–125
Smithies RH, Champion DC, Van Kranendonk MJ (2009) Formation of Paleoarchean continental crust through infracrustal melting of enriched basalt. Earth Planet Sci Lett 281:298–306
Smithies RH, Champion DC, Van Kranendonk MJ, Howard HM, Hickman AH (2005a) Modern style subduction processes in the Mesoarchean: geochemical evidence from the 3.12 Ga Whundo intraoceanic arc. Earth Planet Sci Lett 231:221–237
Smithies RH, Van Kranendonk MJ, Champion DC (2005b) It started with a plume—early Archaean basaltic proto-continental crust. Earth Planet Sci Lett 238:284–297
Smithies RH, Van Kranendonk MJ, Champion DC (2007) The Mesoarchean emergence of modern-style subduction. Gondwana Res 11:50–68
Smithies RH, Witt WK (1997) Distinct basement terranes identified from granite geochemistry in late Archaean granite-greenstones, Yilgarn Craton, Western Australia. Precamb Res 83:185–201
Smrekar SE, Elkins-Tanton L, Leitner JJ, Lenardic A, Mackwell S, Moresi L, Sotin C, Stofan ER (2007) Tectonic and thermal evolution of Venus and the role of volatiles: Implications for understanding the terrestrial planets. In: Esposito LW, Stofan ER, Cravens TE (eds) Exploring Venus as a Terrestrial Planet, AGU Geophys Monogr Ser 176:45–71
Smrekar SE, Hoogenboom T, Stofan ER, Martin P (2010) Gravity analysis of Parga and Hecate chasmata: implications for rift and corona formation. J Geophys Res 115:E07010. doi:10.1029/2009JE003435
Smrekar SE, Parmentier EM (1996) The interaction of mantle plumes with surface thermal and chemical boundary layers: applications to hotspots on Venus. J Geophys Res 101:5397–410
Smrekar SE, Stofan ER (1997) Corona formation and heat loss on Venus by coupled upwelling and delamination. Science 277:1289–1294
Smrekar SE, Sotin C (2012) Constraints on mantle plumes on Venus: Implications for volatile history. Icarus 217:510–523
Sobolev SV, Sobolev AV, Kuzmin DV, Krivolutskaya NA, Petrunin AG, Arndt NT, Radko VA, Vasiliev YR (2011)

Linking mantle plumes, large igneous provinces and environmental catastrophes. Nature 477:312–316
Sokolov SYu, Trifonov VG (2012) Role of the asthenosphere in transfer and deformation of the lithosphere: The Ethiopian–Afar superplume and the Alpine–Himalayan belt. Geotectonics 46:171–184
Sol S, Thomson CJ, Kendall J-M, White D, VanDecar JC, Asudeh I (2002) Seismic tomographic images of the cratonic upper mantle beneath the Western Superior Province of the Canadian Shield—a remnant Archean slab? Phys Earth Planet Int 134:53–69
Solomon SC, Head JW (1982) Mechanisms for lithospheric heat transport on Venus: Implications for tectonic style and volcanism. J Geophys Res 87:9236–9246
Solomatov VS, Moresi L-N (1996) Stagnant lid convection on Venus. J Geophys Res 101(E2):4737–4753
Solomatov VS, Moresi LN (1997) Three regimes of mantle convection with non-Newtonian viscosity and stagnant lid convection on the terrestrial planets. Geophys Res Lett 24:1907–1910
Solomatov VS, Moresi LN (2000) Scaling of time-dependent stagnant lid convection: Application to small-scale convection on Earth and other terrestrial planets. J Geophys Res—Solid Earth 105:21795–21817
Solomon SC, Head JW, Kaula WM, McKenzie D, Parsons B, Phillips RJ, Schubert G, Talwani M (1991) Venus tectonics—initial analysis from Magellan. Science 252:297–312
Solomon SC, Smrekar SE, Duane I, Bindschadler L, Grimm RE, Kaula WM, McGill GE, Phillips RJ, Saunders RS, Schubert G, Squyres SW, Stofan ER (1992) Venus tectonics: An overview of magellan observations. J Geophys Res 97:13,199–13,255
Sorohtin OG, Ushakov SA (2002) Природа Тектонической Активности Земли, Глава 6, Развитие Земли) (Tectonic activity nature of the Earth. Chapter 6, Development of the Earth), Moscow State University Press, 144–199. http://evolbiol.ru/sorohtin.htm. Accessed 3 Feb 2013
Spector A, Grant FS (1970) Statistical models for interpreting aeromagnetic data. Geophysics 35:293–302
Spencer JE (2001) Possible giant metamorphic core complex at the center of Artemis Corona, Venus. GSA Bull 113:333–345
Spiricheva VV, Nikishin AM (1990) Comparison of tessera grabens on Venus and grabens of Baikal region and Basin and Range Province on Earth. Abst Lunar Planet Sci Confer 21:1186–1187
Sproule RA, Lesher CM, Ayer JA, Thurston PC, Herzberg CT (2002) Spatial and temporal variations in the geochemistry of komatiites and komatiitic basalts in the Abitibi greenstone belt. Precamb Res 115:153–186
Squyres SW, Janes DM, Baer G, Bindschadler DL, Schubert G, Sharpton VL, Stofan ER (1992) The morphology and evolution of coronae on Venus. J Geophys Res E 97:13,611–13,634
Stachel T, Banas A, Muehlenbachs K, Kurszlaukis S, Walker EC (2006) Archean diamonds from Wawa (Canada): samples from deep cratonic roots predating cratonization of the Superior Province. Contrib Mineral Petrol 151:737–750
Stanistreet IG, T McCarthyTS, Charlesworth EG, Myers RE, Armstrong RA (1986) Pre-transvaal wrench tectonics along the northern margin of the witwatersrand basin, South Africa. Tectonophysics 131:53–74
Stein M, Hofmann AW (1994) Mantle plumes and episodic crustal growth. Nature 372:63–68
Stern RJ (2004) Subduction initiation: spontaneous and induced. Earth Planet Sci Lett 226:275–292
Stern RJ (2005) Evidence from ophiolites, blueschists, and ultrahigh-pressure metamorphic terranes that the modern episode of subduction tectonics began in Neoproterozoic time. Geology 33:557–560
Stern RJ (2008) Modern-type plate tectonics began in Neoproterozoic time: an alternative interpretation of Earth's tectonic history. In: Condie KC, Pease V (eds) When Did Plate Tectonics begin on Planet Earth? Geol Soc Am Spec Paper 440, pp 265–280
Stern RA, Hanson GN (1991) Archean high-Mg granodiorite: a derivative of light rare earth element-enriched monzodiorite of mantle origin. J Petrol 32:201–238
Stern RA, Percival JA, Mortensen JK (1994) Geochemical evolution of the Minto block: a 2.7 Ga continental magmatic arc built on the Superior proto-craton. Precamb Res 65:115–153
Stevenson R, Henry P, Gariépy C (1999) Assimilation-fractional crystallization origin of Archean Sanukitoid Suites: Western Superior Province, Canada. Precamb Res 96:83–99
Stevenson RK, O'Neil J, Machado N (2004) Isotope (Nd and Sr) and Geochronology studies of Quebec Kimberlites and Lamprophyres. Rapport Final, Sous-projet SC8b, DIVEX. www.divex.ca/projets/doc/SC8b-Machado-2004.pdf. Accessed 3 Feb 2013
Stofan ER, Senske DA, Michaels G (1993) Tectonic Features in Magellan Data, Chapter 8, Guide to Magellan Image Interpretation, JPL-93-94, NASA, pp 20. http://history.nasa.gov/JPL-93-24/ch8.htm. Accessed 1 Feb 2013
Stofan ER, Sharpton VL, Schubert G, Baer G, Bindschadler DL, Janes DM, Squyres SW (1992) Global distribution and characteristics of coronae and related features on Venus: Implications for origin and relation to mantle processes. J Geophys Res 97E:13,347–13,378
Stott G, Mueller W (2009) Superior Province: the nature and evolution of the Archean continental lithosphere. Precamb Res 168:1–3
Stott GM, Corkery T, Leclair A, Boily M, Percival J (2007) A revised terrane map for the Superior Province as interpreted from aeromagnetic data; Institute on Lake Superior Geology Proceedings, 53rd Annual Meeting, Lutsen, MN, v.53, part 1, pp 74–75
Sylvester AG (1988) Strike-slip faults. Geol Soc Am Bull 100:1666–1703
Suppe J, Connors C (1992) Critical-taper wedge mechanics of fold-and-thrust belts on Venus: initial results from Magellan. J Geophys Res 97:3545–13561
Syracuse EM, van Keken PE, Abers GA (2010) The global range of subduction zone thermal models. Phys Earth Planet Int 183:73–90. doi:10.1016/j.pepi.2010.02.004

Tackley PJ (2000a) Self-consistent generation of tectonic plates in time-dependent, three-dimensional mantle convection simulations, 1, Pseudo-plastic yielding. Geochem Geophys Geosyst 1. doi:10.1029/2000GC000036

Tackley PJ (2000b). Self-consistent generation of tectonic plates in time†dependent, three-dimensional mantle convection simulations 2. Strain weakening and asthenosphere Geochem Geophys Geosyst 1, 1026. doi:10.1029/2000GC000043

Tapponnier P, Molnar P (1976) Slip-line field theory and large-scale continental tectonics. Nature 264:319–324

Tapponnier P, Peltzer G, Le Dain A-Y, Armijo R, Cobbold PR (1982) Propagating extrusion tectonics in Asia: New insights from simple experiments with plasticine. Geology 10:611–616

Tchalenko JS (1968) The evolution of kink-bands and the development of compression textures in sheared clays. Tectonophysics 6:159–174

Tchalenko JS (1970) Similarities between shear zones of different magnitudes. Geol Soc Am Bull 81:1625–1640

Taylor SR, McLennan SM (1986) The geochemical composition of the Archaean crust. In: Dawson JB, Carswell DA, Hall J, Wedepohl KH (eds) The Nature of the Lower Continental Crust, Geol Soc London Spec Publ 24:173–178

Telmat H, Mareschal J-C, Gariépy C, David J, Antonuk CN (2000) Crustal models of the eastern Superior Province, Quebec, derived from new gravity data. Can J Earth Sci 37:385–397

Tessalina SG, Bourdon B, Van Kranendonk MJ, Birk J-L, Philippot P (2010) Influence of Hadean crust evident in basalts and cherts from the Pilbara Craton. Nat Geosci 3:214–217

Thébaud N, Rey P (2013) Archean gravity-driven tectonics on hot and flooded continents controls on long-lived hydrothermal systems away from continental margins. Precam Res. 229:93–104 doi:10.1016/j.precamres.2012.03.001

Theriault R (2002) Carte Géologique du Québec, MRNF Québec, DV 2002–06

Thurston PC (2002) Autochthonous development of Superior Province greenstone belts? Precamb Res 115:11–36

Thurston P, Ayer JA, Goutier J, Hamilton MA (2008) Depositional gaps in Abitibi greenstone belt stratigraphy: a key to exploration for syngenetic mineralization. Econ Geol 103:1097–1134

Thurston PC, Ayres LD (1986) Volcanological constraints on Archaean tectonics. Lunar and Planetary Inst. Workshop on the Tectonic Evolution of Greenstone Belts, 126–128

Thurston PC, Chivers KM (1990) Secular variation in greenstone sequence development emphasizing Superior Province, Canada. Precamb Res 46:21–58

Thurston PC, Fryer BJ (1983) The geochemistry of repetitive cyclical volcanism from basalt through rhyolite in the Uchi-Confederation greenstone belt, Canada. Contrib Mineral Petrol 83:204–226

Tomlinson KY, Condie KC (2001) Archean mantle plumes: evidence from greenstone belt geochemistry. In: Ernst RE, Buchan KL (eds) Mantle plumes: their identification through time. Geol Soc Am Spec Paper 352, pp 341–357

Tomlinson KY, Hughes DJ, Thurston PC, Hall RP (1999) Plume magmatism and crustal growth at 2.9 to 3.0 Ga in the Steep Rock and Lumby Lake area, Western Superior Province. Lithos 46:103–136

Tomlinson KY, Stott GM, Percival JA, Stone D (2004) Basement terrane correlations and crustal recycling in the western Superior Province: Nd isotopic character of granitoid and felsic volcanic rocks in the Wabigoon subprovince, N.Ontario, Canada. Precamb Res 132:245–274

Treiman AH (2007) Geochemistry of Venus' surface: Current limitations as future opportunities. In: Esposito LW, Stofan ER, Cravens TE (eds) Exploring Venus as a Terrestrial Planet, Geophys Monogr Ser 176, AGU, Washington, DC. http://www.lpi.usra.edu/science/treiman/venus1.pdf. Accessed 3 Feb 2013

Treloar PJ, Coward MP, Nigel BW, Harris NBW (1992) Himalayan-Tibetan analogies for the evolution of the Zimbabwe Craton and Limpopo Belt. Precamb Res 55:571–587

Tuckwell GW, Ghail RC (2003) A 400-km-scale strike-slip zone near the boundary of Thetis Regio, Venus. Earth Planet Sci Lett 211:45–55

Turcotte DL (1996) Magellan and comparative planetology. J Geophys Res 101:4765–4773

Turcotte DL, Morein G, Roberts D, Malamud BD (1999) Catastrophic resurfacing and episodic subduction on Venus. Icarus 139:49–54

Valley JW, Lackey JS, Cavosie AJ, Clechenko CC, Spicuzza MJ, Basei MAS, Bindeman IN, Ferreira VP, Sial AN, King EM, Peck WH, Sinha AK, Wei CS (2005) 4.4 billion years of crustal maturation: oxygen isotope ratios of magmatic zircon. Contrib Mineral Petrol 150:561–580

Valley JW, Peck WH, King EM, Wilde SA (2002) A cool early Earth. Geology 30:351–354

van der Velden AJ, Cook FA (2005) Relict subduction zones in Canada. J Geophys Res 110, B08403. doi:10.1029/2004JB003333

van der Velden AJ, Cook FA, Drummond BJ, Goleby BR (2006) Reflections of the neoarchean: a global perspective. Archean geodynamics and environments. Geophys Monogr Ser 164:255–265

van Hunen J, Moyen J-F (2012) Archean subduction: fact or fiction? Ann Rev Earth Planet Sci 40:195–219. doi:10.1146/annurev-earth-042711-105255

van Hunen J, van den Berg AP (2008) Plate tectonics on the early Earth: limitations imposed by strength and buoyancy of subducted lithosphere. Lithos 103:217–235

van Keken PE, Kiefer B, Peacock M (2002) High-resolution models of subduction zones: Implications for mineral dehydration reactions and the transport of water into the deep mantle. Geochem Geophys Geosyst 3– art. no. 1056 doi:10.129/2001GC000256

Van Kranendonk MJ (2010) Two types of Archean continental crust: Plume and plate tectonics on early Earth. Am J Sci 310:1187–1209. Doi:10.2475/10.2010.01

Van Kranendonk MJ (2011a) Cool greenstone drips and the role of partial convective overturn in Barberton Greenstone Belt evolution. J Afr Earth Sci 60:346–352

Van Kranendonk MJ (2011b) No arc-accretion tectonics in Yilgarn Craton. West Australian Geologist (WAG) 48:3–4. http://www.wa.gsa.org.au/WAG/WAG_April_May_2011.pdf. Accessed 3 Feb 2013

Van Kranendonk MJ, Hickman AH, Smithies RH, Nelson DR, Pike G (2002) Geology and tectonic evolution of the Archean North Pilbara terrain, Pilbara Craton, Western Australia. Econ Geol 97:695–732

Van Kranendonk MJ, Collins WJ, Hickman A, Pawley MJ (2004) Critical tests of vertical vs. horizontal tectonic models for the Archaean East Pilbara Granite-Greenstone Terrane, Pilbara Craton, Western Australia. Precamb Res 131:173–211

Van Kranendonk MJ, Smithies RH, Hickman AH, Champion DC (2007a) Review: secular tectonic evolution of Archean continental crust: interplay between horizontal and vertical processes in the formation of the Pilbara Craton, Australia. Terra Nova 19:1–38

Van Kranendonk MJ, Smithies RH, Hickman AH, Champion DC (2007b) The East Pilbara Terrane of the Pilbara Craton, Western Australia: formation of a continental nucleus through repeated plume magmatism. In: Van Kranendonk M, Smithies RH, Bennett V (eds) Earth's Oldest rocks, Developments in Precambrian Geology. Elsevier, Amsterdam, pp 307–337

Van Schmus WR (1992) Tectonic setting of the Midcontinent Rift system. Tectonophysics 213:1–15

Van Thienen P, van den Berg AP, Vlaar NJ (2004a) On the formation of continental silicic melts in thermochemical mantle convection models: implications for early Earth. Tectonophysics 394:111–124

Van Thienen P, van den Berg AP, Vlaar NJ (2004b) Production and recycling of oceanic crust in the early Earth. Tectonophysics 386:41–65

Van Thienen P, Vlaar NJ, van den Berg AP (2005) Assessment of the cooling capacity of plate tectonics and flood volcanism in the evolution of Earth, Mars and Venus. Phys Earth Planet Int 150:287–315

Vezolainen AV (2003) Dynamics of equatorial highlands on venus. PhD thesis, New Mexico State University. www.geophysics.nmsu.edu/a_vez/res/phd/diser.pdf. Accessed 3 Feb 2013

Villemaire M, Darbyshire FA, Bastow ID (2012) P-wave tomography of eastern North America: evidence for mantle evolution from Archean to Phanerozoic, and modification during subsequent hot spot tectonism. J Geophys Res Solid Earth 117(12). doi:10.1029/2012JB009639

Vlaar NJ, van Keken PE, van den Berg AP (1994) Cooling of the Earth in the Archaean: consequences of pressure-release melting in a hotter mantle. Earth Planet Sci Lett 121:1–18

Weihed P, Arndt N, Billström K, Duchesne J-C, Eilu P, Martinsson O, Papunen H, Lahtinen R (2005) 8: Precambrian geodynamics and ore formation: The Fennoscandian Shield. Ore Geol Rev 27:273–322

Weijermars R (undated) Structural Geology & Map Interpretation, Chapter 16: Remote-sensing maps, TU Delft OpenCourseWare, http://goo.gl/PDBKf

Weertman J (1979) Height of mountains on Venus and the creep properties of rock. Phys Earth Planet Int 19:197–207

Whalen JB, Percival JA, McNicoll VJ, Longstaffe FJ (2004) Geochemical and isotopic (Nd-O) evidence bearing on the origin of late- to post-orogenic high-K granitoid rocks in the Western Superior Province: implications for Late Archean tectonomagmatic processes. Precamb Res 132:303–326

White DJ, Musacchio G, Helmstaedt HH, Harrap RM, Thurston PC, Velden A van der, Hall K (2003) Images of a lower-crustal oceanic slab: direct evidence for tectonic accretion in the Archean western Superior province. Geology 31:997–1000

Whitehouse MJ, Kalsbeek F, Nutman AP (1998) Crustal growth and crustal recycling in the Nagssugtoqidian orogen of West Greenland: constraints from radiogenic isotope systematics and U-Pb zircon geochronology. Precamb Res 91:365–381

Whitney JA (1988) The origin of granite: the role and source of water in the evolution of granitic magmas. Geol Soc Am Bull 100:1886–1897

Whittington AG, Hofmeister AM, Nabelek PI (2009) Temperature-dependent thermal diffusivity of the Earth's crust and implications for magmatism. Nature 458:319–321

Wilcox RE, Harding TP, Seely DR (1973) Basic wrench tectonics. Am Assoc Pet Geol Bull 57:74–96

Wilkinson L, Cruden AR, Krogh TE (1999) Timing and kinematics of post-Timiskaming deformation within the Larder Lake—Cadillac deformation zone, southwest Abitibi greenstone belt, Ontario, Canada. Can J Earth Sci 36:627–647

Williams H (1990) Subprovince accretion tectonics in the south-central Superior Province. Can J Earth Sci 27:570–581

Willis JJ, Hansen VL (1996) Conjugate shear fractures at "Ki Corona," southeast Parga Chasma, Venus. Lunar Planet Sci 27:1443–1444

Wilson JR, Overgaard G (2005) Relationship between the Layered Series and the overlying evolved rocks in the Bjerkreim-Sokndal Intrusion, Southern Norway. Lithos 83:277–298

Wilson JT (1965) Evidence from ocean islands suggesting movement in the earth. In: Blackett PMS, Bullard E, Runcorn SK (eds) A symposium on continental drift. Philos Trans Royal Soc London A 258:145–167

Windley BF (1984) The Evolving Continents. Wiley, London, p 399

Windley BF, Garde AA (2009) Arc-generated blocks with crustal sections in the North Atlantic craton of West Greenland: crustal growth in the Archean with modern analogues. Earth Sci Rev 93:1–30

Wyborn LAI (1993) Constraints on interpretations of lower crustal structure, tectonic setting and metal-

logeny of the Eastern Goldfields and Southern Cross provinces provided by granite geochemistry. Ore Geol Rev 8:125–140

Wyman DA, Kerrich R (2002) Formation of Archean continental lithospheric roots: the role of mantle plumes. Geology 30:543–546

Wyman DA, Kerrich R (2009) Plume and arc magmatism in the Abitibi subprovince: implications for the origin of Archean continental lithospheric mantle. Precamb Res 168:4–22

Wyman DA, Kerrich R, Polat A (2002) Assembly of Archean cratonic mantle lithosphere and crust: plume-arc interaction in the Abitibi-Wawa subduction-accretion complex. Precamb Res 115:37–62

Yin A, Taylor MH (2011) Mechanics of V-shaped conjugate strike-slip faults and the corresponding continuum mode of continental deformation. GSA Bull 123:1798–1821

Zhai M, Zhao G, Zhang Q (2002) Is the Dongwanzi complex an Archean ophiolite? Science 295:923. doi:10.1126/science.295.5557.923a

Zhang P-Z, et al (2004) Continuous deformation of the Tibetan Plateau from global positioning system data. Geology 32:809–812

Zhao G, Wilde SA, Li S, Sun M, Grant ML, Li X (2008) Response to Note on 'U-Pb zircon constraints on the Dongwanzi ultramafic-mafic body, North China, confirm it is not an Archean ophiolite' by Kusky and Li. Earth Planet Sci Lett 273:231–234

Zheng JP, O'Reilly SY, Griffin WL, Lu FX, Zhang M, Pearson NJ (2001) Relict refractory mantle beneath the eastern North China block: significance for lithosphere evolution. Lithos 57:43–66

Zimmer MM, Plank T, Hauri EH, Yogodzinski GM, Stelling P, Larsen J, Singer B, Jicha B, Mandeville C, Nye CJ (2010) The role of water in generating the calc-alkaline trend: new volatile data for Aleutian magmas and a new tholeiitic index. J Petrol 51:2411–2444

Accreted Turbidite Fans and Remnant Ocean Basins in Phanerozoic Orogens: A Template for a Significant Precambrian Crustal Growth and Recycling Process

10

David A. Foster, Paul A. Mueller, Ben D. Goscombe and David R. Gray

Abstract

Convergent margin settings involving accretion of large turbidite fans with slivers of oceanic basement reflect important cites of continental crustal growth and recycling. Accreted crust consists of an upper layer of recycled arc and/or crustal detritus (turbidites) underlain by a layer of tectonically imbricated upper oceanic crust, and/or thinned continental crust, along with underplated magmatic material. When oceanic crust is converted to lower crust, it represents a juvenile addition to the continent. This two-tiered accreted crust is commonly of average continental crustal thickness and isostatically balanced near sea level. The Paleozoic part of the Tasman Orogen (Lachlan-type) of eastern Australia is the archetypical example of a turbidite-dominated accretionary orogen. The Neoproterozoic Damaran Orogen of SW Africa is similar to the Lachlan-type except that it was incorporated into Gondwana via a continent-continent collision, whereas the Mesozoic Rangitatan Orogen of New Zealand illustrates the transition of convergent margin from a Lachlan-type to more typical accretionary wedge type orogen. The spatial and temporal variations in deformation, metamorphism, and magmatism across these orogens illustrate how large volumes of turbidite and their relict oceanic basement eventually become stable continental crust. The timing of deformation and metamorphism recorded in these rocks reflects the crustal thickening phase, whereas post-tectonic granitoids and volcanic deposits constrain the timing of chemical maturation and cratonization. Cratonization and chemical maturation of

D. A. Foster (✉) · P. A. Mueller
Department of Geological Sciences, University of Florida,
Gainesville, FL 32611–2120, USA
e-mail: dafoster@ufl.edu

B. D. Goscombe
Integrated Terrane Analysis Research, 18 Cambridge Road,
Aldgate, South Australia 5154, Australia

D. R. Gray
Geostructures, Deviot Drive, Deviot,
Tasmania 7275, Australia

Y. Dilek, H. Furnes (eds.), *Evolution of Archean Crust and Early Life*, Modern Approaches in Solid Earth Sciences 7, DOI 10.1007/978-94-007-7615-9_10,

continental crust is fostered in these orogenic settings because turbidites represent fertile sources for magma genesis, particularly for the S-type granites that are common in these orogens. The structural style and lithotectonic assemblages of the three Phanerozoic examples is remarkably similar to the Archean Jardine turbidites, which were accreted to the Wyoming craton by 2.8 Ga. Recognition of similar orogens in the Archean is important for the evaluation of crustal growth models, particularly for those based on detrital zircon age patterns, because crustal growth by accretion of the upper ocean crust or by underplating of mafic magmas does not readily result in the formation of zircon-bearing magmas at the time of accretion. This crust only produces significant zircon when and if it partially melts, which may be long after the actual time of accretion. Consequently, the significance of this process over earth history is distorted compared to more zircon-rich orogenic processes in probability density-based analyses of crustal growth, but is recorded in Lu-Hf model ages of zircons from post-accretion magmas.

10.1 Introduction

Continental growth from transformed oceanic successions in subduction-accretion settings involves large volumes of continental detritus (submarine sediment fans, e.g., Ingersoll et al. 2003; Foster and Gray 2000; Busby 2004; Gray et al. 2007), fragments of juvenile oceanic, back-arc-basin and/or oceanic plateau lithosphere (upper and lower crust, e.g., Sengor and Natal'in 1996, Condie 2008), and juvenile additions to nascent continental crust due to magmatic underplating (e.g. Albarède 1998; Gray et al. 2007). Turbidite fan accretion represents a continental growth mechanism that was active and important throughout earth history with examples in the Phanerozoic of central Asia (Sengor and Natal'in 1996), Proterozoic of SW Laurentia (Karlstrom and Bowring 1988; Karlstrom et al. 2001; Bickford and Hill 2007), and Archean granite-greenstone belts (Percival et al. 2004). Crustal accretion rates in these settings are comparable to magmatic arcs and were the dominant process in some Phanerozoic orogenic zones, for example along the Paleozoic Pacific margin of East Gondwana (e.g., Foster and Gray 2000; Cawood 2005; Gray et al. 2007; Kemp et al. 2009).

Turbidite fan systems on oceanic crust or within oceanic back-arc basins form the basis for constructing new continental crust consisting of a mixture of juvenile basalt from the asthenospheric mantle along with recycled continental detritus (e.g., Patchett and Bridgwater 1984; Foster and Gray 2000; Kemp et al. 2009). It also likely that some of the detritus is sourced from new crust (e.g., island arcs, large igneous provinces) as well as old continents. Turbidite-dominated orogens develop a layered crust with a mafic lower and felsic upper crust. Turbidite-dominated orogens throughout geological time are variable mixtures of recycled continental and mantle-derived end members. Their recognition in the rock record depends on resolving the nature of the lower crust, sources of subduction/accretion related magmas, and provenance of the turbidites.

Much of our understanding of accretion has come from the study of modern or recent accretionary prisms (e.g. Lundberg and Reed 1991; Von Huene and Scholl 1991). In this paper, we investigate some of the parameters of accretion by analyzing ancient accretionary orogens dominated by turbidites. Controls on turbidite fan deformation include the plate tectonic setting, the tectonic position, either on the over-riding plate or subducting plate, the degree of coupling between over-riding and subducting plates that control accretion vs. sediment subduction, the original thickness of the fan, the residence time of the fan on the seafloor, the degree of lithification (diagenesis/metamorphism), the depth of the

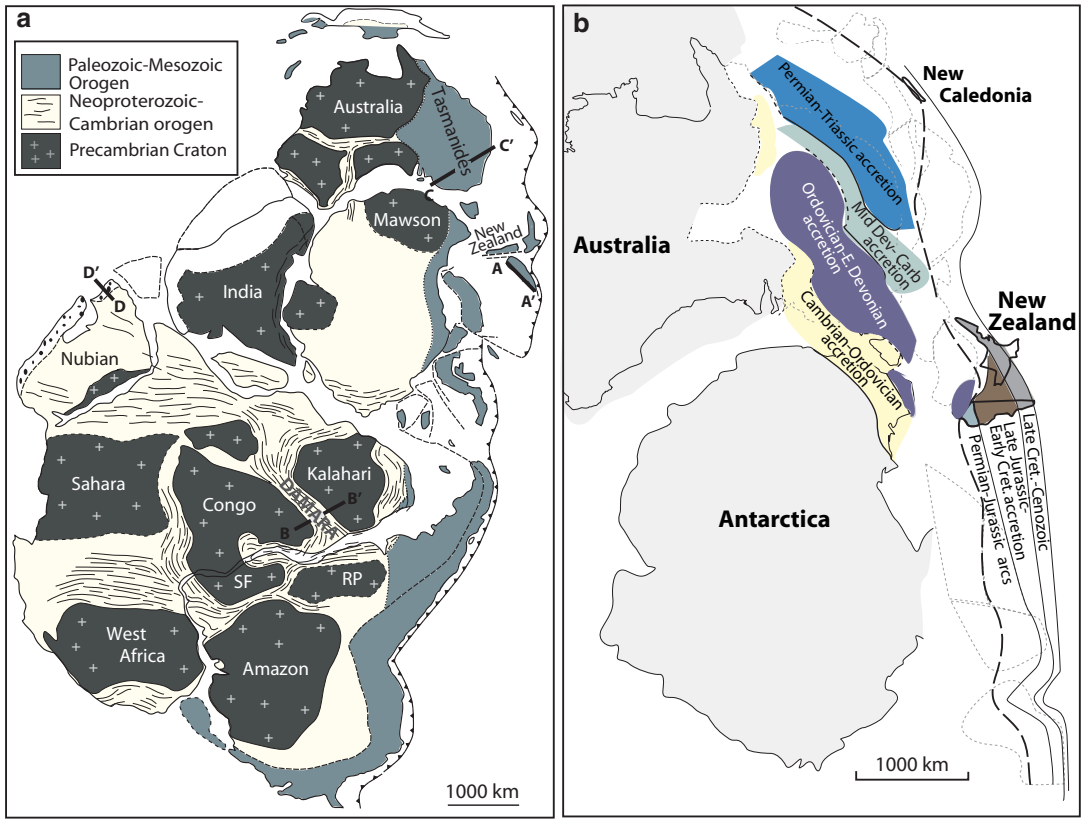

Fig. 10.1 **a** Map of Gondwana showing the distribution of Precambrian cratons and orogenic belts of Neoproterozoic, Paleozoic, Paleozoic-Mesozoic and Mesozoic-Cenozoic ages. The locations of schematic crustal profiles A-A', B-B', C-C', and D-D' in Fig. 10.2 are shown as solid lines (Modified from Gray et al. 2007). **b** Map showing the timing of accretion of oceanic successions along the former eastern margin of Gondwana (Australia and Antarctica segment only). (Map modified from Veevers 2000a, Bradshaw 1989 and Gray et al. 2007)

lower-upper crust boundary in the accretionary wedge, and the availability of fluids. The deformational style of turbidites in ancient orogens includes mélange/broken formation, chevron folding, and fold-nappes and accompanying schistosity. The strain state is typically variable, with either subvertical plane strain or flattening with mostly coaxial increments, or dominantly constrictional involving non-coaxial deformation.

This chapter summarizes the architecture of crustal growth by accretion of turbidite sequences in light of the position of these sequences relative to primary tectonic elements in orogens spanning a range of geologic time, i.e., the Mesozoic Rangitatan (New Zealand) Orogen, the Paleozoic Lachlan Orogen (eastern Australia), the Neoproterozoic Damara Orogen (Namibia), and the Mesoarchean Beartooth orogeny (Fig. 10.1). The paper reviews the widely variable templates of these turbidite-dominated orogens and their similarities using regional to meso-scale structures to delineate their tectonic and magmatic evolution, and discusses implications for these processes for interpretation of crustal growth mechanisms in the Precambrian as well as their expected lack of expression in the global detrital zircon U-Pb age record.

10.2 Orogen Architecture

Figure 10.1 shows examples of turbidite-dominated orogens from Gondwana including the Neoproterozoic-Cambrian Damara Belt of the

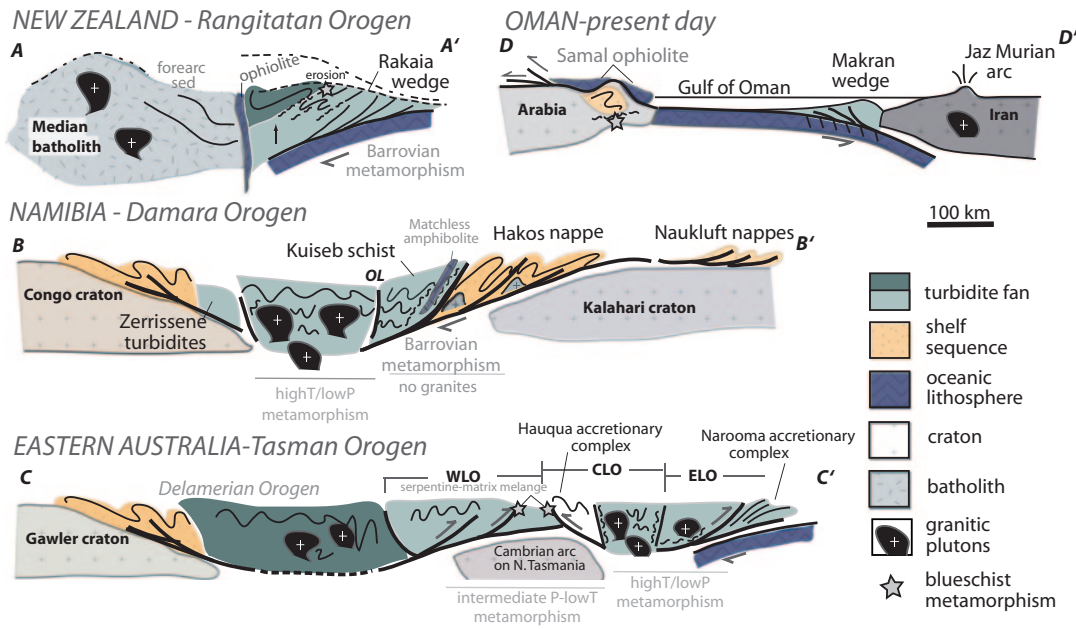

Fig. 10.2 Schematic structural profiles across the Lachlan, Rangitatan, and Damara orogens showing the locations of turbidites with respect to other tectonic elements WLO- Western Lachlan Orogen, CLO - Central Lachlan Orogen, ELO - eastern Lachlan Orogen

Pan African Orogen, the Paleozoic Lachlan Orogen of the composite Tasman Orogen of eastern Australia and the Mesozoic Rangitatan Orogen of New Zealand. The Damara Orogen of Namibia (Fig. 10.2) is a divergent orogen between the Congo and Kalahari cratons with thrusting of the carbonate platform and passive margin sequences to the north and south over the bounding cratons. The south-vergent part is defined by the generally homoclinally dipping schist and a thin-skinned thrust system (Fig. 10.2). The core is dominated by granite with high-T/low-P metamorphism. The location of the granitic magmatism, as well as the structural asymmetry, reflects subduction dipping beneath attenuated Congo craton (Barnes and Sawyer 1980; Miller 1983a, b; Kasch 1983a). The Lachlan Orogen (Fig. 10.2) is made up of an attenuated Ordovician oceanic volcanic arc, a shear-zone bounded high-T/low-P metamorphic complex with similarities to the Chugach metamorphic complex of Alaska (Hudson and Pflaker 1982; Gasser et al. 2011), structurally thickened quartz-rich submarine fans and inverted Siluro-Devonian basins within the arc (Gray and Foster 2004a, b). Evidence of subduction is provided by serpentinite-matrix mélanges containing blueschist blocks and lenses along some of the major fault zones (Spaggiari et al. 2002a, b; 2004a). The Rangitatan Orogen of New Zealand (Fig. 10.2) is made up of a structurally thickened sediment wedge (Caples terrane) abutting arc-forearc sequences (Median batholith) and a deformed turbidite fan system (Torlesse of Rakaia wedge) separated by a steeply dipping, fault-bounded, ophiolite belt (Mortimer 1993, 2004; Gray and Foster 2004c). Structural vergence in the schists suggests NE thrusting of the trench volcaniclastic sedimentary sequence over a subducted quartz-rich sedimentary fan (Mortimer 1993) that lay outboard on now subducted oceanic crust (Coombs et al. 1976). Mafic greenschist-chert sequences are exposed close to the trench-submarine fan boundary (the Caples-Torlesse boundary), where relict blueschist metamorphism is preserved (Yardley 1982). Eventual closure of the Gulf of Oman (Fig. 10.2) would result in a structurally thickened Makran wedge juxtaposed against the Jaz-Murian arc of

Iran producing an orogen section similar to the Rakaia wedge (Gray et al. 2007).

10.3 Eastern Gondwanides—Example Of Phanerozoic Accretion

From about 550 to 90 Ma the East Gondwana margin (Tasmanides) was a classic accretionary margin (Foster and Gray 2000; Cawood 2005; Glen 2005; Rossetti et al. 2011). It shows eastward younging in accretion of submarine fans, fragments of ocean crust, and arc and forearc basin elements from the Cambrian margin of Australia-Antarctica through to New Zealand (Fig. 10.3). The Tasman orogenic system represents at least 10% of the volume of Gondwanan continental crust (Fig. 10.1). Using 100 m.y. timescales (e.g., for development of the Australian part of the Tasmanides: Foster and Gray 2000), this corresponds to approximately 3–4 km^3/yr of apparent continental growth, with ~1.5 km^3/yr of new, mantle-derived material comprising the lower crust (Gray et al. 2007).

In the eastern Australian Tasmanides, accretion occurred in a stepwise fashion with an eastward younging from the Cambrian through the Triassic, reflected by peak deformations of Early Ordovician, early Silurian to mid-Devonian, and Permian-Triassic age in the respective orogenic belts (Foster and Gray 2000; Gray and Foster 2004a). Accretion involved deformation of Neoproterozoic platform and rift basin sequences (Delamerian Orogen), a Cambrian-Orodovician composite turbidite fan overlying Cambrian oceanic crust and an Ordovician island arc (Lachlan Orogen), and Carboniferous-Permian arc, forearc, trench, subduction complex, and foreland basin sequences (New England Orogen) (Gray and Foster 2004a; Cawood 2005). Continental New Zealand records continuous sedimentation and accretionary prism accretion (Rakaia and Pahau Terranes; Bradshaw 1989) in the hanging wall to a long-lived subduction system along the margin of Gondwana from at least Permian to Late Cretaceous times (Fig. 10.1b; Bradshaw 1989; Mortimer 2004).

10.3.1 The Lachlan Orogen, Australia

The Paleozoic Lachlan Orogen as part of the Tasman orogenic system is a composite accretionary orogen that formed along the eastern margin of Gondwana during late Neoproterozoic through Paleozoic times (Figs. 10.1b, 10.3; Foster and Gray 2000; Glen 2005; Gray and Foster 2004b). It is dominated by extensive, Cambrian to Ordovician turbidites that formed a large submarine fan system in the early Paleozoic, comparable in size to the Bengal fan (Fergusson and Coney 1992a). Based on paleocurrent information, the U-Pb ages of detrital zircons $^{40}Ar/^{39}Ar$ ages of detrital muscovites, and isotopic data, the quartz-rich turbidites and black shales were sourced mainly from the Delamerian-Ross Orogen along the margin of Gondwana and other Pan-African aged orogenic belts (Powell 1983, 1984; VandenBerg and Stewart 1992; Gray and Webb 1995; Fergusson and Fanning 2002; Williams et al. 1994; Turner et al. 1996; Foster et al. 1999; Veevers 2000b). The fan accumulated on Middle to Late Cambrian (~505 Ma to ~460 Ma; Fergusson and Coney 1992b; Foster et al. 2005) backarc and forearc crust, consisting of predominantly MORB- to arc-tholeiitic basalt, gabbro, boninite, ultramafic rocks, and calc-alkaline arc rocks (Crawford and Keays 1978, 1987; Foster et al. 2009). Closure of the Lachlan back-arc basin took place from ~450 Ma through 340 Ma, with accretion of structurally thickened submarine fans, accretionary complexes, extinct volcanic arcs, oceanic crust, and the Tasmanian microcontinent (Fergusson and Coney 1992b; Foster et al. 1999; Gray and Foster 2004b).

Structure The Lachlan orogen comprises three thrust-belts that constitute the western, central and eastern parts, respectively. The western Lachlan (WLO) consists largely of an east-vergent thrust system (Fig. 10.3a), whereas the central Lachlan (CLO) is dominated by northwest-trending structures and consists of a southwest-vergent thrust-belt (Howqua accretionary complex in Fig. 10.3a) linked to a fault-bounded, high-T/low-P metamorphic complex (WOMB in Fig. 10.3a). The

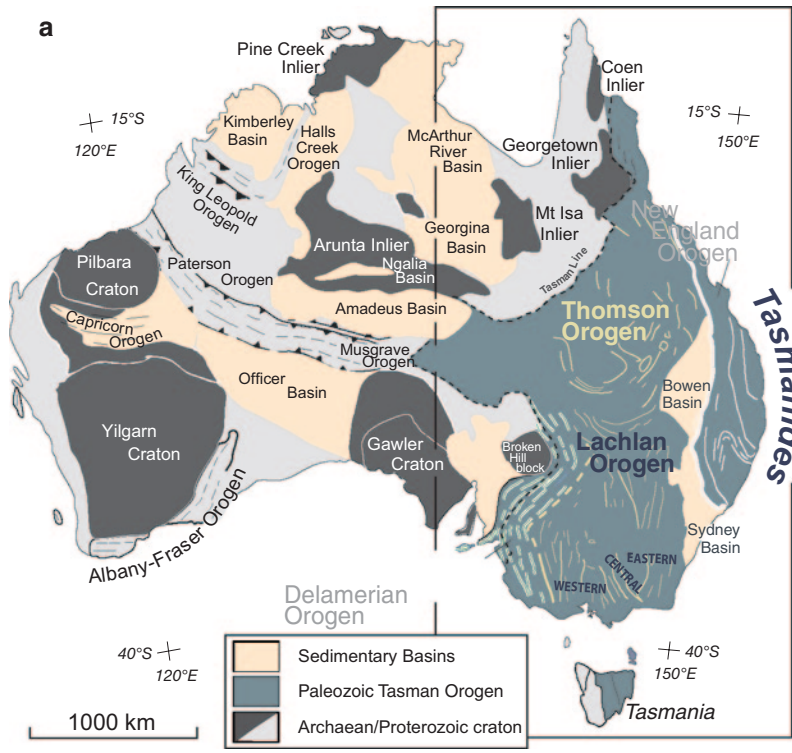

Fig. 10.3 **a** Tectonic map of eastern Australia showing tectonic subdivisions and the major structural elements (Modified from Foster et al. 2009). **b** Map of eastern Australia showing the major lithofacies and tectonostratigraphic elements. (Modified from Gray and Foster 2004a; Foster and Gray 2008). **c** Composite structural profile across the southern Tasmanides at about 37.5° south latitude. The subsection letters refer to specific cross sections in Gray et al. (2006b)

eastern Lachlan (ELO) is dominated by a north-south structural grain and east-directed thrust faults; in the south and in the easternmost part an east-vergent thrust system (Yalmy-Bungonia thrust belt) overrides an older, subduction-related accretionary complex (Narooma accretionary). Shortening via under-thrusting of the back-arc lithosphere for the WLO and CLO (Gray and Foster 2004a) is suggested by the presence of dismembered ophiolite slivers along some major fault zones (Spaggiari et al. 2003a, 2004a), the low-T/intermediate-P metamorphism of meta-sandstone/slate sequences of the WLO and external part of the CLO (Offler et al. 1998; Spaggiari et al. 2003b), the presence of broken formation in the CLO and ELO (Fergusson 1987; Miller and Gray 1997; Watson and Gray, 2001), and a serpentinite-matrix mélange incorporating blueschist blocks (Spaggiari et al. 2002a, b; 2003a).

Metamorphism The turbidite successions of the Lachlan Orogen are generally metamorphosed to greenschist and subgreenschist (anchizonal) conditions (Fig. 10.4a). Most of the turbidites are within the chlorite zone with localized biotite zone conditions in contact aureoles around granitoids. Exceptions include high-T/low-P migmatites and K-feldspar-cordierite-sillimanite gneisses (700 °C and 3–4 kbar) in the Wagga-Omeo Complex and Cooma, Cambalong, Jerangle and Kuark belts of the Eastern Metamorphic belt (Fig. 10.4a). These belts are intimately associated with S-type granitic plutons and anatectic migmatites, and represent deeper parts of the orogenic pile exhumed during extension (e.g. Morand 1990; Collins and Hobbs 2001).

Turbidites from the low-grade parts of the Lachlan Orogen show intermediate pressure series metamorphism based on b_0 values of phengitic micas and chlorite-actinolite assemblages in metabasites (Offler et al. 1998; Gray and Foster 2004b), as well as low-T/intermediate-P blueschist metamorphism (6–7 kbar, <450 °C) of metabaltic blocks in serpentinite/talc-matrix mélanges (Spaggiari et al. 2002a, b). Low-T/intermediate-P metamorphism occurred at 450–440 Ma during the regional deformation of the Lachlan Orogen (Spaggiari et al. 2002a, b; 2003a).

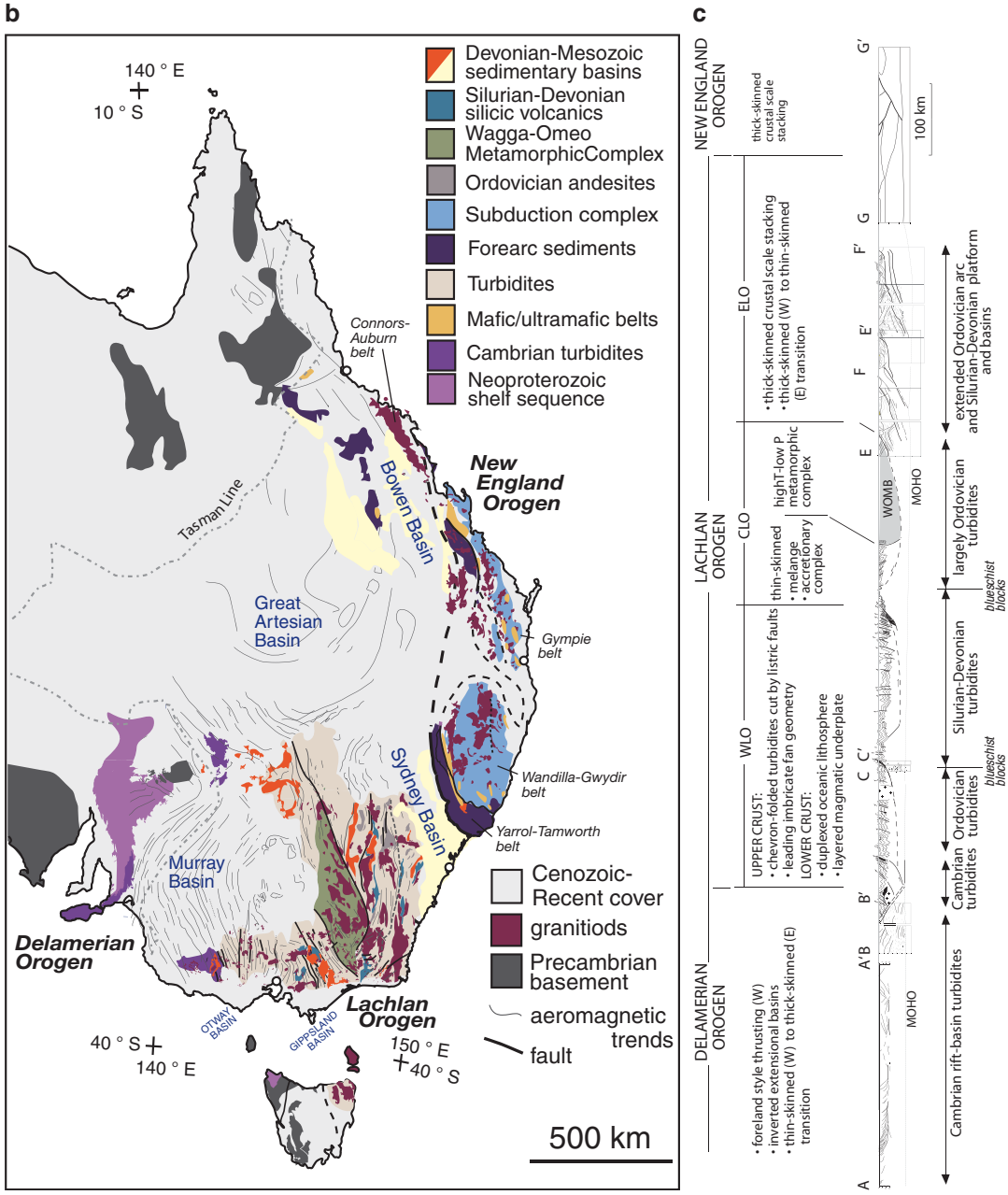

Magmatism Silurian-Devonian granitic rocks form about 20% of the present outcrop in the Lachlan and up to 36% in eastern and central Lachlan. Granitoids form both major batholiths with N-S and NNE orientations roughly parallel to the structural grain, or as single plutons (White and Chappell 1983; Chappell at al. 1988; Chappell and White 1992). Most of the granitic plutons crystallized at about 2 kbar pressure or less and intrude low-grade rocks. The majority are post-tectonic and unmetamorphosed, although the oldest intrusions (Wagga-Omeo Belt, Kosciusko Batholith) are strongly deformed and were emplaced syn- to late-kinematically and at mid-crustal depths (Hine et al. 1978; Keay et al. 2000). Volcanic sequences, mostly dacite-rhyolite, are

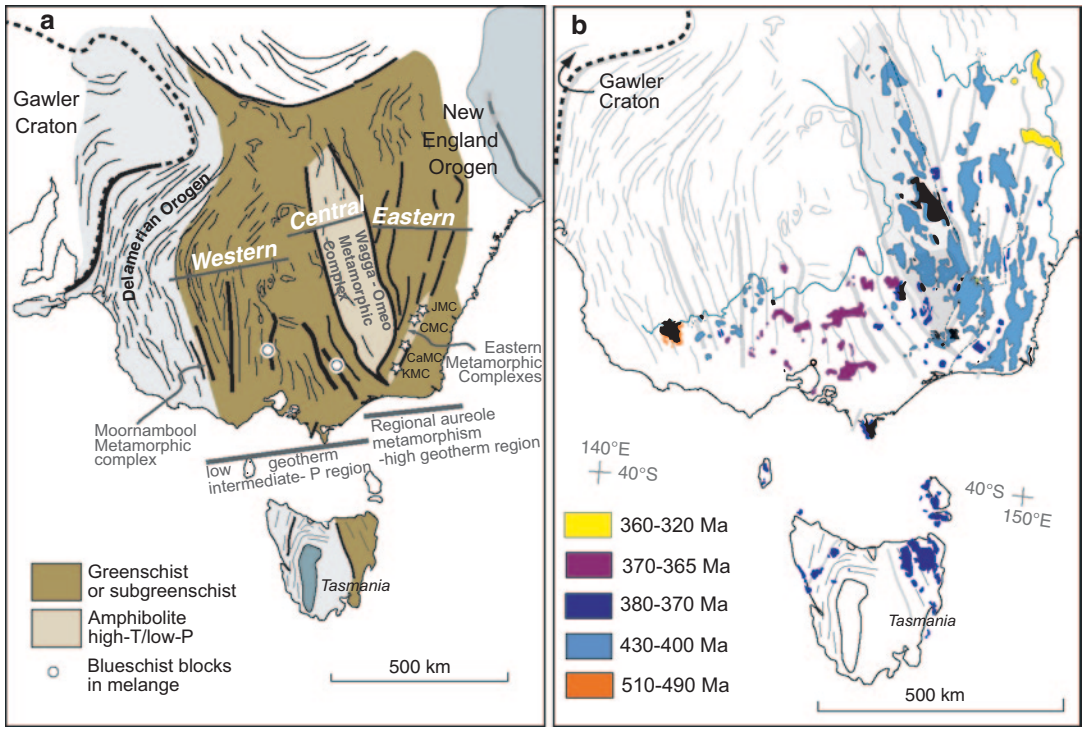

Fig. 10.4 **a** Map of southeastern Australia, showing the distribution of metamorphic rocks. **b** Map of southeastern Australia showing the distribution of granitoid plutons. (Modified from Gray and Foster 2004b; Foster and Gray 2008)

also widespread (15% of area in eastern Lachlan Orogen, significant post-tectonic caldera complexes in western Lachlan Orogen) and associated with shallow granitic plutons. Basaltic to andesitic volcanic rocks comprise the Ordovician Macquarie arc in the eastern Lachlan Orogen (Glen et al. 1998; 2007).

The Lachlan Orogen igneous rocks range from about 430 to 370 Ma (excluding the 480–460 Ma Macquarie Arc), with broad west-to-east younging trends in the eastern (430–370 Ma) and western (410–370 Ma) belts, respectively. Carboniferous (*c*. 320 Ma) granites occur along the eastern edge of the Lachlan Orogen, and are transitional to the Permo-Triassic granites of the younger New England Orogen (Chappell et al. 1988).

S-type granitoids make up roughly half of all exposed granite in the Lachlan Orogen and are concentrated in a NNW-trending belt along the center of the orogen. Granodiorite and granite dominate, and coeval/cogenetic S-type volcanics are locally abundant (Wyborn et al. 1981). Compositions range from Mg-Fe-rich, cordierite-bearing granodiorite (Hine et al. 1978; White and Chappell 1988) to highly fractionated granite (Price et al. 1983). Felsic S-type granites (410–370 Ma) also occur in the western Lachlan Orogen; the youngest (370 Ma) intrusions are associated with extensive caldera complexes (Phillips et al. 1981; Clemens and Wall 1984; Rossiter 2003).

I-type granites form a broad belt in the eastern Lachlan (e.g., 8620 km^2, 419–370 Ma, Bega Batholith), but are also abundant throughout the rest of the orogen. I-type volcanic rocks are locally preserved in grabens (Wyborn and Chappell 1986). Medium-to high-K granodiorites and granites dominate, with lesser tonalite and rare gabbro-diorite (<1%). Trace element patterns in typical I- and S-types are similar and have low Sr/Y ratios, suggesting magma sources with residual plagioclase, but no garnet, similar

to Australian Proterozoic granites (Wyborn et al. 1992), and in post-Archean upper crust in general. A-type granitic rocks are uncommon, widely dispersed, and tend to be post-orogenic (Collins et al. 1982; King et al. 1997). Sr and Nd isotopic data ($^{87}Sr/^{86}Sr$ 0.704–0.720; εNd +4 to −11; e.g., McCulloch and Chappell 1982; Keay et al. 1997; Maas and Nicholls 2002) define a hyperbolic mixing array, typical of trends observed in many Phanerozoic granitic provinces. I-type granites generally give lower $^{87}Sr/^{86}Sr$ and higher εNd than S-types, which trend towards the more evolved compositions of the Paleozoic turbidites ($^{87}Sr/^{86}Sr$ 0.715–0.730, εNd −8 to −12, Adams et al. 2005). Whole rock oxygen isotopes in the I-type (7.9–10‰) and S-type (9.2–12‰) granites of the eastern Lachlan Orogen show correlations with Sr and Nd isotopic ratios, consistent with mixing of high-$\delta^{18}O$ crustal and low-$\delta^{18}O$ mantle-derived components (McCulloch and Chappell 1982). Lu-Hf isotopic data from igneous zircons range from $\varepsilon Hf > +10$ to < -10 with A- and I-types giving higher positive values, approaching depleted mantle, and S-types tending to give more negative values. The εHf values are correlated with $\delta^{18}O$ values of the zircons and whole rock Nd data, such that the positive εHf values correspond to more mantle-like $\delta^{18}O$ values and the strongly negative εHf zircon to $\delta^{18}O$ values of 8–11 (Kemp et al. 2007, 2009).

S-type granites contain zircon xenocrysts with age populations of *c.* 500 and 1000 Ma along with minor populations through to *c.* 3.6 Ga (Williams 1992; Keay et al. 2000; Maas et al. 2001), which are identical to detrital zircon populations in the Early Paleozoic turbidites (Veevers 2000b). The presence of turbidite-derived detrital zircons implicates magma sources at least partly within the early Paleozoic meta-turbidites. Zircon inheritance in I-type granites is typically limited, but with the same age-populations as in the S-type granites (e.g., Chen and Williams 1991; Williams 1992), indicating a recycled sedimentary component was involved in the petrogenesis of the I-types.

The compositions of the granitic rocks are ambiguous in terms of geodynamic setting due to the crustal (sedimentary) components. Mafic dikes, intrusions, and lavas across the orogen, however, show signatures suggesting derivation as back-arc to arc mantle partial melts (Bierlein et al. 2001b; Collins 2002). This suggests that at least some of the granites, e.g., those in the margin-parallel batholiths of the eastern/central Lachlan Orogen, formed within arc/back-arc tectonic settings, albeit with much sedimentary (turbidite) input. The *c.* 370 Ma post-orogenic magmatism in the western Lachlan Orogen is probably related to post-collision lithospheric delamination (Soesoo et al. 1997; Soesoo and Nicholls 1999).

Silurian-Devonian igneous rocks of the Lachlan Orogen were, therefore, derived from a mixture of source components from depleted mantle, either directly or via partial melts of mafic crust, and partial melts of the turbidites (Gray 1984, 1990; Collins 1996, 1998; Kemp et al. 2009). The highest proportions of mantle-derived magmas are found in the post-orogenic A-types, which formed during extension and slab roll back (Kemp et al. 2009). The I-types are variable mixtures with greater proportions of mantle-derived magma than the S-types. This indicates that significant new crustal growth via mantle partial melting occurred during the extensional phases of the orogenic cycle, with variable amounts of growth and recycling occurring during shortening phases (Kemp et al. 2009).

Tectonic Evolution Extensive turbidite fan deposition took place in a marginal basin system on the Gondwana margin between ~490 Ma and 470 Ma, with large turbidite fans spreading out onto Cambrian oceanic crust (Gray and Foster 2004b; Foster et al. 2005). Turbidite deposition occurred at the same time as post-orogenic magmatism, cooling, and erosional exhumation occurred in the Delamerian Orogen (~490–460 Ma; Fig. 10.6b; Turner et al. 1992, 1996). Outboard, subduction-related arc volcanism was initiated at ~485 Ma in the oceanic plate forming the Macquarie magmatic arc (Glen et al. 1998). The Macquarie arc formed some thousands of kilometers from the Gondwanan margin based on palinspastic reconstruction of the WLO and CLO; Fergusson and Coney 1992b; Foster and Gray 2007).

After 460 Ma the back-arc basin system began to close by subduction (Gray et al. 1997;

Soesoo et al. 1997; Foster and Gray 2000), albeit inboard of the main Gondwanan subduction zone. Closure of the Lachlan back-arc basin most likely occurred by double divergent subduction (Gray et al. 1997; Soesoo et al. 1997). In this scenario, multiple oceanic thrust-systems operated in both the eastern and western parts of the basin at the same time (Figs. 10.5 and 10.6). Shortening of the basin thickened and duplexed the oceanic crust, and caused thrusting and chevron folding in the overlying turbidite wedge (Spaggiari et al. 2004a, b). Closure of the southern part of the back arc basin resulted in west-directed shortening and thrusting in northeastern Tasmania and reactivation of Cambrian structures in western Tasmania (Bierlein et al. 2005).

Widespread magmatism in the western part of the WLO at ~400 Ma (Fig. 10.5) was followed by final closure of the marginal basin, which was thrust over the northeastern part of the Tasmanian microcontinent by about 390 Ma (Fig. 10.5). Structural thickening and amalgamation of the WLO and CLO led to cratonization of the inner Lachlan (Foster and Gray 2000). Outboard in the ELO syn-deformational *c*. 440–435 Ma magmatism and high-T/low-P metamorphic belts formed during intermittent east-directed thrusting (Fergusson and Vanden-Berg, 1990) and periods of extension-related volcanism, particularly at *c*. 420 Ma, as part of a Cordilleran-type margin (Zen 1995; Collins 2002). Post-orogenic silicic magmatism in the WLO (central Victorian magmatic province) occurred at *c*. 370–360 Ma, while east-directed thrusting in the ELO caused inversion of former extensional basin faults, and was also followed by post-orogenic magmatism. The late stage magmatism may have been in response to partial removal of mantle lithosphere after closure of the back-arc-basin (Soesoo et al. 1997) or slab roll-back, which started a new cycle of extension and basin formation along the Gondwana margin (Collins 2002). In either case the Lachlan Orogen and related belts were fully accreted to Gondwana by *c*. 330 Ma (Powell 1983).

10.3.2 The Rangitatan Orogen (Rakaia Wedge), New Zealand

The Rangitatan Orogen is a collage of accreted arc and forearc assemblages, and a turbidite-dominated sediment wedge (Rakaia Wedge) that formed along the margin of Gondwana in Jurassic and times (Coombs et al. 1976; Bradshaw 1989; Mortimer 1993). The forearc assemblages are dominated by volcaniclastic deposits from the contemporaneous magmatic arc. The Torless turbidites were deposited on oceanic crust along the Gondwana margin. Detrital zircon U-Pb and detrital mica $^{40}Ar/^{39}Ar$ age distributions age indicate a provenance north of New Zealand (present coordinates) in the New England Orogen of Australia (Adams and Kelly 1998; Adams et al. 1998, 2007). Deformation of the Rakaia wedge and accretion to the Mesozoic arcs in New Zealand occurred when the oceanic plate with the thick turbidite succession was subducted.

Structure The sediment wedge is made up of two distinct structural domains (Fig. 10.7a): (1) the Otago Schist belt characterized by schistosity and transposed layering at the mesoscale, and shear zones and recumbent isoclinal fold-nappes at the regional scale (Mortimer 1993; Gray and Foster 2004c); and (2) the chevron folded, poorly cleaved, younger sediments of the Pahau terrane (Bradshaw 1989). Based on seismic reflection data (Mortimer et al. 2003) the Permian Dun Mountain ophiolite and Maitai mélange (Cawood 1987) form a steeply N-dipping interface between the gently folded, arc and forearc sequences (Median Batholith, Brook Street and Murihiku terranes) to the south, and the deformed submarine fan sediments of the Torlesse composite-terrane to the north (Fig. 10.7b). The Torlesse composite terrane includes a crustal section composed of structurally thickened (~20 km thickness) Permian to Triassic-Jurassic sediments of the Rakaia terrane, structurally overlain by a ~10 km thick wedge of trench sediments (Caples terrane) immediately adjacent to the Livingstone fault (Norris and Craw 1987). In the immediate hanging wall to the Livingstone fault, intensely-deformed monotonous quartzo-feldspathic schist

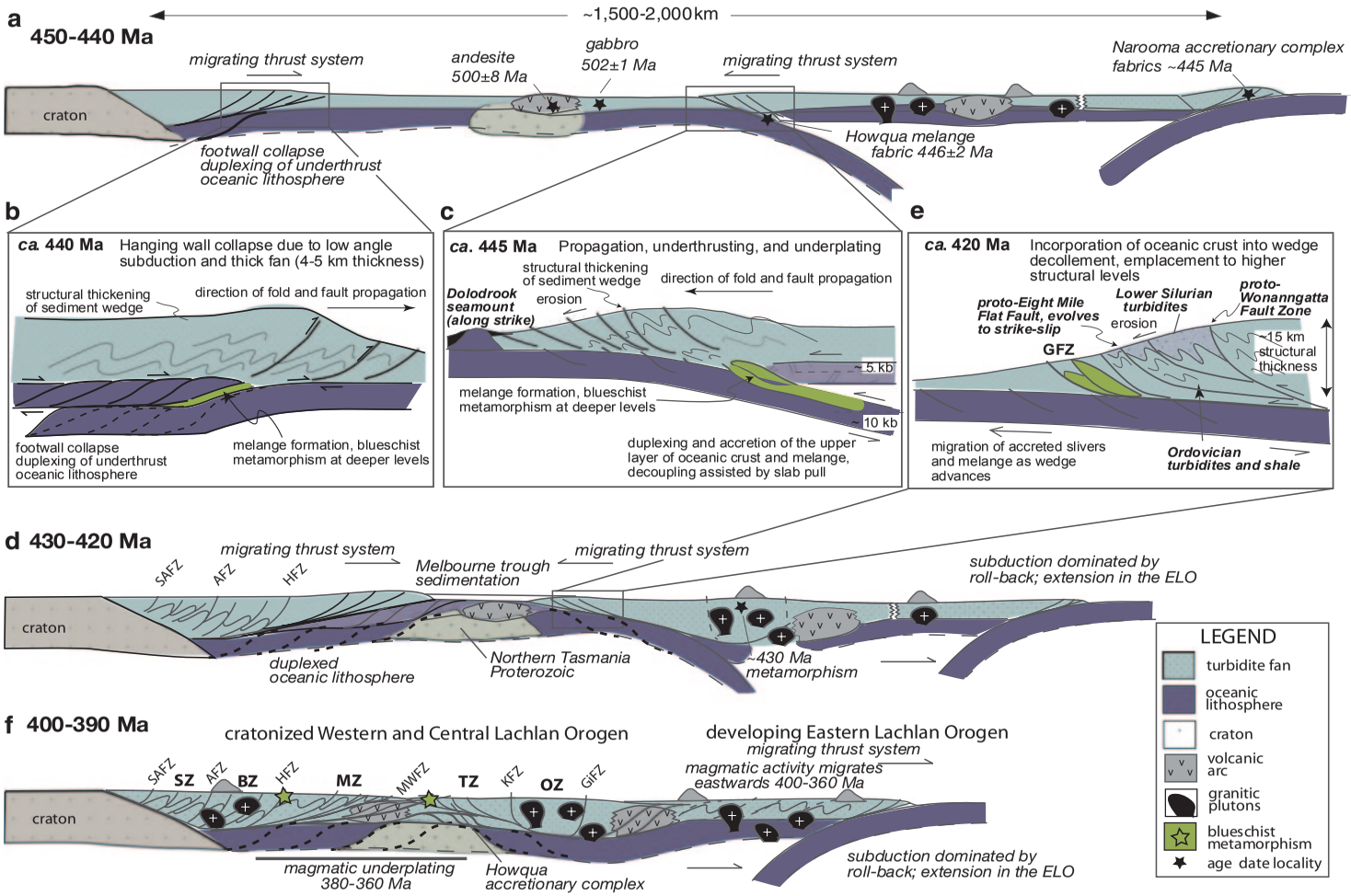

Fig. 10.5 Tectonic evolutionary diagram illustrating the sequential stages in crustal growth for the Lachlan Orogen

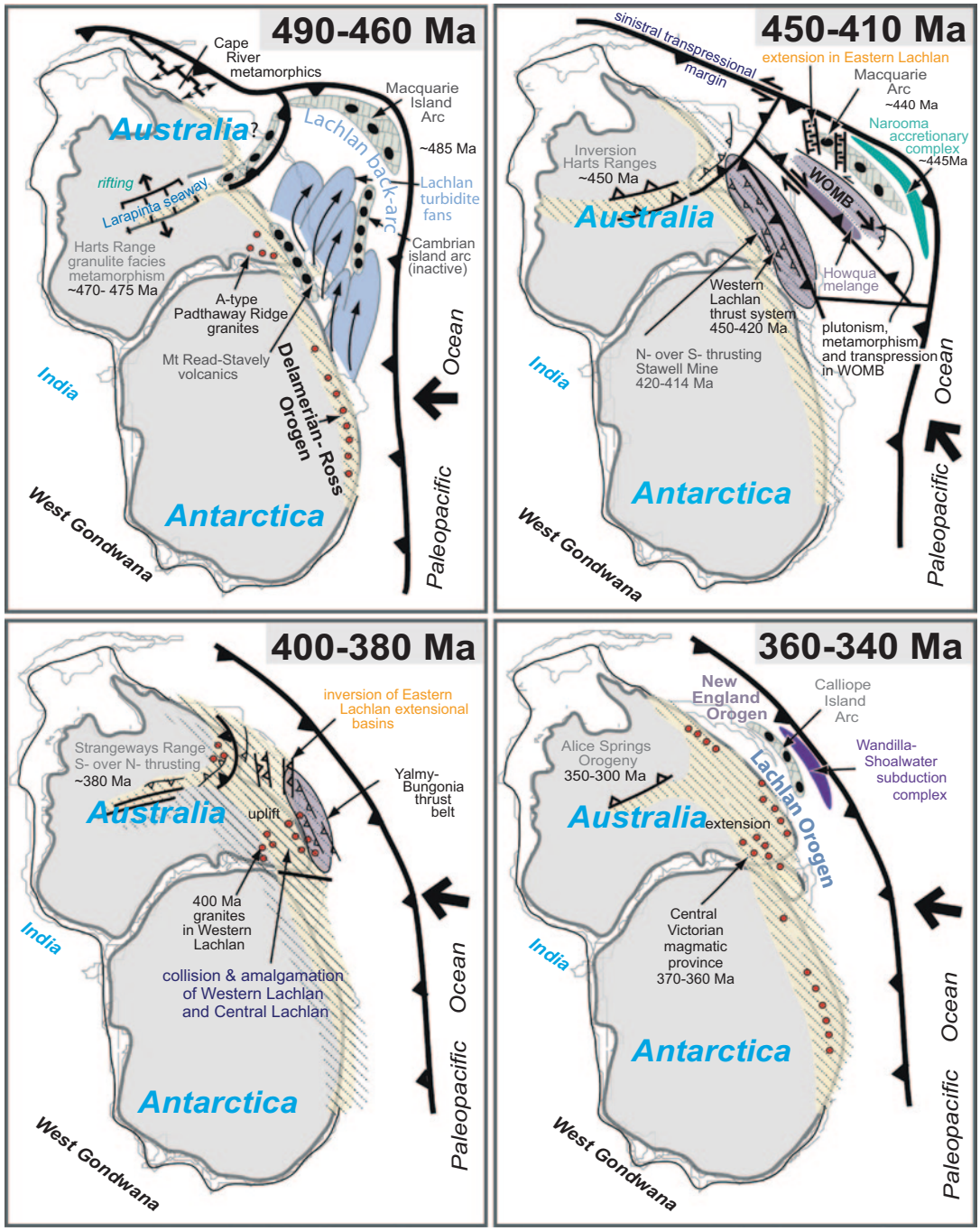

Fig. 10.6 Plate tectonic setting during the development of the Lachlan backarc basin and events leading to the accretion of the Lachlan Orogen

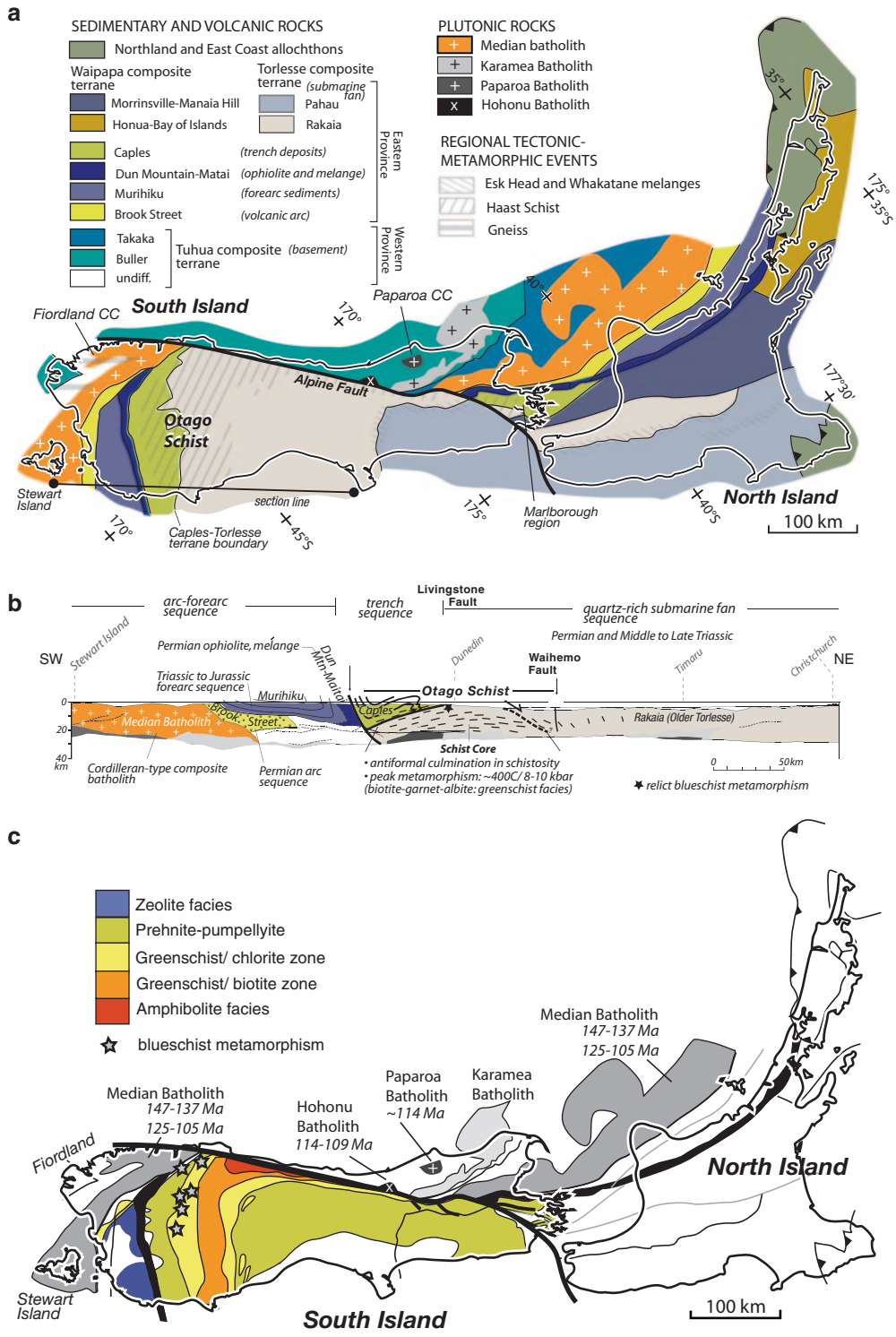

Fig. 10.7 **a** Geologic map of New Zealand showing the key tectonic elements, the main terranes and provinces, the distribution of plutonic rocks and Torlesse terrane components. (Map modified from tectonostratigraphic terrane map of IGNS Qmap Series map). **b** Geological profile showing the crustal architecture of the southern part of the South Island (Based on Mortimer et al. 2003). **c** Metamorphic map of New Zealand also showing the locations and crystallization ages of the granitoids based references in the text

with minor intercalated micaceous schist, greenschist, and metachert (Otago Schist) occupies a domal culmination with a maximum subsurface width of ~220 km and ~20 km of structural relief (Mortimer 1993) (Fig. 10.7b). Northwards beyond the Waihemo Fault, there is a transition into the tectonically imbricated and weakly metamorphosed Permian-Triassic greywacke sequence of the Rakaia (Older Torlesse) terrane. South of the Livingstone fault the crustal section is composed of a ~10–15 km thick succession of Murihiku terrane forearc sediments (Triassic to Jurassic volcanogenic sandstone, siltstone and tuff) overlying a ~10 km thick arc sequence of Brook Street terrane volcanic rocks (layered gabbro-ultramafic sequences, diorites and volcaniclastic sediments, which are the roots of a Permian intra-oceanic arc).

Metamorphism The metamorphosed part of the Rakaia wedge (Otago Schist) is an ~150 km wide, NW-trending metamorphic belt (Fig. 10.7a) that forms a domal culmination (Fig. 10.7b). Prehnite-pumpellyite facies rocks on the northern and southern flanks (Torlesse and Caples Terranes respectively) increase to upper greenschist facies, and then to epidote-amphibolite facies in the broad central portion (Mortimer 1993, 2000). Mineral parageneses indicate peak P-T conditions of 450 °C and 8–10 kbar (Mortimer 2000), suggesting burial to depths of ~20–30 km that place the Otago Schist in a moderate-high P/T metamorphic series (Barrovian-type). Relict blueschist assemblages occur in mafic greenschist/chert sequences close to the Caples-Torlesse boundary, indicating an earlier high-pressure metamorphism (Yardley 1982).

Magmatism Subduction related magmatism in the overriding Gondwana plate formed the Median batholith (Mortimer et al. 1999a). The Median batholith was emplaced into the Paleozoic Gondwanan margin during subduction of the oceanic plate and leading to accretion of the Rakaia wedge (e.g. Muir et al. 1998; Daczko et al. 2001). The granitoids of the Median batholith represent a semi-continuous (230–125 Ma) calc-alkaline, I-type suite, which shows very little evidence of crustal involvement ($^{87}Sr/^{86}Sr \approx 0.7037$; $\varepsilon Nd \approx +4$) (Kimbrough et al. 1993, 1994; Muir et al. 1998; Mortimer et al. 1999b). Collision between the arc and the wedge is marked by the 124–111 Ma Separation Point suite (northern part of South Island) and the lower crustal, 126–119 Ma metadiorites and metagabbros of the Western Fiordland orthogneiss (e.g., McCulloch et al. 1987; Muir et al. 1995, 1998; Klepeis et al. 2003). These I- type suites span a wide range in SiO_2, are distinctly sodic, and have high to very high Sr/Y ratios, resembling Archean TTG or modern adakite suites (Muir et al. 1995). This adakite-like suite probably resulted from partial melting of basaltic protoliths in the subarc crust and mantle after substantial thickening of the arc crust (e.g., Petford and Atherton 1996). Granitic plutons coeval with the Rangitata orogeny, therefore, occur within the Mesozoic arc (Median Tectonic Zone; Wandres and Bradshaw 2005) or along the Paleozoic Gondwanan margin and not within the accreted turbdites. Compared to average Lachlan Orogen granitoids, these are more mafic and almost exclusively I-type, zircon inheritance is absent or much weaker, and continental Sr-Nd-O isotopic signatures are rare. Partial melting of the exposed turbidites apparently did not occur during subduction accretion.

The youngest plutons in the belt are I- and S-type plutons in the Hohonu and Paparoa batholiths in NW South Island, which intrude Paleozoic Gondwana margin metasedimentary rocks. These plutons, known as the Rahu Suite, exhibit xenocrystic zircons (500–1000 Ma), more evolved radiogenic isotopic signatures than the older suite ($^{87}Sr/^{86}Sr$ 0.7062–0.7085, $\varepsilon Nd \approx -5$), and elevated $\delta^{18}O$ (Tulloch 1988; Waight et al. 1998b), suggesting they are mixtures of partial melts of the Mesozoic arc crust and the older Paleozoic continental margin formed after the convergence switched to extension (Tulloch and Kimbrough 2003: Waight et al. (1998a, b)

Tectonic Evolution The Permian-Jurassic Torlesse fan with arc-forearc-trench slope sequences (Brook Street, Maitai, Murihiku and Caples terranes) formed in a convergent margin setting due to subduction of Permian oceanic crust beneath

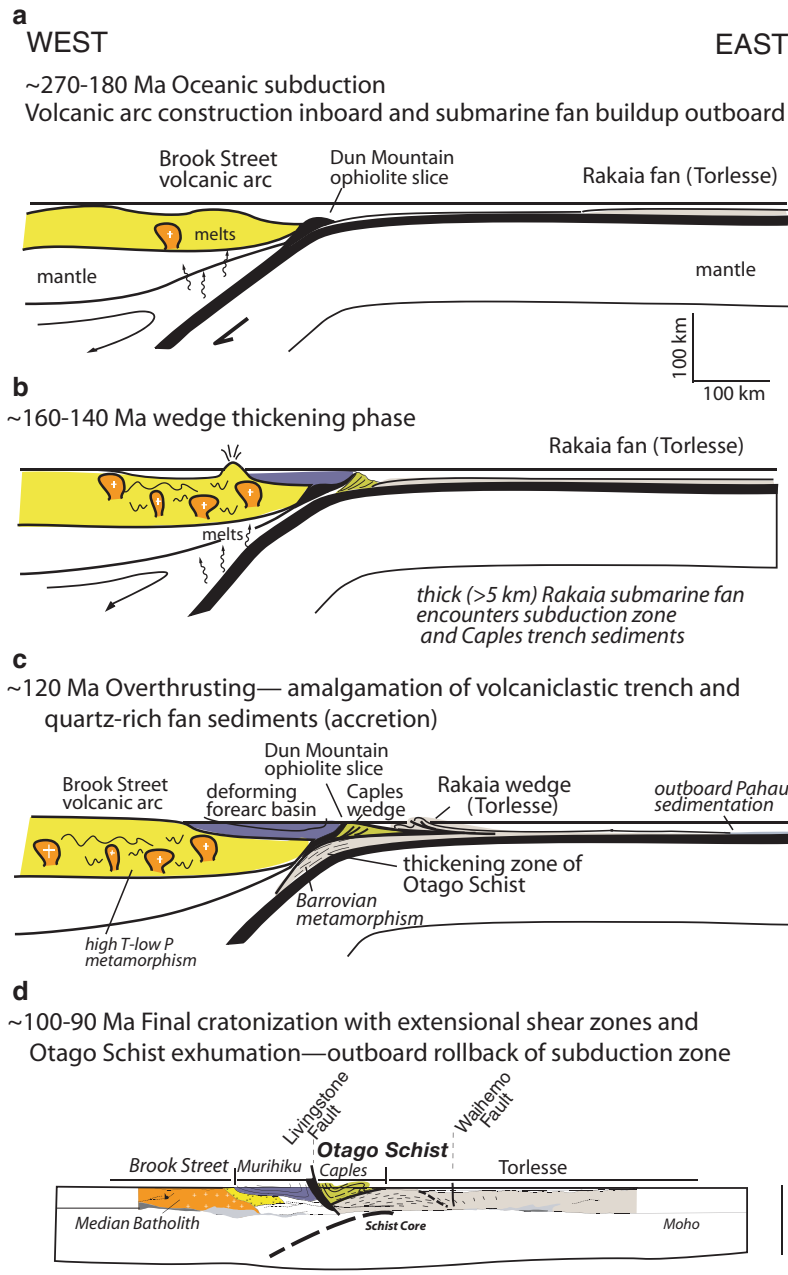

Fig. 10.8 Tectonic evolutionary diagrams illustrating the sequential stages in crustal growth for New Zealand. (Modified from Coombs et al. 1976 and Gray et al. 2007)

the Gondwana margin (Fig. 10.8) (Coombs et al. 1976; Bradshaw 1989; Roser and Cooper 1990). Structural thickening of the Torlesse turbidite fan began in the Late Jurassic (~150–140 Ma), with Early Cretaceous (130–120 Ma) interleaving of Caples and deformed Torlesse sediment and accretion of the turbidite fan to the margin (Bradshaw 1989; Mortimer 1993; Gray and Foster 2004c). This coincided with collision between the Median Tectonic Zone (Median Batholith) and the Gondwana margin, causing onset of adakitic magmatism at 125–118 Ma (Waight et al. 1998b; Kimbrough et al. 1994). Erosional exhumation and core complex development occurred between 110 and 90 Ma as a precursor to Tasman Sea opening (Ireland and Gibson 1998; Spell et al. 2000; Klepeis et al. 2003; Gray and Foster 2004c).

10.4 Gondwana Accretion and Collision: Recycled Turbidites and Crustal Growth in the Neoproterozoic-Cambrian Damara Orogen

The Neoproterozoic-Cambrian Damara Orogen is part of the Pan African orogenic system (e.g. Coward 1981, 1983). Within Namibia it consists of the Inland branch or Damara Belt, and Coastal branches comprising the Kaoko and Gariep Belts in the north and south, respectively (Fig. 10.9a) (Porada et al. 1983; Prave 1996). Metamorphosed turbidites make up a major component of the Damara Belt (Martin and Porada 1977; Hoffmann 1983; Martin 1983; Miller 1983a, b; Kukla et al. 1988; Prave 1996; Gray et al. 2007) and represent a Neoproterozoic submarine fan system and/or accretionary complex that formed in a Neoproterozoic ocean basin (Khomas Ocean) between the Congo and Kalahari cratons (Miller et al. 1983a; Kukla et al. 1988; Kukla and Stannistreet 1991). Detrital zircon U-Pb age distributions and Sm-Nd isotopic compositions of the tubidites indicate that they were sourced from Archean to Neoproterozoic orogenic and magmatic components of the Congo and Kalahari cratons (Foster et al. 2012b).

Structure Khomas oceanic lithosphere is preserved in the thin (200–300 m thick), but laterally extensive (>350 km length) Fig. 10.9b), shear zone-hosted, Matchless amphibolite (Barnes 1983; Killick 2000). This unit consists of intensely deformed basalt, pillow basalt, and gabbro with tholeiitic geochemistry (Schmidt and Weddepohl 1983), and intercalated with banded chert (Killick 2000). Further south, at the margin between the accreted turbidite fan sequences and passive margin sequences of the Kalahari Craton, widely separated serpentinite boudins within the Uis Pass Line shear zone, mark the suture (Barnes 1983). The flanks of the former ocean basin(s) are represented by two craton-verging thrust systems within shelf carbonates (e.g. Hakos and Naukluft nappes in the Southern Margin zone) (Korn and Martin 1959; Coward 1983; Miller 1983b). The Northern zone shelf sequence underwent metamorphism from *c*. 540 through 530 Ma (Goscombe et al. 2004). The deep water Khomas turbidite sequence is metamorphosed to form the Kuiseb schist and subdivided into two structural-metamorphic zones, referred to as the Central and Southern zones (Fig. 10.9b). The Central zone is underlain by attenuated Congo craton (Jacob et al. 1983; Coward 1983; Miller 1983b; Kröner 1984; Kisters et al. 2004), and underwent phases of high-T/low-P metamorphism and deformation (540–530 and 520–505 Ma) with voluminous granitic magmatism between 560 and 470 Ma (Jacob et al. 2000; De Kock et al. 2000; Jung and Metzger 2003a, b ; Gray et al. 2006a; Longridge et al. 2011; Schmitt et al. 2012).

The thicker, basinal sedimentary sequence experienced intermediate-T/intermediate-P (Barrovian) metamorphism and is now part of the ~100 km wide Southern zone (Kasch 1983a; Kukla 1993). This zone consists of homoclinally, N-dipping, Kuiseb schist with transposed foliation and schistosity (Hälbich 1977; Miller 1983b; Kukla et al. 1988; Kukla and Stanistreet 1991) that represents a major shear zone interface transitional into the basement-cored fold- and thrust-nappes of the Southern Margin zone (Fig. 10.9b) (Miller 1983b; Coward 1983). Based on U-Pb ages of metamorphic monazite, Kukla (1993) suggests an age of 525–515 Ma for peak metamorphism in the Kuiseb Schist. The western part of the Northern zone (Ugab domain)

Fig. 10.9 **a** Simplified map of southern Africa showing Pan African orogens and the location of the map shown in **b**. **b** Geologic map of the Damara Orogen, Namibia showing the key tectonic elements, the major structural zones, the distribution of plutonic rocks and Kuiseb schist (former Khomas Ocean turbidites) and the location of the profile A-D in **c**. (Map modified from geological map of Namibia). *NZ*, Northern zone; *CZ*, Central zone; *SZ*, Southern zone; *SMZ*, Southern Margin zone; *AF*, Autseib Fault; *OmSZ*, Omaruru shear zone; *OkSZ*, Okahandja shear zone. **c** Geological profile showing the crustal architecture of the Damara Belt (Inland Branch) of the Damara Orogen. (Modified from Gray et al. 2007 and references therein)

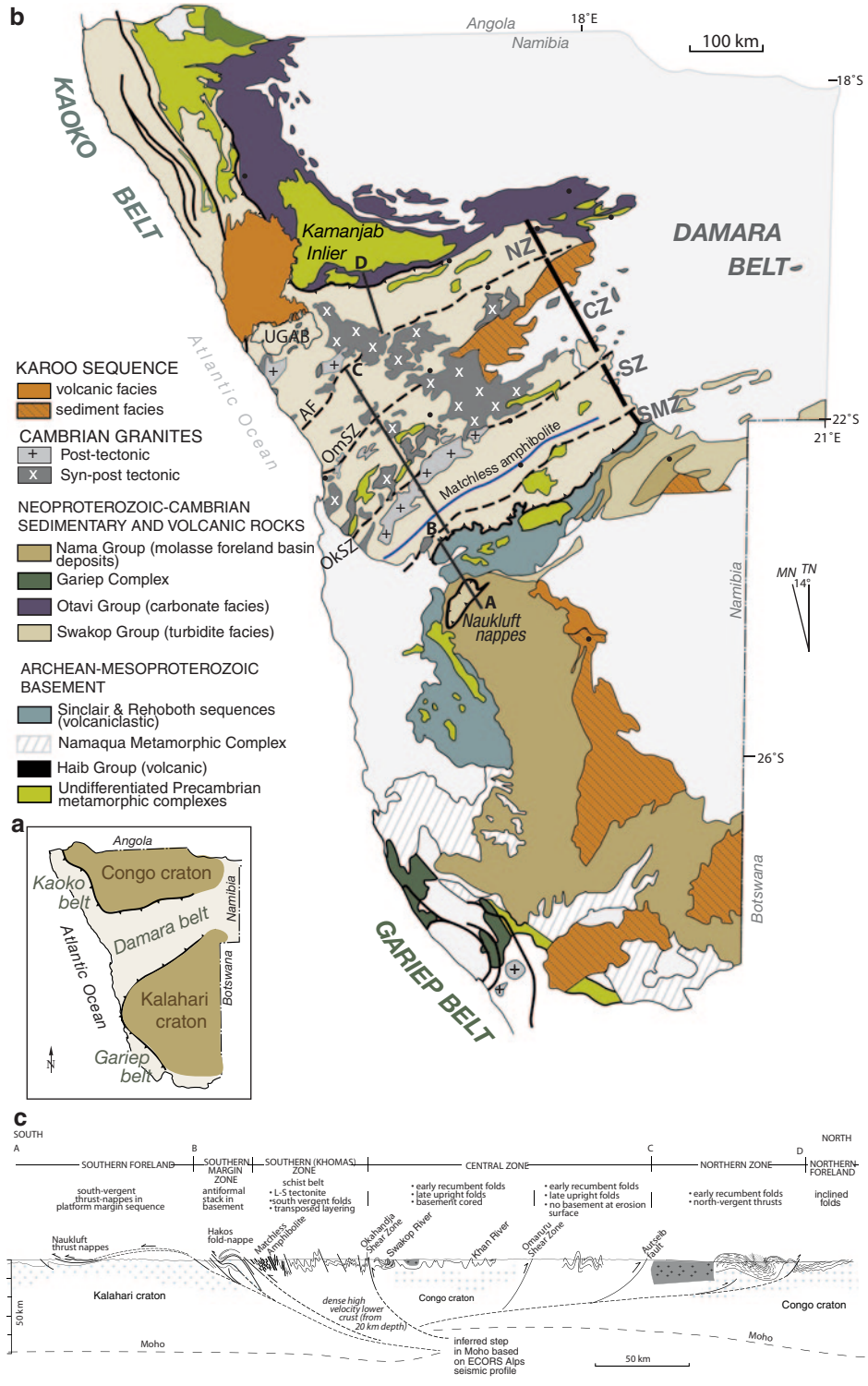
b
Angola
Namibia
18°E
100 km
18°S
22°S
21°E
26°S
KAOKO BELT
DAMARA BELT
Kamanjab Inlier
D
NZ
CZ
SZ
SMZ
UGAB
C
AF
OmSZ
OkSZ
Matchless amphibolite
B
A
Naukluft nappes
Atlantic Ocean
Namibia
Botswana
MN TN
14°
GARIEP BELT
KAROO SEQUENCE
volcanic facies
sediment facies
CAMBRIAN GRANITES
Post-tectonic
Syn-post tectonic
NEOPROTEROZOIC-CAMBRIAN SEDIMENTARY AND VOLCANIC ROCKS
Nama Group (molasse foreland basin deposits)
Gariep Complex
Otavi Group (carbonate facies)
Swakop Group (turbidite facies)
ARCHEAN-MESOPROTEROZOIC BASEMENT
Sinclair & Rehoboth sequences (volcaniclastic)
Namaqua Metamorphic Complex
Haib Group (volcanic)
Undifferentiated Precambrian metamorphic complexes
a
Angola
Congo craton
Kaoko belt
Damara belt
Namibia
Atlantic Ocean
Kalahari craton
Botswana
Gariep belt
c
SOUTH
NORTH
A
B
C
D
SOUTHERN FORELAND
SOUTHERN MARGIN ZONE
SOUTHERN (KHOMAS) ZONE
CENTRAL ZONE
NORTHERN ZONE
NORTHERN FORELAND
south-vergent thrust-nappes in platform margin sequence
antiformal stack in basement
schist belt
• L-S tectonite
•south vergent folds
• transposed layering
• early recumbent folds
• late upright folds
• basement cored
• early recumbent folds
• late upright folds
• no basement at erosion surface
• early recumbent folds
• north-vergent thrusts
inclined folds
Naukluft thrust nappes
Hakos fold-nappe
Matchless amphibolite
Okahandja Shear Zone
Swakop River
Khan River
Omaruru Shear Zone
Autseib fault
Kalahari craton
dense high velocity lower crust (from 20 km depth)
Congo craton
Congo craton
50 km
Moho
inferred step in Moho based on ECORS Alps seismic profile
Moho
50 km

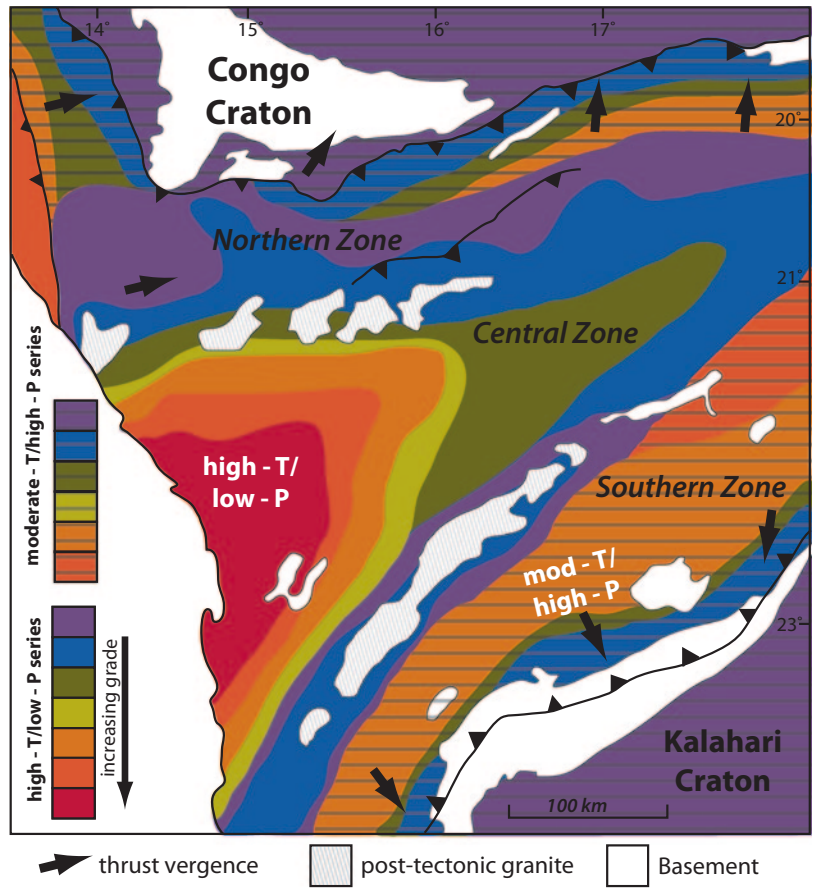

Fig. 10.10 Map of Cambrian metamorphism in the Damara Orogen compiled from sources listed in the text

occurs at the transition between basinal turbidite facies and slope-to-platform carbonates (Miller et al. 1983b; Swart 1992; Passchier et al. 2002), and is intruded by granites of the Central zone (Coward 1983; Maloof 2000; Passchier et al. 2002; Goscombe et al. 2004; Schmitt et al. 2012).

Metamorphism The Damara Belt exhibits elongated sections of intermediate-T/intermediate-P metamorphism and a low-P/high-T metamorphic core (Fig. 10.10). Central zone metamorphism occurred under an elevated geothermal gradient (30–50 °C/km) with clockwise P-T paths (Kasch 1983a; Jung 2000) and includes garnet-cordierite granulites (Puhan 1983; Masberg 2000). The Southern zone metamorphic conditions are moderate-P and T, with peak conditions of ~600 °C and ~10 kbar, but showing a decrease in pressure northwards to ~4 kbar near the Okahandja lineament (Kasch 1983a). The Southern zone has a low thermal gradient (18–22 °C/km), with syn-kinematic staurolite and syn- to post-kinematic garnet in metapelites defining a steep clockwise P-T path. The Northern zone shows high-P/moderate-T with a steep clockwise P-T path; peak conditions are estimated at 635 °C and 8–7 kbar and an average thermal gradient of 21 °C/km (Goscombe et al. 2004).

Magmatism Granitic rocks are a major component of the Damara orogen, comprising approximately 74,000 km^2, or roughly 25% of outcrop (Miller 1983a). Most of the granitic magmatism was concentrated in the Central zone, with minor activity in the Northern zone; the post-tectonic Donkerhuk batholith (5000 km^2) is the only significant granitic complex in the Southern zone. McDermott et al. (1996) divided the granitoids into 3 groups based on geochemical signatures. Group 1 comprises peraluminous leucogranites

and "Salem-type" granites (diverse porphyritic, biotite-rich granites) and minor alaskites (e.g. Rössing: Basson and Greenway 2004). Mildly peraluminous A-type granites with elevated high field strength element compositions (Nd-Zr-Y) compared to the other groups make up Group 2. Group 3 encompasses metaluminous, calcalkaline quartz diorites and granodiorites.

Group 1 granites (96% of the exposed plutons) show a wide range of initial Sr and Nd whole-rock isotope ratios ($^{87}Sr/^{86}Sr$ 0.708–0.740, εNd −2 to −19, Haack et al. 1982; McDermott et al. 1996; Jung et al. 2001, 2003), reflecting involvement of Archean-Mesoproterozoic basement (e.g. Jung et al., 2003). Many of the S-type granites give εNd values about −5, which are similar to Neoproterozoic (Swakop Group) turbidites (Fig. 10.11) (McDermott and Hawkesworth 1990; Jung et al. 2001; Newstead 2010). $\delta^{18}O$ values are typically 11–15‰, similar to both Damara metasediments and pre-Damara basement (Jung et al., 2000, 2003). The elemental and isotopic data for the S-type granites indicate crustal sources within the Damara metasediments and/or pre-Damara basement, with dehydration partial melting at mid-crustal levels (>6 kb).

Group 2 is dominated by A-type granites that are syn- to post-tectonic (525–486 Ma: Jung et al. 1998a, 2000; McDermott et al. 2000). Sr and Nd isotope signatures are less evolved than the S-types ($^{87}Sr/^{86}Sr$ 0.7034–0.709, εNd 0 to −6, as low as −16 for the Sorris Sorris A-type); δ18O is high (10–13‰). Generation of these hot (>800 °C) A-type magmas likely resulted from partial melting of a deep-seated (8–10 kb) tonalitic source, perhaps instigated by mantle-derived magmas, followed by extensive differentiation.

Group 3 includes I-type, metaluminous, hornblende (+/−clinopyroxene) diorite to granodiorite plutons that make up about 2% of the exposed granitoids. Isotopic signatures for this group vary widely ($^{87}Sr/^{86}Sr$ 0.704–0.713, εNd 0 to −20, $\delta^{18}O$ 7–13‰), suggesting a range of magma sources that assimilated crust (Haack et al. 1982; Hawkesworth et al. 1981; Miller 1983a; McDermott et al. 1996; Jung et al. 2002; van de Flierdt et al. 2003). Titanite and zircon U-Pb ages of 555–540 Ma indicate the I-type suite

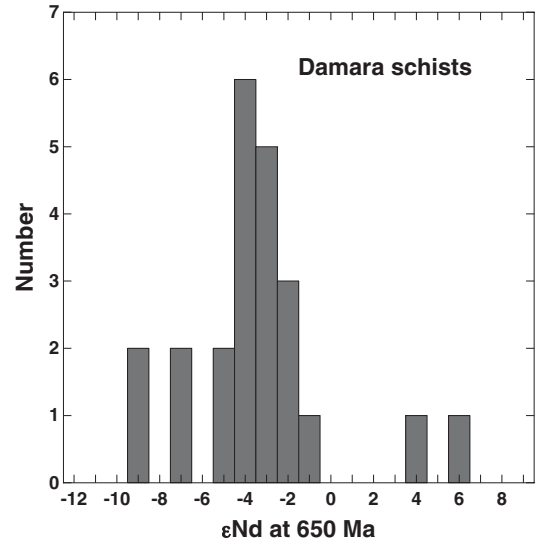

Fig. 10.11 Histogram of Nd isotopic data (at the time of deposition) from Neoproterozoic pelitic schists from the Damara Belt

comprises the oldest intrusive rocks within the Damara Orogen and were emplaced coeval with the onset of high-grade metamorphism (Jung and Mezger 2003a; Jung et al. 2009). A distinct suite of *c.* 540 Ma syenites (with a more limited range of Sr-Nd isotopic ratios, Jung et al. 1998b) was also emplaced at that time. The dioritic rocks with more primitive Sr-Nd-O isotope signatures (Hawkesworth et al. 1981) may have been derived from the mantle with limited crustal assimilation, or be partial melts of mafic lower crustal intrusions of early Pan-African age (Jung et al. 2009). Those with very low initial εNd and high Sr/Y ratios (Goas and Okongava in the Central Zone) may represent partial melts of Archean-Proterozoic mafic lower crust.

The thermal conditions of continent-continent collision, high heat production in Damara metasediments (Haack et al. 1983) and high fertility of the crust combined to produce massive mid/lower crustal melting in the Damara Orogen. The dominance of S-type granites and the absence of clearly mantle-like isotopic signatures indicate the importance of crustal recycling rather than juvenile additions during the Damara Orogeny (McDermott and Hawkesworth 1990; Jung et al. 2003). It is

possible, however, that the widespread magmatism and high-T metamorphism was ultimately the result of primitive magma emplaced at deeper crustal levels. Pervasive crustal melting would have established a density filter preventing further ascent of mafic magmas, and would greatly increase the chance of hybrid magmas forming in the crust. The small volume of I-type granitoids does not rule out greater mantle contributions at depth.

Additional evidence for the proportions of crustal recycling and growth from the depleted mantle in the Damara Orogen comes from the Lu-Hf isotopic composition of detrital zircons within the Neoproterozoic turbidites. Figure 10.12 is a plot of initial εHf against the U-Pb age of detrital zircons from metamorphosed Neoproterozoic turbidites. It is clear from the wide range of Hf isotopic values, and zircon U-Pb ages that extend back to the late Archean, that the turbidites represent a significant recycled component of the Precambrian cratons. The zircon grains with U-Pb ages of about 800–600 Ma are derived from magmatism that occurred during rifting and break-up of the Rodinia supercontinent along the Congo craton margin. The majority of the Neoproterozoic zircons give initial εHf values greater than zero and up to about +10. These data suggest that the majority of the Neoproterozoic magmatism was derived from the depleted mantle, and therefore, a fraction of the Damara turbidites were derived from material that was juvenile. Adding this component to the Gondwana continent during the Damara Orogeny represents new crustal growth within an orogeny that dominantly reworked older crust, and suggests that most of the crustal growth within this orogenic cycle occurred during the rifting phase and not during the accretion phase.

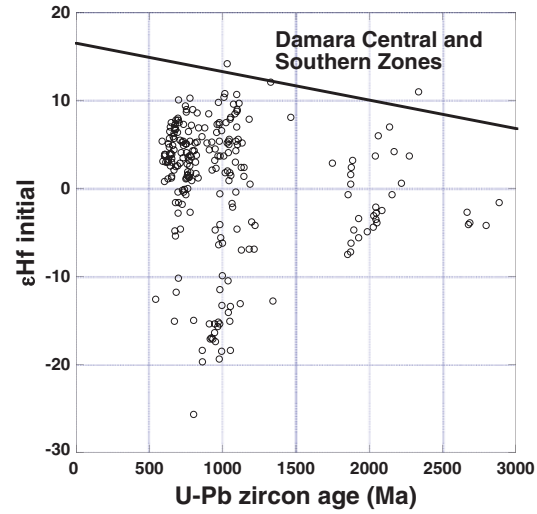

Fig. 10.12 Plot of U-Pb age against initial εHf values for detrital zircons from metamorphosed turbidites from the Damara Belt (data from Foster et al. 2012b)

Tectonic Evolution Rifting of the Congo and Kalahari cratons from parts of Rodinia occurred between 800 and 700 Ma (Miller 1983b; Gray et al. 2008). This produced rift-related rhyolites at about 750 Ma (Hoffman et al. 1996; de Kock et al. 2000) and other volcanic complexes along strike in the Zambezi Belt. Development of an oceanic spreading center and growth of Khomas oceanic crust occurred by about 700 Ma (Miller 1983b). There are conflicting hypotheses for closure of the Khomas Ocean and the nature of the substrate to the turbidites (e.g. Porada 1979, 1983; Martin 1983; Gray et al. 2008). The Khomas basin has either been interpreted as an intracontinental basin between the Congo and Kalahari cratons (Porada 1979, 1983; Martin and Porada 1977; Hawkesworth et al. 1983), or as an open ocean floored by oceanic lithosphere that closed by subduction beneath the Congo craton (Barnes and Sawyer 1980; Miller, 1983b; Kasch 1983b; de Kock 1992; Gray et al. 2008). Basement cored gneiss domes (Puhan 1983; Kröner 1984; Kisters et al. 2004) and isotopic signatures in the granitoids require the presence of attenuated Congo continental crust in the part of the Khomas Ocean basin that now comprises the Central zone, but the Southern zone almost certainly was underlain by oceanic crust. This combination of oceanic and attenuated continental lithosphere suggests a setting similar to the present Japan Sea, which has a complex distribution of attenuated continental crust, rifted crust and oceanic crust (Tamaki 1995).

Closure of the Khomas Ocean involved high-angle convergence with overthrusting at the margins to give a doubly vergent orogen (Fig. 10.13). The distinct metamorphic zonation of the Inland branch, with Barrovian metamorphism on the

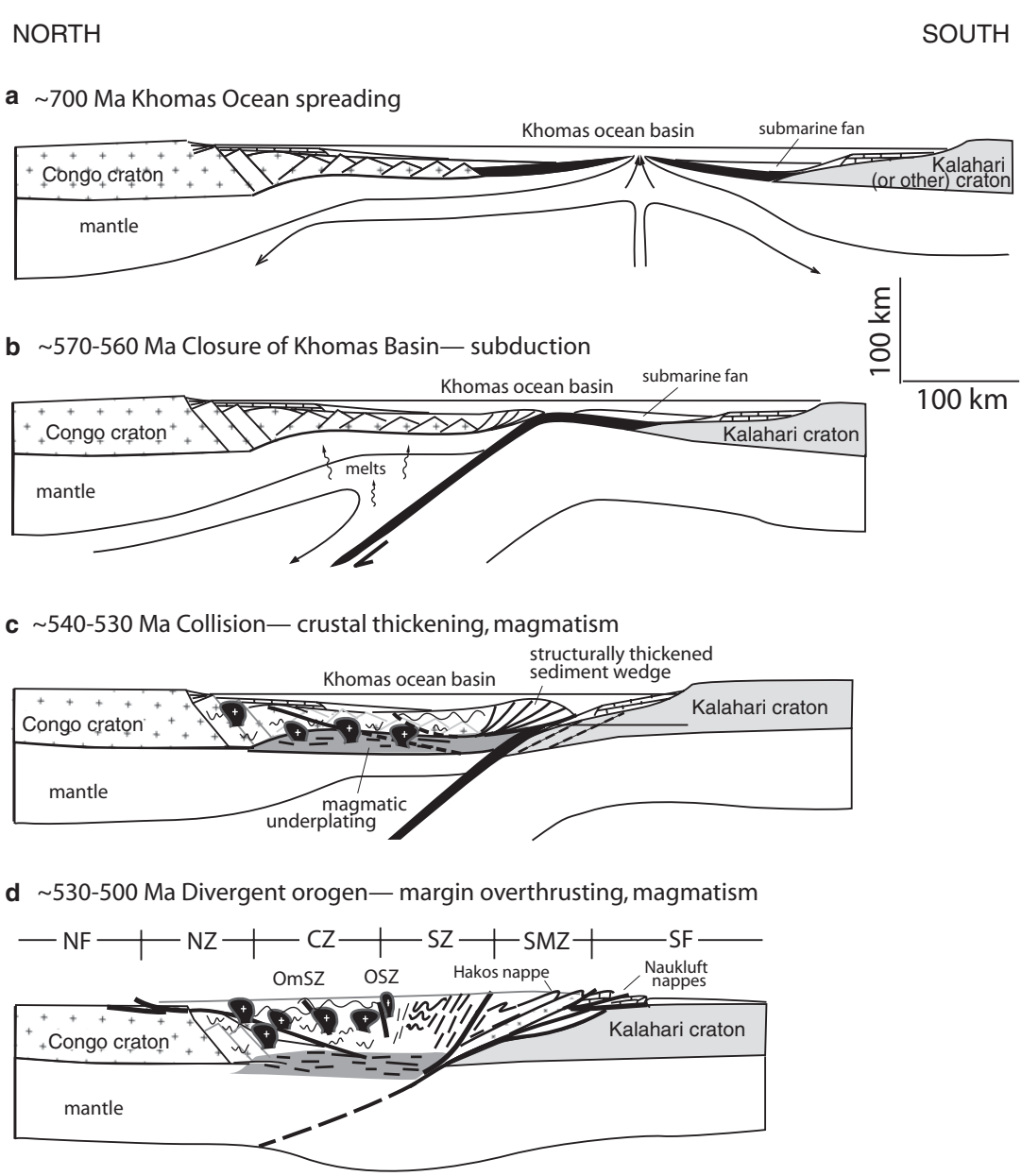

Fig. 10.13 Tectonic evolution diagrams for the Damara Belt of the Damara Orogen highlighting asymmetric rifting and eventual closure of the Khomas Ocean. (Modified from Barnes and Sawyer 1980)

orogen flanks, reflects structural thickening at the craton margins, while Andean- or Cordilleran-style high-T/low-P metamorphic conditions in the Central zone and accretionary prism-like features of the Southern zone Kuiseb schist (Kukla and Stanistreet 1991), and early calcalkaline magmatism reflect subduction beneath this zone (Maloof 2000; Kasch 1983a). The Matchless amphibolite belt is a thrust slice of oceanic crust incorporated within the accretionary wedge, immediately above (north) of the suture at the Uis Pass Line. Arguments against subduction related closure of the Khomas Ocean have been based on granite geochemistry (Hawkesworth et al. 1983), and the apparent lack of blueschists and eclogites (Kröner 1982); high-P metamorphic rocks, however, are exposed along

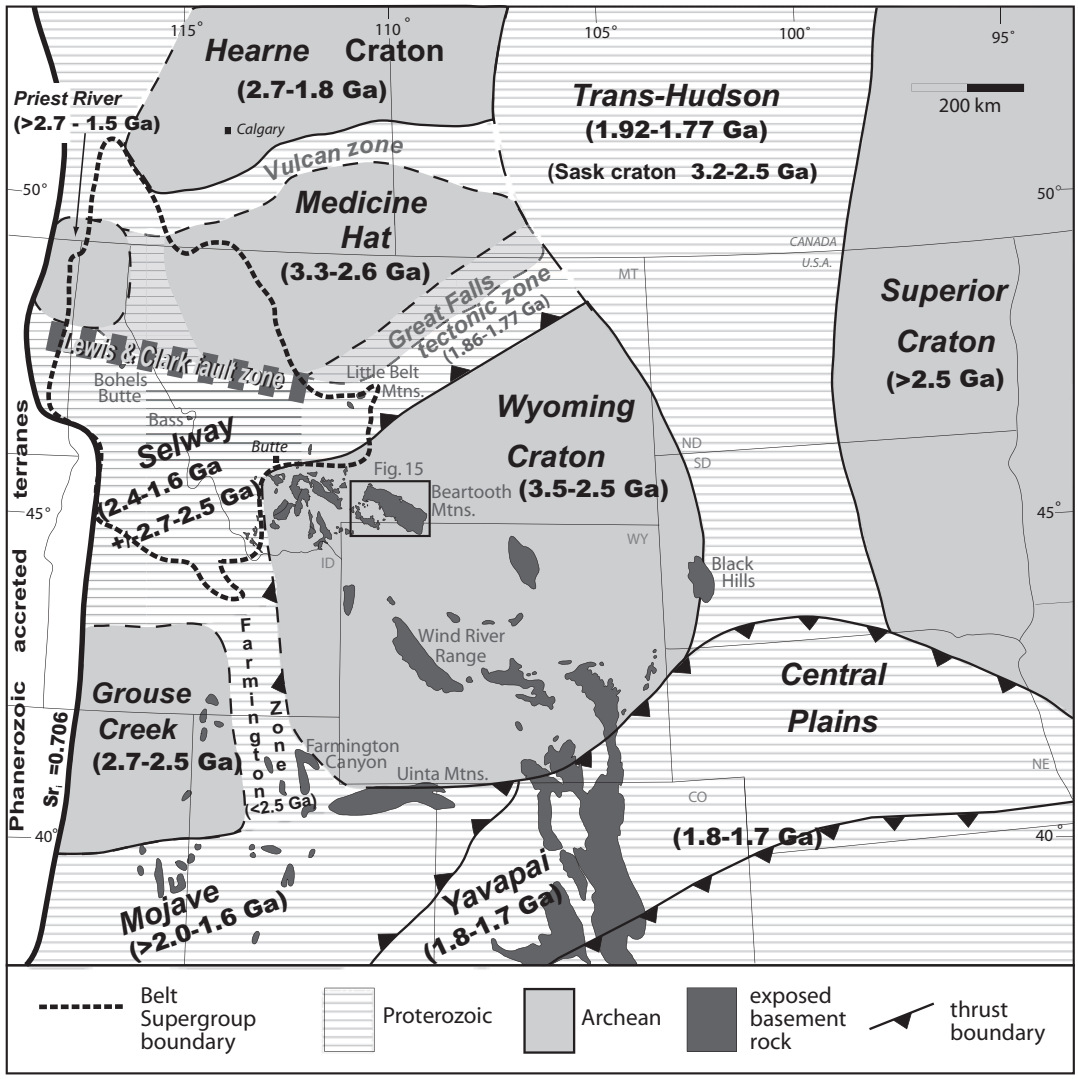

Fig. 10.14 Map of Precambrian cratons and orogenic belts of southwestern North America (southwestern Laurentia) (Modified from Foster et al. 2006). The box shows the area of the map in Fig. 10.15

strike of the suture zone within in the contiguous Zambezi belt (John and Schenk 2003; John et al. 2003; Johnson et al. 2004).

10.5 An Archean Example: The Jardine Turbdites

A series of Mesoarchean tubidites in the NW Wyoming Province of western North America (Fig. 10.14) provide an example for comparing the structural style, metamorphic history and magmatism affecting a turbidite succession that was accreted to a mature Archean continent during subduction at about 2.8 Ga. The Jardine metasedimentary sequence is exposed in the South Snowy block of the Beartooth-Bighorn magmatic zone of the Wyoming Province along the northern margin of Yellowstone National Park (Fig. 10.15) (Mogk et al. 2012; Mueller et al. 2013). This relatively small area in the Wyoming Province preserves most of the components of a turbidite-dominated accretionary margin orogen, which makes it useful for comparison to the

Phanerozoic orogenic belts. A comprehensive review of the NW Wyoming Province comprising the Beartooth Plateau block and the South Snowy block is given by Mueller et al. (2010, 2013), so that only a brief summary is included herein. The metaturbidites comprise a sequence of peltitic schists, quartizites, and banded iron formation (Casella et al. 1982; Mogk et al. 2012). In the least deformed areas the metaclastic rocks preserve primary sedimentary structures typical of middle-to-distal fan turbidites (e.g., graded beds, cross beds, and sole marks). The Jardine metasedimentary sequence was likely deposited as a sequence of turbidites on oceanic crust or thin continental crust along an active continental margin setting (Mogk et al. 2012). Major and trace element abundances, along with Pb- and Nd-isotopic data and detrital zircon age populations of the Jardine turbidites are consistent with derivation from an Archean continental source consisting of mafic to felsic composition igneous lithologies (Mueller et al. 2013). The sediment source was most likely the Wyoming Craton, but not the proximal area in the Beartooth Plateau block.

Metamorphism Metamorphic assemblages in the schists exposed in the western part of the South Snowy block range from chlorite-zone (greenschist facies) to staurolite-andalusite-garnet zone (lower amphibolite facies). Metamorphic grade increases from west to east toward the Beartooth Plateau block; thermobarometry indicates metamorphic temperatures of 572–609 °C and pressures of 3.4–5.9 kbar for the lower amphibolite facies rocks. Plutonic rocks bearing magmatic epidote suggesting pressures of ~8 kbar are juxtaposed against the lower pressure Jardine sequence in the east by the Yellowstone River shear zone. This ductile shear zone separates the Jardine schists of the western South Snowy block from the turbidite-bearing, but TTG-dominated, zone that hosts the Slough Creek batholith in the eastern South Snowy block. Kinematic indicators in the shear zone indicate that pre-accretion, ca. 3.2 Ga gneisses and the syn-accretionary Slough Creek batholith were thrust over the western part of the Jardine turbidites with a cumulative vertical throw of 10–15 km. In the footwall, the lower grade turbidites show progressive deformation characterized by bedding parallel fabrics overprinted by isoclinal folds, and then several generations of kink and upright chevron folds in domains separated by high-strain zones with intense crenulation cleavage.

Magmatism The metasedimentary rocks in the western South Snowy block were intruded by 10 km^2 scale, bulbous, peraluminous granitic plutons, which have U-Pb zircon ages of 2.80–2.81 Ga (Foster et al. 2011; Mogk et al. 2012; Mueller et al. 2013). These granitic rocks are associated with a suite of ca. 2.8 Ga dioritic and granodioritic sheets with TTG compositions that created injection migmatites in the upper amphibolite facies part of the Jardine assemblage. Plutonic rocks of the Slough Creek batholith in the eastern South Snowy block (Fig. 10.15) range in composition from diorite to granite with TTG affinities and comprise a composite plutonic suite of sheet-like intrusions with compositional variations on the 10–100 m scale; magmatic epidote in hornblende-bearing plutons indicates crystallization at ~8 kbar. Crystallization ages determined from U-Pb zircon geochronology are also ~2.8 Ga (Mueller et al. 2013). The ages of the oldest plutons and the youngest detrital zircons constrain the depositional age of the Jardine turbidites to between 2.81 and 2.9 Ga.

The South Snowy block intermediate-to-felsic igneous suites were emplaced within the same time-interval as the subduction-generated, Long Lake magmatic complex in the Beartooth Plateau block and have a range of major element compositions similar to those of the Long Lake suite (Mueller et al. 2010). The western South Snowy block stocks and the Slough Creek batholith in the eastern South Snowy block are, therefore, interpreted to be upper- and middle- crustal equivalents of the Long Lake magmatic complex intruded at about 12 km and 24 km depth, respectively. This connection is particularly strong in terms of whole-rock Pb isotopic compositions, which are one of the most diagnostic geochemical features of the Wyoming Province (Mueller and Frost 2006; Mueller et al. 2013).

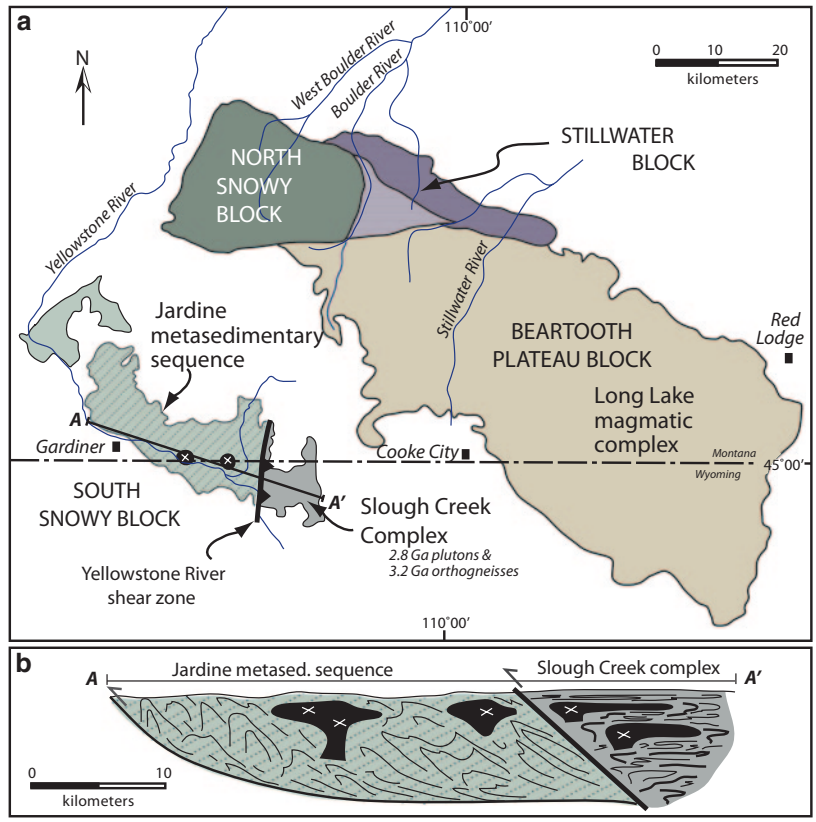

Fig. 10.15 **a** Map of the Beartooth Mountains in the NW part of the Wyoming craton showing the location of the Jardine metasedimentary series and related plutons of the South Snowy Block (see Mueller et al. 2013). **b** Cross section through the Mesoarchean structures of the South Snowy Block

Tectonic History The Jardine turbidites exhibit lithological and compositional similarities to sediments formed in active continental margin settings in contrast to the older passive-margin type (meta)sedimentary rocks preserved as pendants and enclaves in the Beartooth Plateau block (Henry et al. 1982; Wooden and Mueller 1988; Mueller and Wooden 2012). The Jardine turbidites appear to be exotic relative to their current location adjacent to the Beartooth massif. Regardless of their original location, the Jardine turbidites formed part of the upper crust of the NW Wyoming Province by 2.8 Ga. The structural style in the Jardine turbidites is very similar to turbidite dominated Phanerozoic accretionary orogens described above, as is the association with orogenic gold mineralization (Foster and Gray 2008). Another parallel is the timing of plutonism, although compositionally these Archean plutons are dominantly of the TTG association, and thereby similar to the Western Fiordlands orothogneiss. We, therefore, interpret the western South Snowy block assemblage to be a subduction-accretion complex composed of structurally thickened turbidite scraped off of subducting oceanic lithosphere and emplaced against the evolving continental magmatic arc of the northern Wyoming Province. The Yellowstone River shear zone appears to have developed at the juncture between the thick turbiditic sequence and older crust characteristic of crystalline basement within the Beartooth massif, that formed the forearc. This shear zone has some similarities to the backstop or retro-arc shear zones that are typically active during emplacement of turbiditic sequences against older crust in younger orogens, as in the Rakaia wedge example above. In this case, the backstop is the Paleoarchean lithosphere of the Beartooth block. After, and probably very soon after emplacement of the Jardine turbidites, the deformed and accreted Jardine turbidite wedge was intruded by TTG suite magmas, which in some cases assimilated enough sedimentary material to be considered peraluminous

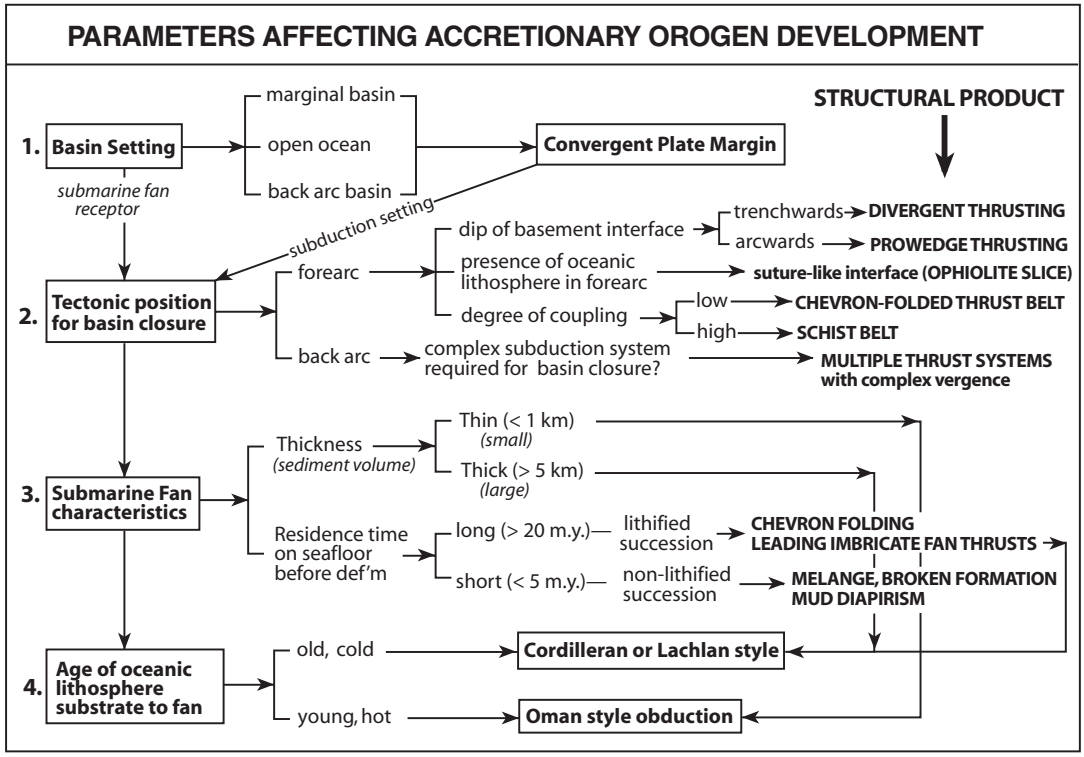

Fig. 10.16 Flow chart for examples of turbidite fan accretion and orogeny

(S-type) granites. It is also clear that parts of the section partially melted, perhaps as the slab rolled back, and continued to drive arc magmatism at 2.8 Ga. In this interpretation the 2.8 Ga plutons intruded into the Jardine schists were emplaced in a setting similar to the post-tectonic magmatism in the Lachlan Orogen.

10.6 Processes of Accretion in Turbidite-Dominated Orogens

Crustal accretion in the Rangitatan, Lachlan, and Damara Orogens involved deformation of submarine turbidite fans and the underlying oceanic basement resulting in marked shortening (>50%) and crustal thickening, but with minimal melting of the accreted oceanic lithosphere. Deformed turbidites now occur either as belts of thrust-imbricated, upright chevron-folded, low-grade turbidites, or zones of higher grade metasedimentary rocks that are characterized by homoclinally dipping schistosity and transposition layering. In these three Phanerozoic-Neoproterozoic examples turbidite deformation resulted from accretion of intra-oceanic plateau (Chatham Rise for the Rangitatan Orogen), convergent margin tectonism driven by closure of marginal basins (western Lachlan Orogen), and closure of an ocean basin by convergence between cratonic nuclei (Damara Orogen). The accreted turbidite fans are a common feature, but each orogen has a unique style or crustal architecture tied to the specific tectonic setting and the position of the turbidites with respect to plate-scale tectonic elements. The Rangitatan, Lachlan, and Damara Orogens show that parameters such as the thickness, structural style, metamorphic history, and tectonic position of the former submarine fan, as well as the age and nature of the underlying substrate, are all important variables for interpreting crustal evolution (Fig. 10.16). All orogens, however, share the critical aspect of proximity to large continental landmasses with active uplift and

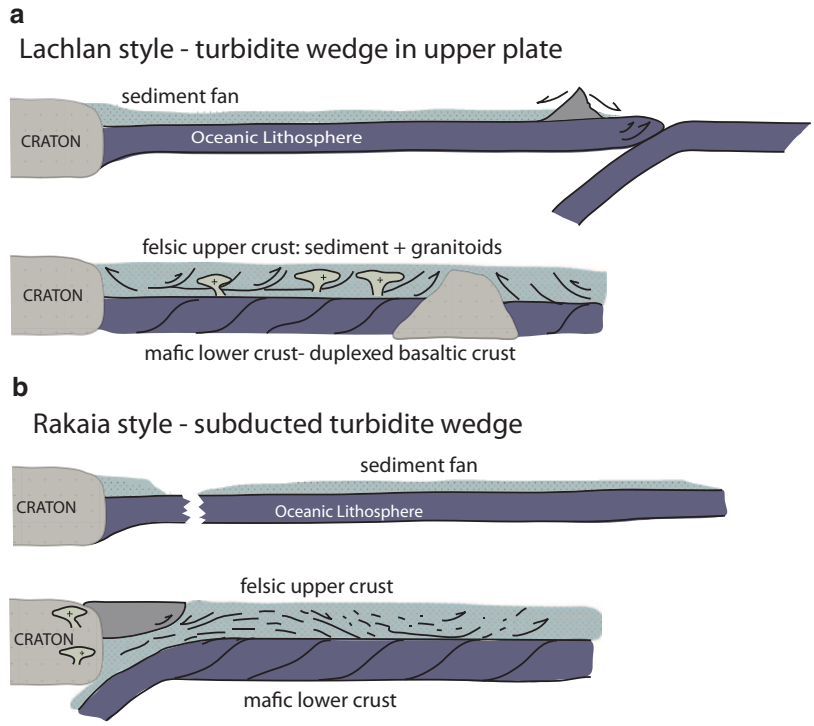

Fig. 10.17 Simple cross sections showing two end-members of continental crust formation from deformed turbidite fans on oceanic crust. The Lachlan-style **a** starts as a thick turbidite fan deposited on mafic back-arc-basin crust. When the marginal basin closes, imbricated basaltic crust forms most of the lower crust and deformed sediments and felsic syn- to post-tectonic plutons form the upper crust. The Rakaia-style, **b** starts with a large sediment fan deposited on oceanic crust or an ocean plateau. A layered crust of continental thickness is formed when the turbidite fan is shortened and metamorphosed as it enters a subduction zone. The lower crust is composed of thickened mafic crust

relatively rapid erosion that supply detritus to the large turbidite fans that characterize these orogens and others like them (see Ingersoll et al. (2003) for other examples).

10.6.1 Settings of Turbidites in Ancient Orogens

In most orogens, tectonic reconstructions are based on recognition and interpretations of key geologic or tectonic elements, as well as the structural architecture and tectonic vergence defined by fault/shear zone dips, the distribution of rock types, and the temporal and spatial distributions of metamorphism and magmatism (e.g. Gray and Foster 2004a, b for the Lachlan Orogen; Mortimer 2004, for the Rakaia Wedge). The thickness of the turbidite successions and the degree of shortening (> 50 %) and thickening (up to 300 %) support an oceanic depositional setting (Fig. 10.17).

The Lachlan Orogen has extensive turbidites, extending over the 750 km width, thrust systems of mixed vergence, and a central high-T/low-P metamorphic complex. How this belt evolved and in what setting has been debated, but there are certain characteristics of the Lachlan Orogen that are important for any tectonic reconstruction (Gray and Foster 2004b). These include: (1) Three simultaneously operating oceanic thrust systems in different parts of a marginal ocean basin that was behind a long-lived, outboard subduction system along the eastern margin of Gondwana. (2) Blueschist blocks in serpentinite-matrix mélanges along major faults in the western and central Lachlan. (3) Mélange and broken formations along faults within the frontal fault system of the central Lachlan (the Howqua accretionary complex). (4) Discordant post-tectonic granitoids in the western Lachlan and large elongate composite granitoid bodies in the central Lachlan (northwest-trending) and eastern Lachlan (north-trending). (5) Shear zone bounded high-T/low-P metamorphic complexes with regional aureole-style metamorphism related to significant high-level S-type granites. These features are consistent with accretion in

the Lachlan Orogen resulting from thickening and imbrication of thick submarine fans and the underlying oceanic lithosphere, in a "Woodlark basin style" double divergent convergent system (Gray et al. 1997; Soesoo et al. 1997; Foster and Gray 2000).

The Lachlan turbidite fans developed on back-arc-basin lithosphere (Foster et al. 2005; 2009) analogous to the Phillippine Sea or Japan Sea (Gray and Foster 2004b). Each of these two modern analogues contains different tectonic elements within the basin that would influence deformational styles when they close in the future, including: microcontinental ribbons (e.g. Tasmania: Cayley et al. 2002; Moore et al. 2013) in the former, and relict arcs (e.g. the Cambrian Licola arc, Spaggiari et al. 2003a, b; and the Ordovician Macquari arc, Glen et al., 2007) in the latter. The ribbon continents and arcs provide significant rigidity contrasts to the basaltic back-arc basing crust during crustal shortening and thickening, which may explain the three different accretionary thrust belts in the Lachlan.

For the Damara Orogen the accretionary prism-like nature of the Southern zone schists (Kukla and Stanistreet 1991; Gray et al. 2006a) as well as their strong similarities to those of the Otago Schist belt in New Zealand (Gray and Foster 2004c) suggest that this orogen is another example of continental growth by subduction-accretion of turbidites. Damara Orogen evolution, however, involves a full Wilson cycle with closing of a ocean basin at least partly floored by attenuated continental crust of the Congo craton and partly underlain by Neoproterozoic lithosphere of the Khomas Ocean.

The Rangitatan Orogen of New Zealand provides the least complicated setting. Representing part of the Mesozoic convergent margin of Gondwana facing a large ocean basin (cf. Busby 2004), the Rangitatan Orogen evolved in a forearc position typical of the modern day Aleutian arc-subduction complex with a turbidite fan accreted via underthrusting (Fuis and Plafker 1991; Finzel et al. 2011). In contrast, the Lachlan Orogen involves closure of a back-arc basin via multiple subduction systems (e.g. Spaggiairi et al. 2004a), while the Damara Belt involves a single subduction system with terminal continent-continent collision (Barnes and Sawyer 1980; Gray et al. 2006a).

10.6.2 Parameters Affecting Accretionary Orogen Development: Sediment Fan Thickness and Timing

Other parameters that affect accretionary orogen development include the thickness of the turbidite fan, the relative depositional age of the fan, the timing of fan shortening and thickening, and the age of the oceanic lithosphere relative to basin closure (Fig. 10.16).

For the Lachlan Orogen, the age of back-arc basin crust is 505–495 Ma (Spaggiari et al. 2003a; Foster et al. 2005, 2009), most of the submarine fan system developed between 490 and 460 Ma (Fergusson and Coney 1992a), and the deformation that caused the back arc basin closure occurred from ~450 to 410 Ma (i.e., some 50 m.y. after oceanic lithosphere formation and some 30–20 m.y. after submarine fan deposition). These conditions favor chevron folding, without the significant stratal disruption and mélange or broken formation typical of shallow levels of modern accretionary complexes (Festa et al. 2012). Folding requires lithification or precompaction of the sediment fan and, therefore, time for burial and dewatering on the seafloor before deformation. Metamorphism due to sediment loading occurs in modern submarine fans including the Bengal Fan (Curray et al. 1982), and leads to closed system quartz vein formation during shortening, as has been documented in the Lachlan Orogen example (Gray et al. 1991).

During accretion parts of oceanic lithosphere are incorporated into the accretionary thrust wedge and preserved as fault-bounded slices (Kimura and Ludden 1995), with the Matchless amphibolite belt in the Damara Orogen providing an excellent example. The temperature, and therefore, age of the oceanic lithosphere is important. The western Lachlan Orogen shows that thick, lithified or partially lithified turbidite fans (4–5 km thicknesses) sitting on old, cold oceanic

lithosphere produce dominantly chevron-folded, thrust-interleaved packages that incorporate fault-bounded, duplexed slivers of the upper parts of the basaltic back-arc basin oceanic lithosphere. This process is inferred to occur by low-angle underthrusting with the turbidites predominantly deforming in the overriding plate (Gray and Foster 1998; Spaggiari et al. 2004a).

In the case of the Rakaia wedge of New Zealand, the age of the underlying oceanic lithosphere as inferred from the Dun Mountain ophiolite is ~280 Ma (Kimbrough et al. 1992) with Permian to Triassic submarine fan sedimentation (~280 through 200 Ma: Bradshaw 1989), and eventual wedge thickening at 160–150 Ma (Gray and Foster 2004c) (i.e., some 120 m.y after oceanic lithosphere formation and some 40 m.y. after fan deposition).

In this respect, plate convergence for significant parts of the Lachlan and the Rakaia wedge of New Zealand involves cold oceanic lithosphere and thick turbidite fans (4–5 km thicknesses), with the deformation of the turbidites in the Rakaia wedge occurring on the down-going slab (Coombs et al. 1976). Deformation and metamorphism of the Kuiseb schist of the Damara belt also occurred on the down-going slab (Barnes and Sawyer 1980, Gray et al. 2007).

Both the Rangitatan (Otago Schist) and Damara Orogens (Kuiseb Schist) show evidence for coupling between the overriding margin and the subducting slab, with the thick turbidite fan sitting on the subducting plate, producing an intensely deformed, highly thickened wedge that underwent Barrovian metamorphism. In both the Rakaia wedge and Southern zone of the Damara, the wedge underwent significant structural thickening by shear-related, non-coaxial deformation at the subduction interface (Mortimer 1993; Gray and Foster 2004b) to produce transpositional layering or schistosity and a pronounced rodding lineation (i.e., S-L tectonites). These are the dominant fabrics produced in this subduction interface environment that have been attributed to underplating in a coaxial flattening strain environment (Lundberg and Reed 1991; Von Huene and Scholl 1991).

In both of these cases, arc magmatism occurs in the overriding plate, but not in the intensely coupled zones. In New Zealand, magmatism occurred on the Gondwana margin side of the Dun Mountain ophiolite and not in the thickened wedge (Fig. 10.7c), most likely because the underlying crust is thin and deformation occurred directly above the subducted slab rather than over the asthenospheric wedge. In the Damara Belt, the composition of the Matchless amphibolite and the chert, pillow basalt, and gabbro association is suggestive of the upper parts of oceanic crust (Killick 2000) tectonically emplaced within the thrust wedge. Most magmatism occurred in the Central zone and where partial melting occurred within the over thickened Precambrian continental basement. Early dioritic intrusions in the Damara may have been partly subduction generated. Their intrusion probably instigated some anatexis of the turbidite and hybridization of magmas. In the Lachlan subduction generated magmatism caused anatexis of turbidites in the Central part of the orogen. Only in the Rakaia wedge were the turbidites not partially melted during subduction and/or tectonic shorting to any significant degree.

10.6.3 The Template of Accretion

The Rangitatan Lachlan, and Damara orogens provide a disconnected history of the tectonic process of turbidite accretion through time from the Mesozoic to the Neoproterozoic, and show that there is no uniform template for the accretionary process that adds these density and compositionally stratified sections to the continent. This is reflected in the crustal architecture of each orogen, as well as the temporal and spatial variations in the development of deformation fabrics, metamorphism, and magmatism. The Lachlan Orogen is composed of three thrust belts with contrasting vergence, whereas the Damara Orogen shows divergent thrust systems, and the Rangitatan Orogen one thrust system and a steeply dipping backstop behind the sediment wedge. For the Jardine sequence and Rakaia wedge, it is clear that turbidite-based accretion even occurs

in scenarios in which the accreted turbiditic sequence is allocthonous to the location of final subduction.

Within the orogenic architecture, the spatial variations in types of metamorphism delineate the tectonic setting. To a first order approximation, the low-T/high-P metamorphic rocks (blueschists and eclogites) define the subduction channel, the moderate-T/moderate-high-P (Barrovian style) metamorphic rocks define the regions of structural thickening above the subduction interface, and the high-T/low-P regional aureole metamorphic rocks intruded by large, elongate composite granitoids define the roots of the magmatic arc.

The Rakaia wedge has relict blueschist metamorphism preserved in intercalated metabasites near the interface between the volcaniclastic trench sediment and the accreted, deformed quartz-rich fan (Yardley 1982), whereas the wedge proper shows Barrovian metamorphism with garnet-oligoclase assemblages in the core of the Otago schist (Mortimer 2000). Similarly, the schistose part of the Damara Orogen shows intermediate-T/intermediate-P (Barrovian-style) metamorphism (Kasch 1983b). The schistose belt dips towards, but verges away from the Central zone belt of large, irregularly shaped, syn-tectonic granitoids and the region of high-T metamorphism (Puhan 1983).

The Lachlan Orogen shows regional low-grade, intermediate-P metamorphism (Gray and Foster 2004b), but has two belts of high-T/low-P metamorphism associated with large, elongate, composite batholiths (Richards and Collins 2002). In the western and central Lachlan blueschist metamorphism is preserved in fault-bounded lenses-shaped block within the serpentinite-matrix mélange of the major faults zones (Spaggiari et al. 2002a, b).

Turbidite-dominated orogens, therefore, develop in convergent margin settings involving subduction of oceanic crust containing large submarine turbidite fans, but have no specific template or orogen design. They have special character reflected by the large volumes of structurally thickened and metamorphosed turbidites, relicts of oceanic crust as fault-bounded slivers, and mafic lower crust consisting of imbricated oceanic crust.

10.7 Implications and Conclusions

10.7.1 Crustal Growth/Recycling

The three Phanerozoic examples, therefore, provide insight into the possible range of processes involved in basin shortening and turbidite fan thickening: Rangitaton—subduction underthrusting, Lachlan—accretionary wedge thickening, and Damara—wedge thrusting and continental collision. All three represent different relative contributions of crustal growth and crustal recycling. The marked shortening and thickening of the crust and the involvement of predominantly oceanic basement are key factors in recognizing ancient subduction-accretion processes in such orogens. The presence of the lower crustal layer of imbricated oceanic crust coupled with the overlying thickened sedimentary succession yields a density structure that is remarkably stable, isostatically balanced near sealevel (O'Halloran and Rey 1999), and hard to identify. Crustal growth is dominated by the mafic lower crustal component, which was originally the depositional substrate of the turbidites (Fig. 10.17). Most of the material in the turbiditic sediment successions was recycled from adjacent continents and arcs. Felsic and mafic magmatism contributes to both crustal growth and chemical maturation of the crust, both new and pre-existing, by recycling and mixing oceanic and continental crust to different degrees. Synorogenic magmatism in the Lachlan added variable amounts of new crust from the mantle with greater amounts in the A- and I- granitoids based on Lu-Hf and O isotopic data from magmatic zircons and whole rock samples (Kemp et al. 2009). The Median batholith in New Zealand comprises significant new crust either directly from subduction-generated partial melting in an Andean setting, or later by remobilization of the young lower arc crust and formation of adakites (Klepeis et al. 2003). In the Damara, granitic magmatism largely regenerated the crustal stack most likely because the

lower crust in part of the Orogen was the thinned edge of the Congo craton. Some of the early dioritic magmatism may have a primitive component, either because it was derived from the mantle or by partial melting of Neoproterozoic mafic lower crust (Jong et al. 2009). It is not possible to estimate how much new crust was accreted to the Wyoming Province along with the Jardine metaturbidites, because the basement is not exposed, and only a relatively small area is preserved. Syn-orogenic plutons were emplaced after accretion of the turbidite, which are a mixture between juvenile and recycled crust (sediment assimilation) along with lower crustal melts (Mueller et al. 2013). These were, however, part of a much larger Andean-style batholith (Long Lake magmatic complex) that did constitute significant crustal growth (Mueller et al. 2010).

Granitic magmatism plays an important role in the differentiation of structurally thickened and accreted turbidite fan systems. Turbidite-dominated orogens tend to be characterized by large volumes of syn- to post-tectonic granite, such as those in all zones of the Lachlan Orogen, and in the Central zone of the Damara Orogen. Turbidites, in particular the more feldspathic (greywacke) and pelitic lithologies, represent fertile sources for crustal melting (Clemens and Vielzeuf 1987; Thompson 1996). There is clear isotopic evidence in both the Lachlan and Damara orogens, for derivation of most of the S-type granites from partial melting of the meta-turbidites or sediment contamination of the I-types. Additional source components are sometimes required to explain the chemical/isotopic constraints, e.g., contributions from underlying Cambrian oceanic crust and syn-magmatic mantle-derived melts (Lachlan Orogen, Keay et al. 1997; Maas et al. 2001), or Precambrian crystalline basement (Damara granitoids, Jung et al. 2003).

It is important to recognize the somewhat unique signature of this style of crustal growth and accretion in the long term geological and isotopic record, particularly that estimated from detrital zircons, which are one of the most utilized records of crustal growth through time (e.g., Condie et al. 2011; Voice et al. 2011). The mafic oceanic basement that makes up the lower crust represents a major fraction of the continental crustal growth in turbidite-dominated orogens, much of which is never remobilized or directly exposed at the surface. In addition, this crust is not zircon bearing by nature and will not be represented in the global detrital zircon U-Pb age record because of the mafic composition and the relatively high density; emplacement in the lower crust means little will be exhumed and eroded. Older Lu-Hf isotopic model ages in younger zircons will reflect the presence of extensive mafic lower crust, but only if partially melted hundreds of millions of years later without mixing with juvenile or continental components (e.g., Kemp et al. 2006; Belousova et al. 2010; Iizuka et al. 2012; Condie et al. 2011; Foster et al. 2012a). Partial melting of the oceanic lower crustal layer some tens of millions of years later will likely not be revealed by detrital zircon Hf isotopic composition because these data will be similar to the signature of juvenile crust. It would appear, rather, that the crustal growth occurred by arc or extensional TTG-like magmatism, when it is actually accretion of the upper part of an ocean or back-arc basin. A similar point could be made for mafic crustal underplates, lower crustal mafic sills, and accreted oceanic plateaus.

10.7.2 Precambrian Comparisons

Perspectives gained by comparing the three Phanerozoic turbidite orogens may be applied to Archean and Proterozoic belts as templates for helping decipher ancient tectonic settings and geodynamics. Belts like the Mesoarchean Jardine metasedimentary sequence and Proterozoic Colorado-Yavapai provinces of Laurentia (e.g. Karlstrom and Bowring 1988) share some comparable styles of deformation, metamorphism, magmatism, and evolution. The microcosm of features in the Jardine metaturbidites appears to closely resemble the evolution of the western Lachlan or Rangatitatan Orogens in that is was likely deposited adjacent to an older continent on

oceanic crust, metamorphosed to lower greenschist facies and deformed by upright chevron folds akin to the western Lachlan. Accretion occurred during subduction which generated a major continental margin magmatic arc; plutons of which eventually intruded and metamorphosed the Jardine schists, but were concentrated in the adjacent Long-Lake and Slough Creek batholiths (see Mueller et al. 2013).

Acknowledgements The research was supported by a variety of Australian Research Council and National Science Foundation Grants (EAR0073638, EAR-0440188, EAR0738874, and EAR0851752). Discussions with Chris Fergusson, Vince Morand, Clive Willman, John Miller, Chris Wilson, Bob Gregory, Roland Maas, Nick Mortimer, Cees Passchier, Rudolph Trouw, Thomas Becker, Charlie Hoffmann, David Mogk, and Darrell Henry have helped shape our understanding of these areas.

References

Adams CJ, Kelly S (1998) Provenance of Permian-Triassic and Ordovician metagraywacke terranes in New Zealand: evidence from $^{40}Ar/^{39}Ar$ dating of detrital micas. Geol Soc Am Bull 110:422–432

Adams CJ, Barley ME, Fletcher IR, Pickard AL (1998) Evidence from U-Pb zircon and $^{40}Ar/^{39}Ar$ muscovite detrital mineral ages in metasandstones for movement of the Torlesse suspect terrane around the eastern margin of Gondwanaland. Terra Nova 10:183–189

Adams CJ, Cambell HJ, Griffin WL (2007) Provenance comparisons of Permian to Jurassic tectostratigraphic terranes in New Zealand: perspectives from detrital zircon age patterns. Geol Mag 144:701–729

Adams CJ, Pankhurst RJ, Maas R, Millar IL (2005) Nd and Sr isotopic signatures of metasedimentary terranes around the South Pacific margin, and implications for their provenance. In Vaughan APM, Leat PT, Pankhurst RJ (eds) Terrane Processes at the Margins of Gondwana. Geological Society of London (Special Publication, 246), London, pp 113–142

Albarède F (1998) The growth of continental crust. Tectonophys 296:1–14

Armstrong RL (1981) The persistent myth of crustal growth. Aust J Earth Sci 38:613–630

Barnes S (1983) Pan-African serpentinites in central south west Africa/Namibia and the chemical classification of serpentinites. In Miller RG (ed) Evolution of the Damara Orogen of South West Africa/Namibia, Geological Society of South Africa Special Publication 11, pp 147–155

Barnes S, Sawyer E (1980) An alternative model for the Damara mobile belt: ocean crust subduction and continental convergence. Precam Res 13:297–336

Basson IJ, Greenway G (2004) The Rössing uranium deposit: a product of late-kinematic localization of uriniferous granites in the Central Zone of the Damara Orogen: Namibia. J Afr Earth Sci 38:413–435

Belousova EA, Kostitsyn YA, Griffin WL, et al (2010) The growth of the continental crust: constraints from zircon Hf-isotopic data. Lithos 119:457–466

Bickford ME, Hill BM (2007) Does the arc accretion model adequately explain the Paleoproterozoic evolution of southern Laurentia?: an expanded interpretation. Geology 35:167–170

Bierlein FP, Arne DC, Keay SM, McNaughton NJ (2001a) Timing relationships between felsic magmatism and mineralisation in the central Victorian gold province, southeast Australia. Aust J Earth Sci 48:883–899

Bierlein FP, Hughes M, Dunphy J, McKnight S, Reynolds P, Waldron H (2001b) Tectonic and economic implications of trace element, 40Ar/39Ar and Sm-Nd data from mafic dykes associated with orogenic gold mineralisation in central Victoria, Australia. Lithos 18:1–31

Bierlein FP, Foster DA, Gray DR, Davidson GJ (2005b) Timing of orogenic gold mineralization in northeast Tasmania – implications for the tectonic and metallogenic evolution of Palaeozoic SE Australia. Min Dep 39:0–903

Bradshaw JD (1989) Cretaceous geotectonic patterns in the New Zealand region. Tectonics 8:803–820

Bradshaw JD (1993) A review of the Median Tectonic Zone: terrane boundaries and terrane amalgamation near the Median Tectonic Line. New Zeal J Geol Geop 36:117–125

Busby C (2004) Continental growth at convergent margins facing large ocean basins: a case study from Mesozoic convergent-margin basins of Baja California, Mexico. Tectonophysics 392:241–277

Casella CJ, Levay J, Eble E, Hirst B, et al (1982) Precambrian Geology of the southwestern Beartooth Mountains, Yellowstone national Park, Montana and Wyoming. In Mueller PA, Wooden JL (eds) Precambrian Geology of the Beartooth Mountains, Montana and Wyoming. Montana Bureau of Mines and Geology (Special Publications, 84), Montana, pp 1–24

Cawood PA (1987) Stratigraphic and structural relations of strata enclosing the Dun Mountain ophiolite belt in the Arthurton-Clinton region, Southland. NZJ Geol Geophys 30:19–36

Cawood PA (2005) Stratigraphic and structural relations of strata enclosing the Dun Mountain ophiolite belt in the Arthurton-Clinton region, Southland, New Zealand. New Zea J Geol Geop 30:19–36

Cawood PA (2005) Terra Australis Orogen: Rodinia breakup and development of the Pacific and Iapetus margins of Gondwana during the Neoproterozoic and Paleozoic. Earth Sci Rev 69:249–279

Cayley RA, Taylor DH, VandenBerg AHM, Moore DH (2002) Proterozoic—early Palaeozoic rocks and the Tyennan Orogeny in central Victoria: the Selwyn block and its tectonic implications. Aust J Earth Sci 49:225–254

Chappell BW, White AJR (1992) I- and S-type granites in the Lachlan Fold Belt. T Roy Soc Edin 83:1–26
Chappell BW, White AJR (2001) Two contrasting granite types: 25 years later. Aust J Earth Sci 48:489–499
Chappell BW, White AJR, Hine R (1988) Granite provinces and basement terranes in the Lachlan Fold Belt, southeastern Australia. Aust J Earth Sci 35:505–521
Chen YD, Williams IS (1991) Zircon inheritance in mafic inclusions from Bega Batholith granites, southeastern Australia: an ion microprobe study. J Geophys Res 95:17787–17796
Claypool AL, Klepeis KA, Clarke GL et al (2001) The evolution and exhumation of Early Cretaceous lower crustal granulites during changes in plate boundary dynamics, Fiordland, New Zealand. Geol Soc Amer Ab Prog 33:265
Clemens JD, Vielzeuf D (1987) Constraints on melting and magma production in the crust. Earth Plan Sci Let 86:287–306
Clemens JD, Wall VJ (1984) Origin and evolution of a peraluminous silicic ignimbrite suite: the Violet Town Volcanics. Contrib Min Pet 88:354–371
Collins WJ (1996) Lachlan Fold Belt granitoids: products of three-component mixing. T Roy Soc Ed-Earth Sci 87:171–182
Collins WJ (1998) Evaluation of petrogenetic models for Lachlan Fold Belt granitoids: implications for crustal architecture and tectonic models. Aust J Earth Sci 45:483–500
Collins WJ (2002) Nature of extensional accretionary orogens. Tectonics 21:1024–1036
Collins WJ, Beams SD, White AJR, Chappell BW (1982) Nature and origin of A-type granites with particular reference to southeastern Australia. Contrib Min Pet 80:189–200
Collins WJ, Hobbs BE (2001) What caused the Early Silurian change from mafic to silicic magmatism in the eastern Lachlan Fold Belt? Aust J Earth Sci 48:25–41
Condie KC (2008) Did the character of subduction change at the end of the Archean? Constraints from convergent-margin granitoids. Geology 36:611–614
Condie KC, Bickford ME, Aster RC, et al (2011) Episodic zircon ages, Hf isotopic composition, and the preservation rate of continental crust. Geol Soc Am Bull 123:951–957
Coombs DS, Cox SC (1991) Low- and very low-grade metamorphism in southern New Zealand. Geol Soc New Zea Misc Pub 58:87
Coombs DS, Landis CA, Norris RJ, et al (1976) The Dun Mountain Ophiolite belt, New Zealand, its tectonic setting, constitution, and origin, with special reference to the southern portion. Am J Sci 276:561–603
Cooper RA, Tulloch AJ (1992) Early Paleozoic terranes in New Zealand and their relationship to the Lachlan Fold Belt. Tectonophysics 214:129–144
Corner B (2000) Crustal framework of Namibia derived from magnetic and gravity data. In Miller RMcG (ed) Henno Martin Commemorative Volume. Communications of Geological Survey of Nambia 12, 13–19
Coward MP (1981) The junction between Pan African Mobile Belts in Namibia: its structural history. Tectonophysics 76:59–73
Coward MP (1983) The tectonic history of the Damaran Belt. In Miller RG (ed) Evolution of the Damara Orogen of South West Africa/Namibia. Geological Society of South Africa (Special Publications, 11), pp 409–421
Crawford AJ, Keays RR (1978) Cambrian greenstone belts in Victoria: marginal sea crust slices in the Lachlan Fold Belt of southeastern Australia. Earth Planet Sci Let 41:197–208
Crawford AJ, Keays RR (1987) Petrogenesis of Victorian Cambrian tholeiites and implications for the origin of associated boninites. J Pet 28:1075–1109
Curray JR, Emmel FJ, Moore DG, Raitt RW (1982) Structure, tectonics, and geological history of the northeastern Indian Ocean. In: Nairn AEM (ed) The ocean basins and margins 5. Plenum Press, New York, pp 399–450
Daczko NR, Klepeis KA, Clarke GL (2001) Evidence of Early Cretaceous collisional-style orogenesis in northern Fiordland, New Zealand, and its effect on the evolution of the lower crust. J Struc Geol 23:693–713
de Kock GS (1992) Forearc basin evolution in the Pan-African Damara Belt, central Namibia: the Hureb Formation of the Khomas Zone. Precam Res 57:169–194
de Kock GS, Eglington B, Armstrong RA et al (2000) U-Pb and Pb-Pb ages of the Naauwpoort Rhyolite, Kawakeup leptite and Okongava Diorite: implications for the onset of rifting and of orogenesis in the Damara Belt, Namibia. In Miller RMcG (ed) Henno Martin Commemorative Volume, Communications Geological Survey of Nambia 12, pp 81–88
Elburg M (1996) U-Pb ages and morphologies of zircon in micrograniteoid enclaves and peraluminous host granite; evidence for magma mingling. Contrib Min Pet 123:177–189
Fergusson CL (1987) Early Palaeozoic backarc deformation in the Lachlan Fold Belt, southeastern Australia: implications for terrane translations in eastern Gondwanaland. In Leitch EC, Scheibner E (eds) Terrane accretion and orogenic belts, (Geodynamics Series) Vol. 19. American Geophysical Union, Washington, DC, pp 39–56
Fergusson CL, Coney PJ (1992a) Implications of a Bengal Fan-type deposit in the Paleozoic Lachlan fold belt of southeastern Australia. Geology 20:1047–1049
Fergusson CL, Coney PJ (1992b) Convergence and intraplate deformation in the Lachlan Fold Belt of southeastern Australia. Tectonophysics 214:417–439
Fergusson CL, Fanning CM (2002) Late Ordovician stratigraphy, zircon provenance and tectonics, Lachlan Fold Belt, southeastern Australia. Aust J Earth Sci 49:423–436
Fergusson CL, VandenBerg AHM (1990) Middle Paleozoic thrusting in the easternLachlan Fold Belt, southeastern Australia. J Struct Geol 12:577–589

Festa A, Dilek Y, Pini GA et al (2012) Mechanisms and processes of stratal disruption and mixing in the development of mélanges and broken formation: redefining and classifying mélanges. Tectonophysics 568–569:7–24

Finzel ES, Trop JM, Ridgeway KD, Enkelmann E (2011) Upper plate proxies for flat-slap subduction processes in southern Alaska. Earth Plan Sci Let 303:348–360

Foden J, Sandiford M, Doherty-Page J, Williams I (1999) Geochemistry and geochronology of the Rathjan Gneiss: implications for the early tectonic evolution of the Delamerian Orogen. Aust J Earth Sci 46:377–389

Foster DA, Gray DR (2000) The structure and evolution of the Lachlan Fold Belt (Orogen) of eastern Australia. An Rev Earth Plan Sci 28:47–80

Foster DA, Mueller PA, Mogk DW, Wooden JL, Vogl JJ (2006) Proterozoic evolution of the western margin of the Wyoming Craton: implications for the tectonic and magmatic evolution of the northern Rocky Mountains. Can J Earth Sci 43:1601-1619

Foster DA, Gray DR (2008) Paleozoic crustal growth, structure, strain rate, and metallogeny in the Lachlan Orogen, Eastern Australia. In Spencer JE, Titley SR (eds) Ores and Orogenesis: Circum-Pacific Tectonics, Geological Evolution, and Ore Deposits. Arizona Geological Society Dig 22, pp 213–225

Foster DA, Gray DR, Bucher M (1999) Chronology of deformation within the turbidite-dominated Lachlan orogen: Implications for the tectonic evolution of eastern Australia and Gondwana. Tectonics 18:452–485

Foster DA, Gray DR, Spaggiari CV (2005) Timing of subduction and exhumation along the Cambrian East Gondwana margin, and the formation of Paleozoic back-arc basins. Geol Soc Am 117:105–116

Foster DA, Gray DR, Kwak TAP, Bucher M (1998) Chronology and tectonic framework of turbidite-hosted gold deposits in the western Lachlan Fold Belt, Victoria: 40Ar–39Ar results. Ore Geol Rev 13:229–250

Foster DA, Gray DR (2007) Strain rate in Paleozoic thrust sheets, the western Lachlan Orogen, Australia: strain analysis and fabric geochronology. In Sears JW, Harms T, Evenchick CA (eds) Whence the mountains? enquiries into the evolution of orogenic systems: a volume in honor of Raymond Price. Geol Soc Am SP 433:349–368

Foster DA, Gray DR, Spaggiari C et al (2009) Palaeozoic Lachlan Orogen, Australia; accretion and construction of continental crust in a marginal ocean setting: isotopic evidence from Cambrian metavolcanic rocks. In Cawood PA, Kroner A (eds) Earth accretionary systems in space and time, Geological Society Special Publication 318, pp 329–349, doi: 10.1144/SP318.12

Foster DA, Mogk DW, Henry DJ, Mueller PA (2011) Evolution of Archean rocks of the south Snowy Block, Yellowstone National Park: results of an REU site project. Geol Soc Am Ab Prog 43:435

Foster DA, Mueller PA, Heatherington A et al (2012a) Lu-Hf systematics of magmatic zircons reveal a Proterozoic crustal boundary under the Cretaceous Pioneer batholith, Montana. Lithos 142–143:216–225. doi: 10.1016/j.lithos.2012.03.005

Foster DA, Goscombe BA Newstead B et al (2012b) Rodinia-Gondwana supercontinent cycle refined be detrtial zircons from the Damara Orogen. Geol Soc Am Ab Prog 44/7:175

Fuis GS, Plfker G (1991) Evolution of deep structure along the Trans-Alaska Crustal Transect, Chugach Mountains and Copper River Basin, Southern Alaska. J Geophys Res 96:4229–4253

Gasser D, Bruand E, Stuwe K, et al (2011) Formation of a metamorphic complex along an obliquely convergent margin: structural and thermochronological evolution of the Chugach metamorphic complex, southern Alaska. Tectonics doi:10.1029/2010TC002776

Glen RA (2005) The Tasmanides of eastern Australia. In Vaughan APM, Leat PT, Pankhurst RJ (eds) Terrane Processes at the Margins of Gondwana, Geological Society of London Special Publication, 246, pp 23–96

Glen RA, Walshe JL, Barron LM, Watkins JJ (1998) Ordovician convergent margin volcanism and tectonism in the Lachlan sector of east Gondwana. Geology 26:751–754

Glen RA, Crawford AJ, Percival IG, Barron LM (2007) Early Ordovician development of the Macquarie Arc, Lachlan Orogen, New South Wales. Aust J Earth Sci 54:167–179

Goscombe B, Gray DR, Hand M (2004) Variation in metamorphic style along the northern margin of the Damara Orogen, Namibia. J Pet 45:1261–1295

Gray CM (1984) An isotopic mixing model for the origin of granitic rocks in southeastern Australia. Earth Plan Sci Let 70:47–60

Gray CM (1990) A strontium isotopic traverse across the granitic rocks of southeastern Australia: petrogenetic and tectonic implications. Aust Earth Sci 37:331–349

Gray CM, Webb J (1995) Provenance of Palaeozoic turbidites in the Lachlan Orogenic Belt: strontium isotopic evidence. Aust J Earth Sci 42:95–105

Gray DR, Gregory RT, Durney DW (1991) Rock-buffered fluid-rock interaction in deformed quartz-rich turbidite sequences, eastern Australia. J Geophys Res 96:19681–19704

Gray DR (1997) Tectonics of the southeastern Australian Lachlan Fold Belt: structural and thermal aspects. In Burg J-P, Ford M (eds) Orogeny through time. Geological Society Special Publication 121, pp 149–177

Gray DR, Foster DA (1998) Character and kinematics of faults within the turbidite-dominated Lachlan Orogen: implications for tectonic evolution of eastern Australia. J Struct Geol 20:1691–1720

Gray DR, Foster DA (2004a) Regional Geology: Tasman Orogen, Australia. Encyclopedia Geology 1:237–252

Gray DR, Foster DA (2004b) Tectonic evolution of the Lachlan Orogen, southeast Australia: historical review, data synthesis and modern perspectives. Aust J Earth Sci 51:773–817

Gray DR, Foster DA (2004c) $^{40}Ar/^{39}Ar$ thermochronologic constraints on deformation, metamorphism and cooling/exhumation of a Mesozoic accretionary

wedge, Otago Schist, New Zealand. Tectonophysics 385:181–210

Gray DR, Foster DA, Bucher M (1997) Recognition and definition of orogenic events in the Lachlan Fold Belt. A J Earth Sci 44:489–581

Gray DR, Willman CE (1991) Thrust-related strain gradients and thrusting mechanisms in a chevron-folded sequence, southeastern Australia. J Struct Geol 13:691–710

Gray DR, Foster DA, Goscombe B et al (2006a) $^{40}Ar/^{39}Ar$ thermochronology of the Pan-African Damara Orogen, Namibia with implications for tectonothermal and geodynamic evolution. Precam Res 150:49–72. doi:10.1016/j.precmres.2006.07.003

Gray DR, Foster DA, Korsch RJ, Spaggiari CV (2006b) Structural style and crustal architecture of the Tasmanides of eastern Australia, example of a composite accretionary orogeny. In Mazzoli S, Butler B (eds) Styles of continental compression. Geological Society of America, (Special Publication 414), pp 119–232

Gray DR, Foster DA, Maas R et al (2007) Continental growth and recycling by accretion of deformed turbidte fans and remnant ocean basins: examples from Neoproterozoic and Phanerozoic orogens. In Hatcher RD et al (eds) The 4D Framework of Continental Crust. Geological Society America Memoirs, 200, pp 63–92 doi:10.1130/2007.1200(05)

Gray DR, Foster DA, Meert JG et al (2008) A Damara Orogen perspective on the assembly of southwestern Gondwana. In Pankhurst RJ et al (eds) West Gondwana: Pre-Cenozoic Correlations Across South Atlantic Region, Geological Society Special Publication 294, pp 257–278, doi:10.1144/SP294.14

Haack U, Hoefs J, Gohn E (1982) Constraints on the origin of Damaran granites by Rb/Sr and δ18O data. Contrib Min Pet 79:279–289

Haack U, Gohn E, Hartmann O (1983) Radiogenic heat generation in Damaran rocks. Geol Surv S Afr SP 11:225–232

Hälbich IW (1977) Structure and tectonics along the southern margin of the Damara mobile belt, South West Africa An Univ Stellenbosch Ser A1 Geology, 2, 149–247

Hawkesworth CJ, Kramers JD, Miller RMG (1981) Old model Nd ages in Namibian Pan-African rocks. Nature 289:278–282

Hawkesworth CJ, Gledhill AR, Roddick JC, et al (1983) Rb-Sr and 40Ar/39Ar studies bearing on models for the thermal evolution of the Damara Belt, Namibia. In Miller RMcG (ed) Evolution of the Damara Orogen of southwest Africa/Namibia. Geological Society South Africa Special Publication 11, 323–338

Henry DJ, Mueller PA, Wooden JL et al (1982) Granulite grade supracrustal assemblages of the Quad Creek area, eastern Beartooth Mountains, Montana. In Mueller PA, Wooden, J L (eds) Precambrian Geology of the Beartooth Mountains, Montana and Wyoming, Montana Bureau of Mines and Geology Special Publication 84, 147–159

Hine R, Williams IS, Chappell BW, White AJR (1978) Contrasts between I-and S- type granitoids of the Kosciusko Batholith. J Geol Soc Aust 25:219–234

Hoffmann K-H (1983) Lithostratigraphy and facies of the Swakop Group of the southern Damara belt, SWA/Namibia. In Miller RG (ed) Evolution of the Damara Orogen of South West Africa/Namibia. Geological Society South Africa Special Publication, 11, 43–63

Hoffman PF, Hawkins DP, Isachsen CE, Bowring SA (1996) Precise U-Pb zircon ages for early Damaran magmatism in the Summas Mountains and Welwitschia Inlier, northern Damara belt, Namibia. Com Geol Sur Namibia 11:47–52

Hudson T, Plafker G (1982) Palaeogene metamorphism of an accretionary flysch terrane, eastern Gulf of Alaska. Geol Soc Am B 93:1280–1290

Ingersoll RV, Dickinson WR, Graham SA (2003) Remnant-ocean submarine fans: Largest sedimentary systems on earth. In Chan MA, Archer AW (eds) Extreme depositional environments: Mega end members in geologic time. Geological Society of American Special Publication 370, 191–208

Ireland TR, Gibson GM (1998) SHRIMP monazite and zircon geochronology of high-grade metamorphism in New Zealand. J Met Geol 16:149–167

Iizuka T, Komiya T, Rino S, et al (2012) Detrital zircon evidence for Hf-isotopic evolution of granitoid crust and continental growth. Geochem Cosmochim Acta 74:2450–2472

Jacob RE, Moore JM, Armstrong RA (2000) Zircon and titanite age determinations from igneous rocks in the Karibib District, Namibia; implications for Navachab vein-style gold mineralization. Com Geol Surv Namibia 12:157–166

Jacob RE, Snowdon PA, Bunting FJL (1983) Geology and structural development of the Tumas basement dome and its cover rocks. In Miller RG (ed) Evolution of the Damara Orogen of South West Africa/Namibia, Geological Society South Africa Special Publication 11, 157–172

John T, Schenk V (2003) Partial eclogitisation of gabbroic rocks in a late Precambrian subduction zone (Zambia); prograde metamorphism triggered by fluid infiltration. Contrib Min Pet 146:174–191

John T, Schenk V, Haase K, et al (2003) Evidence for a Neoproterozoic ocean in south-central Africa from mid-oceanic-ridge-type geochemical signatures and pressure-temperature estimates of Zambian eclogites. Geology 31:243–246

Johnson BD, Veevers JJ (1984) Oceanic palaeomagnetism. In: Veevers JJ (ed) Phanerozoic Earth History of Australia, Oxford Monographs on Geology and Geophysics 2, 17–38

Johnson SP, De Waele B, Tembo F, et al (2004) Subduction of continental crust during Gondwana amalgamation: very-high-pressure metamorphism and metasomatism in the Zambezi Belt. Front Res Earth Evol, 2

Jung S (2000) High-temperature, mid-pressure clockwise P-T paths and melting in the development of regional migmatites: the role of crustal thickening and repeated plutonism. Geol J 35:345–359

Jung S, Hoernes S, Mezger K (2000) Geochronology and petrogenesis of Pan-African syn-tectonic S-type and post-tectonic A-type granite (Namibia) – products of melting of crustal sources, fractional crystallization and wall rock entrainment. Lithos 50:259–287

Jung S, Hoernes S, Mezger K (2002) Synorogenic melting of mafic lower crust; constraints from geochronology, petrology and Sr, Nd, Pb and O isotope geochemistry of quartz diorites (Damara Orogen, Namibia). Contrib Min Pet 143:551–566

Jung S, Mezger K (2003a) U-Pb garnet chronometry in high-grade rocks; case studies from the central Damara Orogen (Namibia) and implications for the interpretation of Sm-Nd garnet ages and the role of high U-Th inclusions. Contrib Min Pet 146:382–396

Jung S, Mezger K (2003b) Petrology of basement-dominated terranes; I, Regional metamorphic T-t path from U-Pb monazite and Sm-Nd garnet geochronology (central Damara Orogen, Namibia). Chem Geol 198:223–247

Jung S, Mezger K, Hoernes S (1998a) Petrology and geochemistry of syn- to post-collisional metaluminous A-type granites – a major and trace element and Nd-Sr-Pb-O isotope study from the Proterozoic Damara Belt, Namibia. Lithos 45:147–175

Jung S, Mezger K, Hoernes (1998b) Geochemical and isotopic studies of syenites from the Proterozoic Damara Belt (Namibia): implications for the origin of syenites. Min Mag 62:729–730

Jung S, Mezger K, Hoernes S (2001) Trace element and isotopic (Sr, Nd, Pb, O) arguments for a mid-crustal origin of Pan-African garnet-bearing S-type granites from the Damara orogen (Namibia). Precam Res 110:325–355

Jung S, Mezger K, Hoernes S (2003) Petrology of basement-dominated terranes II. Contrasting isotopic (Sr, Nd, Pb, O) signatures of basement-derived granites and constraints on the source region of granite (Damara orogen, Namibia). Chem Geol 199:1–28

Jung S, Masberg P, Mihm D, Hoernes S (2009) Partial melting of diverse crustal sources—constraints from Sr-Nd-O isotopic compositions of quartz diorite-granodiorite-leucogranite associations (Kaoko Belt, Namibia). Lithos 111:236–251

Karlstrom KE, Bowring SA (1988) Early Proterozoic orogeny assembly of tectonostratigraphic terranes in southwestern North America. J Geol 96:561–576

Karlstrom KE, Ahall KI, Harlan SS, et al (2001) Long-lived (1.8–1.0 Ga) convergent orogen in southeastern Laurentia; its extensions to Australia and Baltica and implications for refining Rodinia. Precam Res 111:5–30

Kasch KW (1983a) Continental collision, suture progradation and thermal relaxation: a plate tectonic model for the Damara Orogen in central Namibia. In Miller, RG (ed) Evolution of the Damara Orogen of South West Africa/Namibia, Geological Society of South Africa Special Publication 11, 423–429

Kasch KW (1983b) Regional P-T variations in the Damara Orogen with particular reference to early high-pressure metamorphism along the southern margin. In Miller RG (ed) Evolution of the Damara Orogen of South West Africa/Namibia, Geological Society of South Africa Special Publication 11, pp. 243–253

Keay S, Collins WJ, McCulloch MT (1997) A three-component isotopic mixing model for granitoid genesis, Lachlan fold belt, eastern Australia. Geology 25:307–310

Keay S, Steele D, Compston W (2000) Identifying granite sources by SHRIMP U-Pb zircon geochronology: an application to the Lachlan Fold Belt. Contrib Min Pet 137:323–341

Kemp AIS, Hawkesworth CJ, Paterson BA, Kinny PD (2006) Episodic growth of the Gondwana supercontinent from hafnium and oxygen isotopes in zircon. Nature 439:580–583

Kemp AIS, Hawkesworth CJ, Foster GL et al (2007) Magmatic and crustal differentiation history of granitic rocks from Hf-O Isotopes in zircon. Science 315:980–983

Kemp AIS, Hawkesworth CJ, Collins WJ et al (2009) Isotopic evidence for rapid growth in an extensional accretionary orogeny: the Tasmanides, eastern Australia. Earth Plan Sci Let 284:455–466

Killick AM (2000) The Matchless Belt and associated sulphide mineral deposits, Damara Orogen, Namibia. In Miller RMcG (ed) Henno Martin Commemorative Volume, Communication of Geological Survey of Namibia 12, pp 73–80

Kimbrough DL, Mattison JM, Coombs DS et al (1992) Uranium-lead ages for the Dun Mountain Ophiolite belt and Brook Street terrane, South Island, New Zealand. Geol Soc Am B 104:429–443

Kimbrough DL, Tulloch AJ, Geary E, Coombs DS, Mattinson JM (1993) Isotopic ages from the Nelson region of the South Island, New Zealand: crustal structure and definition of the Median Tectonic Zone. Tectonophysics 225:433–448

Kimbrough DL, Tulloch AJ, Coombs DS et al (1994) Uranium-lead ages from the Median Tectonic Zone, South Island New Zealand. New Zea J Geol Geophys 37:393–419

Kimura G, Ludden J (1995) Peeling of oceanic crust in subduction zones. Geology 23:217–220

King PL, White AJR, Chappell BW, Allen CM (1997) Characterization and origin of aluminous A-type granites from the Lachlan Fold Belt, southeastern Australia. J Pet 38:371–391

Kisters AFM, Jordaan LS, Neumaier K, (2004) Thrust-related dome structures in the Karibib district and the origin of orthogonal fabric domains in the south Central Zone of the Pan-African Damara belt, Namibia. Precam Rese 133:283–303

Klepeis KA, Clarke GL, Rushmer T (2003) Magma transport and coupling between deformation and magmatism in the continental lithosphere. GSA Today 13:4–11

Korn H, Martin H (1959) Gravity tectonics in the Naukluft Mountains of South West Africa. Geol Soc Am B 70:1047–1078

Kröner A (1982) Rb-Sr geochronology and tectonic evolution of the Pan African belt of Namibia, southwestern Africa. Am J Sc 282:1471–1507

Kröner A (1984) Dome structures and basement reactivation in the Pan-African Damara belt of Namibia, In Kröner A, Greiling RO (eds) Precambrian tectonics illustrated. Nagele und Obermiller, Stuttgart, pp 191–206

Kukla C (1993) Strontium isotope heterogeneities in amphibolite facies, banded metasediments—a case study from the Late Proterozoic Kuiseb Formation of the southern Damara Orogen, Central Namibia. Geol Sur Namibia Mem 15:p 39

Kukla PA, Stanistreet IG (1991) Record of the Damaran Khomas Hochland accretionary prism in central Namibia: Refutation of an "ensialic" origin of a Late Proterozoic orogenic belt. Geology 19:473–476

Kukla PA, Opitz C, Stanistreet IG, Charlesworth EG (1988) New aspects of the sedimentology and structure of the Kuiseb Formation in the western Khomas Trough, Damara Orogen, South West Africa/Namibia. Com Geol Surv Namibia 4:33–42

Longridge L, Gibson RL, Kinnaird JA, Armstrong RA (2011) Constraining the timing of deformation in the southwestern Central Zone of the Damara Belt, Namibia. In Van Hinsbergen DJJ, Buiter SJH, Torsvik TH, et al (eds) The Formation and Evolution of Africa: A Synopsis of 3.8 Ga of Earth History. Geological Society of London Special Publication 357, pp 107–135.

Lundberg N, Reed DL (1991) Continetal margin tectonics: forearc process. Rev Geophys 29:794–806

Maas R, Nicholls IA (2002) Nd-Sr isotopic evidence for the origin of Devonian granitic and felsic volcanic rocks of the western Lachlan Fold Belt. Geol Soc Austr Ab 67:36

Maas R, Nicholls IA, Greig A, Nemchin A (2001) U-Pb zircon studies of mid- crustal metasedimentary enclaves from the S-type Deddick Granodiorite, Lachlan Fold Belt, SE Australia. J Pet 42:1429–1448

Martin H, Porada H (1977) The intracratonic branch of the Damara orogen in South West Africa. I. Discussion of geodynamic models. Precam Res 5:311–338

Masberg P (2000) Garnet-growth in medium-pressure granulite facies metapelites from the central Damara Orogen: igneous versus metamorphic history. In Miller RMcG (ed) Henno Martin Commemorative Volume. Communications of Geolological Survey of Namibia12, pp 115–124

McCulloch MT, Bradshaw JY, Taylor SR (1987) Sm-Nd and Rb-Sr isotopic and geochemical systematics in Phanerozoic granulites from Fiordland, southwest New Zealand. Contrib Min Pet 97:183–195

McCulloch MT, Chappell BW (1982) Nd isotopic characteristics of S- and I- type granites. Earth Planet Sci Let 58:51–64

McDermott F, Harri NBW, Hawkesworth CJ (2000) Geochemical constraints on the petrogenesis of Pan-African A-type granites in the Damara Belt, Namibia. In Miller RMcG (ed) Henno Martin Commemorative Volume, Communications of Geolological Survey of Namibia12, pp 139–148

McDermott F, Harris NBW, Hawkesworth CJ (1996) Geochemical constraints on crustal anatexis: a case study from the Pan-African granitoids of Namibia. Contrib Min Pet 123:406–423

McDermott F, Hawkesworth CJ (1990) Intracrustal recycling and upper-mantle evolution: a case study from the Pan-African Damara mobile belt, central Namibia. Chem Geol 83:263–280

Maloof AC (2000) Superposed folding at the junction of the inland and coastal belts, Damara Orogen, Namibia. In Miller RMcG (ed) Henno Martin Commemorative Volume, Communications of Geolological Survey of Namibia12, pp 89–98

Martin H (1983) Overview of the geosynclinal, structural and metamorphic development of the intracontinental branch of the Damara Orogen. In: Martin H, Eder FW (eds) Intracontinental Fold Belts. Springer, Berlin, p 473–502

Martin H, Porada H (1977) The intracratonic branch of the Damara Orogen in South West Africa: I. Discussion of Geodynamic models. Precam Res 5:311–338

Miller JMcL, Gray DR (1997) Subduction related deformation and the Narooma anticlinorium, eastern Lachlan Orogen. Austr J Earth Sci 44:237–251

Miller RMcL (1983a) ThePan-African Damara orogen of South West Namibia/Africa. In Miller RMcL (ed) Evolution of the Damara Orogen of southwest Africa/Namibia, Geological Society of South Africa Special Publication 11, 431–515

Miller RMcL (ed) (1983b) Evolution of the Damara Orogen of southwest Africa/Namibia, Geological Society of South Africa Special Publication, p 515

Miller RMcG, Barnes SJ, Balkwill G (1983a) Possible active margin deposits within the southern Damara Orogen: The Kuiseb Formation between Okhahandja and Windhoek. In Miller RMcL (ed) Evolution of the Damara Orogen of southwest Africa/Namibia, Geological Society of South Africa Special Publication, 11, 73–88

Miller RMcG, Freyer EE, Hälbich IW (1983b) Turbidite succession equivalent to the entire Swakop Group. In Miller RMcG (ed) Evolution of the Damara Orogen of southwest Africa/Namibia, Geological Society of South Africa Special Publication, 11, 65–71

Mogk D, Henr D, Mueller P, Foster D (2012) Origins of a continent evidence from a research for undergraduates program in Yellowstone. Yellowstone Sci 20:22–32

Moore DH, Betts PG, Hall H (2013) Towards understanding the early Gondwana margin in southeastern Australia. Gondwana Res 23:1581–1598

Morand VJ (1990) Low-pressure regional metamorphism in the Omeo Metamorphic Complex, Victoria, Australia. J Met Geol 8:1–12

Morand V, Gray DR (1991) Major fault zones related to the Omeo metamorphic complex, northeastern Victoria. Austr J Earth Sci 38:203–221

Mortimer N (1993) Jurassic tectonic history of the Otago Schist, New Zealand. Tectonics 12:237–244

Mortimer N (2000) Metamorphic discontinuities in orogenic belts: example of garnet—biotite—albite zone in the Otago Schist, New Zealand. Int J Earth Sci 89:295–306

Mortimer N (2004) New Zealand's geological foundations. Gondwana Res 7:261–272

Mortimer N, Tulloch AJ, Spark RN et al (1999a) Overview of the Median Batholith, New Zealand: a new interpretation of the geology of the Median Tectonic Zone and adjacent rocks. J Afr Earth Sci 29:259–270

Mortimer N, Gans P, Calvert A, Walker N (1999b) Geology and thermochronometry of the east edge of the Median Batholith (Median Tectonic Zone): a new perspective on Permian to Cretaceous crustal growth of New Zealand. Island Arc 8:404–425

Mortimer N, Davey FJ, Melhush A et al (2003) Geological interpretation of a deep crustal seismic reflection profile across the eastern Province and Median Batholith, New Zealand: crustal architecture of an extended Phanerozoic convergent orogeny. New Zea J Geol Geophys 45:349–363

Mueller P, Frost C (2006) The Wyoming Province: A distinctive Archean craton in Laurentian North America. Can J Earth Sci 43:1391–97

Mueller PA, Wooden JL (2012) Trace Element and Lu-Hf Systematics in Hadean-Archean Detrital Zircons: Implications for Crustal Evolution. J Geology 120:15–29

Mueller PA, Wooden JL, Mogk DW, Henry DJ, Bowes DR (2010) Rapid growth of an Archean continent by arc magmatism. Precambr Res 183:70–88

Mueller PA, Mogk DW, Henry DJ et al (2013) The plume to plate transition: Hadean and Archean evolution of the northern Wyoming Province, U.S.A. In: Dilek Y, Furnes H (eds) Archean Earth and Early Life. Springer, New York, this volume

Muir RJ, Ireland TR, Weaver SD, Bradshaw JD (1996a) Ion microprobe dating of Paleozoic granitoids: Devonian magmatism in New Zealand and correlations with Australia and Antarctica. Chem Geol 127:191–210

Muir RJ, Weaver SD, Bradshaw JD et al (1995) The Cretaceous Separation Point Batholith, New Zealand. Granitoid magmas formed by melting of mafic lithosphere. J Geol Soc Lond 152:689–701

Muir RJ, Ireland TR, Weaver SD et al (1998) Geochronology and geochemistry of a Mesozoic magmatic arc system, Fiordland, New Zealand. J GeolSoc Lond 155:1037–1053

Muir R, Weaver SD, Bradshaw JD et al (1996b) Geochemistry of the Karamea Batholith, New Zealand, and comparisons with the Lachlan Fold Belt granites of southeastern Australia. Lithos 39:1–20

Muir RJ, Ireland TR, Weaver SD et al (1988) Geochronology and geochemistry of a Mesozoic magmatic arc system, Fiordland, New Zealand. J Geol Soc London 155:1037–1053

Murray CG, Fergusson CL, Flood PG et al (1987) Plate tectonic model for the Carboniferous evolution of the New England Fold belt. Austr J Earth Sci 34:213–236

Newstead BL (2010). The Congo-Kalahari cratonic relationship: from Rodinia to Gondwana. M.S. Thesis, University of Florida, Gainesville, p 234

Norris RJ, Craw D (1987) Aspiring terrane: an oceanic assemblage from New Zealand and its implications for Mesozoic terrane accretion in the southwest Pacific. In Leitch EC, Scheibner E, (eds) Terrane Accretion and Orogenic Belts, American Geophysics Union Geodynamics Series 19, pp 169–177

Offler R, McKnight S, Morand V (1998) Tectonothermal history of the western Lachlan Fold Belt, Australia: insights from white mica studies. J Met Geol 16:531–540

O'Halloran GL, Rey P (1999) Isostatic constraints on the central Victorian lower crust: implications for the tectonic evolution of the Lachlan fold belt. Austr J Earth Sci 46:633–639

Passchier CW, Trouw RA, Ribeiro A, Pacuillo FVP (2002) Tectonic evolution of the southern Kaoko Belt, Namibia. J Afr Earth Sci 35:61–75

Patchett PJ, Bridgwater D (1984) Origin of continental crust of 1.9–1.7 Ga age defined by Nd isotopes in the Ketilidian terrain of South Greenland. Contrib Min Pet 87:311–318

Percival JA, Bleeker W, Cook EA et al (2004) PanLITHOPROBE Workshop IV: Intra-orogen correlations and comparative Orogenic anatomy. Geosci Can 31:23–39

Petford N, Atherton M (1996) Na-rich partial melts from newly underplated basaltic crust; the Cordillera Blanca Batholith, Peru. J Pet 37:1491–1521

Phillips GN, Wall VJ, Clemens JC (1981) Petrology of the Strathbogie Batholith—a cordierite-bearing granite. Can Min 19:47–63

Porada H (1979) The Damara-Ribeira orogen of the Pan-African Brasiliano Cycle in Namibia (southwest Africa) and Brazil as interpreted in terms of continental collision. Tectonophysics 57:237–265

Porada H (1983) Geosynclinal model for the geosynclinal development of the Damara Orogen, Namibia, southwest Africa. In: Martin H, Eder FW (eds.) Intracontinental fold belts. Springer, Berlin, pp 503–541

Porada H, Ahrendt H, Behr J, Weber K (1983) The join of the coastal and intracontinental branches of the Damara Orogen, Namibia, South West Africa. In: Martin H, Eder FW (eds.) Intracontinental Fold Belts. Springer, Berlin, pp 901–912

Powell CMcA (1983) Tectonic relationship between the late Ordovician and Late Silurian palaeogeographies of southeastern Australia. J Geol Soc Aust 30:353–373

Powell CMcA (1984) Ordovician to Carboniferous. In: Veevers JJ (ed) Phanerozoic Earth History of Australia, Oxford Mon Geol Geophys 2. Clarendon, Oxford, pp 290–340

Prave AR (1996) Tale of three cratons: tectostratigraphic anatomy of the Damara Orogen in northwestern Namibia and the assembly of Gondwana. Geology 24:1115–1118

Price RC, Brown WM, Woolard CA (1983) The geology, geochemistry and origin of late-Silurian, high-Si igneous rocks of the upper Murray Valley, NE Victoria. J Geol Soc Austr 30:443–459

Price RC, Ireland TR, Maas R, Arculus RJ (2006) SHRIMP zircon geochronology and Sr-Nd isotope constraints on the interface between Brook Street Terrane and the Median Batholith, Bluff Pensinsula and southern Longwoods Range, Southland, New Zealand. New Zea J Geol Geophys 49:291–303

Puhan D (1983) Temperature and pressure of metamorphism in the Central Damara Orogen, in Miller, R.G. ed, Evolution of the Damara Orogen of South West Africa/Namibia. Geological Society of South Africa Special Publication 11, pp 219–223

Richards SW, Collins WJ (2002) The Cooma metamorphic complex, a low-P, high-T (LPHT) regional aureole beneath the Murrumbidgee batholith. J Met Geol 20:119–134

Roser B, Cooper AF (1990) Geochemistry and terrane affiliation of Haast Schist from the western Southern Alps, New Zealand. New Zea J Geol Geophys 94:635–650

Rossetti F, Vignaroli G, Di VG (2011) Long-lived orogenic construction along the paleo-Pacfic margin of Gondwana (Deep Freeze Range, North Victoria Land, Antarctica). Tectonics 30, doe:10.1029/2010TC002804

Rossiter AG (2003) Granitic rocks of the Lachlan Gold Belt in Victoria. In Birch WD (ed) Geol Victoria, Geological Society of Australia Special Publication 23, pp 217–237

Schmidt A, Wedepohl KH (1983) Chemical composition and genetic relations of the Matchless Amphibolite (Damara Orogenic Belt). In Miller RMcG (ed) Evolution of the Damara Orogen of southwest Africa/Namibia, Geological Society of South Africa Special Publication 11, pp 139–145

Schmitt RS, Trouw RAJ, Passchier CW et al (2012) 530 Ma syntectonic syenites and granites in NW Namibia—their relation with collision along the junction of the Damara and Kaoko belts. Gondwana Res 21:362–377

Sengor CAM, Natal'in BA (1996) Turkic-type orogeny and its role in the making of the continental crust. An Rev Earth Plan Sci 24:263–337

Smith AG (1981) Subduction and coeval thrust belts, with particular reference to North America. In McClay KR, Price NJ (eds) Thrust and nappe tectonics, Geological Society Special Publication 9, pp 111–124

Soesoo A, Bons PD, Gray DR, Foster DA (1997) Divergent double sunduction: tectonic and petrologic consequences. Geology 25:755–758

Soesoo A, Nicholls IA (1999) Mafic rocks spatially associated with Devonian felsic intrusions of the southern Lachlan Fold Belt: a possible mantle contribution to crustal evolution processes. Austr J Earth Sci 46:725–734

Spaggiari CV, Gray DR, Foster DA (2002a) Blueschist metamorphism during accretion in the Lachlan Orogen, southeastern Australia. J Met Geology 20:711–726

Spaggiari CV, Gray DR, Foster DA (2003a) Tethyan and Cordilleran-Type Ophiolites of Eastern Australia: implications for the evolution of the Tasmanides. In Dilek Y, Robinson PT (eds) Ophiolites in Earth's History, Geological Society of London Special Publication 218, pp 517–539

Spaggiari CV, Gray DR, Foster DA (2004a) Ophiolite accretion in the Lachlan Orogen, southeastern Australia. J Struct Geol 6:87–112

Spaggiari CV, Gray DR, Foster DA (2004b) Lachlan Orogen subduction-accretion systematics revisited. Austr J Earth Sci 51:549–553

Spaggiari CV, Gray DR, Foster DA, Fanning CM (2002b) Occurrence and significance of blueschists in the southern Lachlan Orogen. Aust J Earth Sci 49:255–269

Spaggiari CV, Gray DR, Foster DA, McKnight S (2003b) Evolution of the boundary between the western and central Lachlan Orogen: implications for Tasmanide tectonics. Austr J Earth Sci 50:725–749

Spell TL, McDougall I, Tulloch AJ (2000) Thermochronologic constraints on the breakup of the Pacific Gondwana margin: The Paparoa metamorphic core complex, South Island, New Zealand. Tectonics 19:433–451

Sporli KB (1978) Mesozoic tectonics, North Island, New Zealand. Geol Soc Am Bull 89:415–425

Swart R (1992) The sedimentology of the Zerrissene turbidite system, Damara Orogen, Namibia. Geological Survey of Namibia Memoirs 13, p 54

Tamaki K (1995) Opening of the Japan Sea. In: Taylor B (ed) Backarc Basins—Tectonic and Magmatism. Plenum, New York, pp 407–420

Thompson AB (1996) Fertility of crustal rocks during anatexis. T Royal Soc Ed 87:1–10

Tulloch AJ, Kimbrough DL (1989) The Paparoa Metamorphic Core Complex, New Zealand: Cretaceous extension associated with fragmentation of the Pacific margin of Gondwana. Tectonics 8:1217–1234

Tulloch AJ (1983) Granitoid rocks of New Zealand—a brief review. Geol Soc Am Mem 159:5–20

Tulloch AJ (1988) Batholiths, plutons and suites: nomenclature for granitoid rocks of Westland-Nelson, New Zealand. New Zea J Geol Geophys 31:505–509

Tulloch AJ, Kimbrough DL (2003) Paired plutonic belts in convergent margins and the development of high Sr/Y magmatism: Peninsular Ranges batholith of Baja California and Median batholith of New Zealand. Geol Soc Am SP 374:1–21

Turner SP, Kelley SP, Morrison RS (1992) Derivation of some A-type magmas by fractionation of basaltic magma: an example from the Padthaway Ridge, South Australia. Lithos 28:151–179

Turner SP, Foden J, Kelley SP et al (1996) Source of the Lachlan fold belt flysch linked to convective removal of the lithospheric mantle and rapid exhumation of the Delamerian-Ross fold belt. Geology 24:941–944

van de Flierdt T, Hoernes S, Jung S et al (2003) Lower crustal melting and the role of open-system processes in the generation of syn-orogenic quartz diorite-granite-leucogranite associations: constraints from Sr-Nd-O isotopes from the Bandombaai Complex, Namibia. Lithos 67:205–226

Vandenberg AHM, Stewart IR (1992) Ordovician terranes of the southeastern Lachlan Fold Belt: stratigraphy, structure and palaeogeographic reconstruction. Tectonophysics 214:159–176

Veevers JJ (2000a) Billion-year earth history of Australia and neighbours in Gondwanaland. Gemoc, Sydney, p 388

Veevers JJ (2000b) Antarctic Beardmore-Ross and Mirny provenances saturate Palaeozoic-Mesozoic East Gondwanaland with 0.6–0.5 Ga zircons. In Veevers JJ (ed) Billion-year earth history of Australia and neighbors in Gondwanaland. Gemoc, Sydney, pp 110–130

Voice PJ, Kowalewski M, Eriksson KA (2011) Quantifying the timing and rate of crustal evolution: global compilation of radiometrically dated detrital zircon grains. J Geol 119:09–126

Von Huene R, Scholl DW (1991) Observations at convergent margins concerning sediment subduction, subduction erosion, and the growth of continental crust. Rev Geophys 29:279–316

Waight TE, Weaver SD, Muir RJ (1998a) Mid-Cretaceous granitic magmatism dating the transition from subduction to extension in southern New Zealand: a chemical and tectonic synthesis. Lithos 45:469–482

Waight TE, Weaver SD, Muir J et al (1998b) The Hohonu Batholith of North Westland, New Zealand: granitoid compositions controlled by source H_2O contents and generated during tectonic transition. Contrib Min Pet 130:225–239

Wandres AM, Bradshaw JD (2005) New Zealand tectonostratigraphy and implications from conglomeratic rocks for the configuration of the SW Pacific margin of Gondwana. In Vaughan APM, Leat PT, Pankhurst RJ (eds) Terrane Processes at the Margins of Gondwana, Geological Society of London Special Publication, 246, pp 179–216

Watson JM, Gray DR (2001) Character, extent and significance of broken formation for the Tabberabbera Zone, central Lachlan Orogen. Austr J Earth Sci 48:943–954

White AJR, Chappell BW (1983) Granitoid types and their distribution in the Lachlan Fold Belt, SE Australia. Geol Soc Am Mem 159:21–34

White AJR, Chappell BW (1988) Some supracrustal (S-type) granites of the Lachlan Fold Belt. T Roy Soc Ed 79:169–182

Williams IS (1992) Some observations on the use of zircon U-Pb geochronology in the study of granitic rocks. T Roy Soc Ed 83:447–458

Williams IS, Chappel BW, McCulloch MT, Crook KA (1991) Inherited and detrital zircons—clues to the early growth of crust in the Lachlan Fold Belt. Geol Soc Austr Ab 29:58

Williams IS, Chappel BW, Crook KAW, Nicoll RS (1994) In search of the provenance of the early Palaeozoic flysch in the Lachlan Fold Belt, southeastern Australia. Geol Soc Austr Ab 37:464

Wooden JL, Mueller PA (1988) Pb, Sr, Nd isotopic compositions of a suite of Late Archean igneous rocks, eastern Beartooth Mountains: implications for crust-mantle evolution. Earth Planet Sci Let 87:59-72

Wyborn D, Chappell BW (1986) The petrogenetic significance of chemically related plutonic and volcanic rock units. Geol Mag 123:619–628

Wyborn D, Chappell BW, Johnston RM (1981) Three S-type volcanic suites from the Lachlan Fold Belt, southeast Australia. J Geophys Res 86:10335–10348

Wyborn LAI, Wyborn D, Warren R, Drummond BJ (1992) Proterozoic granite types in Australia: implications for lower crust composition, structure and evolution. T Roy Soc Ed 83:201–209

Yardley BWD (1982) The early metamorphic history of the Haast Schists and related rocks of New Zealand. Contrib Min Pet 81:317–327

Zen E-An (1995) Crustal magma generation and low-pressure high-temperature regional metamorphism in an extensional environment: possible application to the Lachlan Fold Belt, Australia. Ame J Sci 295:851–874

Biogenicity of Earth's Earliest Fossils

11

J. William Schopf and Anatoliy B. Kudryavtsev

Abstract

The abundant and diverse assemblage of filamentous microbial fossils and associated organic matter permineralized in the ~3465 Ma Apex chert of northwestern Australia—widely regarded as among the oldest records of life—have been investigated intensively. First reported in 1987 and formally described in 1992 and 1993, the biogenicity of the Apex fossils was questioned in 2002 and in three subsequent reports. However, as is shown here by use of analytical techniques unavailable twenty years ago, the Apex filaments are now established to be *bona fide* fossil microbes composed of three-dimensionally cylindrical organic-walled (kerogenous) cells. Backed by a large body of supporting evidence of similar age—other microfossils, stromatolites, and carbon isotopic data—it seems clear that microbial life was present and flourishing on the early Earth ~3500 Ma ago.

J. W. Schopf (✉) · A. B. Kudryavtsev
Department of Earth and Space Sciences and Molecular Biology Institute, University of California, Los Angeles, CA 90095, USA
e-mail: Schopf@ess.ucla.edu

A. B. Kudryavtsev
Center for the Study of Evolution and the Origin of Life, University of California, Los Angeles, CA 90095, USA

NAI PennState Astrobiology Research Center, University Park, PA 16802, USA

Y. Dilek, H. Furnes (eds.), *Evolution of Archean Crust and Early Life*, Modern Approaches in Solid Earth Sciences 7, DOI 10.1007/978-94-007-7615-9_11, © Springer Science+Business Media Dordrecht 2014

11.1 Introduction

The microscopic fossils of the ~3465 Ma Apex chert of the northwestern Australian Pilbara Craton—first reported in a quarter-century ago (Schopf and Packer 1987) and described in detail a few years later (Schopf 1992, 1993)—are widely regarded as among the oldest evidence of life. Though they are not actually the "oldest fossils," supplanted by more recent reports of similar fossil microbes (Ueno et al. 2001a, b, 2004) and megascopic stromatolites ~3496 Ma in age (Walter et al. 1980; Groves et al. 1981; Van Kranendonk 2006), they are nevertheless especially well known, due primarily to their great age and morphological diversity. In some circles they are known also because of a controversy that for more than a decade has swirled about their biological interpretation—a problem that we regard as solved.

We here summarize the history of this controversy, outline the evidence required to establish the biogenicity of putative ancient microbes, and show that these criteria are met by the Apex fossils but not by nonbiologic pseudofossils.

11.1.1 Synopsis of the Controversy

The following is a brief summary of the relevant history:

1. In February 2001, a manuscript was submitted to *Nature* by Brasier et al. that questioned the biological origin of the microbial fossils of the Apex chert, an interpretation proposed a decade earlier (Schopf and Packer 1987; Schopf 1992, 1993). Several months later, in July 2001, we and our colleagues submitted a manuscript to *Nature* reporting our Raman spectroscopy-based finding that confirmed the original optical microscopy-based inference that the Apex fossils are composed of kerogenous organic matter—a finding, at the time, that was something of a "breakthrough," this being the first rigorous application of Raman to rock-embedded organic-walled fossil microbes and a follow-up to our earlier "proof of concept" paper that documented the effectiveness of such studies (Kudryavtsev et al. 2001). Although our paper was formally accepted for publication in November 2001, the *Nature* editor elected to delay its appearance until March 2002 so that it could be published (Schopf et al. 2002) back-to-back with the paper by Brasier et al. (2002).
2. The Brasier et al. article confirmed that the carbon isotopic composition of the Apex organic matter is consistent with a biological origin (Strauss and Moore 1992; Schopf 1993) and that the fossils, like other permineralized Precambrian microbes, are composed of carbonaceous matter (Schopf and Packer 1987; Schopf 1992, 1993; Schopf et al. 2002).
3. Despite these biology-consistent data, Brasier et al. (2002, 2005) interpreted the Apex fossils to be nonbiological, suggesting that they are "graphite" mineral pseudofossils formed by the "self-organization" of nonbiological organic matter produced by Fischer-Tropsch-type abiotic syntheses.
4. Presumably spurred by this controversy, the Apex fossils have subsequently been suggested to be mineralic barium carbonate "biomorphs" (García-Ruíz et al. 2002, 2003), inorganic silica or clay mineral needle-like crystals (Pinti et al. 2009), or hematite-infilled veinlets (Marshall et al. 2011). This last report was followed by a study interpreting the Apex organics to have two differing, perhaps nonbiological origins (Marshall et al. 2012). None of these studies is reported to have been based on examination of the originally described Apex fossils, archived at the Natural History Museum in London (Schopf 1993).

Resolution of this controversy has thus hinged on whether the Apex fossils are cellular and composed of kerogenous organic matter (Schopf and Packer 1987; Schopf 1992, 1993; Schopf et al. 2002, 2007), like similarly chert-permineralized ancient microorganisms, or are solid and mineralic, composed of abiotically derived graphite (Brasier et al. 2002, 2005), barium carbonate (García-Ruíz et al. 2002, 2003), silica or clay minerals (Pinti et al. 2009), or hematite (Marshall et al. 2011), and, if carbonaceous, whether the Apex organic matter has two different origins (Marshall et al. 2012).

11.1.2 Similar Episodes in the History of Precambrian Paleobiology

Though many years ago uncertainty festered, for more than a century, over the "missing" fossil record of Precambrian life—beginning in 1859 with the deep puzzlement about the problem expressed by Darwin in *On the Origin of Species*—the intense interest in the Apex fossils, persisting now for the past decade, is unusual in the recent history of Precambrian paleobiology. In the modern development of the field, perhaps the most comparable example is that following the first detailed report of the now famous ~1900 Ma stromatolite-building fossil microbes of the Gunflint chert by Barghoorn and Tyler (1965)—even though this work was supported two months later by Cloud (1965). In that instance, the skepticism of the scientific community was soon put to rest, perhaps most effectively by a paper of the same year that reported a second example of Precambrian fossil microbes (Barghoorn and Schopf 1965) demonstrating that the first report, of the Gunflint fossils, was not some sort of fluke.

Even though, in 1965, the Gunflint microbes and the stromatolites in which they occur comprised the oldest compelling evidence of life then known, controversy about their biogenicity persisted for only a few years. In those times, however, nearly a half-century ago, the study of Precambrian microbes was dominated by the two widely acknowledged pioneering experts, Barghoorn and Cloud, workers whose findings supported the seminal discoveries of B.V. Timofeev, an "unsung hero" in the initial studies of microscopic Precambrian fossils (for a summary of this history, see Schopf 1999, pp. 35–50). Now, there are far more workers in the field—an increase spurred by the emergence of Precambrian paleobiology as a active field of science and of ever-increasing interest in the astrobiological search for past life on other planets, studies that are based on understanding of Earth's Precambrian fossil record. These developments, coupled with the introduction of an impressive array of new analytical techniques and the multidisciplinary approaches this has fostered, have encouraged divergent opinions.

11.2 Apex Chert Microbial Assemblage

11.2.1 Biologic Diversity

The microbial assemblage of the Apex chert includes 11 taxa of filamentous microorganisms, ranging in width from ~0.5 to ~16.5 μm and differentiated by their medial- and terminal-cell size and shape, described on the basis of measurements of ~1800 cells in 175 specimens (Schopf 1993, Table 1). Shown in Fig. 11.1 are optical photomicrographs and interpretive drawings of seven representative taxa. Although notable in such ancient rocks for their broad range of morphological diversity, they are similar in size, form, mode of preservation, and paleoenvironmental setting to chert-permineralized filamentous fossils reported from numerous other deposits of similar age (Awramik et al. 1983; Walsh and Lowe 1985; Walsh 1992; Rasmussen 2000; Ueno et al. 2001a, b, 2004; Tice et al. 2004; Kiyokawa et al. 2006; Sugitani et al. 2010; Wacey et al. 2011).

11.2.2 Biologic Relations

Although widely assumed to be cyanobacteria, the Apex fossils were formally described as "Bacteria *Incertae Sedis*"—that is, prokaryotes of uncertain affinities belonging to the Bacterial Domain (Schopf 1993, 1999). In the paper in which they were taxonomically defined (Schopf 1993), care was taken to negate a cyanobacterial interpretation since it would have implied that the Apex fossils were capable of oxygen-producing photosynthesis for which there was then, and is now, no compelling evidence (Schopf 1999; Schopf et al. 2007). Although they might be cyanobacteria, as are the majority of similar fossils known from younger Precambrian fossiliferous units (e.g., see the references cited in Mendelson and Schopf 1992), the available evidence is equally consistent with their assignment to non-oxygen-producing bacteria. Moreover, they could be members of an early-evolved microbial lineage that is now extinct or has yet to be

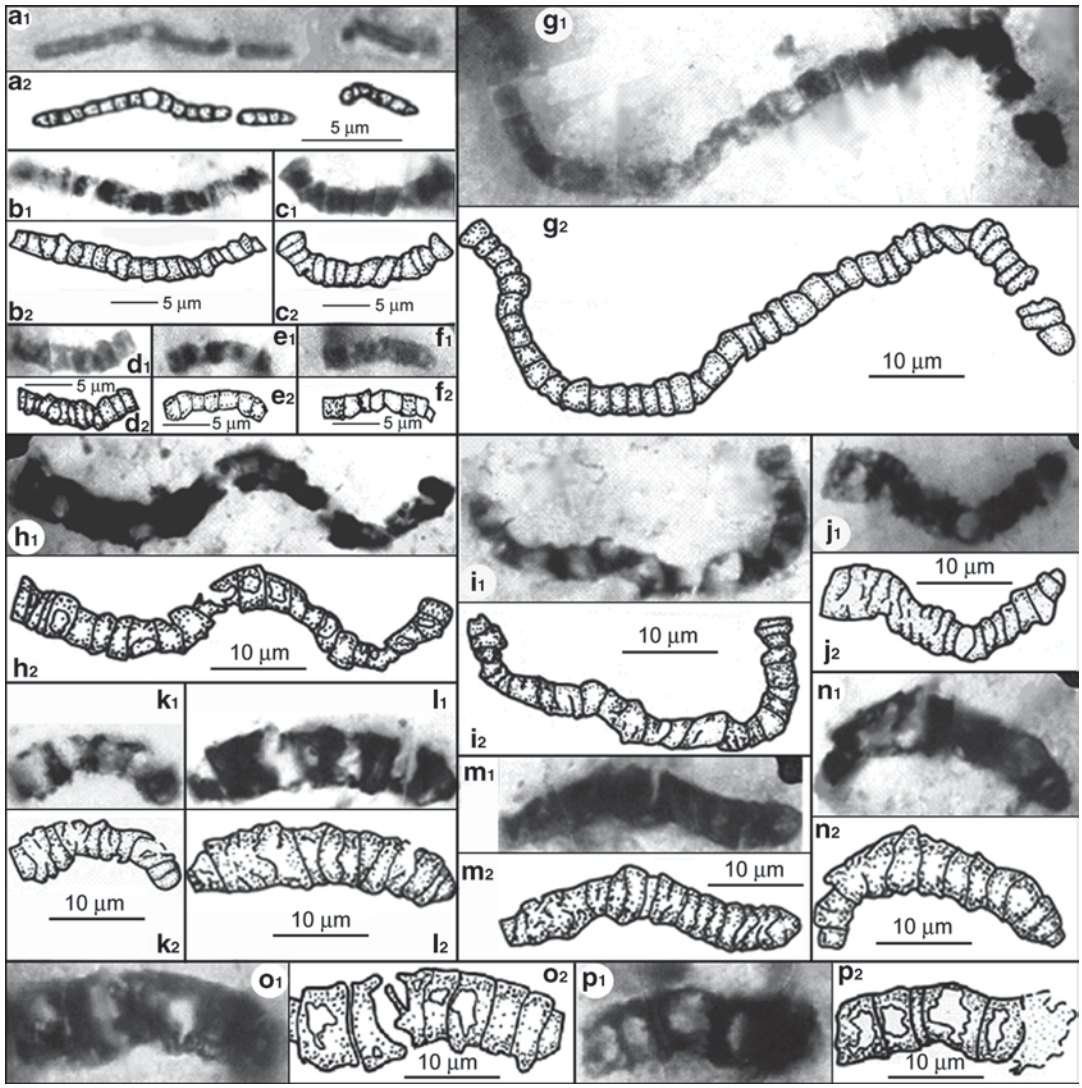

Fig. 11.1 Optical photomicrographs and interpretive drawings illustrating the diversity of filamentous microfossils present in petrographic thin sections of the Apex chert. **a** *Archaeotrichion septatum* (0.5–1.5 µm broad, spheroidal cells). **b**, **c** *Primaevifilum delicatulum* (1–3 µm broad, discoidal cells). **d**–**f** *P. minutum* (1–3 µm broad, quadrate cells). **g**–**i** *P. amoenum* (2–5 µm broad, quadrate to discoidal cells). **j**, **k** *Archaeoscillatoriopsis disciformis* (3–6 µm broad, discoidal cells, rounded end cells). **l**–**n** *P. conicoterminatum* (3–6 µm broad, discoidal cells, conical end cells). **o**, **p** *P. laticellulosum* (6–9 µm broad, short-cylinder to quadrate cells)

recognized in the modern biota. The available evidence is inconclusive.

11.2.3 Mode of Occurrence

Geologically mapped initially as a shallow marine facies (Hickman and Lipple 1978; Hickman 1983), the fossiliferous locality of the Apex chert (Schopf 1993) has more recently been reinterpreted to be a brecciated and altered hydrothermal vein deposit (Van Kranendonk 2006). Though such a setting has been suggested to be unlikely for preservation of delicate fossil microbes (Brasier et al. 2002, 2005; Pinti et al. 2009), microorganisms morphologically comparable

to the Apex filaments are common in modern hydrothermal environments (Pentecost 2003); filamentous microbes similar to *Primaevifilum amoenum*, the most abundant of the described Apex taxa (Schopf 1993), have long been known to occur at deep-sea thermal vents (Jannasch and Wirsen 1981); and chert-permineralized fossil filaments, including specimens so similar to those of the Apex chert that they have been assigned to two of the Apex taxa (Ueno et al. 2004), are present in three other Paleoarchean hydrothermal units of the northwestern Australian Pilbara Craton (Rasmussen 2000; Ueno et al. 2001a, b, 2004; Kiyokawa et al. 2006).

As shown in Fig. 11.2a–c, the Apex fossils typically occur in subrounded millimeter-sized carbonaceous chert granules. Within such clasts the Apex fossils are commonly closely spaced, multiple specimens occurring within a given granular clast (Fig. 11.2d–j). Like some of the microfossils permineralized in other Paleoarchean thermal vent deposits, it is possible that the Apex filaments represent remnants of thermophilic microbes preserved *in situ*, in the Apex chert perhaps permineralized in hydrothermally "milled" and rounded organic-rich clasts. Given their mode of occurrence, however, and its similarity to the fossiliferous chert clasts of younger Precambrian units (Fig. 11.2k), it seems to us at least equally likely that the granule-embedded fossils are allocthonous to the deposit, older than or penecontemporaneous with the Apex chert, fossilized mesophiles emplaced in the unit in reworked detrital granules.

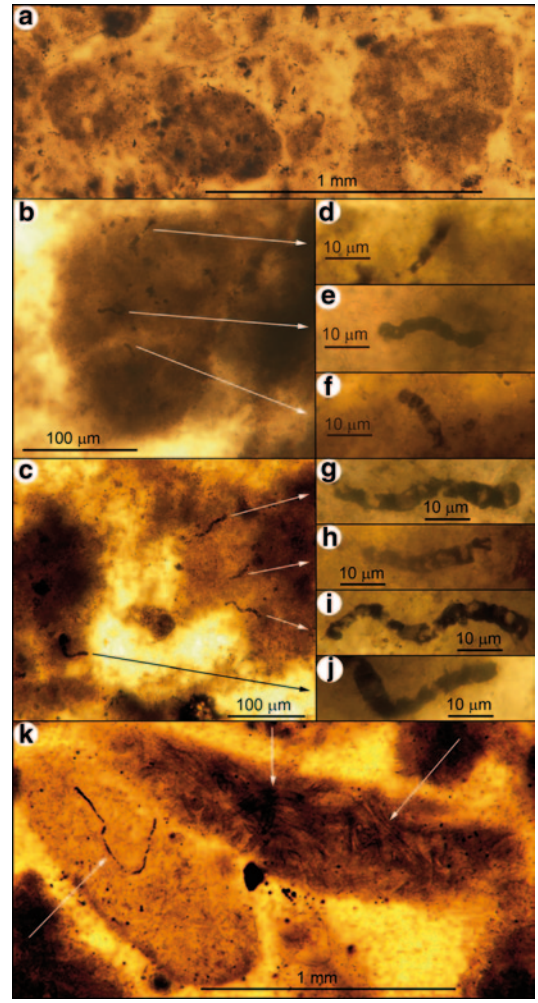

Fig. 11.2 **a**, **b**, **c** Optical photomicrographs of subrounded carbonaceous chert granules, containing cellularly permineralized filamentous fossils embedded in clouds of flocculent organic matter, in petrographic thin sections of the Apex chert. **d** *Primaevifilum minutum*. **e**, **f** *P. delicatulum* **g**–**i** *P. amoenum*. **j** *P. conicoterminatum*. **k** An optical photomicrograph of subrounded fossil-bearing carbonaceous granules in a petrographic thin section of chert from the ~780-Ma-old Auburn Formation of South Australia (Schopf et al. 2005), showing fossiliferous chert granules similar to those of the Apex chert (**a**–**c**) in a younger Precambrian deposit. *Arrows* denote locations of filamentous microfossils

11.3 Establishment of Biogenicity

Establishing the biogenicity of ancient microscopic fossils—the problem of distinguishing bona fide fossil microbes from "fossil-like" mineral grains and other microscopic pseudofossils—posed serious difficulties in the 1960s and '70s when studies of Precambrian microorganisms were just beginning (e.g., Cloud 1973). In the early stages of such studies, the field was plagued by the problem of distinguishing between modern contaminants (air- or water-born pollen, spores, microscopic fungi, micro-algae and the like) and authentic microfossils. This difficulty was resolved by centering investigations on organic-walled three-dimensionally permineralized objects studied in petrographic thin sections

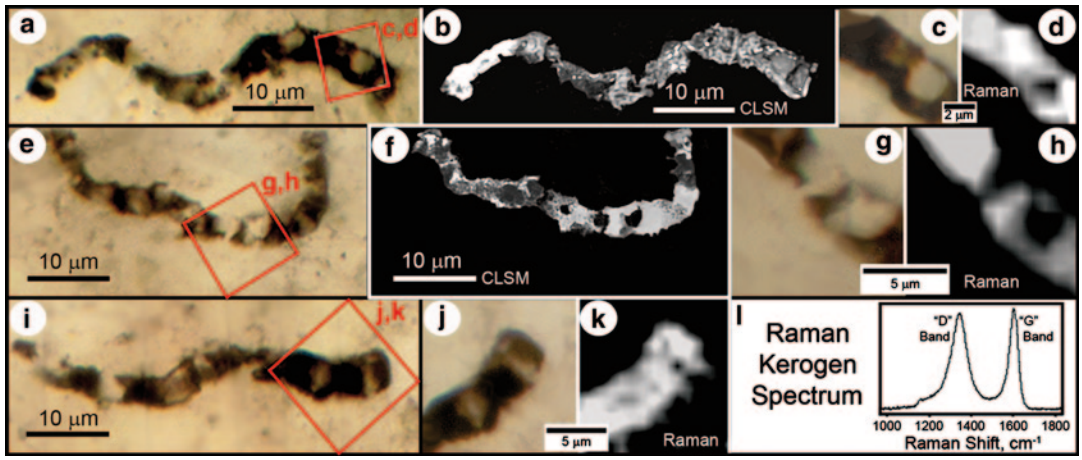

Fig. 11.3 Optical photomicrographs (**a**, **c**, **e**, **g**, **i**, **j**), and CLSM (**b**, **f**) and two-dimensional Raman images (**d**, **h**, **k**) of three specimens of Primaevifilum amoenum in petrographic thin sections of the Apex chert. The *red* rectangle in (**a**) denotes the area in (**c**) and (**d**); that in (**e**), the area in (**g**) and (**h**); and that in (**i**), the area in (**j**) and (**k**). The dark brown color of the fossils (**a**, **c**, **e**, **g**, **i**, **j**) suggests that they are composed of carbonaceous matter, an interpretation supported by their CLSM images (**b**, **f**), derived from laser-induced fluorescence of the interlinked polycyclic aromatic hydrocarbons that comprise their kerogenous cell walls, and that is established both by the 2-D Raman images (**d**, **h**, **k**), acquired at the ~1605^{-1} cm kerogen band, and their Raman spectrum (l)

(such as the Apex fossils shown here), a strategy that demonstrates that such objects are embedded within and indigenous to the investigated rock.

Since those early days, establishment of the biogenicity of microscopic Precambrian fossils has been addressed repeatedly and effectively: comprehensive tabulations have been compiled, separating authentic fossils from non-fossil "lookalikes" (e.g., Schopf and Walter 1983; Mendelson and Schopf 1992), and the characteristics expected of bona fide fossils have been tabulated and discussed in detail in a paper that presents side-by-side comparisons of authentic Precambrian microbes and reported pseudofossils with which they might be confused (Schopf et al. 2010a).

A principal conclusion of such analyses is that of the cascade of mutually reinforcing evidence needed to establish biogenicity, two traits stand out:

1. relatively well-preserved authentic permineralized fossil microorganisms should exhibit cells and cell lumina, discernible walled compartments that typically are devoid of remnants of their originally water-rich cytoplasmic contents; and
2. the three-dimensional walls of such cells should be demonstrably of carbonaceous (kerogenous) composition.

These two prime traits should be expected to be exhibited by permineralized bona fide organic-walled microscopic fossils, backed by additional biogenicity indicators such as the occurrence of specimens ranging from relatively well preserved to partially or completely degraded (for a compilation of such traits, see Schopf et al. 2010a, Table 1).

11.4 Are the Apex Fossils Bona Fide Fossils?

11.4.1 Carbonaceous Composition

Shown here are optical photomicrographs (Fig. 11.3a, e, c, g, i, j), images obtained by confocal laser scanning microscopy, "CLSM" (Fig. 11.3b, f), and two-dimensional (Fig. 11.3d, h, k) and three-dimensional (Fig. 11.4c) Raman images of the Apex fossil Primaevifilum amoenum. CLSM and 2-D and 3-D Raman imagery are techniques relatively new to Precambrian

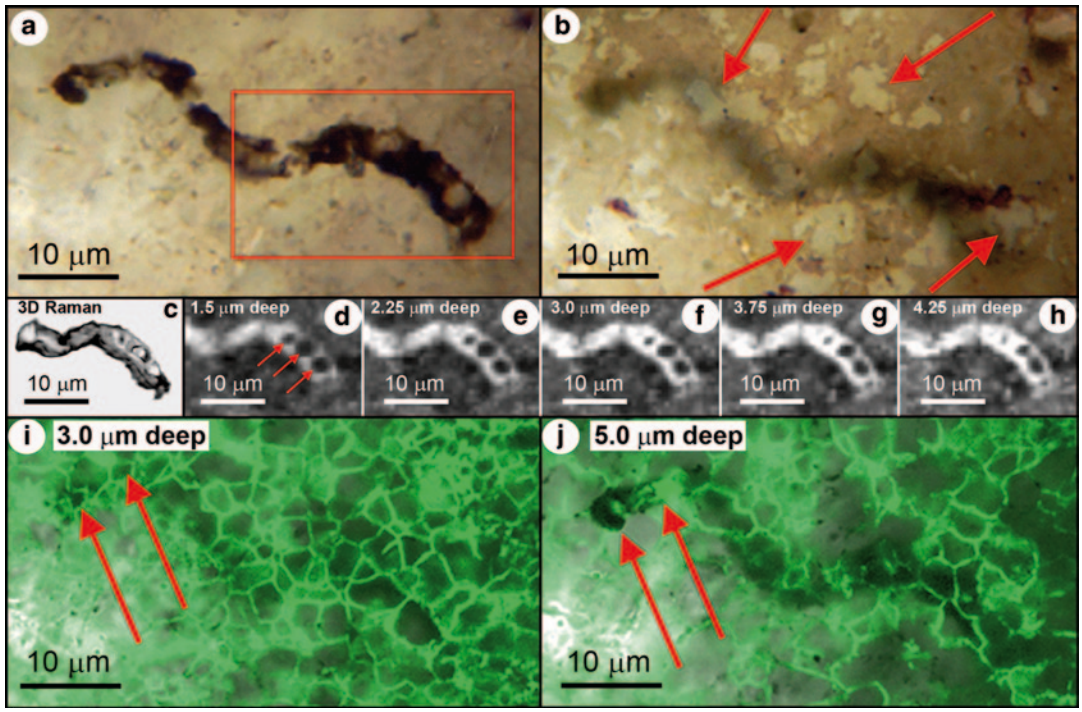

Fig. 11.4 Optical photomicrographs (**a**, **b**), three-dimensional (**c**) and two-dimensional (**d**–**h**) Raman images, and CLSM images (**i**, **j**) of a specimen of Primaevifilum amoenum in a petrographic thin section of the Apex chert. The *red* rectangle in (**a**) denotes the area in (**c**) through (**h**); the Raman images were acquired at the ~1605^{-1} cm kerogen band.The *arrows* in (**b**) point to quartz grains of the fossil-embedding chert matrix, virtually all of which are larger or smaller and more irregularly shaped than the quadrate cells (**a**) of the cylindrical fossil filament (**c**), indicating that it is not composed of organic-coated quartz grains. In (**d**) through (**h**), the box-like cells of the fossil filament are shown in 2-D Raman images (acquired at the ~1605^{-1} cm kerogen band) at the indicated sequentially increasing depths below the upper surface of the fossil images that establish the kerogenous composition of its cell walls (*white*) and the presence of cell lumina, denoted by arrows in (**d**) and shown also in (**e**) through (**h**). The *green* three-dimensional "chicken wire fabric" shown in (**i**) and (**j**) in CLSM images of the fossil-containing area, acquired at the indicated depths below the upper surface of the thin section (in which the *arrows* are provided for orientation), is a product of the laser-induced fluorescence of microscopy immersion oil that penetrated at quartz grain boundaries into the section, an intricate 3-D fabric that differs markedly from the discrete cylindrical fossil and that shows that the filament is not a pseudofossil formed by seepage of organic fluids (e.g., petroleum) into the chert

paleobiology (Kudryavtsev et al. 2001, Schopf et al. 2002, 2005, 2006). The application, effectiveness, and limitations of these techniques for studies of rock-embedded fossils, and the instrumental configurations used to acquire the data presented here, have recently been discussed in detail (Schopf et al. 2010b).

The CLSM images of *P. amoenum* (Fig. 11.3b, f), derived from the laser-induced fluorescence of the interlinked polycyclic aromatic hydrocarbons (PAHs) that comprise the cell walls of this and similarly permineralized organic-walled Precambrian microfossils (Schopf et al. 2005, 2006; Schopf and Kudryavtsev 2010), are consistent with the kerogenous composition of the fossil, as established by its 2-D (Fig. 11.3d, h, k) and 3-D (Fig. 11.4c) Raman images and Raman spectrum (Fig. 11.3l).

11.4.2 Three-Dimensional Cellularity

Raman spectroscopy documents the three-dimensional cellularity of the kerogenous cell walls of a representative specimen of the Apex fossil Primaevifilum amoenum illustrated in

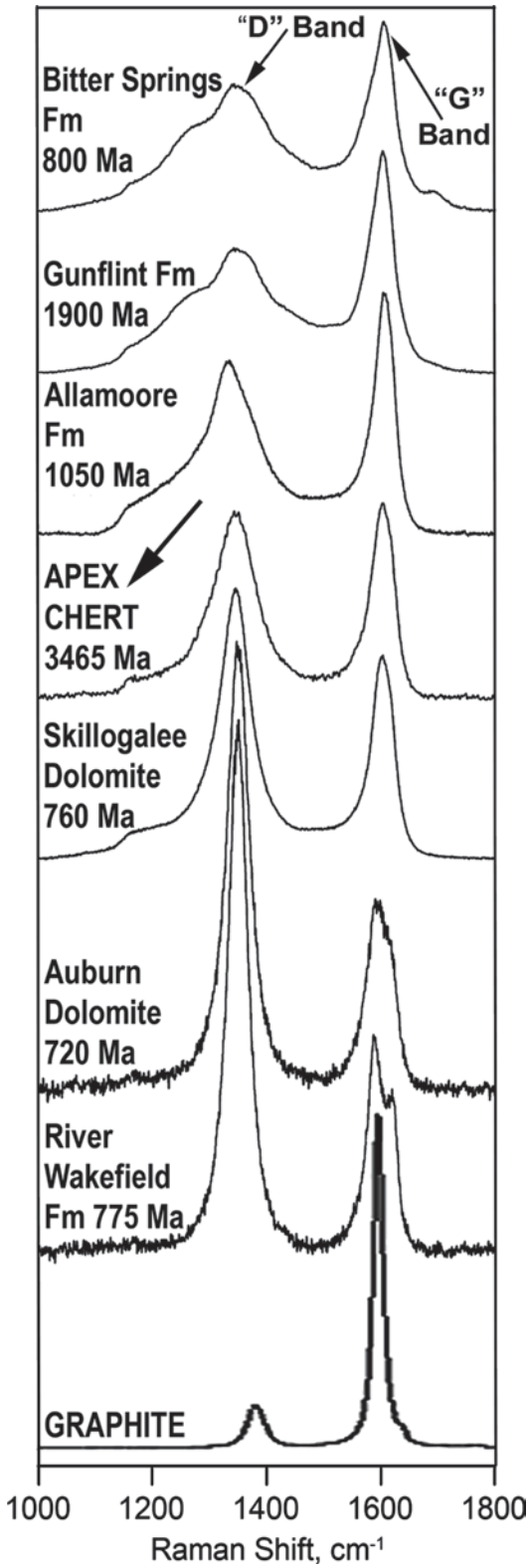

Fig. 11.4c–h. Optical microscopy (Fig. 11.4a, b) shows that the kerogen-defined cells of this specimen are not a result of non-biological organic coating of the irregularly shaped quartz grains in which the Apex fossils are embedded. And CLSM images show that the fossil is not be a result of the penetration of organic fluids (e.g., petroleum) into the chert, a process that results in a three-dimensional "chicken-wire" fabric unlike that of such cellularly permineralized microorganisms (Fig. 11.4i, j).

11.4.3 Organic Geochemical Maturity

Does the composition of the organic matter that comprises the Apex fossils fit with that of microfossils similarly preserved in other Precambrian deposits?

In Fig. 11.5 are compared the Raman spectra of organic-walled fossils chert-permineralized in seven Precambrian units, including the Apex chert (Fig. 11.5, broad arrow), ordered by their geochemical maturation from less mature (top) to more mature (bottom). As these data show, the primary Raman bands of the kerogenous cell walls of such fossils change in relative intensity and width as geochemical alteration results in an increase in the domain-size and orderly stacking of their PAH-dominated graphene layers (Schopf et al. 2005). The spectra illustrated show that the Apex fossils are more geochemically mature than those of the ~800 Ma Bitter Springs and ~1900 Ma Gunflint Formations—but are appreciably better preserved, less geochemically altered, than the partially graphitized fossils of

Fig. 11.5 Raman spectra of kerogen comprising fossils of the Apex chert (*broad arrow*) and similarly permineralized microfossils in six other Precambrian cherts—ordered, from top to bottom, by the changes in the Raman "D" and "G" bands of kerogen (denoted by *narrow arrows* at the top of the figure) that accompany geochemical maturation (Schopf et al. 2005)—compared with the Raman spectrum of graphite (bottom). This comparison demonstrates that the kerogen comprising the Apex fossils is similar to that of other chert-permineralized Precambrian microorganisms and is not graphite

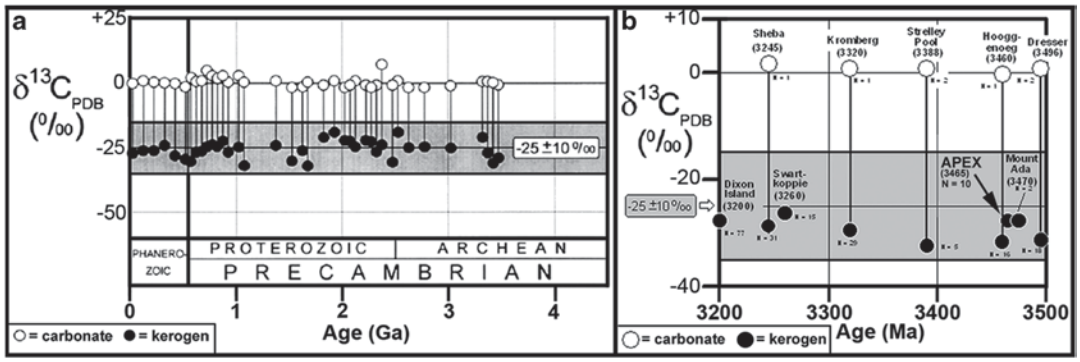

Fig. 11.6 Carbon isotopic composition of biogenic kerogen and co-existing inorganic carbonate carbon. The Precambrian data in **a** measured in 100 geological units (Strauss and Moore 1992; Schopf 2004) and those in **b** based on ~200 measurements of nine Paleoarchean microfossil-bearing cherts (Schopf 2006). These data show that carbon isotopic evidence of CO_2-based autotrophy extends from the present to ~3,500 Ma ago (**a**) and that the carbon isotopic composition of the organic matter of the Apex chert (**b**, *arrow*) is like that of eight other similarly ancient fossil-bearing chert units

the ~720 Ma Auburn and ~775 River Wakefield Formations.

Chert-permineralized carbonaceous fossils from more than a score of Precambrian geological units have been characterized by this same technique (Schopf et al. 2005), results showing that the kerogenous composition of the Apex fossils fits with that of all similarly analyzed permineralized ancient microscopic organisms. Importantly, such data establish that the Apex fossils are not composed of graphite, as proposed by Brasier et al. (2002, 2005), as is evident from comparison of the Raman spectrum of an Apex fossil (Fig. 11.5, broad arrow) with that of graphite (Fig. 11.5, bottom spectrum).

11.4.4 Carbon Isotopic Composition

Throughout the geological record from ~3500 Ma to the present, preserved carbonaceous matter typically exhibits a $\delta^{13}C_{PDB}$ value of -25 ± 10‰ (Fig. 11.6a), a signature of biological (autotrophic) carbon-fixation (cf. House et al. 2003). The carbon isotopic composition of the Apex organics, having an average $\delta^{13}C_{PDB}$ value of −27.7‰ (n = 10; Schopf 2006)—similar to the $\delta^{13}C_{PDB}$ value of −28.8‰ (n = 192; Schopf 2004) of kerogens preserved in eight other 3200–3500 Ma deposits from which microfossils have been reported (Fig. 11.6b)—is consistent with a biological origin. The carbon isotopic composition of the Apex organic matter thus supports interpretation of the fossil assemblage as including CO2-fixing autotrophs, but it is insufficient to establish that such microbes were photoautotrophs, whether oxygenic or anoxygenic (Schopf 1993; House et al. 2003).

11.4.5 Organic Geochemical Composition

As established by Raman spectroscopy (Fig. 11.5; Schopf et al. 2002, 2007), the Apex fossils are composed of carbonaceous matter. This finding, showing the non-graphitic nature of such material and associated organic detritus has been confirmed by numerous other techniques (De Gregorio and Sharp 2003, 2006; De Gregorio et al. 2005, 2009), with these and related studies having rendered implausible an abiotic origin for the organic matter preserved in this and other ancient deposits (cf. Ueno et al. 2004) and indicating that the Apex organics are "consistent with the interpretation that the microbial-like features in the Apex chert are bona fide microfossils" (De Gregorio et al. 2005, p. 1866).

More recently, DeGregorio et al. (2009) used data acquired by transmission electron microscopy (TEM), electron loss near-edge structure spectroscopy (ELNES), synchrotron-based scanning-transmission X-ray microscopy (STXM), STXM-based X-ray absorption near-edge spectroscopy (XANES), and secondary ion mass spectroscopy (SIMS) to characterize the structure, carbon bonding, functional group chemistry, and light element composition of the carbonaceous components of the Apex chert. Highlights of their results can be summarized as follows:

1. The ELNES-detectable peak (at 292 eV) characteristic of graphite and highly disordered graphitic carbon is not present in Apex carbonaceous matter. This finding confirms that the Apex carbonaceous matter is kerogen, as originally inferred (Schopf 1992, 1993), not graphite as postulated by Brasier et al. (2002, 2005).
2. "In addition, Apex carbonaceous matter [is composed of] chemically complex organic materials rather than simple hydrocarbon materials … [and] contains … nitrogen, sulfur, and phosphorous … in which the presence of phosphorus, in particular, implies a biogenic origin" (De Gregorio et al. 2009, p. 632). This result, combined with Raman and ELNES data documenting the presence of carbon, oxygen and hydrogen, shows that the Apex organic matter is composed of all of the biologically definitive elements, C, H, O, N, S and P—a firm indicator of biogenicity.
3. "C-XANES spectra acquired from … Apex carbonaceous matter [show spectral features], including the presence of carboxyl [-COOH] and phenol [$C_{aromatic}$-OH] peaks" (De Gregorio et al. 2009, p. 632), chemical functional groups characteristic of biogenic kerogen that do not occur in graphite.

From this detailed study, De Gregorio et al. (2009, p. 631) conclude that "the Apex microbe-like features represent authentic biogenic organic matter," an interpretation consistent with the reported presence of geochemical biomarkers in the geological unit immediately underlying the Apex chert that "support a scenario according to which life was present on Earth 3.5 By ago" (Derenne et al. 2008, p. 480).

11.5 Suggested Nonbiologic Origins

11.5.1 Abiotic Graphitic Pseudofossils

The data presented here show that the Apex fossils are cellular (Figs. 11.1–11.4), not solid, and are composed of biogenic kerogen, not graphite derived from abiotic organic syntheses. They are not opaque minerals, not contaminants, and not products of permeating organic fluids (Figs. 11.3, 11.4). Further, as discussed below, the Raman-documented molecular structure and geochemical maturity of their carbonaceous components (Figs. 11.3l, 11.5) and that of associated flocculent kerogen (Fig 11.2a–c) are essentially identical, showing that all of the organics of the Apex chert have experienced the same geological history. Although, in comparison with much younger Precambrian fossils, their cells (Figs. 11.1–11.4) and kerogenous constituents (Fig. 11.5) are not particularly well preserved (e.g., see the references cited in Mendelson and Schopf 1992), their biogenicity is consistent with all relevant evidence: their cellular and organismal morphology is like that of modern microbes and other permineralized fossil microscopic organisms; their mode of occurrence and cellular degradation is similar to that of other organic-walled Precambrian microfossils; the biology-consistent carbon isotopic composition of Apex organics fits with thousands of analyses, including those of organic matter in deposits of comparable age; the chemistry of the Apex organics shows it to be biogenic, not abiotic; and the Apex fossils, like those known from geological units of a similar age, are consistent with the history of early life. Moreover, and perhaps most notably, nonbiologically produced particulate organic matter—such as that that postulated to compose the Apex fossils (Brasier et al. 2002, 2005)—has not been reported to occur in the geological record.

11.5.2 Barium Carbonate "Biomorphs"

Millimeter- to micron-sized filamentous, spiral, and radiating "biomorphic" crystallites

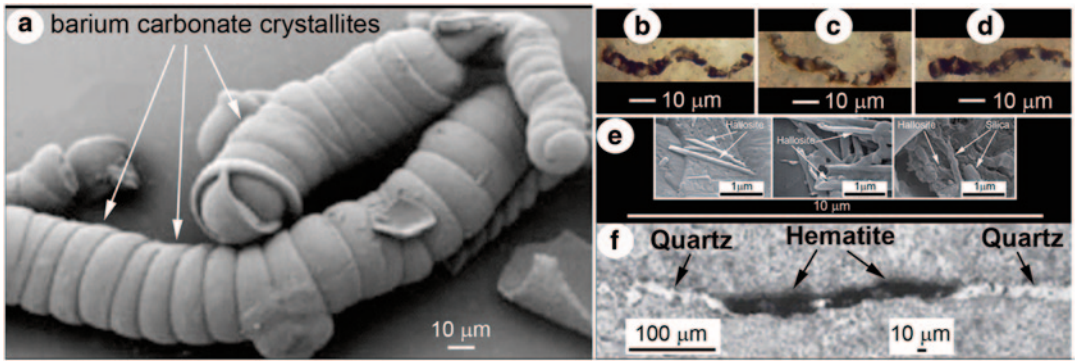

Fig. 11.7 Scanning electron micrographs (**a**, **e**) and optical photomicrographs (**b**–**d**, **f**) comparing (**a**) laboratory synthesized barium carbonate crystallite "biomorphs" (García-Ruíz et al. 2003, Fig. 2A, reprinted by permission); (**b**–**d**) filamentous microfossils of the Apex chert, imaged in petrographic thin sections; (**e**) clay and silica mineral pseudofossils reported from the Apex chert (Pinti et al. 2009, Figs. 1h, 2h and i, reprinted by permission); and (**f**) an Apex chert hematite-infilled pseudofossil veinlet (Marshall et al. 2011, Fig. S2, reprinted by permission). Such barium carbonate (witherite) "biomorphs" (**a**) lack cell-defining kerogenous cell walls (Fig. 11.4d–h) and have not been reported from the geological record. The clay and silica pseudofossils (**e**)—objects that are mineralic, not carbonaceous like the Apex fossils, and are straight and needle-like, not sinuous and cellular as are the Apex fossils—are much too small to be confused with the Apex fossils (**b**–**d**). Unlike the Apex fossils, hematite veinlets (**f**) are rock-transecting planar structures, not rock-embedded cylindrical filaments; are mineralic, rather than carbonaceous; and are solid, rather than cellular. These pseudofossils (**a**, **e**, **f**) differ distinctly from the bona fide fossils of the Apex chert (**b**–**d**)

of co-precipitated barium carbonate ($BaCO_3$, witherite) and silica (SiO_2), the most minute of which resemble certain of the Apex fossils (e.g., Fig. 11.7a), have been synthesized in laboratory experiments by García-Ruíz et al. (2002, 2003). Rather than being composed of organic-walled box-like cells, however, such structures are solid nanocrystals, their surficial cell-like segmentation (Fig. 11.7a) reflecting the presence of grain boundaries that separate adjacent crystallites, not the transverse carbonaceous walls that define microbial filaments.

Although such crystallites can be enveloped by a silica skin (Kunz and Kellermeir 2009; García-Ruíz et al. 2009) capable of absorbing introduced organics on their exterior surfaces (García-Ruíz et al. 2003), their lack of cellular organization—were they to be found in nature—would allow them to be distinguished from bona fide fossils (Schopf et al. 2010a). However, like the graphite pseudofossils proposed by Brasier et al. (2002, 2005) to be composed of abiotically generated organic matter, such witherite-silica "biomorphs" are unknown in the geological record.

11.5.3 Clay Mineral Pseudofossils

Needles composed of hallosite ($Al_2Si_2O_5[OH]_4$), a clay mineral, and of quartz (SiO_2), have been compared with the Apex fossils (Pinti et al. 2009). These mineralic needles, however, are more than 40 times narrower than the carbonaceous Apex fossils (Fig. 11.7e) and, like the "biomorphs" discussed above, the needles are neither cellular nor kerogenous. The authors of this work acknowledge that their "… observations are not applicable to the microfossils of the Apex chert … because [they] did not observe carbonaceous filaments" (Pinti et al. 2009, pp. 640, 642).

11.5.4 Hematite Veinlet Pseudofossils

Hematite- (Fe_2O_3-) infilled secondary veinlets in the Apex chert have also been compared with the Apex fossils (Marshall et al. 2011), primarily because the authors of this work assumed that reports of the carbonaceous composition of the fossils were based on the ~1350 cm^{-1} Raman band of kerogen—which they imagined might have been mistaken for the ~1330 cm^{-1} Raman

band of hematite—rather than the source of the data, the ~1605 cm^{-1} Raman band of kerogen (as specified in Figs. 11.3d, h, k; 11.4c–h). This error of misinterpreting mineral veinlets to be authentic fossils has a well-documented history (Schopf et al. 2010a).

As has been previously discussed (Schopf and Kudryavtsev 2011), the hematite-infilled veinlets described by Marshall et al. (2011) differ markedly from the Apex fossils: the veinlets are mineralic (Fig. 11.7f), not carbonaceous (Fig. 11.3b, d, f, h, k); are rock-transecting planar structures, not rock-embedded cylindrical filaments (Fig. 11.4c–h); are more or less straight (Fig. 11.7f), not sinuous (Fig. 11.7b–d); and are relatively large, having an average diameter of 17 μm and a size-range of 4–65 μm (n = 50; Marshall et al. 2011, p. 240), about three times broader than the Apex fossils (avg. diameter = 6 μm, range = 0.5–19 μm, n = 1788; Schopf 1993).

11.5.5 Multiple Generations of Kerogen

Based on differences in the Raman spectra of samples of Apex kerogen, primarily a difference in the intensity of their Raman "D" bands (Fig. 11.8a, b), Marshall et al. (2012) suggested that the Apex chert contains two generations of carbonaceous matter. However, as is shown here by Raman spectra of particulate and microfossil-comprising kerogens analyzed in single thin sections of Apex, Skillogalee, and River Wakefield fossiliferous cherts (Fig. 11.8c; Schopf et al. 2005), such differences are typical of the spectra of geochemically relatively mature chert-permineralized carbonaceous matter (Fig. 11.5). Such differences are not due to a polarization effect; rather, as is discussed below, they evidence the orientation of Raman-analyzed kerogens composed of stacked, large PAH-domain-dominated graphene layers.

As first shown for highly oriented pyrolytic graphite (HOPG) by Katagiri et al. (1988) and, later, in studies of similar materials (e.g., Compagnini et al. 1997; Kawashima and Katagari 1999; Tan et al. 2004), the intensity of the "D" band (relative to the "G" band) of such carbonaceous matter is a function of the relative contributions of the Raman signatures of the basal planes and edge planes of the material studied. Such signatures are sensitive to the orientation of the analyzed specimen, spectral features of the edge planes being due to molecular discontinuities at the periphery of the large-domain components of their graphene layers (Katagiri et al. 1988).

In chert samples containing geochemically relatively mature permineralized kerogen, randomly oriented particles that comprise flocculent carbonaceous clouds (Fig. 11.2a–c) can be oriented such that molecular discontinuities at the periphery of their stacked large-domain PAHs produce a Raman signature exhibiting edge plane features such as the enhanced kerogen "D" band reported by Marshall et al. (2012). In contrast, in geochemically less altered kerogens the domain size of the PAHs that comprise the graphene layers is very much smaller and, because Raman averages molecular compositions over the ~1-μm-diameter area of the focused laser beam, such edge plane features are not detectable. It is notable, however, that unlike the randomly oriented particles of carbonaceous clouds, the kerogenous cell walls of permineralized fossils are composed of regularly stacked platelets of graphene layers (Kempe et al. 2002, 2005). Thus, in Raman spectra of permineralized organic-walled fossils, such as those of the Apex chert, the relative intensity of the "D" and "G" bands is uniform throughout an individual specimen and is invariant for all fossils of any particular biological community—as has been shown for diverse chert-permineralized carbonaceous fossils (Schopf et al. 2002, 2005, 2007, 2008, 2010a, c)—a Raman signature consistent with their biogenicity.

The minor spectral differences reported by Marshall et al. (2012) are detectable only in geochemically relatively mature kerogens, such as those preserved in the Apex, Skillogalee, and River Wakefield cherts (Fig. 11.8c), but not in less altered kerogens such as those of the Bitter Springs and Gunflint Formations (Fig. 11.5). Raman analyses show that the geochemical maturity of the Apex carbonaceous fossils (Figs. 11.3l,

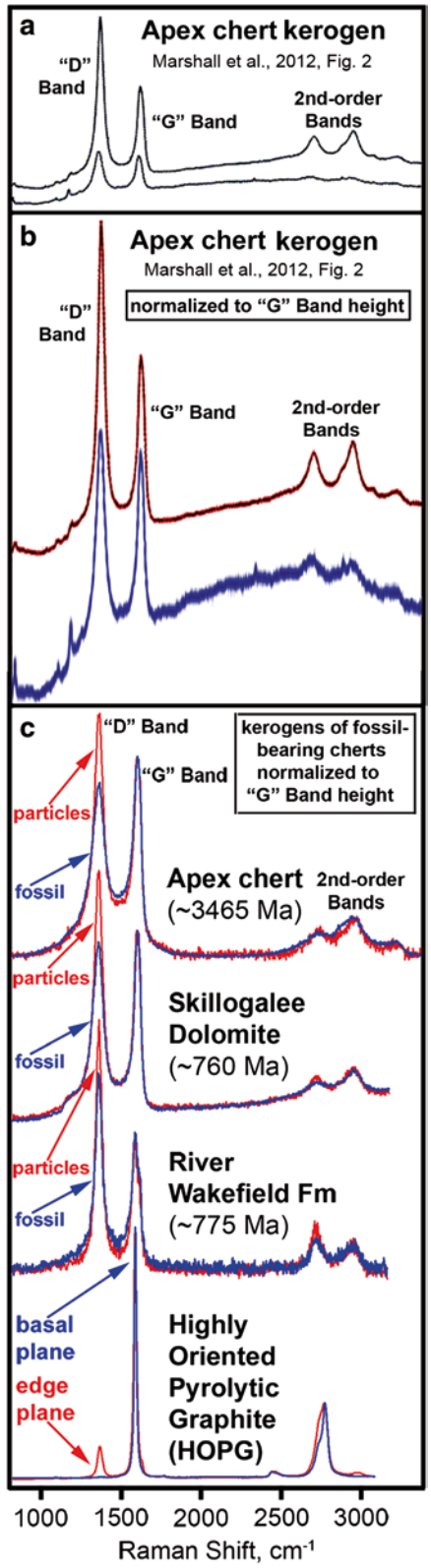

11.5) is the same as that of the associated flocculent kerogen (Fig. 11.2a–c), a characteristic of the co-existing permineralized fossils and particulate kerogens similarly analyzed in more than 20 other Precambrian microbial communities (Schopf and Kudryavtsev 2005, 2010; Schopf et al. 2005, 2008, 2010c). Raman spectra of the Apex kerogens do not evidence two generations of carbonaceous matter.

11.6 Discussion

Studies of rock-embedded carbonaceous microscopic fossils have advanced markedly over the two decades since the Apex microbes were first reported (Schopf and Packer 1987) and formally described (Schopf 1992, 1993). Foremost among such advances are two analytical techniques, both having sub-micron spatial resolution:

1. Raman spectroscopy, a technique that can provide two-dimensional (Figs. 11.3d, h, k; 11.4d–h; Schopf et al. 2002, 2005) and three-dimensional kerogen-derived images (Fig. 11.4c; Schopf and Kudryavtsev 2005, 2010; Schopf et al. 2010b) of permineralized organic-walled microscopic fossils and of their embedding minerals, to a depth of ~150 μm—a thickness equivalent to that of five standard 30-μm-thick petrographic thin

Fig. 11.8 **a** Raman spectra of kerogen analyzed in a petrographic thin section of the Apex chert as reported by Marshall et al. (2012). **b** The spectra in **a** normalized to the height of their kerogen "G" bands. **c** Spectra of permineralized kerogenous fossils and particulate kerogen analyzed in thin sections of cherts of the Apex, Skillogalee, and River Wakefield geological units (the analyses of each derived from specimens in a single thin section) and of highly oriented pyrolytic graphite, "HOPG."The spectra in **a** appear to differ primarily because they were not normalized to the "G" band of kerogen **b**. Differences in the intensity of the "D" band in "G" band-normalized spectra (**c**) are typical of geochemically relatively mature kerogens, such as those of the Apex, Skillogalee, and River Wakefield deposits (**c**), composed of relatively large-domain PAHs that dominate their stacked graphene layers. As documented by Katagiri et al. (1988) for HOPG (**c**, bottom spectrum), such spectral differences are a function of the relative contributions of the Raman signatures of the basal planes and edge planes of the material analyzed

sections—introduced to such studies only a decade ago (Kudryatsev et al. 2001).

2. Confocal laser scanning microscopy, an analytical technique that for carbonaceous fossils is based on detection of laser-induced fluorescence emitted from the interlinked polycyclic aromatic hydrocarbons that comprise their kerogenous cell walls (Fig. 11.3b, f)—a technique, like Raman, applicable to thin section-embedded fossils to depths of ~150 μm—introduced to Precambrian paleobiology some six years ago (Schopf et al. 2006) that has recently been shown effective for studies of permineralized fossil animals, plants, fungi, protists and prokaryotes (Schopf et al. 2010b).

These two new techniques have improved studies of the Precambrian fossil record (Schopf and Kudryatsev 2010) and, as is shown in Fig. 11.3 for fossils of the Apex chert, are especially useful for establishment of biogenicity: applied in situ to the same specimen, and backed by optical microscopy, they can be used together to document a one-to-one correlation of cellular morphology and organic composition, a hallmark of biologic systems. Yet another novel technique, secondary ion mass spectroscopy (SIMS), holds promise for such studies. Since its introduction to investigations of Precambrian microfossils (House et al. 2000), SIMS has been used to document the light-element isotopic composition of thin section surface-exposed microscopic fossils in several Precambrian deposits to provide additional evidence of biogenicity (e.g., Oehler et al. 2006, 2009; Wacey et al. 2011).

Major advances have also been made in techniques used to analyze the chemical composition of ancient organic matter, as shown effectively by De Gregorio et al. (2009) who used ELNES, TEM, STXM, XANES and SIMS to document the biogenicity of the kerogen of the Apex chert, on the basis of which, as noted above, they conclude that the Apex fossils are composed of biogenic organic matter.

Twenty years ago, when the Apex fossils were first described, neither Raman, nor CLSM, nor any of the modern geochemical techniques (e.g., ELNES, TEM, STXM, XANES and SIMS) had been applied to analyses of these or any other Precambrian fossils. Then, the three-dimensional organismal morphology of the Apex filaments, discernible by optical microscopy, could be illustrated only by photomicrographs acquired at varying optical depths that were literally pasted together to demonstrate the typically sinuous organismal form of fossils detected (Schopf 1992, 1993). No analytical technique—provided now by Raman spectroscopy—was available to establish the kerogenous composition of these or any other rock-embedded ancient fossils, an inference that could be drawn (as it had been for the preceding 40 years) based only on the dark brown "organic-like" color of their cell walls (e.g., Barghoorn and Schopf 1965; Barghoorn and Tyler 1965; Cloud 1965).

The application of these new techniques has shown that the biogenic interpretation of the Apex fossils proposed 20 years ago—and, by extension, that of a great many other Precambrian microbes described over the past five decades—remains valid. This is reassuring, for if the early workers had been wrong, if their assumption of organic composition and biogenicity based on the color and optically discernible morphology of such fossils had been mistaken, understanding of the early history of life would be grievously in error. Indeed, if the detailed laboratory work carried out on the Apex fossils and their associated organic matter had proven incapable of establishing biogenicity in rocks from Earth's geological record—where interpretations are backed by decades of studies of Precambrian microscopic fossils, microbially produced stromatolites, and a large body of data documenting the elemental, molecular and carbon isotopic composition of preserved organic matter—how would this science fare in attempts to document evidence of ancient life on other planets such as Mars?

11.7 Conclusion

As summarized here, the ~3465 Ma fossils and associated organic components of the Apex chert have been studied in detail. A host of analytical techniques—most notably, 2-D and 3-D Raman imagery (Figs. 11.3d, h, k, 11.4c–h, 11.5), CLSM imagery (Figs. 11.3b, f, 11.4i, j), and methods used to characterize the chemistry of geochemically

altered organic matter (De Gregorio et al. 2009)—have been applied to the Apex chert, establishing the biogenicity of the exceedingly ancient microbial assemblage and organic matter that it contains. The decade-long controversy over the biogenicity of the Apex fossils has been resolved: "microbial life was present and flourishing on the early Earth ~3500 Ma ago" (Schopf et al. 2010d).

Acknowledgements This paper, invited by the editors of this volume, is a slightly altered recast version of an invited review article published in Gondwana Research (http://dx.doi.org/10.1016/j.gr.2012.07.003), here reprinted with permission from Elsevier. For helpful comments, we thank Malcolm R. Walter, J. Shen-Miller, Ian Foster, Sean Loyd, and the anonymous reviewers of this manuscript.

References

Awramik SM, Schopf JW, Walter MR (1983) Filamentous fossil bacteria from the Archean of Western Australia. Precam Res 20:357–374

Barghoorn ES, Schopf JW (1965) Microorganisms from the Late Precambrian of central Australia. Science 150:337–339

Barghoorn ES, Tyler SA (1965) Microorganisms from the Gunflint chert. Science 147:563–577

Brasier MD, Green OR, Jephcoat AP, Kleppe AK, Van Kranendonk MJ, Lindsay JF, Steele A, Grassineau NV (2002) Questioning the evidence of Earth's oldest fossils. Nature 416:76–81

Brasier MD, Green OR, Lindsay JF, McLoughlin N, Steele A, Stoakes C (2005) Critical testing of Earth's oldest putative fossil assemblage from the ~ 3.5 Ga Apex chert, Chinaman Creek, Western Australia. Precam Research 140:55–102

Cloud P (1965) Significance of the Gunflint (Precambrian) microflora. Science 148:27–45

Cloud P (1973) Pseudofossils: a plea for caution. Geology 1:123–127

Compagnini G, Puglisi O, Foti G (1997) Raman spectra of virgin and damaged graphite edge planes. Carbon 35:1793–1797

De Gregorio BT, Sharp TG (2003) Determining the biogenicity of microfossils in the Apex chert, Western Australia, using transmission electron microscopy. Lunar Planet Sci 34:1267

De Gregorio BT, Sharp TG (2006) The structure and distribution of carbon in 3.5 Ga Apex chert: implications for the biogenicity of Earth's oldest putative microfossils. Amer Mineral 91:784–789

De Gregorio BT, Sharp TG, Flynn GF (2005) A comparison of the structure and bonding of carbon in Apex chert kerogenous material and Fischer-Tropsch-Type carbons. Lunar Planet Sci 36:1866

De Gregorio BT, Sharp TG, Flynn GJ, Wirick S, Hervig RL (2009) Biogenic origin for Earth's oldest putative microfossils. Geology 37:631–634

Derenne S, Robert F, Skrzypczak-Bonduelle A, Gourier D, Binet L, Rouzaud J-N (2008) Molecular evidence for life in the 3.5 billion year old Warrawoona chert. Earth Planet Sci Lett 272:476–480

García-Ruíz JM, Carnerup A, Christy AG, Welham NJ, Hyde ST (2002) Morphology: an ambiguous indicator of biogenicity. Astrobiology 2:353–369

García-Ruiz JM, Hyde ST, Carnerup AM, Christy AG, Van Kranendonk MJ, Welham NJ (2003) Self-assembled silica-carbonate structures and detection of ancient microfossils. Science 302:1194–1197

García-Ruiz JM, Merero-Garcia E, Hyde ST (2009) Morphogenesis of self-assembled nanocrystalline materials of barium carbonate and silica. Science 323:362–365

Groves DI, Dunlop JSR, Buick R (1981) An early habitat of life. Sci Am 245:64–73

Hickman AH (1983) Geology of the Pilbara block and its environs. Geol Surv West Aust Bull 127:1–268

Hickman AH, Lipple SL (1978) Explanatory notes, Marble Bar 1:250,000 Geological Map Series. Geol Surv West Aust, Perth, Australia, 24

House CH, Schopf JW, McKeegan KD, Coath CD, Harrison TM, Stetter KO (2000) Carbon isotopic composition of individual Precambrian microfossils. Geology 28:707–710

House CH, Schopf JW, Stetter KO (2003) Carbon isotopic signatures of biochemistry: fractionation by archaeans and other thermophilic prokaryotes. Org Geochem 3:345–356

Jannasch HW, Wirsen CO (1981) Morphological survey of microbial mats near deep-sea thermal vents. Appl Environ Microbiol 41:528–538

Katagiri G, Ishida H, Ishitani A (1988) Raman spectra of graphite edge planes. Carbon 26:565–571

Kawashima Y, Katagari G (1999) Observation of the out-of-plane mode in the Raman scattering from the graphite edge plane. Phys Rev B 59:62–64

Kempe A, Schopf JW, Altermann W, Kudryavtsev AB, Heckl WM (2002) Atomic force microscopy of Precambrian microscopic fossils. Proc Natl Acad Sci U S A 99:9117–9120

Kempe A, Wirth R, Altermann W, Stark RW, Schopf JW, Heckle WM (2005) Focussed ion beam preparation and in situ nanoscopic study of Precambrian acritarchs. Precam Res 140:36–54

Kiyokawa S, Ito T, Ikehara M, Kitajima F (2006) Middle Archean volcano-hydrothermal sequence: bacterial microfossil-bearing 3.2-Ga Dixon Island Formation, coastal Pilbara terrane, Australia. Geol Soc Amer Bull 118:3–22

Kudryavtsev AB, Schopf JW, Agresti DG, Wdowiak TJ (2001) In situ laser-Raman imagery of Precambrian microscopic fossils. Proc Natl Acad Sci U S A 98:823–826

Kunz W, Kellermeir M (2009) Beyond biomineralization. Science 323:244–245

Marshall CP, Emry JR, Marshall AO (2011) Haematite pseudomicrofossils present in the 3.5-billion-year-old Apex chert. Nature Geosci 4:240–243

Marshall AM, Emry JR, Marshall CP (2012) Multiple generations of carbon in the Apex Chert and implications for preservation of microfossils. Astrobiology 12:160–166

Mendelson CV, Schopf JW (1992) Proterozoic and selected Early Cambrian microfossils and microfossil-like objects. In: Schopf JW, Klein C (eds) The Proterozoic biosphere, a multidisciplinary study. Cambridge University Press, New York, pp 865–951

Oehler DZ, Robert F, Mostefaoui S, Meiborn A, Selo M, McKay DS (2006) Chemical mapping of Proterozoic organic matter at sub-micron spatial resolution. Astrobiology 6:838–850

Oehler DZ, Robert F, Walter MR, Sugatani K, Allwood A, Meiborn A, Mostefaoui S, Selo M, Thomen A, Gibson EK (2009) NanoSIMS: insights into biogenicity and syngenicity of Archean carbonaceous structures. Precam Res 173:70–78

Pentecost A (2003) Cyanobacteria associated with hot spring travertines. Can J Earth Sci 40:1447–1457

Pinti DL, Mineau R, Clement V (2009) Hydrothermal alteration and microfossil artefacts of the 3,465-million-year-old Apex chert. Nature Geosci 2:640–643

Rasmussen B (2000) Filamentous microfossils in a 3235-million-year-old volcanogenic massive sulphide deposit. Nature 405:676–679

Schopf JW (1992) Paleobiology of the Archean. In: Schopf JW, Klein C (eds) The Proterozoic biosphere, a multidisciplinary study. Cambridge University Press, New York, pp 25–39

Schopf JW (1993) Microfossils of the early archean apex chert: new evidence of the antiquity of life. Science 260:640–646

Schopf JW (1999) Cradle of life. Princeton University Press, Princeton, pp 1–367

Schopf JW (2004) Earth's earliest biosphere: status of the hunt. In: Eriksson PG, Altermann W, Nelson DR, Mueller WU, Catuneanu O (eds) The Precambrian earth: tempos and events. Elsevier, New York, pp 516–539

Schopf JW (2006) Fossil evidence of Archaean life. Philos Trans R Soc Lond B Biol Sci 361:869–885

Schopf JW, Kudryavtsev AB (2005) Three-dimensional Raman imagery of precambrian microscopic organisms. Geobiology 3(1):1–12

Schopf JW, Kudryavtsev AB (2010) A renaissance in studies of ancient life. Geol Today 26:141–146

Schopf JW, Kudryavtsev AB (2011) Biogenicity of apex chert microstructures. Nature Geosci 4:346–347

Schopf JW, Packer BM (1987) Early Archean (3.3-billion to 3.5-billion-year-old) microfossils from Warrawoona Group, Australia. Science 237:70–73

Schopf JW, Walter MR (1983) Archean microfossils: new evidence of ancient microbes. In: Schopf JW (ed) Earth's earliest biosphere, its origin and evolution. Princeton University Press, Princeton, pp 214–239

Schopf JW, Kudryavtsev AB, Agresti DG, Wdowiak TJ, Czaja AD (2002) Laser-Raman imagery of Earth's earliest fossils. Nature 416:73–76

Schopf JW, Kudryavtsev AB, Agresti DG, Czaja AD, Wdowiak TJ (2005) Raman imagery: a new approach to assess the geochemical maturity and biogenicity of permineralized Precambrian fossils. Astrobiology 5:333–371

Schopf JW, Tripathi A, Kudryavtsev AB (2006) Three-dimensional confocal optical microscopy of Precambrian microscopic organisms. Astrobiology 6:1–16

Schopf JW, Kudryavtsev AB, Czaja AD, Tripathi AB (2007) Evidence of Archean life: stromatolites and microfossils. Precam Res 158:141–155

Schopf JW, Tewari VC, Kudryavtsev AB (2008) Discovery of a new chert-permineralized microbiota in the Proterozoic Buxa formation of the Ranjit window, Sikkim, India, and its astrobiological implications. Astrobiology 8:735–746

Schopf JW, Kudryavtsev AB, Sugitani K, Walter MR (2010a) Precambrian microbe-like pseudofossils: a promising solution to the problem. Precam Res 179:191–205

Schopf JW, Kudryavtsev AB, Tripathi B, Czaja AD (2010b) Three-dimensional morphological (CLSM) and chemical (Raman) imagery of cellularly mineralized fossils. In: Allison PA, Bottjer DJ (eds) Taphonomy: process and bias through time. Springer, Amsterdam, pp 457–486

Schopf JW, Kudryavtsev AB, Sergeev VN (2010c) Confocal laser scanning microscopy and Raman imagery of the late Neoproterozoic Chichkan microbiota of South Kazakhstan. J Palaeontol 84:402–416

Schopf JW, Walter MR, Hofmann HJ (2010d) Hot rocks, hot topic. New Scientist, 2010(2749):27 (24 February 2010)

Strauss H, Moore TB (1992) Abundances and isotopic compositions of carbon and sulfur species in whole rock and kerogen samples. In: Schopf JW, Klein C (eds) The Proterozoic biosphere, a multidisciplinary study. Cambridge University Press, New York, pp 709–798

Sugitani K, Lepot K, Nagaoka T, Mimura K, Van Kranendonk M, Oehler DZ, Walter MR (2010) Biogenicity of morphologically diverse carbonaceous microstructures from the ca. 3400 Ma Strelley Pool Formation, in the Pilbara Craton, Western Australia. Astrobiology 10:899–920

Tan P-H, Dimovski S, Gogotsi Y (2004) Raman scattering of non-planar graphite: arched edges, polyhedral crystals, whiskers and cones. Phil Trans Roy Soc A. Phys Sci 362:2289–2310

Tice MM, Bostick BC, Lowe DR (2004) Thermal history of the 3.5–3.2 Ga Onverwacht and fig tree groups, Barberton greenstone belt, South Africa, inferred by Raman microspectroscopy of carbonaceous material. Geology 32:37–40

Ueno Y, Isozaki Y, Yurimoto H, Maruyama S (2001a) Carbon isotopic signatures of individual Archean microfossils(?) from Western Australia. Internat Geol Rev 43:196–212

Ueno Y, Maruyama S, Isozaki Y, Yuimoto H (2001b) Early Archaean (ca. 3.5 Ga) microfossils and 13 C depleted carbonaceous matter in the North Pole area, Western Australia: field occurrence and geochemistry. In: Nakasima S, Maruyama S, Brack A, Windley BF (eds) Geochemistry and the origin of life. Universal Academic Press, New York, pp 203–236

Ueno Y, Yoshioka H, Isozaki Y (2004) Carbon isotopes and petrography in ~ 3.5 Ga hydrothermal silica dykes in the North Pole area, Western Australia. Geochim Cosmochim Acta 68:573–589

Van Kranendonk MJ (2006) Volcanic degassing, hydrothermal circulation and the flourishing of early life on Earth: a review of the evidence from c. 3490–3240 Ma rocks of the Pilbara Supergroup, Pilbara Craton, Western Australia. Earth-Sci Rev 74:197–240

Wacey D, Kilburn MR, Saunders M, Cliff J, Brasier MD (2011) Microfossils of sulflur-metabolizing cells in 3.4-billion-year-old rocks of Western Australia. Nature Geosci 4:698–702

Walsh MM (1992) Microfossils and possible microfossils from the Early Archean Onverwacht Group, Barberton Mountain Land, South Africa. Precam Res 54:271–292

Walsh MM, Lowe DR (1985) Filamentous microfossils from the 3500 Myr-old Onverwacht Group, Barberton Mountain Land, South Africa. Nature 314:530–532

Walter MR, Buick R, Dunlop JSR (1980) Stromatolites, 3,400–3,500 Myr old from the North Pole area, Western Australia. Nature 284:443–445

In situ Morphologic, Elemental and Isotopic Analysis of Archean Life

12

David Wacey

Abstract

A number of key questions in Archean palaeobiology require study at the micrometre (μm) to nanometre (nm) scale. These include: identifying the transition from a prebiotic world to one containing life; distinguishing true signs of life from abiotic artifacts; identifying the first appearance of important groups of microbes (e.g. cyanobacteria) and metabolic pathways (e.g. sulfur processing, iron processing, anoxygenic and oxygenic photosynthesis); and, determining the transition from a purely prokaryotic world to one including eukaryotes. Here I outline four complementary *in situ* microanalysis techniques that are now providing new evidence in our quest to solve these important scientific questions. The integrated use of these techniques is illustrated by way of a case study from the 3430 Ma Strelley Pool Formation of Western Australia.

12.1 Introduction

Decoding the record of Archean life requires analysis at a number of spatial scales so that a firm understanding of the geological context of any given sample (e.g. age, environmental setting) can be integrated with analysis of its mineralogy and post-depositional history, and with the morphology, taphonomy and behaviour of candidate biological structures. Traditionally this has been achieved by combining field mapping, hand sample analysis, bulk chemical and isotopic analysis, and optical examination of petrographic thin sections. In many cases, however, even this level of study has provided equivocal results for Archean material (see Wacey 2009 for a review), not least because the earliest life on Earth would have been very small, morphologically simple and likely only subtly different from co-occurring non-biological organic material. However, recent technological advances now provide a new suite of analytical tools that may lead to more confident assessments of biogenicity, antiquity, cell structure and metabolic pathways from the Archean rock record.

In this chapter I will outline four complementary microanalysis techniques that permit *in situ*

D. Wacey (✉)
Centre for Geobiology and Department of Earth Sciences, University of Bergen, Allegaten 41, Bergen 5007, Norway

Centre for Microscopy, Characterisation and Analysis, ARC Centre for Core to Crust Fluid Systems & Centre for Exploration Targeting, The University of Western Australia, 35 Stirling Highway, Crawley, WA 6009, Australia
e-mail: david.wacey@uwa.edu.au

Y. Dilek, H. Furnes (eds.), *Evolution of Archean Crust and Early Life*, Modern Approaches in Solid Earth Sciences 7, DOI 10.1007/978-94-007-7615-9_12, © Springer Science+Business Media Dordrecht 2014

study of Archean material at the micrometre to nanometre scale: (1) Laser Raman micro-spectroscopy; (2) Secondary ion mass spectrometry (SIMS and NanoSIMS) incorporating elemental mapping and isotopic analysis; (3) Transmission electron microscopy (TEM) using focused ion beam (FIB) prepared ultra-thin sections; (4) Three-dimensional serial sectioning and imaging using a focused ion beam and scanning electron microscopy (FIB-SEM). It is important to note that none of these techniques alone provide data that will be a 'smoking gun' for biology. It is the combination of all of these techniques, plus a good understanding of the geological context of a sample that provides the most robust evidence for Archean life. All of these techniques can use a regular petrographic thin section as a starting point and simply extract additional information to build upon observations made using traditional optical microscopy. They are described below in order according to how destructive they are to a given sample, from least destructive (Raman) to most destructive (FIB-SEM), mirroring the logical order in which they would be applied to study material.

The types of data obtained and the combined effectiveness of the four techniques is then demonstrated by way of a case study from the early Archean of Western Australia. Here, SIMS was used to obtain *in situ* carbon isotope data ($\delta^{13}C$) from clusters of candidate microfossils, and sulfur isotope data ($\delta^{34}S$ and $\Delta^{33}S$) from co-occurring pyrite. NanoSIMS was used to obtain *in situ* $\delta^{13}C$ data from individual microfossils and $\delta^{34}S$ data from individual pyrite grains. NanoSIMS and FIB-TEM were used to obtain elemental maps of individual microfossils. FIB-TEM and FIB-SEM were used to investigate the ultrastructure of the microfossil walls and their interaction with fossilizing minerals, and FIB-TEM plus Raman was used to aid interpretation of the antiquity of the microfossils. These data were then integrated with field and petrographic observations to conclude upon the authenticity of the microfossils and their possible modes of life and metabolic pathways.

12.2 Laser Raman Micro-spectroscopy

Laser-Raman micro-spectroscopy is often the first in this suite of *in-situ* techniques to be applied to putative signs of Archean life. This is because it is the only one of these techniques that is truly non-destructive. It can also be applied to standard uncovered thin sections without any further sample preparation, and provides a quick way of identifying mineral phases and providing information about their crystallinity and bonding (see Fries and Steele 2011 for technical details). Hence, Raman is often used as a screening technique to identify the most promising samples on which to perform additional higher-resolution but more destructive analyses. Raman systems are commonly attached to optical microscopes so that Raman data can be compared directly to morphological features in a thin section (Fig. 12.1a). Minerals are identified using a database of characteristic spectra caused by laser excitation of their chemical bonds (e.g. RRUFF database, Downs 2006). Naturally, where the study of Archean life is concerned, the focus of most Raman work has been on carbonaceous minerals and compounds (Brasier et al. 2002; Schopf et al. 2002, 2005; Pasteris and Wopenka 2003; Tice et al. 2004; Schopf and Kudryavtsev 2005, 2009; Marshall et al. 2011; Olcott Marshall et al. 2012).

Raman cannot distinguish between biological and abiotic carbon; at best it gives data consistent with biology. However, very different Raman spectra result from different degrees of order in carbonaceous materials. For example, in perfectly crystalline graphite a single first order peak occurs at 1582 cm^{-1} (known as the 'G' or 'graphite' peak; e.g. Jehlicka et al. 2003; Schopf et al. 2005) and second order peaks occur at ~2695 cm^{-1} and 2735 cm^{-1}. In contrast, imperfectly crystallised graphitic carbons have additional peaks at ~1355 cm^{-1} (known as the 'D' or 'disordered' peak) and ~1620 cm^{-1} ('D′'; occurring as a shoulder to the 'G' peak), and a single broad second order peak around 2700 cm^{-1}.

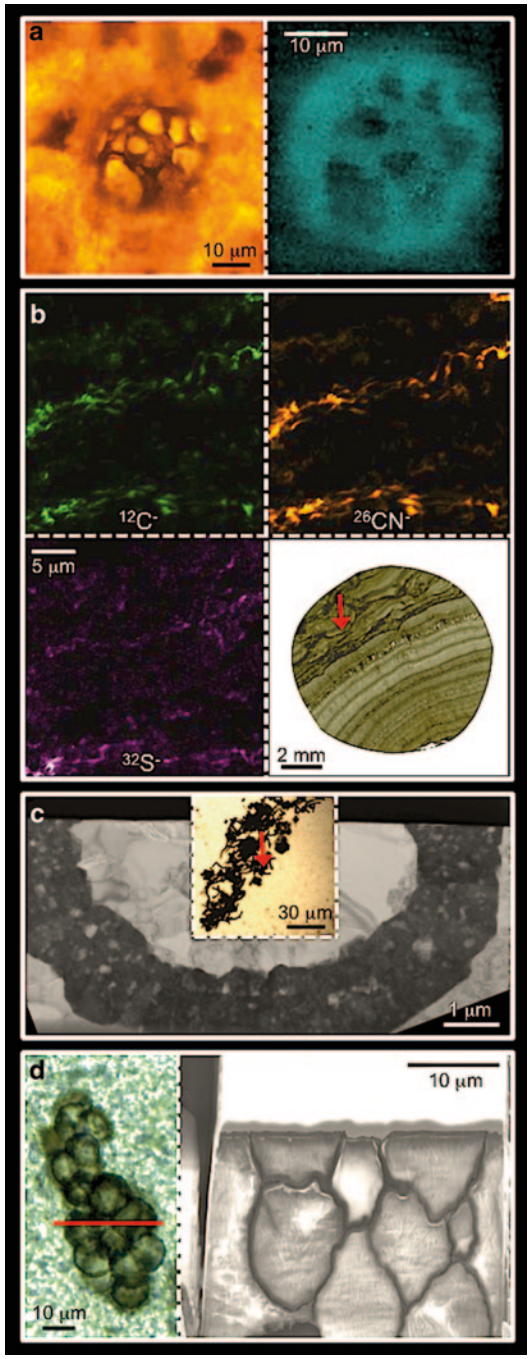

Fig. 12.1 Examples of the type of data obtainable using the *in situ* microanalysis techniques described in this chapter. **a** Optical photomicrograph and correlative laser Raman map of carbon from a microfossil within the ~1.0 Ga Torridon Group, Scotland. **b** NanoSIMS ion images showing the correlation of carbon ($^{12}C^-$), nitrogen ($^{26}CN^-$) and sulfur ($^{32}S^-$) with laminations in a ~2.7 Ga stromatolite from the Tumbiana Formation, Australia. Ion maps come from the area indicated by the *arrow* in the thin section image (*bottom right*). **c** Bright-field TEM image of part of a *Huroniospora* microfossil (from area indicated in optical photomicrograph inset) from the ~1.9 Ga Gunflint chert, Canada. The TEM image shows that microfossil has been pyritised, then silicified, and the pyrite has a porous ultrastructure. **d** Optical photomicrograph of a cluster of cells from the ~1.0 Ga Torridon Group, Scotland, plus FIB-SEM image from area indicated by *red line*. The FIB-SEM image shows the true morphology of the cells below the surface of the thin section and resolves features obscured in optical images

These features have been used in an attempt to determine the syngenicity or antiquity of Archean carbon by comparing data from putative microfossils or microbial mats with that from a database of rocks of different thermal maturities/metamorphic grades (e.g. Wopenka and Pasteris 1993; Tice et al. 2004). Truly ancient carbonaceous microstructures should exhibit the same Raman spectral features as other carbonaceous material in the same rock specimen because both should have undergone the same thermal maturation and geochemical alteration processes. Their spectra should also be consistent with known spectra from equivalent maximum metamorphic grade to the host rock unit.

Raman spectra can also be obtained from multiple points within a sample and combined to form maps with sub-micron spatial resolution (Fig. 12.1a). Maps can be created from any spectral peaks so they need not be merely maps of a given mineral; they could for example show how the ratio of the carbon D to G band varies within a microfossil. Such maps can also be directly correlated with features observed using optical microscopy. For example, a chemical map of carbon can be overlain on an optical image of a putative cell (e.g. Kudryavtsev et al. 2001; Schopf and Kudryavtsev 2005, 2009). 3D chemical visualizations are also obtainable by creating maps at various depths within a thin section and then stacking them together using a 3D software package (e.g. McKeegan et al. 2007). Finally, Raman can be used to look at the distribution and structure of the minerals that host putative microfossils. Many minerals produce spectral peaks that vary in intensity depending on their crystallographic orientation to the laser. This feature can

be used, for example, to image the distribution of quartz crystallographic axes to see whether the biological material occurs between grain boundaries, is enclosed by entire grains, or occurs in cracks (e.g. Fries and Steele 2011).

12.3 Secondary Ion Mass Spectrometry

Secondary ion mass spectrometry (SIMS) can be used to determine the elemental, isotopic or molecular composition of a sample surface, in situ, and at high spatial resolution. This is done by sputtering the surface of a sample with a high intensity ion beam (usually Cs^+ or O^-), then collecting and analysing the ejected secondary ions in a mass specrometer. For those interested in the details of the process and other SIMS applicatons see Ireland (1995), McKibben et al. (1998) or Orphan and House (2009).

12.3.1 Large Radius SIMS

Large radius SIMS instruments come into their own for high precision isotope work. They can be used to date minerals (e.g. zircon by U/Pb decay series; e.g. Ireland 2003) and hence improve the age constraints on Archean rocks containing putative signs of life. They can also be used to obtain stable isotope data for important biological elements such as carbon and sulfur, the application focused upon here. Spatial resolution is good; data with a precision of 0.5 parts per thousand (‰) or better is routinely obtainable from objects >20 µm. With careful tuning, a precision of better than 0.05‰ is possible for some isotopic systems (e.g. $\delta^{33}S$ and $\delta^{34}S$, J Cliff pers comm), and objects as small as 10 µm can be analysed. Sample requirements are straightforward, with analyses possible from polished rock chips or geological thin sections. This means that spatially resolved isotopic data can be obtained directly from microfossils, carbonaceous laminations within microbial mats or stromatolites, and potential biominerals (e.g. pyrite). This is preferential to bulk analyses which may suffer from contamination and/or isotopic homogenisation during processing, preparation and analysis.

SIMS stable isotope data from Archean rocks are still relatively rare but carbon isotope data ($\delta^{13}C$) have been obtained from putative microfossils from the 3490 Ma Dresser Formation (Ueno et al. 2001) and carbonaceous inclusions from 3700–3850 Ma rocks from Greenland (Mojzsis et al. 1996). In both of these studies light $\delta^{13}C$ values (down to −42‰) were interpreted as evidence of biological fractionation of carbon. However, non-biological reactions are able to produce similar $\delta^{13}C$ fractionations (Horita and Berndt 1999; van Zuilen et al. 2003; McCollom and Seewald 2006). Hence, these data are not uniquely biological and demonstrate that a single technique rarely provides compelling evidence for Archean biology.

SIMS has also been used to study Archean sulfur isotope geochemistry. SIMS $\delta^{34}S$ and $\Delta^{33}S$ data have led to a greater understanding of Archean atmospheric chemistry (Mojzsis et al. 2003), cycling of sulfur between the atmosphere, hydrosphere and lithosphere (Kamber and Whitehouse 2007; Philippot et al. 2012) and the origin of sulfate-reducing and sulfur disproportionating microorganisms (Philippot et al. 2007; Wacey et al. 2010a; Bontognali et al. 2012, see case study in Sect. 12.6 for more details).

12.3.2 NanoSIMS

NanoSIMS is a versatile tool capable of both isotopic analysis and fine scale elemental mapping. Although the precision for isotopic anlaysis is not as good as the large radius SIMS (only 1–3‰ for $\delta^{13}C$ and $\delta^{34}S$; Fletcher et al. 2008; Wacey et al. 2010a), NanoSIMS can routinely obtain data from objects only 3–5 µm in size and, with careful optimization, objects as small as 1–2 µm can be analysed. This is critical for Archean palaeobiology where isotopic data can now be obtained from individual microfossils (e.g. Oehler et al. 2010), single grains of potential biominerals (e.g. Wacey et al. 2010a) and single laminations within putative microbial mats and stromatolites (Wacey 2010). Here, the advantage of

increased spatial resolution generally outweighs the reduced precision, since most biological fractionations of carbon and sulfur are large and a 1–3 ‰ precision is still more than adequate to detect these.

In terms of elemental mapping, NanoSIMS is capable of sub-50 nm lateral resolution whilst imaging negatively charged secondary ions and ~150 nm lateral resolution for positive secondary ions with a sensitivity often in the parts per billion (ppb) range. Up to six moveable and one static detector record ion counts from the same sputtered sample volume at up to seven masses simultaneously. This parallel measurement is extremely useful in the analysis of low concentration elements in ancient organic materials that are rapidly sputtered away by the ion beam (Fig. 12.1b).

NanoSIMS data now exist from a variety of Archean environments. Sulfur isotope data from tiny (<15 μm) pyrites within microtubes in c. 3450 Ma basalts record $\delta^{34}S$ values as low as c. −40 ‰, indicating that sulfur processing microbes were a likely component of the early Archean sub-seafloor biosphere (McLoughlin et al. 2012). Carbon isotope data (mean $\delta^{13}C = -26$ ‰) from ambient inclusion trails (AIT) in a c. 3430 Ma sandstone, combined with nm-scale mapping of carbon, nitrogen and biologically-significant trace elements (e.g., Co, Fe, Ni, Zn), showed that AIT might be mediated by microbes (Wacey et al. 2008a, b). This provided the first geochemical data to support a long-standing biological hypothesis for AIT formation (Knoll and Barghoorn 1974) and introduced AIT as a new potential biosignal in ancient rocks. In Neoarchean rocks, NanoSIMS $\delta^{34}S$ and $\delta^{13}C$ data have been combined to show that sulfur-processing and methanotrophic microbes inhabited small hollows and cavities within stromatolites in a terrestrial setting 2750 million-years-ago (Rasmussen et al. 2009). Rasmussen et al. (2008) also used NanoSIMS $\delta^{13}C$ data as part of their evidence for a reassessment of the first appearance of eukaryotes and cyanobacteria in the rock record, concluding that previous evidence from 2700 Ma rocks was actually younger contamination.

NanoSIMS elemental mapping of carbon, nitrogen and sulfur (Fig. 12.1b) has provided supporting evidence for the biogenicity of stromatolites from the ~3430 Ma Strelley Pool Formation of Western Australia (Wacey 2010), and microfossils from these and younger Archean rocks (Oehler et al. 2009, 2010). Such data also lend support to a recent hypothesis that the volcanic rock pumice may have played a key role in the origin of life itself (Brasier et al. 2013). Attempts have also been made to quantify ratios of nitrogen and carbon (N/C) to distinguish different components of microbial communities, and to distinguish biology from co-occurring abiotic organic material (Oehler et al. 2009) although a robust and repeatable methodology for this remains elusive.

12.4 Transmission Electron Microscopy

Transmission electron microscopy (TEM) can be used to image and characterize the structure and chemistry of a sample down to the nm or even atomic scale. TEM actually encompasses a whole suite of sub-techniques that can be performed in a transmission electron microscope (also known as a TEM; see Williams and Carter 2009 for analytical details). In the most basic mode of operation the microscope is used as an imaging tool with versatile spatial resolution, able to resolve objects separated by distances as small as ~0.1 nm, but also image much larger fields of view up to c.10–20 μm (Fig. 12.1c). A true high-resolution image in the TEM (HRTEM or HREM) is a phase contrast image with atomic-scale resolution, allowing the visualization of the arrangement of atoms within a sample. This provides information about the crystallinity of a sample, its lattice structure and any defects it may have. For example, graphite can be quickly visually distinguished from more poorly ordered carbon (Buseck and Bo-Jun 1985; Buseck et al. 1988).

A second sub-technique within the TEM field is electron energy loss spectroscopy (EELS). EELS spectra can be used to identify the elemental composition of nano-areas within a sample,

and the shape and size of the spectra also give an indication of how much of the element is present, what the element is bonded to (e.g. Daniels et al. 2007) and what its oxidation state is (e.g. Calvert et al. 2005). The EELS technique can be taken a step further to produce images of the elemental distribution within a sample by isolating (filtering) specific energy windows (energy-filtered TEM or EFTEM) from an EELS spectrum (e.g. Wacey et al. 2011a, b). A third sub-technique within the TEM offers an alternative method to determine the elemental composition of a sample, energy-dispersive X-ray spectroscopy (EDS). Both qualitative and quantitative elemental analysis is possible using EDS. If elemental maps are required using X-rays, the TEM must be operated in scanning mode (STEM) so that X-rays can be collected at specific points as the beam scans across the sample. Finally, selected area electron diffraction (SAED) within the TEM provides quantitative information on the distances between atomic planes, permitting mineral identification and providing information on crystallinity and crystal orientation.

The study of Precambrian life using TEM is not new, with TEM images of ancient microfossils dating back a number of decades (e.g. Oehler 1976). However, two recent advancements in the field have led to TEM becoming a much more effective tool in this field. These advancements are the integration of TEM images with additional EFTEM, EELS, SAED and EDS data, and the preparation of TEM samples using a focused ion beam (Fig. 12.1c).

Recent integrated data from Archean rocks include images and EELS spectra from carbon in the ~3465 Ma Apex Chert and the ~3430 Ma Strelley Pool Formation of Western Australia (De Gregorio and Sharp 2006; Wacey et al. 2009), showing that this carbon has little order, lacks the characteristic σ^*_1 peak of graphitization, and has similar spectral shape to younger bona fide microfossils (Moreau and Sharp 2004). A point to note is that neither EELS nor HRTEM can distinguish carbon produced biologically from that produced via abiotic reactions such as Fischer-Tropsch type synthesis (Brasier et al. 2002). However, like Raman, these methods do provide vital information on whether the carbon is likely syngenetic with the host rock and whether its structure is at least consistent with a biological precursor.

EFTEM, EDS and SAED were combined by Wacey et al. (2011b) to investigate the distribution of potential biological elements and biominerals associated with pyrite in the Strelley Pool Formation. These data helped provide the earliest potential evidence of iron and sulfur oxidising microbial metabolisms in the rock record. SAED also allows the orientation of crystals to be studied. One potential application of this is to show the orientation of microquartz grains in the vicinity of putative carbonaceous microfossils (see case study in Sect. 12.6), in order to determine whether the carbon is housed between grain boundaries, enclosed within a single grain, or within fractures.

The quality of sample preparation is key to obtaining good TEM data. Ideally, the sample needs to be ultrathin ($\leq$100 nm) in order to extract the maximum structural and chemical information, and images are most easily interpreted if the sample is of approximate constant thickness. Context is also important; for example, one needs to be able to match features seen down the optical microscope with those seen in the TEM (Fig. 12.1c). This was not possible with traditional TEM sample preparation where bulk samples were ground up, or organic material was chemically extracted and placed onto TEM holders; consequently context was lost, sample thickness was very variable, and contamination was always a very real issue. These problems have now largely been solved by the use of focused ion beam (FIB) milling. This procedure uses a highly focused beam of heavy gallium ions to sputter ions from the sample surface, essentially cutting into the sample with very high precision (see Wirth 2009). Hence, small wafers, typically about 15 µm × 10 µm × 0.1 µm, can be cut directly out of thin sections or rock chips (Fig. 12.1c). These are not only uniformly thin but they retain the context of the object of interest and eliminate the possibility of contamination. FIB-TEM sample preparation was used in the case study outlined in Sect. 12.6.

12.5 3D Serial Sectioning, Imaging and Analysis Using a Focused Ion Beam and Scanning Electron Microscopy (FIB-SEM)

The same focused beam of heavy ions used in the TEM sample preparation described above can also be used in other ways to investigate the morphology, and even chemistry, of putative signs of Archean life. Most commonly, FIB milling takes place within a modified scanning electron microscope (SEM), termed a dual-beam instrument (see Wirth 2009). Here, the user can routinely switch between an ion beam (used for milling) and a scanning electron beam (used for imaging). Additional detectors can also be inserted to permit elemental analysis (EDS detector) or phase detection and crystallographic mapping (EBSD detector).

With this set up, FIB milling can simply be used to cut through specific features in a rock chip or thin section so that structures below the surface can be seen, or so that structures on the surface can be better visualized in three dimensions. For example, Westall et al. (2006) used FIB milling to cut through a small portion of a putative microbial mat from the ~3,400 Ma Josefsdal Chert, South Africa. This allowed the internal structure of the mat to be imaged at high spatial resolution.

A logical extension of cutting a single slice into a sample is to mill sequential slices through an object. This is termed FIB-SEM nano-tomography and combines sequential FIB milling with concurrent SEM imaging of each newly milled face (see Wirth 2009; Wacey et al. 2012 for details). This may then be followed by three dimensional volume reconstruction, visualization and analysis of the data. The steps between successive FIB slices can be set by the user and can be smaller than 50 nm so that even fine scale detail within microfossils can be captured (Fig. 12.1d). An image of a single FIB-SEM slice provides nano-scale morphological information about a microfossil (or other object of interest) in the plane normal to the surface of the thin section or rock chip (Fig. 12.1d), while multiple slices can be combined to provide a 3D reconstruction of an entire microfossil (see below). Limitations of this technique include its destructive nature, making it rather unsuitable for samples with very rare or 'type' microfossils, and the time and resources needed to process and reconstruct the raw data into 3D models.

12.6 Case Study—Microfossils from the 3430 Ma Strelley Pool Formation

The effectiveness of combining multiple *in situ* microanalysis techniques has been shown recently in a study reporting well-preserved microfossils from the 3430 Ma Strelley Pool Formation of Western Australia (Wacey et al. 2011a).

Critically, before the putative microfossils were subjected to *in situ* microanalysis, multiple seasons of fieldwork had been completed in order to gain a firm understanding of the geological context of the host rocks. In addition, over 200 thin sections and hand samples had been studied in order to understand the depositional context and post-depositional history of the rocks, and to isolate only the very best and most promising samples for further study. This work had been peer reviewed and published (Wacey et al. 2006, 2010b) and could then be integrated with the *in situ* work.

Optical microscopy revealed a wealth of microstructures in thin sections that resembled biological entities. A number of lines of evidence suggested these were biological and encouraged further study [in what follows the word 'microfossil' will be used to describe microstructures in thin sections that have biology-like morphology, while at the same time recognizing that further tests were required before these could be classed as *bona fide* microfossils]:

- Three distinct morphotypes were present: (1) Tubular microfossils that strongly resembled the protective outer casings (sheaths) of some modern filamentous bacteria (Fig. 12.2). These were about 10–20 µm in diameter and up to 100 µm or so in length; (2) Small spheroidal microfossils, again mostly 10–20 µm in diameter resembling modern colonies of bacterial cells; and (3) Larger spheroidal/ellip-

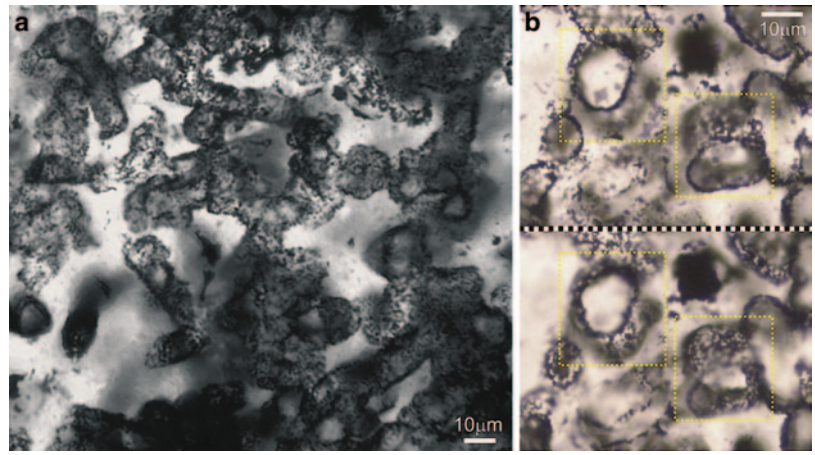

Fig. 12.2 Examples of hollow, tubular, sheath-like microfossils from the 3430 Ma Strelley Pool Formation, Western Australia. **a** Dense patch of tubular microfossils with examples seen in both longitudinal and transverse sections. **b** Transverse cross-sections thorough two tubular microfossils (*boxed*) at two different focal depths in the thin section, permitting differentiation from spheroidal cells or abiotic artifacts. (Modified from Wacey et al. 2011a)

soidal microfossils. These were quite rare, up to 80 μm in size, resembling large individual cells or membrane-like structures that housed several smaller cells. All appeared hollow inside.

- They were arranged in clusters and chains (Fig. 12.2), associated with trace fossil borings into pyrite pebbles and micron-sized pyrite grains, and attached to sand grains just like living biofilms.
- They showed evidence of decay as one would expect biological structures to decay. For example, their cell walls shrink once dead and leave evidence of folding or fracture.

However, cases of Archean microstructures resembling fossils but turning out to be non-biological artifacts or more recent contamination are common (see Wacey 2009 for a review of numerous examples) so a number of questions remained to be answered, for example:

1. What is the chemistry of the microstructures—is there evidence for biologically important elements (e.g. C, N, S) within their cell walls?
2. If so, does the carbon have an isotopic signature and structure consistent with biology?
3. If so, does the carbon have a structure consistent with the age and thermal history of the host rock?
4. What is the relationship between the microstructures and the silica that enclosed them—is this consistent with fossilization of biological structures?
5. Is there evidence for metabolism-like behaviour within the cell walls and/or within surrounding 'waste-products'?
6. What role, if any, does the co-occurring pyrite play?
7. Is the ultrastructure and sub-micron morphology of the microstructures also consistent with biology?

Below I outline how each *in situ* microanalysis technique provided evidence to help answer these questions.

12.6.1 Laser Raman Data

Laser Raman was used to investigate the antiquity of the microfossils and to screen material for carbonaceous composition and structure consistent with biology. Raman maps showed one-to one correlation between microfossil walls and carbonaceous chemistry, and confirmed that quartz was the mineralizing phase (Fig. 12.3). Raman spectra showed that the carbon had a structure both consistent with being derived from a biological precursor and consistent with the known metamorphic grade of the host rock (Fig. 12.3). Additionally, Raman spectra from potential microfossils were similar to spectra from other carbonaceous material within the thin sections, showing that all the carbonaceous material in

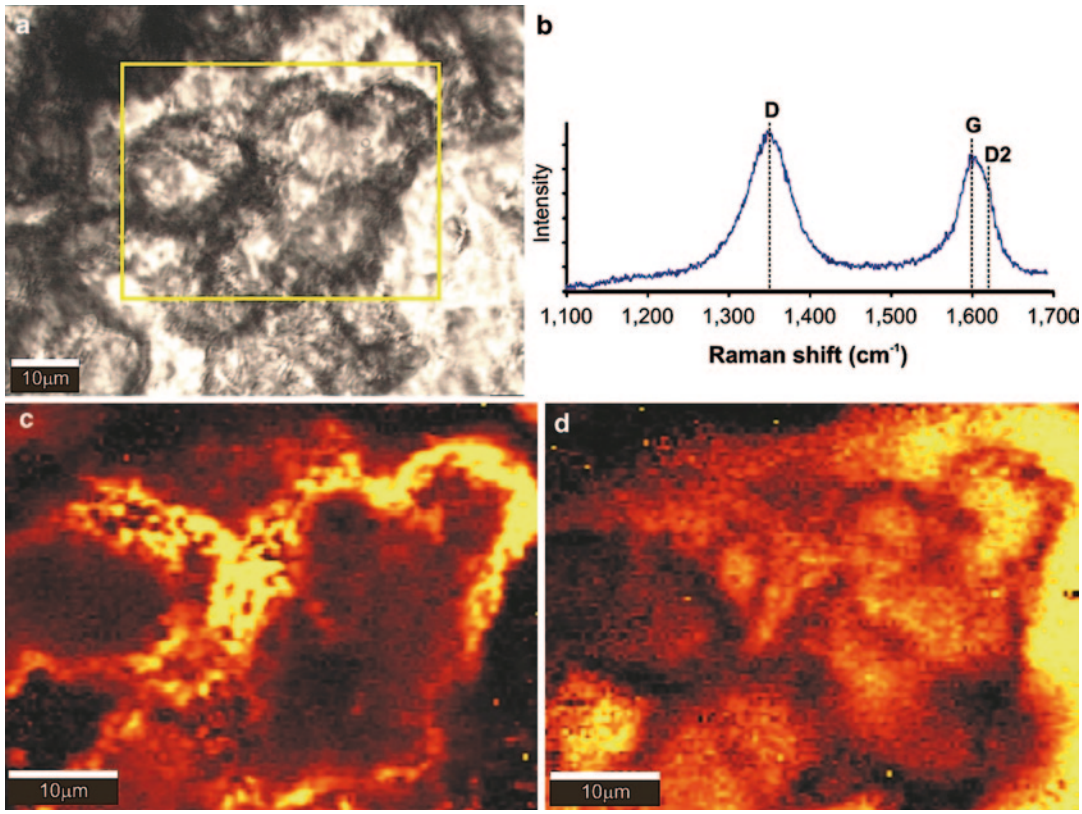

Fig. 12.3 In situ laser Raman micro-spectroscopy of Strelley Pool microfossils. **a** Transmitted light photomicrograph showing area (*boxed*) analysed in (b–d). **b** Part of the first order Raman spectrum from the carbon comprising the cell walls. Two carbon peaks are observed; the ordered 'G' peak at ~1600 cm^{-1}, and the disordered 'D' peak at ~1350 cm^{-1}. A shoulder to the G peak (D2) is also observed at ~1620 cm^{-1}. The position and ratios (area and height) of these peaks is consistent with the known metamorphic grade (lower greenschist facies) of the Strelley Pool sandstone. **c** Map of the intensity distribution of the carbon G peak showing correlation between carbon and the cell walls. **d** Map of the intensity distribution of the quartz 465 cm^{-1} peak showing the mineralizing quartz phase. (From Wacey et al. 2011a)

the thin sections was of similar antiquity and had been subject to the same post-depositional thermal events.

12.6.2 SIMS Data

Large radius SIMS provided *in situ* carbon isotope ($\delta^{13}C$) data from carbonaceous material within the thin sections. Two samples were analysed (SPZ2b and SP9-D2a). SPZ2b contained abundant clusters of microstructures having a cell-like morphology. SP9-D2a also contained abundant carbon but cell-like morphologies were rare. The range of $\delta^{13}C$ values from SPZ2b was −34 to −46‰ (n=44); a similar range was found in SP9-D2a, −33 to −43‰ (n=10). Errors on the sample data (1σ=0.5–1.8‰) were of a similar magnitude to those of previous SIMS $\delta^{13}C$ studies from carbonaceous microstructures (House et al. 2000; Ueno et al. 2001; Williford et al. 2013). There was no statistical difference between the $\delta^{13}C$ data in the two samples. This suggests that all the carbon, whether it has a biological morphology or not, was derived from a similar source. The Strelley Pool data was remarkably similar to that from younger, universally accepted microfossils from the 1900 Ma Gunflint Formation that were also analysed *in situ* (−32.4 to −45.4‰; House et al. 2000). The $\delta^{13}C$ data are consistent with biological fractionations taking place during autotrophic carbon fixation

via either the reductive acetyl-CoA pathway or the Calvin cycle (Schidlowski et al. 1983). It is notable that these $\delta^{13}C$ data are mostly too negative to be attributed to isotopic fractionation by cyanobacteria, and mostly too positive to be attributed to isotopic fractionation by methanogens (cf. Ueno et al. 2006). However, they do mostly lie within the $\delta^{13}C$ range reported for sulfate-reducing bacteria biomass in modern settings (Londry and Des Marais 2003).

Sulfur isotope data from pyrite associated with the microfossils was also obtained using SIMS. $\delta^{34}S$ data showed fractionations from Archean seawater sulfate of up to 15‰, together with non-mass dependent $\Delta^{33}S$ anomalies (−1.65 to +1.43‰) comparable to previous data obtained by ion microprobe from early Archean sedimentary rocks (~±2‰; Mojzsis et al. 2003). Critically, pyrite grains in a single thin section possessed both $+\Delta^{33}S$ and $-\Delta^{33}S$, indicating that these pyrites were incorporating reduced sulfur simultaneously from both the sulfate ($-\Delta^{33}S$) and elemental sulfur ($+\Delta^{33}S$) pools within the sandstone pore water.

12.6.3 NanoSIMS Data

NanoSIMS provided high sensitivity and high spatial resolution ion maps of biologically significant elements, namely carbon and nitrogen. Such maps were obtained from individual microfossils (Fig. 12.4a), showing the co-occurrence of carbon and nitrogen, and a one to one correlation of these elements with features that had been interpreted as microfossil walls using optical microscopy. The ion maps also showed a strong correlation between carbon/nitrogen rich material and tiny pyrite grains (Fig. 12.4b). The isotopic signature ($\delta^{34}S$) of these pyrite grains was also investigated using NanoSIMS. Sixty-six individual grains had a range in $\delta^{34}S$ from −12 to +6‰ (1‰ < 1σ < 4‰), a similar level of fractionation to that observed using large radius SIMS above. Critically, NanoSIMS was able to detect large variations in $\delta^{34}S$ over spatial scales of only a few micrometres (e.g. ~15‰ between grains which are <5 μm apart; Wacey et al. 2010a).

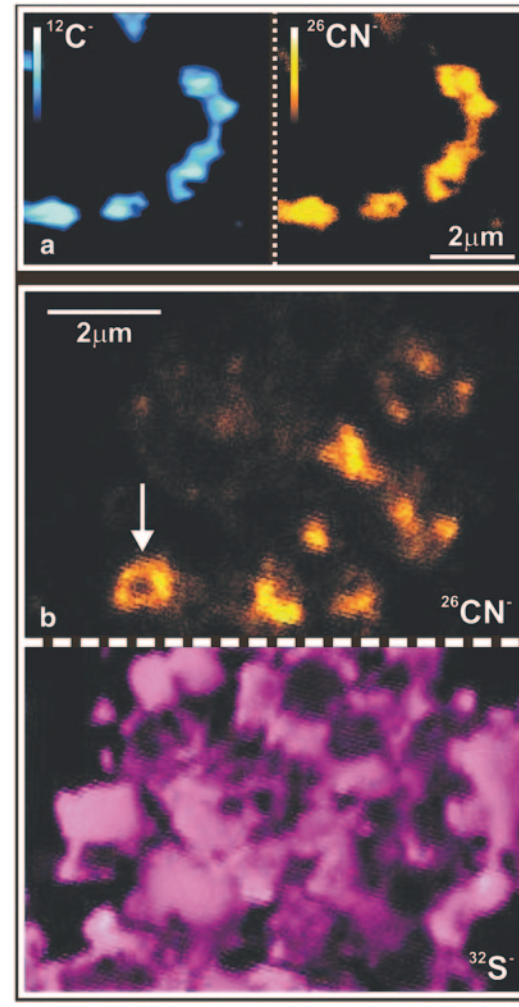

Fig. 12.4 NanoSIMS ion images of Strelley Pool microfossils and associated pyrite. **a** NanoSIMS carbon ($^{12}C^-$) and nitrogen ($^{26}CN^-$) ion maps showing co-occurrence of these elements in part of a microfossil wall. **b** NanoSIMS nitrogen ($^{26}CN^-$) and sulfur ($^{32}S^-$) ion maps showing close correlation between potential microfossils (e.g. *arrow*) and micrometre-sized grains of pyrite. (Part (b) from Wacey et al. 2011a)

Such a large spread of $\delta^{34}S$ at this spatial scale is indicative of microbial S-processing. These data can then integrated with the $\delta^{34}S$ and $\Delta^{33}S$ data from large radius SIMS to conclude that two biological metabolisms were likely active at Strelley Pool, bacterial sulfate reduction and bacterial sulfur disproportionation.

A small number of NanoSIMS $\delta^{13}C$ data were also collected. These data come from individual

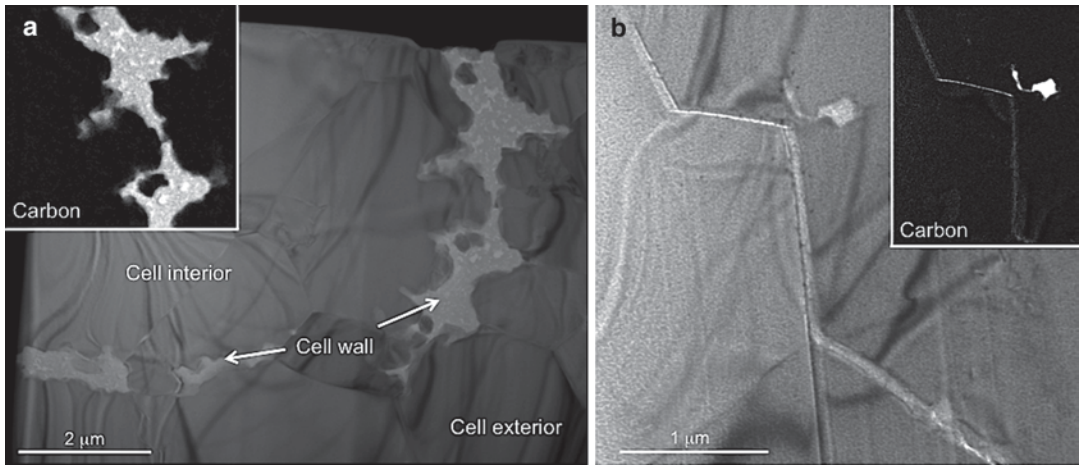

Fig. 12.5 Comparing cell walls and artifacts in the Strelley Pool sandstone using FIB-TEM. **a** Bright-field- and energy-filtered-TEM images of part of a microfossil wall. Carbon is confined to the curved, semi-continuous cell wall and does not occur along the angular boundaries of the numerous quartz grains that fill the hollow centre of the cell. **b** In contrast to (a), carbon occurs along angular quartz grain boundaries suggesting it has been redistributed by crystallization of the quartz and that the carbonaceous microstructure is a non-fossiliferous artifact. (Part (a) modified from Wacey et al. 2011a)

carbonaceous structures that have clear microbial morphology. This contrasts to the large radius SIMS $\delta^{13}C$ data that came from clusters of microfossils and degraded carbon. NanoSIMS $\delta^{13}C$ values range from −27 to −39‰ ($n=7$). Although the precision on these data is relatively poor ($1\sigma=2$–4‰), the range of data is similar to that obtained by large radius SIMS and reinforces the conclusions regarding metabolism made using that technique (see sect. 12.6.2 above).

12.6.4 FIB-TEM Data

FIB-TEM data provided key information about the chemistry and ultrastructure of the microfossil walls at the nanometre-scale and how these walls interacted with the minerals that fossilized them. TEM images and EFTEM mapping showed that structures identified as potential cell walls using optical microscopy were curved semi-continuous features composed of carbon (Fig. 12.5a). EFTEM also showed that the fossilizing material was pure silica and that the carbonaceous microfossil walls had been impregnated and partially permineralized by nano-grains of this mineral. SAED showed that numerous blocky quartz grains precipitated in different crystallographic orientations within the interior of the microfossils. TEM images showed that these quartz grains had very irregular curved boundaries with the microfossil walls and EFTEM showed that no carbon was present in the interior of the microfossil along the angular quartz grain boundaries or triple junctions (Fig. 12.5a). These observations suggested that the microfossil walls existed first and the quartz grains nucleated on these and then grew inwards from the wall, rather than the carbon distribution being controlled by the crystallizing quartz-rich fluids. This allowed the rejection of a null hypothesis that the microstructures formed in an abiotic manner as crystal rim artifacts (cf. Fig. 12.5b; Brasier et al. 2002, 2005). The ultrastructure and chemistry of the microfossil walls in these FIB-TEM sections also closely resembles that of younger well-established microfossils from the 1900 Ma Gunflint Formation (Wacey et al. 2012) giving an extra degree of confidence in their biological interpretation.

HRTEM images revealed the ordering of the carbon, indicating that a mixture of short-range ordered and disordered carbon was present. The ordered regions exhibited the 0.34 nm interlayer spacing of graphite but were far from the order of

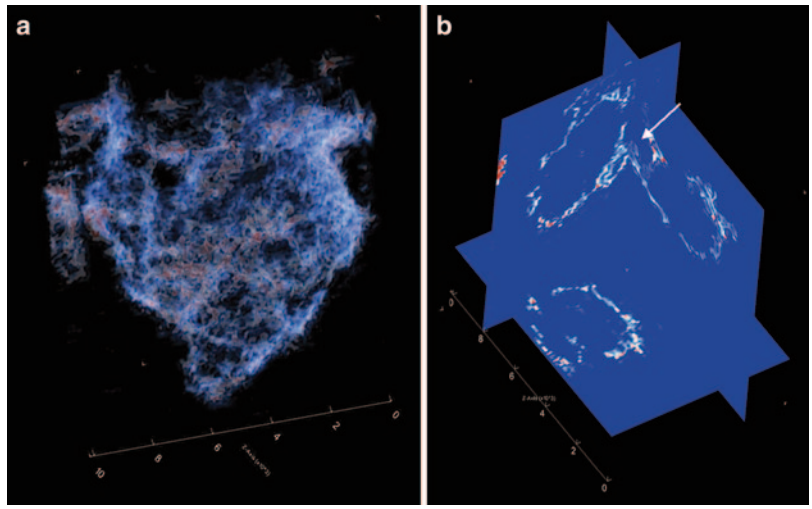

Fig. 12.6 Three-dimensional reconstruction of a putative microfossil from the Strelley Pool Formation. **a** Three-dimensional volume rendering of sixty-five FIB-SEM slices. Each FIB-SEM slice was approximately 10 µm × 10 µm and the step size between slices was 200 nm. **b** Orthogonal slices through the *x*, *y* and *z* axes of the volume rendering in (a) showing spherical to elliptical nature of a putative cell in 3D, and possible attachment of part of second cell (arrow). (Modified from Wacey et al. 2012)

true graphite (cf. Buseck et al. 1988). This was consistent with the metamorphic grade of the rock (greenschist facies), reinforced the Raman data and showed that the carbon could not have been a post-metamorphic contaminant.

TEM images and EFTEM maps were also critical to the interpretation of the metabolic pathways that the microfossils might have employed. Here, TEM images and EFTEM maps showed nano-grains of pyrite occurring within and in close proximity to the microfossil walls. This same pattern is seen today in experiments where bacteria precipitate mineral sulfides (Moreau et al. 2004). This, together with the sulfur isotope data acquired by SIMS, strongly suggested that at least some of these microbes had a sulfur-processing metabolism.

12.6.5 FIB-SEM Data

FIB-SEM data revealed additional information about the ultrastructure of the microfossil walls and overall morphology of the microfossils. These data reinforced the carbonaceous and semi-continuous nature of the partially degraded microfossil walls. Nano-grains of silica were also commonly found within the microfossil walls, confirming observations made using TEM. When non-cellular carbonaceous artifacts were examined by FIB-SEM it was found that they possessed none of the wall-ultrastructure that characterizes the microfossils. For example, instead of thin semi-continuous walls, these artifacts had very thick zones (c.5 µm) comprising nano-particles of carbon.

Multiple FIB-SEM slices through potential microfossils were also combined into nano-tomographic reconstructions (Fig. 12.6a). From such reconstructions, orthogonal slices could be viewed through candidate microfossils, revealing extra details obscured under light microscopy including their true 3D spheroidal/ellipsoidal morphologies (Fig. 12.6b).

12.7 Summary

The study of Archean life has evolved significantly over the past decade. There has been a revolution in our capacity to resolve morphological, chemical and isotopic detail at very fine spatial scales, whilst at the same time maintaining the original context of the structures of interest. Four common ways to do this have been highlighted here, namely laser Raman, SIMS, FIB-TEM and FIB-SEM.

When applied to a promising example of Archean life from the 3430 Ma Strelley Pool Formation of Western Australia, these techniques

combine to provide a large volume of evidence supporting the biogenicity, antiquity and metabolic pathways of these microfossils, given a prior understanding of their geological context and post-depositional history.

Acknowledgments I would like to thank the numerous people who helped to carry out the microanalyses for the case study, in particular, Matt Kilburn, John Cliff, Martin Saunders, Charlie Kong, Len Green, Sarath Menon, Derek Gerstmann, Nicola McLoughlin, Martin Whitehouse, Andrew Steele and Martin Brasier. I acknowledge funding from the Bergen Research Foundation, the University of Bergen, the University of Western Australia and the Australian Research Council. I also acknowledge the facilities, scientific and technical assistance of the Australian Microscopy & Microanalysis Research Facility at the Centre for Microscopy, Characterisation & Analysis, The University of Western Australia, a facility funded by The University, State and Commonwealth Governments.

References

Bontognali TRR, Sessions AL, Allwood AC, Fischer WW, Grotzinger JP, Summons RE, Eiler JM (2012) Sulfur isotopes of organic matter preserved in 3.45-billion-year-old stromatolites reveal microbial metabolism. Proc Nat Acad Sci USA 109:15146–15151

Brasier MD, Green OR, Jephcoat AP, Kleppe AK, Van Kranendonk MJ, Lindsay JF, Steele A, Grassineau NV (2002) Questioning the evidence for Earth's oldest fossils. Nature 416:76–81

Brasier MD, Green OR, Lindsay JF, McLoughlin N, Steele A, Stoakes C (2005) Critical testing of Earth's oldest putative fossil assemblage from the ~3.5 Ga Apex chert, Chinaman Creek, Western Australia. Precamb Res 140:55–102

Brasier MD, Matthewman R, McMahon S, Kilburn MR, Wacey D (2013) Pumice from the ~3460 Ma Apex Basalt, Western Australia: a natural laboratory for the early biosphere. Precamb Res 224:1–10

Buseck PR, Bo-Jun H (1985) Conversion of carbonaceous material to graphite during metamorphism. Geochim et Cosmochim Acta 49:2003–2016

Buseck PR, Bo-Jun H, Miner B (1988) Structural order and disorder in Precambrian kerogens. Org Geochem 12:221–234

Calvert CC, Brown A, Brydson R (2005) Determination of the local chemistry of iron in inorganic and organic materials. J Elec Spect Rel Phenom 143:173–187

Daniels H, Brydson R, Rand B, Brown A (2007) Investigating carbonization and graphitization using electron energy loss spectroscopy (EELS) in the transmission electron microscope (TEM). Phil Mag 87:4073–4092

De Gregorio BT, Sharp TG (2006) The structure and distribution of carbon in 3.5 Ga Apex chert: implications for the biogenicity of Earth's oldest putative microfossils. Am Mineral 91:784–789

Downs R (2006) The RRUFF project: an integrated study of the chemistry, crystallography, Raman and infrared spectroscopy of minerals. Program and abstracts of the 19th general meeting of the International Mineralogical Association. Kobe, Japan, O03–13

Fletcher IR, Rasmussen B, Kilburn MR (2008) NanoSIMS μm-scale in situ measurement of $^{13}C/^{12}C$ in early Precambrian organic matter, with per mil precision. Int J Mass Spec 278:59–68

Fries M, Steele A (2011) Raman spectroscopy and confocal Raman imaging in mineralogy and petrography. Springer Opt Sci 158:111–135

Horita J, Berndt ME (1999) Abiogenic methane formation and isotopic fractionation under hydrothermal conditions. Science 285:1055–1057

House CH, Schopf JW, McKeegan KD, Coath CD, Harrison TM, Stetter KO (2000) Carbon isotopic composition of individual Precambrian microfossils. Geology 28:707–710

Ireland TR (1995) Ion microprobe mass spectrometry: techniques and applications in cosmochemistry, geochemistry, and geochronology. In: Hyman M, Rowe M (eds) Advances in analytical geochemistry. JAI Press, Greenwich, pp 1–118

Ireland TR (2003) Considerations in zircon geochronology by SIMS ZIRCON. Rev Mineral Geochem 53:215–241

Jehlicka J, Urban O, Pokorny J (2003) Raman spectroscopy of carbon and solid bitumens in sedimentary and metamorphic rocks. Spectrochim Acta A 59:2341–2352

Kamber BS, Whitehouse MJ (2007) Micro-scale sulphur isotope evidence for sulphur cycling in the late Archean shallow ocean. Geobiol 5:5–17

Knoll AH, Barghoorn ES (1974) Ambient pyrite in Precambrian chert: new evidence and a theory. Proc Nat Acad Sci USA 71:2329–2331

Kudryavtsev AB, Schopf JW, Agresti DG, Wdowiak TJ (2001) In situ laser-Raman imagery of Precambrian microscopic fossils. Proc Nat Acad Sci USA 98:823–826

Londry KL, Des Marais DJ (2003) Stable carbon isotope fractionation by sulfate-reducing bacteria. Appl Env Microbiol 69:2942–2949

Marshall CP, Emry JR, Olcott Marshall A (2011) Haematite psuedomicrofossils present in the 3.5-billion-year-old Apex Chert. Nature Geosci 4:240–243

McCollom TM, Seewald JS (2006) Carbon isotope composition of organic compounds produced by abiotic synthesis under hydrothermal conditions. Earth Plan Sci Lett 243:64–84

McKeegan KD, Kudryavstev AB, Schopf JW (2007) Raman and ion microscopic imagery of graphitic inclusions in apatite from older than 3830 Ma Akilia supracrustal rocks, west Greenland. Geology 35:591–594

McKibben MA, Shanks III WC, Ridley WI (1998) Applications of Microanalytical Techniques to Understanding Mineralizing Processes. SEG Rev Econ Geol 7:263

McLoughlin N, Grosch EG, Kilburn MR, Wacey D (2012) Sulfur isotope evidence for a Paleoarchean sub-seafloor biosphere, Barberton, South Africa. Geology 40:1031–1034

Mojzsis SJ, Arrenhius G, McKeegan KD, Harrison TM, Nutmam AP, Friend CRL (1996) Evidence for life on Earth 3,800 million years ago. Nature 384:55–59

Mojzsis SJ, Coath CD, Greenwood JP, McKeegan KD, Harrison TM (2003) Mass-independent isotope effects in Archean (2.5–3.8 Ga) sedimentary sulfides determined by ion microprobe analysis. Geochim Cosmochim Acta 67:1635–1658

Moreau JW, Sharp TG (2004) A transmission electron microscopy study of silica and kerogen biosignatures in ~1.9 Ga Gunflint microfossils. Astrobiol 4:196–210

Moreau JW, Webb RI, Banfield JF (2004) Ultrastructure, aggregation-state, and crystal growth of biogenic sphalerite and wurtzite. Am Mineral 89:950–960

Oehler DZ (1976) Transmission electron microscopy of organic microfossils from the late Precambrian Bitter Springs Formation of Australia: techniques and survey of preserved ultrastructure. J Paleont 50:90–106

Oehler DZ, Robert F, Walter MR, Sugitani K, Allwood A, Meibom A, Mostefaoui S, Selo M, Thomen A, Gibson EK (2009) NanoSIMS: insights to biogenicity and syngeneity of Archaean carbonaceous structures. Precamb Res 173:70–78

Oehler DZ, Robert F, Walter MR, Sugitani K, Meibom M, Mostefaoui S, Gibson EK (2010) Diversity in the Archean biosphere: new insights from NanoSIMS. Astrobiol 10:413–424

Olcott Marshall A, Emry JR, Marshall CP (2012) Multiple generations of carbon in the Apex Chert and implications for preservation of microfossils. Astrobiol 12:160–166

Orphan VJ, House CH (2009) Geobiological investigations using secondary ion mass spectrometry: microanalysis of extant and paleo-microbial processes. Geobiol 7:360–372

Pasteris JD, Wopenka B (2003) Necessary, but not sufficient: Raman identification of disordered carbon as a signature of ancient life. Astrobiol 3:727–738

Philippot P, van Zuilen M, Thomazo C, Farquhar J, Van Kranendonk MJ (2007) Early Archaean microorganisms preferred elemental sulfur, not sulfate. Science 317:1534–1537

Philippot P, van Zuilen M, Rollion-Bard C (2012) Variations in atmospheric sulphur chemistry on early Earth linked to volcanic activity. Nature Geosci 5:668–674

Rasmussen B, Fletcher IR, Brocks JJ, Kilburn MR (2008) Reassessing the first appearance of eukaryotes and cyanobacteria. Nature 455:1101–1104

Rasmussen B, Blake TS, Fletcher IR, Kilburn MR (2009) Evidence for microbial life in synsedimentary cavities from 2.75 Ga terrestrial environments. Geology 37:423–426

Schidlowski M, Hayes JM, Kaplan IR (1983) Isotopic inferences of ancient biochemistries: carbon, sulfur, hydrogen, and nitrogen. In: Schopf JW (ed) Earth's earliest biosphere. Princeton University Press, pp 149–186

Schopf JW, Kudryavtsev AB (2005) Three-dimensional Raman imagery of Precambrian microscopic organisms. Geobiol 3:1–12

Schopf JW, Kudryavtsev AB (2009) Confocal laser scanning microscopy and Raman imaging of ancient microscopic fossils. Precamb Res 173:39–49

Schopf JW, Kudryavtsev AB, Agresti DG, Wdowiak TJ, Czaja AD (2002) Laser-Raman imagery of Earth's earliest fossils. Nature 413:73–76

Schopf JW, Kudryavtsev AB, Agresti DG, Czaja AD, Wdowiak TJ (2005) Raman imagery: a new approach to assess the geochemical maturity and biogenicity of permineralized Precambrian fossils. Astrobiol 5:333–371

Tice MM, Bostick BC, Lowe DR (2004) Thermal history of the 3.5-3.2 Ga Onverwacht and Fig Tree Groups, Barberton greenstone belt, South Africa, inferred by Raman microspectroscopy of carbonaceous material. Geology 32:37–40

Ueno Y, Isozaki Y, Yurimoto H, Maruyama S (2001) Carbon isotopic signatures of individual Archean microfossils(?) from Western Australia. Int Geol Rev 43:196–212

Ueno Y, Yamada K, Yoshida N, Maruyama S, Isozaki Y (2006) Evidence from fluid inclusions for microbial methanogenesis in the early Archaean era. Nature 440:516–519

van Zuilen MA, Lepland A, Teranes J, Finarelli J, Wahlen M, Arrhenius G (2003) Graphite and carbonates in the 3.8 Ga old Isua Supracrustal Belt, southern West Greenland. Precamb Res 126:331–348

Wacey D (2009) Early life on Earth: a practical guide. Springer, p 285

Wacey D (2010) Stromatolites in the ~3400 Ma Strelley Pool Formation, Western Australia: examining biogenicity from the macro- to the nano-scale. Astrobiol 10:381–395

Wacey D, McLoughlin N, Green OR, Parnell J, Stoakes CA, Brasier MD (2006) The ~3.4 billion-year-old Strelley Pool sandstone: a new window into early life on Earth. Int J Astrobiol 5:333–342

Wacey D, Kilburn MR, McLoughlin N, Parnell J, Stoakes CA, Brasier MD (2008a) Using NanoSIMS in the search for early life on Earth: ambient inclusion trails in a c. 3400 Ma sandstone. J Geol Soc Lon 165:43–53

Wacey D, Kilburn MR, Stoakes CA, Aggleton H, Brasier MD (2008b) Ambient inclusion trails: their recognition, age range and applicability to early life on earth. In: Dilek Y, Furnes H, Muehlenbachs K (eds) Links between geological processes, microbial activities and evolution of life. Springer, pp 113–133

Wacey D, Kilburn MR, Saunders M (2009) A combined SIMS and TEM study of potential biosignals from Precambrian rocks. Geochim Cosmochim Acta 73:A1397

Wacey D, McLoughlin N, Whitehouse MJ, Kilburn MR (2010a) Two co-existing sulfur metabolisms in a ca. 3,400 Ma sandstone. Geology 38:1115–1118

Wacey D, McLoughlin N, Stoakes CA, Kilburn MR, Green OR, Brasier MD (2010b) The 3426-3350 Ma Strelley Pool Formation in the East Strelley greenstone belt—a field and petrographic guide. Geol Surv WA Record 2010/10:64

Wacey D, Kilburn MR, Saunders M, Cliff J, Brasier MD (2011a) Microfossils of sulfur metabolizing cells in ~3.4 billion year old rocks of Western Australia. Nature Geosci 4:698–702

Wacey D, Saunders M, Brasier MD, Kilburn MR (2011b) Earliest microbially mediated pyrite oxidation in ~3.4 billion-year-old sediments. Earth Planet Sci Lett 301:393–402

Wacey D, Menon S, Green L, Gerstmann D, Kong C, McLoughlin N, Saunders M, Brasier MD (2012) Taphonomy of very ancient microfossils from the ~3400 Ma Strelley Pool Formation and ~1900 Ma Gunflint Formation: new insights using a focused ion beam. Precamb Res 220–221:234–250

Westall F, de Ronde CEJ, Southam G, Grassineau N, Colas M, Cockell C, Lammer H (2006) Implications of a 3.472-3.333 Gyr-old subaerial microbial mat from the Barberton greenstone belt, South Africa for the UV environmental conditions on the early Earth. Phil Trans R Soc B 361:1857–1875

Williams DB, Carter CB (2009) Transmission electron microscopy: a textbook for materials science (2nd edn). Springer Science and Business Media, New York, p 832

Williford KH, Ushikubo T, Schopf JW, Lepot K, Kitajima K, Valley JW (2013) Preservation and detection of microstructural and taxonomic correlations in the carbon isotopic compositions of individual Precambrian microfossils. Geochim Cosmochim Acta 104:165–182

Wirth R (2009) Focused Ion Beam (FIB) combined with SEM and TEM: advanced analytical tools for studies of chemical composition, microstructure and crystal structure in geomaterials on a nanometre scale. Chem Geol 261:217–229

Wopenka B, Pasteris JD (1993) Structural characterisation of kerogens to granulite-facies graphite: applicability of Raman microprobe spectroscopy. Am Mineral 78:533–557

Archaean Soils, Lakes and Springs: Looking for Signs of Life

13

Alexander T. Brasier

Abstract

Microbial life in Archaean non-marine settings like soils, lakes and springs would have faced several challenges. These would have included exposure to UV light; aridity, salinity and temperature changes; and nutrient availability. Current understanding is that none of these challenges would have been insurmountable. Microbial organisms of Archaean marine environments are likely to have been similar in their lifestyles and habits to those of the Archaean terrestrial world. Non-marine stromatolites, microbial filaments, microbial borings and microbially-induced sedimentary structures might therefore have been preserved. But Archaean subaerial surfaces would have been very prone to erosion by wind and rain, so the oldest fossil 'soils' of subaerially weathered surfaces (up to 3.47 Ga) are mostly identified using geochemistry. However, some ancient duricrusts like calcretes have been reported. Archaean lacustrine microbial life may have included stromatolites of the Tumbiana Formation of Western Australia. The case that these were lacustrine rather than marine is critically assessed, with the conclusion that the stratigraphy provides the strongest supporting evidence here. Archaean terrestrial hot springs, though often mentioned in origin of life studies, are not yet known from the rock record. In the Palaeoproterozoic to present these silica and carbonate-precipitating environments are commonly found in proximity to volcanic sediments and faults, where the deposits form terraced mounds, fissure ridges and hydrothermal lakes. It remains plausible that life could have existed and even evolved in these hypothesised Archaean hot-spring settings, and there is cause for optimism that the evidence for this might one day be found.

13.1 Introduction

Archaean lakes have been linked with early life since Charles Darwin first imagined a 'warm little pond' full of primordial soup in his 1871 letter

A. T. Brasier (✉)
Faculty of Earth and Life Sciences, VU University Amsterdam, De Boelelaan 1085,
1081, Amsterdam, The Netherlands
e-mail: a.t.brasier@vu.nl

Y. Dilek, H. Furnes (eds.), *Evolution of Archean Crust and Early Life*, Modern Approaches in Solid Earth Sciences 7, DOI 10.1007/978-94-007-7615-9_13, © Springer Science+Business Media Dordrecht 2014

to Joseph Hooker. But does current knowledge still allow this hypothesis of life in Archaean lakes to be entertained? Could life have evolved or even survived in Archaean non-marine environments, and if so, where and how are the signs of life likely to be preserved?

The radio-isotopically dated lunar cratering record (e.g. Tera et al. 1974) shows a cataclysmic impacting event occurred around 3.9 Ga (±200 Ma), meaning terrestrial environments were likely inhospitable at that time. The sedimentary record only extends to around 3.8 Ga. However it is generally but cautiously (Sweetlove 2011) accepted that the record of (marine) life on Earth extends to at least 3.5 Ga (e.g. Schopf 2006), supported by recent candidates for sulphur metabolising cells in beach sandstones of the Strelley Pool Formation (Wacey et al. 2011). Continued claims that carbonaceous artefacts in the hydrothermal Apex Chert are biogenic microfossils (Schopf and Kudryatsev 2012; 2013) are still refuted on the basis of multiple tests (Pinti et al., in press; Marshall and Marshall, in press), including detailed mapping and petrographic interpretation (M.D. Brasier et al. 2011). The first recorded land surface and possible palaeosol dates to 3.47 Ga (Buick et al. 1995). This review is, therefore, primarily concerned with the possible record of life in non-marine environments in the billion year interval from 3.5 to 2.5 Ga. The volume of literature covering the many topics touched upon here is vast, so only an introductory overview can be presented in such an article as this. Therefore a short summary of the physical challenges that life would face in Archaean non-marine environments is followed by a reminder of what to look for if one is to find any signs of life in Archaean soils, lakes and springs. Some examples of likely Archaean terrestrial sediments and evidence of Archaean terrestrial life are also given, with some predictions and suggestions for future research.

13.2 Hostility of Archaean Non-Marine Environments

Microbes attempting to survive in the Archaean terrestrial world would have faced several challenges, including exposure to ultraviolet (UV) light; aridity and salinity changes; temperature fluctuations; and problems associated with access to nutrients. Nevertheless there would have been many local niches where conditions would have been more habitable (Fig. 13.1).

13.2.1 Ultraviolet Light

The existence of Archaean terrestrial (non-marine) life might have been challenged by a high flux of DNA-damaging UV light in the absence of an ozone layer (e.g. Rothschild 1999). But there is considerable uncertainty on the Earth's early atmospheric composition, and hence it is not easy to judge how hazardous UV light exposure would have been to subaerial life at ground level. One hypothesis, for example, speculates that an atmospheric organic haze (similar to that found around Saturn's moon Titan) might have protected Archaean surface environments from UV radiation (e.g. Domagal-Goldman et al. 2008). In Archaean oceans, life would have been protected by the inability of UV light to penetrate below the surface waters. This would also have been true in deep lakes. The fossil record shows that microbial mats survived in periodically exposed coastal settings around 3.5–3.3 Ga (Westall et al. 2006). UV barriers in coastal environments likely included layers of dust, snow, evaporite minerals and dead organisms (Westall et al. 2006). Glover (1992) similarly suggested shields of mud would have protected coastal microbes. These are all UV shields that could also have been found in fully terrestrial environments. Endolithic niches within the sediment or in primitive 'soils' may have been quite safe for early microbes. For example Cockell and Raven (2007) determined that a thin (mm-thick) layer of ferric iron sediment is also an effective barrier to harmful UV light, and reasonably concluded that this challenge would therefore have been resolvable by Archaean terrestrial life.

13.2.2 Aridity and Salinity

The hazard of desiccation is a particular challenge to be overcome in terrestrial environments. Extra cellular polymeric substances

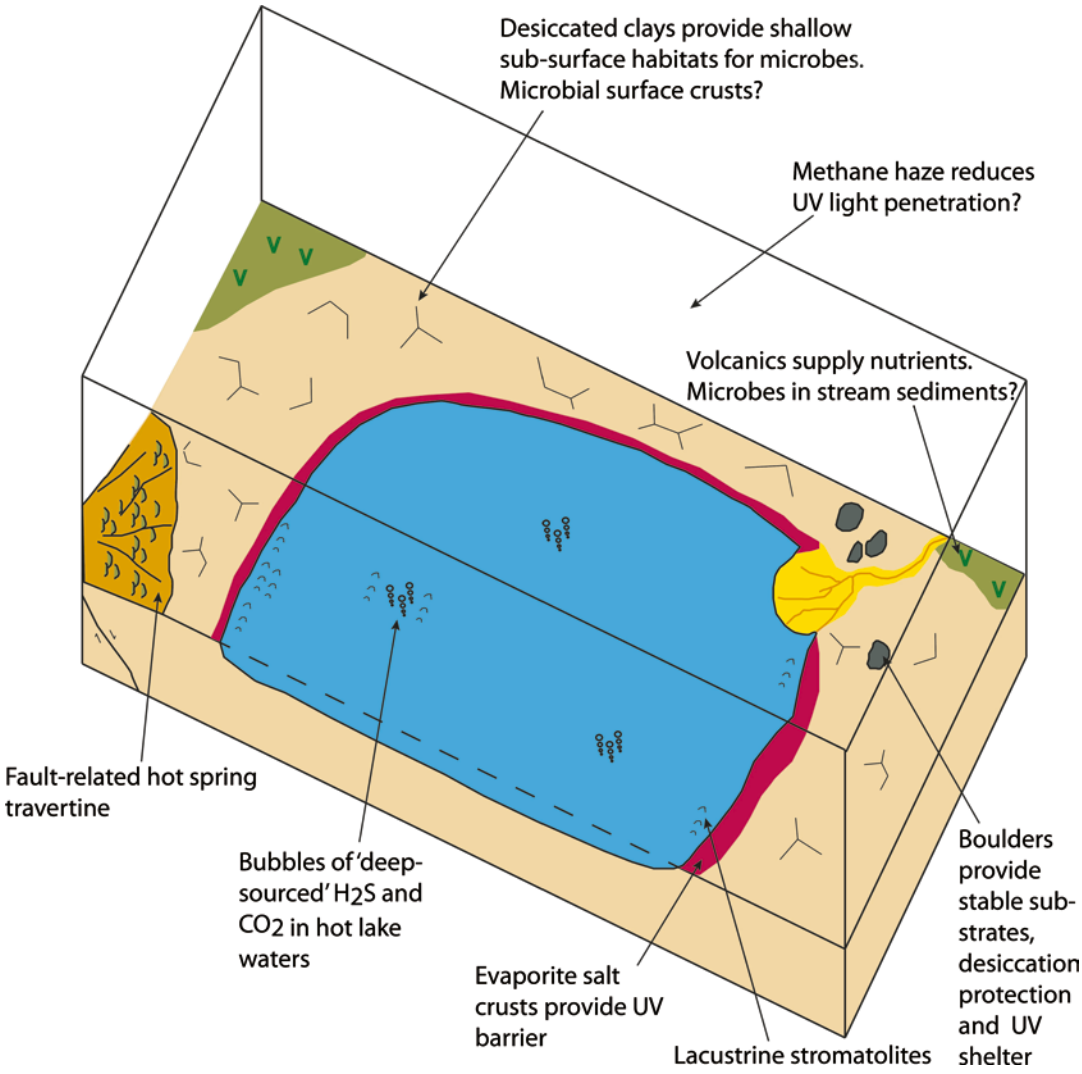

Fig. 13.1 Life in the Archaean terrestrial world, showing some likely habitable niches. Note the presence of volcanics supplying nutrients; salt crusts, desiccated clays and boulders for UV shielding (plus a potential organic haze atmosphere) and protection from desiccation. Extremes of temperature would have affected soils more than subaquatic niches

(EPS) produced by bacteria can help to reduce moisture loss and act as an osmoprotectant, as observed in some modern Alpine bacterial colonies (the latter described by Horath and Bachofen 2009). An endolithic life habit would also minimise water loss, while organisms inhabiting large Archaean lakes would perhaps have been less afflicted by desiccation. But they may have had to cope with fluctuations in lake salinity, particularly in near-coastal brackish systems. On timescales much longer than the lifespan of individual micro-organisms (perhaps thousands of years) then even the most stable of lake systems could have been prone to drying out. Life habits and cycles that enabled survival in any of freshwater rivers, brackish lakes and the sea would likely have been beneficial to the long-term survival of early lacustrine genera. Notably some modern cyanobacterial species like *Schizothrix calcicola* are able to live in all three of these settings. It seems reasonable to assume this phenomenon might also have applied

to Archaean microorganisms with similar life habits and trophic strategies.

13.2.3 Temperature

There is a dispute over the likely temperature of Archaean oceans (with implications for temperatures of terrestrial environments), stemming from interpretation of oxygen isotope values of marine carbonates and cherts (e.g. Knauth and Lowe 1978, 2003; Muehlenbachs 1998). Low chert oxygen isotope values around 7–22‰ VSMOW point towards hot ocean surface temperatures (55–85 °C according to Knauth 2005), whereas temperatures above 37 °C are intolerable to several (but not all) groups of organisms. Most palaeontologists (particularly those working on Phanerozoic rocks, where a discrepancy still exists between temperatures calculated from chert and carbonate oxygen isotope values and expected temperatures) therefore prefer an Archaean world with ocean temperatures no higher than around 37 °C. Even if Archaean oceans were extraordinarily hot, their temperatures would presumably have been more constant (and therefore more bearable to thermophilic bacteria?) than those of most terrestrial surface environments. Large lakes and perhaps some endolithic niches could have provided suitable refugia for organisms intolerant of dramatic temperature fluctuations.

13.2.4 Nutrient Availability

The majority of essential nutrients are found in volcanic rocks and volcanic gases (e.g. CO_2, SO_2, H_2, NO_2 etc) and could therefore be obtained from volcanic rocks, sediments or the atmosphere, while phosphorous could be obtained by osmotrophic organisms directly from minerals like apatite. Fungi are particularly adept at the latter. Whether any microorganisms had evolved this capacity as early as the Archaean is unknown. It is, therefore, possible that living organisms would have depended on dissolved (or volcanically-emitted) nutrients in lakes and ground waters, hindering the colonisation of drier environments until the Neoproterozoic arrival of fungi (Lücking et al. 2009).

13.3 Looking for Fossil Evidence of Ancient Terrestrial Life

The features and lifestyles of organisms that inhabited Archaean terrestrial settings are likely to have been identical or very similar microorganisms to those which inhabited coastal marine or even deep water hydrothermal settings. Therefore many of the features that would identify life in Archaean lakes or soils, for example, are the same as those that apply to the widely studied marine sedimentary record. These include stromatolites, microbial filaments preserved in cherts or carbonates, microbial borings and microbially-induced sedimentary structures (MISS).

13.3.1 Stromatolites

Stromatolites have been the subject of numerous recent reviews (for example Riding 2011; McLoughlin et al. 2013). Often assumed to be biogenic where palaeontological data are sparse (see discussion in Schopf 2006) this is not necessarily the case (McLoughlin et al. 2008). McLoughlin et al. (2013) critically evaluated several criteria used to establish the biogenicity of stromatolitic fabrics. They concluded that a biogenic origin is most easily established in stromatolites with complex morphologies that bear organic remains. There is increasing evidence that microbial assistance commonly aides calcite crystal nucleation in modern non-marine stromatolite-forming settings (Rogerson et al. 2008), yet even some Quaternary laminar carbonates formed around cool water springs are currently hard to conclusively establish as a product of microbial activity (A.T. Brasier et al. 2011a).

13.3.2 Microbial Filaments

Microbial filaments are commonly best preserved in siliceous fabrics (see Cady and Farmer 1996), as these are less prone to early diagenetic recrystallisation than those of carbonate minerals. For example modern *Phormidium* seasonally banded tufas are commonly comprised of low magne-

sian calcite that precipitated around the external surfaces of cyanobacterial filaments (Andrews and Brasier 2005; Brasier et al. 2010). The high initial porosity of these *Phormidium* tufas results from early decay of the organic filaments themselves, and only occasional entombed filaments are found. Chert fabrics have long been seen as more favourable for preservation of organic microbial remains (e.g. Tyler and Barghoorn 1954; Cady and Farmer 1996; Konhauser et al. 2003), although still susceptible to diagenetic alteration (Hinman and Walter 2005) and organic matter preservation still seems to be the exception rather than the rule (see Walter 1996). Even where carbonaceous matter is found in cherts, there are disputes over its possible biogenicity. As with carbonate precipitation (Rogerson et al. 2008) it might well be that silica precipitation around hot springs is facilitated by microbes, or the latter may just provide a stable substrate for mineral growth (Cady and Farmer 1996; Guidry and Chafetz 2003a; Konhauser et al. 2003). Abiogenic silica precipitation can occur as a result of cooling of the depositing waters, evaporation or abrupt raising or lowering of pH (see Jones et al. 1997 and references therein).

13.3.3 Microbial Borings

In the absence of immaculately preserved organic remains, traces like endolithic microbial borings (see McLoughlin et al. 2009; Jones 2010; Cockell and Herrera 2008) are potentially diagnostic signs of ancient primitive life. Such borings as might be preserved in the rock record have been described from modern speleothem-precipitating caves (Jones 2010). These can be produced by several bacterial groups. Dolomite-inhabiting endolithic communities of the Alps, for example, include Cyanobacteria, Actinobacteria, Alpha Proteobacteria and Acidobacteria. As with examples found in modern Antarctica (Friedman 1982), endolithic habits in the Archaean could have afforded microorganisms direct access to nutrients (through osmotrophy), protection from UV light, and respite from desiccation. In younger (Neoproterozoic; Lücking et al. 2009) terrestrial rocks, borings by fungal groups might one day be found. But when seeking fossil endolithic borings, it is important to distinguish between inclusion trails of abiotic origin (Lepot et al. 2009) and ancient bacterial excavations.

13.3.4 Microbially-Induced Sedimentary Structures

Microbially-induced sedimentary structures (MISS; Noffke et al. 1996) are found in tidal flat and shelf sandstones, including those of Archaean age (see for example Noffke et al. 2008). Microbial (mostly photosynthetic cyanobacterial; Noffke 2009) growth, binding, bio-stabilisation, baffling and trapping produce the seventeen types of MISS recognised by Noffke (2009; her Fig. 13.3). To increase confidence that a given MISS occurrence is of a biological origin, Noffke (2009) proposed that six criteria must be met. Briefly these are that the rocks should not have been metamorphosed beyond lower greenschist facies; that stratigraphically, the MISS should occur at the turning points in regression-transgression cycles; that MISS should be found in facies conducive to their formation and preservation (often quartz sands of high purity); that the spatial distribution of MISS corresponds to the ancient 'average hydraulic pattern'; that uniformitarian comparisons with modern examples suggest a biological origin; and that one of nine specific MISS micro-textures is present.

The aim of applying these criteria in a strict way is to reduce the number of doubtful claims of Archaean microbial life where an abiotic process might have caused MISS-like structures. Not all of these criteria can be fairly applied to the non-marine realm. In particular, Noffke (2009) suggests that in all of her sections studied to date, MISS developed 'exclusively' on wide tidal flats during shoreline transgressions. If microbially-induced sedimentary structures are the result of the physical effects of biofilms and microbial mats on sediment stabilisation, baffling and trapping then it seems unlikely that MISS are truly exclusive to shallow marine tidal flat settings, nor does there seem an *a priori* rea-

son why MISS should be exclusive to any particular point in global sea-level cycles. Although seemingly not yet found (Noffke 2009), some forms of MISS –perhaps not identical to or as easily recognisable as the seventeen forms now known from tidal settings—must surely exist and have existed where microbes abounded in sandy lakes, streams, springs and even soils. Ancient terrestrial examples will not necessarily have developed during episodes of global sea-level rise. However humid, wet time intervals (linked to sea-level highstands?) may still have provided more spatially widespread lake and stream habitats for microbes than available during the drier episodes of Earth history. Further, the spatial distribution of terrestrial MISS types is likely to be very complex and less predictable than found in marine lagoonal and tidal flat deposits (described by Noffke 2009), reflecting the relatively high frequency and rapidity of tectonically and climatically-related environmental changes in non-marine settings.

When making claims of ancient terrestrial life, in addition to meeting the several criteria associated with establishing biogenicity (such as Brasier et al. 2005; Noffke 2009; McLoughlin et al. 2013), one must further establish that the setting was non-marine or subaerial at the time the organisms were alive. In the absence of diagnostic fossils this is not always easy or incontrovertible.

13.4 Identifying Archaean 'Soils'

Archaean 'soil' differed from its modern counterparts that are products of biological processes. Retallack (2007) included "rocks altered by hydrolitic weathering" under the palaeosol heading. Often this broad definition is useful in astrobiology and 'deep-time' research, facilitating study of subaerially exposed and weathered surfaces (including Brasier et al. 2013a). The use of soil taxonomy (terms like 'Aridisol' and 'Mollisol') to classify palaeosols in the same way as those of the modern world is highly contentious (see for example Mack et al. 1993; Dahms and Holliday 1998; Retallack 1998). This is because many of the defining characteristics of modern soils require accurate measurement of specific environmental conditions that could only ever be inferred for palaeosols. Nevertheless, the scheme of Mack et al. (1993) was intended for use on soils of all ages and has been quite widely adopted. It has often proven useful in Quaternary palaeoenvironmental studies (e.g. Leeder et al. 2008). Caution is urged in inferring, for example, climatic conditions from a particular soil characteristic because the (potentially and even likely invalid) uniformitarian assumptions that must be made—particularly in studies of pre-Silurian rocks—cannot be overlooked. This may be less of an issue from the late Palaeozoic to the present.

Criteria are required to identify an Archaean soil, and Rye and Holland (1998) applied the following:

1. the unit must be developed on a homogenous parent rock and have been preserved in place;
2. the unit must exhibit changes in mineralogy, texture and chemical composition from the parent rock to the top of the soil that are consistent with soil forming processes;
3. there must be identifiable soft-sediment deformation features (e.g. re-worked soil clasts) along the contact between the unit and the immediately overlying rocks.

To distinguish 'soils' from hydrothermally altered rocks, Grandstaff et al. (1986) recommended the following criteria, some of which are similar to those adopted by Rye and Holland (1998):

1. palaeosols are stratiform, found parallel to bedding;
2. palaeosols are relatively thin (usually < 20 m);
3. palaeosols have transitional lower boundaries and sharp upper boundaries, the latter due to a disconformity or unconformity;
4. palaeosols often exhibit colour variations;
5. palaeosols exhibit the destruction of primary rock textures, often accompanied by the formation of 'soil' textures including clay coatings on grains ('cutans'), calcite or silica nodules, or iron and manganese crusts;
6. palaeosols exhibit the destruction of primary minerals to form clay minerals;
7. palaeosol elemental distributions often show depletion of most cations and enrichment of Al, Ti, Zr and other elements forming insol-

uble compounds. However, this pattern can change according to the geochemical conditions during soil formation, such as with calcrete and silcrete formation;
8. palaeosols may include neptunian dykes of sediment washed down into desiccation cracks;
9. palaeosols may be found as rip-up clasts in overlying sediments

There must be good reason to believe that chemical alteration took place in a subaerial setting and not later during burial. This evidence may come from the stratigraphy, as with the late Archaean Dominion Group palaeosol of South Africa. This palaeosol is directly overlain by fluvial sediments (Grandstaff et al. 1986). These criteria of Grandstaff et al. (1986) and Rye and Holland (1998) are good for identifying subaerially weathered surfaces, if not necessarily 'soils' *sensu stricto*.

If using the criteria of Rye and Holland (1998) then each of the "changes in mineralogy, texture and chemical composition" that are to be expected in an Archaean 'soil' must be defined by the observer. Rye and Holland (1998), for example, looked for 'soils' developed on igneous rocks, and found they usually became increasingly sericite-rich towards their tops. They decided this was a useable criterion for identifying 'soils' amenable to geochemical reconstruction of Archaean palaeoatmospheric compositions. They also looked for invariant ratios between immobile elements (like Ti/Zr and Ti/Al) from the parent rock to the top of the identified 'soil', coupled with loss of the more soluble, mobile elements like Ca, Mg and (in an atmosphere with little free oxygen) Fe^{2+} from the 'soil' tops. The obvious assumption here is that the identified 'soil' is simply comprised of the weathered surface of the bedrock (see Fig. 13.2). This definition excludes 'soil' examples that contain allochthonous materials like wind-blown dust or organic matter. Allochthonous desert dusts constitute a significant proportion of many modern soils (e.g. Goudie and Middleton 2001), and many modern soils are formed in alluvial and fluvial sediments. This might not have been the same in the Archaean because of the absence of plant roots to bind these loose materials together, since these surface materials might easily have been eroded (Fig. 13.2). For the geochemical palaeoenvironmental reconstruction purposes of Rye and Holland (1998), avoiding these allochthonous materials was in any case desirable.

What these Archaean palaeosols or weathered surfaces (e.g. Grandstaff et al. 1986; Rye and Holland 1998) actually tell us about the level of free oxygen in the early atmosphere is not the central focus of this review. However, it is worth noting that iron can be retained in chemically weathered rocks even in reducing conditions: the haematite of Martian dust is a likely example of this. Explanations for production of haematite in the absence of free atmospheric oxygen on Mars include oxidation of iron in hydrothermal environments, where water thermally dissociates and H_2 gas is lost from the system (e.g. Catling and Moore 2003). Iron retention in a palaeosol is therefore not necessarily an indicator of free atmospheric oxygen.

There are rare cases where 'un-weathered' subaerial exposure surfaces are preserved, such as the ashfall tuffs of the Ventersdorp Supergroup, South Africa, which purportedly exhibit the impressions of Archaean raindrops (Som et al. 2012). The lack of their removal by weathering and denudation is testament to the short time these surfaces were exposed to the atmosphere prior to burial. Conceivably the several voids in such rocks could have been inhabited by microbes hiding from UV exposure and desiccation, though that has not been reported in this case.

13.4.1 Morphological Characteristics of Archaean 'Soils'

Many of the features of modern soils would not have been present in the Archaean, making such ancient examples harder to identify (see also Brasier et al. 2013a). Fossil roots, 'one of the best criteria for recognition of paleosols in sedimentary rocks' (Retallack 2007), will not be found in the Precambrian. Vertical horizonation, a feature of modern soils, will also be harder to identify in the most ancient cases. The topsoil ('A') horizon of a modern profile might be dark coloured and

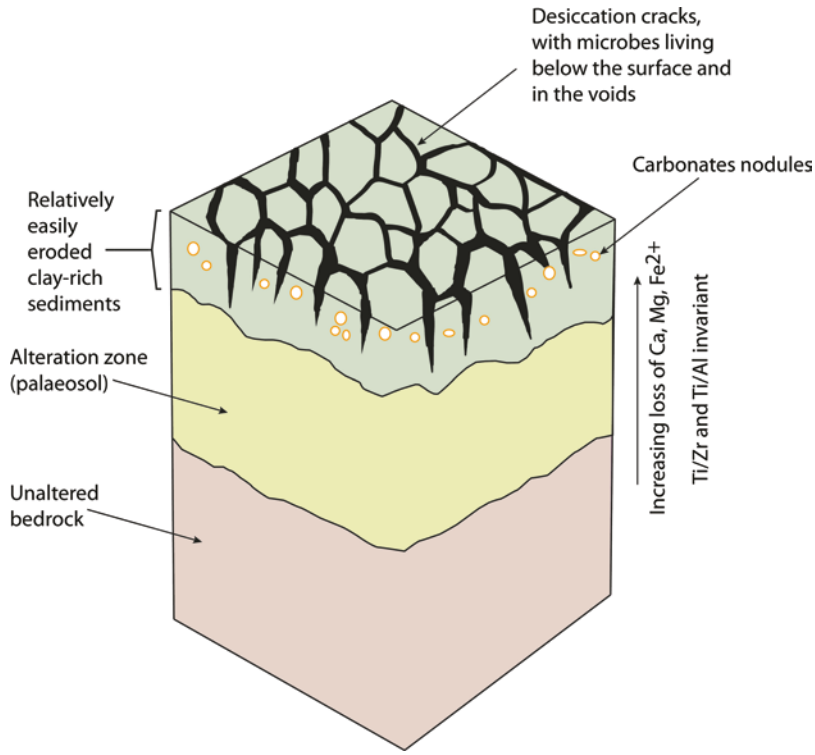

Fig. 13.2 Features of an Archaean soil. Unaltered bedrock passes transitionally into altered 'soil', with increasing loss of Ca, Mg and Fe^{2+} ions towards the soil top (except where duricrust layers form). Unconsolidated sediment would have been easily eroded without the stabilising effect of plant roots, so most Archaean soils are now identified geochemically

organic-rich, and possibly underlain by eluviated (E) and illuviated (B) horizons, becoming transitional (C horizon) to the partially weathered bedrock (R horizon). In the absence of plants, their roots and symbiotic fungi, most Archaean 'soils' would have been more like modern Entisols (or Protosols of Mack et al. 1993): showing only weak development of horizons (Fig. 13.2). However, this does not mean Archaean soils entirely lacked features such as aggregates of clay minerals ('peds') with slickensides and grain-surrounding clay layers ('cutans'), which form through the shrinking and swelling of clay minerals. Nodules or glaebules and pisoliths of authigenic precipitates, commonly carbonates and silica, might also have been present in Archaean soils (see Fig. 13.2 and Brasier 2011). But when searching for an Archaean soil, one must consider the preservation potential of these fabrics. Without plant roots to bind the sediment and remove excess moisture, the unconsolidated surface regolith will have been prone to regular removal by strong winds and rains. Duricrusts like calcretes and silcretes (Brasier et al. 2013a) have a relatively high chance of surviving weathering, denudation, burial and even metamorphism. They might even preserve textural and geochemical evidence of microbial habitation of Earth's early land surfaces (for example Watanabe et al. 2000). This issue of preservation could be the central reason why Archaean soils have so far mostly been identified using geochemical techniques to identify zones of alteration beneath unconformities.

13.4.2 Archaean 'Soil' Examples

The oldest reported exposed land surface (3.47 Ga) belongs to the Pilbara Craton, Western Australia (e.g. Buick et al. 1995; Johnson et al. 2009). This is an angular unconformity beneath rocks of the Warrawoona Group. Chert beds beneath the unconformity surface form steep ridges draped by the overlying succession, indicating at least 10 m of sediment were eroded (Buick et al. 1995). Underlying igneous rocks are more altered (felsics more kaolinitic, mafics less chloritic) within 50 m of the contact, and Buick et al. (1995) suggested

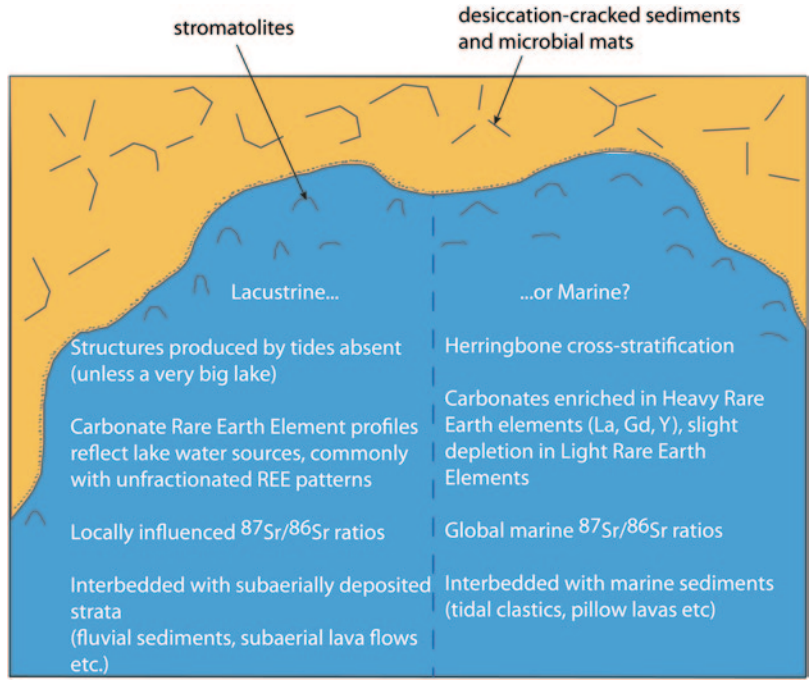

Fig. 13.3 Some criteria for differentiating between lacustrine and marine strata

this alteration zone might be interpreted as Earth's oldest known 'palaeosol'.

Rye and Holland (1998) summarised fifty possible cases of subaerially weathered horzions ('soils') of pre-Devonian age, concluding that fifteen of these met their criteria to be considered 'definite soils'. Of these, the oldest two examples developed on the 2.765 ± 0.1 Ga Mount Roe Basalts, and they were named Mount Roe #1 and Mount Roe #2. The basalts are highly vesicular and do not contain pillow structures, and hence they were interpreted as having erupted subaerially (Rye and Holland 2000). The palaeosols were indentified using the geochemical criteria of Rye and Holland (1998) described above. Expanding on their description and interpretation, Rye and Holland (2000) suggested that Mount Roe #2 contains evidence for terrestrial habitation and even methanotrophy in the form of organic carbon with distinctly light $\delta^{13}C$ compositions (−33 to −51‰ VPDB). They suggested the carbon might represent methanotrophs that were present in the soil, or could originally have been deposited in a hypothesised nearby lake.

Palaeosols of Mpumalanga Province, South Africa, are said to be between 2.7 and 2.6 Ga old (Watanabe et al. 2000). At the Schagen locality, 2.7 Ga serpentinised dunites have been interpreted as having undergone Archaean subaerial alteration to produce a 17 m thick palaeosol including void-filling precipitates of calcite, dolomite and quartz (Watanabe et al. 2000). These authors believed the calcium to be allochthonous (CaO up to 54%); magnesium to be derived from the serpentinites; and bicarbonate ions from the atmosphere, and this may be so. However, carbonatisation of serpentinite to produce dolomite and calcite (sometimes termed 'ophicalcite') could explain the carbonate features Watanabe et al. (2000) describe. Unlike pedogenic calcrete formation, this carbonatisation is a process akin to 'groundwater calcrete' formation, which does not require subaerial exposure or a seasonal climate (see for example Wright and Tucker 1991; Brasier 2011).

Watanabe et al. (2000) claimed 2.6 Ga terrestrial biogenic organic matter in the purported palaeosol they described. The organic matter, which has measured $\delta^{13}C$ of −17.4‰ to −14.3‰ PDB, is found closely associated with clay layers that are presumed to be depositional or derived from a depositional texture. The organic matter is not

concentrated in fissures, potentially reflecting its origin as terrestrial microbial mats formed on the surface of a 'soil' 2.6 billion years ago. Further, Watanabe et al. (2000) claim the crystallinity and H/C index of the organic matter show that it is unlikely to be of hydrothermal origin, and predates a metamorphic event at around 2.0 Ga.

13.5 Lakes

Differentiating Archaean and Proterozoic lacustrine deposits from their marine equivalents is notoriously challenging (Fig. 13.3). The suggestion of continent-flooding epeiric seas (e.g. Kamber et al. 2004) and giant lakes (e.g. Awramik and Buchheim 2009) in the Archaean adds to this complexity. In the absence of diagnostic palaeontology, arguments must be made using sedimentology, stratigraphy, geochemistry, physics or a combination of these. The distinction between marine and non-marine environments is important because this impacts on ones interpretation of the local versus global nature of organism populations and geochemical events.

Westall et al. (2006) claimed anoxygenic photosynthesisers likely built the desiccation-cracked mats of the Josefsdal Chert (Barberton Greenstone Belt) in a coastal marine setting that was periodically subaerial. If so, then life should have been able to withstand the transition from coastal, periodically exposed settings to lakes, streams and soils. Some workers (e.g. Glover 1992) have even postulated that life may have originated in coastal or coastal lacustrine sands. The hypothesis of Glover (1992) was that radiation from heavy minerals concentrated within the sands would provide the necessary heat for polymerisation of organic molecules. Glover (1992) reasonably suggested looking for fossil microbes in the silica cements of such sandstones.

13.5.1 Archaean Lakes: The Tumbiana Formation as an Example?

Stromatolites of the 2.7 Ga Tumbiana Formation (Fortescue Group), Western Australia, have been variously interpreted as lacustrine (Buick 1992; Bolhar and van Kranendonk 2007; Awramik and Buchheim 2009) and as marine (Packer 1990; Thorne and Trendall 2001; Sakurai et al. 2005). These stromatolites were undoubtedly deposited in very shallow waters, as deduced from desiccation cracks, ripples and the topographic relief of the stromatolites themselves.

Buick (1992) suggested that lack of evidence for sulphates in an evaporitic setting reflected a lacustrine rather than marine environment for the Tumbiana Formation. Yet one could ascribe this lack of evidence for sulphate minerals to the low level of free oxygen at this early point in Earth history. The first widespread marine sulphates are not found in the rock record until after 2.4 Ga (e.g. Kah et al. 2004; Melezhik et al. 2005; Schröder et al. 2008; A.T. Brasier et al. 2011b). Further, there is a debate surrounding the presence (e.g. Sakurai et al. 2005) or absence (e.g. Awramik and Buchheim 2009) of sedimentary indicators of (marine) tidal currents, such as herringbone cross-stratification in the Tumbiana Formation.

Packer (1990) reported relatively invariant carbonate carbon isotope values close to 0‰ PDB, and suggested these support a marine origin for the Tumbiana Formation. However, this carbon isotope evidence is not diagnostic. First, in the absence of abundant terrestrial plants, it is likely that marine carbonate (or in some settings volcanic) carbon dominated the dissolved inorganic carbon of Archaean terrestrial waters. Therefore, Archaean terrestrial carbonates are likely to have carbon isotope compositions between approximately 0 and −6‰ VPDB. Cambrian calcretes, for example, have compositions between −1 and −3‰ VDPB (Buggisch et al. 2003). Second, meteoric waters that have long residence times in marine carbonate bedrock are likely to precipitate carbonates with carbon isotopic compositions close to 0‰ VPDB.

Rare Earth Element (REE) patterns cannot on their own allow distinction between marine and lacustrine carbonates (see for example Johannesson et al. 2006), but have been muted as supporting evidence for a lacustrine origin of the Fortescue Group stromatolites by Bolhar and van

Kranendonk (2007). The latter authors believed their shale-normalised REE patterns to have resisted diagenetic alteration, and to show similarities with those of the lacustrine Eocene Green River Formation carbonates. These Fortescue Group stromatolites display no enrichment in either heavy or light rare earth elements relative to the 'post-Archaean Australian shale' they used as a baseline. In contrast, modern marine carbonates are normally enriched in heavy rare earth elements.

Probably the strongest reported evidence that the Tumbiana Formation stromatolites can plausibly be interpreted as non-marine comes from their stratigraphic context, sandwiched between two subaerially-erupted basalts and in close proximity to fluvial sediments (see Buick 1992; Awramik and Buchheim 2009).

13.5.2 Other Potential Archaean Lakes

Kamber et al. (2004) examined the REE and strontium isotope geochemistry of the Archaean Mushandike limestone (Masvingo Greenstone Belt, Zimbabwe), demonstrating a correlation between the REE and Sr data. The $^{87}Sr/^{86}Sr$ values were relatively radiogenic (the lowest being 0.7184), implying input from 3.8 to 3.5 Ga, Rb-rich Archaean gneisses of south-central Zimbabwe. The Mushandike limestone REE pattern was interpreted as reflecting input of locally derived detrital grains to a continent-flooding (marine) epeiric sea.

Stromatolites of the Ventersdorp Group of South Africa reported as terrestrial by Buck (1980) date from around 2.7 Ga (Armstrong et al. 1991). The palaeoenvironmental interpretation of Buck (1980) envisages these stromatolites forming in pools formed by depressions on fluvial floodplains. The evidence for this is based on sedimentary textures and stratigraphy. For example, ripple cross-lamination; 'mud-flake' conglomerates and desiccation cracks require a shallow water to subaerial setting. Poorly-sorted conglomerates and sandstones interpreted as debris flow deposits (partly re-worked by ephemeral streams) are interbedded with the stromatolitic horizons. The stromatolites themselves are commonly desiccated and comprised by layers of either dolomite or chert alternating with mud laminae.

13.6 Terrestrial Springs

Silica or carbonate precipitating (hot) springs can be excellent environments for preservation of (thermophilic) bacterial fossils (see for example Walter and Des Marais 1993; Cady and Farmer 1996; Konhauser et al. 2003). Several authors have suggested life could have thrived or even originated around deep sea hydrothermal vents, including Corliss et al. 1981; Baross and Hoffman 1985; Walter 1996; Ueno et al. 2004; Hoffman 2011, amongst several others. Walter and Des Marais (1993) even suggested looking for Martian thermal springs and their precipitates in the search for extra-terrestrial life. Much less is known or reported of subaerial and sublacustrine hydrothermal springs than submarine examples in 'deep time', with no or very few described Archaean cases and only a few likely deposits documented from Proterozoic rocks (see Brasier 2011). It is noticeable that most recorded ancient spring precipitates were either silica-depositing systems or are now at least part silicified carbonate, perhaps reflecting that most depositing springs precipitated silica, but likely also reflecting the better chances of preservation of a primary silica or silicified deposit.

Heat flow on the young Earth would have been high, and therefore Archaean hot springs should have been common (Walter 1996). On the modern Earth, one can make a distinction between 'ambient temperature' meteogene springs where water is sourced from rainfall, and 'thermogene' springs where a 'deep source', commonly of hot water is involved (see Pentecost 2005). This difference has an important effect on the biology and chemistry of the spring, and therefore on the facies, petrographic and mineralogical properties of any resulting precipitates. In the Archaean it is plausible that all springs would have been 'hot' to any inhabiting organisms (likely >35 °C), and therefore such a distinction is not easy to make and arguably not required (Brasier 2011; Brasier et al. 2013b).

Modern and Phanerozoic hot springs are associated with igneous bodies, commonly with a fault as a conduit for 'deep sourced' fluids rising to the surface. Dissolved H_2S concentrations may be high in such scenarios, as found in some modern Italian cases (Chafetz and Folk 1984). Classic modern examples include Mammoth Hot Springs of Yellowstone National Park in the USA (Tilden 1897; Walter 1976a, b; Pentecost 1990; Fouke 2000; Guidry and Chafetz 2003a, b). Here, regional groundwaters are heated to around 100 °C by near-surface magma chambers and travel to the surface along two major faults. Surface temperatures of the waters are up to around 95 °C (Chafetz and Folk 1984), cooling down with increasing distance (metres or tens of metres) from the spring as they flow over aprons and terraces (see also Walter and Des Marais 1993; Jones et al. 1998; Brasier et al. 2013b). Walter (1976a, b) found that silica 'geyserite' precipitation in Yellowstone National Park springs does not proceed at temperatures below 73 °C. This temperature is commonly taken as the limit above which only thermophilic bacteria are expected (e.g. Jones et al. 1997), with cyanobacteria and thermophilic bacteria found where waters have been able to cool sufficiently.

In carbonate-precipitating 'terraced mounds' (Chafetz and Folk 1984; Guidry and Chafetz 2003a), facies proximal to the spring vent comprise aragonite needle botryoids, with sheets of calcite, calcified bubbles and feather crystals found more distally (Fouke et al. 2000). If Archaean surface temperatures were closer to values found around the vents, then one might not expect such strong temperature-related gradients (and thus aragonite to calcite transitions) around Archaean 'hot' spring mounds. However, chemical gradients, with higher ionic strength solutions proximal to the vent than found in distal locations, might be anticipated. It is, therefore, plausible that bacteria with different trophic strategies would have inhabited their own specific zones around Archaean terrestrial spring vents. Indeed, such chemical gradients might have actively encouraged microbial diversification.

Several different types of 'hot spring' settings have been documented. Facies models relevant to early Earth history described by Brasier et al. (2013b) were inspired by models like those of Pedley (1990), Pentecost and Viles (1994), Jones et al. (1998) and Guidry and Chafetz (2003a) that are of most relevance to the Quaternary. Archaean settings could include 'terraced mounds' similar to those of Mammoth Hot Springs, but also 'fissure ridges' (elongate, narrow ridges from which waters escape and precipitate minerals) and 'hydrothermal lakes' (Brasier et al. 2013b). Where no deep-sourced fluids were involved (as might be interpreted where there are no volcanic sediments in the stratigraphy, or no fault conduit for fluids) then the 'perched springline', 'fluviatile' and 'lacustrine' facies models of Brasier et al. (2013b) might be more relevant. However, Brasier (2011) noted that high atmospheric pCO_2 levels on the early Earth would not have favoured carbon dioxide degassing (and thus carbonate precipitation) from surface waters. Some calcite precipitation might still have occurred around springs where the precipitating waters had very high pCO_2 from 'deep sources' like subducted sediments or volcanics. Silica precipitation also seems to be more common in settings with significant volumes of volcanic rock, so it is likely that the majority of Archaean terrestrial hot springs that could have preserved evidence of ancient terrestrial life were 'hot spring-like' settings in volcanic areas.

Some selected petrographic features of spring carbonates that might be observed in any Archaean examples are tabulated in Brasier (2011). Petrographic studies of modern silica 'geyserite' precipitates have revealed columnar and stratiform stromatolitic fabrics (Walter 1976a; b; Jones et al. 1997, 1998; Hinman and Walter 2005) plus spicules, oncoids, peloids and breccias (Campbell et al. 2001; Guidry and Chafetz 2003b; Konhauser et al. 2003).

Diagenesis of siliceous precipitates involves transformation from opal-A to opal-CT and quartz, often as a result of exposure to high temperatures. Hinman and Walter (2005) compared siliceous hot spring deposits of Artist Point, Yellowstone National Park with those of Steamboat Springs, Nevada. They found that the latter exhibited similar but fewer 'original' petrographic characteristics, and ascribed this to differences

in the early diagenetic histories of the two deposits. Hot springs can have complex diagenetic histories because of heating of facies deposited at 'cooler' temperatures by hot waters (even affecting facies only a few centimetres below the surface); temporal fluctuations in the amount of hot-spring activity; and contributions from subsurface waters of different compositions and temperatures (Guidry and Chafetz 2003b).

Stratigraphically underlying the mineral precipitates of an ancient hot spring, one might look for hydrothermal breccias. In silica-depositing environments these are likely to be chert cemented, as found in a Jurassic example from Patagonia (Guido and Campbell 2009). As a further example of the field occurrence of an ancient 'hot-spring' deposit, the succession containing the famous Devonian Rhynie Chert and its flora and fauna includes a lava flow preserved beneath subaerially deposited tuffaceous sandstones. In turn, these underlie the interbedded shales and thin sandstones that contain the Rhynie Chert (Trewin and Rice 1992).

13.6.1 Archaean Spring Examples?

For all that is written of hydrothermal activity in the Archaean, the oldest reported hydrothermal travertines are Palaeoproterozoic, with seemingly no reports of any Archaean terrestrial springs (Melezhik and Fallick 2001; Pirajno and Grey 2002; Rainbird et al. 2006). The Kuetsjärvi Sedimentary Formation travertines of the Pechenga Basin, Fennoscandian Russia, were documented by Melezhik and Fallick (2001), Melezhik et al. (2004) and Brasier et al. (2013b). They date from between 2.2 and 2.06 Ga. Purported hydrothermal travertines include laminated dolomitic carbonate sheets of 1–15 cm thickness, and dolomitic mounds of 1–10 cm height. Some silica in these specimens was also interpreted as an original 'sinter' precipitate (Melezhik and Fallick 2001). The interpretation that the fluids were likely 'deep sourced' and hot-spring-like is based on association with volcanic sediments and carbon isotope values around −6‰ VPDB (Melezhik and Fallick 2001).

The pervasively silicified Bartle Member of the Killara Formation of Western Australia also contains some interpreted Palaeoproterozoic terrestrial hot spring sediments (Pirajno and Grey 2002). Chert veins within continental tholeiitic volcanics lower in the Killara Formation were interpreted as evidence for the conduits of hydrothermal fluids that fed chert layers of the Bartle Member (Pirajno and Grey 2002). These authors also reported that the cherts contain 'microdubiofossils'. The 1.79 Ga Kunwak Formation of northern Canada includes likely hydrothermal travertine, interpreted as such and described as laminar colloform calcite by Rainbird et al. (2006). Swallow tail shapes of gypsum crystals are consistent with H_2S-rich depositing waters, and there is also an association between hot spring deposits and volcanic sediments here.

13.7 Discussion: Finding Signs of Life in Archaean Soils, Lakes and Springs

Returning to the question asked at the beginning of this review, it seems likely that life could have survived (perhaps even evolved) in Archaean non-marine environments. Big Archaean lakes like that envisaged by Awramik and Buchheim (2009) could have provided reasonably stable environments for microorganisms to flourish. Individual lakes would have grown their own disparate populations, each facing specific geochemical conditions unique to their environment, and therefore helping to drive evolution and increase global diversity through natural selection. Notably one does not require global glaciations or meteorite impacts to cause a crisis in a lake of any size. Major catastrophes in terrestrial environments could have been a change in the direction from which rainfall arrives; the incision of a river; a succession of cold winters. These are all factors that can dramatically affect the physical characteristics of a lake, challenging life to adapt and evolve, and are common occurrences in geological history.

But with the exception of some plausible lacustrine stromatolites, well-preserved evidence of early terrestrial life (even early terrestrial soil)

is scarce. There is a time gap of around 800 million years between (carbon isotopic and stromatolitic) suggestions of life on land at around 2.7 Ga and the likely maximum age for life on land at around 3.5 Ga. Given that most recorded Archaean terrestrial deposits are siliceous or silicified, carbonaceous microbial filaments are most likely to be found in silicified lacustrine or fluvial sandstones. Hopefully, further searching in such environments will help to uncover some of this missing record.

13.8 Conclusions

The challenges faced by life in coastal marine environments from ~3.5 Ga onwards would have been very similar to those faced by microorganisms in Archaean lakes. These include exposure to UV radiation; desiccation, temperature fluctuations and access to nutrients. Current studies suggest that each of these challenges would have been resolvable, probably with endolithic and sub-aquatic life habits favoured over the most exposed surface settings. The features and effects of organisms that inhabited terrestrial Archaean environments will have been similar to those found in marine environments. Therefore, visual evidence to look for in non-marine settings should include stromatolites, microbial filaments (often in cherts), microbial borings and microbially-induced sedimentary structures.

There are some reports of truly ancient duricrusts like calcretes and silcretes, but without any protective vegetation cover the Archaean subaerial world would have been very prone to erosion by wind and rain. The more easily eroded Archean regolith is seemingly scarcely preserved. Archaean 'soils' or subaerially weathered surfaces, including an example as old as 3.47 Ga, are therefore most commonly identified using geochemical criteria.

It seems to be generally accepted that life could have survived in Archaean lakes. Yet differentiating lacustrine from marine environments is a major challenge in the Archaean. Stratigraphic evidence that an environment was lacustrine remains the most robust, backed up by potential geochemical indicators like strontium isotopes and rare earth element profiles of authigenic carbonates.

Hot springs are commonly mentioned in discussions of the origin of life, but despite well-reasoned suggestions that they should have been common, no Archaean terrestrial hot springs are yet known. The oldest likely cases are Palaeoproterozoic. Most ancient preserved hot spring deposits are siliceous or at least part silicified, generally associated with volcanic sedimentary rocks. Although themselves subject to diagenesis, siliceous fabrics are commonly more robust than those of carbonates. Whether or not life originated in the dynamic niches around 'deep-sourced' sub-lacustrine hot springs, there is hope that such deposits and their fossilised biota might one day be found.

References

Andrews JE, Brasier AT (2005) Seasonal records of climatic change in annually laminated tufas: short review and future prospects. J Quatern Sci 20(5):411–421

Armstrong RA, Compston W, Retief EA, Williams IS, Welke HJ (1991) Zircon ion microprobe studies bearing on the age and evolution of the Witwatersrand triad. Precambr Res 53(3–4):243–266

Awramik SM, Buchheim HP (2009) A giant, late Archean lake system: the Meentheena member (Tumbiana Formation; Fortescue Group), Western Australia. Precambr Res 174(3–4):215–240

Baross JA, Hoffman SE (1985) Submarine hydrothermal vents and associated gradient environments as sites for the origin and evolution of life. Origins Life Evol B 15(4):327–345

Bolhar R, Van Kranendonk MJ (2007) A non-marine depositional setting for the northern Fortescue Group, Pilbara Craton, inferred from trace element geochemistry of stromatolitic carbonates. Precambr Res 155(3–4):229–250

Brasier AT (2011) Searching for travertines, calcretes and speleothems in deep time: Processes, appearances, predictions and the impact of plants. Earth-Science Rev 104(4):213–239. doi:10.1016/J.Earscirev.2010.10.007

Brasier AT, Andrews JE, Marca-Bell AD, Dennis PF (2010) Depositional continuity of seasonally laminated tufas: Implications for $d^{18}O$ based palaeotemperatures. Glob Planet Change 71:160–167. doi:10.1016/j.gloplacha.2009.03.022

Brasier AT, Andrews JE, Kendall AC (2011a) Diagenesis or dire genesis? The origin of columnar spar in tufa stromatolites of central Greece and the role of

chironomid larvae. Sedimentology 58(5):1283–1302. doi:10.1111/J.1365-3091.2010.01208.X

Brasier AT, Fallick AE, Prave AR, Melezhik VA, Lepland A (2011b) Coastal sabkha dolomites and calcitised sulphates preserving the Lomagundi-Jatuli carbon isotope signal. Precambr Res 189:193–211. doi:10.1016/j.precamres.2011.05.011

Brasier AT, Melezhik VA, Fallick AE (2013a) Caliche. Reading the archive of Earth's oxygenation. In: Melezhik VA, Prave A, Fallick AE et al. (eds) Global events and the Fennoscandian Arctic Russia—Drilling Early Earth Project, vol 3. Frontiers in Earth Sciences, vol 8 Springer, Berlin, pp 1419–1434. doi:10.1007/978-3-642-29670-3_9

Brasier AT, Salminen P, Karhu J, Melezhik VA, Fallick AE (2013b) Earth's earliest travertines. In: Melezhik VA, Prave A, Fallick AE et al. (eds) Reading the archive of Earth's oxygenation: Global events and the Fennoscandian Arctic Russia—Drilling Early Earth Project, vol 3. Frontiers in Earth Sciences, vol 8 Springer, Berlin, pp 1435–1456. doi: 10.1007/978-3-642-29670-3_9

Brasier MD, Green OR, Lindsay JF, McLoughlin N, Steele A, Stoakes C (2005) Critical testing of earth's oldest putative fossil assemblage from the 3.5 Ga Apex Chert, Chinaman Creek, western Australia. Precambr Res 140 (1–2):55–102. doi:10.1016/J.Precamres.2005.06.008

Brasier MD, Green OR, Lindsay JF, Stoakes CA, Brasier AT, Wacey D (2011) Geology and putative microfossil assemblage of the c.3460 Ma 'Apex Chert', Western Australia—a field and petrographic guide. Geol Surv West Aust. Rec 2011/7:1–66

Buck SG (1980) Stromatolite and ooid deposits within the fluvial and lacustrine sediments of the Precambrian Ventersdorp Supergroup of South Africa. Precambr Res 12(1–4):311–330

Buggisch W, Keller M, Lehnert O (2003) Carbon isotope record of late Cambrian to early Ordovician carbonates of the Argentine Precordillera. Palaeogeogr Palaeoclimatol Palaeoecol 195(3–4):357–373

Buick R (1992) The antiquity of oxygenic photosynthesis—evidence from stromatolites in sulfate-deficient Archean lakes. Science 255(5040):74–77

Buick R, Thornett JR, Mcnaughton NJ, Smith JB, Barley ME, Savage M (1995) record of emergent continental-crust similar-to-3.5 billion years ago in the Pilbara Craton of Australia. Nature 375(6532):574–577

Cady SL, Farmer JD (1996) Fossilization processes in siliceous thermal springs: Trends in preservation along thermal gradients. Ciba Foundation Symposium 202:150–173

Campbell KA, Sannazzaro K, Rodgers KA, Herdianita NR, Browne PRL (2001) Sedimentary facies and mineralogy of the late Pleistocene Umukuri silica sinter, Taupo Volcanic Zone, New Zealand. J Sed Res 71(5):727–746

Catling DC, Moore JA (2003) The nature of coarse-grained crystalline hematite and its implications for the early environment of Mars. Icarus 165(2):277–300. doi:10.1016/S0019-1035(03)00173-8

Chafetz HS, Folk RL (1984) Travertines: depositional morphology and the bacterially constructed constituents. J Sed Petrol 54(1):289–316

Cockell CS, Herrera A (2008) Why are some microorganisms boring? Trends Microbiol 16(3):101–106. doi:10.1016/J.Tim.2007.12.007

Cockell CS, Raven JA (2007) Ozone and life on the Archaean earth. Philos T R Soc A 365(1856):1889–1901. doi:10.1098/Rsta.2007.2049

Corliss JB, Baross JA, Hoffman SE (1981) An hypothesis concerning the relationship between submarine hot springs and the origin of life. Oceanol Acta 4(Suppl):59–69

Dahms DE, Holliday VT (1998) Soil taxonomy and paleoenvironmental reconstruction: A critical commentary. Quatern Int 51(2):109–114

Domagal-Goldman SD, Kasting JF, Johnston DT, Farquhar J (2008) Organic haze, glaciations and multiple sulfur isotopes in the Mid-Archean Era. Earth Planet Sci Lett 269(1–2):29–40

Fouke BW, Farmer JD, Des Marais DJ, Pratt L, Sturchio NC, Burns PC, Discipulo MK (2000) Depositional Facies and Aqueous-Solid Geochemistry of Travertine-Depositing Hot Springs (Angel Terrace, Mammoth Hot Springs, Yellowstone National Park, U.S.A.). J Sed Res 70(3):565–585. doi:10.1306/2dc40929-0e47-11d7-8643000102c1865d

Friedmann EI (1982) Endolithic microorganisms in the antarctic cold desert. Science 215(4536):1045–1053. doi:10.1126/science.215.4536.1045

Glover JE (1992) Sediments of Early Archean Coastal Plains—a Possible Environment for the Origin of Life. Precambr Res 56(1–2):159–166

Goudie AS, Middleton NJ (2001) Saharan dust storms: nature and consequences. Earth-Science Rev 56(1–4):179–204

Grandstaff DE, Edelman MJ, Foster RW, Zbinden E, Kimberley MM (1986) Chemistry and mineralogy of Precambrian paleosols at the base of the Dominion and Pongola Groups (Transvaal, South Africa). Precambr Res 32(2–3):97–131

Guido DM, Campbell KA (2009) Jurassic hot-spring activity in a fluvial setting at La Marciana, Patagonia, Argentina. Geol Mag 146(04):617–622. doi:10.1017/S0016756809006426

Guidry SA, Chafetz HS (2003a) Anatomy of siliceous hot springs: examples from Yellowstone National Park, Wyoming, USA. Sed Geol 157(1–2):71–106. doi:10.1016/S0037-0738(02)00195-1

Guidry SA, Chafetz HS (2003b) Depositional facies and diagenetic alteration in a relict siliceous hot-spring accumulation: Examples from Yellowstone National Park, USA. J Sed Res 73(5):806–823

Hinman NW, Walter MR (2005) Textural preservation in siliceous hot spring deposits during early diagenesis: Examples from Yellowstone National Park and Nevada, USA. J Sed Res 75(2):200–215

Hoffman A (2011) Archaean Hydrothermal Systems in the Barberton Greenstone Belt and Their Significance as a Habitat for Early Life. In: Golding SD, Glikson M (eds) Earliest Life on Earth: Habitats, Environ-

ments and Methods of Detection. Springer, pp 51–78. doi:10.1007/978-90-481-8794-2_3

Horath T, Bachofen R (2009) Molecular Characterization of an Endolithic Microbial Community in Dolomite Rock in the Central Alps (Switzerland). Microb Ecol 58(2):290–306. doi:10.1007/S00248-008-9483-7

Johannesson KH, Hawkins DL, Cortes A (2006) Do Archean chemical sediments record ancient seawater rare earth element patterns? Geochimet Cosmochimica Acta 70(4):871–890. doi:10.1016/J.Gca.2005.10.013

Johnson IM, Watanabe Y, Stewart B, Ohmoto H (2009) Earth's oldst (~3.4 Ga lateritic paleosol in the Pilbara Craton, Western Australia. Geochimica et Cosmochimica Acta 73(13, Suppl 1):A601

Jones B (2010) Microbes in caves: agents of calcite corrosion and precipitation. In: Pedley HM, Rogerson M (eds) Tufas and Speleothems: Unravelling the Microbial and Physical Controls, vol Special Publication 336. Geological Society of London, London, pp 7–30. doi:10.1144/SP336.2

Jones B, Renaut RW, Rosen MR (1997) Biogenicity of silica precipitation around geysers and hot-spring vents, North Island, New Zealand. J Sed Res 67(1):88–104

Jones B, Renaut RW, Rosen MR (1998) Microbial biofacies in hot-spring sinters; a model based on Ohaaki Pool, North Island, New Zealand. J Sed Res 68(3):413–434

Kah LC, Lyons TW, Frank TD (2004) Low marine sulphate and protracted oxygenation of the Proterozoic biosphere. Nature 431:834–838

Kamber BS, Bolhar R, Webb GE (2004) Geochemistry of late Archaean stromatolites from Zimbabwe: evidence for microbial life in restricted epicontinental seas. Precambr Res132(4):379–399. doi:10.1016/J.Precamres.2004.03.006

Knauth LP (2005) Temperature and salinity history of the Precambrian ocean: implications for the course of microbial evolution. Palaeogeography, Palaeoclimatology, Palaeoecology 219(1–2):53–69. doi:10.1016/J.Palaeo.2004.10.014

Knauth LP, Lowe DR (1978) Oxygen Isotope Geochemistry of Cherts from Onverwacht Group (3.4 Billion Years), Transvaal, South-Africa, with Implications for Secular Variations in Isotopic Composition of Cherts. Earth Planet Sci Lett 41(2):209–222

Knauth LP, Lowe DR (2003) High Archean climatic temperature inferred from oxygen isotope geochemistry of cherts in the 3.5 Ga Swaziland Supergroup, South Africa. Geol Soc Am Bull 115(5):566–580

Konhauser KO, Jones B, Reysenbach AL, Renaut RW (2003) Hot spring sinters: keys to understanding Earth's earliest life forms. Can J Earth Sci 40(11):1713–1724. doi:10.1139/E03-059

Leeder MR, Mack GH, Brasier AT, Parrish RR, McIntosh WC, Andrews JE, Duermeijer CE (2008) Late-Pliocene timing of Corinth (Greece) rift-margin fault migration. Earth Planet Sci Lett 274(1–2):132–141

Lepot K, Philippot P, Benzerara K, Wang GY (2009) Garnet-filled trails associated with carbonaceous matter mimicking microbial filaments in Archean basalt. Geobiology 7(4):393–402. doi:10.1111/j.1472-4669.2009.00208.x

Lücking R, Huhndorf S, Pfister DH, Plata ER, Lumbsch HT (2009) Fungi evolved right on track. Mycologia 101(6):810–822

Mack GH, James WC, Monger HC (1993) Classification of paleosols. Geol Soc Am Bull 105:129–136

Marshall AO, Marshall CP (In Press) Comment on "Biogenicity of Earth's earliest fossils: a resolution of the controversy" by JW Schopf and AB Kudryatsev. Gondwana Res. doi:10.1016/j.gr.2012.12.006

Mcloughlin N, Wilson LA, Brasier MD (2008) Growth of synthetic stromatolites and wrinkle structures in the absence of microbes—implications for the early fossil record. Geobiology 6(2):95–105. doi:Doi 10.1111/J.1472-4669.2007.00141.X

McLoughlin N, Furnes H, Banerjee NR, Muehlenbachs K, Staudigel H (2009) Ichnotaxonomy of microbial trace fossils in volcanic glass. J Geol Soc 166:159–169. doi:10.1144/0016-76492008-049

McLoughlin NJ, Melezhik VA, Brasier AT, Medvedev PV (2013) Palaeoproterozoic stromatolites from the Lomagundi-Jatuli interval of the Fennoscandian Shield. In: Melezhik VA, Prave A, Fallick AE et al. (eds) Reading the archive of Earth's oxygenation: Global events and the Fennoscandian Arctic Russia—Drilling Early Earth Project (FAR-DEEP). Frontiers in Earth Sciences 8:1298–1351. Springer, Berlin. doi:10.1007/978-3-642-29670-3_8

Melezhik VA, Fallick AE (2001) Palaeoproterozoic travertines of volcanic affiliation from a ^{13}C-rich rift lake environment. Chem Geol 173(4):293–312

Melezhik VA, Fallick AE, Grillo SM (2004) Subaerial exposure surfaces in a Palaeoproterozoic ^{13}C-rich dolostone sequence from the Pechenga Greenstone Belt: palaeoenvironmental and isotopic implications for the 2330–2060 Ma global isotope excursion of ^{13}C/^{12}C. Precambr Res 133(1–2):75–103

Melezhik VA, Fallick AE, Rychanchik DV, Kuznetsov AB (2005) Palaeoproterozoic evaporites in Fennoscandia: implications for seawater sulphate, the rise of atmospheric oxygen and local amplification of the δ^{13}C excursion. Terra Nova 17(2):141–148

Muehlenbachs K (1998) The oxygen isotopic composition of the oceans, sediments and the seafloor. Chem Geol 145(3–4):263–273

Noffke N (2009) The criteria for the biogeneicity of microbially induced sedimentary structures (MISS) in Archean and younger, sandy deposits. Earth-Science Reviews 96(3):173–180. doi:10.1016/J.Earscirev.2008.08.002

Noffke N, Gerdes G, Klenke T, Krumbein WE (1996) Microbially induced sedimentary structures—examples from modern sediments of siliciclastic tidal flats. Zentralblatt für Geologie und Palaontologie Teil 1:307–316

Noffke N, Beukes N, Bower D, Hazen RM, Swift DJP (2008) An actualistic perspective into Archean worlds-

(cyano-)bacterially induced sedimentary structures in the siliciclastic Nhlazatse Section, 2.9 Ga Pongola Supergroup, South Africa. Geobiology 6(1):5–20. doi 10.1111/J.1472-4669.2007.00118.X

Packer BM (1990) Sedimentology, paleontology, and stable-isotope geochemistry of selected formations in the 2.7-billion-year-old Fortescue Group, Western Australia. University of California, Los Angeles

Pedley HM (1990) Classification and environmental models of cool freshwater tufas. Sed Geol 68(1–2):143–154

Pentecost A (1990) The formation of travertine shrubs; Mammoth Hot Springs, Wyoming. Geol Mag 127(2):159–168

Pentecost A (2005) Travertine. Springer-Verlag, Berlin, p 445

Pentecost A, Viles H (1994) A Review and Reassessment of Travertine Classification. Geographie Physique et. Quaternaire 48(3):305–314

Pinti DL, Mineau R, Clement V (In Press) Comment on "Biogenicity of Earth's earliest fossils: a resolution of the controversy" by JW Schopf and AB Kudryatsev. Gondwana Res doi:10.1016/j.gr.2012.12.012

Pirajno F, Grey K (2002) Chert in the Palaeoproterozoic Bartle Member, Killara Formation, Yerrida Basin, Western Australia: a rift-related playa lake and thermal spring environment? Precambr Res 113(3–4):169–192

Rainbird RH, Davis WJ, Stern RA, Peterson TD, Smith SR, Parrish RR, Hadlari T (2006) Ar-Ar and U-Pb Geochronology of a Late Paleoproterozoic Rift Basin: Support for a Genetic Link with Hudsonian Orogenesis, Western Churchill Province, Nunavut, Canada. J Geol 114:1–17

Retallack GJ (1998) Core concepts of paleopedology. Quatern Int 51-2:203–212

Retallack GJ (2007) Soils and Global Change in the Carbon Cycle over Geological Time. In: Holland HD, Turekian KK (eds) Treatise on Geochemistry, vol 5. Pergamon, Oxford, pp 1–28

Riding R (2011) The Nature of Stromatolites: 3,500 Million Years of History and a Century of Research. In: Reitner J (ed) Advances in Stromatolite Geobiology, vol 131. Lecture Notes in Earth Sciences. Springer-Verlag, Berlin, pp 29–74

Rogerson M, Pedley HM, Wadhawan JD, Middleton R (2008) New insights into biological influence on the geochemistry of freshwater carbonate deposits. Geochim Cosmochim Acta 72(20):4976–4987

Rothschild LJ (1999) The influence of UV radiation on protistan evolution. J Eukaryot Microbiol 46(5):548–555

Rye R, Holland HD (1998) Paleosols and the evolution of atmospheric oxygen: A critical review. Am J Sci 298(8):621–672

Rye R, Holland HD (2000) Life associated with a 2.76 Ga ephemeral pond?: Evidence from Mount Roe #2 paleosol. Geology 28(6):483–486

Sakurai R, Ito M, Ueno Y, Kitajima K, Maruyama S (2005) Facies architecture and sequence-stratigraphic features of the Tumbiana Formation in the Pilbara Craton, northwestern Australia: Implications for depositional environments of oxygenic stromatolites during the Late Archean. Precambr Res 138(3–4):255–273. doi: 10.1016/J.Precamres.2005.05.008

Schopf JW (2006) Fossil evidence of Archaean life. Philosophical Transactions of the Royal Society B 361 (1470):869–885. doi: 10.1098/Rstb.2006.1834

Schopf JW, Kudryavtsev AB (2012) Biogenicity of Earth's oldest fossils: A resolution of the controversy. Gondwana Res 22:761–771. doi:10.1016/j.gr.2012.07.003

Schopf JW, Kudryavtsev AB (2013) Reply to the comments of DL Pinti, R Mineau and of AO Marshall and CP Marshall on "Biogenicity of Earth's oldest fossils: A resolution of the controversy". Gondwana Res 23(4):1656–1658. doi:10.1016/j.gr.2012.12.005

Schröder S, Bekker A, Beukes NJ, Strauss H, Van Niekerk HS (2008) Rise in seawater sulphate concentration associated with the Paleoproterozoic positive carbon isotope excursion: evidence from sulphate evaporites in the ~2.2–2.1 Gyr shallow-marine Lucknow Formation, South Africa. Terra Nova 20(2):108–117. doi:10.1111/j.1365-3121.2008.00795.x

Som SM, Catling DC, Harnmeijer JP, Polivka PM, Buick R (2012) Air density 2.7 billion years ago limited to less than twice modern levels by fossil raindrop imprints. Nature 484(7394):359–362. doi:10.1038/nature10890

Sweetlove L (2011) New candidates for oldest fossils. Nature. doi:10.1038/news.2011.491

Tera F, Papanast DA, Wasserburg GJ (1974) Isotopic Evidence for a Terminal Lunar Cataclysm. Earth Planet Sci Lett 22(1):1–21

Thorne AM, Trendall AF (2001) Geology of the Fortescue Group, Pilbara Craton, Western Australia. Geol Surv West Aust. Bull 144:1–249

Tilden JE (1897) On Some Algal Stalactites of the Yellowstone National Park. Bot Gaz 24(3):194–199

Trewin NH, Rice CM (1992) Stratigraphy and sedimentology of the Devonian Rhynie chert locality. Scot J Geol 28:37–47

Tyler SA, Barghoorn ES (1954) Occurrence of Structurally Preserved Plants in Pre-Cambrian Rocks of the Canadian Shield. Science 119(3096):606–608

Ueno Y, Yoshioka H, Maruyama S, Isozaki Y (2004) Carbon isotopes and petrography of kerogens in similar to 3.5-Ga hydrothermal silica dikes in the North Pole area, Western Australia. Geochim Cosmochim Acta 68(3):573–589. doi:10.1016/S0016-7037(00)00462-9

Wacey D, Kilburn MR, Saunders M, Cliff J, Brasier MD (2011) Microfossils of sulphur-metabolizing cells in 3.4-billion-year-old rocks of Western Australia. Nat Geosci 4(10):698–702. doi:10.1038/Ngeo1238

Walter MR (1976a) Geyserites of Yellowstone National Park: An Example of Abiogenic "Stromatolites". In: Walter MR (ed) Stromatolites, vol 20. Developments in Sedimentology. Elsevier, Amsterdam, pp 87–112. doi:10.1016/S0070-4571(08)71131-2

Walter MR (1976b) Hot Spring Sediments of Yellowstone National Park. In: Walter MR (ed) Stromatolites, vol 20. Developments in Sedimentology. Elsevier, Amsterdam, pp 489–498. doi:10.1016/S0070-4571(08)71131-2

Walter MR (1996) Ancient hydrothermal ecosystems on Earth: a new palaeobiological frontier. In: Evolution of Hydrothermal Ecosystems on Earth (and Mars?). Ciba Foundation Symposium 202, vol 202. Wiley, Chichester, pp 112–127

Walter MR, Des Marais DJ (1993) Preservation of biological information in thermal spring deposits: developing a strategy for the search for fossil life on Mars. Icarus 101(1):129–143

Watanabe Y, Martini JEJ, Ohmoto H (2000) Geochemical evidence for terrestrial ecosystems 2.6 billion years ago. Nature 408:574–578

Westall F, Ronde CEJ de, Southam G, Grassineau N, Colas M, Cockell CS, Lammer H (2006) Implications of a 3.472–3.333 Gyr-old subaerial microbial mat from the Barberton greenstone belt, South Africa for the UV environmental conditions on the early Earth. Philos T R Soc B 361(1474):1857–1875. doi:10.1098/Rstb.2006.1896

Wright VP, Tucker ME (1991) Calcretes: an Introduction. In: Wright VP, Tucker ME (eds) Calcretes. Blackwell Scientific Publications, Oxford, pp 1–22

14 Rare Earth Elements in Stromatolites—1. Evidence that Modern Terrestrial Stromatolites Fractionate Rare Earth Elements During Incorporation from Ambient Waters

Karen H. Johannesson, Katherine Telfeyan, Darren A. Chevis, Brad E. Rosenheim and Matthew I. Leybourne

Abstract

Ancient chemical sediments may provide critical information about early microbial life and ancient environmental conditions. For example, the rare earth element (REE) content and fractionation patterns of Archean and Proterozoic banded iron formations (BIF) and other chemical sediments are thought to preserve the REE patterns of ancient seawater, and as such have been employed to investigate secular trends in seawater chemistry through geologic time. Recently it was suggested that REEs could provide evidence for distinguishing between biotic and abiotically precipitated chemical sediments. However, it is important to underscore that very little is actually known about how stromatolites and other microbialites obtain their REE concentrations and fractionation patterns, including what biological processes, if any, the REEs may record. Here, we present REE concentration and fractionation patterns for modern, lacustrine stromatolites and the ambient waters within which they form. We show that the REE patterns of the stromatolites are highly fractionated compared to the ambient waters. Specifically, the stromatolites exhibit heavy REEs (HREE) enrichments relative to upper crustal proxies (i.e., shale composites), whereas the ambient waters are substantially depleted in the HREEs. We propose that surface complexation and subsequent preferential incorporation of HREEs by organic ligands associated with bacterial cell walls, microbialite biofilms, and/or exopolymeric substances may explain the HREE enrichments of the stromatolites.

K. H. Johannesson (✉) · K. Telfeyan · D. A. Chevis · B. E. Rosenheim
Department of Earth and Environmental Sciences, Tulane University, New Orleans, Louisiana 70118, USA
e-mail: kjohanne@tulane.edu

M. I. Leybourne
ALS Geochemistry, North Vancouver, British Columbia V7H 0A7, Canada

14.1 Introduction

Rare earth elements (REE) have long been employed for investigating the petrogenesis of igneous rocks and for tracing circulation and mixing of oceanic water masses (Jakeš and Gill 1970; Hanson 1980; Piepgras and Wasserburg 1987;

Y. Dilek, H. Furnes (eds.), *Evolution of Archean Crust and Early Life*, Modern Approaches in Solid Earth Sciences 7, DOI 10.1007/978-94-007-7615-9_14, © Springer Science+Business Media Dordrecht 2014

McKenzie and O'Nions 1991). The efficacy of the REEs as tracers of geochemical processes largely reflects their uniform trivalent charge (Ce^{4+} and Eu^{2+} can also occur), and the gradual decrease in their ionic radii with increasing atomic number (i.e., the lanthanide contraction) that accompanies the progressive filling of the 4*f*-electron shell across the lanthanide series. As a consequence, the REEs exhibit strong fractionation as a group due to size and charge, as well as substantial "within-group" fractionation resulting from the lanthanide contraction (see Johannesson et al. 2005, and references therein). These unique properties can thus facilitate investigations of both complex and subtle geochemical processes that other, single element or single compound (i.e., molecules) tracers cannot discern (Quinn et al. 2004; Johannesson et al. 2005).

Many researchers have argued that the REE concentrations of Archean and Proterozoic banded iron formations (BIF) provide a record of paleo-ocean chemistry, and consequently, that REE can be used to study secular trends in ocean chemistry through geologic time (Derry and Jacobsen 1990; Shimuzu et al. 1990; Danielson et al. 1992; Bau and Möller 1993). For example, the general enrichments in shale-normalized concentrations of the heavy REEs (HREE) relative to the light REEs (LREE) that characterizes many BIFs closely resemble the HREE enrichments of modern seawater, suggesting that similar chemical processes have influenced REEs in seawater throughout geologic history (Derry and Jacobsen 1990; Bau and Möller 1993; Bau and Dulski 1996; van Kranendonk et al. 2003; Bolhar et al. 2004; Yamamoto et al. 2004; Friend et al. 2008; Nutman et al. 2010; Planavsky et al. 2010). On the other hand, the positive shale-normalized Eu anomalies and lack of Ce anomalies that characterize BIF's are thought to reflect the importance of high-temperature (>250 °C) hydrothermal discharges along the seafloor (i.e., so-called "mantle-flux") and the substantially lower PO_2 levels, respectively, in the Archean and early Proterozoic oceans and atmosphere as compared to today. Recently, shale-normalized REE patterns of some Archean chemical sediments, including the 3.45 Ga rocks of the Warrawoona Group in Western Australia and the 3.7 Ga rocks of the Isua Greenstone Belt of Greenland, have been cited as evidence for their formation as biochemical precipitates (e.g., microbialites) within shallow marine environments (Van Kranendonk et al. 2003; Bolhar et al. 2004; Alexander et al. 2008; Friend et al. 2008; Nutman et al. 2010; Planavsky et al. 2010), thus supporting the presence of early microbial life forms. Some researchers have even argued that the REE contents and shale-normalized REE fractionation patterns of ancient chemical sediments (presumably microbialites) can be used to distinguish between biotically and abiotically precipitated chemical sediments (Allwood et al. 2006; Guido et al. 2010).

Despite these observations, it is important to underscore that very little is actually known about how microbialites, including stromatolites, obtain their REE concentrations and fractionation patterns. Claims that REEs can be used to discriminate between abiotic vs. biotic origins of ancient chemical sediments (e.g., Allwood et al. 2006; Guido et al. 2010) appear to be largely based on solid-liquid partitioning coefficients determined for Holocene reefal microbialites that are nearly uniform across the REE series suggesting little to no fractionation during uptake from seawater (Webb and Kamber 2000). Although intriguing such partitioning coefficients provide no mechanistic understanding of REE uptake and incorporation into microbialites, and certainly tell us nothing about biological vs. abiological processes that may have been important during the uptake and incorporation of REEs in ancient chemical sediments. For example, REE concentrations and fractionation patterns of modern and fossilized microbialites likely reflect a complex combination of REE adsorption onto microbialite organic matter (bacterial cells, extracellular polymeric substances [EPS]), incorporation into carbonate minerals that precipitate indirectly due to metabolic processes that generate alkalinity (e.g., dissimilatory anaerobic respiration, photosynthesis), carbonate minerals that form as a result of the influence of EPS (i.e., changes in saturation states), and detrital mineral grains trapped by the growing microbialites (e.g., Firsching and Mohammadzadel 1986; Carroll 1993; Meinrath and

Takeishi 1993; Zhong and Mucci 1995; Elzinga et al. 2002; Anderson and Pedersen 2003; Takahashi et al. 2005, 2007). To sort out the relative contribution of these potential constituents, careful analysis of the REE contents and fractionation patterns of each potential constituent, as well as associated pore waters, combined with process-oriented investigations of REE cycling within living microbialites is required. Here, we take an initial step towards this objective by examining the REE concentrations and fractionation patterns of modern stromatolitic microbialites from the Cuatro Ciénegas bolson (i.e., Four Marshes basin) in the Chihuahua Desert of México, and show that the fractionation patterns of these microbialites are poor proxies for the ambient waters within which they are "growing".

14.2 Background

14.2.1 Microbialites and Stromatolites

Microbialites are sedimentary deposits that form by the interaction of benthic microbial communities and chemical and detrital sediments (Burne and Moore 1987). Stromatolites are a type of microbialite that are characterized by macroscopic laminated fabrics that may or may not contain interlayered abiotic precipitates (e.g., Riding 2010; Monty 1977; Semikhatov et al. 1979). Other related microbialites include thrombolites, which possess a clotted macroscopic fabric, and leiolites, which do not have characteristic macroscopic fabrics (Burne and Moore 1987; Dupraz et al. 2009, and references therein). Microbialites, and in particular, stromatolites can form by a number of processes including trapping of detrital sediments on bacteria and associated EPS produced by microbes (Decho 1990, 2000; Costerston et al. 1995), biologically induced precipitation of calcium carbonate that results from microbial metabolic processes (e.g., photosynthesis, sulfate reduction), modification of carbonate mineral saturation indices by ionic interactions (i.e., Ca^{2+}) with EPS, as well as entirely abiotic mechanisms (Semikhatov et al. 1979; Lyons et al. 1984; Burne and Moore 1987; Lowe 1994; Grotzinger and Rothman 1996; Reid et al. 2000; Visscher et al. 2000; Braissant et al. 2003, 2007; Ben Chekroun et al. 2004; Dupraz et al. 2004, 2009; Dupraz and Visscher 2005; Ludwig et al. 2005; Wright and Wacey 2005; Wacey 2009).

Modern genomic techniques demonstrate that microbialite communities are more diverse than originally thought (Burns et al. 2004; Papineau et al. 2005; Ley et al. 2006; Baumgartner et al. 2006; Dupraz et al. 2009; Stolz et al. 2009; Paerl and Yannarell 2010). For simplicity, however, the principal microbial guilds include oxygenic photoautotrophs (primarily cyanobacteria), anoxygenic photoautotrophs (purple and green sulfur bacteria), fermenters, aerobic heterotrophs (chemoorgano-heterotrophs), anaerobic heterotrophs (chiefly sulfate reducing bacteria, SRB), aerobic chemolithoautotrophs (sulfide oxidizers), and methanogens (Visscher and Stolz 2005; Konhauser 2007; Gerdes 2010; Fig. 14.1). Because the diversity and metabolic complexity of microbialites communities is beyond the scope of the current study, the reader is referred to Dupraz et al. (2009) for an excellent recent review. In brief, however, cyanobacteria are chiefly responsible for carbon fixation, which they accomplish by converting CO_2 via photosynthesis into organic matter for cell growth (Dupraz et al. 2009; Stolz et al. 2009). Fermenting bacteria and aerobic heterotrophs subsequently break down organic matter produced by the cyanobacteria-driven primary production (i.e., cells, EPS) into smaller organic molecules that anaerobic heterotrophs, such as SRB, use as electron donors during respiration (Konhauser 2007; Dupraz et al. 2009; Fenchel et al. 2012, and references therein). Oxidation of the organic matter produces alkalinity, which leads to the precipitation of calcium carbonate minerals (Lyons et al. 1984; Walter et al. 1993; Visscher et al. 2000; van Lith et al. 2003; Dupraz et al. 2004; Dupraz and Visscher 2005; Baumgartner et al. 2006). In addition to this microbial induced $CaCO_3$ precipitation, the EPS matrix can influence carbonate precipitation by uptake of free Ca^{2+} ions onto organic functional groups (Kempe and Kazmierczak 1994; Arp et al. 1999a, b; Dupraz et al. 2009). The EPS can also inhibit carbonate precipitation

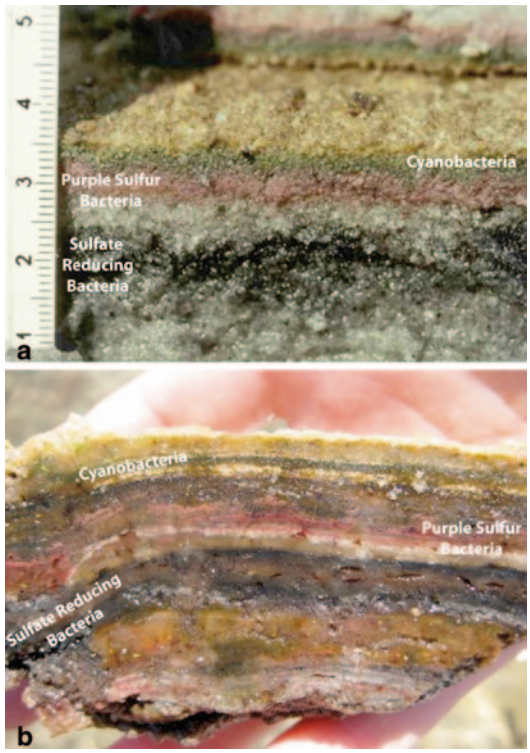

Fig. 14.1 Cross-sections through two examples of microbialites showing layering of mineral material and some microbial guilds. *Bottom* image is a modern marine stromatolites from Shark Bay, Australia (www.physorg.com/news201502581.html)

or alternatively trap detrital carbonate grains and promote stromatolite growth via accretion (Ferris et al. 1989; Reid et al. 2000; Kawaguchi and Decho 2002; Gautret and Trichet 2005).

Understanding the uptake of trace elements by microbialites is especially important with regards to the REEs as microbial carbonates might provide proxies for evaluating paleo-seawater chemistry (e.g., Webb and Kamber 2000). Specifically, Holocene reefal microbialites from the Great Barrier Reef appear to incorporate REEs from ambient seawater at substantially higher concentrations than other commonly employed biogeochemical precipitates, and with little fractionation across the REE series. It was previously shown that uptake of REEs by corals does not significantly fractionate the REEs (Sholkovitz and Shen 1995). Nonetheless, with the exception of Holocene microbialites from the Great Barrier Reef, there appear to be no other investigations of REE uptake by microbialites from other environmental settings.

14.2.2 Rare Earth Element Fractionation Patterns of Modern Seawater—A Review

Input-normalized REE fractionation patterns of modern seawater samples are characterized by enrichments in the HREEs compared to the LREEs and large, negative Ce anomalies (Elderfield and Greaves 1982; Elderfield 1988; Bertram and Elderfield 1993; Fig. 14.2a). In addition to these characteristics, input-normalized REE fractionation patterns of modern seawater also exhibit a number of more subtle features including elevated, normalized La values compared to other LREEs (e.g., Pr, Nd), variable Eu anomalies, positive Gd anomalies, and substantial Y/Ho ratios (Fig. 14.2a; Zhang et al. 1994; Bau et al. 1995; Nozaki et al. 1997). We note that the input-normalized REE patterns represent the relative concentration of each REE in the sample (i.e., seawater) as compared to their chief source concentration, which in the case of the oceans is detrital material produced from weathering of continental crust (e.g., Taylor and McLennan 1985; Goldstein and Jacobsen 1988). Because the composition of the upper continental crust is closely approximated by the composition of shales (Taylor 1964; Taylor and McLennan 1985), average shale composites, such as Post Archean Australian Shale (PAAS; Nance and Taylor 1976) are commonly used for input-normalization of dissolved REE concentrations in modern seawater (Elderfield 1988). Other less significant sources of REEs to modern oceans include atmospheric deposition of dust and aerosols originating from continental regions, as well as hydrothermal inputs along the seafloor (e.g., mid-ocean ridges; Elderfield and Greaves 1982; Klinkhammer et al. 1983; Goldstein and Jacobsen 1988; Sholkovitz et al. 1993). Submarine groundwater discharge may also be important in some coastal settings (Duncan and Shaw 2003; Johannesson and Burdige 2007; Johannesson et al. 2011).

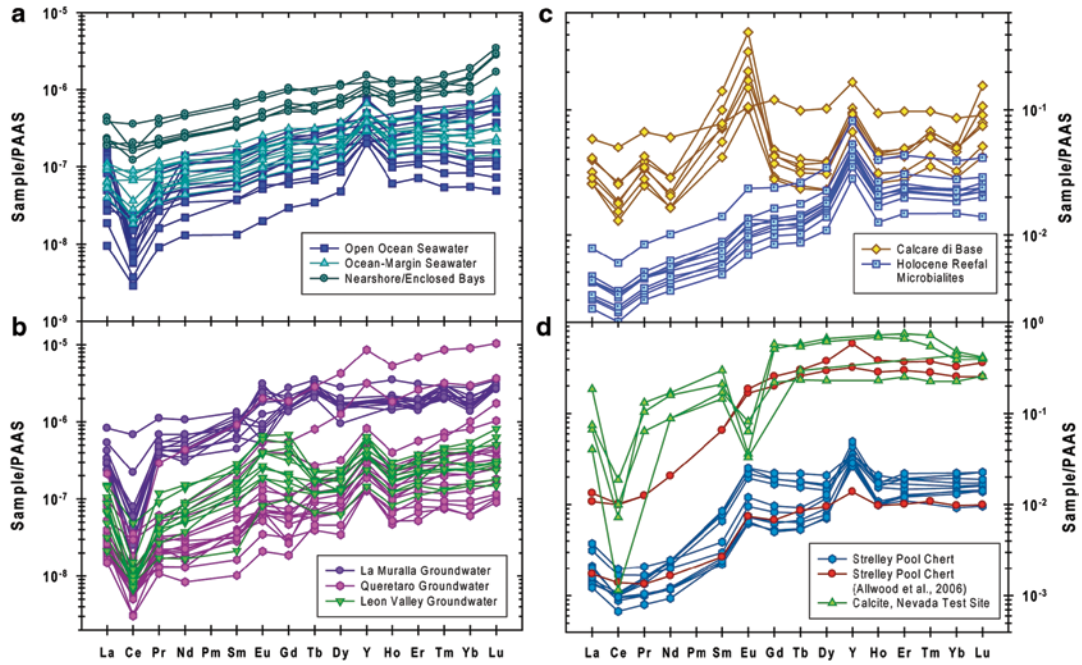

Fig. 14.2 Shale-normalized REE data for **a** modern seawater samples, **b** various groundwaters from central México (Johannesson et al. 2005, 2006), **c** Holocene reefal microbialites from the Great Barrier Reef (Webb and Kamber 2000) and carbonate rocks from the Messinian Calcare di Base (Guido et al. 2010), and **d** Archean stromatolitic chemical sediments of the Strelley Pool Chert, and modern, secondary vein calcite from Yucca Mountain, Nevada (Zhou 2004). In panel (**d**) the *blue* Strelley Pool Chert REE data are from Van Kranendonk et al. (2003), whereas the *red* Strelley Pool Chert data are from Allwood et al. (2006). Note, the *red* Strelley Pool Chert samples that are enriched 250-fold over those shown in *blue*, and which plot within the range of secondary calcites of Yucca Mountain are interpreted by Allwood et al. (2006), and other researchers, as evidence of microbial precipitation. For the source of seawater data in panel (**a**), see Johannesson et al. (2006)

The fact that shale-normalized REE fractionation patterns for seawater are not flat (i.e., shale-like) demonstrates that dissolved REEs in the oceans are fractionated with respect to their chief source, the upper continental crust. The HREE enrichment that characterizes modern seawater reflects competition between solution and surface complexation reactions, whereby formation of strong aqueous complexes with carbonate ions preferentially stabilizes HREEs in solution, lowering the activity of the free metal ion (e.g., Yb^{3+}), and thus inhibiting surface complexation of the HREEs compared to the LREEs (Cantrell and Byrne 1987; Byrne and Kim 1990; Koeppenkastrop and DeCarlo 1992, 1993; Quinn et al. 2004, 2006). The presence of negative Ce anomalies (Fig. 14.2a) reflects abiotic and biologically mediated oxidation of Ce^{3+} to Ce^{4+}, and subsequent removal of markedly less soluble tetravalent Ce from solution (Moffett 1990, 1994; Sholkovitz and Schneider 1991; DeCarlo et al. 1998). Positive Eu anomalies, which are uncommon in modern seawater but are have been reported in many Archean chemical sediments (Figs. 14.2, 14.3), are generally attributed to input from hydrothermal discharges along mid-ocean ridges (e.g., see Klinkhammer et al. 1983, 1994).

Many of the more subtle features revealed by shale-normalized REE patterns of modern seawater are thought to reflect the progressive filling of the 4-*f* electron shell across the REE series, which conveys small differences in the chemical properties of the REEs (Byrne and Kim 1990). For example, enrichments in La compared to other LREEs (i.e., Pr and Nd), signify greater stability of La in seawater, which is thought to reflect its

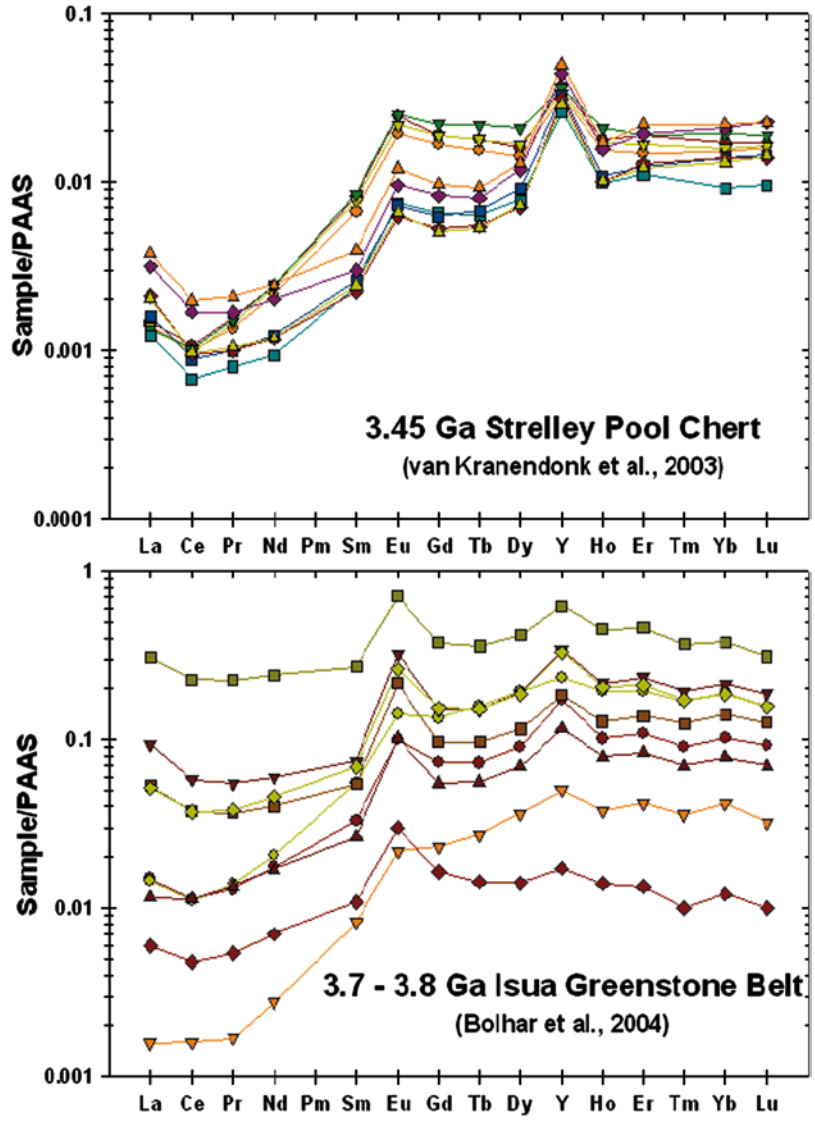

Fig. 14.3 Shale-normalized REE data for examples of Archean chemical sediments with broadly similar REE patterns to those of modern seawater. The *top panel* shows examples of the 3.45 Ga Strelley Pool Chert from Western Australia (Van Kranendonk et al. 2003), whereas the *bottom panel* presents data for the 3.7–3.8 Ga Isua Greenstone Belt in Greenland. (Bolhar et al. 2004)

empty 4-*f* electron shell (Byrne and Kim 1990; DeBaar et al. 1991). Furthermore, the anomalous behavior of Gd likely reflects its half-filled 4-*f* electron shell, which appears to influence solution and surface complexation of Gd compared to its nearest neighbors, Eu and Tb (Byrne and Kim 1990; Kim et al. 1991; Byrne and Li 1995; Byrne et al. 1996). Therefore, shale-normalized patterns for modern seawater typically have positive La and Gd anomalies (Fig. 14.2a).

Modern seawater is also characterized by large, superchondritic Y/Ho ratios (Høgdahl et al. 1968; Zhang et al. 1994; Bau et al. 1995; Nozaki et al. 1997). Molal Y/Ho ratios for seawater samples analyzed by Nozaki et al. (1997) and Bau (1996) range from ~80 to ~150, with a mean (± standard deviation) of 108 ± 12 (n = 93). In contrast, molal Y/Ho ratio of crustal rocks and chondrites are astonishingly similar, ranging between ~48 and ~50 (Nozaki et al. 1997). The open-ocean seawater samples shown in Fig. 14.2a that have accompanying Y data have molal Y/Ho ratios from 92 to 168, and exhibit a mean (± SD) = 108 ± 23 (Johannesson et al. 2006). The molal Y/Ho ratios are lower for the ocean-margin seawater (i.e., Y/Ho = 80–107; Fig. 14.2a)

and enclosed bays (Y/Ho = 65–70; Fig. 14.2a), reflecting increased input from proximal continental sources. Because the ionic radii of Ho^{3+} and Y^{3+} are almost identical, both are expected to exhibit similar geochemical behavior in natural waters (e.g., Zhang et al. 1994; Nozaki et al. 1997). However, the fact that Y/Ho ratios are not constant in the oceans and vary with depth (Høgdahl et al. 1968; Nozaki et al. 1997) indicates that biogeochemical processes fractionate these trace elements. Although the Y/Ho fractionation is incompletely understood, a number of mechanisms have been advanced to explain the differences in Y and Ho behavior in seawater including variable solution and surface complexation behavior, different Y- and Ho-phosphate mineral solubilities, and fractionation during chemical weathering of continental source regions (Zhang et al. 1994; Bau et al. 1995; Bau 1999; Nozaki et al. 1997).

Despite the numerous, well-documented features of shale-normalized REE patterns of modern seawater, these fractionation patterns are indeed not unique to seawater (e.g., Johannesson et al. 2006; Johannesson 2012). In fact, many terrestrial waters, including river waters, groundwaters, and lake waters, also exhibit shale-normalized REE patterns that closely resemble modern seawater, including superchondritic Y/Ho ratios (e.g., Michard and Albarède 1986; Sholkovitz 1992; Johannesson and Lyons 1994; Johannesson et al. 1994, 1996, 2000, 2005, 2006, 2011; Tricca et al. 1999; Barrat et al. 2000; Dia et al. 2000; Johannesson and Hendry 2000; Leybourne et al. 2000; Négrel et al. 2000; Aubert et al. 2001; Yan et al. 2001; Biddau et al. 2002; De Carlo and Green 2002; Pokrovsky and Schott 2002; Shiller 2002; Duncan and Shaw 2003; Bau et al. 2004; Leybourne and Cousens 2005; Tang and Johannesson 2005, 2006; Han and Liu 2007; Bozau et al. 2008; Leybourne and Johannesson 2008; Rönnback et al. 2008; Pourret et al. 2010; Fig. 14.2b). Moreover, it is well known that the shale-normalized REE patterns that characterize modern seawater are initiated during chemical weathering of continental rocks, and enhanced during transport to the oceans in rivers and estuaries by the effects of solution and surface complexation reactions acting on dissolved REEs (Hoyle et al. 1984; Goldstein and Jacobsen 1988; Elderfield et al. 1990; Sholkovitz 1995; Byrne and Liu 1998; Sholkovitz and Szymczak 2000; Quinn et al. 2006; Johannesson et al. 2011; Schijf and Marshall 2011). Consequently, without a clear understanding of the mechanisms and processes that control REE uptake in modern microbialites, it is premature to assume that REE patterns of ancient chemical sediments presumably formed at least in part by microbial processes, unequivocally record the REE patterns of the ancient waters within which they formed (Johannesson et al. 2006).

14.2.3 REE Fractionation Patterns of Modern and Ancient Chemical Sediments

A number of studies have discussed the similarities in shale-normalized REE patterns of chemical sediments (thought to be fossil microbialites) and modern seawater, relying heavily on these similarities to reconstruct the paleo-environment within which the sediment formed (e.g., Van Kranendonk et al. 2003; Bolhar et al. 2004, 2005; Alexander et al. 2008; Friend et al. 2008; Nutman et al. 2010; Plavansky et al. 2010). Previously, the broad similarity between shale-normalized REE patterns of reefal microbialites and modern seawater was cited as evidence that microbialites quantitatively incorporate REEs from ambient water during formation (Webb and Kamber 2000). It was then concluded from these observations that ancient carbonate rocks with high REE concentrations and low Si and Al contents must represent ancient microbial carbonates that additionally preserve the REE fractionation patterns of the ancient, ambient seawater within which they formed (Webb and Kamber 2000). Nevertheless, the simple fact that the many terrestrial waters have shale-normalized REE fractionation patterns that are identical to modern seawater demonstrate that such conclusions represent over interpretations of the REE data of these ancient rocks.

Van Kranendonk et al. (2003), followed by Allwood et al. (2006), investigated stromatolitic

rocks of the 3.43–3.45 Ga Strelley Pool Chert from Western Australia (Figs. 14.2d, 14.3). These authors present: (1) convincing sedimentary evidence for the biogenicity of these Archean carbonate rocks; and (2) REE data as additional support for a shallow marine origin for these rocks. The shale-normalized REE signatures of stromatolitic and laminated dolomitic rocks of the Strelley Pool Chert exhibit substantial depletions in LREEs compared to both middle REEs (MREE) and HREEs, possess positive La, Eu, and Y anomalies, and have either small or negligible Ce anomalies (Figs. 14.2d, 14.3). The lack of significant negative Ce anomalies, a common feature of Archean chemical sediments, suggests suboxic or anoxic conditions, the positive La anomalies and large Y/Ho ratios suggest deposition in shallow waters, and the positive Eu anomalies imply that input from hydrothermal sources (i.e., mantle-flux) was important during the formation of the Strelley Pool Chert (Van Kranendonk et al. 2003). Van Kranendonk et al. (2003) interpreted the primary sedimentary structures and the shale-normalized REE signatures as evidence that the Strelley Pool Chert precipitated from seawater as microbial carbonate sediments within a shallow, peritidal setting. More critically, Allwood et al. (2006) argued that the ~250-fold enrichment of REEs in carbonate layers over adjacent chert layers represents a biogenic signal in the Strelley Pool Chert. This same criterium was recently applied to carbonates of the Messinian Calcare di Base in Sicily (Fig. 14.2c) to argue for microbial precipitation based on REE contents (Guido et al. 2010). Formation within Archean seawater was also advanced for the early Archean rocks (~3.7–3.8 Ga) from southwest Greenland based on their shale-normalized REE patterns (Appel 1983; Bolhar et al. 2004; Friend et al. 2008; Nutman et al. 2010; Fig. 14.3).

For comparison, shale-normalized REE patterns for secondary calcites from south-central Nevada, USA, are plotted in Fig. 14.2d. These data demonstrate that REE patterns for authigenic, secondary calcite collected from vadose-zone fractures within rhyolite and quartz latite tuffs in Nevada (Zhou 2004), also closely resemble those of modern seawater, groundwaters, as well as modern and ancient chemical sediments (Fig. 14.2). Furthermore, the REE patterns of these secondary calcites from southern Nevada clearly demonstrate that authigenic, and probably abiotic, carbonate minerals originating in the vadose zone within terrestrial (i.e., sialic) environments can also exhibit seawater-like REE patterns. More importantly, the argument that the elevated REE contents of the Strelley Pool Chert carbonates is a biogenic (i.e., microbial) signature seems questionable given the similarly REE enriched secondary calcites from Nevada, some of which appear to have formed at temperature in excess of 80 °C (Wilson et al. 2003). Clearly, more detailed study of REE uptake by and incorporation into biotic and abiotic carbonate minerals seems warranted to sort out the important processes responsible for the variety of REE fractionation patterns recorded by ancient and modern chemical sediments.

14.3 Geological Setting

The Cuatro Ciénegas bolson (Four Marshes basin) is a 1200 km^2 desert basin located within the Chihuahuan Desert in the northeast Mexican state of Coahuila (Fig. 14.4). The Cuatro Ciénegas bolson is an important discharge zone of the Cupido-Aurora aquifer in terms of the number of springs and the numerous endemic species that are supported by these springs (70 endemic species; Minckley 1969, 1984; Wolaver et al. 2008). Cuatro Ciénegas is located on the eastern edge of the 26,000 km^2, internally drained Bolson de Mapimi, and within the Coahuila marginal fold belt (Laramide) on the eastern flank of the Sierra Madre Oriental, which is characterized by steeply folded Cretaceous marine sedimentary, chiefly carbonate, rocks (Murray 1961; Lesser Jones 1965; Baker 1970; Lehmann et al. 1999).

Groundwaters discharging from springs within the Cuatro Ciénegas bolson are primarily Ca–SO_4–HCO_3 waters of circumneutral pH ($6.5 \leq pH \leq 8.5$; Minckley and Cole 1968; Minckley 1969; Winsborough 1990; Johannesson et al. 2004a). Groundwaters are dilute to mildly brackish with ionic strength ranging from 0.036

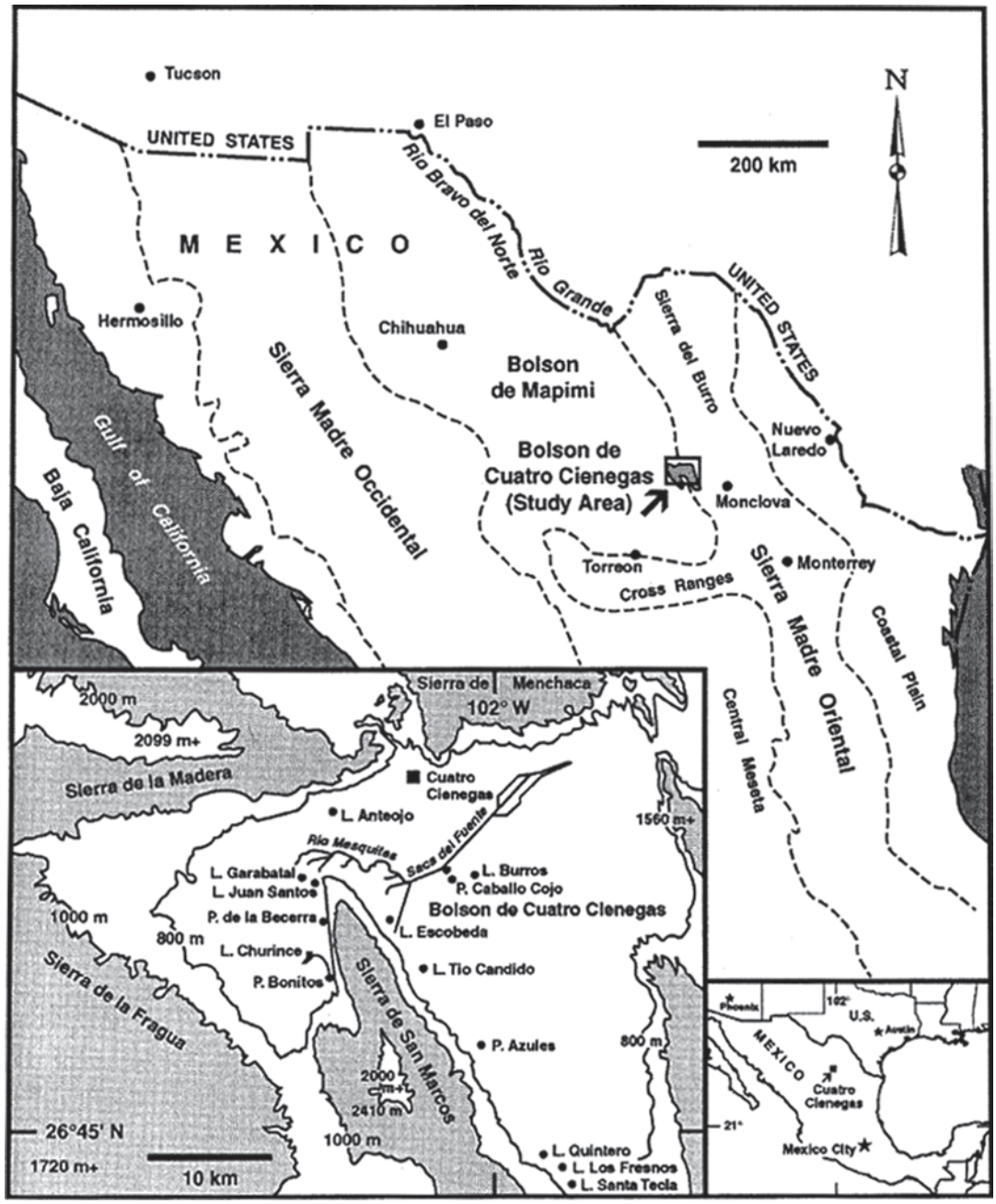

Fig. 14.4 Map of northern México showing the location of the Cuatro Ciénegas bolson in Coahuila, México. Insert map shows details of the Cuatro Ciénegas bolson, including various springs, lagunas, streams, and canals. (Map is from Johannesson et al. 2004a)

to 0.127 moles kg^{-1} (Johannesson et al. 2004a). Cuatro Ciénegas waters are especially notable because they have the lowest P concentrations yet reported for terrestrial waters (Minckley and Cole 1968; Breitbart et al. 2009). Previous analysis of stable oxygen and hydrogen isotopes of spring waters and Cl mass balance calculations indicates that recharge occurs both locally in

Fig. 14.5 Panel (**a**) is a photograph of a typical groundwater discharge point (i.e., Pozo Azul) in the Cuatro Ciénegas bolson. Stromatolites are partially visible along the *lower* portion of the photograph, despite the wind-disturbed water surface. Panel (**b**) shows oncolites collected from the Rio Mesquites. (Photographs by KH Johannesson)

surrounding mountain ranges, as well as further away in neighboring basins (Lesser y Associados 2001; Johannesson et al. 2004a; Wolaver et al. 2008).

Stromatolitic and thrombolytic microbialites are common in many of the springs (pozos), lagunas, and streams within the Cuatro Ciénegas bolson (Fig. 14.5). Although recognized decades before (e.g., Winsbrough and Golubić 1987; Winsborough et al. 1994), these microbialites have recently been the subject of intense investigation regarding the diversity of their microbial communities (Garcia-Pichel et al. 2004; Souza et al. 2006; Falcón et al. 2007; Escalante et al. 2008; Breitbart et al. 2009). Calcite is the predominant mineral within the microbialites although minor amounts of gypsum and silica also occur (Winsborough et al. 1994). The diverse microbial community consists of cyanobacteria (*Calothrix* sp.), anoxygenic photoautotrophs such as the green sulfur bacteria *Chlorobium tepidum* and the purple sulfur bacteria *Rhodopseudomonas palustris*, as well as sulfate reducing bacteria including *Desulfovibrio gigas* and *Desulfovibrio salexigens* (Falcón et al. 2007). Phosphorus-scavenging bacteria have also been sequenced and shown to be essential for stromatolite survival (Souza et al. 2008; Breitbart et al. 2009). Indeed, the adaptability of the stromatolite-forming microbial communities to the low-phosphorus conditions has enabled their persistence in Cuatro Ciénegas at the expense of potential predators, such as snails that have thus far been unable to adapt (Souza et al. 2008; Breitbart et al. 2009). These researchers also identified bacterial genes associated with CO_2 fixation and a large population responsible for building the extracellular polymeric substances (EPS).

14.4 Methods

14.4.1 Sample Collection

For this study we focused on two sites within the Cuatro Ciénegas bolson where stromatolites were previously reported (Winsborough 1990). The sites included the groundwater discharge area and associated marshes of the El Mojarral West system located at the northeastern corner of the Sierra de San Marcos Mountains, as well as the Rio Mesquites, into which waters from El Mojarral, and numerous other springs, flow and that historically drained the bolson to the east

(e.g., Minckley and Cole 1968; Winsborough and Golubić 1987; Winsborough 1990; Wolaver et al. 2008; Breibart et al. 2009). Water and stromatolites samples were collected at both sites for REE analysis. It should be noted that because the Cuatro Ciénegas bolson is an official biological preserve within México, we were limited in the amount of samples we could collect.

High density linear polyethylene (HDPE) sample bottles and Teflon® tubing used during water sample collection and filtration were thoroughly cleaned using trace element cleaning procedures before transport to the field for sample collection (Johannesson et al. 2004b; Willis and Johannesson 2011). Water samples were immediately filtered through 0.45 μm Gelman Sciences in-line groundwater filter capsules (polyether sulfone membrane) using a peristaltic pump and Teflon® tubing. Each water sample was pumped directly through the in-line filter capsule and into another "trace clean" 1 L HDPE bottle, which was rinsed three times with the filtered water sample to "condition" the bottle before filling the bottle with the filtered water sample. The filtered water sample was then immediately acidified to pH < 2 using ultra-pure HNO_3 (Seastar Chemical, Baseline). After collection, all samples were stored ~4 °C prior to analysis. One water sample from El Mojarral West was not filtered prior to acidification.

14.4.2 Preparation of Cuatro Ciénegas Waters for REE Analysis

All water samples collected for REE analysis were transported back to Tulane University where sample aliquots were then loaded onto Poly-Prep columns (Bio-Rad Laboratories) packed with AG 50W-X8 (100–200 mesh, hydrogen form, Bio-Rad Laboratories) cation-exchange resin at approximately 1 ml min^{-1} to separate the REEs from the major solutes and interfering ions (Johannesson et al. 2005). Iron and Ba were subsequently eluted from the columns using a 1.75 M ultra-pure HCl solution (Seastar Chemicals, Baseline, sub-boiling, distilled in quartz) and a 2 M ultra-pure HNO_3 solution (Seastar Chemicals, Baseline), respectively (Elderfield and Greaves 1983; Greaves et al. 1989; Klinkhammer et al. 1994; Stetzenhach et al. 1994). The REEs were then eluted from the columns using 8 M ultra-pure HNO_3 (Seastar Chemicals, Baseline) and collected in Teflon® beakers. The eluent was subsequently taken to dryness by heating the Teflon® beakers on a hot plate, and the residue then redissolved in 10 ml of a 2% v/v ultra-pure HNO_3 solution.

14.4.3 Preparation of Microbialite Samples for REE Analysis

Stromatolite samples were digested by lithium metaborate fusion according to methods presented in Guo et al. (2005). Specifically, 0.1 g samples of ground stromatolite (agate mortar and pestle) was mixed with 0.4 g of $LiBO_2$ and heated in a graphite crucible at 1050 °C for 20–30 min. The fused beads were then transferred to Teflon® beakers and dissolved in 15–30 ml HNO_3 (2% v/v) on a combination hot plate/stir plate using an acid-washed Teflon® stir bar. Upon dissolution (~1 h), the solution was filtered to remove graphite particles. Before analysis, samples were evaporated to near dryness and redissolved in 10 ml of HNO_3 (2% v/v).

14.4.4 REE Analysis

Each 10 ml sample was spiked with 10 ppb of ^{115}In as an internal standard to monitor instrument drift, which varied less than ±10%, and analyzed for the REEs by high resolution (magnetic sector) inductively coupled plasma mass spectrometry (HR-ICP-MS, Finnigan MAT Element II) at Tulane University. We monitored ^{139}La, ^{140}Ce, ^{141}Pr, ^{143}Nd, ^{145}Nd, ^{146}Nd, ^{147}Sm, ^{149}Sm, ^{151}Eu, ^{153}Eu, ^{155}Gd, ^{157}Gd, ^{158}Gd, ^{159}Tb, ^{161}Dy, ^{163}Dy, ^{165}Ho, ^{166}Er, ^{167}Er, ^{169}Tm, ^{172}Yb, ^{173}Yb, and ^{175}Lu (low- and medium-resolution mode) as many of these isotopes are free of isobaric interferences, and because monitoring more than one isotope provides an additional check for potential interferences (Stetzenbach

Table 14.1 Major (mmol kg^{-1}) and minor (μmol kg^{-1}) solute concentrations in waters collected from the El Mojarral spring and marsh system and the Rio Mesquites, both of which contain stromatolites, within the Cuatro Ciénegas basin. In addition, mean concentration for these solutes used in the aqueous complexation modeling of the REEs are presented. The data are from Winsborough (1990) and Evans (2005)

	El Mojarral West	Rio Mesquites	Mean Cuatro Ciénegas
pH	7.12	6.7	7.2 (range 6–8.5)
Temp. (°C)	33.3	30.4	31.1
(mmol kg^{-1})			
Ca	9.3	9.6	9.6
Mg	4.5	5	4.7
Na	6.2	7.4	7.2
K	0.21	0.28	0.25
Cl	2.9	4	3.4
HCO_3	2.68	2.47	3.23
SO_4	14.3	15.5	15
(μmol kg^{-1})			
HPO_4	0.03	0.06	0.86
H_4SiO_4	305	343	599
Fe	0.072	0.041	0.073
Mn	0.0009	–	0.011

et al. 1994; Shannon and Wood 2005). The HR-ICP-MS was calibrated and the concentrations of REEs in the samples confirmed with a series of REE calibration standards of known concentrations (1 ng kg^{-1}, 2 ng kg^{-1}, 5 ng kg^{-1}, 10 ng kg^{-1}, 100 ng kg^{-1}, 500 ng kg^{-1}, and 1000 ng kg^{-1}). The calibration standards were prepared from NIST traceable High Purity Standards (Charleston, SC). In addition, check standards were prepared using Perkin Elmer multi-element solutions and the NIST Standard Reference Material (SRM) "Trace Elements in Water No. 1643b and National Research Council Canada (Ottawa, Ontario, Canada) SMR for river waters (SRLS-3) were analyzed for each sample run to check for accuracy. Analytical precision of the REE analyses was always better than 4 % relative standard deviation (RSD), and generally better than 2 % RSD.

14.4.5 REE Solution Complexation Modeling

Solution complexation of the REEs in waters from the Cuatro Ciénegas bolson was modeled using the React program of the Geochemist's Workbench® (release 8.0; Bethke 2008; Bethke and Yeakel 2010). The Lawrence Livermore National Laboratory database (i.e., *thermo.dat*; Delany and Lundeen 1989) provided with the software was modified to include aqueous complexation reactions for REEs with inorganic ligands, which required addition of the most up-to-date stability constants for these reactions (e.g., Lee and Byrne 1992; Liu and Byrne 1998; Schijf and Byrne 1999, 2004; Klungness and Byrne 2000; Luo and Byrne 2000, 2001, 2004). We used mean concentration values of major cations and anions for the El Mojarral West and Rio Mesquites, as well as mean values of these parameters calculated from data for waters from Cuatro Ciénegas that were presented in Winsborough (1990) and Evan (1995). The major ion concentrations used in the solution complexation modeling are presented in Table 14.1.

14.5 Results

14.5.1 REE Concentrations of Cuatro Ciénegas Waters and Stromatolites

Rare earth element concentrations for water and stromatolites from the El Mojarral West springs and marsh system, as well as the Rio Mesquites are presented in Table 14.2. In addition, another stromatolite sample from Laguna Garabatal, which is located along the northwestern side of the Sierra de San Marcos Mountains (Fig. 14.4), is also listed in Table 14.2.

Table 14.2 Rare earth element concentrations in surface waters and stromatolites of the Cuatro Ciénegas Bolson, Coahuila, México. Rare earth element concentrations in the water samples are in pmol kg^{-1}, whereas those for the stromatolites are in ppb (μg kg^{-1})

	El Mojarral West[a]	El Mojarral West	Rio Mesquites 1	Rio Mesquites 2	El Mojarral West	Rio Mesquites	Laguna Garabatal
Sample Type	Water pmol kg^{-1}	Water pmol kg^{-1}	Water pmol kg^{-1}	Water pmol kg^{-1}	Stromatolite ppb	Stromatolite ppb	Stromatolite ppb
La	943	826	940	624	424	1364	1402
Ce	1863	1689	1908	1292	768	2895	2612
Pr	213	194	222	228	88.4	304	288
Nd	864	1043	935	966	345	1212	1178
Sm	141	134	158	112	70.9	245	227
Eu					13.2	39.3	20.9
Gd	113	111	146	127	80.1	252	200
Tb	13.7	13.2	16.1	12.8			
Dy	84.1	77.2	91.7	67.6	65	231	194
Ho	11	9.96	11.8	8.37			
Er	30.3	28	33.6	24.2	38.4	123	99.9
Tm	4.58	3.89	4.5	3.34			
Yb	25.9	24.4	29.1	20.7	37.5	125	101
Lu	3.7	3.51	4.24	2.99			
Ce/Ce^*	0.96	0.97	0.96	0.77	1.03	0.91	0.94
Eu/Eu^*					0.73	0.81	0.46
$(Yb/Nd)_{SN}$	0.411	0.321	0.427	0.293	1.24	1.18	0.982

[a] water sample was not filtered
$Ce/Ce^* = [Ce/(0.5La + 0.5Pr)]_{SN}$
$Eu/Eu^* = [Eu/(0.5Sm + 0.5Gd)]_{SN}$
SN shale-normalized

Concentrations of the REEs in the Cuatro Ciénegas waters are substantially higher than those measured in water discharging from a similar, carbonate-rock dominated regional flow system in southern Nevada, USA (i.e., the Ash Meadows—Death Valley system; Johannesson et al. 1997). For example, Nd concentrations in Cuatro Ciénegas waters range from 864 pmol kg^{-1} to 1043 pmol kg^{-1} [mean (±SD) Nd = 952 ± 74 pmol kg^{-1}], whereas Nd concentrations in spring waters from the Ash Meadows—Death Valley system range between 25 pmol kg^{-1} and 33 pmol kg^{-1} [mean (±SD) Nd = 28.9 ± 4.2 pmol kg^{-1}; Johannesson et al. 1997]. Shale-normalized REE patterns of Cuatro Ciénegas waters are enriched in the LREEs relative to the HREEs (Fig. 14.6). The shale-normalized Yb/Nd ratio, which is a measure of the relative fractionation of HREEs compared to the LREEs, ranges from 0.293 to 0.427 [mean Yb/Nd_{SN} (±SD) = 0.363 ± 0.066] for the Cuatro Ciénegas waters. By comparison, groundwaters from the broadly similar Ash Meadows—Death Valley system are all enriched in the HREEs over the LREEs when normalized to shale. Specifically, the Yb/Nd_{SN} ratios of waters from the Ash Meadows—Death Valley all exceed unity [mean Yb/Nd_{SN} (±SD) = 1.69 ± 1.1; Johannesson et al. 1997]. An interesting feature of the El Mojarral West water samples is the similarity between the REE concentrations and shale-normalized fractionation patterns of the filtered and unfiltered water samples, which indicate that REEs are not transported in Cuatro Ciénegas waters with particulate matter, but occur in ionic form or associated with colloids (Table 14.2, Fig. 14.6).

As expected the REE contents of the stromatolites from the Cuatro Ciénegas bolson are orders of magnitude higher than in the waters (Table 14.2, Fig. 14.6). Neodymium concentrations in the stromatolites range from 345 μg kg^{-1} up to 1212 μg kg^{-1} (i.e., 2392–8403 nmol kg^{-1}).

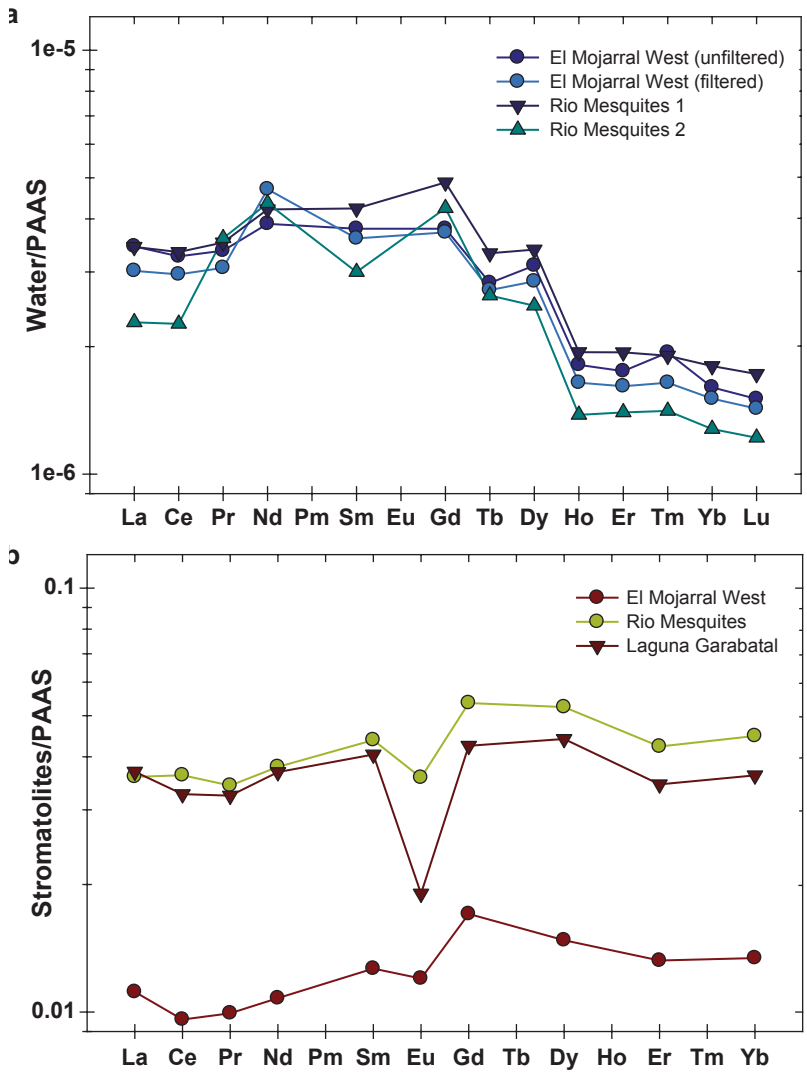

Fig. 14.6 Shale-normalized REE patterns for **a** waters from El Mojarral West and the Rio Mesquites and **b** stromatolites collected for these locations within the Cuatro Ciénegas bolson. The waters and stromatolites are normalized to Post Archean Australian Shale. (i.e., PAAS; Nance and Taylor 1976)

To the best of our knowledge, there are no other published data for the REE content of modern terrestrial stromatolites with which to compare our data. Nonetheless, we can compare the REE contents of these Cuatro Ciénegas stromatolites with measurements made by Takahashi et al. (2005) of modern microbial mats from terrestrial hot spring environments as well as the reefal microbialites analyzed by Webb and Kamber (2000). Takahashi et al. (2005) report the Nd contents of two microbial mats from the Nakabusa hot springs in Japan (7.51 mg kg^{-1} and 4.98 mg kg^{-1}), which exceed the Nd contents of the Cuatro Ciénegas stromatolites by a factor of close to 7, on average. The mean ± SD of the Nd content of the 52 reefal microbialite analyzed by Webb and Kamber (2000) is 160 ± 40.4 μg kg^{-1}, which is almost 6-fold lower than the mean Nd content of the Cuatro Ciénegas stromatolites (912 μg kg^{-1}).

Shale-normalized REE fractionation patterns for the Cuatro Ciénegas stromatolites are also presented in Fig. 14.6. The shale-normalized fractionation patterns of the stromatolites differ dramatically from the local waters in that the stromatolites exhibit enrichments in the HREEs compared to the LREEs, which is in contrast to the LREE enriched patterns of the Cuatro Ciénegas waters (Fig. 14.6). The HREE enrichments of the Cuatro Ciénegas stromatolites are

demonstrated by their shale-normalized Yb/Nd ratios, which range from ~1 to 1.24 [mean Yb/Nd_{SN} (±SD) = 1.13 ± 0.14; Table 14.2]. In addition to the HREE enrichments, the stromatolite REE patterns all exhibit varying degrees of negative Eu anomalies, and the stromatolites from El Mojarral West and Laguna Garabatal have small negative Ce anomalies (Fig. 14.6; Table 14.2). The negative Eu anomalies may be a feature of the Cuatro Ciénegas waters, however, because the water samples were analyzed using the low-resolution mode of the ICP-MS, we were unable to confidently separate the large false positive Eu counts during the analysis caused by isobaric interference from BaO^+ generated in the plasma stream. Nonetheless, the negative Eu anomalies recorded in the Cuatro Ciénegas stromatolites almost certainly reflects the depletion of Eu observed in continental rocks, which are the ultimate source of the REEs in both the Cuatro Ciénegas waters and the associated stromatolites (Hanson 1980; Johannesson and Lyons 1994).

The REE concentrations of stromatolites from the El Mojarral West system are depleted compared to the REE content of the stromatolites collected from Laguna Garabatal and Rio Mesquites (Table 14.2, Fig. 14.6). Moreover, the shale-normalized fractionation patterns of the Laguna Garabatal and Rio Mesquites stromatolites are more similar in shape than the El Mojarral West stromatolite. We have not quantified the REE concentration of waters from the Laguna Garabatal groundwater discharge zone, and thus cannot comment on the possibility that differences in REE concentrations in Laguna Garabatal waters influence the REE patterns of the stromatolites. However, the REE concentrations, and in particular, the shale-normalized fractionation patterns of waters from El Mojarral West and the Rio Mesquites are remarkably similar, indicating that the differences in the REE contents and fractionation patterns of the stromatolites are not simply due to the REE concentrations in the ambient waters. These observations are counter to those put forth by other researchers who have argued that ancient stromatolites record the REE signature of the ancient seawater within which they formed. This point is even more obvious by simple comparison of the shale-normalized REE patterns of the Cuatro Ciénegas waters and stromatolites (Fig. 14.6).

14.5.2 Aqueous Complexation of REEs of Cuatro Ciénegas Waters

The results of the aqueous complexation modeling for the REEs are shown in Fig. 14.7 for waters from the El Mojarral West system and the Rio Mesquites. Because pH of waters from Cuatro Ciénegas range from ~6.5 up to ~8.3 (Winsborough 1990; Johannesson et al. 2004a; Evans 2005), we also computed the speciation of REEs in a model, average Cuatro Ciénegas water (Table 14.1) for varying pH between 6 and 8.5 (Fig. 14.8). The mean pH of the Cuatro Ciénegas water data presented in Winsborough (1990), Johannesson et al. (2004a), and Evans (2005) is ~7.2, which is also delineated as vertical dashed lines on Fig. 14.8.

The aqueous complexation modeling for waters from the El Mojarral West system (pH 7.12) indicates that REE chiefly occur in solution as carbonato complexes (i.e., $LnCO_3^+$, where Ln indicates any of the REEs). The only exceptions are La and Pr, which the model predicts occur in solution principally complexed by sulfate ions ($LnSO_4^+$), followed by the carbonato complex (Fig. 14.7). The dicarbonato complex (i.e., $Ln(CO_3)_2^-$) is also important for the HREEs in El Mojarral West waters. In comparison, the model predicts that REEs primarily occur in solution in the Rio Mesquites (pH 6.7) as sulfate complexes, except for REEs heavier than Er, which occur chiefly as carbonato complexes (Fig. 14.7). The difference in REE complexation between El Mojarral West and Rio Mesquites waters chiefly reflects the differences in pH. Specifically, the change from predominantly $LnSO_4^+$ complexes to $LnCO_3^+$ complexes in average Cuatro Ciénegas waters occurs around pH 7 for LREEs like Nd and pH 6.3 for HREEs such as Yb (Fig. 14.8). It is important to note that for average Cuatro Ciénegas waters, LREEs are predicted to occur chiefly as carbonato complexes, followed by sulfate complexes, whereas HREE occur primarily

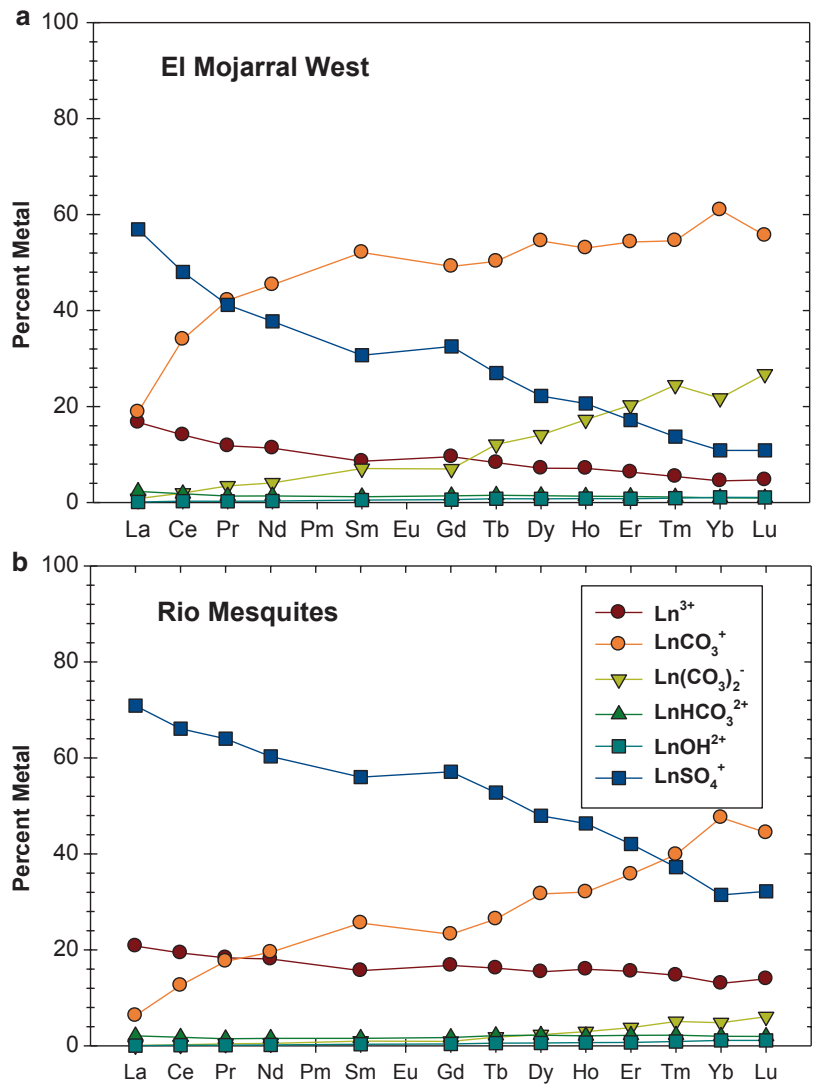

Fig. 14.7 Results of the solution complexation modeling for REEs in waters of **a** El Mojarral West and **b** the Rio Mesquites. Data used in the modeling are presented in Tables 14.1 and 14.2. Ln represents any of the REEs (i.e., lanthanides)

as carbonato complexes followed by dicarbonato complexes (Fig. 14.8).

14.6 Discussion

If REE contents, and in particular, REE fractionation patterns, of microbialites can be used as tracers of secular trends in seawater and/or terrestrial waters compositions throughout geologic time, then either: (1) uptake of the REEs from the ambient water by microbialites must not fractionate the REEs relative to the ambient water; or (2) any processes that do fractionate the REEs during such uptake must be delineated and understood. The current paradigm is that uptake of REE from ambient waters by microbialites does not lead to significant fractionation of the REEs. Again, this paradigm appears to largely rest on a study of reef microbialites from the Great Barrier Reef where solid-liquid partitioning coefficients between these microbial carbonates and the ambient seawater were shown to be fairly uniform across the REE series (Table 14.3; Webb and Kamber 2000). Nevertheless, despite what appears to be a general acceptance of this paradigm of unfractionated uptake of REEs from ambient waters by microbialites, the data presented here for the microbialites of the

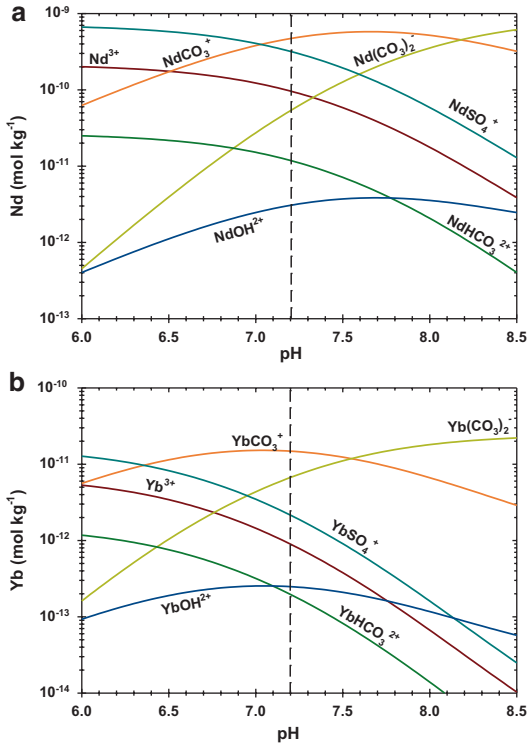

Fig. 14.8 Solution complexation model for **a** Nd and **b** Yb over the range of pH observed in waters from the Cuatro Ciénegas bolson. The model was computed using the average major solute composition of waters from the Cuatro Ciénegas bolson taken from Winsborough (1990), Johannesson et al. (2004b), and Evans (2005). The vertical *dashed line* in each panel represents the mean pH of Cuatro Ciénegas waters based on the analyses in these previous studies

Cuatro Ciénegas bolson clearly points to fractionation of the REEs during incorporation into these modern, terrestrial microbialites (Fig. 14.6). More specifically, if REEs were not fractionated from the ambient waters during incorporation into the Cuatro Ciénegas stromatolites, then the shale-normalized fractionation patterns of the stromatolites would resemble the shale-normalized REE fractionation patterns of the ambient waters, which is clearly not the case (Fig. 14.6). Again, the waters are strongly depleted in the HREEs relative to the LREEs when normalized to shale, whereas the stromatolites are enriched in the HREEs relative to the LREEs.

The marked difference in the REE fractionation patterns between the Cuatro Ciénegas stromatolites and the ambient waters within which they formed is further emphasized when their REE content is normalized to the REE concentrations of the ambient waters (Fig. 14.9). The idea here is that if the Cuatro Ciénegas stromatolites incorporate REEs from the ambient waters without fractionation, their ambient water-normalized REE fractionation patterns should be flat. Both stromatolite samples exhibit similar, highly fractionated ambient water-normalized REE patterns. More specifically, the stromatolites have relatively flat or decreasing ambient water-normalized patterns between La and Nd, but are strongly enriched in REEs heavier than Nd compared to the waters. For example, the ambient water-normalized Yb/Nd ratios are 3.27 and 3.46 for the El Mojarral West and Rio Mesquites stromatolites, respectively.

Assuming that uptake of REEs from the ambient water is the principal source of REEs in the stromatolites, the ambient water-normalized REE patterns for the El Mojarral West and the Rio Mesquites stromatolites are essentially equivalent to solid-liquid partitioning coefficients for these microbialites (e.g., Takahashi et al. 2005). The ambient water-normalized REE values for both Cuatro Ciénegas stromatolite samples are compared to solid-liquid partitioning coefficients calculated for the microbiolites from the Great Barrier Reef, and for sorption of REEs onto the cell walls of a variety of bacteria in Table 14.3. The Yb/Nd ratios for the ambient water-normalized stromatolites samples from Cuatro Ciénegas are similar in magnitude to the Yb/Nd ratios of solid-liquid partitioning coefficients describing REE sorption onto bacterial cell waters, but not those of the reef microbialites. Consequently, the similar enrichments in the HREEs between the Cuatro Ciénegas stromatolites and the bacterial cell walls suggests that the microbial component of these stromatolites plays an important role in REE uptake from the ambient waters.

Because aqueous complexation modeling indicates that typically more than ~80% of each REE is complexed by carbonate and sulfate ions in Cuatro Ciénegas waters (Figs. 14.7, 14.8), the formation of these solution complexes may impact the uptake of REEs by the microbialites

Table 14.3 Solid-liquid distribution/partitioning coefficients for REEs in Cuatro Ciénegas stromatolites, Holocene reefal microbialites from the Great Barrier Reef, and bacterial cell walls

	Rio Mesquites[a] ($\times 10^3$)	El Mojarral West[a] ($\times 10^3$)	Holocene Reefal Microbialites[b]	Bacteria Cell Walls[c] ($\times 10^3$)
La	3.9	11.1	272 ± 92	3.95 ± 1.64
Ce	3.43	11.6	452 ± 140	5.91 ± 2.27
Pr	2.79	10.6	313 ± 115	6.89 ± 2.44
Nd	2.52	8.81	284 ± 85	7.19 ± 2.42
Sm	3.5	11.9	330 ± 92	12 ± 3.63
Eu			317 ± 93	12.2 ± 3.77
Gd	3.74	14.3	297 ± 80	10.4 ± 3.37
Tb			270 ± 74	10.1 ± 3.39
Dy	5.02	17.6	263 ± 68	9.26 ± 3.12
Ho			258 ± 67	8.25 ± 2.81
Er	7.93	25.2	262 ± 69	8.9 ± 3.16
Tm				12.7 ± 4.76
Yb	8.72	28.8	324 ± 80	23.8 ± 10.1
Lu			334 ± 88	35.2 ± 16
Yb/Nd	3.46	3.27	1.14 ± 0.44	3.31 ± 1.79

[a] Content of REEs in stromatolites from Table 14.2 normalized to the mean values of the corresponding waters
[b] Estimated from Fig. 14.3A of Webb and Kamber (2000)
[c] Distribution coefficients (K_d) between bacteria and water at pH 4 from Table 14.1 of Takahashi et al. (2007). The data represent the mean ± SD *K*d (units g/g) for five separate experiments involving both gram positive and negative bacteria (i.e., *Pseudomonas fluorescens*, *Shewanella putrefaciens*, *Alcaligenes faecalis*, *Bacillus subtilis*, and *Escherichia coli*)

(Takahashi et al. 2005, 2007). Consequently, the REE content of the El Mojarral West and Rio Mesquites stromatolites are normalized to the computed free metal ion concentration for each REE in the ambient waters (i.e., $[Ln^{3+}]_F$, where Ln indicates any of the lanthanides), to correct for the potential impact of solution complexation. The resulting fractionation patterns are shown in Fig. 14.9b and the corresponding solid-liquid partitioning coefficients are included in Table 14.3. The solution complexation corrected REE fractionation patterns for the El Mojarral West and Rio Mesquites stromatolites are even more enriched in the HREEs than the uncorrected, ambient water-normalized patterns (compare Fig. 14.9a and b). For example, the Yb/Nd ratios for the solution complexation corrected fractionation patterns are 8.25 and 4.81 for the El Mojarral West and the Rio Mesquites stromatolites, respectively.

Takahashi et al. (2005) used a similar solution complexation corrected approach to calculate solid-liquid partitioning coefficients for REEs in microbial mats of the Nakafusa hot springs in Japan. They subsequently explained the LREE enrichment of the ambient (hot spring) water-normalized fractionation patterns of the microbial mats as the result of the formation of strong aqueous REE carbonate and hydroxyl complexes, which were able to outcompete surface ligands on bacterial cell walls within the microbial mat for the HREEs (Takahashi et al. 2005). That is, the increase in the stability constants with increasing atomic number across the REE series that characterizes both carbonate and hydroxyl ions (e.g., Klungness and Byrne 2000; Luo and Byrne 2004), decreases the dissolved, free REE ion concentrations across the series, limiting the activity of free HREE ions that are available to complex with surface ligands on bacterial cell walls within the microbial mat. However, because Cuatro Ciénegas stromatolites are substantially enriched in the HREEs compared to the ambient waters (Fig. 14.9), the same argument cannot be made for the origins of REE fractionation patterns of the Cuatro Ciénegas stromatolites.

Instead, in the case of the Cuatro Ciénegas stromatolites we suggest that uptake of REEs

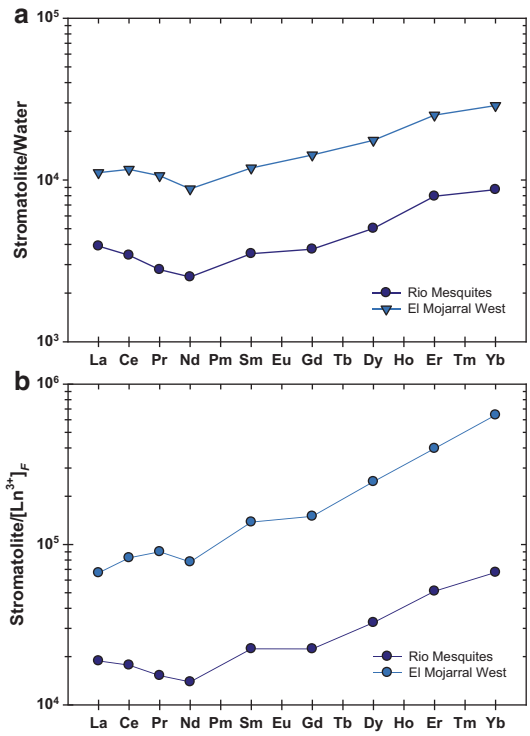

Fig. 14.9 REE fractionation patterns for the REE contents of stromatolites from the Cuatro Ciénegas bolson normalized to **a** the average REE concentrations of the corresponding waters (Table 14.2) and **b** the computed free metal concentration (i.e., Ln^{3+}) in Fig. 14.7

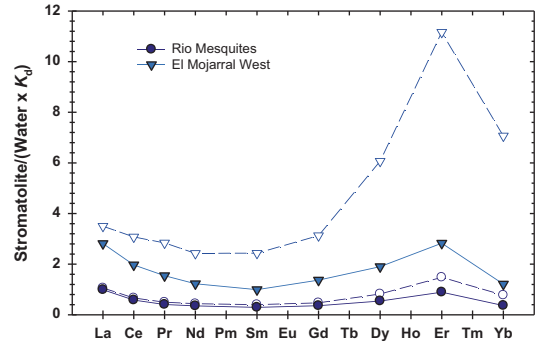

Fig. 14.10 REE fractionation patterns for stromatolites of the Cuatro Ciénegas bolson normalized to the corresponding waters corrected for REE adsorption to bacterial cell walls ($K_d \times [REE]_{solution}$). *Solid* symbols represent the product of the total REE concentration and the solid-liquid partitioning coefficient for REE sorption onto bacterial cells (see Takahashi et al. 2007), whereas the *open* symbols represent the product of the partitioning coefficient and the weakly complexed (Ln_{Tot}—$\{LnCO_3^+ + Ln(CO_3)_2^-\}$, where Ln represents each REE individually). See text for details

by surface functional groups on bacteria and exopolymeric substances produced by the various bacteria associated with these microbialites plays an important role in fractionating the REEs within the associated waters. Specifically, Takahashi et al. (2005, 2007) demonstrated that surface functional groups on bacterial cell walls preferentially sorb the HREEs relative to the LREEs. These surface sites likely outcompete the relatively weak sulfate, bicarbonate, and chloride complexes of the REEs, as well as the hydroxide complexes in the neutral pH Cuatro Ciénegas waters, which leads, in part to the HREE enrichments of the bulk stromatolites. We can test this hypothesis by comparing the REE contents of the Cuatro Ciénegas stromatolites to the product of the ambient water and the solid-liquid partitioning coefficients for REEs and bacterial cell walls (Table 14.3). More specifically, because the partitioning coefficients is defined as

$$K_d = \frac{[REE]_{solid}}{[REE]_{solution}} \tag{14.1}$$

where $[REE]_{solid}$ is the amount of each REE adsorbed by the bacterial cell wall, and hence associated with the bulk stromatolite, and $[REE]_{solution}$ is the amount of each REE in solution, the product $K_d \times [REE]_{solution}$ will be the same as $[REE]_{solid}$ if adsorption to bacterial cells in the growing stromatolite is the chief mechanism of REE uptake by the microbialite from the ambient water. For this case, the $[REE]_{solid}/(K_d \times [REE]_{solution})$ ratio will equal unity, and the resulting fractionation pattern will be flat.

Figure 14.10 presents the $[REE]_{solid}/(K_d \times [REE]_{solution})$ ratios for Cuatro Ciénegas stromatolites and waters. For each stromatolite sample we plot the bulk stromatolite REE contents normalized to $K_d \times [REE]_{solution}$ for the whole water (solid symbols) and to the water minus the fraction of REE complexed as strong carbonate complexes. The REE fractionation patterns for the Rio Mesquites are relatively flat indicating that uptake of REE by bacteria likely played an important role in fractionating the REEs from the ambient water during formation of

the microbialite (Fig. 14.10). By comparison, the El Mojarral West stromatolite exhibits more fractionation of the HREEs than the Rio Mesquites, especially when the strong HREE complexing carbonate complexes are excluded. Nonetheless, because the REE fractionation patterns presented in Fig. 14.10 are plotted on a linear scale as opposed to the logarithmic scale used in the other REE fractionation patterns of this contribution, the enrichments in HREEs depicted on Fig. 14.10 are substantially lower than those depicted in, for example, Fig. 14.9. The additional REE fractionation still apparent in Fig. 14.10 may reflect surface complexation of dissolved REEs with other organic ligands associated with the microbialites biofilms/exopolymeric substances (e.g., Xu et al. 2011). For example, a number of naturally occurring organic ligands are known to strongly complex the HREEs (Tang and Johannesson 2003; Yamamoto et al. 2005, 2010; Sonke and Salters 2006; Davranche et al. 2005, 2008, 2011; Pourret et al. 2007; Stern et al. 2007; Marsac et al. 2010; Tang and Johannesson 2010; Roberts et al. 2012; Zoll and Schijf 2012).

14.7 Implications and Conclusions

Although our investigation is limited to only a few stromatolites and associated ambient water samples from one modern, terrestrial environment (i.e., the Cuatro Ciénegas bolson in north-central México), the implications of our results may be profound with regards to deciphering the meaning of the REE contents and fractionation patterns of ancient chemical, and presumably, microbial sediments. As mentioned above, REEs have been employed as proxies for investigating secular trends in ocean chemistry through geologic time, and it is generally considered that the REE contents of Archean and Proterozoic banded iron formations (BIF) and putative microbialites (i.e., stromatolites) provide a record of paleo-ocean chemistry. Specifically, the shale-normalized REE fractionation patterns of ancient chemical sediments are generally believed to preserve the REE fractionation patterns of the ancient seawater within which they formed (e.g., Derry and Jacobsen 1990; Shimuzu et al. 1990; Danielson et al. 1992; Bau and Möller 1993). Thus, the current paradigm is that ancient chemical sediments and putative microbialites incorporated REEs into their structures directly from ancient seawater without fractionation. Hence, the relative distribution of REE in ancient chemical sediments informs us directly about their relative distribution in the ancient waters within which they precipitated. However, our results for stromatolites from the Cuatro Ciénegas bolson, which reveal substantial REE fractionation during uptake from ambient waters, calls into question the universality of the current paradigm regarding uptake without fractionation of the REE by ancient chemical sediments and putative microbialites. Indeed, the large fractionation of the HREEs in the Cuatro Ciénegas stromatolites compared to the HREE-depleted ambient waters is suggestive of, although does not prove, a possible component of REE adsorption onto the microbial cell walls and/or exopolymeric substances produced by the bacterial communities associated with these interesting microbialites. Such processes could have also been important in the Late Archean and throughout the Proterozoic, however, it is unknown if similar uptake mechanisms were active in the Early Archean (e.g., see Wacey 2009, for review).

Recently, some researchers have also argued that the REE contents and shale-normalized REE fractionation patterns of ancient chemical sediments can be used to distinguish between biotic and abiotically precipitated chemical sediments (Allwood et al. 2006; Guido et al. 2010). These arguments also appear to be based on the assumption of REE uptake from ambient waters without fractionation, as well as an enrichment of the REEs by factor of ~250 over ambient waters that directly result from some "vital" effect. Again, study of the modern, terrestrial stromatolites of the Cuatro Ciénegas bolson shows that uptake of REEs from the ambient waters by these microbialites leads to substantial fractionation of the REEs. Moreover, probable abiotic secondary carbonates from the vadose zone be-

neath Yucca Mountain in southern Nevada, also exhibit seawater-like REE patterns with similar overall enrichments to those reported for putative Early Archean microbialites from Western Australia (Fig. 14.2d; Wilson et al. 2003; Zhou 2004). Therefore, these interpretations of REEs as indicators of biotic versus abiotic origins of ancient chemical sediments also seem premature given our very poor understanding of the specific processes responsible for REE uptake by modern microbialites as demonstrated in this contribution.

Nevertheless, we recognize that without additional sampling of the waters and stromatolites of the Cuatro Ciénegas bolson, we can only hypothesize as to the mechanisms responsible for the substantial fractionation of the REEs between the ambient waters and the currently forming stromatolites, as well as the general importance of REE fractionation during uptake for other microbialites, ancient and modern. Moreover, because similar investigations of REEs in marine and other terrestrial microbialites appear to be limited to the current contribution and an earlier investigation of Holocene reefal microbialites (i.e., Webb and Kamber 200), we cannot confidently evaluate the range of possible explanations for our results indicating substantial REE fractionation during microbialite uptake versus the apparent lack of REE fractionation during uptake in the reefal microbialites. Clearly, more investigation of REE uptake by stromatolites and other microbialites from a wide variety of environmental settings in necessary before the processes acting to incorporate and fractionate, in some cases, REEs during uptake from the ambient waters by microbialites can be confidently deciphered. Such studies are critical to understanding the REE fractionation patterns of ancient chemical sediments, including putative microbialites.

Acknowledgements We would like to thank Drs. Barbara Winsborough and Brad Wolaver who collected the stromatolite samples for this project. Funds provided to Johannesson by a number of NSF grants (INT-9912159, EAR-0303761, and EAR-0805331) were instrumental to this project, and the authors thank the National Science Foundation for this invaluable assistance.

References

Alexander BW, Bau M, Andersson P, Dulski P (2008) Continentally-derived solutes in shallow Archean seawater: rare earth element and Nd isotope evidence in iron formation from the 2.9 Ga Pongola Supergroup, South Africa. Geochim Cosmochim Acta 72:378–394

Allwood AC, Walter MR, Kamber BS, Marshall CP, Burch IW (2006) Stromatolite reef from the Pilbara Craton of Western Australia. Nature 441:714–718

Anderson CR, Pedersen K (2003) In situ growth of *Gallionella* biofilms and partitioning of lanthanides and actinides between biological material and ferric oxyhydroxides. Geobiol 1:169–178

Appel PWU (1983) Rare earth elements in the Early Archaean Isua iron-formation, West Greenland. Precambrian Res 20:243–258

Arp G, Reimer A, Reitner J (1999a) Calcification in cyanobacterial biofilms of alkaline salt lakes. Eur J Phycol 34:393–403

Arp G, Theil V, Reimer A, Michaelis W, Reitner J (1999b) Biofilm exopolymers control microbialite formation at thermal springs discharging into alkaline Pyramid Lake, Nevada, USA. Sed Geol 126:159–176

Aubert D, Stille P, Probst A (2001) REE fractionation during granite weathering and removal by waters and suspended loads: Sr and Nd isotopic evidence. Geochim Cosmochim Acta 65:387–406

Baker CL (1970) Geologic reconnaissance in the Eastern Cordilleran of Mexico. Geol Soc Am, Special Paper 131

Barrat JA, Boulègue J, Tiercelin JJ, Lesourd M (2000) Strontium isotopes and rare-earth element geochemistry of hydrothermal carbonate deposits from Lake Tanganyika, East Africa. Geochim Cosmochim Acta 64:287–298

Bau M (1996) Controls on the fractionation of isovalent trace elements in magmatic and aqueous systems: evidence from Y/Ho, Zr/Hf, and lanthanide tetrad effect. Contrib Mineral Petrol 123:323–333

Bau M (1999) Scavenging of dissolved yttrium and rare earths by precipitating iron oxyhydroxide: experimental evidence for Ce oxidation, Y–Ho fractionation, and lanthanide tetrad effect. Geochim Cosmochim Acta 63:67–77

Bau M, Dulski P (1996) Distribution of yttrium and rare-earth elements in the Penge and Kuruman iron-formations, Transvaal Supergroup, South Africa. Precambrian Res 79:37–55

Bau M, Möller P (1993) Rare earth element systematics of the chemically precipitated component of Early Precambrian iron formations and the evolution of the terrestrial atmosphere-hydrosphere-lithosphere. Geochim Cosmochim Acta 57:2239–2249

Bau M, Dulski P, Möller P (1995) Yttrium and holmium in South Pacific seawater: vertical distribution and possible fractionation behavior. Chem Erde 55:1–15

Bau M, Alexander B, Chesley JT, Dulski P, Brantley SL (2004) Mineral dissolution in the Cape Cod aquifer,

Massachusetts, USA: I. Reaction stoichiometry and impact of accessory feldspar and glauconite on strontium isotopes, solute concentrations, and REY distributions. Geochim Cosmochim Acta 68:1199–1216

Baumgartner LK, Reid RP, Dupraz C, Decho AW, Buckley DH, Spear JR, Przekop KM, Visscher PT (2006) Sulfate reducing bacteria in microbial mats: changing paradigms, new discoveries. Sed Geol 185:131–145

Ben Chekroun K, Rodriguez-Navarro C, Gonzalez-Munoz MT, Arias JM, Cultrone G, Rodriguez-Gallegos M (2004) Precipitation and growth morphology of calcium carbonate induced by Myxococcus xanthus: implications for recognition of bacterial carbonates. J Sed Res 74:868–876

Bertram CJ, Elderfield H (1993) The geochemical balance of the rare earth elements an neodymium isotopes in the oceans. Geochim Cosmochim Acta 57:1957–1986

Bethke CM (2008) Geochemical and biogeochemical reaction modeling. Cambridge University Press, Cambridge, p 543

Bethke CM, Yeakel S (2010) Geochemist's Workbench® Release 8.0. Reaction modeling guide. University of Illinois, Urbana, p 84

Biddau R, Cidu R, Frau F (2002) Rare earth elements in waters from the albitite-bearing granodiorites of Central Sardinia, Italy. Chem Geol 182:1–14

Bolhar R, Kamber BS, Moorbath S, Fedo CM, Whitehouse MJ (2004) Characterisation of early Archaean chemical sediments by trace element signatures. Earth Planet Sci Lett 222:43–60

Bolhar R, Van Kranendonk MJ, Kamber BS (2005) A trace element study of siderite-jasper banded iron formation in the 3.45 Ga Warrawoona Group, Pilbara Craton—formation from hydrothermal fluids and shallow seawater. Precambrian Res 137:93–114

Bozau E, Göttlicher J, Stärk H-J (2008) Rare earth element fractionation during the precipitation and crystallisation of hydrous ferric oxides from anoxic lake water. Appl Geochem 23:3473–3486

Braissant O, Cailleau G, Dupraz C, Verrecchia EP (2003) Bacterial induced mineralization of calcium carbonate in terrestrial environments: the role of exopolysaccharides and amino acids. J Sed Res 73:485–490

Braissant O, Decho AW, Dupraz C, Glunk C, Przekop KM, Visscher PT (2007) Exopolymeric substances of sulfate-reducing bacteria: interactions with calcium at alkaline pH and implication for formation of carbonate minerals. Geobiol 5:401–411

Breitbart M, Hoare A, Nitti A, Siefert J, Haynes M, Dinsdale E, Edwards R, Souza V, Rohwer F, Hollander D (2009) Metagenomic and stable isotopic analyses of modern freshwater microbialites in Cuatro Ciénegas, Mexico. Environ Microbiol 11:16–34

Burne RV, Moore LA (1987) Microbialites: organosedimentary deposits of benthic microbial communications. Palaios 2:241–254

Burns BP, Goh F, Allen M, Nellan BA (2004) Microbial diversity of extant stromatolites in the hypersaline marine environment of Shark Bay, Australia. Environ Microbiol 6:1096–1101

Byrne RH, Kim K-H (1990) Rare earth element scavenging in seawater. Geochim Cosmochim Acta 54:2645–2656

Byrne RH, Li B (1995) Comparative complexation behavior of the rare earths. Geochim Cosmochim Acta 59:4575–4589

Byrne RH, Liu X (1998) A coupled riverine-marine fractionation model for dissolved rare earths and yttrium. Aquatic Geochem 4:103–121

Byrne RH, Liu X, Schijf J (1996) The influence of phosphate coprecipitation on rare earth distributions in natural waters. Geochim Cosmochim Acta 60:3341–3346

Cantrell KJ, Byrne RH (1987) Rare earth element complexation by carbonate and oxalate ions. Geochim Cosmochim Acta 51:597–605

Carroll SA (1993) Precipitation of Nd-Ca carbonate solids at 25 °C. Geochim Cosmochim Acta 57:3383–3393

Costerton JW, Lewandowski Z, Caldwell DE, Korber DR, Lappin-Scott HM (1995) Microbial biofilms. Ann Rev Microbiol 49:711–745

Danielson A, Möller P, Dulski P (1992) The europium anomalies in banded iron formation and the thermal history of the oceanic crust. Chem Geol 97:89–100

Davranche M, Pourret O, Gruau G, Dia A, Le Coz-Bouhnik M (2005) Adsorption of REE(III)-humate complexes onto MnO_2: experimental evidence for cerium anomaly and lanthanide tetrad effect suppression. Geochim Cosmochim Acta 69:4825–4835

Davranche M, Pourret O, Gruau G, Dia A, Jin D, Gaertner D (2008) Competitive binding of REE to humic acid and manganese oxide: impact of reaction kinetics on Ce anomaly development and REE adsorption. Chem Geol 247:154–170

Davranche M, Grybos M, Gruau G, Pédrot M, Dia A, Marsac R (2011) Rare earth element patterns: a tool for identifying trace metal sources during wetland soil reduction. Chem Geol 284:127–137

De Baar HJW, Schijf J, Byrne RH (1991) Solution chemistry of the rare earth elements in seawater. Eur J Solid State Inorg Chem 28:357–373

De Carlo EH, Green WJ (2002) Rare earth elements in the water column of Lake Vanda, McMurdo Dry Valleys, Antarctica. Geochim Cosmochim Acta 66:1323–1333

De Carlo EH, Wen X-Y, Irving M (1998) The influence of redox reactions on the uptake of dissolved Ce by suspended Fe and Mn oxide particle. Aquatic Geochem 3:357–392

Decho AW (1990) Microbial exopolymer secretions in ocean environments: their role(s) in food webs and marine processes. Oceanogr Marine Biol Rev 28:73–154

Decho AW (2000) Exopolymer microdomains as a structuring agent for heterogeneity within microbial biofilms. In: Riding RE, Awramik SM (eds) Microbial sediments. Springer-Verlag, Berlin, pp 1–9

Delaney JM, Lundeen SR (1989) The LLNL thermochemical database. Lawrence Livermore National Laboratory Report UCRL–21658

Derry LA, Jacobsen SB (1990) The chemical evolution of Precambrian seawater: evidence from REEs in

banded iron formations. Geochim Cosmochim Acta 54:2965–2977
Dia A, Gruau G, Olivié-Lauquet G, Riou C, Molénat J, Curmi P (2000) The distribution of rare earth elements in groundwaters: assessing the role of source-rock composition, redox changes and colloidal particles. Geochim Cosmochim Acta 64:4131–4151
Duncan T, Shaw TJ (2003) The mobility of rare earth elements and redox sensitive elements in the groundwater/seawater mixing zone of a shallow coastal aquifer. Aquatic Geochem 9:233–255
Dupraz C, Visscher PT (2005) Microbial lithification in marine stromatolites and hypersaline mats. Trends Microbiol 13:429–438
Dupraz C, Visscher PT, Baumgartner LK, Reid RP (2004) Microbe-mineral interactions: early carbonate precipitation in a hypersaline lake (Eleuthera Island, Bahamas). Sedimentology 51:745–765
Dupraz C, Reid RP, Braissant O, Decho AW, Norman RS, Visscher PT (2009) Processes of carbonate precipitation in modern microbial mats. Earth-Sci Rev 96:141–162
Elderfield H (1988) The oceanic chemistry of the rare-earth elements. Phil Transactions R Soc London A 325:105–126
Elderfield H, Greaves MJ (1982) The rare earth elements in seawater. Nature 296:214–219
Elderfield H, Greaves MJ (1983) Determination of rare earth elements in sea water. In: Wong CS, Boyle E, Bruland KW, Burton JD, Goldberg ED (eds) Trace metals in sea water. Plenum Press, New York, pp 427–445
Elderfield H, Upstill-Goddard R, Sholkovitz ER (1990) The rare earth elements in rivers, estuaries, and coastal seas and their significance to the composition of ocean waters. Geochim Cosmochim Acta 54:971–991
Elzinga EJ, Reeder RJ, Withers SH, Peale RE, Mason RA, Beck KM, Hess WP (2002) EXAFS study of rare-earth element coordination in calcite. Geochim Cosmochim Acta 66:2875–2885
Escalante AE, Eguiarte LE, Espinosa-Asuar L, Forney LJ, Noguez AM, Souza Saldivar A (2008) Diversity of aquatic prokaryotic communities in the Cuatro Cienegas basin. FEMS Microbiol Ecol 65:50–60
Evans SB (2005) Using chemical data to define flow systems in Cuatro Cienegas, Coahuila, Mexico. Thesis, University of Texas, Austin
Falcón LI, Cerritos R, Eguiarte LE, Souza V (2007) Nitrogen fixation in microbial mats and stromatolite communities from Cuatro Cienegas, Mexico. Microbiol Ecol 54:363–373
Fenchel T, King GM, Blackburn H (2012) Bacterial Biogeochemistry: the ecophysiology of mineral cycling, 3rd edn. Academic Press, Amsterdam, p 303
Ferris FG, Schultze S, Witten TC, Fyfe WS, Beveridge TJ (1989) Metal interactions with microbial biofilms in acidic and neutral pH environments. Appl Environ Microbiol 55:1249–1257
Firsching FH, Mohammadzadel J (1986) Solubility products of the rare-earth carbonates. J Chem Eng Data 31:40–42
Friend CRL, Nutman AP, Bennett VC, Norman MD (2008) Seawater-like trace element signature (REE + Y) of Eoarchaean chemical sedimentary rocks from southern West Greenland, and their corruption during high-grade metamorphism. Contrib Mineral Petrol 155:229–246
Garcia-Pichel F, Al-Horani FA, Farmer JD, Ludwig R (2004) Balance between microbial calcification and metazoan bioerosion in modern stromatolitic oncolites. Geobiol 2:49–57
Gautret P, Trichet J (2005) Automicrites in modern cyanobacterial stromatolitic deposits of Rangiroa, Tuamotu Archipelago, French Polynesia: biochemical parameters underlying their formation. Sed Geol 178:55–73
Gerdes G (2010) What are microbial mats? In: Seckbach J, Oren A (eds) Microbial mats: modern and ancient microorganisms in stratified systems. Cellular Origin, Life in Extreme Habitats and Astrobiology 14:5–25
Goldstein SJ, Jacobsen SB (1988) Rare earth elements in river waters. Earth Planet Sci Lett 89:35–47
Greaves MJ, Elderfield H, Klinkhammer GP (1989) Determination of rare earth elements in natural waters by isotope-dilution mass spectrometry. Anal Chim Acta 218:265–280
Grotzinger JP, Rothman DH (1996) An abiotic model for stromatolite morphogenesis. Nature 383:423–425
Guido A, Mastandrea A, Tosti F, Russo F (2010) Importance of rare earth elements patterns in discrimination between biotic and abiotic mineralization. In: Reitner J, Quéric N-V, Arp G (eds) Advances in stromatolite geobiology. Lecture notes in earth sciences 131. Springer, Berlin, pp 433–442
Guo C, Stetzenbach KJ, Hodge VF (2005) Determination of 56 trace elements in three aquifer-type rocks by ICP-MS and approximation of the solubilities of these elements in a carbonate system by water-rock concentration ratios. In: Johannesson KH (ed) Rare earth elements in groundwater flow systems. Springer, Dordrecht, pp 39–65
Han G, Liu C-Q (2007) Dissolved rare earth elements in river waters draining karst terrains in Guizhou Province, China. Aquatic Geochem 13:95–107
Hanson GN (1980) Rare earth elements in petrogenetic studies of igneous systems. Ann Rev Earth Planet Sci 8:371–406
Høgdahl OT, Bowen BT, Melson S (1968) Neutron activation analysis of lanthanide elements in seawater. Adv Chem Ser 73:308–325
Hoyle J, Elderfield H, Gledhill A, Greaves M (1984) The behaviour of the rare earth elements during the mixing of river and sea waters. Geochim Cosmochim Acta 48:143–149
Jakeš P, Gill J (1970) Rare earth elements and the island arc tholeiitic series. Earth Planet Sci Lett 9:17–28
Johannesson KH (2012) Rare earth element geochemistry of scleractinian coral skeleton during meteoric diagenesis: a sequence through neomorphism of aragonite to calcite by Webb et al., Sedimentology, 56, 1433–1463: Discussion. Sedimentology 59:729–732

Johannesson KH, Burdige DJ (2007) Balancing the global oceanic neodymium budget: evaluating the role of groundwater. Earth Planet Sci Lett 253:129–142

Johannesson KH, Hendry MJ (2000) Rare earth element geochemistry of groundwaters from a thick till and clay-rich aquitard sequence, Saskatchewan, Canada. Geochim Cosmochim Acta 64:1493–1509

Johannesson KH, Lyons WB (1994) The rare earth element geochemistry of Mono Lake water and the importance of carbonate complexing. Limnol Oceanogr 39:1141–1154

Johannesson KH, Lyons WB, Bird DA (1994) Rare earth element concentrations and speciation in alkaline lakes from the western U.S.A. Geophys Res Lett 21:773–776

Johannesson KH, Stetzenbach KJ, Hodge VF, Lyons WB (1996) Rare earth element complexation behavior in circumneutral pH groundwaters: assessing the role of carbonate and phosphate ions. Earth Planet Sci Lett 139:305–319

Johannesson KH, Stetzenbach KJ, Hodge VF, Kreamer DK, Zhou X (1997) Delineation of ground-water flow systems in the Southern Great Basin using aqueous rare earth element distributions. Ground Water 35:807–819

Johannesson KH, Zhou X, Guo C, Stetzenbach KJ, Hodge VF (2000) Origin of rare earth element signatures in groundwaters of circumneutral pH from southern Nevada and eastern California, USA. Chem Geol 164:239–257

Johannesson KH, Cortés A, Kilroy KC (2004a) Reconnaisance isotopic and hydrochemical study of Cuatro Ciénegas groundwater, Coahuila, México. J South Am Earth Sci 17:171–180

Johannesson KH, Tang J, Daniels JM, Bounds WJ, Burdige DJ (2004b) Rare earth element concentrations and speciation in organic-rich blackwaters of the Great Dismal Swamp, Virginia, USA. Chem Geol 209:271–294

Johannesson KH, Cortés A, Ramos Leal JA, Ramírez AG, Durazo J (2005) Geochemistry of rare earth elements in groundwaters from a rhyolite aquifer, central México. In: Johannesson KH (ed) Rare earth elements in groundwater flow systems. Springer, Dordrecht, pp 187–222

Johannesson KH, Hawkins DL Jr, Cortés A (2006) Do Archean chemical sediments record ancient seawater rare earth element patterns? Geochim Cosmochim Acta 70:871–890

Johannesson KH, Chevis DA, Burdige DJ, Cable JE, Martin JB, Roy M (2011) Submarine groundwater discharge is an important net source of light and middle REEs to coastal waters of the Indian River Lagoon, Florida, USA. Geochim Cosmochim Acta 75:825–843

Kawaguchi T, Decho AW (2002) Characterization of extracellular polymeric secretions (EPS) from modern soft marine stromatolites (Bahamas) and its inhibitory effect on $CaCO_3$ precipitation. Preparative Biochem Biotechnol 32:51–63

Kempe S, Kazmierczak J (1994) The role of alkalinity in the evolution of ocean chemistry, organization of living systems, and biocalcification processes, vol 13. Bull l'Institute Océanogr, Monaco, pp 61–117

Kim K-H, Byrne RH, Lee JH (1991) Gadolinium behavior in seawater: a molecular basis for gadolinium anomalies. Mar Chem 36:107–120

Klinkhammer G, Elderfield H, Hudson A (1983) Rare earth elements in seawater near hydrothermal vents. Nature 305:185–188

Klinkhammer G, German CR, Elderfield H, Greaves MJ, Mitra A (1994) Rare earth elements in hydrothermal fluids and plume particulates by inductively coupled plasma mass spectrometry. Mar Chem 45:170–186

Klungness GD, Byrne RH (2000) Comparative hydrolysis behavior of the rare earth elements and yttrium: the influence of temperature and ionic strength. Polyhedron 19:99–107

Koeppenkastrop D, DeCarlo EH (1992) Sorption of rare earth elements from seawater onto synthetic mineral particles: an experimental approach. Chem Geol 95:251–263

Koeppenkastrop D, DeCarlo EH (1993) Uptake of rare earth elements from solution by metal oxides. Environ Sci Technol 27:1796–1806

Konhauser K (2007) Introduction to geomicrobiology. Blackwell Publishing, Malden, p 425

Lee JH, Byrne RH (1992) Examination of comparative rare earth element complexation behavior using linear free-energy relationships. Geochim Cosmochim Acta 56:1127–1137

Lehmann C, Osleger DA, Montañez IP, Sliter W, Arnaud-Vanneau A, Banner J (1999) Evolution of the Cupido and Coahuila carbonate platforms, early Cretaceous, northeastern Mexico. Geol Soc Am Bull 111:1010–1029

Lesser Jones H (1965) Confined fresh water aquifers in limestone, exploited in the north of Mexico with deep wells below sea level. In: Proceedings Dubrovnik Symposium, 1965, Hydrology of Fractured Rocks. vol 2. International Association of Scientific Hydrology, pp 526–539

Lesser y Asociados (2001) Sinopsis del estudio de evaluación hidrogeologógica e isotópica en el Valle del Hundido, Coahuila. Guadalajara, Jalisco. Comisin Nacional del Agua, Subdirección General Técnica, Gerencia de Aguas Subterráneas, Mexico

Ley RE, Harris JK, Wilcox J, Spear JR, Miller SR, Bebout BM, Maresca JA, Bryant DA, Sogin ML, Pace NR (2006) Unexpected diversity and complexity of the Guerrero Negro hypersaline microbial mat. Appl Environ Microbiol 72:3685–3695

Leybourne MI, Cousens BL (2005) Rare earth elements (REE) and Nd and Sr isotopes in groundwater and suspended sediments from the Bathurst Mining Camp, New Brunswick: water-rock reactions and elemental fractionation. In: Johannesson KH (ed) Rare earth elements in groundwater flow systems. Springer, Dordrecht, pp 253–293

Leybourne MI, Johannesson KH (2008) Rare earth elements (REE) and yttrium in stream waters, stream sediments, and Fe-Mn oxyhydroxides: fractionation, speciation, and controls over REE + Y patterns in the surface environment. Geochim Cosmochim Acta 72:5962–5983

Leybourne MI, Goodfellow WD, Boyle DR, Hall GM (2000) Rapid development of negative Ce anomalies in surface waters and contrasting REE patterns in groundwaters associated with Zn-Pb massive sulphide deposits. Appl Geochem 15:695–723

Liu X, Byrne RH (1998) Comprehensive investigation of yttrium and rare earth element complexation by carbonate ions using ICP-mass spectrometry. J Sol Chem 27:803–815

Lowe DR (1994) Abiological origin of described stromatolites older than 3.2 Ga. Geology 22:387–390

Ludwig R, Al-Horani FA, deBeer D, Jonkers HM (2005) Photosynthesis-controlled calcification in a hypersaline microbial mat. Limnol Oceanogr 50:1836–1843

Luo Y-R, Byrne RH (2000) The ionic strength dependence of rare earths and yttrium fluoride complexes at 25 °C. J Sol Chem 29:1089–1099

Luo Y-R, Byrne RH (2001) Yttrium and rare earth element complexation by chloride ions at 25 °C. J Sol Chem 30:837–845

Luo Y-R, Byrne RH (2004) Carbonate complexation of yttrium and the rare earth elements in natural waters. Geochim Cosmochim Acta 68:691–699

Lyons WB, Long DT, Hines ME, Gaudette HE, Armstrong PB (1984) Calcification of cyanobacterial mats in solar lake, Sinai. Geology 12:623–626

Marsac R, Davranche M, Gruau G, Dia A (2010) Metal loading effect on rare earth element binding to humic acid: experimental and modelling evidence. Geochim Cosmochim Acta 74:1749–1761

McKenzie D, O'Nions RK (1991) Partial melt distributions from inversion of rare earth element concentrations. J Petrol 32:1021–1091

Meinrath G, Takeishi H (1993) Solid-liquid equilibria of Nd^{3+} in carbonate systems. J Alloys Compounds 194:93–99

Michard A, Albarède F (1986) The REE content of some hydrothermal fluids. Chem Geol 55:51–60

Minckley WL (1969) Environments of the Bolsón of Cuatro Ciénegas, Coahuila, México, with special reference to the aquatic biota. University of Texas El Paso Science Series. Texas Western Press, El Paso

Minckley WL, Cole GA (1968) Preliminary limnologic information on waters of the Cuatro Cienegas Basin, Coahuila, Mexico. Southwest. Naturalist 13:421–431

Minckley WL (1984) Cuatro Ciénegas fishes: research review and a local test of diversity versus habitat size. J Arizona-Nevada Acad Sci 19:13–21

Moffett JW (1990) Microbially mediated cerium oxidation in sea water. Nature 345:421–423

Moffett JW (1994) The relationship between cerium and manganese oxidization in the marine environment. Limnol Oceanogr 39:1309–1318

Monty CLV (1977) Evolving concepts on the nature and the ecological significance of stromatolites. In: Flügel E (ed) Fossil algae. Springer-Verlag, Berlin, pp 15–35

Murray GE (1961) Geology of the Atlantic and Gulf Coastal Province of North America. Harper and Brothers, New York

Nance WB, Taylor SR (1976) Rare earth element patterns and crustal evolution—I. Australian post-Archean sedimentary rocks. Geochim Cosmochim Acta 40:1539–1551

Négrel Ph, Guerrot C, Cocherie A, Azaroual M, Brach M, Fouillac Ch (2000) Rare earth elements, neodymium and strontium isotopic systematics in mineral waters: evidence from the Massif Central, France. Appl Geochem 15:1345–1367

Nozaki Y, Zhang J, Amakawa H (1997) The fractionation between Y and Ho in the marine environment. Earth Planet Sci Lett 148:329–340

Nutman AP, Friend CRL, Bennett VC, Wright D, Norman MD (2010) ≥ 3700 Ma pre-metamorphic dolomite formed by microbial mediation in the Isua supracrustal belt (W. Greenland): simple evidence for early life? Precambrian Res 183:725–737

Paerl HW, Yannarell AC (2010) Environmental dynamics, community structure and function in a hypersaline microbial mat. In: Seckbach J, Oren A (eds) Microbial mats: modern and ancient microorganisms in stratified systems, cellular origin, life in extreme habitats and astrobiology, vol 14. Springer, Dordrecht, pp 423–442

Papineau D, Walker J, Mojzsis SJ, Pace NR (2005) Composition and structure of microbial communities from stromatolites of Hamelin Pool in Shark Bay, Western Australia. Appl Environ Microbiol 71:4822–4832

Piepgras DJ, Wasserburg GJ (1987) Rare earth element transport in the western North Atlantic inferred from Nd isotopic observations. Geochim Cosmochim Acta 51:1257–1271

Planavsky N, Bekker A, Rouxel O, Kamber B, Hofmann A, Knudsen A, Lyons TW (2010) Rare earth element an yttrium compositions of Archean and Paleoproterozoic Fe formations revisited: Ne perspectives on the significance and mechanisms of deposition. Geochim Cosmochim Acta 74:6387–6405

Pokrovsky OS, Schott J (2002) Iron colloids/organic matter associated transport of major and trace elements in small boreal rivers and their estuaries (NW Russia). Chem Geol 190:141–179

Pourret O, Davranche M, Gruau G, Dia A (2007) Organic complexation of rare earth elements in natural waters: evaluating model calculations from ultrafiltration data. Geochim Cosmochim Acta 71:2718–2735

Pourret O, Gruau G, Dia A, Davranche M, Molénat J (2010) Colloidal controls on the distribution of rare earth elements in shallow groundwaters. Aquatic Geochem 16:31–59

Quinn KA, Byrne RH, Schijf J (2004) Comparative scavenging of yttrium and the rare earth elements in seawater: competitive influences of solution and surface complexataion. Aquatic Geochem 10:59–80

Quinn KA, Byrne RH, Schijf J (2006) Sorption of yttrium and rare earth elements by amorphous ferric hydroxide: influence of solution complexation with carbonate. Geochim Cosmochim Acta 70:4151–4165

Reid RP, Visscher PT, Decho AW, Stolz JF, Bebout BM, Dupraz C, MacIntyre IG, Paerl HW, Pinckney JL, Prufert-Bebout L, Steppe TF, Des Marais DJ (2000) The role of microbes in accretion, lamination and early lithification of modern marine stromatolites. Nature 406:989–992

Riding R (2010) The nature of stromatolites: 3,500 million years of history and a century of research. In: Reitner J, Quéric N-V, Arp G (eds) Advances in stromatolite geobiology. Lecture Notes in Earth Sciences 131. Springer, Berlin, pp 29–74

Roberts NL, Piotrowski AM, Elderfield H, Eglinton TI, Lomas MW (2012) Rare earth element association with foraminifera. Geochim Cosmochim Acta 94:57–71

Rönnback P, Åström M, Gustafsson J-P (2008) Comparison of the behaviour of rare earth elements in surface waters, overburden groundwaters and bedrock groundwaters in two granitoidic settings, Eastern Sweden. Appl Geochem 23:1862–1880

Schijf J, Byrne RH (1999) Determination of stability constants for the mono- and difluoro-complexes of Y and the REE, using a cation-exchange resin and ICP-MS. Polyhedron 18:2839–2844

Schijf J, Byrne RH (2004) Determination of $SO_4\beta_1$ for yttrium and the rare earth elements at I = 0.66 m and t = 25 °C–Implications for YREE solution speciation in sulfate-rich waters. Geochim Cosmochim Acta 68:2825–2837

Schijf J, Marshall KS (2011) YREE sorption on hydrous ferric oxide in 0.5 M NaCl solutions: a model. Mar Chem 123:32–43

Semikhatov MA, Gebelein CD, Cloud P, Awramik SM, Benmore WC (1979) Stromatolite morphogenesis—progress and problems. Can J Earth Sci 16:992–1015

Shannon WM, Wood SA (2005) The analysis of picogram quantities of rare earth elements in natural waters. In: Johannesson KH (ed) Rare earth elements in groundwater flow systems. Springer, Dordrecht, pp 1–37

Shiller AM (2002) Seasonality of dissolved rare earth elements in the lower Mississippi River. Geochem Geophys Geosyst 3(11):1068. doi:10.1029/2002GC000372

Shimizu H, Umemoto N, Masuda A, Appel PWU (1990) Sources of iron-formations in the Archean Isua and Malene supracrustals, West Greenland: evidence from La—Ce and Sm—Nd isotopic data and REE abundances. Geochim Cosmochim Acta 54:1147–1154

Sholkovitz ER (1992) Chemical evolution of rare earth elements: fractionation between colloidal and solution phases of filtered river water. Earth Planet Sci Lett 114:77–84

Sholkovitz ER (1995) The aquatic chemistry of rare earth elements in rivers and estuaries. Aquatic Geochem 1:1–34

Sholkovitz ER, Schneider DL (1991) Cerium redox cycles and rare earth elements in the Sargasso Sea. Geochim Cosmochim Acta 55:2737–2743

Sholkovitz ER, Shen GT (1995) The incorporation of rare earth elements in modern coral. Geochim Cosmochim Acta 59:2749–2756

Sholkovitz ER, Szymczak R (2000) The estuarine chemistry of rare earth elements: comparison of the Amazon, Fly, Sepik and Gulf of Papua systems. Earth Planet Sci Lett 179:299–309

Sholkovitz ER, Church TM, Arimoto R (1993) Rare earth element composition of precipitation, precipitation particles, and aerosols. J Geophys Res 98:20587–20599

Sonke JE, Salters VJM (2006) Lanthanide—humic substances complexation. I. Experimental evidence for a lanthanide contraction effect. Geochim Cosmochim Acta 70:1495–1506

Souza V, Espinosa-Asuar L, Escalante AE, Eguiarte LE, Farmer J, Forney L, Lloret L, Rodríguez-Martínez JM, Soberón X, Dirzo R, Elser JJ (2006) An endangered oasis of aquatic microbial biodivsersity in the Chihuahuan desert. Proc Natl Acad Sci U S A 103:6565–6570

Souza V, Eguiarte LE, Siefert J, Elser JJ (2008) Microbial endemism: does phosphorus limitation enhance speciation? Nature Rev Microbiol 6:559–564

Stern JC, Sonke JE, Salters VJM (2007) A capillary electrophoresis-ICP-MS study of rare earth element complexation by humic acids. Chem Geol 246:170–180

Stetzenbach KJ, Amano M, Kreamer DK, Hodge VF (1994) Testing the limits of ICP-MS: determination of trace elements in ground water at the parts-per-trillion level. Ground Water 32:976–985

Stolz JF, Reid RP, Visscher PT, Decho AW, Norman RS, Aspden RJ, Bowlin EM, Franks J, Foster JS, Paterson DM, Przekop KM, Underwood GJC, Prufert-Bebout L (2009) The microbial communities of the modern marine stromatolites at Highborn Cay, Bahamas. Atoll Res Bull 567:1–29

Tang J, Johannesson KH (2003) Speciation of rare earth elements in natural terrestrial waters: assessing the role of dissolved organic matter from the modeling approach. Geochim Cosmochim Acta 67:2321–2339

Tang J, Johannesson KH (2005) Rare earth element concentrations, speciation, and fractionation along groundwater flow paths: the Carrizo Sand (Texas) and Upper Floridan aquifers. In: Johannesson KH (ed) Rare earth elements in groundwater flow systems. Springer, Dordrecht, pp 223–251

Tang J, Johannesson KH (2006) Controls on the geochemistry of rare earth elements along a groundwater flow path in the Carrizo Sand aquifer, Texas, USA. Chem Geol 225:156–171

Tang J, Johannesson KH (2010) Ligand extraction of rare earth elements from aquifer sediments: implications for rare earth element complexation with organic matter in natural waters. Geochim Cosmochim Acta 74:6690–6705

Takahashi Y, Châtellier X, Hattori KH, Kato K, Fortin D (2005) Adsorption of rare earth elements onto bacterial cell walls and its implication for REE sorption onto natural microbial mats. Chem Geol 219:53–67

Takahashi Y, Hirata T, Shimizu H, Ozaki T, Fortin D (2007) A rare earth element signature for bacteria in natural waters. Chem Geol 244:569–583

Taylor SR (1964) Abundance of chemical elements in the continental crust: a new table. Geochim Cosmochim Acta 28:1273–1285

Taylor SR, McLennan SM (1985) The continental crust: its composition and evolution. Blackwell, Oxford, p 312

Tricca A, Stille P, Steinmann M, Kiefel B, Samuel J, Eikenberg J (1999) Rare earth elements and Sr and Nd isotopic compositions of dissolved and suspended loads from small river systems in the Vosges mountains (France), the river Rhine and groundwater. Chem Geol 160:139–158

Van Kranendonk MJ, Webb GE, Kamber BS (2003) Geological and trace element evidence for a marine sedimentary environment of deposition and biogenicity of 3.45 Ga stromatolitic carbonates in the Pilbara Craton, and support for a reducing Archean ocean. Geobiol 1:91–108

Van Lith Y, Warthmann R, Vasconcelos C, McKenzie JA (2003) Sulfate-reducing bacteria induce low-temperature Ca-dolomite and high Mg-calcite formation. Geobiol 1:71–79

Visscher PT, Stolz JF (2005) Microbial mats as bioreactors: populations, processes and products. Paleogeogr Paleoclimatol Paleoecol 219:87–100

Visscher PT, Reid RP, Bebout BM (2000) Microscale observations of sulfate reduction: correlation of microbial activity with lithified micritic laminae in modern marine stromatolites. Geology 28:919–922

Wacey D (2009) Early life on earth: a practical guide. Springer, Dordrecht, p 274

Walter LM, Bischof SA, Patterson WP, Lyons TW (1993) Dissolution and recrystallization in modern shelf carbonates: evidence from pore water and solid phase chemistry. Phil Trans Royal Soc London A 344:27–36

Webb GE, Kamber BS (2000) Rare earth elements in Holocene reefal microbialites: a new shallow water proxy. Geochim Cosmochim Acta 64:1557–1565

Willis SS, Johannesson KH (2011) Controls on the geochemistry of rare earth elements in sediments and groundwaters of the Aquia aquifer, Maryland, USA. Chem Geol 285:32–49

Wilson NSF, Cline JS, Amelin YV (2003) Origin, timing, and temperature of secondary calcite-silica mineral formation at Yucca Mountain, Nevada. Geochim Cosmochim Acta 67:1145–1176

Winsborough BM (1990) Some ecological aspects of modern freshwater stromatolites in lakes and streams of the Cuatro Cienegas Basin, Coahuila, Mexico. Dissertation, University of Texas, Austin

Winsborough BM, Golubić S (1987) The role of diatoms in stromatolite growth: two examples from modern freshwater settings. J Phycol 23:195–201

Winsborough BM, Seeler J-S, Golubić S, Folk RL, Maquire B (1994) Recent fresh-water lacustrine stromatolites, stromatolitic mats and oncoids from Northeastern Mexico. In: Bertand-Sarfati J, Monty C (eds) Phanerozoic Stromatolites II. Kluwer Academic Publishers, Amsterdam, pp 71–100

Wolaver BD, Sharp JM Jr, Rodriguez JM, Ibarra Flores JC (2008) Delineation of regional arid karstic aquifers: an integrative data approach. Ground Water 46:396–413

Wright DT, Wacey D (2005) Precipitation of dolomite using sulfate-reducing bacteria from the Coorong Region, South Australia: significance and implications. Sedimentology 52:987–1008

Xu C, Zhang S, Chuang C-X, Miller EJ, Schwehr KA, Santschi PH (2011) Chemical composition and relative hydrophobicity of microbial exopolymeric substances (EPS) isolated by anion exchange chromatography and their actinide-binding affinities. Mar Chem 126:27–36

Yamamoto K, Itoh N, Matsumoto T, Tanaka T, Adachi M (2004) Geochemistry of Precambian carbonate intercalated in pillows and its host basalt: implications for the REE composition of circa 3.4 Ga seawater. Precambrian Res 135:331–344

Yamamoto Y, Takahashi Y, Shimizu H (2005) Systematics of stability constants of fulvate complexes with rare earth ions. Chem Lett 34:880–881

Yamamoto Y, Takahashi Y, Shimizu H (2010) Systematic change in relative stabilities of REE-humic complexes at various metal loading levels. Geochem J 44:39–63

Yan XP, Kerrich R, Hendry MJ (2001) Distribution of the rare earth elements in porewaters from a clay-rich aquitard sequence, Saskatchewan, Canada. Chem Geol 176:151–172

Zhang YS, Amakawa H, Nozaki Y (1994) The comparative behaviours of yttrium and lanthanides in the seawater of the North Pacific. Geophys Res Lett 21:2677–2680

Zhong S, Mucci A (1995) Partitioning of rare earth elements (REEs) between calcite and seawater solutions at 25 °C and 1 atm, and high dissolved REE concentrations. Geochim Cosmochim Acta 59:443–453

Zhou X (2004) Trace element geochemistry of groundwater flow systems in Southern Nevada and Eastern California. Dissertation, University of Nevada, Las Vegas

Zoll AM, Schijf J (2012) A surface complexation model of YREE sorption on Ulva lactuca in 0.5–5.0 M NaCl solutions. Geochim Cosmochim Acta 97:183–199

Index

Y. Dilek, H. Furnes (eds.), *Evolution of Archean Crust and Early Life*, Modern Approaches in Solid Earth Sciences 7, DOI 10.1007/978-94-007-7615-9, © Springer Science+Business Media Dordrecht 2014